

Physics of Atomic Nuclei

Nuclear and Particle Physics – An Introduction 2e

2009

Print ISBN: 978-0-470-74275-4

Adobe PDF ISBN: 978-0-470-74398-0

Vital eBook PDF ISBN: 978-1-118-30406-8

*CourseSmart ISBN: 978-1-118-30407-5

ePub ISBN: 978-1-119-96511-4

eMobi ISBN: 978-1-119-96512-1

Iliadis, C.

Nuclear Physics of Stars

2 Edition

2015

Print ISBN: 978-3-527-33648-7

Adobe PDF ISBN: 978-3-527-33649-4

eMobi ISBN: 978-3-527-33650-0

ePub ISBN: 978-3-527-33651-7

ISBN: 978-3-527-69266-8

Lilley, J.

Nuclear Physics – Principles & Applications

2001

Print ISBN: 978-0-471-97936-4

ePub ISBN: 978-1-118-72332-6

eMobi ISBN: 978-1-118-72333-3

Griffiths, D.

Introduction to Elementary Particles

2 Edition

2008

Print ISBN: 978-3-527-40601-2

Kratz, J., Lieser, K.H.

Nuclear and Radiochemistry Fundamentals and Applications

3 Edition

2013

Print ISBN: 978-3-527-32901-4

ISBN: 978-3-527-65333-1

eMobi ISBN: 978-3-527-65334-8

ePub ISBN: 978-3-527-65335-5

Adobe PDF ISBN: 978-3-527-65336-2

Stock, R. (ed.)

Encyclopedia of Nuclear Physics and its Applications

2013

Print ISBN: 978-3-527-40742-2

eMobi ISBN: 978-3-527-64925-9

ePub ISBN: 978-3-527-64926-6

Adobe PDF ISBN: 978-3-527-64927-3

Nagashima, Y.

Beyond the Standard Model of Elementary Particle Physics

2014

Print ISBN: 978-3-527-41177-1

ISBN: 978-3-527-66502-0

eMobi ISBN: 978-3-527-66503-7

ePub ISBN: 978-3-527-66504-4

Adobe PDF ISBN: 978-3-527-66505-1

Physics of Atomic Nuclei

*Vladimir Zelevinsky
Alexander Volya*

WILEY-VCH
Verlag GmbH & Co. KGaA

Authors

Prof. Vladimir Zelevinsky

Michigan State University
Department of Physics and Astronomy
Cyclotron 640 South Shaw Lane
MI
United States

Prof. Alexander Volya

Florida State University
Department of Physics
208 Keen Building
FL
United States

Cover

Atomic model: fotolia_©morena
Background: fotolia_©agsandrew

All books published by Wiley-VCH are carefully produced. Nevertheless, authors, editors, and publisher do not warrant the information contained in these books, including this book, to be free of errors. Readers are advised to keep in mind that statements, data, illustrations, procedural details or other items may inadvertently be inaccurate.

Library of Congress Card No.: applied for

British Library Cataloguing-in-Publication Data
A catalogue record for this book is available from the British Library.

Bibliographic information published by the Deutsche Nationalbibliothek

The Deutsche Nationalbibliothek lists this publication in the Deutsche Nationalbibliografie; detailed bibliographic data are available on the Internet at <<http://dnb.d-nb.de>>.

© 2017 Wiley-VCH Verlag GmbH & Co. KGaA,
Boschstr. 12, 69469 Weinheim, Germany

All rights reserved (including those of translation into other languages). No part of this book may be reproduced in any form – by photostriking, microfilm, or any other means – nor transmitted or translated into a machine language without written permission from the publishers. Registered names, trademarks, etc. used in this book, even when not specifically marked as such, are not to be considered unprotected by law.

Print ISBN: 978-3-527-41350-8

ePDF ISBN: 978-3-527-69360-3

ePub ISBN: 978-3-527-69363-4

Mobi ISBN: 978-3-527-69362-7

oBook ISBN: 978-3-527-69361-0

Cover Design Adam-Design, Weinheim, Germany

Typesetting SPi Global, Chennai, India

Printing and Binding

Printed on acid-free paper

Contents

Dedication *xiii*

Preface *xv*

1 Building Blocks and Interactions 1

- 1.1 What Are the Nuclei Made Of? 1
- 1.2 Proton and Neutron 3
- 1.3 Strong Interactions 4
- 1.4 Electromagnetic Interactions and Charge Distribution 5
- 1.5 Magnetic Properties 10
- 1.6 Weak Interactions 11
- 1.7 Neutron Decay 13
- 1.8 Nuclear World 15
- References 19

2 Isospin 21

- 2.1 Quantum Numbers in the Two-Body Problem 21
- 2.2 Introducing Isospin 23
- 2.3 Isospin Invariance 25
- 2.4 Space–Spin Symmetry and Isospin Invariance 26
- 2.5 Glimpse of a More General Picture 30
- 2.6 Relations between Cross Sections 31
- 2.7 Selection Rules 35
- 2.8 Isobaric Mass Formulae 38
- References 41

3 Two-Body Dynamics and the Deuteron 43

- 3.1 Low-Energy Nuclear Forces 43
- 3.2 Example: Argonne Potential 45
- 3.3 Meson Exchange 48
- 3.4 Deuteron: Central Forces and *s*-Wave 51
- 3.5 Tensor Forces and *d*-Wave 55
- 3.6 Magnetic Dipole Moment 58
- 3.7 Electric Quadrupole Moment 59
- References 65

4	Two-Body Scattering	67
4.1	Scattering Problem	67
4.2	Phase Shifts	69
4.3	Scattering Length	71
4.4	Sign of the Scattering Length	78
4.5	Resonance Scattering at Low Energies	80
4.6	Effective Radius	82
4.7	Scattering of Identical Particles	83
4.8	Coulomb Scattering	86
4.9	Coulomb-Nuclear Interference	87
	References	89
5	Liquid Drop Model	91
5.1	Binding Energies	91
5.2	Shape Variables	95
5.3	Microscopic Variables	97
5.4	Multipole Moments	98
5.5	Kinetic Energy and Inertial Parameters	100
5.6	Shape Vibrations	102
5.7	Stability of the Charged Spherical Liquid Drop	104
	References	111
6	Vibrations of a Spherical Nucleus	113
6.1	Sound Waves	113
6.2	Isovector Modes	117
6.3	Giant Resonance and Linear Response	119
6.4	Classification of Normal Modes	121
6.5	Quantization of Nuclear Vibrational Modes	125
6.6	Multiphonon Excitations	128
6.7	Angular Momentum Classification	132
	References	134
7	Fermi Gas Model	135
7.1	Mean Field and Quasiparticles	135
7.2	Perfect Fermi Gas	137
7.3	Ground State	138
7.4	Correlation Between Particles	142
7.5	Asymmetric Systems and Chemical Equilibrium	143
7.6	Pressure and Speed of Sound	146
7.7	Gravitational Equilibrium	148
7.8	Nuclear Matter Equation of State	150
	References	151
8	Spherical Mean Field	153
8.1	Introduction	153
8.2	Magic Numbers	153
8.3	Separation Energy	155

8.4	Periodicity of Nuclear Spectra	156
8.5	Harmonic Oscillator Potential	157
8.6	Orbital Momentum Representation	160
8.7	Square Well Potential	162
8.8	Spin–Orbit Coupling	163
8.9	Realistic Level Scheme	165
8.10	Semiclassical Origins of Shell Structure	166
	References	168
9	Independent Particle Shell Model	169
9.1	Shell Model Configurations	169
9.2	Particle–Hole Symmetry	171
9.3	Magnetic Moment	172
9.4	Quadrupole Moment	174
9.5	Recoil Corrections	177
9.6	Introduction to Group Theory of Multiparticle Configurations	178
	References	183
10	Light Nuclei	185
10.1	A Short Walk along the Beginning of the Nuclear Chart	185
10.2	Halo in Quantum Systems	190
10.3	Nuclear Halos	192
10.4	One-Body Halo	193
10.5	Two-Body Halos	195
10.6	Efimov States	199
	References	202
11	Many-Body Operator Formalism	203
11.1	Secondary Quantization	203
11.2	Physical Observables: One-Body Operators	208
11.3	Two-Body Operators	209
11.4	Interparticle Interaction	210
11.5	Interaction in a Spherical Basis	213
11.6	Recoupling of Angular Momentum	215
	References	222
12	Nuclear Deformation	223
12.1	Idea of Nuclear Deformation	223
12.2	Collective Model	224
12.3	Adiabatic Approximation	226
12.4	Onset of Deformation	228
12.5	Quadrupole Deformation in the Body-Fixed Frame	230
12.6	Quadrupole Shape Variables	232
12.7	Variety of Quadrupole Shapes	233
12.8	Empirical Deformation	235
12.9	Single-Particle Quantum Numbers	239
12.10	Anisotropic Harmonic Oscillator	240
12.11	Asymptotic Quantum Numbers	245

12.12	Nilsson Potential	246
12.13	More Examples	247
	References	250
13	Pairing Correlations	251
13.1	Physical Evidence	251
13.2	Seniority Scheme	256
13.3	Multipole Moments in the Seniority Scheme	260
13.4	Degenerate Model	261
13.5	Canonical Transformation	265
13.6	BCS Theory: Trial Wave Function	269
13.7	Energy Minimization	271
13.8	Solution for the Energy Gap	273
13.9	Excitation Spectrum	276
13.10	Condensation Energy	278
13.11	Transition Amplitudes	279
	References	281
14	Gamma-Radiation	283
14.1	Introduction	283
14.2	Electromagnetic Field and Gauge Invariance	283
14.3	Photons	285
14.4	Interaction of Radiation with Matter	288
14.5	Radiation Probability	291
14.6	Electric Dipole Radiation	292
14.7	Electric Quadrupole Radiation	295
14.8	Magnetic Dipole Radiation	296
14.9	Photoabsorption	298
14.10	Multipole Expansion	299
	References	303
15	Nuclear Gamma-Transitions and Related Electromagnetic Processes	305
15.1	Single-Particle Transitions	305
15.2	Collective Transitions	308
15.3	Nuclear Isomerism	310
15.4	Isospin	312
15.5	Structural Selection Rules	315
15.6	Monopole Transitions	318
15.7	Internal Electron Conversion	320
15.8	Coulomb Excitation	322
15.9	Nuclear Photoeffect	326
15.10	Electron Scattering	330
	References	335
16	Nuclear Rotation	337
16.1	Introduction: Rotational Bands	337

16.2	Finite Rotations	345
16.3	Rotation Matrices as Functions on the Group	346
16.4	Euler Angles	347
16.5	Angular Momentum in Euler Angles	351
16.6	Eigenfunctions of Angular Momentum	354
16.7	Rigid Rotor	355
16.8	Symmetry Properties	357
16.9	Simplest Solutions	358
16.10	Ground-State Band	359
16.11	Intensity Rules	360
16.12	Electric Quadrupole Moment	363
16.13	Magnetic Moment	366
16.14	Symmetry Properties Revisited	367
16.15	Coriolis Mixing and Decoupling Parameter	368
16.16	Classical Rotation and Routhian	370
16.17	Cranked Rotation	372
16.18	Moment of Inertia	375
16.19	Adiabatic Expansion	377
16.20	Rotation of a Perfect Fermi Gas	379
16.21	Perfect Bose Gas and Ideal Liquid	381
16.22	Pairing Effects	384
16.23	Band Crossing	385
	References	388
17	Self-Consistent Field	391
17.1	Exchange Interaction	391
17.2	Hartree–Fock Equations	395
17.3	Operator Formulation	397
17.4	Single-Particle Density Matrix	398
17.5	Hartree–Fock–Bogoliubov Approximation	400
17.6	General Canonical Transformation	402
17.7	Solutions	404
17.8	Generalized Density Matrix	407
17.9	Pairing and Particle Number Conservation	409
17.10	Effective Interaction	411
17.11	Skyrme Functionals	413
17.12	Generalization to Nonzero Temperature	418
	References	419
18	Collective Modes	421
18.1	Schematic Model	421
18.2	Random Phase Approximation	426
18.3	Canonical Form of the RPA	427
18.4	Model with Factorized Forces	430
18.5	Collective Modes as Bosons	432
18.6	Mapping of Dynamics	433
18.7	Normalization and the Mass Parameter	435

18.8	Symmetry Breaking	438
18.9	Generator Coordinate Method	444
	References	446
19	Bosons, Symmetries and Group Models	447
19.1	Introduction	447
19.2	Low-Lying Quadrupole Excitations as Interacting Bosons	448
19.3	Algebra of Boson Operators	450
19.4	Subgroups and Casimir Operators	452
19.5	$s-d$ Model	455
19.6	Irreducible Representations and Quantum Numbers	458
19.7	Vibrational Limit	461
19.8	$O(6)$ Limit	466
19.9	$SU(3)$ Limit	468
19.10	Shapes and Phase Transitions in the IBM	470
	References	473
20	Statistical Properties	475
20.1	Introduction	475
20.2	Level Density: General Properties	478
20.3	Darwin–Fowler Method	480
20.4	Relation to Statistical Thermodynamics	482
20.5	Thermodynamics of a Nuclear Fermi Gas	483
20.6	Statistics of Angular Momentum	486
20.7	Shell Model Monte Carlo Approach	488
20.8	Thermodynamics of Compound Reactions	490
20.9	Statistical Description of Resonances	492
	References	497
21	Nuclear Fission	499
21.1	Introduction	499
21.2	Alpha-Decay	502
21.3	Neutron Fission	505
21.4	Photofission	509
21.5	Fission as a Large-Amplitude Collective Motion	510
21.6	Nonadiabatic Effects and Dissipation	512
21.7	Fission Isomers	514
21.8	Parity Violation in Fission	518
	References	522
22	Heavy-ion Reactions: Selected Topics	525
22.1	Introduction	525
22.2	Experimental Indications	526
22.3	Macroscopic Description	530
22.4	Equilibration as a Diffusion Process	534
22.5	Toward a Microscopic Description	540
22.6	Sketch of a More General Approach	541

22.7	A Simple Model	545
22.8	Nuclear Multifragmentation	547
22.9	More about Fusion Reactions	550
	References	553
23	Configuration Interaction Approach	555
23.1	Center-of-Mass Problem	555
23.2	Matrix Elements of Two-Body Interactions	558
23.3	<i>Ab initio</i> Approach	559
23.4	Three-Body Forces	564
23.5	Semiempirical Effective Interactions	565
23.6	Shell-Model Hamiltonian, Properties and Solutions	570
23.7	Effective Non-Hermitian Hamiltonian	571
23.8	From Isolated to Overlapping Resonances	576
23.9	Realistic Nuclear Calculations	581
	References	583
24	Weak Interactions	585
24.1	Introduction	585
24.2	Beta-Spectrum in the Simplest Case	587
24.3	Nuclear Transitions	590
24.4	Dirac Formalism	595
24.5	Four-Fermion Theory	599
24.6	Nuclear Structure Effects	601
24.7	Parity Violation	604
24.8	Electric Dipole Moment	607
24.9	Nuclear Enhancement	609
24.10	On the Way to Electroweak Theory	612
24.11	Higgs Mechanism	616
24.12	Neutrino: Oscillations	618
24.13	Neutrino: Majorana or Dirac?	620
	References	623
25	Nucleus as a Chaotic System	627
25.1	Introduction	627
25.2	Strength Function	628
25.3	Level Density Revisited	633
25.4	Complexity of Wave Functions	636
25.5	Correlations between Classes of States	639
25.6	Invariant Entropy	643
25.7	Random Matrix Ensembles	646
25.8	Thermalization	650
	References	652
	General Nuclear Data Resources	655
	Index	657

In loving memory of the great physicist, teacher, and friend Spartak T. Belyaev.

Preface

Nuclear physics is currently enjoying a renaissance due to the availability of new experimental facilities and significant computational advances. There is a renewed interest in the studies of nuclei far from stability, fundamental symmetries, astrophysics, atomic physics, and related fields. Nuclear science connects and expands ideas from different areas which include low- and high-energy physics, few- and many-body dynamics, and classical and quantum statistical mechanics.

There are well-known books devoted to the physics of atomic nuclei, including the classical texts *Theoretical Nuclear Physics* by J. Blatt and V. Weisskopf, *Nuclear Structure* by A. Bohr and B.R. Mottelson, and *The Nuclear Many-Body Problem* by P. Ring and P. Schuck. Although many years have passed since their first publication, they are still informative to students as well as to experienced researchers. One can also find numerous books for those just starting their studies in nuclear science, or for more seasoned researchers in other fields who wish to connect their work to some aspects of nuclear physics.

We hope that the present text will be useful to students who wish to not only grasp the basic framework of nuclear physics but to clearly understand the logical threads that permeate the field and thus to maintain a broader perspective. Starting from basic principles, we try to show the path to modern, often unsolved, problems. Our goal is to give our readers a solid understanding of the fundamentals and to go beyond the majority of available textbooks.

Although the text is new, it is based on lectures by V.Z. at the Budker Institute of Nuclear Physics in Novosibirsk (a small part of which was collected in a short book coauthored with V.F. Dmitriev), the Niels Bohr Institute in Copenhagen, and Michigan State University, as well as in courses taught by A.V. at Florida State University. We have provided many problems, some of them with solutions, which should be considered an essential part of the text.

Throughout the text our goal is to explain the underlying physics and to establish the relationship between theoretical equations and experimental observables. The explanations are based on quantum mechanics, an understanding of which is a prerequisite to reading this text. In many places, we supply additional details via references to the two-volume textbook *Quantum Physics* by V.Z. (Wiley, 2011); they are referred to as [QP, I or II, ...] where I or II indicates the volume, and the ellipsis contains the section or equation number. Any modern quantum mechanics textbook is also suitable.

In our presentation, we try to maintain a practitioner's perspective by highlighting methods and algorithms from computational physics and presenting results from

numerical investigations. Owing to the rapidly evolving nature of programming languages and hardware platforms, we do not endorse or provide any specific codes. Links to software can be found using search engines, software repositories, and the web pages of various research groups, including those of the authors (some guidance is provided at the end of the book). Most figures in the text are original and are based on freely accessible experimental data (a list of the relevant data centers is provided) and on the described computational methods.

The last few chapters go beyond the standard menu of nuclear physics courses and are selected from the viewpoint of our own scientific interests. Here we do not hesitate to introduce concepts which could be perceived as nontraditional. Regrettably, in the single volume we could only scratch the surface of the theory of nuclear reactions. The same goes for the details of modern theoretical efforts, so we limited this discussion to short explanations and references to the original articles and reviews.

Over the course of many years, we have greatly benefited from discussions with excellent scientists in various countries; unfortunately, it is impossible to give them individual credit here. We are grateful to Valerie Molière for suggesting to organize our work into a publishable manuscript. The careful editorial work of Samanaa Srinivas and Sujisha Kunchi Parambathu is especially acknowledged. Of course, in such an extensive text, it is hardly possible to avoid ambiguities and errors. We would be extremely grateful to our readers for any constructive feedback.

The work on the book consumed significant time and effort on our part. We are deeply grateful to our families for their patience and support.

East Lansing, Michigan, United States
Tallahassee, Florida, United States
September 2016

*Vladimir Zelevinsky
Alexander Volya*

1

Building Blocks and Interactions

Our job in physics is to see things simply, to understand a great many complicated phenomena in a unified way, in terms of a few simple principles.

S. Weinberg, *Nobel Lecture, 1979.*

1.1 What Are the Nuclei Made Of?

The standard textbook statement reads “Nuclei consist of *protons* and *neutrons*.” For the major part of what we are going to discuss in the course, this simple notion is approximately true. Indeed, complex nuclei in the Universe were mostly “cooked” in stars by the processes of consecutive addition of neutrons and protons and their mutual transformations. It is relatively easy to extract these particles back from the nuclei since the *separation energy* per particle is typically only 6–8 MeV, less than 1% of the mass of the proton (p) or neutron (n) that is of order $\sim 1 \text{ GeV} = 10^3 \text{ MeV}$.

In many nuclei with an abnormal ratio between the proton and neutron numbers, the separation energy is even significantly lower than the value mentioned earlier. And still the statement of our first sentence has a limited range of validity. In general, the answer to the question of nuclear constituents depends on the kind of phenomena we are interested in. Various experimental studies emphasize different aspects of nuclear structure. Different patterns can be resolved at different *energy scales* by specifically adjusted experimental tools.

The *nuclear forces* that keep the nucleus together are induced through exchange by mediating quanta – *mesons*, similar to how the *electromagnetic* interactions are generated by the exchange of *photons*. Roughly speaking, at energies small compared to the masses of particles that are capable of serving as mediators of nuclear forces, the nucleus indeed looks as an object composed of protons and neutrons. (Note that such a range of energies does not exist in the case of electromagnetic interactions carried by *massless* photons.)

Protons and neutrons have very similar nuclear properties, and they are called by a unifying term “*nucleons*” (N). The mesons of the lightest family, *pions* ($\pi^{+,0,-}$), are approximately seven times lighter than the nucleons. Corresponding energies $E < m_\pi c^2 \approx 140 \text{ MeV}$ define a domain of *low-energy* nuclear physics where the nucleus can be considered as being made of *nonrelativistic* nucleons. In this domain, mesons are *virtual* particles hidden in nucleon–nucleon interactions, and they rarely appear

as autonomous entities. Here, we have in mind the *excitation energy* of a nucleus with respect to its *ground state* rather than the total mass or *binding energy* of a complex nucleus or energy of the beams used by experimentalists for inducing nuclear reactions and producing excited nuclei.

The area of low-energy nuclear physics where the main new results of the near future are to be obtained is related to *radioactive beam facilities*. The nucleus appears here as a self-bound *many-body* nucleonic system with its own intrinsic degrees of freedom, *single-particle* and *collective*. Such systems, along with complex atoms and molecules, micro- and nanodevices of condensed matter physics, and artificial systems, such as cold atoms in traps or future quantum computers, are called *mesoscopic*. They occupy an intermediate place between macroscopic and microscopic worlds. The peculiarity of this class of physical systems is twofold: they are sufficiently large to reveal generic *statistical* regularities; at the same time they are sufficiently small to allow physicists to study, theoretically and experimentally, individual *quantum states*. This area is the subject of our main interest.

At higher energies, one can directly see mesons and intrinsic excitations of nucleons – *nucleon resonances*, as well as heavier relatives of nucleons containing *strange* quarks – *hyperons*. Relativistic effects become more and more important. This is the region of *intermediate energy* nuclear physics that can be characterized by energies up to few gigaelectronvolts. One of the most effective tools for studying this field is electron scattering (e.g., at Thomas Jefferson National Accelerator Facility) with the wavelength short enough for resolving individual nucleons and some features of their intrinsic structure inside the nucleus.

Finally, at even higher energies and in processes with high momentum transfer, it is possible to resolve deep constituents of nucleons and mesons: *quarks* and *gluons*. Physicists expect that at densities several times higher than the normal nuclear density, the nucleons melt forming a quark–gluon soup. Such a phase of hot and dense nuclear matter supposedly existed at the early stages of the Universe and can be recreated in relativistic heavy ion collisions. Important results in this direction were obtained at the Super Proton Synchrotron (CERN) and at Relativistic Heavy Ion Collider (RHIC, Brookhaven); they are being reinforced by research work at the Large Hadron Collider (LHC) also at CERN. Such experiments detect collision products of heavy nuclei, as gold on gold, at very high energies up to 200 GeV – 10 TeV per nucleon. This area can be called *high-energy* nuclear physics. The energy of 10 TeV ($1 \text{ TeV} = 10^3 \text{ MeV}$) used in proton accelerators is in fact *macroscopic* being equal to 16 erg; in cosmic rays, rare events were detected at energy of the order 10^8 erg.

As a whole, nuclear physics covers a huge energy range from electronvolts (an upper limit for the hypothetical neutrino mass that might be measured in nuclear beta-decay and energy of slow neutrons used in many applications) and kiloelectronvolts (gamma-ray energies in low-energy nuclear transitions and energies of astrophysical nuclear reactions) to gigaelectronvolts and teraelectronvolts (RHIC and LHC). Although we start here with basic features of a more broad picture, our topics are taken mostly from low-energy physics. The main theoretical tools will be nonrelativistic quantum mechanics and quantum statistics. Nevertheless, even at this stage, some relativistic effects are to be included. As a whole, nuclear structure and reactions give an exceedingly rich material for learning how quantum mechanics works in the real world and for understanding mesoscopic physics in general.

1.2 Proton and Neutron

We start with a short description of main nuclear constituents, nucleons. Their properties will be taken as an empirical input to the physics of nuclei. A free proton and a free neutron have nearly equal masses. In convenient energy units ($1 \text{ MeV} = 1.602 \times 10^{-6} \text{ erg} = 1.602 \times 10^{-13} \text{ J}$),

$$M_p c^2 = 938.272 \text{ MeV}, \quad M_n c^2 = 939.565 \text{ MeV}, \quad (1.1)$$

so that their relative mass difference is $\delta M/M_p = 0.14\%$. Since the free neutron is slightly heavier, it turns out to be unstable and undergoes *beta-decay* into the proton, electron, and electron antineutrino (Section 1.4). The *half-life* of the neutron is $t_{1/2} \approx 615 \text{ s}$; the *mean lifetime* τ that appears in the *exponential decay* law,

$$N(t) = N(0)e^{-t/\tau}, \quad (1.2)$$

is $\tau = t_{1/2}/\ln 2 = 881.5 \text{ s}$. The exact lifetime is currently being debated. The number quoted is a result of averaging of several conflicting experimental data. Experiments with neutron beams [1] and with ultracold neutrons in a magnetic bottle [2] produce results that differ by as much as 8 s. Nuclei can be stable against neutron decay only because the nuclear forces prefer an optimal ratio between the proton and neutron numbers so that the spontaneous neutron decay inside the nucleus may be energetically forbidden. Moreover, nuclei with proton excess may undergo beta-decay in the opposite direction transforming protons into neutrons.

Joint requirements of relativity and quantum theory put limitations to a notion of a free particle. For a particle of mass m , an attempt to localize its wave packet within a time interval Δt gets meaningless when the corresponding energy uncertainty $\Delta E \sim \hbar/\Delta t$ becomes comparable to the mass (1.1). For the nucleons, the characteristic time is

$$\Delta t_N \sim \frac{\hbar}{Mc^2} \approx 0.7 \times 10^{-24} \text{ s}. \quad (1.3)$$

At times shorter than Δt_N due to the large energy uncertainty, the nucleon wave function loses its *single-particle* nature and acquires components with particle–antiparticle pairs. The minimum localization length is of the order of

$$\lambda_N \sim c\Delta t_N \sim \frac{\hbar}{Mc} \approx 2 \times 10^{-14} \text{ cm}. \quad (1.4)$$

For any particle of mass m , the Compton wavelength \hbar/mc , as in Eq. (1.4), defines the limit of spatial localization when it is still possible to keep the single-particle character of the description.

The nucleons have *spin* 1/2. Therefore, they are *fermions*, particles that obey Fermi statistics, that is, many-body wave functions have to be *antisymmetric* with respect to interchange of *all* (space and spin) variables of any pair of *identical* nucleons. Because of the similarity between the proton and the neutron with respect to strong (nuclear) forces, it will be possible and useful to introduce higher, *isobaric*, symmetry and approximately consider them as different charge states of the nucleon. It is necessary to mention that relativistic theory introduces *antiparticles* with the same masses and the same lifetimes as the corresponding particles. Antiprotons and antineutrons have been discovered and studied. The striking predominance of particles and absence of antiparticles in the observable Universe is still not fully understood.

1.3 Strong Interactions

Nucleons take part in all known interactions. The main features of the nuclear world are shaped by *strong* interactions that are responsible for nuclear forces and stability of matter. Usually all particles participating in strong interactions are called *hadrons*. Nucleons are the lightest fermions among hadrons. The *mesons* mediating strong interactions are hadrons with an integer spin. Particles with an integer spin are *bosons*. According to current concepts, low-energy nuclear forces are manifestations of interactions at a more fundamental level between the constituents of hadrons, quarks, and gluons. These interactions are described by the *quantum chromodynamics* (QCD).

As far as we know, there are two additive quantities, *charges*, which are absolutely conserved in all observed processes, *electric* charge and *baryonic* charge. Only hadrons can have a nonzero baryonic charge B . In this case, they are called *baryons*; mesons are hadrons with $B = 0$. The proton and the neutron have the same baryonic charge that is taken to be equal to +1; this is a signature of the isobaric symmetry. If the baryonic charge is strictly conserved, the lightest baryon – proton – has to be stable. Experiments searching for proton decay did not find such events. All charges of antiparticles are of the same magnitude and of the opposite sign relative to those of corresponding particles.

Neutrons carry no electric charge and protons have an elementary electric charge $+e$. Thus, a nucleus with the electric charge Ze and baryonic charge B is treated, within the above-discussed limitations of low energy, as built of Z protons and N neutrons that comprise the mass number $A = Z + N = B$. These two quantum numbers, Z and B , are sufficient to characterize a nuclear species, *nuclide*. However, standard excessive notations, when a nuclide is designated as ${}^A_Z Y_N$, with Y being a chemical symbol of the element (of course, equivalent to the knowledge of Z), do no harm. The nuclides with the same A but different Z (different proton–neutron composition) form a set of *isobars*, those with the same Z but different N are *isotopes* of the same *chemical element*, while the nuclides with the same N and different Z are *isotones*.

On the nucleon level, “strong” interactions are indeed strong: for a pair of nucleons at a distance of the order of the nucleon Compton wavelength (1.4), typical interaction energy is of the order of Mc^2 . However, these interactions have a relatively *short range* $r_0 \simeq (1 \div 2) \text{ fm} \simeq 10^{-13} \text{ cm}$ and rapidly die away at $r > r_0$. The shortest range of interactions still keeping identity of the nucleons corresponds to the size of the distribution of quark–gluon matter inside the nucleons, $\simeq 0.8 \text{ fm}$. At short distances, the interaction is similar to the *hard-core repulsion*. At larger distances the interaction is *attractive*, this allows the nucleus to be self-bound and determines a typical interparticle distance inside the nucleus.

The longest range of nuclear forces can be estimated with the aid of the uncertainty relation used in Eq. (1.4). Assume that the interaction is mediated by field quanta being emitted by one particle and absorbed by another particle (Figure 1.1). Let a quantum of the intermediate field have mass m . The creation of a virtual particle of mass m is associated with the energy uncertainty $\Delta E \sim mc^2$. This determines the lifetime $\Delta t \sim \hbar/mc^2$ of such a fluctuation and the maximum possible propagation distance

$$\Delta R \sim c\Delta t \sim \frac{\hbar}{mc}. \quad (1.5)$$

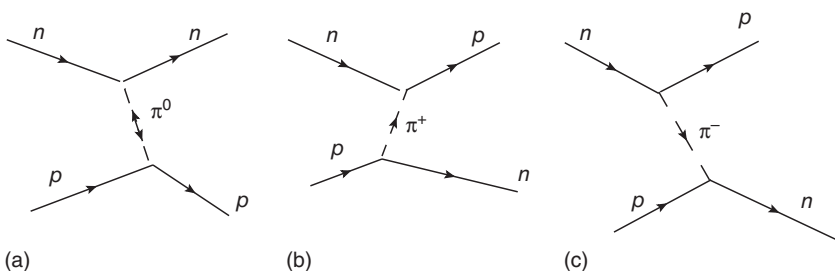


Figure 1.1 Meson exchange as a mechanism of the nucleon interaction.

Hence, the range of nuclear forces is defined by the Compton wavelength of the *lightest* particle that can mediate the strong interaction. The lightest meson is the neutral pion π^0 with $mc^2 = 135$ MeV that corresponds to $\hbar/mc = 1.46$ fm. (It is useful to know that $\hbar c = 197.327$ MeV fm.) The shortest time relevant for nuclear processes is determined by the lifetime of such fluctuations or by the flight time across the size of the range of nuclear forces, 1 fm = 10^{-13} cm, at the speed of light, $\Delta t \sim 1$ fm/c = 0.3×10^{-23} s. Of course, typical times of flight increase for slower particles and larger nuclear sizes; the latter can reach 10^{-12} cm for the heaviest nuclei.

1.4 Electromagnetic Interactions and Charge Distribution

Nucleons also interact with *electromagnetic* fields. Protons have positive electric charge $+e$ equal in magnitude and opposite in sign to the charge of electrons. Therefore, protons repel each other via Coulomb forces. Due to the long-range nature of the electric force (the electrostatic potential $\sim 1/r$), it prevails at large distances beyond the radius of the strong force. However, at distances $r \sim \lambda_N$, the Coulomb energy

$$\frac{e^2}{\lambda_N} \sim \frac{e^2}{\hbar c} Mc^2 \equiv \alpha Mc^2 \quad (1.6)$$

is small compared to Mc^2 . The dimensionless *fine structure constant*

$$\alpha = \frac{e^2}{\hbar c} \approx 1/137 \quad (1.7)$$

is characteristic for the relative strength of electromagnetic interactions. Its smallness allows one to take into account these interactions in a regular *perturbative* manner prescribed by *quantum electrodynamics* (QED), which is the most precise branch of modern theoretical physics. Due to the relative weakness of electromagnetic forces, the best *nondemolishing* probes of nuclear structure and charge distribution rely on electromagnetic interactions (electron scattering, muonic atoms, etc.). Electron scattering from nuclear targets reveals that charge and currents inside the nucleons can be characterized by the nucleon *charge radius* ~ 0.8 fm. It is harder to get precise quantitative information on the distribution of nuclear matter.

Problem 1.1 Estimate the energy shift of the ground atomic state for the electron and the negative muon as a function of the nuclear size.

Solution

For a nucleus of finite size, the electrostatic potential $\varphi(\mathbf{r})$ acting onto atomic electrons is different from the potential $\varphi_0(\mathbf{r}) = Ze/r$ of the point charge Ze . The difference

$$\delta\varphi(\mathbf{r}) = \varphi(\mathbf{r}) - \frac{Ze}{r} \quad (1.8)$$

can be considered as a source of perturbation that induces the shift of energy levels of atomic electrons

$$\delta E_e = \int d^3r \delta\varphi(\mathbf{r})\rho_e(\mathbf{r}). \quad (1.9)$$

The shift can be measured by the displacement of atomic spectral lines. Here $\rho_e(\mathbf{r})$ is the unperturbed electron charge density

$$\rho_e(\mathbf{r}) = -e|\psi_e(\mathbf{r})|^2 \quad (1.10)$$

expressed in terms of the electron wave function $\psi_e(\mathbf{r})$. For s -electrons the wave function is real and spherically symmetric so that the integral in (1.9) contains only the isotropic (monopole) component of the nuclear electrostatic potential. Outside the nuclear volume, according to the Gauss theorem, this component is the same as for the point-like charge, so that the integrand in (1.9) vanishes outside the nucleus. Inside the nucleus, the electron s -wave function is practically a constant $\psi_e(0)$, and this value can be taken outside the integral leading to

$$\delta E_e = -e|\psi_e(0)|^2 \int d^3r \left(\varphi(r) - \frac{Ze}{r} \right). \quad (1.11)$$

Using the explicit expression for the potential inside the uniformly charged sphere of radius R with the total charge Ze ,

$$\varphi(r) = \frac{Ze}{2R} \left(3 - \frac{r^2}{R^2} \right), \quad r \leq R, \quad (1.12)$$

and calculating the integral in Eq. (1.11), we come to

$$\delta E_e = \frac{2\pi}{5} |\psi_e(0)|^2 Ze^2 R^2. \quad (1.13)$$

It is customary to introduce the mean square charge radius of the nucleus via its charge density $\rho_{ch}(\mathbf{r})$,

$$\overline{r_{ch}^2} = \frac{1}{Ze} \int d^3r \rho_{ch}(\mathbf{r})r^2. \quad (1.14)$$

For a nucleus as a uniformly charged sphere of radius R ,

$$\overline{r_{ch}^2} = \frac{3}{5} R^2, \quad (1.15)$$

so that our result (1.13) can be written as

$$\delta E_e = \frac{2\pi}{3} |\psi_e(0)|^2 Ze^2 \overline{r_{ch}^2}. \quad (1.16)$$

It is easy to see that in this form the result is quite general and applicable to any spherically symmetric charge distribution inside the nucleus. To show this, we can use the identity with the Laplace operator

$$\nabla^2 r^2 = 6 \quad (1.17)$$

and to rewrite the integral in (1.11) with the aid of the twofold integration by parts as

$$I \equiv \int d^3r \left(\varphi - \frac{Ze}{r} \right) \frac{\nabla^2 r^2}{6} = \frac{1}{6} \int d^3r r^2 \nabla^2 \left(\varphi - \frac{Ze}{r} \right). \quad (1.18)$$

Here the integrated parts disappear because at the surface the potential φ is continuously matched to that of the point charge. Now, we have

$$\nabla^2 \frac{Ze}{r} = -4\pi Ze \delta(\mathbf{r}), \quad (1.19)$$

so that, being multiplied by r^2 , this term vanishes, and

$$\nabla^2 \varphi = -4\pi \rho_{ch}(\mathbf{r}) \quad (1.20)$$

for any charge distribution. As a result, we obtain

$$I = -\frac{2\pi}{3} \int d^3r r^2 \rho_{ch}(\mathbf{r}) = -\frac{2\pi Ze}{3} \overline{r_{ch}^2}, \quad (1.21)$$

which leads to the general expression (1.16).

In a hydrogen-like atom with the nuclear charge Ze , an unperturbed energy of the electron 1s-state $E_e = Ze^2/2a$, where $a = a_B/Z$ is the radius of the orbit, and a_B is the Bohr radius (see Eq. (1.33)). In this case,

$$|\psi_e(0)|^2 = \frac{1}{\pi a^3}, \quad (1.22)$$

and the energy shift is determined by the ratio of nuclear and atomic sizes squared,

$$\frac{\delta E_e}{E_e} = \frac{4\overline{r_{ch}^2}}{3a^2} = \frac{4Z^2\overline{r_{ch}^2}}{3a_B^2}. \quad (1.23)$$

In complex atoms, because of the screening by other electrons, $|\psi_e(0)|^2$ increases $\sim Z$ rather than $\sim Z^3$ in (1.22). But the shift of levels is still measurable. Usually one is interested in the relative difference of electron terms for the isotopes of the same chemical element. This *isotopic shift* reveals the change of the nuclear charge distribution induced by the change of the neutron number. Large changes are seen if the adjacent isotopes with nuclear spin $J = 0$ have very different shapes. As the deformation axis is uniformly distributed in space, the deformation of the nucleus with $J = 0$ gives rise to an apparent increase in the mean square radius.

The effect calculated earlier is absent for p, d, \dots and higher orbital electron states because then the radial electron wave function is vanishingly small inside the nucleus. The deformed nucleus has nonzero higher *multipole moments* of the charge distribution, most frequently the quadrupole moment Q . Then the perturbation of the potential is also deformed and can be felt by the nonspherical electron states. The order of magnitude of the quadrupole effect is $\sim eQ/a^3$, which again contains the ratio of nuclear and atomic radii squared. However, in such cases, one needs to consider the *quadrupole hyperfine structure* of atomic spectra.

The effect is much stronger for *muons* being, according to (1.23), enhanced roughly by $(m_\mu/m_e)^2 \approx 4 \times 10^4$. In heavy nuclei, the radius of the lowest muon orbit is already inside the nucleus so that the distortion of the hydrogen-like muon wave function is large and the perturbative approach fails. The energy shifts of states in muon atomic

spectra (in the X-ray range) provide one of the best ways of measuring the nuclear charge radius. One can use even heavier negatively charged particles, such as pions, kaons, or antiprotons. But in those cases, the strong interactions are to be taken into account; they allow nuclear absorption of pions and kaons and annihilation of antiprotons.

Problem 1.2 A *charge form-factor* is a Fourier image of the spatial charge distribution density $\rho(\mathbf{r})$. Calculate the charge form-factor $F_{ch}(\mathbf{q})$ as a function of the wave vector \mathbf{q} for the neutral hydrogen atom in its ground state assuming the point-like proton. How this form-factor is changed by a finite size of the proton? At what values of the momentum transfer q , one can detect this change?

Solution

The electron wave function in the ground state of the hydrogen atom is spherically symmetric [in accordance with (1.22)],

$$\psi(r) = \frac{1}{\sqrt{\pi a_B^3}} e^{-r/a_B}, \quad a_B = \frac{\hbar^2}{me^2}. \quad (1.24)$$

The atomic charge density consists of nuclear and electronic parts,

$$\rho(\mathbf{r}) = \rho_p(\mathbf{r}) + \rho_e(\mathbf{r}) = \rho_p(\mathbf{r}) - e|\psi(\mathbf{r})|^2. \quad (1.25)$$

The electron contribution to the atomic form-factor [QP, II, 3.4] is

$$F_e(\mathbf{q}) = -\frac{e}{\pi a_B^3} \int d^3 r e^{i(\mathbf{q} \cdot \mathbf{r}) - 2r/a_B}. \quad (1.26)$$

A straightforward evaluation of the integral (it depends only on the magnitude q of the vector \mathbf{q}) gives

$$F_e(q) = -\frac{e}{[1 + (qa_B/2)^2]^2}. \quad (1.27)$$

As it should be, $F_e(0) = -e$, the total charge of the electron cloud. When the wavelength of the probe becomes much smaller than the atomic size, $qa_B \gg 1$, the form-factor goes to zero $\sim (qa_B)^{-4}$, which points to the absence of any singularities or accumulation of charges at smaller scales: there are no substructures. In contrast, the *point-like* proton has its charge concentrated in a vanishingly small volume so that its form-factor does not depend on q at all,

$$\rho_p(\mathbf{r}) = e\delta(\mathbf{r}) \Leftrightarrow F_p(\mathbf{q}) = e. \quad (1.28)$$

In this approximation, the wavelength $\sim 1/q$ of the probe is always greater than the proton size and the probe sees the proton as a point. The full atomic form-factor is given by

$$F_H(q) = F_p(q) + F_e(q) = e \left\{ 1 - \frac{1}{[1 + (qa_B/2)^2]^2} \right\}. \quad (1.29)$$

At the wavelength greater than the Bohr radius, $qa_B \ll 1$, the electron cloud screens the proton, the atom looks as a neutral object and the form-factor vanishes. As the wavelength gets shorter, the form-factor grows $\sim e(qa_B)^2$. When $qa_B \gg 1$, only the charge of

the point-like proton contributes to the form-factor; the electronic contribution disappears since at high momentum one is probing very small distances and only an infinitesimal part of the electron charge is found localized in ever-decreasing spatial region.

For a proton, viewed as a small sphere of radius r_p , instead of (1.28), the charge form-factor is

$$F_p(q) = \frac{e}{(4\pi/3)r_p^3} \int_{r \leq r_p} d^3r e^{i(\mathbf{q} \cdot \mathbf{r})}, \quad (1.30)$$

or, after simple calculation,

$$F_p(q) = \frac{3e}{x^3} (\sin x - x \cos x), \quad x = qr_p. \quad (1.31)$$

This can also be expressed using the spherical Bessel function $j_1(x)$, which is derived from the expansion of the plane wave in (1.30) over spherical waves. The parameter x represents the ratio of the wavelength $\sim 1/q$ to the proton size r_p . For long wavelengths, $x \ll 1$, the point charge limit (1.28) is recovered since $\sin x \approx x - x^3/6$ and $\cos x \sim 1 - x^2/2$. For short wavelengths, $x \gg 1$, the form-factor (1.31) goes to zero as $\cos x/x^2$ with oscillations (again, there are no substructures inside the proton in this approximation). The momentum transfer for an experiment designed to see the proton size corresponds to the wavelength of the order of this size, $x \geq 1$, or at least

$$q \sim \frac{1}{r_p}, \quad \hbar q \sim \frac{\hbar}{r_p} = 250 \text{ MeV}/c. \quad (1.32)$$

We can note parenthetically that the quantity α , Eq. (1.7), naturally defines three fundamental length scales. The Bohr radius

$$a_B = \frac{\hbar^2}{me^2} = 0.529 \text{ \AA}, \quad (1.33)$$

where m is the electron mass and $1 \text{ \AA} = 10^{-8} \text{ cm}$, determines the typical atomic size: this is the mean radius of the lowest orbit in the hydrogen atom and at the same time the typical outer radius of neutral complex atoms because the outermost electron is moving in the screened field of the ion with the effective charge +1 as in the hydrogen atom. Multiplying a_B by α we come to the deeper scale, that of the *electron Compton wavelength*,

$$\lambda_e = \alpha a_B = \frac{\hbar}{mc} = 3.862 \times 10^{-11} \text{ cm}. \quad (1.34)$$

At this scale, similar to what was discussed earlier, the quantum relativistic effects restrict the possible localization of the particle, in this case of the electron. Finally, the next step leads to the *classical electron radius*

$$r_e = \alpha \lambda_e = \alpha^2 a_B = \frac{e^2}{mc^2} = 2.818 \times 10^{-13} \text{ cm}. \quad (1.35)$$

This length does not contain the Planck constant \hbar and determines the intrinsic limit of validity of classical electrodynamics: the Coulomb self-energy of the electron as a small particle of radius r_e would reach its total rest energy mc^2 .

Charged pions π^\pm transfer electric charge from one nucleon to another as shown in Figure 1.1b,c. As a result of such transfer, proton and neutron interchange their roles. Consider for instance a process of $n-p$ scattering at small scattering angles in the

center-of-mass frame. “Normally” the neutron would continue its motion after scattering close to the forward direction. However, after scattering that involves interaction mediated by a charged pion, the particle moving forward will be the proton. This is a reason to say that nuclear forces are of *exchange* character. It is easy to understand that in the exchange by neutral pions (Figure 1.1a) in the interaction of two neutrons (or two protons), there are two possibilities in final states. The crucial difference is that now we deal with *identical particles*, and these two outputs are in fact *indistinguishable*. According to quantum mechanical laws, one has to add in this case the *amplitudes* of two possible processes, direct and exchange. The presence of exchange interactions of identical particles is extremely important in all many-body systems. In particular, the exchange part of the Coulomb interaction between electrons is mostly responsible for the macroscopic magnetic ordering in ferromagnets. The existence of charged mesons as mediators of nuclear forces along with the isobaric symmetry extends the idea of exchange interactions to the nucleons that differ by their electric charge.

1.5 Magnetic Properties

Protons and neutrons have intrinsic *magnetic moments* μ_p and μ_n . Their interaction with electron magnetic moments is responsible for the *hyperfine* magnetic structure of atomic and molecular levels. The magnetic moments are known with high accuracy,

$$\mu_p = 2.792847351 \pm 0.000000028 \text{ } \mu_N, \quad \mu_n = -1.9130427 \pm 0.0000005 \text{ } \mu_N, \quad (1.36)$$

where the characteristic unit is the *nuclear magneton* (n.m.),

$$\mu_N = \frac{e\hbar}{2M_p c} = 1 \text{ n.m.} = 5.05 \times 10^{-24} \text{ erg Gs}^{-1} = 3.152 \times 10^{-14} \text{ MeV T}^{-1}. \quad (1.37)$$

These magnetic moments characterize the nucleons at rest and should be ascribed to spin and intrinsic quark structure rather than to orbital motion. Proton orbital motion creates orbital magnetism with the classical gyromagnetic ratio of the magnetic moment to the mechanical moment $\hbar\ell$ equal to $g^{(\ell)} = e/2M_p c$; this defines the magnetic moment of 1 nm. Because of internal strong interactions, the spin gyromagnetic ratios differ from the Dirac limit of 2 [QP, II, 13.5]. Instead of (1.36), if proton was a structureless Dirac particle, its magnetic moment would be 1 n.m. and the magnetic moment of a structureless neutron would vanish. The magnetic moment of the neutron reflects the distribution of charge and currents inside the neutron although the total charge is zero. The hyperfine structure splitting in atoms is small because the nuclear magneton is inversely proportional to the large nucleon mass $M \approx 1840 m_e$.

Problem 1.3 Calculate the angular frequency of spin precession for electrons, protons, and neutrons in the magnetic field 0.1 T.

Solution

If the magnetic dipole $\boldsymbol{\mu}$ is not aligned along the magnetic field \mathbf{B} , it feels a torque

$$\mathbf{T} = [\boldsymbol{\mu} \times \mathbf{B}]. \quad (1.38)$$

In the presence of torque, the vector $\hbar\mathbf{J}$ of the angular momentum is not conserved. Its equation of motion takes the form

$$\hbar \frac{d\mathbf{J}}{dt} = \mathbf{T}. \quad (1.39)$$

The magnetic moment operator $\boldsymbol{\mu}$ is proportional to that of the total angular momentum (spin) of the particle,

$$\boldsymbol{\mu} = g\mathbf{J}, \quad (1.40)$$

where g is the gyromagnetic ratio in units of the corresponding magnetons $e\hbar/2mc$ for a particle of mass m (Bohr magneton μ_B for the electron and nuclear magneton μ_N for the nucleons). From those preliminaries, we find the equation of motion for the magnetic moment:

$$\frac{d\boldsymbol{\mu}}{dt} = \frac{g}{\hbar} [\boldsymbol{\mu} \times \mathbf{B}]. \quad (1.41)$$

As follows from (1.41), the magnetic moment precesses around the field direction, and the vector of the precession frequency is given by

$$\boldsymbol{\omega} = \frac{g\mathbf{B}}{\hbar}. \quad (1.42)$$

For electrons, protons, and neutrons $J = s = 1/2$, and

$$g_e = 2\mu_B, \quad g_p = 5.58\mu_N, \quad g_n = -3.83\mu_N. \quad (1.43)$$

This determines

$$\omega_e = 1.76 \times 10^{10} \text{ s}^{-1}, \quad \omega_p = 2.68 \times 10^7 \text{ s}^{-1}, \quad \omega_n = 1.83 \times 10^7 \text{ s}^{-1}.$$

The methods of *nuclear spectroscopy* are almost exclusively based on electromagnetic interactions. Stationary states of any quantum system form a discrete spectrum. The gamma-transitions between the discrete levels carry away energy and angular momentum. The measurements of intensity, branching, lifetime of excited states, angular distribution, and polarization of gamma-rays allow the experimentalists to recreate the nuclear level scheme with the corresponding quantum numbers.

1.6 Weak Interactions

The weak processes, Figure 1.2, are mediated by *intermediate vector bosons* – very short-lived and massive particles with spin 1 – two charged W^\pm bosons with mass $m_W = 80.4$ GeV and a neutral Z^0 boson with mass $m_Z = 91.2$ GeV. Together with the massless photon γ , these four intermediate bosons are responsible for all phenomena of electromagnetic and weak interactions that are naturally combined in the *electroweak theory*. Similar to electromagnetism, in the combined electroweak theory we have the interaction of *currents*, for example, of the nucleon current with the electron-neutrino (*lepton*) current in the examples of Figure 1.2.

At energies much lower than $m_W c^2$, the manifestations of electromagnetic and weak physics are quite different. The range of forces is inversely related, Eq. (1.5), to the mass

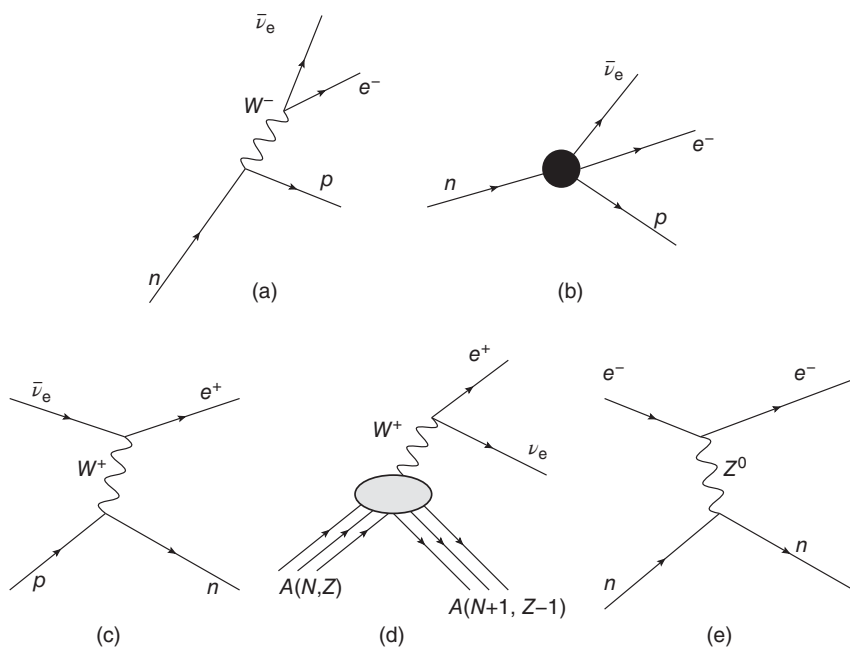


Figure 1.2 Examples of weak processes: (a) neutron beta-decay and (b) its contact image, (c) neutrino proton scattering, (d) positron decay of a nucleus, and (e) electroweak electron scattering.

of the agent mediating the interaction. In contrast to electromagnetic forces of infinite range ($m_\gamma = 0$), the weak interactions have the range

$$\Delta R_{\text{weak}} \simeq \frac{\hbar}{m_W c} \simeq 2 \times 10^{-16} \text{ cm.} \quad (1.44)$$

Such distances are much smaller than those of importance in nuclear phenomena at not very high energies. Therefore, in many applications, the weak processes can be considered as resulting from a *contact*, point-like interaction (Figure 1.2b). The corresponding interaction strength is much weaker than that due to strong and electromagnetic forces. At distances of the order of the proton Compton wavelength (1.4) used in earlier estimates, Eq. (1.6), the intensity of the weak interaction between two nucleons is of the order of $10^{-5} Mc^2$. Typical *cross sections* of reactions due to the weak interaction are smaller than 10^{-40} cm^2 , well below normal nuclear cross sections of the order of milibarns or even barns (1 barn = 10^{-24} cm^2).

Thus, we can definitely ignore the contribution of the weak interactions to the total energy of a nuclear system. But the weak interaction is extremely important because it (i) makes possible some processes that would not be allowed with strong and electromagnetic forces only and (ii) violates some fundamental symmetries. The whole nuclear and chemical evolution of the Universe at some stages could only proceed via weak processes. Weak interactions can be studied both in elementary processes and in complex nuclei. There are physical mechanisms that may enhance weak effects in the many-body nuclear environment. Such cases are especially interesting as amplifiers of the weak interactions, and, on the other hand, as bright signatures of those many-body

mechanisms at work. The main manifestation of weak interaction is in weak nuclear decays that are very slow compared to characteristic nuclear times. As weak interactions violate specific symmetry properties, they can be observed by the characteristic effects of such violations.

Finally, we need to mention *gravitational forces*. They are extremely weak for two nucleons at typical nuclear distances but become exceedingly important on an astrophysical scale because of their long-range character that covers huge masses of matter in stars and galaxies.

1.7 Neutron Decay

From the single-nucleon point of view, the most prominent effect of the weak interaction is instability of the free neutron. The excess of mass, Eq. (1.1), of the neutron compared to the proton makes the neutron unstable. Therefore, the decay $n \rightarrow p + (\text{something})$ is energetically allowed. This “something” should carry the negative electric charge, $e = -1$. The only available light negative charge carrier is the electron. But then the angular momentum conservation requires the presence of another electrically neutral particle of half-integer spin. This particle has to be light since the decay energy is only $(M_n - M_p - m_e)c^2 = 783 \text{ keV}$. This role is played by the *neutrino* (ν). The neutron decay is the simplest example of the β -decay,

$$n \rightarrow p + e^- + \bar{\nu}_e. \quad (1.45)$$

The β -decay (1.45), Figure 1.2a, is studied in detail; the mean life time $\tau_n \approx 15 \text{ min}$ of the neutron, huge on a nuclear scale, is due to the weakness of the underlying interaction and very limited energy release in the process.

As reflected in the notations for the neutrino, historically it was assumed that in weak interactions the *leptonic charge* is conserved. The class of particles called leptons includes electron ($m_e c^2 = 0.511 \text{ MeV}$) and its heavy analogs, *muon* μ , $m_\mu c^2 = 105.658 \text{ MeV}$, and τ -*lepton*, $m_\tau = 1784 \text{ MeV}$, together with their antiparticles, and the corresponding neutrinos and antineutrinos. Each lepton is coupled to its own neutrino, such as $\bar{\nu}_e$ in the case of (1.45), where it appears along with the electron. For each *generation* of leptons, e , μ , or τ , the specific leptonic charge is assigned, +1 for a lepton and -1 for a corresponding antilepton. Hadrons have zero leptonic charge. To conserve the leptonic charge, the particle accompanying the electron in (1.45) has to be an antilepton, that is, *electron antineutrino* (antiparticles can be denoted by the same symbols as particles with the bar added).

Apparently the neutrinos have no magnetic moments; for example, for the magnetic moment of the electronic neutrino, the experimental upper boundary is $|\mu_{\nu_e}/\mu_e| < 4 \times 10^{-10}$. Thus, neutrinos participate in weak and gravitational interactions only. Therefore, they have an astronomical mean free path in matter. The first direct observation of the interaction with matter of electron antineutrinos, produced from the processes like (1.45) in the nuclear reactor, was carried out [3], with the reaction, Figure 1.2c,

$$\bar{\nu}_e + p \rightarrow n + e^+. \quad (1.46)$$

Here, as compared to the beta-decay in (1.46), we reversed the direction of the processes and transferred the electron to the opposite side of the equation substituting it

by the positron. Such substitutions are always allowed from the viewpoint of charge conservation, although not all possibilities are energetically open. The cross section of the reaction (1.46) is very low, $\approx 10^{-43}$ cm².

The similar process

$$\bar{\nu}_e + n \rightarrow p + e^- \quad (1.47)$$

turned out [4] to be forbidden; actually the reaction was sought for not on a free neutron (such a target did not exist) but on the nucleus ^{37}Cl ($Z = 17, N = 20$) that was expected to be transformed into ^{37}Ar ($Z = 18, N = 19$). From Eq. (1.45) we see that the possible process with the lepton number conservation should be initiated by the electron neutrino rather than by the antineutrino,

$$\nu_e + n \rightarrow p + e^- \quad (1.48)$$

The absence of the reaction (1.47) was interpreted as a fact that neutrino and antineutrino are different particles and the lepton number is a convenient tool to differentiate between them.

Later it turned out that this interpretation might be doubtful. The process (1.48) can be forbidden by the property of the weak interaction based on *left currents*: neutrinos in such processes are always left-polarized while antineutrinos are right-polarized. Here polarization is the sign of conserved *helicity*, spin projection on the linear momentum. The left-polarized particle cannot induce the reaction (1.48). The distinction would be absolute if the neutrinos were *massless*. However, later discovered *neutrino oscillations* show that electronic, muonic, and tau neutrino appearing in weak interactions are not stationary being linear combinations of stationary neutrino mass eigenstates. Then neutrinos have nonzero mass, their helicities are not absolute, and the idea of the conserved leptonic quantum number is of a limited applicability. A massive neutrino can still be identical to its antiparticle (the so-called *Majorana particles*) but this can be established only by an experiment. The electronic neutrino mass is very low, not greater than 1 eV. Its precise measurement is a difficult experimental task. For almost all practical purposes in ordinary nuclear physics, we can set $m_{\nu_e} = 0$. The problem of the neutrino mass, extremely important both theoretically and for the search of missing *dark matter* in the Universe, attracts many researchers (another direction in the problem of dark matter is related to the search for the so-called weakly interacting massive particles, WIMPs).

Similar to (1.45) weak decays of the *proton* are energetically forbidden. If the electric and baryonic charges are strictly conserved, the *lightest* particles with nonzero values of those charges – the electron and the proton, respectively, – must be absolutely stable. In some theories, however, the conservation of baryonic charge can be violated, so that the proton can decay, for example, into a positron and neutral pion π^0 . In the models combining strong, electromagnetic, and weak interactions (*grand unification*), the baryon and lepton numbers are not necessarily separately conserved, and the proton decay processes such as $p \rightarrow e^+ + \pi^0$ are allowed. Until now, in spite of continuing efforts, there is no experimental indication for the existence of such decays, and it was possible only to establish a lower boundary: the lifetime of the proton is longer than 10^{34} years. The proton decay could be a missing ingredient for the understanding of the above-mentioned *baryonic asymmetry* of the Universe (absence of antimatter); other ingredients are violation of *CP* symmetry (combined charge conjugation *C*, transforming particles into antiparticles, and spatial inversion *P*) and a nonstationary situation

that was present at the early stages of the expanding Universe [5]. Other ideas of explaining the matter–antimatter asymmetry of the Universe are related to neutrino physics.

1.8 Nuclear World

Every nuclide can be conveniently placed as a small cell on a *nuclear chart*, Figure 1.3, with its electric charge Z as the vertical coordinate and the neutron number $N = A - Z = B - Z$ as the horizontal coordinate. The symmetric nuclei $N = Z$ find themselves along the diagonal, while the perpendicular diagonal combines the nuclei with the same A (isobars); all isotopes of the same chemical element are located on the same horizontal line and all isotones on a vertical line.

A lot of detailed information about nuclei can be found in nuclear databases [6]. The majority of nuclear systems are *unstable*. They widely differ by their lifetimes. Usually only *particle-stable* nuclides, even if they undergo slow radioactive decay, are included in the nuclear charts. Particle-unstable species can be formed in nuclear reactions and usually emit neutrons during time $\sim 10^{(21-23)}$ s after the formation. Proton-unstable nuclei (*proton emitters*) sometimes can live longer if the energy of the proton is low and its path outside requires a long penetration through the Coulomb barrier of the residual nucleus. The spectroscopy of long-lived proton emitters can be studied experimentally. The lines on the nuclear chart showing the boundary of particle-unstable nuclei are called *drip lines*. The proton drip line is measured approximately up to $Z = 20$, and the neutron drip line is measured up to exotic oxygen isotope ^{26}O (the last particle-stable oxygen isotope is ^{24}O). At the drip lines, the particle *separation energy*, the difference of the ground-state binding energies of the parent and daughter nuclei is zero or negative (in stable nuclei, one needs to invest positive energy to extract a particle, which is similar to the atomic ionization potential).

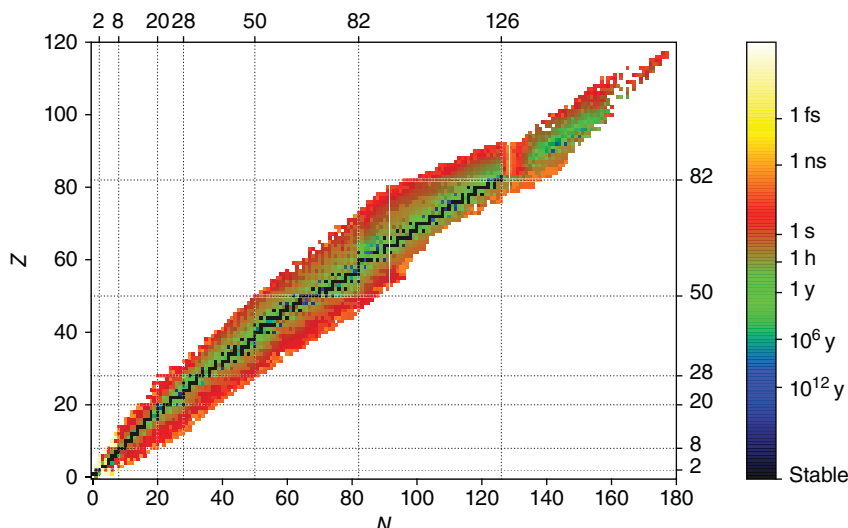


Figure 1.3 Nuclear chart. Colors represent ground-state lifetimes.

Estimates and extrapolations from the properties of well-known nuclei show that probably there can exist up to 8000 particle-stable nuclides. Only about 3300 of them were experimentally observed; this number steadily grows due to the efforts of many devoted laboratories. We should note that it has been an unfortunate tradition that only the discovery of a new chemical element – which means the progress along the Z -coordinate of the nuclear chart – was celebrated in the past as a real discovery repeatedly awarded by Nobel Prizes in chemistry; in contrast, the motion along the N -coordinate – related to the discovery of new isotopes – has been less known but often it requires great experimental efforts [7].

Less than 300 nuclides can be called stable. In fact, many of them are energetically allowed to undergo *fission* into two smaller but more tightly bound nuclear fragments. Similar to proton decay, the fission rate is determined by the probability of Coulomb barrier penetration. For nuclei in the middle of the chart, beyond the iron–nickel region, the fission probability is extremely small and often can be ignored. At the same time, *alpha-decay* with the emission of the *alpha-particle*, the nucleus of ${}^4\text{He}$, and fission define the finite lifetime of very heavy elements with large electric charge. This determines the end at the right upper corner of the nuclear chart; the heaviest observed nuclide is ${}^{294}_{118}(\text{Og})_{176}$ recently named *Oganesson* to recognize the Dubna physicist Yu. Oganessian. At the left lower end, we can start with the nucleons p and n , or with the lightest $A = 2$ system, the *deuteron* ${}^2\text{H}_1$.

The region of studied nuclei occupies a band around the *valley of stability*. This valley deviates down from the $N = Z$ diagonal. This means that the growing Coulomb repulsion establishes the most energetically favorable ratio $N/Z > 1$ for the stable nuclei. Nuclei on both sides of the valley of stability improve the value of this ratio by *beta-decay* that keeps the same A but moves the nuclei closer to the stability line. This is a typical route of the *nucleosynthesis* in the stellar environment. The lifetimes for various types of beta-decay are large compared to the typical nuclear times, recall the neutron beta-decay (1.48), so that it is possible to study the spectroscopy of both, initial and final, nuclei.

Among observed nuclei, we can distinguish three classes: about one-quarter of nuclei are *even–even* with respect to both N and Z ; one-half have an *odd mass number* A when N or Z is odd; and the rest are *odd–odd*. The even–even nuclei are the most stable, while there are only very few stable nuclei among the odd–odd ones. This reveals the *pairing* effect that amounts to extra binding existing mainly between two identical nucleons. As we will see later, this effect is similar to the Cooper pairing of electrons responsible for superconductivity in condensed matter physics; sometimes heavy nuclei are termed *superfluid*.

One of the main tools of nuclear spectroscopy is the study of *gamma-rays* emitted in the transitions (with no change in A or Z) of a nucleus between its energy levels. Various combinations of possible initial and final states in a nucleus produce many gamma-rays. The typical experimental problem is that of combining the observed transitions into a consistent *level scheme*, whereas the theoretical task is to interpret this scheme from the viewpoint of underlying many-body structure. The highest number of gamma-transitions, 1319, is known in ${}^{53}_{25}\text{Mn}_{28}$. The largest number of energy levels, 578, is established for ${}^{40}_{20}\text{Ca}_{20}$. At the same time, for approximately 1100 nuclides no gamma-rays were measured, and for about 800 nuclides only the ground state is known.

The loosely bound nuclei, for example, the *halo nucleus* ^{11}Li with two outer neutrons at relatively large distances from the center, have no excited states and therefore decay after any excitation exceeds the binding energy. This nucleus also gives an example of a *Borromean system* as the neighboring ^{10}Li is unbound and the excitation releases a pair of neutrons.

Medium and heavy stable nuclei on average display a simple mass dependent on the size: the mean square radius of nuclear density on average depends on the mass number A as

$$R = r_0 A^{1/3}, \quad r_0 \approx 1.2 \text{ fm}. \quad (1.49)$$

This means that the nuclear volume is roughly proportional to the mass number, that is, the nuclear matter in equilibrium is *incompressible* being characterized by a typical bulk density. The parameter $A^{1/3}$ does not exceed 7 in the heaviest nuclei so that the sizes of nuclei are between 1 and 10 fm. The simple rule (1.49) is violated in loosely bound nuclei, like ^{11}Li , where the outer nucleons can form nuclear *skins* and *halos*. The study of the nuclei away from the valley of stability is currently considered as the main goal of nuclear research.

Typical velocities of the nucleons inside the nucleus are about 0.2 of the speed of light. Therefore, the periods of nucleonic motion inside the nucleus are of the order of 10^{-22} s. The timescale for neutron emission from a particle-unstable nucleus should be on average of the same order.

Problem 1.4 Estimate kinetic energy of electrons necessary to reveal the diffraction on the nuclear boundary of the alpha-particle and the uranium nucleus.

Solution

With $R = 1.2A^{1/3}$ fm, the wavelength $2\pi\hbar/p$ is of the order of the nuclear radius at electron kinetic energy equal to ≈ 660 and 170 MeV for ^4He and ^{238}U , respectively. In both cases, the electron is ultrarelativistic and it is possible to neglect its rest mass.

Nuclear transformations (beta-decay, alpha-decay, gamma-emission, fission) that proceed relatively slowly compared to typical periods of internal motion probe the structure of the nucleus as if it would be stable. For gamma-emission, usually the lifetime τ is greater than 10^{-18} s; strong (intensive, *collective*) transitions proceed in picoseconds. Some exceptionally long-lived excited states are called *isomers*. The record here belongs to the nucleus ^{180}Ta , where the isomeric state at excitation energy 77 keV has an amazingly long lifetime greater than 10^{15} years, while the beta-decaying ground state of the same isotope has a half-life time of only 8 h. Usually, one can understand specific structural reasons for the hindered transitions. Beta-decay is typically slow, $\tau > 10^{-8}$ s. All slow nuclear transformations are conventionally combined under the name of *radioactivity*, in distinction to faster *nuclear reactions* or gamma-radiation.

Nuclear quantum states are characterized by certain energy defined within the limits of the uncertainty relation, $\Delta E \sim \hbar/\tau$, where τ is the mean lifetime. The states also have exactly conserved quantum numbers of total angular momentum J (called usually *nuclear spin*) and its projection $J_z = M$ onto a quantization axis. If one can ignore the effects of the weak interactions, parity Π is also conserved. Angular momentum

and parity are conserved in electromagnetic interactions. Therefore, the quantum numbers of the initial and final states restrict the character of the possible gamma-radiation between these states: the triangle rule should be fulfilled,

$$\mathbf{J} = \mathbf{J}' + \boldsymbol{\lambda}, \quad (1.50)$$

where \mathbf{J} and \mathbf{J}' refer to the initial and final nuclear states, whereas $\boldsymbol{\lambda}$ is the angular moment carried away by the emitted photon (*multipolarity*). The radiation of high multipoles is strongly suppressed, and the main observed modes are electric and magnetic dipole, $\lambda = 1$, and electric quadrupole, $\lambda = 2$. The highest experimentally observed multipolarity of nuclear gamma-radiation is that of the electric radiation in ^{53}Fe with $\lambda = 6$ (half-life of about 2.6 min). In the previously mentioned isotope ^{180}Ta , the difference of spins between the excited ($J^\pi = 9^-$) and ground ($J^\pi = 1^+$) states is too large, which makes the gamma-radiation highly improbable; this isomeric state decays through a weak process.

Problem 1.5 The ratio of intensities of two components of the hyperfine structure of the spectral line $(^2P_{1/2}) \rightarrow (^2S_{1/2})$ in the sodium atom is close to 10:6. Find the ground-state spin of the nucleus ^{23}Na .¹

Solution

The hyperfine splitting of the upper term $^2P_{1/2}$ is negligibly small (the valence electron in the p -state has zero probability to be in the nuclear volume). The lower term $^2S_{1/2}$ is split into two hyperfine components with total atomic angular momenta $F_> = J + 1/2$ and $F_< = J - 1/2$ where J is the nuclear spin. The number of magnetic sublevels is, respectively, $2F_> + 1 = 2J + 2$ and $2F_< + 1 = 2J$. These sublevels are populated statistically, that is, the intensities are proportional to the statistical weights (number of sublevels). Therefore, the ratio of intensities is

$$\frac{10}{6} = \frac{2J + 2}{2J} = \frac{J + 1}{J} \Rightarrow J = \frac{3}{2}. \quad (1.51)$$

Problem 1.6 In the Stern–Gerlach experiment, an atomic beam traverses a weak but strongly nonuniform transverse magnetic field. For atoms of the isotopes ^{13}C and ^{133}Cs , the beam was split into 2 and 16 components, respectively. The atomic terms are correspondingly $(^3P_0)$ and $(^2S_{1/2})$. Determine nuclear spins.

Solution

Each subset of atoms with a given value of total angular momentum F , $\mathbf{F} = \mathbf{J}_e + \mathbf{J}$, where \mathbf{J}_e is the total angular momentum of atomic electrons and \mathbf{J} is the nuclear spin, is split into $2F + 1$ deflected beams. The total number of hyperfine components is

$$\sum_F (2F + 1) = (2J_e + 1)(2J + 1). \quad (1.52)$$

¹ Atomic levels given in parentheses are labeled in terms of their total spin S , total orbital momentum L , and total angular momentum J as $(^{2S+1}L_J)$.

From here, we find

$$\begin{aligned} {}^{13}\text{C} : J_e &= 0, 2J + 1 = 2, J = \frac{1}{2}; \\ {}^{133}\text{Cs} : J_e &= \frac{1}{2}, 2J + 1 = 8, J = \frac{7}{2}. \end{aligned}$$

Problem 1.7 Molecules LiF have the total angular momentum of electron shells $J_e = 0$. In the magnetic resonance measurement with the static magnetic field $\mathcal{B} = 0.5$ T, two resonance peaks at the frequencies of the time-dependent transverse magnetic field $v_{\text{Li}} = 8.3$ MHz and $v_{\text{F}} = 20.0$ MHz are observed corresponding to the ${}^7\text{Li}$ and ${}^{19}\text{F}$ nuclides, respectively. Determine the magnetic moments of these nuclei.²

Solution

Nuclear spins are $J = 3/2$ and $J = 1/2$ for ${}^7\text{Li}$ and ${}^{19}\text{F}$, respectively. From (1.40), we find

$$\mu = gJ = \frac{\hbar\omega}{\mathcal{B}}J = \frac{2\pi\hbar\nu}{\mathcal{B}}J, \quad (1.53)$$

or

$$\mu = \frac{4\pi\nu McJ}{e\mathcal{B}} \mu_N \quad (1.54)$$

with the proton mass M . This gives

$$\mu({}^7\text{Li}) = 3.26 \mu_N, \quad \mu({}^{19}\text{F}) = 2.62 \mu_N.$$

References

- 1 A.T. Yue *et al.*, Phys. Rev. Lett. **111**, 222501 (2013).
- 2 A.P. Serebrov *et al.*, Phys. Lett. B **605**, 72 (2005).
- 3 F. Reines and C.L. Cowan, Phys. Rev. **113**, 273 (1959).
- 4 R. Davis, Phys. Rev. **97**, 766 (1955).
- 5 A.D. Sakharov, JETP Lett. **5**, 24 (1967); republished as A.D. Sakharov, Sov. Phys. Usp. **34**, 392 (1991).
- 6 National Nuclear Data Center – Brookhaven National Laboratory, www.nndc.bnl.gov.
- 7 M. Thoennessen, Rep. Prog. Phys. **75**, 056301 (2013).

²Take the nuclear ground-state spin values from the isotope tables.

2

Isospin

Even though nothing is “spinning” in this charge space, we can use the mathematics of a system with two internal quantum states to make a one-to-one parallel between the two-spin state system and the two-charge state system.

K.T. Hecht, *Quantum Mechanics*.

2.1 Quantum Numbers in the Two-Body Problem

The simplest interacting nuclear systems (pp , nn , or pn) consist of $A = 2$ nucleons. The total momentum \mathbf{P} of a pair is conserved and completely decoupled from the relative motion, which is the goal of our study. In the nonrelativistic case, center-of-mass motion can be separated by the transformation of the nucleon coordinates \mathbf{r}_1 and \mathbf{r}_2 to the center-of-mass coordinate \mathbf{R} and the relative coordinate \mathbf{r} ,

$$\mathbf{R} = \frac{1}{2}(\mathbf{r}_1 + \mathbf{r}_2), \quad \mathbf{r} = \mathbf{r}_1 - \mathbf{r}_2, \quad (2.1)$$

where we do not distinguish the proton and neutron masses. The conjugate momenta for these coordinates are

$$\mathbf{P} = \mathbf{p}_1 + \mathbf{p}_2, \quad \mathbf{p} = \frac{1}{2}(\mathbf{p}_1 - \mathbf{p}_2). \quad (2.2)$$

The kinetic energy term of the transformed nonrelativistic Hamiltonian contains global energy and relative energy,

$$K = \frac{\mathbf{p}_1^2}{2M} + \frac{\mathbf{p}_2^2}{2M} = \frac{\mathbf{P}^2}{4M} + \frac{\mathbf{p}^2}{M}. \quad (2.3)$$

The corresponding masses are the total mass $2M$ and the reduced mass $m \equiv M/2$. Global motion of a free nucleus is described by a plane wave with momentum \mathbf{P} and does not need to be discussed. The situation is more complicated in the relativistic case where the very concept of a simultaneous wave function describing a many-body system has to be modified. The separation of the center-of-mass motion also becomes a practical problem for few-body and many-body systems since the usual mean field approximation assumes the fixed position of the center and violates the translational invariance.

Wave functions of relative motion of two particles have radial, angular, and spin parts. The complete set of states can be constructed using the spherical harmonics $Y_{\ell m}(\mathbf{n})$ for

the angular part $[\mathbf{n}(\theta, \varphi)]$ is the unit vector along $\mathbf{r} = r\mathbf{n}$. This defines the parity quantum number $\Pi = (-)^\ell$. We use the standard spectroscopic symbols $s, p, d, f, g, h, i, j, \dots$ for the values $0, 1, 2, 3, 4, 5, 6, 7, \dots$ of the orbital momentum ℓ . The spin function χ_{SS_z} of the two-nucleon system can belong to the $S = 0$ (singlet) or $S = 1$ (triplet) values of the total spin

$$\mathbf{S} = \mathbf{s}_1 + \mathbf{s}_2 \equiv \frac{1}{2}(\boldsymbol{\sigma}_1 + \boldsymbol{\sigma}_2), \quad (2.4)$$

where $\boldsymbol{\sigma}_a$ is the vector of Pauli matrices acting on the spin variable of the particle a . The symmetry with respect to the exchange of the spin variables is tested by the spin-exchange *Bartlett operator*

$$\mathcal{P}^\sigma = \frac{1}{2} [1 + (\boldsymbol{\sigma}_1 \cdot \boldsymbol{\sigma}_2)]. \quad (2.5)$$

The triplet states are symmetric and the singlet state is antisymmetric under spin exchange,

$$\mathcal{P}^\sigma = (-)^{S+1}. \quad (2.6)$$

In a two-nucleon system, the space inversion changes the sign of the relative coordinate (2.1); therefore, it is equivalent to the exchange of the space coordinates, $\mathbf{r}_1 \leftrightarrow \mathbf{r}_2$, given by the *Majorana operator* \mathcal{P}^r . The eigenvalues of this operator are parity quantum numbers Π defined by the orbital momentum ℓ ,

$$\mathcal{P}^r = (-)^\ell = \Pi. \quad (2.7)$$

The result of exchanging both, spin and orbital, coordinates of a pair is given by the *Heisenberg exchange operator*,

$$\mathcal{P} = \mathcal{P}^r \mathcal{P}^\sigma = (-)^{\ell+S+1}. \quad (2.8)$$

In general, the relative orbital momentum ℓ and the spin \mathbf{S} of the pair are not necessarily conserved vectors. In the presence of the *spin-orbit coupling*, they are not individually conserved. But the rotational invariance guarantees the conservation of the total angular momentum

$$\mathbf{J} = \ell + \mathbf{S}. \quad (2.9)$$

The state with given values of ℓ and S can be coupled, according to (2.9), to $J = \ell$ for the spin singlet and to $J = \ell, \ell \pm 1$ for the spin triplet (in the exceptional case of $\ell = 0$, only $J = S$ is possible). As in atomic spectroscopy, the resulting state will be denoted as $^{2S+1}(\ell)_J$, where (ℓ) stands for the symbol of the orbital momentum. Using this nomenclature, all possible two-nucleon states can be classified as in Table 2.1.

Since the only *exact constants of motion* are J and (ignoring parity-violating weak interactions) parity $\Pi = (-)^\ell$, in the study of nuclear levels it is usually convenient to use the reduced symbolics J^Π indicating only those quantum numbers. In a two-nucleon system, parity of *singlet* states $(-)^\ell = (-)^J$ is uniquely determined by J . For *triplet* states, the quantum numbers J and Π do not completely determine a state: there are two possibilities with different $\ell = J \pm 1$. In general, only the states $J^\Pi = 0^+$ and $J^\Pi = 0^-$ are uniquely determined by angular momentum and parity (they are, in spectroscopic notations, 1s_0 and 3p_0 , respectively). Let us rearrange the states according to the exact quantum numbers J^Π of the strong interaction (Table 2.2).

Table 2.1 Two-nucleon states $^{2S+1}(\ell)_J$.

	ℓ	0	1	2	3	4
Singlets, $S = 0$	$J = \ell$	1s_0	1p_1	1d_2	1f_3	1g_4
Triplets, $S = 1$	$J = \ell - 1$		3p_0	3d_1	3f_2	3g_3
	$J = \ell$		3p_1	3d_2	3f_3	3g_4
	$J = \ell + 1$	3s_1	3p_2	3d_3	3f_4	3g_5

Table 2.2 Two nucleon states J^Π .

	0 ⁺	0 ⁻	1 ⁺	1 ⁻	2 ⁺	2 ⁻	3 ⁺	3 ⁻	4 ⁺
Singlets	1s_0			1p_1	1d_2			1f_3	1g_4
Triplets		3p_0	$^3s_1, ^3d_1$	3p_1	3d_2	$^3p_2, ^3f_2$	$^3d_3, ^3g_3$	3f_3	3g_4

In principle, the interaction can mix the states with the same J^Π but with different ℓ or S . There are two possible types of superpositions compatible with the conservation of J^Π . First, one can mix the triplet and singlet states with the same ℓ , for example, 1p_1 and 3p_1 (vertical mixing in Table 2.2). Second, the superposition is allowed for the triplet states with $\ell = J \pm 1$ (horizontal mixing). Note that the states available for the vertical mixing have opposite permutational symmetry (2.8), namely the same behavior with respect to P^r but the opposite behavior with respect to P^{σ} . In contrast, the horizontal mixing combines two states of the same symmetry. Therefore, the underlying physics is very different. Only the horizontal mixing takes place actually and the only possible *bound* two-nucleon state is the *deuteron*, $d \equiv {}^2_1\text{H}_1$, with the proton–neutron wave function as a superposition ${}^3s_1 + {}^3d_1$ (see Table 2.2). All other combinations of quantum numbers allowed by quantum mechanics correspond to the continuum spectrum, that is, to the states of the *scattering problem*. Systems of two *identical* nucleons, such as diproton ${}^2\text{He}$ or dineutron 2n , are unbound.

2.2 Introducing Isospin

Apart from fundamental symmetries associated with the basic properties of space and time, specific interactions reveal additional symmetries that, in general, can be only *approximate* being violated by other parts of Hamiltonian. If the violation is relatively weak, it makes sense to start with the ideal picture where the symmetry is considered to be exact and noninvariant interactions are turned off. This gives rise to a useful hierarchy of approximations capable of organizing and ordering empirical data.

As discussed in Chapter 1, the main properties of the proton and the neutron are quite similar. They have the same spin 1/2 and baryon charge $B = 1$, almost equal masses and their *strong interactions* (nuclear forces) are nearly identical. The difference of *electromagnetic* properties is of minor importance at this stage as it is the strong interaction that governs the most significant part of internal nuclear dynamics.

We come to an idea to treat the *nucleons* of two sorts as different states of the same strongly interacting object. This object has now an intrinsic degree of freedom, which defines its proton or neutron appearance. Thus, we have a “two-level” system – the *nucleon* – with two basis states

$$|p\rangle = \begin{pmatrix} 0 \\ 1 \end{pmatrix}, \quad |n\rangle = \begin{pmatrix} 1 \\ 0 \end{pmatrix}. \quad (2.10)$$

The states (2.10) have a certain electric charge, $Q_p = 1$ and $Q_n = 0$ in units of e , that is, they are the eigenstates of the charge operator Q . Referring to the basis (2.10) in analogy to the usual spin as the z -representation, we can say that this “quantization axis” in a new additional space is related to the interaction with the electromagnetic field that allows one to distinguish between the two charge states of the nucleon.

Let us call the spinor space span by the basis vectors (2.10) nucleon *charge space*. All operators in this space are matrices 2×2 as in the case of spinors of a spin-1/2 particle. We can construct the full set of matrices acting in this two-dimensional space using as a basis the unit matrix and matrices $\tau_{1,2,3}$ are defined exactly as the Pauli matrices $\sigma_{1,2,3}$ in spin space. Evidently, the charge operator is diagonal in this basis,

$$Q = \begin{pmatrix} 0 & 0 \\ 0 & 1 \end{pmatrix} = \frac{1}{2}(1 - \tau_3). \quad (2.11)$$

The off-diagonal operators induce transitions between the charge states of the nucleon. The operator raising the charge is

$$\tau_- = \begin{pmatrix} 0 & 0 \\ 1 & 0 \end{pmatrix}, \quad \tau_-|p\rangle = 0, \quad \tau_-|n\rangle = |p\rangle; \quad (2.12)$$

the lowering operator is

$$\tau_+ = \begin{pmatrix} 0 & 1 \\ 0 & 0 \end{pmatrix} = (\tau_-)^\dagger, \quad \tau_+|p\rangle = |n\rangle, \quad \tau_+|n\rangle = 0. \quad (2.13)$$

The operators τ_\pm are built of the Pauli matrices,

$$\tau_\pm = \tau_1 \pm i\tau_2, \quad (2.14)$$

in the same way as raising and lowering components $J_\pm = J_x \pm iJ_y$ of any angular momentum operator. We can combine the matrices $\tau_{1,2,3}$ into the matrix “vector” τ , which is completely analogous to the vector σ of spin Pauli matrices. Continuing the spin analogy, we speak about the *isospin* of the nucleon

$$\mathbf{t} = \frac{1}{2}\boldsymbol{\tau} \quad (2.15)$$

that acts in 2×2 charge (iso-) space with the natural basis (2.10), where the basis states have a certain charge

$$Q = \frac{1}{2} - t_3. \quad (2.16)$$

In the isospin language, the proton and neutron are the states with different projections of the isospin onto the axis 3 of isospace,

$$t_3|p\rangle = -\frac{1}{2}|p\rangle, \quad t_3|n\rangle = \frac{1}{2}|n\rangle. \quad (2.17)$$

By historical reasons, the isospin projections are defined in nuclear physics, Eq. (2.11), in the way opposite to their action on the charge eigenvalue. In particle physics, a more natural definition is used with the proton having, instead of what is defined in Eqs. (2.10) and (2.17), the isospin projection $+1/2$ and the neutron having the projection $-1/2$. This formal difference comes from the fact that the majority of nuclei have $N > Z$; therefore, the definition (2.17) supplies them with the “more pleasant” positive total projection. No difference in physical predictions can arise if any convention is applied consistently. The correct full spelling of the abbreviation “isospin” is *isobaric* spin, which unifies the *isobars*, the states with the same mass number, similar to the proton and the neutron or nuclei with the same sum $A = Z + N$ of the proton, $Z = Q$, and neutron, N , numbers. It is incorrect to decipher the term “isospin” as *isotopic* that would relate the *isotopes* having the same electric charge Z at different masses A (the different isotopes belong to the same chemical element). The isospin as a working instrument in nuclear physics was first used by Wigner [1].

2.3 Isospin Invariance

The *charge symmetry* transformation is the one reversing the sign of the projection t_3 : $p \leftrightarrow n$. For this purpose, one can use an appropriate operator of the rotation, for example, by an angle π in the plane (1–3) of isospin space. We can also introduce all possible rotation operators in isospace built of the τ -matrices instead of σ -matrices. Such transformations comprise a group *isomorphic* to the $SU(2)$ group. Using the basis states (2.10) as building bricks, we can obtain the multiplets (*irreducible representations*) with any isospin, exactly copying angular momentum algebra.

We have introduced the additional degree of freedom associated with isospin without actually increasing the dynamical contents of the theory. At this point, we obtain merely another classification of the available states. Real physics enters the game with the idea of symmetry of the underlying Hamiltonian in isospin space. We need to take care of a right number of proton–neutron degrees of freedom: the introduction of isospin should not increase this number.

The *mirror symmetry* of strong interactions implies invariance under the charge symmetry transformation. By virtue of this symmetry, the proton and neutron states are to be degenerate. As their electromagnetic properties are different, this is equivalent to the statement that their mass difference comes exclusively from electromagnetic interactions, supposedly on the quark level. The charge symmetry transformation is a particular case of $SU(2)$ operations. More broad *isospin invariance* assumes that the strong Hamiltonian is invariant under *all* elements of the isospin group. In this case, we have full rotational invariance in isospin space, and the stationary states of a many-body system can be labeled by the conserved quantum number T of the total isospin,

$$\mathbf{T} = \sum_a \mathbf{t}_a, \quad (2.18)$$

that is, an analog of the total angular momentum in the isospace related to the eigenvalues of the isospin “length,” $\mathbf{T}^2 = T(T+1)$.

Since the algebraic properties of spin and isospin are identical, the allowed values of T are quantized to be integer (half-integer) in a system of an even (odd) number

of nucleons. It gives rise to *isomultiplets* with given T that contain $2T + 1$ states with projections $T_3 = -T, \dots, +T$ or, equivalently, with the charge [see (2.11)]

$$Q = \sum_a \left(\frac{1}{2} - t_{3a} \right) = \frac{A}{2} - T_3. \quad (2.19)$$

The isospin invariance of the strong interaction Hamiltonian \hat{H}_s can be written as the conservation law

$$[\hat{T}, \hat{H}_s] = 0. \quad (2.20)$$

In the case of stationary states, all $2T + 1$ states of a multiplet would have the same energy in the limit of exact isospin invariance. Let us emphasize that the states within a given isomultiplet belong to *different* nuclei (the same A but different Z). They are frequently called *isobaric analog states* (IAS). The conservation law (2.20) is certainly the same for the component T_3 related to the electric charge, Eq. (2.19).

If we forget for a moment about electromagnetic interactions that single out the axis 3 and violate the isotropy of isospace, we can classify all nuclear states by isomultiplets. The allowed values of the magnitude T of the isospin of the nucleus (A, Z) cannot be less than the value of projection T_3 , Eq. (2.21), and they cannot exceed the maximum value $A/2$ (in the case of $T_3 = A/2$, the nucleus would consist of neutrons only and all its states would be *isospin-aligned* having the same value of $T = T_3$). All states in a given nucleus (the *vertical* scale) have the same projection

$$T_3 = \frac{1}{2}(N - Z) = \frac{A}{2} - Z. \quad (2.21)$$

They belong to various isomultiplets (the *horizontal* scale). In general,

$$\frac{1}{2}|N - Z| \leq T \leq \frac{1}{2}(N + Z). \quad (2.22)$$

An example of the family of nuclear isomultiplets is given in Figure 2.1.

Problem 2.1 Assuming isospin invariance of nuclear forces, what nucleus, ${}^8_8\text{O}_6$, or ${}^{14}_7\text{N}_7$, has a greater number of quantum states?

Solution

According to the rule (2.22), states of the ${}^{14}\text{N}$ nucleus can have the isospin value T from 0 to 7, while the states of the ${}^{14}\text{O}$ nucleus can have T from 1 to 7. All states with $1 \leq T \leq 7$ are isobaric analogs corresponding to the projections $T_3 = 1$ in ${}^{14}\text{O}$ and $T_3 = 0$ in ${}^{14}\text{N}$ within the same isobaric multiplet. The states $T = T_3 = 0$ in ${}^{14}\text{N}$ have no analogs in ${}^{14}\text{O}$. The ${}^{14}\text{C}$ nucleus is mirror with respect to ${}^{14}\text{O}$ and has the same isospin properties.

2.4 Space–Spin Symmetry and Isospin Invariance

We have enumerated two-nucleon states in Tables 2.1 and 2.2 without mentioning whether the nucleons are different, as in the deuteron case, or *identical*. However, in the latter case, only *antisymmetric* states with the value $\mathcal{P} = -1$ of the exchange operator (2.8) are allowed by the Fermi statistics. Therefore, only a subclass of the states

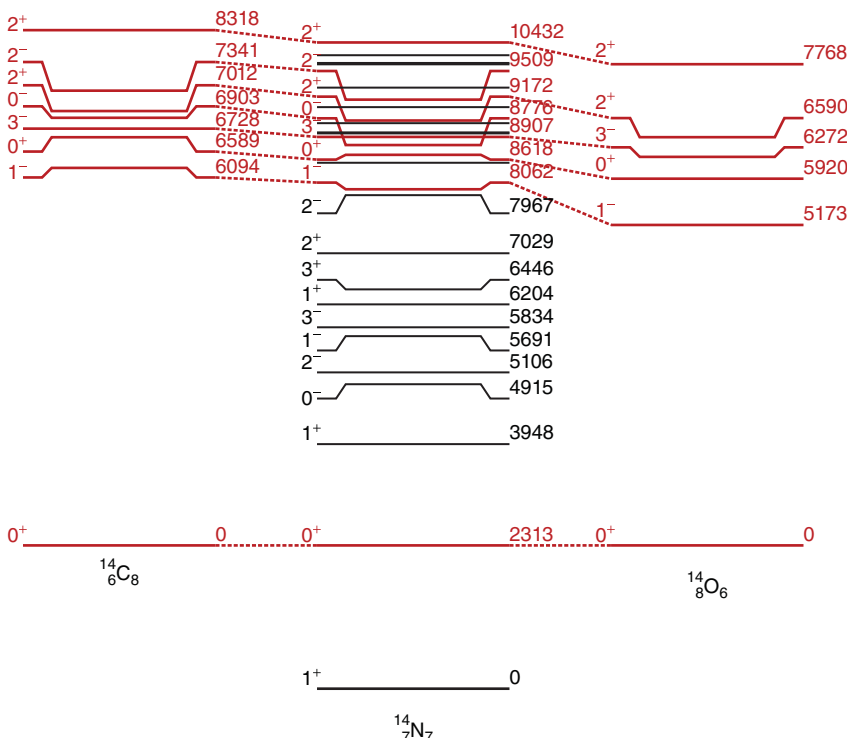


Figure 2.1 Family of nuclear isomultiplets in $A = 14$ nuclei. Selected states are marked with their spins and parity on the left, and their excitation energy in kiloelectronvolts is shown on the right. Isobaric analog states with $T = 1$ are shown in red and are connected by dashed lines.

is selected for $n-n$ or $p-p$ systems, where the orbital (\mathcal{P}^r) and spin (\mathcal{P}^σ) symmetries are *complementary*, namely

$$\text{Even singlets: } 0^+(^1s_0), \quad 2^+(^1d_2), \quad 4^+(^1g_4), \dots; \quad (2.23)$$

and

$$\text{Odd triplets: } 0^-(^3p_0), \quad 1^-(^3p_1), \quad 2^-(^3p_2 + ^3f_2), \quad 3^-(^3f_3), \dots. \quad (2.24)$$

The naive expectation would be that, due to the charge independence of nuclear forces, the existence of the bound deuteron ($A = 2, Z = 1$) would imply the existence of the bound states $n-n$ ($Z = 0$, dineutron) and $p-p$ ($Z = 2$, diproton or ${}^2\text{He}$). Such bound states apparently do not exist. The reason can be understood in the following way.

The deuteron, with the binding energy of 2.225 MeV, has no excited bound states. If the nuclear forces are charge independent, then the hypothetical bound states $n-n$ and $p-p$ should have the same quantum numbers ${}^3s_1 + {}^3d_1$ as the only bound $n-p$ state. However, Eqs. (2.23) and (2.24) show that such states are *forbidden* by the Fermi statistics. Inversely, a bound state with some quantum numbers in a system of identical nucleons would have its analog in a $n-p$ system that does not exist. The idea of *charge independence* has to be formulated as the equivalence of the nuclear forces *in the same quantum states* of different proton–neutron systems.

Problem 2.2 Pions π^- with spin 0 and negative electric charge can be captured on a hydrogen-like orbit around a nucleus and form a Coulomb *mesoatom* (see Problem 1.1 for the muon with mass of the same order as the pion). The process ends up either by the decay of the pion into a muon and muonic antineutrino,

$$\pi^- \rightarrow \mu_- + \bar{\nu}_\mu, \quad (2.25)$$

or by the nuclear capture of the pion. Consider the deuterium π -mesoatom where the pion capture from the ground mesoatomic state (a process governed by the strong interaction) leads to the nuclear dissociation into two neutrons,

$$\pi^- + d \rightarrow n + n. \quad (2.26)$$

Show that the process (2.26) is possible only if the pion has negative intrinsic parity (*pseudoscalar particle*).

Solution

With the spinless pion in the ground s -wave of the mesoatom and the deuteron spin (total angular momentum) equal to 1, the total angular momentum of the initial state in the capture process (2.26) is $J_i = 1$. Therefore, the final state of two neutrons must also have the angular momentum $J_f = 1$. Equation (2.24) allows for two neutrons only one combination of quantum numbers with $J = 1$, namely 3p_1 with negative parity ($\ell = 1$). Parity of the initial state coincides with intrinsic pion parity because $\ell = 0$ for the lowest s -orbit in the mesoatom, and the deuteron state is also even. Therefore, parity conservation in the process (2.26) proves that the *pion has negative intrinsic parity*.

The nuclear forces are strongly dependent on space and spin symmetry of the state under consideration. Now we can show that the isospin invariance and the isospin conservation are physically equivalent to the statement that in the nuclear interactions *space–spin symmetry* of the wave function is conserved.

Let us construct the isospin states for the two-nucleon system. It can be done in exact analogy to the spin states. For $A = 2$, one can build the *isotriplet* $T = 1$ with the substates $T_3 = 1$ (two neutrons), $T_3 = -1$ (two protons), and $T_3 = 0$ (neutron and proton), and the *isosinglet* $T = T_3 = 0$ (neutron and proton). Introducing the notation Ω_{TT_3} for the isospin wave function, we have the correct combinations of the two-body states:

$$\Omega_{1-1} = |p_1 p_2\rangle, \quad \Omega_{11} = |n_1 n_2\rangle, \quad \Omega_{10} = \frac{1}{\sqrt{2}}(|n_1 p_2\rangle + |p_1 n_2\rangle), \quad (2.27)$$

$$\Omega_{00} = \frac{1}{\sqrt{2}}(|n_1 p_2\rangle - |p_1 n_2\rangle). \quad (2.28)$$

The isotriplet state Ω_{10} is symmetric with respect to the transformation of charge symmetry, $p \leftrightarrow n$, while the isosinglet state Ω_{00} is antisymmetric. It is natural to introduce the exchange operator P^τ that interchanges the charge variables of the nucleons. Its eigenvalues in triplet and singlet states are 1 and -1 , respectively, so that, similar to the spin case (2.6), one can write

$$P^\tau = \frac{1}{2}[1 + (\boldsymbol{\tau}_1 \cdot \boldsymbol{\tau}_2)] = (-)^{T+1}. \quad (2.29)$$

Now we can add the charge variables to the coordinate and spin variables and construct the full two-nucleon wave function as a product of the coordinate, ψ , spin, χ , and isospin, Ω , parts,

$$\Phi(1, 2) = \psi(\mathbf{r}_1, \mathbf{r}_2) \chi_{SS_z} \Omega_{TT_3}. \quad (2.30)$$

The point is that we should not increase the number of degrees of freedom. Therefore, it must exist a rule for proper combination of the space–spin and isospin factors.

If the nucleons are identical, the space–spin part $\psi\chi$ is antisymmetric in accordance with the Fermi statistics. As seen from Eq. (2.27), in this case the isospin part Ω is symmetric and the full wave function (2.30) is *antisymmetric* with respect to the *complete interchange* of all variables $P^\ell P^\sigma P^\tau$. Owing to the isospin invariance, the strong forces are the same for the state Ω_{10} , Eq. (2.27), of the $n-p$ system. Therefore, we assign the states of the $n-p$ system, which are antisymmetric in the space and spin variables, to the isospin $T = 1$. They have their analogs in the case of identical nucleons, and the total wave function Φ is antisymmetric. Any state appears in three charge forms, which is a signature of $T = 1$.

The $n-p$ states, which have the symmetric space–spin function $\psi\chi$, have no analogs for identical nucleons and cannot belong to the isodoublet. The necessary isospin function in this case is Ω_{00} , which is antisymmetric in charge variables. As a result, the full function (2.30) is again *antisymmetric*.

We came to the *generalized Pauli principle*: the full two-nucleon function is antisymmetric with respect to the interchange of all, space, spin, and isospin, variables. The combination of Eqs. (2.8) and (2.29) allows one to write down this statement as a selection rule for the physical two-body states with correct statistics,

$$P^\ell P^\sigma P^\tau = (-)^{\ell+S+T} = -1. \quad (2.31)$$

Returning to the enumeration of possible states, we now can add the isospin quantum number. All states permissible for two identical nucleons, *even singlets and odd triplets* (2.23), (2.24), have $T = 1$; all remaining states, *odd singlets and even triplets*, including the deuteron state, have $T = 0$,

$$T = 1 : \quad ^1s_0, \quad ^3p_{0,1,2}, \quad ^1d_2, \dots; \quad (2.32)$$

$$T = 0 : \quad ^3s_1, \quad ^1p_1, \quad ^3d_{1,2,3}, \dots. \quad (2.33)$$

At given ℓ , that is, at given parity, spin triplets and singlets always belong to different values of T . If there is no accidental degeneracy, a stationary state, being characterized by a certain isospin T , has, as a consequence, a certain spin S . The vertical mixing of the two-nucleon states in Table 2.2 does not occur.

As it is clear from Eq. (2.31), the isospin conservation is simply conservation of the space–spin symmetry. For the two-nucleon case, the isospin and space–spin symmetries are complementary in the sense of Eq. (2.31). However, the isospin formalism is extremely convenient and powerful in the many-body problems where the symmetry properties are more complicated [2]. Loosely speaking, even in the many-body case, the state with maximum T has more identical nucleons and, as a consequence, reveals less space–spin symmetry.

2.5 Glimpse of a More General Picture

We have already argued that the introduction of the isospin does not increase the number of nuclear degrees of freedom or the number of possible states. This is just a convenient classification associated with the invariance (2.20) of strong interactions [3]. As shown earlier, this classification is actually related to the permutational symmetry of the many-body wave function in the coordinate and spin variables. If the effects violating the isospin invariance, in particular, due to electromagnetic interactions, can be treated as small corrections, we have an approximate isospin symmetry.

The idea of isospin invariance can be naturally extended to higher hadron multiplets (Figure 2.2). Thus, strong interactions are invariant under the transformations within the triplet of spinless *pions*, $\pi^{-0,+}$. The pions are classified as the states with isospin $T = 1$ and $T_3 = +1, 0, -1$, respectively. Many-pion wave functions should be classified using *Bose-statistics* because pions are spin-zero particles. Again, the electromagnetic effects lead to slightly different masses of neutral and charged pions and different lifetimes. For the neutral pion, the main decay channel is the electromagnetic decay into two photons that is impossible for the charged pions. Charged pions decay much slowly by weak interactions into the muon (a heavier analog of the electron) and the corresponding muonic neutrino, for example, $\pi^+ \rightarrow \mu^+ \nu_\mu$; electromagnetic and weak processes do not preserve the isospin symmetry. For meson multiplets, such as that of the pions, $Q = -T_3$ (symmetry with respect to the center of the multiplet). For baryons, this symmetry is shifted by the baryon charge $B = A$, so that for nucleons ($B = 1$) and mesons ($B = 0$), the general rule for identifying the members of the isomultiplet can be written as

$$Q = \frac{B}{2} - T_3. \quad (2.34)$$

Excited nucleons, as for example, *hyperons*, have additional quantum numbers related to their quark structure. For example, $\Sigma^{+,0,-}$ -hyperons are characterized by the *strangeness* $S = -1$, and the role of the baryon charge in the relations as (2.34) is played by the *hypercharge* $Y = B + S$ (for the nucleons $S = 0$, $Y = B = 1$, for the Λ - and Σ -hyperons $S = -1$, $Y = 0$). Then

$$Q = \frac{Y}{2} - T_3. \quad (2.35)$$

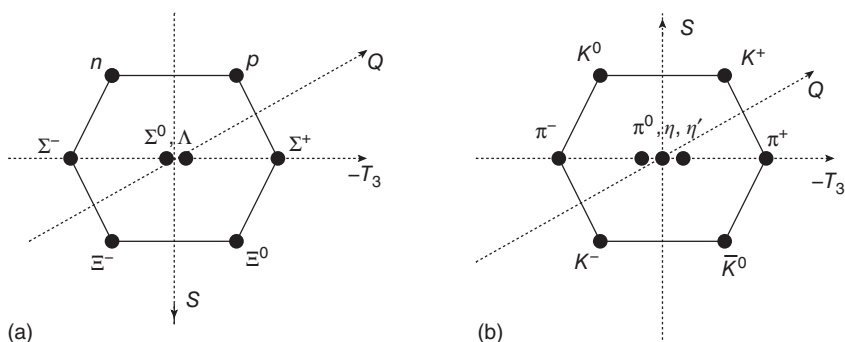


Figure 2.2 Octets of baryons and pseudoscalar mesons.

The concept of isospin $SU(2)$ invariance is generalized to *higher symmetries* in QCD where it is related to the fact that the two lightest quarks, u (up) and d (down), have similar masses and interactions. Furthermore, in the approximation that neglects the difference of the u, d quarks from the s (strange) quark, the carrier of the strangeness, we have already three fundamental objects so that the corresponding (approximate) invariance group is $SU(3)$ or even $SU(6)$ if the interactions do not depend on spins.

Of course, the absolute conservation of the electric charge does not permit the existence of such systems as a superposition of the proton and the neutron (the so-called *superselection rule*). However, all members of the isomultiplets with different electric charges (2.19) at a given baryon charge can exist and should have nearly identical properties with respect to strong forces. Although electromagnetic, first of all Coulomb, effects violate isospin invariance, still in many cases this symmetry holds up to a good accuracy and gives a guidance for reconstruction of the Hamiltonian of strong interactions.

As already mentioned, rotational symmetry in usual space and isomorphic isobaric symmetry in charge space are described by transformations of the $SU(2)$ group. This is a group of unitary matrices 2×2 with the determinant equal to 1. Such matrices determine transformations of elementary objects, in this case of two-component spinors corresponding to spin 1/2 or isospin 1/2, forming the *fundamental representation* of the $SU(2)$ group. Objects with higher spins or isospins can be built by combining an appropriate number of spinors. This construction can be generalized for higher symmetries. The basic symmetry of QCD, *color symmetry*, is described by the $SU(3)$ group of transformations in fundamental space of three colored *quarks*. *Color* is introduced as a new intrinsic quantum number that should not be confused with the *flavor* (characteristic of u, d, s , or heavier quarks). The interaction between the quarks requires $3 \times 3 - 1 = 8$ color states for the particles (gluons) changing color of the quarks (we subtracted the identity operator). Only “white,” or colorless, particles (*singlets* with respect to color $SU(3)$ transformations), such as nucleons (three quarks of complementary colors) or mesons (quark+antiquark) can be observed as free asymptotic states.

2.6 Relations between Cross Sections

Isospin invariance of nuclear forces extended to all hadrons built of u and d quarks allows one to predict relations between cross sections of various reactions with particles, which belong to given isobaric multiplets. The reactions under study are to be taken at identical center-of-mass energies and scattering angles for the same spin states. Of course, it is assumed that the processes are driven by the strong forces.

As an example consider reactions involving the triplet ($T = 1$) of pions, $\pi^{-, 0, +}$. Already from *charge symmetry*, without taking into account full isospin invariance, one can make some predictions. This transformation reflects t_3 changing $p \leftrightarrow n, \pi^+ \leftrightarrow \pi^-, \pi^0 \leftrightarrow \pi^0$. This immediately leads to equality of cross sections for production of π^+ and π^- in np collisions

$$p + n \rightarrow n + n + \pi^+, \quad p + n \rightarrow p + p + \pi^-. \quad (2.36)$$

In more complicated cases, we need to use the full isospin invariance. The initial and final states are to be presented as superpositions of isospin eigenfunctions Ω_{TT_3} . Effects

of the Coulomb interactions and Coulomb-nuclear interference are to be considered separately.

Problem 2.3 Compare cross sections for production of pion and deuteron in np and pp collisions,

$$(a) \ n + p \rightarrow \pi^0 + d; \quad (b) \ p + p \rightarrow \pi^+ + d. \quad (2.37)$$

Solution

Since the deuteron has $T = 0$, in both cases the final state has isospin $T_f = T_\pi = 1$. Therefore, the reactions are possible only for initial isospin $T_i = 1$. The pp system always has $T = 1$, while, according to (2.27) and (2.28),

$$|np\rangle = \frac{1}{\sqrt{2}}(\Omega_{10} + \Omega_{00}). \quad (2.38)$$

The fraction of the state $T = 1$ is only $1/2$. Since at $T = 1$ both reactions should have equal amplitudes because of isospin invariance (the final states represent different projections of $T = 1$ while the physics of strong interactions does not depend on the orientation in isospace), we predict $\sigma_b = 2\sigma_a$.

In fact, relations between different reactions in the same isospin channel are determined by the Clebsch–Gordan coefficients (CGC), which are the same for the isospin $SU(2)$ group as for angular momentum. In the case (2.38), the CGC = $1/\sqrt{2}$. There exists a simple way to connect different reactions between the members of the same isomultiplets avoiding the calculation of CGC, the so-called *Shmushkevich factory*. As an example, consider all possible charge channels for pion–nucleon scattering (without and with charge exchange):

			–	0	+	
(1)	$\pi^+ p \rightarrow \pi^+ p$	(1')	$\pi^- n \rightarrow \pi^- n$	1	0	1
(2)	$\pi^0 p \rightarrow \pi^0 p$	(2')	$\pi^0 n \rightarrow \pi^0 n$	0	2	0
(3)	$\pi^0 p \rightarrow \pi^+ n$	(3')	$\pi^0 n \rightarrow \pi^- p$	1	0	1
(4)	$\pi^- p \rightarrow \pi^- p$	(4')	$\pi^+ n \rightarrow \pi^+ n$	1	0	1
(5)	$\pi^- p \rightarrow \pi^0 n$	(5')	$\pi^+ n \rightarrow \pi^0 p$	0	2	0

(2.39)

The reactions (1')–(5') are charge mirrors of the reactions 1–5 and have the same cross sections, $\sigma_n = \sigma_{n'}$. Now we imagine that all reactions (2.39) proceed simultaneously inside a black box starting with the completely *isospin-unpolarized* state when all members of the nucleon and pion multiplets are supplied evenly, that is, all initial isospin projections are equiprobable. Owing to the isospin invariance, no direction in the charge space can be singled out as a result of reactions – the state will remain *isospin-unpolarized*. This means that populations of various meson states will remain equal. In turn, this is possible only if the cross sections satisfy the condition

$$\sigma_1 + \sigma_3 + \sigma_4 = 2(\sigma_2 + \sigma_5). \quad (2.40)$$

We can in addition recall the *detailed balance principle* based on time reversal invariance. It tells us that $\sigma_3 = \sigma_{3'} = \sigma_5$, and we arrive at a nontrivial result

$$\sigma_2 = \frac{1}{2} (\sigma_1 + \sigma_4 - \sigma_5). \quad (2.41)$$

Because of the fast decay $\pi^0 \rightarrow 2\gamma$, we cannot in practice perform the reactions (2) and (3). Nevertheless, we can predict their cross sections in terms of the experimentally observed reactions with charged pions.

Problem 2.4 Derive the relation between the cross sections of pion production in nucleon collisions,

$$\sigma(np \rightarrow np\pi^0) + \sigma(pp \rightarrow pp\pi^0) = \sigma(np \rightarrow pp\pi^-) + \frac{1}{2}\sigma(pp \rightarrow pn\pi^+). \quad (2.42)$$

More detailed results can be obtained with the explicit use of CGC applied to isospin states. Take as an example pion–nucleon scattering. The pion plus nucleon system can have $T = 1/2$ with $T_3 = \pm 1/2$ and $T = 3/2$ with $T_3 = \pm 1/2, \pm 3/2$. Under the assumption of exact isospin invariance of nuclear forces, T is conserved. Therefore, there exist only two independent amplitudes of πN scattering, $f_{1/2}$ and $f_{3/2}$ (no dependence on the isospin projections).

Problem 2.5 Express observable cross sections of charged pion scattering by nucleons via amplitudes $f_{1/2}$ and $f_{3/2}$ for scattering in states with certain T .

Solution

It is sufficient to consider only pion scattering off the proton since the scattering off the neutron can be obtained by charge symmetry (in reality it is hard to create a pure neutron target, and information on scattering by neutrons can be extracted indirectly from the experiments on nuclei containing both protons and neutrons). For the coupling of isospin 1 of pions with nucleon isospin 1/2, we use the CGC, which can be found for the vector coupling of orbital momentum 1 and spin 1/2 [QP, I, 23.2], and construct the pion–nucleon states as correct combinations of states Ω_{TT_3} with definite isospin:

$$\begin{aligned} |\pi^+ p\rangle &= \Omega_{3/2 -3/2}; \quad |\pi^- n\rangle = \Omega_{3/2 3/2}; \\ |\pi^- p\rangle &= \sqrt{\frac{1}{3}} \Omega_{3/2 1/2} + \sqrt{\frac{2}{3}} \Omega_{1/2 1/2}; \quad |\pi^0 n\rangle = \sqrt{\frac{2}{3}} \Omega_{3/2 1/2} - \sqrt{\frac{1}{3}} \Omega_{1/2 1/2}; \\ |\pi^0 p\rangle &= \sqrt{\frac{2}{3}} \Omega_{3/2 -1/2} + \sqrt{\frac{1}{3}} \Omega_{1/2 -1/2}; \\ |\pi^+ n\rangle &= \sqrt{\frac{1}{3}} \Omega_{3/2 -1/2} - \sqrt{\frac{2}{3}} \Omega_{1/2 -1/2}. \end{aligned} \quad (2.43)$$

From this, we define the transition amplitudes (elements of the scattering matrix),

$$\begin{aligned} \langle \Omega_{3/2 T_3} | \hat{f} | \Omega_{3/2 T_3} \rangle &= f_{3/2}, \quad \langle \Omega_{1/2 T_3} | \hat{f} | \Omega_{1/2 T_3} \rangle = f_{1/2}; \\ M(\pi^+ p \rightarrow \pi^+ p) &= \langle \Omega_{3/2 -3/2} | \hat{f} | \Omega_{3/2 -3/2} \rangle = f_{3/2}; \\ M(\pi^- p \rightarrow \pi^0 n) &= \left\langle \sqrt{\frac{1}{3}} \Omega_{3/2 1/2} + \sqrt{\frac{2}{3}} \Omega_{1/2 1/2} | \hat{f} | \sqrt{\frac{2}{3}} \Omega_{3/2 1/2} \right. \\ &\quad \left. - \sqrt{\frac{1}{3}} \Omega_{1/2 1/2} \right\rangle \end{aligned} \quad (2.44)$$

$$\begin{aligned}
&= \frac{\sqrt{2}}{3} [\langle \Omega_{3/2}^{1/2} | \hat{f} | \Omega_{3/2}^{1/2} \rangle - \langle \Omega_{1/2}^{1/2} | \hat{f} | \Omega_{1/2}^{1/2} \rangle] \\
&= \frac{\sqrt{2}}{3} (f_{3/2} - f_{1/2});
\end{aligned} \tag{2.45}$$

$$M(\pi^- p \rightarrow \pi^- p) = \frac{1}{3} (f_{3/2} + 2f_{1/2}); \quad M(\pi^0 p \rightarrow \pi^0 p) = \frac{1}{3} (2f_{3/2} + f_{1/2}). \tag{2.46}$$

The cross sections are proportional to $|M|^2$.

Experiments reveal that in all cases of πN scattering, there is a pronounced broad resonance centered at pion energy around 190 MeV. The resonance cross sections are related as

$$\sigma(\pi^+ p \rightarrow \pi^+ p) : \sigma(\pi^- p \rightarrow \pi^0 n) : \sigma(\pi^- p \rightarrow \pi^- p) = 9 : 2 : 1. \tag{2.47}$$

This is precisely what should have been expected if the interaction in the $T = 3/2$ state was much stronger in the resonance region than in the $T = 1/2$ state, $|f_{3/2}| \gg |f_{1/2}|$. We conclude that at this energy the pion–nucleon interaction proceeds mainly through an intermediate state with $T = 3/2$. Analyzing the angular distribution of scattered particles, one discovers that the angular momentum of this state is also $J = 3/2$ (*3–3 resonance*). The resonance can be described by the Breit–Wigner formula [QP, II, Ch. 10] with energy $E \approx 1236$ MeV and width $\Gamma \approx 120$ MeV. We see that there exists a quasistationary state, called Δ -resonance, or *delta-isobar*, as a spin–isospin excitation of the nucleon with quantum numbers $J = 3/2$ and $T = 3/2$. In quark language, this is the state with parallel alignment of spins and isospins of three constituent quarks. According to isospin invariance, there have to be $2T + 1 = 4$ states with projections $T_3 = \pm 1/2, \pm 3/2$ and electric charges defined from $-T_3 = Q - B/2 = Q - 1/2$,

	Δ^{++}	Δ^+	Δ^0	Δ^-
T_3	$(\pi^+ p)$	$(\pi^0 p), (\pi^+ n)$	$(\pi^0 n), (\pi^- p)$	$(\pi^- n)$

Problem 2.6 Establish the isospin of the final state in the decay $K^+ \rightarrow \pi^+ \pi^0$. This decay is governed by weak interactions and does not preserve isospin. However, the spatial structure of the *final* state (spins are equal to zero) determines its isospin.

Solution

In a two-pion system, the vector coupling allows for isospins $T = 0, 1, 2$. The value $T_3 = -1$ excludes $T = 0$. In the case of $T = 1$, the wave functions of the two pions would be antisymmetric in charge space as it should be in vector coupling of two vectors into their cross-product. Because of the Bose statistics for pions (spin 0) considered in a generalized sense as identical particles with different charge states, the total wave function (spatial charge) has to be symmetric, which would require the spatial wave function for $T = 1$ to be antisymmetric as well. This is equivalent to negative parity of the two-pion state, that is, an odd value of the orbital momentum ℓ . However, ℓ has to be equal to zero because of the angular momentum conservation (spin of K^+ is zero). Because of this contradiction, the only possibility is $T = 2$.

2.7 Selection Rules

In coordinate (or momentum) space, tensor operators have certain selection rules [QP, I, Ch. 22] for transitions between the states $|JM\rangle$ with definite quantum numbers of the rotation group (we do not indicate other quantum numbers). Fully analogous selection rules emerge for matrix elements between the states $|TT_3\rangle$ with definite isospin quantum numbers for the operators with certain isospin tensor properties.

To give the first impression of such selection rules, we consider an arbitrary *one-body* operator, Q , a sum of certain single-particle operators q_a over all particles $a = 1, \dots, A$ in the system,

$$Q = \sum_a q_a. \quad (2.49)$$

With two sorts of particles in the nucleus, we have two types of operators, q_n and q_p . Therefore, the operator (2.49) can be presented with the help of isospin projection operators that single out neutrons or protons,

$$Q = \sum_n q_n + \sum_p q_p = \sum_a \left(q_n \frac{1 + \tau_{3a}}{2} + q_p \frac{1 - \tau_{3a}}{2} \right). \quad (2.50)$$

Now we express a one-body operator as a sum,

$$Q = Q^{(\tau=0)} + Q^{(\tau=1)}, \quad (2.51)$$

of the two parts with different tensor properties in isospin space; τ is the tensor rank of the corresponding operator, analogous to the rank λ of the spherical functions $Y_{\lambda\mu}$.

The *isoscalar* part, $\tau = 0$, is given by the average contributions of neutrons and protons,

$$Q^{(\tau=0)} = \sum_a \frac{q_n + q_p}{2}. \quad (2.52)$$

The matrix elements of isoscalar operators have trivial selection rules, $\Delta T = \Delta T_3 = 0$. The *isovector* part, $\tau = 1$, contains the difference of neutron and proton characteristics,

$$Q^{(\tau=1)} = \sum_a \frac{q_n - q_p}{2} \tau_{3a}. \quad (2.53)$$

This is the third component of an operator that transforms as a vector in isospin space. The corresponding selection rules are $\Delta T = 0, \pm 1$, $\Delta T_3 = 0$, which means that the proton–neutron symmetry can change in such a transition.

As an important example, we can mention the electric multipoles

$$M_{\lambda\mu} = \sum_a e_a r_a^\lambda Y_{\lambda\mu}(\mathbf{n}_a). \quad (2.54)$$

Such an operator can be decomposed into the isoscalar,

$$M_{\lambda\mu}^{(\tau=0)} = \frac{e}{2} \sum_a r_a^\lambda Y_{\lambda\mu}(\mathbf{n}_a), \quad (2.55)$$

where the neutron and proton contributions act coherently, and the isovector

$$M_{\lambda\mu}^{(\tau=1)} = -\frac{e}{2} \sum_a r_a^\lambda Y_{\lambda\mu}(\mathbf{n}_a) \tau_{3a}, \quad (2.56)$$

with opposite contributions of neutrons and protons.

The special case is the *electric dipole*,

$$\mathbf{d} = \sum_a e_a \mathbf{r}_a. \quad (2.57)$$

The spherical components d_μ of this vector, $\mu = 0, \pm 1$, differ from $M_{1\mu}$ only by a constant factor $\sqrt{4\pi/3}$. The isoscalar part of the dipole,

$$\mathbf{d}^{(\tau=0)} = \frac{e}{2} \sum_a \mathbf{r}_a = \frac{e}{2} A \mathbf{R}, \quad (2.58)$$

is proportional to the center-of-mass vector,

$$\mathbf{R} = \frac{1}{A} \sum_a \mathbf{r}_a, \quad (2.59)$$

and cannot influence any intrinsic transition. Then we are left with the isovector part $\mathbf{d}^{(\tau=1)}$. However, the electric dipole moment for a system with a nonzero total charge depends on the choice of the coordinate origin. With respect to the center-of-mass as the origin, according to Eq. (2.53), we have

$$\mathbf{d}^{(\tau=1)} = \frac{e}{2} \left\{ - \sum_n (\mathbf{r}_n - \mathbf{R}) + \sum_p (\mathbf{r}_p - \mathbf{R}) \right\}. \quad (2.60)$$

Using Eq. (2.59), we see that the operator (2.60) counts neutrons and protons with the *effective dipole charges*,

$$e_n = -\frac{Z}{A} e, \quad e_p = \frac{N}{A} e. \quad (2.61)$$

This result means that the neutrons have to *recoil* at the proton displacement in order to keep the center-of-mass intact.

The isospin selection rules considerably influence probabilities of nuclear processes. As an example, consider the electric dipole transitions without change of isospin, $\Delta T = 0$. Such transitions turn out to be forbidden in *self-conjugate* nuclei with $N = Z$ and therefore $T_3 = 0$, and this can be shown in various ways. As follows from the quantum mechanical vector model [QP, I, 22.8], a matrix element for such a transition has to be proportional to the CGC $C_{10 \ 70}^{T0}$ or the corresponding $3j$ -symbol that vanishes: this is a special case of a more general geometric property valid for integer positive J_1, J_2, J_3 ,

$$\begin{pmatrix} J_1 & J_2 & J_3 \\ 0 & 0 & 0 \end{pmatrix} = 0 \quad \text{if } J_1 + J_2 + J_3 = \text{odd}. \quad (2.62)$$

This result reflects parity conservation as it is easy to understand in the case when the three angular momenta are orbital momenta of three spherical functions: the matrix element that contains the integral of their product has to be invariant under inversion of coordinates when every spherical function Y_{JM} receives a factor $(-)^J$. In the isospin case, the “inversion” is the *charge symmetry* transformation $C_T, p \leftrightarrow n$. For a many-body system, this leads to $N \leftrightarrow Z$, and therefore $T_3 \leftrightarrow -T_3$. A self-conjugate nucleus with $N = Z$ transforms into itself (maybe with change of sign as $C_T^2 = 1$). Hence, such a system has a certain “*charge parity*.” The dipole operator in the matrix element is the isovector with the selection rule $\Delta T = \Delta T_3 = 0$ that has to change the charge symmetry of the

system being antisymmetric with respect to the transformation $p \leftrightarrow n$. Due to charge parity conservation this amplitude has to vanish.

To find the eigenvalue of charge parity for a self-conjugate system of isospin T , we can explicitly present the operator C_T changing $T_3 \rightarrow -T_3$ as rotation through 180° around a transverse axis in isospin space, for example,

$$C_T = e^{-i\pi T_2}. \quad (2.63)$$

Using the algebra of Pauli matrices, we have for one-nucleon states

$$C_T = e^{-i\pi t_2} = e^{-i\pi \tau_2/2} = \cos\left(\frac{\pi}{2}\right) - i \sin\left(\frac{\pi}{2}\right) \tau_2 = -i\tau_2. \quad (2.64)$$

This operator acts according to

$$C_T |n\rangle = |p\rangle, \quad C_T |p\rangle = -|n\rangle, \quad (2.65)$$

or, in isospinors,

$$C_T \Omega_{1/2\tau} = (-)^{1/2-\tau} \Omega_{1/2-\tau}. \quad (2.66)$$

The self-conjugate system, $T_3 = 0$, is the eigenstate of charge symmetry. For two-particle wave functions (2.27) and (2.28), the explicit action of the operator (2.65) gives

$$C_T \Omega_{00} = \Omega_{00}, \quad C_T \Omega_{10} = -\Omega_{10}. \quad (2.67)$$

Thus, the eigenvalue of the charge symmetry operator is here

$$C_T = (-)^T. \quad (2.68)$$

For the definition (2.63), this differs by sign from the isospin exchange operator P^τ , Eq. (2.29). The result (2.68) is valid for any value of isospin. Indeed, for any state with $T_3 = 0$,

$$C_T = \langle T0 | e^{-i\pi T_2} | T0 \rangle = d_{00}^T(\pi), \quad (2.69)$$

the standard matrix element of finite rotation [QP, I, 21.1,2] around the y -axis for the angle equal to π . This d -function is just the Legendre polynomial,

$$C_T = P_T(\pi) = (-)^T, \quad (2.70)$$

similar to parity $(-)^{\ell}$ of spherical functions.

Until now, we limited ourselves to the one-body operators of type (2.49), which have the $\tau = 1$ part (2.53) that acts as the third component of an isovector. The weak interaction processes induced by the *charged currents* (exchange by charged intermediate bosons W^\pm) change the charge of the nucleus and therefore the projection T_3 . The most probable weak processes are those induced by the Fermi operators,

$$F^{(\pm)} = \sum_a \tau_{\pm,a}, \quad (2.71)$$

and Gamow-Teller operators,

$$(GT)_i^{(\pm)} = \sum_a \sigma_{i,a} \tau_{\pm,a}. \quad (2.72)$$

The operators $F^{(-)}$ and $(GT)^{(-)}$ transform $n \rightarrow p$; they work in β^- decays while the operators $F^{(+)}$ and $(GT)^{(+)}$ work in β^+ decays and weak processes of electron capture. Both types of operators have the properties of the (\pm) -components of the isovector, T_\pm .

Fermi operators simply coincide with T_{\pm} and therefore act only within a given isobaric multiplet, $\Delta T = 0$. They do not change any other quantum numbers of the nucleus so that raising and lowering matrix elements are just those of angular momentum. The Gamow–Teller operators have general isovector selection rules, $\Delta T = 0, \pm 1$, except for the $(T = 0) \rightarrow (T = 0)$ transition that is forbidden. With respect to coordinate space, Fermi transitions are related to the usual electromagnetic transitions; in fact the latter comprise the third component of the same *electroweak current* (*conserved vector current*, CVC). The matrix elements of this current should be universal for all transitions without changing the usual quantum numbers that is indeed fulfilled with high accuracy. The Gamow–Teller processes are caused by the *axial vector current* as seen from the presence of the spin operators. These matrix elements are not strictly universal being *renormalized* in the nuclear medium.

2.8 Isobaric Mass Formulae

The idea of isospin invariance allows one to establish relations between isobaric analog states, that is, corresponding states in different nuclei that belong to the same isospin multiplet.

In the limit of exact isobaric invariance, all members of the multiplet have the same energy. In reality, the multiplets are split. A trivial correction comes from the mass difference between the proton and the neutron. The contribution of the rest masses to the total nuclear energy is

$$H_0 = \sum_n M_n c^2 + \sum_p M_p c^2 \Rightarrow c^2 \sum_a \left(M_n \frac{1 + \tau_{3a}}{2} + M_p \frac{1 - \tau_{3a}}{2} \right). \quad (2.73)$$

As earlier, we can separate the isoscalar and the third component of the isovector,

$$\frac{1}{c^2} H_0 = \frac{M_n + M_p}{2} \sum_a 1 + \frac{M_n - M_p}{2} \sum_a \tau_{3a} = \frac{M_n + M_p}{2} A + (M_n - M_p) T_3. \quad (2.74)$$

The isoscalar term determines the main part of the nuclear mass, which is common for all multiplet members. The isovector term gives the linear shift in energy to states of the same isospin along the fixed- A diagonal line of the nuclear chart; it does not mix states with different isospin, which is similar to the static magnetic field in the Zeeman effect.

A similar consideration is valid for kinetic energy:

$$K = \sum_n \frac{\mathbf{p}_n^2}{2M_n} + \sum_p \frac{\mathbf{p}_p^2}{2M_p} = \sum_a \frac{\mathbf{p}_a^2}{2} \left(\frac{1 + \tau_{3a}}{2M_n} + \frac{1 - \tau_{3a}}{2M_p} \right). \quad (2.75)$$

Combining again the terms of different tensor nature in charge space, we find

$$K = \frac{1}{4M_n M_p} \sum_a \mathbf{p}_a^2 [(M_n + M_p) - (M_n - M_p)\tau_{3a}]. \quad (2.76)$$

The isoscalar term is the total kinetic energy with the effective mass equal to the reduced mass of the neutron and the proton. The second term is again the third component of an isovector, but in this case it is not a component of the total isospin, thus it can

mix the multiplets with different values of T (still keeping the same T_3). This mixing is small being proportional to $(m_n - m_p)/(m_n + m_p) \approx 7 \times 10^{-4}$, so that the isospin purity is essentially preserved.

The main effect violating isospin comes from the *Coulomb interaction* [4],

$$U_C = \frac{1}{2} \sum_{a \neq b} \frac{e_a e_b}{r_{ab}} \Rightarrow e^2 \sum_{a \neq b} \frac{(1 - \tau_{3a})(1 - \tau_{3b})}{8r_{ab}}, \quad (2.77)$$

where $r_{ab} = |\mathbf{r}_a - \mathbf{r}_b|$. The isospin operators in (2.77) can be decomposed into isoscalar, isovector, and isotensor parts, similarly to what is usually done for the product of two vectors in usual space [QP, I, 16.9]. To have an irreducible second-rank isotensor, we make it *traceless* eliminating the isoscalar, as it is done for the quadrupole moment. This decomposition leads to

$$U_C = \sum_{a \neq b} \frac{e^2}{8r_{ab}} \left[\left(1 + \frac{1}{3} (\boldsymbol{\tau}_a \cdot \boldsymbol{\tau}_b) \right) - (\tau_{3a} + \tau_{3b}) + \left(\tau_{3a}\tau_{3b} - \frac{1}{3} (\boldsymbol{\tau}_a \cdot \boldsymbol{\tau}_b) \right) \right]. \quad (2.78)$$

The isoscalar term preserves T but shifts all levels of an isomultiplet by the same energy that depends on T . The isovector term not only splits the multiplet in proportion to $T_3 = (N - Z)/2$ but also it can mix multiplets with $\Delta T \leq 1$. Finally, the isotensor term gives the quadrupole-type splitting, similar to the quadrupole hyperfine structure [QP, I, 23.8] and proportional, according to the Wigner–Eckart theorem [QP, I, 22.7] applied in isospace, to $T_3^2 - T(T+1)/3$. As dictated by the selection rules, this shift occurs only in the multiplets with $T \geq 1$. Apart from that, the isotensor term can mix different iso-multiplets with $\Delta T \leq 2$.

The strong nuclear forces also have a small charge-dependent component, probably not greater than 2–3% in comparison to the main isospin-invariant part. The most general form of two-body charge-dependent forces is

$$U'_s = \frac{1}{2} \sum_{a \neq b} (X_1(\tau_{3a} + \tau_{3b}) + X_2\tau_{3a}\tau_{3b}), \quad (2.79)$$

where X_1 and X_2 are functions of spatial and spin variables symmetric with respect to permutations of the interacting particles. Again we have here the isovector and isotensor parts. Combining all those effects we see that *inside the isobaric multiplet*, the nuclear mass can be expressed by the *isobaric multiplet mass equation* (IMME) [5],

$$M = a(A, T) + b(A, T)T_3 + c(A, T)T_3^2. \quad (2.80)$$

The fulfillment of this relation would evidence that the isospin mixing is small and can be neglected compared to the (mainly Coulomb) splitting within the multiplet. This can be empirically tested for multiplets with $T \geq 3/2$, which have at least four members.

Problem 2.7 Show that the mass equation (2.80) implies the relation between the masses $M(T_3)$ of the four members of a multiplet with $T = 3/2$,

$$M(-1/2) - M(1/2) = \frac{1}{3} [M(-3/2) - M(3/2)]. \quad (2.81)$$

For many experimentally known isobaric families (more than 400), the relation (2.81) is well satisfied, with the difference between the left and the right sides typically not exceeding 20 keV, while the coefficient c in the mass formula (2.80) is always around 200 keV and goes down with A (a characteristic measure of Coulomb mixing that weakens for larger nuclei). In rough agreement with (2.78), the coefficient b is negative and grows in magnitude approximately as A/R_c , where R_c is the mean radius of the charge distribution measured by electron scattering or other electromagnetic methods. This confirms that the main effect is the average Coulomb splitting within the multiplet. One can also see odd–even staggering effects due to pairing correlations. The situation is generally more complex for excited and loosely bound states [6] when the spatial wave functions of neutrons and protons can be quite different. In a similar spirit, many mass formulae were widely used in theory of elementary particles based on isospin and higher symmetries.

In some cases, the main violation of the isospin invariance comes from the so-called *antianalog states*. As a simple example (suggested by N. Auerbach), take a nucleus (N, Z) with a neutron excess, $N > Z$, so that the isospin of the ground state $|N, Z; \text{g.s.}\rangle$ is given by its minimal possible value, $T = (N - Z)/2$. In the neighboring nucleus $(N - 1, Z + 1)$ one neutron is substituted by a proton, and among the levels of this nucleus there exist an isobaric analog state. Using the lowering matrix element, we obtain

$$|\text{analog}\rangle \equiv |N - 1, Z + 1; \text{IAS}\rangle = \frac{1}{\sqrt{2T}} T_- |N, Z; \text{g.s.}\rangle, \quad (2.82)$$

Assume that in the mother nucleus, the neutron excess is concentrated on two single-particle levels so that $N - Z = 2T = n_1 + n_2$. If the core structure does not change in the transition between the two nuclei, we can consider only this neutron excess so that $|N, Z; \text{g.s.}\rangle$ reduces to $|n_1, n_2\rangle$ while the change of the isospin projection can be realized by annihilating any of the excess neutrons and creating a proton with exactly the same space–spin wave function that certainly does not violate the Pauli principle,

$$|\text{analog}\rangle = \frac{1}{\sqrt{2T}} [\sqrt{n_1}|n_1 - 1, p_1; n_2\rangle + \sqrt{n_2}|n_1; n_2 - 1, p_2\rangle]. \quad (2.83)$$

The orthogonal state with the same T_3 but isospin $T - 1$ is the so-called *antianalog*,

$$|\text{antianalog}\rangle = \frac{1}{\sqrt{2T}} [\sqrt{n_2}|n_1 - 1, p_1; n_2\rangle - \sqrt{n_1}|n_1; n_2 - 1, p_2\rangle]. \quad (2.84)$$

The Coulomb admixture of this state can be responsible for a noticeable violation of the isospin purity, especially if the two groups of neutrons in the mother wave function differ significantly by spatial structure.

Problem 2.8 Show that if the single-particle Coulomb matrix element is that of the mean Coulomb potential U_C , the mixture of the analog and antianalog states is given by the difference of U_C for the states 1 and 2,

$$\langle \text{antianalog} | U_C | \text{analog} \rangle = \frac{\sqrt{n_1 n_2}}{2T} [(U_C)_{11} - (U_C)_{22}]. \quad (2.85)$$

References

- 1 E. Wigner, Phys. Rev. **51**, 106 (1937).
- 2 A. Frank, J. Jolie, and P. Van Isacker, *Symmetries in Atomic Nuclei*, Springer-Verlag, Heidelberg, 2009.
- 3 C. Amsler *et al.*, (Particle Data Group), Phys. Lett. B **667**, 1 (2008).
- 4 N. Auerbach, Phys. Rep. **98**, 273 (1983).
- 5 W. Benenson and E. Kashy, Rev. Mod. Phys. **51**, 527 (1979).
- 6 Y.H. Lam, B. Blank, N.A. Smirnova, J.B. Bueb, and M.S. Antony, At. Data Nucl. Data Tables **99**, 680 (2013).

3

Two-Body Dynamics and the Deuteron

... the two-nucleon problems are the basic problems of nuclear physics and are our best source of knowledge regarding the nature of nuclear forces.

J.M. Blatt and V.F. Weisskopf, *Theoretical Nuclear Physics*.

3.1 Low-Energy Nuclear Forces

In the domain of low-energy nuclear physics, as it was defined in Section 3.1, we can mostly (not always) limit ourselves with consideration of nucleon degrees of freedom only. Using nonrelativistic quantum mechanics, we attempt to describe the nucleon–nucleon interaction by a Hamiltonian expressed in terms of nucleon variables, namely coordinates \mathbf{r} , momenta \mathbf{p} , and spins \mathbf{s} . Moreover, forces containing momentum dependence are of relativistic origin, and in the zeroth approximation we can ignore them. In this limit, the Hamiltonian of a two-nucleon system can depend on $\mathbf{r}_1, \mathbf{r}_2$ and $\mathbf{s}_1, \mathbf{s}_2$ only. Now we use all known symmetries to restrict a possible form of the low-energy Hamiltonian.

The center of mass of the two-nucleon system is moving freely with the momentum \mathbf{P} , as shown in Eq. (2.2). In the center-of-mass frame, the Hamiltonian is a function of the relative coordinate \mathbf{r} , Eq. (2.1), only. This is strictly correct only if there are no other particles around, then the two-body interaction can depend on the position of their center-of-mass with respect to the density of the system as a whole. At present, we restrict ourselves to the pure two-body problem.

The rotational symmetry requires the Hamiltonian to be a scalar. Therefore, a *central potential* $U_c(r)$ with arbitrary dependence on $r = |\mathbf{r}|$ is always allowed. Other scalars have to include spin operators. Due to the special properties of spin 1/2, any function of $\boldsymbol{\sigma}$ can be reduced to a linear one, that is, spin operators can appear only as vector components σ_{1k}, σ_{2k} or tensor components $\sigma_{1k}\sigma_{2l}$. The only nontrivial scalar here is the scalar product $(\boldsymbol{\sigma}_1 \cdot \boldsymbol{\sigma}_2)$. Being multiplied by a coordinate scalar $U_\sigma(r)$, it gives the *spin–spin* forces. Another method to obtain a scalar is to contract the spin operator with a coordinate operator of the same tensor structure. Combinations like $(\mathbf{r} \cdot \boldsymbol{\sigma})$ are pseudoscalars rather than genuine scalars. They are invariant under rotations as scalars but change sign under inversion of coordinates (they would also violate time reversal invariance). Such terms cannot be present in the Hamiltonian assuming that parity is conserved in strong interactions.

To construct a spin-dependent Hamiltonian, we have to take a *bilinear* combination of spins that does not change sign under spatial inversion or time reversal. Then we are left with the scalar operator $(\boldsymbol{\sigma}_1 \cdot \mathbf{n})(\boldsymbol{\sigma}_2 \cdot \mathbf{n})$ where the unit vector $\mathbf{n} = \mathbf{r}/r$ is used. Such an operator is responsible for the *tensor* forces that have *noncentral* character depending on the spin orientation relative to the axis of the system. With respect to the coordinate variables, we have here the symmetric tensor of the second-rank $n_k n_l$ that is still reducible under rotations. Its *scalar* part does not depend on orientation of \mathbf{n} and can be extracted by the angular averaging,

$$\overline{n_k n_l} \equiv \frac{1}{4\pi} \int d\Omega n_k n_l = \frac{1}{3} \delta_{kl}. \quad (3.1)$$

Thus, the average part of the above-mentioned operator is $(1/3)(\boldsymbol{\sigma}_1 \cdot \boldsymbol{\sigma}_2)$ and actually belongs to the spin–spin forces. It is convenient to define a pure tensor operator

$$S_{12}(\mathbf{n}) = 3(\boldsymbol{\sigma}_1 \cdot \mathbf{n})(\boldsymbol{\sigma}_2 \cdot \mathbf{n}) - (\boldsymbol{\sigma}_1 \cdot \boldsymbol{\sigma}_2) \quad (3.2)$$

that has zero angular average,

$$\int d\Omega S_{12}(\mathbf{n}) = 0. \quad (3.3)$$

The tensor operator (3.2) is responsible for the *noncentral* forces, analogous to those known in electrodynamics as the interaction of magnetic (or electric) dipole moments, although the radial dependence is different.

To summarize, the general *momentum-independent* interaction of two spin-1/2 particles may contain only three types of forces: central, spin, and tensor, each with its own radial dependence,

$$H_s(\mathbf{r}, \boldsymbol{\sigma}_1, \boldsymbol{\sigma}_2) = U_c(r) + U_\sigma(r)(\boldsymbol{\sigma}_1 \cdot \boldsymbol{\sigma}_2) + U_t(r)S_{12}. \quad (3.4)$$

Note that the interaction (3.4) is automatically symmetric under the spin exchange,

$$[\mathcal{P}^\sigma, H_s] = 0. \quad (3.5)$$

Thus, the spin symmetry defined according to (2.6) by the spin value S is conserved, and triplet states cannot mix with the singlet states.

The expression (3.4) can be applied to the nucleon–nucleon interaction in any quantum state. However, the interaction should not be exactly the same for the states of different space–spin symmetry, or, equivalently, for the isospin values $T = 0$ and $T = 1$. The spin operator structure is universal but the radial functions $U_c(r)$, $U_\sigma(r)$, and $U_t(r)$ can vary. We can conveniently describe this difference adding to (3.4) the same structures multiplied by the operator $(\boldsymbol{\tau}_1 \cdot \boldsymbol{\tau}_2)$ that takes values +1 and −3 for isotriplet and isosinglet states, respectively. Each term in (3.4) gives rise to two terms as, for example,

$$U_c(r) \rightarrow U_c(r) + U_{ct}(r)(\boldsymbol{\tau}_1 \cdot \boldsymbol{\tau}_2) = U_c(r) - U_{ct}(r) + 2U_{ct}(r)\mathcal{P}^\tau, \quad (3.6)$$

where we expressed $(\boldsymbol{\tau}_1 \cdot \boldsymbol{\tau}_2)$ using the isospin exchange operator \mathcal{P}^τ , as shown in Eq. (2.29). Similar to that, a spin–isospin term $U_{\sigma\tau}(r)(\boldsymbol{\sigma}_1 \cdot \boldsymbol{\sigma}_2)(\boldsymbol{\tau}_1 \cdot \boldsymbol{\tau}_2)$ can be added and expressed with the help of the exchange operators \mathcal{P}^σ and \mathcal{P}^τ . As a result, instead of the first two terms in (3.4) with the isotropic radial dependence, we now have four terms,

$$H'_s = U_c(r) + U_\sigma(r)(\boldsymbol{\sigma}_1 \cdot \boldsymbol{\sigma}_2) + U_{ct}(r)(\boldsymbol{\tau}_1 \cdot \boldsymbol{\tau}_2) + U_{\sigma\tau}(r)(\boldsymbol{\sigma}_1 \cdot \boldsymbol{\sigma}_2)(\boldsymbol{\tau}_1 \cdot \boldsymbol{\tau}_2), \quad (3.7)$$

which can be rearranged, using the generalized Pauli principle $\mathcal{P}^r = -\mathcal{P}^r \mathcal{P}^\sigma$, Eq. (2.31), into a combination of Wigner (central), Majorana ($\propto \mathcal{P}^r$), Bartlett ($\propto \mathcal{P}^\sigma$), and Heisenberg ($\propto \mathcal{P}^r \mathcal{P}^\sigma$) forces,

$$H'_s = U_W(r) + U_M(r)\mathcal{P}^r + U_B(r)\mathcal{P}^\sigma + U_H(r)\mathcal{P}^r\mathcal{P}^\sigma, \quad (3.8)$$

where the new radial potentials are

$$\begin{aligned} U_W(r) &= U_c(r) - U_\sigma(r) - U_{ct}(r) + U_{\sigma t}(r), \\ U_B(r) &= 2[U_\sigma(r) - U_{\sigma t}(r)], \\ U_H(r) &= -2[U_{ct}(r) - U_{\sigma t}(r)], \\ U_M(r) &= -4U_{\sigma t}(r). \end{aligned} \quad (3.9)$$

The tensor operator S_{12} , Eq. (3.2), can be expressed in terms of the total spin (2.4),

$$S_{12} = 2[3(\mathbf{S} \cdot \mathbf{n})^2 - \mathbf{S}^2]. \quad (3.10)$$

From Eq. (3.10), we see that the S_{12} operator gives zero acting on any singlet state ($S = 0$). This also follows from the general tensor recoupling rules because S_{12} is a scalar made of the coordinate tensor $n_j n_k$ and the quadrupole spin tensor $3\sigma_{1j}\sigma_{2k} - \delta_{jk}(\sigma_1 \cdot \sigma_2)$. The spin tensor acting onto a state with $S = 0$ could give only a nonexistent state with $S = 2$. Therefore, S_{12} has nonzero matrix elements within the triplet subspace only. Since for the triplet states $(\sigma_1 \cdot \sigma_2) = 1$, we have

$$S_{12}(\sigma_1 \cdot \sigma_2) = (\sigma_1 \cdot \sigma_2)S_{12} = S_{12}. \quad (3.11)$$

From hence the spin exchange is not effective for the tensor forces, and only the isospin exchange brings in a new structure. The isospin exchange can be reduced again to the Majorana operator that gives two tensor terms,

$$H''_s = [U_{tW}(r) + U_{tM}(r)\mathcal{P}^r]S_{12}. \quad (3.12)$$

3.2 Example: Argonne Potential

The most general construction $H'_s + H''_s$ with no momentum operators consists of six radial potentials that can be combined in various methods. These potentials are usually obtained by fitting experimental data on nucleon–nucleon interactions and properties of the deuteron and of other light nuclei. The radial functions are also restricted by theoretical arguments, which will be partly discussed later. The series of the so-called *Argonne* potentials [1, 2] is among the successful examples of phenomenologically constructed nucleon forces. Figure 3.1 shows the Argonne v_4 potential. This is a four-function parametrization of the nucleon–nucleon interaction containing only the isotropic part H'_s , Eqs. (3.7)–(3.9). The four curves correspond to the quantum numbers of the total spin S and isospin T of the pair. The appropriate combinations can be easily found from (3.7), for example,

$$\begin{aligned} H'_s(S = 1, T = 0) &= U_c(r) + U_\sigma(r) - 3[U_{ct}(r) + U_{\sigma t}(r)], \\ H'_s(S = 0, T = 1) &= U_c(r) - 3U_\sigma(r) + U_{ct}(r) - 3U_{\sigma t}(r). \end{aligned} \quad (3.13)$$

The main qualitative features of the potential curves are their short-range character (the interaction becomes very weak at $r > 2$ fm), strong dependence on S and T , and

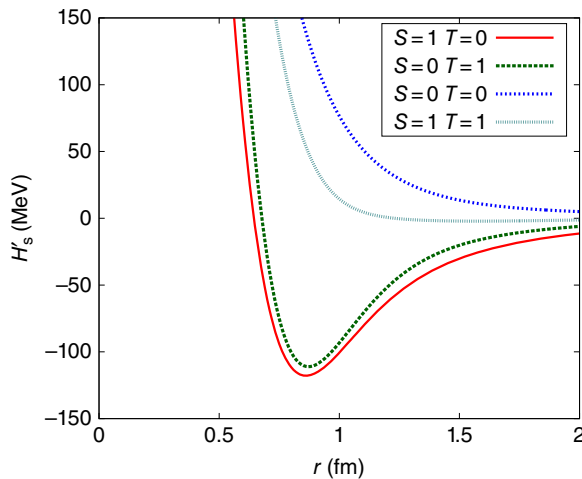


Figure 3.1 Radial dependence of the H'_s part of the Argonne v_4 potential for various combinations (S, T) of spin and isospin of the nucleon–nucleon pair.

sharp repulsion at $r \simeq 0.7$ fm. The states with odd $S + T$ correspond to even- ℓ coordinate functions. A noticeable attraction exists only in such states. The deepest attractive well in the triplet isosinglet state ($S = 1, T = 0$) creates a bound state of the deuteron with the wave function that is mainly a superposition of 3s_1 and 3d_1 parts. The well for the singlet isotriplet states ($S = 0, T = 1$) is not sufficient for supporting a bound state, but it is responsible for the so-called *virtual* (almost bound) state of the $n-p$ system, dineutron or ${}^2\text{He}$, that would become bound if the attraction had been slightly stronger. The odd- ℓ states with even $S + T$ reveal no attraction. Except for the repulsive core, the interaction in the space-odd states is rather weak and it is neglected in some models (Serber forces, which, being proportional to the combination $1 + P^r$ of the Wigner and Majorana forces with equal weights, provide the nucleon–nucleon interaction only in states with even values of ℓ). The tail of the potential is determined, according to the arguments of Eq. (1.5), by exchange of pions as the lightest mesons. This point will be illustrated in the following section.

The form of the short-range part of the potential is the least known. In fact, this is only a potential representation of the complicated short-range interactions taking place via exchange by heavy mesons or already on the level of quark–gluon dynamics. Although early phenomenological potentials introduced a hard impenetrable core, later a “soft core” was usually used. In the Argonne potentials, the core is modeled with a Woods–Saxon form

$$U_{s.c.}(r) = \frac{C}{1 + \exp[(r - r_c)/a_c]} \quad (3.14)$$

that appears in nuclear physics in various contexts. This functional dependence being a formal analog of the momentum distribution for a Fermi gas shows a smooth transition from a constant value near the origin to zero at $r \gg r_c$. At the core radius $r = r_c$, the potential is approximately one-half of the value at the origin if $r_c \gg a_c$, where a_c characterizes the diffuseness region – width of the function (3.14) – similar to the temperature in the Fermi gas case. The parameters used in the Argonne potentials are $r_c = 0.5$ fm and $a_c = 0.2$ fm; the amplitude C is different for different parts of the potential reaching 2 GeV for the main central part (strong repulsion).

The next step in the construction of the nucleon–nucleon forces includes the dependence on the relative momentum \mathbf{p} . In the first order (linear with respect to \mathbf{p}), it can enter only being multiplied by the spin components since this is the only way to make the Hamiltonian time reversible. The scalar product $(\mathbf{s} \cdot \mathbf{p})$ is actually a pseudoscalar and cannot be combined with any radial function to make a parity conserving expression. The same conclusion holds for the symmetric tensor $s_j p_k + s_k p_j$. The only remaining possibility is the antisymmetric tensor that is equivalent to $[\mathbf{p} \times \mathbf{s}]$. This vector product of the axial and polar vectors is a polar vector. Its scalar product with the radius vector \mathbf{r} is a genuine scalar that can be rearranged into the form

$$[\mathbf{r} \times \mathbf{p}] \cdot \mathbf{s} = (\boldsymbol{\ell} \cdot \mathbf{s}), \quad (3.15)$$

where all invariance properties are evident.

For a two-nucleon system, we have two possible (linear in momentum) terms of type (3.15), which have different spin exchange symmetry,

$$H_p = U_{\ell s}(r)(\boldsymbol{\ell} \cdot (\mathbf{s}_1 + \mathbf{s}_2)) + U'_{\ell s}(r)(\boldsymbol{\ell} \cdot (\mathbf{s}_1 - \mathbf{s}_2)). \quad (3.16)$$

The first term gives the *spin-orbit* interaction,

$$H_{\ell s} = U_{\ell s}(r)(\boldsymbol{\ell} \cdot \mathbf{S}). \quad (3.17)$$

The second term does not contradict any fundamental law but changes the spin symmetry of the wave function. It will mix singlet and triplet $n-p$ states belonging, as shown in Eqs. (2.32) and (2.33), to different isospins. The physical source of such a term is the magnetic spin–orbit interaction that feels different magnetic moments of neutrons and protons and therefore violates the charge symmetry. In the consideration of the strong interactions, this term, as a rule, is neglected.

The strong spin–orbit interaction (3.17) is usually included into phenomenological potentials. Again, it can be different in isotriplet and isosinglet states so that one adds two new potential functions increasing their number to eight. In addition, there are terms of the *second order* in momentum. In the Argonne v_{14} potential, six possible terms containing the second power of the orbital momentum operator,

$$\begin{aligned} & \boldsymbol{\ell}^2, \quad \boldsymbol{\ell}^2(\sigma_1 \cdot \sigma_2), \quad \boldsymbol{\ell}^2(\tau_1 \cdot \tau_2), \quad \boldsymbol{\ell}^2(\sigma_1 \cdot \sigma_2)(\tau_1 \cdot \tau_2), \\ & (\boldsymbol{\ell} \cdot \mathbf{S})^2, \quad (\boldsymbol{\ell} \cdot \mathbf{S})^2(\tau_1 \cdot \tau_2), \end{aligned} \quad (3.18)$$

are added so that the full potential counts 14 radial functions. This explains the notation v_{14} . The $\boldsymbol{\ell}^2$ terms make fine-tuning of the wave functions mixed by the tensor forces (as s - and d -waves). The spin–orbit terms of the second order, the lower line of Eq. (3.18), discriminate the interactions for the triplet states with the same ℓ but different J (see Table 2.2). The equivalent parameters are introduced into other phenomenological potentials such as the *Paris potential* [3] or *Nijmegen potential* [4]. We come back to low-energy nucleon–nucleon forces discussing the scattering problem.

We conclude this section showing, Figure 3.2, the radial functions of the Argonne v_{18} potential for the proton–neutron system in states with different quantum numbers. In addition to 14 radial functions (3.18), the popular 18-function parametrization of the nucleon–nucleon interaction, v_{18} , includes four isospin-dependent charge symmetry breaking components.

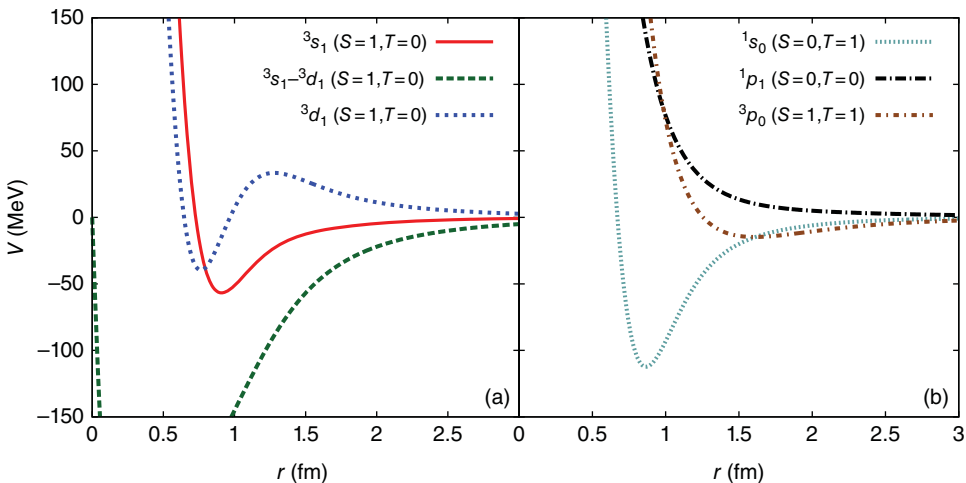


Figure 3.2 The radial behavior of the Argonne potential v_{18} for proton–neutron states of different quantum numbers. The potentials for the diagonal and off-diagonal parts associated with the deuteron quantum numbers are shown separately in panel (a).

The Argonne v_{28} includes, apart from the functions introduced in v_{14} , the same amount of functions related to the possible transition of a nucleon into the excited state of the Δ -resonance with quantum numbers $S = T = 3/2$ (Eq. (2.48)). These terms could be rather important in the nucleon scattering at higher energies.

Argonne potentials give an excellent description of the main deuteron properties, which will be discussed later. It is remarkable that the central (diagonal 3S_1) part, Figure 3.2a, is shallow compared to 1S_0 , Figure 3.2b. The main attraction that binds the proton and neutron in a deuteron is generated by the tensor forces, the off-diagonal $^3S_1 - ^3D_1$ component in Figure 3.2a.

3.3 Meson Exchange

As discussed in Section 1.3, mesons can serve as *mediators* of strong forces (Figure 1.1). The lightest mesons – pions – generate the long-range components of the forces. In order to understand the character of the emerging forces, we follow an analogy with the Coulomb force mediated by electromagnetic field. The full development of meson physics requires the formalism of quantum field theory [5, 6]. Here, we restrict ourselves to the limit of a *static source* when the interacting nucleons are considered to be at rest. This approximation is meaningful because of the heavy mass of the nucleon compared to the pion mass, and we can neglect the recoil of the nucleon in the processes of emission and absorption of mesons.

The free meson field $\phi^\alpha(\mathbf{r}, t)$, where α labels the isospin (charge) characteristic $t_3 = -Q$ of the meson, satisfies the Klein–Gordon equation,

$$\left(\nabla^2 - \frac{1}{c^2} \frac{\partial^2}{\partial t^2} - \mu^2 \right) \phi^\alpha = 0, \quad (3.19)$$

where the typical length $1/\mu$ is given by the meson *Compton wavelength*,

$$\mu = \frac{mc}{\hbar}, \quad (3.20)$$

and m is the meson mass. In order to describe the meson field generated by a nucleon source, Eq. (3.19) should also include the corresponding source density ρ^α of the same isospin in the right-hand side. In the static limit, ϕ^α depends only on coordinates

$$(\nabla^2 - \mu^2)\phi^\alpha(\mathbf{r}) \propto \rho^\alpha(\mathbf{r}). \quad (3.21)$$

The coefficient of proportionality in Eq. (3.21) is the *coupling constant*, the strength of interaction of the meson field with the nucleon source.

In the Coulomb case, the mass μ of the mediator, the photon, is zero, while the density of the static point-like electric charge e_1 at the origin is $\delta(\mathbf{r})$. In the absolute (Gaussian) system of units, we have the Poisson equation

$$\nabla^2\phi = -4\pi e_1\delta(\mathbf{r}). \quad (3.22)$$

The well-known spherically symmetric solution of this equation is given by

$$\phi(\mathbf{r}) = \frac{e_1}{r}, \quad (3.23)$$

or, if the charge is located at an arbitrary point \mathbf{r}_1 ,

$$\phi(\mathbf{r}) = \frac{e_1}{|\mathbf{r} - \mathbf{r}_1|}. \quad (3.24)$$

The second charge e_2 located at \mathbf{r}_2 feels the field generated by the first charge, and e_2 again plays the role of a coupling constant. In this way, we come to the interaction between the charges:

$$U(\mathbf{r}_1, \mathbf{r}_2) = e_2\phi(\mathbf{r}_2) = \frac{e_1e_2}{|\mathbf{r}_1 - \mathbf{r}_2|} \equiv \frac{e_1e_2}{r}. \quad (3.25)$$

In the meson case, the source density is to be constructed of the nucleon variables with the same symmetry properties as the meson field generated by this source. Pions are pseudoscalar particles (negative intrinsic parity) so that the density has to be pseudoscalar as well. The only possible pseudoscalar operator is the scalar product $(\boldsymbol{\sigma} \cdot \mathbf{V})$ of the axial spin vector and a polar vector \mathbf{V} . As spin $\boldsymbol{\sigma}$, the vector \mathbf{V} should also be \mathcal{T} -odd in order to keep the density invariant under time reversal. Therefore, we introduce the momentum operator $\mathbf{p} = -i\hbar\nabla$ acting on the coordinate of the source; in order to make the whole source real and to get the right dimensionality of the entire expression, we write the coefficient of proportionality as $-ig/\hbar\mu$, where g is a real coupling constant of the same dimension as the electric charge. Finally, the isospin superscript α in the left-hand side requires the nucleon isospin matrix τ^α in the right-hand side. This reveals three possible charge operators in the source creating three charge states of the pion. Correspondingly, the meson field acts as an isospin operator on the nucleon variables. The constant g , as well as the mass μ , is the same for all identical nucleons and, according to isospin invariance, for all members of an isobaric multiplet.

As a result, we obtain the field equation (3.21) in the form similar to (but more complicated than) (3.22),

$$(\nabla^2 - \mu^2)\phi^\alpha(\mathbf{r}) = -\frac{g}{\mu} \tau^\alpha(\boldsymbol{\sigma} \cdot \nabla)\delta(\mathbf{r} - \mathbf{r}_1), \quad (3.26)$$

where, as in Eq. (3.24), we assume the nucleon acting as a point source located at \mathbf{r}_1 . Similar to the Green function of the scattering problem,

$$(\nabla^2 - \mu^2) \frac{e^{-\mu r}}{r} = -4\pi\delta(\mathbf{r}), \quad (3.27)$$

the solution for the meson field (3.26) is given by

$$\phi^\alpha(\mathbf{r}) = \frac{g}{4\pi\mu} \tau^\alpha(\boldsymbol{\sigma} \cdot \nabla) \frac{e^{-\mu|\mathbf{r}-\mathbf{r}_1|}}{|\mathbf{r} - \mathbf{r}_1|}. \quad (3.28)$$

The interaction of the second nucleon with the meson field should contain the coupling constant combined with the same operators, so instead of (3.25) we have

$$U_\pi(\mathbf{r}_1, \mathbf{r}_2) = \frac{g}{\mu} \tau_2^\alpha(\boldsymbol{\sigma}_2 \cdot \nabla) \phi^\alpha(\mathbf{r}_2), \quad (3.29)$$

where we use the subscripts 1 and 2 for the variables of the two nucleons. The isospin index α has to be summed over since the isospin-invariant interaction can proceed through any type of pions with the same strength. This leads to the isoscalar operator $(\boldsymbol{\tau}_1 \cdot \boldsymbol{\tau}_2)$; the full result is the *pion-exchange potential* U_π that is explicitly symmetric with respect to the nucleons ($r = |\mathbf{r}_1 - \mathbf{r}_2|$),

$$U_\pi = \frac{g^2}{4\pi\mu^2} (\boldsymbol{\tau}_1 \cdot \boldsymbol{\tau}_2)(\boldsymbol{\sigma}_1 \cdot \nabla)(\boldsymbol{\sigma}_2 \cdot \nabla) \frac{e^{-\mu r}}{r}. \quad (3.30)$$

Problem 3.1 Perform the explicit differentiation and prove that

$$U_\pi = U_{\text{long range}}(r) + U_{\text{contact}}(r), \quad (3.31)$$

$$U_{\text{long range}}(r) = mc^2 \frac{g^2}{4\pi\hbar c} (\boldsymbol{\tau}_1 \cdot \boldsymbol{\tau}_2) \frac{1}{3} \left\{ (\boldsymbol{\sigma}_1 \cdot \boldsymbol{\sigma}_2) + \left[1 + \frac{3}{\mu r} + \frac{3}{(\mu r)^2} \right] S_{12} \right\} \frac{e^{-\mu r}}{\mu r}, \quad (3.32)$$

$$U_{\text{contact}}(r) = -mc^2 \frac{g^2}{4\pi\hbar c} (\boldsymbol{\tau}_1 \cdot \boldsymbol{\tau}_2) \frac{4\pi}{3\mu^3} (\boldsymbol{\sigma}_1 \cdot \boldsymbol{\sigma}_2) \delta(\mathbf{r}). \quad (3.33)$$

Solution

It is convenient to use $\partial_{x_i} = (x_i/r)\partial_r$. One should also remember that the Laplace operator ∇^2 acting on the singularity $1/r$ gives $-4\pi\delta(\mathbf{r})$, as in Eq. (3.22).

The exponential fall $\sim \exp(-\mu r)$ shows, in agreement with simple uncertainty arguments (1.5), that the interaction range is limited by the Compton wave length $1/\mu$ of the mediating meson. Since pions are the lightest strongly interacting particles (hadrons), they define the long-range part of nuclear forces. The phenomenological nuclear potentials usually contain the long-range part with the pion-exchange tail similar to what we have found in this approximate static consideration (spin–spin and tensor parts). The spin–spin part corresponds to attraction in the isosinglet spin-triplet channel. However, the empirically extracted strength of this interaction, $g^2/4\pi\hbar c \approx 0.08$, is too weak for creating a bound state (the critical strength for the Yukawa potential $\exp(-\mu r)/r$ equals 0.22). The main part of the internucleon attraction apparently comes from the *two-pion-exchange* channels, which are often modeled by a scalar *sigma-meson*.

At smaller distances, heavier mesons contribute to the interaction. In the vicinity of the origin, nucleons start to overlap, and their quark structure enters the game. Quark

dynamics along with the Pauli principle create the strong repulsive core. Therefore, the contact term (3.33) can only be an approximate description of reality since the nucleons do not keep their identity at $r \rightarrow 0$, and at very short distances we need to go over to the quark–gluon language of the quantum chromodynamics (QCD). On the other hand, such short distances turn out to be much smaller than typical distances between the nucleons in nuclei. As a result, this part of interaction can be modeled by a repulsive core, as in Eq. (3.14).

Here, it is appropriate to mention the *chiral effective field theory* that is currently being developed. In this approach, the nucleonic interactions are constructed using the QCD symmetries and fitting the contact constants using the scattering data. Consideration of details of this theory is outside of our framework, and we limit ourselves to a few pedagogical Refs. [7–9]. It is necessary to mention that any QCD-based theory also predicts three-body and higher order many-body forces, which might be important in detailed description of heavier nuclei [10, 11]. For example, the adjusted two-body forces v_{18} perfectly reproduce nucleon–nucleon scattering and properties of the two-nucleon systems but predict for the tritium nucleus ${}^3\text{H}$ (three-nucleon system) the binding energy of 7.65 MeV, whereas the experimentally measured binding energy is 8.48 MeV. Modification of such “*ab initio*” forces inside the nuclear medium where the conditions for meson exchange are different from those in vacuum is yet an unsolved problem.

3.4 Deuteron: Central Forces and s-Wave

The lightest nucleus, the deuteron, ${}^2\text{H}$, has binding energy $\epsilon_d = 2.225$ MeV that is quite low on a nuclear scale. In a quantum bound state generated by a finite-range potential, the wave function is localized within the region of size r_0 and exponentially decreases at larger distances. The localization length *does not coincide* with the potential range R due to the quantum penetration into a classically forbidden region under the potential curve. The deuteron is *loosely bound*, and therefore its wave function has a rather long tail. The smaller the binding energy, the further the wave function penetrates under the barrier (Figure 3.3).

As can be recalled from basic quantum mechanics [QP, I, Ch.3 and 17.6], in order to support a bound state, an attractive three-dimensional potential well must be deeper than a critical depth U_{cr} . However, a bound state *always* exists in an attractive one-dimensional or two-dimensional potential that goes to zero at infinity. For the one-dimensional case, it is easy to understand. To find the localization length r_0 , we

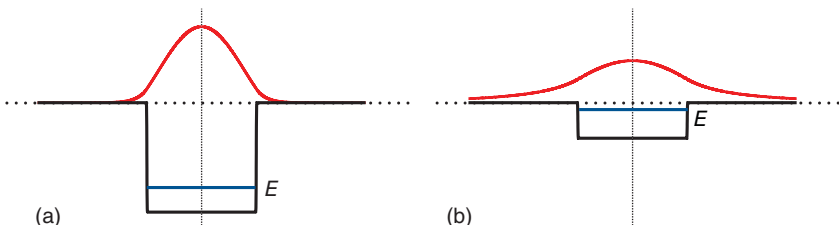


Figure 3.3 Schematic behavior of the ground state bound wave functions in the deep (a) and shallow (b) potential wells.

estimate the ground-state energy as a sum of the average (positive) kinetic energy E_{kin} and the average (negative) potential energy E_{pot} . The spatial localization in the interval $\Delta x \sim r_0$ implies the uncertainty relation,

$$p \sim \Delta p \sim \frac{\hbar}{r_0} \quad \Leftrightarrow \quad E_{\text{kin}} \sim \frac{p^2}{m} \sim \frac{\hbar^2}{mr_0^2}. \quad (3.34)$$

The potential energy is gained only within the potential range R , so that in the one-dimensional case the fraction of time spent inside the potential is then $E_{\text{pot}} \sim (-\bar{U})R/r_0$, where $\bar{U} > 0$ is a typical depth of the well. At large r_0 , the potential energy prevails thus allowing for a bound state to exist. The minimization of $E = E_{\text{kin}} + E_{\text{pot}}$ with respect to r_0 gives $r_0 \sim \hbar^2/m\bar{U}R$ with negative total energy, $|E| \sim \hbar^2/mr_0^2 \sim m(\bar{U}R/\hbar)^2$. A more accurate estimate leads to nearly the same result with $\bar{U}R$ substituted by the integral $\int dx U(x)$. In the two-dimensional case, the binding energy in a shallow well is exponentially small and cannot be obtained by such a simple estimate.

The three-dimensional case is essentially reduced to the one-dimensional case after elimination of angular variables. But the radial variable is restricted to the region $r > 0$ and the effective infinitely high wall at $r = 0$ invalidates the arguments in the preceding section. The levels are pushed up from the well by this repulsive wall. At $\bar{U} < U_{\text{cr}}$, no bound states remain. The exact borderline U_{cr} depends on the shape of the potential.

An important example is given by the Yukawa potential, see Eqs. (3.27) and (3.28), where it appears due to the meson exchange,

$$U(r) = -f^2 \frac{e^{-\mu r}}{r}. \quad (3.35)$$

Such a potential emerges, for example, as a result of the screening of the Coulomb potential $\sim 1/r$ by free electrons in metals or in plasmas where μ is an inverse of the screening radius. As the electron density increases, the screening radius decreases, and the upper hydrogen-like atomic levels disappear one by one in the continuum until there remains no bound states at all. This is observed by a gradual disappearance of spectral lines in plasmas. For given μ and mass m , the critical strength of the potential (when there is just one level with zero binding energy) is $f_{\text{cr}}^2/(\hbar c) = 0.84\mu/m$, where m is the reduced mass of interacting particles.

Let us first ignore the tensor forces. The wave function for relative $n-p$ motion is a product of the coordinate, $\psi(\mathbf{r})$, and spin-triplet, χ_{1S_z} , parts. The coordinate dynamics is governed by the Schrödinger equation with the reduced mass $m = M/2$, Eq. (2.3), and the effective central potential $U(r) = H'_s$ for the isosinglet spin-triplet states (3.7),

$$\left\{ -\frac{\hbar^2}{2m} \nabla^2 + U(r) \right\} \psi(\mathbf{r}) = E\psi(\mathbf{r}). \quad (3.36)$$

For a central field, the orbital momentum ℓ is a good quantum number, and the angular dependence is given by the spherical function $Y_{\ell m}(\mathbf{n})$. It is convenient to single out the factor $1/r$ from the radial function,

$$\psi_{\ell m}(r, \mathbf{n}) = R_\ell(r) Y_{\ell m}(\mathbf{n}), \quad R_\ell(r) = \frac{u_\ell(r)}{r}. \quad (3.37)$$

The factor $1/r$ describes the probability current decreasing at large distances r due to the increasing surface area $\sim r^2$ in such a way that the total flux is conserved. The remaining

function $u_\ell(r)$ satisfies the radial equation of the one-dimensional type

$$u_\ell'' + \frac{2m}{\hbar^2} \left[E - U(r) - \frac{\hbar^2 \ell(\ell+1)}{2mr^2} \right] u_\ell = 0. \quad (3.38)$$

The difference compared to the genuine one-dimensional case is in the centrifugal potential and in the restriction of motion by the region $r > 0$ plus the boundary condition

$$u_\ell(0) = 0 \quad (3.39)$$

at the origin. For a nonsingular potential, the radial behavior of the regular solution of (3.38) near the origin is

$$u_\ell(r) \sim r^{\ell+1}, \quad r \rightarrow 0. \quad (3.40)$$

Due to the centrifugal barrier, all waves with $\ell > 0$ are suppressed near the origin while the s -wave function u_0/r goes to a constant limit. Far away from the origin, the short-range potential dies away and the centrifugal term is small as well. Then Eq. (3.38) shows the universal asymptotics of the solution,

$$u(r) \sim e^{\pm ikr}, \quad k = \frac{\sqrt{2mE}}{\hbar}. \quad (3.41)$$

For a bound state, the energy eigenvalue is negative, $E = -\epsilon$, where ϵ is positive *binding energy*, and we have to select the asymptotic function decaying into the classically forbidden region,

$$u(r) \sim e^{-\kappa r}, \quad \kappa = \frac{\sqrt{2m\epsilon}}{\hbar}. \quad (3.42)$$

The inverse quantity

$$r_d = \frac{1}{\kappa} = \frac{\hbar}{\sqrt{2m\epsilon}} = \frac{\hbar}{\sqrt{M\epsilon}} \quad (3.43)$$

is the natural length characteristic for the tail of a loosely bound state. At small ϵ , this length is considerably larger than the force radius R . In this case, the probability for being in the exterior, classically forbidden, region may exceed the probability for the interior region. The length (3.43) is fully defined by the binding energy being equal to 4.32 fm for the deuteron.

For the s -wave, the angular part is simply a normalization constant $Y_{00} = 1/\sqrt{4\pi}$. The radial Schrödinger equation for a bound state is

$$u_0'' - \left[\kappa^2 + \frac{2m}{\hbar^2} U(r) \right] u_0 = 0. \quad (3.44)$$

The asymptotic solution (3.42) is valid outside of the potential range, $r \geq R$. The interior solution for $r < R$ has to be found, usually numerically, for a given potential $U(r)$ using the boundary condition (3.40). It should be continuously matched to the exterior solution (3.42) at a distance $r = R$, where nuclear forces are already weak and can be neglected. Since the common amplitude depends on the normalization, it is convenient

to write down the continuity condition in terms of the *logarithmic derivatives*. Denoting this derivative of the interior function ($r = R - 0$) as λ , the matching condition reads

$$\lambda \equiv \left(\frac{u'_0}{u_0} \right)_{r=R-0} = -\kappa. \quad (3.45)$$

Equation (3.45) determines the eigenvalue of the bound state energy ϵ . For the existence of the solution, it is necessary that $\lambda < 0$. Only then one can match the inner function with the *decreasing* outer solution (3.42). The critical potential U_{cr} corresponds to $\lambda = 0$ when the bound level just appears with the zero binding energy. Actually, for the small binding energy, only the exterior part of the wave function is important so the parameter λ extracted from the binding energy is the single information on the interior part.

It is easy to solve the problem exactly for the square well (Figure 3.4), with the stepwise potential equal to a constant, $-U_0$, at $r < R$ and to zero outside the well. An intrinsic function satisfying the condition (3.39) for the square well is

$$u_0(r) = A \sin kr, \quad k = \frac{\sqrt{2m(U_0 - \epsilon)}}{\hbar} \quad (3.46)$$

so that the logarithmic derivative (3.45) is $\lambda = k \cot kR$. At the critical depth, this derivative is zero together with ϵ , that is,

$$kR = \pi/2 \quad \Rightarrow \quad U_{\text{cr}} = \pi^2 \hbar^2 / 8mR^2. \quad (3.47)$$

This gives 36 MeV for $R = 1.7$ fm. The presence of the infinite repulsive core of radius r_c would simply shift this function from the origin to the point $r = r_c$.

As the potential depth exceeds the critical value (Figure 3.4), the logarithmic derivative on the boundary becomes negative and the level sinks into the well. To have the bound level at the actual deuteron energy, one would need to make the square well much deeper as the next term of the matching equation (3.45) gives $U_0 - U_{\text{cr}} \propto \sqrt{U_{\text{cr}} \epsilon}$. The nucleon–nucleon potential for the singlet (isotriplet) configuration, Figure 3.2, cannot support a bound state.

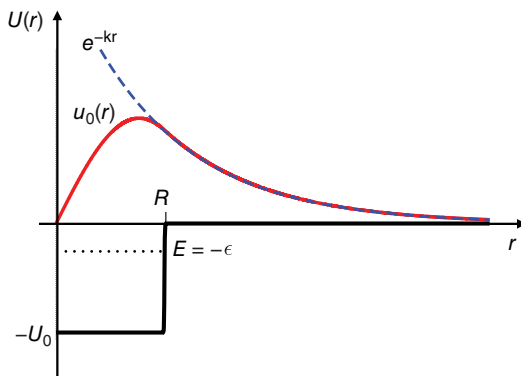


Figure 3.4 The radial potential of the square well and the wave function for the depth exceeding the critical value.

Problem 3.2 Find the dependence of binding energy on the depth of the square potential well for a loosely bound state.

Solution

In the dimensionless variables

$$\xi = kR, \quad \eta = \kappa R, \quad \xi^2 + \eta^2 = \frac{2mU_0R^2}{\hbar^2} \equiv b^2, \quad (3.48)$$

the matching condition reads

$$\tan \xi = -\frac{\xi}{\eta}. \quad (3.49)$$

Every new level appears at $\eta = 0$, or $\xi = \pi/2, 3\pi/2, \dots$. In the situation with the shallow first bound state, $U_0 = U_{\text{cr}} + \delta U$, the binding energy, κ , and η are small, the parameter b , Eq. (3.48), slightly exceeds the critical value of $\pi/2$; From Eq. (3.42), we find

$$\epsilon \approx \frac{\pi^2}{16} \frac{(\delta U)^2}{U_{\text{cr}}}. \quad (3.50)$$

With $U_{\text{cr}} \approx 36$ MeV and $\epsilon = 2.2$ MeV, this estimate gives the effective depth of the deuteron potential well $U = U_{\text{cr}} + \delta U \approx 47$ MeV.

3.5 Tensor Forces and *d*-Wave

Taking into account the tensor forces (3.12), we come to the Schrödinger equation with the *noncentral spin-dependent potential*

$$U(r) = U_0(r) + U_t(r)S_{12}, \quad (3.51)$$

where $U_t(r) = U_{tW}(r) + U_{tM}(r)$ for the space-even states under consideration. The tensor operator S_{12} given by Eqs. (3.2) or (3.10) is a scalar constructed as a product of the spin quadrupole tensor and the coordinate quadrupole tensor. As we discussed, it cannot mix singlet and triplet states, but it mixes the orbital states, $\Delta\ell = 2$, of the same parity with the same total angular momentum. For the deuteron with $J = 1$, we have the superposition ${}^3s_1 + {}^3d_1$ (see Table 2.2).

The *s*-wave part of the deuteron wave function was discussed in the preceding section. Owing to the mixing with the *d*-wave, the radial *s*-function is modified. As for the *d*-wave, the general rules dictate that the 3d_1 state can be represented by the angular momentum coupling $[Y_2(\mathbf{n})\chi_1]_{1M}$ of spin 1 and orbital momentum $\ell = 2$ to the total deuteron spin $J = 1$ and its projection $J_z = M$. The same coupling can be equivalently presented in a convenient form

$$\Theta_M = \frac{1}{\sqrt{32\pi}} S_{12} \chi_{1M}. \quad (3.52)$$

Problem 3.3 Show that the function (3.52) has the correct deuteron quantum numbers and it is properly normalized.

Solution

Indeed, Θ_M is a triplet spin state (S_{12} does not change spin symmetry). The total angular momentum quantum numbers J and M are equal to those in a spin function χ_{1M} since the operator S_{12} is a scalar and preserves these quantum numbers. The angular dependence in (3.52) is given by the components of the vector \mathbf{n} in S_{12} . A symmetric tensor of the second rank is equivalent under rotations to the set of the spherical harmonics $Y_{2\mu}$. Another way to prove it is to check by a direct calculation that $\nabla^2(r^2\Theta_M) = 0$. A regular solution $\Theta(\theta, \varphi)$ of the Laplace equation $\nabla^2(r^\ell\Theta) = 0$ is a linear combination of the spherical functions $Y_{\ell\mu}$. Thus, we have in (3.52) a spin-triplet d -wave.

The coefficient in (3.52) is chosen to normalize the function according to

$$\langle \Theta_{M'} | \Theta_M \rangle = \delta_{M'M}. \quad (3.53)$$

The normalization integral in (3.53), due to Hermiticity of S_{12} , is

$$\frac{1}{32\pi} \int d\Omega \langle S_{12} \chi_{1M'} | S_{12} \chi_{1M} \rangle = \frac{1}{32\pi} \int d\Omega \langle \chi_{1M'} | S_{12}^2 | \chi_{1M} \rangle. \quad (3.54)$$

To compute S_{12}^2 , note that within the triplet Eq. (3.10) gives

$$S_{12} = 2[3(\mathbf{S} \cdot \mathbf{n})^2 - 2]. \quad (3.55)$$

For any direction \mathbf{n} , the projection $(\mathbf{S} \cdot \mathbf{n})$ has eigenvalues 0 or ± 1 , and therefore within the triplet an identity holds

$$(\mathbf{S} \cdot \mathbf{n})^2[(\mathbf{S} \cdot \mathbf{n})^2 - 1] = 0. \quad (3.56)$$

Taking the square of the operator (3.55) and eliminating $(\mathbf{S} \cdot \mathbf{n})^4$ by virtue of (3.56), we derive the identity

$$S_{12}^2 = 8 - 2S_{12} \quad (3.57)$$

valid within the triplet. Since the operator S_{12} is a combination of $Y_{2\mu}(\mathbf{n})$, its angular integral vanishes, and we get from (3.57)

$$\int d\Omega S_{12}^2 = 8 \int d\Omega = 32\pi. \quad (3.58)$$

Then Eq. (3.54) reduces to Eq. (3.53) confirming the proper normalization of the d -wave (3.52).

The complete deuteron wave function now contains two radial parts and, separating out the spherical wave factor $1/r$, it can be written as

$$\Psi_M = \frac{1}{\sqrt{4\pi}} \frac{1}{r} \left(u_0(r) + \frac{1}{\sqrt{8}} u_2(r) S_{12} \right) \chi_{1M}. \quad (3.59)$$

If the total function (3.59) is normalized to unity, for the radial functions u_0 and u_2 we obtain

$$\int_0^\infty dr|u_0|^2 + \int_0^\infty dr|u_2|^2 = 1. \quad (3.60)$$

The two integrals (3.60) can be interpreted as the *weights* W_s and W_d of the *s*- and *d*-waves, respectively. However, the exact values of these quantities depend on the interior part of the wave function including short distances where the potential description is approximate. In this sense, a more model-independent estimate of the relative importance of the *s*- and *d*-contributions can be achieved via the *asymptotic ratio* of the amplitudes of the *s*- and *d*-waves that can be introduced as follows.

In the exterior region when r exceeds the range of the nuclear forces, both radial functions u_0 and u_2 correspond to free motion with orbital momenta $\ell = 0$ and $\ell = 2$ respectively. Therefore, independent of the short-range behavior, here we have two *decoupled* partial wave equations (3.38),

$$\begin{aligned} u_0'' + \frac{2mE}{\hbar^2}u_0 &= 0, \\ u_2'' - \frac{6}{r^2}u_2 + \frac{2mE}{\hbar^2}u_2 &= 0. \end{aligned} \quad (3.61)$$

For the bound deuteron case, we have $2m = M$ and $E = -\epsilon$. Analogous to (3.42), we can find the asymptotic solution of (3.61) exponentially decreasing at large r as

$$\begin{aligned} u_0(r) &= A_0 e^{-\kappa r}, \\ u_2(r) &= A_2 e^{-\kappa r} \left[\frac{1}{(\kappa r)^2} + \frac{1}{\kappa r} + \frac{1}{3} \right]. \end{aligned} \quad (3.62)$$

The amplitudes A_0 and A_2 are to be determined by the matching to the interior wave function. Their ratio $\eta = A_2/A_0$ does not depend on the common normalization and characterizes the relative probability of the *d*-wave. Its value extracted from the experimental data is [2] $\eta = 2.6\%$.

In the interior region, the tensor forces of the full potential in Eq. (3.51) do not conserve the orbital momentum and mix *s*- and *d*-waves. Therefore, we get a coupled set of differential equations for $u_0(r)$ and $u_2(r)$. Looking for the solution in the form (3.59), we plug it into the Schrödinger equation (3.36) with the potential (3.51). The quadratic term in S_{12} is calculated with the aid of (3.57). After that we equate separately the terms with S_{12} and those that do not contain S_{12} . This leads to the equations sought for,

$$\begin{aligned} u_0'' - [\kappa^2 + \tilde{U}_0(r)]u_0 - \sqrt{8}\tilde{U}_t(r)u_2 &= 0, \\ u_2'' - [\kappa^2 + \frac{6}{r^2} + \tilde{U}_0(r) - 2\tilde{U}_t(r)]u_2 - \sqrt{8}\tilde{U}_t(r)u_0 &= 0. \end{aligned} \quad (3.63)$$

Here the tilded potentials include the factor $2m/\hbar^2$. In the asymptotic region, these equations decouple. The radial dependences of diagonal and off-diagonal interaction terms (not including centrifugal term) in (3.63) are shown in Figure 3.2a for v_{18} . Figure 3.5 shows the typical picture of the *s*- and *d*-wave radial functions calculated with the Argonne v_{18} potential.

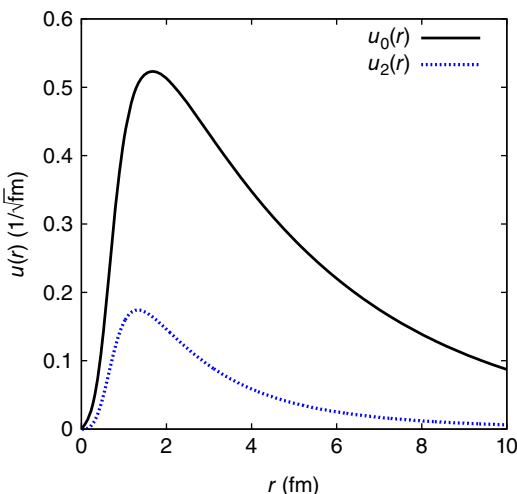


Figure 3.5 Deuteron wave functions $u_0(r)$ and $u_2(r)$ found using Argonne v_{18} potential.

3.6 Magnetic Dipole Moment

The experimental value for the magnetic dipole moment of the deuteron is 0.857 n.m. It is only 0.023 n.m. smaller than the algebraic sum of the magnetic moments (1.36) of the free neutron and proton. The experimental errors are certainly less than this difference.

As any tabular value of the multipole moment, the magnetic moment is conventionally defined by the expectation value of the corresponding operator in the substate with the maximum angular momentum projection, $|J = M = 1\rangle$. If there were no orbital contribution to the magnetic moment, the operator μ would be equal to the sum of the spin contributions. In this $\ell = 0$ situation, $J = M = 1$ means a complete alignment of the constituent spins. As a result, we would have the tabular value of the multipole moment being equal to the algebraic sum of the spin magnetic moments. The small difference can be attributed to the d -wave contribution (plus some relativistic corrections and effects of meson or/and quark currents, which are outside of the proton–neutron model and are rather weak here due to the large distance between the nucleons in the deuteron).

To calculate the deuteron magnetic moment, we separate global motion introducing the center-of-mass frame (2.1), (2.2) where $\mathbf{R} = 0$. In the new variables, we have

$$\mathbf{r}_p = \frac{\mathbf{r}}{2}, \quad \mathbf{r}_n = -\frac{\mathbf{r}}{2}, \quad \mathbf{p}_p = \frac{\mathbf{P}}{2} + \mathbf{p}, \quad \mathbf{p}_n = \frac{\mathbf{P}}{2} - \mathbf{p}. \quad (3.64)$$

Only the proton contributes to the orbital magnetism, and the proton orbital momentum is

$$[\mathbf{r}_p \times \mathbf{p}_p] = (1/2)[\mathbf{r} \times (\mathbf{P}/2 + \mathbf{p})]. \quad (3.65)$$

The term containing \mathbf{P} describes the convection current due to the motion of the deuteron as a whole. It is irrelevant for the problem of the intrinsic magnetic moment where only the relative orbital momentum $\hbar\ell = [\mathbf{r} \times \mathbf{p}]$ enters with the factor 1/2. Finally, the required magnetic moment operator is (in nuclear magnetons)

$$\mu = g_n^{(s)} \mathbf{s}_n + g_p^{(s)} \mathbf{s}_p + \frac{1}{2} \ell. \quad (3.66)$$

Let us rewrite Eq. (3.66) as a sum of spin-symmetric and spin-antisymmetric terms,

$$\boldsymbol{\mu} = \frac{g_n^{(s)} + g_p^{(s)}}{2} \mathbf{S} + \frac{g_p^{(s)} - g_n^{(s)}}{2} (\mathbf{s}_p - \mathbf{s}_n) + \frac{1}{2} \boldsymbol{\ell}. \quad (3.67)$$

The asymmetric term with the difference of spins changes the spin symmetry and has zero expectation value in a state of a certain spin symmetry. It is responsible for the *magnetic dipole* (M1) transitions from the triplet deuteron state to a singlet state in the continuum. Using the spin gyromagnetic ratios from (1.43), we come to the expectation value of the deuteron magnetic moment,

$$\langle \boldsymbol{\mu} \rangle = (\mu_n + \mu_p) \langle \mathbf{S} \rangle + \frac{1}{2} \langle \boldsymbol{\ell} \rangle, \quad (3.68)$$

or, introducing the total angular momentum $\mathbf{J} = \mathbf{S} + \boldsymbol{\ell}$,

$$\langle \boldsymbol{\mu} \rangle = (\mu_n + \mu_p) \langle \mathbf{J} \rangle - \left(\mu_n + \mu_p - \frac{1}{2} \right) \langle \boldsymbol{\ell} \rangle. \quad (3.69)$$

It is clear that the presence of the *d*-wave with $\ell \neq 0$ is the source of the correction to the trivial first term.

Now we can apply the standard vector model [QP, I, 22.8]. For $J = M = 1$, Eq. (3.69) gives

$$\mu = \mu_n + \mu_p - \left(\mu_n + \mu_p - \frac{1}{2} \right) \frac{\langle (\mathbf{J} \cdot \boldsymbol{\ell}) \rangle}{2}. \quad (3.70)$$

For $J = S$,

$$\langle (\mathbf{J} \cdot \boldsymbol{\ell}) \rangle = \frac{1}{2} \langle \ell(\ell+1) \rangle. \quad (3.71)$$

Here the mean value

$$\langle \ell(\ell+1) \rangle = 0 \cdot W_s + 6W_d \quad (3.72)$$

is entirely due to the admixture W_d of the *d*-wave. Finally,

$$\mu = \mu_n + \mu_p - \left(\mu_n + \mu_p - \frac{1}{2} \right) \frac{3}{2} W_d. \quad (3.73)$$

From Eq. (3.73), we can extract $W_d \approx 4\%$. Unfortunately, as we already mentioned, there are other effects that influence the magnetic moment and make the conclusion less certain.

3.7 Electric Quadrupole Moment

The quadrupole moment of the charge distribution is a symmetric tensor given (in Cartesian coordinates) by the sum over charged particles

$$Q_{jk} = \sum_a e_a (3r_{ja}r_{ka} - \mathbf{r}_a^2 \delta_{jk}). \quad (3.74)$$

The subtracted sum of diagonal terms with $j = k$ in (3.74) eliminates a scalar part (trace $Q_{xx} + Q_{yy} + Q_{zz}$ vanishes). The remaining five independent components form an irreducible tensor of the second rank. We have already used the quadrupole tensors constructed of the spin vector and radius vector in the tensor operator (Eqs. (3.2) and (3.10)).

In spherical components, the quadrupole operator is a superposition of the spherical harmonics $Y_{2\mu}$, and the connection is clear from the $Q_{zz} \equiv Q_{20}$ component,

$$\begin{aligned} Q_{zz} &= \sum_a e_a r_a^2 (3 \cos^2 \theta_a - 1) \\ &= 2 \sum_a e_a r_a^2 P_2(\cos \theta_a) = \sqrt{\frac{16\pi}{5}} \sum_a e_a r_a^2 Y_{20}(\mathbf{n}_a), \end{aligned} \quad (3.75)$$

where $\mathbf{n}_a = \mathbf{r}_a / r_a$.

As seen from (3.75), the quadrupole moment manifests the angular anisotropy, or *deformation*, of the charge distribution. The positive Q_{zz} shows the elongate (*prolate*) distribution along the z -axis while $Q_{zz} < 0$ reveals the *oblate* distribution concentrated near the equatorial plane xy . The expectation value of the quadrupole tensor vanishes if the distribution is isotropic. The observed value of the deuteron quadrupole moment is positive and equal to $Q/e = 0.286 \text{ fm}^2$. However, the mean square radius of the deuteron charge distribution is $\sqrt{\langle r^2 \rangle} = 1.96 \text{ fm}$. The quadrupole moment is small compared to the $\langle r^2 \rangle$ that shows a small nonsphericity. This agrees with the small weight of the d -wave estimated from the magnetic moment. Of course, a pure s -wave state would lead to the isotropic distribution with $Q = 0$.

Neglecting the contribution of the intrinsic charge distribution inside the nucleons and taking into account that the deuteron wave function depends on the relative coordinate \mathbf{r} , while $\mathbf{r}_p = \mathbf{r}/2$, the tabular quadrupole moment of the deuteron is

$$Q = \frac{e}{4} \langle 3z^2 - r^2 \rangle, \quad (3.76)$$

where the diagonal matrix element has to be taken over the deuteron state Ψ_M of Eq. (3.59) with $J = M = 1$.

Problem 3.4 Find the quadrupole moment (3.76) in terms of the s -wave and d -wave radial functions $u_0(r)$ and $u_2(r)$.

Solution

The calculation of (3.76) is similar to what has been done for the normalization (3.53,3.54). We have to calculate

$$Q = \frac{e}{16\pi} \left\langle \left(u_0 + \frac{1}{\sqrt{8}} u_2 S_{12} \right) \chi_{11} \middle| 3 \cos^2 \theta - 1 \middle| \left(u_0 + \frac{1}{\sqrt{8}} u_2 S_{12} \right) \chi_{11} \right\rangle. \quad (3.77)$$

The term $\propto u_0^2$ does not contribute because, as it should be for the isotropic distribution, the angular integral vanishes. We are left with the interference term $\propto u_0 u_2$ and with the pure d -wave contribution $\propto u_2^2$,

$$Q = \frac{e}{16\pi} \int d^3 r (3 \cos^2 \theta - 1) \left\{ \frac{2}{\sqrt{8}} u_0 u_2 \langle \chi_{11} | S_{12} | \chi_{11} \rangle + \frac{1}{8} u_2^2 \langle \chi_{11} | S_{12}^2 | \chi_{11} \rangle \right\}. \quad (3.78)$$

Using the same trick as in (3.57), the matrix element of S_{12}^2 reduces to the matrix element of S_{12} and a constant that does not contribute due to the angular integral. Therefore,

Eq. (3.78) transforms to

$$Q = \frac{e}{8\pi} \int d^3r (3\cos^2\theta - 1) \left(\frac{1}{\sqrt{8}} u_0 u_2 - \frac{1}{8} u_2^2 \right) \langle \chi_{11} | S_{12} | \chi_{11} \rangle. \quad (3.79)$$

To calculate the spin matrix element, use the form (3.55) of the tensor operator and note that

$$\langle \chi_{11} | (\mathbf{S} \cdot \mathbf{n})^2 | \chi_{11} \rangle = \langle \chi_{11} | S_z^2 \cos^2\theta + \frac{1}{2}(\mathbf{S}^2 - S_z^2) \sin^2\theta | \chi_{11} \rangle = \frac{1}{2}(1 + \cos^2\theta), \quad (3.80)$$

where θ is the polar angle of the vector \mathbf{n} . The spin matrix element in (3.79) is therefore

$$\langle \chi_{11} | S_{12} | \chi_{11} \rangle = 3\cos^2\theta - 1 = 2P_2(\cos\theta), \quad (3.81)$$

that could have been guessed directly from the definition (3.2). Using the normalization of the Legendre polynomials,

$$\int d\theta P_l(\cos\theta) P_l(\cos\theta) = \frac{4\pi}{2l+1} \delta_{ll}, \quad (3.82)$$

we come to the result for the quadrupole moment of the deuteron,

$$Q = \frac{\sqrt{2}}{10} e \int dr r^2 \left(u_0 u_2 - \frac{1}{\sqrt{8}} u_2^2 \right). \quad (3.83)$$

The contributions to (3.83) come mainly from the interior region where the d -wave is relatively weak. The u_2^2 term gives less than 10% of the total sum. The main interference term $\propto u_0 u_2$ leads to the positive Q , that is, prolate deformation of the deuteron. In terms of the asymptotic functions (3.62), this term is proportional to $A_0 A_2 = A_0^2 \eta$. Therefore, the quadrupole moment is a physical measure of the asymptotic d/s ratio.

The calculations of the deuteron properties with the most advanced phenomenological nucleon–nucleon forces are in almost perfect agreement with experiment (see Table 3.1). The slight, by a few percent, underprediction of values for the quadrupole and magnetic moments can be attributed to relativistic corrections and explicit meson exchange currents.

Table 3.1 Selected static deuteron properties from experiment and from phenomenological nucleon–nucleon forces Argonne v_{18} [2].

	Experiment	Argonne v_{18}
e (MeV)	2.224575(9)	2.224575
$\sqrt{\langle r^2 \rangle}$ (fm)	1.953(3)	1.967
Q (e fm 2)	0.2859(3)	0.270
μ/μ_N	0.857406(1)	0.847
η	0.0256(4)	0.0250
W_d (%)		5.76
A_0 ($\sqrt{\text{fm}}$)	0.8781(44)	0.8850

Problem 3.5 Consider, in addition to nuclear $n-p$ forces, the interaction of the neutron magnetic moment with the Coulomb field of the proton.

- a) Show that, for nonrelativistic relative $n-p$ motion, this interaction leads to the new Hamiltonian term that has the following structure:

$$H' = V(r)(\ell \cdot \mathbf{s}_n), \quad (3.84)$$

where ℓ and \mathbf{s}_n are the operators of the relative orbital momentum and of the neutron spin, respectively. Find the coordinate dependence of $V(r)$.

- b) Determine the constants of motion in the $n-p$ system in the presence of the additional interaction (3.84).
c) Construct the matrix of the interaction (3.84) in the basis of the unperturbed $n-p$ wave functions with given values of ℓ , total spin S , and total angular momentum J . Estimate the shift of the deuteron binding energy due to this interaction.
d) Write down the Schrödinger equations for the radial wave functions outside the range of nuclear forces. Are there any new effects expected in the $n-p$ scattering?

Solution

- a) The effect can be estimated similar to what is usually done for the relativistic spin-orbit interaction in atoms. Owing to the motion of the proton relative to the neutron, the Coulomb field $\mathcal{E} = e\mathbf{r}/r^3$ gives rise to the magnetic field

$$\mathcal{B} = \frac{1}{c}[\mathcal{E} \times \mathbf{v}] = \frac{1}{mc}[\mathcal{E} \times \mathbf{p}] = \frac{e}{mcr^3}[\mathbf{r} \times \mathbf{p}] = \frac{2e\hbar}{Mcr^3}\ell, \quad (3.85)$$

where \mathbf{v} , $\mathbf{p} = m\mathbf{v}$, and \mathbf{r} are relative velocity, momentum, and coordinate, respectively; $m = M/2$ is the reduced mass; M is the nucleon mass; and $\hbar\ell = [\mathbf{r} \times \mathbf{p}]$ is the quantized relative orbital momentum. The neutron magnetic moment is

$$\mu_n = g_n \mathbf{s}_n \quad (3.86)$$

where we use the neutron spin gyromagnetic ratio $g_n = -3.83 \mu_N$ in nuclear magnetons (see (1.43)). Now the interaction Hamiltonian of the neutron magnetic moment with the magnetic field (3.85) would be $-(\mathcal{B} \cdot \mu_n)$ if we did not take into account the Thomas factor 1/2 which comes from the Dirac equation or proper relativistic transformation taking into account the Coriolis force (anyway, we obtained the correct order of magnitude). With this factor,

$$H' = -\frac{e\hbar g_n}{Mcr^3}(\ell \cdot \mathbf{s}_n). \quad (3.87)$$

This interaction, contrary to nuclear forces, has a long range, it decreases as a power law, $V(r) \propto r^{-3}$.

- b) The interaction (3.87) explicitly distinguishes the neutron from the proton and therefore violates charge symmetry, charge independence, and isospin invariance. Being a scalar, it conserves the total angular momentum J and its projection M_J . The orbital momentum ℓ is preserved by the Hamiltonian (3.87); but the orbital waves ℓ and $\ell + 2$ for $J = \ell + 1$ and $S = 1$ are still mixed by the tensor forces. Parity $(-)^{\ell}$ is also conserved. However, the total spin \mathbf{S} ceases to be a constant of motion. The triplet,

$S = 1$, and singlet, $S = 0$, states are, respectively, spin symmetric and spin antisymmetric. The operator

$$\mathbf{s}_n = \frac{1}{2}\mathbf{S} + \frac{1}{2}(\mathbf{s}_n - \mathbf{s}_p) \quad (3.88)$$

contains the antisymmetric term that changes spin symmetry of the wave functions transforming a singlet into a triplet and back.

- c) Consider states with a given value of ℓ . They can be classified into singlets ($S = 0, J = l$) and triplets ($S = 1, J = \ell, \ell \pm 1$). Let $\Phi_{JM_J}^{\ell S}$ be the corresponding normalized spin-angular wave function. In the lowest order of perturbation theory, we neglect all admixtures of comparatively highly excited states with radial excitations due to $V(r)$. Since ℓ and J are conserved by the interaction (3.84), the triplet states with $J = \ell \pm 1$ do not acquire any admixture due to the Hamiltonian (3.87), whereas the singlet and triplet states $J = \ell$ can mix with each other. Thus, for the states with $J = \ell \pm 1$, the spin symmetry persists and the Hamiltonian (3.87) has only diagonal matrix elements determined by the first term of (3.88),

$$(\boldsymbol{\ell} \cdot \mathbf{s}_n) \Rightarrow \frac{\langle (\boldsymbol{\ell} \cdot \mathbf{S}) \rangle}{2} = \frac{J(J+1) - \ell(\ell+1) - S(S+1)}{4}. \quad (3.89)$$

This gives

$$(\boldsymbol{\ell} \cdot \mathbf{s}_n) \Phi_{\ell+1 M_J}^{\ell 1} = \frac{\ell}{2} \Phi_{\ell+1 M_J}^{\ell 1}, \quad (3.90)$$

$$(\boldsymbol{\ell} \cdot \mathbf{s}_n) \Phi_{\ell-1 M_J}^{\ell 1} = -\frac{\ell+1}{2} \Phi_{\ell-1 M_J}^{\ell 1}. \quad (3.91)$$

The deuteron wave function ($S = 1$) is a superposition ${}^3s_1 + {}^3d_1$, or in the new notations, $\Phi_{1M_J}^{01} + \Phi_{1M_J}^{21}$. Equation (3.90) determines the expectation value (equal to zero) for the deuteron s -wave while the d -wave component, $\Phi_{1M_J}^{21}$ with $J = 1 = l - 1$, according to (3.91), leads to the energy shift of the deuteron bound state

$$\delta E = -\frac{3}{2} \int_0^\infty dr u_2^2(r) V(r). \quad (3.92)$$

Estimating the integral in (3.92) as the weight W_d of the d -wave multiplied by the mean value of $V(r)$ and taking the mean square radius of the deuteron as $r \approx 2$ fm, we obtain $\delta E \approx 1$ keV, which is small but should be taken into account at current experimental precision.

The states $\Phi_{\ell M_J}^{\ell S}$ with $S = 0$ and $S = 1$ are mixed by the new interaction. Using the decomposition (3.88) and the eigenvalue (3.89) of the first item, we obtain

$$(\boldsymbol{\ell} \cdot \mathbf{s}_n) \Phi_{\ell M_J}^{\ell 0} = \frac{1}{2} \boldsymbol{\ell} \cdot (\mathbf{s}_n - \mathbf{s}_p) \Phi_{\ell M_J}^{\ell 0} \equiv a \Phi_{\ell M_J}^{\ell 1}, \quad (3.93)$$

$$(\boldsymbol{\ell} \cdot \mathbf{s}_n) \Phi_{\ell M_J}^{\ell 1} = -\frac{1}{2} \Phi_{\ell M_J}^{\ell 1} + \frac{1}{2} \boldsymbol{\ell} \cdot (\mathbf{s}_n - \mathbf{s}_p) \Phi_{\ell M_J}^{\ell 1} \equiv -\frac{1}{2} \Phi_{\ell M_J}^{\ell 1} + b \Phi_{\ell M_J}^{\ell 0}, \quad (3.94)$$

where

$$b = \langle \Phi_{\ell M_J}^{\ell 0} | \frac{1}{2} \boldsymbol{\ell} \cdot (\mathbf{s}_n - \mathbf{s}_p) | \Phi_{\ell M_J}^{\ell 1} \rangle = a^*. \quad (3.95)$$

We find the mixing matrix element a (it can be taken to be real) acting twice by the same operator,

$$\langle \Phi_{\ell M_j}^{\ell 0} | \left(\frac{1}{2} \boldsymbol{\ell} \cdot (\mathbf{s}_n - \mathbf{s}_p) \right)^2 | \Phi_{\ell M_j}^{\ell 0} \rangle = a^2. \quad (3.96)$$

Since the Clebsch–Gordan coefficients for the spin singlet reduce to 1, the wave function in (3.96) is a product of a spherical function and the spin singlet function,

$$\Phi_{\ell M_j}^{\ell 0} = Y_{\ell M_j} \chi_{00}. \quad (3.97)$$

Equation (3.96) can be written as

$$a^2 = \sum_{i k} \frac{1}{4} \langle Y_{\ell M_j} | \ell_i \ell_k | Y_{\ell M_j} \rangle \langle \chi_{00} | (s_{ni} - s_{pi})(s_{nk} - s_{pk}) | \chi_{00} \rangle. \quad (3.98)$$

The spin matrix element for the symmetric χ_{00} state is a symmetric tensor. Owing to the absence of any preferred direction,

$$\langle \chi_{00} | (s_{ni} - s_{pi})(s_{nk} - s_{pk}) | \chi_{00} \rangle = x \delta_{ik}, \quad (3.99)$$

where the new constant x can be found by taking the trace and expressing the scalar product $(\mathbf{s}_n \cdot \mathbf{s}_p)$ as in (3.89),

$$x = \frac{1}{3} \langle \chi_{00} | (\mathbf{s}_n - \mathbf{s}_p)^2 | \chi_{00} \rangle = 1. \quad (3.100)$$

Finally,

$$a^2 = \sum_{i k} \frac{1}{4} \langle Y_{\ell M_j} | \ell_i \ell_k | Y_{\ell M_j} \rangle \delta_{ik} = \frac{1}{4} \langle Y_{\ell M_j} | \ell^2 | Y_{\ell M_j} \rangle = \frac{\ell(\ell+1)}{4}, \quad (3.101)$$

$$a = \frac{1}{2} \sqrt{\ell(\ell+1)}. \quad (3.102)$$

The correct combinations of the wave functions, diagonal with respect to H' , are the eigenvectors of the 2×2 matrix with the off-diagonal radial elements $a \langle V(r) \rangle$ and diagonal elements equal to zero and $-\langle V(r) \rangle / 2$ for $S = 0$ and $S = 1$, respectively, where $\langle V(r) \rangle$ represents the matrix element of the potential evaluated for a corresponding radial function.

- d) In the asymptotic region, one can neglect all short-range nuclear forces. Then the problem can be solved without perturbation theory. The total wave function including the radial dependence is

$$\Psi_{JM_j}^{\ell S} = \Phi_{JM_j}^{\ell S} \mathcal{R}_{J\ell S}(r). \quad (3.103)$$

Outside the range of nuclear forces, only the centrifugal potential and the interaction (3.87) enter the equation. Considering energy of relative motion $E > 0$ in the continuum, introducing the dimensionless coordinate $\rho = kr$, where the wave number k is defined by $E = \hbar^2 k^2 / M$, and separating the spin-angular part Φ , we have four radial equations, two decoupled equations for $S = 1, J = \ell \pm 1$,

$$\left\{ \mathcal{K}_\ell(\rho) - \lambda \frac{\ell}{2\rho^3} + 1 \right\} \mathcal{R}_{\ell+1 \ell-1} = 0, \quad (3.104)$$

$$\left\{ \mathcal{K}_\ell(\rho) + \lambda \frac{\ell+1}{2\rho^3} + 1 \right\} \mathcal{R}_{\ell-1 \ell 1} = 0, \quad (3.105)$$

and two coupled equations for $S = 0$ or 1 and $J = \ell$,

$$(\mathcal{K}_\ell(\rho) + 1) \mathcal{R}_{\ell\ell 0} - \lambda \frac{\sqrt{\ell(\ell+1)}}{2\rho^3} \mathcal{R}_{\ell\ell 1} = 0, \quad (3.106)$$

$$\left\{ \mathcal{K}_\ell(\rho) + 1 + \lambda \frac{1}{2\rho^3} \right\} \mathcal{R}_{\ell\ell 1} - \lambda \frac{\sqrt{\ell(\ell+1)}}{2\rho^3} \mathcal{R}_{\ell\ell 0} = 0. \quad (3.107)$$

Here the radial operator for the partial wave with the orbital momentum l is used,

$$\mathcal{K}_\ell(\rho) = \frac{1}{\rho^2} \frac{d}{d\rho} \rho^2 \frac{d}{d\rho} - \frac{\ell(\ell+1)}{\rho^2}, \quad (3.108)$$

and the dimensionless constant of the new interaction is introduced,

$$\lambda = -\frac{eg_n}{\hbar c} k. \quad (3.109)$$

References

- 1 R.B. Wiringa, R.A. Smith, and T.L. Ainsworth, Phys. Rev. C **29**, 1207 (1984).
- 2 R.B. Wiringa, V.G.J. Stoks, and R. Schiavilla, Phys. Rev. C **51**, 38 (1995).
- 3 M.B. Lacombe *et al.*, Phys. Rev. C **21**, 861 (1980).
- 4 V.G.J. Stoks, R.A.M. Klomp, C.P.F. Terheggen, and J.J. de Swart, Phys. Rev. C **49**, 2950 (1994).
- 5 G.E. Brown and A.D. Jackson, *The Nucleon-Nucleon Interaction*, North Holland, Amsterdam, 1976 [Ch. 1–3].
- 6 T. Ericson and W. Weise, *Pions and Nuclei*, Clarendon Press, Oxford, 1988 [Ch. 2, 3].
- 7 M. Hjort-Jensen, T.T.S. Kuo, and E. Osnes, Phys. Rep. **261**, 125 (1995).
- 8 E. Epelbaum, H.-W. Hammer, and U.-G. Meissner, Rev. Mod. Phys. **81**, 1773 (2009).
- 9 R. Machleidt and D.R. Entem, Phys. Rep. **503**, 1 (2011).
- 10 G.E. Brown and A.M. Green, Nucl. Phys. **A137**, 1 (1969).
- 11 E. Epelbaum, A. Nogga, W. Gl'ockle, H. Kamada, U.-G. Meissner, and H. Witala, Phys. Rev. C **66**, 064001 (2002).

4

Two-Body Scattering

*We used to think that if we knew one, we knew two, because one and one are two.
We are finding that we must learn a great deal more about “and”.*

A. Eddington, *New Pathways in Science*.

4.1 Scattering Problem

The deuteron is the only bound two-nucleon state. Any additional information on $n-p$ forces, and all information on the interaction of identical nucleons, comes from scattering experiments. First let us briefly refresh our knowledge on quantum scattering [QP, II, Chapters 3, 7, 8].

Here, we limit our consideration by *elastic scattering* when the exit channel contains the same particles as the entrance channel and the relative kinetic energy E is preserved. As earlier, we consider the two-body problem in the center-of-mass frame, where \mathbf{r} is the relative distance between the particles. Assuming that at sufficiently large distances r one can neglect the interaction forces and consider free motion, we can write the *asymptotic* form of the wave function of relative motion as a combination of the incident plane wave and outgoing spherical wave:

$$\psi(\mathbf{r}) \approx e^{i(\mathbf{k} \cdot \mathbf{r})} + f(\mathbf{k}', \mathbf{k}) \frac{e^{ikr}}{r}, \quad (4.1)$$

where $k = k' = \sqrt{2mE/\hbar^2}$ is the wave vector, m is the reduced mass, and $f(\mathbf{k}', \mathbf{k})$ is the *scattering amplitude* that has the dimension of length. This expression does not take into account the spin part of the wave function, assuming that it does not change in the process. Later we extend the theory for spin-dependent scattering. The *differential cross section* of scattering is given by

$$\frac{d\sigma}{d\Omega} = |f(\mathbf{k}', \mathbf{k})|^2. \quad (4.2)$$

The scattering angle θ is that between \mathbf{k} and \mathbf{k}' .

In a *central field*, the orbital momentum ℓ of relative motion is conserved and we consider the scattering of individual *partial waves* with a certain value of ℓ . The expansion

of the plane wave over spherical functions can be written as

$$e^{i(\mathbf{k} \cdot \mathbf{r})} = e^{ikr \cos \theta} = \sum_{\ell=0}^{\infty} (2\ell + 1) i^\ell j_\ell(kr) P_\ell(\cos \theta), \quad (4.3)$$

where we took the initial propagation vector \mathbf{k} along the polar z -axis, $j_\ell(kr)$ are *spherical Bessel functions*, and P_ℓ are Legendre polynomials. At large distances, $kr \gg \ell$, the asymptotics of the radial functions are given by

$$j_\ell(x) \approx \frac{\sin(x - \ell\pi/2)}{x}. \quad (4.4)$$

The scattering amplitude $f(\theta)$ can also be expanded over partial waves,

$$f(\theta) = \sum_{\ell} (2\ell + 1) P_\ell(\cos \theta) f_\ell. \quad (4.5)$$

Now we collect the incoming and outgoing waves in Eq. (4.1) as a sum of partial waves to get the asymptotics

$$\psi(\mathbf{r}) \approx \frac{i}{2kr} \sum_{\ell} (2\ell + 1) P_\ell(\cos \theta) [(-)^{\ell} e^{-ikr} - (1 + 2ikf_\ell)e^{ikr}]. \quad (4.6)$$

The incoming spherical wave $\propto e^{-ikr}$ is not changed by scattering. In contrast, the outgoing wave $\propto e^{ikr}$ is distorted. Its amplitude is not equal to unity; instead it acquired the factor

$$S_\ell = 1 + 2ikf_\ell. \quad (4.7)$$

The numbers (4.7) are the elements of the *S-matrix* transforming the incident wave into the scattered wave. In elastic scattering off a central potential, each partial wave is scattered independently, and the *S-matrix* is diagonal in the ℓ -representation; for non-central forces, we would have the matrix $S_{\ell\ell'}$. The elements of the *S-matrix* are complex numbers

$$S_\ell = e^{2i\delta_\ell}, \quad (4.8)$$

which can depend only on the energy of relative motion. With no absorption, the flux conservation in each partial wave requires

$$|S_\ell|^2 = 1, \quad (4.9)$$

so that the *scattering phase shifts* δ_ℓ are real. The scattering process in this case results simply in the extra phase shift $2\delta_\ell$ of the partial wave due to the interaction (difference between the actual phase and the unperturbed phase of free motion).

The differential elastic cross section (4.2) is the product of two expansions, (4.5) and the conjugate function f^* . It is complicated because all partial waves interfere at the detector located at a certain angle. The interference disappears in the *total* cross section due to the orthogonality of the partial waves in the angular integrals. Expressing the scattering amplitude (4.5) as

$$f(\theta) = \frac{1}{2ik} \sum_{\ell} (2\ell + 1) P_\ell(\cos \theta) (S_\ell - 1), \quad (4.10)$$

we obtain the total elastic cross section as the sum of the *partial cross sections*

$$\begin{aligned}\sigma_{\text{el}} &= \sum_{\ell\ell'} (2\ell + 1)(2\ell' + 1) f_\ell f_{\ell'}^* \int d\theta P_\ell(\cos \theta) P_{\ell'}(\cos \theta) \\ &= 4\pi \sum_\ell (2\ell + 1) |f_\ell|^2 = \frac{\pi}{k^2} \sum_\ell (2\ell + 1) |S_\ell - 1|^2.\end{aligned}\quad (4.11)$$

4.2 Phase Shifts

The whole description of elastic scattering in a central field is reduced now to the determination of the phase shifts δ_ℓ , Eq. (4.8).

Writing $S_\ell - 1$ as $2i \exp(i\delta_\ell) \sin \delta_\ell$, we express the scattering amplitude (4.10) as

$$f(\theta) = \frac{1}{k} \sum_\ell (2\ell + 1) P_\ell(\cos \theta) e^{i\delta_\ell} \sin \delta_\ell. \quad (4.12)$$

The asymptotics (4.6) becomes now

$$\psi(\mathbf{r}) \approx \frac{1}{kr} \sum_\ell i^\ell (2\ell + 1) P_\ell(\cos \theta) e^{i\delta_\ell} \sin \left(kr - \frac{\ell\pi}{2} + \delta_\ell \right). \quad (4.13)$$

In terms of the phase shifts, the elastic cross section is expressed as

$$\sigma_{\text{el}} = \frac{4\pi}{k^2} \sum_\ell (2\ell + 1) \sin^2 \delta_\ell. \quad (4.14)$$

The phase shift $\delta_\ell = n\pi$ at some energy corresponds to the absence of scattering in a given partial wave at this energy, $S_\ell = 1$. The maximum scattering (*resonance*) occurs at $\delta_\ell = \pi/2$. At the resonance, the cross section is defined not by the geometrical parameters of the system but by the wavelength $\lambda = 2\pi/k$ of the wave,

$$\sigma_\ell^{\max} = \frac{4\pi}{k^2} (2\ell + 1). \quad (4.15)$$

In order to determine the phase shifts theoretically for a given potential, one has to solve the radial Schrödinger equation, find the radial function $u_\ell(r)/r$, where $u_\ell(r)$ is regular at the origin, and determine the phase shift δ_ℓ from the asymptotics $u_\ell(r) \sim \sin(kr - \ell\pi/2 + \delta_\ell)$. Then the full wave function $\psi(\mathbf{r})$ can be found as the superposition of the partial waves with the coefficients $i^\ell \exp(i\delta_\ell)$. In practice, it might be convenient to find the mutually complex conjugate solutions $u_\ell^{(\pm)}$ with the asymptotic behavior $\sim \exp(\pm ikr)$. These functions form a complete set of functions in the continuum. Their behavior at the origin is defined by the asymptotics. Now one can look for their superposition, compare with (4.6),

$$u_\ell(r) = A_\ell [u_\ell^{(-)}(r) - (-)^\ell S_\ell u_\ell^{(+)}(r)] \quad (4.16)$$

that would be regular at the origin. This requirement determines S_ℓ .

The partial wave expansion is especially convenient at *low energy* when phases decrease with ℓ and practically the series can be truncated. The region of low energy is determined here by the ratio of the range R of the potential to the wavelength $\lambda = 2\pi/k$ of relative motion. When kR is small, the phase difference between the waves moving

in different directions is small, and the axis of the incident beam is not singled out. This means that the scattering is nearly isotropic so that the contribution of the s -wave, and, maybe, of few other lowest partial waves should be the most important.

If the potential $U(x)$ in the Schrödinger equation has no singularity at the origin or it is less singular than the centrifugal energy $\sim \ell(\ell + 1)/x^2$, where we use the dimensionless variable $x = kr$, then it is possible to find the phase shifts *modulo* 2π by the equation

$$\sin \delta_\ell = - \int_0^\infty dx \frac{U(x)}{E} u_\ell(x) v_\ell(x), \quad (4.17)$$

through the solutions $u_\ell(x)$ and the free motion solution $v_\ell(x) = x j_\ell(x)$ for the same energy. For sufficiently large ℓ when the phase shift is small, one can substitute $u_\ell(x)$ in the integrand by the free function v_ℓ . This would be obvious in the classical case when large ℓ correspond to large impact parameters $b_\ell \simeq \ell/k > R$, which define the trajectory lying outside of the interaction region. But the same conclusion is valid in the quantum case. The effective potential $U_\ell = U + \hbar^2 \ell(\ell + 1)/2mr^2$ strongly suppresses both u_ℓ and v_ℓ under the barrier where they are proportional to $r^{\ell+1}$. The turning points for both cases (free motion and motion in the potential) almost coincide if they are further from the origin than R . In this case, the influence of the potential U is weak everywhere, and we can expect smallness of the phase shifts (Figure 4.1).

Turning points $E = U_\ell(r)$ are located at $r_\ell > R$ if

$$U(r_\ell) \ll \frac{\hbar^2 \ell(\ell + 1)}{2mr_\ell^2} \approx E < \frac{\hbar^2 \ell(\ell + 1)}{2mR^2}. \quad (4.18)$$

This is fulfilled at

$$\ell(\ell + 1) > \frac{2mE}{\hbar^2} R^2 = (kR)^2 \quad (4.19)$$

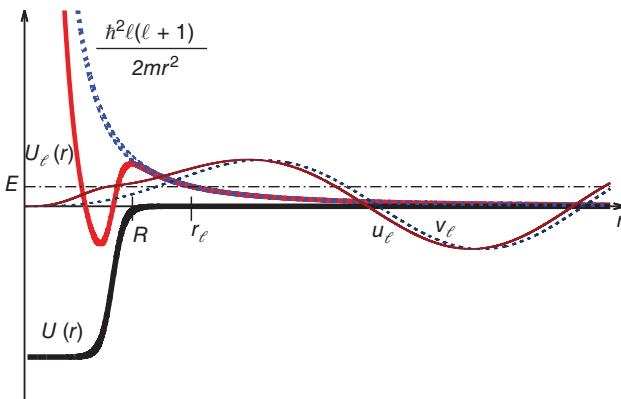


Figure 4.1 Illustration showing a nonsingular short-range potential $U(r)$ of radius R and the effective potential $U_\ell(r)$ that coincides with the centrifugal potential in the vicinity of the origin. The turning point for scattering at low energy E is r_ℓ . The free solution v_ℓ (for centrifugal potential in dashed blue) and the full solution u_ℓ (for full potential in red) are shown.

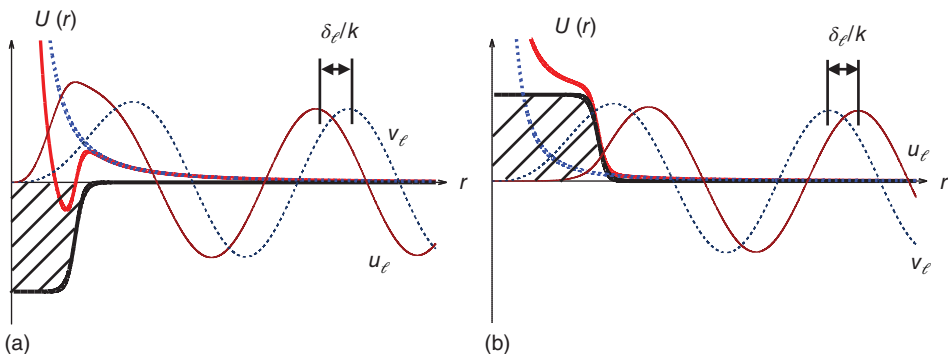


Figure 4.2 The radial function for the (a) attractive and (b) repulsive potentials with no bound states in the attraction case.

which is in fact the above-mentioned classical statement concerning the impact parameter, $\sim \ell/k > R$. If this is the case, the phase shifts δ_ℓ are small, $\sin \delta_\ell \approx \delta_\ell$, and we obtain from (4.17)

$$\delta_\ell \approx - \int_0^\infty dx \frac{U(x)}{E} v_\ell^2(x). \quad (4.20)$$

This expression has a simple meaning: the presence of the potential superimposed onto the unperturbed wave function v_ℓ changes its oscillation in time by the mean value of the potential measured in the natural time units $\sim 1/E$.

At sufficiently low energies, $kR \ll 1$, this result is valid for all $\ell \neq 0$. A practical conclusion is that, in the low-energy scattering, only the s -wave may have a significant phase shift. As energy increases, the higher partial waves enter the game. The integrand in (4.20) is restricted by the potential range R . In the low-energy limit, the behavior here is determined by the centrifugal term and therefore by the regular spherical Bessel function $v_\ell(x) = x j_\ell(x) \propto x^{\ell+1}$. Then Eq. (4.20) gives for the low-energy phase shifts ($\ell \neq 0$),

$$\delta_\ell \propto k^{2\ell+1} \propto E^{\ell+1/2}. \quad (4.21)$$

Indeed, at low energy (4.19), we limit ourselves to the lowest members of the partial wave expansion. More accurate estimates are necessary for long-range potentials, which fall off as a power law, $U \propto 1/r^\alpha$, including the Coulomb case.

Note that for the attractive potential, $U < 0$, the phase shifts are positive while they are negative for the repulsive potential, $U > 0$. This is easy to understand from the comparison of the actual solution with the free motion case: a particle spends more time in the attractive region (Figure 4.2).

4.3 Scattering Length

Now we apply the general theory to the nucleon–nucleon scattering. Historically, the initial information about nuclear forces was learned from $n-p$ scattering at low energies. We know that the term “low energy” in the scattering problem usually means that the wavelength $1/k = \hbar/mv$ of relative motion (in our case $m = M/2$ is the reduced mass for two nucleons) is large compared to the force range R ,

$$kR < 1. \quad (4.22)$$

In $n-p$ scattering, this region covers energies E up to ~ 5 MeV in the center-of-mass frame (~ 10 MeV in the proton rest frame). In the low-energy region, only the s -wave scattering, $\ell = 0$, can have a significant phase shift δ_0 and contribute to the scattering cross section. The nucleon–nucleon interactions for odd parity states are much weaker (Section 3.2); therefore, the p -wave scattering is suppressed, so actually the $n-p$ cross section is nearly isotropic up to $E \approx 10-15$ MeV.

At ultralow energy that can be studied with the neutrons from a nuclear reactor, the results may depend on material structure of the target. For a proton chemically bound in the target, the binding affects the scattering picture. The chemical binding energy is of the order of several electronvolts, so we should first assume that the kinetic energy of incident neutrons is substantially higher, allowing the chemical binding energy to be ignored. The problem of chemical environment is important for the experiment with molecular hydrogen discussed in the next section.

Let us consider the s -wave scattering by a short-range potential in more detail. The results turn out to be universal in a sense that they can be described by a small number of physical parameters that are not sensitive to the details of shape of the potential.

The elastic cross section for the s -wave (since below we discuss the s -scattering only, the subscript $\ell = 0$ will be omitted) can be expressed in terms of the scattering amplitude,

$$f = e^{i\delta} \frac{\sin \delta}{k}, \quad \sigma = 4\pi|f|^2 = \frac{4\pi}{k^2} \sin^2 \delta. \quad (4.23)$$

Our partial wave analysis was derived for the central potential $U(r)$. In reality, even for momentum-independent interactions, we have, Section 3.1, six independent potential structures. At this stage, we will not consider a small mixture of orbital momenta due to the tensor forces and fix $\ell = 0$. In the space-even states, there are only two different potentials, for the spin singlet, $S = 0$, and therefore $T = 1$, and for the spin triplet, $S = 1$ and $T = 0$. The second case, see Figure 3.1, has a deeper well that supports the deuteron bound state (although tensor forces are still necessary to bind the deuteron, Figure 3.2), whereas the spin-singlet case has no bound states. We have to consider both cases, and the corresponding phase shifts, δ_s and δ_t , are different.

For any specific shape of the short-range potential, we can find the radius R such that at $r > R$ the potential is vanishingly small and can be neglected. Outside the potential, the solution $\psi(r) = u(r)/r$ of the scattering problem has a universal form,

$$u(r) = \frac{e^{i\delta}}{k} \sin(kr + \delta), \quad r > R, \quad (4.24)$$

where the phase shift δ depends on energy or on k . The condition for matching the external function (4.24) with the potential region can be formulated as in the bound state problem with the use of the logarithmic derivative λ of the inner wave function,

$$\left(\frac{u'}{u} \right)_{r=R-0} \equiv \lambda = k \cot(kR + \delta). \quad (4.25)$$

Thus, the phase shift δ is determined by the single intrinsic quantity λ . One particular case is seen immediately: for a very strong repulsive potential, the wave function is close to zero at the boundary $r = R$, while its derivative is finite so that $\lambda \rightarrow \infty$ and the phase shift is

$$\delta = -kR, \quad (4.26)$$

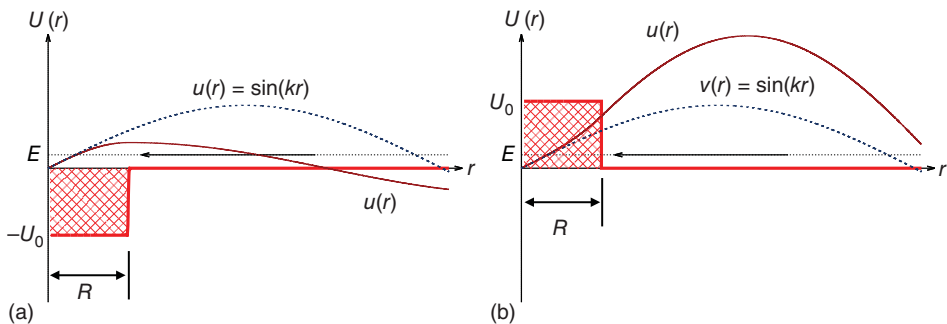


Figure 4.3 The square well potential $U(r)$ and the corresponding radial eigenfunction: (a) the attractive potential for Problem 4.1 and (b) the repulsive square well potential for Problem 4.2.

the wave does not penetrate inside and correspondingly acquires a smaller phase. Two following simple examples illustrate physics of the s -wave scattering (Figure 4.3).

Problem 4.1 Calculate the scattering cross section of a particle by a square attractive potential (depth U_0 , radius R) at low energies.

Solution

The Schrödinger equation at $\ell = 0$ is (for the function $u \propto r\psi$)

$$u'' + k^2 u = 0, \quad k^2 = \frac{2mE}{\hbar^2}, \quad r > R; \quad (4.27)$$

$$u'' + k'^2 u = 0, \quad k'^2 = \frac{2m(E + U_0)}{\hbar^2}, \quad r < R. \quad (4.28)$$

Given that the solution must vanish at the origin and that the remote asymptotic is of the form (4.24),

$$u = A \sin k'r, \quad r < R; \quad u = \sin(kr + \delta), \quad r > R. \quad (4.29)$$

The unknown coefficient A and the phase shift δ are to be found from the matching at $r = R$. The logarithmic derivative gives

$$\delta = \tan^{-1} \left(\frac{k}{k'} \tan(k'R) \right) - kR. \quad (4.30)$$

The partial cross section (4.14) is

$$\sigma_0 = \frac{4\pi}{k^2} \sin^2 \delta. \quad (4.31)$$

At very low energy

$$k \rightarrow 0, \quad k'^2 \rightarrow k_0^2 = \frac{2mU_0}{\hbar^2}. \quad (4.32)$$

If $k_0 R$ is not very close to $\pi/2$, at low energy the phase shift goes to zero linearly in k ,

$$\delta \approx kR \left(\frac{\tan(k_0 R)}{k_0 R} - 1 \right). \quad (4.33)$$

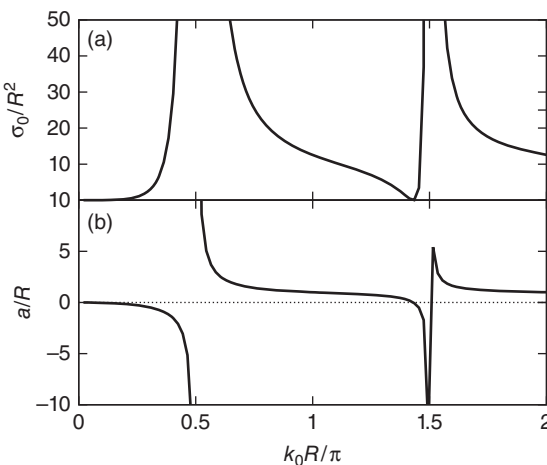


Figure 4.4 (a) The s-wave cross section (in units of R^2 at zero energy); (b) the scattering length (in units of R) for a square well potential of radius R are shown as a function of depth in units k_0R/π .

The scattering amplitude (4.12) and the cross section (4.31) are finite. They are expressed via the *scattering length*

$$\alpha = -\lim_{k \rightarrow 0} f = -\lim_{k \rightarrow 0} \frac{\delta}{k} = -R \left(\frac{\tan(k_0 R)}{k_0 R} - 1 \right), \quad (4.34)$$

$$\lim_{k \rightarrow 0} \sigma_0 = 4\pi \alpha^2. \quad (4.35)$$

In the shallow well, $k_0 R \ll 1$, $\tan(k_0 R) \approx k_0 R [1 + (k_0 R)^2/3]$,

$$\alpha = -R \frac{(k_0 R)^2}{3}, \quad \sigma_0 = 4\pi R^2 \frac{(k_0 R)^4}{9} = \frac{16\pi}{9} \frac{m^2 U_0^2 R^6}{\hbar^4}, \quad (4.36)$$

that is, the cross section is much less than the geometrical one, $4\pi R^2$. This result can be derived using the first Born approximation [QP, II, 7.5]. In this limit, the scattering length is actually defined by the *volume* of the well.

Let us deepen the well keeping k small but finite (see Figure 4.4). At $k_0 R = \pi/2$, we get to the *resonance*. The quantity

$$\frac{1}{\gamma} \equiv \frac{\tan(k' R)}{k'} \quad (4.37)$$

is small as compared to R . We can neglect term $-kR$ in (4.30) and get the cross section near the resonance:

$$\delta = \tan^{-1} \frac{k}{\gamma}, \quad \sigma_0 = \frac{4\pi}{\gamma^2 + k^2}. \quad (4.38)$$

For the resonance well and $k \rightarrow 0$, the cross section grows. The resonance condition shows the appearance of the bound state in the well. At small energy, the inner wave function within the deep well is only slightly energy dependent, being very similar for the newborn bound state and for the positive but small energy. Going further to a deeper well, we see the decreasing cross section; the resonance description (4.38) is not valid any longer but we can return to the nonresonant formulae, which show the zero of the cross section (4.34) at $\tan(k_0 R) = k_0 R$. At each appearance of the new bound state, there is a new resonance so that the cross section rapidly oscillates between very small and

very large values as a function of the depth. The Wigner formula for the resonance cross section (4.38) is valid for the near-critical well depth when a small change leads to the appearance or disappearance of the discrete level.

Problem 4.2 Calculate the scattering cross section of a particle by a repulsive potential barrier (height U_0 , radius R) at low energy.

Solution

In the inner region under the barrier, $E < U_0$, we have

$$u = A \sinh(k'R), \quad k'^2 = \frac{2m(U_0 - E)}{\hbar^2}. \quad (4.39)$$

The scattering phase is given by

$$\delta = \tan^{-1} \left[\frac{k}{k'} \tanh(k'R) - kR \right]. \quad (4.40)$$

Since $\tanh x$ changes from -1 to 1 , there are no resonances, and in the low-energy limit

$$\alpha = -R \left(\frac{\tanh(k_0 R)}{k_0 R} - 1 \right) > 0, \quad k_0^2 = \frac{2mU_0}{\hbar^2}, \quad (4.41)$$

note the positive sign of the scattering length;

$$\sigma_0 = 4\pi R^2 \left(\frac{\tanh(k_0 R)}{k_0 R} - 1 \right)^2. \quad (4.42)$$

For the infinite wall, as follows from (4.26),

$$U_0 \rightarrow \infty, \quad \alpha \rightarrow R, \quad \delta \rightarrow -kR; \quad (4.43)$$

the cross section is equal to the surface of the sphere,

$$\sigma_0 \rightarrow 4\pi R^2. \quad (4.44)$$

The factor of 4 shows a typical wave effect: the wave of the large length interacts with the whole surface while a classical particle feels only the area πR^2 of the impenetrable obstacle. The resonance behavior reappears for overbarrier energies $E > U_0$.

Problem 4.3 For the scattering of a nucleon from a nucleus at low energy, a better model can be that of a surface interaction with the possibility of penetration inside. The simplest example is given by the potential of a spherical shell,

$$U(r) = g\delta(r - R). \quad (4.45)$$

Calculate the cross section for low-energy particles.

Solution

The regular intrinsic ($0 \leq r < R$) wave function for the s -wave is

$$u_{<}(r) = A \sin(kr), \quad k = \sqrt{\frac{2mE}{\hbar^2}}. \quad (4.46)$$

Outside the well ($r > R$), the function also describes free motion but it acquires the phase,

$$u_>(r) = B \sin(kr + \delta). \quad (4.47)$$

The matching of the solutions at the singular point $r = R$ of the potential gives

$$u'_> - u'_< = \frac{2mg}{\hbar^2} \quad u(R) = \frac{2mgA}{\hbar^2} \sin(kR), \quad (4.48)$$

or, with the explicit form (4.47),

$$\cot(kR + \delta) - \cot(kR) = \frac{2mg}{k\hbar^2} \equiv \frac{w}{k}. \quad (4.49)$$

Equation (4.49) determines the phase shift δ . The cross section of s -scattering,

$$\sigma(E) = \frac{4\pi}{k^2} \sin^2 \delta, \quad (4.50)$$

has zeros at $kR = n\pi$ and maxima in between (Figure 4.5).

These exact solutions show that the s -wave phase shift at small k is proportional to k (see Eq. (4.21)). The coefficient of proportionality, with the negative sign, is the *scattering length*,

$$\lim_{k \rightarrow 0} \frac{\delta(k)}{k} = -a. \quad (4.51)$$

For Problem 4.3, $a/R = Rw/(1 + Rw)$, and for the strong repulsion, $Rw \gg 1$, the scattering length approaches R , as in Eq. (4.43). According to the connection (4.23) between the phase shift and the scattering amplitude f , the scattering length is the limiting value of f at low energies,

$$\lim_{k \rightarrow 0} f = \lim_{k \rightarrow 0} \frac{e^{i\delta} \sin \delta}{k} = -a. \quad (4.52)$$

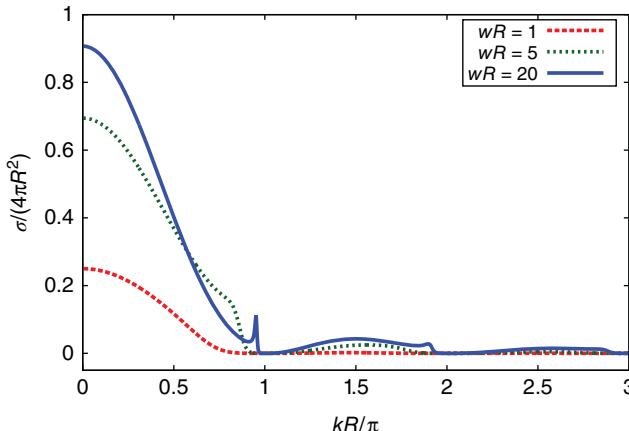


Figure 4.5 The cross section as a function of momentum for Problem 4.3.

The magnitude of the cross section (4.23) in this limit is

$$\lim_{k \rightarrow 0} \sigma = 4\pi a^2. \quad (4.53)$$

For the impenetrable wall, the scattering length coincides with the radius R of the wall. However, in general, the value of the scattering length can considerably differ from the range of the potential R . The scattering length can be directly determined from the behavior of the outer wave function (4.24) that, in the limit $k \rightarrow 0$, can be written near the boundary as a linear function

$$u(r) \approx r - a. \quad (4.54)$$

Therefore, the scattering length is given by the value of the radial coordinate at the point where the extrapolation of the wave function (4.54) goes to zero. The various possible cases are illustrated in Figure 4.6.

For the shallow well with no bound states (Figure 4.6a) the inner wave function is increasing at the boundary, $\lambda > 0$, and the extrapolation (4.54) leads to $a < 0$. Making the well deeper, we increase the intrinsic wave vector and shift the intersection point to the left. Eventually, the absolute value of the scattering length exceeds the force range R . At the critical depth corresponding to the appearance of the bound state, the scattering length goes to $-\infty$ (Figure 4.6b; see also Figure 4.4). If the well supports a bound state, the limiting behavior of the phase shift at zero energy has to be defined as $\lim_{k \rightarrow 0} \delta = \pi - ka$. As soon as the well becomes even more deep, the bound state goes down in energy. Then the inner wave function has a negative derivative at the boundary, $\lambda < 0$, and the scattering length returns to the real axis from $+\infty$ (Figure 4.6c).

If the bound state has very low binding energy, it might be difficult to establish its presence empirically. The sign of the scattering length clarifies the situation. However, the scattering cross section alone is not sufficient. As seen from (4.53), the cross section gives no information about the sign of a . Moreover, the experiment with unpolarized neutrons and protons can measure only the *average* value for the singlet and triplet cross sections: for a given nucleon – nucleon collision, the initial state has probability 1/4 and 3/4 to be singlet or triplet, respectively. The observable cross section is

$$\bar{\sigma} = \frac{1}{4}\sigma_s + \frac{3}{4}\sigma_t. \quad (4.55)$$

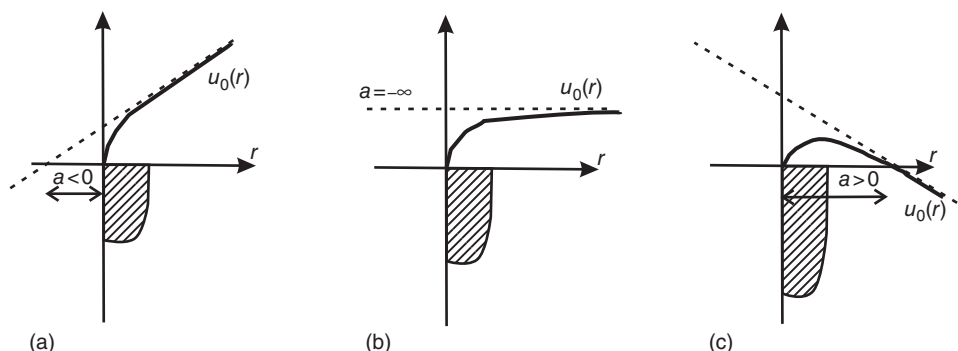


Figure 4.6 The radial wave functions for (a) the negative, (b) almost infinite, and (c) positive scattering length.

4.4 Sign of the Scattering Length

Historically, the important experiment for the determination of the signs of the singlet, a_s , and triplet, a_t , $p-n$ scattering lengths was performed, following the suggestion by Schwinger and Teller, as a measurement [1] of neutron scattering in *para*- and *ortho*-hydrogen. This example is instructive and we discuss it next.

The molecular hydrogen H_2 can exist in two forms, *para*- and *ortho*-, which differ in the total nuclear spin $S = \mathbf{s}_1 + \mathbf{s}_2$ of two protons forming the molecule. The nuclear spin is $S = 0$ and $S = 1$ for *para*- and *ortho*-hydrogen, respectively. Since the $n-p$ forces depend on the total spin of the $n-p$ system, the neutron scattering by the molecule H_2 is different for those cases.

We can note parenthetically that the hydrogen molecules provide us with a bright example of the manifestation of Fermi statistics. The molecular wave function has to be antisymmetric under proton interchange. The electronic and vibrational wave functions of the ground state are symmetric in proton coordinates. The nuclear spin function is antisymmetric for *para*-hydrogen and symmetric for *ortho*-hydrogen, as in (2.6). The proper total antisymmetry has to be ensured by the complementary symmetry of the angular wave function of the molecular orientation, symmetric for *para*-hydrogen and antisymmetric for *ortho*-hydrogen. Diatomic molecules have rotational spectra corresponding to the rotation around an axis perpendicular to the molecular axis. The orientational wave function is simply $Y_{LM}(\mathbf{n})$ with the unit vector \mathbf{n} describing the direction of the molecular axis in space. This function acquires the factor $(-)^L$ under proton interchange (for a two-particle system, this is equivalent to spatial inversion). Therefore, only the states with even $L = 0, 2, \dots$ are allowed for the *para*-hydrogen molecule, and only odd $L = 1, 3, \dots$ are allowed for the *ortho*-hydrogen molecule. This means that the rotational spectrum of *ortho*-hydrogen starts with $L = 1$ that brings additional rotational energy compared to the ground state of *para*-hydrogen ($L = 0$). The rotational energy difference between the $L = 0$ and $L = 1$ states is 0.02 eV. At room temperature, which is higher than the rotational energy intervals, the hydrogen gas is a statistical mixture of the two modifications with the ratio *ortho*:*para* = 3 : 1 equal to the ratio of a number of magnetic substates. At low temperatures, the molecules relax to the *para*-hydrogen phase. To keep a considerable fraction of the *ortho*-hydrogen molecules at low temperatures, the cooling has to be faster than the relaxation time.

Let us consider for simplicity the neutron scattering by the hydrogen molecule at a very low energy when it is impossible to excite even the lowest rotational molecular levels. Here we see an example when the chemical structure of the target mentioned in the previous section has to be accounted for in a nuclear experiment. At such energies, only the *elastic* scattering is possible. We should go to this limit because due to the allowed rotational levels, the *inelastic* neutron scattering is different for *ortho*- and *para*-hydrogen even without spin-dependent nuclear forces.

To get a result valid for any spin state, let us write the effective scattering length for the $n-p$ interaction as

$$a = \frac{1}{2}(1 - \mathcal{P}^\sigma)a_s + \frac{1}{2}(1 + \mathcal{P}^\sigma)a_t. \quad (4.56)$$

Here a_s and a_t are the singlet and triplet $n-p$ scattering lengths, respectively, and \mathcal{P}^σ is the spin-exchange operator. The combinations $(1/2)(1 \mp \mathcal{P}^\sigma)$ in (4.56) project out of

any spin state its singlet or triplet part. Using the explicit expression (2.5) of the spin exchange operator, we obtain the effective $n-p$ scattering length as an operator acting on the spin variables,

$$\alpha = \frac{1}{4}[3\alpha_t + \alpha_s + (\alpha_t - \alpha_s)(\boldsymbol{\sigma}_n \cdot \boldsymbol{\sigma}_p)]. \quad (4.57)$$

Now we can apply Eq. (4.57) to the scattering by molecular hydrogen.

The mean distance between the protons in the hydrogen molecule is 0.75 Å. Under the simplifying assumption that the neutron wavelength exceeds this distance, which means that both protons see the neutron wave function nearly at the same phase, we obtain the *coherent* interaction with the protons. Then we have to add the *amplitudes* in Eq. (4.57) for both protons and introduce the effective scattering length,

$$A = \alpha(1) + \alpha(2) = \frac{1}{2}[3\alpha_t + \alpha_s + (\alpha_t - \alpha_s)(\boldsymbol{\sigma}_n \cdot \mathbf{S})], \quad (4.58)$$

where \mathbf{S} is the total nuclear spin of the molecule. Taking into account the phase difference due to the displacement between the protons in the molecule, we also obtain terms that are antisymmetric in proton spins. These terms are responsible for ortho–para and para–ortho transitions. The elastic scattering, as well as para–para and ortho–ortho excitations, is governed by the symmetric terms.

The elastic scattering is described by the matrix element $\langle m'M'|A|mM\rangle$, where m, m' and M, M' are initial and final spin projections for the neutron and the molecule, respectively. If the neutron and initial molecular hydrogen gas are unpolarized, the observed elastic cross section with no final polarization measured is proportional to this matrix element squared, *averaged over initial polarizations and summed over final polarizations*,

$$\sigma_{\text{el}} \propto \frac{1}{2(2S+1)} \sum_{mMm'M'} |\langle m'M'|A|mM\rangle|^2. \quad (4.59)$$

A standard way for calculating such sums is the following. The sum over initial and final spin states is reduced to a trace in the spin space (we will use this in other situations as well):

$$\sum_{fi} |A_{fi}|^2 = \sum_i \left(\sum_f A_{fi}^* A_{fi} \right) = \sum_i (A^\dagger A)_{ii} = \text{Tr}(A^\dagger A). \quad (4.60)$$

Using the algebra of angular momentum operators, the quadratic term in spin matrices in (4.60) gives

$$(\boldsymbol{\sigma}_n \cdot \mathbf{S})^2 = S_j S_k (\delta_{jk} + i\epsilon_{jkl}(\boldsymbol{\sigma}_n)_l) = \mathbf{S}^2 - (\boldsymbol{\sigma}_n \cdot \mathbf{S}). \quad (4.61)$$

The trace of any angular momentum component is equal to zero. As a result, we have

$$\text{Tr}(A^\dagger A) = 2(2S+1) \frac{1}{4} [(3\alpha_t + \alpha_s)^2 + S(S+1)(\alpha_t - \alpha_s)^2]. \quad (4.62)$$

To compare the cross sections for $n-p$ and $n-\text{H}_2$ scattering, we should account for different recoil factors (reduced masses): $m = (1/2)M$ for the scattering from free protons, and $m = (2/3)M$ for the scattering from the molecule. The scattering amplitude that contains the wave vector of relative motion is proportional to the reduced mass, and the cross section is proportional to the reduced mass squared. For the neutron

scattering of a proton bound in a heavy molecule, the reduced mass is close to the nucleon mass M and the cross section is four times larger than for a free proton. Thus, for the two types of molecular hydrogen, we find the elastic neutron scattering cross sections as

$$\sigma_{\text{para}} = 4\pi \left(\frac{4}{3}\right)^2 \frac{1}{4} (3a_t + a_s)^2 = \frac{16\pi}{9} (3a_t + a_s)^2. \quad (4.63)$$

and

$$\sigma_{\text{ortho}} = \frac{16\pi}{9} [(3a_t + a_s)^2 + 2(a_t - a_s)^2]. \quad (4.64)$$

The cross section for free protons (4.55) is

$$\bar{\sigma} = 4\pi \left(\frac{3}{4}a_t^2 + \frac{1}{4}a_s^2\right) = \frac{\pi}{4} [(3a_t + a_s)^2 + 3(a_t - a_s)^2]. \quad (4.65)$$

A combination of different measurements allows one to determine the scattering lengths with their signs: $a_t \approx 5.44$ fm, $a_s \approx -23.72$ fm. Due to the opposite signs of the triplet and singlet lengths, the *ortho*-hydrogen cross section significantly exceeds that for *para*-hydrogen. Returning to our illustration (Figure 4.6) of the meaning of the scattering length, we realize that the result above agrees with the presence of the loosely bound triplet state (the deuteron) and absence of the bound singlet state.

4.5 Resonance Scattering at Low Energies

The large negative value of the *spin-singlet* scattering length shows that the potential well is almost ready to support a bound singlet *s*-wave state. In such cases, it is said usually that there is a *virtual level*. To characterize the energy dependence of the scattering amplitude and the cross section beyond the limit $k \rightarrow 0$, especially in the case of a loosely bound or virtual state, we include the next term of the low-energy expansion [2].

For elastic scattering in the central field, the condition (4.9) of flux conservation (*unitarity* of the S -matrix) allows one to convert the expression (4.7) for the partial amplitudes f_ℓ into an equation

$$\text{Im } f_\ell = k|f_\ell|^2, \quad \text{or} \quad \text{Im} \left(\frac{1}{f_\ell} \right) = -k. \quad (4.66)$$

Therefore, the general form of the amplitude f_ℓ compatible with the unitarity is $1/f_\ell = g_\ell - ik$, or

$$f_\ell = \frac{1}{g_\ell - ik} \quad (4.67)$$

where g_ℓ is (for real energies) a *real* function with the dimension of inverse length. Simple algebra with the use of the relation $f_\ell = \exp(i\delta_\ell) \sin \delta_\ell/k$ defines the function $g_\ell(k)$ as

$$g_\ell = k \cot \delta_\ell. \quad (4.68)$$

Being real for real energies, g_ℓ can be represented by a series in powers of E , that is, powers of k^2 . At low energies, as shown in (4.21), $\delta_\ell \propto k^{2\ell+1}$. Therefore, $f_\ell \propto k^{2\ell}$, and the expansion of g_ℓ begins with the term $\sim 1/k^{2\ell}$. For the *s*-wave scattering, the function

$g_0(k)$ starts with a constant, $g_0 \rightarrow \gamma$ in the low-energy limit. Comparing Eq. (4.67) with the definition of the scattering length, we can make an identification

$$g_0(0) = \gamma = -\frac{1}{a}. \quad (4.69)$$

In this approximation, we can take into account the next term in the denominator of Eq. (4.67), which is imaginary and linear in k . Then

$$f_0 = -\frac{1}{(1/a) + ik} \equiv -\frac{1}{\gamma + ik}. \quad (4.70)$$

This shows the cross section beyond the limiting value (4.53),

$$\sigma = \frac{4\pi}{\gamma^2 + k^2}, \quad (4.71)$$

along with its energy dependence [compare with Eq. (4.38)].

The *analytical continuation* of the S -matrix into the complex energy plane defines the poles corresponding to the energies of the *bound* states. The pole of (4.67) on the upper imaginary axis of k corresponds to $k \rightarrow ik$ where κ determines the binding energy $\epsilon = \hbar^2 \kappa^2 / 2m$. If there is a solution of the equation $\kappa = -g_0(ik)$ for small κ , $\kappa R < 1$, we have a loosely bound state, and Eq. (4.69) shows that $\kappa \approx 1/a = -\gamma$. In this situation, the cross section (4.71) at energy $E = \hbar^2 k^2 / 2m$ is uniquely defined by the small binding energy [3],

$$\sigma(E) = \frac{2\pi\hbar^2}{m} \frac{1}{E + \epsilon}. \quad (4.72)$$

This is the so-called *resonance scattering* off a subthreshold resonance. The cross section would be infinite if it would be possible to use the incident beam of negative energy $E = -\epsilon$. Since the binding energy is small, the beam is nearly “in the resonance.” However, the phase shift δ_0 is here close to π in contrast to the genuine resonance with $\delta \approx \pi/2$ that was mentioned earlier.

Equation (4.71) is in fact more general being valid even if there is no bound level. Indeed, as we mentioned earlier, the part of the wave function inside a deep well behaves continuously, and there is no sharp change in observables when state transitions from bound to virtual. In this case, $\gamma^2 \equiv 2m|\epsilon|/\hbar^2$ defines an energy $|\epsilon|$ of the *virtual level* that would become a real bound state if the well were a little deeper. With the substitution $\epsilon \rightarrow |\epsilon|$, the resonance formula (4.72) is still applicable. This is the situation in the singlet $n-p$ scattering. The singlet scattering length a_s is large and negative showing that the well depth is close to the critical value for the appearance of a bound state. The corresponding virtual energy defined through the cross section at zero energy E , or through the scattering length,

$$\epsilon_{\text{virt}} = \frac{2\pi\hbar^2}{m\sigma} = \frac{\hbar^2}{2ma_s^2}, \quad (4.73)$$

is very small, $\epsilon_{\text{virt}} \approx 70$ keV. Therefore, at low energies, the singlet $n-p$ scattering exceeds significantly the triplet one.

4.6 Effective Radius

The next term of the low-energy expansion of the scattering amplitude (4.67), or the function g_0 , Eqs. (4.68) and (4.69), is quadratic in k (see Figure 4.7),

$$g_0(k) = k \cot \delta_0(k) = -\frac{1}{a} + \frac{1}{2} r_0 k^2 + O(k^4). \quad (4.74)$$

This definition introduces a new length parameter r_0 that is called the *effective radius*. The correction connected with the effective radius is more important than the small contribution of the p -wave that would result in the corrections $\sim (kR)^3$ to the scattering amplitude.

In this advanced approximation, the scattering amplitude (4.67) can be presented as

$$f_0(k) = \frac{1}{(-1/a) + (r_0 k^2/2) - ik}. \quad (4.75)$$

For the pole $k = ik$ of the analytical continuation, we have now

$$\kappa = \frac{1}{a} + \frac{1}{2} r_0 \kappa^2. \quad (4.76)$$

Of course, the values of the effective radius in the $p-n$ scattering are different for the triplet and singlet states. The relation (4.76) allows one to calculate the triplet effective radius r_{0t} in terms of the triplet scattering length a_t and the deuteron binding energy $\epsilon = \hbar^2 \kappa^2 / 2m$.

The experimental data give $r_{0t} = 1.7$ fm and $r_{0s} = 2.7$ fm. When the scattering length is large, the effective radius is positive and has a magnitude close to the range R of the forces. Therefore, it is preferable as a measure of the force range in contrast to the scattering length that is very sensitive to the existence of a bound state, changes sign,

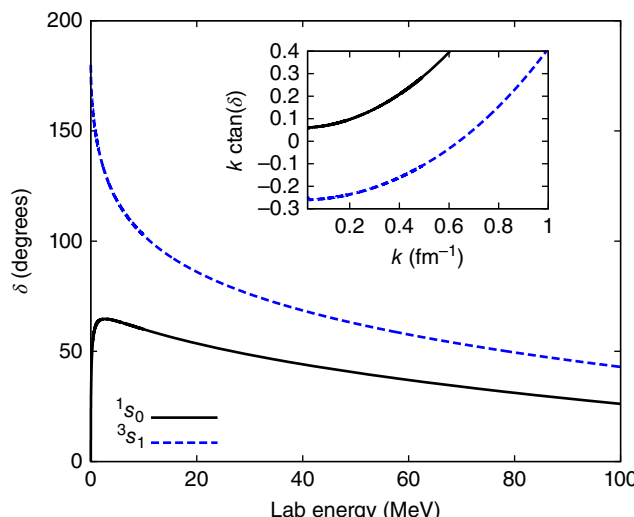


Figure 4.7 Phases of the nucleon–nucleon interaction in singlet and triplet s -states as a function of energy. Inset shows the parabolic, Eq. (4.74), low-energy behavior of g_0 as a function of momentum k . Phase shift analysis used data from Ref. [4].

and might be quite different from R . For the square well potential, the scattering length is shown in Figure 4.4 as a function of depth. Each time a new bound state emerges (at $k_0 R/\pi = 1/2, 3/2, \dots$), the scattering length jumps from $-\infty$ to $+\infty$; it can be shown [5] that in the same region the effective radius coincides with the potential radius R . This allows us to translate the experimental data on the effective radius into information about the range of nuclear forces.

Problem 4.4 Calculate the effective range r_0 for the square well potential of Problem 4.1.

Both the scattering length and effective radius do not provide specific information concerning the shape and detailed behavior of the potential. The high-order terms in the expansion (4.74) would be more informative. But they are shadowed by the contributions from higher partial waves. Therefore, practically the low-energy expansion is hardly useful beyond the approximation of the effective radius.

4.7 Scattering of Identical Particles

Theory of $p-p$ scattering is more cumbersome than that of the $n-p$ scattering. There are two additional aspects that complicate the problem: identity of colliding particles and Coulomb interaction.

The symmetry requirements for a system of identical particles leave their fingerprints in the scattering picture. Even in classical mechanics, looking at the scattering cross section with the registration of two identical particles by two detectors (Figure 4.8), we have two cases when a particle arrives at a detector located at an angle θ with respect to the incident direction of mutual motion in the center-of-mass frame. In the case (a), the detector registers a particle 1 after its scattering by an angle θ ; the particle 2, due to the momentum conservation, would be registered by a detector in the direction $\pi - \theta$. In the case (b), the particle 1 is scattered by an angle $\pi - \theta$, while the detector sees the particle 2 that is indistinguishable from the particle 1.

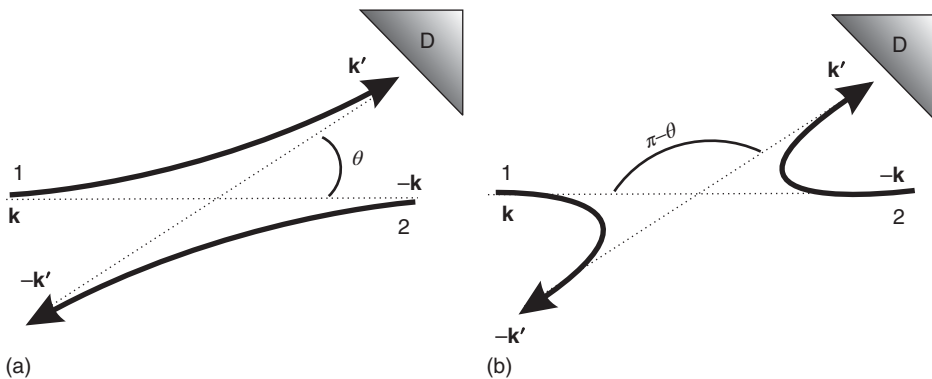


Figure 4.8 Detecting two identical particles.

The classical cross section is a sum of two elementary cross sections, for the *direct*, $\mathbf{k} \rightarrow \mathbf{k}'$, and *exchange*, $\mathbf{k} \rightarrow -\mathbf{k}'$, processes,

$$d\sigma_{\text{cl}}(\mathbf{k}', \mathbf{k}) = d\sigma(\mathbf{k}', \mathbf{k}) + d\sigma(-\mathbf{k}', \mathbf{k}). \quad (4.77)$$

If the interaction is due to a central potential, the cross section depends on the polar angle θ only and (4.77) reduces to

$$d\sigma_{\text{cl}}(\theta) = d\sigma(\theta) + d\sigma(\pi - \theta), \quad (4.78)$$

therefore

$$d\sigma_{\text{cl}}(\pi/2) = 2 d\sigma(\pi/2). \quad (4.79)$$

The quantum result will differ from the classical one by the interference of the direct and exchange amplitudes. The wave function of proper symmetry for two identical particles in their center-of-mass frame has a form

$$\frac{1}{\sqrt{2}}(1 \pm \mathcal{P}_{12})\psi(\mathbf{r}; s_1, s_2) = \frac{1}{\sqrt{2}}[\psi(\mathbf{r}; s_1, s_2) \pm \psi(-\mathbf{r}; s_2, s_1)], \quad (4.80)$$

where \mathcal{P}_{12} is the exchange operator (2.8) and the sign \pm refers to bosons or fermions.

Let us consider a case when the space and spin variables are separated, so that the wave function is a product $\psi(\mathbf{r}, s_1, s_2) = \psi(\mathbf{r})\chi(s_1, s_2)$. Then the function (4.80) goes into

$$\begin{aligned} & \frac{1}{\sqrt{2}}[\psi(\mathbf{r})\chi(s_1, s_2) \pm \psi(-\mathbf{r})\chi(s_2, s_1)] \\ &= \frac{1}{\sqrt{2}}[(\psi_S + \psi_A)(\chi_S + \chi_A) \pm (\psi_S - \psi_A)(\chi_S - \chi_A)] \end{aligned} \quad (4.81)$$

with

$$\psi_{S,A} = \frac{1}{2}[\psi(\mathbf{r}) \pm \psi(-\mathbf{r})], \quad \chi_{S,A} = \frac{1}{2}[\chi(s_1, s_2) \pm \chi(s_2, s_1)]. \quad (4.82)$$

This general consideration gives for the Bose statistics

$$\psi_B(\mathbf{r}; s_1, s_2) = \sqrt{2}(\psi_S\chi_S + \psi_A\chi_A) \quad (4.83)$$

and for the Fermi statistics

$$\psi_F(\mathbf{r}; s_1, s_2) = \sqrt{2}(\psi_A\chi_S + \psi_S\chi_A); \quad (4.84)$$

symmetries of space and spin parts are complementary.

In the elastic scattering of identical particles, the asymptotic wave function can be written as

$$\psi(\mathbf{r}; s_1, s_2) \approx \left[e^{i(\mathbf{k} \cdot \mathbf{r})} + f(\mathbf{k}', \mathbf{k}) \frac{e^{ikr}}{r} \right] \chi(s_1, s_2), \quad (4.85)$$

where vectors \mathbf{r} and $\mathbf{k}' = k(\mathbf{r}/r)$ change signs under interchange of the particles corresponding to the cases a and b of Figure 4.8. Coordinate functions of correct symmetry (4.82) are

$$\psi_{S,A}(\mathbf{r}) \approx \frac{1}{2} \left\{ e^{i(\mathbf{k} \cdot \mathbf{r})} \pm e^{-i(\mathbf{k} \cdot \mathbf{r})} + \frac{e^{ikr}}{r} [f(\mathbf{k}', \mathbf{k}) \pm f(-\mathbf{k}', \mathbf{k})] \right\}. \quad (4.86)$$

For spinless bosons, $\chi_A = 0$, $\chi_S = 1$, and from (4.85) and (4.86) we obtain $\psi_B(\mathbf{r}) = \sqrt{2}\psi_S(\mathbf{r})$. The incident part of the wave function is then $(1/\sqrt{2})[\exp(i\mathbf{k} \cdot \mathbf{r}) + \exp(-i\mathbf{k} \cdot \mathbf{r})]$. This defines the incident flux $(1/2)\hbar k/m$ in each wave, \mathbf{k} and $-\mathbf{k}$, but it makes no sense to indicate which particle is moving from the left and which is moving from the right. The scattered part of the wave function is $(1/\sqrt{2})[\exp(ikr)/r][f(\mathbf{k}', \mathbf{k}) + f(-\mathbf{k}', \mathbf{k})]$. The total current of particles scattered through an angle θ across an area $d\mathcal{A}$ consists of the currents for both particles,

$$\mathbf{j}_{\text{scatt}} d\mathcal{A} = \frac{\hbar k}{m} \left| \frac{1}{\sqrt{2}} [f(\mathbf{k}', \mathbf{k}) + f(-\mathbf{k}', \mathbf{k})] \right|^2 \frac{\mathbf{r}}{r} \frac{1}{r^2} d\mathcal{A}. \quad (4.87)$$

Now we obtain the cross section

$$\begin{aligned} \left(\frac{d\sigma}{do} \right)_{S=0} &= |f(\mathbf{k}', \mathbf{k}) + f(-\mathbf{k}', \mathbf{k})|^2 \\ &= |f(\mathbf{k}', \mathbf{k})|^2 + |f(-\mathbf{k}', \mathbf{k})|^2 + 2\text{Re}[f^*(\mathbf{k}', \mathbf{k})f(-\mathbf{k}', \mathbf{k})]. \end{aligned} \quad (4.88)$$

For the central field, the interference pattern is determined by

$$\left(\frac{d\sigma}{do} \right)_{S=0} = |f(\theta)|^2 + |f(\pi - \theta)|^2 + 2\text{Re}[f^*(\theta)f(\pi - \theta)]. \quad (4.89)$$

The cross section for $\theta = \pi/2$ is enhanced by a factor 2 as compared to the classical cross section (4.78),

$$\left(\frac{d\sigma(\pi/2)}{do} \right)_{S=0} = 4 \left| f\left(\frac{\pi}{2}\right) \right|^2. \quad (4.90)$$

In the fermion case (spin 1/2) both, symmetric (triplet, χ_S) and antisymmetric (singlet, χ_A), spin states are possible. Selecting the complementary space functions, we obtain, analogous to (4.87) and (4.89),

$$\left(\frac{d\sigma_{1/2}}{do} \right)_t = |f(\mathbf{k}', \mathbf{k}) - f(-\mathbf{k}', \mathbf{k})|^2, \quad (4.91)$$

$$\left(\frac{d\sigma_{1/2}}{do} \right)_s = |f(\mathbf{k}', \mathbf{k}) + f(-\mathbf{k}', \mathbf{k})|^2. \quad (4.92)$$

In the triplet state (4.91), the interference term has the sign opposite to that for bosons or for singlet fermions. Here, the cross section in the central field vanishes for $\theta = \pi/2$. In the partial wave expansion only even ℓ survive for bosons or spin-singlet fermions; only odd ℓ remain for spin-triplet fermions.

If all four spin states in the collision of identical fermions of spin 1/2 are equiprobable, the observed cross section, in comparison with the $n-p$ case (4.55), is equal to

$$\overline{\frac{d\sigma_{1/2}}{do}} = \frac{1}{4} \left(\frac{d\sigma_{1/2}}{do} \right)_s + \frac{3}{4} \left(\frac{d\sigma_{1/2}}{do} \right)_t. \quad (4.93)$$

Using our previous results (Eqs. (4.91) and (4.92)), we obtain

$$\overline{\frac{d\sigma_{1/2}}{do}} = |f(\mathbf{k}', \mathbf{k})|^2 + |f(-\mathbf{k}', \mathbf{k})|^2 - \text{Re}[f^*(\mathbf{k}', \mathbf{k})f(-\mathbf{k}', \mathbf{k})]. \quad (4.94)$$

For the angle $\theta = \pi/2$ in the central field, Eq. (4.94) means that

$$\frac{d\sigma_{1/2}(\pi/2)}{d\theta} = \left| f\left(\frac{\pi}{2}\right) \right|^2 = \frac{1}{2} \frac{d\sigma_{\text{cl}}}{d\theta}. \quad (4.95)$$

If the forces are known as it is the case for the Coulomb interaction, one can make conclusions about the value of the spin of the particles.

We should point out that the cross section *integrated over angles* has to be calculated according to

$$\sigma = \frac{1}{2} \int d\theta \frac{d\sigma}{d\theta} \quad (4.96)$$

to avoid the double counting.

4.8 Coulomb Scattering

For a pure Coulomb interaction (no nuclear forces), the Schrödinger equation can be solved exactly [QP, I, 18.7]. Due to the very slow decrease in the potential, the boundary condition (4.1) for the asymptotic wave function is not correct anymore. The wave front of the scattered wave is distorted even at large distances from the center. The actual asymptotic behavior is

$$\psi^C(\mathbf{r}) \approx e^{ikz+i\eta \ln k(r-z)} + f^C(\theta) \frac{e^{ikr-i\eta \ln kr}}{r}, \quad (4.97)$$

where the *Sommerfeld parameter* is, for a collision of particles with the charge e ,

$$\eta = \frac{e^2}{\hbar v} = \frac{me^2}{k\hbar^2}, \quad (4.98)$$

and the Coulomb scattering amplitude can be written as

$$f^C(\theta) = -\frac{e^2}{2mv^2 \sin^2(\theta/2)} \frac{\Gamma(1+i\eta)}{\Gamma(1-i\eta)} e^{-i\eta \ln [\sin^2(\theta/2)]}. \quad (4.99)$$

Here Γ stands for the gamma-function that, in this case, has a complex argument.

For the opposite charges (attraction case), the Coulomb parameter η changes sign, which corresponds to the complex conjugation in Eqs. (4.97) and (4.99). The gamma-function $\Gamma(x)$ has poles on the real axis in the integer points $x = -n+1, n=1, 2, \dots$. For the conjugate scattering amplitude, those are the poles of $\Gamma(1-i\eta)$, that is, the points where $-i\eta = -n$, or the points on the positive imaginary axis of k , $k = i\kappa_n = ime^2/\hbar^2 m$. According to the general rules of analyticity [QP, II, 8.4], these points coincide with the bound states in the Coulomb field,

$$\epsilon_n = -\frac{\hbar^2 \kappa_n^2}{2m} = -\frac{me^4}{2\hbar^2 n^2} \quad (4.100)$$

(the energy spectrum of the hydrogen atom).

The distortion of the wave front gives corrections to the current j associated with the asymptotic wave function. These corrections, however, do not contribute to the main terms $j \sim 1/r^2$. The cross section can still be determined by

$$\frac{d\sigma^C}{d\theta} = |f^C(\theta)|^2 = \left\{ \frac{e^2}{2mv^2} \right\}^2 \frac{1}{\sin^4(\theta/2)}, \quad (4.101)$$

which is nothing but the Rutherford cross section. Here, the exact results of classical and quantum mechanics coincide. Moreover, the Born approximation gives also the exact result. The classical case corresponds to the formal limit of $\hbar \rightarrow 0$, that is, $\eta \gg 1$. The Born approximation is valid at $\eta \ll 1$. But the exact result (4.101) expressed through the relative velocity v does not depend on \hbar at all.

Such simple features disappear even in the pure Coulomb case if the particles are identical. Equation (4.99) describes the direct process only. The exchange process with $\theta \rightarrow (\pi - \theta)$ is given by the same expression with $\sin(\theta/2) \rightarrow \cos(\theta/2)$. For the proton–proton scattering, the cross section averaged over the polarizations should be calculated as in Eq. (4.94),

$$\frac{d\sigma^C}{d\theta} = \left(\frac{e^2}{Mv^2} \right)^2 \left\{ \frac{1}{\sin^4 \theta/2} + \frac{1}{\cos^4 \theta/2} - \frac{\cos[\eta \ln(\tan^2 \theta/2)]}{(\sin^2 \theta/2)(\cos^2 \theta/2)} \right\}. \quad (4.102)$$

At both, forward, $\theta \approx 0$, and backward, $\theta \approx \pi$, angles, the cross section is dominated by one term, direct or exchange, respectively. For the intermediate angles, the interference term is important. In the classical limit $\eta \gg 1$, the numerator of the interference term rapidly oscillates. An experiment with classical resolution feels only a mean value of this term that is equal to zero, and the average result reduces to the classical sum (4.78) of cross sections. However, in the quantum (Born) limit of $\eta \ll 1$, the cosine in the numerator of the third term is close to unity for almost all angles, and the combination of three terms leads to

$$\frac{d\sigma^C}{d\theta} \approx \left(\frac{2e^2}{Mv^2} \right)^2 \frac{4 - 3\sin^2 \theta}{\sin^4 \theta}. \quad (4.103)$$

4.9 Coulomb-Nuclear Interference

Now we can include the *nuclear p–p* interaction. At low energies, only the *s*-wave is sensitive to the nuclear potential. The Coulomb amplitude was expressed in Eq. (4.99) without the partial wave expansion. The complicated angular dependence shows that the final picture is a result of the superposition of many partial waves. Only one of them is considerably perturbed by the nuclear forces. To insert the result of the nuclear scattering, first we expand the Coulomb amplitude in partial waves,

$$f^C(\theta) = \frac{1}{2ik} \sum_{\ell} (2\ell + 1) (e^{2i\delta_{\ell}^C} - 1) P_{\ell}(\cos \theta). \quad (4.104)$$

The Coulomb phase shifts can be found by the calculation of integrals of the Coulomb amplitude (4.99) with the Legendre polynomials,

$$e^{2i\delta_{\ell}^C} = \frac{\Gamma(l + \ell + i\eta)}{\Gamma(1 + \ell - i\eta)}. \quad (4.105)$$

The gamma-functions can be reduced to those in Eq. (4.99) by the use of the recurrence relation $\Gamma(x + 1) = x\Gamma(x)$.

Switching on the nuclear interaction we change the Coulomb phase shifts, $\delta_{\ell}^C \rightarrow \delta_{\ell}^C + \delta_{\ell}$. The extra term is the additional shift due to the nuclear forces. In general, owing to the Coulomb repulsion, it is not equal to a pure nuclear phase shift because the probability

of being at small distances is suppressed compared to the case with no Coulomb interaction. For example, in contrast to a normal s -wave phase for the short-range potential (4.51) that behaves $\sim -ka$ in the low-energy limit, this additional phase shift is exponentially small,

$$\delta_0 \propto e^{-2\pi e^2/hv} \equiv e^{-2\pi\eta}. \quad (4.106)$$

This factor is actually the probability $|\psi(0)|^2$ for two protons to approach small distances against the Coulomb repulsion. The exponential smallness is due to the necessity to tunnel under the Coulomb barrier as in an elementary α -decay problem [QP, I, (2.66)] (the so-called Gamow factor).

Since the additional phase shift appears at low energies for $\ell = 0$ only, the resulting amplitude can be written as

$$f(\theta) = f^C(\theta) + \frac{1}{2ik} \left[e^{2i(\delta_0^C + \delta_0)} - e^{2i\delta_0^C} \right]. \quad (4.107)$$

For the Coulomb amplitude f^C , we can again use the full expression (4.99).

To calculate the cross section, we need to specify the symmetry of the spin wave function of the protons. For $\ell = 0$, the singlet state is the only allowed one. The appropriate cross section is given by Eq. (4.92). Instead of (4.102), we now obtain

$$\frac{d\sigma}{d\theta} = \frac{d\sigma^C}{d\theta} - \left(\frac{e^2}{Mv^2} \right)^2 \left\{ \frac{2}{\eta} \sin \delta_0 \left[\frac{\cos \delta'(\theta)}{\sin^2 \theta / 2} + \frac{\cos \delta''(\theta)}{\cos^2 \theta / 2} \right] + \frac{4}{\eta^2} \sin^2 \delta_0 \right\}, \quad (4.108)$$

where

$$\delta'(\theta) = \delta_0 + \eta \ln(\sin^2 \theta / 2), \quad \delta''(\theta) = \delta_0 + \eta \ln(\cos^2 \theta / 2). \quad (4.109)$$

The main new feature of the result (4.108) is the *Coulomb-nuclear interference*. The presence of the cross term $\sim \sin \delta_0$ allows one to measure the sign of the nuclear phase shift, which is opposite (attraction in the singlet state 1s_0) to that for the Coulomb repulsion. Figure 4.9 shows the differential cross section of the $p-p$ scattering at low energy

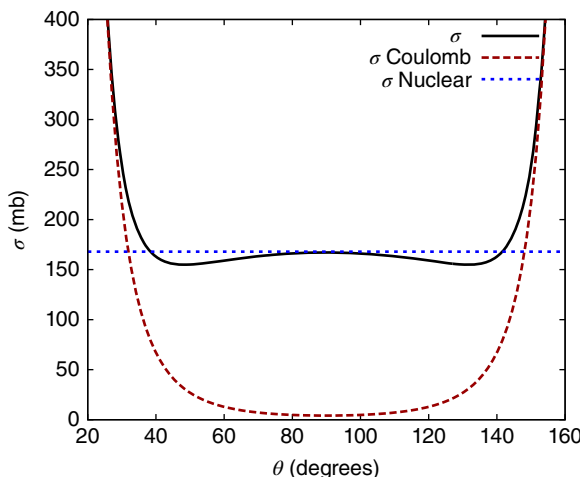


Figure 4.9 The differential cross section of $p-p$ scattering, solid line (black); Coulomb scattering, dashed line (blue); pure nuclear s -wave scattering, dotted line (brown).
Source: Phase shift analysis from Ref. [4]. For further reading, see Ref. [6].

(2.0 MeV in the center-of-mass frame). As it should be for identical particles, the angular distribution is symmetric with respect to 90° . In forward and backward directions, the Coulomb scattering dominates. At intermediate angles, there are two minima displaying the result of the destructive Coulomb-nuclear interference.

This interference remains one of the main tools for determining the nuclear phase shifts at higher energies. The Coulomb scattering is concentrated in a narrow cone around the beam axis; the cone is narrowing as energy increases. Therefore, the Coulomb-nuclear interference is also seen at smaller and smaller angles.

Theory of the scattering length and effective radius can be generalized to include the Coulomb interaction. This allows one to relate the parameters of the nuclear $p-p$ spin-singlet potential to the observed effective parameters distorted by the Coulomb interaction. The values found from such an analysis are $a_s(p-p) = -17.2$ fm and $r_{0s}(p-p) = 2.7$ fm. The effective radius is the same as for the $n-p$ scattering, while the scattering length seems to differ from the $n-p$ value. However, one should have in mind that in both cases the scattering length is negative and very large, that is, the virtual singlet level is very close to zero energy. In such a situation, the scattering length is a very sensitive function of the potential. The difference in the $n-p$ and $p-p$ nuclear singlet potentials is indeed small in agreement with the *charge independence* of nuclear forces.

References

- 1 R.B. Sutton *et al.*, Phys. Rev. **72**, 1147 (1947).
- 2 L. Landau and Ya. Smorodinsky, J. Phys. (U.S.S.R.) **8**, 154 (1944).
- 3 E.P. Wigner, Phys. Rev. **43**, 252 (1933).
- 4 V.G.J. Stoks, R.A.M. Klomp, M.C.M. Rentmeester, and J.J. de Swart, Phys. Rev. C **48**, 792 (1993). See also Ref. [4] in chapter 3 and <http://nn-online.org>.
- 5 H.A. Bethe and P. Morrison, *Elementary Nuclear Theory*, John Wiley & Sons, Inc., New York, 1956.
- 6 J.D. Jackson and J.M. Blatt, Rev. Mod. Phys. **22**, 77 (1950).

5

Liquid Drop Model

The liquid drop model was historically the first model to describe nuclear properties.

K. Heyde, *Basic Ideas and Concepts in Nuclear Physics*.

5.1 Binding Energies

Here we turn to the *global properties* of the nuclear chart. Scattering experiments show that nuclei have nearly uniform inner density and the nuclear size grows on average as $A^{1/3}$, so that the nuclear volume is proportional to the particle number A . These are important indications towards *hydrodynamic* features of nuclear matter. The short-range nuclear forces are *saturated* at normal nuclear density that corresponds to a certain interparticle distance of the order of the mean attraction range. Addition of extra nucleons does not change the central density, they occupy mostly the surface increasing the average radius. The nuclear matter is similar to *incompressible* liquid. This idea finds its natural expression in the *liquid drop model* of complex nuclei going back to N. Bohr: the nucleus is treated as a droplet of continuous medium. Such a model exists in various versions but, as a rule, only *macroscopic* features are considered here, with rare references to microscopic structure.

We start with the regularities of nuclear binding energies. There are many elaborate fits to the binding energies that use a large number of parameters. We limit ourselves here to a simple classical Bethe – Weizsäcker semiempirical *mass formula* that is reasonably successful in describing data around the line of stability and in predicting binding energies of new isotopes away from this line (although not very far away) as was tested many times in the history of nuclear physics [1]. The model also served as an example for developing similar approaches in atomic and molecular physics [2].

The nuclear *mass defect* [total ground state energy of the nucleus (A, Z) minus rest masses of Z protons and N neutrons] is expressed as a sum of several universal contributions smoothly changing as a function of the mass number $A = Z + N$ and charge Z . The *binding energy*, by definition, is given by

$$B(A, Z) = (ZM_p + NM_n) c^2 - E_{\text{tot}}(A, Z). \quad (5.1)$$

For particle-stable nuclei, this quantity is positive. The data can be parameterized as

$$B(A, Z) = b_V A - b_S A^{2/3} - b_{\text{symm}} \frac{(N - Z)^2}{2A} - b_C \frac{Z^2}{A^{1/3}} + b_p [(-)^N + (-)^Z] \frac{1}{\sqrt{A}}. \quad (5.2)$$

There are five coefficients b_i with dimension of energy in this simple version of the mass formula. Their values are found from the fit to hundreds of experimental masses. The quality of the fit can be seen in Figure 5.1, but one has to have in mind that there are many versions of the liquid drop fits that can differ slightly by the numerical values of the parameters [3].

The main binding term $b_V \approx 15$ MeV gives the volume energy per particle (if the density is constant, the volume $V \propto A$). In the limit of very large A , assuming $N = Z$ but without the Coulomb interaction, this would be the predominant term. The medium in this limit is referred to as *symmetric nuclear matter*. In order to extract a particle from the bound state in nuclear matter, $A \rightarrow A - 1$, one would need to invest in average the *separation energy* equal to b_V , an analog of the work function for electrons in solids.

In statistical mechanics, the quantity of such type, the derivative $(\partial E / \partial A) = -b_V$ of energy (of free energy at nonzero temperature) with respect to the particle number, is called the *chemical potential* μ (counted from the mass of the free particle). Independence of the chemical potential of the particle number is a typical feature of the *thermodynamic limit* of macroscopic systems, regardless of their aggregate state (solid, liquid, or gaseous). From Figure 5.1, it is seen that the actual separation energy for most nuclei is smaller than the limiting value b_V by a factor close to 2. This means that for *finite* nuclei, the correctional factors in the mass formula are equally important. The A -dependence is not negligible as well. However, this dependence is smooth almost everywhere except for the region of the lightest nuclei. Systems, such as atomic nuclei, that have many degrees of freedom and manifest some macroscopic properties but still do not fully reach the thermodynamic limit and allow one to study individual quantum states are often called *mesoscopic*.

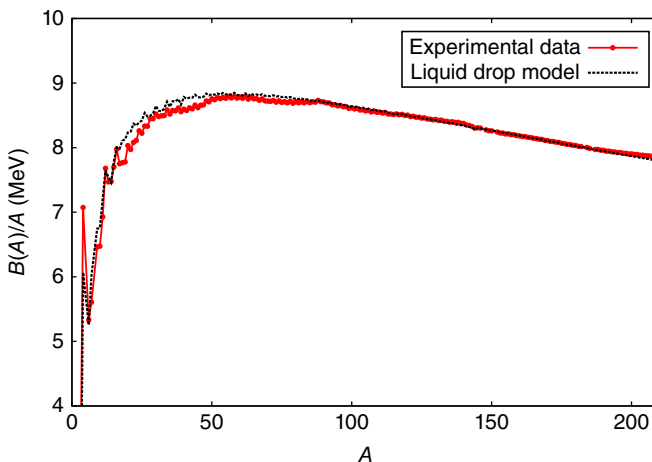


Figure 5.1 Experimental binding energies per particle (red solid line); the dotted black line represents the semiempirical mass formula (5.2) with the following values of the parameters: $b_V = 15.2$ MeV, $b_S = 15.8$ MeV, $b_C = 0.686$ MeV, $b_{\text{symm}} = 44.7$ MeV, and $b_p = 5$ MeV.

The following term in the mass formula, $b_S \approx 16$ MeV, is related to the presence of the surface with the area proportional to $R^2 \propto A^{2/3}$. The coefficient r_0 in the relation,

$$R = r_0 A^{1/3}, \quad (5.3)$$

is the length of the order of average interparticle distance. In various parameterizations (and for different quantities), r_0 is fixed in slightly different ways but typically $r_0 \approx 1.2 \div 1.3$ fm. The quantity

$$\sigma = \frac{b_S}{4\pi r_0^2} \quad (5.4)$$

can be interpreted as the *surface tension*. As in an elementary consideration, it arises due to the unsaturated interaction of the outer particles that diminishes the binding energy.

Problem 5.1 Using the radius of nuclear matter, the value (5.3) with $r_0 = 1.25$ fm, find the surface tension of nuclear matter and compare the result with that of liquid mercury, $\sigma_{\text{Hg}} = 470$ erg cm $^{-2}$.

Solution

Taking the surface energy b_S from the mass formula, we obtain

$$\sigma = \frac{b_S}{4\pi r_0^2} = 1.4 \times 10^{20} \text{ erg cm}^{-2} = 0.3 \times 10^{18} \sigma_{\text{Hg}}. \quad (5.5)$$

The next two terms in the mass formula discriminate between neutrons and protons. The *symmetry energy*, $b_{\text{symm}} \approx 45$ MeV, prefers to equalize the number of protons and neutrons. The nucleon–nucleon interaction is stronger in the space-even, spin-triplet states ($T = 0$) that partially explains the origin of this term, as mentioned earlier. Another part of extra energy comes due to a simple reason that identical nucleons are not allowed to occupy the same energetically favorable states (see Chapter 7). The symmetry term is proportional to the squared isospin projection T_3^2 .

Problem 5.2 Using the fact that the nuclide ^{197}Au is beta-stable, determine the limits of possible values for the coefficient of symmetry energy in the mass formula.

Solution

The nucleus (A, Z) is beta-stable if its mass is smaller than the masses of its neighbors $(A, Z \pm 1)$. In the opposite case, because of the pairing, the situation is possible when the *double beta-decay* is allowed with the jump from an even–even nucleus to an even–even neighbor. This will be explained in the section on weak interactions. Here, we consider only a single beta-decay. In the simplest version of the mass formula, we need to look at the change of Coulomb and symmetry energy taking into account the mass difference between the neutron and the proton. This gives the double inequality

$$b^{(+)} > b_{\text{symm}} > b^{(-)}, \quad (5.6)$$

$$b^{(\pm)} = \frac{A \left[(6/5)(e^2/R_c)(Z \pm 1/2) - (m_n - m_p)c^2 \right]}{2(N - Z \mp 1)}. \quad (5.7)$$

With $R_c = 1.25 A^{1/3}$ fm, this leads to $43 \text{ MeV} < b_{\text{symm}} < 46 \text{ MeV}$.

The Coulomb term is relatively weak, $b_C \approx 0.7$ MeV, but its influence grows very fast for heavy nuclei. The dependence on Z and A corresponds to a simple classical estimate of the Coulomb energy of the uniformly charged sphere

$$E_C = \frac{3}{5} \frac{(Ze)^2}{R} = \frac{3}{5} \frac{e^2}{r_0} \frac{Z^2}{A^{1/3}}. \quad (5.8)$$

The interplay of the symmetry and Coulomb term determines the most energetically favorable relation between the proton and neutron numbers at given A , the *valley of beta-stability*. Other nuclei with the same A will be unstable with respect to beta-decay when the daughter nucleus returns closer to the stability line.

Problem 5.3 In the following table, you see total binding energies of nuclei (in megaelectronvolts) grouped in mirror pairs. Suggest a method to estimate the *charge radius* R_c of nuclei, fit your results by $R_c = r_c A^{1/3}$, and determine (for instance by the least square fit) the parameter r_c .

Nuclides	Binding energy	Nuclides	Binding energy
${}^3\text{H}$	8.482	${}^3\text{He}$	7.718
${}^5\text{He}$	27.410	${}^5\text{Li}$	26.330
${}^7\text{Li}$	39.246	${}^7\text{Be}$	37.601
${}^{11}\text{Be}$	76.207	${}^{11}\text{C}$	73.442
${}^{13}\text{C}$	97.110	${}^{13}\text{N}$	94.107
${}^{15}\text{N}$	115.494	${}^{15}\text{O}$	111.952
${}^{17}\text{O}$	131.764	${}^{17}\text{F}$	128.221
${}^{19}\text{F}$	147.803	${}^{19}\text{Ne}$	143.782
${}^{21}\text{Ne}$	167.407	${}^{21}\text{Na}$	163.078
${}^{23}\text{Na}$	186.566	${}^{23}\text{Mg}$	181.727
${}^{25}\text{Mg}$	205.589	${}^{25}\text{Al}$	200.527
${}^{27}\text{Al}$	224.953	${}^{27}\text{Si}$	219.361
${}^{29}\text{Si}$	245.012	${}^{29}\text{P}$	239.286

Solution

For mirror nuclei with charges $Z + 1$ and Z , the difference of Coulomb energies can be approximately presented as

$$\Delta E_C = \frac{3}{5} \frac{e^2}{R_c} [(Z + 1)^2 - Z^2]. \quad (5.9)$$

Here we assume exact isospin invariance of nuclear forces and neglect quantum exchange corrections as well as the classical correction $Z^2 \rightarrow Z(Z - 1)$. From (5.9), we find for each mirror pair (using $e^2/\hbar c = 1/137$)

$$R_c = \frac{6}{5 \times 137} (\hbar c) \frac{Z + 1/2}{\Delta E_C(\text{MeV})} \text{ fm} = 1.73 \frac{Z + 1/2}{\Delta E_C(\text{MeV})} \text{ fm}. \quad (5.10)$$

Having the set of data $\{R_c(i), A(i)\}$, we can try to fit them according to $R_c = r_c A^{1/3}$. A one-parameter fit is given by the minimization of the deviation function

$$D(r_c) = \sum_i [R_c(i) - r_c A^{1/3}(i)]^2. \quad (5.11)$$

The parameter r_c corresponds to the point where

$$\frac{\partial D(r_c)}{\partial r_c} = 0. \quad (5.12)$$

Using this condition and our set of data, we obtain

$$r_c = \frac{\sum_i R_c(i) A^{1/3}(i)}{\sum_i A^{2/3}(i)} = 1.44 \text{ fm}. \quad (5.13)$$

This value is greater than that found from the charge density because the extra charge that determines the isobaric energy difference is physically associated with the outer nucleon orbitals.

The last term of the mass formula, $b_p \approx 6 \text{ MeV}$, describes the *pairing correlations* between identical nucleons. Odd- A nuclei lose $\sim 6/\sqrt{A} \text{ MeV}$ due to the presence of an unpaired nucleon; odd–odd nuclei lose twice as much. The pairing correlations give rise to many coherent phenomena in low-energy nuclear physics being similar to the Cooper pairing in superconductors (see Chapter 13).

The mass formula well describes the increase in binding from the low deuteron value of 1.1 MeV per nucleon to the most strongly bound nuclei around iron and nickel (^{62}Ni has maximum binding energy per particle). The subsequent decrease is mainly due to the electrostatic energy that cannot be fully compensated by the smaller charge/mass ratio because of the increase in the symmetry energy in the case of the large neutron excess. The accuracy of the formula for stable nuclei is better than 200 keV per particle.

What is left outside the mass formula is the manifestation of *quantum effects*; they can be seen in Figure 5.2 as the *modulation* of the binding energy curve of Figure 5.1. The only quantum phenomena taken here into account are Pauli exclusion principle and pairing. In reality, groups of nuclei periodically appear along the nuclear chart that reveal a stronger binding than in average. This evidently reminds the periodicity of properties of chemical elements in a function of the filling of electron orbits in atoms. Leaving aside these *shell effects*, which are similar to shell effects in quantum chemistry, we have a reasonable although schematic description of a finite quantum system with strong intrinsic interactions in terms of *global* classical variables. It is necessary to point out that at this stage, we still did not incorporate any specific models. The mass formula in the most natural way leads to the idea of a liquid drop.

5.2 Shape Variables

Now we can try to go further and consider the *dynamical* features of nuclei described by the mass formula. It is important to make a reasonable choice of *dynamic variables*. These variables are of *collective* nature as the mass formula does not consider

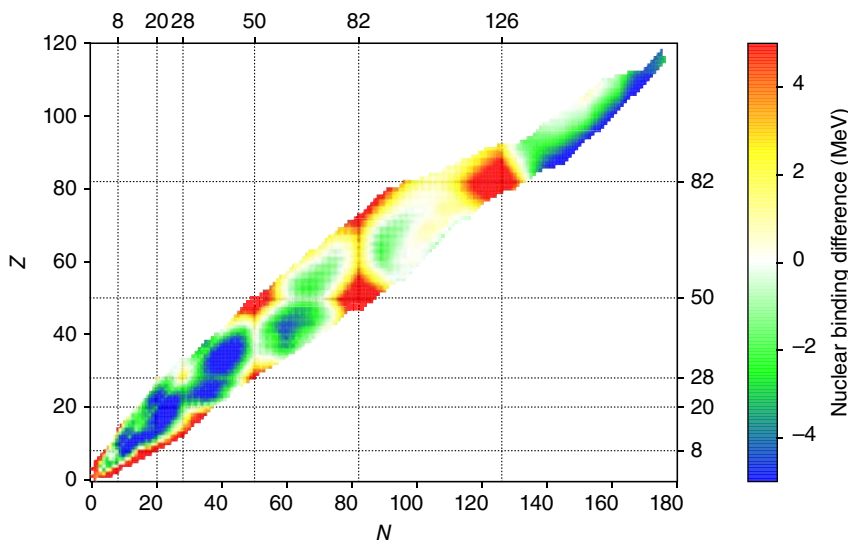


Figure 5.2 Difference between experimental nuclear binding energy and semiempirical mass formula. The nuclei with the so-called *magic* numbers of protons and neutrons, shown by grid lines, are significantly more bound due to the shell effects.

single-particle motion of the constituents. To extend this approach to dynamics, we have to stay on a level of continuous medium, although some features associated with individual particles will be useful.

In such a medium, the excitations should resemble the *propagating waves*. In a finite system, the spectrum of frequencies or wave numbers is *discrete*. The wavelengths should be sufficiently long; otherwise the notion of a continuous medium with unresolved individual constituents breaks down. The lowest limit for the wavelength is of the order of the mean interparticle distance r_0 that is close to the range of nuclear forces. Thus, the macroscopic description can be valid only if the wave length is large or the wave number k is small enough,

$$\frac{1}{k} > r_0 \simeq \frac{R}{A^{1/3}}. \quad (5.14)$$

For a stable substance that forms a self-sustaining drop, the *excitations*, at least at relatively low excitation energy, can be associated only with changes of shape. Let the ground state with energy described by the mass formula correspond to *spherical shape*. (Later we include the deformed ground states as well.) In the center-of-mass frame of the nucleus, the stationary states have certain values of energy and angular momentum (usually called *nuclear spin*). We assume that the ground state has quantum numbers $J^\pi = 0^+$ to $J^\Pi = 0^+$ of angular momentum and parity. This is the case for all *even-even* nuclei (N and Z are both even). In odd- A nuclei, the angular momentum is half-integer due to the single-particle contribution of the nucleon spin.

From the Kramers theorem [QP, I, 20.5], we know that the nucleon orbits are degenerate due to the *time-reversal invariance*. Therefore, in the low-lying states, the *time-conjugated orbits* are mostly occupied pairwise and angular momenta of the partners are compensated. The single-particle properties are outside of the global

continuous-medium description, thus compelling us to limit our consideration to even–even nuclei. The excitations of the spherical drop should have a certain angular momentum λ and orientation characterized by the angular momentum projection μ onto an arbitrarily chosen axis. Therefore, we expect that the excited states are similar to *surface waves*. The angular momentum of the wave has to be sufficiently low to avoid the violation of the condition (5.14),

$$\lambda \simeq kR < A^{1/3}. \quad (5.15)$$

For simplicity, we assume the sharp edge of the nuclear surface. This assumption, being more or less justified for stable heavy nuclei, is made only to simplify estimates and can be lifted by considering, instead of the external boundary, a family of similar equipotential surfaces. In a collective wave of deformation, the radius of the sphere R becomes a function of the direction $\mathbf{n}(\theta, \varphi)$ and can be represented by a superposition of the spherical harmonics,

$$R(\mathbf{n}) = R_0 \left[1 + \sum_{\lambda\mu} \alpha_{\lambda\mu} Y_{\lambda\mu}(\mathbf{n}) \right], \quad (5.16)$$

where the equilibrium radius is denoted as R_0 . The coefficients of the expansion (5.16), $\alpha_{\lambda\mu}$, are time-dependent parameters describing the excitations of the drop. In the same way, one can describe *static deformation* introducing time-independent components of $\alpha_{\lambda\mu}$. Many nuclei turn out to be deformed even in the ground state, but at this stage, we limit ourselves to a spherical equilibrium shape.

The deformation parameters $\alpha_{\lambda\mu}$ are the *dynamical variables* of the model. They are complex but, as the radius (5.16) is real, their complex conjugation properties are the same as those of the spherical functions,

$$\alpha_{\lambda\mu}^* = (-)^{\mu} \alpha_{\lambda-\mu}. \quad (5.17)$$

For each multipolarity λ , we have a set of $(2\lambda + 1)$ variables, $\mu = 0, \pm 1, \dots, \pm \lambda$. The corresponding wave-like excitations carry the angular momentum λ , its projection μ onto a quantization axis z fixed in space, and *natural parity* $(-)^{\lambda}$.

5.3 Microscopic Variables

The liquid drop description does not explicitly contain nucleonic degrees of freedom and information about nucleon configurations. We define observable quantities in terms of the particles and then relate them to the collective variables of the liquid drop model (LDM).

The *matter density* is one of the main characteristics of any many-body system. The local density can be different for different intrinsic states, and it can change because the system is being excited as in thermal expansion of macroscopic bodies. Experimental information for nuclei exists mostly about the density distribution in the ground states, which will be denoted as $|0\rangle$. In the nonrelativistic proton–neutron model, we assume that the nucleons carry the matter distribution. Then the ground state density is the expectation value of the density operator,

$$\rho(\mathbf{r}) = \langle 0 | \hat{\rho}(\mathbf{r}) | 0 \rangle = \langle 0 | \sum_a \delta(\mathbf{r} - \mathbf{r}_a) | 0 \rangle. \quad (5.18)$$

In the same model, we can introduce the *charge density*, using the operator

$$\rho^{\text{ch}}(\mathbf{r}) = \langle 0 | \sum_a e_a \delta(\mathbf{r} - \mathbf{r}_a) | 0 \rangle, \quad (5.19)$$

or the neutron density, $\rho(\mathbf{r}) - \rho^{\text{ch}}(\mathbf{r})$.

It is common to use density operators for the one-body quantities described in Section 2.7. In this way, we can introduce the *isoscalar and isovector densities*. The matter density $\rho(\mathbf{r})$, Eq. (5.18), counts all nucleons with the same weight, and therefore it is isoscalar. The charge density (5.19) contains the isoscalar part equal to $(e/2)\rho(r)$ and the isovector part that in fact shows the difference between local proton and neutron densities. Further modification can be made by considering the Fourier transforms and inserting the nucleon intrinsic form-factors, which can be studied in the experiments with a large momentum transfer to the nucleus. In the shape oscillations, we deal with the components of density in modes of rotational symmetry ($\lambda\mu$).

The one-body operators for the quantities $q(\mathbf{r})$, which depend only on coordinates, could be written as the integrals with the density operator,

$$\sum_a q_a(\mathbf{r}_a) = \int d^3 r q(\mathbf{r}) \rho(\mathbf{r}). \quad (5.20)$$

Here $q(\mathbf{r})$ is a non-operator function and the entire operator character is transferred to the density operator. The subdivision into the isoscalar and isovector components can be performed in both parts of (5.20). For the momentum-dependent quantities, one needs to be careful with the order of noncommutative operators. For example, the current operator, which satisfies the continuity equation together with the density operator (5.18), should be written as an *anticommutator* $[\dots, \dots]_+$,

$$\mathbf{j}(\mathbf{r}) = \frac{1}{2} \sum_a \left\{ \frac{\mathbf{p}_a}{m_a} \delta(\mathbf{r} - \mathbf{r}_a) + \delta(\mathbf{r} - \mathbf{r}_a) \frac{\mathbf{p}_a}{m_a} \right\} \equiv \sum_a \frac{1}{2m_a} [\mathbf{p}_a, \delta(\mathbf{r} - \mathbf{r}_a)]_+. \quad (5.21)$$

We have to stress that by using one-body operators to represent the physical observables, a strong assumption of validity of the pure nucleon model should be made. The whole charge is concentrated in protons, or, if the neutron intrinsic form-factor is taken into account, in nucleons, which has been mentioned earlier in charge-exchange interactions. If charge-exchange interactions are considered explicitly, the charge partly is located in the mesons or other mediators of nuclear forces. If the mesons are excluded from the explicit consideration by introducing an effective interaction, this interaction, in general, depends on relative velocity of interacting nucleons and therefore generates *two-body*, or in general many-body, components in addition to the current operator (5.21).

5.4 Multipole Moments

In the simplest approach, Eq. (5.16) describes a surface of a drop with constant intrinsic density ρ . The excitations of the drop are in fact the excitations of underlying nucleons, which form this density of matter. The multipole moments allow for the translation between the languages of nucleon motion and collective waves.

The *monopole* term in (5.16), $\lambda = 0$, describes the *breathing mode* with changing density. Owing to the incompressibility of nuclear matter, such excitations require high energy. For low-energy excitations, we can approximately consider the density and consequently the total volume as a constant. This condition determines the monopole variable α_{00} in terms of all other variables. Consider the small amplitude motion of the surface around the spherical equilibrium. The volume of the slightly deformed sphere, $R = R(\theta, \varphi)$, is equal to ($d\Omega$ is the element of solid angle)

$$V = \int d\Omega \int_0^{R(\theta, \varphi)} dr r^2 = \frac{1}{3} \int d\Omega R^3(\theta, \varphi). \quad (5.22)$$

With the expansion (5.8) substituted into Eq. (5.22), we need to calculate the integrals of the products of spherical functions. In the small amplitude case, we neglect the terms of the third order in amplitudes $\alpha_{\lambda\mu}$ and use the orthogonality of the spherical functions to get

$$V = \frac{R_0^3}{3} \left(4\pi + 3\sqrt{4\pi} \alpha_{00} + 3 \sum_{\lambda\mu} |\alpha_{\lambda\mu}|^2 \right). \quad (5.23)$$

An excitation keeps the volume $(4\pi/3)R_0^3$ unchanged if the following condition is fulfilled:

$$\alpha_{00} = -\frac{1}{\sqrt{4\pi}} \sum_{\lambda\mu} |\alpha_{\lambda\mu}|^2. \quad (5.24)$$

Hence, for an incompressible drop, the monopole amplitude is of the second order, and its own contribution to the sum in the right-hand side of (5.23) can be neglected in this approximation.

The *multipole moments* of the charge or matter distribution are originally defined, Eq. (2.54), through the corresponding density ρ as

$$\mathcal{M}_{\lambda\mu} = \int d^3r \rho(\mathbf{r}) r^\lambda Y_{\lambda\mu}(\mathbf{n}). \quad (5.25)$$

In our model, the multipole moments (5.25) become collective dynamic variables expressed in terms of $\alpha_{\lambda\mu}$. Again assuming the smallness of $\alpha_{\lambda\mu}$ and integrating as in Eqs. (5.22) and (5.23), we obtain

$$\mathcal{M}_{\lambda\mu} = \rho R_0^{\lambda+3} \alpha_{\lambda\mu}^*, \quad (5.26)$$

that is, in the small amplitude limit, the deformation parameters $\alpha_{\lambda\mu}$ are in fact collective multipole moments. Since the density is normalized according to $\int d^3r \rho = A$, Eq. (5.26) can be rewritten as

$$\mathcal{M}_{\lambda\mu} = \frac{3}{4\pi} A R_0^\lambda \alpha_{\lambda\mu}^*. \quad (5.27)$$

For the charge density we obtain, instead of (5.27), the *electric multipole* moments,

$$\mathcal{M}(E\lambda, \mu) = \frac{3}{4\pi} Ze R_0^\lambda \alpha_{\lambda\mu}^*. \quad (5.28)$$

The $\lambda = 1$ integrals in Eq. (5.25) are nothing but the spherical components of the center-of-mass vector,

$$\mathbf{R} = \int d^3r \rho(\mathbf{r}) \mathbf{r}. \quad (5.29)$$

This means that the amplitudes $\alpha_{1\mu}$ are the coordinates of the small displacement of the center of mass. They are not related to physical excitations and represent a *ghost*, or *spurious*, mode. We set them equal to zero. We have already discussed in Section 2.7 that only the isovector part of the dipole moment can induce physical excitations. The definitions started with Eq. (5.25) contain only isoscalar quantities.

The first genuine excitation modes in this scheme are associated with the *quadrupole* and *octupole* degrees of freedom, $\lambda = 2$ and $\lambda = 3$, respectively. Almost all even–even nuclei have the first excited states with $J^\pi = 2^+$. As a rule, these states have a relatively large intensity of the quadrupole (E2) radiation transition to the ground state 0^+ . There are many examples of the low-lying 3^- states with strong octupole (E3) transitions to the ground state. The enhancement of the radiative transition probability implies coherent motion of many particles and correspondingly *collective* character of the transition, in line with our collective model. Making more specific assumptions, we can evaluate the corresponding frequencies.

5.5 Kinetic Energy and Inertial Parameters

The mass formula does not contain any information concerning the inertial properties of the shape variables. The inertial parameters turn out to be sensitive to interactions inside the system and can be calculated from general physical arguments only in special cases (e.g., according to the *Galilean invariance*, the mass parameter related to the nonrelativistic translational motion of the system as a whole is equal to the total mass M regardless of the details of the interactions).

As a natural first attempt, we use the *hydrodynamic model* to find the kinetic energy and inertial parameters related to the time dependence $\alpha_{\lambda\mu}(t)$. We assume that the *velocity field* $\mathbf{v}(\mathbf{r}, t)$ is *irrotational*,

$$\operatorname{curl} \mathbf{v} = 0. \quad (5.30)$$

There are several arguments in favor of this idea. In normal fluids, creation of vortices requires additional energy so that we can expect the irrotational flow in the lowest part of the excitation spectrum. The second argument, related to quantum mechanics, refers to the current defined in terms of the wave function and its gradient. If it makes sense to speak about the *macroscopic wave function* $\Psi(\mathbf{r}, t)$ of the whole system [QP, I, 14.2], we can consider the corresponding current \mathbf{j} and, introducing the real amplitude and phase instead of the complex wave function,

$$\Psi(\mathbf{r}, t) = \sqrt{\rho(\mathbf{r}, t)} e^{(i/\hbar)\phi(\mathbf{r}, t)}, \quad (5.31)$$

express the mass current in a hydrodynamic form,

$$M\mathbf{j} = \rho \nabla \phi. \quad (5.32)$$

Then we can identify

$$\mathbf{v} = \nabla \phi \quad (5.33)$$

that implies the irrotational flow (5.30) if the phase $\phi(\mathbf{r}, t)$, which plays the role of the *potential* for the velocity field, is a single-valued function of coordinates.

A weak point of this derivation is the possibility to model the wave function of the many-body system by a collective wave function depending on one coordinate \mathbf{r} only. In fact, nuclei are far away from this limiting behavior characterizing an *ideal superfluid*. Collective motion is associated with virtual coherent excitation of single-particle degrees of freedom, and the hydrodynamic approach assumes their local equilibration. In reality, the single-particle motion does exist in nuclei being the basis of the shell model. Therefore, the hydrodynamic model can serve only as a guideline based on the symmetry properties of a drop while its quantitative estimates might be unrealistic.

Still it is instructive to look at what follows from the hypothesis of the irrotational flow (5.30). For the incompressible fluid, the continuity equation reduces to

$$M \operatorname{div} \mathbf{j} = 0 = \rho \operatorname{div} \mathbf{v}. \quad (5.34)$$

Therefore, the velocity potential ϕ satisfies the Laplace equation

$$\nabla^2 \phi = 0. \quad (5.35)$$

The solution has to be regular at the origin. At the surface of the drop given at each moment by Eq. (5.16) with time-dependent amplitudes $\alpha_{\lambda\mu}(t)$, the radial component of the gradient of the potential (5.33) must coincide with the radial velocity of the surface,

$$(v_r)_{\text{surf}} = \left(\frac{\partial \phi}{\partial r} \right)_{\text{surf}} = \frac{\partial R(\theta, \varphi)}{\partial t}. \quad (5.36)$$

The surface velocity is a sum of the terms containing the *collective velocities* $\dot{\alpha}_{\lambda\mu}(t)$.

At the origin, the regular solution of the Laplace equation is

$$\phi(\mathbf{r}) = \sum_{\lambda\mu} \phi_{\lambda\mu} \left(\frac{r}{R_0} \right)^{\lambda} Y_{\lambda\mu}(\mathbf{n}). \quad (5.37)$$

Here the sum includes multipolarities $\lambda \geq 2$ because the monopole excitation is excluded by the assumption of incompressibility, and the ghost dipole translation is irrelevant for our purposes. The complex amplitudes $\phi_{\lambda\mu}$ have the same conjugation properties as in (5.17). They are to be found from the boundary condition (5.36) taken, in the small amplitude approximation, at the unperturbed surface $r = R_0$. For each multipolarity $\lambda \geq 2$, we obtain

$$\phi_{\lambda\mu} = \frac{1}{\lambda} R_0^2 \dot{\alpha}_{\lambda\mu}. \quad (5.38)$$

The kinetic energy of the perfect fluid is (here we need the mass density $M\rho$)

$$K = \frac{M}{2} \int d^3r \rho \mathbf{v}^2. \quad (5.39)$$

We calculate it using $\rho = \text{constant}$ inside the surface and the solution for the velocity field from Eqs. (5.33), (5.37), and (5.38). First, we have

$$K = \frac{M\rho}{2} \int d^3r (\nabla \phi)^2 = \frac{M\rho}{2} \int d^3r \nabla(\phi \nabla \phi), \quad (5.40)$$

where the Laplace equation (5.35) was taken into account. The volume integral (5.40) can be transformed to the surface integral. Since the integrand is already the quantity of

the second order in amplitudes, which are treated as small, the surface again is that of the unperturbed sphere $R = R_0$, and the normal component of \mathbf{v} is $\partial\phi/\partial r$,

$$K = \frac{M\rho}{2} \int d\mathcal{A} \cdot (\phi \nabla \phi) = \frac{M\rho R_0^2}{2} \int do \left(\phi \frac{\partial \phi}{\partial r} \right)_{\text{surf}}. \quad (5.41)$$

Finally, using the expansion (5.37) with the coefficients (5.38) and integrating over angles, we get

$$K = \frac{1}{2} \sum_{\lambda\mu} B_\lambda |\dot{\alpha}_{\lambda\mu}|^2, \quad (5.42)$$

where the *mass (inertia) parameters* are

$$B_\lambda = \frac{M}{\lambda} \rho R_0^5. \quad (5.43)$$

Introducing the mean square velocity of the surface in a mode with given λ ,

$$\overline{(v^2)_\lambda} = \int \frac{do}{4\pi} (\dot{R}^2)_\lambda = \frac{R_0^2}{4\pi} \sum_\mu |\dot{\alpha}_{\lambda\mu}|^2, \quad (5.44)$$

we can write the kinetic energy for the λ -mode as

$$K_\lambda = \frac{3}{2\lambda} M A \overline{(v^2)_\lambda}. \quad (5.45)$$

The kinetic energy (5.42) is our first example of the *collective Hamiltonian*. This is a part of the total Hamiltonian of the system derived in the approximation of decoupling between the collective mode and remaining, intrinsic, degrees of freedom. The form of Eq. (5.42) is more general than the model we used; the specific features of the model enter via the mass parameters B_λ . Kinetic energy is usually the quadratic form in the velocities, the rotational invariance leads to the sum $\sum_\mu |\dot{\alpha}_{\lambda\mu}|^2$ with coefficients B_λ that cannot depend on μ but can be different for different modes λ and depend on the invariants built of the coordinates $\alpha_{\lambda\mu}$. For small deformations around the spherical shape, as it was accepted in the above derivation, the coefficients are to be calculated at the equilibrium, that is, they do not depend on the coordinates. The situation would be more complicated for the deformed ground state. In this case, the unperturbed shape is characterized by the tensors of static deformation, and the general rotationally invariant quadratic form would be

$$K = \frac{1}{2} \sum_{\lambda\lambda'\mu\mu'} B_{\lambda\mu,\lambda'\mu'} \dot{\alpha}_{\lambda\mu}^* \dot{\alpha}_{\lambda'\mu'}, \quad (5.46)$$

where the mass parameters form a tensor built of the coordinates in such a way that makes the whole operator (5.46) rotationally invariant.

5.6 Shape Vibrations

The time-dependent distortion of the equilibrium nuclear shape is limited by a *restoring force*. Assuming small deviations from the equilibrium, we can calculate the emerging force in the linear approximation. This leads to the potential energy U being quadratic

in coordinates. For a spherical ground state shape, the same arguments of rotational invariance define

$$U = \frac{1}{2} \sum_{\lambda\mu} C_\lambda |\alpha_{\lambda\mu}|^2. \quad (5.47)$$

Along with kinetic energy (5.42), this expression forms the classical Hamiltonian of shape variables in the small amplitude approximation.

To bring the Hamiltonian to its traditional form, we introduce *collective momenta*,

$$\pi_{\lambda\mu} = B_\lambda \dot{\alpha}_{\lambda\mu}, \quad (5.48)$$

and rewrite the Hamiltonian as

$$H = \frac{1}{2} \sum_{\lambda\mu} \left\{ \frac{1}{B_\lambda} |\pi_{\lambda\mu}|^2 + C_\lambda |\alpha_{\lambda\mu}|^2 \right\}. \quad (5.49)$$

The Hamilton equations of motion are

$$\dot{\alpha}_{\lambda\mu} = \frac{\partial H}{\partial \pi_{\lambda\mu}^*} = \frac{1}{B_\lambda} \pi_{\lambda\mu}, \quad (5.50)$$

which is the definition (5.48) of $\pi_{\lambda\mu}$, and

$$\dot{\pi}_{\lambda\mu} = -\frac{\partial H}{\partial \alpha_{\lambda\mu}^*} = -C_\lambda \alpha_{\lambda\mu}. \quad (5.51)$$

The canonically conjugate coordinates for $\pi_{\lambda\mu}$ are $\alpha_{\lambda\mu}^*$ (and the conjugate momenta for $\alpha_{\lambda\mu}$ are $\pi_{\lambda\mu}^*$) because of their properties as tensor operators. The spherical functions $Y_{\lambda\mu}$ raise the angular momentum projection, $\Delta M = \mu$. The same is valid for the multipole operators (5.25), and, according to (5.26), for the conjugate coordinate $\alpha_{\lambda\mu}^*$. The equations of motion for $\alpha_{\lambda\mu}$ and $\pi_{\lambda\mu}$ are constructed in such a way that their right- and left-hand sides have the same selection rules, namely $\Delta M = -\mu$, they lower the angular momentum projection. It is important to observe such phase relationships in all equations.

Each excitation $(\lambda\mu)$ is now presented as a normal mode of *harmonic vibrations*. In the approximation of small amplitudes, the modes are completely decoupled. Although we used classical Hamilton equations, here the quantization is trivial because the Heisenberg equations of motion for quantum operators look exactly the same in the case of harmonic oscillators. We come to this question later introducing the secondary quantization (Chapter 11).

The shape vibrations described by the Hamiltonian (5.49) have the spectrum of frequencies

$$\omega_\lambda = \sqrt{\frac{C_\lambda}{B_\lambda}}. \quad (5.52)$$

The spectrum is *degenerate* because the frequency is the same for all projections μ at a given λ (different orientations of the angular momentum carried by a surface wave). This is a consequence of spherical symmetry of the equilibrium state. The solution of equations of motion is a superposition of $\cos \omega_\lambda t$ and $\sin \omega_\lambda t$, or $\exp(\pm i\omega_\lambda t)$, defined by the initial conditions. The system is stable if all frequencies are real. Otherwise one of

the solutions will indefinitely grow with time. The stability should be guaranteed by the *positive* restoring force C_λ .

5.7 Stability of the Charged Spherical Liquid Drop

To calculate the restoring force, we have to know the potential energy landscape as a function of shape variables. This is a very complicated problem of quantum dynamics. However, in the LDM, it can be relatively easily solved if we assume that the mass formula is valid not only for ground state binding energies but also in the process of deformation.

It is already mentioned, Eq. (5.15), that the multipolarity of deformation should be low in order to apply the LDM or any collective model. If the deformation is small, it cannot be locally distinguished from the common change of the radius. Therefore, the change of the surface energy should be described by the same surface tension (5.4) as in the global surface energy. Any deviation from the spherical shape at fixed volume increases the surface area and surface energy. Thus, the surface tension always provides us with the restoring force.

In contrast to the surface energy, the electrostatic repulsion prefers the deformation that would increase distances between the charge elements. In heavy nuclei, the gain of Coulomb energy (5.8) becomes comparable with the loss of surface energy. Their balance defines the stability of the drop. Too heavy nuclei cannot be stable because of too strong Coulomb repulsion. In the following Problems we present straightforward but rather lengthy calculations of the change of energy associated with the deformation parameterized by the shape variables $\alpha_{\lambda\mu}$. Such calculations were originally carried out for a classical charged drop by Rayleigh in his seminal book on *The Theory of Sound* in 1877 [4]. (By the way, there are also examples of inaccurate calculations in the literature, still usually with the correct final answer.)

Problem 5.4 Find the restoring force C_λ^{surf} due to the surface tension.

Solution

In the approximation of small amplitudes, we neglect all terms of higher than second order in $\alpha_{\lambda\mu}$. The first-order terms vanish as always at the equilibrium. The only nonzero linear term is related to the monopole deformation α_{00} , but due to the volume conservation it is also effectively of the second order, Eq. (5.24).

We have to calculate the change of the surface area under a small deformation described by the radius (5.16). The general recipe of differential geometry gives the surface area parameterized by the angular coordinates θ and φ as an integral

$$S = \int \sqrt{g} d\theta d\varphi, \quad (5.53)$$

where g is the determinant of the metric tensor $g_{ik} = g_{ki}$ that expresses the length element dl on the surface,

$$dl^2 = g_{\theta\theta} d\theta^2 + 2g_{\theta\varphi} d\theta d\varphi + g_{\varphi\varphi} d\varphi^2. \quad (5.54)$$

In spherical polar coordinates R, θ, φ

$$dl^2 = dR^2 + R^2 d\theta^2 + R^2 \sin^2 \theta d\varphi^2. \quad (5.55)$$

Here the radius $R(\theta, \varphi)$ is to be taken on the surface (5.16) so that

$$dR = (\partial R / \partial \theta) d\theta + (\partial R / \partial \varphi) d\varphi, \quad (5.56)$$

and the length element is

$$dl^2 = \left[R^2 + \left(\frac{\partial R}{\partial \theta} \right)^2 \right] d\theta^2 + \left[R^2 \sin^2 \theta + \left(\frac{\partial R}{\partial \varphi} \right)^2 \right] d\varphi^2 + 2 \frac{\partial R}{\partial \theta} \frac{\partial R}{\partial \varphi} d\theta d\varphi. \quad (5.57)$$

The standard mathematical notation is

$$dl^2 = E d\theta^2 + G d\varphi^2 + 2Fd\theta d\varphi, \quad (5.58)$$

then the determinant we need in Eq. (5.53) is given by

$$g = EG - F^2 = R^4 \sin^2 \theta \left\{ 1 + \frac{1}{R^2} \left[\left(\frac{\partial R}{\partial \theta} \right)^2 + \frac{1}{\sin^2 \theta} \left(\frac{\partial R}{\partial \varphi} \right)^2 \right] \right\}. \quad (5.59)$$

Finally, the area of the deformed surface is expressed by the integral (5.53),

$$S = \int d\theta d\varphi R^2 \sin \theta \sqrt{1 + \frac{1}{R^2} \left[\left(\frac{\partial R}{\partial \theta} \right)^2 + \frac{1}{\sin^2 \theta} \left(\frac{\partial R}{\partial \varphi} \right)^2 \right]}, \quad (5.60)$$

where we have to use the function $R(\theta, \varphi)$ from (5.16).

The deviations from the sphere are assumed to be small,

$$R = R_0 [1 + f(\theta, \varphi)], \quad f(\theta, \varphi) \ll 1. \quad (5.61)$$

Expanding the integrand \sqrt{g} in Eq. (5.60) in powers of f up to the second order, we get

$$\sqrt{g} \approx R_0^2 \sin \theta \left\{ (1 + f)^2 + \frac{1}{2} \left[\left(\frac{\partial f}{\partial \theta} \right)^2 + \frac{1}{\sin^2 \theta} \left(\frac{\partial f}{\partial \varphi} \right)^2 \right] \right\}. \quad (5.62)$$

Here $R_0^2 \sin \theta$ along with the differentials of the angles forms a standard element of a spherical area $R_0^2 d\Omega$ covered by the solid angle $d\Omega = \sin \theta d\theta d\varphi$. The integral of $(1 + f)^2$, due to the orthogonality of spherical functions, reduces to

$$R_0^2 \int d\Omega (1 + f)^2 = R_0^2 \left[4\pi + 2\sqrt{4\pi} \alpha_{00} + \sum_{\lambda\mu} |\alpha_{\lambda\mu}|^2 \right]. \quad (5.63)$$

The first term in square brackets gives the unperturbed area S_0 of the sphere. The second term contains the monopole amplitude which, due to the condition of the volume conservation, is actually of second order, Eq. (5.24). Therefore

$$R_0^2 \int d\Omega (1 + f)^2 = S_0 - R_0^2 \sum_{\lambda\mu} |\alpha_{\lambda\mu}|^2. \quad (5.64)$$

The remaining terms in Eq. (5.62) can be written with the aid of the *angular gradient* operator ∇ . Their contribution to the area is

$$\frac{R_0^2}{2} \int d\Omega (\nabla f)^2 = \frac{R_0^2}{2} \int d\Omega [\nabla(f\nabla f) - f\nabla^2 f]. \quad (5.65)$$

The first term in Eq. (5.65) vanishes because of the periodicity of spherical functions. For the second term, we recall that the angular part of the Laplace operator is, with the opposite sign, proportional to the square of the angular momentum operator, and the spherical functions are its eigenfunctions,

$$\nabla^2 Y_{\lambda\mu} = -\lambda(\lambda+1)Y_{\lambda\mu}. \quad (5.66)$$

Using again the orthogonality, we come finally to

$$S = S_0 + R_0^2 \sum_{\lambda\mu} \left[\frac{\lambda(\lambda+1)}{2} - 1 \right] |\alpha_{\lambda\mu}|^2 = S_0 + \frac{R_0^2}{2} \sum_{\lambda\mu} (\lambda-1)(\lambda+2) |\alpha_{\lambda\mu}|^2. \quad (5.67)$$

As expected, the deformation increases the surface area, except for the case $\lambda = 1$, which corresponds to the displacement as a whole with no distortion. If the surface energy is written as

$$E_S = \sigma S = \sigma S_0 + \frac{1}{2} \sum_{\lambda\mu} C_\lambda^{\text{surf}} |\alpha_{\lambda\mu}|^2, \quad (5.68)$$

the restoring force for the multipolarity λ is found as

$$C_\lambda^{\text{surf}} = (\lambda-1)(\lambda+2)\sigma R_0^2. \quad (5.69)$$

As a result, the change of the surface area in the λ -mode gives rise to the restoring force parameter of the order

$$\sigma \overline{[(R - R_0)^2]} \sim \sigma R_0^2 \sum_{\mu} |\alpha_{\lambda\mu}|^2. \quad (5.70)$$

As it should be, $C_\lambda^{\text{surf}} > 0$.

Problem 5.5 Find the change of the electrostatic energy under small deformation of the liquid drop.

Solution

The Coulomb energy for the charge density $\rho(\mathbf{r})$ is given by the integral

$$E_C = \frac{1}{2} \int d^3r \rho \phi, \quad (5.71)$$

where $\phi(\mathbf{r})$ is the corresponding electrostatic potential

$$\phi(\mathbf{r}) = \int d^3r' \frac{\rho(\mathbf{r}')}{|\mathbf{r} - \mathbf{r}'|}. \quad (5.72)$$

The density is normalized to the total charge,

$$\int d^3r \rho = eZ. \quad (5.73)$$

In the uniformly charged unperturbed sphere of radius R_0 , the charge density is angle independent and can be written with the help of the step function $\Theta(r - R_0)$ equal to 1 for $0 < r < R_0$ and 0 for $r > R_0$,

$$\rho(\mathbf{r}) = \rho_0 \Theta(r - R_0), \quad \rho_0 = \frac{3eZ}{4\pi R_0^3}. \quad (5.74)$$

After the sphere has been deformed according to (5.16), the density of the incompressible fluid has got the same value ρ_0 but within the region with the boundary (5.61),

$$\rho(\mathbf{r}) = \rho_0 \Theta(r - R_0 - R_0 f). \quad (5.75)$$

Considering again small deformations f and using the derivative of the step function $\Theta'(x) = -\delta(x)$, we can formally present the new charge density as

$$\rho(\mathbf{r}) \approx \rho_0 \Theta(r - R_0) + \rho^{(1)} + \rho^{(2)}, \quad (5.76)$$

where the first- and second-order variations are, respectively,

$$\rho^{(1)} = \rho_0 (-R_0 f)(-\delta(r - R_0)) = \rho_0 R_0 f \delta(r - R_0), \quad (5.77)$$

and

$$\rho^{(2)} = -\frac{1}{2} \rho_0 (R_0 f)^2 \delta'(r - R_0). \quad (5.78)$$

Similar to the expansion (5.78), we expand the potential:

$$\phi = \phi_0 + \phi^{(1)} + \phi^{(2)}, \quad (5.79)$$

where, as in (5.72), each term corresponds to its counterpart in the expansion of the charge density (5.78).

Now we are looking for the expansion of the electrostatic energy (5.71) up to the second order,

$$E_C = \frac{1}{2} \int d^3 r \left\{ \rho_0 \phi_0 + [\rho^{(1)} + \rho^{(2)}] \phi_0 + \rho_0 [\phi^{(1)} + \phi^{(2)}] + \rho^{(1)} \phi^{(1)} \right\}, \quad (5.80)$$

or, due to the symmetry which follows from the correspondence between ρ and ϕ , Eq. (5.80),

$$E_C = \int d^3 r \left\{ \frac{1}{2} [\rho_0 \phi_0 + \rho^{(1)} \phi^{(1)}] + [\rho^{(1)} + \rho^{(2)}] \phi_0 \right\}. \quad (5.81)$$

Let us first calculate the integral

$$I = \int d^3 r (\rho^{(1)} + \rho^{(2)}) \phi_0. \quad (5.82)$$

Since the unperturbed potential is spherically symmetric, the angular integration is trivial with the use of the expansion (5.16),

$$I = \rho_0 \int dr r^2 \phi_0(r) \left[\delta(r - R_0) R_0 \sqrt{4\pi} \alpha_{00} - \frac{1}{2} \delta'(r - R_0) R_0^2 \sum_{\lambda\mu} |\alpha_{\lambda\mu}|^2 \right]. \quad (5.83)$$

Two terms here are related by the volume preservation (5.24), so that

$$I = \sqrt{4\pi} \alpha_{00} \rho_0 R_0 \int dr r^2 \phi_0(r) \left[\delta(r - R_0) + \frac{R_0}{2} \delta'(r - R_0) \right]. \quad (5.84)$$

Using the properties of the delta-function, we obtain

$$\int dr r^2 \phi_0 \delta'(r - R_0) = - \int dr \delta(r - R_0) \frac{d}{dr} (r^2 \phi_0), \quad (5.85)$$

and, with the unperturbed potential on the surface, $\phi_0(R_0) = Ze/R_0$, and the unperturbed charge density (5.74),

$$I = \frac{1}{2} \sqrt{4\pi} \alpha_{00} \rho_0 R_0^2 Ze = \frac{3}{8\pi} \sqrt{4\pi} \alpha_{00} \frac{(Ze)^2}{R_0}. \quad (5.86)$$

Another integral we need to calculate is

$$I' = \frac{1}{2} \int d^3r \rho^{(1)} \phi^{(1)}. \quad (5.87)$$

The first-order density correction (5.77) appears only at the unperturbed surface $r = R_0$. Therefore, in the expression of the potential according to (5.72), both radial arguments r and r' are equal to R_0 . Using the standard multipole expansion,

$$\frac{1}{|\mathbf{r} - \mathbf{r}'|} = \sum_{\lambda\mu} \frac{4\pi}{2\lambda + 1} \frac{r_\lambda^\lambda}{r_\lambda^{\lambda+1}} Y_{\lambda\mu}(\mathbf{r}) Y_{\lambda\mu}^*(\mathbf{r}'), \quad (5.88)$$

we come to

$$I' = \frac{1}{2} \rho_0^2 R_0^5 \sum_{\lambda\mu} \frac{4\pi}{2\lambda + 1} |\alpha_{\lambda\mu}|^2. \quad (5.89)$$

Combining Eqs. (5.86) and (5.89), we find the change of the Coulomb energy due to the deformation,

$$\delta E_C = -\frac{3}{4\pi} \frac{(Ze)^2}{R_0} \sum_{\lambda\mu} \frac{\lambda - 1}{2\lambda + 1} |\alpha_{\lambda\mu}|^2. \quad (5.90)$$

Electrostatic repulsion energy favors deformation; again the dipole displacement, $\lambda = 1$, does not influence the energy balance. The Coulomb force parameter in the collective Hamiltonian is found to be

$$C_\lambda^{\text{Coul}} = -\frac{3}{2\pi} \frac{(Ze)^2}{R_0} \frac{\lambda - 1}{2\lambda + 1} = -\frac{5(\lambda - 1)}{2\pi(2\lambda + 1)} E_C. \quad (5.91)$$

This change in the λ -mode is of the order of

$$\frac{Z^2 e^2}{R_0} \frac{[(R - R_0)/R_0]^2}{[(R - R_0)/R_0]^2} \sim \frac{Z^2 e^2}{R_0} \sum_{\mu} |\alpha_{\lambda\mu}|^2. \quad (5.92)$$

The calculation of the change in Coulomb energy assumed the uniform charge distribution within the distorted surface with a sharp edge. The diffuseness of the nuclear surface changes the total energy but practically does not change the elastic properties and the magnitude of the restoring force.

Combining the surface and Coulomb energies, we obtain the full macroscopic restoring force for the multipolarity λ ,

$$C_\lambda = C_\lambda^{\text{surf}} + C_\lambda^{\text{Coul}} = \frac{\lambda - 1}{4\pi} \left[(\lambda + 2)E_S - \frac{10}{2\lambda + 1} E_C \right]. \quad (5.93)$$

From here we predict the point of absolute instability of a spherical drop against the deformation of multipolarity λ : the vibrational frequency (5.52) of the λ -mode goes to zero if the Coulomb energy reaches the critical value

$$E_C^{\text{crit}} = \frac{(2\lambda + 1)(\lambda + 2)}{10} E_S. \quad (5.94)$$

The first instability occurs for the quadrupole mode, $\lambda = 2$, at

$$E_C = 2E_S. \quad (5.95)$$

Equation (5.95) determines the *critical fissility*:

$$\frac{3}{5} \frac{e^2}{r_c} \frac{Z^2}{A^{1/3}} = 2b_S A^{2/3} \Leftrightarrow x_{\text{crit}} \equiv \left(\frac{Z^2}{A} \right)_{\text{crit}} = \frac{10 b_S}{3(e^2/r_c)} \approx 49, \quad (5.96)$$

where the numerical value corresponds to the standard parameters of the mass formula. Heavy nuclei are already rather close to the limit (5.96). For example, $x(^{238}\text{U}) = 35.5$, $x(^{244}\text{Cf}) = 39.3$.

Problem 5.6 Derive the equation $Z = Z_s(A)$ for the charge Z_s of the most stable nucleus at a given mass number A . Find maximum values of Z and A for which a nucleus on the valley of beta-stability is still stable with respect to fission.

Solution

The most stable isobar for given A corresponds to the minimum mass,

$$\left(\frac{\partial M(Z, A)}{\partial Z} \right)_A = 0. \quad (5.97)$$

With the standard values of the coefficients in the mass formula, this gives

$$Z = \frac{A}{1.97 + 0.015 A^{2/3}}. \quad (5.98)$$

The fission instability corresponds to the conditions (5.95) and (5.96). Combining the critical value of the fissility parameter x with the path along the line of stability (5.98), we find $A = 368$, $Z = 135$. In fact, the observed superheavy nuclei (the heaviest confirmed case corresponds to $Z = 118$) decay by alpha-emission.

Problem 5.7 For $A = 20, 40, 80, 120, 200$, predict the beta-stable elements and compare the result with the data.

Solution

Using (5.98) and taking into account the pairing term in the semiempirical mass formula, we obtain

A	$Z(\text{prediction})$	$Z(\text{exp})$	
20	10	10	Ne
40	18	18, 20	Ar, Ca
80	36	34, 36	Se, Kr
120	52	50, 52	Sn, Te
200	80	80	Hg

We have found that spherical superheavy nuclei with a large ratio x of Coulomb to surface energy would be absolutely unstable with respect to quadrupole deformation. Once started, the deformation will increase pulling the nucleus toward the region of large

values of the shape parameters α . Then our analysis based on the linear approximation to the equations of motion becomes invalid. The consideration can be extended to the region of large deformations. It allows one to find the shape of the potential energy that shows the potential barrier at $x < x_{\text{crit}}$ and the steep descent at $x > x_{\text{crit}}$.

This consideration qualitatively explains nuclear *fission* that is, according to the mass formula, energetically possible long before the critical point but delayed by the potential barrier. Although the total energy of two separated spheres with particle numbers A_1 and A_2 and charges Z_1 and Z_2 can be lower than the total energy of the nucleus with $A = A_1 + A_2$ and $Z = Z_1 + Z_2$, the fission process is connected with *tunneling* of large fragments through the potential barrier and therefore it is very slow. It can be accelerated if started not spontaneously from the ground state but by nuclear excitation that brings the energy of the nucleus to the vicinity of the top of the barrier or higher (*induced fission*). However, the specific predictions of the barrier shape in the LDM are not quite reliable because the quantum shell effects can create new potential wells at large deformations.

In the subcritical region, the LDM predicts shape vibrations with the frequencies (5.52). If the surface contribution is much larger than that of Coulomb repulsion, the energy of the first excited state 2_1^+ of the harmonic oscillator corresponding to $\lambda = 2$ is

$$E(2_1^+) = \hbar\omega_2 \approx \hbar\sqrt{\frac{32\pi}{3} \frac{\sigma}{AM}} \approx \frac{36}{\sqrt{A}} \text{ MeV}. \quad (5.99)$$

This energy is a smooth function of the mass number; the $A^{-1/2}$ dependence is characteristic for the *surface modes*. The comparison with the abundant experimental data on the low-lying 2^+ states shows a different picture, Figure 5.3.

The energies of the first 2^+ states are significantly lower than those predicted by the LDM. Only in ^{208}Pb we find that $E(2_1^+) = 4.1$ MeV is higher than 2.5 MeV predicted by

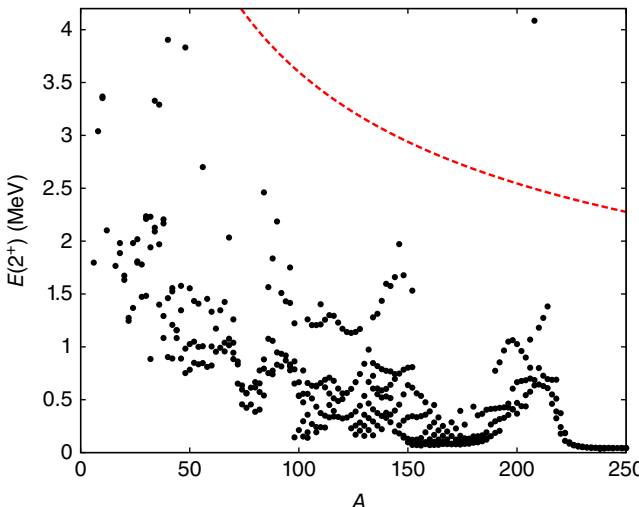


Figure 5.3 Energies of the first 2^+ states in stable even–even nuclei as a function of the nuclear mass. Dashed red line shows prediction in Eq. (5.99).

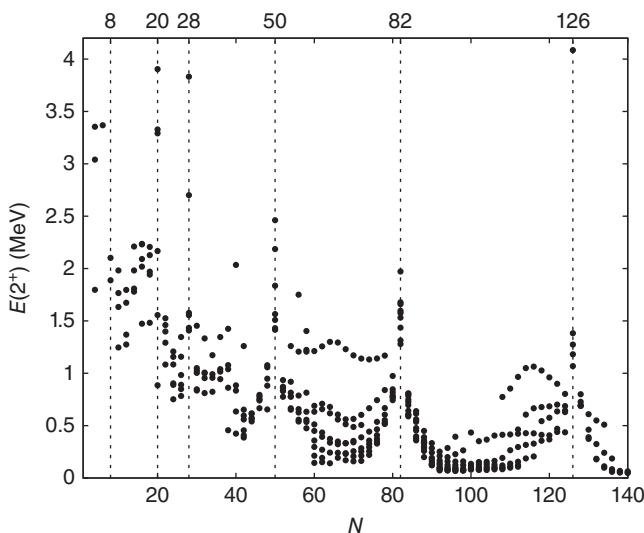


Figure 5.4 Energies of the first 2^+ states in stable even–even nuclei as a function of the neutron number.

Eq. (5.99). It is even more interesting to know that the energy $E(2_1^+)$ clearly displays the oscillatory behavior along the nuclear chart (see Figure 5.4). This modulation of the average decrease can be explained by the quantum shell effects, obviously outside of the LDM framework, and by residual interactions beyond the mean field picture.

We have to stress that we discussed here the classical version of the LDM and the corresponding observables. The new development is mainly directed to the readjustement of this approach for nuclei far from stability, astrophysical processes, and so on [5–9].

References

- 1 K. Heyde, *Basic Ideas and Concepts in Nuclear Physics*, Institute of Physics, Bristol, 2004.
- 2 M.Ya. Amusia and Y. Kornyushin, Contemp. Phys. **41**, 219 (2000).
- 3 M.V. Kirson, Nucl. Phys. **A798**, 29 (2004).
- 4 J.W.S. Rayleigh, *The Theory of Sound*, Vols I and II, Cambridge University Press, Cambridge, MA, 2011.
- 5 P. Danielewicz, Nucl. Phys. **A727**, 233 (2003).
- 6 A.S. Botvina and I.N. Mishustin, Nucl. Phys. **A843**, 98 (2010).
- 7 M.B. Tsang *et al.*, Phys. Rev. C **86**, 015803 (2012).
- 8 S. Furusawa, K. Sumiyoshi, S. Yamada, and H. Suzuki, Astrophys. J. **772**, 1 (2013).
- 9 F. Sammarruca, Symmetry **6**, 851 (2014).

6

Vibrations of a Spherical Nucleus

... we start by considering the macroscopic collective motions of the system, and we introduce the degrees of freedom completely phenomenologically.

S.T. Belyaev, *Collective Excitations in Nuclei*.

6.1 Sound Waves

We discussed the simplest vibrational excitations of the incompressible nuclear drop as *surface waves*. The next step in the application of hydrodynamic concepts to nuclei is related to the propagation of the sound waves *in the nuclear volume*. Since the normal sound waves are propagating oscillations of density ρ and pressure P , we need to lift the assumption of incompressibility.

We again limit ourselves to the low amplitude waves assuming the small deviations of density, $\delta\rho$, and pressure, δP , from their equilibrium values, ρ and

$$P = -\frac{\partial E}{\partial V}. \quad (6.1)$$

The continuity equation for these small quantities can be written as

$$\frac{\partial \delta\rho}{\partial t} + \rho \operatorname{div} \mathbf{v} = 0, \quad (6.2)$$

whereas the equation of motion for a fluid element takes a form

$$M\rho \frac{\partial \mathbf{v}}{\partial t} = -\nabla P. \quad (6.3)$$

By introducing the speed of sound as

$$c_s^2 = \frac{1}{M} \frac{\partial P}{\partial \rho}, \quad (6.4)$$

two linearized equations (6.2) and (6.3) lead to the wave equation

$$\frac{1}{c_s^2} \frac{\partial^2 \delta\rho}{\partial t^2} - \nabla^2 \delta\rho = 0. \quad (6.5)$$

If our discussion is limited to the low-lying excitations, we can consider a nucleus at temperature close to zero. Then it does not matter whether the derivative in Eq. (6.4) is taken for an adiabatic or isothermal process (the specific heat at constant volume or

at constant pressure is the same at zero temperature). For the same reason, in Eq. (6.1) we used energy instead of thermodynamic free energy. Unfortunately, up to now, the compressibility of nuclear matter and therefore the speed of sound are not known with sufficient accuracy.

To solve the wave equation (6.5), we need to impose the appropriate boundary condition on the nuclear surface. In the linear approximation, we still consider this surface to be spherical, $R = R_0$. The stationary solution $\sim \exp(-i\omega t)$ with a certain frequency ω can be found with arbitrary angular symmetry ($\lambda\mu$) corresponding to a wave with an angular momentum λ and its projection μ . The separation of angular variables using spherical functions $Y_{\lambda\mu}$ gives the same equation for the radial part as the Schrödinger equation for free motion with the wave number $k = \omega/c_s$. The standard solution is given by the spherical Bessel function $j_\lambda(kr)$ regular at the origin. Thus, we can write down the solution for each λ -mode as

$$\delta\rho_{\lambda\mu}(\mathbf{r}, t) = A_{\lambda\mu}\rho j_\lambda(kr)Y_{\lambda\mu}(\mathbf{n})e^{-i\omega t}. \quad (6.6)$$

The gradient of the function (6.6) determines, according to (6.3), the velocity field in the sound wave. The dimensionless amplitudes $A_{\lambda\mu}$ can be found from initial conditions.

The boundary condition on the nuclear surface requires the absence of pressure as it should be for a self-sustained system with no external forces. For each λ -mode, we find a series of eigenfrequencies $\omega_\lambda^{(n)} = c_s k_\lambda^{(n)}$, where the wave number $k_\lambda^{(n)}$ is a root of the spherical Bessel function on the free surface,

$$j_\lambda(k_\lambda^{(n)}R_0) = 0. \quad (6.7)$$

Since $R_0 \propto A^{1/3}$, one important conclusion is that the wave numbers and the frequencies behave with the mass number A as

$$\omega_\lambda^{(n)} = \frac{(\text{const})_\lambda^{(n)}}{A^{1/3}}, \quad (6.8)$$

in contrast to the $\sim A^{-1/2}$ rule for the surface waves (5.99). The dispersion law (6.8) agrees with the natural idea of a standing wave with the wavelength $2\pi/k$ determined by the size of the system. As a consequence of the different A -dependence, the surface waves in a large system are of considerably lower frequencies.

In the volume sound wave, the velocity field is equal, according to (6.3), to $\mathbf{v} = (-i/\omega)(c_s^2/\rho)\nabla\delta\rho$. With the boundary condition (6.7), the density gradient $\nabla\delta\rho$ does not vanish on the surface in contrast to the quantity $\delta\rho$ itself. But the velocity on the surface creates, as in Eq. (5.36), motion of the surface and, therefore, time dependence of the shape variables $\alpha_{\lambda\mu}$, see Eq. (5.38), with the external, much higher, frequencies of the sound waves. This induced surface motion generates the multipole moments (5.27). At the same time, the sound wave is accompanied by its own volume multipole moment (5.25),

$$\delta\mathcal{M}_{\lambda\mu}(t) = \int d^3r \delta\rho_{\lambda\mu}(\mathbf{r}, t) r^\lambda Y_{\lambda\mu}(\mathbf{n}). \quad (6.9)$$

Using the boundary condition (6.7) and properties of the radial functions $j_\lambda(kr)$, one can show [1] that the multipole moment (6.9) exactly cancels the surface multipole moment induced by the sound wave. Thus, in this approximation, the net multipole moment generated by the volume sound waves vanishes; surface and volume waves are effectively decoupled.

In more elaborate approaches, there is a coupling between surface and volume excitations. The surface waves create the additional pressure at the surface that modifies the boundary conditions for the volume sound. As a result, one should consider a coupled set of hydrodynamic equations that has two families of solutions: high-frequency ones mainly concentrated inside the volume, and low-frequency ones with the maximum strength near the surface but with a tail of excitation deeply in the volume.

Problem 6.1 *Sum rules.* Consider a many-body system of nonrelativistic particles interacting through a potential that depends only on coordinates \mathbf{r}_a of individual particles of masses m_a . Let $|n\rangle$ be a complete set of stationary *many-body* states with energies E_n and

$$Q = \sum_a q_a, \quad q_a = q(\mathbf{r}_a), \quad (6.10)$$

be an arbitrary *one-body* operator also depending on coordinates \mathbf{r}_a . Fix one of the many-body states $|i\rangle$ and call an *energy-weighted sum rule* (EWSR) the following sum over all states $|n\rangle$ allowed by the selection rules for the transition from the state $|i\rangle$:

$$S_i[Q] \equiv \frac{1}{2} \sum_n (E_n - E_i) \{ |\langle n|Q|i\rangle|^2 + |\langle n|Q^\dagger|i\rangle|^2 \}. \quad (6.11)$$

- a) Express $S_i[Q]$ in terms of the properties of the initial state $|i\rangle$ and apply the result to the following specific cases:
- b) The monopole operator, $Q \Rightarrow \sum_a r_a^2$;
- c) The dipole operator with excluded excitation of the center-of-mass motion, $Q \Rightarrow \sum_a (d_z)_a$, where $(d_z)_a = e_a(z_a - R_z)$, and \mathbf{R} is the coordinate of the center-of-mass of the nucleus with Z protons and N neutrons;
- d) Fourier component of the density operator, $Q \Rightarrow \rho_{\mathbf{k}} = \sum_a \exp(i\mathbf{k} \cdot \mathbf{r}_a)$.

Solution

- a) After rearrangement of terms in the right-hand side of (6.11), we express the energy-weighted sum with the aid of the double commutator (since $[Q, H]$ is proportional to the time derivative of the operator Q , this commutator in fact expresses the equation of motion)

$$S_i[Q] = \frac{1}{2} \langle i | [[Q, H], Q^\dagger] | i \rangle. \quad (6.12)$$

Thus, the calculation of the sum requires the knowledge of the initial wave function only. For the momentum-independent interaction, the operator does not commute only with the kinetic part of the Hamiltonian and the result can be found explicitly as an anticommutator:

$$[Q, H] = \sum_{ab} \frac{1}{2m_b} [q_a, \mathbf{p}_b^2] = \sum_a \frac{i\hbar}{2m_a} [(\nabla_a q_a), \mathbf{p}_a]_+. \quad (6.13)$$

The second commutator reduces (6.12) to

$$S_i[Q] = \sum_a \frac{\hbar^2}{2m_a} \langle i | \nabla_a q_a |^2 | i \rangle. \quad (6.14)$$

- b) For the monopole operator $\nabla q = 2\mathbf{r}$, so that

$$S_i \left[\sum_a r_a^2 \right] = \sum_a \frac{2\hbar^2}{m_a} \langle i | r_a^2 | i \rangle. \quad (6.15)$$

For the system of A particles of mass M , this is proportional to the mean square radius $A \langle r^2 \rangle_i$ in the state $|i\rangle$,

$$S_i \left[\sum_a r_a^2 \right] = \frac{2\hbar^2}{M} A \langle r^2 \rangle_i. \quad (6.16)$$

- c) The dipole operator of the nucleus, after the center-of-mass was separated, see Eq. (2.61), describes the excitation of protons against neutrons:

$$D_z \equiv \sum_a d_{za} = e \sum_p z_p - e \frac{Z}{A} \left(\sum_p z_p + \sum_n z_n \right) = e_p \sum_p z_p + e_n \sum_n z_n, \quad (6.17)$$

where the *effective proton and neutron charges* are

$$e_p = \frac{N}{A} e, \quad e_n = -\frac{Z}{A} e. \quad (6.18)$$

The sum rule (6.14) in this case is universal for all states $|i\rangle$:

$$S_i[D_z] = \sum_a \frac{\hbar^2 e_a^2}{2m_a}. \quad (6.19)$$

With the effective charges (6.18), this gives

$$S_i[D_z] = \frac{\hbar^2 e^2}{2M} (Ze_p^2 + Ne_n^2) = \frac{\hbar^2 e^2}{2M} \frac{NZ}{A}. \quad (6.20)$$

In an atom, the center-of-mass frame is attached to the nucleus, and the dipole sum rule (6.19) for Z electrons (Thomas–Reiche–Kuhn sum rule) reads

$$S_i[D_z]_{\text{TRK}} = \frac{\hbar^2 e^2}{2m_e} Z. \quad (6.21)$$

In the nucleus, the dipole strength related to the nuclear motion as a whole ($m_e \Rightarrow AM$, $e \Rightarrow Ze$) provides the center-of-mass contribution (no intrinsic excitations),

$$S_{\text{c.m.}} = \frac{\hbar^2 (Ze)^2}{2AM}. \quad (6.22)$$

The total sum of global (6.22) and intrinsic (6.20) strength recovers the TRK sum rule (6.21) with $m_e \Rightarrow M$,

$$S_{\text{dip}} = \frac{\hbar^2 e^2}{2M} \left(\frac{NZ}{A} + \frac{Z^2}{A} \right) = \frac{\hbar^2 e^2}{2M} Z. \quad (6.23)$$

- d) In this case, we again get the universal sum rule independent of the choice of the state $|i\rangle$,

$$S_i[\rho_{\mathbf{k}}] = \sum_a \frac{\hbar^2 k^2}{2m_a}, \quad (6.24)$$

or, for a system of A identical particles of mass M ,

$$S_i[\rho_{\mathbf{k}}] = \frac{\hbar^2 k^2}{2M} A. \quad (6.25)$$

In the long wavelength limit, $kr_a \ll 1$, the expansion of the exponent in $\rho_{\mathbf{k}}$ leads to the result equivalent to the dipole sum rule.

6.2 Isovector Modes

As was pointed out in Sections 2.7 and 5.3, the one-body quantities, such as density or multipole moments, can be of isoscalar or isovector nature. This distinction is important as long as isospin can be considered a good quantum number. The surface modes and the volume sound waves discussed in the preceding sections do not distinguish between protons and neutrons. These excitations belong to the isoscalar type (5.18), where the whole nuclear density is involved *coherently*. In other words, in such modes, protons and neutrons are moving *in phase*.

A more general description of nuclei has to account for the existence of two components, proton and neutron “fluids,” in nuclear matter. This is especially important for nuclei that are far from stability due to a large neutron excess. The isovector excitations are the modes that arise in two-fluid hydrodynamics due to the possibility of *counter-phase* motion of protons against neutrons. The corresponding multipole moments are the isovector quantities. Recall that for the dipole mode, only isovector excitations correspond to physical collective motion with multipolarity $\lambda = 1$.

Any attempt to create a local nonequilibrium relation between the proton and neutron densities increases energy; the restoring force tends to bring the system back. As was understood by A.B. Migdal, 1944, the force is provided by the *symmetry term* in the mass formula. In the mass formula, the symmetry term is introduced in a *global* form. Using the same ideas as for isoscalar modes, we expect that the excessive energy appears in a *local* element of the medium where the equilibrium conditions are violated. This element has to be sufficiently small to allow one to use the differential equations of hydrodynamics but sufficiently large to neglect the discrete nature of the elementary constituents. Interparticle interactions have to be strong enough to ensure the motion of this element as a whole. These conditions are approximately fulfilled in nuclei with a relatively large number of particles.

Considering the continuous nuclear medium with $N = Z$ as being in the local equilibrium with $\rho_p = \rho_n = \rho/2$, we write down the *local* analog of the symmetry energy near the equilibrium as

$$E_{\text{symm}} = \frac{1}{2} b_{\text{symm}} \int d^3r \frac{[\rho_p(\mathbf{r}) - \rho_n(\mathbf{r})]^2}{\rho(\mathbf{r})} \approx \frac{b_{\text{symm}}}{2\rho} \int d^3r [\rho_n(\mathbf{r}) - \rho_p(\mathbf{r})]^2. \quad (6.26)$$

Here the coefficient b_{symm} characterizes the properties of nuclear matter and therefore coincides with the same parameter in the mass formula. Equation (6.26) is our first example of the *energy density functional*. In the uniform limit, $\rho_p = Z/V$ and $\rho_n = N/V$, this expression goes over to the symmetry energy (5.2) of the LDM.

At zero temperature, we can find pressure as the energy derivative with respect to the volume, Eq. (6.1). Therefore, the derivation along the same steps as in Eqs. (6.2)–(6.5) leads to the wave equation with the speed of isovector sound

$$c_s^{(1)} = \sqrt{\frac{b_{\text{symm}}}{M}}. \quad (6.27)$$

With the normal value of $b_{\text{symm}} \approx 45$ MeV, this gives $c_s^{(1)} \approx 0.2c$.

The solution of the wave equation has the same form with the wave number k_λ and frequency $\omega_\lambda = c_s^{(1)} k_\lambda$ as in Eq. (6.6). But the widely accepted boundary condition for the isovector case differs from that for the isoscalar modes (6.7). Since the amount of

energy needed for removal of protons from the volume filled by neutrons is rather large, it is assumed that the surface is actually fixed and the radial current on the surface is absent. The current is proportional to the density gradient. This leads to the boundary condition with the zero derivative on the surface,

$$\left[\frac{\partial j_\lambda(k_\lambda^{(n)} r)}{\partial r} \right]_{r=R_0} = 0. \quad (6.28)$$

Of course, the volume wave equation determines the spectrum with the typical volume A -dependence (6.8).

The lowest isovector dipole mode corresponds to the lowest root of (6.28), $k_1^{(0)} R_0 = 2.08$, which gives energy of the first excited state 1^-

$$\hbar\omega_1^{(0)} = \hbar c_s^{(1)} k_1^{(0)} = 2.08 \frac{\hbar c_s^{(1)}}{R_0} \approx \frac{79}{A^{1/3}} \text{ MeV}. \quad (6.29)$$

All photonuclear processes with gamma-rays absorbed by a nucleus of medium or heavy mass display a strong peak in the cross section at the energy close to the value (6.29). The photoabsorption has a dipole character. The absence of significant shell modulation in the A -dependence (compare Figures 5.3 and 5.4 for the lowest quadrupole excitation) manifests a *universal* nature of the peak. Being identified with the isovector sound, this collective excitation is called *giant dipole resonance* (GDR). Figure 6.1 shows an example of the experimental data set.

Two aspects of Figure 6.1 deserve special attention. First, the observed peak is rather broad (the full width at half-maximum height is $\Gamma(\text{FWHM}) \approx 4$ MeV). This reminds the resonance curve for a *damped oscillator*. The quality of this oscillator is not very

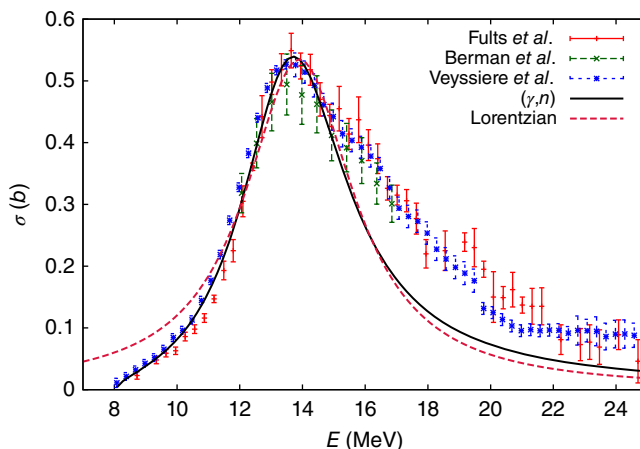


Figure 6.1 Total photoabsorption cross section by ^{197}Au , data from Refs [2–4]. Experimental results are fit with the Lorentzian function, with the peak at energy 13.9 MeV and width 4.2 MeV. The peak in the experimentally observed cross section mainly comes from the (γ, n) reaction, the theoretical cross section for this reaction is also shown assuming the same width and centroid for GDR. The reaction is only possible for gamma energies above threshold given here by the neutron separation energy of about 8 MeV. At higher energies, above 14 MeV, other reactions, such as $(\gamma, 2n)$, contribute.

high, $\hbar\omega/\Gamma \approx 4$. This means that in fact the dipole oscillator can perform only several periods of oscillations. Its damping is caused by the “friction” due to the coupling to incoherent motion of individual nucleons that is not taken into account in the global hydrodynamic description. Second, the bell-shaped solid curve in Figure 6.1 that takes as input parameters only the position of the resonance, its width and the cross section in the maximum, is in a rather good agreement with data within the error bars. The excess of data at the right-hand side of the curve can be related to the increase in the nuclear level density and growth of open decay channels. The integral area covered by the curve turns out to be close to a universal value predicted by the *sum rule* (6.20).

6.3 Giant Resonance and Linear Response

Here we consider the estimate of the frequency of the giant dipole resonance similar to that of Eq. (6.29) but using more detailed arguments.

Our starting point is again the local symmetry energy (6.26) as a part of the general *energy density functional*. We combine this idea with that of the *linear response* to an external perturbation of given symmetry. Let us apply a weak uniform electric field $\mathcal{E} = \mathcal{E}_z$ to the spherical nucleus in the ground state when protons and neutrons have equilibrium densities ρ_p° and ρ_n° , respectively. The field will modify the equilibrium conditions *polarizing* the nucleus by pushing the protons along the z -axis. Because of nuclear incompressibility, we expect that the neutrons will also move keeping the total density $\rho = \rho_p^\circ + \rho_n^\circ$ fixed. The distortion of the densities can be written as

$$\rho_p = \rho_p^\circ + \alpha \rho z, \quad \rho_n = \rho_n^\circ - \alpha \rho z, \quad (6.30)$$

where we limit ourselves by a linear dipole term that will be proportional to the external field. The coefficient α has to be determined by the equilibrium condition in the presence of the field.

With the deformation (6.30), the center of mass is still at rest but the dipole polarization appears. The centers of protons and neutrons are now displaced,

$$z_p = \int d^3r \rho_p z = \alpha \rho \langle z^2 \rangle V = \frac{\alpha \rho}{3} \langle r^2 \rangle V, \quad (6.31)$$

where V is the nuclear volume; similarly

$$z_n = -\frac{\alpha \rho}{3} \langle r^2 \rangle V. \quad (6.32)$$

With effective dipole charges (6.18) and the mean square radius $\langle r^2 \rangle = (3/5)R^2$, the induced dipole moment is

$$d = e_p z_p + e_n z_n = \frac{e \alpha \rho}{3} \langle r^2 \rangle V = \frac{e \alpha \rho}{5} R^2 V. \quad (6.33)$$

It is customary to introduce the *static polarizability* α defined as the coefficient of proportionality between the external field and induced polarization:

$$d = \alpha \mathcal{E} \quad \Leftrightarrow \quad \alpha = \frac{e \alpha \rho R^2 V}{5 \mathcal{E}}. \quad (6.34)$$

The value of α is determined by the minimum of the symmetry energy (6.26) that increases because of the proton–neutron separation,

$$E_{\text{symm}} = \frac{b_{\text{symm}}}{2\rho} \int d^3r [(\rho_n^\circ - a\rho z) - (\rho_p^\circ + a\rho z)]^2. \quad (6.35)$$

The linear in az term vanishes in the integration, and the rest gives

$$E_{\text{symm}} = E^\circ + \frac{2}{5} b_{\text{symm}} V \rho R^2 a^2. \quad (6.36)$$

Adding here the negative contribution of the interaction energy with the dipole field (induced dipole alignment),

$$E_{\text{dip}} = -\mathcal{E}d, \quad (6.37)$$

we obtain the total change of energy

$$\delta E = \frac{1}{5} VR^2 \rho (2a^2 b_{\text{symm}} - ae\mathcal{E}). \quad (6.38)$$

The minimum of this function with respect to a is reached at

$$a = \frac{e\mathcal{E}}{4 b_{\text{symm}}} \quad (6.39)$$

that corresponds to the polarizability (6.34)

$$\alpha = \frac{e^2 R^2 A}{20 b_{\text{symm}}}. \quad (6.40)$$

However, we can calculate the same polarizability by using the perturbation Hamiltonian (6.37),

$$\hat{H}' = -\mathcal{E}\hat{d}, \quad (6.41)$$

where \hat{H}' and \hat{d} are now quantum operators. The perturbed wave function Ψ'_0 of the ground state contains components of excited states Ψ_n admixed by the dipole perturbation,

$$\Psi_0 \rightarrow \Psi'_0 = \Psi_0 + \sum_{n \neq 0} \frac{H'_{n0}}{E_0 - E_n} \Psi_n, \quad (6.42)$$

where E_n in the denominator are unperturbed energies of excited states of opposite parity with respect to the ground state. The expectation value of the electric dipole in the perturbed state (6.42) determines the polarizability,

$$\alpha = \frac{\langle \Psi'_0 | d | \Psi'_0 \rangle}{\mathcal{E}} = 2 \sum_{n \neq 0} \frac{|d_{n0}|^2}{E_n - E_0}. \quad (6.43)$$

Another element of the derivation is the energy-weighted sum rule for the dipole operator,

$$S[d] \equiv \sum_n |d_{n0}|^2 (E_n - E_0). \quad (6.44)$$

Without velocity-dependent interactions, this sum has a universal value (6.20). Now we make a crucial assumption that the dipole strength is *saturated* in a relatively narrow

energy window of the isovector GDR located at $E_r - E_0 \approx E_r$. This assumption is reasonable for stable nuclei where the GDR is known to have the width small compared to the resonance energy, but it might be less justified for nuclei far from stability where the significant fraction of the dipole strength is shifted down in energy (*pygmy*-branch of the giant resonance). Assuming the saturation and comparing the two sum rules, polarizability (6.43) and TRK (6.20), we relate α and E_r ,

$$\alpha \approx \frac{2S[d]}{E_r^2} = \frac{NZ}{A} \frac{\hbar^2 e^2}{ME_r^2}. \quad (6.45)$$

Finally, our estimate for α based on symmetry energy, Eq. (6.40), along with Eq. (6.45), provides the resonance energy

$$E_r^2 = 20 \frac{NZ}{A^2} \frac{\hbar^2}{MR^2} b_{\text{symm}}. \quad (6.46)$$

With $b_{\text{symm}} = 46$ MeV, $R = r_0 A^{1/3}$, $r_0 = 1.2$ fm, and $NZ/A^2 \approx 0.24$ (for heavy stable nuclei), we find

$$E_r \approx \frac{78}{A^{1/3}} \text{ MeV}, \quad (6.47)$$

in agreement with the experimental data and the hydrodynamic estimate (6.29).

6.4 Classification of Normal Modes

Experiments show many *giant modes* of both isoscalar and isovector types revealing the strong response of the nucleus to external agents with certain symmetry. The response is typically concentrated in a relatively narrow region of excitation energy and therefore justifies the word “resonance.” Such modes of excitation may include also spin degrees of freedom that can be added to the hydrodynamic description. The A -dependence roughly agrees with the $A^{-1/3}$ rule.

The giant resonances are universal and only weakly correlate with the peculiarities of the individual nuclei. In this sense, we can say that the hydrodynamic approach sets the framework for the classification of normal modes of nuclear excitation. A more detailed analysis shows that the apparent success of the hydrodynamic approach up to great extent is stipulated by the requirements of *symmetry* rather than by the specific dynamic contents of the LDM. The most striking discrepancy between the LDM and reality is revealed in the low-lying “surface” modes, which are very sensitive to the details of the ground state. The microscopic theory discussed later shows the reasons for successes as well as failures of the hydrodynamic approach.

The full classification of possible normal modes of collective excitations can be based solely by the requirements of symmetry. The most general one-body operator, *generalized multipole moment*, $\mathcal{M}_{JM;TT_3}^{\lambda S}$, carries the quantum numbers of the total angular momentum (JM), orbital momentum (λ), spin (S), and isospin quantum numbers (TT_3). After quantization, Section 6.6, we introduce the corresponding quanta with their creation and annihilation operators. The total angular momentum J follows from the vector coupling of \mathbf{L} and \mathbf{S} . The general multipole moment is given by the sum over the particles,

$$\mathcal{M}_{JM;TT_3}^{\lambda S} = \sum_a f_\lambda(r_a) [Y_\lambda(a) \otimes \mathcal{O}_S(a)]_{JM} \mathcal{T}_{TT_3}(a), \quad (6.48)$$

where the standard notation for vector coupling is used,

$$[Y_\lambda(a) \otimes \mathcal{O}_S(a)]_{JM} \equiv \sum_{\mu\nu} C_{\lambda\mu}^{JM} {}_{S\nu} Y_{\lambda\mu}(\mathbf{n}_a) \mathcal{O}_{S\nu}(a). \quad (6.49)$$

The excitation (6.48) changes parity by $(-)^{\lambda}$.

The spin operators $\mathcal{O}_{S\nu}(a)$ change the state of the particle a . There are two types of possible spin operators:

$$\mathcal{O}_{S\nu} = \begin{cases} 1, & S = 0, \quad \nu = 0, \quad (\text{nonspin-flip}) \\ \vec{\sigma}, & S = 1, \quad \nu = 0, \pm 1, \quad (\text{spin-flip}). \end{cases} \quad (6.50)$$

a constant that does not change the spin state, and vector $\vec{\sigma}$ that can change the spin state; the vector operator has three possible components, Cartesian (x, y, z) or spherical, $\nu = 0, \pm 1$. Similar to that, we have the classification of isospin operators,

$$\mathcal{T}_{TT_3} = \begin{cases} 1, & T = 0, \quad T_3 = 0, \quad (\text{isoscalar}) \\ \vec{\tau}, & T = 1, \quad T_3 = 0, \pm 1, \quad (\text{isovector}). \end{cases} \quad (6.51)$$

The components $T_3 = \pm 1$ describe beta-decay or *charge-exchange* excitation, while in gamma-radiation we have $T_3 = 0$. Since our particles have spin 1/2 and isospin 1/2, the corresponding operators can always be expressed as linear functions of $\vec{\sigma}$ or $\vec{\tau}$ [QP, I, 20.2].

The radial form-factor of the excitation can vary; usually for multipole operators in the long wavelength limit $f_\lambda(r_a) = r_a^\lambda$ and it might be more useful to use $f_\lambda(r_a) = j_\lambda(kr_a)$ for shorter wavelengths. The operators r^λ correspond to the first term of the long wavelength expansion of the spherical Bessel functions. Correspondingly, there exists the following nomenclature: *allowed* transitions ($\lambda = 0$), *first-forbidden* ($\lambda = 1$), *second-forbidden* ($\lambda = 2$), and so on. This terminology makes sense with respect to beta-decay when the emitted electron-neutrino pair has very low momenta so that $kR \ll 1$.

In allowed (*monopole*) transitions, $\lambda = 0$, the resulting angular momentum is determined by the spin character of the operator, $J = S$. The general definition (6.48) reduces then to

$$\mathcal{M}_{S\nu;TT_3}^{\text{OS}} = \frac{1}{\sqrt{4\pi}} \sum_a f_0(r_a) \mathcal{O}_{S\nu}(a) \mathcal{T}_{TT_3}(a); \quad (6.52)$$

the isoscalar monopole resonance with $S = T = 0$ has the radial form-factor $f_0(r_a) = r_a^2$.

In weak interaction processes, we mostly deal with the Fermi transitions, $S = 0, T_3 = \pm 1$,

$$F_\pm = \sum_a t_\pm(a) = T_\pm, \quad (6.53)$$

and Gamow-Teller transitions, $S = 1, \nu = 0, \pm 1, T_3 = \pm 1$,

$$(\text{GT})_{\nu;\pm} = \sum_a \sigma_\nu(a) T_\pm(a); \quad (6.54)$$

both have no radial dependence. The Fermi operator (6.53) reduces to the raising or lowering component of the total isospin and causes the transition to the neighboring nucleus within the same isobaric multiplet; only the isospin projection is changed. The final state is an *isobaric analog state* (IAS) with respect to the parent one. With isospin

invariance of strong interactions, the spin and spatial quantum numbers are unchanged by the Fermi transition. As discussed in Chapter 2, the energy of the daughter state differs from the original value by the change of Coulomb energy. For Gamow–Teller transitions, in addition the spin-flip is possible, and the isospin of the state can change by ± 1 . Here several final states, usually at energy higher than the IAS, can be populated and energy change cannot be fully reduced to Coulomb energy.

Problem 6.2 Under the assumption of exact isospin invariance, there exist the exact *sum rules* for Fermi (6.53) and Gamow–Teller (6.54) transitions.

- a) The Fermi sum rule determines the total strength of all Fermi transitions from a given initial state $|i\rangle$ with isospin quantum numbers T and T_3 to all final states $|f\rangle$,

$$B^\pm(F) \equiv \sum_f |\langle f | F_\pm | i \rangle|^2. \quad (6.55)$$

Calculate this sum rule, consider particular cases of $T = |T_3|$ in the initial state and explain your results.

- b) The Gamow–Teller strength of the initial state $|i\rangle$ is defined as

$$B^\pm(\text{GT}) = \sum_f \sum_v |\langle f | (\text{GT})_{v;\pm} | i \rangle|^2. \quad (6.56)$$

Calculate the sum rule for a given initial state $|i\rangle = |TT_3\rangle$,

$$S(\text{GT}) \equiv B^-(\text{GT}) - B^+(\text{GT}). \quad (6.57)$$

Solution

- a) Using the completeness of all possible states $|f\rangle$, we transform the Fermi strength $B(F)$ into the expectation value of the quadratic operator in the initial state $|i\rangle$:

$$B^\pm(F) = \sum_f \langle i | F_\pm | f \rangle \langle f | F_\mp | i \rangle = \langle i | F_\pm F_\mp | i \rangle, \quad (6.58)$$

where the Hermitian conjugation was used,

$$\langle f | F_\pm | i \rangle = \langle i | F_\pm^\dagger | f \rangle^* = \langle i | F_\mp | f \rangle^*. \quad (6.59)$$

The Fermi operator F is nothing but the lowering, F_- , or raising, F_+ , component of the total isospin operator of the system,

$$F_\pm = T_\pm = T_1 \pm iT_2. \quad (6.60)$$

Therefore, its matrix elements are determined by the same algebra as for angular momentum. For the state $|i\rangle = |TT_3\rangle$, we find

$$B^\pm(F) = (T \mp T_3)(T \pm T_3 + 1). \quad (6.61)$$

In the ground state of a nucleus with a neutron excess, we have, as a rule, $T_3 = T \geq 0$. Then

$$B^+(F) \rightarrow 0, \quad B^-(F) \rightarrow 2T = 2T_3 = N - Z. \quad (6.62)$$

In this case, we cannot increase the isospin projection with the aid of the decay $p \rightarrow n$ because then a “new” neutron would occupy the orbital already filled by an

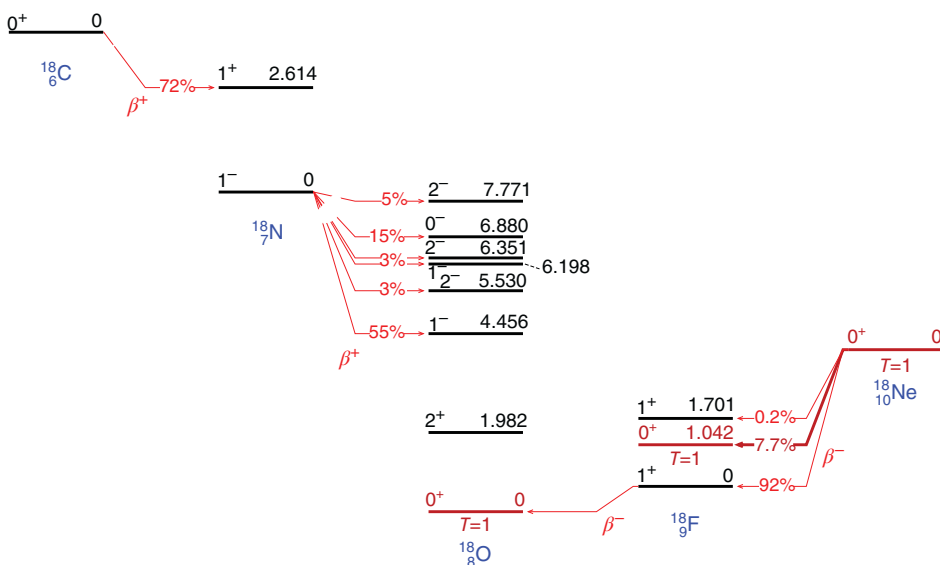


Figure 6.2 Scheme of the Fermi and Gamow–Teller decays of ground states in $A = 18$ nuclei. Data from the evaluation [5].

“old” neutron. In the inverse direction, the process is possible for any of the excess neutrons (there are $N - Z$ of them), each is the transformation of unit strength. For nuclei close to the proton drip line, we can have $N < Z$. In this case, the roles of B^+ and B^- are interchanged.

In Figure 6.2, the allowed beta-decay and branching ratios are shown for the ground states of $A = 18$ nuclei. The ground state of ^{18}Ne , which is a $T_3 = 1$ state of the isobaric $T = 1$ triplet, decays to the isobaric analog 0^+ state in ^{18}F at 1.042 MeV with about 1 out of 13 chance (7.7%). This *superallowed* beta-decay goes via the Fermi transition exclusively (the Gamow–Teller operator cannot couple two states with zero total angular momentum). The partial half-life for this decay is about 1.66 s, and with $B^-(F) = 2$ it can be used to infer information about the strength of weak interaction.

- b) Analogous to the Fermi case, Eq. (6.58), the Gamow–Teller strength is given by

$$B^\pm(\text{GT}) = \sum_v (-)^v \langle i | (\text{GT})_{-v;\mp} (\text{GT})_{v;\pm} | i \rangle. \quad (6.63)$$

Here we used the Hermiticity property of tensor operators (6.54),

$$(\text{GT})_{v;\pm}^\dagger = (-)^v (\text{GT})_{-v;\mp}, \quad (6.64)$$

with \pm in isospin space transforming into \mp , whereas the vector components are transformed as for spherical functions. In the explicit form, the strengths can be written as sums over the particles a and b ,

$$B^\pm(\text{GT}) = \sum_{ab} \sum_v (-)^v \langle i | (\sigma_a)_{-v} (\sigma_b)_v t_a^\mp t_b^\pm | i \rangle = \sum_{ab} \langle i | (\vec{\sigma}_a \cdot \vec{\sigma}_b) t_a^\mp t_b^\pm | i \rangle, \quad (6.65)$$

where we used the scalar product of two vectors in spherical components,

$$(\mathbf{a} \cdot \mathbf{b}) = \sum_{\mu} (-)^{\mu} a_{-\mu} b_{\mu}. \quad (6.66)$$

The sum rule (6.57) now takes the form

$$S(\text{GT}) = B^-(\text{GT}) - B^+(\text{GT}) = \sum_{ab} \langle i | (\vec{\sigma}_a \cdot \vec{\sigma}_b) (t_a^+ t_b^- - t_a^- t_b^+) | i \rangle. \quad (6.67)$$

By renaming in the last term $a \leftrightarrow b$, the isospin part in the matrix element reduces to the commutator (the spin part is symmetric in a and b):

$$t_a^+ t_b^- - t_b^- t_a^+ = 2\delta_{ab}(t_a)_3. \quad (6.68)$$

Since $(\vec{\sigma}_a)^2 = 3$, this simplifies the sum rule (6.67) to

$$B^-(\text{GT}) - B^+(\text{GT}) = 6 \sum_a (t_a)_3 = 6T_3 = 3(N - Z). \quad (6.69)$$

The interpretation of this result is similar to the Fermi case, Eq. (6.62); the factor 3 comes from three spin projections of the GT operator.

Dipole (“first-forbidden”) transitions are produced by the $\lambda = 1$ operators, where we can distinguish a non-spin-flip vector, $S = 0, J = 1$,

$$\mathcal{M}_{1\mu;1T_3}^{10} = \sum_a r_a Y_{1\mu}(\mathbf{n}_a) \tau_{T_3}(a), \quad (6.70)$$

and three axial-vector ($S = 1$) spin-flip operators, $J = 0, 1, 2$,

$$\mathcal{M}_{JM;1T_3}^{11} = \sum_a r_a [Y_1(a) \otimes \sigma(a)]_{JM} \tau_{T_3}(a). \quad (6.71)$$

In Eq. (6.70), the $T_3 = 0$ isovector term describes the GDR, while the similar isoscalar, $T = T_3 = 0$, as we know, would correspond to the center-of-mass displacement. The terms $T_3 = \pm 1$ in (6.70) and (6.71) describe dipole and *spin-dipole* charge-exchange modes, respectively. The classification can be obviously extended to higher multipoles.

6.5 Quantization of Nuclear Vibrational Modes

In Chapter 5, we considered the classical Hamiltonian describing the surface vibrations of the nucleus around equilibrium spherical shape. The vibrations were treated in the harmonic approximation. As it is clear from our arguments, we used the LDM and assumptions of irrotational flow only to illustrate a possible source of the effective mass and restoring force. The form of the harmonic Hamiltonian is quite general being based solely on the symmetry consideration. Therefore, it does not depend on the specific model for the origin of vibrations; such model would define the numerical values of the parameters only. Next, we perform a transition to the *quantized* vibrational Hamiltonian. It will make possible to predict the vibrational spectra and to compare them with the data.

Our dynamical variables are the collective coordinates $\alpha_{\lambda\mu}$ and the conjugate momenta $\pi_{\lambda\mu}$. The complication compared to the one-dimensional textbook case of

harmonic oscillator comes from the fact that the variables are now *complex* subject to the constraint (5.17). This, in turn, is related to the rotational symmetry. The subscripts $(\lambda\mu)$ correspond to an object carrying the angular momentum λ and its projection μ . The spherical functions $Y_{\lambda\mu}$ with their φ -dependence $\sim e^{i\mu\varphi}$, considered as operators, *increase* the angular momentum projection of the state, on which they act, by μ . The same is valid for the multipole operators $\mathcal{M}_{\lambda\mu}$, Eq. (5.25), which, in our definition, are proportional to the *conjugate* collective coordinate $a_{\lambda\mu}^*$. When $a_{\lambda\mu}$ and $\pi_{\lambda\mu}$ become quantum operators, according to this definition, they act as the *conjugate* spherical functions and therefore *lower* the angular momentum projection by μ .

In order to keep rotational invariance, we generalize the case of the one-dimensional Heisenberg–Weyl algebra in such a way that both parts of the equation have the same properties of annihilating or creating the angular momentum projection. The annihilation, $a_{\lambda\mu}$, and creation, $a_{\lambda\mu}^\dagger$, operators for the mode $(\lambda\mu)$ are introduced with an arbitrary scale factor η ,

$$a_{\lambda\mu} = \sqrt{\frac{\hbar}{2\eta}} (a_{\lambda\mu} + (-)^\mu a_{\lambda-\mu}^\dagger), \quad \pi_{\lambda\mu} = -i\sqrt{\frac{\hbar\eta}{2}} (a_{\lambda\mu} - (-)^\mu a_{\lambda-\mu}^\dagger). \quad (6.72)$$

It follows from this definition that Hermitian conjugate coordinates and momenta satisfy the relations

$$a_{\lambda\mu}^\dagger = (-)^\mu a_{\lambda-\mu}, \quad \pi_{\lambda\mu}^\dagger = (-)^\mu \pi_{\lambda-\mu} \quad (6.73)$$

generalizing corresponding properties (5.17) of the classical case. The inverse transformation can be easily found with the help of (6.73),

$$a_{\lambda\mu} = \frac{1}{\sqrt{2\hbar\eta}} (\eta a_{\lambda\mu} + i\pi_{\lambda\mu}), \quad a_{\lambda\mu}^\dagger = \frac{1}{\sqrt{2\hbar\eta}} (\eta a_{\lambda\mu}^\dagger - i\pi_{\lambda\mu}^\dagger). \quad (6.74)$$

The commutation relations between the operators also reflect the requirements of rotational invariance. All coordinates for different modes commute with each other and also with all momenta. The coordinates also commute with the momenta related to different modes. The commutator of a coordinate with its own conjugate momentum is $(i\hbar)$ times the unit operator. Acting onto a state, this commutator does not change any quantum numbers. The operators in this commutator should be combined in such a way that their joint action give a *scalar* with respect to rotations. In order to get the unit operator, the commutator has to contain the product of operators with the zero total projection,

$$[a_{\lambda\mu}, \pi_{\lambda'\mu'}^\dagger] = (-)^\mu [a_{\lambda\mu}, \pi_{\lambda'-\mu'}] = i\hbar \delta_{\lambda'\lambda} \delta_{\mu'\mu}. \quad (6.75)$$

Equations (6.74) and (6.75) lead to the commutation relations between the creation and annihilation operators,

$$[a_{\lambda\mu}, a_{\lambda'\mu'}] = 0, \quad [a_{\lambda\mu}^\dagger, a_{\lambda'\mu'}^\dagger] = 0, \quad (6.76)$$

$$[a_{\lambda\mu}, a_{\lambda'\mu'}^\dagger] = \delta_{\lambda'\lambda} \delta_{\mu'\mu}. \quad (6.77)$$

Again both parts of (6.77) have the same angular momentum selection rules.

To summarize, the operator $a_{\lambda\mu}$ *annihilates* a quantum with quantum numbers $(\lambda\mu)$. It changes the angular momentum of a system according to quantum vector coupling rules, $\mathbf{J}_f = \mathbf{J}_i - \vec{\lambda}$, and annihilates the projection μ so that $M_f = M_i - \mu$. The operator

$a_{\lambda\mu}^\dagger$ creates a quantum, the final angular momentum satisfies $\mathbf{J}_f = \mathbf{J}_i + \vec{\lambda}$, and the final projection is $M_f = M_i + \mu$. To make an annihilation operator to create the projection or a creation operator to annihilate the projection, we should perform the transformation to the “hole-type” operators, for example take $(-)^{\mu} a_{\lambda-\mu}^\dagger$ instead of $a_{\lambda\mu}^\dagger$ as in (6.72). For the coordinates and momenta, this would be the Hermitian conjugation (6.73). This phase reflects the tensor operator transformation under time reversal [QP, I, 20.6] that includes the reversal of the angular momentum projection.

To express the vibrational Hamiltonian (5.49) in terms of the creation and annihilation operators, we choose the scale parameter η in (6.72) and (6.74) as $\eta_\lambda = \sqrt{B_\lambda C_\lambda}$. Substituting the coordinates in the potential energy and momenta in the kinetic energy by the operators (6.72), the terms $\sim aa$ and $\sim a^\dagger a^\dagger$ cancel out and the Hamiltonian (5.49) turns out to be *diagonal* in the number of quanta,

$$H = \sum_{\lambda\mu} \hbar\omega_\lambda \left(N_{\lambda\mu} + \frac{1}{2} \right). \quad (6.78)$$

Here the *number operators* with integer eigenvalues are

$$N_{\lambda\mu} = a_{\lambda\mu}^\dagger a_{\lambda\mu}, \quad (6.79)$$

and the *normal frequencies* ω_λ are given by the classical expression (5.52). The frequency spectrum (6.78) is degenerate in projections μ .

As in the one-dimensional case, the full solution of the quantal problem in the harmonic approximation can be interpreted in terms of the new bosons, *vibrational quanta*, which are usually called *phonons*, in analogy to the quanta of sound waves in condensed matter. As we will see later, in reality the harmonic approximation is an oversimplification. The anharmonic Hamiltonian can be also expressed through the same operators, but in general it is not diagonal in a phonon number. It describes the interaction processes when the phonons can be created, transformed, and annihilated.

The quantum Heisenberg equations of motion for the creation and annihilation operators with the harmonic Hamiltonian (6.78) follow from the commutation relations (6.76), (6.77) or ladder relations:

$$i\hbar\dot{a}_{\lambda\mu} = [a_{\lambda\mu}, H] = \hbar\omega_\lambda a_{\lambda\mu}, \quad (6.80)$$

$$i\hbar\dot{a}_{\lambda\mu}^\dagger = [a_{\lambda\mu}^\dagger, H] = -\hbar\omega_\lambda a_{\lambda\mu}^\dagger. \quad (6.81)$$

The operator equations of motion for the coordinates and momenta (6.72) are a straight operator generalization of the classical equations for harmonic vibrations.

Equations (6.80) and (6.81) have the standard *ladder form* showing that $a_{\lambda\mu}$ decreases the energy of the system by $\hbar\omega_\lambda$ while $a_{\lambda\mu}^\dagger$ increases the energy by the same amount (we assume $\omega_\lambda > 0$). The operator solution gives

$$a_{\lambda\mu}(t) = e^{-i\omega_\lambda t} a_{\lambda\mu}(0), \quad a_{\lambda\mu}^\dagger(t) = e^{i\omega_\lambda t} a_{\lambda\mu}^\dagger(0). \quad (6.82)$$

Obviously, this is a quantal analog of a classical normal mode.

The stationary states of the phonon system are labeled by the phonon numbers $N_{\lambda\mu}$ but, due to the rotational degeneracy, there are several (in some cases many) states with different sets of $\{N_{\lambda\mu}\}$ having the same total energy. In the following, we consider the classifications of phonon states more closely.

6.6 Multiphonon Excitations

The recipe of phonon quantization used in Section 6.5 leads to the *Bose statistics* for vibrational quanta. Real nuclear excitations can obey this statistics only approximately. The restoring force ceases to be linear when the deviation from equilibrium exceeds a certain value. On the microscopic level, as we will see later, one cannot form exact bosons using the underlying nucleon degrees of freedom. Indeed, the constituent fermions taking part in two vibrational modes still should obey the Pauli principle. The multiphonon states with a large number of phonons become unphysical due to underlying Pauli blocking. Even earlier, the phonon states may in fact lose their pure collective character being mixed with neighboring noncollective many-body wave functions. However, for collective modes with many coherent nucleonic contributions, the boson approximation can be reasonable, at least as long as the amplitude of vibrations is not large.

The majority of even–even nuclei have the typical sequence of low-lying states: ground state 0^+ (*phonon vacuum*) and the first excited state 2_1^+ (one *quadrupole phonon*, $\lambda = 2$, of course coming as a degenerate multiplet of $2\lambda + 1$ states with different projections μ). We have already seen, Figure 5.3, a regular trend of energy of the 2_1^+ state as a function of the nuclear mass. Another characteristic signature of the collective character of this state is the strong intensity of gamma-radiation to the ground state. In terms of the phonon operators $a_{\lambda\mu}$, the ground state $|0\rangle$ satisfies

$$a_{\lambda\mu}|0\rangle = 0, \quad (6.83)$$

for all types of phonons. In the harmonic approximation, the one-phonon state is built with the aid of the creation operator, for example,

$$|2_1^+ \mu\rangle = a_{2\mu}^\dagger |0\rangle. \quad (6.84)$$

It is fivefold degenerate with respect to the projection μ .

The matrix element of the transition between the one-quantum state and vacuum has to contain the annihilation operator $a_{2\mu}$ of the quadrupole quantum. The physical electromagnetic excitation and de-excitation are induced by the charge multipole moment (5.28), that is, by the *coordinate* $\alpha_{\lambda\mu}^*$ that, in the quantum case, contains the phonon creation and destruction operators. The relations (6.74) show that the annihilation operator enters the coordinate with the factor inversely proportional to $\sqrt{\omega_\lambda}$, as the classical vibrational amplitude. For *soft* collective modes, the amplitude grows along with the transition probabilities.

Problem 6.3 Consider a transition $i \rightarrow f$ between two states of the nucleus with spins J_i and J_f , respectively. The transition probability is proportional to the squared matrix element $|\langle J_f M_f | T_{\lambda\mu} | J_i M_i \rangle|^2$ where $T_{\lambda\mu}$ is a Hermitian tensor operator of rank λ responsible for the process. Define the *reduced transition probability*

$$B(T_\lambda; i \rightarrow f) = \sum_{\mu M_f} |\langle J_f M_f | T_{\lambda\mu} | J_i M_i \rangle|^2 \quad (6.85)$$

as a sum of squared matrix elements over *final* projections M_f and operator projections μ . According to the Wigner–Eckart theorem, the entire dependence of the matrix element of a tensor operator on the magnetic quantum numbers is concentrated in the

vector coupling coefficients (we use here the $3j$ -symbols),

$$\langle J_f M_f | T_{\lambda\mu} | J_i M_i \rangle = (-)^{J_f - M_f} \begin{pmatrix} J_f & \lambda & J_i \\ -M_f & \mu & M_i \end{pmatrix} (f \| T_\lambda \| i), \quad (6.86)$$

where the projections satisfy the conservation law $M_i + \mu = M_f$ corresponding to the creation of the projection (such formal rules are to be strictly followed).

- a) Express the quantity (6.85) in terms of the *reduced matrix element* ($f \| T_\lambda \| i$) and show that it does not depend on the *initial* projection M_i .
- b) Establish the *detailed balance* relation between the reduced transition probabilities of the direct, $i \rightarrow f$, and inverse, $f \rightarrow i$, processes.

Solution

- a) Using the orthogonality condition and performing the summation over μ and M_f , we obtain the reduced transition probability

$$B(T_\lambda; i \rightarrow f) = \frac{1}{2J_i + 1} |(f \| T_\lambda \| i)|^2. \quad (6.87)$$

This quantity is independent of M_i and therefore convenient being a characteristic for the transition strength rather than for the initial population of various magnetic substates.

- b) The reduced (double-barred) matrix element is, up to a phase, the same for the direct and inverse transitions, so that the detailed balance gives

$$B(T_\lambda; f \rightarrow i) = \frac{2J_i + 1}{2J_f + 1} B(T_\lambda; i \rightarrow f). \quad (6.88)$$

The ratio of reduced transition probabilities is merely proportional to the statistical weight of the final state.

Problem 6.4 Calculate the reduced transition probability $B(E\lambda; i \rightarrow f)$ for the transition from the ground state of zero spin to the one-phonon state and for the inverse process of de-excitation of the one-phonon state [$T_{\lambda\mu} \Rightarrow \mathcal{M}_{\lambda,\mu}$].

Solution

The electric multipole moment (5.28) created by the surface deformation of rank λ is related to the collective multipole coordinate via

$$\mathcal{M}_{\lambda,\mu} = \frac{3}{4\pi} ZeR_0^\lambda \alpha_{\lambda\mu}^\dagger; \quad (6.89)$$

both parts are defined as operators raising the angular momentum projection. Then, in terms of operators creating (a^\dagger) and annihilating (a) vibrational quanta, ($\eta_\lambda = \sqrt{B_\lambda C_\lambda}$),

$$\mathcal{M}_{\lambda,\mu} = \frac{3}{4\pi} ZeR_0^\lambda \sqrt{\frac{\hbar}{2\eta_\lambda}} \left(a_{\lambda\mu}^\dagger + (-)^\mu a_{\lambda-\mu} \right) \equiv A_\lambda \left(a_{\lambda\mu}^\dagger + (-)^\mu a_{\lambda-\mu} \right). \quad (6.90)$$

All operators labeled with the dagger create the projection indicated in the corresponding subscript.

The reduced transition probability (6.85) for the operator (6.90) is

$$B(E\lambda; i \rightarrow f) = A_\lambda^2 \sum_{\mu M_f} |\langle J_f M_f N_f | a_{\lambda\mu}^\dagger + (-)^\mu a_{\lambda\mu} | J_i M_i N_i \rangle|^2. \quad (6.91)$$

Here N_f and N_i show numbers of quanta in the final and initial states, respectively. For the transition from the ground state, $N_i = 0, J_i = M_i = 0$, only the creation operator $a_{\lambda\mu}^\dagger$ contributes, and the selection rules pick only one final state $J_f = \lambda, M_f = \mu, N_f = 1$ the matrix element being equal to one. The sum over remaining projections μ gives their number $2\lambda + 1$,

$$B(E\lambda; 0_\lambda \rightarrow 1_\lambda) = (2\lambda + 1)A_\lambda^2. \quad (6.92)$$

For the inverse transition, we have one quantum $J_i = \lambda, M_i = \mu_i$ in the initial state and the vacuum state in the end, $J_f = M_f = N_f = 0$,

$$\langle 000_\lambda | \mathcal{M}_{\lambda,\mu} | \lambda \mu_i 1_\lambda \rangle = A_\lambda(-)^{\mu_i} \delta_{\mu_i, -\mu_i}. \quad (6.93)$$

Then in the definition of the reduced probability (6.91), the sums in fact reduce to one term only, $M_f = 0, \mu = -\mu_i$, and

$$B(E\lambda; 1_\lambda \rightarrow 0_\lambda) = A_\lambda^2. \quad (6.94)$$

The detailed balance (6.88) is obviously fulfilled.

If the bosonic approximation is justified, we need to construct *multiphonon* states and look for their counterparts in the experiment. First, we construct proper *two-phonon* states. For the total (integer) angular momentum J , the states of two quanta of multipolarity λ are

$$|JM; 2\rangle = K_J \sum_{\mu\mu'} C_{\lambda\mu \lambda\mu'}^{JM} a_{\lambda\mu}^\dagger a_{\lambda\mu'}^\dagger |0\rangle, \quad (6.95)$$

where $|0\rangle$ represents the vacuum state and K_J is the normalization constant to be found from the orthonormality

$$\langle J'M'; 2 | JM; 2 \rangle = \delta_{J'J} \delta_{M'M}. \quad (6.96)$$

The orthogonality follows from the general properties of the eigenfunctions of Hermitian operators ensured by the Clebsch–Gordan coefficients (CGC). For $J' = J$ and $M' = M$, the matrix element in (6.96) contains two nonzero terms because of two possible ways to contract the creation and annihilation operators. These two contributions differ in ordering the (JM) pairs in one of the CGC. According to the symmetry properties of the CGC, the two items differ by the phase $(-)^{\lambda+\lambda-J} = (-)^J$. This leads to

$$K_J = \frac{1}{\sqrt{2}} \frac{1 + (-)^J}{2}. \quad (6.97)$$

Only even values of J are allowed for two-phonon states by the Bose symmetry of quanta. The factor $1/\sqrt{2}$ is the prototype of the general $1/\sqrt{N!}$ that appears in the normalization of N -boson states.

In the *quadrupole* case, $\lambda = 2$, the two-phonon states form the *triplet* $0_2^+, 2_2^+, 4_1^+$. Here, J^Π indicate the angular momentum and parity while the lower right index simply counts the states with the same J^Π in the order of increasing energy, starting with the ground state 0_1^+ . In the harmonic approximation, the triplet states would be *degenerate* at the doubled energy of the single-phonon state 2_1^+ . This is usually not the case in reality. But the anharmonic effects are not very large in many cases, Figure 6.3, and still allow us to

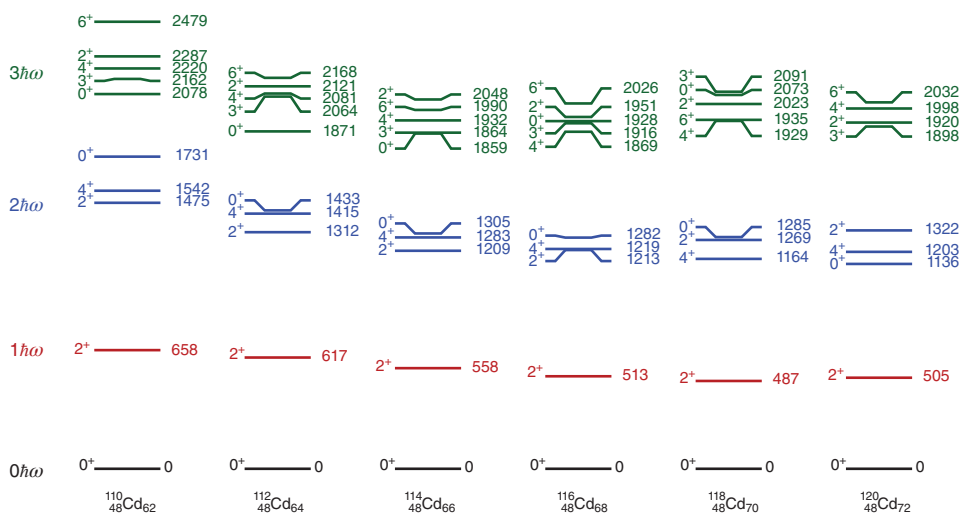


Figure 6.3 Example of the collective one, two, and three quadrupole phonon multiplets in isotopes of Cd. Experimental data from Ref. [6] and references therein; level energies are given in kiloelectronvolts.

identify clearly the two-phonon triplets and three-phonon quintuplets $0_3^+, 2_3^+, 3_1^+, 4_2^+, 6_1^+$. The *octupole* phonons have $\lambda = 3$ and negative parity. Their double excitations again can have only even values of angular momentum, $J = 0, 2, 4, 6$, and positive parity. Such states, as well as double excitations of the GDR and other highly excited modes, are also known experimentally. In general, the full problem of not only listing but explicitly constructing all possible multiphonon states is complex and can be solved by using the elements of group theory. We return to this formalism later.

Problem 6.5 Find the reduced transition probabilities for de-excitation of different two-phonon states $|JM; 2\rangle$ by the radiative transitions to the one-phonon state.

Solution

The reduced transition probability is given by

$$B(J; 2 \rightarrow \lambda; 1) = A_\lambda^2 \sum_{\mu\mu'} |\langle \lambda\mu'; 1 | a_{\lambda\mu} | JM; 2 \rangle|^2. \quad (6.98)$$

Since $\langle \lambda\mu'; 1 | = \langle 0 | a_{\lambda\mu'}$, the matrix element in (6.98) can be rewritten as a scalar product of the two-phonon states with the help of coupling two annihilation operators on the left side of the matrix element to all possible total angular momenta J' ,

$$\langle 0 | a_{\lambda\mu'} a_{\lambda\mu} | JM; 2 \rangle = \sum_{J'M'} C_{\lambda\mu' \lambda\mu}^{J'M'} \frac{1}{K_{J'}} \langle J'M'; 2 | JM; 2 \rangle. \quad (6.99)$$

The orthonormality leaves only $J' = J, M' = M$; the sum over μ and μ' in (6.98) is equal to 1, $K_J^2 = 1/2$, and as a result

$$B(J; 2 \rightarrow \lambda; 1) = \frac{1}{K_J} A_\lambda^2 = 2A_2^2 \quad (6.100)$$

for all allowed (even) values of J , in the quadrupole case $J = 0, 2, 4$. From comparison with (6.94), in units of the reduced transition probability from the one-phonon state to the ground state,

$$\frac{B(J; 2 \rightarrow \lambda; 1)}{B(\lambda; 1 \rightarrow 0; 0)} = 2, \quad (6.101)$$

as in a one-dimensional harmonic oscillator (the *stimulated radiation*). For the higher states, N identical phonons can build various angular momenta J , and their de-excitation probabilities for transitions $|N, J\rangle \rightarrow |N - 1, J'\rangle$ in general depend on J and J' . However, between the *aligned* states with the largest possible spins, $J = N\lambda$ and $J' = (N' - 1)\lambda$, the reduced transition probability still equals N in the same units as in (6.101). This is easy to see taking the initial state of N quanta with the maximum projection $M = J = \lambda N$; then all quanta are equivalent, and the result is the same as in the one-dimensional case. Recall that the reduced transition probability does not depend on the choice of the initial projection.

6.7 Angular Momentum Classification

The Bose statistics of phonons requires that multiphonon wave functions be fully symmetric under phonon permutations. As we have already seen for the two-phonon states, Eq. (6.97), this imposes restrictions on allowed quantum numbers of total angular momentum J : the two-phonon states can have only even values of J .

Let us consider states with phonon number $N > 2$. In reality, such states are not always seen in experimental spectra because of the *fragmentation* phenomenon. The collective multipole strength is spread over few states of a simpler nature; this is a quantum equivalent of classical *damping* of collective vibrations. However, it is important to be able to classify the basis states in a correct way. The simplest procedure of finding the allowed values of J goes as follows. As a generic example, we consider the three-phonon multiplet of quadrupole phonons with angular momentum $\lambda = 2$ of individual phonons.

The maximum possible angular momentum projection of an N -phonon state is $M_{\max} = N\lambda$. This determines the maximum value of the angular momentum, $J_{\max} = M_{\max}$, that is, equal to 6 in our case. The configuration of projections for quadrupole phonons is, obviously,

$$(\mu_1, \mu_2, \mu_3) = (2, 2, 2). \quad (6.102)$$

This state, of course, is fully symmetric and in the quantized form can be written as [the normalization factor for N identical bosons is $1/\sqrt{N!}$]

$$|JM = 66\rangle = \frac{1}{\sqrt{6}} a_{22}^\dagger a_{22}^\dagger a_{22}^\dagger |0\rangle, \quad (6.103)$$

where $|0\rangle$ is the phonon vacuum and the Bose symmetry of the creation operators $a_{2\mu}^\dagger$ guarantees the correct symmetry of the state. The total angular momentum operator in the secondary quantized form is

$$\mathbf{J} = \sum_{\mu\mu'} a_{\lambda\mu}^\dagger a_{\lambda\mu'} \langle \lambda\mu | \mathbf{J} | \lambda\mu' \rangle, \quad (6.104)$$

where the last factor is the usual matrix element of the corresponding component of angular momentum. Lowering the projection M by the operator J_- , we must obtain the state $|JM = 65\rangle$. Using explicitly the right-hand side of Eq. (6.104) we get, in notations (6.102), the superposition of states $(1,2,2)$, $(2,1,2)$, and $(2,2,1)$. This superposition is automatically *symmetric*; it belongs to the same multiplet with $J = J_{\max}$. Since this is the *only* state with the projection $M = M_{\max} - 1$, we do not have any state for starting another multiplet. Therefore, *the multiplets with $J = J_{\max} - 1$ are forbidden*.

Although the application of J_- in the form (6.104) always creates symmetrized states, for the purpose of counting it is sufficient to lower the projection of only one phonon having in mind that the actual combination has to be symmetric. Using such notations, we have at the next step, $J_z = M_{\max} - 2$, two possibilities, $(0,2,2)$ and $(1,1,2)$. One (symmetrized) combination belongs to the first multiplet $J = J_{\max}$, while the second (symmetrized and orthogonal to the first one) combination opens the new multiplet with $J = J_{\max} - 2 = 4$. The next step gives three states: $(-1,2,2)$, $(0,1,2)$, and $(1,1,1)$. Here we list configurations assuming $\mu_1 \leq \mu_2 \leq \mu_3$ with understanding that the actual states are permutation symmetric. Filling in the two open earlier multiplets, we have the third state to start the multiplet with $J = 3$. Continuing in this way, see Table 6.1, we get the

Table 6.1 List of configurations for three bosons with spin 2. (total angular momentum projection M and number of states with given M are shown).

μ_1	μ_2	μ_3	M	#
2	2	2	6	1
1	2	2	5	1
0	2	2	4	
1	1	2	4	2
-1	2	2	3	
0	1	2	3	3
1	1	1	3	
-2	2	2	2	
-1	1	2	2	
0	0	2	2	4
0	1	1	2	
-2	1	2	1	
-1	0	2	1	
-1	1	1	1	4
0	0	1	1	
-2	0	2	0	
-1	1	2	0	
-2	1	1	0	5
0	0	1	0	
0	0	0	0	

full set of allowed states for three quadrupole phonons:

$$[2 \otimes 2 \otimes 2]_{JM} \Rightarrow J = 0, 2, 3, 4, 6. \quad (6.105)$$

A standard check of correctness for such a procedure is provided by calculating the total number of states that must satisfy

$$\sum_J (2J+1) = \frac{(N+\Omega-1)!}{N!(\Omega-1)!}, \quad (6.106)$$

where the right-hand side determines the total number of possible states for N bosons on Ω orbitals. In our case of $N = 3, \Omega = 2\lambda + 1 = 5$, we come to $1 + 5 + 7 + 9 + 13 = 35$, in agreement with (6.106).

Problem 6.6 Find the allowed angular momentum multiplets for four quadrupole phonons.

Solution

$$[2 \otimes 2 \otimes 2 \otimes 2]_{JM} \Rightarrow J = 0, 2^2, 4^2, 5, 6, 8. \quad (6.107)$$

In (6.107), we see that it is possible to have few multiplets with the same J (*equivalent irreducible representations of the $SU(2)$ group*). In such cases, one might need to introduce *additional quantum numbers* to distinguish different states of the same J . Similar procedures work for the construction of possible rotationally invariant higher order terms for anharmonic phonon Hamiltonians.

References

- 1 A. Bohr and B.R. Mottelson, *Nuclear Structure*, Vol. 1, Benjamin, New York, 1969.
- 2 S.C. Fultz *et al.*, Phys. Rev. **127**, 1273 (1962).
- 3 B.L. Berman *et al.*, Phys. Rev. C **36**, 1286 (1987).
- 4 A. Veyssiére *et al.*, Nucl. Phys. **A159**, 561 (1970).
- 5 D.R. Tilley *et al.*, Nucl. Phys. **A595**, 1 (1995).
- 6 J.C. Batchelder *et al.*, Phys. Rev. C **89**, 054321 (2014).

7

Fermi Gas Model

... the simplest and most naive approximation, in which the force to which any one particle is exposed is taken to be due to the average force field created by the other particles.

K. Gottfried and T.-M. Yan, *Quantum Mechanics: Fundamentals*.

7.1 Mean Field and Quasiparticles

In this chapter, our viewpoint will be seemingly opposite to the approach of Chapters 5 and 6, where we were interested in the properties of the nucleus as a drop of a continuous medium. Now we look at the system with the aid of the microscope that is capable of resolving *individual constituents*. In fact, these viewpoints do not contradict each other, but they rather complement, clarify, and improve each other indicating the complex interplay between the collective and single-particle degrees of freedom. This interplay is at the core of quantum physics of many-body systems.

It is discussed in Chapter 5 that the nuclear matter exists in the form of self-sustaining droplets. Particles are bound and evaporation of a particle requires additional energy. Nuclear matter reveals surface tension and elastic properties. All this information tells us that the interaction between the constituents is crucial. However, a significant part of the interaction is *averaged out* due to the fact that the system has many degrees of freedom that interact simultaneously. Another averaging factor comes from the Fermi statistics. The most stable, coherent part of the interaction can be presented as a *mean field* created by all particles and influencing motion of each of them.

The idea of the mean field in many-body systems is known for more than 100 years. Nowadays, we are aware of many examples demonstrating how fruitful this idea is. In various modifications, the concept of the mean field is the base of practically all quantitative theories of many-body systems. In such an approach, the interaction between the constituents is subdivided into two components: the mean field and the *residual* part. At this stage, we did not introduce any guideline dictating the principles of the mean field separation. But we can have in mind the global properties known from the experiment. They show the environment where the dynamics of the individual particles take place.

The first step in implementing this idea is to consider the mean field as an *external* field with the properties established by experiment. Such a field is not *self-consistent* as it should be. We do not know how the change in motion of a particle changes the field acting onto all other particles. This is a shortcoming of the approach. But the hope is that the field is created by many particles and only a synchronous *coherent* excitation of many of them can change the field considerably. After averaging, the incoherent excitations of individual particles and random collision-like processes usually will have little influence onto the mean field. Their main effect is in establishing the equilibrium including the effective temperature of the system determined by the full excitation energy. Exceptional cases are possible when the mean field is *unstable* and small effects can induce a *phase transition* to a more stable configuration. On the next stage, we would like to introduce the self-consistent interplay between the field and the single-particle degrees of freedom.

Another aspect of the problem is that the particles and their residual interactions in the mean field are not the same as in vacuum. The particles are “*dressed*” by the part of the interaction that was already taken into account by formation of the mean field. In fact, we have new objects moving in this field: a bare particle is accompanied by a cloud of changes in the medium induced by its presence. L. Landau called these objects *quasiparticles*. This term is used also in a different sense (“Bogoliubov quasiparticles” in theory of pairing correlations, Chapter 13). Therefore, often we call our objects *particles*, keeping in mind that they are not original nucleons.

At this stage of our discussion, the properties of the quasiparticles have to be taken from experiment. Their number is equal to a number of the original “bare” particles and the dressing keeps unchanged exact quantum numbers – spin, electric charge, isospin – and Fermi statistics, whereas some quantitative characteristics can change. The quasiparticles acquire an effective mass, they have renormalized magnetic moments, and so on. At slow velocities the whole cloud of a quasiparticle is moving together; at sharp excitation we can recover bare particles as a seed inside the cloud. This is similar to the deep-inelastic scattering of high-energy electrons from hadrons that gives evidence of *partons* – quarks and gluons inside the nucleon structure [1]. By this and other reasons, the mean field and *effective forces* between quasiparticles could be velocity dependent.

The forces responsible for the formation of the mean field originate from the nucleon–nucleon interaction renormalized by the presence of other nucleons and by the change of the meson-mediated forces in the medium. The mean field is generated by the most smooth and regular component of this interaction. For example, the mean interparticle distance at realistic density is greater than the radius of the repulsive core and the mean field is the result of averaging over the short-range collisions. Effectively, it is equivalent to the elimination of high Fourier components of the wave function. This is another reason why for the explicit derivation of the properties of the mean field we need effective forces. We need also to mention that the mesons that carry the interaction are not explicitly present in the mean field being also substituted by effective forces. This picture makes sense only at excitation energy smaller than the mass of real mesons.

To start with, we take the mean field as given and study the behavior of independent fermions in this field. Later we come to the effects of the residual interaction, coupling between the field and single-particle motion, and to the determination of the mean field itself. As our first prototype, we consider a perfect Fermi gas in a box.

7.2 Perfect Fermi Gas

In this section, we assume the simplest form of the mean field: a cubic box of size $L = V^{1/3}$, where V is the volume of the system. The particles are confined to this volume and move freely inside. In such a primitive model, the particles do not interact if we forget that the confinement is just due to their interaction.

In fact, if the volume V and the number of particles A are large enough, the exact shape of the volume is of minor significance, and we use it just for correct counting. The main results depend on the *density* $n = A/V$. This is the so-called *thermodynamic*, or macroscopic, limit when our main observables are either *extensive*, proportional to A or V as, for example, volume energy in the mass formula (5.2), or *intensive* as matter or energy density, pressure, or temperature. The intensive quantities are *local* properties of the state of matter. In the thermodynamic limit, they depend on local density: recall, for example, the symmetry energy of the nucleus in the form (6.26). As we discussed in connection with the mass formula, the real nuclei are mesoscopic objects that do not fully reach the thermodynamic limit.

One aspect that was also seen in the mass formula, and that is usually absent in condensed matter applications, is that the uncompensated electric charge violates the normal scaling laws of the thermodynamic limit. The electrostatic energy grows faster than proportional to A or V . This explains the sharp decline of the binding energy of superheavy elements and fission instability. The *multifragmentation* phenomenon (Section 22.8), the decay into light fragments of the highly excited nuclear system formed in a heavy ion collision, is also strongly influenced by macroscopic Coulomb repulsion. Such behavior is related to the long-range character of Coulomb forces, and their influence is stretched over the entire volume of the system. The similar situation is known in astrophysics where massive astronomical objects and their constituents interact through long-range gravitational forces.

Each single-particle orbit in the Fermi gas model is characterized by the momentum \mathbf{p} and spin–isospin quantum numbers. The single-particle stationary states are the plane waves normalized in the volume V ,

$$\psi_{\mathbf{p}\sigma\tau}(\mathbf{r}) = \frac{1}{\sqrt{V}} e^{(i/\hbar)(\mathbf{p}\cdot\mathbf{r})} \chi_\sigma \Omega_\tau, \quad (7.1)$$

where spin and isospin parts are shown explicitly. The energy ϵ of the single-particle state (7.1) is a function of quantum numbers. Initially, we assume this function to be spin independent and isospin independent (the same for protons and neutrons) and isotropic in the momentum space, $\epsilon = \epsilon(p)$. Usually, this function is taken as quadratic,

$$\epsilon(p) = \frac{p^2}{2m^*}, \quad (7.2)$$

with the parameter of the *effective mass* m^* expressing the difference from the free motion case. This is the simplest example of the velocity-dependent influence of the mean field. But we can also assume more complicated functions $\epsilon(p)$ including those different for protons and neutrons. The single-particle states form degenerate time-conjugate pairs, in this case (\mathbf{p}, σ) and $(-\mathbf{p}, -\sigma)$.

The density of *single-particle* states plays an important role in determining the physical properties of the system. We denote this density as $v(\epsilon)$, keeping the standard

notation $\rho(E)$ for the level density of the whole *many-body* system at total energy E . If single-particle energies do not depend on spin-isospin quantum numbers, the latter enter the level density via a common degeneracy factor $g = (2s + 1)(2t + 1) = 4$. The momentum components p_i of the plane waves (7.1) are conveniently quantized by periodic boundary conditions, $p_i = (2\pi\hbar/L_i) \times (\text{integer})$, where the integer numbers can be positive or negative. Then the single-particle level density [QP, I, 3.7,8] is given by

$$\nu(\epsilon) = \int \frac{d^3 p d^3 r}{(2\pi\hbar)^3} \delta(\epsilon - \epsilon(p)) = V \frac{g}{2\pi^2 \hbar^3} p^2 \left(\frac{dp}{d\epsilon} \right)_{\epsilon(p)=\epsilon}, \quad (7.3)$$

or, for the quadratic spectrum (7.2),

$$\nu(\epsilon) = V \frac{gm^*}{2\pi^2 \hbar^3} p(\epsilon). \quad (7.4)$$

Here we have integrated over the angles in the momentum space so that $\nu(\epsilon)d\epsilon$ is the total number of single-particle states in the energy interval $[\epsilon, \epsilon + d\epsilon]$.

Any stationary state of the Fermi gas is uniquely determined by the set of the *occupation numbers* $\{n_{\mathbf{p}\sigma\tau}\}$ for all single-particle orbits. These numbers are equal to 0 or 1 defining empty and filled orbits, respectively. The wave function of the entire system is a *Slater determinant* built on the occupied orbits [QP, II, 15.4]. The total number of particle is fixed,

$$\sum_{\mathbf{p}\sigma\tau} n_{\mathbf{p}\sigma\tau} = A. \quad (7.5)$$

We can also make partial summations calculating number of protons, number of neutrons,

$$Z = \sum_{\mathbf{p}\sigma} n_{\mathbf{p}\sigma-1/2}, \quad N = \sum_{\mathbf{p}\sigma} n_{\mathbf{p}\sigma1/2}, \quad (7.6)$$

or, for example, in a certain range of momenta, we can sum over protons with the spin projection $+1/2$.

The energy associated with each Slater determinant state is the sum of energies ϵ over all occupied orbits,

$$E = E(\{n_{\mathbf{p}\sigma\tau}\}) = \sum_{\mathbf{p}\sigma\tau} \epsilon(\mathbf{p}\sigma\tau) n_{\mathbf{p}\sigma\tau}. \quad (7.7)$$

It is a functional of the occupation numbers n . In the same manner, an arbitrary one-body operator Q (5.20) has an expectation value in the determinantal state

$$\langle Q \rangle = \sum_{\mathbf{p}\sigma\tau} q(\mathbf{p}\sigma\tau) n_{\mathbf{p}\sigma\tau}, \quad (7.8)$$

where $q(\mathbf{p}\sigma\tau)$ is the expectation value of the operator Q in the single-particle state (7.1).

7.3 Ground State

If the single-particle energies $\epsilon(p)$ monotonously increase with the momentum p , the ground state of the Fermi gas obviously corresponds to the uniform occupation of A lowest orbitals (7.1) with no holes left.

Let us assume that a large particle number that is a multiple of g occupies completely all quartets (here $g = 4$) of lowest in energy degenerate single-particle states ("orbitals"). The boundary between occupied and empty states is called the *Fermi surface* Σ_F . This surface is a sphere $p = p_F$ in momentum space that includes exactly A orbitals. Using the standard recipe for the transformation of sums over quantized momentum components into integrals, from Eq. (7.5) we have

$$A = V g \int_{p < p_F} \frac{d^3 p}{(2\pi\hbar)^3} = \frac{Vg}{(2\pi\hbar)^3} \frac{4}{3} \pi p_F^3. \quad (7.9)$$

Thus, the *Fermi momentum* p_F is determined only by the density $n = A/V$ regardless of the dispersion law $\epsilon(p)$,

$$p_F = \hbar k_F = \hbar \left(6\pi^2 \frac{n}{g} \right)^{1/3}. \quad (7.10)$$

The wave vector $k_F = p_F/\hbar$ determines the de Broglie wave length $\lambda_F = 1/k_F$ of particles at the Fermi surface. If the mean interparticle distance \bar{r} is defined as

$$V = \frac{4\pi}{3} \bar{r}^3 A \quad \rightsquigarrow \quad \bar{r} = \left(\frac{3}{4\pi n} \right)^{1/3}, \quad (7.11)$$

it is of the order of λ_F ,

$$\frac{\bar{r}}{\lambda_F} = k_F \bar{r} = \left(\frac{9\pi}{2g} \right)^{1/3} \quad (7.12)$$

which gives $k_F \bar{r} = 1.52$ for $g = 4$. Therefore, at the Fermi surface Σ_F , the wave packets of particles are just on the brink of overlap. The average density of nuclear matter $n = 0.17 \text{ fm}^{-3}$ (approximately the central density in heavy nuclei) defines $k_F = 1.36 \text{ fm}^{-1}$, $p_F = \hbar k_F = 270 \text{ MeV}/c$, which corresponds to the velocity at the Fermi surface $v_F \approx 0.27 c$.

Problem 7.1 The Λ -hyperon is a heavy analog of the neutron, where one of the d -quarks is substituted by the strange s -quark; its mass is $m_\Lambda = 1115.7 \text{ MeV}/c^2$. It has spin 1/2 and isospin $T = 0$ (see Figure 2.2). This particle decays due to the weak interaction to a nucleon and pion (either to $p\pi^-$ or to $n\pi^0$) with the mean lifetime 260 ps. The Λ -particle produced in a nuclear reaction can live for some time inside a nucleus, forming a *hyper-nucleus*. Eventually it decays either by the same channels as in vacuum or by the weak interaction with the nucleons of the host nucleus, $\Lambda + N \Rightarrow N + N$. The probabilities of these processes can be suppressed by the Pauli principle that blocks final states already occupied by the nucleons. Using the conservation laws, estimate energy and momentum of the newborn nucleon. Taking the Pauli exclusion principle into account, what should be the main type of Λ -decay (mesonic or non-mesonic) in a nucleus?

Solution

The kinetic energy of the nucleon from the mesonic decay can be estimated as

$$K_N \approx \frac{(M_\Lambda - M_N)^2 - m_\pi^2}{2M_\Lambda} c^2 \approx 5 \text{ MeV}. \quad (7.13)$$

This corresponds to the momentum of the newborn nucleon

$$p_N = \sqrt{2M_N K_N} \approx 100 \text{ MeV}/c. \quad (7.14)$$

For a nucleus that is not too light, this momentum is below the Fermi surface, so that the mesonic decay is suppressed. For the non-mesonic process, assuming for the estimate that two nucleons in the final state share evenly the kinetic energy,

$$K_N \approx \frac{M_\Lambda - M_N}{2} \approx 90 \text{ MeV} \quad \Leftrightarrow \quad p_N \approx 400 \text{ MeV}/c. \quad (7.15)$$

Indeed, observations confirm that the non-mesonic decay dominates for $A > 10$.

The states on Σ_F have energy

$$\epsilon_F = \epsilon(p_F). \quad (7.16)$$

This *Fermi energy* determines the borderline in energy space. For the quadratic spectrum (7.2), the Fermi energy is

$$\epsilon_F = \frac{p_F^2}{2m^*} = \frac{1}{2} \left(\frac{6\pi^2}{g} \right)^{2/3} \frac{\hbar^2 n^{2/3}}{m^*}. \quad (7.17)$$

Since the condition (7.10) in fact contains the density n/g per intrinsic (spin-isospin) degree of freedom, the result does not change if neutrons and protons are treated as two different gases of the same density $n/2$.

The Fermi energy is of the same order of magnitude as the degeneracy temperature T_d . This is the value of temperature, below which the notion of a classical gas of spatially separated distinguishable particles is getting invalid. The thermal de Broglie wavelength,

$$\lambda_{\text{th}} \sim \frac{\hbar}{p_{\text{th}}} \sim \frac{\hbar}{\sqrt{mT}}, \quad (7.18)$$

grows as temperature decreases and at

$$T_d \sim \frac{\hbar^2}{m} n^{2/3} \quad (7.19)$$

it reaches the size of the mean distance between the particles, $\bar{r} \sim n^{-1/3}$. When $\lambda_{\text{th}} \geq \bar{r}$, the wave packets of individual particles overlap, and their quantum indistinguishability makes it necessary to go over to quantum statistics (Bose or Fermi depending on spin of the particles). For the above-mentioned value of k_F , the Fermi energy is $\epsilon_F = 38(m/m^*)$ MeV. There are indications that the effective mass on Σ_F is of the order $0.7m$, which would lead to $\epsilon_F \approx 55$ MeV. It is impossible to excite a nucleus up to a temperature of this order since it will cease to exist as a bound system much earlier. As a result, we are always working at temperatures much lower than $T_d \sim \epsilon_F$. The nuclear Fermi gas is highly *degenerate*, and quantum statistical laws related to antisymmetry of wave functions and Pauli exclusion principle are crucial.

An external excitation of a degenerate Fermi system with a low frequency, $\omega \ll \epsilon_F/\hbar$, first acts on the particles near Σ_F . Particles in deeply lying orbitals are *frozen* because the energy $\hbar\omega$ is not sufficient to bring them into empty states above the Fermi level. The response of the system to a perturbation depends critically on the number of particles and available empty levels near Σ_F , which, in turn, are determined by the single-particle level density $\nu_F = \nu(\epsilon_F)$. In the case of the quadratic dispersion law, we obtain from (7.4)

$$\nu_F = V \frac{gm^*}{2\pi^2\hbar^3} p_F, \quad (7.20)$$

or, comparing (7.20) with (7.9) and (7.17),

$$v_F = \frac{3}{2} \frac{A}{\epsilon_F}. \quad (7.21)$$

The level density (7.4) at any energy ϵ is scaled in this case as

$$v(\epsilon) = v_F \sqrt{\frac{\epsilon}{\epsilon_F}}. \quad (7.22)$$

For a nonquadratic dispersion law, we can still use the expression (7.20) for the single-particle level density if we define the velocity on Σ_F as $v_F = (de/dp)_F$ and the effective mass as $m^* = p_F/v_F$.

Having the single-particle level density $v(\epsilon)$ at our disposal, we can calculate the mean values of the observables like (7.8) in the obvious way,

$$\langle Q \rangle = \frac{1}{2} \sum_{\sigma} \frac{1}{2} \sum_{\tau} \int \frac{d\omega}{4\pi} \int d\epsilon v(\epsilon) q(\mathbf{p}\sigma\tau) n_{\mathbf{p}\sigma\tau}. \quad (7.23)$$

This is valid for any momentum-dependent one-body operator Q and for any state (not necessarily the ground state of the Fermi gas) if the occupation numbers are replaced by their *expectation values*, which can be noninteger but always between 0 and 1.

The total ground state energy for the occupied Fermi sphere is given by Eq. (7.7),

$$E_0 = \int_0^{\epsilon_F} d\epsilon v(\epsilon) \epsilon. \quad (7.24)$$

For the quadratic spectrum, we have with the aid of (7.21) and (7.22)

$$E_0 = \frac{2}{5} v_F \epsilon_F^2 = \frac{3}{5} A \epsilon_F. \quad (7.25)$$

As it should be for an extensive quantity, the energy is linear in a particle number with average energy per particle equal to

$$\bar{\epsilon} = \frac{3}{5} \epsilon_F. \quad (7.26)$$

Note that in our formulae we assumed that the lowest single-particle energy corresponds to the bottom of the box, which was taken as the origin of the energy scale. To mimic the situation in a bound nucleus, we need to consider all energies ϵ of occupied single-particle states as negative. It means that, for example, instead of (7.2) we have to write

$$\epsilon(p) = \frac{p^2}{2m^*} - U_0 \quad (7.27)$$

where U_0 is the depth of the potential well, $U_0 > 0$. The Fermi energy ϵ_F is negative, its absolute value being the separation energy of particles from Σ_F . Almost all our results remain unchanged. The total energy (7.24) acquires an extra negative term $-AU_0$. Using Eq. (7.25) for kinetic energy, we obtain the volume part of the total energy as

$$E_0 = -A \left(U_0 - \frac{3}{5} \epsilon_F \right). \quad (7.28)$$

This can be used for a crude estimate of the depth of the potential well (our first candidate for the nuclear mean field). Using for E_0/A the value of the volume coefficient b_V from the mass formula, we obtain $U_0 \simeq 40 \div 50$ MeV depending on the effective mass m^* .

7.4 Correlation Between Particles

Although in our approximation, particles moving in the mean field do not have direct dynamical interactions, their quantum motion is correlated, this is still a *degenerate quantum many-body* system. The correlations are *kinematic*, they are caused by the Fermi statistics, and therefore they are not related to any forces.

Correlations in the coordinate space are calculated in [QP,II, Problem 19.2]. The typical correlation length is determined by Fermi motion, $\sim 1/k_F$, which is slightly smaller than the mean interparticle distance. These correlations exist only between the identical particles with the same spin projections, whereas the particles with different intrinsic quantum numbers are essentially independent in this approximation. The *density correlator* is defined as the expectation value in the ground state,

$$C(r) = \langle n(\mathbf{r}_1, \sigma) n(\mathbf{r}_2, \sigma) \rangle, \quad r = |\mathbf{r}_1 - \mathbf{r}_2|. \quad (7.29)$$

In fulfillment of the Pauli exclusion principle, the correlation function is negative (*correlational hole*) and, at the relative distance $r \neq 0$, is given by the function

$$C(r) = -\frac{k_F^6}{4\pi^4} \frac{[\sin x - x \cos x]^2}{x^6}, \quad x = k_F r. \quad (7.30)$$

These kinematic correlations rapidly fall down at $x > 1$. This means that, for particles with coinciding spin projections, the most important interactions will be those with the radius of action of order of the average distance between the particles that is determined by the mean density. The correlation function (7.30) is shown in Figure 7.1.

The realistic interactions depend on the relative energy of interacting (colliding) particles. Therefore, it is useful to know the distribution of particles with respect to their relative momentum. For two fermions with momenta (we use the wave vectors) \mathbf{k}_1 and \mathbf{k}_2 , we define the total momentum of the pair, $\mathbf{K} = \mathbf{k}_1 + \mathbf{k}_2$, and their relative momentum $\mathbf{k} = [\mathbf{k}_1 - \mathbf{k}_2]/2$. Both momenta, \mathbf{k}_1 and \mathbf{k}_2 , are confined inside the Fermi surface:

$$k_1 = |\mathbf{k} + \mathbf{K}/2| \leq k_F, \quad \text{and} \quad k_2 = |- \mathbf{k} + \mathbf{K}/2| \leq k_F. \quad (7.31)$$

This sets the geometric conditions for the allowed angle between \mathbf{k}_1 and \mathbf{k}_2 ; these conditions depend on the total momentum K .

If $K/2$ is smaller than $k_F - k$, any relative direction is allowed, and the integral over the solid angle of \mathbf{k} equals 4π . The maximum possible magnitude of the total momentum is

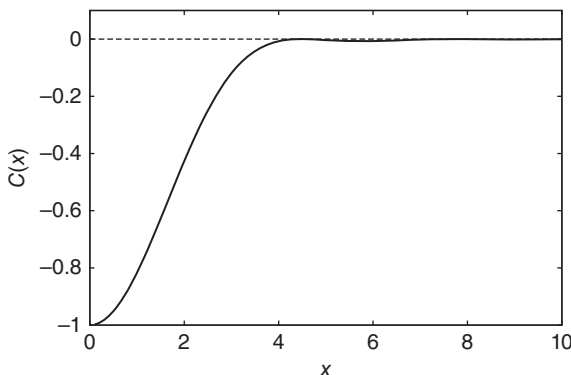


Figure 7.1 Correlation function (for $r \neq 0$) of two fermionic densities as a function of $x = k_F r$.

determined by

$$\frac{1}{2} K_{\max} = \sqrt{k_F^2 - k^2}. \quad (7.32)$$

In between, for

$$k_F - k \leq \frac{1}{2} K_{\max} \leq \sqrt{k_F^2 - k^2}, \quad (7.33)$$

the integral over the solid angle covers only a part of 4π ,

$$\Delta\Omega = 4\pi \frac{k_F^2 - k^2 - K^2/4}{k^2}. \quad (7.34)$$

It follows from here that, for a given value of k , the allowed values of the total momentum correspond to

$$I_k = \left[\int d^3K \right]_k = 4\pi \left\{ \int_0^{2(k_F-k)} dK K^2 + \int_{2(k_F-k)}^{2\sqrt{k_F^2-k^2}} dK K^2 \frac{k_F^2 - k^2 - K^2/4}{k^2} \right\}. \quad (7.35)$$

The integration leads to

$$I_k = \frac{32\pi}{3} k_F^3 \left(1 - \frac{3k}{2k_F} + \frac{k^3}{2k_F^3} \right). \quad (7.36)$$

This allowed phase space volume for the total momentum determines the probability $W(k)$ of the relative momentum k . If we normalize it according to

$$\int_0^{k_F} dk k^2 W(k) = 1, \quad (7.37)$$

then the result follows from (7.36):

$$W(k) = \frac{24}{k_F^3} \left(1 - \frac{3k}{2k_F} + \frac{k^3}{2k_F^3} \right). \quad (7.38)$$

This distribution is shown in Figure 7.2. The maximum of the distribution corresponds approximately to $0.6k_F$ or to a relative energy ~ 30 MeV in the center-of-mass frame of interacting nucleons.

7.5 Asymmetric Systems and Chemical Equilibrium

It is easy to introduce corrections for a difference in proton and neutron numbers. The neutron excess gives rise to the positive symmetry energy in the mass formula because equalizing the Fermi energies for protons and neutrons would reduce the total kinetic energy.

Problem 7.2 The part of the symmetry energy term in the mass formula is determined by the fact that, according to the Pauli principle, the kinetic energy of a

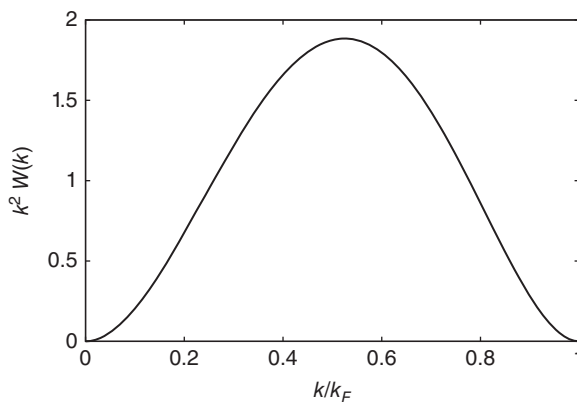


Figure 7.2 Distribution function $k^2 W(k)$ of the relative momentum in Fermi gas at zero temperature.

two-component Fermi gas is minimized when the particle numbers of the two components are equal. Find the corresponding contribution, b_{sym} , to the symmetry energy coefficient.

Solution

In the Fermi gas model with the quadratic dispersion law, the total kinetic energy is

$$E_0 = \frac{3}{5} [N\epsilon_F^n + Z\epsilon_F^p]. \quad (7.39)$$

Fermi energies for neutrons and protons moving in the common volume V are different,

$$\epsilon_F^n = \epsilon_\circ N^{2/3}, \quad \epsilon_F^p = \epsilon_\circ Z^{2/3}, \quad \epsilon_\circ = \frac{\hbar^2}{2M} \left(\frac{3\pi^2}{V} \right)^{2/3}. \quad (7.40)$$

For small asymmetry, $T_3 = (N - Z)/2 \ll A$, $N = (A/2) + T_3$, $Z = (A/2) - T_3$, the energy (7.39) is

$$E_0 = \frac{3}{5} \epsilon_\circ \left[\left(\frac{A}{2} + T_3 \right)^{5/3} + \left(\frac{A}{2} - T_3 \right)^{5/3} \right]. \quad (7.41)$$

Keeping terms up to the second order in T_3 ,

$$E_0 = \frac{3}{5} A \epsilon_F \left(1 + \frac{20}{9} \frac{T_3^2}{A^2} \right), \quad (7.42)$$

where $\epsilon_F = \epsilon_\circ (A/2)^{2/3}$ is the Fermi energy of a symmetric nucleus, $N = Z = A/2$. The second term in Eq. (7.42) is to be identified with the symmetry energy

$$E_{\text{sym}} = b_{\text{sym}} \frac{(N - Z)^2}{2A}. \quad (7.43)$$

It leads to

$$b_{\text{sym}} = \frac{2}{3} \epsilon_F. \quad (7.44)$$

The semiempirical mass formula gives $b_{\text{sym}} \approx 48 \text{ MeV} \approx (4/3)\epsilon_F$. This implies that only a half of the symmetry energy comes from kinetic energy; the rest is due to the interaction of particles ignored in the Fermi gas model.

The $n-p$ interaction is slightly stronger than that in the pairs of identical particles. Therefore, the average potential acting upon single-particle motion is different for neutrons and protons depending on the neutron excess in the core that creates the mean field. The isospin-invariant formulation of this fact can depend only on the isoscalar combination $(\mathbf{t} \cdot \mathbf{T})$, where \mathbf{t} is the isospin of the considered particle, and \mathbf{T} is the total isospin of the field created by all other particles, that is, the isospin of the rest of the nucleus. In accordance with this, we write the global nuclear potential as

$$U = U_0 + \frac{U_1}{A} (\mathbf{t} \cdot \mathbf{T}^{\text{core}}). \quad (7.45)$$

The expectation value of this potential in the ground state contains only t_3 of the valence nucleon and $T_3^{\text{core}} = (N - Z)/2$,

$$U = U_0 + t_3 \frac{N - Z}{2A} U_1. \quad (7.46)$$

The total potential symmetry energy can be obtained by summing all potentials (7.46) acting on individual nucleons and dividing by 2 in order to avoid the double counting if it is assumed that this potential is generated by the two-body nucleon–nucleon interaction,

$$U_{\text{sym}}^{\text{pot}} = \frac{1}{2} \left[N \times \frac{1}{2} + Z \times \frac{-1}{2} \right] \frac{N - Z}{2A} U_1 = \frac{1}{8} \frac{U_1}{A} (N - Z)^2. \quad (7.47)$$

This gives the potential part of the symmetry energy coefficient in the mass formula

$$b_{\text{sym}} = \frac{1}{4} U_1 \approx 25 \text{ MeV}, \quad (7.48)$$

where the estimate is performed with the empirical value $U_1 \approx 100 \text{ MeV}$ for heavy nuclei, $A \sim 200$, $Z \sim 80$. Thus, the symmetry energy in heavy nuclei is generated by two nearly equal parts: by the Pauli principle (kinetic part) and by the stronger $p-n$ interaction (potential part).

The Coulomb energy acting only onto protons can be accounted for taking instead of (7.27) a sum of the proton and neutron contributions with the bottom of the proton well shifted up by the average Coulomb energy per particle E_C/Z . The most energetically favorable proton/neutron ratio is also influenced by the difference of their masses that acts to slightly counterbalance the Coulomb repulsion among protons. The total energy including rest masses is, in this improved approximation,

$$E_0 = -N \left[U_0 - \frac{3}{5} \epsilon_F(n) - M_n c^2 \right] - Z \left[\left(U_0 - \frac{E_C}{Z} \right) - \frac{3}{5} \epsilon_F(p) - M_p c^2 \right]. \quad (7.49)$$

The minimization of energy (7.44) with respect to Z at fixed $A = Z + N$ gives a reasonable estimate for the *line of beta-stability*. Nuclei with the ratio Z/N deviating from this line undergo beta-decay that preserves A but changes the proton–neutron composition toward the stability.

The derivative of total energy with respect to a particle number (the derivative should be taken at fixed volume, which will be marked by a subscript) is a *chemical potential* μ . For a one-component Fermi gas, Eq. (7.25) determines [recall that, according to (7.17), $\epsilon_F \propto (A/V)^{2/3}$]

$$\mu = \left(\frac{\partial E_0}{\partial A} \right)_V = \frac{5}{3} \frac{E_0}{A} = \epsilon_F. \quad (7.50)$$

Thus, at zero temperature, the chemical potential of the Fermi gas is equal to the Fermi energy. This result is independent of the dispersion law. Indeed, Eq. (7.24) leads to

$$\mu = \left(\frac{\partial E_0}{\partial A} \right)_V = \frac{\partial E_0}{\partial \epsilon_F} \frac{\partial \epsilon_F}{\partial A} = \epsilon_F v_F \frac{\partial \epsilon_F}{\partial A}. \quad (7.51)$$

But, as follows from Eq. (7.5) written in the integral form similar to (7.24),

$$A = \int^{\epsilon_F} d\epsilon v(\epsilon) \Rightarrow \frac{\partial A}{\partial \epsilon_F} = v_F, \quad (7.52)$$

so that we come to $\mu = \epsilon_F$ as in (7.50). This is essentially the condition of *statistical equilibrium*: the mean energy required for the extraction of a particle from the system, which is just the definition of the chemical potential, has to be equal to the Fermi energy.

For the case of asymmetric ($N \neq Z$) two-component gas, we obtain from (7.49) two chemical potentials for protons and neutrons separately. Redefining them to include the rest mass, we have

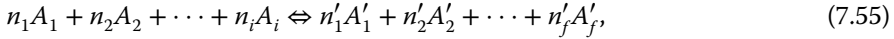
$$\mu_p = \frac{\partial E_0}{\partial Z} = M_p c^2 + \epsilon_F(p) + \frac{\partial E_C}{\partial Z}, \quad \mu_n = \frac{\partial E_0}{\partial N} = M_n c^2 + \epsilon_F(n). \quad (7.53)$$

The above-mentioned minimization of the total energy gives the condition

$$\mu_p = \mu_n. \quad (7.54)$$

This means that in stable nuclei, the Coulomb repulsion increases all proton-level energies so that the Fermi surfaces of protons and neutrons for $N > Z$ coincide.

The equality of chemical potentials (7.54) is nothing but the condition of *chemical equilibrium*. Let a reaction (chemical or nuclear),



transforming initial species A_1, \dots, A_i into final species A'_1, \dots, A'_f and vice versa, be possible. Here n_j and n'_j are the numbers of objects of each sort participating in the reaction (*stoichiometric* coefficients in chemistry). In equilibrium, the rates of the direct and reverse reactions are balanced to ensure the stationary concentrations of all species. Looking for minimum of energy, or *free energy* at $T \neq 0$, we find the equilibrium relation between the chemical potentials of all reagents,

$$n_1 \mu_1 + \cdots + n_i \mu_i = n'_1 \mu'_1 + \cdots + n'_f \mu'_f. \quad (7.56)$$

If Eq. (7.54) is fulfilled, a nucleus is stable with respect to reactions transforming $n \Leftrightarrow p$ (decays by *weak interaction*). Weak decays are much slower than typical nuclear processes. As a result, there exist many nuclides unstable with respect to beta-decay but sufficiently long-lived to be considered as stable on a nuclear timescale.

7.6 Pressure and Speed of Sound

Due to the Pauli principle, the filled Fermi sphere contains (at zero temperature!) many particles with different momenta and exerts pressure onto the volume walls. Increasing the size in the x -direction by dx , we decrease all momenta and therefore decrease the

energy by dE , which is the work of the force $F = -dE/dx$. The force F/A referred to the unit area in the yz -plane, perpendicular to the displacement, is *pressure*, recall Eq. (6.1),

$$P = \frac{F}{A} = -\frac{dE}{A dx} = -\frac{dE}{dV}. \quad (7.57)$$

This derivative has to be calculated at the fixed particle number A . For the quadratic dispersion law, the Fermi energy (7.17) is proportional to $n^{2/3} = (A/V)^{2/3}$, so that Eq. (7.25) gives

$$P = \frac{2 E_0}{3 V} = \frac{2}{3} n \bar{\epsilon} \propto n^{5/3}. \quad (7.58)$$

As density increases, the Fermi energy can exceed the rest energy Mc^2 . Then particles in the top layer of the Fermi sphere become *relativistic* that modifies all expressions. With further increase, we come to the *ultrarelativistic* limit when one can neglect the rest mass and use $\epsilon(p) \approx cp$. The definition of the Fermi momentum is still the same, Eq. (7.10), so that in this case $\epsilon_F \propto n^{1/3}$. Then we have the level density $v_F \propto \epsilon_F^2 \propto n^{2/3}$ and the ground state energy (7.24) $E_0 \propto \epsilon_F^4 \propto n^{4/3}$. It is easy to see that for the linear dispersion law $P = (1/3)(E_0/V)$ and pressure is growing with density as $n^{4/3}$. Thus, in the ultrarelativistic limit, the density dependence of pressure becomes weaker, and this is important for the properties of dense matter, for example, in stellar evolution.

Since pressure of the Fermi gas depends on density, the perfect gas reveals *elastic properties*. The speed of sound is given by the usual expression (6.4) where the derivative has to be calculated at the fixed particle number A . Introducing the energy density $e = E_0/V$ and density $n = A/V$, we can rewrite the definition of pressure (7.57) explicitly in terms of extensive quantities,

$$P = n \frac{\partial e}{\partial n} - e. \quad (7.59)$$

Then the speed of sound, Eq. (6.4), is equal

$$c_s^2 = \frac{1}{M} \frac{\partial P}{\partial n} = \frac{n}{M} \frac{\partial^2 e}{\partial n^2}. \quad (7.60)$$

Here M is a bare particle mass determining the mass density Mn . Often it is useful to define the speed of sound in terms of the chemical potential $\mu = (\partial E_0 / \partial A)_V = (\partial e / \partial n)$,

$$c_s^2 = \frac{A}{M} \frac{\partial \mu}{\partial A}. \quad (7.61)$$

For a gas with the quadratic dispersion law, $e \propto n^{5/3}$, we obtain with the help of Eq. (7.25)

$$c_s^2 = \frac{n}{M} \left(\frac{5}{3} \times \frac{2}{3} \right) \frac{e}{n^2} = \frac{10}{9} \frac{E_0}{MA} = \frac{2}{3} \frac{\epsilon_F}{M}. \quad (7.62)$$

The Fermi energy (7.17) contains the *effective mass* m^* so that the result is

$$c_s^2 = \frac{p_F^2}{3Mm^*} = \frac{1}{3} v_F^2 \frac{m^*}{M}. \quad (7.63)$$

If the mass renormalization is weak, $m^* \approx M$, the speed of sound is $c_s \approx v_F/\sqrt{3}$.

Our calculation is formally correct, but we have to remember that the application of the hydrodynamic approach implies that there is a thermodynamic equilibrium inside a small element satisfying equations of motion (6.2,3). In the propagation process of the

density and pressure wave, the *local equilibrium* conditions corresponding to a variable density should be established. The mechanism of equilibration is not considered in the theory of perfect gases. The underlying assumption is that such a mechanism is provided by particle collisions. The efficiency of this mechanism depends on the collision rate, but it does not influence the equilibrium properties. For given external parameters, the equilibrium is always the same corresponding to minimum energy or, at $T \neq 0$, free energy. The collision rate determines the *relaxation time* necessary to establish the equilibrium. However, for the sound propagation, the time τ of local equilibration has to be short enough compared to a period $\sim 1/\omega_s$ of the sound wave. From therefore sound can propagate only as a *low-frequency* wave,

$$\omega_s \tau \ll 1. \quad (7.64)$$

In a perfect Fermi gas at $T \rightarrow 0$, the collisions are strongly suppressed. Due to energy–momentum conservation, the orbitals above Σ_F are inaccessible for final particles, whereas inside Σ_F the Pauli principle makes any redistribution of fermions impossible. The effective collisions are possible only for thermally excited particles. Their number goes to zero along with temperature. Consequently, the collision rate decreases and τ grows violating the propagation condition (7.64). As a result, the sound in a perfect Fermi gas at low temperature is strongly absorbed giving rise to uncorrelated motion of individual particles. This damping is possible due to a resonance between the single-particle excitations and the waves with the velocity lower than Fermi velocity as in Eq. (7.63).

Our calculation was also not fully consistent in another aspect. The quasiparticle energies include, for example, in the form of effective mass, the interaction effects. Effects of the same order change the energy of quasiparticles perturbed by the wave: in Eq. (7.61), the local change of density in the field of the sound wave changes not only the numerical value of the local kinetic Fermi energy but also the energy (7.2) of each particle. Such effects transform a Fermi gas into a *Fermi liquid* [2].

7.7 Gravitational Equilibrium

The properties of the Fermi statistics define the fate on some stellar objects and many observational facts in astrophysics [3, 4]. In *white dwarf* stars, the gravitational collapse is counteracted by the Fermi pressure of the *electron gas*. If the electron density is not too high, the electrons form a *non-relativistic* degenerate Fermi gas and we can make estimates for zero temperature. For a star of mass M_\star , the equilibrium condition, in concordance to the virial theorem [QP, I, 7.7], is that the potential gravitation energy is balanced by the electron kinetic energy. For order-of-magnitude estimates we can write down the equilibrium condition as

$$E_{\text{kin}} \sim N_e \epsilon_{F_e} \sim E_{\text{grav}} \sim \frac{GM_\star^2}{R_\star}, \quad (7.65)$$

where N_e is the number of electrons, ϵ_{F_e} their Fermi energy, G Newtonian gravitational constant, and R_\star radius of a star. The electron charge is compensated by the charge Z of

nuclei. Neglecting the mass difference between protons and neutrons and the electron contribution to the total mass M_\star we have the number of nuclei equal to M_\star / AM_p , where A is the atomic weight of the nuclei. If Z is the charge of the nucleus, the number of electrons should be equal to $N_e = ZM_\star / AM_p$, and the condition of equilibrium (7.64) takes the form

$$\frac{Z}{A} \frac{M_\star}{M_p} \frac{\hbar^2 n_e^{2/3}}{m_e} \sim \frac{GM_\star^2}{R_\star}, \quad (7.66)$$

where the typical electron energy is taken as their Fermi energy, m_e is the electron mass. The electron density n_e can be estimated as N_e / R_\star^3 .

Now the balance estimate (7.66) leads to the value of the white dwarf radius

$$R_\star \sim \frac{\hbar^2 (Z/A)^{5/3}}{G m_e M_p^{5/3} M_\star^{1/3}}. \quad (7.67)$$

For $Z/A \approx 1/2$ and M_\star as a solar mass, 2×10^{33} g, this gives about 2×10^4 km, a little bigger than the exact calculation, but with the correct parametric dependence. With increasing mass M_\star , the radius is going down.

Our estimates can be prolonged to higher densities when the electron gas becomes *relativistic* with changes briefly discussed after Eq. (6.62). We go essentially through the same steps as above but the Fermi energy is now

$$\epsilon_{F_e} = cp_{F_e} \sim c\hbar n_e^{1/3} \propto R_\star^{-1}, \quad (7.68)$$

and the comparison with gravitational energy excludes R from the result,

$$\hbar c \left(\frac{M_\star Z}{AM_p} \right)^{4/3} \sim GM_\star^2. \quad (7.69)$$

This determines the limiting mass M_\star when it is still possible, due to the Fermi pressure of the relativistic electron gas, to withstand the gravitational force,

$$M_\star \sim \left(\frac{\hbar c}{G} \right)^{3/2} \left(\frac{Z}{AM_p} \right)^2. \quad (7.70)$$

This mass is called the *Chandrasekhar limit*. It is impossible to hold against the gravitational collapse for the mass beyond this limit just by using the degenerate relativistic electron gas. Equation (7.70) gives for this limit approximately $2(Z/A)^2$ of the solar mass. The full calculation with correct numerical factors gives a result about three times larger providing the limit of 1.4 solar masses.

In the *neutron stars* [5], which are most probably the remnants of the supernova explosion, the neutron is effectively stable because of too high Fermi energy of the electrons emerging as a result of the neutron beta-decay. Then the gravitational collapse is prevented by the Fermi pressure of the neutron gas plus repulsive short-range nuclear interaction between neutrons. This is again possible only if the mass of the star does not exceed some upper limit, the so-called *Tolman–Oppenheimer–Volkoff (TOV) limit*. For this calculation, one has to use the results of general relativity so we avoid it here. Different estimates put this limit below three solar masses. Recently, a mass of the neutron

star was measured [6] using the spectra of its white dwarf companion to be 2.01 ± 0.04 of solar masses. Above the TOV limit, a neutron star either will collapse to a black hole or undergo a phase transition to something like a quark star.

7.8 Nuclear Matter Equation of State

Here we briefly discuss the relation between the simple models (liquid drop and Fermi gas) and a more realistic picture of interacting nuclear matter. Although the gas occupies the whole volume allowed by external conditions, the liquid should have a property of *saturation*. It means that its energy dependence on volume has a minimum at some equilibrium density. This property is generated by the interparticle forces: further increase in density is energetically unfavorable because of repulsive short-range forces, while decrease in density would diminish the influence of attractive forces. If the minimum is clearly developed, the liquid cannot be easily compressed, the property of nuclear matter used in the liquid-drop model of Chapter 5.

Let us consider this connection from the perspective of statistical mechanics where in the microcanonical ensemble the total internal energy is a function of the particle number A and volume V . We discuss here the ground state properties or the zero temperature limit, therefore

$$dE_0 = \left(\frac{\partial E_0}{\partial A} \right)_V dA + \left(\frac{\partial E_0}{\partial V} \right)_A dV. \quad (7.71)$$

Here

$$\epsilon_F = \mu = \left(\frac{\partial E_0}{\partial A} \right)_V \quad (7.72)$$

which is the definition of the chemical potential that at zero temperature coincides with the Fermi energy (7.50).

In the Fermi gas model at saturation density, adding a particle to Σ_F in the system of A particles, we obtain again the ground state of the system with $A + 1$ particle,

$$E_0(A + 1) = E_0(A) + \epsilon_F. \quad (7.73)$$

For sufficiently large A , this is equivalent to

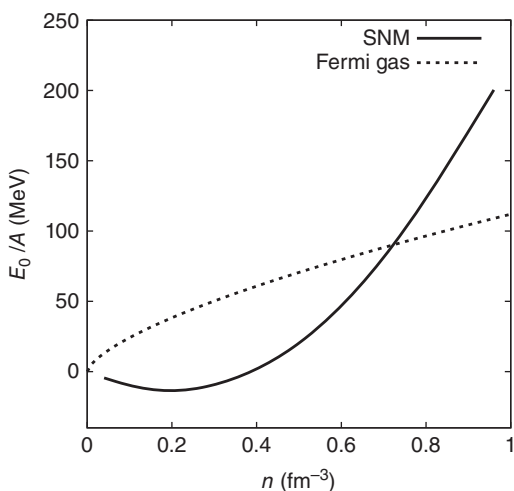
$$dE_0 = \epsilon_F dA. \quad (7.74)$$

Therefore, the second (pressure) term in (7.71) must be zero; this expresses the saturation condition that, for a given particle number, the binding energy reaches its minimum at the saturation density n_0

$$\frac{\partial(E_0/A)}{\partial n} = 0. \quad (7.75)$$

As suggested at the beginning of this discussion, the saturation property emerges due to the interactions that generally modify the *equation of state* of the nuclear matter from that of Fermi gas (7.25). Therefore, the behavior of energy per nucleon is quite different from $E_0/A \propto n^{2/3}$ (see Figure 7.3). The nuclear equation of state has a minimum of energy per particle at the saturation density n_0 . From the liquid-drop model systematics, we know that $n_0 = 0.17 \text{ fm}^{-3}$ and the energy per nucleon for symmetric matter

Figure 7.3 Equation of state for Fermi gas and for symmetric nuclear matter (SNM). The latter is obtained theoretically in Ref. [7] using the Argonne v_{18} nucleon–nucleon potential with added three-body interactions.



at this point is $-b_V \approx 15$ MeV. Various measurements, such as frequencies of nuclear monopole vibrations and the breathing modes that are associated with compressions, allow to determine the second derivative at the minimum, known as the compressibility coefficient (sometimes called *incompressibility*)

$$K = 9n_0^2 \frac{\partial^2(E_0/A)}{\partial n^2}. \quad (7.76)$$

There is no complete agreement between various measurements and theories in relation to the compressibility; it is believed that K is between 200 and 300 MeV. The lower and higher limits are, respectively, referred to as corresponding to the soft and hard equations of state.

Heavy-ion reactions provide access to the equation of state for dilute matter, $n < 2n_0$, where one can use a phenomenological expansion [8]

$$E_0/A = \sum_{p=2,3,4,5} a_p \left(\frac{n}{n_0} \right)^{p/3}. \quad (7.77)$$

At low densities, $n \sim 0.4 n_0$, nuclear matter undergoes a *liquid–gas phase transition*. The nuclear equation of state at higher densities and for asymmetric matter is less known but it remains a subject of active research.

References

- 1 R.P. Feynman, *Photon-Hadron Interactions*, Advanced Book Classics, Westview Press, Reading, MA, 1998.
- 2 L.P. Pitaevskii and E.M. Lifshitz, *Statistical Physics, Part 2: Theory of the Condensed State*, Vol. 9 of the Course of Theoretical Physics by L.D. Landau, and E.M. Lifshitz, Butterworth-Heinemann, 1980.
- 3 M.L. Kutner, *Astronomy: A Physical Perspective*, Cambridge University Press, Cambridge, 2003.

- 4 S.E. Woosley, A. Heger, and T.A. Weaver, Rev. Mod. Phys. **74**, 1015 (2002).
- 5 P. Haensel, A.Y. Potekhin, and D.G. Yakovlev, *Neutron Stars*, Springer-Verlag, New York, 2007.
- 6 P.B. Demorest, T. Pennucci, S.M. Ransom, M.S. Roberts et al., Nature **467**, 1081 (2010).
- 7 A. Akmal, V.R. Pandharipande, and D.G. Ravenhall, Phys. Rev. C **58**, 1804 (1998).
- 8 J. Kapusta, Phys. Rev. C **29**, 1735(1984).

8

Spherical Mean Field

Wigner, too, believed in the liquid drop model but he recognized, from the work of Maria Mayer, the very strong evidence for the closed shells. It seemed a little like magic to him, and that is how the words “Magic Numbers” were coined.

From a talk by S. Moszkowski presented at the APS meeting in Indianapolis, May 4, 1996, cited by G. Audi in the paper “*The History of Nuclidic Masses and of their Evaluation*,” arXiv:physics/0602050.

8.1 Introduction

The smooth behavior of binding energy according to the mass formula cannot explain the modulations visible in Figures 5.1 and 5.4. Now we examine the clustering of single-particle levels called *shell structure*.

The existence of the single-particle shells is well known from atomic systems starting with the lightest hydrogen atom. This phenomenon is in the core of the periodic table of chemical elements. Many mesoscopic systems, such as atomic clusters, cold atoms in traps, and electrons in quantum dots, reveal a similar modulation of the level density. From theoretical point of view, the shell structure reflects deep properties of the dynamics. In this chapter, we discuss the main observable features of nuclear shells.

The simplest approach to the shell structure is the *independent particle shell model*. This is nothing but a Fermi gas model for *realistic nuclear potentials* taken as a mean field. Here we take into account individual properties of the single-particle mean-field orbitals going beyond the average statistical description of Chapter 7. Historically the idea of nuclear shells was juxtaposed to Bohr’s picture of the *compound nucleus*. Now we understand the validity of both seemingly opposite pictures: the compound nucleus features emerge naturally with an increase in the level density; they correspond to the emergence of the many-body *quantum chaos* that does not contradict to the ordered shell structure of the mean field. Let us briefly enumerate the brightest experimental facts indicating the reality of nuclear shells.

8.2 Magic Numbers

In atomic physics, the most stable atoms are those of noble gases. This can be seen in Figure 8.1 where atomic ionization energy, which is the energy it takes to remove

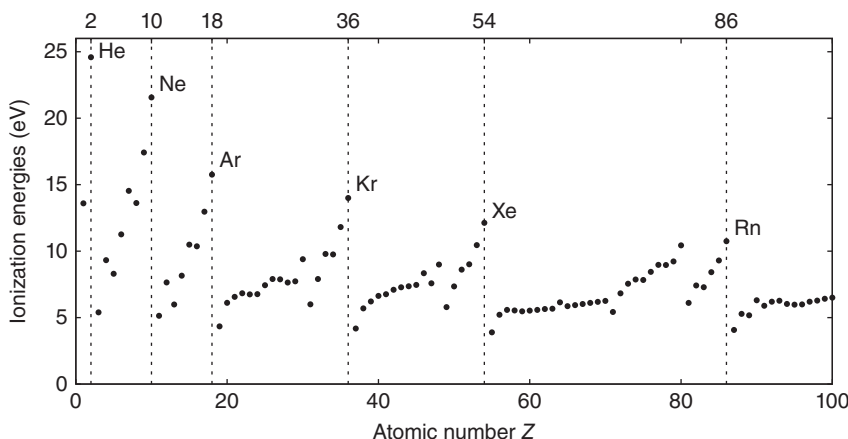


Figure 8.1 Atomic ionization energies.

one electron, is shown. They have a number of electrons (equal to the nuclear charge) exactly fitted to the complete filling of a given shell. The atomic shell is a set of electron orbitals labeled by the quantum numbers n, ℓ, m_ℓ, m_s . At fixed n , these orbitals are close in energy $\epsilon_{n\ell}$, nearly degenerate in magnetic quantum numbers m_ℓ and m_s , and separated from other shells by a wider spacing.

In nuclear physics, we also see that a certain number of protons and neutrons lead to especially stable nuclear systems. Those *magic numbers* for nuclei along the valley of stability are

$$2, 8, 20, 50, 82, 126. \quad (8.1)$$

Since the shape of the mean field is nearly the same for protons and neutrons, the magic numbers turn out to be the same as well. The most stable are the *doubly-magic* nuclei, such as $^4_2\text{He}_2$, $^{16}_8\text{O}_8$, $^{40}_{20}\text{Ca}_{20}$, $^{208}_{82}\text{Pb}_{126}$. The formally double-magic tin isotopes $^{100}_{50}\text{Sn}_{50}$ and $^{132}_{50}\text{Sn}_{82}$ have too exotic neutron/proton ratios and turned out to be radioactive but still reveal some features of “magicity.” Figure 5.2 showed the increased binding energy in the vicinity of the doubly-magic nuclei. By analogy with the atomic case, we conclude that the list (8.1) contains a number of particles for the closed *major shells*. The major shells are separated by relatively large energy gaps that suppress the probability of the ground state to involve particle excitations into the neighboring major shells.

There are also less pronounced but still noticeable effects of the closure of *subshells* at numbers of protons or neutrons equal to 6, 28, 40, and others. The energy spacings between the subshells within a given major shell are narrower than between the major shells.

Nuclei with magic Z have an increased number of stable (in nuclear sense, which means with respect to the spontaneous emission of nucleons but not to the beta-decay) isotopes with different N , whereas nuclei with magic N have an increased number of isotones with different Z . Probably the record is set by the proton-magic tin isotopes, $Z = 50$, which were observed to cover not only the entire interval between the two magic

neutron numbers, from $^{100}_{50}\text{Sn}_{50}$ to $^{132}_{50}\text{Sn}_{82}$, but also stretch far beyond (the exact upper boundary for particle-stable tin isotopes is not established yet).

8.3 Separation Energy

Nuclei with one nucleon on top of the filled major shell (analog of alkali atoms) have diminished nucleon *separation energy* defined as the difference of binding energies for neighboring nuclei. The nucleon separation energy is given by

$$\begin{aligned} S_n(A, Z) &= B(A, Z) - B(A - 1, Z), \\ S_p(A, Z) &= B(A, Z) - B(A - 1, Z - 1), \end{aligned} \quad (8.2)$$

for neutrons and protons, respectively. Systematics of neutron separation energies for even Z , odd N nuclei is shown in Figure 8.2, this and other examples of separation energies are discussed in Ref. [1] (Figures 2.14–2.16).

The separation energies are analogous to atomic ionization potentials, Figure 8.1, and their knowledge allows one to estimate the energy gap between the major shells in heavy nuclei as ~ 4 MeV. Shell effects are particularly noticeable in the systematics of two nucleon separation energies because this form of presentation minimizes effects associated with pairing correlations so that odd and even mass nuclei can be shown on the same plot. Systematics of two neutron separation energies is shown in Figure 8.3.

Another related phenomenon is an abnormally small neutron capture cross section by closed-shell nuclei. This is important for the process of nucleosynthesis in the universe since the heavy elements are generated mainly by neutron capture with the subsequent beta-decay of unstable nuclei with neutron excess in the direction of the valley of stability. Neutron numbers corresponding to closed shells in heavy nuclei show maxima

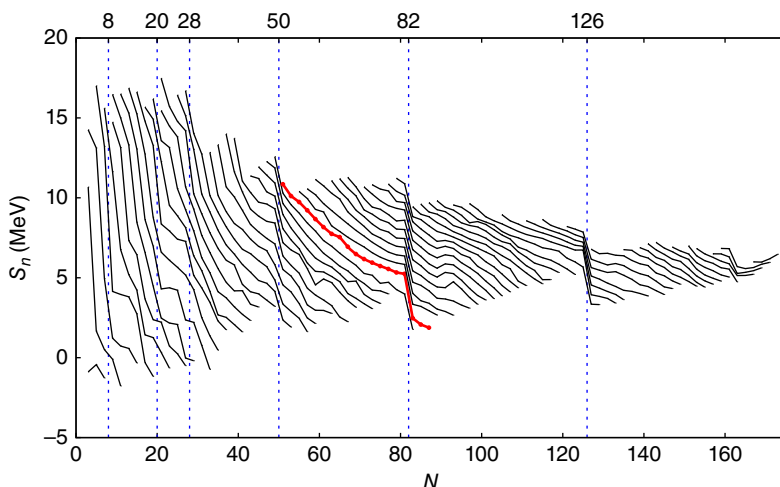


Figure 8.2 Neutron separation energies as a function of neutron numbers, isotopic chains are connected by lines, a specific example of tin isotopes, $Z = 50$, is highlighted.

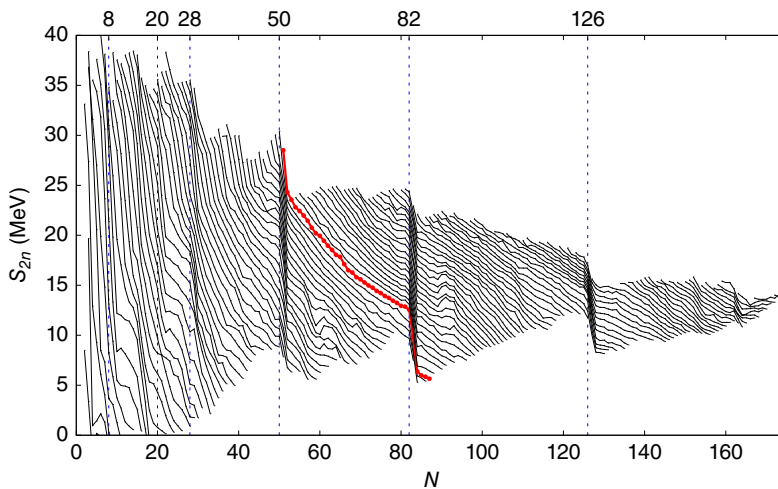


Figure 8.3 Two-neutron separation energies, $S_{2n}(A, Z) = \mathcal{B}(A, Z) - \mathcal{B}(A - 2, Z)$, as a function of neutron numbers. As in Figure 8.2, isotopic chains are connected by lines and example of tin isotopes is highlighted.

on the curves [1], Figures 2.19 and 2.20, of relative abundance of different elements in nature, see the astrophysical discussion of solar abundances [2].

8.4 Periodicity of Nuclear Spectra

Along with global binding energy, many nuclear observables manifest periodicity associated with the shell occupation.

All even–even nuclei have quantum numbers $J^\pi = 0^+$ of the ground state. As we already mentioned in Chapter 5, this is, at least partly, related to the time-reversal invariance: an even number of fermions fill a certain number of degenerate time-conjugate pairs of orbitals. The fact that such a pairwise occupation (*pairing correlations*) is energetically preferable is also connected to the residual short-range nucleon attraction, which should be the strongest for spatially overlapped orbits that is just the case for time-conjugate single-particle states.

The first excited state in even–even nuclei almost always has spin-parity quantum numbers 2^+ . The excitation energy $E(2_1^+)$ of this state is, recall Figure 5.4, a complicated function of a neutron number with sharp peaks near the magic nuclei. This behavior cannot be understood if we neglect the shell structure. Only the global trend with the decrease in excitation energies in heavier nuclei is related to general volume properties.

The elasticity of the nucleus (the restoring force for deviations from the equilibrium spherical shape) clearly depends on the abundance of *valence* nucleons on top of the closed magic core. With a growing number of valence nucleons, the 2_1^+ energy drops off steeply and then stabilizes at the level by an order of magnitude lower than the surface vibration frequencies predicted for the liquid drop (see Figures 5.3 and 5.4). This means that nuclei remote from the closed shells are very soft and presumably have quadrupole excitations of nonhydrodynamic nature. In fact, nuclei lose equilibrium spherical shape and become deformed, which will be discussed later.

There are many more examples of the periodic dependence of observables on the shell occupation, some of them are mentioned in other chapters. Thus, for the same (not very high) excitation energy, the level density in near-magic nuclei is considerably *lower* than in nuclei far away from the closed shells. The many-body level density is mainly of *combinatorial* character being determined by a number of combinations of single-particle excitations (transfer of a particle to another orbit) having nearly the same total energy. Such a combinatorial number is low in near-magic nuclei where the majority of possible excitations carry a large intershell energy.

One should however note that some effects are apparently insensitive to shell structure. The giant dipole isovector resonance, Section 6.2, is one of such examples. Its energy, being close to the global hydrodynamic estimate of Eqs. (6.29) and (6.47), does not reveal noticeable shell modulations. Nevertheless, this global sound-like mode is influenced by the shell structure in a different way via width and deformation splitting to be discussed later.

8.5 Harmonic Oscillator Potential

Considering the shell structure, we start with the simplest analytically solvable model of the mean nuclear field, namely the *isotropic harmonic oscillator* potential. It will present a reference point for more elaborate applications of the shell model and provide us with opportunities for some rough but reasonable estimates. The drawbacks of the model are in its unrealistic features that include *excessive symmetry* leading to full degeneracy inside a major shell and *absence of continuum spectrum* as the potential energy goes to infinity at large distances. After discussing the harmonic oscillator potential, we briefly compare it with the square potential well.

The single-particle Hamiltonian $\hat{\epsilon}$ in this model has a form

$$\hat{\epsilon} = \frac{\mathbf{p}^2}{2M} + \frac{1}{2}M\omega_o^2\mathbf{r}^2. \quad (8.3)$$

Its eigenvalues are

$$\epsilon_N = \hbar\omega_o \left(N + \frac{3}{2} \right), \quad (8.4)$$

the zero point energy $(3/2)\hbar\omega_o$ is included here. The integer $N \geq 0$ is the main quantum number, which gives the total number of oscillator quanta.

The energy eigenvalues (8.4) are degenerate. The degree of degeneracy is easily found from the fact that the Hamiltonian (8.3) permits the separation of variables in Cartesian coordinates. Here and in the following, we denote the single-particle quantum states by round parentheses leaving the angular brackets for the many-body states. Then stationary single-particle wave functions (orbitals) are given by the products

$$|n_x, n_y, n_z\rangle = |n_x\rangle |n_y\rangle |n_z\rangle \quad (8.5)$$

of standard wave functions of linear harmonic oscillators for each Cartesian coordinate. All combinations of partial quantum numbers n_x, n_y, n_z with the same sum,

$$n_x + n_y + n_z = N, \quad (8.6)$$

have the same energy (8.4) and form the N th major shell. This is an extreme example of shell structure when all orbitals within a major shell are precisely degenerate. The degree

of degeneracy is the number of combinations of three nonnegative integers having the same sum N , Eq. (8.6).

Problem 8.1 Find the degree of degeneracy of the N th major shell in the field of the isotropic harmonic oscillator.

Solution

$$A(N) = \sum_{n_x=0}^N \sum_{n_y=0}^{N-n_x} 1 = \frac{1}{2} (N+1)(N+2). \quad (8.7)$$

The total degeneracy should also include the spin factor 2 and the isospin factor 2 if neutrons and protons are treated together.

If we have, for one kind of nucleons, completely filled shells up to (including) the *Fermi surface* $N = N_F$, the total number of particles is

$$A = 2 \sum_{N=0}^{N_F} \frac{1}{2} (N+1)(N+2) = \frac{1}{3} (N_F+1)(N_F+2)(N_F+3). \quad (8.8)$$

Thus, the model predicts the magic numbers

$$2, 8, 20, 40, 70, 112. \quad (8.9)$$

Only three lightest of the numbers (8.9) coincide with what we need for explaining the data (8.1) for nuclei close to stability. At large N , the result (8.8) agrees with simple semiclassical estimates.

Problem 8.2 Find the mean square radius for the wave function of a particle in the state $|n_x, n_y, n_z\rangle$ of the isotropic harmonic oscillator.

Solution

For the state $|n\rangle$ of a *linear* oscillator, the mean squared coordinate is given by

$$\langle n | x^2 | n \rangle = \frac{\hbar}{M\omega_0} \left(n + \frac{1}{2} \right). \quad (8.10)$$

Therefore, for the radial coordinate of the *three-dimensional* oscillator, we get

$$\langle n_x, n_y, n_z | r^2 | n_x, n_y, n_z \rangle = \frac{\hbar}{M\omega_0} \left(N + \frac{3}{2} \right). \quad (8.11)$$

This quantity is the same for all degenerate states within a major shell although the shapes and orientations of the corresponding wave functions are different. A similar conclusion is valid for the momentum squared; recall that by the *virial theorem*, the expectation values of kinetic and potential energy are equal for any stationary state of a harmonic oscillator, as well as in the equilibrium thermal ensemble.

To model the nuclear structure by the harmonic oscillator, the parameters of the Hamiltonian are to be adjusted to global features of the nuclear mean field. The

adjustment condition is that the mean square radius of the nucleus as a whole found in the model agrees with what is known from nuclear density,

$$\overline{r^2} \approx \frac{3}{5} r_0^2 A^{2/3}. \quad (8.12)$$

The left-hand side of Eq. (8.12) can be explicitly calculated by averaging the expectation value (8.11) over all filled orbits,

$$\overline{r^2} = \frac{1}{A} \sum_{N=0}^{N_F} \frac{\hbar}{M\omega_o} \left(N + \frac{3}{2} \right) A(N), \quad (8.13)$$

where the capacity of an orbit is defined by Eq. (8.7) but we have to take into account the spin-isospin degeneracy,

$$\overline{r^2} = \frac{1}{A} \frac{\hbar}{M\omega_o} 4 \sum_{N=0}^{N_F} \left(N + \frac{3}{2} \right) \frac{1}{2} (N+1)(N+2). \quad (8.14)$$

The summation in Eq. (8.14) gives

$$\overline{r^2} = \frac{\hbar}{2AM\omega_o} (N_F + 1)(N_F + 2)^2(N_F + 3). \quad (8.15)$$

Combining Eqs (8.12) and (8.15) and using $r_0 = 1.2$ fm, we come to the estimate of the oscillator frequency

$$\hbar\omega_o = \frac{5}{4} \left(\frac{3}{2} \right)^{1/3} \frac{\hbar^2}{Mr_0^2} A^{-1/3} \approx \frac{41}{A^{1/3}} \text{ MeV}. \quad (8.16)$$

Problem 8.3 Find the level density $\nu(\epsilon)$ for a Fermi gas in the potential field of the anisotropic harmonic oscillator,

$$U(x, y, z) = \frac{M}{2} (\omega_x x^2 + \omega_y y^2 + \omega_z z^2). \quad (8.17)$$

Solution

The energy spectrum $\epsilon(n_x, n_y, n_z)$ of a particle in a field (8.17) is

$$\epsilon(n_x, n_y, n_z) = \hbar [\omega_x(n_x + 1/2) + \omega_y(n_y + 1/2) + \omega_z(n_z + 1/2)]. \quad (8.18)$$

In the limit of high excitation energies we disregard the zero point energy 3/2 and replace summation over all possible combinations of number of quanta with an integral

$$\nu(\epsilon) = g \int_0^\infty dn_x dn_y dn_z \delta(\epsilon - \hbar (\omega_x n_x + \omega_y n_y + \omega_z n_z)), \quad (8.19)$$

where g is the spin-isospin degeneracy of each state. The integral (8.19) can be evaluated by introducing stretched variables $\eta_k = \hbar\omega_k n_k$. The integral, once the delta function is used to remove η_z integration, simply measures the area of the triangle in the first quadrant of the $(\eta_x \eta_y)$ -plane where $\eta_x + \eta_y \leq \epsilon$. The final answer is

$$\nu(\epsilon) = \frac{g}{2} \frac{\epsilon^2}{\hbar^3 \omega_x \omega_y \omega_z}. \quad (8.20)$$

8.6 Orbital Momentum Representation

Although the solution for the harmonic oscillator (8.3) in Cartesian coordinates is trivial, it can be inconvenient for generalization to a potential deviating from the harmonic oscillator. A generic feature of many potentials is that the potential energy, including one in Eq. (8.3), has central symmetry and therefore the orbital momentum of a particle is a constant of motion. Owing to the large degeneracy (8.7), we can combine anisotropic wave functions (8.5) within a major shell with a given N to form three-dimensional functions with the angular part being an eigenfunction of the orbital momentum ℓ^2 and its projection ℓ_z . After that we can add the spin function χ , and using the vector coupling coefficients, construct the single-particle states with quantum numbers jm of the total angular momentum and its projection. Without spin-orbital coupling, the new functions with correct behavior under rotations still have the same energies (8.4) as their counterparts (8.5) in the Cartesian basis.

We can note parenthetically that the Coulomb potential $\sim 1/r$ and the harmonic oscillator potential $\sim r^2$ are the exceptional examples of three-dimensional potentials, which allow one to separate variables and find complete sets of good quantum numbers in different representations. In both cases, this opportunity is related to the additional symmetry properties. In the Coulomb field one can find, both classically and quantum mechanically, an integral of motion, the so-called Runge–Lenz vector [QP, I, 18.4]. As any vector, it does not commute with ℓ , and therefore it has no definite value in normal hydrogen-like states with quantum numbers ℓ and ℓ_z . But, due to its existence, one can build combinations of degenerate states within the same shell (separation of variables in parabolic coordinates), which are similar to classical Kepler orbits with a given orientation of the elliptical trajectory in the motion plane. In the isotropic harmonic oscillator case, the extra symmetry is due to the possibility of exchanging the excitation quanta between the Cartesian axes keeping their sum (8.6), and hence energy (8.4), fixed. From the mathematical point of view, this symmetry of redistributing the quanta between equivalent axes is described by the $SU(3)$ group of transformations generated by unitary 3×3 matrices. It is the generalization of the $SU(2)$ group of spin or isospin (Chapter 2). In classical mechanics, the exceptional symmetry of the Coulomb and harmonic oscillator potentials is manifested by the fact that they are the only potentials where all bound states have closed periodic trajectories.

In the Coulomb field, the degenerate orbits in a shell with a given main quantum number n' , which defines their energy $\propto -1/n'^2$, can have all orbital momenta ℓ from 0 to $n' - 1$. The stationary superpositions found in parabolic coordinates are linear combinations of different ℓ and therefore have no certain parity. In particular, we find here an example of a stationary state, as a superposition of $2s_{1/2}$ and $2p_{1/2}$ atomic orbitals, that can have a nonzero dipole moment with no parity nonconservation in the Hamiltonian. This explains the abnormal features of the Stark effect (linear level splitting in a uniform static electric field) in the hydrogen atom [QP, I, 24.4].

The situation is different for the harmonic oscillator. The three-dimensional states (8.5) have certain parity,

$$\Pi = (-)^{n_x+n_y+n_z} = (-)^N. \quad (8.21)$$

It is important that *all states in a major shell* have the same parity. Therefore, it is clear that the linear combinations of the major shell orbits with proper rotational symmetry should have only even (odd) ℓ for even (odd) N .

It is easy to see that the maximum possible orbital momentum in a major shell is $\ell = N$ (each quantum carries the orbital momentum 1, and the maximum projection is equal to N). The next possible orbital values of the same parity are $N - 2, N - 4, \dots, 0$ (or 1) for even (odd) N ; thus $\ell = N - 2n$ where $n = 0, 1, \dots$.

Problem 8.4 Check this result by counting the total number of states in a major shell and confirm Eq. (8.7).

Solution

$$A(N) = \sum_{\ell=0}^N (2\ell + 1) \frac{1 + (-)^{\ell+N}}{2} = \frac{1}{2} (N+1)(N+2). \quad (8.22)$$

Here, we took into account that each ℓ -level is degenerate in projections ℓ_z .

The single-particle level scheme of equidistant degenerate major shells for the harmonic oscillator potential is presented in Figure 8.4, left side. The possible values of the orbital momentum and the capacities of the shells that determine the magic numbers (8.9) are indicated. The symbolic notations used on this scheme include

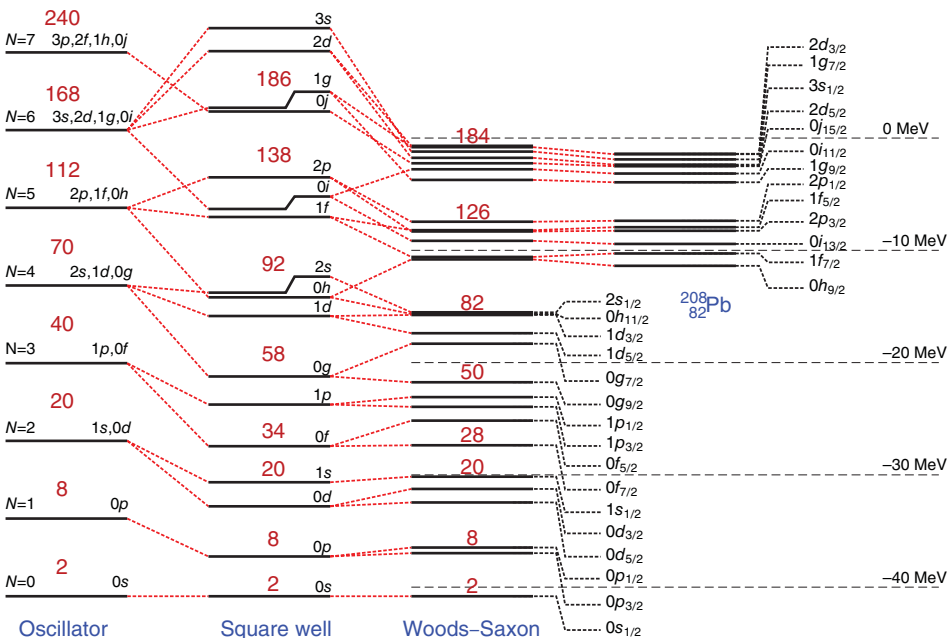


Figure 8.4 Single-particle levels for the isotropic harmonic oscillator on the left, next to the right levels for the square well potential, then for the realistic Woods–Saxon potential, and finally on the right single-particle states in ^{208}Pb , deduced from spectra of ^{207}Pb and ^{209}Pb (see Ref. [3] and references therein). Energy scale is indicated, ground states for oscillator and square well potentials are aligned with the ground state of the Woods–Saxon potential. In this example, the oscillator frequency, the square well radius, and the parameters of the Woods–Saxon potential were selected targeting neutron orbits in the ^{208}Pb nucleus. Shell gaps are marked with corresponding magic numbers (cumulative numbers of states below the gap).

the spectroscopic symbol of the orbital momentum and the radial quantum number showing the number of radial nodes of the coordinate wave function not including $r = 0$ and $r = \infty$; for example, the lowest levels on the scheme would be designated in this manner as $0s$; $0p$; $0d, 1s$; $0f, 1p$, and so on. Using number of nodes for the radial quantum number n , the total number of quanta is $N = 2n + \ell$. Sometimes, an alternative enumeration, which is analogous to that of Coulomb problem, is used where the radial quantum number $n' = n + 1$ enumerates, starting from 1, the appearances of a given ℓ with increasing excitation energy. Unless explicitly stated otherwise, we will not use this alternative enumeration.

8.7 Square Well Potential

As mentioned earlier, the harmonic oscillator potential is not quite realistic due to its excessive symmetry and related degeneracy. Another undesirable feature is the incorrect asymptotic behavior of single-particle wave functions. Indeed, the oscillator wave functions fall off too rapidly, $\propto \exp(-m\omega r^2/2\hbar)$, whereas at large distances (beyond the potential radius, the notion nonexistent for the oscillator field), the wave function of a neutral particle has to decay as $\exp(-\kappa r)$, where the penetration length $1/\kappa$ is determined by the binding energy, $\kappa = \sqrt{2m|\epsilon|/\hbar^2}$. The actual nuclear density is a rather flat function inside the nucleus. The mean-field potential in the nuclear interior is expected to be of approximately the same shape as the density. This is also the case in the phenomenological *optical potential* describing the absorption of external nucleons in the reaction processes. The square well potential, $U(r) = -U_0$ for $0 < r < R$ and $U = 0$ for $r > R$, is another simple case that allows an analytical solution and has a flat bottom.

The radial wave function with the orbital momentum ℓ is, inside the well (compare the s -wave case in Chapter 4), given by the *spherical Bessel function*,

$$\frac{u_\ell(r)}{r} = A j_\ell(kr), \quad k = \sqrt{\frac{2M(U_0 - |\epsilon|)}{\hbar^2}}. \quad (8.23)$$

For a bound state, this function has to be continuously matched to the exponentially decaying *Hankel function* in the classically forbidden region outside the well,

$$\frac{u_\ell(r)}{r} = B h_\ell^{(1)}(ikr), \quad \kappa = \sqrt{\frac{2M|\epsilon|}{\hbar^2}}. \quad (8.24)$$

In particular, for the s -wave,

$$h_0^{(1)}(ikr) = -\frac{e^{-\kappa r}}{\kappa r}. \quad (8.25)$$

The resulting level sequence for the *infinite* well is shown in Figure 8.4. When applied to a *finite* well, this implies a limit of a finite distance of very deep level energies ϵ from the bottom. It corresponds to $\kappa \rightarrow \infty$ when the tail penetrating into the forbidden region disappears, and the levels are given by the roots of the spherical Bessel function (8.23) on the boundary, $r = R$,

$$j_\ell(kR) = 0. \quad (8.26)$$

The main difference compared to the harmonic oscillator case is that the degeneracy is lifted (except for the rotational degeneracy in the orbital momentum projection ℓ_z). The

level density becomes much more uniform although the shell gaps are still noticeable. The levels with a higher orbital momentum are shifted down deeper than the levels with lower ℓ . The reason is that, due to the flat bottom, the additional attraction in the square well as compared to the oscillator potential is stronger at larger distances from the origin. The states with larger ℓ are localized further from the center and feel stronger attraction than in the oscillator field. This effect agrees with empirical data. In the so-called Nilsson potential to be discussed later, Section 12.12, the same effect is mimicked by the addition of the term proportional to ℓ^2 to the harmonic oscillator field.

One can notice that in higher shells the *intruders* appear: levels with high ℓ , as for example $0h$, increase their binding energy up to such an extent that they get into the previous shell where the aboriginal population carries opposite parity. The splitting of oscillator degeneracy in the square well changes the magic numbers starting from the shell $N = 3$, but the resulting sequence still does not coincide with the empirical sequence, Eq. (8.1). The interpolation in the middle of Figure 8.4 corrects too strong attraction for large ℓ making the boundaries of the well less steep but does not bring the proper magic numbers. Approximately the same level sequence as in the middle part of Figure 8.4 is given by the realistic Woods–Saxon type potential, see the following, with a flat bottom and smooth boundary.

The approximation (8.26) of a very deep well is invalid for *loosely bound* states. As we know from the analysis of the deuteron *s*-wave, Section 3.4, bound levels appear in the well one by one as the depth of the well increases. The sequence of loosely bound levels that can be found from exact matching conditions is slightly different from the sequence of Figure 8.4, right. Weakly bound states with large ℓ feel a stronger centrifugal barrier and turn out to be effectively more localized. However, this difference exists only for rather high shells, for example, in contrast to what we see for the deep well, Figure 8.4, $2s$ level emerges in shallow potential earlier than $0h$. This change in ordering can be observed in Figure 8.5 where for lighter nuclei the smaller potential radius makes states less bound and effects of finite depth more important.

8.8 Spin–Orbit Coupling

In the above-mentioned consideration, we did not take into account any spin-dependent forces. In a nucleus with one nucleon on top of the magic core, spin–spin and tensor forces (Section 3.1) between the nucleon and core nucleons do not contribute to the single-particle energy because in the core all spins are compensated so that the net result of such interactions averages to zero. This is however not the case for the spin–orbit forces. The effective mean-field potential acting upon a nucleon can contain a spin–orbit term

$$U_{\ell s} = f(r)(\ell \cdot \mathbf{s}). \quad (8.27)$$

Using the invariance arguments similar to those of Section 3.1, we can prove that this is the only possible term of the *first order* in nuclear momentum.

The spin–orbit interaction is well known in atoms. For an atomic electron, this is the relativistic correction of the *second order* in v/c . It is originated by the interaction of the electron spin magnetic moment with the magnetic field seen by the electron in an electrostatic field of the nucleus $U(r)$. The electron is moving in the electric field

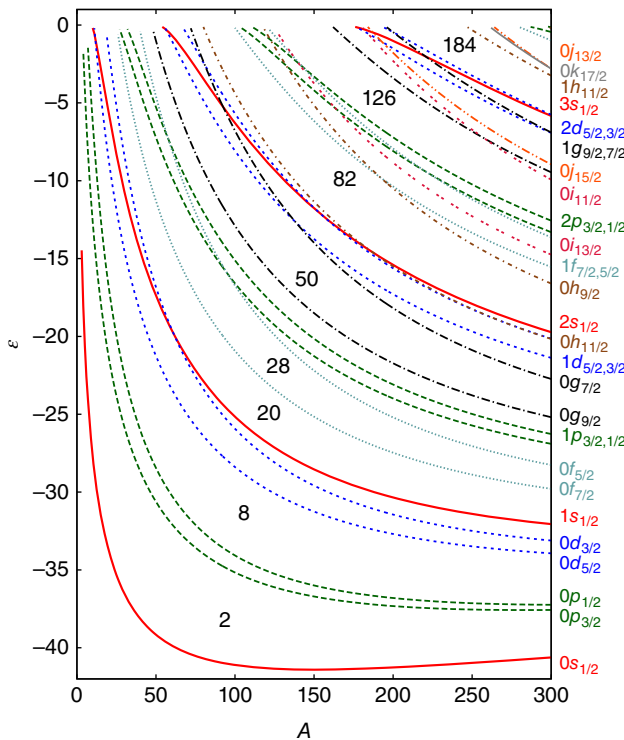


Figure 8.5 Energies of the neutron single-particle levels in a spherical mean field given by the Woods–Saxon potential are shown along the line of stability as a function of the mass number A . Levels are labeled on the right. The main quantum number is the number of nodes of radial wave functions at finite values of r . Gaps that correspond to magic numbers are labeled. Parameters of the Woods–Saxon potential are taken from Ref. [3].

$\mathcal{E} = -\nabla\phi = -(1/e)\nabla U$, but in its own frame there is a magnetic field defined by the Lorentz transformation $\mathbf{B} = -(1/mc)[\mathbf{p} \times \mathcal{E}]$. The interaction energy of the electron spin magnetic moment $\mu = \mu_B 2s$ (the factor 2 corresponds to the spin gyromagnetic ratio) is

$$U_{\ell s} = -(\mu \cdot \mathbf{B}) = -\frac{\hbar}{m^2 c^2} (\mathbf{s} \cdot [\mathbf{p} \times \nabla U(\mathbf{r})]). \quad (8.28)$$

Actually, it is easy to understand that the operator form (8.28) is the only possible one without violation of rotational invariance or parity. In a spatially uniform system, there is no force defining the direction that would be necessary for constructing a scalar (8.28). Therefore, $U_{\ell s}$ contains the gradient of the potential field, and in nuclei it should be concentrated near the nuclear surface.

In a field with central symmetry, we have $\nabla U(r) = (dU/dr)(\mathbf{r}/r)$ so that the spin–orbit interaction for the atomic electron is found to be

$$U_{\ell s} = \frac{\hbar^2}{m^2 c^2} \frac{1}{r} \frac{dU}{dr} (\boldsymbol{\ell} \cdot \mathbf{s}), \quad (8.29)$$

or, for the Coulomb field $U(r) = -Ze^2/r$,

$$U_{\ell s} = \frac{Ze^2 \hbar^2}{m^2 c^2 r^3} (\boldsymbol{\ell} \cdot \mathbf{s}). \quad (8.30)$$

This estimate is not quite correct as it does not take into account Thomas precession, the Coriolis force for an electron accelerating in the Coulomb field. The exact result follows from the Dirac equation and differs from (8.30) by a factor 1/2. Thus, for atomic electrons, the spin–orbit coupling is the second order ($\sim 1/c^2$) effect that becomes relatively strong only in heavy atoms.

As a result of the spin–orbit interaction (8.27), a single-particle level with the orbital momentum $\ell \neq 0$ and spin 1/2 is split according to the total angular momentum j into a *spin–orbit doublet* $j = \ell \pm 1/2$ (states with “parallel” or “antiparallel” orientation of vectors ℓ and s). Calculating the expectation value of the operator $(\ell \cdot s) = [j(j+1) - \ell(\ell+1) - s(s+1)]/2$ for the doublet terms, we find the energy shifts

$$\begin{aligned}\Delta\epsilon_{\ell s} &= \frac{\ell}{2} \langle f(r) \rangle_\ell, \quad j = \ell + \frac{1}{2}, \\ \Delta\epsilon_{\ell s} &= -\frac{\ell+1}{2} \langle f(r) \rangle_\ell, \quad j = \ell - \frac{1}{2}.\end{aligned}\tag{8.31}$$

For a given radial function, the splitting (8.31) increases with ℓ being proportional to $(2\ell+1)$.

In the *atomic* case (8.30), the interaction prefers the antiparallel spin–orbit orientation so that the doublet member with smaller j is shifted down in energy. In the *nuclear* case, apart from electromagnetic effects similar to those for electrons, there are stronger effects induced by nuclear forces. The presence of the strong spin–orbit interaction is supported by the polarization data for nucleons scattered off the nuclear optical potential. The microscopic mechanism is not yet completely clear, but presumably it emerges from various components of the meson exchange potential with a special role played by the vector meson exchange. When compared to the atomic spin–orbit interaction, using Eq. (8.29) with an additional factor of 1/2 and with the nucleon mass instead of the electron mass, the empirical nuclear spin–orbit interaction not only has an opposite sign but also turns out to be about 30 times stronger. The opposite sign to that in the atomic case implies that the “parallel” levels with larger $j = \ell + 1/2$ have lower energy. In the presence of strong spin–orbit coupling, a better classification of nucleonic single-particle states, *jj-coupling*, should use the total angular momentum j .

8.9 Realistic Level Scheme

As a result of the spin–orbital splitting, the single-particle levels in the spherical mean field are characterized by the set of quantum numbers $(nljm\tau)$ where m is an eigenvalue of j_z . The orbital momentum ℓ defines parity of the orbit $(-)^{\ell}$. The energy of the orbital does not depend on m resulting in the $(2j+1)$ -fold degeneracy of a j -multiplet.

The lower component of the spin–orbit doublet, $j = \ell + 1/2$, is shifted down from its position in a spin-independent potential (see Figure 8.4). The shift can be strong enough to bring this level as an *intruder* into the previous oscillator shell filled by the states of opposite parity. The presence of intruders regroups the levels into the new shells. This allows one to reproduce exactly the empirical magic numbers (8.1). The $0f_{7/2}$ level is shifted down by the spin–orbit interaction so that it becomes noticeably isolated from the spin–orbit partner $0f_{5/2}$ and forms its own shell responsible for the magic number 28, Eq. (8.1). This makes both calcium isotopes $^{40}_{20}\text{Ca}_{20}$ and $^{48}_{20}\text{Ca}_{28}$ double-magic.

The empirical intensity of the spin–orbit coupling turns out to be approximately

$$U_{\ell s} \simeq -20 (\boldsymbol{\ell} \cdot \mathbf{s}) \frac{1}{A^{2/3}} \text{ MeV}. \quad (8.32)$$

This estimate agrees with (8.29) multiplied by the above-mentioned factor ~ 15 if $(1/r)(dU/dr)$ is estimated as $\sim 50/R^2$ MeV.

Figure 8.4 shows the typical level scheme and new shells with correct magic numbers arising from the spin–orbital splitting. The exact ordering of j -levels (subshells) within a given major shell depends on many additional factors in a specific nucleus. The spacings between the subshells and even between the major shells can vary as well.

For more accurate description, one should solve the Schrödinger equation for a particle in a field

$$U = U(r) + f(r)(\boldsymbol{\ell} \cdot \mathbf{s}) \quad (8.33)$$

where the potentials $U(r)$ and $f(r)$ contain fitted parameters. Typically, the central field has a form of the Woods–Saxon type,

$$U(r) = U_0 w(r), \quad w(r) = \frac{1}{1 + \exp[(r - R)/a]}, \quad (8.34)$$

with the parameters close to those extracted from the nuclear density and from the nucleon scattering: radius $R = r_0 A^{1/3}$, $r_0 = 1.2 \div 1.3$ fm, diffuseness $a = 0.6 \div 0.7$ fm. The depth of the potential is about $U_0 = 50$ MeV for nuclei with $N = Z$, but for the nonzero isospin, it contains an additional contribution from isospin dependence of interaction, thus scaling U_0 by a factor $\sim 1 - 4x \mathbf{t} \cdot \mathbf{T}/A \approx 1 \pm x(N - Z)/A$, where plus and minus signs stand for proton and neutron, respectively (compare Eq. (7.45)). For neutrons, for example, the presence of this extra term diminishes the depth of the potential in neutron-rich nuclei. The typical values of this parameter are $x = 0.6 \div 0.9$.

The spin–orbit potential is usually concentrated on the surface in accordance with the arguments of the preceding section. It can be chosen as a derivative of the central part, similar to (8.29),

$$f(r) = -\lambda \frac{\hbar^2}{2M^2c^2} \frac{1}{r} \frac{dU}{dr} (\boldsymbol{\ell} \cdot \mathbf{s}), \quad (8.35)$$

where, as mentioned earlier, the scaling factor $\lambda = 24 \div 36$. Using this form with the scaling parameter λ is very common; the situation with isospin dependence of the spin–orbit interaction is unclear – it has different signs in different schemes of deriving the mean field. The neutron single-particle levels calculated for ^{208}Pb are shown in Figure 8.4, the same figure contains also experimentally determined levels deduced from the single-particle excitations found around the Fermi surface. The evolution of the neutron single-particle levels in the Woods–Saxon potential as a function of the nuclear mass is shown in Figure 8.5.

8.10 Semiclassical Origins of Shell Structure

Variations in the density of single-particle states and resulting shell structure have a close relation to the classical periodic orbits. Even for irregular potentials, without any symmetries, classical periodic orbits represent special trajectories around which the motion

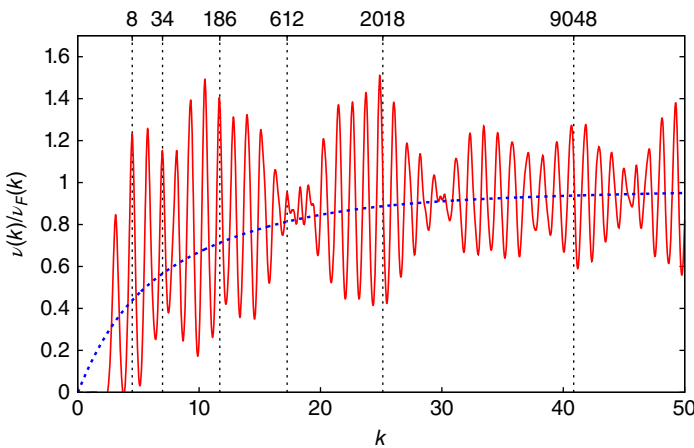


Figure 8.6 Density of states in the infinite square well potential of unit radius. The density of states as a function of the wave vector is shown relative to the density of states in the Fermi gas model. Grid lines indicate several magic numbers. Averaged behavior with asymptotic convergence to unity is shown with a smooth dashed line.

is regular and nonchaotic in the sense of sensitivity to initial conditions. In view of the semiclassical Bohr–Sommerfeld quantization, this means that for each closed trajectory of length L there is a periodic set of eigenstates $k_n = 2\pi n/L$ with $n = 1, 2, \dots$. For low-lying spectrum, only the shortest trajectories are important.

Let us consider an example of an infinitely deep spherical potential discussed in Section 8.7. In Figure 8.6, the density of states $v(k)$ is shown relative to the density of states in the Fermi gas model $v_F(k) = (2/3\pi)k^2$, which is a number of states per absolute value of the wave vector \mathbf{k} , where radius of the well defines the unit of length. The behavior of the density of states exhibits multiple oscillations, on top of the shell structure discussed earlier there is an additional beat frequency or the *supershell structure* [4] seen clearly in large atomic clusters [5].

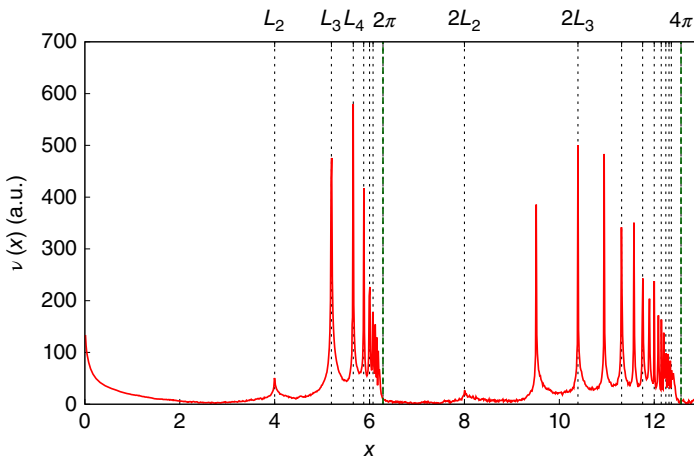


Figure 8.7 Fourier transform of the density of states in the infinite square well potential of unit radius.

The Fourier transform of this pattern $v(x)$, shown in Figure 8.7 as a function of length x (canonically conjugate to the \mathbf{k} variable), reveals multiple peaks responsible for the regular oscillations in the density of states. It is easy to identify these peaks with periodic orbits. Specific cases that correspond to regular q -sided polygons inside a circle where $x = L_q = 2Rq \sin(\pi/q)$ are identified in the figure. The general theory of semiclassical density of states and its relation to the resonances and classical periodic orbits can be found in the book [6].

References

- 1 A. Bohr and B. Mottelson, *Nuclear Structure*, World Scientific, Singapore, 1997.
- 2 K. Lodders, *Astrophys. J.* **591**, 1220 (2003).
- 3 N. Schwierz, I. Wiedenhöver, and A. Volya, arXiv:0709.3525.
- 4 R.B. Balian and C. Bloch, *Ann. Phys.* **69**, 76 (1971).
- 5 K. Nishioka, K. Hansen, and B. Mottelson, *Phys. Rev. B* **42**, 9377 (1990).
- 6 M. Brack and R.K. Bhaduri, *Semiclassical Physics*, Addison-Wesley, Reading, MA, 1997.

9

Independent Particle Shell Model

It is customary in physics to begin with a physical problem and then to search for the appropriate mathematical apparatus.

M.E. Rose, in *Spectroscopic and Group Theoretical Methods in Physics*,
John Wiley & Sons, New York, 1968.

9.1 Shell Model Configurations

Let us consider a system of A nucleons in a given spherically symmetric mean field characterized by the single-particle Hamiltonian $\hat{\epsilon}$. We start with *independent* nucleons; this consideration will later deliver the convenient basis for incorporating the interactions between the particles. The eigenstates of the mean field determine the set of bound single-particle orbits and, in general, continuum states. Here we restrict our consideration to bound orbitals. The shell model analysis starts with determining the nucleon *configuration space*, which includes valence single nucleon orbits, usually near Fermi surface, and the number of valence nucleons.

The *single-particle* orbits $|\lambda\rangle$ are labeled by the complete set of quantum numbers. In the *spherical* field with spin–orbit coupling, these numbers are $\lambda = \{n, \ell, j, m, \tau\}$, where $m = j_z$ and τ is the isospin projection. Single-particle energies ϵ_λ are degenerate with respect to the projection m ; the parity of the orbital is fixed as $(-)^{\ell}$. The simplest *many-body* state allowed by the Fermi statistics is the *Slater* determinant defined by a set $\{n_\lambda\}$ of *occupation numbers* (equal to 0 or 1) selected for all single-particle orbits $|\lambda\rangle$ in such a way that we come to a given total particle number,

$$\sum_{\lambda} n_{\lambda} = A. \quad (9.1)$$

In the independent particle shell model, each determinant is stationary because there is no interaction that could relocate particles and change the configuration. The complete set of the many-body states for all possible occupation numbers (of course, in practice the single-particle space is always truncated) defines the so-called spherical *m-scheme* basis.

For noninteracting particles, the energy of a Slater determinant state is simply a sum of energies over single-particle states occupied by nucleons

$$E(\{n_\lambda\}) = \sum_{\lambda} \epsilon_{\lambda} n_{\lambda}. \quad (9.2)$$

Because of spherical symmetry, many of these states have the same energy. Therefore, determinants are naturally combined into the sets in such a way that for each kind of particles, τ , the states within a given set differ only by the redistribution of the identical particles within the spherical orbits $|n\ell j\rangle$ occupying different m -states, at fixed total occupancies of each $(n\ell j)$ -level. A *partition* contains all possible redistributions of this type, namely a specific way that A nucleons are distributed over the $(n\ell j)$ -levels. Each partition gives rise to many determinantal states, and all determinants of a given partition are *degenerate* having the same energy.

The next stage is absent in a simple Fermi gas model, but we need to have it in mind in applications to actual nuclei. The number of m -scheme states (the dimension of the configuration space) allowed by the Pauli exclusion principle grows very fast with a number of particles. A partition, as a rule, is *reducible* with respect to rotations. The states belonging to the same partition [the same distribution of the total particle number over the $(n\ell j)$ -levels], but with different populations of m -states inside the partition, in general are not eigenfunctions of the total angular momentum J and, at a given J , may differ by the coupling scheme of individual vectors \mathbf{j} to the total \mathbf{J} . For a finite self-bound quantum system, such as the nucleus, J is an exact quantum number. Therefore, the stationary states are certain *combinations* of the m -scheme states belonging to the same partition, which have definite values of J and of the total projection $M = \sum m$. Rotations change quantum numbers m of orbits participating in a superposition $|JM\rangle$ of single-particle states with different values of m but with the same other quantum numbers. The many-body states with a good total angular momentum are usually *superpositions* of the Slater determinants rather than single determinants.

Due to the strong spin–orbit interaction, it is common to use the *j–j coupling*. First, we make proper single-particle states with a given $j = \ell \pm 1/2$ and then we look for the superpositions that would be the eigenstates of J^2 , where the operator of the total angular momentum of the many-body system is

$$\mathbf{J} = \sum_a \mathbf{j}_a. \quad (9.3)$$

In principle, it should be done with the aid of the Clebsch–Gordan coefficients [QP, I, 22.6] and the related higher coefficients of angular momentum recoupling. In practice, such procedures very soon become too cumbersome and one uses the appropriate numerical algorithms. Total parity is a product of single-particle parities,

$$\Pi = (-)^{\sum_a \ell_a}. \quad (9.4)$$

The simplest and exceptional case is of course a closed shell nucleus. This configuration has an even number, $2j + 1$, of particles for any occupied j -orbital, and as all m -states are occupied, it allows a unique value $J = 0$ with positive parity. The situation is also obvious for nuclei with one valence nucleon above the closed shell core. Let the valence nucleon be located on the level with the single-particle angular momentum j . This one-particle configuration contains $(2j + 1)$ degenerate m -states, and each of them already has correct quantum numbers $J = j$, $J_z = m$ as the core does not contribute. In this case, we have only one multiplet $|JJ_z\rangle \equiv |jm\rangle$. In general, each partition gives rise to many J -multiplets. In practice, one can avoid the complicated angular momentum recoupling algebra and work in the m -scheme paying the price of a higher dimensionality. The solution, if correct, will reveal degeneracies in energy of many-body

multiplets, each of a corresponding dimension $(2J + 1)$. We should add here that each m -scheme state has a good total magnetic quantum number M , which is just a sum of m 's of all occupied states. Therefore, blocks of states with a given total $J_z = M$ and parity can be treated separately.

9.2 Particle–Hole Symmetry

It is easy to understand that in the spherical shell model, there exist such symmetry. Consider a j -level with $2j$ particles and one empty single-particle state, *a hole*. If a state with a projection m is empty, the configuration as a whole has uniquely defined quantum numbers $J = j$, $J_z \equiv M = -m$ because the addition of the last particle with quantum numbers jm would complete the shell leading to a unique state $J = J_z = 0$. Since a hole can be in any m , we have a hole multiplet of $(2j + 1)$ states with $J = j$.

By the same logic, the full complementarity exists between *many-particle* and *many-hole* states. For any state $|JM\rangle$ of n particles on a j -level, there exists a complementary state $|J-M\rangle$ of $(2j + 1 - n)$ particles occupying the holes in the original state and completing the shell. Therefore, we have symmetry of states with respect to the half-occupied level and it might be convenient to use the hole language if the level is more than half-occupied. This inversion of the sense of rotation, $M \rightarrow -M$, corresponds to using the time-conjugated orbits.

Another important consequence of particle–hole symmetry concerns the multipole moments. The closed shell has $J = 0$ and, therefore, does not carry any multipole moments except for the monopole one, $\lambda = 0$. Let us calculate the trace (sum of the diagonal matrix elements) of a one-body multipole operator $\mathcal{M}_{\lambda\mu}$ in space of the single-particle orbits belonging to the same j -level. The trace does not depend on the choice of the basis. In the basis $|jm\rangle$, the trace is nothing but the expectation value of the operator $\mathcal{M}_{\lambda=\mu=0}$ for the fully occupied shell, and therefore it is equal to zero for $\lambda > 0$,

$$\sum_m \langle jm | \mathcal{M}_{\lambda 0} | jm \rangle = 0, \quad \lambda \neq 0. \quad (9.5)$$

It follows from (9.5) that the multipole moments of a state $|jm\rangle$ with a single valence particle and of a state of $2j$ particles with a hole in the state $|jm\rangle$ are equal in magnitude and have opposite signs,

$$\langle \mathcal{M}_{\lambda 0} \rangle_{jm; \text{particle}} = -\langle \mathcal{M}_{\lambda 0} \rangle_{jm; \text{hole}}. \quad (9.6)$$

Traditionally, the tabular values of multipole moments \mathcal{M}_λ are their expectation values $\langle JJ | \mathcal{M}_{\lambda 0} | JJ \rangle$ taken for the state $|J, J_z = J\rangle$ with the maximum projection of the angular momentum. In the particle case, it corresponds to the projection $m = j$ while in the hole case the projection $J = j$ of the total angular momentum corresponds to the projection $m = -j$ of the empty state. From hence the observable multipole moments of one-particle and one-hole states are

$$\mathcal{M}_\lambda^{\text{particle}} = \langle \mathcal{M}_{\lambda 0} \rangle_{jj; \text{particle}}, \quad \mathcal{M}_\lambda^{\text{hole}} = \langle \mathcal{M}_{\lambda 0} \rangle_{j-j; \text{hole}}. \quad (9.7)$$

Combining this with (9.6), we get

$$\mathcal{M}_\lambda^{\text{hole}} = -\langle \mathcal{M}_{\lambda 0} \rangle_{j-j; \text{particle}}. \quad (9.8)$$

But the single-particle states $|jm\rangle$ and $|j-m\rangle$ are time-conjugate. If the operator $\mathcal{M}_{\lambda\mu}$ is invariant under time reversal (" \mathcal{T} -even"), its expectation values for the orbits $\pm m$ are the same. In this case,

$$\mathcal{T}\text{-even: } \mathcal{M}_\lambda^{\text{hole}} = -\mathcal{M}_\lambda^{\text{particle}}. \quad (9.9)$$

An important example is the electric quadrupole moment. According to Eq. (9.9), it is of opposite sign for particles and holes. Contrary to that, for a \mathcal{T} -odd operator changing sign under time reversal,

$$\mathcal{T}\text{-odd: } \mathcal{M}_\lambda^{\text{hole}} = \mathcal{M}_\lambda^{\text{particle}}. \quad (9.10)$$

\mathcal{T} -odd quantities like magnetic moment have the same value for particles and holes.

9.3 Magnetic Moment

Even in the framework of the simple shell model with no interaction, the calculation of the electromagnetic multipole moments requires additional assumptions. The even–even nucleus has the zero ground-state magnetic moment because its spin $J = 0$. We assume that the magnetic moment of the odd- A nucleus in its ground state is determined by the last odd particle while the remaining particles are paired and cancel their orbital and spin currents.

Let a particle with spin s move in a central field where its orbit is characterized by an orbital momentum ℓ . The energy of the orbit depends, in general, on the mutual orientation of the quantum vectors ℓ and \mathbf{s} through the spin–orbit interaction. For nucleons in nuclei, the spin–orbit coupling is strong, and one has to introduce the total angular momentum of the nucleon, $\mathbf{j} = \ell + \mathbf{s}$, and to use the corresponding basis of states $|(ls)jj_z = m\rangle$. Since the lengths of the three vectors are fixed, we can find the average mutual orientations,

$$\langle \mathbf{j} \cdot \ell \rangle = \frac{j(j+1) + \ell(\ell+1) - s(s+1)}{2}, \quad \langle \mathbf{j} \cdot \mathbf{s} \rangle = \frac{j(j+1) + s(s+1) - \ell(\ell+1)}{2}. \quad (9.11)$$

Of course, the scalar quantities (9.11) are the same for all the states $|(\ell s)jm\rangle$ with different m .

The next assumption concerns the choice of the magnetic moment operator. For a particle in a central field, it is usually assumed (in units of the corresponding magneton)

$$\boldsymbol{\mu} = g^s \mathbf{s} + g^\ell \ell. \quad (9.12)$$

Using the vector model together with the scalar quantities (9.11), we obtain the *effective operator* of the magnetic moment within the multiplet of states $|jm\rangle$,

$$\boldsymbol{\mu} = g(j, \ell, s) \mathbf{j}, \quad (9.13)$$

where the gyromagnetic ratio (Lande factor) is

$$\begin{aligned} g(j, \ell, s) &= g^\ell \frac{\langle (\mathbf{j} \cdot \ell) \rangle}{j(j+1)} + g^s \frac{\langle (\mathbf{j} \cdot \mathbf{s}) \rangle}{j(j+1)} \\ &= \frac{1}{2j(j+1)} \left\{ (g^\ell + g^s) j(j+1) + (g^\ell - g^s)[\ell(\ell+1) - s(s+1)] \right\}. \end{aligned} \quad (9.14)$$

As we mentioned, the tabular value corresponds to the state with $j_z = m = j$, that is, the magnetic moment is equal to $\mu = gj$; for the case under consideration, the noninteracting shell model predicts $J = j, M = m$.

For a free nucleon at rest $\ell = 0, j = s = 1/2$. Therefore, spin gyromagnetic ratios are determined by the empirical magnetic moments μ_p and μ_n

$$g_p^s = 2\mu_p = 5.58, \quad g_n^s = 2\mu_n = -3.82 \quad (9.15)$$

(in nuclear magnetons). Since the neutron does not carry electric charge, we assume that orbital gyromagnetic ratios for the nucleons are (in the same units)

$$g_p^\ell = 1, \quad g_n^\ell = 0. \quad (9.16)$$

The total angular momentum of the nucleon can be $j = \ell \pm 1/2$. With the use of (9.13) and (9.15), we find the single-particle magnetic moments for these two cases:

$$\mu_p(j) = j - \frac{1}{2} + \mu_p, \quad \mu_n(j) = \mu_n, \quad j = \ell + \frac{1}{2}, \quad (9.17)$$

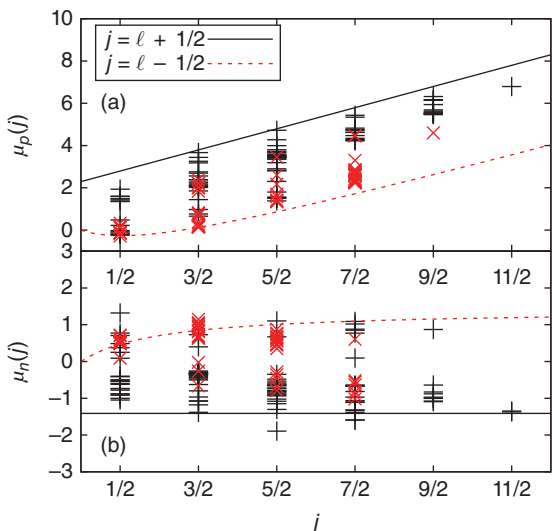
where μ_p and μ_n are the free values from Eq. (9.15), and

$$\mu_p(j) = \frac{(2j+3)j - 2j\mu_p}{2(j+1)}, \quad \mu_n(j) = -\frac{j}{j+1}\mu_n, \quad j = \ell - \frac{1}{2}. \quad (9.18)$$

The dependence of the magnetic moments on j as given by (9.17) and (9.18) is plotted in Figure 9.1 (Schmidt lines). In the semiclassical limit of large $j \approx \ell \gg s$, the neutron magnetic moment, containing only the spin contribution due to (9.16), is equal to $\pm\mu_n$ for all j , for parallel or antiparallel mutual orientation of \mathbf{s} and \mathbf{j} , respectively; the proton magnetic moment is linearly increasing as $j \pm \mu_p$ due to the orbital part. Note that under the assumption that only the unpaired nucleon defines the observable magnetic moment of the ground state, the Schmidt lines are universal and carry no information on the characteristics of the central field.

The empirical data for the nuclei close to the line of stability do not always agree with these extreme single-particle predictions (see Figure 9.1). The average deviation of the

Figure 9.1 Schmidt lines for the magnetic moments in the independent particle spherical shell model: (a) for protons and (b) for neutrons. Solid black line shows $j = \ell + 1/2$ and dashed red line $j = \ell - 1/2$ case, relevant experimental points are shown in corresponding colors.



data from the Schmidt lines is about 1 nm but always in the direction inside the region formed by these lines. The proximity of one or another line often allows us to determine the orbital moment ℓ of the unpaired orbit. The main physical effects responsible for the deviations are related to the interaction of particles. The interaction makes the actual ground state wave functions of the odd- A nuclei more complex than under the idealized assumption of the limiting version of the independent particle shell model; this effect is called *configuration mixing*.

In addition, the operator form (9.12) borrowed from the one-particle physics is not the most general one. In the many-body system, another contribution is possible. Any contribution to the magnetic moment should be an axial vector changing sign under time reversal. Using the spin σ and unit coordinate vectors $\mathbf{n} = \mathbf{r}/r$, we can construct

$$\boldsymbol{\mu}^{(2)} = g^{(2)}(r)(\boldsymbol{\sigma} \cdot \mathbf{n})\mathbf{n} \quad (9.19)$$

that satisfies the correct transformation properties for any radial form-factor $g^{(2)}(r)$. The nontrivial part of this operator that cannot be reduced to the spin term of (9.12) also can be rewritten as a result of the vector coupling $[\sigma \otimes Y_2(\mathbf{n})]_{1\mu}$. The operator (9.19) has new selection rules with respect to the orbital momentum, $\Delta\ell = 0, \pm 2$, and can, in contrast to the simple operator (9.12), induce the so-called M1 ℓ -*forbidden* magnetic transitions. Physically, such terms can emerge owing to the tensor forces (recall Section 3.5). Finally, we cannot exclude the possibility that inside the many-body system, the gyromagnetic ratios (9.15) and (9.16) can be *renormalized* to different numerical values. They are produced by the meson clouds and meson exchange currents around the nucleons, and these clouds should be distorted inside the nucleus by the presence of other nucleons.

Problem 9.1 Calculate the contribution to the magnetic moment of a single nucleon on the j -level from the operator (9.19).

Solution

According to the vector model, the effective operator for a single j -level can be written as $xj\mathbf{j}$. Then, since $(\mathbf{n} \cdot \boldsymbol{\ell}) = 0$,

$$(\boldsymbol{\mu}^{(2)} \cdot \mathbf{j}) = xj(j+1) = g^{(2)}(r)(\boldsymbol{\sigma} \cdot \mathbf{n})(\mathbf{n} \cdot \mathbf{j}) = g^{(2)}(r)(\boldsymbol{\sigma} \cdot \mathbf{n})(\mathbf{n} \cdot \mathbf{s}) = \frac{1}{2} g^{(2)}(r). \quad (9.20)$$

Finally,

$$\boldsymbol{\mu}^{(2)} = xj = \frac{\langle g^{(2)}(r) \rangle}{2(j+1)}. \quad (9.21)$$

9.4 Quadrupole Moment

The tabular quadrupole moment is the expectation value of the operator Q_{zz} , Eqs. (3.74) and (3.75), in the state with the maximum possible projection $J_z = J$ of the angular momentum. Let us calculate this quantity for a nucleus with one valence nucleon on a j -level above a magic core. According to the single-particle shell model, the whole quadrupole moment is carried by this last nucleon because the core is spherical. Then $J = j$, and the quadrupole moment is

$$Q = \langle jj | r^2(3\cos^2\theta - 1)jj \rangle. \quad (9.22)$$

The electric quadrupole moment for the single proton differs only by the charge factor e .

The spin-angular wave function in (9.22) can be obtained in a standard way using the Clebsch–Gordan coefficients, which couple spin 1/2 and orbital momentum ℓ to total angular momentum $j = \ell \pm 1/2$. The straight forward integration over angles leads to

$$Q = -\langle r^2 \rangle \frac{2j-1}{2j+2}. \quad (9.23)$$

Problem 9.2 Derive Eq. (9.23).

Solution

Here we show how one can calculate this value with no tables of the Clebsch–Gordan coefficients at hand but using the algebraic method typical for problems of this type. In the spirit of the vector model, compare Problem 9.1, we construct an effective quadrupole operator acting in the space of states belonging to certain values of j and ℓ (one of the members of the spin–orbit doublet $j = \ell \pm 1/2$). The quadrupole tensor Q_{ik} , Eq. (3.74), is symmetric and traceless ($Q_{ii} = 0$; always the summation over the repeated subscripts is implied) second-rank tensor. The effective operator has to be built using the angular momentum components j_i . Up to a constant factor, the only possible combination is

$$Q_{ik} = \alpha \left(j_i j_k + j_k j_i - \frac{2}{3} \delta_{ik} \mathbf{j}^2 \right). \quad (9.24)$$

Here α is a constant that is the main subject of our interest because it is linked to the observable quadrupole moment (9.22). From (9.24), we obtain

$$\langle jm | Q_{zz} | jm \rangle = \frac{2}{3} \alpha [3m^2 - j(j+1)], \quad (9.25)$$

Then the observable quadrupole moment is ($m = j$)

$$Q = \frac{2}{3} \alpha j(2j-1). \quad (9.26)$$

The form (9.24) of the effective quadrupole operator is valid for a multiplet with any angular momentum, integer or half-integer. Note that, according to (9.26), we automatically guarantee the selection rules that do not allow a quadrupole moment for the states with angular momenta $j = 0$ and $j = 1/2$.

To determine the constant α and hence the quadrupole moment (9.26), we write down the original single-particle operator (3.74) in a tensor form in terms of the components of the radial vector $\mathbf{n} = \mathbf{r}/r$,

$$Q_{ik} = r^2 (3n_i n_k - \delta_{ik}). \quad (9.27)$$

The matrix elements of the operator (9.27), diagonal with respect to j , have to coincide with those of the effective operator (9.24). If we multiply the exact operator (9.27) by the angular momentum components j_i , from the left, and j_k , from the right, with the summation over i and k , we are still within the multiplet of states with given j . Therefore, the result should be the same as for the effective operator (9.24),

$$A(j) \equiv j_i Q_{ik} j_k = \langle r^2 \rangle [3(\mathbf{j} \cdot \mathbf{n})^2 - \mathbf{j}^2], \quad (9.28)$$

where the average over the radial wave function is taken. But the vector ℓ is perpendicular to the radius vector and $(\ell \cdot \mathbf{n}) = 0$. Since $\mathbf{j} = \ell + \mathbf{s}$,

$$(\mathbf{j} \cdot \mathbf{n})^2 = (\mathbf{s} \cdot \mathbf{n})^2 = \frac{1}{4} (\boldsymbol{\sigma} \cdot \mathbf{n})^2 = \frac{1}{4}. \quad (9.29)$$

It gives for the quantity (9.28)

$$A(j) = \langle r^2 \rangle \left[\frac{3}{4} - j(j+1) \right] = -\frac{1}{4} \langle r^2 \rangle (2j-1)(2j+3). \quad (9.30)$$

The same procedure with the effective operator (9.24) gives (keep track of the order of noncommuting operators!)

$$A(j) = a \left(\frac{1}{3} \mathbf{j}^4 + j_i j_k j_i j_k \right). \quad (9.31)$$

The second term here can be transformed using the angular momentum commutation relations,

$$j_i j_k j_i j_k = j_i [j_k, j_i] j_k + \mathbf{j}^4 = i \epsilon_{kin} j_i j_n j_k + \mathbf{j}^4. \quad (9.32)$$

Applying the commutation relations again to the first term in the right-hand side of (9.32), we obtain

$$i \epsilon_{kin} j_i ([j_n, j_k] + j_k j_n) = i \epsilon_{kin} j_i (i \epsilon_{nkm} j_m + j_k j_n). \quad (9.33)$$

The first term in (9.33) reduces, with the use of cyclic invariance of ϵ_{ikl} , to

$$- \epsilon_{kin} \epsilon_{kmn} j_i j_m = -2 \delta_{im} j_i j_m = -2 \mathbf{j}^2. \quad (9.34)$$

The second term in (9.33) gives, using the asymmetry properties and the same commutator,

$$i \epsilon_{kin} \frac{1}{2} [j_i, j_k] j_n = \frac{i}{2} \epsilon_{kin} i \epsilon_{ikm} j_m j_n = \mathbf{j}^2. \quad (9.35)$$

The result for the quantity (9.31) is

$$A(j) = a \left(\frac{4}{3} \mathbf{j}^4 - \mathbf{j}^2 \right) = \frac{a}{3} j(j+1)(2j-1)(2j+3). \quad (9.36)$$

Combining this with Eq. (9.30), we find

$$a = -\frac{3}{4} \frac{\langle r^2 \rangle}{j(j+1)}. \quad (9.37)$$

By means of Eq. (9.26), this is equivalent to (9.23). The result is valid for both components of the spin-orbit doublet $j = \ell \pm 1/2$.

The quadrupole moment of a single-particle state above the closed core, according to (9.23), is always *negative* as it should be for the orbit with the maximum projection j_z that classically would correspond to motion in the equatorial plane perpendicular to the quantization axis and, consequently, to *oblate* (pancake) shape with $Q < 0$. In the classical limit of $j \gg 1$, which is possible only for $\ell \gg 1$, Eq. (9.23) gives $Q = -\langle r^2 \rangle$ in accordance with the vanishing value of $\cos \theta$ in the equatorial plane.

Protons starting a new shell usually indeed lead to a negative quadrupole moment of a nucleus. We use the unit of *barn*, $1 \text{ b} = 10^{-24} \text{ cm}^2$, for the dimension of the area (it is also used for reaction cross sections). The examples can be ^{63}Cu and ^{65}Cu , where the odd proton should be on the $1p_{3/2}$ level (the extra neutrons form a spherical pair with zero total angular momentum) and $Q = -0.211(4) \text{ b}$ and $-0.195(4) \text{ b}$, respectively; ^{121}Sb ($1d_{5/2}$) and ^{123}Sb ($0g_{7/2}$) with $Q = -0.36(4) \text{ b}$ and $Q = -0.49(5) \text{ b}$, respectively; ^{209}Bi ($0h_{9/2}$), $Q = -0.37(3) \text{ b}$. The numerical value is of the same order of magnitude as predicted by (9.23), $\langle r^2 \rangle \sim (3/5)R^2$, although there is no exact quantitative agreement.

The quadrupole moment is a *time-even* quantity and, as we proved in (9.9), it should have an opposite value for a state with one hole in a nearly filled shell. In two potassium isotopes, $^{39}_{19}\text{K}_{20}$ and $^{41}_{19}\text{K}_{22}$, with one proton hole in the *sd*-shell, the quadrupole moment is positive and has almost the same value, +0.0585(6) b and +0.060(5) b, respectively, being only slightly perturbed by the extra neutron pair in ^{41}K . The ground states of both these isotopes have spin 3/2, which agrees with the shell model level $0d_{3/2}$ closing the *sd*-shell. The absolute value of the quadrupole moment is significantly higher than 0.04 b predicted by (9.23). Other examples of the positive hole quadrupole moment are ^{11}B (proton hole $0p_{3/2}$, $Q = +0.0407(3)$ b) and ^{113}In (proton hole $0g_{9/2}$, $Q = +0.80(4)$ b).

It is common for the magnitude of empirical quadrupole moments to be substantially larger than single-particle predictions of Eq. (9.23). Even in nuclei with one particle or one hole, their magnitudes are usually higher than according to the single-particle shell model. With several valence nucleons, the quadrupole moments of nuclei are mostly positive and in many cases exceed the single-particle estimates by one to two orders of magnitude. Evidently, here we need to have another mechanism producing the quadrupole moments. The large magnitude can be provided only by the correlated quadrupole moments of several particles.

One of the examples where the predictions of the single-particle shell model seem to come true can be found in sulfur isotopes. From Figure 8.4, we notice that if the orbit occupation proceeds in accordance with the spherical shell model, both protons and neutrons in the $^{32}_{16}\text{S}_{16}$ fill completely $d_{5/2}$ and $s_{1/2}$ shells. In the isotopes $^{33}_{16}\text{S}_{17}$ and $^{35}_{16}\text{S}_{19}$, we have one neutron and one neutron hole in the next $0d_{3/2}$ level, respectively. The corresponding quadrupole moments are found to be $-0.084(8)$ b and $+0.0471(9)$ b. Note however that the experiment measures the *electric* quadrupole moment, which should vanish for an odd neutron!

9.5 Recoil Corrections

A more accurate consideration shows that there exists a small contribution from an odd neutron to the quadrupole (and other multipole) moments of the charge distribution. Such contributions are due to the recoil of protons when the neutron is displaced. Indeed the center of mass should be fixed to avoid the admixture of spurious (false) excitations of motion as a whole to physical wave functions. In the definition (3.74) of the electric quadrupole moment, the sum goes only over proton coordinates. But since we are not interested in motion of the nucleus as a whole, the coordinates should be reckoned from the center of mass \mathbf{R} . For example, instead of $\sum_a e_a z_a^2$ in the quadrupole moment Q_{zz} , it should be $\sum_a e_a (z_a - R_z)^2$, where R_z is the z -coordinate of the center of mass, $R_z = (1/A) \sum_a z_a$. Here the summation goes over all particles, protons and neutrons. As a result, we obtain a new operator

$$\sum_a e_a z_a^2 - \frac{2}{A} \sum_a z_a \sum_b e_b z_b + \frac{1}{A^2} \left(\sum_a z_a \right)^2 \sum_b e_b. \quad (9.38)$$

In the last item, $\sum_b e_b$ gives the total charge Z . The sum in front of Z contains contributions of all particles. In the single-particle shell model for a nucleus with one valence neutron, only this contribution survives for the single-neutron matrix element, and we get $(Z/A^2)z^2$, much smaller than the single-proton contribution z^2 .

Thus, the neutron contribution to electric multipole moments is not zero, but we expect it to be small by the recoil factors. An example when it seems to be true is given by ^{17}O with the odd neutron in the $0d_{5/2}$ level and the quadrupole moment, $Q = -0.02578 \text{ b}$, by an order of magnitude smaller than typical values for an odd proton; in ^{17}F , the magnitude of the quadrupole moment is 0.10 b . In reality, however, in many cases, an odd neutron and an odd proton induce comparable quadrupole moments.

The recoil effect is however extremely important for the *electric dipole* operator. Introducing again the center of mass, we have

$$\mathbf{d} = \sum_a e_a (\mathbf{r}_a - \mathbf{R}) = \sum_a e_a \mathbf{r}_a - Ze\mathbf{R} = \sum_a e_a \mathbf{r}_a - \frac{Z}{A} e \sum_b \mathbf{r}_b. \quad (9.39)$$

The first sum runs over protons only. Subdividing the second sum into proton and neutron parts, we present the dipole operator in the form

$$\mathbf{d} = e \left[\frac{N}{A} \sum_p \mathbf{r}_p - \frac{Z}{A} \sum_n \mathbf{r}_n \right]. \quad (9.40)$$

Protons and neutrons contribute to the electric dipole operator on equal footing with *effective charges* N/A for protons and $-Z/A$ for neutrons. It is clear that, in a system with particles of one sort only, there is no intrinsic dipole operator as it reduces to the center of mass (recall sum rules and Problem 6.1). The dipole polarization implies that there is a displacement of protons against neutrons with the center of mass fixed. The dipole operator, in contrast to the quadrupole moment, does not create any static asymmetry (there are no diagonal matrix elements). Due to parity conservation, it is seen only in dipole transitions that are of isovector character as follows from (9.40) as well.

The empirical results show strong enhancement of quadrupole moments that definitely cannot be caused by a single neutron or neutron hole. Other particles should contribute to quadrupole asymmetry. Since they belong to a closed core and a redistribution of particles inside a core is impossible due to the Pauli principle, the only possibility to provide the core with a quadrupole moment is to make a *mixture of configurations*. In the wave function of the core, new components appear corresponding to the excitation of particles to higher shells. The valence particles interact with the core and generate core excitations usually referred to as *core polarization* [1]. Even if the effect is small for each core particle, the total polarization multipole moment is a *coherent* sum of such small contributions and the resulting summarized effect can be large compared to the original “bare” single-particle quadrupole moment. Such a polarization has nothing in common with the electric charge and in general has to be of the same order for protons and neutrons.

9.6 Introduction to Group Theory of Multiparticle Configurations

Classification of degenerate multiparticle configurations as symmetry group representations [2] offers many advantages. For example, rotational symmetry is an exact symmetry, therefore states of different angular momenta are never mixed by the Hamiltonian and one could reduce the number of basis states by considering each set

of states with a fixed J separately, the so-called J -scheme. The smallest separate sets of states transforming among themselves under rotations form *irreducible representations* of the rotation group. Even for nonexact symmetries, such as isospin symmetry or $SU(3)$ symmetry of the harmonic oscillator potential mentioned in Chapter 8, the symmetry-based classification may offer better understanding of the nature of low-lying states and transitions between them and better convergence of solutions and systematic strategy for basis truncation. A symmetry classification can be helpful in dealing with other issues such as the center-of-mass problem, which we discuss later.

Assume that the valence space consists of Ω degenerate single-particle orbits. A simple A -particle wave function can be built as a product of A single-particle wave functions. There are many, determined by combinatorics, different many-body states that one can make this way. For noninteracting particles, all these states would have the same energy, Eq. (9.2). It is obvious that without any change to the total energy, the Ω single-particle wave functions can be linearly mixed using an arbitrary unitary $\Omega \times \Omega$ matrix with complex elements. Thus, the problem is said to be symmetric with respect to $\mathcal{U}(\Omega)$ group.

To give a glimpse on the general picture, it is instructive to review a familiar $SU(2)$ group of angular momentum, the “ S ” in the name implies that this is a “special” unitary group, a subgroup of matrices that have the unit determinant (as opposed to an arbitrary complex number of absolute value one). Approaching this group for a two-state system ($\Omega = 2$) with some number of particles, we arrive at the so-called **Schwinger representation** for angular momentum [QP, I, 20.2]. In this representation, the many-body wave function is a product of f_1 functions of type 1 with the spin projection $m = +1/2$ and f_2 functions of type 2 that have $m = -1/2$ (total of $A = f_1 + f_2$ functions, one for each particle). This state is symmetric with respect to the first f_1 variables and separately with respect to the second f_2 variables. Using symmetry operations that linearly mix functions 1 and 2, we can obtain various other wave functions, but all the new functions will retain the same permutational symmetry. This permutational symmetry is expressed with a Young diagram, or pattern, as $[f_1, f_2]$. As interchanging $1 \leftrightarrow 2$ is among symmetry operations, in order to identify an irreducible representation uniquely we should establish ordering, and as a rule we select $f_1 \geq f_2$. Thus, we established that a two-component Young pattern that labels irreducible representations of the permutational group can be used to label irreducible representations of $\mathcal{U}(2)$, where the highest allowed projection for this permutational symmetry is $j = (f_1 - f_2)/2$. If we are just interested in identifying an irreducible representation of the rotational $SU(2)$ group, we can take a minimum number of functions in a stretched state so that $f_2 = 0$, and our j is formally labeled as $[2j, 0]$. Numerical algorithms can be found in [3].

The procedure can be generalized to the $\mathcal{U}(\Omega)$ group, and thus irreducible representations of this group are labeled with Ω components of a Young pattern $[f_1, f_2, \dots, f_\Omega]$ where f_q are nonnegative integers forming an ordered list $f_{q-1} \geq f_q$. The Young schemes are often visualized as patterns of boxes where f_q is the number of boxes in the q th row from the top, for example,

$$[4, 2, 1] = \begin{array}{c} \square \quad \square \quad \square \quad \square \\ \square \quad \square \\ \square \end{array} .$$

Since $\mathcal{U}(\Omega - 1)$ is a subgroup of $\mathcal{U}(\Omega)$, an irreducible representation $[f_1^{(\Omega)}, \dots, f_\Omega^{(\Omega)}]$ of $\mathcal{U}(\Omega)$ contains irreducible representations of $\mathcal{U}(\Omega - 1)$; all of them can be found by

listing all possible Young patterns $[f_1^{(\Omega-1)}, f_2^{(\Omega-1)}, \dots, f_{\Omega-1}^{(\Omega-1)}]$ that satisfy the betweenness condition $f_k^{(\Omega)} \geq f_k^{(\Omega-1)} \geq f_{k+1}^{(\Omega)}$. In fact, going through this *canonical reduction* procedure $\mathcal{U}(\Omega) \supset \mathcal{U}(\Omega-1) \dots \supset \mathcal{U}(1)$, all states can be enumerated and it can be shown that the number of states in a given irreducible representation is

$$\dim([f_1, f_2, \dots, f_\Omega]) = \prod_{1 \leq q < q' \leq \Omega} \left(1 + \frac{f_q - f_{q'}}{q' - q} \right). \quad (9.41)$$

Let us now examine how to count and organize states according to their symmetries. For example, as we already discussed in Section 6.7, under rotational symmetry all \mathcal{N} many-body m -scheme states form different irreducible representations. If $D(J)$ is a number of states with spin J and $\dim(J) = 2J + 1$ is a number of states in each irreducible representation, then we can reorganize all states into blocks so that

$$\mathcal{N} = \sum_J D(J) \dim[J]. \quad (9.42)$$

Let us further elaborate on the procedure used to find $D(J)$ and deduce the number and types of irreducible representations present. For the $SU(2)$ group, we demonstrated this procedure in Table 6.1. The question is answered by first counting the number of states with different M projections. Since each J state has all projections $M = -J, -J + 1, \dots, J$ and if $d(M)$ is a number of m -scheme configurations with given M , then the number of irreducible representations for each J can be found as

$$D(J = M) = d(M) - d(M + 1), \quad (9.43)$$

working our way from the highest absolute value M_{\max} for which $d(M_{\max} + 1) = 0$ down until we reach zero $J \geq 0$. The same approach can be used when states are to be classified according to several combined $SU(2)$ symmetries. For example, classifications according to angular momentum and isospin or according to spin and orbital angular momentum are very common.

These procedures can be generalized. Let us take another look at the $SU(3)$ symmetry of a spherically symmetric harmonic oscillator potential mentioned in Chapter 8: the symmetry involves exchanging quanta in the x , y , and z directions. In this case, the number of irreducible representations can be determined by going through all many-body states and counting occurrences of particular distributions of quanta along three Cartesian directions $d(n_1, n_2, n_3)$. Then number of irreducible representations of each kind can be found using equation

$$\begin{aligned} D([f_1 = n_1, f_2 = n_2, f_3 = n_3]) \\ = d(n_1, n_2, n_3) + d(n_1 + 1, n_2 + 1, n_3 - 2) + d(n_1 + 2, n_2 - 1, n_3 - 1) \\ - d(n_1 + 2, n_2, n_3 - 2) - d(n_1 + 1, n_2 - 1, n_3) - d(n_1, n_2 + 1, n_3 - 1). \end{aligned} \quad (9.44)$$

which is a generalization of Eq. (9.43). Similar to the $SU(2)$ case, in order to identify irreducible representations in $SU(3)$, it is sufficient to use two labels (λ, μ) where $\lambda = f_1 - f_2 \geq 0$ and $\mu = f_2 - f_3 \geq 0$. From Eq. (9.41), we obtain the number of states in each irreducible representation,

$$\dim((\lambda, \mu)) = \dim([\lambda + \mu, \mu, 0]) = \frac{1}{2}(\lambda + 1)(\mu + 1)(\lambda + \mu + 2). \quad (9.45)$$

When we discuss many-body states in a harmonic oscillator field, the classification according to angular momentum (rotational subgroup $O(3)$) is the most convenient.

Summarizing the result, the states can be enumerated using an auxiliary nonnegative integer K , which is of the same parity but not greater than $\min(\lambda, \mu)$,

$$K = \min(\lambda, \mu), \mu - 2, \dots, 1 \text{ or } 0. \quad (9.46)$$

For each K , we have a set of angular momentum states

$$\begin{aligned} L = & K, K + 1, \dots, K + \max(\lambda, \mu) && \text{if } K > 0; \\ L = & \max(\lambda, \mu), \max(\lambda, \mu) - 2, \dots && \text{if } K = 0. \end{aligned} \quad (9.47)$$

Problem 9.3

- The exotic ${}^7\text{He}$ nucleus can be considered as an alpha-particle core and three neutrons in the $0p$ -shell. Classify these configurations according to their total angular momentum and identify excitation energies of these configurations assuming that the spin-orbit splitting between $0p_{3/2}$ and $0p_{1/2}$ orbitals is ϵ .
- In atoms, the spin-orbit interaction is weak, which makes LS -coupling more relevant. The nitrogen atom has the lowest electron configuration $1s^2 2s^2 2p^3$, where similar to ${}^7\text{He}$ three identical spin $1/2$ particles are in the p -shell. Determine possible quantum numbers L, S, J for this configuration.
- Consider three identical spin $1/2$ particles in the p -shell of a harmonic oscillator potential. Classify these configurations according to $SU(3)$ oscillator symmetry.

Solution

- There are $\Omega = 3 \times 2 = 6$ *single-particle* states in the system and the total number of fermionic three-particle states is

$$\mathcal{N} = \frac{6!}{3!3!} = 20. \quad (9.48)$$

The following table lists all possible distributions of three particles among six levels labeled with their m projections, $m = 3/2, 1/2, -1/2, -3/2$ for $p_{3/2}$ and $m = 1/2'$ and $-1/2'$ for $p_{1/2}$ orbital. Last three columns show the total magnetic projection of angular momentum, configuration (partition of particles among the levels), and energy of this configuration. The excitation energy is determined by the number of particles in the $p_{1/2}$ state.

m_1	m_2	m_3	M	Configuration	E
3/2	1/2	1/2'	5/2	$(p_{3/2})^2 p_{1/2}$	ϵ
3/2	1/2	-1/2	3/2	$(p_{3/2})^3$	0
3/2	-1/2	1/2'	3/2	$(p_{3/2})^2 p_{1/2}$	ϵ
3/2	1/2	-1/2'	3/2	$(p_{3/2})^2 p_{1/2}$	ϵ
3/2	1/2'	-1/2'	3/2	$p_{3/2}(p_{1/2})^2$	2ϵ
3/2	1/2	-3/2	1/2	$(p_{3/2})^3$	0
3/2	1/2'	-3/2	1/2	$(p_{3/2})^2 p_{1/2}$	ϵ
3/2	-1/2	-1/2'	1/2	$(p_{3/2})^2 p_{1/2}$	ϵ
1/2	1/2'	-1/2	1/2	$(p_{3/2})^2 p_{1/2}$	ϵ
1/2	1/2'	-1/2'	1/2	$p_{3/2}(p_{1/2})^2$	2ϵ

Using Eq. (9.43), we determine that there is one state with $J = 5/2$ that belongs to $(p_{3/2})^2 p_{1/2}$ configuration, there are three states with $J = 3/2$, one of those states $(p_{3/2})^3$ is the ground state, one is $(p_{3/2})^2 p_{1/2}$, and one has two particles on $p_{1/2}$ orbit, namely $p_{3/2}(p_{1/2})^2$. Finally, there is one more state in this configuration space with $J = 1/2$ and $(p_{3/2})^2 p_{1/2}$ structure. We can verify Eq. (9.42) that $1 \times 6 + 3 \times 4 + 1 \times 2 = 20$.

- b) Here the enumeration is slightly more complicated because we want to classify states based on $SU(2) \times SU(2)$ symmetry for orbital angular momentum and spin, therefore we need to list orbital momentum and spin projections separately and then combine them in the way allowed by Fermi statistics. The available $\Omega = 3 \times 2 = 6$ *single-particle* states (m_l, m_s) are

$$\begin{aligned} (a) & (1, 1/2); \quad (a') (1, -1/2); \\ (b) & (0, 1/2); \quad (b') (0, -1/2); \\ (c) & (-1, 1/2); \quad (c') (-1, -1/2). \end{aligned}$$

Now we fill in those states by three particles forming the many-body states. Start with the maximum possible total orbital momentum projection $M_L = 2$. There are three ways of doing this, all including (a) and (a'): $(aa'b), M_S = 1/2$, and $(aa'b'), M_S = -1/2$. Since always the situation will be symmetric for positive and negative M_L and M_S , we can limit ourselves to the states with positive values of both projections,

$$M_L = 2 : (aa'b), \quad M_S = 1/2. \quad (9.49)$$

Therefore, the state with $L = 2$ and $S = 1/2$ is allowed, its symbol being 2D ; the corresponding total angular momentum can be $J = 3/2$ or $5/2$. For $M_L = 1$, we have

$$M_L = 1 : (aa'c), \quad M_S = 1/2; \quad (abb'), \quad M_S = 1/2. \quad (9.50)$$

One of these states belongs to the previous multiplet, another one opens the new one with $L = 1$ and $S = 1/2$, that is, 2P with $J = 1/2$ or $3/2$. Finally, the combinations allowed for $M_L = 0$ include

$$M_L = 0 : (abc); \quad (abc'); \quad (ab'c); \quad (a'bc), \quad (9.51)$$

with the spin projection $M_S = 3/2$ for the first one, and $M_S = 1/2$ for the three remaining cases. This shows a new (third) multiplet with $L = 0$ and $S = 3/2$ that should be labelled as 4S , and here $J = S$. Three leftover states with $M_L = 0$ fill the three open multiplets. Now we can list all possible terms of the configuration p^3 :

$${}^2D_{3/2,5/2}; \quad {}^2P_{1/2,3/2}; \quad {}^4S_{3/2}. \quad (9.52)$$

Indeed, counting all states (9.52) with various J and M_J , we obtain

$$\mathcal{N} = \sum_J (2J + 1) = 4 + 6 + 2 + 4 + 4 = 20. \quad (9.53)$$

- c) Spin is not a part of the harmonic oscillator symmetry, and we can classify the states according to $SU(3) \times SU(2)$, keeping spin separately. This means that in the Young pattern, we can allow at most two nucleons to be in the symmetric state. In the p -shell, one quantum of oscillator excitation can be in one of three spatial directions,

thus we can have two possible Young patterns $[f] = [2, 1, 0]$, which gives $(\lambda, \mu) = (1, 1)$, and $[f] = [1, 1, 1]$ giving another irreducible representation $(\lambda, \mu) = (0, 0)$. As spin is a separate symmetry, all states in a given $SU(3)$ irreducible representation should have the same spin.

In $(\lambda, \mu) = (1, 1)$ irreducible representation ($[f] = [2, 1, 0]$), two particles are in a symmetric state and thus must be in the antisymmetric spin state with spin zero. The third (spin-unpaired) particle makes all states with quantum numbers $(\lambda, \mu) = (1, 1)$ to have $S = 1/2$. According to the above-discussed Elliott's classification (9.47), this $SU(3)$ irreducible representation contains two angular momentum states with $L = 1$ and $L = 2$. The second irreducible representation $(\lambda, \mu) = (0, 0)$ is an $L = 0$ state with $S = 3/2$. The reclassification in terms of angular momentum recovers the result obtained in part (b).

We can confirm these results by counting irreducible representations using Eq. (9.44) while ignoring spin. For example, $d(1, 1, 1) = 8$ because in this configuration there are eight different ways that spins can be oriented, while $d(2, 1, 0) = 2$ because there are two choices of spin direction for the particle with one quantum along the y -axis. This counting leads to $D((\lambda, \mu) = (0, 0)) = 4$ and $D((\lambda, \mu) = (1, 1)) = 2$ which, of course, reflects the spin degeneracy. Once again with Eq. (9.45), we verify $\mathcal{N} = 20 = 4 \times 1 + 2 \times 8$.

References

- 1 Bohr, A. and Mottelson, B.R. (1975) *Nuclear Structure*, Vol. II, Benjamin, Reading, MA.
- 2 Hamermesh, M. (1962) *Group Theory and Its Application to Physical Problems*, Addison Wesley, Reading, MA.
- 3 Alex, A., Kalus, M., Huckleberry, A., and von Delft, J. (2011) A numerical algorithm for the explicit calculation of $SU(N)$ and $SL(N,C)$ Clebsch-Gordan coefficients. *J. Math. Phys.* **52**, 023507, <https://arxiv.org/abs/1009.0437>.

10

Light Nuclei

... a basic reason behind the successes of nuclear physics: our good fortune to have been able to extract essential regularities from the nuclear many-body problem without a deeper understanding of why – at least at the outset.

From J.S. Vaagen *et al.*, in *New Perspectives in Nuclear Structure*, ed. A. Covello, World Scientific, Singapore, 1996, p. 39.

10.1 A Short Walk along the Beginning of the Nuclear Chart

Now we can start looking in more detail at the shell model at work. Since it is impossible to review an immense amount of available information, we limit ourselves in this chapter to primitive examples leaving more complicated physical phenomena for the future.

The shell-model configurations are the simplest in light nuclei. But even here, we encounter many cases when (i) for a given configuration, several values of the total spin are possible and (ii) there are different configurations close in energy leading to *configuration mixing*. Only for the ground states of doubly-magic nuclei and adjacent nuclei with one valence particle or one hole, the shell model is capable of predicting the ground state unambiguously. For many particles (holes), the ground state spin is $J_0 = 0$ in even–even nuclei and agrees – usually but not always – with the *pairing* idea. In an odd- A nucleus, the ground state spin is expected to be equal to the value of j for the orbit occupied by the last unpaired nucleon. There are also some empirical rules for the ground states in odd–odd nuclei, but those rules lack clear theoretical justification. (The number of stable odd–odd nuclei is rather small.) To choose between the configurations, it is assumed usually that the state with the minimum isospin value $T = |T_3|$ has the lowest energy. As was discussed for the deuteron, Chapter 3, such states have maximum symmetry in space-spin variables that is favorable for the attraction forces.

Let us take a look at the beginning of the nuclear chart (Figure 10.1), looking selectively at the shell-model properties. Low-lying states of some light nuclei are shown in Figures 10.2 and 10.3. As the deuteron properties were discussed in Chapter 3, we start with the first doubly-magic, $Z = N = 2$, nucleus.

$^4_{\alpha}He_2$ (*alpha-particle*). In accordance with the expectations, the ground state spin-parity quantum numbers are 0^+ . The α -particle has enhanced binding energy and, with the

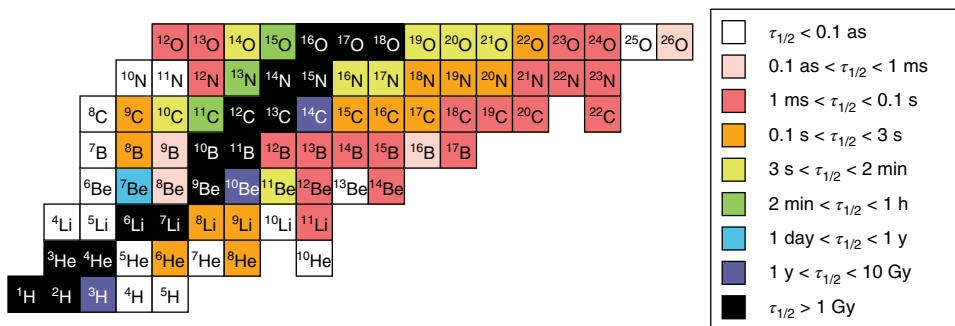
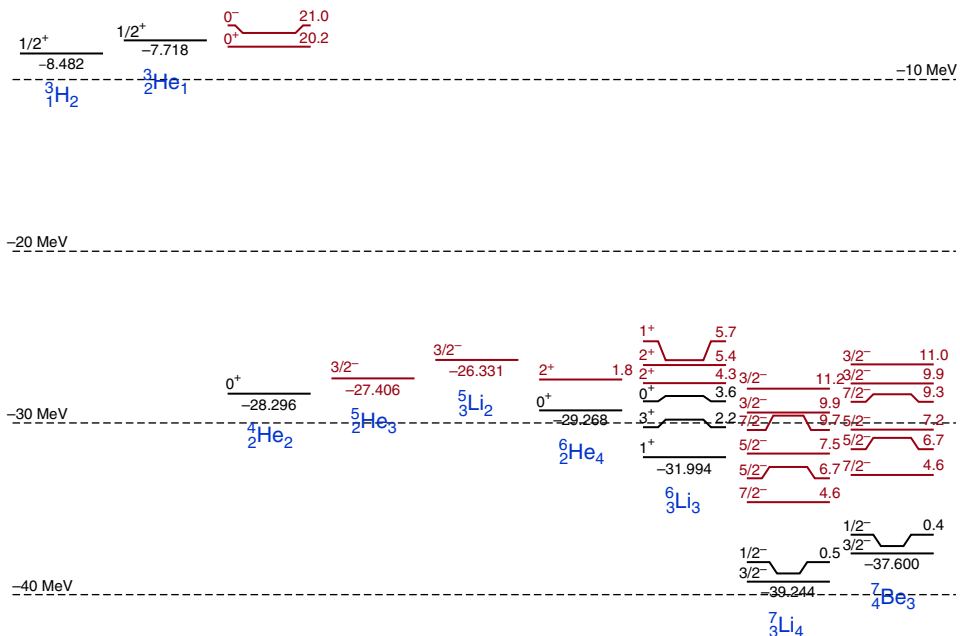


Figure 10.1 Chart of light nuclei.

Figure 10.2 Low-lying energy spectra of light nuclei, $A \leq 7$. States that are unstable with respect to nuclear decay are shown in red.

lowest excited state being at the level around 20 MeV of excitation, it is exceptionally stable. These properties confirm the doubly-magic nature of this nucleus and allow the α -particle to be emitted as a whole in many cases of alpha-decay, as well as a by-product of reactions with heavier nuclei. All four nucleons can be accommodated in the $0s$ -state that becomes completely filled. Such a configuration is usually denoted as $(0s)^4$. There are indications that this is not the whole truth, and the ground state in reality is more complex having an admixture of higher configurations. In particular, due to the tensor forces there might be a small fraction of the d -states giving a configuration with $L = 2$ and $S = 2$ that cannot appear in the extreme limit of a single closed shell $(0s)^4$. Of course, the amount of admixture is defined relative to $0s$ state of the mean field, which

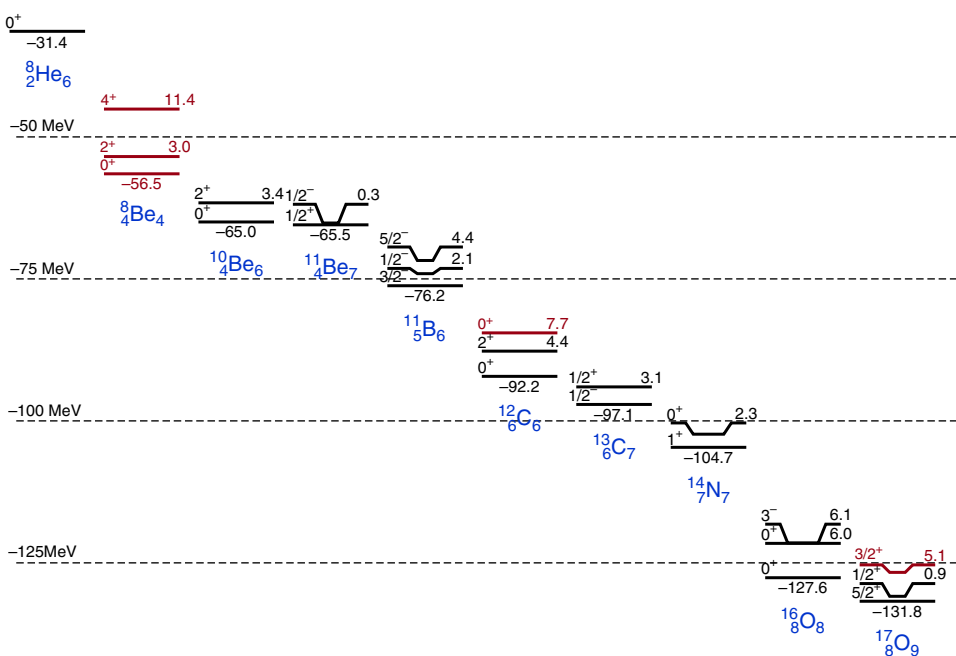


Figure 10.3 Low-lying energy spectra of light nuclei, $A \geq 8$.

for four nucleons can be rather ambiguous. Numerical studies show that for harmonic oscillator potential (see Section 8.5), the optimal value of $\hbar\omega_o \approx 28$ MeV, which is in good agreement with estimate (8.16).

$^3\text{H}_2$ (*tritium*). The configuration corresponds to a proton hole in the doubly magic ^4He . Therefore, we expect the configuration $(0s)^3$ with spin $J = j = 1/2$, which is indeed the case. Using the *particle-hole symmetry* (9.10) and the Schmidt line (9.18) for a proton with $j = \ell + 1/2$, we predict the magnetic moment $\mu = \mu_p = 2.79$ n.m., whereas the experimental value is 2.98 n.m.

$^3\text{He}_1$. This is a *mirror nucleus* with respect to ^3H . The properties of the mirror partners are similar due to the isospin invariance. The ground state spin is $1/2$. The magnetic moment is that of the neutron hole. The Schmidt value (9.17) is $\mu = \mu_n = -1.91$ nm; the experimental value is -2.13 nm. The shift from the Schmidt value is almost the same as in ^3H but in the opposite direction. The part of this shift is again due to the d -wave admixture. ^3He is stable while tritium is beta-radioactive and decays into ^3He but with the quite small energy release, only about 18 keV (essentially the extra weight of two neutrons compared to two protons minus extra Coulomb energy of two protons); the decay is slow, with the halife of 12 years. Because of the very small energy release, this beta-decay is used in the experiments directed to the measurement of the neutrino mass.

$^5\text{Li}_2$ and $^5\text{He}_3$. Both are *particle-unstable*, which is explained by the abnormally weak binding of the valence nucleons to the doubly-magic alpha-core. In the experiments on scattering of neutrons and protons off ^4He , the observed low-lying resonances with spins $3/2^-$ and $1/2^-$ correspond to short-lived states of ^5He and ^5Li with the extra nucleon

on an unbound p -orbit in the continuum. The sequence of spins and the energy splitting between the resonances agree with the shell-model predictions for $0p_{3/2}$ and $0p_{1/2}$ spin–orbit doublet. The Schmidt magnetic moments in this case, $j = 3/2 = 1 + 1/2$, would be $\mu(^5\text{Li}) = 1 + \mu_p = 3.79$ n.m. and $\mu(^5\text{He}) = \mu_n = -1.91$ n.m.

$^6\text{Li}_3$. In this odd–odd nucleus, we have for the first time two valence particles and we cannot predict uniquely the ground state spin. If, in accordance with the shell model, valence proton and neutron occupy $0p_{3/2}$ levels, the total nuclear spin can take values 0, 1, 2, and 3. The experiment gives $J = 1$ suggesting the *alpha-deuteron* model: extra proton and neutron form a deuteron analog in the triplet spin state. The experimental magnetic moment is 0.82 n.m. (it was 0.86 n.m. for the deuteron, Section 3.6). To calculate the magnetic moment in the framework of the shell model, we should repeat our derivation of the Schmidt lines in Section 9.3 taking, instead of the spin–orbit coupling, the jj -coupling (9.3) of spins of two valence nucleons,

$$\mathbf{J} = \mathbf{j}_p + \mathbf{j}_n. \quad (10.1)$$

The magnetic moment is given by

$$\vec{\mu} = g^{(\text{odd } p)} \mathbf{j}_p + g^{(\text{odd } n)} \mathbf{j}_n, \quad (10.2)$$

where the gyromagnetic ratios coincide with those calculated above for ^5Li and ^5He . The vector model gives the effective magnetic moment operator similar to (9.13),

$$\vec{\mu} = g(J, j_p, j_n) \mathbf{J}, \quad (10.3)$$

with the Lande factor

$$g(J, j_p, j_n) = \frac{(g^{(\text{odd } p)} + g^{(\text{odd } n)})}{2} + \frac{(g^{(\text{odd } p)} - g^{(\text{odd } n)})}{2} \frac{[j_p(j_p + 1) - j_n(j_n + 1)]}{J(J + 1)}. \quad (10.4)$$

This equation can be applied to any odd–odd nucleus under assumption that the magnetic moment is due to the last unpaired proton and neutron only. In our case of a symmetric nucleus ^6Li , we have $j_p = j_n$ and

$$\mu = \frac{J}{2} [g^{(\text{odd } p)} + g^{(\text{odd } n)}]. \quad (10.5)$$

Using here the gyromagnetic ratios equal to the magnetic moments of ^5Li and ^5He divided by $j_p = j_n = 3/2$, we obtain $\mu = 0.63$ n.m. Note that if the valence proton and valence neutron would have a significant probability to be promoted (both of them, to ensure positive parity) to the $1s$ -level, then the same Eq. (10.5) would bring us much closer to the experimental value. For the pure $(1s_{1/2})^2$ configuration with $J = 1$, the result is simply $\mu = \mu_p + \mu_n = 0.88$ n.m. (parallel spins and no orbital contribution as for the deuteron in the pure s -wave approximation). Apparently, to utilize the deuteron-like attraction, the valence nucleons prefer to form a wave packet of several configurations.

$^6\text{He}_4$. This is our first experience with an *exotic nucleus*. The heavy helium isotope, with a large neutron-to-proton ratio equal to 2, ^6He , is unstable undergoing beta-decay to ^6Li . The wave function of ^6He is not well described by a standard shell model; it is better to think of the *cluster structure* of the alpha-core and the correlated neutron pair spread over few single-particle states on top of the core. Each of these states is already in

the continuum, but the energy of the pair correlation keeps the pair bound to the core. This can be considered as the simplest analog of the Cooper pair in superconductors; we discuss the pairing effects in more detail. We return to the large spatial size and other *halo* features later in this chapter. The similar cluster structure *alpha + deuteron* is probably responsible for the mixture of configurations in ${}^6\text{Li}$.

${}^7\text{Li}_4$. In this nucleus, two neutrons and one proton on top of the closed alpha-core are presumably in the $0p_{3/2}$ level. There are several possible states of three valence nucleons with different values of J and different permutational symmetries. To predict the ground state and its property, additional assumptions are needed. The ground state spin is $3/2^-$, and the magnetic moment is equal to 3.26 n.m. If the neutrons were paired with each other, the resulting magnetic moment would coincide with that for a proton in the $p_{3/2}$ level which is, according to the Schmidt rule, 3.79 nm. The mirror isotope, ${}^7\text{Be}_3$, supplies one of the best confirmation of charge symmetry as seen from the comparison of the low-lying energy spectra (Figure 10.2).

${}^8\text{He}_6$. This heaviest particle-stable helium isotope sets a record of the neutron/proton ratio that equals to 3 here. Four valence neutrons supposedly have more spherically symmetric configuration around the alpha-core than the neutron pair in ${}^6\text{He}$. This might be a reason for a *smaller* mean square charge radius; roughly speaking, the neutron shell slightly squeezes the proton charge distribution. Note that all odd helium isotopes heavier than alpha-particle are unbound.

${}^8\text{Be}_4$. This nucleus is the best example of the cluster structure. It can be considered as a nuclear molecule made of two alpha-particles. Because of the very tight structure of alpha-particles, their coupling is not sufficient for creating a genuine bound state so that ${}^8\text{Be}$ is in fact unstable, but its half-life time with respect to the decay into two alpha-particles, 7×10^{-17} s, is relatively long. Among 11 particle-stable beryllium isotopes only one, ${}^9\text{Be}_5$, is stable. The extra neutron stabilizes the core of two alpha-particles in a way qualitatively similar to collectivized electrons responsible for the molecular binding.

${}^5\text{B}_5$. Here we have, above an alpha-cluster, three protons and three neutrons, according to the shell model, in $0p_{3/2}$ states. Two remaining holes in this orbit can have spins 0, 1, 2, or 3. The ground state spin is 3. To explain this, we need additional assumptions about residual forces between the valence nucleons in an odd–odd nucleus. In some theories, *three-body nucleon forces* are responsible for the important part of additional interaction. In this specific case, one can assume that we have a contribution of three *quasideuteron pairs*, which prefer to align their spins to the maximum value $J = 3$. Accepting $J = 3$, we can apply Eq. (10.5) and predict the shell-model magnetic moment $\mu = 1.88$ n.m. to compare with the experimental value 1.80 n.m.

Next pair of mirror nuclei, ${}^5\text{B}_6$ and ${}^4\text{Be}_7$, contradicts to the simple independent particle shell model. In ${}^{11}\text{B}$, the ground state has spin $3/2^-$ in agreement with the configuration containing one proton $p_{3/2}$ hole. But the magnetic moment of this hole would be 3.79 n.m. while the empirical value is 2.69 n.m. The situation is even worse in ${}^{11}\text{Be}$ where the ground state spin is $1/2^+$ with positive parity that is impossible for a valence nucleon in a p -orbit (*level inversion*). There are residual interactions and alpha-cluster effects that lead to a considerable admixture of higher configurations and, possibly, to the *deformation* of the mean field. It is also useful to apply the ideas of quantum chemistry

and consider the admixtures of crystal-like geometrical structures built on overlapping alpha-clusters [1, 2].

$^{12}_6C_6$. According to the shell model, in the ^{12}C nucleus the $0p_{3/2}$ level is filled, which predicts that its spin-orbit partner $0p_{1/2}$ will be half-filled in the next isotope. The traces of possible triple-alpha cluster structure are seen in the existence of the so-called Hoyle state [3, 4], a resonance at excitation energy 7.65 MeV, slightly higher than the threshold for the decay into three alpha-particles. The cluster structure of the Hoyle state is supported by the fact that the rotational band based on this state has the moment of inertia considerably larger than the ground state [5]. It is also qualitatively understandable that cluster states are often located close to thresholds of corresponding decays – this allows for their stretched geometry that helps keeping their specific structure. The Hoyle state plays a crucial role in the *triple-alpha process* [6] of stellar nucleosynthesis.

$^{13}_6C_7$. Indeed, the ground spin here is $1/2^-$ and the magnetic moment of the ground state is 0.70 n.m. as compared to the Schmidt value for the odd neutron in $j = l - 1/2$ state equal to $(1/3)\mu_n = 0.64$ n.m.

$^{14}_7N_7$. Again we encounter the problem of finding the energetically favorable value of the total angular momentum for the valence proton and neutron, supposedly in the $0p_{1/2}$ level. Similar to 6Li , the *deuteron-like* state with $J = 1$ turns out to be preferable. The magnetic moment is given by Eq. (10.5) together with proton and neutron gyromagnetic ratios from (9.15), $\mu = 0.37$ n.m., whereas the empirical value is 0.40 n.m. The first excited state 0^+ at excitation energy 2.31 MeV almost equal to the deuteron binding energy is similar to the 1s_0 singlet virtual two-nucleon state. While the ground state has $T = T_3 = 0$ and has no analogs in the neighboring isobars with the same A , $^{14}_6C_8$ and $^{14}_8O_6$, the excited state 0^+ is analogous to the ground states of $^{14}_6C_8$ and $^{14}_8O_6$; they form the *isobaric triplet* with $T = 1$ and $T_3 = 0, \pm 1$ (see Figure 2.1 in Chapter 2 and Ref. [7]). The long lifetime for beta-decay of ^{14}C is traditionally used in geochronology (radioactive dating) [8].

$^{16}_8O_8$. This is a good example of a doubly-magic nucleus, $Z = N = 8$. The next major shell consists of the $0d_{5/2,3/2}$ spin-orbit doublet and $1s_{1/2}$ level. Nevertheless, even here the cluster structures are present with some probability and revealed in excited levels. The experiments with a superthin jet as a nuclear target in the electron storage ring [9] registered the events of the complete splitting $^{16}O \Rightarrow 2^8Be \Rightarrow 4^4He$.

$^{17}_8O_9$. This isotope is one of the best shell-model examples of a nucleus with one particle above the doubly-magic core. The ground state spin is $5/2^+$ in agreement with the lowest position of the $d_{5/2}$ level within the sd shell. The magnetic moment should be equal to the free neutron magnetic moment -1.91 n.m.; in reality $\mu = -1.89$ n.m.

We did not mention here the halo nuclei with loosely bound neutrons as ^{11}Li that will be discussed next.

10.2 Halo in Quantum Systems

The distribution of matter in an isolated quantum system is determined by the quantum mechanical wave function. A surface is well defined only on a macroscopic scale.

Textbooks in quantum mechanics show standard pictures of electron clouds in atoms and molecules. Always the density is smoothly decreasing from its typical internal value to zero far outside.

The diffuseness of the nuclear surface is characterized by the parameter α (do not confuse with the scattering length!) in the empirical density distribution, Eq. (8.34). For stable nuclei, the transitional layer is relatively thin, and the nucleus can be approximately treated as a *leptodermous* system with a rather sharp boundary. However, if the separation energy of a nucleon or a group of nucleons (nucleon cluster) becomes low, the wave function of a system reveals a significant probability of finding a nucleon or a cluster at a large distance from the core of the system. The disobedient cluster almost feels free but cannot leave the parent nucleus being still bound although only weakly. At large distances, the cluster is mainly outside the core and a simple potential two-body description is possible. Then the situation is similar to what has been discussed with respect to the deuteron *s*-wave (Section 3.4).

Consider a neutral cluster in the *s*-state relative to the core. Let $\psi(r)$ be the wave function of cluster motion relative to the core with energy $-\epsilon$ below the separation threshold. This function is exponentially decaying,

$$r\psi(r) \equiv u(r) = Be^{-\kappa r}, \quad \kappa = \sqrt{\frac{2mc}{\hbar^2}}, \quad (10.6)$$

at distances r greater than the range R of the cluster–core interaction. Here B is defined by the overall normalization and by proper matching with the interior wave function, and m is the reduced mass of the cluster–core system. Equation (10.6) brightly manifests the effect of quantum tunneling into a classically forbidden region. The penetration length $1/\kappa$ is defined solely by the separation energy and goes to infinity when this energy vanishes (at threshold), and the cluster is freed with the infinite scattering length (Section 4.3). At small binding energy, a cluster spends an appreciable amount of time far from the core forming a *halo* of the matter density. The relative time outside and inside the system is determined by the ratio $1/\kappa R$ of the penetration length to the force range; this ratio can be very big. One can say that the effective interaction range (here the system size) is $1/\kappa$, which is much larger than the force range R .

Examples of spatially stretched loosely bound systems are well known in physics. In the hydrogen-like atoms, an electron on a highly excited orbit (Rydberg state) is weakly bound and its wave function is extended far away from the nucleus. The lifecycle of pionic or muonic atoms starts usually with meson capture to an orbit with a very high main quantum number. There are recent experimental results confirming the existence of a weakly bound *dimer* of two ${}^4\text{He}$ atoms that can have a size of $10^2 \div 10^3$ Å and binding energy 10^{-7} eV [10].

The important difference of those examples versus the nuclear case is that in atomic and molecular physics we usually deal with the Coulomb or van der Waals forces, which are of the *long-range* type. Such forces decrease relatively slow, as an inverse power of the distance. Even at large distances, the attractive forces still influence the wave function or classical trajectory. For example, this leads to the divergence of the total cross section in the Rutherford scattering. In the Rydberg states, we gradually go to the classical limit of weak binding as for the Kepler orbits of remote planets in the solar system. This is also a reason for the *continuous* transition from the statistics of highly excited bound Rydberg states to the gas statistics in the continuum [11]. Because the

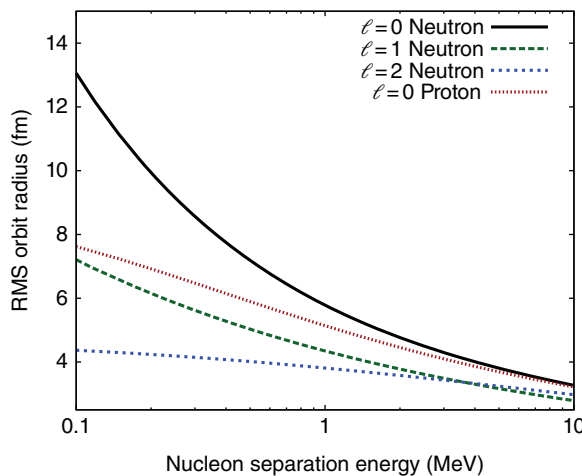


Figure 10.4 Root-mean-square radius of the outer nucleon orbit as a function of the binding energy (nucleon separation energy).

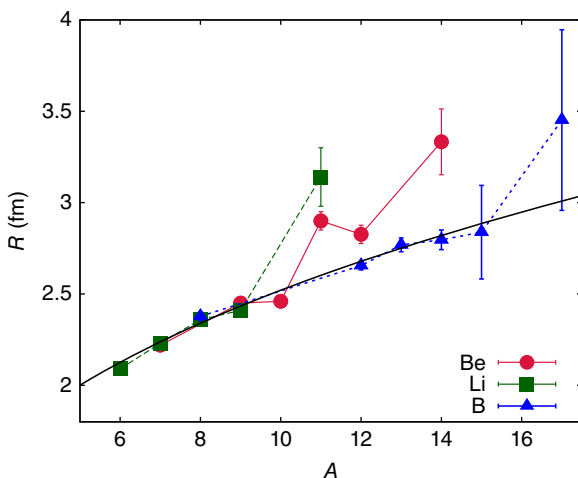
wave function at large distances falls off faster than the potential, this motion occurs in the *classically allowed* though remote region. The *short-range* character of nuclear forces makes the halo phenomenon with a significant probability to find a system far away in the *classically forbidden* region a distinct signature of quantum tunneling. To get similar effects with the Coulomb interaction, the latter should be *screened* transforming to the short-range Yukawa potential (see brief discussion in Section 3.4). The screening takes place in metals or plasmas with a considerable concentration of free charge carriers.

For protons or charged clusters, the Coulomb barrier makes the appearance of the long tail of the wave function much less probable. The centrifugal barrier plays a similar role. The radial wave function in this case vanishes at the origin and has only a small probability to penetrate the barrier. Therefore, it is effectively localized being *confined* to a narrow region inside the barrier. The higher the orbital momentum, the stronger the confinement of a particle that prevents the development of an appreciable halo. The centrifugal potential $\sim \ell(\ell + 1)/r^2$ acts in the same way as other long-range repulsive forces. The situation is illustrated by Figure 10.4, where the root-mean-square radius of the outer halo orbit is shown as a function of the separation energy. In this example, we use the Woods–Saxon potential with the parameters that would be appropriate for ^{11}Be ; the depth of the potential is varied in order to change the binding energy of the state. The increase in size of the weakly bound orbit is a generic phenomenon, the effect is the strongest for neutral particles in *s*-waves where it is related to the divergence of the scattering length and cross section.

10.3 Nuclear Halos

The investigated halo systems in nuclear physics appear in loosely bound nuclei near the so-called *drip lines*. As seen from the mass formula, if we move on the nuclide chart across the valley of beta-stability, the proton/neutron ratio changes becoming more and more energetically unfavorable. The valley of stability is roughly determined by the balance of symmetry energy, Coulomb energy, and neutron–proton mass difference (Section 5.1). Fine-tuning is added by the shell effects and pairing correlations.

Figure 10.5 The systematics of interaction radii for the chains of lithium, beryllium, and boron isotopes determined from the scattering cross sections as a function of mass number (see [12, 13] and references therein). The systematic behavior $R = r_0 A^{1/3}$ is shown with a solid line.



Isotopes with a proton/neutron ratio different from the most favorable, which are still stable with respect to strong interactions and have rather long lifetimes, return to the stability valley by the weak interaction processes changing $|N - Z|$ in the right direction (electron or positron beta-decay and orbital capture of atomic electrons). The drip lines correspond to large deviations from stability when the separation energy for a proton (proton drip line) or a neutron (neutron drip line) vanishes. Then the nucleus is getting unstable with respect to fast particle emission. As a precursor of the drip lines, loosely bound nuclei with low but still positive separation energy may display halo effects. In such cases, the long tails of the wave function become responsible for the observed halo phenomena.

For light nuclei, the halo phenomenon is illustrated by Figure 10.5 where interaction radii determined from the scattering cross sections are shown. When compared to the standard liquid drop systematics, ^{11}Li , ^{11}Be , ^{14}Be , and ^{17}B appear to be exceptionally large.

With extensively developing techniques of experiments using radioactive nuclear beams, this topic is one of the hot issues of nuclear physics. In principle, it becomes even possible to look for the structure and halo effect in *excited* nuclear states if their lifetime for beta-processes and radiation is not too short. The excited states, even in stable nuclei, could be very close to the threshold and reveal stronger halo effects if their wave function has a significant single particle or cluster component.

10.4 One-Body Halo

This is the case discussed earlier when the halo is created by a single nucleon. The terminology can be misleading because sometimes this situation is called “two-body halo” as the system decays into two-body channels after being gently excited. The significant component of the nucleon wave function should be an *s*-wave to make the appearance of the halo possible. The absence of the halo effect in the carbon isotopes ^{17}C and ^{19}C , where the separation energy of the last neutron is less than 1 MeV, is presumably due to the $d_{5/2}$ neutron orbit.

The best known case for the neutron halo is ^{11}Be that was mentioned as an anomalous example (parity inversion) in our glimpse of the shell model for light nuclei (Section 10.1). As we noticed, the residual interactions change the sequence of neutron levels in the mean-field potential. In one of the possible explanations, the ground state $1/2^+$ of ^{11}Be with the small separation energy 0.5 MeV has a complicated wave function as a superposition of states, including an intruder $1s_{1/2}$ orbit and a combination of the neutron on the $0d_{5/2}$ level, with the excited 2^+ state of the ^{10}Be core. The excited state $1/2^-$ in ^{11}Be is close to the “normal” shell-model $0p_{1/2}$ neutron state, which has even lower neutron binding energy of 0.18 MeV only.

The experimentally measured mean square radius of the ^{10}Be core is $\langle r^2 \rangle^{1/2} = 2.30 fm. Radii of the halo nuclei cannot be measured directly unless one manages to create a target consisting of this isotope. They are measured indirectly by the interaction of the beam of nuclei under study with nuclear targets in *inverse kinematics* [14]. It is possible to produce in nuclear reactions beta-radioactive nuclei with lifetimes as short as milliseconds, form their secondary beams, and look for their interactions with stable nuclear targets. The cross section for the interaction of the high-energy beam with a stable light target can be calculated in the *eikonal approximation* [QP, II, 7.12]. The enhancement of the interaction cross section, up to 20%, gives a distinct signal of the presence of the matter density outside the “normal” nuclear volume for given A . For heavy targets, the strong Coulomb field plays a major role leading to the excitation and breakup of a weakly bound halo nucleus. Figure 10.6 shows the density distribution for ^{11}Be assuming the last neutron in a $1s_{1/2}$ orbit of a realistic mean-field potential. The contributions of the core and of the halo are shown separately.$

The mean square radius of the halo subsystem (A_h nucleons) can be found if the radii of the total nucleus (A nucleons) and of the core ($A_c = A - A_h$ nucleons) are known.

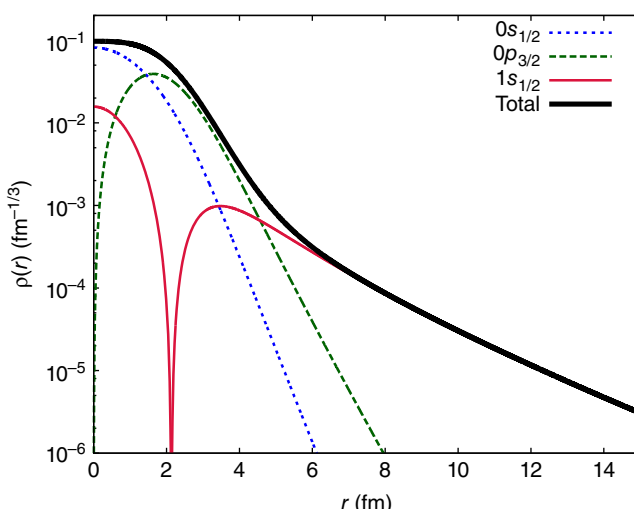


Figure 10.6 Neutron density distribution (solid black line) of ^{11}Be . Calculations use the Woods–Saxon potential adjusted to reproduce ^{11}Be with a $1s_{1/2}$ state bound only by 0.5 MeV. The contributions to the density from particles on different orbitals are shown highlighting the halo nature of the weakly bound state.

Let \mathbf{R}_c and \mathbf{R}_h refer to the center of mass of the core and of the halo, respectively. The center-of-mass radius, \mathbf{R} , of the total system and the radius of the halo relative to the core, \mathbf{r} , are defined as

$$\mathbf{R} = \frac{1}{A} (A_c \mathbf{R}_c + A_h \mathbf{R}_h), \quad \mathbf{r} = \mathbf{R}_h - \mathbf{R}_c, \quad (10.7)$$

or, inversely,

$$\mathbf{R}_c = \mathbf{R} - \frac{A_h}{A} \mathbf{r}, \quad \mathbf{R}_h = \mathbf{R} + \frac{A_c}{A} \mathbf{r}. \quad (10.8)$$

Setting the origin at the point of the total center of mass, as we did in the calculation of the deuteron magnetic moment in Section 3.6, we have

$$\mathbf{R}_c = -\frac{A_h}{A} \mathbf{r}, \quad \mathbf{R}_h = \frac{A_c}{A} \mathbf{r}. \quad (10.9)$$

For any particle a taken in the core, its mean square radius from the core center is $\langle (\mathbf{r}_a - \mathbf{R}_c)^2 \rangle$. If the core particles are considered to be uncorrelated with the halo position, the cross terms here vanish after averaging. The same procedure should be applied to particles of the halo. Then the mean square radius of the composite system is given by

$$\begin{aligned} A \langle r^2 \rangle_{\text{tot}} &= \sum_{a(\text{core})} \langle (\mathbf{r}_a - \mathbf{R}_c)^2 \rangle + \sum_{a(\text{halo})} \langle (\mathbf{r}_a - \mathbf{R}_h)^2 \rangle \\ &= A_c \langle r^2 \rangle_c + A_c \left(\frac{A_h}{A} \right)^2 \langle r^2 \rangle + A_h \left(\frac{A_c}{A} \right)^2 \langle r^2 \rangle + A_h \langle r^2 \rangle_h. \end{aligned} \quad (10.10)$$

Finally,

$$\langle r^2 \rangle_{\text{tot}} = \frac{A_c}{A} \langle r^2 \rangle_c + \frac{A_c A_h}{A^2} \langle r^2 \rangle + \frac{A_h}{A} \langle r^2 \rangle_h. \quad (10.11)$$

In the Woods–Saxon model used for Figure 10.6, the single-neutron halo in ^{11}Be has a radius $\langle r^2 \rangle^{1/2} = 7.17$ fm under assumption of $1s_{1/2}$ state being bound by 0.5 MeV. The size of the halo particle does not have much effect in this case, but we can still assume that the single neutron has an rms size $\langle r^2 \rangle_h^{1/2} = 0.6$ fm. Together with the earlier mentioned value $\langle r^2 \rangle_c^{1/2} = 2.30$ fm for the core ^{10}Be , Eq. (10.11) gives 3.01 fm for ^{11}Be to be compared with the experimental value of 2.90 ± 0.05 fm.

There are also other candidates to be studied in search for the one-body halos like $^{8}\Lambda\text{B}_3$. An exotic hypernucleus $^{3}_{\Lambda}\text{H}$, “hypertriton” or strange deuteron [15], is a bound state $p + n + \Lambda$ where Λ -hyperon is an analog of the neutron but with the specific intrinsic quantum number of *strangeness*. The separation energy of the Λ -particle is 0.13 ± 0.05 MeV.

10.5 Two-Body Halos

Here we refer to the systems with two nucleons in the halo. The most famous example is the heavy lithium isotope $^{11}_3\text{Li}_8$. The breakup threshold is only 0.31 MeV, and the decay proceeds into the three-body channel $n + n + ^9\text{Li}$. Apparently, the halo is produced by two outer neutrons above the ^9Li core. As the adjacent isotope $^{10}_3\text{Li}_7$ with the odd number of neutrons is particle-unstable, the stability of ^{11}Li is again due to the pair correlations

of external neutrons. The core nucleus has a typical for the $0p$ -shell nuclei mean square radius $\langle r^2 \rangle^{1/2} = 2.32 \pm 0.02$ fm, whereas the indirectly measured mean square radius of ^{11}Li is approximately 3.2 fm, in obvious contradiction to a normal trend of the smooth radius increase $\sim A^{1/3}$, see Figure 10.5.

When considered in the shell-model framework, the core nucleus ^9Li has its magnetic moment and electric quadrupole moment due to the third proton in the $0p_{3/2}$ -shell. The Schmidt value of the magnetic moment is 3.79 n.m. Experimental data for the magnetic moment are close to this value for both ^9Li and ^{11}Li being equal to 3.44 and 3.67 n.m., respectively. Estimating the electric quadrupole moment of ^9Li by the contribution of the valence proton with $j = 3/2$ and the above value of $\langle r^2 \rangle$, we would get $Q = -21.5$ mb. The magnitude and the negative sign of the single-proton quadrupole moment in the beginning of a shell were discussed in Section 9.4. Empirically the quadrupole moment is greater by absolute value, $Q(^9\text{Li}) = -27.4 \pm 1.0$ mb, and it has the close magnitude for the halo nucleus $Q(^{11}\text{Li}) = -31 \pm 5$ mb. Taking in Eq. (9.21) the empirical value of $\langle r^2 \rangle$ for ^{11}Li , we would get $Q = -41$ mb. We can conclude that ^9Li is a relatively rigid core that does not strongly change with two halo neutrons added.

The halo-like nature of ^{11}Li is indicated by the anomalous increase in the interaction cross sections of the lithium isotopes with a nuclear target. The sharp increase is characteristic for the total cross section that includes two neutron removal processes. The increase is not seen in *charge changing* channels influencing the core. This is interpreted as an evidence of a normal spatial size and rigidity of the core along with a big size of the wave functions of the outer neutrons.

Rich information can be obtained from the experiments on nuclear and Coulomb dissociation of halo nuclei on stable targets. If dissociation can be considered as a very fast process, the *sudden approximation* can be applied. In our case, this means that an instant perturbation breaks the loosely bound system exciting it to the continuum. But the wave function had no time to change and the fragments continue their way with the same momentum distribution as in the bound system before breakup. If this is correct, a measurement of this distribution gives the Fourier transform of the original bound state wave function. For large spatial extension, the uncertainty relation leads to an abnormally narrow momentum distribution of the fragments.

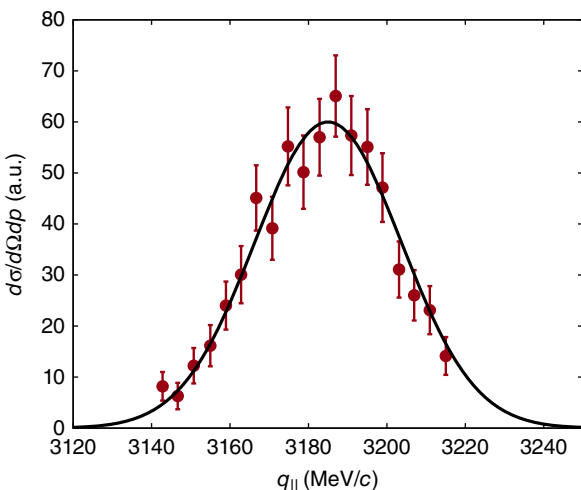
The single-particle wave function $\psi(r)$ of the s -wave halo neutron should have the form (10.6) outside the core region. If we assume that the core region does not contribute to the narrow part of the momentum distribution $w(q)$, the latter is given by a simple Fourier transform squared,

$$w(q) = \left| \int d^3r e^{-i(\mathbf{q} \cdot \mathbf{r})} \psi(\mathbf{r}) \right|^2 \propto \frac{1}{(q^2 + \kappa^2)^2}. \quad (10.12)$$

In many experiments, only the momentum distribution along a single axis is measured. This *longitudinal momentum distribution* is less sensitive to the recoil effects, which can distort the sudden wave function. Then we have to integrate the three-dimensional distribution, given in (10.12) as a function of $q^2 = q_{||}^2 + q_{\perp}^2$, over the two transverse components. This gives the so-called Breit–Wigner shape

$$w_l(q_{||}) = \int d^2q_{\perp} w(q) \propto \frac{1}{q_{||}^2 + \kappa^2} \quad (10.13)$$

Figure 10.7 Longitudinal momentum distribution of ${}^9\text{Li}$ in arbitrary units as obtained in ${}^{11}\text{Li}$ dissociation on the Ta target [16]. Solid line shows Gaussian fit with $\sigma = 18.7 \text{ MeV}/c$.



with the width (full width at half maximum, FWHM) $\Gamma = 2\kappa$ solely defined by the binding energy. For the separation energy $\sim 0.3 \text{ MeV}$ and the reduced mass $m = (10/11)M$, the width in the momentum units would be $\hbar\Gamma \approx 45 \text{ MeV}/c$.

Figure 10.7 shows the experimental data for the longitudinal distribution of the core nuclei ${}^9\text{Li}$ after the removal of two halo neutrons. Here the cross section is fit by the Gaussian,

$$w_l(q_{||}) = \text{const} \frac{1}{\sqrt{2\pi\sigma^2}} e^{-q_{||}^2/2\sigma^2}. \quad (10.14)$$

The Breit–Wigner and Gaussian shapes are quite similar in the central part, which is the one of primary interest here because anyway, as was mentioned earlier, the wings of the momentum distribution reflect non-halo properties. The width (FWHM) of the Gaussian distribution is $\Gamma = \sqrt{8 \ln 2} \sigma = 2.35 \sigma$. The experimental value of σ is translated into $\hbar\Gamma = 44 \text{ MeV}/c$ in perfect agreement with the estimate from the separation energy.

The most interesting unsolved questions are associated with the mechanism of the breakup, especially in the interaction with different targets, lifetime and nature of the final continuum state after the breakup, and the correlations between the two halo neutrons. The extreme model of the strongly correlated neutron pair (*dineutron*) seems to disagree with data. The single-neutron momentum distribution was measured to have a width of $\Gamma_1 \sim 26 \text{ MeV}/c$. For uncorrelated neutrons, the width of the distribution of the neutron pair would be the convolution of the single-neutron Gaussians. In such a convolution, the widths are added in quadratures which result in $\Gamma_2 = \sqrt{2} \Gamma_1 \simeq 37 \text{ MeV}/c$. This value is closer to what is observed for the recoil nucleus ${}^9\text{Li}$. The weakness or absence of neutron correlations raises the question of the nature of binding in ${}^{11}\text{Li}$, whereas ${}^{10}\text{Li}$ is unbound. Apparently, the wave function of the halo neutrons is a superposition of various configurations, where the neutrons are coupled with quantum numbers $J^\pi = 0^+$ of the pair but the pair is spread over few single-particle orbitals, mainly $1s$ and $0p$. Such a migrating pair reminds a Cooper pairing effect

that spreads the correlated pair wave functions over single-particle levels in superconductors (for electrons) and heavier nuclei (for nucleons). We discuss nuclear pairing correlations in detail later, Chapter 13.

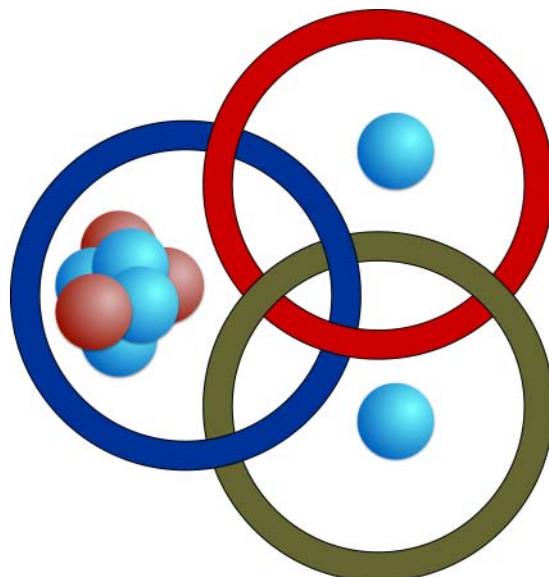
The two-neutron halos were observed also in ^{14}Be and ^{17}B . The considerable enhancement of the reaction cross section was discovered in $^{17}\text{Ne}_7$, where the two last nucleons, in this case protons, occupy the $1s_{1/2}$ orbit with the separation energy less than 1 MeV.

Referring to the rigid properties of the ^9Li core, one can use the *three-body model* ($^9\text{Li} + 2n$) of ^{11}Li . Neglecting the core excitations might be a reasonable starting approximation for near-threshold phenomena. In the three-body model, the nucleus ^{11}Li belongs to the family of the so-called *Borromean systems*. This means that the three-body system is bound although the possible two-body subsystems, ^{10}Li and dineutron, are unbound. The origin of the term (see the illustration in Figure 10.8) is explained in the following quotation:

The Borromean rings, the heraldic symbol of the Princes of Borromeo, are carved in the stone of their castle in Lake Maggiore in northern Italy. The three rings are interlocked in such a way that if any of them were removed, the other two would also fall apart.

Frequently the nucleus ^6He is also considered as a member of the same family being composed of $\alpha + n + n$. Again the jump of the mean square radius from 1.46 fm for ^4He (alpha-particle) to 2.5 fm in ^6He is quite remarkable (one should have in mind however that the alpha-particle is a very compact object). In both cases, ^{11}Li and ^6He , the daughter nucleus after one neutron removal, ^{10}Li and ^5He , respectively, is unstable with respect to the emission of the second neutron of the pair. In both cases, the neutrons form a pair with total angular momentum 0. The neutron pairing correlations can be at least one of the reasons of stability of the Borromean nuclei. However, ^6He apparently has no neutron halo. It does not manifest an enhancement of the scattering cross section.

Figure 10.8 Illustration of the Borromean character of ^{11}Li .



The neutron excess here probably forms what is called *neutron skin* with a normal density distribution of the valence neutron excess and no long halo tail. The nucleus ^9Be can also be called Borromean if treated as a bound state of two alpha-particles and the last neutron. As we already know, ^5He is unstable whereas ^8Be is a long-lived “molecular resonance” (but not a bound state) of two alpha-particles.

10.6 Efimov States

An interesting quantum phenomenon of appearance of bound states in a three-particle system that does not support any two-particle bound states was predicted by Efimov [17]. Here we discuss briefly the main physics of the phenomenon.

We mentioned in Section 3.4 that the three-dimensional Schrödinger equation for relative motion of a pair of particles interacting through an attractive potential might have no bound states if the potential is not strong enough. The Efimov states in a three-body system emerge if the pair forces in subsystems are close to their critical value. Let us consider the low-energy scattering when we can limit ourselves to the s -wave case. As we saw in Section 3.4, the critical strength of the pair potential is $U_{\text{cr}} \sim \text{const}(\hbar^2/mR^2)$, where m is a reduced mass of the pair and R is the range of interaction. This estimate follows from the uncertainty principle; the constant here is the number of the order of unity depending on the precise shape of the potential; for a square well it equals $\pi^2/8$. We are interested in the case when this constant is slightly less than its critical value. The conclusion of the existence of *three-body* bound states will be valid in the case of the overcritical value of the constant as well.

Proximity of the bound state (*virtual level* in the language of scattering theory, Section 4.5) leads to the resonance scattering in the two-body system. This was the case for the spin singlet s -wave $n-p$ scattering when the cross section was much higher than in the spin triplet state just due to the existence of the very close virtual level. The virtual level reveals itself in the large magnitude of the (negative) scattering length a (Section 4.3). The scattering length [QP, II, 8.7] is very sensitive to the properties of the potential in the near-critical situation. It goes to $-\infty$, when the virtual level becomes real, and then jumps to $+\infty$ (Figure 4.4).

Near the critical point for both virtual and real levels, the low-energy s -wave cross section $4\pi a^2$, Eq. (4.53), is very large. One can say that the particles effectively interact at distances $\sim |a|$, which are much greater than the range R of the potential. At the critical point, this length represents a huge size of the loosely bound state, which is a manifestation of the halo.

The physical mechanism leading to the formation of Efimov states in a three-body system is related to the large range of interaction in two-body subsystems. The resonance in the two-body scattering corresponds to a long lifetime of an intermediate two-body cluster even if it is unbound. After it decays, the released fragment can be picked up by the third particle. This repeating exchange keeps all particles together similar to the mechanism of molecular binding by the collectivized electrons.

A primitive prototype of the effect is a system of two fixed centers each of them being incapable of binding the third particle. For low energies, $kR \ll 1$, where R is the short force range between each center and the particle, we can look for the s -wave only. As we discussed for the deuteron (Section 4.3), the logarithmic derivative λ of the

internal wave function taken at the potential boundary should be negative, $\lambda = -\kappa$, Eq. (3.45), to ensure the existence of the bound state with the asymptotics (10.6). Let λ be positive. Now we put an identical center at a large distance d from the first one, $d \gg R$. Outside of both potential regions, the bound state wave function of the particle would be a combination of two s -waves decaying as in (10.6),

$$\psi(\mathbf{r}) = \frac{\exp[-\kappa|\mathbf{r} - \mathbf{r}_1|]}{|\mathbf{r} - \mathbf{r}_1|} + \frac{\exp[-\kappa|\mathbf{r} - \mathbf{r}_2|]}{|\mathbf{r} - \mathbf{r}_2|} \quad (10.15)$$

where \mathbf{r}_1 and \mathbf{r}_2 are the coordinates of the centers, $|\mathbf{r}_1 - \mathbf{r}_2| = d$. Near the first center (but still outside the potential range which is possible if $d \gg R$) we can expand the first exponent and put $\mathbf{r} = \mathbf{r}_1$ in the second term to get

$$\psi(\mathbf{r}) \approx \frac{1}{|\mathbf{r} - \mathbf{r}_1|} - \kappa + \frac{e^{-\kappa d}}{d}. \quad (10.16)$$

We see that in the region around the first center, we have effectively the s -wave solution where the radial function $u = r\psi$ is presented in a linear form analogous to what we have used for the definition of the scattering length in Section 4.3. The role of the second center is reduced to the effective change of the logarithmic derivative of the external function. Instead of the matching condition $\lambda = -\kappa$ as in the one-center problem, we have now

$$\lambda = \frac{e^{-\kappa d}}{d} - \kappa. \quad (10.17)$$

The first term in the right-hand side of (10.17) is just the “Yukawa term” corresponding to the exchange between the centers by the object with the “mass” $\kappa c/\hbar$ (see Section 1.2 and Eq. (3.3)). The equation for κ , that is, for the binding energy, can be easily solved graphically (Figure 10.9). The solution exists even for positive λ if the distance between the centers is not too large, $d < 1/\lambda$. Two centers support each other in organizing the common three-body bound state.

Efimov’s analysis is much more general (no fixed centers, three particles come on equal footing) but requires some properties of the three-body problem, which we do not discuss here. We limit ourselves to the qualitative explanation. The size of the system is characterized by the global radial variable r that, for identical particles, is defined as $r^2 = r_{12}^2 + r_{23}^2 + r_{31}^2$. In the case of different particles, the definition contains the mass

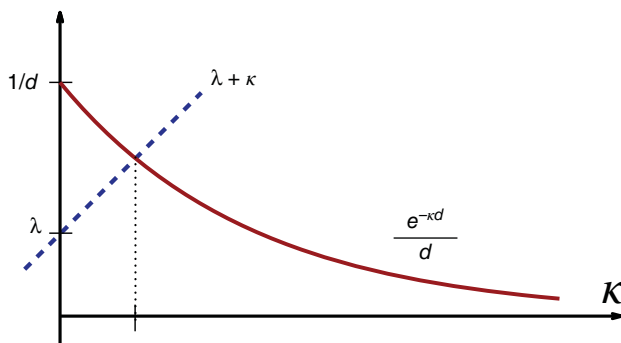


Figure 10.9 The solution of Eq. (10.17).

ratios. There are two typical scales in the problem, short-range R , radius of the potential, and long-range a , scattering length ($|a|$ if the scattering length is negative). It is assumed that the resonances, or loosely bound states, exist in the two-body subsystems so that the interaction range is determined by $a \gg R$.

In the interval between R and a , the attraction appears due to the same exchange mechanism. Independent of details of potentials at $r \leq R$, the attraction is *universal*. In this intermediate region, both edges, R and a , are remote so that one can consider them as displaced to 0 and ∞ , respectively. Then the exchange attraction as a function of r is proportional to \hbar^2/mr^2 as this is the only available quantity with the dimension of energy; m is the analog of the reduced mass. This estimate follows also from the uncertainty relation for the particle localized between these distances similar to what we have discussed in the beginning of this section. The attraction stretches from the inner boundary $r = R$ to the outer boundary $r = a$ (Figure 10.10).

The potential $\sim 1/r^2$ gives rise to bound states. We can use semiclassical phase space arguments to estimate the number of discrete states in a given potential,

$$\mathcal{N}_{\text{discr}} \propto \int \frac{d^3 p d^3 r}{(2\pi\hbar)^3} \propto \frac{m^{3/2}}{\pi^2 \hbar^3} \int d^3 r \left(\frac{\hbar^2}{mr^2} \right)^{3/2} \propto \frac{1}{\pi} \ln \left(\frac{|a|}{R} \right), \quad (10.18)$$

where the classical phase space volume integral is restricted by the requirement that for bound states the energy $\epsilon = p^2/2m - \hbar^2/mr^2 \leq 0$. The logarithmically diverging integral is taken between the natural limits R and $|a|$. A more exact analysis gives the same result (10.18) and determines the proportionality factor equal to 1. It means that one bound state will exist if $a \approx e^\pi R \approx 20R$. The known nuclear halo states do not satisfy such a hard criterion. But the search continues. Near the drip lines, one can encounter extremely loosely bound nuclei that can be an embodiment of this effect. For other ideas, the reader is referred to the article [18]. Similar effects are expected in other systems [19], including neutron matter in stars since the low-energy neutron interaction is close to the *unitary limit* when the scattering length is very big because of the proximity of threshold for the formation of a bound state. Recently, the Efimov states were discovered experimentally in atomic physics [20–22]. In scattering involving complex atoms with internal degrees of freedom, one can technically adjust the scattering length,

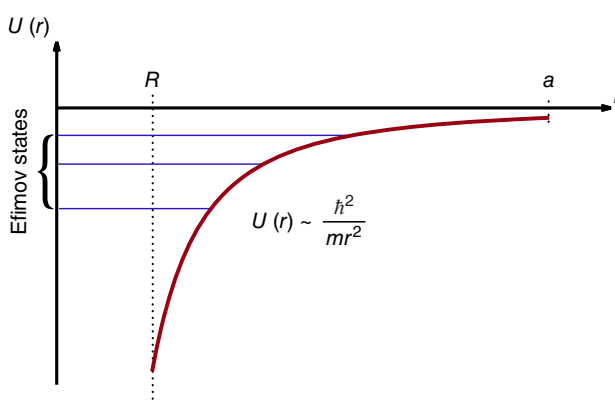


Figure 10.10 Effective three-body long-range interaction, according to Ref. [18].

including the change of its sign, with the help of a magnetic field, the so-called *Feshbach resonance*.

References

- 1 J.A. Wheeler, Phys. Rev. **52**, 1083 (1937).
- 2 W. von Oertzen, in *Nuclei Far from Stability and Astrophysics*, eds. D.N. Poenaru, H. Rebel, and J. Wentz, Springer-Verlag, Dordrecht, 2001.
- 3 F. Hoyle, *A Life in Science*, Cambridge University Press, Cambridge, 2011.
- 4 E. Epelbaum, H. Krebs, T. Laehde, D. Lee, and U.-G. Meissner, Phys. Rev. Lett. **109**, 252501 (2012).
- 5 M. Gai *et al.*, J. Phys. Conf. Ser. **436**, 012007 (2013).
- 6 D.A. Ostlie and B.W. Carroll, *An Introduction to Modern Stellar Astrophysics*, Addison Wesley, San Francisco, CA, 2007.
- 7 A. Bohr and B.R. Mottelson, *Nuclear Structure*, Vol. **1**, Benjamin, New York, 1969.
- 8 G. Faure and D. Mensing, *Isotopes - Principles and Applications*, 3rd edn, John Wiley & Sons, Hoboken, NJ, 2005.
- 9 V.F. Dmitriev, D.M. Nikolenko, S.G. Popov, I.A. Racheck, D.K. Toporkov, E.P. Tsentalovich, B.B. Wojtsekhowski, and V.G. Zelevinsky, Nucl. Phys. **A464**, 237 (1987).
- 10 R. Grisenti, W. Schoellkopf, J. Toennies, G. Hegerfeldt, T. Koehler, and M. Stoll, Phys. Rev. Lett. **85**, 2284 (2000).
- 11 S.T. Belyaev, in *Plasma Physics and Problem of Controllable Thermonuclear Reactions*, Proceedings of Geneva Conference, Moscow, 1958, Vol. **3**, p. 66.
- 12 I. Tanihata, J. Phys. G: Nucl. Part. Phys. **22**, 157 (1996).
- 13 I. Tanihata *et al.*, Prog. Part. Nucl. Phys. **68**, 215 (2013).
- 14 W. Mittig and P. Roussel-Chomaz, Nucl. Phys. **A693**, 495 (2001).
- 15 A. Cobis, A.S. Jensen, and D.V. Fedorov, J. Phys. G **23**, 401 (1997).
- 16 N.A. Orr *et al.*, Phys. Rev. Lett. **69**, 2050 (1992).
- 17 V. Efimov, Phys. Lett. B **33**, 563 (1970).
- 18 V. Efimov, Nat. Phys. **5**, 533 (2009).
- 19 H.-W. Hammer and L. Platter, Annu. Rev. Nucl. Part. Sci. **60**, 207 (2010).
- 20 T. Kraemer *et al.*, Nature **440**, 315 (2006).
- 21 M. Zaccanti *et al.*, Nat. Phys. **5**, 586 (2009).
- 22 S.-K. Tung, K. Jimenez-Garcia, J. Johansen, C.V. Parker, and C. Chin, Phys. Rev. Lett. **113**, 240402 (2014).

11

Many-Body Operator Formalism

... the general mathematical setting should be presented in a self-contained manner to enable the reader to gain fluency in the language without having to learn its vocabulary and grammar from a variety of other sources.

G.G. Emch, Algebraic Methods in Statistical Mechanics
and Quantum Field Theory

11.1 Secondary Quantization

Evidently, the independent particle shell model is not sufficient for realistic description of complex nuclei. It accounts only for average view of nuclear dynamics leaving aside *correlations* between the particles. The correlations, or *residual interactions*, contain effects of the Pauli principle, Section 7.4, and dynamic processes – incoherent nature. An appropriate formalism for the description of various features of many-body dynamics is provided by the *secondary quantization*. We have already used the quantized operators for collective modes assuming their boson character in analogy with the harmonic oscillator. However, the underlying nuclear interactions are those of fermions, and the boson description of collective excitations can only be approximate.

The secondary quantization deals with systems and states of a variable particle number, introducing operators that create and annihilate particles. For fermions, the formalism has to guarantee the *antisymmetry* of wave functions in accordance with the requirements of the statistics and, at the same time, allow one to consider the processes with a variable particle number. We review here some most relevant to our discussion topics, additional details can be found in [QP, II, 17].

The starting point is the *occupation number representation*. Let $|\lambda\rangle$ be an arbitrary complete set of *single-particle* states with certain quantum numbers such as (\mathbf{p}, σ) used for the Fermi gas in free space. At this stage, we do not need to specify a Hamiltonian governing the dynamics. We use only the completeness of the set $|\lambda\rangle$ and assume that the states $|\lambda\rangle$ are orthonormal,

$$\langle \lambda | \lambda' \rangle = \delta_{\lambda\lambda'}, \quad (11.1)$$

although this restriction can also be lifted because it is possible to work with nonorthogonal sets as well (see Problem 11.4). The Kronecker symbol in (11.1), as usual, has to be

understood as the Dirac δ -function for continuous quantum numbers λ . Of course, in practice, some sets $|\lambda\rangle$ can be more convenient than others. Sometimes, the states $|\lambda\rangle$ can be called orbits or *orbitals*, as we have already done in the past.

Now we can construct *many-body* states

$$|\{n_\lambda\}\rangle = |n_1, n_2, \dots, n_\lambda, \dots\rangle \quad (11.2)$$

by introducing the sets of integers n_λ , which show how many particles are put into each orbit $|\lambda\rangle$. We assume that the orbits $|\lambda\rangle$ are ordered in some (arbitrary) way, and they always appear in this order in the specification of the many-body state of Eq. (11.2). In order to distinguish between the single-particle and many-body states, we use the parentheses in the definition of the former and the angular brackets for the latter. It is also often convenient to use instead of λ arabic numerals 1, 2, ..., where the number combines all single-particle quantum numbers of an orbital.

The numbers n_λ are *occupation numbers* in a given basis $|\lambda\rangle$. According to the type of the statistics, they could be only 0 and 1 for Fermi statistics and any nonnegative integers for Bose statistics. We see later that the formalism ensures this requirement automatically. We include in the consideration all states with different total particle numbers fixed by the condition

$$\sum_\lambda n_\lambda = A. \quad (11.3)$$

With the occupation numbers chosen in conformity with the type of statistics, the set of many-body states (11.2) is complete in Fock space, the extension of quantum-mechanical Hilbert space for problems with variable particle numbers. Due to identity of particles, we do not need to indicate which particle occupies the orbit $|1\rangle$, which one occupies the orbit $|2\rangle$, and so on. As soon as all properties of single-particle orbits are known, the occupation number representation contains *full information*. The only variables in this representation are the integer occupation numbers n_λ , and the quantum operators have to be defined as acting on these “coordinates.” Any many-body state can be expanded over the complete set (11.2). The *expectation values* of the occupation numbers in a general superposition will be *fractional*, between 0 and 1 for fermions and arbitrary nonnegative numbers for bosons. An arbitrary unitary transformation of the basis (11.1) is always possible leading in general to fractional occupation numbers in the new basis. Interaction processes transmit particles between orbitals. Then the many-body states $|\{n_\lambda\}\rangle$ are not stationary in an interacting system, but still this basis is complete and accounts properly for the permutational symmetry.

The elementary actions in Fock space are produced by *creation*, a_λ^\dagger , and *annihilation*, a_λ , operators, that create and annihilate the particle in the state $|\lambda\rangle$ from the vacuum state $|0\rangle$, namely $|\lambda\rangle = a_\lambda^\dagger|0\rangle$ and $|0\rangle = a_\lambda|\lambda\rangle$. The vacuum state $|0\rangle$ of Fock space does not contain particles at all, so that

$$a_\lambda|0\rangle = 0 \quad \text{for all } \lambda. \quad (11.4)$$

From here, it follows that under basis transformation

$$|\lambda\rangle \rightarrow |\nu\rangle = \sum_\lambda |\lambda\rangle (\lambda|\nu), \quad (11.5)$$

where $(\lambda|\nu) = (\nu|\lambda)^*$ are transformation coefficients, the creation operators are transformed in the same way as states in Eq. (11.5),

$$a_\nu^\dagger = \sum_\lambda (\lambda|\nu) a_\lambda^\dagger. \quad (11.6)$$

The annihilation operators are transformed according to the conjugate equations,

$$a_\nu = \sum_\lambda (\nu|\lambda) a_\lambda. \quad (11.7)$$

For states with more than one particle, we should introduce additional rules related to permutational symmetry. Using the *anticommutators* for fermions, $[\dots, \dots]_+$, instead of the commutators, $[\dots, \dots]_-$, for bosons, we write down the main algebraic relations as

$$[a_\lambda, a_{\lambda'}]_+ = [a_\lambda^\dagger, a_{\lambda'}^\dagger]_+ = 0, \quad [a_\lambda, a_{\lambda'}^\dagger]_+ = \delta_{\lambda\lambda'}. \quad (11.8)$$

As earlier, in the case of single-particle variables with continuous spectrum, the δ -symbols in all commutation relations are to be substituted by the δ -functions. The first two equalities of (11.8) give for $\lambda = \lambda'$

$$a_\lambda^\dagger a_\lambda^\dagger = 0, \quad a_\lambda a_\lambda = 0. \quad (11.9)$$

This ensures the *Pauli principle*: it is forbidden for two identical fermions to populate the same orbit. One can verify, see also [QP, II, 17], that commutation or anticommutation relations (11.8) are preserved under unitary transformations of basis (11.6) and (11.7).

The occupation *number operators* are defined in the same way for bosons and fermions; for fermions, using the last anticommutator in (11.8), we obtain

$$N_\lambda = a_\lambda^\dagger a_\lambda, \quad 1 - N_\lambda = a_\lambda a_\lambda^\dagger. \quad (11.10)$$

Simple algebra then leads to

$$N_\lambda^2 = a_\lambda^\dagger a_\lambda a_\lambda a_\lambda^\dagger = a_\lambda^\dagger (1 - a_\lambda^\dagger a_\lambda) a_\lambda, \quad (11.11)$$

or, using (11.9),

$$N_\lambda^2 = N_\lambda. \quad (11.12)$$

Hence, the eigenvalues of an occupation number operator are 0 and 1 as it should be for Fermi statistics.

The basis of the many-body system (11.2) of A fermions can be constructed as a simple product of the creation operators a_λ^\dagger for all occupied orbits,

$$|\Phi\rangle = \prod_{\lambda(n_\lambda=1)} a_\lambda^\dagger |0\rangle. \quad (11.13)$$

Any permutation of the creation operators changes the common sign of the state vector due to the anticommutativity (11.8), so that the wave function reveals correct permutational symmetry. It is antisymmetrized and fully corresponds to a *Slater determinant* in a “primary quantization.” All operators can be represented as consisting of the simplest blocks, such as $a_\lambda, a_\lambda^\dagger$, or $a_\lambda^\dagger a_{\lambda'}$ (annihilation, creation, or transfer of a particle).

One subtle thing should be mentioned. We said in defining the many-body states (11.2) that the set of single-particle orbits $|\lambda\rangle$ has to be ordered in some way. This is of no importance for the Bose case because of symmetry of the operators. But in the antisymmetric Fermi case, it involves more complicated matrix elements of the creation and annihilation operators. It is easy to understand by simple examples that the matrix elements should be taken as

$$\begin{aligned} a_\lambda |\dots, n_\lambda, \dots\rangle &= (-)^{\varphi_\lambda} \sqrt{n_\lambda} |\dots, n_\lambda - 1, \dots\rangle, \\ a_\lambda^\dagger |\dots, n_\lambda, \dots\rangle &= (-)^{\varphi_\lambda} \sqrt{1 - n_\lambda} |\dots, n_\lambda + 1, \dots\rangle, \end{aligned} \quad (11.14)$$

where the square roots express the Pauli principle limitations, and the phase

$$\varphi_\lambda = \sum_{\lambda' < \lambda} n_{\lambda'} \quad (11.15)$$

is determined by a number of transpositions that are necessary for bringing the external operator a_λ or a_λ^\dagger into its natural place in the pre-ordered sequence of orbits.

Problem 11.1 Show that the expectation values of fermion occupancies, $\langle N_1 \rangle = \langle a_1^\dagger a_1 \rangle$, in state (11.2) built using arbitrary single-particle basis $|\lambda\rangle$, are between 0 and 1.

Solution

Let the occupation numbers n_λ in the orthonormal reference basis $|\lambda\rangle$ be 0 or 1. The basis $|1\rangle$ is the result of a unitary transformation when a single-particle state is transformed as

$$|1\rangle = \sum_\lambda |\lambda\rangle (\lambda|1), \quad \sum_\lambda (1|\lambda)(\lambda|2) = \delta_{12}. \quad (11.16)$$

The mean occupation numbers are

$$\langle N_1 \rangle = \langle a_1^\dagger a_1 \rangle = \sum_{\lambda \lambda'} (\lambda|1)(1|\lambda') \langle a_\lambda^\dagger a_{\lambda'} \rangle, \quad (11.17)$$

here we used transformations (11.6) and (11.7). By initial assumption, the many-body state used here for averaging has certain occupation numbers n_λ equal to 0 or 1. If $n_{\lambda'} = 0$, the corresponding term in (11.17) vanishes. If $n_{\lambda'} = 1$, the mean value in (11.17) does not vanish only when the creation operator a_λ^\dagger restores the particle removed by the operator $a_{\lambda'}$. This means that the matrix element here $\langle a_\lambda^\dagger a_{\lambda'} \rangle = n_\lambda \delta_{\lambda \lambda'}$. Then

$$\langle N_1 \rangle = \sum_\lambda |(\lambda|1)|^2 n_\lambda \leq \sum_\lambda |(\lambda|1)|^2 = 1. \quad (11.18)$$

The operator N_1 is nonnegatively defined; therefore, its expectation value in any state is nonnegative. However, in basis other than $|1\rangle$, this operator is generally not diagonal, $\langle \{n'_\lambda\} | a_1^\dagger a_1 | \{n_\lambda\} \rangle \neq 0$.

Problem 11.2 Prove that the expectation value of the total particle number (11.3) is the same in all single-particle bases.

Problem 11.3 Prove algebraic identities [some of them are valid for both types of statistics; in others the upper (lower) sign refers to bosons (fermions)]:

$$[a_1, a_2^\dagger a_3] = \delta_{12} a_3, \quad [a_1^\dagger, a_2^\dagger a_3] = -\delta_{13} a_2^\dagger, \quad (11.19)$$

$$[a_1, a_2^\dagger a_3^\dagger] = \delta_{12} a_3^\dagger \pm \delta_{13} a_2^\dagger, \quad (11.20)$$

$$[a_1^\dagger a_2, a_3^\dagger a_4] = \delta_{23} a_1^\dagger a_4 - \delta_{14} a_3^\dagger a_2, \quad (11.21)$$

$$[a_1 a_2, a_3^\dagger a_4^\dagger] = \delta_{23} \delta_{14} \pm \delta_{24} \delta_{13} + \delta_{24} a_3^\dagger a_1 + \delta_{13} a_4^\dagger a_2 \pm \delta_{23} a_4^\dagger a_1 \pm \delta_{14} a_3^\dagger a_2. \quad (11.22)$$

Here we use the digital notations, 1, 2, ... for the orbits in the orthogonal basis, and in all cases we compute commutators rather than anticommutators.

To calculate matrix elements of the operators between the many-body states (11.13), it is enough to be able to calculate the vacuum expectation values. They do not vanish only if numbers of creation and annihilation operators are equal. Due to the vacuum condition (11.4), vacuum expectation values are equal to zero if the operators are put into the *normal form* with all creation operators *on the left* from all annihilation operators. For an arbitrary sequence of operators in the original matrix element, one should bring them into the normal form by permutations. The result consists only of δ -symbols produced in this process. For example,

$$\langle 0 | a_1 a_2^\dagger | 0 \rangle = \delta_{12}, \quad (11.23)$$

$$\langle 0 | a_1 a_2 a_3^\dagger a_4^\dagger | 0 \rangle = \langle 0 | \overbrace{a_1 a_2}^{\square} \overbrace{a_3^\dagger a_4^\dagger}^{\square} | 0 \rangle + \langle 0 | \overbrace{a_1 a_2}^{\square} \overbrace{a_3^\dagger}^{\square} a_4^\dagger | 0 \rangle = \delta_{23} \delta_{14} \pm \delta_{24} \delta_{13}. \quad (11.24)$$

This equation also demonstrates the recipe for obtaining an arbitrary vacuum expectation value. One needs to form all *pairwise contractions* $a_1^\dagger a_2^\dagger$ (in this order!) possible for the initial operator, write δ_{12} for each pair and take a sum of the contributions from all such contractions. The final sign of each contribution is + for bosons, whereas for fermions it is determined by parity of the permutations that bring the partners of a given contraction near to each other.

It is easy to see that the state (11.13) does not require any normalization factor in contrast to the Slater determinant in the coordinate or momentum representation. Indeed, the inner product $\langle \Phi | \Phi \rangle$ includes the creation operators (11.13) in the ket-vector and the sequence of the Hermitian conjugate annihilation operators taken in the opposite order in the bra-vector. Therefore, the scalar product reduces to the product of all occupation numbers n_1 over occupied orbitals,

$$\langle \Phi | \Phi \rangle = \prod_{1;\text{occ}} n_1 = 1. \quad (11.25)$$

The states $|\Phi\rangle$ and $|\Phi'\rangle$ that differ in the occupancy of at least one orbital are automatically orthogonal. When the occupied orbitals are the same but their ordering may differ, the result can be ± 1 . For example, for two particles, the product of two arbitrary states (11.13), one of which, $|\Phi_{12}\rangle$, has orbits $|1\rangle$ and $|2\rangle$ occupied, while in the second one, $|\Phi_{34}\rangle$, the occupied orbitals are $|3\rangle$ and $|4\rangle$, is given by Eq. (11.24) with the sign minus between the two terms. This can be written as a determinant

$$\langle \Phi_{12} | \Phi_{34} \rangle = \begin{vmatrix} \delta_{14} & \delta_{13} \\ \delta_{24} & \delta_{23} \end{vmatrix}. \quad (11.26)$$

Such a determinant can be directly generalized for $A > 2$ particles.

Problem 11.4 Consider a normalized but *nonorthogonal* single-particle basis $|1\rangle$, so that $\langle 1|2\rangle = \Theta_{12}$ and $\Theta_{11} = 1$. Let $|\Phi\rangle$ be a many-fermion state, where A particles are distributed over A nonorthogonal orbitals $|1\rangle$. Find the analogs of the commutation relations (11.8) for the fermion operators a_1 and a_2^\dagger . Construct the normalized wave function of this many-body state in the secondary quantized form.

Solution

The new commutation relations are

$$[a_1, a_2]_+ = [a_1^\dagger, a_2^\dagger]_+ = 0, \quad [a_1, a_2^\dagger]_+ = \Theta_{12}. \quad (11.27)$$

The states are built by A creation operators acting on the vacuum as in (11.13). But the scalar product, instead of (11.26), is given by the determinant built of the overlap factors, for example, for two particles,

$$\langle \Phi_{12} | \Phi_{34} \rangle = \begin{vmatrix} \Theta_{14} & \Theta_{13} \\ \Theta_{24} & \Theta_{23} \end{vmatrix}. \quad (11.28)$$

11.2 Physical Observables: One-Body Operators

To apply the developed formalism to physical problems, we need to express all operators in the form of secondary quantization. Consider first an operator Q of the one-body type that is given by the sum of the contributions q_a of all identical particles. We can take the complete set $|q\rangle$ of eigenstates of the single-particle operator \hat{q} ,

$$\hat{q}|q\rangle = q|q\rangle, \quad (11.29)$$

as a new single-particle basis. In this basis, the secondary quantized form of the many-body operator Q is obvious: it is given by a sum over all orbits $|q\rangle$ of contributions equal to an eigenvalue q for a given orbit multiplied by an occupation number n_q . This is an eigenvalue of the operator

$$Q = \sum_q q N_q = \sum_q q a_q^\dagger a_q. \quad (11.30)$$

Now we use the transformation of the single-particle basis to find the form of Q for the arbitrary choice of the basis $|\lambda\rangle$,

$$Q = \sum_{q\lambda\lambda'} q(\lambda|q)a_\lambda^\dagger(q|\lambda')a_{\lambda'} = \sum_{\lambda\lambda'} \left(\sum_q (\lambda|q)q(q|\lambda') \right) a_\lambda^\dagger a_{\lambda'}. \quad (11.31)$$

Since the sum in (11.31) is equal to the matrix element of the operator q ,

$$\sum_q (\lambda|q)q(q|\lambda') = (\lambda|q|\lambda'), \quad (11.32)$$

we come to the general expression for any one-body operator in the form invariant under basis transformations,

$$Q = \sum_{12} (1|q|2)a_1^\dagger a_2. \quad (11.33)$$

Such an operator is presented by a sum of diagonal terms and terms transferring a single particle from one orbit to another; the transition amplitudes $|2\rangle \rightarrow |1\rangle$ are equal to the single-particle matrix elements $\langle 1|q|2\rangle$.

An important example is given by the *density operators*

$$\hat{\rho}(q) = \sum_a \delta(q - \hat{q}_a), \quad (11.34)$$

where the sum runs over the particles a . The density operator defines the probability amplitude to get a value q for a single-particle variable \hat{q}_a in a system of identical particles. In the particular case $q \rightarrow \mathbf{r}$, this is the usual spatial density which appears in the continuity equation; for example, the electric charge density should be written as $\rho_e(\mathbf{r}) = \sum_a e_a \delta(\mathbf{r} - \mathbf{r}_a)$. By its meaning, the operator (11.34) coincides with N_q used in (11.30). The secondary quantized form of the density operator is therefore trivial in the eigenbasis $|q\rangle$ of the operator \hat{q} but more complicated in an arbitrary basis,

$$\hat{\rho}(q) = N_q = a_q^\dagger a_q = \sum_{\lambda\lambda'} (q|\lambda)^*(q|\lambda') a_\lambda^\dagger a_{\lambda'}. \quad (11.35)$$

Frequently, one has to deal with coordinate and momentum representations, where the corresponding creation operators are a_r^\dagger and a_p^\dagger ; the spin and isospin characteristics can be added to \mathbf{r} and \mathbf{p} if needed. (In the coordinate representation, the notations $\psi^\dagger(\mathbf{r})$ and $\psi(\mathbf{r})$ instead of a_r^\dagger and a_r are also often used.) If the coordinate plane waves are normalized in the finite volume V , the relation between the representations is given by

$$a_r^\dagger = \frac{1}{\sqrt{V}} \sum_{\mathbf{p}} e^{(i/\hbar)(\mathbf{p}\cdot\mathbf{r})} a_{\mathbf{p}}^\dagger, \quad a_{\mathbf{p}}^\dagger = \int d^3 r e^{-(i/\hbar)(\mathbf{p}\cdot\mathbf{r})} a_r^\dagger. \quad (11.36)$$

Thus, the spatial density operator is

$$\hat{\rho}(\mathbf{r}) \equiv N_r = a_r^\dagger a_r = \frac{1}{V} \sum_{\mathbf{p}\mathbf{p}'} e^{(i/\hbar)(\mathbf{p}'-\mathbf{p})\cdot\mathbf{r}} a_{\mathbf{p}}^\dagger a_{\mathbf{p}'}^\dagger. \quad (11.37)$$

The operator diagonal in the coordinate representation is highly off-diagonal in the momentum representation.

11.3 Two-Body Operators

Consider now an operator depending on the variables of *pairs* of identical particles. The most important example is the two-body interaction Hamiltonian. The generic structure of a two-body operator is

$$F = \sum_{a\neq b} f_{ab}. \quad (11.38)$$

In secondary quantization, it takes an invariant form

$$F = \sum_{1234} (12|f|34) a_1^\dagger a_2^\dagger a_4 a_3 \quad (11.39)$$

with the transparent physical meaning of encoding all pair transitions $(3,4) \rightarrow (1,2)$ characterized by the amplitudes f . For two fermions, $(12|f|34)$ is the matrix element between normalized pair states $|34\rangle = a_3^\dagger a_4^\dagger |0\rangle$ and $|12\rangle = a_1^\dagger a_2^\dagger |0\rangle$. Note the ordering of

the subscripts: pair state is annihilated in a reversed order. To see how the expression (11.39) emerges, assume that f_{ab} depends on variables q_a and q_b of interacting particles $f_{ab} = f(q_a, q_b)$. Then we can rewrite (11.38) including the self-action term $a = b$ as a function of the corresponding operators,

$$\begin{aligned} F &= \sum_{ab} f(\hat{q}_a, \hat{q}_b) - \sum_a f(\hat{q}_a, \hat{q}_a) \\ &= \int dq dq' f(q, q') \left\{ \sum_{ab} \delta(\hat{q}_a - q) \delta(\hat{q}_b - q') - \delta(q - q') \sum_a \delta(\hat{q}_a - q) \right\}. \end{aligned} \quad (11.40)$$

Introducing the density operator (11.34), (11.35) for a variable q , this is transformed to

$$F = \int dq dq' f(q, q') \{N_q N_{q'} - \delta(q - q') N_q\}. \quad (11.41)$$

The operator in curly brackets in Eq. (11.41) is, by virtue of the commutation relations,

$$a_q^\dagger a_q a_{q'}^\dagger a_{q'} - \delta(q - q') a_q^\dagger a_q = \pm a_q^\dagger a_{q'}^\dagger a_q a_{q'}. \quad (11.42)$$

The transposition of the last two operators makes the common sign plus so that the operator (11.41) takes a form

$$F = \int dq dq' f(q, q') a_q^\dagger a_{q'}^\dagger a_{q'} a_q. \quad (11.43)$$

The transformation to an arbitrary basis gives Eq. (11.39), where the coefficients $(12|f|34)$ are the matrix elements of the two-body operator f for the transition $(3,4) \rightarrow (1,2)$,

$$(12|f|34) = \int dq dq' \psi_1^*(q) \psi_2^*(q') f(q, q') \psi_4(q') \psi_3(q). \quad (11.44)$$

Here $\psi_1(q) = (q|1)$ are the transformation functions of the basis, that is, the wave functions of the states $|1\rangle$ in the q -representation. Note again the order of the arguments in the integrand (11.44) and its relation to Eq. (11.39).

11.4 Interparticle Interaction

The two-body operators mainly appear in the consideration of interaction between the particles. In a system of not very high density, the most important interactions occur pairwise so that here we limit ourselves by this case. If the many-body interactions are needed, the treatment can be extended in a straightforward manner.

If the interaction of particles a and b can be described by an operator U_{ab} , the total interaction Hamiltonian in a system of many particles is, according to Eq. (11.38),

$$H' = \frac{1}{2} \sum_{a \neq b} U_{ab}, \quad (11.45)$$

where the factor 1/2 is needed as each pair a, b ($a \neq b$) must be counted only once. For identical particles, this gives rise to the secondary quantized form (11.39),

$$H' = \frac{1}{2} \sum_{1234} (12|U|34) a_1^\dagger a_2^\dagger a_4 a_3. \quad (11.46)$$

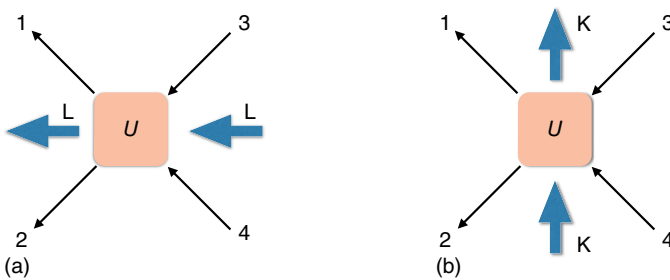


Figure 11.1 The interaction block in the particle–particle channel (a) and in the particle–hole channel (b). The arrows L and K correspond to the angular momentum transfer in a given channel, Sections 11.5 and 11.6.

The interaction structure, Figure 11.1a, describes a two-body collision with the pair of particles undergoing the transition $(3,4 \rightarrow 1,2)$. This representation of the process will be referred to as the *particle–particle channel*.

For a Hermitian Hamiltonian, $H'^\dagger = H'$, the two-body matrix elements satisfy the condition

$$(12|U|34) = (43|U|21)^*. \quad (11.47)$$

Another property of matrix elements follows from the commutation relations of single-particle operators: for any statistics of the particles, the simultaneous permutation of initial and final particles does not change the amplitude of the process,

$$(12|U|34) = (21|U|43). \quad (11.48)$$

Under the permutation of only initial (or only final) particles, the original matrix element, given by integral (11.44), does not have any symmetry. However, the total sum (11.46) contains only symmetrized (for bosons) or antisymmetrized (for fermions) part. Therefore, it might be convenient to introduce the matrix elements of a certain symmetry,

$$(12|\bar{U}|34) = (12|U|34) \pm (21|U|34), \quad (11.49)$$

and write down the full interaction operator as

$$H' = \frac{1}{4} \sum_{1234} (12|\bar{U}|34) a_1^\dagger a_2^\dagger a_4 a_3. \quad (11.50)$$

As an example, we consider the case when the interaction can be described with the aid of a *potential* that depends on the relative distance r between the particles and does not carry any dependence on additional quantum number of particles as spin or isospin. The set of suitable single-particle quantum characteristics is in this case $|1\rangle = |\mathbf{r}_1, \sigma_1\rangle$, and the potential *vertex* has the following structure in coordinate space (isospin can also be easily included):

$$(12|U|34) = \delta_{\sigma_1 \sigma_4} \delta_{\sigma_2 \sigma_3} \delta(\mathbf{r}_1 - \mathbf{r}_4) \delta(\mathbf{r}_2 - \mathbf{r}_3) U(|\mathbf{r}_1 - \mathbf{r}_2|). \quad (11.51)$$

The total interaction Hamiltonian is given by

$$H' = \frac{1}{2} \sum_{\sigma_1 \sigma_2} \int d^3 r_1 d^3 r_2 U(|\mathbf{r}_1 - \mathbf{r}_2|) a_{\mathbf{r}_1 \sigma_1}^\dagger a_{\mathbf{r}_2 \sigma_2}^\dagger a_{\mathbf{r}_2 \sigma_2} a_{\mathbf{r}_1 \sigma_1}. \quad (11.52)$$

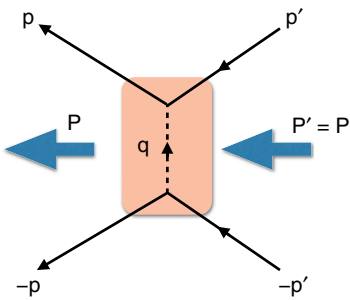


Figure 11.2 The interaction vertex U_q in the momentum representation; in the uniform medium, the total momentum $\mathbf{P} = \mathbf{P}'$ of the pair remains unchanged in the process.

The momentum representation is suitable for spatially uniform systems when every collision preserves the total momentum of the pair. Using again the normalization in a volume V , Eq. (11.28), we transform the Hamiltonian (11.52) as follows:

$$H' = \frac{1}{2V^2} \sum_{\sigma_1 \sigma_2} \sum_{\mathbf{p}_1 \mathbf{p}_2 \mathbf{p}'_1 \mathbf{p}'_2} \int d^3 r_1 d^3 r_2 U(|\mathbf{r}_1 - \mathbf{r}_2|) e^{(i/\hbar)[\mathbf{r}_1 \cdot (\mathbf{p}_1 - \mathbf{p}'_1) + \mathbf{r}_2 \cdot (\mathbf{p}_2 - \mathbf{p}'_2)]} a_{\mathbf{p}_1 \sigma_1}^\dagger a_{\mathbf{p}_2 \sigma_2}^\dagger a_{\mathbf{p}'_2 \sigma_2} a_{\mathbf{p}'_1 \sigma_1}. \quad (11.53)$$

Instead of the four momenta \mathbf{p}_a of the particles in the process, we introduce, Figure 11.2, the total momenta \mathbf{P}' and \mathbf{P} in the particle–particle channel and the relative momenta \mathbf{p}' and \mathbf{p} before and after the collision, respectively [compare (7.31)],

$$\mathbf{p}_1 = \frac{\mathbf{P}}{2} + \mathbf{p}, \quad \mathbf{p}_2 = \frac{\mathbf{P}}{2} - \mathbf{p}, \quad \mathbf{p}'_1 = \frac{\mathbf{P}'}{2} + \mathbf{p}', \quad \mathbf{p}'_2 = \frac{\mathbf{P}'}{2} - \mathbf{p}'. \quad (11.54)$$

The integral over the coordinates in Eq. (11.53) is now decomposed into the product of two independent integrals, over the coordinate $\mathbf{R} = (\mathbf{r}_1 + \mathbf{r}_2)/2$ of the center-of-mass and the relative distance $\mathbf{r} = \mathbf{r}_1 - \mathbf{r}_2$ of the pair,

$$\begin{aligned} & \int d^3 r_1 d^3 r_2 U(|\mathbf{r}_1 - \mathbf{r}_2|) e^{(i/\hbar)[\mathbf{r}_1 \cdot (\mathbf{p}_1 - \mathbf{p}'_1) + \mathbf{r}_2 \cdot (\mathbf{p}_2 - \mathbf{p}'_2)]} \\ &= \int d^3 R e^{(i/\hbar)\mathbf{R} \cdot (\mathbf{P} - \mathbf{P}')} \int d^3 r U(r) e^{(i/\hbar)\mathbf{r} \cdot (\mathbf{p} - \mathbf{p}')}. \end{aligned} \quad (11.55)$$

The center-of-mass integral reveals the momentum conservation,

$$\int d^3 R e^{(i/\hbar)\mathbf{R} \cdot (\mathbf{P} - \mathbf{P}')} = V \delta_{\mathbf{P}\mathbf{P}'}, \quad (11.56)$$

whereas the scattering result is determined by the Fourier component of the potential corresponding to the momentum transfer $\mathbf{q} = \mathbf{p} - \mathbf{p}'$, as in the Born approximation,

$$U_{\mathbf{q}} = \int d^3 r U(r) e^{(i/\hbar)\mathbf{r} \cdot \mathbf{q}}. \quad (11.57)$$

Finally, the interaction Hamiltonian in the momentum representation is

$$H' = \frac{1}{2V} \sum_{\sigma_1 \sigma_2} \sum_{\mathbf{p} \mathbf{p}'} U_{\mathbf{p}-\mathbf{p}'} a_{\mathbf{p}+\mathbf{P}/2, \sigma_1}^\dagger a_{-\mathbf{p}+\mathbf{P}/2, \sigma_2}^\dagger a_{-\mathbf{p}'+\mathbf{P}/2, \sigma_2} a_{\mathbf{p}'+\mathbf{P}/2, \sigma_1}. \quad (11.58)$$

11.5 Interaction in a Spherical Basis

In nuclear applications, the natural single-particle basis is provided by the mean field. The nuclear shell model usually uses the spherical basis $|1m_1\rangle$ with spin–orbital coupling, where 1 combines all quantum numbers except for projections of total angular momentum, $j_z = m$. The two-body Hamiltonian takes the form

$$H' = \frac{1}{2} \sum_{1234; \{m\}} (1m_1, 2m_2 | U | 3m_3, 4m_4) a_{1m_1}^\dagger a_{2m_2}^\dagger a_{4m_4} a_{3m_3}. \quad (11.59)$$

If isospin invariance is taken into account explicitly, one can also single out the isospin projection $t_3 = \tau$ of each particle.

The angular momentum conservation puts constraints on the amplitudes. Indeed, if the interaction U is rotationally invariant, the total angular momentum L of the initial pair (3,4) has to be equal to that of the final pair (1,2) as illustrated in Figure 11.1a. The initial decoupled state $|3m_3, 4m_4\rangle$ is a superposition of coupled states with a certain value of L and total projection $L_z = \Lambda = m_3 + m_4$,

$$|3m_3, 4m_4\rangle = \sum_{L\Lambda} C_{j_3m_3 j_4m_4}^{L\Lambda} |34; L\Lambda\rangle. \quad (11.60)$$

A similar representation is valid for the final state,

$$(1m_1, 2m_2) = \sum_{L'\Lambda'} C_{j_1m_1 j_2m_2}^{L'\Lambda'} (12; L'\Lambda'). \quad (11.61)$$

In these definitions, we use the standard Clebsch–Gordan coefficients [QP, I, 22] and order the single-particle states in such a way that, as in Figure 11.1a, the quantum numbers of the pair as a whole 1 and 3 would correspond, for distinguishable particles, to the first particle, and 2 and 4 to the second particle. The order of indexes can also be understood as follows: pair state $|3, 4\rangle$ annihilated by $a_4 a_3$ in (11.46) is created from vacuum by $a_3^\dagger a_4^\dagger$. Matrix elements of U , as of any scalar operator, do not change rotational quantum numbers, $L' = L$, $\Lambda' = \Lambda$. Moreover, the matrix elements do not depend on the projection Λ . Therefore, the process amplitude can be written as

$$(1m_1, 2m_2 | U | 3m_3, 4m_4) = \sum_{L\Lambda} C_{j_1m_1 j_2m_2}^{L\Lambda} C_{j_3m_3 j_4m_4}^{L\Lambda} U_L (12; 34), \quad (11.62)$$

with effective matrix elements $U_L (12; 34)$, where the m -dependence was eliminated. Now we can combine the Clebsch–Gordan coefficients with the creation and annihilation operators and form the *pair creation* operators,

$$P_{L\Lambda}^\dagger (12) = \sum_{m_1 m_2} C_{j_1m_1 j_2m_2}^{L\Lambda} a_{1m_1}^\dagger a_{2m_2}^\dagger, \quad (11.63)$$

and Hermitian conjugate *pair annihilation* operators,

$$P_{L\Lambda} (12) = \sum_{m_1 m_2} C_{j_1m_1 j_2m_2}^{L\Lambda} a_{2m_2} a_{1m_1}. \quad (11.64)$$

Thus, the rotationally invariant interaction in the particle–particle channel can be brought to the form

$$H' = \frac{1}{2} \sum_{1234; L\Lambda} U_L (12; 34) P_{L\Lambda}^\dagger (12) P_{L\Lambda} (34). \quad (11.65)$$

As an easy generalization, we get for the isospin-invariant interaction

$$P_{L\Lambda;tt_3}^\dagger(12) = \sum_{m_1 m_2, \tau_1 \tau_2} C_{j_1 m_1 j_2 m_2}^{L\Lambda} C_{1/2\tau_1 1/2\tau_2}^{tt_3} a_{1m_1 \tau_1}^\dagger a_{2m_2 \tau_2}^\dagger, \quad (11.66)$$

$$P_{L\Lambda;tt_3}(12) = \sum_{m_1 m_2, \tau_1 \tau_2} C_{j_1 m_1 j_2 m_2}^{L\Lambda} C_{1/2\tau_1 1/2\tau_2}^{tt_3} a_{2m_2 \tau_2} a_{1m_1 \tau_1}, \quad (11.67)$$

$$H' = \frac{1}{2} \sum_{1234; L\Lambda; tt_3} U_{Lt}(12; 34) P_{L\Lambda;tt_3}^\dagger(12) P_{L\Lambda;tt_3}(34), \quad (11.68)$$

where t is the total isospin of the pair (0 or 1 for nucleons), and

$$(1m_1 \tau_1, 2m_2 \tau_2 | U | 3m_3 \tau_3, 4m_4 \tau_4) \\ = \sum_{L\Lambda, tt_3} C_{j_1 m_1 j_2 m_2}^{L\Lambda} C_{1/2\tau_1 1/2\tau_2}^{tt_3} C_{1/2\tau_3 1/2\tau_4}^{tt_3} C_{j_3 m_3 j_4 m_4}^{L\Lambda} U_{Lt}(12; 34), \quad (11.69)$$

The nucleon pair operators, Eqs. (11.66) and (11.67), have simple symmetry properties that follow from the Fermi statistics and complementarity between spin-spatial and isobaric variables (Chapter 2). If we permute two creation operators in the sum of Eq. (11.66), the result gets sign minus. Now we recover the correspondence between the Clebsch–Gordan coefficients and the order of the operators interchanging the lower pairs of indices of both coefficients, which brings in the phases $(-)^{j_1+j_2-L}$ and $(-)^{1/2+1/2-t}$. As a result, we obtain the same operator P^\dagger but with the opposite order of nonrotational quantum numbers 1 and 2:

$$P_{L\Lambda,tt_3}^\dagger(12) = (-)^{j_1+j_2+L+t} P_{L\Lambda,tt_3}^\dagger(21). \quad (11.70)$$

In particular, for a pair on the same single-particle orbit, $I=2$, the sum $L+t$ must be an *odd* integer. This agrees with the correspondence discussed in Chapter 2 – pairs of equivalent fermions ($t=1$) can have only *even* total angular momentum L . Quasideuteron pairs ($t=0$) can have only *odd* values of L . In the same way, we would obtain only *even* L for boson pairs (no isospin).

It can be useful to give a few additional comments about symmetries in angular momentum coupling. Rather than couple, with the Clebsch–Gordan coefficients, several angular momenta into a certain final value, as illustrated in Figure 11.3a, from the symmetry perspective it makes sense to consider the coupling schemes where multiple angular momenta add up to a net total of zero,

$$\mathbf{j}_1 + \mathbf{j}_2 + \mathbf{j}_3 + \dots = 0. \quad (11.71)$$

The most trivial constriction, $\mathbf{j}_1 + \mathbf{j}_2 = 0$, Figure 11.3b, is well known. It is a scalar made out of two equal angular momenta,

$$\sum_{m_1, m_2} \begin{pmatrix} j_1 & j_2 \\ m_1 & m_2 \end{pmatrix} |j_1 m_1; j_2 m_2\rangle = \delta_{j_1 j_2} \sum_m (-)^{j_2-m} |j_1 m; j_2 - m\rangle. \quad (11.72)$$

The coefficient here, referred to as a $2j$ -symbol, is, up to a normalization, the simple Clebsh–Gordan coefficient

$$\begin{pmatrix} j_1 & j_2 \\ m_1 & m_2 \end{pmatrix} = (-1)^{j_1-m_1} \delta_{j_1 j_2} \delta_{m_1 -m_2} = \sqrt{2j_1 + 1} C_{j_1 m_1 j_2 m_2}^{00}. \quad (11.73)$$

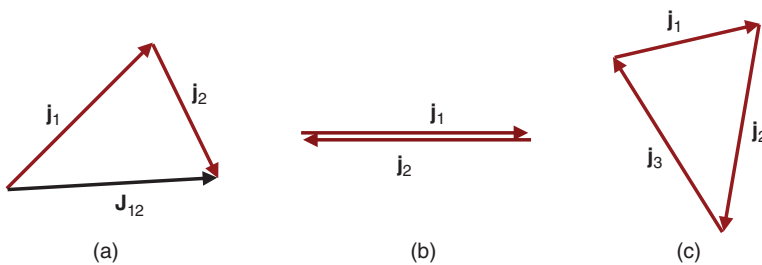


Figure 11.3 Graphical illustration of angular momentum coupling: (a) Clebsch–Gordan coefficient $j_1 + j_2 = J_{12}$, (b) $2j$ symbol $j_1 + j_2 = 0$, (c) $3j$ symbol $j_1 + j_2 + j_3 = 0$.

If the relation is viewed as $j_2 = -j_1$, then action of the $2j$ -symbol amounts to flipping the angular momentum, or to time reversal. Thus, time-reversed state is

$$|\tilde{j} m\rangle = \sum_{m'} \begin{pmatrix} j & j \\ m & m' \end{pmatrix} |j m'\rangle = (-)^{j-m} |j - m\rangle. \quad (11.74)$$

In our discussions of operators, we always define creation operators as “adding” angular momentum to states, and corresponding annihilation operators with the reversed structure as “removing” angular momentum. As an example, we can recall the quantization of vibrational modes, Eq. (6.73).

A construction that involves a triangle of angular momentum vectors, $j_1 + j_2 + j_3 = 0$ is shown in Figure 11.3c. A scalar out of three angular momenta is made with the so-called $3j$ -symbol [QP, I, 22.6],

$$\sum_{m_1, m_2, m_3} \begin{pmatrix} j_1 & j_2 & j_3 \\ m_1 & m_2 & m_3 \end{pmatrix} |j_1 m_1; j_2 m_2; j_3 m_3\rangle \quad (11.75)$$

If we take $j_3 = -J_{12}$, the $3j$ -symbol is equivalent to the Clebsh–Gordan coefficient,

$$\begin{pmatrix} j_1 & j_2 & j_3 \\ m_1 & m_2 & m_3 \end{pmatrix} = \frac{(-1)^{j_1-j_2-m_3}}{\sqrt{2j_3+1}} C_{j_1 m_1 j_2 m_2}^{j_3 m_3}. \quad (11.76)$$

Unlike Clebsh–Gordan coefficients, the $3j$ -symbols have many symmetries: sequential permutation of angular momentum vectors, such as $(1, 2, 3) \rightarrow (2, 3, 1)$, leads to the identical $3j$ -symbol; since $m_1 + m_2 + m_3 = 0$ reversing all three items adds a phase $(-1)^{j_1+j_2+j_3}$; the same reversed triangle and the same phase emerge if any two angular momentum vectors are interchanged.

A triangle of three vectors is the largest possible rigid construction. As obvious from geometrical considerations, the structures with more vectors in (11.71) would not be uniquely defined unless some additional intermediate couplings are specified. These intermediate couplings can be specified in different ways, and relations between them are established by recoupling coefficients that we discuss next.

11.6 Recoupling of Angular Momentum

The interaction in the particle–particle channel was constructed as a scalar coupling of four single-particle operators in both spin-spatial and isospin space. These operators

are first coupled in pairs, and two pairs give a total tensor operator of zero rank. The same result can be achieved by changing the order of the vector couplings, for example, according to the *particle-hole* scheme, $[[a^\dagger a]_K [a^\dagger a]_K]_{00}$, where the brackets indicate the order of coupling of two pairs in the intermediate spin K (see Figure 11.1b).

A possibility of recoupling first emerges for *three* subsystems with spins j_1, j_2, j_3 that do not add up to zero. The state of the total system with angular momentum quantum numbers J, M can be built, for instance, according to the scheme

$$\mathbf{j}_1 + \mathbf{j}_2 = \mathbf{J}_{12}, \quad \mathbf{J}_{12} + \mathbf{j}_3 = \mathbf{J};$$

this scheme can be denoted as $[[j_1 j_2]_{J_{12}} j_3]JM$. We can write down explicitly this process of vector coupling as

$$|[[j_1 j_2]_{J_{12}} j_3]JM\rangle = \sum_{m_1 m_2 m_3 M_{12}} C_{j_1 m_1 j_2 m_2}^{J_{12} M_{12}} C_{J_{12} M_{12} j_3 m_3}^{JM} |j_1 m_1; j_2 m_2; j_3 m_3\rangle. \quad (11.77)$$

It is important that the coupling is fully defined by the choice of the intermediate angular momentum J_{12} : each value of J_{12} appears in the subsystem $\mathbf{j}_1 + \mathbf{j}_2$ only once as a new quantum number labeling the total state of three subsystems. Note that we used in Eq. (11.77) an excessive indication of the summation indices: for a given total projection M , only m_1 and m_2 are taken independently, the remaining projections are determined by the conservation laws. Usually, it is just simpler to use such a system of notations.

Problem 11.5 Show that the states (11.77) with different choices of J_{12} are orthonormalized,

$$\langle [[j_1 j_2]_{J'_{12}} j_3]J' M' | [[j_1 j_2]_{J_{12}} j_3]JM \rangle = \delta_{J_{12} J'_{12}} \delta_{J' M'} \delta_{MM'}. \quad (11.78)$$

Using the orthogonality properties of the Clebsch–Gordan coefficients, we can inversely express the decoupled state $|j_1 m_1; j_2 m_2; j_3 m_3\rangle$ in terms of the states (11.77) coupled via various intermediate momenta,

$$|j_1 m_1; j_2 m_2; j_3 m_3\rangle = \sum_{JM J_{12} M_{12}} C_{j_1 m_1 j_2 m_2}^{J_{12} M_{12}} C_{J_{12} M_{12} j_3 m_3}^{JM} |[[j_1 j_2]_{J_{12}} j_3]JM\rangle. \quad (11.79)$$

On the other hand, the intermediate coupling may be performed in a different way,

$$\mathbf{j}_2 + \mathbf{j}_3 = \mathbf{J}_{23}, \quad \mathbf{J}_{23} + \mathbf{j}_1 = \mathbf{J},$$

or, explicitly,

$$|[j_1 [j_2 j_3]_{J_{23}}]JM\rangle = \sum_{m_1 m_2 m_3 M_{23}} C_{j_1 m_1 J_{23} M_{23}}^{JM} C_{j_2 m_2 j_3 m_3}^{J_{23} M_{23}} |j_1 m_1; j_2 m_2; j_3 m_3\rangle. \quad (11.80)$$

If we express the decoupled state here in terms of the previous way of coupling, Eq. (11.79), we obtain an interrelation between the two coupling schemes,

$$\begin{aligned} |[j_1 [j_2 j_3]_{J_{23}}]JM\rangle &= \sum_{J' M' J_{12} M_{12} m_1 m_2 m_3 M_{23}} C_{j_1 m_1 j_2 m_2}^{J_{12} M_{12}} C_{J_{12} M_{12} j_3 m_3}^{J' M'} \\ &\times \left(C_{j_1 m_1 J_{23} M_{23}}^{JM} C_{j_2 m_2 j_3 m_3}^{J_{23} M_{23}} |[[j_1 j_2]_{J_{12}} j_3]J' M'\rangle \right). \end{aligned} \quad (11.81)$$

Since the total angular momentum quantum numbers J, M have to be the same in both parts of the Eq. (11.81), the sum of the Clebsch–Gordan coefficients has to be a rotational scalar. It can be found, with the aid of orthogonality (11.78), as an overlap of states implementing different intermediate couplings,

$$\langle [j_1 j_2]_{J_{12}} j_3 J' M' | [j_1 j_2 j_3]_{J_{23}} J M \rangle = \delta_{J'} \delta_{M' M} \\ \times \sum_{m_1 m_2 m_3 M_{12} M_{23}} C_{j_1 m_1 j_2 m_2}^{J_{12} M_{12}} C_{J_{12} M_{12} j_3 m_3}^{JM} C_{j_1 m_1 J_{23} M_{23}}^{JM} C_{j_2 m_2 j_3 m_3}^{J_{23} M_{23}}. \quad (11.82)$$

As always for scalars, this overlap does not depend on M . Angular momentum recoupling (11.82) determines the so-called Racah coefficient W , or, equivalently, the $6j$ -symbol denoted by the two-line array in the curly brackets,

$$W(j_1 j_2 J j_3; J_{12} J_{23}) \sqrt{(2J_{12} + 1)(2J_{23} + 1)} \\ = \sum_{m_1 m_2 m_3 M_{12} M_{23}} C_{j_1 m_1 j_2 m_2}^{J_{12} M_{12}} C_{J_{12} M_{12} j_3 m_3}^{JM} C_{j_1 m_1 J_{23} M_{23}}^{JM} C_{j_2 m_2 j_3 m_3}^{J_{23} M_{23}}; \quad (11.83)$$

$$W(j_1 j_2 J j_3; J_{12} J_{23}) \equiv (-)^{j_1 + j_2 + j_3 + J} \begin{Bmatrix} j_1 & j_2 & J_{12} \\ j_3 & J & J_{23} \end{Bmatrix}. \quad (11.84)$$

The coupling of angular momenta and possible intermediate couplings can be shown graphically; in Figure 11.4, we show the coupling $\mathbf{j}_1 + \mathbf{j}_2 + \mathbf{j}_3 = \mathbf{J}$ graphically with head-to-tail drawing of the vector additions. The original three vectors are shown in red, their total sum, \mathbf{J} , is in black, and two intermediate sums, \mathbf{J}_{12} and \mathbf{J}_{23} , are in blue. In order to elucidate the illustration, the projections onto the plane formed by \mathbf{j}_1 and \mathbf{j}_2 are shown. Two angular momenta add up to each given value of the final angular momentum uniquely; in other words, each irreducible representation occurs only once. This group property makes a triangle of three vectors defined by their lengths as a rigid (fully determined) figure. A sum of more than two angular momenta, where magnitudes are given but relative angles can vary, may lead to the same magnitude of the final total angular momentum in more than one way. Thus, additional information is needed, this is provided by the intermediate angular momentum values that make the shape of the coupling diagram rigid. The $6j$ -symbol is a transformation coefficient between different coupling schemes of three angular momenta, each $6j$ -symbol is fully determined by a tetrahedral shape in Figure 11.4, where only the lengths of sides are used to define the shape. Given lengths of all sides, the number of equivalent tetrahedral shapes is just the number of ways that four triangles can be sequentially selected. Any two faces share a unique edge; therefore, we get $4! = 24$ possibilities (this equals the number of symmetry operations for a regular tetrahedron). In addition, there are two choices for selecting the first and second sides when making a first face. This is leading to a total of 48 possibilities. Therefore, the $6j$ -symbol (11.84) is highly symmetric, for example, its value is unchanged by interchange of any two columns or by exchange of upper and lower values in any two columns.

In the problems with spin–orbit coupling, a commonly encountered recoupling emerges in the transition between j - and ℓs -schemes. For an interaction of two particles in a particular angular momentum channel $\mathbf{j}_1 + \mathbf{j}_2 = \mathbf{L}$, for each of the particles we

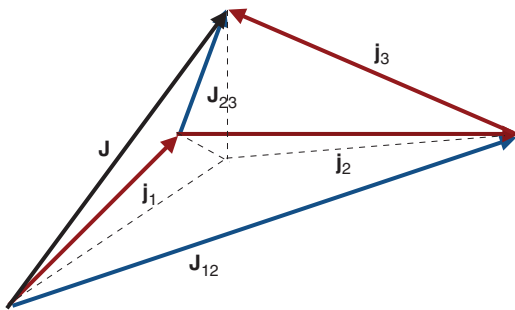


Figure 11.4 Graphical illustration of coupling of three angular momenta. The tetrahedral shape defines the $6j$ -symbol.

have $\mathbf{j} = \ell + \mathbf{s}$. Frequently, it may be more convenient to separate coordinate and spin dependence by recoupling

$$\underbrace{\ell_1 + s_1}_{j_1} + \underbrace{\ell_2 + s_2}_{j_2} = \mathbf{L} = \underbrace{\ell_1 + \ell_2}_{\ell} + \underbrace{s_1 + s_2}_{\mathbf{s}}.$$

Various recoupling relations and tensor decomposition of interactions, as well as useful additional information, can be found in the classical book [1].

Problem 11.6 The $0f_{7/2}$ single-particle orbit is well separated from adjacent orbits in the nuclear spherical mean-field potential (Chapter 8). Using the formalism of secondary quantization, write down the most general two-body interaction Hamiltonian for identical nucleons occupying this orbit. Experimental data for states in $N = 28$ isotones are presented in Table 11.1: using binding energies for states in ^{49}Sc and ^{50}Ti , determine the phenomenological parameters of the effective Hamiltonian. Using this Hamiltonian, make predictions for energies of states in ^{51}V .

Solution

The general two-body interaction Hamiltonian within the $f_{7/2}$ space can be written as

$$H = \epsilon N + \sum_{L=0,2,4,6} U_L \sum_{\Lambda} P_{L\Lambda}^{\dagger} P_{L\Lambda}, \quad (11.85)$$

where N is the total number of valence particles, ϵ is the single-particle energy. The two-body interactions are described by the pair scattering matrix elements U_L . Two particles each with angular momentum j can form pairs with any angular momentum from 0 unto $2j$, but identical nucleons can only be in the antisymmetric state, which forbids odd values of L . Therefore, $L = 0, 2, 4$, and 6 are the only allowed values. It is convenient to define pair operators so that they create a normalized state, then if nucleons come from the same spherical orbit an additional factor $1/\sqrt{2}$ is needed to assure that $\langle 0 | P_{L\Lambda} P_{L\Lambda}^{\dagger} | 0 \rangle = 1$,

$$P_{L\Lambda}^{\dagger} = \frac{1}{\sqrt{2}} \sum_{m_1 m_2} C_{jm_1 jm_2}^{L\Lambda} a_{jm_1}^{\dagger} a_{jm_2}^{\dagger}. \quad (11.86)$$

The systems with one and two valence particles provide empirical values for the parameters. Binding energy of the $J = 7/2$ state in ^{49}Sc , which is the proton separation energy in this case, suggests $\epsilon = -9.626$ MeV, this agrees well with the

Table 11.1 Experimental information about states in $N = 28$ isotopes.

J	E_x	Binding	J	E_x	Binding	J	E_x	Binding
0	^{48}Ca	0	0	^{52}Cr	40.355	7/2	^{53}Mn	46.915
7/2	^{49}Sc	9.626	2	1.434	38.921	5/2	0.378	46.537
0	^{50}Ti	21.787	4	2.370	37.986	3/2	1.290	45.625
2	1.554	20.233	4	2.768	37.587	11/2	1.441	45.474
4	2.675	19.112	2	2.965	37.390	9/2	1.620	45.295
6	3.199	18.588	6	3.114	37.241	15/2	2.693	44.222
7/2	^{51}V	29.851	5	3.616	36.739	0	^{54}Fe	55.769
5/2	0.320	29.531	8	4.750	35.605	2	1.408	54.360
3/2	0.929	28.922				4	2.538	53.230
11/2	1.609	28.241				6	2.949	52.819
9/2	1.813	28.037				7/2	^{55}Co	60.833
15/2	2.700	27.151				0	^{56}Ni	67.998

States identified by their spin are listed along with their excitation energy and with total binding energy relative to the ^{48}Ca core. All energies are in units of megaelectronvolts.

prediction of the mean-field model discussed in Chapter 8. For two particles, the Hamiltonian gives energies $E_{J=L} = 2\epsilon + U_L$: comparing this with energies of states in ^{50}Ti , we determine $U_0 = -2.535$ MeV, $U_2 = -0.981$ MeV, $U_4 = 0.140$ MeV, and $U_6 = 0.664$ MeV. This set of parameters can be used to make predictions for all states listed in Table 11.1. For example, using this Hamiltonian for ^{51}V , we obtain results shown in Table 11.2, they agree well with the data. Three identical nucleons on a single $j = 7/2$ shell can couple to total angular momenta $J = 3/2, 5/2, 7/2, 9/2, 11/2$, and $15/2$. Luckily, there is only one state with each angular momentum (a special property of the level $j = 7/2$). Therefore, it does not matter how these states are constructed, all coupling schemes would lead to the same state. Moreover, all states of good angular momentum are automatically eigenstates of the Hamiltonian, and thus energies of the states are just expectation values of the Hamiltonian. For example, the most aligned $J = 15/2$ state is just $|15/2 M = 15/2\rangle = a_{j=3/2}^\dagger a_{j=5/2}^\dagger a_{j=7/2}^\dagger |0\rangle$. The energy of this state $\langle 15/2 M | H | 15/2 M \rangle = 3\epsilon + \frac{15}{22}U_4 + \frac{51}{22}U_6$. The state with $J = 7/2$ and the magnetic projection M can be made from vacuum using the operator $P_{00}^\dagger a_{j,m=M}^\dagger$ (this needs to be normalized). The energy of $J = 7/2$ state is $\langle 7/2 M | H | 7/2 M \rangle = 3\epsilon + \frac{3}{4}U_0 + \frac{5}{12}U_2 + \frac{3}{4}U_4 + \frac{13}{12}U_6$.

A better approach for defining the phenomenological Hamiltonian would be to fit all energies in Table 11.2 with five parameters U_L . However, it turns out that some interaction matrix elements and specific linear combinations of them are more important as they lead to *collective* features. The U_0 matrix element turns out to be related to pairing, which in large systems leads to collective superfluid or superconducting phenomena.

Another important component of interaction is the *monopole*. Let us take out an average part \tilde{U} from all interaction matrix elements U_L so that $U_L = U'_L + \tilde{U}$, correspondingly $H = H' + \tilde{H}$. The monopole Hamiltonian \tilde{H} , where all nucleon pairs

Table 11.2 Comparison of predicted and observed excitation and binding energies for the states in ^{51}V .

J	E_x	Binding	E_x	Binding
		Experiment		
7/2	0	29.851	0	30.364
5/2	0.320	29.531	0.367	29.997
3/2	0.929	28.922	1.185	29.179
11/2	1.609	28.241	1.797	28.567
9/2	1.813	28.037	1.948	28.416
15/2	2.700	27.151	3.120	27.243

All energies are in units of megaelectronvolts.

interact with the same strength, just counts the number of pairs,

$$\tilde{H} = \tilde{U} \sum_{L=0,2,4,6} \sum_{\Lambda} P_{L\Lambda}^\dagger P_{L\Lambda} = \tilde{U} \frac{N(N-1)}{2}. \quad (11.87)$$

This interaction is *collective* because its contribution to energy strongly increases with the particle number. In the particle–hole channel, the monopole Hamiltonian corresponds to the interaction part with $K = 0$ (Figure 11.1b). As $[a^\dagger a]_0 \propto N$, the interaction in the $K = 0$ channel gives $[a^\dagger a]_0 [a^\dagger a]_0 \propto N^2$. The monopole interaction drives an overall binding of the system; when the shell is completely filled, this is the only remaining interaction term that, along with single-particle energies, contributes to the total energy. The energy of a completely filled state, where $N = \Omega = 2j + 1$, is $E = \epsilon\Omega + \sum_L (2L + 1)U_L$. Indeed, each interaction term $P_{L\Lambda}^\dagger P_{L\Lambda}$, where the pair is removed and then added back, gives exactly the same unit contribution to the sum in (11.87). The “average” monopole part is defined in such a way that $\tilde{U}\Omega(\Omega - 1)/2 = \sum_L (2L + 1)U_L$. Since $\sum_L (2L + 1) = \Omega(\Omega - 1)/2$, which is just a number of two-nucleon states in a single j -shell, the monopole part emerges as the weighted average

$$\tilde{U} = \frac{\sum_L (2L + 1)U_L}{\sum_L (2L + 1)}. \quad (11.88)$$

We discuss the mean field later, here we just mention that the recovered dependence of energy on the particle number suggests that the effective single-particle energy changes with the number of particles roughly as $\epsilon(N) \sim \epsilon + \tilde{U}N$.

Problem 11.7 Derive the normalization property of the $6j$ -coefficients,

$$\sum_J (2J + 1) \left\{ \begin{matrix} j_1 & j_2 & J \\ j_3 & j_4 & x \end{matrix} \right\} \left\{ \begin{matrix} j_3 & j_4 & J \\ j_1 & j_2 & y \end{matrix} \right\} = \frac{\delta_{xy}}{2x + 1}. \quad (11.89)$$

Problem 11.8 Prove that

$$\begin{Bmatrix} J & j_1 & j_2 \\ 0 & j_2 & j_1 \end{Bmatrix} = \frac{(-)^{J+j_1+j_2}}{\sqrt{(2j_1+1)(2j_2+1)}}. \quad (11.90)$$

Many other useful relations and the exact expressions for $6j$ and similar symbols of higher order that enter with the vector coupling of many angular momenta can be found, for example, in Refs [2, 3].

Problem 11.9 Consider a single j -level discussed in problem 11.6, define multipole operator in the particle–hole channel are as

$$\mathcal{M}_{K\kappa}^\dagger = \sum_{m_1 m_2} (-)^{j-m_2} C_{jm_1 j-m_2}^{K\kappa} a_{jm_1}^\dagger a_{jm_2}. \quad (11.91)$$

Prove the following properties

- a) Behavior of multipoles under Hermitian conjugation is similar to that of spherical harmonics

$$(\mathcal{M}_{K\kappa})^\dagger = (-)^\kappa \mathcal{M}_{K-\kappa}. \quad (11.92)$$

- b) Particle number operator N is related to $K=0$ multipole

$$N = \sqrt{2j+1} \mathcal{M}_{0\ 0}. \quad (11.93)$$

- c) Angular momentum operator \mathbf{J} is related to $K=1$ multipole as

$$J_\kappa = \frac{\sqrt{j(j+1)(2j+1)}}{\sqrt{3}} \mathcal{M}_{1\ \kappa}. \quad (11.94)$$

Here J_κ is a spherical component of angular momentum operator related to usual Cartesian and raising and lowering operators as

$$J_0 = J_z, \quad J_{\pm 1} = \mp \frac{1}{\sqrt{2}} (J_x \pm iJ_y) = \mp \frac{J_\pm}{\sqrt{2}}. \quad (11.95)$$

Problem 11.10 Consider a Hamiltonian for a single j -level and define particle-pair operators $P_{L\Lambda}$ according to Eq. (11.86) and multipole operators as in Eq. (11.91). Show that (summation over L includes only even values $L = 0, 2, \dots, 2j-1$)

$$H = \sum_L U_L \sum_\Lambda P_{L\ \Lambda}^\dagger P_{L\ \Lambda} = \epsilon N - \sum_K \frac{\tilde{U}_K}{2} \sum_\kappa \mathcal{M}_{K\kappa}^\dagger \mathcal{M}_{K\kappa}, \quad (11.96)$$

where the matrix elements in the particle–hole channel are

$$\tilde{U}_K = \sum_L (2L+1) \begin{Bmatrix} j & j & L \\ j & j & K \end{Bmatrix} U_L. \quad (11.97)$$

Commutations required to reorder operators, such as those in Eq. (11.42), also give rise to the one-body term (single-particle energy)

$$\epsilon = -\frac{\tilde{U}_0}{2} = \frac{1}{2\Omega} \sum_L (2L+1) U_L. \quad (11.98)$$

Note that the number operator N is the only one-body scalar possible in this space.

Problem 11.11 Interactions in the particle–hole channel are subject to additional constraints that reflect Pauli principle. For a single j -shell Hamiltonian (11.96), only even L are allowed, meaning that $U_L = 0$ for $L = 1, 3, \dots, 2j$. Show that in the particle–hole channel, the same condition is expressed as the relation between different amplitudes,

$$\tilde{U}_K = \sum_{K'} (-)^{K+K'} (2K'+1) \left\{ \begin{matrix} j & j & K' \\ j & j & K \end{matrix} \right\} \tilde{U}_{K'} . \quad (11.99)$$

Analogous relations are known in the macroscopic Fermi-liquid theory [4].

References

- 1 A. De Shalit and I. Talmi, *Nuclear Shell Theory*, Academic Press, New York, 1963.
- 2 A. Messiah, *Quantum Mechanics*, North-Holland, Amsterdam, 1962.
- 3 A.R. Edmonds, *Angular Momentum in Quantum Mechanics*, Princeton University Press, Princeton, NJ, 1968.
- 4 G. Baym and C. Pethick, *Landau Fermi-Liquid Theory*, Wiley-VCH, Weinheim, 2004.

12

Nuclear Deformation

*And, as imagination bodies forth
 The forms of things unknown, the poet's pen
 Turns them to shapes, and gives to airy nothing
 A local habitation and a name.*

W. Shakespeare, A Midsummer Night's Dream

12.1 Idea of Nuclear Deformation

As we have already mentioned, the mean field in general and the shell model in particular serve as a base for practically all microscopic calculations in nuclear structure. We have seen the simplest examples of how the primitive single-particle shell model explains configurations, spins, and magnetic moments of many light nuclei. We also pointed out that there are many cases when the shell model predictions in this oversimplified form are far from reality.

When applied to medium and heavy nuclei, the independent particle shell model with spin–orbit coupling works satisfactorily mainly in magic and near-magic nuclei not far from the valley of stability. The magic numbers come out correctly; in their vicinity, the model successfully predicts spins and magnetic moments of ground states and reasonably well describes low-lying excited states of single-particle nature (promotion of individual particles to adjacent empty orbits). As number of valence nucleons increases, we encounter serious practical difficulties in our attempts to classify nuclear states in terms of simple single-particle configurations.

In even–even nuclei, we need an additional postulate of *pairing* which leads to quantum numbers 0^+ of the ground state. However, this postulate is not sufficient for explaining the low-lying excited states as a result of single-particle excitations. The situation is even more complicated in odd- A nuclei. The pairing hypothesis makes it tempting to ascribe the ground state spin J and magnetic moment to the j -orbit of the last unpaired nucleon, but these predictions are frequently not accurate. In some regions of the periodic table, such as $A = 150 \div 190$ and $A > 220$, these expectations do not work at all. The magnetic moments of odd- A nuclei are usually closer to one of the Schmidt lines that determines $\ell = j \pm 1/2$ if the nuclear spin $J = j$ is known. But it is impossible to speak about good quantitative agreement.

The most striking contradictions to the spherical single-particle shell model are found, as we discussed earlier, in electric quadrupole moments of odd- A nuclei. The very fact that many such nuclei, and almost all nuclei far from the closed spherical shells, reveal large quadrupole moments of the same order of magnitude for odd protons and odd neutrons, tells us that the nonspherical distribution is most probably due to the *core polarization*. The polarized core loses spherical shape by means of its interaction with valence nucleons. The core is spherical near the closed shells when the polarizing influence of a small number of valence nucleons is not sufficiently strong to deform the core.

We know from general selection rules that for even–even nuclei in their ground states the quadrupole moment automatically vanishes because the ground state spin is equal to zero. It is important to understand that this is not directly related to nuclear shape. The *rotational invariance* implies that the total Hamiltonian of the system is invariant under rotations of the system as a whole. It follows from here that stationary states of the system have a certain total angular momentum (*nuclear spin*). Zero spin shows that the orientation of the system is equiprobable in all directions in space. Then all intrinsic directions which could in principle exist in the system are averaged out and all observed multipole moments, except $\lambda = 0$, vanish. This is the case even for an intrinsically deformed system if its total wave function corresponds to $J = 0$.

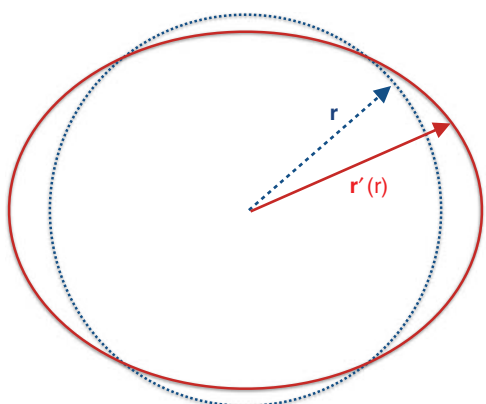
In contrast, a state with $J \neq 0$ can have a certain angular momentum projection onto a quantization axis that was chosen in some way. This brings a special direction in space, and the wave function is *anisotropic*; remember that all observable multipole moments are, by definition, referred to a state with the maximum projection $J_z = J$. This underscores the deep meaning of the *vector model* (see [QP, I, 22.8] and examples discussed in Chapters 3.6 and 9.3) where all observables are substituted by effective operators expressed in terms of the only vector operator characterizing the state, namely the total angular momentum \mathbf{J} . In the absence of the angular momentum, all observables, except for scalar (monopole) quantities, disappear. Thus, for a $J = 0$ state, we need other signatures that would characterize the shape of the system. These signatures come not from this state itself but rather from the whole structure of the energy spectrum and matrix elements of the multipole operators connecting the ground state with excited states.

As was first pointed out by Rainwater [1], a valence nucleon on the orbit $|jm\rangle$ in the field of a spherical core exerts pressure on the core as on the walls of the container. In a semiclassical picture, the particle orbit with a certain orientation singles out a plane, and the particle prefers to deform the core in such a way that increase the overlap between the orbit and the matter distribution in the core. The spherical core is unstable against deformation if there exist single-particle orbits that diminish their energy in the deformed field stronger than the core itself increases its energy getting deformed. The presence of several valence particles amplifies the effect and augments the probability of deformation.

12.2 Collective Model

Let us formalize this idea in a simplest way considering a particle above the spherical core. The core generates the mean-field potential $U(\mathbf{r})$ that depends only on r if there is no feedback from the particle. Try to deform the core preserving the density or the volume. The core deformation can be described as a transformation \hat{D} , which converts

Figure 12.1 Illustration showing original (dashed) circular shape being deformed.



$\mathbf{r} \rightarrow \mathbf{r}'(\mathbf{r}) = \hat{D}\mathbf{r}$ (see illustration in Figure 12.1). Now a particle at each point \mathbf{r} feels a new potential that arrived at this point from the point $\hat{D}^{-1}\mathbf{r}$ together with the deformed matter distribution,

$$U(\mathbf{r}) \Rightarrow U'(\mathbf{r}) = U(\hat{D}^{-1}\mathbf{r}). \quad (12.1)$$

We can borrow from the liquid drop model the description of deformation in terms of the shape variables $\alpha_{\lambda\mu}$. Extending this idea, we can visualize the deformation assuming that there is a displacement of any matter element inside the drop described by the same shape parameters. Then the equipotential surfaces are similar, and the potential energy of the particle located at the point \mathbf{r} is, according to (12.1),

$$U'(\mathbf{r}) = U'(r, \theta, \varphi) = U\left(r\left[1 + \sum_{\lambda\mu} \alpha_{\lambda\mu} Y_{\lambda\mu}(\theta, \varphi)\right]^{-1}\right). \quad (12.2)$$

Considering the case of small deformations, we can make an expansion in the deformation parameters,

$$U'(\mathbf{r}) \approx U\left(r\left[1 - \sum_{\lambda\mu} \alpha_{\lambda\mu} Y_{\lambda\mu}(\theta, \varphi)\right]\right) \approx U(r) - r \frac{dU}{dr} \sum_{\lambda\mu} \alpha_{\lambda\mu} Y_{\lambda\mu}(\theta, \varphi). \quad (12.3)$$

Here the derivative dU/dr is taken for the unperturbed spherical potential. The presence of this derivative shows that the influence of the deformation onto motion of valence nucleons occurs essentially on the nuclear surface. In the nuclear interior, where the original potential is rather flat, the displacement does not change the energy of a particle. However, at the surface with a considerable gradient of the potential, $(dU/dr) > 0$, the particle really feels the angular dependence of the potential energy that is proportional to the deformation parameters. In this approximation, the *radial* dependence is the same for all multipoles ($\lambda\mu$) being separated from the *angular* modulation.

The single-particle problem is now that of motion in the external field (12.3) parameterized by $\alpha_{\lambda\mu}$. The single-particle Hamiltonian H_{s-p} in the unperturbed field was a sum of the isotropic potential energy $U(r)$ and kinetic energy K . The deformation adds the coupling of the particle to the shape variables,

$$H_{s-p} + H_{\text{coulpl}} = K + U(r) - \kappa(r) \sum_{\lambda\mu} Y_{\lambda\mu}(\theta, \varphi) \alpha_{\lambda\mu}. \quad (12.4)$$

The radial form-factor is here

$$\kappa(r) = r \frac{dU}{dr}. \quad (12.5)$$

For simplicity, one can even use the “surface-delta” approximation

$$\kappa(r) \approx R_0 U_0 \delta(r - R_0). \quad (12.6)$$

The spin–orbit potential is assumed to be included into kinetic energy. In a more careful analysis, we can also consider its change due to the shape distortion.

To complete the formulation of a dynamical problem, we have to convert the field parameters $\alpha_{\lambda\mu}$ into dynamical variables adding their own dynamics. In our small-amplitude approximation and with the spherical core, the only choice is the vibrational collective Hamiltonian (5.49), which we call here H_0 . We come to the *collective model* of Bohr and Mottelson [2],

$$H = H_0(\alpha, \pi) + H_{s-p} + H_{coup}(\alpha). \quad (12.7)$$

The model can be straightforwardly generalized to a case of several valence nucleons, but their interaction introduces new effects that should be analyzed separately.

12.3 Adiabatic Approximation

In the collective model, the core is characterized only by the shape variables. The shape degrees of freedom are expected to be the slowest ones. They describe coherent motion of many particles with no significant distortion of their relative interactions. It is similar to a long wavelength excitation in condensed matter when the adjacent parts of the medium are moving in phase and one does not spend considerable energy for breaking short-range links. Typical frequencies of surface collective motion are expected to be lower than the frequencies related to motion of a single valence nucleon at the Fermi surface.

This gives rise to the *adiabatic approximation* borrowed from the molecular and solid state physics; correspondingly this form of the collective model is sometimes called the *quasimolecular model*. We first neglect dynamics of slow variables β (nuclear skeleton in molecules, crystal lattice in solids, or shape in our case) and consider fast variables ξ (electrons in molecules and solids or valence nucleons here) at an arbitrary *frozen* configuration of slow degrees of freedom. Then we come to a wave function of fast variables at a given (*nonequilibrium*) value of slow variables. It is assumed that the fast variables have sufficient time to adjust themselves to a given shape before the shape is noticeably changed: they are in equilibrium with the ongoing slow shape evolution as in the adiabatic process that slowly changes the external conditions in thermodynamics.

Formally, we have to solve the Schrödinger equation

$$[H_0(\beta) + H_{s-p}(\xi) + H_{coup}(\xi; \beta)]\Psi(\xi, \beta) = E\Psi(\xi, \beta), \quad (12.8)$$

but we first solve equation

$$[H_{s-p}(\xi) + H_{coup}(\xi; \beta)]\psi(\xi; \beta) = \epsilon(\beta)\psi(\xi; \beta) \quad (12.9)$$

for particles in an external field described by the set of fixed parameters β , in our case shape variables α . At each value $\beta = \beta_0$, we find a set of functions $\psi(\xi; \beta_0)$ and instant

energy levels (*energy terms*) $\epsilon(\beta_0)$. This set is complete, and in principle it is possible to look for the exact solution $\Psi(\xi, \beta)$ of the whole problem including the β -variables as an expansion over the basis functions belonging to the set found at a specific value of β_0 . But in the adiabatic case, the transitions between the terms are suppressed so it is convenient to use the *traveling* basis. We expect that a single term in the expansion would give a good approximation. Then the term energy $\epsilon(\beta)$ enters an equation for the slow mode as an *additional* potential energy. The total wave function is approximated by a single term of this complete expansion,

$$\Psi(\xi, \beta) \approx \phi_{\text{coll}}(\beta)\psi(\xi; \beta), \quad (12.10)$$

where the collective part satisfies the Schrödinger equation

$$[H_0(\beta) + \epsilon(\beta)]\phi_{\text{coll}}(\beta) = E\phi_{\text{coll}}(\beta). \quad (12.11)$$

Practically this is not that simple because in nuclear structure, we have no such small parameters as the ratio m/M of electron to ion mass in molecules or solids that would explicitly justify the adiabatic approximation.

Problem 12.1 Estimate rotational, vibrational, and electronic excitations in molecules and show that they form an hierarchy of excitation energies, or frequencies,

$$\Delta E_{\text{rot}} : \Delta E_{\text{vib}} : \Delta E_{\text{el}} \simeq \frac{m}{M} : \sqrt{\frac{m}{M}} : 1. \quad (12.12)$$

/See [QP, I, 5.7]. Actually, even in molecules, the situations are known where the adiabatic approximation does not work./

Let us consider a magic nucleus with a single extra valence nucleon. The nucleon is in the upper shell, and its typical excitation frequencies correspond to a transition between the j -subshells. The intershell distance $\Delta\epsilon_{\text{sh}}$ compared to the Fermi energy ϵ_F is of the order of

$$\Delta\epsilon_{\text{sh}} \sim \hbar\omega_0 \approx \frac{\epsilon_F}{A^{1/3}}. \quad (12.13)$$

Each major shell contains several, $\sim A^{1/3}$, j -levels (see estimates in Chapter 8). Therefore, the excitation energy of the outer nucleon within the same major shell is of the order of

$$\Delta\epsilon_j \approx \frac{\epsilon_F}{A^{2/3}}. \quad (12.14)$$

Hence, $\Delta\epsilon_j \approx 1.5 \div 2$ MeV, it is less or of the order of the liquid drop vibrational energy even for the lowest multipolarity 2^+ . Therefore, in magic nuclei, we have almost the inverse situation with respect to a hierarchy of frequencies (recall Figures 5.3 and 5.4).

The collective frequencies rapidly drop when we move away from the magic core, while the single-particle excitation energies are still defined by the shell model level scheme, Eq. (12.14). Then we restore the normal hierarchy of single-particle and collective energies and can apply the adiabatic approximation. However, the presence of a number of valence nucleons and their interactions introduce a new dimension into the problem. Thus, there is no real domain of validity for the extreme single-nucleon adiabatic collective model. Still it is instructive to briefly look at the predictions of such

an idealized model. Some features of the model *reappear* after we include the pairing correlations that increase the energies of single-particle excitations, which acquire the *energy gap* in their spectrum. The existence of the gap related to pair breaking again makes the situation adiabatic. In addition, the pattern of symmetry and deformed shapes in the adiabatic approximation is practically the same as in more elaborate approaches.

12.4 Onset of Deformation

Applying the ideas of the adiabatic approximation, we have to average the particle–core interaction energy (12.4) over the particle wave function at the fixed core deformation. This defines energy terms $\epsilon(\beta)$. Together with the original core energy, they define the total core Hamiltonian, Eq. (12.11), and we are interested in the final equilibrium shape of the core.

The Hamiltonian (12.4) was derived in the lowest order with respect to the shape parameters $\alpha_{\lambda\mu}$. Within the same accuracy, we can directly find the deformation-dependent shift of the particle energy for the single-particle state with quantum numbers $(nljm)$,

$$\Delta\epsilon_{nljm} = -\kappa_{nl} \sum_{\lambda\mu} \langle Y_{\lambda\mu} \rangle_{jm} \alpha_{\lambda\mu}. \quad (12.15)$$

Here κ_{nl} is an average value of $\kappa(r)$ over the radial part of the unperturbed particle wave function, and the spherical harmonics are averaged over the spin-angular part. The shape variables $\alpha_{\lambda\mu}$ are proportional to the multipole moments $\mathcal{M}_{\lambda\mu}^{(\text{core})}$ of the core, Eq. (5.27). The expectation value $\langle Y_{\lambda\mu} \rangle$ is proportional to that of the multipole moment of the particle. Therefore, we have effectively the *multipole–multipole interaction* between the core and the valence particles,

$$H^{(\text{particle–core})} = - \sum_{\lambda\mu} \kappa_{nl}^{(\lambda)} \mathcal{M}_{\lambda\mu}^{(\text{particle})} \mathcal{M}_{\lambda\mu}^{(\text{core})*}, \quad (12.16)$$

where the effective coupling constant for the multipolarity λ and for the particle on the orbit (nl) is

$$\kappa_{nl}^{(\lambda)} = \frac{4\pi\kappa_{nl}}{3A\langle r^\lambda \rangle_{nl} R_0^\lambda}. \quad (12.17)$$

This quantity is a smooth function of the quantum numbers (nl) and in many cases, as it can be tested by a direct calculation in the surface-delta model (12.6), can be considered as an effective constant.

The first-order expectation value (12.15) does not vanish for the term $\mu = 0$ only. In this order we can get only the *axial* deformation $\alpha_{\lambda 0}$ (no φ -dependence in (5.16)),

$$\Delta\epsilon_{nljm} = -\kappa_{nl} \sum_{\lambda} \sqrt{\frac{2\lambda+1}{4\pi}} \langle P_{\lambda} \rangle_{jm} \alpha_{\lambda 0} \quad (12.18)$$

where the Legendre polynomials are introduced. The restoring force for the core deformation in the liquid drop model (5.93) has the smallest value for the quadrupole case $\lambda = 2$. Let us consider this “softest” mode corresponding to the quadrupole–quadrupole interaction (12.16).

Inserting the quadrupole moment q_{zz} of the particle (small q refers to the single-particle contribution), the energy shift (12.18) can be presented as

$$\Delta\epsilon_{nljm} = -\kappa_{nl}\sqrt{\frac{5}{16\pi}} \frac{\langle jm|q_{zz}|jm\rangle}{\langle r^2 \rangle_{nl}} \alpha_{20}. \quad (12.19)$$

The matrix element of q_{zz} in (12.19) was found in (9.25). This gives the *splitting* of the magnetic substates of a j -level under quadrupole deformation of the core,

$$\Delta\epsilon_{nljm} = \kappa_{nl}\sqrt{\frac{5}{64\pi}} \frac{3m^2 - j(j+1)}{j(j+1)} \alpha_{20}. \quad (12.20)$$

There is still a double degeneracy of the states with projections $\pm m$ of the angular momentum on the deformation axis. It is related to time-reversal invariance and Kramers theorem. The pair of time-conjugate orbits for $j = 1/2$ does not split.

In the *prolate* field of the core, $\alpha_{20} > 0$, the orbits with small values of $|m| = 1/2$ have the lowest energy. This is just another formulation of the original Rainwater's idea: such orbits are elongated along the quantization axis, and they prefer to deform the field along their own directions. The sign of the interaction, $\kappa_{nl} > 0$, is defined by the attractive nucleon potential that leads to $dU/dr > 0$ in (12.3). For the *oblate* field, $\alpha_{20} < 0$, the orbits with the largest $|m| = j$ lower their energy trying to deform the field in the equatorial plane where these orbits are mostly concentrated.

Generalizing this result for several valence nucleons (still noninteracting among themselves), we get their total energy change due to the core deformation,

$$\Delta E^{(\text{particles})} = \zeta \alpha_{20}, \quad (12.21)$$

where the intensity of pressure from particles onto the core is measured by

$$\zeta = \sqrt{\frac{5}{64\pi}} \sum_{nljm} \kappa_{nl} \frac{3m^2 - j(j+1)}{j(j+1)} n_{nljm}. \quad (12.22)$$

The result strongly depends on the occupation numbers n_{nljm} for the orbits in the valence shell. This shows that the problem must be solved *self-consistently*: particles create the mean deformed field, which in turn defines their motion. Fully occupied j -levels do not contribute to the sum in (12.22). The contribution of the hole states is opposite to that of the particle states (Section 9.2). Therefore, the sign of ζ also depends on the valence shell occupation, $\zeta < 0$ for $\langle m^2 \rangle < (1/3)j(j+1)$.

The total potential energy of the drop together with the valence nucleons consists of the liquid drop energy (5.47) and the particle energy (12.22). For a given (though arbitrary) direction of the quantization axis, this determines the virtual deformation direction,

$$U(\alpha_{20}) = \frac{1}{2} C_2 \alpha_{20}^2 + \zeta \alpha_{20}, \quad (12.23)$$

where the symbol of the absolute value is omitted because $\alpha_{\lambda\mu=0}$ are real, see (5.17). The influence of the valence particles displaces the equilibrium position of the α_{20} -oscillator from the origin in (5.47) to the point of finite deformation

$$\langle \alpha_{20} \rangle = -\frac{\zeta}{C_2}. \quad (12.24)$$

The negative sign of ζ defines the prolate shape with $\langle \alpha \rangle > 0$, when the particle occupation creating the prolate shape is energetically favorable. In this sense, our approach delivers *consistent* results. For a softer core with a small restoring force coefficient C_2 , the resulting deformation is bigger.

It follows from the results of our adiabatic approximation that already near-magic nuclei should be deformed. Only doubly-magic nuclei are spherical in this extreme model. This conclusion disagrees with the empirical evidence, see Fig. 12.3. The manifestations of deformation appear in nuclei that are relatively remote from closed spherical shells. The model is definitely far from being completely satisfactory due to quite a few crude approximations: noninteracting valence particles, adiabaticity, and first-order perturbation theory. However, it is nice that now we see that there exists a natural mechanism for producing the self-consistent nuclear deformation.

Additional physical problems have to be mentioned at this point.

- If the resulting deformation (12.24) is too small, we are not able to distinguish between the static deformation of the mean field and its zero-point quantum vibrations, which are always present in the ground state wave function of the shape variables. This is especially important at small frequencies where the system is getting unstable and the zero-point amplitude grows.
- For sufficiently large deformation, perturbation theory does not work, and one should go beyond the first-order consideration. Nonaxial deformations become in principle competitive.
- In our consideration, the deformation axis was arbitrary. Actual theory must be formulated in such a way that the rotational invariance be preserved. The single-particle energies are split with respect to the axis related to the mean field rather than fixed in the laboratory. The probability distribution for the direction of the deformation in space is governed by the wave function corresponding to a certain value of the rotational angular momentum \mathbf{J} of the nucleus. For $J \neq 0$, the rotational energy depending on the deformation should be included into the collective Hamiltonian (12.23). It can change the equilibrium conditions and the mean field shape as a function of J .

12.5 Quadrupole Deformation in the Body-Fixed Frame

In the following, we concentrate on the practically most important case of quadrupole deformation, $\lambda = 2$. To describe single-particle motion in the deformed field, it is important to separate actual intrinsic deformation from the complications due to the specific choice of the coordinate frame.

The quadrupole deformation in general is described by *five complex amplitudes* $\alpha_{2\mu}$ subject to the conjugation condition (5.17). Therefore, we have five real parameters defining the deformation of the core and the interaction (12.4) of the particle with the deformed core. The core deformation is defined in (5.16) with respect to a *laboratory* frame that is chosen without any relation to the intrinsic properties of the system. We call this frame a *space-fixed* frame.

If we rotate the coordinate frame, the angles θ, φ of any given point are changed but the shape of the nucleus does not. A spherical function $Y_{2\mu}$ transforms into combinations of the same functions with various μ as it should be for any tensor operator implementing

an irreducible representation of the rotation group. After the rotation, the equation of an equipotential surface will look the same, but it will contain new combinations of the previous deformation parameters $\alpha_{2\mu}$. Of course, this frame is as good as the original frame. This means that there is an arbitrariness in the choice of the deformation parameters: only some of them do really characterize nuclear shape while the others reflect irrelevant information related to an accidental choice of the coordinate frame.

We can separate shape information selecting the frame related to the natural directions that exist in the deformed system (intrinsic, or *body-fixed* frame). The natural choice combines the coordinate axis with the main axis of the spheroidal deformation. An arbitrary three-dimensional rotation of the coordinate frame can be characterized by *three* parameters. For example, one can fix the direction of the rotation axis by its two angles in the space-fixed frame and then define the rotation angle around this axis. Another parametrization uses the three Euler angles. At present, we do not need to specify explicitly these three parameters. In any parametrization, the parameters have to be selected in a proper way in order to bring the coordinate frame into the new position coinciding with the coordinate frame of the main body-fixed axes. After that, we have only *two remaining deformation parameters* describing the *invariant shape* (A. Bohr, 1952).

In the rotated frame, the shape of the equipotential surfaces is written as in (5.16) but with the new parameters $a_{2\mu} \equiv a_\mu$ instead of the old parameters $\alpha_{2\mu}$,

$$\delta R(\theta', \varphi') \equiv R(\theta', \varphi') - R_0 = R_0 \sum_{\mu=-2}^2 a_\mu Y_{2\mu}(\theta', \varphi'), \quad (12.25)$$

where the angles θ' and φ' are taken with respect to the new frame. The variables a_μ are combinations of $\alpha_{2\mu}$ with the coefficients depending on three rotation angles. By specific choice of those angles, we put *three constraints* onto the deformation parameters. Let us make it explicitly.

Equation (12.25), with the use of the spherical functions $Y_{2\mu}$, reads

$$\begin{aligned} \frac{\delta R(\theta', \varphi')}{R_0 \sqrt{5/4\pi}} &= a_0 \left(\frac{3}{2} \cos^2 \theta' - \frac{1}{2} \right) \\ &+ \sqrt{\frac{3}{2}} \sin \theta' \cos \theta' (a_{-1} e^{-i\varphi'} - a_1 e^{i\varphi'}) \\ &+ \sqrt{\frac{3}{8}} \sin^2 \theta' (a_2 e^{2i\varphi'} + a_{-2} e^{-2i\varphi'}). \end{aligned} \quad (12.26)$$

Now we can choose the new axes as the main axes of the spheroidal deformation. The body should be invariant under reflection in three coordinate planes perpendicular to the main axes. Reflection in the equatorial plane $z' = 0$ changes the polar angle $\theta' \rightarrow \pi - \theta'$ without changing the azimuthal angle φ' . Then $\cos \theta'$ changes its sign. To have invariant shape, we need to get rid of the term linear in $\cos \theta'$. Therefore, we set

$$a_1 = 0, \quad a_{-1} = 0. \quad (12.27)$$

Reflection in the vertical plane $x' = 0$ does not change θ' but changes $\varphi' \rightarrow \pi - \varphi'$. Then the two terms corresponding to $Y_{2\pm 2}$ transform into each other. To keep the expression invariant, we set the third constraint

$$a_2 = a_{-2}. \quad (12.28)$$

We are left with the *two invariant parameters*, a_0 and a_2 , which characterize the intrinsic quadrupole deformation regardless of the orientation of the system.

12.6 Quadrupole Shape Variables

Following A. Bohr, we introduce the standard quadrupole shape variables β and γ according to

$$a_0 = \beta \cos \gamma, \quad a_2 = a_{-2} = \frac{1}{\sqrt{2}} \beta \sin \gamma. \quad (12.29)$$

Now nuclear shape in main deformation axes can be written as

$$\delta R(\theta', \varphi') = R_0 \sqrt{\frac{5}{4\pi}} \beta \left\{ \cos \gamma \left(\frac{3}{2} \cos^2 \theta' - \frac{1}{2} \right) + \frac{\sqrt{3}}{2} \sin \gamma \sin^2 \theta' \cos 2\varphi' \right\}. \quad (12.30)$$

In general, there is no axial symmetry because of the φ' -dependence in (12.30). Axial symmetry appears in the particular case when $a_2 = a_{-2} = 0$, or $\sin \gamma = 0$. Thus, the parameter γ regulates the degree of nonaxiality. As for the parameter β , it defines the common scale of the deformation.

Being intrinsic characteristics, the deformation parameters β and γ can be expressed in the invariant way in terms of the shape variables $\alpha_{2\mu}$ taken in any frame. Indeed, let us construct the invariant combinations using the variables $\alpha_{2\mu}$. These variables carry the angular momentum 2 and its projection μ (see Section 11.5); now we construct the tensor products of these variables which are invariant under rotations.

The simplest (*bilinear*) combination $C^{(2)}$ is readily built following Eq. (11.72),

$$C^{(2)} = \sum_{\mu} (-)^{2-\mu} \alpha_{2\mu} \alpha_{-2-\mu} \equiv [\alpha^2]_{00}. \quad (12.31)$$

Using the complex conjugation condition (5.17), we get

$$C^{(2)} = \sum_{\mu} |\alpha_{\mu}|^2. \quad (12.32)$$

In the body-fixed frame attached to the main axes ($\alpha_{2\mu} \rightarrow a_{\mu}$), this invariant quantity is equal to

$$C^{(2)} = (a_0^2 + a_2^2 + a_{-2}^2) = \beta^2. \quad (12.33)$$

Thus, β^2 is an *invariant* of the global deformation. The liquid drop potential energy (5.47) of small quadrupole deformation is simply proportional to β^2 .

Going further, we can construct the next (*trilinear*) invariant using the definition of the $3j$ -symbols (11.75), which allows to express $C^{(3)}$ in the fully symmetric form with respect to three variables α ,

$$C^{(3)} = \sum_{\mu\mu'\mu''} \begin{pmatrix} 2 & 2 & 2 \\ \mu & \mu' & \mu'' \end{pmatrix} \alpha_{2\mu} \alpha_{2\mu'} \alpha_{2\mu''}. \quad (12.34)$$

Problem 12.2 Show that (12.34) is the only possible invariant of the third order and calculate its value in the body-fixed frame.

Solution

This is equivalent to the question of how many states with total angular momentum 0 are possible in a system of three identical quadrupole bosons. From the direct counting of the symmetric states [QP, I, Problem 18.1], we know that the allowed states are those with angular momenta 0, 2, 3, 4 and 6, each of them appearing only once. In the intrinsic frame specified by Eqs. (12.27)–(12.29), we obtain

$$C^{(3)} = -\sqrt{\frac{2}{35}} \beta^3 \cos 3\gamma. \quad (12.35)$$

Since we have at our disposal only two shape parameters and they uniquely define the invariants $C^{(2)}$ and $C^{(3)}$, we made a conclusion that all possible invariants of higher orders are functions of those two, rather than new, independent quantities. Therefore, we can formulate an important result that any rotationally invariant function of quadrupole variables $\alpha_{2\mu}$ is in fact a function of two invariants β^2 and $\beta^3 \cos 3\gamma$. For example, if we are interested in the higher terms of potential energy beyond the simple harmonic approximation (5.47), we can write the series of *anharmonic* terms

$$\begin{aligned} H_{\text{anharm}} = & X_3 \beta^3 \cos 3\gamma + X_4 \beta^4 \\ & + X_5 \beta^5 \cos 3\gamma + X_6 \beta^6 + X'_6 \beta^6 \cos^2 3\gamma + \dots \end{aligned} \quad (12.36)$$

Of course, here we still limit ourselves to the quadrupole degree of freedom and ignore possible momentum-dependent higher order terms.

12.7 Variety of Quadrupole Shapes

The functions of the nonaxiality parameter γ are necessarily periodic in this variable with the period 120° . This is related to the fact that the body-fixed frame is not defined uniquely. There exist discrete transformations leaving the system invariant but changing the parameters, namely the angles of the body-fixed frame with respect to the space-fixed frame and parameter γ ; the parameter β is fixed by the global deformation. The choice of parameters is made for the specific definition of the main axes that can be changed.

The available symmetry transformations are $3! = 6$ permutations of the main axes x', y', z' and $2^3 = 8$ possibilities of selecting the positive direction along each axis. Therefore, we have 48 discrete symmetry operations. If we restrict ourselves to the *right-oriented* triplets of unit coordinate vectors \mathbf{e}_i ,

$$[\mathbf{e}_{x'} \times \mathbf{e}_{y'}] = +\mathbf{e}_{z'} \Rightarrow [\mathbf{e}_i \times \mathbf{e}_j] = \epsilon_{ijk} \mathbf{e}_k, \quad (12.37)$$

then the direction of the third axis is defined by the choice of the directions for the first two axes, and the number of symmetry operations is reduced to 24. This symmetry group being isomorphic to the group of rotations transforming a cube into itself is also a frequent guest in theory of molecules and crystals.

To understand the geometry of the quadrupole shapes, let us write down the equations for the deformation (12.30) along the main axes, expressing it in terms of the ratio

$$r(\theta', \varphi') \equiv \sqrt{\frac{4\pi}{5}} \frac{\delta R(\theta', \varphi')}{R_0}. \quad (12.38)$$

The z' -axis, $\theta' = 0$, coincides with the polar axis. The deformation along this axis, which we call axis 3, is

$$r_3 = r(0, 0) = \beta \cos \gamma. \quad (12.39)$$

Analogously we get for the perpendicular, $\theta' = \pi/2$, axes $x' \equiv 1$ and $y' \equiv 2$,

$$r_1 = r\left(\frac{\pi}{2}, 0\right) = \beta \left[-\frac{1}{2} \cos \gamma + \frac{\sqrt{3}}{2} \sin \gamma \right], \quad (12.40)$$

$$r_2 = r\left(\frac{\pi}{2}, \frac{\pi}{2}\right) = -\beta \left[\frac{1}{2} \cos \gamma + \frac{\sqrt{3}}{2} \sin \gamma \right]. \quad (12.41)$$

For any deformation,

$$r_1 + r_2 + r_3 = 0, \quad (12.42)$$

which shows that, in the linear approximation, the nuclear volume is preserved by the deformation.

The equations for the deformation along the main axes can be jointly expressed as

$$r_k = \beta \cos \left(\gamma - k \frac{2\pi}{3} \right), \quad k = 1, 2, 3. \quad (12.43)$$

In particular, the axially symmetric (around the 3 axis) case of $\gamma = 0$ gives

$$r_3 = \beta, \quad r_1 = r_2 = -\frac{1}{2} \beta. \quad (12.44)$$

The sign of β is defined in such a way that $\beta > 0 (< 0)$ characterizes the prolate (oblate) deformation with respect to the 3 axis. Taking, instead of $\gamma = 0$, the value of this parameter equal to $\gamma = \pi/3$, we would have

$$r_2 = -\beta, \quad r_1 = r_3 = \frac{1}{2} \beta. \quad (12.45)$$

Now the axis 2 is the symmetry axis. For $\beta < 0$, this is the same axially symmetric shape as in (12.43) but with the renamed axes. If we decide to keep always $\beta > 0$, the shape in (12.44) is prolate while that in (12.45) is oblate. Therefore, it might be convenient to consider β as a positive radial variable and γ as an azimuthal angle in the deformation plane.

From (12.43), we see that the change $\gamma \rightarrow \gamma - 2\pi/3$ simply interchanges the axes in a cyclic way. If, by some reason of convenience, we prefer to keep the numeration of the axes, the whole range 2π of the variable γ contains six regions by 60° each. The boundary rays between the sectors correspond to the axial symmetry around different axes with prolate or oblate shape. The change of symmetry in the plane $r(\beta, \gamma)$ is shown in Figure 12.2.

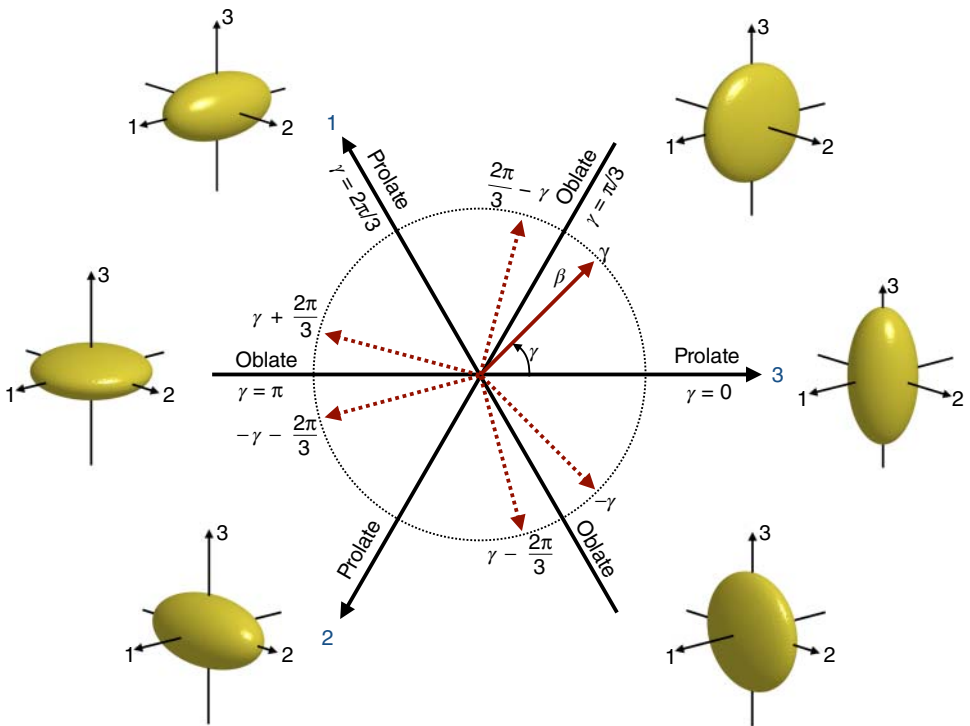


Figure 12.2 A polar diagram in the deformation plane (β, γ) . Components of a radius vector of a point (β, γ) along three nonorthogonal axes show the values $r_k(\beta, \gamma)$. Any quadrupole shape can be identified within a region $\beta \geq 0$ and $0 \leq \gamma \leq \pi/3$; on a full polar plane, symmetry, transformations allow for six equivalent representations as illustrated. Values of γ multiples of 60° correspond to restoration of axial symmetry along axis whose number is indicated and direction points toward prolate shape; the shapes are illustrated.

12.8 Empirical Deformation

Different equivalent parameterizations of deformation are also used in the literature. For axial symmetry (12.44), the parameter δ is defined via the (mass rather than electric charge) quadrupole moment Q_0 in the body-fixed frame and the mean square radius $\langle r^2 \rangle$ as

$$Q_0 = \frac{4}{3}A\langle r^2 \rangle\delta; \quad (12.46)$$

the electric quadrupole moment in the same approximation of the uniform deformation differs from (12.46) by a factor Z/A .

The relation between the quadrupole tensor Q_μ and the general multipole moment $\mathcal{M}_{2\mu}$, Eq. (5.25), is given by

$$Q_\mu = \sqrt{\frac{16\pi}{5}}\mathcal{M}_{2\mu}. \quad (12.47)$$

In the linear approximation (small deformations), the multipole moment \mathcal{M}_{20} is expressed, Eq. (5.27), through the deformation parameter α_{20} that reduces to β ,

Eq. (12.29), in the body-fixed frame for the axial symmetry case. As a result, we have

$$Q_0 = \sqrt{\frac{16\pi}{5}} \mathcal{M}_{20} = \sqrt{\frac{16\pi}{5}} \frac{3}{4\pi} A R_0^2 \beta. \quad (12.48)$$

In the same approximation of small deformations, $\langle r^2 \rangle = (3/5)R_0^2$, which can be considered as a definition of the radius R_0 that was used starting with Eq. (12.25). Finally, the connection between β and δ reads

$$\delta = \sqrt{\frac{45}{16\pi}} \beta = 0.95\beta. \quad (12.49)$$

The parameter δ has a direct meaning being related to the nuclear anisotropy measured by the quadrupole moment. For axial deformations preserving the volume or density, the mean square radius in (12.46) is defined from $\langle x'^2 + y'^2 + z'^2 \rangle$ that is proportional to the combination $R_{\parallel}^2 + 2R_{\perp}^2$ of squared longitudinal (z') and transverse (x', y') nuclear radii. The quadrupole moment Q_0 is given by another combination, $\langle 3z'^2 - r^2 \rangle$, which is proportional to $2(R_{\parallel}^2 - R_{\perp}^2)$. Therefore, the definition (12.46) is equivalent to

$$\delta = \frac{3}{2} \frac{R_{\parallel}^2 - R_{\perp}^2}{R_{\parallel}^2 + 2R_{\perp}^2}. \quad (12.50)$$

In the limit of small deformations, we can use the average radius $R_0 \approx (1/3)(R_{\parallel} + 2R_{\perp})$ and the elongation $\Delta R = R_{\parallel} - R_{\perp}$ to get from (12.50)

$$\delta \approx \frac{\Delta R}{R_0}. \quad (12.51)$$

We will not discuss here how one can obtain the intrinsic deformation from the experiment. To do it, we need to define the transition from the space-fixed frame to the body-fixed frame more precisely. We just mention a variety of techniques that include measurements of electrostatic moments using electromagnetic radiation, Coulomb excitation, electron scattering, hyperfine splitting in electron and muonic atomic levels; strongly interacting probes such as protons, neutrons, and alpha-particles can also be used to probe mass moments. Here, we show the systematics of the quadrupole deformations near the ground state. In Figure 12.3, the map of deformations is shown that comes from theoretical predictions well adjusted to reproduce abundant experimental data. The shell boundaries where nuclei tend to be spherical are clearly seen. For heavy nuclei, away from shell closures, the deformation parameter exhibits a rather smooth behavior, and nearly all nuclei tend to have prolate shapes. Shapes of light nuclei are rather irregular, which is generally due to cluster effects and another physics beyond the mean field.

As we mentioned, the spherical shell model turns out to be useless in the regions of mass number $150 \leq 190$ (rare-earth elements) and $A \geq 220$ (actinides) as well as in a number of smaller islands of the nuclide chart. In these areas, the nuclei are deformed so that single-particle motion differs from that in a spherical field [4]. Figure 12.4 shows the δ parameter related to the intrinsic quadrupole moment (12.46) that can be extracted from experiment (see [2, 3] and references therein). The typical value of δ in the region of the well-developed deformation is 0.3. This is still rather small keeping the linear approximation reasonable. The deformations less than 0.1 correspond to ill-defined shape

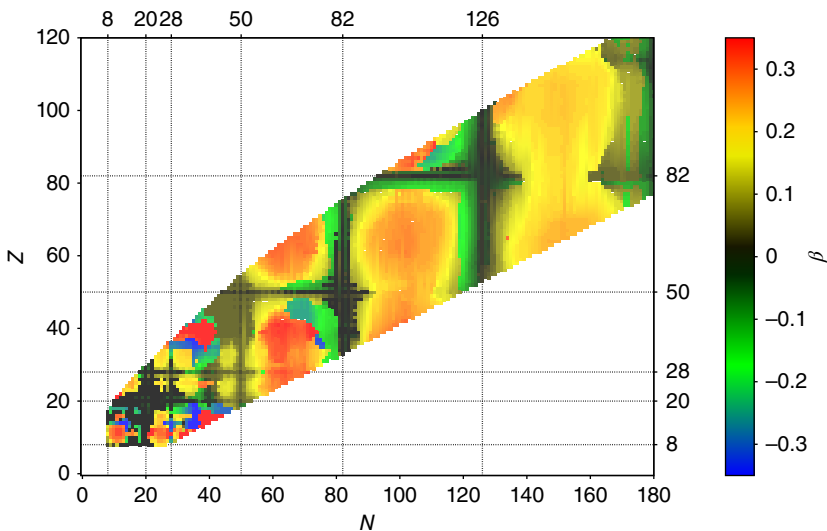


Figure 12.3 Nuclear chart showing quadrupole deformation parameters β as predicted by the model discussed in Ref. [3].

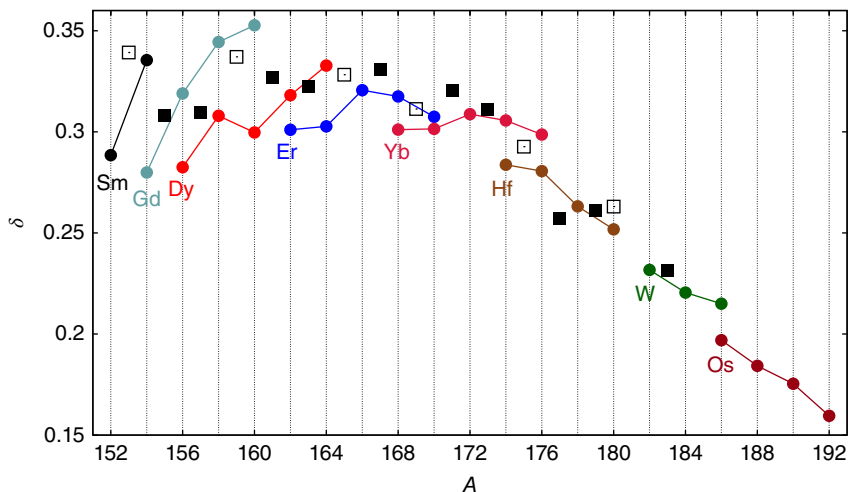


Figure 12.4 Quadrupole deformation parameters δ for rare-earth elements: even–even nuclei (circles), odd–neutron nuclei (black squares), and odd–proton nuclei (open squares).

with large zero-point vibrations. The majority of significant cases among stable nuclei indicate *prolate* deformation, $\delta > 0$, which is of the same order for even–even and odd- A nuclei [5, 6].

Larger deformations were observed in many light nuclei (Figure 12.3). They are caused by big admixtures to the wave functions of components built of alpha-clusters. Thus, ^9Be has the value $\delta = 1.2$. This nucleus has distinct quasimolecular structure. The last neutron stabilizes the decaying two-alpha construction of ^8Be similar to the molecular

ion H_2^- , where the collectivized electron binds two protons together (again a Borromean system). The geometry of this wave function implies the strong intrinsic deformation.

The average deformation $\delta \approx 0.3$ corresponds to the ratio $1 + \delta = 1.3$ of the longitudinal to transverse axes. At high angular momenta, very large deformations with the axis ratio $2:1$ were observed. Such nuclei are called *superdeformed*. The superdeformation becomes energetically favorable [7] due to the special shell effects for this “resonance” axis ratio. The *hyperdeformation* with the axis ratio $3:1$ was also predicted but not reliably observed yet. Two-dimensional analogs of such deformed structures exist in physics of cold atoms in harmonic oscillator traps [8]. Of course, the linear approximation with respect to deformation parameters becomes invalid in all cases of strong deformation.

In a general case of *triaxial* deformation, keeping the same definition (12.49), we have instead of (12.46) two components of the intrinsic quadrupole moment corresponding to the parametrization (12.29),

$$Q_0 = \frac{4}{3} A \langle r^2 \rangle \delta \cos \gamma, \quad (12.52)$$

and

$$Q_2 \equiv \sqrt{\frac{16\pi}{5}} \frac{1}{2} (\mathcal{M}_{22} + \mathcal{M}_{2-2}) = \frac{4}{3} A \langle r^2 \rangle \delta \frac{1}{\sqrt{2}} \sin \gamma. \quad (12.53)$$

Knowing the intrinsic quadrupole moments, we extract the parameter of nonaxiality via

$$\tan \gamma = \sqrt{2} \frac{Q_2}{Q_0}. \quad (12.54)$$

Transforming the spherical functions in the definition of the multipole moments $\mathcal{M}_{2\mu}$ into Cartesian coordinates, we express the intrinsic quadrupole moments in terms of the expectation values of squared particle coordinates along the main deformation axes,

$$Q_0 = \sum_a \langle 2z_a'^2 - x_a'^2 - y_a'^2 \rangle, \quad (12.55)$$

$$Q_2 = \sqrt{\frac{3}{2}} \sum_a \langle x_a'^2 - y_a'^2 \rangle. \quad (12.56)$$

Of course, Q_2 vanishes in the case of axial symmetry. Experimentally, the triaxial deformation of the ground states is observed [9] in osmium isotopes, on the way from typical axially deformed rare-earth nuclei to the spherical region close to the doubly-magic lead isotope.

Features of triaxiality are observed in ^{24}Mg . In the simplest spherical oscillator shell model, this nucleus has the ^{16}O core and eight valence nucleons in the $N = 2$ oscillator shell. Core polarization and other residual interactions favor the ground state structure where one neutron pair with total zero spin is placed in a state with Cartesian oscillator quantum numbers $n_x = n_y = 0$, $n_z = 2$, and the second $S = 0$ neutron pair in a state $n_x = 1$, $n_y = 0$, $n_z = 1$. The configuration of protons is identical to that of neutrons leading to a ground state formally classified by $SU(3)$ symmetry as $(\lambda, \mu) = (8, 4)$ (see Section 9.6). Nucleons of the core do not contribute to deformation. Using Eq. (8.10) in Eqs. (12.55) and (12.56), we obtain

$$Q_0 = \frac{\hbar}{M\omega_o} (2\lambda + \mu), \quad Q_2 = \sqrt{\frac{3}{2}} \frac{\hbar}{M\omega_o} \mu, \quad (12.57)$$

where the axes are selected in such a way that $\lambda = n_z - n_x$ and $\mu = n_x - n_y$. As a result, we can estimate triaxiality of the state as

$$\tan \gamma = \frac{\sqrt{3} \mu}{2\lambda + \mu}. \quad (12.58)$$

For ^{24}Mg , this gives $\gamma \approx 19^\circ$. It is important, see Eqs. (9.46) and (9.47), that spatial rotations are a part of $SU(3)$ group, which allows us to consider the same irreducible representation of the $SU(3)$ group in the space-fixed and body-fixed frame. This example highlights the possibility of a deformed many-body state emerging in a spherical basis, which will be discussed later.

12.9 Single-Particle Quantum Numbers

Our next problem is to populate the deformed mean field by nucleons and construct the corresponding analog of the shell model. Here we assume that the mean nuclear field acquired a static *axially symmetric* quadrupole deformation. In the adiabatic approximation, the particles are moving in an external deformed field and, for not very large deformations, the potential acting onto the particle can be presented as a sum of the spherical and linear deformation parts (12.4). The main new effects onto single-particle motion are related to the violation of spherical symmetry.

In the first nonvanishing approximation (12.20), the single-particle j -levels are split according to the value of the projection of the angular momentum onto the symmetry axis of the potential. This projection is frequently denoted as Ω but we keep the same notation m as for the spherical field remembering that this is the projection onto the *body-fixed* axis coinciding with the symmetry axis of the deformed field. Also we can now omit primes in the notations for the particle coordinates in the body-fixed frame.

The first-order perturbative estimate can be insufficient at realistic deformation. The quadrupole perturbation has the form (12.4)

$$H_{\text{coupl}} = -\kappa(r) \sqrt{\frac{5}{4\pi}} \beta P_2(\cos \theta), \quad (12.59)$$

where the radial dependence $\kappa(r) = r(dU/dr)$ comes from the deformation of the density distribution that induces, through the short-range forces, the deformation of the potential. Apart from the splitting of j -levels, the nonspherical field (12.59) is also mixing different j -levels of the same parity with the obvious selection rules $|\Delta j| \leq 2$; $\Delta \ell = 0, \pm 2$. The resulting single-particle orbits in the deformed field are complicated superpositions of the spherical shell-model states. The only quantum numbers which, strictly speaking, survive after onset of axial quadrupole deformation are the projection m and parity.

Since the time-reversal invariance is not violated, the Kramers theorem states that the double degeneracy of the states $\pm m$ still holds. Due to the Kramers degeneracy, particles occupy single-particle orbits in the deformed but time-reversal invariant potential *pairwise*, neutrons and protons independently. Therefore, we expect to have zero spin in the ground state of even–even nuclei (another argument in favor of this result is the residual pairing interaction, Chapter 13). For an odd mass number, the last unpaired

particle on the orbit with $j_z = m$ is responsible for the total spin projection onto the symmetry axis that is usually called K : in this case, $K = m$.

It seems natural to identify in this case the single-particle angular momentum with the total angular momentum of the nucleus (nuclear spin). However, we should remember that the whole consideration of the deformed mean field takes place in the *body-fixed* frame. We should know, apart from the intrinsic wave function, the orientational wave function of the deformed body. This wave function carries the rotational angular momentum that, along with the intrinsic angular momentum of the particles, comprises the total nuclear spin. Nevertheless, our original guess was correct. Rotation as a whole requires additional energy growing with the magnitude of the rotational angular momentum. If the minimum energy corresponds to the zero rotational angular momentum (uniform distribution of the deformation axes in space), the intrinsic moment is the only one contributing to the nuclear spin. Indeed, the even–even nuclei still have the zero ground state spin, while the spin of deformed odd- A nuclei, as a rule, agrees with the extreme single-particle deformed shell model.

With no spin–orbit coupling, the orbital momentum projection ℓ_z and the spin projection s_z would be conserved separately as well as their sum j_z . This would give rise to the quantum numbers that are usually called, as in molecular physics, $\ell_z = \Lambda$ and $s_z = \Sigma$ so that $j_z = m = \Lambda + \Sigma$.

12.10 Anisotropic Harmonic Oscillator

This natural generalization of the spherical harmonic oscillator for the case of the quadrupole deformation is the simplest analytically solvable model for the deformed mean field.

The parabolic spherical potential $U(r) = (1/2)M\omega_0^2 r^2$ gives in Eq. (12.59) $\kappa(r) = 2U(r)$, and

$$H_{\text{coupl}} = -M\omega_0^2 r^2 \sqrt{\frac{5}{4\pi}} \beta P_2(\cos \theta) = -\frac{2}{3} \delta M\omega_0^2 r^2 P_2(\cos \theta). \quad (12.60)$$

Adding the nonperturbed spherical term and expressing $r^2 P_2(\cos \theta)$ in Cartesian coordinates, we come to the potential of the anisotropic harmonic oscillator,

$$U(r) = \frac{M}{2} (\omega_x^2 x^2 + \omega_y^2 y^2 + \omega_z^2 z^2), \quad (12.61)$$

where for our axially symmetric deformation

$$\omega_x^2 = \omega_y^2 \equiv \omega_\perp^2 = \omega_0^2 \left(1 + \frac{2}{3}\delta\right), \quad \omega_z^2 \equiv \omega_\parallel^2 = \omega_0^2 \left(1 - \frac{4}{3}\delta\right) \quad (12.62)$$

but one can also consider the more general case with no axial symmetry when all three frequencies ω_k are different. From (12.62), we can find the deformation parameter in terms of the oscillator frequencies, compare Eq. (12.50),

$$\delta = \frac{3}{2} \frac{\omega_\perp^2 - \omega_\parallel^2}{\omega_\parallel^2 + 2\omega_\perp^2}. \quad (12.63)$$

The unperturbed frequency ω_0 in (12.62) is still given by the same expression (8.16) as in spherical nuclei.

The separation of variables in the Cartesian coordinates determines the single-particle energy spectrum labeled by numbers of quanta n_x, n_y , and n_z along main axes, Eq. (8.18), a number of quanta n_x, n_y , and n_z along different main axes,

$$\epsilon(n_x, n_y, n_z) = \hbar \left[\omega_x \left(n_x + \frac{1}{2} \right) + \omega_y \left(n_y + \frac{1}{2} \right) + \omega_z \left(n_z + \frac{1}{2} \right) \right]. \quad (12.64)$$

In the axially symmetric case, only two quantum numbers, $n_{\parallel} = n_z$ and $n_{\perp} = n_x + n_y$, enter the energy expression,

$$\epsilon(n_{\parallel}, n_{\perp}) = \hbar \left[\omega_{\parallel} \left(n_{\parallel} + \frac{1}{2} \right) + \omega_{\perp} (n_{\perp} + 1) \right]. \quad (12.65)$$

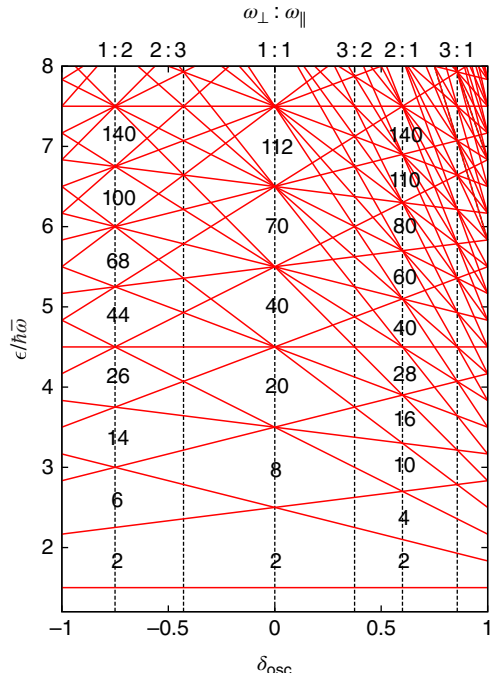
Due to the axial symmetry, there is still a degeneracy. The states with the same n_{\perp} and different distribution of quanta between the x - and y -axes can be labeled by the orbital momentum projection Λ .

Problem 12.3 For an axially symmetric deformed harmonic oscillator field, find a number of degenerate single-particle orbits for a given $n_{\perp} = n_x + n_y$. Using the symmetry arguments, determine the allowed values of the orbital momentum projection onto the symmetry axis $\ell_z = \Lambda$, and check that the count using n_{\perp} and Λ gives the same degree of degeneracy.

The full picture of the single-particle spectrum for the anisotropic axially symmetric harmonic oscillator (12.65) has remarkable structure shown in Figure 12.5. The energy terms

$$\epsilon(n_{\parallel}, n_{\perp}) = \hbar \bar{\omega} \left[N + \frac{3}{2} - \frac{1}{3} \delta_{\text{osc}} (2n_{\parallel} - n_{\perp}) \right] \quad (12.66)$$

Figure 12.5 Single-particle levels (energy in units of $\hbar \bar{\omega}$) for the axially symmetric harmonic oscillator field as a function of the oscillator deformation parameter (12.67). A similar picture for the two-dimensional oscillator is discussed in relation to quantum dots in Ref. [8]; see also [QP, I, 11.4].



are *linear* functions of the oscillator deformation parameter starting in the spherical field at the degenerate value (8.4) for the main quantum number $N = n_{\parallel} + n_{\perp}$ and the mean frequency $\bar{\omega} = (1/3)(\omega_{\parallel} + 2\omega_{\perp})$,

$$\delta_{\text{osc}} = \frac{\omega_{\perp} - \omega_{\parallel}}{\bar{\omega}} \equiv 3 \frac{\omega_{\perp} - \omega_{\parallel}}{2\omega_{\perp} + \omega_{\parallel}}. \quad (12.67)$$

The central part of Figure 12.5 gives the normal isotropic harmonic oscillator shell structure as in Figure 8.4, left. It is marked by the strong degeneracy and large gaps between the major shells. Although not that bright, the shell structure revisits at special values of the deformation parameter. These values correspond to the ratio of frequencies $\omega_{\perp}/\omega_{\parallel}$ equal to that of simple prime numbers ($2:1, 1:2, 3:1$, etc.). Corresponding deformation parameters (12.67) are $\delta_{\text{osc}} = 0.6, -0.75, 0.86$, and so on. We already mentioned that the case $2:1$ was discovered as *superdeformation*; there is also some evidence for *hyperdeformation* corresponding to the ratio $3:1$. The new magic numbers in the case of the superdeformed ($2:1$) oscillator are $2, 4, 10, 16, 28, 40, 60, 80, 110, 140, \dots$. As mentioned in Section 8.10, the quantum shell structure in some sense is a precursor of the periodic trajectories in classical mechanics. It arises due to the *resonances* between the different degrees of freedom.

Problem 12.4 Consider a system of many ($A \gg 1$) identical fermions of mass M in the field of the anisotropic harmonic oscillator with an arbitrary set of frequencies $\omega_k, k = x, y, z$. Let particles occupy the *lowest states* (12.64). Their distribution can be described by the sums over the occupied orbits of the oscillator quanta along each axis,

$$W_k = \sum_{\text{occupied}} \left(n_k + \frac{1}{2} \right), \quad k = x, y, z. \quad (12.68)$$

In the following calculations, you may substitute sums by integrals and consider n_k as large numbers (what is the accuracy of such an approximation?).

- Calculate the Fermi energy ϵ_F .
- Show that the mean square values of the coordinates x_k and velocities $v_k = p_k/M$ of the particles are equal, respectively, to

$$\sum_{\text{occupied}} \langle x_k^2 \rangle = \frac{\hbar}{M\omega_k} W_k \quad (12.69)$$

and

$$\sum_{\text{occupied}} \langle v_k^2 \rangle = \frac{\hbar\omega_k}{M} W_k. \quad (12.70)$$

- Calculate the sums W_k and show that they satisfy the condition

$$W_x \omega_x = W_y \omega_y = W_z \omega_z = C; \quad (12.71)$$

find the value of the constant C . Discuss the physical meaning of these conditions from the viewpoint of distribution of coordinates and distribution of velocities.

- Show that the self-consistent deformation parameters of a configuration with given values of sums W_k is given by

$$\delta \cos \gamma = \frac{3}{4} \frac{2W_z^2 - W_x^2 - W_y^2}{W_x^2 + W_y^2 + W_z^2} \quad \text{and} \quad \tan \gamma = \frac{\sqrt{3}(W_x^2 - W_y^2)}{2W_z^2 - W_x^2 - W_y^2}. \quad (12.72)$$

Solution

The semiclassical level density for the anisotropic harmonic oscillator is given (see Problem 8.3 and [QP, I, Problem 3.11]) by

$$\nu(\epsilon) = \frac{g\epsilon^2}{2\hbar^3\omega_x\omega_y\omega_z}. \quad (12.73)$$

The integral of the level density up to Fermi energy ϵ_F is equal to the total number of particles A ,

$$A = \frac{g}{6\hbar^3\omega_x\omega_y\omega_z} \epsilon_F^3. \quad (12.74)$$

This determines Fermi energy in terms of the average frequency

$$\bar{\omega} = (\omega_x\omega_y\omega_z)^{1/3}, \quad (12.75)$$

$$\epsilon_F = \hbar\bar{\omega}\left(\frac{6}{g} A\right)^{1/3}. \quad (12.76)$$

This result is in agreement with the standard estimates for the harmonic oscillator, which show that the frequency should scale as $A^{-1/3}$: then ϵ_F becomes A -independent as a property of the Fermi gas representing nuclear matter.

In the semiclassical approximation ($n_k \gg 1/2$),

$$W_x = g \int dn_x dn_y dn_z n_x \Theta(\epsilon_F - \hbar(\omega_x n_x + \omega_y n_y + \omega_z n_z)) \quad (12.77)$$

where we use the step function $\Theta(a)$ equal to zero for negative values of the argument a and one for $a > 0$. With the transformation to the *stretched coordinates*, $\hbar\omega_k n_k = \xi_k$, we obtain

$$W_x = \frac{g}{\hbar^4\bar{\omega}^3\omega_x} \int d\xi_x d\xi_y d\xi_z \xi_x \Theta(\epsilon_F - \xi_x - \xi_y - \xi_z). \quad (12.78)$$

The restriction of the integration area,

$$0 \leq \xi_x + \xi_y + \xi_z \leq \epsilon_F, \quad (12.79)$$

is symmetric with respect to all three coordinates. Therefore, the integrals in (12.78) would have the same value for y or z sums, and we can make the substitution

$$\xi_x \Rightarrow \frac{1}{3}(\xi_x + \xi_y + \xi_z) \quad (12.80)$$

in the integrand (12.78),

$$W_x = \frac{g}{3\hbar^4\bar{\omega}^3\omega_x} I(\epsilon_F), \quad (12.81)$$

reducing the problem to that of calculating the integral

$$I(\epsilon) = \int d\xi_x d\xi_y d\xi_z (\xi_x + \xi_y + \xi_z) \Theta(\epsilon - \xi_x - \xi_y - \xi_z) \quad (12.82)$$

that depends on the parameter ϵ (we need the value of I at $\epsilon = \epsilon_F$). Since the derivative of $\Theta(a)$ is $\delta(a)$, we can use the property of the delta-function to obtain

$$\frac{dI}{d\epsilon} = \epsilon \int d\xi_x d\xi_y d\xi_z \delta(\epsilon - \xi_x - \xi_y - \xi_z). \quad (12.83)$$

The new integral in (12.83) is proportional to the level density $v(\epsilon)$ that, after the same transformation of variables, takes the form

$$v(\epsilon) = \frac{g}{\hbar^3 \bar{\omega}^3} \int d\xi_x d\xi_y d\xi_z \delta(\epsilon - \xi_x - \xi_y - \xi_z). \quad (12.84)$$

On the other hand, the level density was calculated as in Eq. (12.73). This gives

$$\frac{dI}{d\epsilon} = g \frac{\epsilon^3}{2} \Leftrightarrow I(\epsilon_F) = g \frac{\epsilon_F^4}{8}. \quad (12.85)$$

Thus, the sum we are interested in turned out to be equal to

$$W_x = \frac{g \epsilon_F^4}{24 \hbar^4 \bar{\omega}^3 \omega_x}. \quad (12.86)$$

This proves the statement of the problem,

$$W_k = \frac{C}{\omega_k}, \quad C = \frac{1}{4} \left(\frac{6}{g} \right)^{1/3} \bar{\omega} A^{4/3} = \frac{\epsilon_F A}{4 \hbar}, \quad (12.87)$$

where the value (12.76) of Fermi energy was used. This result is valid as well if one does not neglect the zero point energies $\hbar \omega_k / 2$.

For a stationary state $|n_k\rangle$ of a one-dimensional harmonic oscillator with a frequency ω_k , the simple quantum mechanical calculation determines the expectation values for mean square position, momentum, and velocity of a particle (no summation over k):

$$\langle x_k^2 \rangle = \frac{\langle p_k^2 \rangle}{M^2 \omega_k^2} = \frac{\langle v_k^2 \rangle}{\omega_k^2} = \frac{\hbar}{M \omega_k} \left(n_k + \frac{1}{2} \right). \quad (12.88)$$

This gives immediately

$$\sum_{\text{occupied}} \langle x_k^2 \rangle = \frac{\hbar}{M \omega_k} W_k = \frac{\hbar C}{M \omega_k^2}, \quad (12.89)$$

$$\sum_{\text{occupied}} \langle v_k^2 \rangle = \frac{\hbar \omega_k}{M} W_k = \frac{\hbar C}{M}. \quad (12.90)$$

The results (12.89) and (12.90) are typical for the *statistical equilibrium*: the coordinate distribution ensures that the highest potential energy of occupied orbits be the same in all directions; similarly, the kinetic energy is also the same. As the masses of particles are isotropic, the velocity distribution is isotropic as well.

Problem 12.5 Looking at Figure 12.5, find the lowest configuration of ${}^{20}\text{Ne}$. For this configuration, calculate sums W_k , the deformation parameter δ , and the electric quadrupole moment (the experimental value is $Q_0 = 54 \text{ fm}^2$).

Problem 12.6 Assuming that the lowest configuration of the valence nucleons in ${}^{24}\text{Mg}$ contains two filled orbits ($n_x = n_y = 0, n_z = 2$) and ($n_x = 1, n_y = 0, n_z = 1$) above the core ${}^{16}\text{O}$, calculate the ratio of the mean square lengths $\langle x^2 \rangle : \langle y^2 \rangle : \langle z^2 \rangle$, the deformation parameters δ and γ , and the intrinsic quadrupole moments (12.55) and (12.56). The experiment gives $Q_0 = 57 \text{ fm}^2$.

Solution

The intrinsic quadrupole moments are expressed in terms of the sums (12.68):

$$Q_0 = 2X_z - X_x - X_y = \frac{\hbar}{m} \left(2 \frac{W_z}{\omega_z} - \frac{W_x}{\omega_x} - \frac{W_y}{\omega_y} \right), \quad (12.91)$$

$$Q_2 = \sqrt{\frac{3}{2}} \left(\frac{W_x}{\omega_x} - \frac{W_y}{\omega_y} \right). \quad (12.92)$$

For ^{24}Mg with the suggested distribution of particles over deformed orbitals, these sums are equal to

$$W_x = 20, \quad W_y = 16, \quad W_z = 28, \quad (12.93)$$

where the spin–isospin factor $g = 4$ was included and we did not neglect the zero point vibration contribution $1/2$ because here the quantum numbers are not large. Using the semiclassical estimate (12.87) for the constant C , which of course cannot be very accurate for such a light nucleus, we obtain the oscillator frequencies

$$\hbar\omega_x = \frac{\hbar C}{W_x} \approx \frac{\epsilon_F A}{4W_x} = 10.8 \text{ MeV}, \quad (12.94)$$

$$\hbar\omega_y = 13.5 \text{ MeV}, \quad \hbar\omega_z = 7.7 \text{ MeV}. \quad (12.95)$$

Thus, this configuration of the ^{24}Mg nucleus possesses a significant triaxial deformation. Then we obtain from (12.91), $Q_0 = 175 \text{ fm}^2$ and $Q_2 = 34 \text{ fm}^2$. The image of shape can be provided by the ratios

$$\langle x^2 \rangle : \langle y^2 \rangle : \langle z^2 \rangle \approx 1 : 0.6 : 2. \quad (12.96)$$

In comparison to Eqs. (12.57) and (12.58), the result here is self-consistent and oscillator frequencies in different directions are allowed to change, thus permitting the valence state to polarize the whole oscillator mean field.

12.11 Asymptotic Quantum Numbers

As we know from our experience with the spherical shell model, the harmonic oscillator field should be improved by adding the spin–orbit coupling and flattening the bottom of the potential well. The flattening of the potential lifts the degeneracy of states (12.65) originating from the same pair of quantum numbers $(n_{||}, n_{\perp})$. Keeping the axial symmetry we still label the states by the orbital momentum projection Λ , but the states with different values of Λ have now different energy, similar to what we have seen in the transition from the isotropic harmonic oscillator to the square well (Figure 8.4). The states with larger Λ values have lower energy due to the enhanced attraction at larger distances from the origin. The states corresponding to the projections $\pm\Lambda$ are still pairwise, or rather fourfold, due to the spin projection $\pm\Sigma$, degenerate.

In the presence of the spin–orbit coupling, Λ and Σ cease to be separate integrals of motion. Only their sum $m = \Lambda + \Sigma$ is strictly conserved for any axial deformation. The levels remain double degenerate in sign of m . Similar to the spherical case (Section 8.8), the spin–orbit coupling prefers the states with the *parallel* alignment of Λ and Σ .

The spin–orbit terms in the Hamiltonian relatively weakly depend on deformation, whereas the main effect (12.60) grows as the deformation increases. Therefore, for the well-developed axial deformation, single-particle orbits can be approximately labeled by the *asymptotic quantum numbers* $[Nn_{\parallel}\Lambda]m$, where the main quantum number is $N = n_{\parallel} + n_{\perp}$. Strictly speaking, the asymptotic quantum numbers in square brackets are not conserved; N is not conserved since the matrix elements of the deformed potential (12.60) not only can change, due to the Legendre polynomial P_2 , the orbital momentum by $\Delta\ell = \pm 2$, but also, due to the factor r^2 , can change the main quantum number by $\Delta N = \pm 2$. But these admixtures of remote, $\delta\epsilon \approx 2\hbar\omega_{\text{o}}$, major shells are rather small because of the large energy denominators in perturbation theory.

Thus, the qualitative picture of the web of single-particle orbits as a function of the quadrupole deformation can be understood as a transition from the spherical coupling scheme characterized by the quantum numbers $(n\ell jm)$ to the asymptotic quantum numbers $[Nn_{\parallel}\Lambda]m$. Note that in the spherical limit it is customary to use the radial quantum number so that here $N = 2n + \ell$ (Section 8.6). At small deformations, we have a star of levels with different $|m|$ coming from the spherical degenerate point $(n\ell j)$ in accordance with the linear dependence on deformation (12.20). At large deformations, the energy behavior is again approximately linear, now in asymptotic quantum numbers (12.66).

The above-described qualitative properties based on the symmetry and corresponding quantum numbers are similar for all specific choices of the single-particle potential with the axial quadrupole deformation. The deformed Woods–Saxon potential is one of the most popular. Historically, the phenomenological Nilsson potential, 1955, turned out to be a convenient approximation to realistic deformed potentials. It is however invalid for the levels excited considerably over the Fermi surface because the oscillator potential cannot correctly describe the behavior of loosely bound orbitals and the continuum effects.

12.12 Nilsson Potential

This is the same anisotropic harmonic oscillator potential (12.61) with two added terms,

$$H'_N = \hbar\omega_{\text{o}}[v_{\ell\ell}(\vec{\ell}^2 - \langle \vec{\ell}^2 \rangle_N) + v_{\ell s}(\vec{\ell} \cdot \mathbf{s})]. \quad (12.97)$$

As we discussed, the $v_{\ell\ell}$ term makes the parabolic oscillator well closer to a realistic flat potential. In this version, the constants $v_{\ell\ell}$ and $v_{\ell s}$ are assumed to be independent of deformation although in more elaborate approaches this dependence does exist. The values of the constants are to be in agreement with the results for near-magic spherical nuclei. Therefore, in the $v_{\ell\ell}$ -term, a constant is subtracted equal to the average value of the operator $\vec{\ell}^2$ within the major spherical shell,

$$\langle \vec{\ell}^2 \rangle_N = \frac{1}{A(N)} \sum_{\ell=0}^N \frac{1 + (-)^{\ell+N}}{2} (2\ell + 1)\ell(\ell + 1) = \frac{1}{2}N(N + 3), \quad (12.98)$$

where $A(N)$ is the total number of states in the major shell (8.7). The subtraction keeps the average intershell spacing intact. Both constants $v_{\ell\ell}$ and $v_{\ell s}$ are negative to ensure the desired effects. Their typical numerical values are $v_{\ell\ell} \simeq -0.03$ and $v_{\ell s} \simeq -0.12$. It is easy to see that these values agree with our estimates for spherical nuclei. Parameters for protons and neutrons and for different mass regions can be slightly different.

The eigenvalues and the eigenfunctions of the Nilsson Hamiltonian can be found by a numerical diagonalization of the Hamiltonian matrix in a suitable basis, for example, in the spherical harmonic oscillator basis of functions $|n\ell\Lambda\Sigma\rangle$. Analytical estimates match the numerical computations at small and large deformations.

12.13 More Examples

We conclude this chapter by several examples of realistic single-particle level schemes. In Figure 12.6, we show a typical single-particle level scheme that follows from the

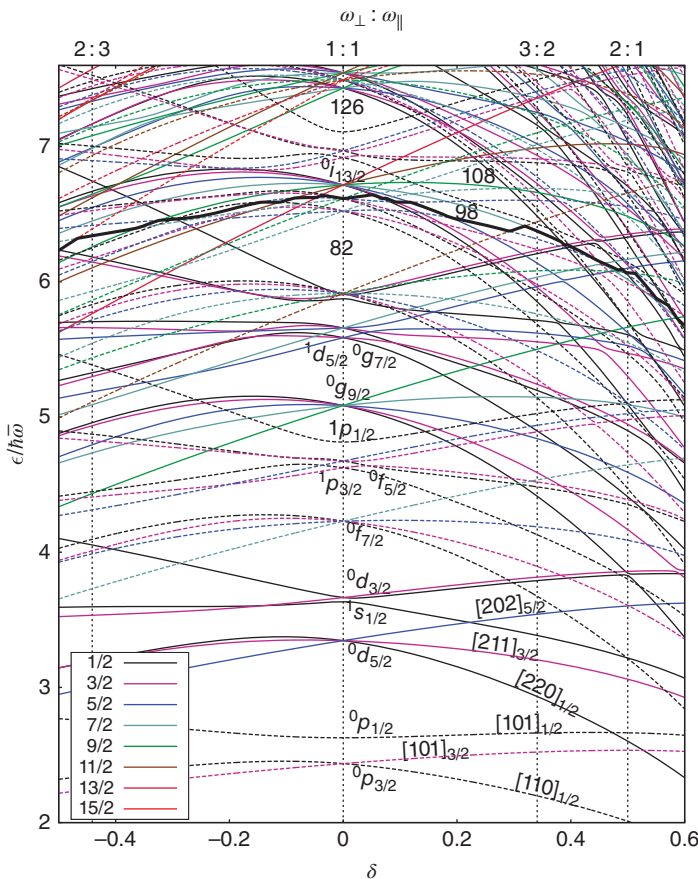


Figure 12.6 Energy levels (in units of $\hbar\omega$ from Eq. (12.75)) in the Nilsson potential as a function of the deformation parameter (12.63). Vertical grid lines indicate several values of deformation corresponding to commensurate frequencies. The plot is generated using $v_{ee} = -0.0268$ and $v_{es} = -0.127$, which are considered to be appropriate parameters for the neutron potential when the number of neutrons is between 82 and 126. Levels are colored based on the value of the projection m as indicated in the legend. Solid lines correspond to positive parity, dashed lines represent states of negative parity. Some spherical orbitals are indicated along the line $\delta = 0$; selected shell gaps, both spherical and deformed, are marked by the corresponding magic numbers. Asymptotic quantum numbers are given on the right for a few low-lying states. The position of the Fermi surface for $N = 98$ is shown with a thick solid line.

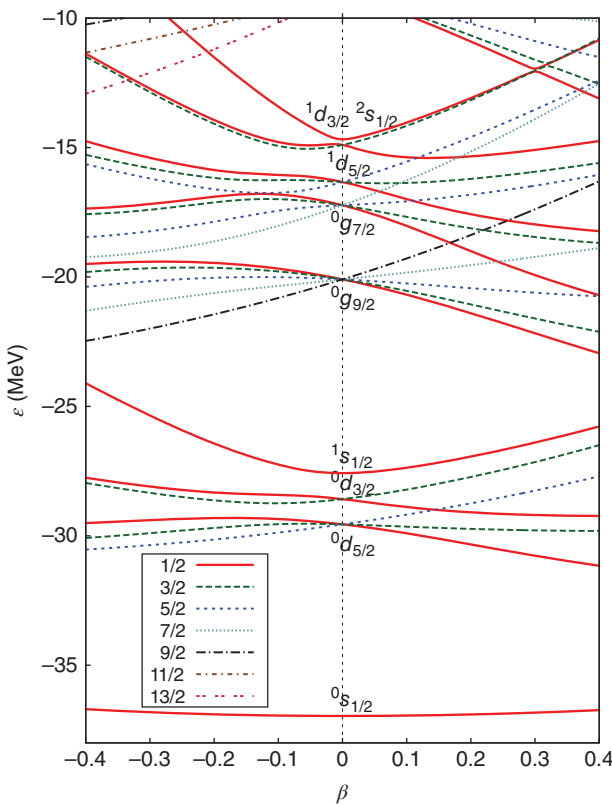


Figure 12.7 Evolution of single-particle levels of positive parity in the axially symmetric deformed Woods–Saxon potential adjusted to mass $A \sim 200$ as a function of quadrupole deformation.

Nilsson potential, whereas Figure 12.7 shows the lowest positive parity states in the realistic Woods–Saxon potential. Both examples target neutron states, and there is no substantial qualitative difference for protons. These similar figures highlight the important differences between the deformed and spherical level schemes: (i) lifting of degeneracies, except for the twofold Kramers degeneracy, and (ii) significantly more uniform level density. Only in few places, we see considerable shell gaps, for example, at $N=98$ and 108 in Figure 12.6; the numbers $N=86$ and 116 correspond to shell gaps in certain superdeformed nuclei. These “magic” numbers do not coincide with what is predicted by the pure anisotropic harmonic oscillator, Figure 12.5, because of the new terms in (12.97).

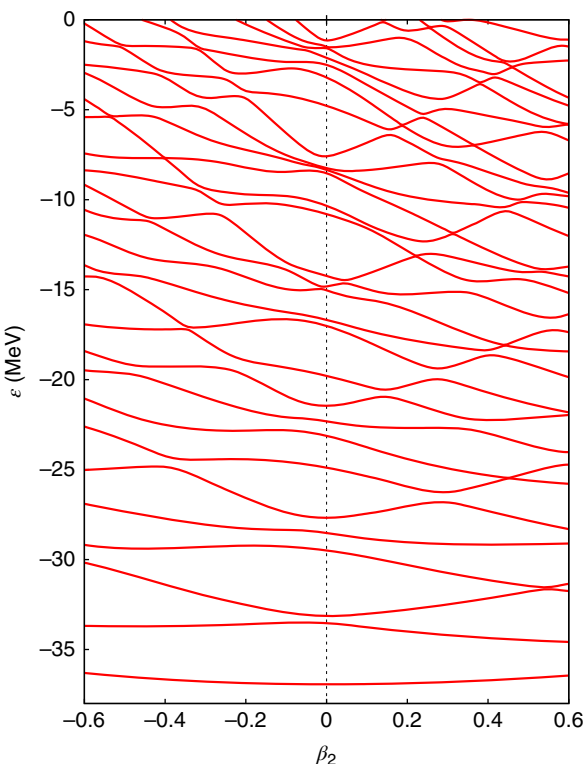
In Problem 12.6, we observed that the lowest-energy configuration is obtained for prolate deformation when the last two pairs of neutrons occupy the lowest Nilsson levels [220]1/2 and [211]3/2. This justifies the assumption used for that problem. In confirmation of Eq. (12.20), we note that the states with lowest $|m|$ are lowered toward prolate deformation, while the opposite is true for oblate deformation. From the spherical limit, the levels fan into prolate and oblate regions with some asymmetry. Prolate deformation is clearly preferred for situations with only a few valence particles above major spherical shells. In the opposite limit, for more than half-filled shells, the oblate state is possible (see also Eq. (9.6)); however, a substantial lowering of intruder levels coming from the

next major shell may still lead to preference of prolate deformation. A careful examination of Figure 12.6 shows that the Fermi surface is often slightly lower on the prolate side. The Fermi surface for $N = 98$ neutrons is shown as an example. As one can see from Figure 12.3, most nuclear ground states are observed and/or predicted to be prolate.

The qualitative feature that plays a serious role in physics of nuclear states, in particular in the rare-earth region, is the steep decrease in energy of some orbitals with increasing deformation. The neutron level $i_{13/2}$ corresponds to $\ell = 6$ and positive parity. In the spherical shell model (Figure 8.5), this level is an *intruder* coming to the shell $82 \leq N \leq 126$ from the next major shell. The surrounding spherical levels have negative parity. The deformation splits the $i_{13/2}$ level into Kramers doublets $\pm m$ but cannot mix it with other close levels due to their opposite parity. Even at fairly high deformations typical for the rare-earth nuclei, $\delta \approx 0.3$, the lower components of the $i_{13/2}$ level can be described as almost pure i -states because of a large difference in orbital momenta compared to the states of positive parity that come up from the low-lying major shells.

A glimpse of the complicated level scheme of Figure 12.6 shows another interesting feature. Some terms $\epsilon(\delta)$ with the same quantum numbers (m and parity that is equal to parity of the main quantum number N) cross each other. Careful examination of both Figures 12.6 and 12.7 shows multiple *avoided level crossings*. For example, in Figure 12.7, the level $m = 1/2$ of the orbit $2s_{1/2}$ shown by the solid line that would have asymptotic quantum numbers [400]1/2 moves up with increasing deformation. At $\beta \approx 0.3$ and energy $\epsilon \approx -12$ MeV, this level encounters the down-going level of the same $m = 1/2$

Figure 12.8 Evolution of $m = 1/2$ single-particle levels as a function of the quadrupole deformation in a Woods–Saxon potential with fixed octupole deformation $\beta_3 = 0.1$.



and positive parity from the just discussed $0i_{13/2}$ orbit ([660]1/2). The levels approach each other but actually never cross. This results from the fact that there is some small matrix element in the Hamiltonian that mixes these states. The mutual admixtures are very small except for the region of immediate contact, when the spacing between the levels is comparable with the small mixing matrix element, of the order of 100 keV, which is almost invisible on the scale of the figure. The fact that this crossing is avoided is hard to see in Figure 12.6 (around $\delta \approx 0.25$ and $\epsilon/\hbar\bar{\omega} \approx 6.2$) because in the Nilsson model $\Delta N = 2$ mixing is weak.

As commented in Section 8.10, there is close connection between classical periodic orbits, symmetries, and shell effects. The irregular shape of the potential makes the classical particle-in-a-well problem chaotic. In quantum mechanics, the level dynamics with avoided level crossings is a crucial issue that is responsible for destruction of approximate constants of motion and transition to *quantum chaos* that will be discussed in the end of the course. Let us, nevertheless, present yet another Figure 12.8 where we take the same example as in Figure 12.7 but introduce quadrupole deformation ($\beta_2 = \beta$) on top of an octupole deformation with a fixed parameter $\beta_3 = a_{30} = 0.1$. Here the body-fixed axis 3 remains the axis of symmetry, thus projection m is a good quantum number; however, parity of intrinsic states is no longer conserved. The additional irregularity in the shape has a profound effect, multiple avoided crossings create a turbulent dynamics of levels nearly eliminating all hints of regular picture seen in Figure 12.7.

References

- 1 J. Rainwater, Phys. Rev. **79**, 432 (1950).
- 2 A. Bohr and B.R. Mottelson, *Nuclear Structure*, Vol. 2, Chapter 4, 2; Chapter 5; Chapter 6, App. 2, World Scientific, Singapore, 1998.
- 3 P. Moeller *et al.*, At. Data Nucl. Data Tables **59**, 185 (1995).
- 4 S. Åberg, H. Flocard, and W. Nazarewicz, Annu. Rev. Nucl. Part. Sci. **41**, 321 (1991).
- 5 I. Hamamoto and B.R. Mottelson, Phys. Rev. C **79**, 034317 (2009).
- 6 M. Horoi and V. Zelevinsky, Phys. Rev. C **81**, 034306 (2010).
- 7 R.V.F. Janssens and T.L. Khoo, Annu. Rev. Nucl. Part. Sci. **41**, 321 (1991).
- 8 S. Reimann and M. Manninen, Rev. Mod. Phys. **74**, 1283 (2002).
- 9 J.M. Allmond, R. Zaballa, A.M. Oros-Peusquens, W.D. Kulp, and J.L. Wood, Phys. Rev. C **78**, 014302 (2008).

13

Pairing Correlations

... the pairing became a part of a “standard nuclear paradigm” and its manifestations are well known in practically all low-energy nuclear phenomena.

S.T. Belyaev, in *Fifty Years of Nuclear BCS*,
World Scientific, Singapore, 2013, p. 9

13.1 Physical Evidence

The semi-empirical mass formula (5.2) displays pairing correlations of nucleons via differences of binding energies for even–even, odd- A , and odd–odd nuclei. As shown in Figure 13.1, the difference of neutron separation energies between even- N and odd- N nuclei is nearly constant along the isotope chain although these energies change considerably; note also a steep fall near the magic number $N = 82$.

Extra binding energy can be explained by the character of the *residual interaction* between the particles in the common mean field. As we discussed, the short-range attraction prefers the nucleons with strongly overlapped wave functions. The best candidate is the nucleon pair in *time-conjugate orbits*. This agrees with the fact that the ground states of all even–even nuclei have quantum numbers $J^{\Pi} = 0^+$.

One could also attempt to explain the 0^+ spin parity of ground states as being associated with the Kramers degeneracy, which is a direct consequence of time-reversal invariance [QP, I, 20.5]. Since the time-conjugate orbits are degenerate, the sequential filling of single-particle orbitals in the order of increasing energy has to proceed *pair-wise* even without pairing interaction. In spherical nuclei, the single-particle degeneracy corresponds to j -levels and cannot unambiguously relate to odd–even staggering. Nevertheless, this mechanism may work in deformed nuclei where the degeneracy is indeed twofold (see Chapter 12). However, in this case, the odd–even mass staggering would be only of the order of a spacing between split double-degenerate Nilsson-like orbitals, $\sim \epsilon_F/A$, a few hundred kiloelectronvolts. In reality, see Figure 13.1 as an example, the pairing effects are typically of the order of $\epsilon_F A^{-2/3} \sim 2$ MeV being clearly of collective nature. The presence of these effects influences all properties of low-lying nuclear states.

The traditional explanation of the zero ground state spin by coherent pairing correlations going back to the founders of the modern nuclear shell model was recently put in doubt by the observation [1] that even a randomly taken but *rotationally invariant* interaction leads to the zero ground state spin of an even–even system with a large probability in the shell model calculations, usually greater than 50% (though not 100%).

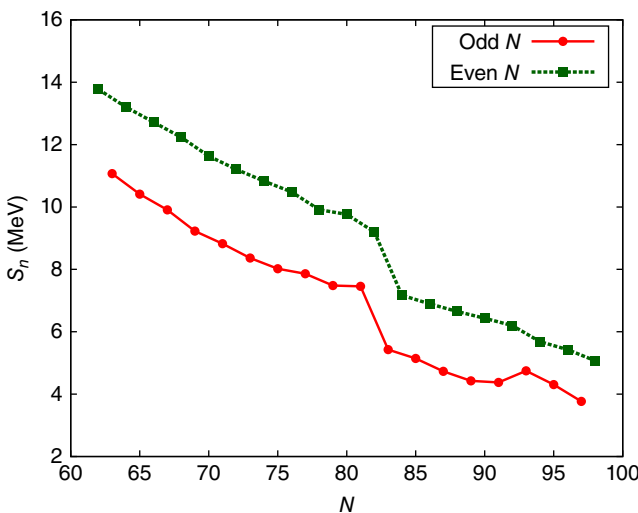


Figure 13.1 The neutron separation energy as a function of a neutron number for Ce isotopes.

This happens in spite of the fact that the multiplicity of the states with $J = 0$ among all possible states allowed by Fermi statistics for a given set of nucleon orbitals is usually small, only few percent. The predominance of the zero ground state spin in the ensemble of random interactions is supposedly related to the averaging over all characteristics except for the constants of motion as total spin and isospin. The structure of a typical ground state in this case is in general different from the one built upon the coherent pairing. The physics of random interactions and complicated (*chaotic*) wave functions will be discussed more in detail later, Section 25.5.

Let us assume that the residual interaction of two nucleons above a magic core can be described by an effective potential $U(\mathbf{r} - \mathbf{r}')$. It can be expanded over Legendre polynomials depending on the angle ϑ between \mathbf{r} and \mathbf{r}' ,

$$U(\mathbf{r} - \mathbf{r}') = \sum_L U_L(r, r') P_L(\cos \vartheta). \quad (13.1)$$

In the extreme limit of very short-range forces $\sim \delta(\mathbf{r} - \mathbf{r}')$, all values of L contribute to the sum (13.1). Indeed, the angular δ -function appears when the weights U_L of different waves depend on L through the statistical factor $(2L + 1)$ only, namely,

$$\delta(\mathbf{r} - \mathbf{r}') = \frac{\delta(r - r')}{rr'} \sum_L \frac{2L + 1}{4\pi} P_L(\cos \vartheta). \quad (13.2)$$

At large L , the Legendre polynomials give the significant contribution only in a small angle between \mathbf{r} and \mathbf{r}' , $\vartheta \sim 1/L$. For particles near the nuclear surface, $r \sim r' \sim R$, this interaction is noticeable if the distance between them is small, $\Delta r \sim R\vartheta \sim R/L$. Inversely, the low- L harmonics of (13.1) have a smooth angular dependence and are compatible with the long-range interaction, $\Delta r \sim R$. We can expect therefore that the long-range and short-range residual interactions are responsible for different physical phenomena.

As discussed in Chapter 11, two identical nucleons on the same spherical j -shell can couple to different (*only even*) total angular momenta $J = 0, 2, \dots, 2j - 1$. The

corresponding wave functions, in the secondary quantized form, can be written as in (12.83),

$$|JM\rangle = \frac{1}{\sqrt{2}} \sum_{mm'} C_{jmjm'}^{JM} a_m^\dagger a_{m'}^\dagger |0\rangle. \quad (13.3)$$

Here we create two particles above the inert core that is treated as a “vacuum” $|0\rangle$. The role of the core is reduced to the mean field that provides the j -levels for the valence nucleons. The factor $1/\sqrt{2}$ in Eq. (13.3) comes from the normalization that assumes that the state $|0\rangle$ is normalized. Two possible pairwise contractions of four Fermi operators in Eq. (11.24) are equal due to the symmetry of the Clebsch–Gordan coefficient that acquires the phase factor $(-)^{2j+J} = (-)^{J+1}$ under the permutation of m and m' . For odd J , these two terms cancel each other and such a state is not allowed; for even J , we get a factor 2 (see also Eq. (11.86)).

Problem 13.1 Consider identical particles on a single j -level interacting with a residual δ -force $U(\mathbf{r} - \mathbf{r}') = V \delta(\mathbf{r} - \mathbf{r}')$. Show that the matrix element of the two-body interaction in Eq. (13.1) is

$$U_L = \frac{V\mathcal{R}}{8\pi} \frac{(2j+1)^2}{2L+1} \left| C_{j1/2 \ j-1/2}^{L0} \right|^2, \quad (13.4)$$

where \mathcal{R} is an integral of four identical radial parts $u(r)/r$

$$\mathcal{R} = \int \left| \frac{u(r)}{r} \right|^4 r^2 dr. \quad (13.5)$$

Solution

Since the radial parts of the wave functions involved are all the same, the problem is reduced to the angular part. The permutational symmetry is contained in the symmetry of Clebsch–Gordan coefficients, thus, as long as L is even, direct and exchange terms are equal; this extra factor of 2 cancels the $1/\sqrt{2}$ normalization of the pair states. If we evaluate U_L in a two-particle state $|L\Lambda\rangle$ as $U_L = (2L+1)^{-1} \sum_\Lambda \langle L\Lambda | U | L\Lambda \rangle$, then, with the summation over Λ , the expression has no angular dependence (note that the δ interaction contributes only when particles are at the same angle but does not constrain an absolute orientation in space). Therefore, we are free to pick any particular orientation and multiply the result by 4π . We can select the forward angle where spherical functions are particularly simple [QP I, Eq. (16.143)], $Y_{\ell m}(\theta = 0) = \delta_{m0} \sqrt{(2\ell+1)/4\pi}$. Combining these arguments, we obtain

$$U_L = \frac{V\mathcal{R}(2\ell+1)^2}{4\pi(2L+1)} \sum_{\Lambda mm'} \left| C_{jm jm'}^{L\Lambda} C_{\ell 0 \ 1/2m}^{jm} C_{\ell 0 \ 1/2m'}^{jm'} \right|^2. \quad (13.6)$$

Due to antisymmetry only the $m = -m' = \pm 1/2$ terms with $\Lambda = 0$ can contribute, and the answer in (13.3) is obtained using that

$$C_{\ell 0 \ 1/2m}^{jm} = (-)^{\ell+1/2-j} \sqrt{\frac{2j+1}{2(2\ell+1)}}. \quad (13.7)$$

Only small changes are required to extend these results to a general case with different spherical orbits and nonidentical nucleons, detailed discussions and some examples can

be found in the textbook [2]. From the result (13.4), we see that the δ -interaction favors $L = 0$,

$$U_0 = V\mathcal{R} \frac{(2j+1)}{8\pi}, \quad (13.8)$$

and, in the asymptotic limit $1 \ll L \ll j$, the matrix elements U_L become small, [QP,I, Problem 16.17],

$$U_L \propto \frac{(2j+1)}{2L+1} \left| C_{j1/2 \ j-1/2}^{L0} \right|^2 \sim P_L^2(1/(2j+1)) \sim \frac{2}{\pi L}. \quad (13.9)$$

The $J = 0$ combination of the two-nucleon states containing the Clebsch–Gordan coefficient with $m' = -m$,

$$|00\rangle = \sqrt{\frac{1}{2(2j+1)}} \sum_m (-)^{j-m} a_m^\dagger a_{-m}^\dagger |0\rangle, \quad (13.10)$$

is especially important because all $(m, -m)$ components correspond to the time-conjugate orbits completely overlapped in space. Time conjugation for the fermions is defined in (11.74) and [QP, I, 20.6], the definition contains the same phase as in (13.10) which of course agrees with the meaning of the time-reversible state with $J = 0$.

In the case of δ -like forces, the state (13.10) is singled out by the strongest short-range interaction among all possible pair states (13.3). The attraction is weakened as the total angular momentum of the pair grows (13.9). If the short-range component of the residual forces dominates, we expect that nuclei with two nucleons above the core will have a typical sequence of the excited states $0^+, 2^+, 4^+, \dots$ with the 0^+ state considerably below the rest because of the pronounced pairing correlation. This turns out to be the case. Figure 13.2 shows the low-lying levels of ^{210}Po with two protons above the doubly-magic nucleus ^{208}Pb and on the right the spectrum for the δ -interaction. The levels on the figure

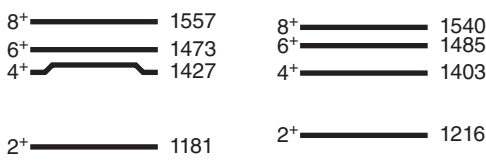


Figure 13.2 Energy spectrum of the lowest states in ^{210}Po is shown on the left and the spectrum of two protons on $j = 9/2$ orbit interacting by the δ -force (13.3) of strength $V\mathcal{R} = -4033$ keV (13.4) is on the right. Spin and parity for each state are shown on the left and excitation energy in units of kiloelectronvolts is on the right.



supposedly correspond to the intrinsic excitation of the valence pair to higher angular momenta. Note the large spacing between the ground state 0^+ and the first excited state 2^+ . The next levels are much closer to each other due to the small differences in the short-range residual interaction between, let say 4^+ and 6^+ . Such a characteristic spectrum of the lowest excited levels in near-magic even–even nuclei is called *the seniority scheme*; the meaning of this term will be explained in the following.

As a typical pattern (see Figure 13.2), we observe in all even–even non-magic nuclei a rarefied level density at low excitation energy. The level density grows rather steeply from energy that roughly coincides with the pairing energy in the mass formula, $\sim 12/\sqrt{A}$ MeV. Accepting the pairing hypothesis, we expect that the increase in the level density occurs at the energy sufficient to break a pair labeled as 2Δ in Figure 13.3. A variety of possibilities to recouple the nucleons of the broken pair into higher angular momenta ensures the increase in the level density. The levels below this threshold should have another nature. Such slow motion can be related to collective vibrations and rotations of a nucleus as a whole, which only weakly perturb the pair structure. This idea is confirmed by generic spectra of odd- A and odd–odd nuclei where the unpaired nucleon or nucleons can be easily transferred to other orbits without breaking pairs. As a result, we see there the enhanced and more uniform level density at low excitation energy. The discussed differences in spectra are shown in Figure 13.4 using an example of Ni isotopes.

The idea of nucleon pairing was used by M. Goeppert-Mayer and J.H.D. Jensen in their promotion of the shell model. Assuming that in spherical nuclei the nucleons are coupled to pairs with zero angular momentum, one can predict ground state spins of odd- A nuclei. The spin value should coincide with the single-particle momentum j of the last valence nucleon. This value, in turn, is determined by the level sequence in the shell model. A vast amount of experimental information supports this idea. The same should be valid for magnetic moments where the isotropic pairs do not contribute. Then

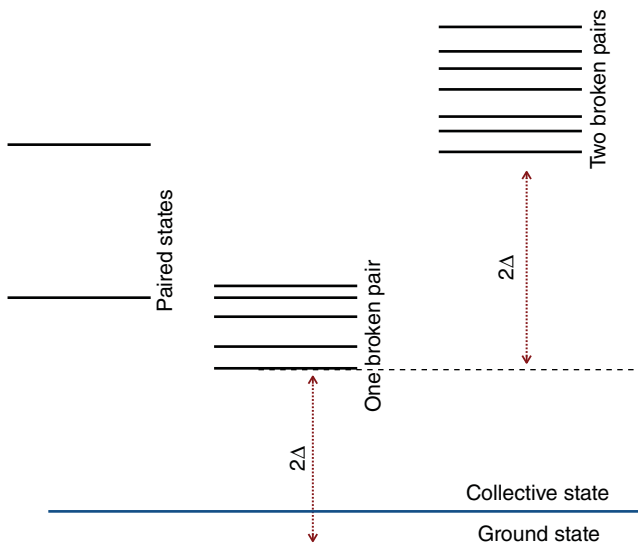


Figure 13.3 A typical spectrum of an even–even non-magic spherical nucleus.

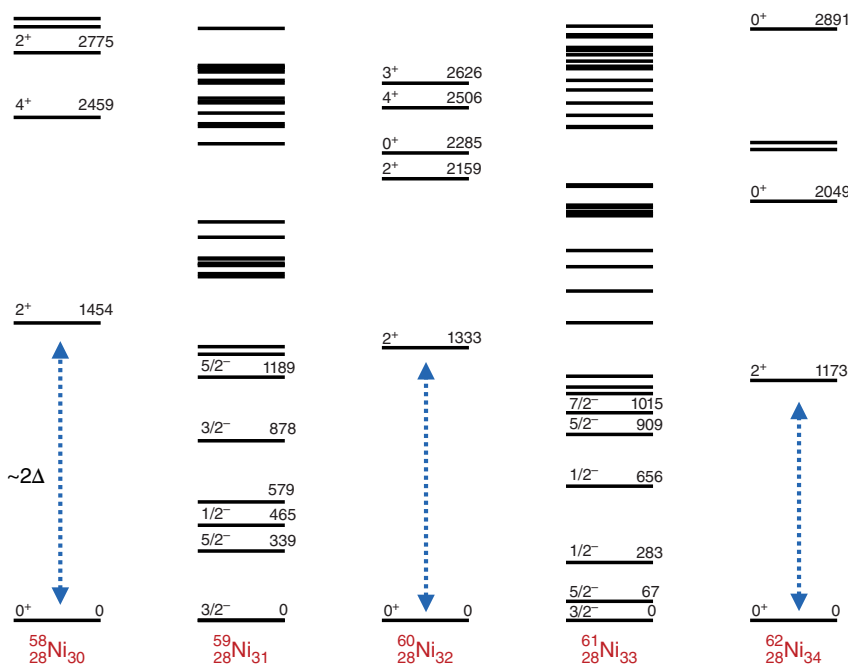


Figure 13.4 The low-lying levels in nickel isotopes showing a gap in the spectra of even–even nuclei.

the Schmidt values, Figure 9.1, are applicable to all spherical odd- A nuclei rather than to nuclei with one valence nucleon above the magic core only. In Chapter 10, we have seen how this works for the lightest nuclei. Many radiative transitions in odd- A nuclei also can be interpreted as single-particle transitions on the paired background. A more accurate treatment of pairing renormalizes the characteristics of low-lying nuclear spectra.

As became clear after the fundamental work by Bardeen *et al.* (BCS) [3], the phenomenon of *superconductivity* in solids is also based on pairing correlations. Electron pairs (Cooper pairs) created due to the electron attraction mediated by the lattice deformation acquire *quasibosonic* properties and behave similar to, but still different from, a Bose condensate. The analogy between superconductivity and nuclear pairing was suggested by Bohr *et al.* [4]. The idea turned out to be extremely fruitful. It was demonstrated by Belyaev [5], that nuclear superconductivity, or superfluidity, changes all features of nuclear structure. The latest development of the pairing physics is summarized in the collection of papers [6] *50 Years of Nuclear BCS*.

13.2 Seniority Scheme

The simplest approach to the description of pairing correlations assumes that in an even system, the nucleons are pairwise coupled to angular momentum $L = 0$ as in the case of one pair (13.10). Two comments are appropriate here.

First, in heavy nuclei with $N \neq Z$, protons and neutrons near the Fermi surface occupy different orbits. Therefore, the short-range attraction acts mainly between *identical*

nucleons ($T_3 = \pm 1$ pairs). In relatively light nuclei, one can expect considerable effects of the proton–neutron pairing ($T = 1$, $T_3 = 0$ isovector pairs or $T = T_3 = 0$ isoscalar, *quasideuteron correlations*). The effects of the isoscalar type are seen in nuclei as ^{10}B or ^{22}Na , where the wave function probably contains a significant component of three deuteron-like pairs on top of the $N = Z$ core, alpha-particle, and ^{16}O , respectively, with aligned spins of those pairs resulting in the ground state quantum numbers 3^+ . The $n-p$ correlations can also show up near drip lines in heavier neutron-deficit nuclei, where proton and neutron numbers are closer or even equal to each other, for example, around $_{50}^{100}\text{Sn}_{50}$. Unfortunately, this exotic nucleus is in the region barely accessible for experiments. Along the line $N = Z$, even quartic correlations of alpha-type can be appreciable.

Second, the state (13.10) constructed for a single spherical j -shell is the simplest example. The pairing effects are seen in deformed nuclei as well, where the spherical j -level scheme is destroyed by the mean-field deformation. The main feature is pairing between the *time-conjugate* nucleon orbits.

It is convenient to introduce a special notation that does not presume the existence of spherical symmetry being based exclusively on time-reversal invariance. For each single-particle state $|\lambda\rangle$, the time-conjugate state will be designated $|\tilde{\lambda}\rangle$. With our phase convention in the spherical basis (11.74) the single-particle time conjugation in an arbitrary basis can be defined through the expansion over the complete set of spherical states,

$$|\lambda\rangle = \sum_{jm} C_{jm}^\lambda |jm\rangle \Rightarrow |\tilde{\lambda}\rangle = \sum_{jm} (C_{jm}^\lambda)^*(-)^{j-m} |j-m\rangle. \quad (13.11)$$

It is important that the second time reversal brings back the original state with the opposite sign for the fermions (when the single-particle angular momentum j is half-integer),

$$|\tilde{\tilde{\lambda}}\rangle = \sum_{jm} C_{jm}^\lambda (-)^{2j} |jm\rangle = -|\lambda\rangle. \quad (13.12)$$

In a general case, the two-particle paired state (13.10) can be obtained from the vacuum by the action of the pair operator

$$P^\dagger = \frac{1}{2} \sum_{\lambda} a_\lambda^\dagger a_\lambda^\dagger, \quad (13.13)$$

where the definition of the operator for the time-conjugate orbit includes all phase factors assuming

$$a_{\tilde{\lambda}}^\dagger = -a_\lambda^\dagger, \quad (13.14)$$

and similarly for the annihilation operator a_λ . The sum in P^\dagger includes Ω terms, where Ω is a capacity of the relevant single-particle space [even number of states $|\lambda\rangle$]. For a single j -level, $\Omega = 2j + 1$. Terms corresponding to λ and to $\tilde{\lambda}$ are in fact equal to each other as follows from (13.14) and Fermi statistics. Therefore, it is possible, as it is done by many authors, to remove the factor $1/2$ in front of (13.13) and carry out the summation over pair-states, which is a half of single-particle states, only $\Omega/2$ “positive” ones.

The one-pair state [generalization of (13.10)] is proportional to $P^\dagger |0\rangle$. To normalize it, we introduce the Hermitian conjugate operator of pair annihilation P and calculate

$$\langle 0 | P P^\dagger | 0 \rangle = \frac{1}{4} \sum_{\lambda \lambda'} \langle 0 | a_{\tilde{\lambda}} a_\lambda a_{\lambda'}^\dagger a_{\tilde{\lambda}'}^\dagger | 0 \rangle. \quad (13.15)$$

Using the Wick theorem (pairwise contractions), we come to

$$\langle 0|PP^\dagger|0\rangle = \frac{1}{4} \sum_{\lambda\lambda'} (\delta_{\lambda\lambda'} \delta_{\tilde{\lambda}\tilde{\lambda}'} - \delta_{\lambda\tilde{\lambda}'} \delta_{\tilde{\lambda}\lambda'}), \quad (13.16)$$

where all phase factors are included in the definition of the tilded subscripts. The summation over λ' leaves $\delta_{\lambda\lambda} = 1$ in the first term and, due to (13.12), $\delta_{\lambda\tilde{\lambda}} = -1$ in the second one. As a result,

$$\langle 0|PP^\dagger|0\rangle = \frac{1}{2} \Omega, \quad (13.17)$$

that leads to the normalization of the one-pair state

$$|2; s=0\rangle = \sqrt{\frac{2}{\Omega}} P^\dagger |0\rangle. \quad (13.18)$$

The normalization coincides with that in (13.10) in the case of a single j -level. We denote in (13.18) the many-body states $|N; s\rangle$ for the total particle number in the shell, N , and *seniority*, s , that shows the number of unpaired particles.

Now we continue to fill the shell with pairs. Since they have integer (zero) spin, they are *quasibosons* and we can repeatedly create them. At the same time, they are not real bosons and their coexistence in the same space is distorted by the Fermi statistics of the constituents; we mentioned briefly the statistics of composite objects in Chapter 1. The repeated actions of the pair creation operator P contain the overlapped terms with the same ($\lambda, \tilde{\lambda}$), which do not work because of the Pauli exclusion principle. A slightly similar situation takes place in relation to the Holstein–Primakoff bosonic representation [QP, I, Problem 16.8] of angular momentum operators.

To go further, first let us use the rules for fermion operators to calculate the commutator

$$[P, P^\dagger] = \frac{\Omega}{2} - \hat{N}, \quad (13.19)$$

where \hat{N} is the operator of the total particle number. This agrees with (13.17), where \hat{N} acting onto the vacuum gives zero. Equation (13.19) helps to calculate the normalization of the two-pair state,

$$\langle 0|P^2(P^\dagger)^2|0\rangle = \langle 0|P([P, P^\dagger] + P^\dagger P)P^\dagger|0\rangle. \quad (13.20)$$

The operator \hat{N} in the commutator (13.19) acts in Eq. (13.20) on the state with one pair and gives 2, the remaining operators reduce to Eq. (13.17). In the second term in (13.20), we again form the commutator and use $P|0\rangle = 0$. Collecting all items, we get

$$\langle 0|P^2(P^\dagger)^2|0\rangle = 2 \left(\frac{\Omega}{2} - 1 \right). \quad (13.21)$$

It is instructive to discuss the meaning of the result (13.21). If the space capacity is large and particle number is relatively small, $\Omega/2 \gg N$, then, by including the factor $\sqrt{\Omega/2}$ into the definition of P and P^\dagger and neglecting \hat{N} in (13.19), we would reduce the pair operators to normal bosons. In this approximation, the matrix element (13.21) would be equal to $2!(\Omega/2)^2$. The difference between this bosonic limit and the *quasibosonic* result (13.21) is due to the *Pauli blocking* effect. We have $\Omega/2$ different possibilities for

the first pair and only $\Omega/2 - 1$ for the second pair as two orbits (one pair state) are already occupied by the first pair. For large $\Omega/2$, the difference is not significant, and the picture of the Bose condensate of pairs is qualitatively valid.

Problem 13.2 Derive the general result for the state $|N; s = 0\rangle$ that has $n = N/2$ pairs and seniority zero (N is even),

$$\langle 0|P^n(P^\dagger)^n|0\rangle = \frac{n!(\Omega/2)!}{[(\Omega/2) - n]!}. \quad (13.22)$$

Again the factor $n!$ is the remnant of the Bose condensate, while the two other factorials reflect the *Pauli blocking* increasing as the shell is getting filled by the pairs.

In an odd- A system, one orbit $|\lambda\rangle$ is filled by the unpaired valence particle. But the presence of the single unpaired particle blocks actually the whole *pair state* $(\lambda, \tilde{\lambda})$ that becomes inaccessible for pairs. In our nomenclature, the three-particle state with one pair has seniority $s = 1$ and is to be denoted as $|3; s = 1_\lambda\rangle$, where the unpaired orbit is indicated explicitly. The normalization of the state can be easily found from

$$\langle 0|a_\lambda P P^\dagger a_\lambda^\dagger|0\rangle = \frac{\Omega}{2} - 1. \quad (13.23)$$

Here for calculation we again use the commutator (13.19) where \hat{N} gives 1 when applied to a one-particle state. The simple meaning of Eq. (13.23) is that the particle removes one pair state from the available volume (compare Eq. (13.17)). The addition of extra pairs gives the same as in (13.22), but the available volume is diminished by one pair state,

$$\langle 0|a_\lambda P^n(P^\dagger)^n a_\lambda^\dagger|0\rangle = \frac{n![(\Omega/2) - 1]!}{[(\Omega/2) - 1 - n]!}. \quad (13.24)$$

Equation (13.24) defines the normalization of the state $|N = 2n + 1; s = 1_\lambda\rangle$; the result does not depend on the choice of the unpaired orbit λ .

The same result (13.24) is valid if *both* orbits, λ and $\tilde{\lambda}$, are occupied by unpaired particles. This state is different from the pair state, (13.10) or (13.18), where the pair is uniformly distributed over available space rather than blocks a specific couple of time-conjugate orbits. As one pair state is already blocked by a single particle, the presence of the time-conjugate partner does not change the situation. Therefore, as in (13.24),

$$\langle 0|a_\lambda a_\lambda P^n(P^\dagger)^n a_\lambda^\dagger a_{\tilde{\lambda}}^\dagger|0\rangle = \frac{n![(\Omega/2) - 1]!}{[(\Omega/2) - 1 - n]!}. \quad (13.25)$$

Finally, two unpaired particles on the orbits λ and λ' , which belong to *different* time-conjugate pairs, block two pair states leading to

$$\langle 0|a_{\lambda'} a_\lambda P^n(P^\dagger)^n a_\lambda^\dagger a_{\lambda'}^\dagger|0\rangle = \frac{n![(\Omega/2) - 2]!}{[(\Omega/2) - 2 - n]!}. \quad (13.26)$$

The states with two unpaired particles are $|N = 2n + 2; s = 2_{\lambda, \lambda'}\rangle$. In a similar manner, the states with higher seniority can be constructed. Note that at this stage, we did not introduce the Hamiltonian explicitly so that the seniority scheme gives simply a basis convenient for describing pairing correlations.

13.3 Multipole Moments in the Seniority Scheme

We expect that the ground state wave function of an odd- A nucleus is close to that of a pure state with seniority $s = 1$. Then it is of practical interest to compute the expectation values of multipole moments for those pure states. Here, we consider the spherical shell model assuming a valence particle in a state $|j, m = j\rangle$ as required by the definition of the multipole moment because the isotropic pairs do not contribute to the angular momentum.

The multipole moments belong to the class of the one-body operators expressed in Section 11.2 in the secondary quantized form. Only the diagonal terms in the $|jm\rangle$ basis do contribute to the expectation value so that the effective operator can be written as

$$\hat{Q} = \sum_m (m|q|m) a_m^\dagger a_m. \quad (13.27)$$

Let an even core contain n pairs. We need to calculate the matrix element

$$Q(n) = \langle N = 2n + 1; s = 1_j | \hat{Q} | N = 2n + 1; s = 1_j \rangle. \quad (13.28)$$

It is convenient to transform to the “hole” representation using in (13.27) $a_m^\dagger a_m = 1 - a_m a_m^\dagger$. For any multipole moment, except for scalar ones, the trace

$$\text{Tr}_j Q = \sum_{m=-j}^j (m|q|m) = 0. \quad (13.29)$$

In the matrix element (13.28), one can transfer the operator a_m to the left and the operator a_m^\dagger to the right commuting them with P^n and $(P^\dagger)^n$, respectively (free of charge because P and P^\dagger contain only pairs of Fermi operators). Including the norm (13.24) of the state with seniority 1, we obtain

$$Q = - \sum_m (m|q|m) \frac{\langle 0 | a_j a_m P^n (P^\dagger)^n a_m^\dagger a_j^\dagger | 0 \rangle}{\langle 0 | a_j P^n (P^\dagger)^n a_j^\dagger | 0 \rangle}. \quad (13.30)$$

The matrix element in the numerator (13.30) is equal to zero due to the Pauli principle for $m = j$ and it is given by Eqs. (13.25) and (13.26) for $m = \tilde{j}$ and for $m \neq j, \tilde{j}$, respectively. Taking the ratio of the norms from (13.24)–(13.26), we get

$$Q = -(\tilde{j}|q|\tilde{j}) - \frac{(\Omega/2) - 1 - n}{(\Omega/2) - 1} \sum_{m \neq j, \tilde{j}} (m|q|m). \quad (13.31)$$

Because of the vanishing trace, the sum in (13.31) is equal to $-(j|q|j) - (\tilde{j}|q|\tilde{j})$. Finally,

$$Q = (j|q|j) - \frac{n}{(\Omega/2) - 1} [(j|q|j) + (\tilde{j}|q|\tilde{j})]. \quad (13.32)$$

The first term is a normal result of the single-particle shell model (recall Section 9.4 for the quadrupole moment). The additional contribution proportional to the number n of pairs reflects their distortion owing to the presence of the unpaired particle.

The final result depends on the character of the multipole operator, similar to what we have seen in Section 9.2. For *time-even* operators, their expectation values in time-conjugate states are equal, and ($\Omega = 2j + 1$)

$$Q = (j|q|j) \left(1 - \frac{2n}{j - (1/2)} \right). \quad (13.33)$$

In the beginning, $n = 0$, and in the end, $n = j - (1/2)$, of the shell, (13.33) coincides with the shell model result for single-particle, $Q = (j|q|j)$, and single-hole, $Q = -(j|q|j)$, states. As a function of n , all time-even multipole moments are predicted to interpolate linearly between these limits. Their absolute magnitude is lower than at the edges, and they change the sign near the half-occupied shell. We already discussed, Section 9.4, that, for the quadrupole moment, this prediction turns out to be incorrect. There are long-range residual forces responsible for the large quadrupole moment and the trend to deformation.

For *time-odd* operators, the time-conjugate orbits have opposite expectation values, and the result (13.32) coincides with the pure single-particle, or single-hole, value. This means, for example, that the magnetic moment is not influenced by the presence of pairs and, for the states of seniority 1, should still be equal to the Schmidt value.

13.4 Degenerate Model

Here we consider the exactly solvable model that was apparently originally studied by G. Racah, 1949. It seems to be the first reasonable microscopic model of superconductivity although this was not understood at that time.

Assume that near the Fermi surface, particles interact through forces of the pairing type. The strength of interaction measured by the pairing effects in the mass formula is small compared to e_F and even compared to the distance between major shells. In the rough approximation, we consider all single-particle levels in some interval around the Fermi surface degenerate at energy ϵ . Total number of orbits in this layer is Ω .

Pairing interaction U_p is of attractive type and leads to the scattering processes of pairs between time-conjugate orbits $(\lambda, \tilde{\lambda})$. As a result, the particles either remain in the same pair of orbits or scatter to another pair $\lambda', \tilde{\lambda}'$. The states with broken pairs do not provide a sufficient overlap of the particle wave functions and, referring to the information of two-particle spectra, Figure 13.2, we simply assume that the interaction is turned off if the particle orbits are not time-conjugate to each other.

We substitute the scattering matrix elements induced by the pairing interaction,

$$U_{\lambda'\lambda}^P \equiv (\lambda', \tilde{\lambda}' | U_p | \lambda, \tilde{\lambda}), \quad (13.34)$$

by their average constant value ($G > 0$),

$$\overline{U_{\lambda'\lambda}^P} = -G. \quad (13.35)$$

The short range of the interaction implies that the individual matrix elements (13.34) are small being inversely proportional to the nuclear volume or to the mass number A . Indeed, the single-particle wave functions in the integrand are normalized to the nuclear volume while the forces do not vanish at small interparticle distances only. A crude estimate based on average experimental data gives $G \simeq (20 - 25)/A$ MeV. Using our experience with two-body operators in the secondary quantized form, we postulate the pairing Hamiltonian for the degenerate model as

$$H = e\hat{N} - GP^\dagger P. \quad (13.36)$$

The product of pair creation and annihilation operators (13.13) contains each of the above mentioned pair-scattering processes once.

The diagonalization of the Hamiltonian (13.36) can be performed by using operator methods. It goes without calculations that the operators P and P^\dagger form a *ladder structure* [QP, I, 11.6] with the particle number operator \hat{N} ; the ladder step is ± 2 ,

$$[P, \hat{N}] = 2P, \quad [P^\dagger, \hat{N}] = -2P^\dagger. \quad (13.37)$$

The algebra is closed by the commutator (13.19). Three operators,

$$\mathcal{L}_- = P, \quad \mathcal{L}_+ = P^\dagger, \quad \mathcal{L}_z = \frac{1}{2} \left(\hat{N} - \frac{\Omega}{2} \right), \quad (13.38)$$

form the algebra $SU(2)$ isomorphic to that of angular momentum. The “momentum” vector $\vec{\mathcal{L}}$ is called *quasispin*. The quasispin projection \mathcal{L}_z is determined by the particle number and the volume of available single-particle space. Therefore, \mathcal{L}_z is an exact constant of motion that takes the same value for all states in a given nucleus. As shell is getting filled, \mathcal{L}_z changes from $-(\Omega/4)$ for the empty shell, $N = 0$, to $+(\Omega/4)$ for the full shell, $N = \Omega$. For $N = (\Omega/2)$ (half-filled shell), $\mathcal{L}_z = 0$.

Another constant of motion is the square of the quasispin,

$$\vec{\mathcal{L}}^2 = \mathcal{L}_z^2 - \mathcal{L}_+ \mathcal{L}_-. \quad (13.39)$$

It takes values $\mathcal{L}(\mathcal{L} + 1)$ where \mathcal{L} is integer or half-integer depending on the value of \mathcal{L}_z . In a given nucleus, different states have different \mathcal{L} that can vary from $\mathcal{L}_{\min} = |\mathcal{L}_z|$ to the maximum value $\mathcal{L}_{\max} = (\mathcal{L}_z)_{\max} = \Omega/4$,

$$\frac{1}{2} \left| N - \frac{\Omega}{2} \right| \leq \mathcal{L} \leq \frac{\Omega}{4}. \quad (13.40)$$

Thus, each N -particle state can be characterized by the quasispin quantum numbers \mathcal{L} and \mathcal{L}_z . The expectation value of the Hamiltonian (13.36) determines, according to (13.39), the energy of the state,

$$E(\mathcal{L}, N) = eN + \frac{G}{4} \left(N - \frac{\Omega}{2} \right) \left(N - \frac{\Omega}{2} - 2 \right) - G\mathcal{L}(\mathcal{L} + 1). \quad (13.41)$$

At a given N , the ground state is the one with the maximum value of $\mathcal{L} = \Omega/4$. Let us assume, for example, that $\Omega/4$ is an integer and the particle number N is even. Then \mathcal{L}_z and \mathcal{L} are integers and the ground state has $\mathcal{L} = \Omega/4$.

The seniority quantum number s introduced earlier equals to twice the deviation of the quasispin \mathcal{L} from its maximum value,

$$s = 2 \left(\frac{\Omega}{4} - \mathcal{L} \right), \text{ equivalently } \mathcal{L} = \frac{1}{4}(\Omega - 2s). \quad (13.42)$$

As follows from (13.40), s changes from 0 in the ground state to the total particle number N for less than half-filled shell, $N < \Omega/2$, or to the hole number, $\Omega - N$, if $N > \Omega/2$. For even N , the seniority is even as well. As a function of seniority, the energy spectrum (13.41) takes a form

$$E_s(N) = eN + \frac{G}{4}(N - s)(N + s - \Omega - 2). \quad (13.43)$$

It is seen from (13.43) that the seniority quantum number describes the shrinkage of phase space available for interacting pairs due to the blocking of s orbits by s (for $N < \Omega/2$) particles, which do not participate in pairing correlations. Compared to the

ground state with $s = 0$, a nonzero value of s corresponds in (13.43) to the changes $N \rightarrow N - s$, $\Omega \rightarrow \Omega - 2s$, which reduce a number of states accessible for the pair transfer and effectively quench attraction.

In a given nucleus, the excitation energy of states with nonzero seniority is

$$E_s(N) - E_0(N) = \frac{G}{4} s(\Omega - s + 2). \quad (13.44)$$

As long as $s \ll \Omega$, excitation energy (13.44) increases as $G\Omega s/4$, that is, proportional to a number of broken pairs (see Figure 13.2). The loss of binding for the first pair breakup, $s = 2$,

$$2\Delta = G \frac{\Omega}{2}, \quad (13.45)$$

is pair binding energy. This defines the *energy gap* in the pair excitation spectrum that is seen in the experiment. Note that the effect is proportional to the phase space volume Ω . The collective nature of binding is due to the coherent combination of all available states in the pair wave function, Eqs. (13.13) and (13.18). Using empirical estimates of G and Δ from the pairing term in the mass formula, we get $\Omega \simeq \sqrt{A}$.

Let us add an odd particle to an even system, $N \rightarrow N + 1$. For a new (odd) particle number, the quasispin L is half-integer and s is odd. The maximum possible quasispin value is $L_{\max} = (\Omega/4) - (1/2)$ that corresponds to $s = 1$, that is, one unpaired particle blocking one pair state. The ground state energy $E_{s=1}(N + 1)$ of the odd system follows from (13.43) at $N \rightarrow N + 1$ and $s = 1$. It can be expressed via the ground state energy of the even parent as

$$E_1(N + 1) = E_0(N) + \epsilon + \frac{GN}{2}. \quad (13.46)$$

The loss of energy again has collective nature being proportional to a number of pairs $N/2$; each of the pairs has lost one state for possible scattering.

The comparison of the ground state energies $E_0(N)$ and $E_0(N + 2)$ of two consecutive even systems shows that

$$E_0(N + 2) - E_0(N) = 2\epsilon + GN - G \frac{\Omega}{2}. \quad (13.47)$$

This means that due to the pairing, the ground state of the odd system is shifted up from the average ground state energy of even neighbors by a half-value of the gap (13.45),

$$E_1(N + 1) = E_0(N) + \frac{E_0(N + 2) - E_0(N)}{2} + G \frac{\Omega}{4} = \frac{E_0(N) + E_0(N + 2)}{2} + \Delta. \quad (13.48)$$

This describes the *odd–even effect in the mass formula* as the loss of pairing energy because of the Pauli blocking in an odd system.

Let us now take another look at a single j -level model introduced in Chapter 11 (Problems 11.6, 11.9, and 11.10). This is a classic nuclear example of a degenerate model, where due to spherical symmetry many single-particle states that belong to the same j -orbit are degenerate in energy. Of course, quasispin is no longer a good quantum number for a general Hamiltonian (11.85) or (11.96), but for low-lying states mixing is

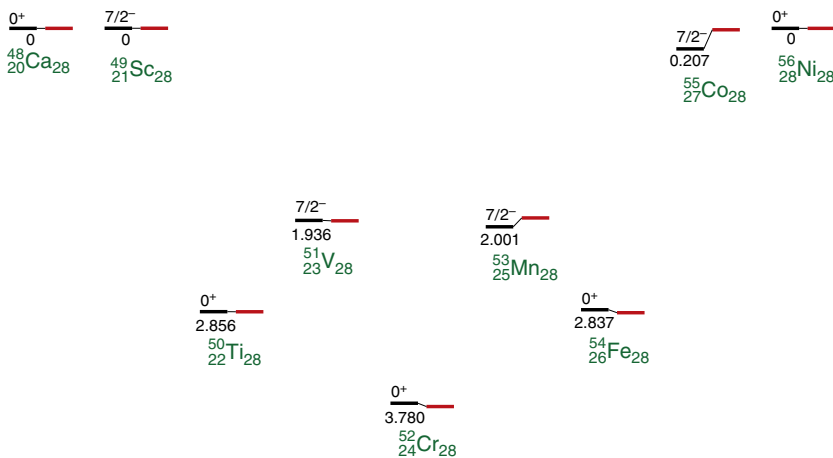


Figure 13.5 Ground state energies of $N = 28$ isotopes. All energies are shown relative to the single-particle and monopole contributions. Here $\epsilon = -9.626$ MeV and $\tilde{U}_0 = 0.3225$ MeV, being set by ^{49}Sc and ^{56}Ni , respectively. The red levels show energies of the states in the seniority model. The pairing strength is $U'_0 = -2.857$ MeV.

usually small. The most coherent components of the Hamiltonian, such as mean-field, monopole, and pairing interactions, are built from operators (generators) of the quasispin algebra (13.37) (note that, from (13.18), $P_{00}^\dagger = \sqrt{2/\Omega} P^\dagger$) and conserve quasispin.

Problem 13.3 Show that for identical fermions, the expectation value of the general two-body Hamiltonian for a single j -level of type (11.85) in a seniority $s = 0$ or $s = 1$ state is just a combination of single-particle energy, monopole, and pairing parts

$$\langle N; s | H | N; s \rangle = \epsilon N + \frac{\tilde{U}}{2} N(N-1) + U'_0 \frac{(N-s)(\Omega-N-s)}{2(\Omega-2)}. \quad (13.49)$$

Here \tilde{U} is the strength of the monopole component (11.88) and $U'_0 = U_0 - \tilde{U}$.

The $f_{7/2}$ shell discussed in Problem 11.6 is among the best examples of a degenerate model; in Figure 13.5, experimental ground state energies for $N = 28$ isotopes are compared with the results for the degenerate model (13.49).

Problem 13.4 Show that within a single j -level model, a one-body operator that carries an even angular momentum J is a quasispin vector and the operators with odd J are quasispin scalars.

Solution

Two single-nucleon creation and annihilation operators are two components of the $\mathcal{L} = 1/2$ quasispin doublet with projections $\mathcal{L}_z = 1/2$, and $-1/2$, respectively. A one-body operator of type $(a^\dagger a)_J$, therefore, can carry quasispin 0 or 1. For quasispin 1, all three operators with quasispin projections $\mathcal{L}_z = -1, 0$, and 1 must exist. This is true only if J is even because only in that case $(a^\dagger a^\dagger)_J$ is allowed by the Pauli principle. Therefore, if J is even, the one-body operator is a quasivector; and if J is odd, the operator is a quasiscalar.

Problem 13.5 Show that, for $j = 7/2$ valence space with identical nucleons, seniority is a good quantum number for any two-body Hamiltonian.

Solution

In order to break pairs and mix seniorities, a Hamiltonian must contain a second-rank quasitensor $\mathcal{L} = 2$ of type $(a^\dagger a^\dagger aa)$, which is simultaneously a rotational scalar $J = 0$. A scalar operator of type $(a^\dagger a^\dagger a^\dagger a^\dagger)$ should also exist as another member of the multiplet. Within $j = 7/2$ model space, four single-particle operators $(a^\dagger a^\dagger a^\dagger a^\dagger)_j$ can couple to angular momentum $J = 0$ only in one way proportional to $(P^\dagger)^2$. This means that there are no other scalar terms in the Hamiltonian that could form a second-rank quasitensor and change seniority by 2.

The quasispin symmetry introduces selection rules for transitions. As follows from Problem 13.4, in one-body transitions, seniority cannot change by more than 2. For example, in ^{52}Cr , the first excited 2_1^+ state has seniority 2 and the second excited 2_2^+ state has seniority 4. As a result, the electromagnetic transition from 2_2^+ to the ground state 0^+ is seniority-forbidden. Indeed, $B(\text{E2}, 2_2^+ \rightarrow 0^+) = 0.06 \pm 0.05 e^2 \text{ fm}^4$ which is very strongly suppressed compared with the allowed transition $B(\text{E2}, 2_1^+ \rightarrow 0^+) = 118 \pm 35 e^2 \text{ fm}^4$.

Problem 13.6 Using the Wigner–Eckart theorem in quasispin space, evaluate the matrix element $\langle N; 0|a_\lambda|N + 1; 1_\lambda\rangle$ in the seniority scheme.

Solution

States of the same seniority but with a different particle number are all members of the same quasispin multiplet; therefore, the Wigner–Eckart theorem can be used to relate matrix elements. Let us view the state $|N; 0\rangle$ as $|\mathcal{L} \mathcal{L}_z\rangle$ in the quasispin representation, where $\mathcal{L} = \Omega/4$ and $\mathcal{L}_z = N/2 - \Omega/4$, then $|N + 1; 1_\lambda\rangle$ is $|\mathcal{L} - 1/2 \mathcal{L}_z + 1/2\rangle$. Using the Wigner–Eckart theorem, the whole particle number dependence is expressed through the Clebsh–Gordan coefficient

$$\langle N; 0|a_\lambda|N + 1; 1_\lambda\rangle \propto C_{1/2 \ -1/2 \ \mathcal{L}-1/2 \ \mathcal{L}_z+1/2}^{\mathcal{L} \ \mathcal{L}_z} \propto \sqrt{\mathcal{L} - \mathcal{L}_z} \propto \sqrt{\Omega - N}. \quad (13.50)$$

The $N = 0$ case $\langle 0; 0|a_\lambda|1; 1_\lambda\rangle = 1$ allows one to obtain the final answer

$$\langle N; 0|a_\lambda|N + 1; 1_\lambda\rangle = \sqrt{\frac{\Omega - N}{\Omega}}. \quad (13.51)$$

13.5 Canonical Transformation

Presence of pairing correlations influences probabilities of all processes in the system. The simplest example is given by a *pair transfer*. In the reaction between two nuclei, a pair of nucleons can be transferred from one nucleus to another, keeping the correlation between the constituents. This process, being an analog of the Josephson effect in superconductors [QP, I, 14.5], can be microscopically described by the pair operators P and P^\dagger . Adding or subtracting the condensate pair, these operators do not change the seniority.

The quasispin algebra (13.38) allows one to use the angular momentum matrix elements for the transfer amplitudes between the states of the same seniority,

$$\begin{aligned}\langle N+2; s|P^\dagger|N; s\rangle &= \frac{1}{2}\sqrt{(\Omega-N-s)(N-s+2)}, \\ \langle N-2; s|P|N; s\rangle &= \frac{1}{2}\sqrt{(\Omega-N-s+2)(N-s)}.\end{aligned}\quad (13.52)$$

At small $s \sim 1$ and far away from the shell edges, these matrix elements are approximately equal to each other, their common value being

$$\langle N+2; s|P^\dagger|N; s\rangle \approx \langle N-2; s|P|N; s\rangle \approx \frac{1}{2}\sqrt{N(\Omega-N)}.\quad (13.53)$$

We obtained a *coherent effect* of enhancement for the condensate pair transfer due to the boson-stimulated radiation or absorption of pairs.

Now we can proceed to the single-particle processes in the presence of the condensate. The pairing Hamiltonian (13.36) generates the equations of motion for the fermion creation and annihilation operators

$$[\alpha_\lambda^\dagger, H] = -\epsilon\alpha_\lambda^\dagger + GP^\dagger\alpha_\lambda, \quad [\alpha_\lambda, H] = \epsilon\alpha_\lambda + Ga_\lambda^\dagger P = (\epsilon - G)\alpha_\lambda + GPa_\lambda^\dagger,\quad (13.54)$$

where the commutation rules for Fermi operators were used. In the second equation, we made use of the commutator $[\alpha_\lambda^\dagger, P] = -\alpha_\lambda$ that brings all fermion operators to the right. We can take the matrix element $\langle N+2; 0| \dots |N+1; 1_\lambda \rangle$ in the first of these operator equations and the matrix element $\langle N; 0| \dots |N+1; 1_\lambda \rangle$ in the second one. Let us define the matrix elements of α and α^\dagger as

$$u_\lambda(N) = \langle N; 0|\alpha_\lambda|N+1; 1_\lambda \rangle, \quad v_\lambda(N) = \langle N; 0|\alpha_\lambda^\dagger|N-1; 1_\lambda \rangle.\quad (13.55)$$

In both cases, 1_λ means the state with one unpaired particle in the orbit λ . The action of P^\dagger as in (13.53) takes us from $N \rightarrow N+2$, therefore, let us define $\Delta(N) = G\langle N+2; 0|P^\dagger|N; 0 \rangle$. We already know from Figure 13.5 and Problem 13.3 that ground states are nearly pure seniority states: $s = 0$ for even systems and $s = 1$ for odd-particle systems. If we adopt this approximation, we can evaluate

$$\begin{aligned}\langle N+2; 0|P^\dagger\alpha_\lambda|N+1; 1_\lambda \rangle &= \langle N+2; 0|P^\dagger|N; 0 \rangle \langle N; 0|\alpha_\lambda|N+1; 1_\lambda \rangle \\ &= \Delta(N)u_\lambda(N).\end{aligned}\quad (13.56)$$

Similarly, we can proceed in the second case in Eq. (13.54). The commutator gives the matrix element of the α or α^\dagger operator multiplied by the difference of energies. After that we come to the set of linear equations for matrix elements (13.55)

$$\begin{aligned}[E_1(N+1) - E_0(N+2) + \epsilon]v_\lambda(N+2) - \Delta(N)u_\lambda(N) &= 0, \\ [E_1(N+1) - E_0(N) - \epsilon + G]u_\lambda(N) - \Delta^*(N)v_\lambda(N+2) &= 0.\end{aligned}\quad (13.57)$$

For a degenerate model with energies ϵ independent on λ , the matrix elements also do not depend on λ and we can omit this subscript. The normalization constant can be defined from the basic anticommutator $\alpha_\lambda^\dagger\alpha_\lambda + \alpha_\lambda\alpha_\lambda^\dagger = 1$, where taking a single intermediate state as in (13.56) we obtain $|u(N)|^2 + |v(N)|^2 = 1$. In the same approximation as in (13.56), using number operators $a_\lambda^\dagger a_\lambda$, we find

$$u(N) = \sqrt{\frac{\Omega-N}{\Omega}}, \quad v(N) = \sqrt{\frac{N}{\Omega}}.\quad (13.58)$$

The single-particle amplitudes are not equal to 1 or 0 as it would be in the independent particle model. In the presence of the condensate, the amplitudes are the numbers between 0 and 1 (the so-called *coherence factors*).

We can bring equations (13.57) to a simpler form if we introduce two parameters $\mu(N)$ and $e(N)$ so that

$$E_0(N+2) = E_0(N) + 2\mu(N), \quad E_1(N+1) = E_0(N) + \mu(N) + e(N) - G/2 \quad (13.59)$$

and express single-particle energy relative to the chemical potential $\mu(N)$, $e'(N) = e - \mu(N) - G/2$,

$$\begin{aligned} [e(N) + e'(N)]v(N+2) - \Delta(N)u(N) &= 0, \\ [e(N) - e'(N)]u(N) - \Delta^*(N)v(N+2) &= 0. \end{aligned} \quad (13.60)$$

This set of equations has a nontrivial solution when $e^2(N) = e'^2(N) + |\Delta(N)|^2$. The necessary equation for self-consistency comes from the definition of Δ ,

$$\Delta = \frac{G}{2} \sum_{\lambda} \langle N+2, 0 | a_{\lambda}^{\dagger} a_{\lambda}^{\dagger} | N; 0 \rangle = \frac{G}{2} \sum_{\lambda} v_{\lambda}(N+2) u_{\lambda}^*(N). \quad (13.61)$$

For degenerate model, this gives

$$\Delta^2 = \frac{G^2}{4} (N+2)(\Omega - N). \quad (13.62)$$

Using this and Eq. (13.60) to solve for combinations $e(N) \pm e'(N)$, allow one to find $e'(N)$ and the resulting chemical potential

$$\mu(N) = e - \frac{G}{4}(\Omega - 2N). \quad (13.63)$$

This reproduces the results obtained earlier using quasispin symmetry arguments (see Eqs. (13.47) and (13.59)).

In these considerations, it is possible to neglect the difference between the condensates containing N or $N \pm 2$ particles. For example, in Eq. (13.60), the approximation $v(N+2) \approx v(N)$ leads to a closed solution for the amplitudes

$$v^2 = \frac{1}{2} \left(1 - \frac{e'}{e} \right), \quad u^2 = \frac{1}{2} \left(1 + \frac{e'}{e} \right), \quad (13.64)$$

which is an important result that will be discussed at the end of this chapter. The N -dependence is smooth and this approximation is justified for $N \gg 1$. We can simplify the whole analysis going to the approximate description that does not use the states with the exact particle number. Instead, one can use the *average particle number* for several adjacent systems, an analog of the grand canonical ensemble of statistical mechanics. This does not lead to any problems in macroscopic superconductors. In nuclei, this approach describes average properties of neighboring nuclei and might not be sufficiently accurate for individual nuclei, especially close to the drip lines, or in the case of sharp differences in the properties of neighboring nuclei, such as emergence of deformation.

The “average” ground state $|\emptyset\rangle$ is a superposition of ground states of even nuclei $|N; 0\rangle$ in an interval ΔN around \bar{N} such that $1 \ll \Delta N \ll N$. The single-particle excitation

$|s = 1_\lambda\rangle$ with quantum numbers λ is generated from the even ground state $|\emptyset\rangle$ by the action of the new Fermi operator b_λ^\dagger ,

$$b_\lambda^\dagger |\emptyset\rangle = |s = 1_\lambda\rangle. \quad (13.65)$$

Note that here the amplitude is equal to 1. The object generated by the operator b_λ^\dagger or annihilated by the conjugate operator b_λ is an approximate elementary excitation of a system, and it is usually called a *quasiparticle*. As mentioned earlier, this term here has a quite specific meaning being different from the general concept of quasiparticles used in many-body physics irrespective of the presence of pairing correlations.

According to (13.58), the amplitudes for creating a genuine particle from the condensate or a hole in the conjugate orbit are given by

$$a_\lambda^\dagger |N; 0\rangle = \sqrt{\frac{\Omega - N}{\Omega}} |N + 1; 1_\lambda\rangle, \quad a_{\bar{\lambda}}^\dagger |N; 0\rangle = \sqrt{\frac{N}{\Omega}} |N - 1; 1_{\bar{\lambda}}\rangle. \quad (13.66)$$

Neglecting the difference of the condensate particle numbers in the two cases of (13.66), we can combine these expressions to get the quasiparticle operator

$$b_\lambda^\dagger = u_\lambda a_\lambda^\dagger + v_\lambda a_{\bar{\lambda}}^\dagger, \quad (13.67)$$

where the parameters u_λ and v_λ do not actually depend on λ in our degenerate model and coincide with the results (13.58) of equations of motion,

$$u_\lambda = \sqrt{\frac{\Omega - N}{\Omega}}, \quad v_\lambda = \sqrt{\frac{N}{\Omega}}. \quad (13.68)$$

The Hermitian conjugate operator is

$$b_\lambda = u_\lambda^* a_\lambda + v_\lambda^* a_{\bar{\lambda}}^\dagger. \quad (13.69)$$

The transformation from particles (a, a^\dagger) to quasiparticles (b, b^\dagger) invented by N.N. Bogoliubov, 1958, is a powerful tool in many-body quantum theory. In the presence of the condensate, there are two ways to create a single-particle excitation with quantum numbers λ : directly generate a particle with such quantum numbers, the first term in (13.67), or remove the time-conjugate partner from the condensate pair, the second term in (13.67). The actual elementary excitation is given by the linear combination (13.67) of these two amplitudes. It is normalized in a natural way,

$$|u_\lambda|^2 + |v_\lambda|^2 = 1. \quad (13.70)$$

In a time-reversal invariant system, the amplitudes u_λ and v_λ can be taken real and coinciding for λ and $\bar{\lambda}$. However, one has to be careful with the relative signs of amplitudes owing to the time-reversal rule (13.14) because the time-reversed quasiparticle operators (in a \mathcal{T} -invariant system) are

$$b_{\bar{\lambda}}^\dagger = u_\lambda a_{\bar{\lambda}}^\dagger - v_\lambda a_\lambda, \quad b_{\bar{\lambda}} = u_\lambda a_{\bar{\lambda}} - v_\lambda a_\lambda^\dagger. \quad (13.71)$$

The situation is more complicated if there is no \mathcal{T} -invariance, for example, with an external magnetic field. Then the transformation amplitudes become in general complex.

The quasiparticles are still *fermions*. Due to the normalization (13.70), the anticommutator is preserved,

$$[b_\lambda, b_{\lambda'}^\dagger]_+ = \delta_{\lambda\lambda'}. \quad (13.72)$$

The remaining anticommutators are preserved as well. For example,

$$[b_\lambda, b_{\lambda'}]_+ = u_\lambda^* v_{\lambda'}^* \delta_{\lambda\lambda'} + v_\lambda^* u_{\lambda'}^* \delta_{\bar{\lambda}\bar{\lambda'}}. \quad (13.73)$$

Here the δ -symbols differ in sign as in (13.16) so that

$$[b_\lambda, b_{\lambda'}]_+ = \delta_{\bar{\lambda}\lambda'}(v_\lambda u_{\bar{\lambda}} - u_\lambda v_{\bar{\lambda}})^*. \quad (13.74)$$

The result vanishes after a proper choice of phases for time-conjugate orbits (automatically in the \mathcal{T} -invariant case). Therefore, the Bogoliubov transformation is a *canonical* one.

The operator (13.67) creates an elementary Fermi excitation, while its conjugate operator (13.69) acting onto the ground state gives zero,

$$b_\lambda |\emptyset\rangle = 0, \quad (13.75)$$

as seen from (13.69), (13.68), and (13.66) taking into account again the rule $a_\lambda = -a_{\bar{\lambda}}$ and identifying the condensates in both terms of (13.66). Therefore, the condensate ground state is a vacuum state for quasiparticles.

The inverse transformation to (13.67) and (13.69) can be easily found,

$$a_\lambda = u_\lambda b_\lambda - v_\lambda b_{\bar{\lambda}}^\dagger, \quad a_\lambda^\dagger = u_\lambda b_\lambda^\dagger - v_\lambda b_{\bar{\lambda}}. \quad (13.76)$$

Taking into account (13.75), the expectation value of the fermion number operator in the ground state $|\emptyset\rangle$ turns out to be

$$n_\lambda = \langle \emptyset | \hat{n}_\lambda | \emptyset \rangle = v_\lambda^2 \langle \emptyset | b_\lambda b_{\bar{\lambda}}^\dagger | \emptyset \rangle = v_\lambda^2. \quad (13.77)$$

In the degenerate model (13.68), the mean occupation numbers are uniform over the whole space,

$$n_\lambda = \frac{N}{\Omega}. \quad (13.78)$$

Thus, the amplitudes u_λ and v_λ characterize the particle distribution in the ground state,

$$v_\lambda = \sqrt{n_\lambda}, \quad u_\lambda = \sqrt{1 - n_\lambda}. \quad (13.79)$$

Except for the amplitudes (13.68), which in this specific case do not depend on single-particle quantum numbers, the majority of results are similar for an arbitrary nondegenerate scheme of single-particle levels. Any operator for the original fermion system can be translated into the quasiparticle language with the aid of the canonical transformation that allows one to calculate all matrix elements of physical quantities. The price one has to pay for this simplification is the particle number nonconservation.

13.6 BCS Theory: Trial Wave Function

Being armed with the results for the solvable degenerate model, we can develop a more general approach applicable to realistic nondegenerate situations. This was done first in the BCS paper on microscopic theory of superconductivity [3]. Although this method is also approximate, it can be shown to give exact results in the asymptotic limit of large macroscopic systems. In nuclei, as we have already mentioned, in some cases its accuracy is not sufficient.

We consider a general *pairing Hamiltonian* for a Fermi system. It consists of independent particle energies ϵ_λ and pairing interaction with pair matrix elements (13.34). The single-particle level scheme ϵ_λ is arbitrary, but the pairing strength is assumed to

be small compared to the Fermi energy ϵ_F . The pairing is efficient in the energy layer near the Fermi surface Σ_F . The single-particle level density v_F at Σ_F , Section 7.2, plays an important role in final results.

The single-particle orbits are divided into Kramers doublets $(\lambda, \tilde{\lambda})$, which are degenerate due to the assumed \mathcal{T} -invariance. We will proceed with a variational procedure: construct a trial ground state wave function that accounts for the existence of the pair condensate and minimize the ground state energy E_0 with respect to the parameters of the wave function.

The pairing interaction scatters a pair from one doublet state to another. For the broken pair, the interaction is much weaker and we neglect it as we did earlier. In this approximation, pairs always travel over available space as a whole. The ground state wave function is a superposition of components with different occupancies of the doublet states. We consider these occupancies as variational parameters. The corresponding amplitudes are just the earlier introduced v_λ and u_λ , Eq. (13.79).

In the \mathcal{T} -invariant system, the occupancies of both doublet components are equal. For each doublet, $v_\lambda = v_{\tilde{\lambda}}$ gives the probability amplitude of finding both doublet states occupied, whereas $u_\lambda = u_{\tilde{\lambda}}$ gives the probability amplitude for both doublet states being empty. The sum of probabilities is 1, Eq. (13.70), because we neglect the probabilities of the partial occupation of only one of the doublet states. The appropriate wave function can be written as a product over all doublet states

$$|\emptyset\rangle = \prod_\lambda \{u_\lambda - v_\lambda P_\lambda^\dagger\} |\emptyset\rangle. \quad (13.80)$$

Here the operator

$$P_\lambda^\dagger = a_\lambda^\dagger a_{\tilde{\lambda}}^\dagger \quad (13.81)$$

is the analog of (13.13) for a given doublet and, distinctly from (13.13), each doublet is represented by only one factor in the infinite product (13.80) where $|\emptyset\rangle$ stands for an absolute vacuum, with no particles at all.

The obvious shortcoming of the simple function (13.80) is that it does not conserve the particle number. In this infinite product, there is a nonzero amplitude coming from multiplication of all u factors that correspond to the empty state $|\emptyset\rangle$; the product of all v -factors gives infinitely many particles; all intermediate cases are present as well. However, this is a standard situation in statistical mechanics of macroscopic systems, where it is impossible to guarantee the exact conservation of a giant particle number. The appropriate recipe of statistical mechanics recommends to use the grand canonical ensemble where the system is considered to be open and the particle number is fluctuating around the mean value \bar{N} . The desired mean value is ensured by the introduction of the chemical potential μ : the Hamiltonian H is substituted by

$$H' = H - \mu \hat{N}. \quad (13.82)$$

All eigenstates depend on μ that is chosen afterwards in such a way that the expectation value of \hat{N} in the ground state is equal to the mean particle number,

$$\langle \hat{N} \rangle_\mu = \bar{N}. \quad (13.83)$$

This equation specifies the necessary value of μ . In equilibrium macroscopic systems, the fluctuations of the particle number grow as $\Delta N \sim \sqrt{N}$ and their *relative* role is

small, $\Delta N/\bar{N} \sim 1/\sqrt{N}$. This is the same approximation as earlier when we neglected the difference of condensates. In nuclear problems, it might be desirable to improve the approximation removing the fictitious fluctuations of the particle number. One way of doing this is to project a component with the desired value of N out of the wave function (11.80) that has no certain value of the particle number, but this violates the variational character of the method. A more advanced way (but also more complicated in practice) is to follow exactly the particle number in all quantities and come to recurrence relations between the matrix elements referring to different nuclei (similar to Eq. (13.60), [7]). In the current consideration, we proceed as in statistical mechanics introducing the chemical potential (13.82).

The Hamiltonian generalizing (13.36) can be written in terms of single-particle energies ϵ_λ and matrix elements (13.34) as

$$H' = \sum_\lambda 2\epsilon'_\lambda \hat{n}_\lambda + \sum_{\lambda\lambda'} U_{\lambda\lambda'}^P P_\lambda^\dagger P_{\lambda'}, \quad (13.84)$$

where sums are again taken over the doublets. The single-particle energies are now shifted by the chemical potential, $\epsilon'_\lambda = \epsilon_\lambda - \mu$. Practically, the pairing is concentrated near Σ_F so that the chemical potential is close to its unperturbed value ϵ_F .

13.7 Energy Minimization

Let us calculate the expectation value

$$E_0 = \langle \emptyset | H' | \emptyset \rangle \quad (13.85)$$

for the shifted Hamiltonian (13.84) in the trial state (13.80). In the independent particle term, the operator \hat{n}_λ is simply substituted by its expectation value v_λ^2 . In the interaction term, let us consider an item with the pair transfer $\lambda' \rightarrow \lambda$, where $\lambda \neq \lambda'$. It gives the nonzero contribution to (13.85) if in the initial state (the right-hand side of the matrix element) the doublet λ' is filled, amplitude $v_{\lambda'}$, and the doublet λ is empty, amplitude u_λ . On the other hand, in the final state (left-hand side of the matrix element), the doublet λ' has to be empty, amplitude $u_{\lambda'}$, while the doublet λ is filled by the transferred pair, amplitude v_λ . The factors of the product (13.80) that do not participate in a considered process go through without changes and give 1 due to the normalization (13.70).

We come to the total energy as a sum of independent particle energies and contributions of all possible pair scattering processes weighted with the coherence factors,

$$E_0 = \sum_\lambda 2\epsilon'_\lambda v_\lambda^2 + \sum_{\lambda\lambda'} U_{\lambda\lambda'}^P u_\lambda v_\lambda u_{\lambda'} v_{\lambda'}. \quad (13.86)$$

The diagonal interaction terms, $\lambda' = \lambda$, give $\sum_\lambda U_{\lambda\lambda}^P v_\lambda^4$, with a single summation instead of the double summation in (13.86). Therefore, their contribution is smaller by a factor $\sim \Omega$ and can be omitted (a slight renormalization of single-particle energies analogous to a weak monopole component arising from the pairing interaction).

In order to perform minimization with respect to u_λ and v_λ that are linked by the normalization condition (13.70), we express them through the occupation numbers n_λ as in (13.79),

$$E_0 = \sum_\lambda 2\epsilon'_\lambda n_\lambda + \sum_{\lambda\lambda'} U_{\lambda\lambda'}^P \sqrt{n_\lambda(1-n_\lambda)n_{\lambda'}(1-n_{\lambda'})}. \quad (13.87)$$

All n_λ are independent because the care of particle number conservation is taken (in average) by the chemical potential.

The direct variation of energy (13.87) gives a set of equations

$$\frac{\partial E_0}{\partial n_\lambda} = 0 \quad (13.88)$$

calculated for each λ . The subscripts λ and λ' in (13.87) are equivalent and each of them can coincide with the external λ in (13.88). We keep only one contribution multiplying the result by 2. The direct differentiation leads to

$$2\epsilon'_\lambda + 2\frac{1 - 2n_\lambda}{2\sqrt{n_\lambda(1 - n_\lambda)}} \sum_{\lambda'} U_{\lambda\lambda'}^P \sqrt{n_{\lambda'}(1 - n_{\lambda'})} = 0. \quad (13.89)$$

Let us introduce the notation

$$\Delta_\lambda = - \sum_{\lambda'} U_{\lambda\lambda'}^P \sqrt{n_{\lambda'}(1 - n_{\lambda'})} = - \sum_{\lambda'} U_{\lambda\lambda'}^P u_{\lambda'} v_{\lambda'}. \quad (13.90)$$

The sign minus is chosen because we are interested in the case of attraction when matrix elements are mostly negative. The minimization condition (13.89) takes a form

$$2\epsilon'_\lambda \sqrt{n_\lambda(1 - n_\lambda)} = \Delta_\lambda (1 - 2n_\lambda). \quad (13.91)$$

It is worthwhile to introduce another notation

$$E_\lambda = +\sqrt{\epsilon_\lambda'^2 + \Delta_\lambda^2}. \quad (13.92)$$

Then, after simple algebra, we arrive at the solution of the quadratic equation for the occupation numbers,

$$n_\lambda = \frac{1}{2} \left(1 \pm \frac{\epsilon'_\lambda}{E_\lambda} \right). \quad (13.93)$$

The quantity Δ_λ , Eq. (13.90), accumulates the pairing effects. With *no pairing interaction*, $E_\lambda \rightarrow |\epsilon'_\lambda|$, so that

$$n_\lambda \rightarrow n_\lambda^\circ = \frac{1}{2} \left(1 \pm \frac{\epsilon'_\lambda}{|\epsilon'_\lambda|} \right). \quad (13.94)$$

The single-particle energies ϵ'_λ are positive above μ and negative below μ . Therefore, we have to choose the minus sign in (13.94). It will guarantee the correct occupation numbers equal to 1 far below μ and 0 far above μ . Of course, this is just another definition of the Fermi energy, $\mu = \epsilon_F$.

In the presence of pairing forces, the quantity E_λ is different from $|\epsilon'_\lambda|$ in the region $\delta\epsilon \sim \Delta$ near Σ_F , where $\Delta \ll \epsilon_F$ is an average value of Δ_λ . Outside this region, we can neglect Δ_λ and come back to the unperturbed occupancy (13.94). Here, we again have to select the lower sign in (13.93). Consequently, the solution of the minimization problem is

$$v_\lambda^2 = n_\lambda = \frac{1}{2} \left(1 - \frac{\epsilon'_\lambda}{E_\lambda} \right), \quad u_\lambda^2 = 1 - n_\lambda = \frac{1}{2} \left(1 + \frac{\epsilon'_\lambda}{E_\lambda} \right). \quad (13.95)$$

However, this is merely a formal solution since the quantity Δ_λ entering E_λ depends on the occupation numbers through the definition (13.90).

13.8 Solution for the Energy Gap

The unknown quantity Δ_λ is usually called the *energy gap* because, as we see, its value defines the minimum excitation energy near Σ_F , where the unperturbed energy $\epsilon' = \epsilon - \mu$ is small. To find Δ_λ , we have to substitute the parameters (13.95) into (13.90), which leads to a nonlinear equation for Δ_λ .

The combination that enters Eq. (13.90) is

$$u_\lambda v_\lambda = \sqrt{n_\lambda(1-n_\lambda)} = \frac{\Delta_\lambda}{2E_\lambda}. \quad (13.96)$$

It disappears in the normal (no-pairing) limit when all occupation numbers are 1 or 0. Equations (13.96) and (13.90) lead to the integral equation for Δ_λ ,

$$\Delta_\lambda = - \sum_{\lambda'} U_{\lambda\lambda'}^P \frac{\Delta_{\lambda'}}{2E_{\lambda'}}. \quad (13.97)$$

This main equation of the BCS theory always has a trivial solution $\Delta_\lambda = 0$ corresponding to a normal Fermi gas. To find a *nontrivial* solution (if it does exist), we have to assume some properties of the pairing potential that define the existence and symmetry of Δ_λ .

In *uniform* macroscopic systems, pairs are characterized by the total momentum \mathbf{P} conserved in scattering processes, and the relative momentum \mathbf{p} (Figure 11.2). The total momentum of each pair should be zero for the ground state with no current. The absolute values of \mathbf{p} and \mathbf{p}' are close to p_F , and the scattering is described by the angle between the initial, \mathbf{p}' , and final, \mathbf{p} , relative momentum. As a function of this angle, the matrix elements $U_{\mathbf{p}\mathbf{p}'}^P$ can be expanded over Legendre polynomials. The condensate will be formed by pairs in the state of relative motion (partial wave) corresponding to the maximum attraction. Usually, this occurs in the *s*-wave, and therefore in the singlet spin state. (In superfluid ${}^3\text{He}$ pairing occurs in the spin triplet *p*-state with several thermodynamic phases which differ in coupling between spin and orbital momentum [8].) For the *s*-wave pairing, the interaction matrix element does not depend on the scattering angle and can be substituted by an effective constant.

The situation is qualitatively similar in nuclei although the matrix elements vary for different combinations λ and λ' . Still the approximation (13.35) by an effective constant within some energy region around Σ_F (and zero outside this region) may give a reasonable estimate,

$$U_{\lambda\lambda'}^P \approx -G\theta_\lambda\theta_{\lambda'}, \quad (13.98)$$

where the cut-off factors θ_λ truncate the pairing space by the energy layer $-\xi \leq \epsilon'_\lambda \leq +\xi$ near Σ_F . In this approximation

$$\Delta_\lambda = G\theta_\lambda \sum_{\lambda'} \frac{\Delta_{\lambda'}}{2E_{\lambda'}} \theta_{\lambda'} \quad (13.99)$$

so that Δ_λ is a constant within the layer,

$$\Delta_\lambda = \theta_\lambda \Delta. \quad (13.100)$$

The nontrivial value of Δ satisfies the equation

$$1 = G \sum_\lambda \frac{1}{2E_\lambda} \theta_\lambda \quad (13.101)$$

where Δ enters the denominator through E_λ , Eq. (13.92).

To solve Eq. (13.101), one can substitute the summation over the layer by the integration over single-particle energies with the level density $v'(\epsilon) \approx v'_F$ at Σ_F . This level density counts degenerate doublets and therefore differs from v_F by a factor 1/2. The subtle point of this substitution is that in the discrete spectrum, Eq. (13.101) might have no solutions, which would mean that $\Delta = 0$. The interaction has to be *sufficiently strong* to ensure the formation of the condensate [9]. Indeed, the minimum value of the denominator in (13.101) is $|\epsilon'_\lambda|$. Then the *critical pairing strength* G_c is defined by

$$1 = G_c \sum_\lambda \frac{\theta_\lambda}{2|\epsilon'_\lambda|}. \quad (13.102)$$

A nontrivial solution is absent if $G < G_c$. If one would have performed the transition to the continuous spectrum, then the corresponding integral over ϵ' in (13.102) with the level density that is finite at Σ_F would have a logarithmic singularity. Then $G_c = 0$, and the condensate appears at an *arbitrary weak* interaction strength. This means that in macroscopic Fermi systems, the normal Fermi state is *unstable* with respect to attraction forces causing the formation of the pair condensate (Cooper phenomenon).

In a finite system, the substitution of the sum by the integral is justified only if the pairing strength is *overcritical*, otherwise one loses all pairing correlations. With strong pairing and such a continuous approximation, the integration reduces to

$$1 = G \int_{-\xi}^{+\xi} d\epsilon' \frac{v'(\epsilon')}{2\sqrt{\epsilon'^2 + \Delta^2}} \approx Gv'_F \int_0^\xi d\epsilon' \frac{1}{\sqrt{\epsilon'^2 + \Delta^2}} \quad (13.103)$$

and can be easily performed,

$$1 = Gv'_F \ln \frac{\xi + \sqrt{\xi^2 + \Delta^2}}{\Delta} \approx Gv'_F \ln \frac{2\xi}{\Delta}, \quad (13.104)$$

where we assumed $\Delta^2 \ll \xi^2$. This approximation is sound because ξ is of the order of the width of the major shell $\epsilon_F A^{-1/3}$ while a typical value of Δ in medium nuclei is ~ 1 MeV. Finally, the model gives the solution for the gap parameter,

$$\Delta \approx 2\xi \exp \left(-\frac{1}{Gv'_F} \right). \quad (13.105)$$

The result is a *nonanalytical* function of the strength G at $G \rightarrow 0$ (an *essential singularity* does not allow Taylor expansion) and cannot be derived in perturbation theory even at small G . However, again we need to recall that this conclusion is valid for macroscopic systems only, whereas for finite systems, the whole method does not work in the case of weak pairing.

Going back to the parameters (13.95) of the wave functions, we come to a simple picture of single-particle occupancies for the constant (or slightly changing as a function of λ) energy gap Δ . The occupation numbers, instead of the sharp discontinuity in a normal Fermi gas, smoothly decrease from 1 well below Σ_F to 0 well above Σ_F (Figure 13.6). The width of the transition region is of the order of Δ , that is, less than that of the interaction layer $\sim 2\xi$.

The precision experiments using electron scattering to measure the charge distribution in nuclei show a more smooth picture than it would be for the normal case with

Figure 13.6 The occupation numbers near the Fermi surface in a paired system.

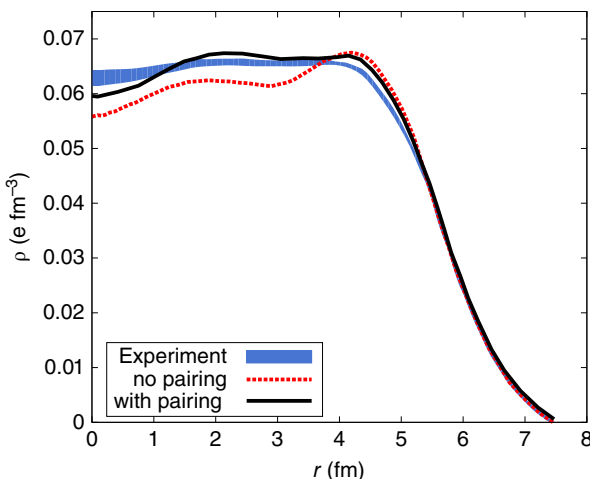
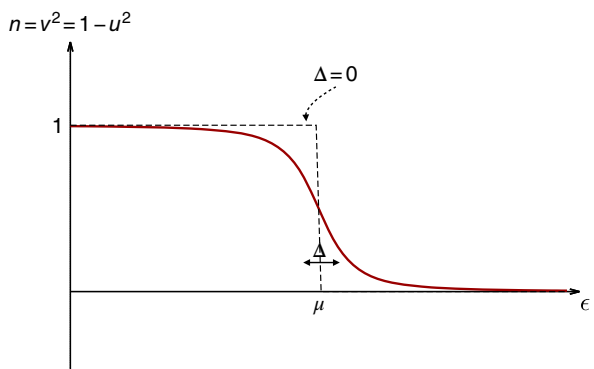


Figure 13.7 Charge density distribution in ^{140}Ce ; the results of electron scattering (the width corresponds to the experimental errors) are compared with the mean field calculations without (dashed line) and with (solid line) pairing.

completely filled and completely empty orbits. In Figure 13.7, the distribution function that follows from pairing correlations agrees better with the data for ^{140}Ce [10] than the independent particle model with the mean field derived from the same self-consistent calculation but neglecting the pairing. Here, pairing correlations lead to partial occupancy of $2s_{1/2}$ orbit that otherwise would be unoccupied in the Fermi state. Protons on the s -orbit increase the interior charge density.

The results of this variational approach can be obtained in many other ways. We could use the canonical transformation method assuming the structure of the quasiparticle operators given by (13.67) and (13.69). One has to express the Hamiltonian in terms of the new operators b, b^\dagger using the inverse transformation (13.76). With the help of commutation relations, the transformed Hamiltonian is brought to the normal form with respect to the new operators b and b^\dagger . The interaction terms, bilinear in operators, have two types of structure, $b^\dagger b$ and $(bb + b^\dagger b^\dagger)$. The second type corresponds to the *dangerous diagrams* of creating and annihilating two quasiparticles. Their presence would make a system unstable. The choice of the parameters u, v of the canonical

transformation that nullifies the dangerous terms determines the stable ground state. For the pairing Hamiltonian, the resulting parameters coincide with those found by the variational method.

We can check straightforwardly that the quasiparticle operators found in the degenerate model have exactly the same properties in the realistic many-orbital case if defined with the appropriate amplitudes u, v . Indeed, let us act by the quasiparticle creation operator b_λ^\dagger , Eq. (13.67), onto the ground state (13.80). The term $u_\lambda a_\lambda^\dagger$ puts the particle in the empty state with the amplitude u_λ^2 . The term $v_\lambda a_\lambda^\dagger$ annihilates the time-conjugate partner from the condensate pair. The superposition of these two amplitudes gives, in agreement with (13.65),

$$b_\lambda^\dagger |\emptyset\rangle = a_\lambda^\dagger \prod_{\lambda' \neq \lambda} \{u_{\lambda'} - v_{\lambda'} P_{\lambda'}^\dagger\} |\emptyset\rangle, \quad (13.106)$$

which is exactly the state (13.65) with $s = 1$. In the same way, we check that our ground state satisfies the vacuum condition for quasiparticles (13.75).

13.9 Excitation Spectrum

The energy E_λ introduced in the process of the solution, Eq. (13.92), has an important physical meaning justifying its notation. This energy is related to an extra valence particle that blocks the pair levels and reduces the total gain due to the condensate formation.

Let us add a particle in the orbit λ to the paired even system and calculate the energy W_λ of the resulting state. First, the energy of the occupied orbit, relative to the Fermi energy, is added (ϵ'_λ) instead of the removed pair term $2\epsilon'_\lambda v_\lambda^2$ in (13.86). But near Σ_F , the orbit energy ϵ'_λ is small anyway, the extra particle sits almost on the Fermi surface.

Second, there exists another effect connected with the blocking of a pair state available for scattering of other pairs. This contribution turns out to be finite at Σ_F due to the summation over many pair states. This effect comes from the second term in (13.86) where we have now to cross out the contributions of the blocked orbit in both sums, over λ and over λ' , which give equal effects. As a result, the total change of energy associated with the extra particle is

$$W_\lambda = \epsilon'_\lambda (1 - 2v_\lambda^2) - 2u_\lambda v_\lambda \sum_{\lambda'} U_{\lambda\lambda'}^P u_{\lambda'} v_{\lambda'}. \quad (13.107)$$

The sum in (13.97) is equal to $-\Delta_\lambda$, Eq. (13.90). Using the values of the parameters (13.92), (13.95), and (13.96), we come to

$$W_\lambda = \epsilon'_\lambda \left(1 - 1 + \frac{\epsilon'_\lambda}{E_\lambda}\right) - 2 \frac{\Delta_\lambda}{2E_\lambda} (-\Delta_\lambda) = E_\lambda. \quad (13.108)$$

Thus, the quantity E_λ can be called *quasiparticle energy*. It is the amount of energy added to the system in the excitation produced by the quasiparticle creation operator (13.65). It is identical to the energy e used in Eq. (13.64) of the degenerate model. Now the meaning of the term *energy gap* becomes more clear. At Σ_F , the self-energy of the added particle goes to zero, but the minimum excitation energy is finite and equal to Δ . Note that it comes exclusively from the blocking effect of the extra particle onto all other pairs.

In a normal macroscopic system, the single-particle excitation energy near Σ_F goes linearly as a function of momentum,

$$W_p = \epsilon(p) - \epsilon_F \approx v_F(p - p_F), \quad p > p_F. \quad (13.109)$$

The same is valid for the hole excitations,

$$W_p = \epsilon_F - \epsilon(p) \approx v_F(p_F - p), \quad p < p_F; \quad (13.110)$$

in both cases, v_F is the Fermi velocity. This energy has two branches, for particles and holes, which join at Σ_F where the excitation energy vanishes (Figure 13.8). In the paired system, we have a smooth behavior with a gap Δ at Σ_F . The excitations have mixed particle–hole nature as embodied in the quasiparticle canonical transformation. It can be shown that such a pattern is necessary for superfluidity in macroscopic systems.

To excite an *even* system, we need to break one of the pairs. If the partners occupy after that the single-particle orbits λ and λ' , the associated excitation energy is

$$W_{\lambda\lambda'} = E_\lambda + E_{\lambda'}. \quad (13.111)$$

Obviously, such excitations start from higher threshold equal to $(W_{\lambda\lambda'})_{\min} = 2\Delta$ demonstrating the emergence of two quasiparticles. The presence of the gap 2Δ in the excitation spectrum is directly related to the superconductivity in macroscopic Fermi systems with attraction between the fermions. The Landau criterion [QP, II, 21.5] for the critical velocity (the upper limit for a speed of superfluid motion) gives $v_{cr} = \min(W/P) \Rightarrow \Delta/p_F$, where the minimum excitation energy (13.111) is in our case 2Δ , and the maximum momentum $P = 2p_F$ for the excitation breaking a pair.

Summarizing these features of the excitation spectrum in a paired system, we can use the seniority scheme developed originally for the degenerate model. We classified the states by the number s of unpaired particles. The energy gap in that model was given by Eq. (13.45). Now we can extend this description to the realistic case. The ground state has $s = 0$, the first excited states in an even system correspond to $s = 2$, whereas the ground state of an odd- A nucleus can be described as having $s = 1$. The excitation spectrum of the even system has a gap 2Δ ; the excitation spectrum of the odd system has

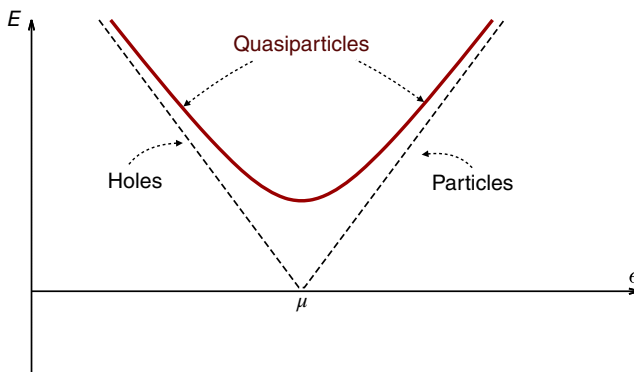


Figure 13.8 Single-particle excitation spectrum near the Fermi surface in a paired system.

no gap as the unpaired particle can be excited to another orbit with no strong distortion of the condensate (see Figures 13.2 and 13.3). At energy $\sim 2\Delta$ in the odd system, the set of three-quasiparticle states, $s = 3$, is located, and the level density is sharply growing. This construction can easily be continued.

However, the states with high s become less and less correlated. Each time, one should solve the equation for the gap, similar to (13.90) but with new occupation numbers, including the blocking effect. If the probability of finding an unpaired particle in the orbit λ is f_λ [do not confuse this function with the pair occupancies n_λ present already in the ground state (13.80)], the probability of finding the doublet state $(\lambda, \tilde{\lambda})$ empty and accessible for the pair scattering is

$$p_\lambda = 1 - f_\lambda - f_{\tilde{\lambda}}. \quad (13.112)$$

Then instead of the main equation (13.90), we obtain

$$\Delta_\lambda = - \sum_{\lambda\lambda'} U_{\lambda\lambda'}^P \frac{\Delta_{\lambda'}}{2E_{\lambda'}} p_{\lambda'}. \quad (13.113)$$

This happens as the excitation energy (that can also be expressed with the aid of *temperature* T) grows increasing the probabilities $f_\lambda(T)$ of thermally excited quasiparticles. The nontrivial solution $\Delta \neq 0$ decreases with temperature and vanishes at critical temperature T_c that can be found from (13.113) with $\Delta \rightarrow 0$. In macroscopic systems, it is observed as a phase transition from superconducting to normal state. In finite systems like nuclei, there is no sharp phase transitions but Δ gradually decreases. When it becomes less than the mean spacing between the orbit energies in a normal system, it makes no sense to speak about the gap in the spectrum.

The quasiparticle excitations in the even system that are pushed above threshold 2Δ increase the *level density* in that region. The new level density $\nu_{q-p}(E)$ of the unpaired particles with energies (13.102) $E = \sqrt{\epsilon^2 + \Delta^2}$ is, as usual, the number of levels dN/dE per unit energy interval. In terms of the unperturbed level density $\nu(\epsilon)$, we find

$$\nu_{q-p}(E) = \frac{dN}{d\epsilon} \frac{d\epsilon}{dE} = \nu \frac{E}{\sqrt{E^2 - \Delta^2}}. \quad (13.114)$$

This level density in a macroscopic system would have an (integrable) singularity at threshold of pair breaking due to accumulation of quasiparticle states. Unfortunately, this effect is not easily observable because other interactions and levels of collective nature smooth out all singularities.

13.10 Condensation Energy

Now we can show that the “superconducting” state with the nontrivial solution for Δ is energetically favorable compared to the normal solution with $\Delta = 0$. In the model with constant matrix elements (13.97), the ground state energy E_0 (with the insignificant shift by $\mu\bar{N}$) is

$$E_0 = 2 \sum_{\lambda} \epsilon'_\lambda v_\lambda^2 - G \left(\sum_{\lambda} u_\lambda v_\lambda \theta_\lambda \right)^2. \quad (13.115)$$

The first term here can be substituted by the integral as in (13.103),

$$E_0^{(1)} \approx v'_F \int_{-\xi}^{\xi} d\epsilon' \epsilon' \left(1 - \frac{\epsilon'}{\sqrt{\epsilon'^2 + \Delta^2}} \right). \quad (13.116)$$

The second term in (13.115) is, as seen from (13.99), $\Delta^2/2G$. Using (13.103), we write it again in the integral form

$$E_0^{(2)} = -\frac{\Delta^2}{G} \approx -\frac{1}{2} \Delta^2 v'_F \int_{-\xi}^{\xi} \frac{d\epsilon'}{\sqrt{\epsilon'^2 + \Delta^2}}. \quad (13.117)$$

To find the condensation energy E_c , we have to calculate the difference between the ground state energies of paired and normal systems, the latter being equal to the sum of all single-particle energies in the interaction layer below Σ_F ,

$$E_{\text{norm}} \approx 2v'_F \int_{-\xi}^0 d\epsilon' \epsilon'. \quad (13.118)$$

It is convenient to collect all terms and then to perform the integration that gives

$$E_c = E_0^{(1)} + E_0^{(2)} - E_{\text{norm}} = v'_F \left(\xi^2 - \xi \sqrt{\xi^2 + \Delta^2} \right). \quad (13.119)$$

This energy is negative for any nonzero value of the gap parameter. Therefore, the non-trivial solution is *energetically favorable*.

In the approximation $\xi^2 \gg \Delta^2$ that was used in (13.104),

$$E_c = -\frac{1}{2} \Delta^2 v'_F. \quad (13.120)$$

This result has a simple physical meaning: the pairing is effective in changing the single-particle energy spectrum in the interval of the order Δ . This interval contains $v_F \Delta$ states. Each of them acquires extra binding energy of the order of Δ . If both proton and neutron subsystems are paired, it should be taken into account in the level density v'_F . For nuclei far from the line of stability, we have essentially two Fermi surfaces, for neutrons and protons, and two pair condensates.

In macroscopic superconductors, the condensation energy per unit volume (the level density contains the volume as a factor) is equal to the magnetic field energy density $B_c^2/8\pi$ that is needed to destroy superconductivity. Therefore, Eq. (13.120) directly determines the critical magnetic field B_c .

13.11 Transition Amplitudes

As we discussed in relation to the transfer processes (13.53), the coherence factors determined by the condensate properties strongly influence the transition probabilities. Here we look at the matrix elements of one-body operators, which define multipole moments and radiation transitions.

The general one-body operator that does not change the particle number can be written as

$$V = \sum_{\lambda\lambda'} V_{\lambda\lambda'} a_\lambda^\dagger a_{\lambda'}, \quad (13.121)$$

where the sum goes over all single-particle orbits. To find its action in the paired system, we perform the canonical transformation (13.76) to quasiparticles. The resulting operator contains terms $V_{\Delta s}$ with different seniority selection rules Δs .

First, we consider the contributions $\sim b^\dagger b$ that conserve the number of quasiparticles, $\Delta s = 0$. There are two terms of this type,

$$V_0 = \sum_{\lambda\lambda'} V_{\lambda\lambda'} \left(u_\lambda u_{\lambda'} b_\lambda^\dagger b_{\lambda'} + v_\lambda v_{\lambda'} b_{\tilde{\lambda}}^\dagger b_{\tilde{\lambda}'} \right). \quad (13.122)$$

The second item in (13.122) can be brought to the normal form,

$$b_{\tilde{\lambda}} b_{\tilde{\lambda}'}^\dagger = \delta_{\lambda\lambda'} - b_{\tilde{\lambda}}^\dagger b_{\tilde{\lambda}}. \quad (13.123)$$

In this way, we extract the nonoperator term (diagonal expectation value)

$$\bar{V} = \sum_{\lambda} V_{\lambda\lambda} n_{\lambda} \quad (13.124)$$

that is determined by the occupation numbers $n_{\lambda} = v_{\lambda}^2$. Two operator terms with $\Delta s = 0$ are combined into the operator that is responsible for the processes of quasiparticle transfer by the field V ,

$$\hat{V}_0 = \sum_{\lambda\lambda'} V_{\lambda\lambda'} \left(u_\lambda u_{\lambda'} b_\lambda^\dagger b_{\lambda'} - v_\lambda v_{\lambda'} b_{\tilde{\lambda}'}^\dagger b_{\tilde{\lambda}} \right). \quad (13.125)$$

In the second term (13.125), we can change the summation variables, $\tilde{\lambda} \rightarrow \lambda'$, $\tilde{\lambda}' \rightarrow \lambda$ making the operators identical to those in the first term. In a \mathcal{T} -invariant system, the amplitudes u, v do not change under time reversal. The final result depends on the properties of the field V with respect to time reversal.

For \mathcal{T} -even field, $V_{\lambda\lambda'} = V_{\tilde{\lambda}\tilde{\lambda}}$, the matrix element $M_{\lambda\lambda'}$ of quasiparticle transfer $b_{\lambda}^\dagger b_{\lambda'}$ is equal to

$$M_{\lambda\lambda'}^{(+)} = V_{\lambda\lambda'} (u_\lambda u_{\lambda'} - v_\lambda v_{\lambda'}). \quad (13.126)$$

In the \mathcal{T} -odd case, $V_{\lambda\lambda'} = -V_{\tilde{\lambda}\tilde{\lambda}}$, the matrix element contains a different coherence factor

$$M_{\lambda\lambda'}^{(-)} = V_{\lambda\lambda'} (u_\lambda u_{\lambda'} + v_\lambda v_{\lambda'}). \quad (13.127)$$

The diagonal matrix element of the \mathcal{T} -odd multipole moment is not influenced by the pairing correlations,

$$M_{\lambda\lambda}^{(-)} = V_{\lambda\lambda} (u_{\lambda}^2 + v_{\lambda}^2) = V_{\lambda\lambda}. \quad (13.128)$$

For example, the magnetic moment of the quasiparticle on a given orbit keeps the Schmidt value as we have found in the seniority scheme (13.32).

The amplitude of creating two quasiparticles by the same field (pair breaking) is given by the term $\Delta s = 2$,

$$V_2 = - \sum_{\lambda\lambda'} V_{\lambda\lambda'} u_\lambda v_{\lambda'} b_\lambda^\dagger b_{\tilde{\lambda}'}^\dagger. \quad (13.129)$$

To generate quasiparticles $b_{\tilde{\mu}}^\dagger b_{\mu}^\dagger$, there are two possibilities: $\lambda = \mu, \lambda' = \mu'$, and $\lambda = \tilde{\mu}', \lambda' = \mu$. Again for the \mathcal{T} -even field V , we get the matrix element

$$P_{\lambda\lambda'}^{(+)} = V_{\lambda\lambda'} (u_\lambda v_{\lambda'} + u_{\lambda'} v_\lambda). \quad (13.130)$$

In the \mathcal{T} -odd case, the amplitude is

$$P_{\lambda\lambda'}^{(-)} = V_{\lambda\lambda'}(u_\lambda v_{\lambda'} - u_{\lambda'} v_\lambda). \quad (13.131)$$

Here the creation of the diagonal pair $\lambda = \lambda'$ is forbidden. This is the pair with the condensate quantum numbers and therefore \mathcal{T} -even while the field is \mathcal{T} -odd. These results are indispensable for calculating the response of the paired system to any external field.

References

- 1 C. Johnson, G. Bertsch, and D. Dean, Phys. Rev. Lett. **80**, 2749 (1998).
- 2 R.D. Lawson, *Theory of the Nuclear Shell Model*, Clarendon Press, Oxford, 1980.
- 3 J. Bardeen, L.N. Cooper, and J.R. Schriffer, Phys. Rev. **106**, 162 (1957); 108, 1175 (1957).
- 4 A. Bohr, B.R. Mottelson, and D. Pines, Phys. Rev. **110**, 936 (1958).
- 5 S.T. Belyaev, Kgl. Dansk. Vid. Selsk. Mat.-Fys. Medd. **31**, No. 11 (1959).
- 6 R. Broglia and V. Zelevinsky, eds. *Fifty Years of Nuclear BCS. Pairing in Finite Systems*, World Scientific, Singapore, 2013.
- 7 A. Volya and V. Zelevinsky, in *Fifty Years of Nuclear BCS. Pairing in Finite Systems*, World Scientific, Singapore, 2013, p. 73.
- 8 D. Vollhardt and P. Wölfle, *The Superfluid Phases of Helium 3*, Taylor and Francis, London, 1990.
- 9 S.T. Belyaev, in *Fifty Years of Nuclear BCS. Pairing in Finite Systems*, World Scientific, Singapore, 2013, p. 3.
- 10 A.H. Wapstra and G. Audi, Nucl. Phys. **A432**, 55 (1985).

14

Gamma-Radiation

The subject is ever fresh. There are always important new applications and examples.

J.D. Jackson, *Classical Electrodynamics*

14.1 Introduction

Electromagnetic radiation by nuclei is one of the most informative sources of our knowledge on properties of nuclear states. Gamma-ray energies allow one to reconstruct a level scheme in the region of discrete spectrum or narrow resonances. Contrary to the spectrum of black-body radiation, one can observe intensities of discrete transitions that are directly related to matrix elements of multipole moments between nuclear states that are very sensitive to nuclear structure. Transitions connecting continuum states with discrete ones or with other states in the continuum carry information on the strength distribution. This information characterizes excited nuclear matter. Gamma-rays weakly interact with nucleons, and usually one can neglect a probability of their reabsorption. Therefore, we get unperturbed signals of nuclear properties. In the inverse processes of photoexcitation or electroexcitation, the external field is weak compared to strong interaction inside the system, so that one can consider only single-step processes when nuclear structure is not distorted.

We start with the theory of *spontaneous radiation* by quantum systems. Here we revisit the subject of quantization of electromagnetic field that allows us to introduce photons emitted in individual radiative events; more in-depth discussions can be found in [QP, II, 4] and in a number of classic textbooks [1–4].

14.2 Electromagnetic Field and Gauge Invariance

Throughout the text, we use the absolute system of units. The electromagnetic field is described by the four-vector electromagnetic potentials (ϕ, \mathbf{A}) that determines electric, \mathcal{E} , and magnetic, \mathcal{B} , fields,

$$\mathcal{E} = -\nabla\phi - \frac{1}{c} \frac{\partial \mathbf{A}}{\partial t}, \quad (14.1)$$

$$\mathcal{B} = [\nabla \times \mathbf{A}]. \quad (14.2)$$

Electromagnetic fields carry energy

$$E = \frac{1}{8\pi} \int d^3r (\mathcal{E}^2 + \mathcal{B}^2) \quad (14.3)$$

and momentum

$$\mathbf{P} = \frac{1}{c^2} \int d^3r \mathbf{S} \equiv \frac{1}{4\pi c} \int d^3r [\mathcal{E} \times \mathcal{B}], \quad (14.4)$$

where the Poynting vector \mathbf{S} gives the momentum density. The important difference between electric and magnetic fields is in their behavior under discrete space-time transformations. The electric vector is a polar vector while the magnetic vector is an axial vector (pseudovector). They behave differently under time reversal as well. Electric fields are generated by charges and do not change sign while magnetic fields are generated by currents and change sign along with them. Maxwell equations are invariant under both \mathcal{P} - and \mathcal{T} -transformations. As seen from (14.1) and (14.2), the scalar potential ϕ is a \mathcal{T} -even scalar and \mathbf{A} is a polar \mathcal{T} -odd vector (it is also generated by currents).

Electromagnetic potentials are not defined uniquely by electromagnetic fields. Keeping intact the vector character of $\mathbf{A}(t, \mathbf{r})$, one can make a *gauge transformation* adding a gradient of an arbitrary single-valued scalar function of time and space coordinates,

$$\mathbf{A}(t, \mathbf{r}) \Rightarrow \mathbf{A}'(t, \mathbf{r}) = \mathbf{A}(t, \mathbf{r}) + \nabla f(t, \mathbf{r}). \quad (14.5)$$

If the scalar potential is simultaneously transformed according to

$$\phi(t, \mathbf{r}) \Rightarrow \phi'(t, \mathbf{r}) = \phi(t, \mathbf{r}) - \frac{1}{c} \frac{\partial f(t, \mathbf{r})}{\partial t} \quad (14.6)$$

with the same gauge function $f(t, \mathbf{r})$ as in (14.5), the fields do not change. We can use the gauge freedom to simplify the calculations. For our purposes, the *radiation gauge* seems to be convenient. First, we can always get rid of the scalar potential taking $f(t, \mathbf{r}) = c \int^t dt' \phi(t', \mathbf{r})$ so that $\phi'(t, \mathbf{r}) = 0$. Then, since we are interested in the radiation field in free space, where $\operatorname{div} \mathcal{E} = 0$, we can choose the vector potential \mathbf{A} subject to the additional condition

$$\operatorname{div} \mathbf{A} = 0. \quad (14.7)$$

As a result, only two components of \mathbf{A} are physically independent.

In the following, we see that this is equivalent to the statement that electromagnetic waves in free space are *transversely* polarized. This, in turn, is related to the fact that the quanta that appear after the field is quantized, *photons*, have zero mass. For massless particles, there exists no rest frame. Their wave function is axially symmetric with respect to the motion axis. It is characterized by *helicity* that is Lorentz invariant for a massless particle. The two possible values of photon helicity, ± 1 , correspond to right (left) circular polarization. Their combinations describe two possible linear polarizations in the plane perpendicular to the motion axis. The longitudinal polarization along the wave vector, $\mathbf{A} \parallel \mathbf{k}$, which would have zero helicity, is not allowed for a real massless photon. In general, for massless particles of spin s , only two helicities, $\pm s$, are allowed (only angles 0 and π are relativistically invariant).

14.3 Photons

Consider free electromagnetic field in a large normalization volume V . The vector potential satisfies the *wave equation*

$$\left(\frac{1}{c^2} \frac{\partial^2}{\partial t^2} - \nabla^2 \right) \mathbf{A} = 0. \quad (14.8)$$

The plane wave with the wave vector \mathbf{k} ,

$$\mathbf{A}_k(t, \mathbf{r}) = \mathbf{A}_k e^{i(\mathbf{k} \cdot \mathbf{r}) - i\omega t}, \quad (14.9)$$

is a solution of the wave equation if the wave frequency ω satisfies the dispersion law,

$$\omega = \omega_k \equiv c|\mathbf{k}| \equiv ck. \quad (14.10)$$

The components of the wave vectors are quantized, $k_i = (2\pi/L)n_i$, where L is a size of the volume $V = L^3$, and n_i are integer (positive or negative).

The supplementary gauge condition (14.7) requires that the amplitude vector \mathbf{A}_k be orthogonal to the wave vector,

$$(\mathbf{k} \cdot \mathbf{A}_k) = 0, \quad (14.11)$$

which is just the *transversality* condition. To describe the wave polarization, we introduce two unit vectors $\mathbf{e}_{k\lambda}$ labeled by an additional subscript λ taking one of two values. The polarization vectors are orthogonal to the wave vector,

$$(\mathbf{e}_{k\lambda} \cdot \mathbf{k}) = 0; \quad (14.12)$$

they are also taken to be mutually orthogonal. In general, they are complex and their scalar products are defined with the complex conjugation, as in the case of complex wave functions,

$$(\mathbf{e}_{k\lambda}^* \cdot \mathbf{e}_{k\lambda'}) = \delta_{\lambda\lambda'}. \quad (14.13)$$

Two standard choices are *linear* polarizations described by real vectors \mathbf{e}_{k1} , \mathbf{e}_{k2} along $x \equiv 1$ and $y \equiv 2$ axes in the plane perpendicular to the wave vector direction $z \equiv 3$, or *circular* polarizations with the complex polarization vectors

$$\mathbf{e}_{k\pm} = \mp \frac{1}{\sqrt{2}} (\mathbf{e}_{k1} \pm i\mathbf{e}_{k2}). \quad (14.14)$$

In both cases, three unit vectors, $\mathbf{e}_{k\lambda}$ and \mathbf{k}/k , form a right-handed triplet. The frequencies (14.10) do not depend on polarization.

The solution (14.9) can be represented by a sum of two polarizations with some scalar amplitudes,

$$\mathbf{A}_k(t, \mathbf{r}) = \sum_{\lambda} A_{k\lambda} \mathbf{e}_{k\lambda} e^{i(\mathbf{k} \cdot \mathbf{r}) - i\omega_k t}. \quad (14.15)$$

Finally, since the vector potential is real, a physical field should contain a complex conjugate (c.c.) term along with (14.15). The most general solution of the wave equation is

an arbitrary superposition of partial solutions,

$$\mathbf{A}(t, \mathbf{r}) = \sum_{\mathbf{k}\lambda} (A_{\mathbf{k}\lambda} \mathbf{e}_{\mathbf{k}\lambda} e^{i(\mathbf{k}\cdot\mathbf{r}) - i\omega_{\mathbf{k}} t} + A_{\mathbf{k}\lambda}^* \mathbf{e}_{\mathbf{k}\lambda}^* e^{-i(\mathbf{k}\cdot\mathbf{r}) + i\omega_{\mathbf{k}} t}). \quad (14.16)$$

The potential (14.16) generates electric and magnetic fields according to Eq. (14.1) with $\phi = 0$ and (14.2),

$$\mathcal{E}(t, \mathbf{r}) = \frac{i}{c} \sum_{\mathbf{k}\lambda} \omega_{\mathbf{k}} (A_{\mathbf{k}\lambda} \mathbf{e}_{\mathbf{k}\lambda} e^{i(\mathbf{k}\cdot\mathbf{r}) - i\omega_{\mathbf{k}} t} - (\text{c.c.})) , \quad (14.17)$$

$$\mathcal{B}(t, \mathbf{r}) = i \sum_{\mathbf{k}\lambda} [\mathbf{k} \times (A_{\mathbf{k}\lambda} \mathbf{e}_{\mathbf{k}\lambda} e^{i(\mathbf{k}\cdot\mathbf{r}) - i\omega_{\mathbf{k}} t} - (\text{c.c.}))]. \quad (14.18)$$

The field can be quantized by a direct analogy with the harmonic oscillator or nuclear shape vibrations. The time dependence of the coordinate operators for the normal vibrational modes was (Section 6.5)

$$\alpha_{\lambda\mu}(t) = \sqrt{\frac{\hbar}{2\eta}} \left\{ a_{\lambda\mu} e^{-i\omega_{\lambda} t} + (-)^{\mu} a_{\lambda-\mu}^{\dagger} e^{i\omega_{\lambda} t} \right\}. \quad (14.19)$$

The expansion (14.16) has the same structure. It is a superposition of independent normal modes with quantum numbers of momentum and polarization instead of the angular momentum quantum numbers in (14.19). The coefficients of the general solution presented as a sum of normal modes are annihilation and creation operators for quanta with quantum numbers of a given normal mode. The annihilating term carries time dependence $e^{-i\omega_{\lambda} t}$, whereas the creation term carries time dependence $e^{i\omega_{\lambda} t}$ where in both cases the energy of a quantum $\hbar\omega$ is positive. This is a general recipe to quantize a system of independent oscillators, and the procedure is applicable to the electromagnetic field as well.

Thus, we postulate that in quantum theory, the amplitudes $A_{\mathbf{k}\lambda}$ and $A_{\mathbf{k}\lambda}^*$ are substituted by operators proportional to annihilation and creation operators,

$$A_{\mathbf{k}\lambda} \Rightarrow \hat{A}_{\mathbf{k}\lambda}, \quad A_{\mathbf{k}\lambda}^* \Rightarrow \hat{A}_{\mathbf{k}\lambda}^*. \quad (14.20)$$

Their commutation relations and the corresponding type of statistics are to be established with the help of physical arguments. After the substitution (14.20), electric and magnetic fields (14.17, 14.18) also become operators. The quantized energy (14.3) gives the Hamiltonian \hat{H} .

Problem 14.1 Express the field Hamiltonian in terms of the operators (14.20) and prove that it is a constant of motion.

Solution

Using the operator definitions of the fields in the energy expression (14.3), we get four terms for electric energy and similar four terms for magnetic energy with the summation $\sum_{\mathbf{k}\lambda\mathbf{k}'\lambda'}$. These terms have different operator structure. To calculate them, first perform spatial integration using the orthogonality of plane waves,

$$\int d^3r e^{i(\mathbf{k}\pm\mathbf{k}')\cdot\mathbf{r}} = V\delta_{\mathbf{k},\mp\mathbf{k}'}. \quad (14.21)$$

In both cases (\pm), the frequencies are equal, $\omega_{\mathbf{k}} = \omega_{\mathbf{k}'}$. The terms as $\hat{A}\hat{A}^{\dagger}$ and $\hat{A}^{\dagger}\hat{A}$ turn out to be time independent. The terms with the operators $\hat{A}\hat{A}$ or $\hat{A}^{\dagger}\hat{A}^{\dagger}$ depend on time

$\propto \exp(\mp 2i\omega_{\mathbf{k}}t)$, which would contradict to energy conservation. However, such terms vanish due to the cancellation of electric and magnetic contributions. Indeed, electric terms have the polarization-dependent amplitudes

$$-\frac{\omega_{\mathbf{k}}^2}{c^2}(\mathbf{e}_{\mathbf{k}\lambda} \cdot \mathbf{e}_{-\mathbf{k}\lambda'}) = -k^2(e_{\mathbf{k}\lambda} \cdot \mathbf{e}_{-\mathbf{k}\lambda'}). \quad (14.22)$$

For analogous magnetic terms, we obtain with simple vector algebra

$$-[\mathbf{k} \times \mathbf{e}_{\mathbf{k}\lambda}] \cdot [(-\mathbf{k}) \times \mathbf{e}_{-\mathbf{k}\lambda'}] = k^2(\mathbf{e}_{\mathbf{k}\lambda} \cdot \mathbf{e}_{-\mathbf{k}\lambda'}) - (\mathbf{k} \cdot \mathbf{e}_{-\mathbf{k}\lambda'})(\mathbf{k} \cdot \mathbf{e}_{\mathbf{k}\lambda}). \quad (14.23)$$

The last item in (14.23) vanishes because of the field transversality and the first item cancels the electric contribution (14.22). Then the time-dependent terms (in fact, energy transfer between the electric and magnetic fields) disappear in total energy, as it should be. In the remaining terms, the polarization vectors form the scalar product (14.13) and the orthogonality of different polarizations selects $\lambda' = \lambda$. The magnetic and electric contributions add up to

$$\hat{H} = \frac{V}{4\pi c^2} \sum_{\mathbf{k}\lambda} \omega_{\mathbf{k}}^2 (\hat{A}_{\mathbf{k}\lambda}^\dagger \hat{A}_{\mathbf{k}\lambda} + \hat{A}_{\mathbf{k}\lambda} \hat{A}_{\mathbf{k}\lambda}^\dagger). \quad (14.24)$$

We normalize our operators according to

$$\hat{A}_{\mathbf{k}\lambda} = \sqrt{\frac{2\pi\hbar c^2}{\omega_{\mathbf{k}} V}} a_{\mathbf{k}\lambda}, \quad \hat{A}_{\mathbf{k}\lambda}^\dagger = \sqrt{\frac{2\pi\hbar c^2}{\omega_{\mathbf{k}} V}} a_{\mathbf{k}\lambda}^\dagger \quad (14.25)$$

to bring the Hamiltonian to the sum of the independent photon energies $\hbar\omega_{\mathbf{k}}$,

$$\hat{H} = \frac{1}{2} \sum_{\mathbf{k}\lambda} \hbar\omega_{\mathbf{k}} (a_{\mathbf{k}\lambda}^\dagger a_{\mathbf{k}\lambda} + a_{\mathbf{k}\lambda} a_{\mathbf{k}\lambda}^\dagger). \quad (14.26)$$

At this point, we have to decide the type of statistics. The decision is easy because the Fermi choice with anticommutators would lead to the Hamiltonian containing no operators at all (just an infinite constant sum over all modes). Therefore, we have to select Bose statistics, postulating the commutation relations

$$[a_{\mathbf{k}\lambda}, a_{\mathbf{k}'\lambda'}] = [a_{\mathbf{k}\lambda}^\dagger, a_{\mathbf{k}'\lambda'}^\dagger] = 0, \quad [a_{\mathbf{k}\lambda}, a_{\mathbf{k}'\lambda'}^\dagger] = \delta_{\mathbf{k}\mathbf{k}'} \delta_{\lambda\lambda'}. \quad (14.27)$$

The photon number operator is defined for each mode $(\mathbf{k}\lambda)$ as usual,

$$\hat{n}_{\mathbf{k}\lambda} = a_{\mathbf{k}\lambda}^\dagger a_{\mathbf{k}\lambda}, \quad (14.28)$$

and the Hamiltonian takes a standard form for the gas of noninteracting Bose quanta, photons,

$$\hat{H} = \sum_{\mathbf{k}\lambda} \hbar\omega_{\mathbf{k}} \left(\hat{n}_{\mathbf{k}\lambda} + \frac{1}{2} \right). \quad (14.29)$$

Here, in distinction to an oscillator or nuclear vibrational modes, we quantized a *field*, a system with *infinite* number of degrees of freedom. Indeed, to specify the initial value of the vector potential $\mathbf{A}(\mathbf{r})$, we should define its magnitude and direction for all points \mathbf{r} of continuous space. Correspondingly, we have an infinite amount of normal modes that give rise to photons with different quantum numbers $(\mathbf{k}\lambda)$.

The zero-point vibrational energy, the item $1/2$ for each mode in (14.29), gives an infinite sum. But this does not bring any physical difficulties because this energy is a nonoperator constant that can be identified with the vacuum energy. All physical states have positive energy relative to the vacuum that is defined in a standard way as the state that is annihilated by the action of annihilation operators for all modes. The basis states in Fock space $|\{n_{\mathbf{k}\lambda}\}\rangle$ are constructed with the aid of the creation operators with integer photon numbers $n_{\mathbf{k}\lambda}$ as eigenvalues of the operators (14.28). Each photon $(\mathbf{k}\lambda)$ carries momentum $\mathbf{p} = \hbar\mathbf{k}$, polarization λ , and energy $\hbar\omega_{\mathbf{k}}$. The dispersion law (14.10) shows that photons are *massless*.

The final quantized form of the vector potential is

$$\hat{\mathbf{A}}(t, \mathbf{r}) = \sum_{\mathbf{k}\lambda} \sqrt{\frac{2\pi\hbar c^2}{\omega_{\mathbf{k}} V}} (a_{\mathbf{k}\lambda} \mathbf{e}_{\mathbf{k}\lambda} e^{i(\mathbf{k}\cdot\mathbf{r}) - i\omega_{\mathbf{k}} t} + a_{\mathbf{k}\lambda}^\dagger \mathbf{e}_{\mathbf{k}\lambda}^* e^{-i(\mathbf{k}\cdot\mathbf{r}) + i\omega_{\mathbf{k}} t}). \quad (14.30)$$

The field operators are easily obtained from (14.17) and (14.18). All these quantities are linear in creation and annihilation operators. Therefore, they have selection rules $\Delta n = \pm 1$, and their matrix elements between the states with different photon numbers are the same as for harmonic oscillators; we have the photon absorption, $\sim a$, and spontaneous and stimulated emission, $\sim a^\dagger$.

We have quantized the electromagnetic field in plane waves. As we know from the general secondary quantization formalism, it is possible to make a unitary transformation to an arbitrary basis adjusted to any field geometry like spherical, cylindrical waves or waves in a cavity of arbitrary shape. The procedure is the same: find a complete set of solutions (vector normal modes) for the wave equation in any coordinates, write a general solution as a superposition of all normal modes and declare the coefficients of the superposition Bose operators. Similar to (14.25), they should be normalized to define the photon energy in accordance with the spectrum of the quantized normal modes in a given geometry with certain boundary conditions.

14.4 Interaction of Radiation with Matter

Consider a nonrelativistic system of charged particles interacting with electromagnetic fields. The interaction makes the system capable of absorbing and emitting photons. To describe the interaction, we turn it on in the so-called *minimal* way. Let $H_0(\mathbf{r}_a, \mathbf{p}_a)$ be the original Hamiltonian of the many-body system with no field. The interaction is obtained by a substitution $\mathbf{p}_a \Rightarrow \mathbf{p}_a - (e_a/c)\mathbf{A}(\mathbf{r}_a)$ for all particles so that the new Hamiltonian includes the terms depending on the field variables,

$$H_0 \Rightarrow H'_0 = H_0 \left(\mathbf{r}_a, \mathbf{p}_a - \frac{e_a}{c} \mathbf{A}(\mathbf{r}_a) \right) + \sum_a e_a \phi(\mathbf{r}_a). \quad (14.31)$$

We also added potential energy of charged particles, the last term in (14.31). This procedure is obviously consistent with relativity since the four-vector of energy-momentum $(E, c\mathbf{p})$ is transformed by adding another four-vector, that of electromagnetic potential (ϕ, \mathbf{A}) . It is easy to check, for example, that, for a particle in a uniform constant magnetic field \mathcal{B} defined by the vector potential $\mathbf{A} = (1/2)[\mathcal{B} \times \mathbf{r}]$, one gets from (14.31) correct classical or quantum operator equations of motion with the Lorentz force $e\mathcal{E} + (e/c)[\mathbf{v} \times \mathcal{B}]$.

This description is applicable to the electromagnetic field from any source including the radiation field. In the *radiation gauge*, we can omit the scalar potential and write down the part of the nonrelativistic Hamiltonian of the system describing the interaction with the radiation field as

$$H = \sum_a \frac{1}{2m_a} \left(\mathbf{p} - \frac{e_a}{c} \hat{\mathbf{A}}(\mathbf{r}_a) \right)^2, \quad (14.32)$$

where $\hat{\mathbf{A}}(\mathbf{r}_a)$ is the quantized vector potential (14.30) taken at the point \mathbf{r}_a of the particle a . Here we assumed that the interaction between particles depends on their coordinates so that the minimal inclusion of the electromagnetic field affects only the kinetic energy part. In the presence of velocity-dependent interactions, for example, spin-orbit forces, the minimal substitution is to be made in the interaction term as well. Another effect of the electromagnetic field not included in (14.32) is interaction of spins of the particles with the magnetic field. In relativistic theory, as in the Dirac equation, such terms appear naturally [QP, II, 13.5]. Within the framework of nonrelativistic approach, we simply add such terms:

$$H' = - \sum_a g_a^{(s)} (\mathbf{s}_a \cdot \mathbf{B}(\mathbf{r}_a)), \quad (14.33)$$

where the spin gyromagnetic ratios $g_a^{(s)}$ are taken from experiment, and the quantized magnetic field is given by Eqs. (14.2) and (14.30).

Problem 14.2 Find the contribution to the operator of the static magnetic moment of the nucleon that emerges from the minimal substitution in the spin-orbit part of the mean field.

Solution

Let the spin-orbit part of the mean field be given by

$$U_{\ell s} = -f(r)(\boldsymbol{\ell} \cdot \mathbf{s}). \quad (14.34)$$

Since $\boldsymbol{\ell} = [\mathbf{r} \times \mathbf{p}] / \hbar$, in the presence of the field with the vector potential \mathbf{A} , the spin-orbit part acquires the new term,

$$U'_{\ell s} = \frac{ef(r)}{\hbar c} [\mathbf{r} \times \mathbf{A}] \cdot \mathbf{s}. \quad (14.35)$$

For a static magnetic field \mathbf{B} , the convenient gauge is

$$\mathbf{A} = \frac{1}{2} [\mathbf{B} \times \mathbf{r}], \quad (14.36)$$

With simple vector algebra, Eqs. (14.35) and (14.36) lead to

$$U'_{\ell s} = \frac{ef(r)}{2\hbar c} [\mathbf{r} \times [\mathbf{s} \times \mathbf{r}]] \cdot \mathbf{B}. \quad (14.37)$$

According to the definition (14.33), this is equivalent to the new contribution to the magnetic moment operator,

$$\mu' = -\frac{ef(r)}{2\hbar c} [\mathbf{r} \times [\mathbf{s} \times \mathbf{r}]]. \quad (14.38)$$

Again using vector algebra, we present this contribution as a sum of the renormalization of the spin gyromagnetic ratio and the term of the spin-quadrupole type,

$$\mu' = -\frac{er^2f(r)}{2\hbar c} (\mathbf{s} - (\mathbf{s} \cdot \mathbf{n})\mathbf{n}), \quad \mathbf{n} = \frac{\mathbf{r}}{r}. \quad (14.39)$$

Problem 14.3 Calculate the contribution of the operator found in Problem 14.2 to the magnetic moment of a single nucleon on the j -orbit.

The standard averaging, see Problem 9.1, gives (in n.m.)

$$\mu' = \pm \frac{2j+1}{4(j+1)} \frac{m\langle r^2f(r) \rangle}{\hbar^2}, \quad (14.40)$$

where \pm refers to $\ell = j \pm 1/2$. This contribution is of the order of the ratio of the spin-orbit splitting $\langle f(r) \rangle$ to $\hbar^2/m\langle r^2 \rangle$.

The electromagnetic interaction is relatively weak compared to the main strong forces. The relevant parameter is the fine structure constant $\alpha = e^2/\hbar c = 1/137$. As a rule, this interaction can be taken into account in the lowest nonvanishing order of perturbation theory. Looking for the transition probabilities of radiative processes, we keep first the main, linear in the vector potential, term of (14.32),

$$H^{(1)} = - \sum_a \frac{e_a}{2m_a c} (\mathbf{p}_a \cdot \hat{\mathbf{A}}(\mathbf{r}_a) + \hat{\mathbf{A}}(\mathbf{r}_a) \cdot \mathbf{p}_a). \quad (14.41)$$

This Hamiltonian is linear in creation and annihilation operators describing the single-photon emission and absorption. For a static magnetic field, using again Eq. (14.36), this can be reduced to $-\sum_a g_a^{(\ell)} (\ell_a \cdot \mathbf{B})$, where $g_a^{(\ell)} = e_a \hbar / (2m_a c)$ is the orbital gyromagnetic ratio (a magneton) for the particle a , and combined with the spin contribution (14.33).

Due to the interaction of radiation with matter, stationary states of the “bare” system are not stationary anymore. The same is valid for the states of the radiation field with a certain number of photons. This number is also changed by emission and absorption. The states of the system that would be stationary without interaction with electromagnetic field acquire a finite *lifetime* τ . It leads to the energy uncertainty. The energy of a state is defined only within its *width* $\Gamma \sim \hbar/\tau$. The energy spectrum can still be considered as *quasidiscrete* if the widths are small compared with level spacings, and the levels do not overlap. Strictly speaking, only a ground state of a stable system is stationary. If the whole system would be kept for a long time inside a real physical box (*cavity*), it would make sense to speak about genuine stationary states. They would be superpositions of the bare states “a system with no photons,” “a system in another state + one photon,” and so on. Roughly speaking, emitted photons being reflected from the boundaries have a probability to be reabsorbed, reemitted again, and so on. The total energy of the whole system can be well defined. However, we have only a fictitious normalization volume that can be considered as arbitrarily large so the emission process is irreversible and the probability of equilibration via reabsorption is zero. In such a situation, the language of quasistationary states with the finite lifetime is physically more appropriate.

We did not yet fix the gauge in Eq. (14.41). The radiation gauge (14.7) is convenient because under this condition, two terms in (14.41) are equal to each other (their commutator is just $\text{div}\mathbf{A}$). Then

$$H' = - \sum_a \frac{e_a}{m_a c} (\mathbf{p}_a \cdot \hat{\mathbf{A}}(\mathbf{r}_a)) + H'_{\text{sp}}, \quad (14.42)$$

and we can use the quantized form (14.30) derived in the same gauge. This form is a nonrelativistic version of the relativistic Hamiltonian corresponding to the interaction of the electromagnetic field with the current \mathbf{j} ,

$$H' = -\frac{1}{c} \int d^3r (\mathbf{j}(\mathbf{r}) \cdot \hat{\mathbf{A}}(\mathbf{r})). \quad (14.43)$$

The first term in Eq. (14.42) describes the radiation processes induced by the convection current of charged particles. The total current includes also spin and magnetization effects as well as the charge transfer by the virtual particles as charged pions mediating nuclear forces. All components of the current can radiate according to the general interaction Hamiltonian (14.43). They all come together in relativistic theory; in our consideration, we introduce various terms separately.

14.5 Radiation Probability

Let the nucleus be in an excited initial state $|i\rangle$. (We have in mind the states that would be stationary without the interaction with the radiation field.) To find the probability of radiation with the transition to a final state $|f\rangle$, we use the quantum mechanical golden rule [QP, II, 2.1] derived for weak perturbations. This rule gives the probability of radiation per second (transition rate w_f); multiplied by the photon energy $\hbar\omega$, it determines the *intensity* of radiation. The inverse quantity $\tau_f = 1/w_f$ determines the mean lifetime with respect to a given transition.

Let us calculate the probability to emit the photon with quantum numbers $(\mathbf{k}\lambda)$. The joint system of particles and radiation field undergoes the transition

$$|i; n_{\mathbf{k}\lambda}\rangle \rightarrow |f; n_{\mathbf{k}\lambda} + 1\rangle. \quad (14.44)$$

The golden rule with the perturbation (14.42) leads to the transition rate

$$w_f = \frac{2\pi}{\hbar} \left| \langle f; n_{\mathbf{k}\lambda} + 1 | \sum_a \frac{e_a}{m_a c} (\mathbf{p}_a \cdot \hat{\mathbf{A}}(\mathbf{r}_a)) | i; n_{\mathbf{k}\lambda} \rangle \right|^2 \delta(E_i - \hbar\omega_{\mathbf{k}} - E_f). \quad (14.45)$$

Here the vector potential (14.30) is taken without the time-dependent exponent because the unperturbed time dependence is already fully accounted for by the derivation of the golden rule.

In the emission matrix element, the only contribution comes from the creation operator $a_{\mathbf{k}\lambda}^\dagger$ in (14.30). The matrix element of this operator is equal to $\sqrt{n_{\mathbf{k}\lambda} + 1}$, containing stimulated and spontaneous radiation. Therefore, we find

$$w_f = \frac{4\pi^2}{V\omega_{\mathbf{k}}} (n_{\mathbf{k}\lambda} + 1) \left| \langle f | \sum_a \frac{e_a}{m_a} (\mathbf{p}_a \cdot \mathbf{e}_{\mathbf{k}\lambda}^*) e^{-i(\mathbf{k}\cdot\mathbf{r}_a)} | i \rangle \right|^2 \delta(E_i - \hbar\omega_{\mathbf{k}} - E_f). \quad (14.46)$$

The emitted photon can have any direction, and we have to count available final states. The density of final states for a photon ($\omega = \omega_{\mathbf{k}}$) is

$$d\rho_f d(\hbar\omega) = \frac{Vd^3k}{(2\pi)^3} = \frac{V\omega^2}{(2\pi c)^3 \hbar} d\omega d(\hbar\omega). \quad (14.47)$$

Using the δ -function in (14.46) to integrate over photon energy, we come to the differential transition rate for the fixed direction in the solid angle $d\Omega$ and for the fixed polarization λ ,

$$\frac{dw_{fi}}{d\Omega} = \frac{\omega_{\mathbf{k}}}{2\pi c^3 \hbar} (n_{\mathbf{k}\lambda} + 1) \left| \langle f | \sum_a \frac{e_a}{m_a} (\mathbf{p}_a \cdot \mathbf{e}_{\mathbf{k}\lambda}^*) e^{-i(\mathbf{k} \cdot \mathbf{r}_a)} | i \rangle \right|^2. \quad (14.48)$$

The observable transition rate does not depend on the auxiliary volume V . Note that the radiation probability is actually a quantity of the form-factor type for the current component in the plane perpendicular to the radiation direction. The exponent gives the relative phase for the radiation by different constituents, and their contributions are coherently superimposed.

The states of the radiating systems have their own quantum numbers. For a finite system, the initial and final states can be characterized by the total angular momentum and its projection, J_i, M_i and J_f, M_f , respectively. Some of the transitions can be forbidden due to the selection rules related to the properties of the electromagnetic field. For example, all single-photon transitions with $J_f = J_i = 0$ (the so-called 0–0 transitions) are strictly forbidden by the angular momentum conservation. Indeed, the emitted photon carries helicity ± 1 (it can be in a superposition of these spiral states). This means that the projection of the angular momentum of the system onto the direction of radiation \mathbf{k} is changed by ± 1 , which is impossible for the 0–0 transition.

14.6 Electric Dipole Radiation

The important practical case is connected to the long wavelength radiation: $\lambda \sim 1/k \gg R$ where R is a size of the system. In nuclei the condition

$$kR \ll 1 \quad (14.49)$$

is equivalent to $\hbar\omega \ll 165 A^{-1/3}$ MeV, which is usually fulfilled. In the limit (14.49), one can substitute the exponent in the matrix element (14.48) by unity as all particles are confined in the volume of size $\sim R$. The rate of spontaneous radiation in a given direction is given then by

$$dw_{fi} = \frac{\omega_{\mathbf{k}}}{2\pi c^3 \hbar} \left| \langle f | \sum_a \frac{e_a}{m_a} (\mathbf{p}_a \cdot \mathbf{e}_{\mathbf{k}\lambda}^*) | i \rangle \right|^2 d\Omega. \quad (14.50)$$

In the long wavelength limit, the phase differences are lost and particles can radiate coherently.

If we neglect the possible effects of velocity-dependent and exchange forces, the velocity operator for a particle a in the unperturbed system is simply

$$\dot{\mathbf{r}}_a = \frac{1}{i\hbar} [\mathbf{r}_a, H_0] = \frac{1}{i\hbar} \left[\mathbf{r}_a, \frac{p_a^2}{2m_a} \right] = \frac{\mathbf{p}_a}{m_a}. \quad (14.51)$$

Taking the matrix element $\langle f | \dots | i \rangle$ of the operator relation (14.51) between the stationary states of the unperturbed Hamiltonian with energies E_f and E_i , we link the matrix elements of the particle momentum \mathbf{p}_a to those of the coordinate \mathbf{r}_a ,

$$(\mathbf{p}_a)_{fi} = \frac{m_a}{i\hbar} (E_i - E_f) (\mathbf{r}_a)_{fi} = -im_a\omega_k(\mathbf{r}_a)_{fi}. \quad (14.52)$$

Thus, the matrix element in (14.50) becomes that of the dipole operator, and we obtain the rate of the electric dipole (E1) radiation as

$$dw_{fi} = \frac{\omega_k^3}{2\pi c^3 \hbar} \left| (\mathbf{e}_{k\lambda}^* \cdot \mathbf{d}_{fi}) \right|^2 do, \quad (14.53)$$

or its intensity

$$dI_{k\lambda} = \frac{\omega_k^4}{2\pi c^3} \left| (\mathbf{e}_{k\lambda}^* \cdot \mathbf{d}_{fi}) \right|^2 do. \quad (14.54)$$

This result is similar to the one known from classical radiation theory. It could be derived if from the very beginning, instead of the current-related form of the Hamiltonian (14.42), one would use the dipole interaction with the electric field,

$$H_{\text{dip}} = -(\mathcal{E} \cdot \mathbf{d}), \quad (14.55)$$

and calculate the transition rate with the operator \mathcal{E} given by quantization of Eq. (14.17). Our derivation shows which approximations are necessary along this road to guarantee that the results from the two forms be identical. Note that in a natural frame with the z -axis along the emitted photon, only transverse components d_x and d_y can radiate. These terms have the selection rules $\Delta M = \pm 1$ with respect to the total angular momentum projection onto the \mathbf{k} -axis. The missing projection is carried away as the photon helicity.

Now we can sum over two polarizations possible for a given wave vector \mathbf{k} . The matrix element \mathbf{d}_{fi} is a vector defined for a fixed pair of states f, i . Let θ be a polar angle of this vector in a frame with \mathbf{k} along the z -axis. We can choose real vectors of linear polarization \mathbf{e}_{k1} and \mathbf{e}_{k2} in such a way that the vector \mathbf{d}_{fi} is in the plane formed by the vectors \mathbf{k} and \mathbf{e}_{k1} . Then $(\mathbf{e}_{k2} \cdot \mathbf{d}_{fi}) = 0$, and the vector \mathbf{d}_{fi} has components along \mathbf{k} , equal to $|\mathbf{d}_{fi}| \cos \theta$, and along \mathbf{e}_{k1} , equal to $|\mathbf{d}_{fi}| \sin \theta$ (see Figure 14.1). In this way, we obtain the transition rate and the angular distribution of the radiation with respect to the direction of \mathbf{d}_{fi} ,

$$dw_k = dw_{k1} = \frac{\omega_k^3}{2\pi c^3 \hbar} |\mathbf{d}_{fi}|^2 \sin^2 \theta do. \quad (14.56)$$

The integral rate of radiation from a given transition is the inverse lifetime

$$\tau_f^{-1} = w_{fi} = \frac{\omega^3}{2\pi c^3 \hbar} |\mathbf{d}_{fi}|^2 \int do \sin^2 \theta = \frac{4\omega^3}{3c^3 \hbar} |\mathbf{d}_{fi}|^2. \quad (14.57)$$

In Eq. (14.56), we found the angular distribution of the radiation relative to the “direction of oscillations” in the quantum antenna represented by the vector \mathbf{d}_{fi} . One can also find the angular distribution of radiation in the *laboratory frame* with the z -axis as the quantization axis of angular momentum. In general, one has to calculate the Poynting vector (14.4) of the emitted wave. This is a straightforward but cumbersome procedure. We just illustrate the results by a simple example.

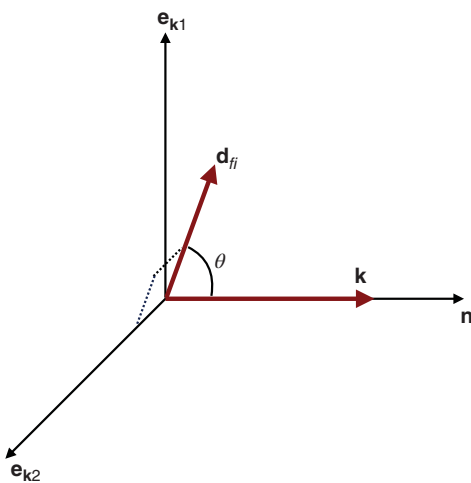


Figure 14.1 Illustration showing relative orientation of polarization vectors, wave vector, and matrix element of dipole moment.

Let us fix the initial projection M_i , sum the radiation probability over two polarizations, and consider different possibilities for the final projection M_f . As seen from (14.53) and (14.56),

$$\sum_{\lambda} |(\mathbf{e}_{k\lambda}^* \cdot \mathbf{d}_{fi})|^2 = |[\mathbf{n} \times \mathbf{d}_{fi}]|^2, \quad (14.58)$$

where $\mathbf{n} = \mathbf{k}/k$ is the direction of radiation. We want to find the distribution of probabilities for the angles $(\theta_{\mathbf{k}}, \varphi_{\mathbf{k}})$ in the lab frame.

A spherical component $(d_{fi})_{\mu}$ [QP, I, 14.8] of the vector \mathbf{d}_{fi} generates the transition with $\Delta M = \mu$. For $\Delta M = 0$, only $(d_{fi})_0 = d_{fi}^z$ is effective. The corresponding coefficient in (14.58) is

$$\Delta M = 0 : \quad n_x^2 + n_y^2 = \sin^2 \theta. \quad (14.59)$$

The transverse components are

$$d_{fi}^x = \frac{1}{\sqrt{2}} [(d_{fi})_{-1} - (d_{fi})_1], \quad d_{fi}^y = \frac{i}{\sqrt{2}} [(d_{fi})_{-1} + (d_{fi})_1]. \quad (14.60)$$

In the process with $\Delta M = 1$ (the result is the same for $\Delta M = -1$), we need only the component $(d_{fi})_1$. Calculating terms in the vector product (14.58), which contain the matrix element $|d_{fi}|^2$, we obtain the angular distribution for this case,

$$\Delta M = \pm 1 : \quad \frac{1}{2} (2n_z^2 + n_x^2 + n_y^2) = \frac{1}{2} (1 + \cos^2 \theta). \quad (14.61)$$

In all cases, the angular distribution has no azimuthal asymmetry; this asymmetry can appear only if the photon polarization is registered.

The observed angular distribution depends on the initial population of different substates M_i . For example, consider the electric dipole radiation for the transition between states 1^- and 0^+ . In this case, all Clebsch–Gordan coefficients are equal to unity. If $g(M_i)$ are relative occupancies for $M_i = 0, \pm 1$, the angular distribution takes the form

$$F(\theta) = g(0)\sin^2 \theta + \frac{g(1) + g(-1)}{2} (1 + \cos^2 \theta). \quad (14.62)$$

For the *unpolarized* initial state, $g(0) = g(1) = g(-1) = 1/3$, and the angular distribution (14.62) becomes *isotropic*. The angular distribution for the dipole radiation summed over polarizations in the general case has a simple form (14.62)

$$F_1(\theta) \propto 1 + \beta_1 \cos^2 \theta \quad (14.63)$$

with the asymmetry coefficient β_1 depending on the initial nuclear polarization. For any radiation multipolarity L , the angular distribution can be presented as a sum over the *even* powers of $\cos \theta$,

$$F_L(\theta) = \sum_{\ell=0}^L \beta_\ell \cos^{2\ell} \theta. \quad (14.64)$$

The presence of odd powers of $\cos \theta$ would imply *parity nonconservation*.

A dipole transition can connect the states $|f\rangle$ and $|i\rangle$ only if the dipole *selection rules* are fulfilled. For the E1 multipolarity, we have the restriction $\Delta J = 0, \pm 1$. Apart from that, the initial and final states should have opposite parity. If the selection rules for E1 transitions are not satisfied, the emission is forbidden in this, lowest in the parameter kR , approximation.

14.7 Electric Quadrupole Radiation

If dipole radiation is not allowed, the photon emission can still occur due to the next terms of the expansion of the exponent in (14.48). They contain extra factor $-i(\mathbf{k} \cdot \mathbf{r})$ in the amplitude and therefore lead to a suppression of the emission probability by $\sim (kR)^2$.

Let us consider a typical next order term of the amplitude (14.48). It can be rewritten as

$$-i \frac{e}{m} (\mathbf{e}^* \cdot \mathbf{p})(\mathbf{k} \cdot \mathbf{r}) \equiv -i \frac{e}{2m} (F_+ + F_-), \quad (14.65)$$

where another term is added and subtracted to get

$$F_\pm = (\mathbf{e}^* \cdot \mathbf{p})(\mathbf{k} \cdot \mathbf{r}) \pm (\mathbf{e}^* \cdot \mathbf{r})(\mathbf{k} \cdot \mathbf{p}). \quad (14.66)$$

Here only longitudinal components of \mathbf{r} and transverse components of \mathbf{p} or vice versa enter so that the operators \mathbf{p} and \mathbf{r} effectively commute. By virtue of the equation of motion (14.51) (again, if there is no velocity-dependent forces), we obtain

$$F_+ = m(\mathbf{e}^* \cdot \dot{\mathbf{r}})(\mathbf{k} \cdot \mathbf{r}) + (\mathbf{e}^* \cdot \mathbf{r})m(\mathbf{k} \cdot \dot{\mathbf{r}}) = m \frac{d}{dt} ((\mathbf{e}^* \cdot \mathbf{r})(\mathbf{k} \cdot \mathbf{r})). \quad (14.67)$$

Since $(\mathbf{e}^* \cdot \mathbf{k}) = 0$, we can reduce (14.67) to the time derivative of the single-particle electric quadrupole tensor q_{lj} ,

$$\begin{aligned} F_+ &= me_l^* k_j \frac{d}{dt} (r_l r_j) \\ &= me_l^* k_j \frac{d}{dt} \left(r_l r_j - \frac{1}{3} \delta_{lj} r^2 \right) = me_l^* k_j \frac{d}{dt} \left(\frac{1}{3e} q_{lj} \right). \end{aligned} \quad (14.68)$$

The corresponding matrix element in the radiation probability (14.48) becomes

$$-\frac{i}{2} \langle f | \sum_a \frac{e_a}{m_a} F_+(a) | i \rangle = -\frac{i}{6} e_l^* k_j \langle f | \dot{Q}_{lj} | i \rangle, \quad (14.69)$$

where the total quadrupole moment $Q_{lj} = \sum_a q_{lj}(a)$ has appeared. Using, as in (14.52), the equation of motion and introducing the transition frequency,

$$i\hbar\dot{Q} = [Q, H_0] \Rightarrow \dot{Q}_{fi} = -i\omega_{\mathbf{k}} Q_{fi}, \quad (14.70)$$

we come to the spontaneous emission transition rate (14.48)

$$\frac{dw_{fi}}{do} = \frac{\omega_{\mathbf{k}}}{2\pi c^3 \hbar} \left| -\frac{1}{6} \omega_{\mathbf{k}} (e_{k\lambda}^*)_l k_j (Q_{lj})_{fi} \right|^2 = \frac{\omega_{\mathbf{k}}^3}{72\pi c^3 \hbar} \left| (e_{k\lambda}^*)_l k_j (Q_{lj})_{fi} \right|^2. \quad (14.71)$$

Thus, this term describes the *electric quadrupole* (E2) radiation. Again it is possible to show that this result is in precise correspondence with the classical quadrupole radiation.

Similar to the dipole case, only components Q_{xz} and Q_{yz} of the quadrupole tensor Q_{lj} radiate that is again associated with helicity ± 1 of the emitted photon. As for the selection rules related to angular momentum and parity, we know that for the quadrupole tensor, $\Delta J = 0, \pm 1, \pm 2$ and parity does not change. Therefore, E1 and E2 transitions cannot happen between the same pair of states if parity is conserved.

The transition rate for the E2 radiation increases with photon energy as ω^5 while it was proportional to ω^3 in the E1 case. In both cases, the initial state having a choice between several final states allowed for the photon emission selects the state at a larger energy distance if the corresponding matrix elements are comparable. If the final states of different parities are available, in the long wavelength limit, the dipole radiation is preferable. Very rough estimates with the matrix elements evaluated as $(eR)^2$ and $k^2 e^2 R^4$ for the dipole and quadrupole cases, respectively, and all numerical factors neglected give for the transition rate

$$w_{\text{dip}} \sim \alpha (kR)^2 \omega, \quad w_{\text{quad}} \sim \alpha (kR)^4 \omega. \quad (14.72)$$

The fine structure constant $\alpha = e^2/\hbar c$ enters as a signature of a relative weakness of electromagnetic interactions. Due to the small factors α and $(kR)^2$, the lifetimes are very long compared to the period $1/\omega$ of the emitted photon. The radiation widths $\Gamma_{\gamma} = \hbar\omega$ are small compared to typical times of nuclear processes driven by strong interactions, so that the states that can decay only by photon emission can usually be considered as nearly stationary.

The estimates (14.72) are based on the fact that the transition operators (dipole or quadrupole moment) are one-body quantities. They are sums of terms changing only one single-particle orbit, and the estimates (14.72) are made for *single-particle* transitions. If the wave functions reflect coherent many-body motion, the particles can make their transitions synchronously, which will cause a strong enhancement of the transition probability. In other cases, correlations between particles can quench the transition strength. The extreme example is the isoscalar dipole transition. The corresponding moment is simply the vector of the center of mass, which cannot lead to any internal excitation. More examples will be given later.

14.8 Magnetic Dipole Radiation

We did not yet take into account the antisymmetric term F_- in the second-order matrix element (14.65). Using vector algebra as in (14.23), we obtain

$$F_- = [\mathbf{k} \times \mathbf{e}^*] \cdot [\mathbf{r} \times \mathbf{p}] = [\mathbf{k} \times \mathbf{e}^*] \cdot \hbar \boldsymbol{\ell}, \quad (14.73)$$

where the orbital momentum ℓ was introduced. As seen from (14.18), the vector $-i[\mathbf{k} \times \mathbf{e}_{\mathbf{k}\lambda}^*]$ is just a part of the quantized magnetic field vector associated with creation of the photon with quantum numbers $(\mathbf{k}\lambda)$.

The matrix element resulting from the term F_- is the same as the one that would follow from the interaction

$$H_{\text{orb}} = -(\boldsymbol{\mu}_\ell \cdot \mathbf{B}) \quad (14.74)$$

of the orbital magnetic moment

$$\boldsymbol{\mu}_\ell = \sum_a \frac{e_a \hbar}{2m_a c} \ell_a \equiv \sum_a g_a^{(\ell)} \ell_a \quad (14.75)$$

with the magnetic field of the emitted photon. As we know, the spin term

$$H_{\text{spin}} = -(\boldsymbol{\mu}_s \cdot \mathbf{B}), \quad \boldsymbol{\mu}_s = \sum_a g_a^{(s)} \mathbf{s}_a, \quad (14.76)$$

should be added on equal footing with the orbital contribution.

Combining the orbital and spin magnetic moments into the total operator $\boldsymbol{\mu} = \boldsymbol{\mu}_\ell + \boldsymbol{\mu}_s$, we obtain for the rate of *magnetic dipole* (M1) radiation

$$d\omega_{fi} = \frac{\omega_{\mathbf{k}}}{2\pi c^3 \hbar} \left| -ic[\mathbf{k} \times \mathbf{e}_{\mathbf{k}\lambda}^*] \cdot \boldsymbol{\mu}_{fi} \right|^2 = \frac{\omega_{\mathbf{k}}^3}{2\pi c^3 \hbar} \left| [\mathbf{n} \times \mathbf{e}_{\mathbf{k}\lambda}^*] \cdot \boldsymbol{\mu}_{fi} \right|^2. \quad (14.77)$$

where $\mathbf{n} = \mathbf{k}/k$. This result is very similar to that for the electric dipole radiation (14.53). The only difference is that the magnetic vector $\boldsymbol{\mu}_{fi}$ is projected onto the vector corresponding to the polarization, which is complementary to that of the emitted photon. Again only $\Delta M = \pm 1$ is possible for the angular momentum projection along \mathbf{k} ; all properties of the classical magnetic dipole radiation are reproduced. As in the E1 case, the probability grows with the radiation frequency $\propto \omega^3$. Angular distributions (for the same initial population of magnetic substates) are always identical for electric and magnetic radiation of the same multipolarity; these cases can be distinguished by the photon polarization.

The angular momentum and parity restrictions for the M1 radiation follow from the character of the magnetic moment as an axial vector. The selection rule is $\Delta J = 0, \pm 1$; parity does not change. In many cases, both M1 and E2 radiations are allowed between the same initial and final states. Then we have their interference for the emission in a given direction. As in the scattering problem, the interference terms vanish in the total intensity integrated over the angles.

Making the same rough estimate as in (14.72), we obtain

$$\omega_{\text{magn}} \sim \alpha(kR)^2 \left(\frac{\hbar/mc}{R} \right)^2 \omega. \quad (14.78)$$

The ratio of the Compton wavelength of particles to the size of the system can be estimated as \bar{p}/mc via the typical momentum $\bar{p} \sim \hbar/R$ from the uncertainty relation. Then the extra factor in (14.78) is simply $(v/c)^2$. This estimate fails for the nuclei, where $R \sim r_0 A^{1/3}$ and the typical momentum is $p_F \sim \hbar/r_0 \gg \bar{p}$. The lowest order magnetic transitions (M1) in general are comparable to the next order electric transitions (E2). For low-energy collective transitions, the E2 radiation is more probable.

14.9 Photoabsorption

Now we consider an inverse process, absorption of photons by a nonrelativistic system of particles. A photon of the incident beam is annihilated in the interaction with the system getting excited. This is described by the first term of the quantized vector potential (14.30). The suitable characteristic of the process is the *cross section* of photoabsorption, which is the ratio of the transition rate to the incident photon flux.

The process we are interested in can be written, compare (14.44), as

$$|i; n_{\mathbf{k}\lambda}\rangle \rightarrow |f; n_{\mathbf{k}\lambda} - 1\rangle \quad (14.79)$$

with the final state $|f\rangle$ of the system having increased energy $E_f = E_i + \hbar\omega_{\mathbf{k}}$. The matrix element of the photon absorption is equal to $\sqrt{n_{\mathbf{k}\lambda}}$. The golden rule determines the transition rate

$$\begin{aligned} w_{fi} &= \frac{2\pi}{\hbar} \left| \langle f; n_{\mathbf{k}\lambda} - 1 | \sum_a \frac{e_a}{m_a c} (\mathbf{p}_a \cdot \hat{\mathbf{A}}(\mathbf{r}_a)) | i; n_{\mathbf{k}\lambda} \rangle \right|^2 \delta(E_i - E_f + \hbar\omega_{\mathbf{k}}) \\ &= \frac{4\pi^2}{V\omega_{\mathbf{k}}} n_{\mathbf{k}\lambda} \left| \langle f | \sum_a \frac{e_a}{m_a} (\mathbf{p}_a \cdot \mathbf{e}_{\mathbf{k}\lambda}) e^{i(\mathbf{k} \cdot \mathbf{r}_a)} | i \rangle \right|^2 \delta(E_i - E_f + \hbar\omega_{\mathbf{k}}). \end{aligned} \quad (14.80)$$

The incident flux is the photon density multiplied by the speed of light, $(n_{\mathbf{k}\lambda}/V)c$. The photoabsorption cross section for the specific transition $i \rightarrow f$ is therefore

$$\sigma_{fi}(E_{\gamma}) = \frac{4\pi^2 \hbar}{E_{\gamma} c} \left| \sum_a \frac{e_a}{m_a} \langle f | (\mathbf{p}_a \cdot \mathbf{e}_{\mathbf{k}\lambda}) e^{i(\mathbf{k} \cdot \mathbf{r}_a)} | i \rangle \right|^2 \delta(E_{\gamma} - E_{fi}) \quad (14.81)$$

where $E_{\gamma} = \hbar\omega_{\mathbf{k}}$ and $E_{fi} = E_f - E_i$. The interaction of nucleon spins with the magnetic field of the incident wave can be added as in (14.76).

The δ -function in (14.81) shows an infinitely narrow energy dependence of resonant absorption. The infinite cross section is a result of our approximation. In reality, the excited states have a finite lifetime τ and, consequently, the energy uncertainty, or the width $\Gamma \sim \hbar/\tau$, because later they reemit the absorbed photon or get rid of the excitation in another possible way. Therefore, the sharp δ -function in (14.81) or other similar expressions should be substituted by the smooth bell-shaped resonance curve of a finite width. Usually, the line shape is taken as a Lorentzian. Here we assume that this *absorption line* is narrow, and all matrix elements and kinematic factors can be treated as constant within the line width. Then the total transition strength is preserved, and one can integrate over photon energy and find the integral cross section

$$\int dE_{\gamma} \sigma_{fi}(E_{\gamma}) = \frac{4\pi^2 \hbar}{E_{fi} c} \left| \sum_a \frac{e_a}{m_a} \langle f | (\mathbf{p}_a \cdot \mathbf{e}_{\mathbf{k}\lambda}) e^{i(\mathbf{k} \cdot \mathbf{r}_a)} | i \rangle \right|^2. \quad (14.82)$$

As in the radiation problem, we can utilize the long wavelength approximation expanding the exponent in (14.82) and using the equations of motion (14.52). The lowest order term is given by the dipole absorption,

$$\int dE_{\gamma} \sigma_{fi} = \frac{4\pi^2 E_{fi}}{\hbar c} |(\mathbf{e}_{\mathbf{k}\lambda} \cdot \mathbf{d}_{fi})|^2. \quad (14.83)$$

Using the *dipole sum rule*, Problem 6.1 and [QPI,7.9], valid under the assumption of absence of velocity-dependent and exchange forces,

$$\sum_f E_{f0} |d_{f0}^z|^2 = \frac{\hbar^2 e^2}{2M} \frac{NZ}{A}, \quad (14.84)$$

where we take the effective charges for electric dipole transitions, we can estimate the total photoabsorption cross section summed over all transitions $|0\rangle \rightarrow |f\rangle$ from the ground state (the result is formally the same for an arbitrary initial state $|i\rangle$). Taking in (14.83) the polarization vector along the z -axis, we come to the total dipole photoabsorption cross section

$$\sigma_{\text{tot}} = \sum_f \int dE_\gamma \sigma_{fi} = 2\pi^2 \frac{e^2 \hbar}{Mc} \frac{ZN}{A}. \quad (14.85)$$

This universal prediction,

$$\sigma_{\text{tot}} = 0.06 \frac{ZN}{A} \text{ barn} \cdot \text{MeV}, \quad (14.86)$$

on average well agrees with experiment in spite of crudeness of approximations made in the derivation. One should remember that it includes only dipole absorption and does not include the electroproduction of mesons [5, 6].

14.10 Multipole Expansion

Although we were able to get through all calculations for E1, E2, and M1 multipoles using only elementary techniques, the task becomes more complicated for higher multipoles. The processes of high multipolarity are much slower due to the increasing power of the small parameter (kR) . The probability of the radiation of multipolarity (EL) is proportional to $(kR)^{2L+1}$ as follows from simple single-particle estimates. By similar estimates, the magnetic multipole radiation (ML) is suppressed by a factor $\sim (v/c)^2$ compared to the (EL) radiation. Usually, the lowest allowed multipolarity is the most probable albeit there are important exceptions, especially in the cases of coherent many-body enhancement. But, due to the selection rules in angular momentum and parity, the low-order multipole radiation can be forbidden. The general formalism of multipole expansion is needed.

We limit ourselves here with explaining the framework of this theory [6]. The starting point is the Hamiltonian (14.43) for the current interacting with the radiation field. The physical properties of the system are accumulated in the specific features of the current. Contrary to that, the electromagnetic field is expressed universally. We use the quantized form (14.30). Here the exponent plays the role of the “orbital” wave function of the photon, whereas the polarization vectors $\mathbf{e}_{k\lambda}$ characterize the intrinsic state of the photon, that is, its spin that is equal to 1 (\mathbf{e} is a vector with three components being equivalent by rotational properties to a tensor of rank 1), but the transversality of the field puts additional restrictions.

Thus, the photon is an object with the momentum \mathbf{k} and spin $\mathbf{e}_{k\lambda}$. We can expand the plane wave into partial waves with a certain orbital momentum ℓ . Each partial wave can be combined with the spin vector \mathbf{e} into a state with the total angular momentum of

the photon \mathbf{L} , which can take values $L = \ell, \ell \pm 1$. These states have parity $(-)^{\ell}$ determined by the transformation of the given partial wave. The component with $L = \ell$ and parity $(-)^L$ after multiplication in the matrix element by the polar vector of the current \mathbf{j} that changes sign under spatial inversion gives the magnetic multipole operator (ML) with multipolarity L and parity $(-)^{L+1}$. The components with $L = \ell \pm 1$ and parity $(-)^{L+1}$ in the matrix element are combined into the electric multipole operator (EL) with multipolarity L and parity $(-)^L$ in accordance with the properties of static multipole moments.

The final expression for the probability of the radiative transition $i \rightarrow f$ integrated over angles of the emitted photon and summed over its polarizations is [2]

$$w_{fi} = \frac{8\pi(L+1)}{L[(2L+1)!!]^2\hbar} k^{2L+1} \sum_{LM} \left\{ \left| (\mathcal{M}(\text{EL}, M))_{fi} \right|^2 + \left| (\mathcal{M}(\text{ML}, M))_{fi} \right|^2 \right\} \quad (14.87)$$

where the multipole matrix elements for electric and magnetic transitions are expressed via the current operator $\mathbf{j}(\mathbf{r})$,

$$\mathcal{M}(\text{ML}, M) = \int d^3r (\mathbf{j} \cdot \hat{\ell}) \Phi_{LM}, \quad (14.88)$$

$$\mathcal{M}(\text{EL}, M) = \int d^3r \left[(\nabla \mathbf{j}) \frac{1}{k} \frac{\partial}{\partial r} r - k(\mathbf{r} \cdot \mathbf{j}) \right] \Phi_{LM}, \quad (14.89)$$

$\hat{\ell} = -i[\mathbf{r} \times \nabla]$ is the orbital momentum operator and the function Φ_{LM} came from the partial wave expansion of the plane wave,

$$\Phi_{LM} = -i \frac{(2L+1)!!}{L+1} \frac{1}{ck^L} j_L(kr) Y_{LM}(\mathbf{n}), \quad (14.90)$$

$j_L(kr)$ are spherical Bessel functions. Of course, for a given pair of states (f, i) with certain parity and for a given multipolarity L , only one, either electric or magnetic, term in (14.87) works.

In the long wavelength approximation, we can use the limiting values of spherical Bessel functions at small arguments. Then the magnetic multipoles (14.88) become

$$\mathcal{M}(\text{ML}, M) = -\frac{i}{c(L+1)} \int d^3r (\mathbf{j}(\mathbf{r}) \cdot \hat{\ell}) r^L Y_{LM}(\mathbf{n}). \quad (14.91)$$

For the orbital current, this expression coincides with the orbital part of static magnetic multipoles. The presence of spin implies magnetization currents. In macroscopic electrodynamics, such a current is $c[\nabla \times \mathbf{m}]$ where \mathbf{m} stands for the magnetization density. The analogous quantity for a quantum system of particles is

$$\mathbf{m}(\mathbf{r}) = \sum_a g_a^s \mathbf{s}_a \delta(\mathbf{r} - \mathbf{r}_a). \quad (14.92)$$

The induced spin current is

$$\mathbf{j}_{\text{spin}} = c \sum_a g_a^s [\nabla \times \mathbf{s}_a] \delta(\mathbf{r} - \mathbf{r}_a). \quad (14.93)$$

Being substituted into (14.91), this current reproduces the spin part of static magnetic multipoles.

In the long wavelength limit, the second term of the electric multipole (14.89) is by a factor $(kR)^2$ smaller than the first one. In the first term, $\text{div} \mathbf{j}$ reduces to the time derivative

of the charge density ρ^{ch} with the aid of the continuity equation. This time derivative can be expressed through the operator equation of motion as in (14.70); the difference of energies between the initial and final states gives $\hbar\omega_{\mathbf{k}}$. Performing the expansion of the spherical Bessel functions, we come to

$$\mathcal{M}(\text{EL}, M) = \int d^3r \rho^{\text{ch}}(\mathbf{r}) r^L Y_{LM}(\mathbf{n}) \quad (14.94)$$

which is a standard definition of the electric multipoles. As it was already discussed, the *isoscalar* dipole operator, $L = 1$, in the long wavelength approximation (14.94) would reduce to the center of mass that is not related to intrinsic excitations. The nonzero dipole isoscalar transitions can be generated by the next term, $\propto (kR)^3$, of the spherical Bessel function $j_1(kr)$ in the general expression of the photon wave function (14.90). Their concentration around the excitation energy of roughly 6–10 MeV forms the so-called *pygmy dipole resonance* in medium-mass nuclei [7]. This energy corresponds in average to the distance between the neighboring shells of opposite parity as required for the dipole transitions.

It is easy to check that our results derived earlier coincide with those given by general theory. For example, for the dipole radiation, we get from (14.87)

$$w_{fi} = \frac{16\pi}{9\hbar} k^3 \sum_M \left| (\mathcal{M}(\text{E1}, M))_{fi} \right|^2. \quad (14.95)$$

The multipole operator $\mathcal{M}(\text{E1})$ in (14.95) differs from the dipole operator by the factor $\sqrt{3/4\pi}$. The sum over projections M in (14.95) is the same as the scalar product of the vector \mathbf{d}_{fi} by itself in (14.57). Then (14.95) coincides with (14.57).

Usually, the angular momentum projection M_f of the final state is not measured. Then we have to sum the transition rate over all M_f defining the *reduced transition probability*

$$B(\text{EL}; i \rightarrow f) = \sum_{MM_f} \left| (\mathcal{M}(\text{EL}, M))_{fi} \right|^2. \quad (14.96)$$

According to the Wigner–Eckart theorem, the entire dependence of the matrix element on the magnetic quantum numbers is concentrated in the Clebsch–Gordan coefficients. We can use their orthogonality and perform the summation over M and M_f . The reduced transition probability is then related to the reduced matrix element of the multipole operator,

$$B(\text{EL}; i \rightarrow f) = \frac{1}{2J_i + 1} |\langle f || \mathcal{M}(\text{EL}) || i \rangle|^2. \quad (14.97)$$

This quantity is convenient because it does not depend on the initial population of various projections M_i . Note that for the inverse transition induced by the same operator, the *detailed balance* relation is valid,

$$B(\text{EL}; f \rightarrow i) = \frac{2J_i + 1}{2J_f + 1} B(\text{EL}; i \rightarrow f). \quad (14.98)$$

The reduced transition probability determines the partial lifetime of a given initial state with respect to a specific radiative decay (all M_f summed up),

$$\tau_{i \rightarrow f}^{-1} = \sum_{M_f} w_{fi} = \frac{8\pi}{\hbar} \frac{L + 1}{L[(2L + 1)!!]^2} k^{2L+1} B(\text{EL}; i \rightarrow f). \quad (14.99)$$

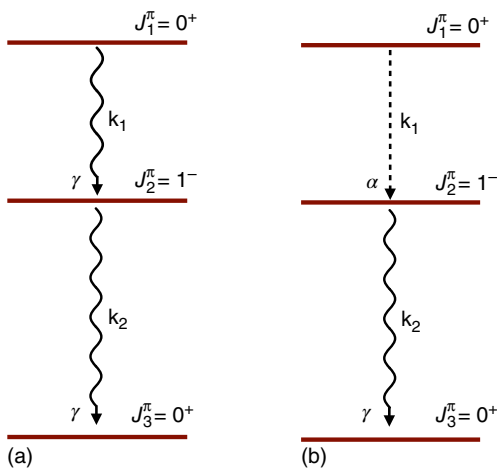


Figure 14.2 Sequence of transitions discussed in Problem 14.4.

Here the kinematic factors are singled out. They are associated with the geometry and phase space volume of the emitted photon. Information concerning structure of the radiating system is concentrated in the reduced transition probability. With the substitution $EL \rightarrow ML$, the same expressions are valid for magnetic multipoles.

Problem 14.4

- A nucleus undergoes a cascade of gamma-transitions, see Figure 14.2a, from the initial state 1 with spin $J_1 = 0$ and positive parity to the intermediate state 2 with $J_2 = 1$ and negative parity and then to the final state 3 with $J_3 = 0$ and positive parity. What is the probability distribution for the angle θ between the directions of the photons \mathbf{k}_1 and \mathbf{k}_2 , emitted in the first and second transitions, respectively?
- Solve the same problem when in the first step an alpha-particle is emitted followed by the photon in the second decay, all quantum numbers are the same as in part (a) (see Figure 14.2b).

Solution

- Only dipole radiation could contribute in this case, and the rate of electric dipole radiation E1 summed over final polarizations is

$$\frac{d\omega}{d\Omega} = \frac{\omega_k^3}{2\pi c^3 \hbar} |\mathbf{n}_1 \times \mathbf{d}_{fi}|^2. \quad (14.100)$$

Initial $J_1 = 0$ state is fully symmetric and we can select quantization axis along the direction of the emitted photon $\mathbf{n}_1 = \mathbf{k}_1/k_1$. Then in the intermediate state, only projections $M_2 = \pm 1$ are populated because only transverse components of d_x and d_y of the dipole operator can radiate. The second photon originates from the same magnetic substates and since the final magnetic projection $M_3 = 0$, again only d_x and d_y radiate. The angular distribution for this radiation has the form

$$|\mathbf{n}_2 \times \mathbf{d}_{fi}|^2 \sim \frac{1}{2}(1 + \cos^2 \theta). \quad (14.101)$$

Note that in this case the Wigner–Eckart theorem states that matrix elements of the dipole operator are the same for all magnetic projections. Being normalized, the probability to find two photons at an angle θ is

$$P(\theta) = \frac{3}{16\pi}(1 + \cos^2(\theta)). \quad (14.102)$$

- b) If α -particle is radiated first, we can again select the quantization axis along the direction of α -particle. However, α has no spin and the entire angular dependence is in the relative angular momentum, which has to be a p -wave in this case. The projection of the angular momentum onto the quantization axis is zero because angular momentum is perpendicular to this axis. After the first decay, the sublevel with $M_2 = 0$ is populated in the intermediate state, and it radiates a photon that does not change the magnetic projection. The corresponding angular dependence is proportional to $\sin^2(\theta)$. The normalized probability is

$$P(\theta) = \frac{3}{8\pi}\sin^2\theta. \quad (14.103)$$

The identical answer can be obtained if we choose the quantization axis along the direction of photon, \mathbf{k}_2 . In this frame, the α -particle in the transition $1 \rightarrow 2$ must populate states with $M_2 = \pm 1$. This means that the α -decay is described by the spherical function $Y_{1,\pm 1}$. Thus, probability is

$$P(\theta) = |Y_{1,\pm 1}|^2 = \frac{3}{8\pi}\sin^2\theta. \quad (14.104)$$

References

- 1 M.E. Rose, *Multipole Fields*, John Wiley & Sons, Inc., New York, 1955.
- 2 A. Bohr and B.R. Mottelson, *Nuclear Structure*, Vol. 1, Benjamin, New York, 1969.
- 3 A.I. Achiezer and V.B. Beresteckij, *Quantum Electrodynamics*, Interscience, New York, 1965.
- 4 V.B. Beresteckij, E.M. Lifshitz, and L.P. Pitaevskii, *Quantum Electrodynamics*, vol. 4 of *Course of Theoretical Physics* (eds L.D. Landau and E.M. Lifshitz), 2nd edn, Butterworth-Heinemann, Oxford, 2008.
- 5 J.S. Levinger, *Nuclear Photo-Disintegration*, Oxford University Press, Oxford, 1960.
- 6 A.I. Akhiezer, A.G. Sitenko, and V.K. Tartakovskii, *Nuclear Electrodynamics*, Springer-Verlag, Berlin, 1994.
- 7 N. Paar, D. Vretenar, E. Khan, and G. Coln, Rep. Prog. Phys. **70**, 691 (2007).

15

Nuclear Gamma-Transitions and Related Electromagnetic Processes

In this section we discuss the interaction of nuclei, or any finite quantum mechanical system, with electromagnetic fields. Much of what we know about nuclei comes from such interactions.

J.D. Walecka, *Theoretical Nuclear and Subnuclear Physics*

15.1 Single-Particle Transitions

In the independent particle model, stationary wave functions of the nucleons are simple Slater determinants. Occupation numbers of single-particle orbits are equal to 1 or 0. Excited states differ from the ground state by a number of particle–hole excitations (redistribution of filled and empty orbits). A particle excited above the Fermi surface Σ_F can radiate and fall into lower energy states, including hole states below Σ_F . The amplitude of radiation in this process is given by a pure single-particle matrix element $|\lambda\rangle \rightarrow |\lambda'\rangle$ where only occupation numbers of this pair of orbits are changed,

$$|i\rangle \equiv |n_{\lambda'} = 0, n_{\lambda} = 1\rangle \rightarrow |f\rangle \equiv |n_{\lambda'} = 1, n_{\lambda} = 0\rangle. \quad (15.1)$$

In the language of secondary quantization, this transition is described by the fermion transfer operator $a_{\lambda'}^{\dagger}a_{\lambda}$. However, in this trivial example, we do not need to use secondary quantization.

Let us consider a single-particle radiation transition of electric multipole type in the spherical shell model with spin–orbit coupling. The particle wave functions are products of the radial and spin-angular parts,

$$\psi_{n\ell jm}(\mathbf{r}, \sigma) = \frac{u_{n\ell}(r)}{r} [Y_{\ell}(\mathbf{n})\chi(\sigma)]_{jm} \quad (15.2)$$

where the symbol $[A_L B_{L'}]_{JM}$ stands for the vector coupling of two subsystems A and B with angular momenta L and L' , respectively, into the total angular momentum J and projection M ; χ is the single-particle spinor. The quantum numbers of the final orbit are $(n' \ell' j' m')$.

The electric multipole operator (14.94) is simply $er^L Y_{LM}(\mathbf{n})$ so that the radial integral separates from the spin-angular part. The resulting reduced probability can be written as

$$B(\text{EL}) = \frac{e^2}{4\pi} \left| \int dr u_{n'\ell'}(r) r^L u_{n\ell} \right|^2 S_{\ell'j',\ell j}^{\text{EL}} \quad (15.3)$$

where the *statistical factor*

$$S_{\ell'j',\ell j}^{\text{EL}} = 4\pi \sum_{m'M} |\langle [Y_{\ell'}\chi']_{j'm'} | Y_{LM} | [Y_\ell\chi]_{jm} \rangle|^2 \quad (15.4)$$

can be calculated in terms of a sum of the Clebsch–Gordan coefficients.

We discussed already the geometrical selection rules. In a single-particle transition, they require the triangle condition ($j'Lj$) for the total angular momentum and $(-)^{\ell'+L+\ell} = +1$ for parity conservation. As electric multipole operators do not depend on spin variables, the new selection rule of pure orbital nature arises from the statistical factor. The angular integral S^{EL} includes only three spherical functions. It is equal to

$$\int d\theta Y_{\ell'\mu'}^* Y_{LM} Y_{\ell\mu} = \sqrt{\frac{(2L+1)(2\ell+1)}{4\pi(2\ell'+1)}} C_{L0\ell0}^{\ell'0} C_{LM\ell\mu}^{\ell'\mu'} \quad (15.5)$$

and can be brought into the form symmetric with respect to all three spherical functions by the transformation to the $3j$ -symbols (11.76). Equation (15.5) implies the additional orbital selection rule given by the triangle ($\ell'L\ell$).

Problem 15.1 Derive Eq. (15.5).

Solution

According to the Wigner–Eckart theorem, in the expansion of the product of two spherical functions over spherical functions of the same angles, the coefficients should be proportional to the Clebsch–Gordan coefficients (CGC), which carry the triangle condition and conservation of the total projection. Therefore, the expansion must look like

$$Y_{LM}(\mathbf{n}) Y_{\ell\mu}(\mathbf{n}) = \sum_{\ell'\mu'} \gamma_{\ell'} C_{LM\ell\mu}^{\ell'\mu'} Y_{\ell'\mu'}(\mathbf{n}), \quad (15.6)$$

or, due to the orthogonality of the CGC,

$$\gamma_{\ell'} Y_{\ell'\mu'}(\mathbf{n}) = \sum_{M\mu} C_{LM\ell\mu}^{\ell'\mu'} Y_{LM}(\mathbf{n}) Y_{\ell\mu}(\mathbf{n}). \quad (15.7)$$

Equation (15.7) has to be satisfied for all directions \mathbf{n} . For \mathbf{n} along the polar axis ($\theta = 0$), only Y_{L0} does not vanish because in this direction the azimuthal angle φ is not defined and any single-valued function of φ as $Y_{\ell\mu} \propto \exp(i\mu\varphi)$ has to vanish. Physically it is equivalent to the statement that a particle moving along the z -axis does not have angular momentum projection along this axis. Thus,

$$Y_{\ell\mu}(\mathbf{e}_z) = \delta_{\mu 0} Y_{\ell 0} = \delta_{\mu 0} \sqrt{\frac{2\ell+1}{4\pi}} P_\ell(\cos \theta = 1) = \delta_{\mu 0} \sqrt{\frac{2\ell+1}{4\pi}}. \quad (15.8)$$

From here,

$$\gamma_{\ell'} \sqrt{2\ell'+1} = C_{L0\ell0}^{\ell'0} \sqrt{\frac{(2\ell+1)(2L+1)}{4\pi}} \quad (15.9)$$

which, being substituted into (15.6), is equivalent to (15.5). Using the backward direction $\theta = \pi$ in this derivation, we easily show that the parity selection rule follows as well,

$$C_{L0\ell0}^{\ell'0} = 0 \quad \text{if} \quad \ell + L + \ell' = (\text{odd}). \quad (15.10)$$

Problem 15.2 Show that when parity rule $(-)^{\ell'+L+\ell} = +1$ is satisfied, the statistical factor in Eq. (15.5) can be expressed as

$$S_{\ell'j',\ell j}^{\text{EL}} = (2L+1) \left| C_{L0\ j1/2}^{j'1/2} \right|^2. \quad (15.11)$$

To get a reference point, the so-called Weisskopf single-particle units are used for estimating the transition probabilities. They are “derived” by setting the statistical factor (15.4) to unity and taking for the radial integral the mean value of r^L inside a sphere with the nuclear radius R ,

$$\int dr u_{n'\ell'}(r) r^L u_{n\ell}(r) \simeq \frac{3}{L+3} R^L. \quad (15.12)$$

The Weisskopf unit is, according to this estimate,

$$B_W(\text{EL}) = \frac{e^2}{4\pi} \left(\frac{3}{L+3} \right)^2 R^{2L}. \quad (15.13)$$

As a rule, the single-particle transition probabilities are overestimated in this way as we neglect the oscillatory behavior of the wave functions inside the nuclear volume.

In the case of the electric dipole transitions, we have to use the effective charges (9.40) removing an unphysical admixture of the global translation to the genuine internal excitation. For other multipolarities, the effective neutron charge due to the recoil effects is small and formally calculated single-neutron electric multipole transitions vanish. Practically it is not the case, especially for electric quadrupole transitions where the situation is similar to what we discussed in Section 9.4 for static quadrupole moments. The physical reason is that in reality the transitions are not pure single-particle even in near-magic nuclei. A valence particle interacts with the core and the stationary states are superpositions including, apart from the main shell-model component, admixtures of the states where the core is excited. This important effect of *core polarization* takes place in both initial and final states of a given transition. The resulting transition probabilities differ from the single-particle estimates. This difference is formally described by the *effective charge* that is related to the core polarization rather than to the recoil corrections. The examples for the E2 transitions in near-magic nuclei, both proton-odd and neutron-odd, can be found in Ref. [1], Vol. 1, Table 3.2.

As a number of valence particles grow, pairing correlations suppress all electric multipole single-particle transitions by the coherence factors $(uu' - vv')^2$ (Section 13.11 for \mathcal{T} -even operators). The core polarization becomes stronger and eventually deforms a nucleus (Section 12.4). Transition probabilities in deformed nuclei include rotational degrees of freedom and have to be discussed separately.

The magnetic dipole operator $\mathcal{M}(M1, M)$ is given by the usual expression as a sum of the orbital and spin magnetic moments. For a single-particle transition, we can add and subtract $g^{(l)}\mathbf{s}$ in order to write down the M th spherical component of this vector as

$$\mathcal{M}(M1, M) = \sqrt{\frac{3}{4\pi}} \mu_N (g^{(\ell)}\mathbf{j} + (g^{(s)} - g^{(\ell)})\mathbf{s})_M. \quad (15.14)$$

The first term is proportional to the total angular momentum of the particle and cannot cause single-particle transitions. In the second term, the operator is simply spin \mathbf{s} that does not change the orbital wave function. The only allowed single-particle magnetic

dipole transition in the spherical independent-particle shell model is that between the members of the spin-orbit doublet $j = \ell \pm 1/2$, which have the same orbital momentum ℓ and parity $(-)^{\ell}$. The transition is of the spin-flip type.

For higher magnetic multipole transitions along with similar estimates as for electric multipole transitions, one can employ the so-called Moszkowski units,

$$B_M(ML) = \frac{\mu_N^2}{4\pi} \left(\frac{3L}{L+2} \right)^2 \left(g^{(s)} - \frac{2g^{(l)}}{L+1} \right)^2 R^{2L-2}. \quad (15.15)$$

There exist also a simplified Weisskopf unit for magnetic transitions defined as

$$B_W(ML) = \frac{10\mu_N^2}{\pi} \left(\frac{3}{L+3} \right)^2 R^{2L-2}. \quad (15.16)$$

These estimates are applied to single-proton as well as to single-neutron transitions.

The M1 operators are less sensitive to pairing correlations; their expectation values do not change at all in the seniority model. In the BCS theory, the coherence factors for the \mathcal{T} -odd operators (Section 13.11) are $(uu' + vv')^2$, which are usually close to 1. However, the core polarization is important here as well. It leads to renormalized “effective” gyromagnetic ratios in the M1 operator. This polarization in the magnetic case is especially effective if the core contains only the lower energy component of a spin-orbit doublet; then the virtual M1 transitions of the core particles to the empty upper level of the doublet can lead to a significant renormalization.

The single-particle M1 transitions between the upper level of the spin-orbit doublet and the lower level of another doublet of the same parity and with $\Delta j = 1$ as, for example, $p_{3/2} \leftrightarrow f_{5/2}$, are allowed by angular momentum and parity. Such transitions are *ℓ -forbidden* because the single-particle M1 operator (15.14) cannot induce $|\Delta\ell| = 2$. The M1 ℓ -forbidden transitions become possible with the emergence of additional structures like (9.19) in the magnetic dipole operator due to the strong (tensor) or electromagnetic interactions. The core polarization is also effective bringing in the admixtures to the wave functions that make the transition possible.

15.2 Collective Transitions

Frequently the gamma-transitions turn out to be strongly enhanced compared to the single-particle estimates. Similar to our conclusions concerning the origin of the enhancement of static quadrupole moments in Section 9.4, the electromagnetic transitions can be considerably amplified by the coherent radiation of many particles. The mechanism of enhancement can be understood with the simple schematic model. If residual interaction effects are taken into account, the particle-hole excitations cease to be really stationary states. An excited particle interacts with the particles in the core. The two-body interaction has nonzero matrix elements between the original particle-hole state and the state where the particle and the hole are shifted to new orbits. Also new particle-hole pairs can be created as a result of the interaction.

Let us assume that the stationary state (we call it *collective*) is a superposition of various “simple”, for example, single-particle (particle-hole) excitations $|k\rangle$,

$$|\Psi_{\text{coll}}\rangle = \sum_k C_k |k\rangle. \quad (15.17)$$

Of course, all components $|k\rangle$ have the same quantum numbers of angular momentum and parity. The coefficients C_k of the superposition are normalized according to

$$\sum_k |C_k|^2 = 1. \quad (15.18)$$

Let N_c be a number of amplitudes C_k contributing considerably to the collective superposition. Due to the normalization condition, a typical magnitude of the amplitudes is

$$\overline{|C_k|^2} = \frac{1}{N_c}. \quad (15.19)$$

At large N_c , the amplitudes are small.

Now we can evaluate the matrix element of the multipole excitation of the collective state (15.17) from the ground state (or the matrix element of de-excitation of the collective state). The collective state and all states $|k\rangle$ have the same angular momentum quantum numbers $\lambda\mu$. The excitation from the ground state $|0\rangle$ is implemented by the multipole operator $\mathcal{M}_{\lambda\mu}$. Each individual simple state $|k\rangle$ can be reached by a transition amplitude

$$\mathcal{M}_k = \langle k; \lambda\mu | \mathcal{M}_{\lambda\mu} | 0 \rangle. \quad (15.20)$$

Let the typical magnitude of the amplitudes (15.20) be $\overline{\mathcal{M}}$. The amplitude of the collective excitation is

$$\langle \Psi_{\text{coll}}; \lambda\mu | \mathcal{M}_{\lambda\mu} | 0 \rangle = \sum_k C_k^* \mathcal{M}_k. \quad (15.21)$$

This can be treated as a scalar product of two multidimensional vectors in a large space of dimension N_c . If the vector \mathbf{C} of the collective state components and the vector \mathcal{M} of transition amplitudes are uncorrelated, most probably the individual products in the sum (15.21) have *random signs* and cancel each other. Since the average magnitude of the components \mathbf{C} is $\sim N_c^{-1/2}$, each term in (15.21) is of the order of $\mathcal{M}N_c^{-1/2}$. The sum of a large number N_c of random items grows in average $\propto N_c^{1/2}$. Then the whole sum does not increase with N_c being of the order of a typical single-particle amplitude $\overline{\mathcal{M}}$.

However, one can imagine an exceptional situation when the vectors \mathbf{C} and \mathcal{M} are correlated being *aligned* nearly in the same direction in multidimensional space. In this case, the sum is *coherent* and contains a big number $\sim N_c$ of small terms $\sim \mathcal{M}N_c^{-1/2}$. As a result of the coherent coupling, the total amplitude is enhanced,

$$\langle \Psi_{\text{coll}} | \mathcal{M} | 0 \rangle \simeq \sqrt{N_c} \overline{\mathcal{M}}, \quad (15.22)$$

and the excitation probability is enhanced by the factor N_c in comparison with the single-particle probability,

$$B(\mathcal{M}) \simeq N_c |\overline{\mathcal{M}}|^2 \simeq N_c B_{s-p}(\mathcal{M}). \quad (15.23)$$

Hence, the enhancement is determined by the degree of *collectivization*, a number of coherent components in the wave function of the collective excitation. Known collective transitions, mostly E1, E2, and E3, are enhanced by one to two orders of magnitude relative to single-particle estimates.

We have to stress that the enhancement occurs for a specific multipole operator only. The simple states are mixed into a collective superposition (15.17) by the residual interaction that itself is similar to the multipole–multipole interaction (Section 12.2). Then

the admixture coefficients are proportional to the matrix elements of multipole operators that have the properties analogous to the matrix elements of $\mathcal{M}_{\lambda\mu}$.

In the situation of collective enhancement, another approach can be very promising. Instead of the complicated wave function (15.17) with many components, one can consider the collective excitation as a new entity, a quasiparticle of a different kind, for example, as a surface or volume wave that definitely has collective nature. We used this idea in our global description of nuclear drops and boson quantization of collective vibrational modes (Section 6.5). The electric multipole moment associated with the surface vibrations can be simply expressed in terms of creation and annihilation operators of collective phonons,

$$\mathcal{M}(\text{EL}, M) = \frac{3}{4\pi} Z e R_0^L \sqrt{\frac{\hbar}{2(B_L C_L)^{1/2}}} (\alpha_{LM}^\dagger + (-)^M \alpha_{L-M}). \quad (15.24)$$

Here the parameter η in (6.72) is chosen in agreement with the proper normalization of the phonon Hamiltonian (5.49); B_L and C_L are the mass parameter and the restoring force for the mode under consideration; the frequency is $\omega_L = \sqrt{C_L/B_L}$, Eq. (5.52).

The reduced probability of the excitation of the phonon state from the ground state is directly given by Eqs. (14.96) and (15.24),

$$B(\text{EL}) = (2L + 1) \left(\frac{3}{4\pi} Z e R_0^L \right)^2 \frac{\hbar}{2B_L \omega_L}. \quad (15.25)$$

The de-excitation probability does not contain the factor $(2L + 1)$, see Eq. (14.98). The enhancement of the collective transition probability in this model relative to the single-particle estimate (15.13) is due to the factor $Z^2/B_L \propto Z^2/A$ if one takes the estimate similar to (5.43) for the mass parameter. The estimates based on the hydrodynamic models are not reliable for low-frequency modes. But such a factor would emerge anyway for low multipolarities when surface motion should coherently move many nucleons although probably instead of the total proton number Z , one can expect a smaller number corresponding to outer shells only. The appearance of ω_L^{-1} in the denominator (15.25) is also of general nature. It will appear in any model working with phonons as quanta of collective vibrations. The softness of the vibrational mode implies the large amplitude $\propto \omega^{-1/2}$ that is to be squared in the transition probability. It is another reflection of collectivity leading to a strong enhancement of the transition strength.

15.3 Nuclear Isomerism

We discussed repeatedly selection rules that follow from general invariance principles: the angular momentum and parity conservation. Here we give examples of selection rules related to specific features of nuclear wave functions.

Since electric multipole operators act only on the orbital functions, they bring in geometrical selection rules for the orbital angular momentum. This is important in cases when the orbital momentum is a good quantum number, primarily for the single-particle transitions. Specific phenomena stipulated by these selection rules arise in the regions of the periodic table where the single-particle levels are populated that belong to *intruders*, Section 8.8, orbits coming from the next higher major shell due to the strong

spin-orbit coupling. They have parity opposite to the main part of the orbits in the given shell and angular momenta ℓ, j differing by several units. A particle excited to such an intruder orbit (it might happen in a reaction or beta-decay from above) can return down by gamma-radiation of high multipolarity only. Due to small excitation energy, this radiation is highly suppressed so that the excited state can have an abnormally long lifetime.

The especially long-lived excited nuclear states are called *isomers*. Their lifetimes can reach days and even years. Practically, we have to deal with different “stable” nuclear species. Historically, first isomer states were discovered in 1921 as two types of the element called at that time “uranium X_2 ,” with lifetimes 6.7 h and 1.14 min. In fact, those are two different quantum states of protactinium ^{234}Pa ($Z = 91$). Isomeric states can be artificially excited by various reactions.

The isomeric states appear most frequently in the *islands of isomerism* near the ends of major shells, that is, just at the intruder location. The single-particle nature in many cases can be confirmed by the fact that isomeric states in odd- A nuclei often survive also in neighboring nuclei differing by a pair of nucleons of the opposite kind. For example, each of proton-odd isotopes $^{107,109}\text{Ag}$ has a very similar isomeric state (the same excitation energies and lifetimes). This also takes place in isotopes $^{113,115}\text{In}$. Magnetic and quadrupole moments within such pairs are quite similar as well. Here we deal with a proton single-particle spectrum on the background of the paired neutron system whose properties are insensitive to the exact number of pairs.

The well-known islands of isomerism are located at N or Z near 45 and near 75. The spherical shell model clearly demonstrates the origin of the phenomenon: we have a close contact of $0g_{9/2}$ and $1p_{1/2}$ orbits below the magic number 50 and of $0h_{11/2}$ and $2s_{1/2}$ below the magic number 82. The ground state of $^{115}_{49}\text{In}_{56}$ has one proton hole in the $0g_{9/2}, \ell = 4$ orbit. Indeed the ground state spin of this nucleus is $9/2$. The first excited state corresponds to the hole transfer to the orbit $1p_{1/2}$ with $\ell = 1$ (a particle from this orbit occupies the former hole state in the $g_{9/2}$ orbit). The de-exciting gamma-transition should have $\Delta j = 4, \Delta\ell = 3$ and change parity. The lowest options are E5 or M4 transitions the latter being more probable. Due to small energy difference, the lifetime with respect to the M4 transition is quite long.

Figure 15.1 shows the low-lying levels of the sequence of the neutron-odd tellurium isotopes located in the end of the $N = 4$ major shell. Here the intruder $0h_{11/2}, \ell = 5$ orbit is adjacent to the $1d_{3/2}, \ell = 2$ and $2s_{1/2}, \ell = 0$ orbits. It turns out to be energetically favorable to place each new neutron pair on the $h_{11/2}$ orbit with large capacity because it increases the pairing energy. Therefore, these isotopes have ground state spins $1/2$ or $3/2$ but never $11/2$ as the $h_{11/2}$ level is populated pairwise only. The isomeric states with $J = 11/2$ have a lifetime from half a year to an hour. The lifetime is monotonously decreases as transition energy increases. The transition $h_{11/2} \rightarrow d_{3/2}$ has $\Delta j = 4, \Delta\ell = 3$ with changing parity and occurs as M4. Its energy dependence $\sim E_\gamma^9$ explains rapid fall off of the lifetime.

The isomers can appear also rather accidentally if, due to some details of nuclear structure, a state of two or several quasiparticles with large angular momentum turns out to be located below the states with small angular momentum. Then possible gamma-transitions have large multipolarity and become strongly hindered. Such states form traps on the way of nuclear de-excitation. A very interesting type of isomerism emerges in the heaviest elements where potential energy as a function of deformation can have

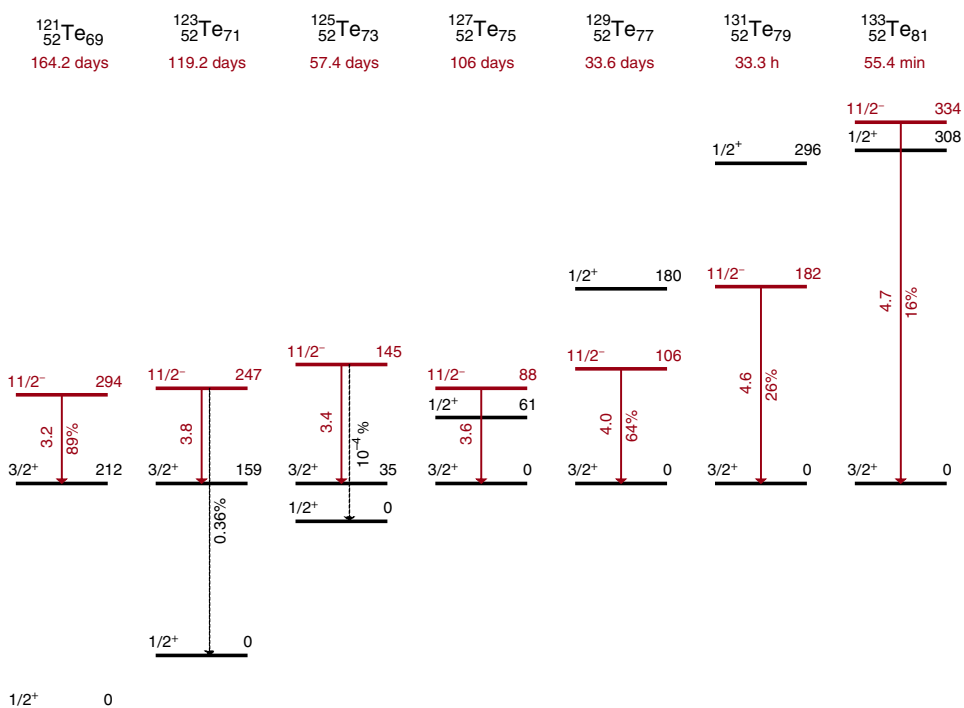


Figure 15.1 Low-lying levels of odd tellurium isotopes; lifetimes refer to $J = 11/2$ isomers. The isomeric state decays slowly via the M4 isomeric transition $11/2^-$ to $3/2^+$ shown by the red arrow with reduced $B(M4)$ values in Weisskopf units being indicated. In cases where competition with other decay modes (beta-decay) is significant, the branching fraction that corresponds to the electromagnetic part is shown. In ^{123}Te and ^{125}Te , the weak E5 branch has been seen, this is shown by black arrows, where relative intensity is indicated.

two or more local minima separated by potential barriers. Wave functions localized mainly in one of the minima have only a small probability to make a gamma-transition to the lower minima because of a small overlap of the many-body wave functions (*shape isomerism*). In some cases, the nucleus has a larger probability to undergo spontaneous fission than to make a radiative transition to the lower potential minimum. In such cases, we can speak about *fissioning isomers*.

15.4 Isospin

Specific nuclear selection rules are caused by the isospin invariance. We know that one-body operators consist, from the isospin point of view, of isoscalar and isovector parts. In addition to angular momentum and parity selection rules, we have similar requirements in isospace: $\Delta T = 0$ and $\Delta T = 0, \pm 1$ for the isoscalar and isovector parts, respectively. Of course, T_3 is always the same for all states in a given nucleus.

In the isovector part of the dipole operator, protons and neutrons contribute with opposite signs. In general, it would have the selection rules $\Delta T = 0, \pm 1$. However, nuclei with $N = Z$ and, therefore, $T_3 = 0$, are exceptional because in this case the transitions

with no change of isospin, $\Delta T = 0$, are forbidden. Take any isovector operator $O_{t=1,\tau}$. Here the notations show the tensor rank $t = 1$ in isospace (isovector) and projections $\tau = 0, \pm 1$ allowed for $t = 1$. Within the excitation spectrum of a given nucleus, only $\tau = 0$ is possible so we are interested in the isospin matrix element $(O_{10})_{fi}$ with $\Delta T_3 = 0$. Isospin invariance implies that the Wigner–Eckart theorem is valid in isospace similar to ordinary space, and the matrix element is proportional to the CGC,

$$(O_{10})_{fi} = \langle T_f T_3 | O_{10} | T_i T_3 \rangle \propto C_{10T_i T_3}^{T_f T_3}. \quad (15.26)$$

In a nucleus with $T_3 = 0$, the transition without changing isospin, $T_f = T_i$ is forbidden because the matrix element vanishes due to the “isoparity” selection rule (15.10).

As an example, one can refer to the low-lying E1 transitions in the $N = Z$ nucleus ^{14}N (see Figure 15.2). The ground state ^{14}N has a configuration similar to $^{12}\text{C} + \text{deuteron}$ that corresponds to $J^\Pi = 1^+$ and $T = 0$. The first excited state has $J^\Pi = 0^+$ and $T = 1$ being analogous to $^{12}\text{C} + \text{spin-singlet nucleon pair}$; its excitation energy 2.31 MeV is very close to the deuteron binding energy. This excited state belongs to the *isotriplet*; two other, charged, components of this triplet are ground states of ^{14}C and ^{14}O with $T_3 = -1$ and $T_3 = +1$, respectively. The excited state of ^{14}N at energy 5.69 MeV has quantum numbers $J^\Pi = 1^-, T = 0$. By angular momentum and parity, E1 transitions from this

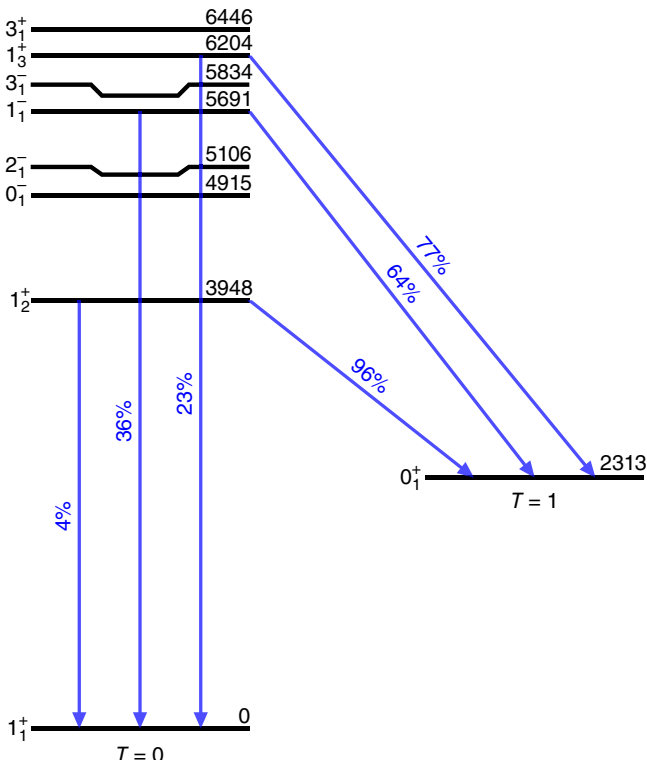


Figure 15.2 Level scheme for ^{14}N with $T = 0$ and $T = 1$ states shown separately; arrows indicate dipole transitions in ^{14}N with branching ratios for the transitions from the common initial state. States are labeled with their spin and parity on the left and excitation energy in kiloelectronvolts on the right.

level are allowed to both the ground state and the first excited state. At comparable values of matrix elements, the ratio of probabilities would be determined by the dipole factor $k^3 \propto E_\gamma^3$ of Eq. (14.99) in favor of the ground state transition, $(5.69/3.38)^3 = 4.77$. In the experiment (Figure 15.2), this ratio is 0.56, mainly because the transition is isospin-forbidden.

We have already mentioned that the isoscalar part of the E1 operator is totally excluded only in the lowest order of the long wavelength approximation. Expanding the exponent in (14.48) and taking the second term of the series, similar to that done for monopole transitions in the following, Eqs. (15.37) and (15.38), we obtain the operator

$$\mathbf{d}' = \sum_a e_a \mathbf{r}_a r_a^2 \quad (15.27)$$

that has E1 selection rules and a nonzero *isoscalar* part. But the corresponding transition amplitude has an extra suppression factor $(kR)^2$. Moreover, the operator \mathbf{d}' contains a large part coming from the diagonal contributions of mean square radii $\langle r_a^2 \rangle$. These contributions result in an effective operator again proportional to the isoscalar dipole moment. Therefore, it is worthwhile to define the so-called Schiff moment that, in terms of the charge density $\rho_{\text{ch}}(\mathbf{r})$, is usually written, with a conventional normalization factor, as

$$\mathbf{S} = \frac{1}{10} \int d^3r \rho_{\text{ch}}(\mathbf{r}) \mathbf{r} [r^2 - \langle r_{\text{ch}}^2 \rangle]. \quad (15.28)$$

This operator can excite the dipole state mostly around excitation energy $\sim 3\hbar\omega$ in oscillator units (*isoscalar giant dipole resonance*) [2]. Another important role of the Schiff moment is to excite through weak interaction with atomic electrons the electric dipole moment of the atom (the dipole moment of the nucleus, which can exist only in the case of \mathcal{P} - and \mathcal{T} -violation, will not show up in the external electric field being screened by the redistribution of the electrons).

The *magnetic dipole* operator also can be divided into isoscalar and isovector parts and again it turns out that the isovector part prevails in transitions but this time just numerically rather than by virtue of some conservation law. Neglecting orbital contributions of neutrons ($g_p^{(\ell)} = 1, g_n^{(\ell)} = 0$), we have for the standard part of the M1 operator

$$\boldsymbol{\mu} = \frac{1}{2} \mu_N \sum_a \{(1 + \tau_{3a})(g_p^{(s)} \mathbf{s}_a + \boldsymbol{\ell}_a) + (1 - \tau_{3a})g_n^{(s)} \mathbf{s}_a\}. \quad (15.29)$$

In the orbital term we add and subtract \mathbf{s}_a to get total nucleon angular momenta \mathbf{j}_a , which combine together the angular momentum \mathbf{J} of the nucleus. Collecting isoscalar and isovector terms, we obtain (in n.m.)

$$\begin{aligned} \boldsymbol{\mu} &= \frac{1}{2} \mathbf{J} + \frac{1}{2} \sum_a \{(g_p^{(s)} + g_n^{(s)} - 1)\mathbf{s}_a + \tau_{3a}[(g_p^{(s)} - g_n^{(s)})\mathbf{s}_a + \boldsymbol{\ell}_a]\} \\ &= \frac{1}{2} \mathbf{J} + \sum_a \left\{ 0.38 \mathbf{s}_a + \tau_{3a} \left(4.70 \mathbf{s}_a + \frac{1}{2} \boldsymbol{\ell}_a \right) \right\}. \end{aligned} \quad (15.30)$$

The total angular momentum cannot excite the system, and the remaining isoscalar term is by order of magnitude weaker than the isovector one due to the cancellation of neutron and proton contributions (we used the numerical values for gyromagnetic ratios). We can apply again the arguments associated with Eq. (15.26) to show that in nuclei with $N = Z$, the M1 transitions with $\Delta T = 0$ are suppressed. The quenching of

M1 transitions can be seen in the example of ^{14}N , Figure 15.2, where we can look at the dipole transitions without changing parity (branching ratios of the transitions from the states 6.20 MeV and, especially, 3.95 MeV).

The isospin invariance holds only approximately being violated mainly by the Coulomb interaction. There are also small isospin-nonconserving nuclear forces apparently generated by the electromagnetic effects on the quark level. Therefore, the isospin selection rules are only approximate. In average, the isospin impurity is expected to increase at high excitation energies because any state mixing becomes stronger in the region of the dense spectrum. However, this statement is also not absolute; there are highly excited states with very pure isospin. The continuum effects also help in keeping isospin invariance because the quasistationary states can decay before any mixing with the states of other isospin takes place.

15.5 Structural Selection Rules

Selection rules of different nature are related to structure of nuclear wave functions. In our approximation, all multipole moments are *one-body* operators. Each term in these operators can change an orbit of not more than one particle; in secondary quantization, the operators are of the type $a_{\lambda}^{\dagger}a_{\lambda}$. Take two shell-model configurations that differ by the orbits of two or larger number of particles. Such configurations cannot be connected by any multipole transition unless we include new *many-body* terms in the electromagnetic current. With a one-body current, the de-excitation path in this case would consist of several steps each of them changing the configuration by one transfer operator $a^{\dagger}a$. Here, we can say that a structural selection rule does not permit single-step transitions.

With pairing taken into account, the classification of states changes. The particles and holes are mixed and it is more convenient to speak in terms of quasiparticles. The multipole operators, as any one-body operators, can create or annihilate pairs of quasiparticles (13.126), (13.127) as well as transfer a quasiparticle to another orbit (13.124), (13.125). The magnitudes of the matrix elements are usually suppressed by the coherence factors, sometimes significantly (all of them ≤ 1). This is related to the smeared distribution function with partial occupancies of the single-particle orbits. But the selection rules still exist since the transitions are possible only with the change of seniority $\Delta s = 0$ or $\Delta s = 2$. As mentioned earlier (Section 13.4), a good example of this is the second 2^+_2 $s = 4$ state in ^{52}Cr , whose decay to the $s = 0$ ground state 0^+ is strongly hindered.

In reality, the situation is more complicated. Residual interactions outside of independent particle shell model mix configurations. The stationary states are superpositions of the configurations with different numbers of particles and holes with respect to the unperturbed Fermi surface (or different seniorities in the pairing classification). Among these superpositions, there are *coherent* combinations that lead to the enhancement of transitions as was discussed earlier. But the number of such collective states is small. The remaining states being orthogonal to collective ones, as a rule, are built as incoherent superpositions of shell-model configurations. We can apply the ideas of statistical estimates (15.17) – (15.23) used for collective states to this case as well.

Consider a stationary state $|\Psi\rangle$ given by a superposition (15.17) with N principal components. This number rapidly grows with excitation energy reaching $10^4 \div 10^6$ for the states near continuum threshold (excitation energy $6 \div 8$ MeV). Again a typical magnitude of the coefficients in the superposition is $\overline{|C_k|^2} \simeq 1/\sqrt{N}$. For the transition

from such a state to a simple low-lying, for example ground, state we again use Eq. (15.21). Now, however, the majority of matrix elements \mathcal{M}_k vanish because of structural selection rules. To have a nonvanishing contribution to the matrix element $\langle 0 | \dots | \Psi \rangle$, the contributing configuration $|k\rangle$ should have only one particle–hole pair in a different position compared to the state $|0\rangle$. Moreover, this pair should have a nonzero probability of possessing correct quantum numbers ($\lambda\lambda'$) while in general the complicated state $|\Psi\rangle$ includes particle–hole pairs in all possible states under the only condition that together they are coupled to the correct value of the total angular momentum. The number n of possible “proper” pairs is practically small compared to N , and one can only overestimate it by writing $n \simeq A^{2/3}$ (a combination of any j level in the major shell with any other).

Applying such estimates to Eq. (15.21), we obtain for the resulting matrix element of the multipole operator between a simple state and a very complicated excited state

$$\langle 0 | \mathcal{M} | \Psi \rangle \simeq \frac{n}{\sqrt{N}} \overline{\mathcal{M}}. \quad (15.31)$$

The old result (15.22) for the coherent superposition corresponds to $n \simeq N$. Thus, as excitation energy and complexity of states grow, the typical multipole matrix elements for de-excitation to a simple state decrease $\propto N^{-1/2}$ (the so-called *N-scaling*). This does not mean that the lifetime of highly excited states becomes longer and longer. Quenching of matrix elements for individual transitions is compensated by the abundance of available final states that increases along with N . Instead of being concentrated on a single final state, the transition strength is now *fragmented* – spread over many of them.

This scenario of increasing complexity is of very general nature and applied to nearly all quantum many-body systems. Specific structural selection rules may work for some sequences of states, *bands*. In this case, we have an organized chain of states connected by strong transitions of a preferred multipolarity. Interband transitions are usually suppressed compared to intraband transitions.

The simple example of such type is given by the low-lying vibrational modes. Similar to the coordinate of the one-dimensional oscillator, the multipole operator (15.24) of the vibrational mode creates and annihilates vibrational quanta. We have a selection rule for the phonon number $\Delta n = \pm 1$ analogous to the photon selection rules in gamma-radiation and photoabsorption. It is strictly valid in the harmonic approximation for vibrations if the multipole moments (15.24) are linear in phonon operators. The multipolarity of transitions coincides here with the angular momentum L of a phonon. For a collective state, the transition probability is much greater than single-particle estimates.

There are specific predictions that follow from the phonon selection rules. Consider states with two quadrupole ($L = 2$) phonons, Problems 6.4 and 6.5; for other multipoles, the results are quite similar. Since the total wave function has to be symmetric under permutations of identical bosons, only three values of the total angular momentum are allowed, $J = 0, 2, 4$. Due to the phonon selection rule, the two-phonon states can decay only to the one-phonon state that has the angular momentum $J = L = 2$ (usual notation 2_1^+). For the two-phonon states with $J = 0$ and $J = 4$, this is the only possibility allowed for the quadrupole transitions by the ordinary selection rules for angular momentum. But the state $J = 2$ usually designated as 2_2^+ can have a nonzero quadrupole transition to the ground state $J = 0$. This *crossover* transition, Figure 15.3, is forbidden

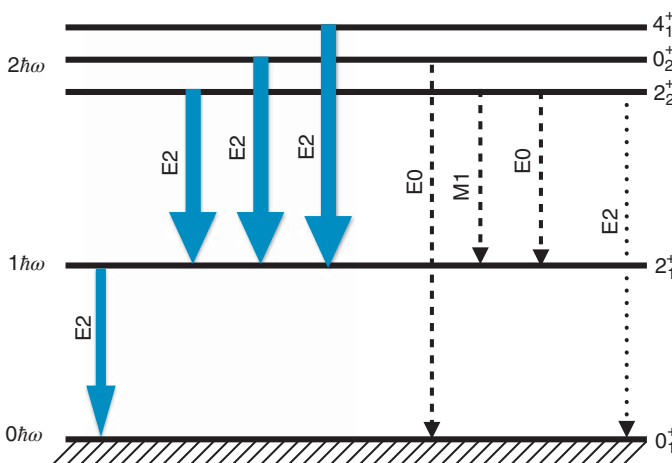


Figure 15.3 Typical level scheme for a low-lying quadrupole vibrational mode. Solid lines show collective enhanced transitions; dashed lines refer to some of the possible noncollective transitions. The E2 transition to the most right, labeled by dotted arrow, is a noncollective crossover transition.

only by the phonon selection rule. Since the harmonic approximation is not good in many cases and phonon selection rules are not exact, the crossover transition is allowed due to *anharmonicity* but it is always by one to two orders of magnitude weaker than the normal phonon transition $2_2^+ \rightarrow 2_1^+$. Here we refer to the reduced E2 probabilities extracted from empirical transition rates by dividing the energy factor ω^5 out.

The geometrical selection rules also allow M1 transitions between the 2_2^+ and 2_1^+ phonon states. Such transitions exist but they do not reveal collective enhancement. The simplest 1^+ operator in the quadrupole phonon model is the phonon angular momentum, which is not related to transitions. Again, we have to include higher order terms to explain M1 transitions between the phonon states. Finally, we can mention that E0 conversion transitions (next section) are also allowed between the states with the same angular momentum.

The brightest example of band-like transitions is provided by the *rotational* states as it is known from molecular physics as well. Rotational bands will be discussed separately.

Remarkable structural selection rules appear if different mean-field shapes can *coexist* in the same nucleus in the same energy range. One can construct independent particle models based on each configuration. Populating one of such states, one can observe de-excitation processes of two types, within the same class of states or between the classes. The latter transitions have to be hindered. Indeed, the Slater determinants built on different bases are nonorthogonal, but their overlap is small. It is a product of A single-particle overlaps (more precisely, a determinant of the overlap matrix, Problem 11.4) and each overlap gives a factor less than 1. The probability amplitude of inducing the transition between such different states with the aid of a one-body operator is very low. In some sense, the situation is not much different from what we have discussed in relation to transitions between simple and complicated states. In the shell-model basis constructed on one of the shapes, its own Slater determinant is a simple state while the simple determinant of orbits adjusted to another shape is extremely complicated in the first basis; the complexity of states has only *relative* meaning.

A strong hindrance of gamma-transitions to the states of different shape makes a nucleus to look for another way of de-excitation. In actinides, several *fissioning shape isomers* are known. They are strongly deformed and prefer to undergo spontaneous fission, usually a very slow process, rather than to return by radiation to a potential well corresponding to normal deformation.

15.6 Monopole Transitions

As the 0–0 transitions with emission of a single photon are strictly forbidden by helicity conservation, a nucleus in an excited state with spin $J_i = 0$ has to find either another mechanism of de-excitation to $J_f = 0$ or a partner with $J_f \neq 0$ as a final state.

One option is provided by the Hamiltonian (14.32). Until now, we did not take into account the term quadratic in the vector potential,

$$H'' = \sum_a \frac{e_a^2}{2m_a c^2} \mathbf{A}^2(\mathbf{r}_a). \quad (15.32)$$

For a static external magnetic field $\mathbf{B} = [\nabla \times \mathbf{A}]$, this term adds positive energy $\propto \mathbf{B}^2$, which is equivalent to the diamagnetic effect. If \mathbf{A} in (15.32) is the quantized radiation field (14.30), this term induces *two-photon* processes, radiation $\sim a_{\mathbf{k}}^\dagger a_{\mathbf{k}'}^\dagger$, and absorption $\sim a_{\mathbf{k}} a_{\mathbf{k}'}$. The total helicity of two emitted photons can be equal to zero, which opens the possibility of 0–0 transitions. But the two-photon processes are allowed also in the second order of perturbation theory for a linear term in the Hamiltonian.

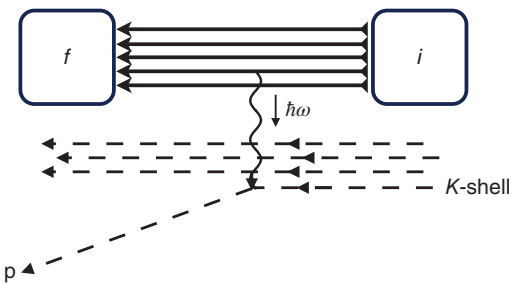
The two-photon radiation is known to be important for the transition $2s_{1/2} \rightarrow 1s_{1/2}$ in a hydrogen atom because the competing process of the single-photon M1 radiation is in fact caused by the spin flip of the electron that does not act on the orbital degrees of freedom and is therefore strongly suppressed by the orthogonality of the radial wave functions. The M1 radiation occurs only via small relativistic effects; it would give the lifetime 2×10^5 s for the $2s_{1/2}$ level. The two-photon radiation as the second-order process also has a low transition rate; however, in reality, this is the process that determines the lifetime of $2s_{1/2}$ hydrogen level equal to 0.15 s.

Other options for nuclear 0–0 transitions utilize *virtual* photons which being emitted by a nucleus transform into the excitation of atomic electrons or of the electron–positron vacuum. In the second case, a virtual photon creates an electron–positron pair, which is possible only if $\hbar\omega > 2m_e c^2$. In the first case, it is sufficient to have the nuclear excitation energy greater than the atomic ionization potential to knock out an atomic electron from the atom. This process is called *internal conversion* (Figure 15.4). It can occur in any (not necessarily 0–0) nuclear transition competing with the real photon emission. The energy transfer from a nucleus to atomic electrons does not require a real transversely polarized photon (this case is sometimes called internal photoeffect) and can be accomplished by Coulomb interaction. Therefore, the ban on 0–0 transitions is lifted.

Here we discuss the main features of the internal conversion acting through the Coulomb interaction between an electron (coordinate \mathbf{r}) and protons in the nucleus (coordinates \mathbf{r}_a)

$$H_C = \sum_a \frac{ee_a}{|\mathbf{r} - \mathbf{r}_a|}. \quad (15.33)$$

Figure 15.4 Internal electron conversion, nucleons are drawn by solid lines, atomic electrons by dashed lines; wavy line corresponds to interaction (exchange by a virtual quantum).



This approximation is good for not very large transition energies $E_i - E_f = \hbar\omega$ as we neglect retardation effects that is justified for wavelengths greater than the radius of the lowest atomic orbits (K -shell with $\ell = 0$).

The *monopole*, E0, transitions are generated by the part of the Coulomb interaction related to the finite nuclear size. Consider (15.33) as an operator acting on both nuclear and electron variables,

$$U(\mathbf{r}) = e \int d^3 r' \frac{\rho_{ch}(\mathbf{r}')}{|\mathbf{r} - \mathbf{r}'|}. \quad (15.34)$$

Here the nuclear charge density ρ_{ch} performs the nuclear transitions, whereas the coordinate \mathbf{r} and the charge e belong to the atomic electron. We can carry out the Fourier transformation to the operator ρ_{ch} of nuclear charge density using the Fourier transform of the Coulomb potential,

$$U(\mathbf{r}) = 4\pi e \int \frac{d^3 q}{(2\pi)^3} \frac{e^{-i(\mathbf{q} \cdot \mathbf{r})}}{q^2} \rho_q^{ch}. \quad (15.35)$$

For each nuclear transition $i \rightarrow f$, we have the effective electron perturbation

$$U_{fi}(\mathbf{r}) = 4\pi e \int \frac{d^3 q}{(2\pi)^3} \frac{e^{-i(\mathbf{q} \cdot \mathbf{r})}}{q^2} (\rho_q^{ch})_{fi}. \quad (15.36)$$

We are interested in the *long wavelength limit* when the essential Fourier components are small, $qR \ll 1$. The behavior of ρ_q^{ch} at small q is known, compare the expansion of the form-factor,

$$\rho_q^{ch} = \int d^3 r e^{i(\mathbf{q} \cdot \mathbf{r})} \rho_{ch}(\mathbf{r}) = \int d^3 r \left(1 + i(\mathbf{q} \cdot \mathbf{r}) - \frac{1}{2}(\mathbf{q} \cdot \mathbf{r})^2 + \dots \right) \rho_{ch}(\mathbf{r}). \quad (15.37)$$

The first term is equal to the total charge Ze and does not generate transitions, the second term can generate electric dipole transitions. The third term contains both the quadrupole and the monopole component as

$$(\mathbf{q} \cdot \mathbf{r})^2 = q_i q_j \left(r_i r_j - \frac{1}{3} \delta_{ij} r^2 \right) + \frac{1}{3} q^2 r^2. \quad (15.38)$$

Note that here the operator \mathbf{r} enters via its longitudinal component with respect to the momentum of the virtual quantum. We obtained from the last term in (15.38) the E0 operator responsible for the monopole transitions,

$$-\frac{1}{6} q^2 \int d^3 r r^2 \rho_{ch}(\mathbf{r}) = -\frac{1}{6} q^2 \sum_a e_a r_a^2 \equiv -\frac{1}{6} (\widehat{E0}) q^2, \quad (15.39)$$

as an analog of the mean-square charge radius but for transitions rather than for a static expectation value. It has desired selection rules $\Delta J = 0$, parity does not change. In particular, 0–0 transitions can be accomplished in this way.

The effective operator for the electron excitation accompanying the nuclear transition is

$$U_{fi}(\mathbf{r}) = 4\pi e \int \frac{d^3q}{(2\pi)^3} \frac{e^{-i(\mathbf{q}\cdot\mathbf{r})}}{q^2} \left(-\frac{1}{6} (\hat{E0})_{fi} q^2 \right) = -\frac{2}{3} \pi e \delta(\mathbf{r}) (\hat{E0})_{fi}. \quad (15.40)$$

Thus, this perturbation is felt only by the electron wave function in the nuclear interior, literally speaking at the origin; this singles out *s*-wave electronic orbitals.

This operator treated as a perturbation can excite an atomic electron to the continuum. Using the Born formula and neglecting the electron interaction with the atom in the final state (all approximations are discussed in the next section), we can take the final state as a plane wave. Simple algebra gives for the monopole conversion probability integrated over electron angles,

$$w_{fi}(E0) = \frac{8\pi}{9} \frac{m_e e^2 p}{\hbar^4} |\psi(0)|^2 (\hat{E0})_{fi}^2 \quad (15.41)$$

Here the final electron momentum p is defined by the energy conservation and $\psi(0)$ is the initial electron wave function at the origin. Only the *s*-states have a noticeable probability to emit an electron; the probability rapidly falls off with an increase in radial quantum number. The *K*-shell conversion is the most probable although *s*-states of the next atomic shells, *L* and *M*, still can supply conversion electrons.

15.7 Internal Electron Conversion

With the interaction (15.33), only the internal conversion of electric multipole radiation is possible. Retardation effects and magnetic interaction make possible the internal conversion of magnetic multipole radiation as well. But it requires taking into account relativistic spin–orbit interaction in atomic wave functions. Otherwise, the electron spin is decoupled and the ML transition, by the angular momentum conservation, changes the electron orbital momentum from 0 at the *K*-shell to *L*. Electron parity becomes $(-)^L$, whereas it should be opposite for the ML transition.

Let us consider (electric) transitions of multipolarities $L > 0$ that allow a comparison with radiative transitions. In contrast to E0 transitions, where the electron probes the nuclear volume, here the main events take place outside of the nucleus. The standard multipole expansion of the electrostatic potential in the region outside the nucleus gives

$$H_C = \sum_{LM} \frac{4\pi e}{2L+1} \frac{1}{r^{L+1}} Y_{LM}^*(\mathbf{n}) \mathcal{M}(EL, M) \quad (15.42)$$

where $\mathbf{n} = \mathbf{r}/r$. The monopole, $L = M = 0$, term of (15.42) creates a normal spherical Coulomb field binding the electrons. The higher terms induce the synchronized transitions in the nucleus and in the atomic shells (Figure 15.4). For a nuclear transition $i \rightarrow f$, the matrix element over nuclear wave functions is the same as that determining the radiation probability (14.94).

Let us estimate the probability of internal conversion with the *K*-electron (initial energy e_0) emitted into continuum (a final state $|e\rangle$ with energy ϵ). Having two electrons

on the K -orbit in a heavy atom (this is equivalent to summation over electron spin states) and using the golden rule, we obtain for the EL transition

$$\begin{aligned} dw_{fi} &= 2 \frac{2\pi}{\hbar} |(H_C)_{fi}|^2 \delta(\epsilon - \epsilon_0 - E_{if}) d\rho_e d\epsilon \\ &= \frac{4\pi}{\hbar} \left(\frac{4\pi e}{2L+1} \right)^2 \left| \sum_M \left(e \left| \frac{1}{r^{L+1}} Y_{LM}^* \right| K \right) (\mathcal{M}(\text{EL}, M))_{fi} \right|^2 d\rho_e. \end{aligned} \quad (15.43)$$

For the sake of simplicity, we neglect the electron interaction with the atom in the final state taking the state $|e\rangle$ as a plane wave with the momentum $\hbar\mathbf{q}$. The magnitude q is determined by the energy conservation and we need to include the corresponding level density in the continuum. For the nonrelativistic electron (this approximation works only if $E_{if} = \hbar\omega \ll m_e c^2$), it is $d\rho_e = V m_e \hbar q d\omega / (2\pi\hbar)^3$.

The K -orbit wave function does not depend on angles,

$$\psi_K = \frac{1}{\sqrt{\pi a_0^3}} e^{-r/a_0}, \quad (15.44)$$

where the orbit radius for the nucleus of charge Z is

$$a_0 = \frac{a_B}{Z} = \frac{\hbar^2}{m_e e^2 Z}. \quad (15.45)$$

The angular integral in the electron matrix element in (15.44) picks up the partial wave with quantum numbers (LM) from the expansion of $\exp[-i(\mathbf{q} \cdot \mathbf{r})]$. This reflects the transfer of the angular momentum L from the nucleus to the electron. After the angular integration, we obtain

$$\left(e \left| \frac{1}{r^{L+1}} Y_{LM}^* \right| K \right) = (-i)^L 4 \sqrt{\frac{\pi}{V a_0^3}} Y_{LM}^*(\mathbf{q}) \int \frac{dr}{r^{L-1}} j_L(qr) e^{-r/a_0}. \quad (15.46)$$

Under our conditions, the electron wavelength $\sim 1/q$ is small compared to the atomic radius (15.44), $qa_0 > 1$. Moreover, we consider $qa_0 > L$ because we are mostly interested in low multipolarities. Then the function $j_L(qr)$ suppresses the integrand before we reach the atomic boundary $r \sim a_0$. Therefore, the exponent can be substituted by unity, and the integral reduces to

$$\int_0^\infty \frac{dr}{r^{L-1}} j_L(qr) = q^{L-2} \int_0^\infty \frac{dx}{x^{L-1}} j_L(x) = \frac{q^{L-2}}{(2L-1)!!}. \quad (15.47)$$

Now we substitute (15.46) and (15.47), along with the final electron density of states, into (15.43), sum over projections M_f of the nuclear final state and integrate the product of spherical functions $\int d\Omega_{\mathbf{q}} Y_{LM}^*(\mathbf{q}) Y_{LM'}(\mathbf{q}) = \delta_{MM'} \delta_{LL'}$ over the angles of \mathbf{q} . The result is the total probability of the internal conversion for a given nuclear multipole transition,

$$w_{\text{conv}}(\text{EL}; fi) = 128\pi \frac{m_e e^2}{\hbar^3 a_0^3} \frac{q^{2L-3}}{[(2L+1)!!]^2} \sum_{M_f M} |(\mathcal{M}(\text{EL}, M))_{fi}|^2. \quad (15.48)$$

The radiation probability for the same nuclear transition is given by Eq. (14.87), where one needs to sum over the projections M_f . It allows one to find the *conversion coefficient* for the K -shell

$$\alpha_K(\text{EL}) = \frac{w_{\text{conv}}(\text{EL}; fi)}{w_{\text{rad}}(\text{EL}; fi)}. \quad (15.49)$$

In the ratio, information on nuclear matrix elements cancels out. In our approximation, the electron kinetic energy is large compared to its binding energy, $\hbar\omega \approx \hbar^2 q^2 / 2m$, so that the result can be written as

$$\alpha_K(\text{EL}) = \frac{16L}{L+1} \frac{m_e e^2}{\hbar^2 a_0^3} \frac{q^{2L-3}}{k^{2L+1}} = \frac{L}{L+1} Z^3 \alpha^4 \left(\frac{2m_e c^2}{\hbar\omega} \right)^{L+5/2}. \quad (15.50)$$

In the right-hand side, α stands for the fine structure constant. The internal conversion coefficients strongly increase with the nuclear charge and multipolarity of the transition; they prefer low-frequency transitions.

The result (15.50) is derived under many simplifying assumptions. It is easy to see that they are mutually consistent but restrict the domain of validity of (15.50).

- i) The initial atomic wave function was considered in the nonrelativistic approximation, $v_e/c \sim Z\alpha \ll 1$. This does not permit to use the results for large Z .
- ii) The emitted electron is nonrelativistic, $\hbar^2 q^2 < m_e c^2$; this leaves us with low-energy nuclear excitations only.
- iii) $\hbar\omega < m_e c^2 \approx 500 \text{ keV}$.
- iv) A stronger limitation comes from using the nonretarded interaction, $(2\pi c/\omega) > a_0$. It leads to $\hbar\omega < 2\pi Z a_0 m_e c^2 \approx Z \times 25 \text{ keV}$. This practically excludes small Z because of absence of nuclear excitations at such low energy.
- v) We neglected the electron binding energy and its Coulomb interaction in the final state that is justified for $\hbar\omega > (m_e e^4 Z^2 / 2\hbar^2) = Z^2 \times 13.6 \text{ eV}$. For $Z \approx 50$, this limits nuclear excitation energies from below, $\hbar\omega > 35 \text{ keV}$.
- vi) The approximation $qa_0 > 1$ in computing the integral (15.46) is valid if (iv) is fulfilled.

All these approximations can be lifted. The internal conversion coefficients for various atomic shells are calculated and tabulated [3, 4] using relativistic electron wave functions and taking into account the finite nuclear size (recall that the expansion (15.42) can be used only outside the nucleus). The relative magnitudes of the conversion coefficients for different shells turn out to be rather sensitive to the multipolarity of the nuclear transition; their measurement helps establish this multipolarity.

15.8 Coulomb Excitation

Electromagnetic excitation of a nucleus by the field of another nucleus is a powerful tool for studying nuclear structure, especially excited collective states. It is a unique method for studying short-lived isotopes in the experiments with inverse kinematics (scattering of a fast radioactive projectile by a heavy nuclear target that serves as a source of the Coulomb field). In a collision of two nuclei with a large impact parameter there is no overlap of nuclear densities, and short-range nuclear forces are not efficient. To avoid a violent nuclear collision, the impact parameter should be larger than the sum of nuclear radii $R_1 + R_2$.

We discuss shortly the nonrelativistic problem although currently major experimental efforts are applied to physics of relativistic nuclear collisions in order to study nuclear matter at high density. In contrast to that, in Coulomb excitation, we assume that nuclei perturb each other only through long-range electromagnetic interactions. Let v be the

relative velocity of two nuclei at infinity that determines the energy of relative motion $E = mv^2/2$, where m is the reduced mass. The strength of Coulomb interaction can be measured by the parameter

$$\eta = \frac{Z_1 Z_2 e^2}{\hbar v} = Z_1 Z_2 \alpha \frac{c}{v}, \quad (15.51)$$

where $Z_{1,2}$ are charges of the nuclei. For $Z_1 Z_2 > 137$, the parameter (15.51) $\eta > 1$ and can easily be $\eta \gg 1$. This means that the Coulomb interaction is effectively strong and cannot be accounted for by perturbation theory.

This situation allows for the use of the semiclassical approximation when the Coulomb interaction is taken into account exactly in determining the classical Rutherford trajectory of relative motion $\mathbf{R}(t)$, where \mathbf{R} is the distance between the centers of the colliding nuclei (Figure 15.5). The relative energy E is assumed to be large enough to allow one to neglect the feedback from the intrinsic excitations to relative motion. Then the trajectory is fixed by energy and impact parameter or deflection angle. The classical distance of closest approach,

$$R_0 = 2Z_1 Z_2 e^2 / mv^2, \quad (15.52)$$

is larger than $R_1 + R_2$ at relative energy lower than the Coulomb barrier

$$E_B = \frac{Z_1 Z_2 e^2}{R_1 + R_2}. \quad (15.53)$$

The excitation is generated by the time-dependent field and the probability of the process is determined by the presence in this field of Fourier harmonics with the excitation frequencies $\omega = (E_f - E_i)/\hbar$. If motion is too slow, the field acts adiabatically, the intrinsic wave function is changing reversibly and the probability of excitation is low. The corresponding *adiabaticity parameter* is the ratio ξ of timescales for the Coulomb collision, $\sim R_0/v$, and for the nuclear excitation, $\sim 1/\omega$. At $\xi = R_0\omega/v > 1$, the situation is adiabatic and transition probabilities are small.

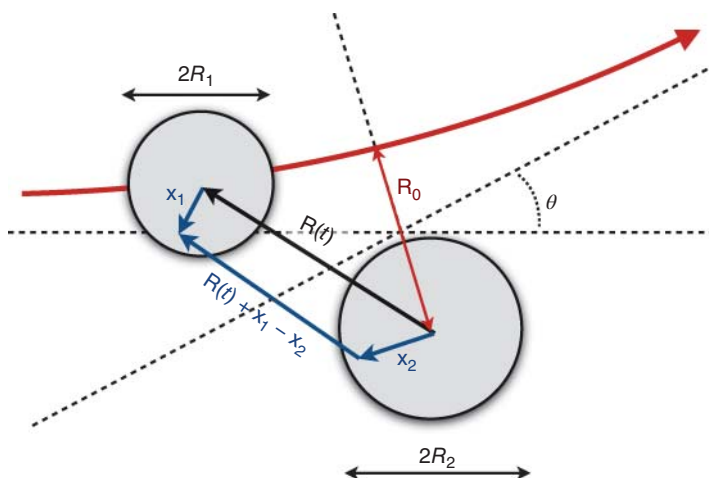


Figure 15.5 Classical Coulomb trajectory $\mathbf{R}(t)$ for a nucleus–nucleus collision.

The interaction Hamiltonian responsible for the excitation processes in the nonrelativistic case can be written as

$$H' = \int d^3x_1 d^3x_2 \frac{\rho_1^{\text{ch}}(\mathbf{x}_1)\rho_2^{\text{ch}}(\mathbf{x}_2)}{|\mathbf{R}(t) + \mathbf{x}_1 - \mathbf{x}_2|} - \frac{Z_1 Z_2 e^2}{R(t)}, \quad (15.54)$$

where charge densities of unperturbed nuclei depend on the distances from the corresponding centers of each nucleus $\mathbf{x}_{1,2}$ (see Figure 15.5). We subtracted the interaction between nuclei as a whole that determines the trajectory $\mathbf{R}(t)$ but does not contribute to intrinsic excitations. Next, we carry out the multipole expansion as in (15.42) for a large distance between the centers, $R \gg x_{1,2}$,

$$H' = \int d^3x_1 d^3x_2 \rho_1^{\text{ch}}(\mathbf{x}_1)\rho_2^{\text{ch}}(\mathbf{x}_2) \sum_{L>0,M} \frac{4\pi}{2L+1} \frac{x_{12}^L}{R^{L+1}(t)} Y_{LM}(\mathbf{x}_{12})Y_{LM}^*(\mathbf{R}). \quad (15.55)$$

Here $\mathbf{x}_{12} \equiv \mathbf{x}_2 - \mathbf{x}_1$.

This Hamiltonian is rather complicated due to the correlations associated with the mutual excitation of the nuclei. It becomes much simpler if we are interested in the excitation of one of the partners only. Let the “projectile” 2 (or the target at inverse kinematics) be not excited; we also neglect effects related to its structure as an extended object. Then the field of the nucleus 2 is the same as if this would be a point charge, $\rho_2^{\text{ch}}(\mathbf{x}_2) \approx Z_2 e \delta(\mathbf{x}_2)$, and the Hamiltonian is expressed in terms of the electric multipole moments (14.94) of the “target” 1,

$$H' = Z_2 e \sum_{L>0,M} \frac{4\pi}{2L+1} \frac{1}{R^{L+1}(t)} Y_{LM}^*(\mathbf{R}(t)) \mathcal{M}(\text{EL}, M). \quad (15.56)$$

The Hamiltonian (15.56) is time dependent as the trajectory of relative motion is considered as a given function of time. Then we have to repeat our derivation of the transition rate from Chapter 14. Now the transition amplitude $i \rightarrow f$ with the excitation by $\hbar\omega = E_f - E_i$ is the Fourier component for the transition frequency of the interaction Hamiltonian taken along the unperturbed trajectory,

$$S_{fi} = -\frac{i}{\hbar} \int_{-\infty}^{\infty} dt H'_{fi}(t) e^{i\omega t}. \quad (15.57)$$

For the unpolarized initial nuclei and with no final polarization registered, the transition rate is to be averaged over the initial spin projections and summed over the final projections of the target,

$$w_{fi} = \frac{1}{2J_i + 1} \sum_{M_f M_i} |S_{fi}|^2; \quad (15.58)$$

the polarization state of the projectile is supposed to be unchanged.

The trajectory enters the result via the time integral

$$I_{LM}(\omega) = \int_{-\infty}^{\infty} dt \frac{1}{R^{L+1}(t)} Y_{LM}(\mathbf{R}(t)) e^{i\omega t}. \quad (15.59)$$

This Fourier component becomes small, $\propto \exp(-\text{const} \cdot \xi)$, if the trajectory changes too slowly as compared to the needed transition frequency and the adiabaticity parameter $\xi > 1$.

The intrinsic matrix elements of multipole moments appear in the transition rate (15.58) in sums over magnetic quantum numbers

$$\Sigma_{LM,L'M'} = \frac{1}{2J_i + 1} \sum_{M_f M_i} (\mathcal{M}(EL, M))_{fi} (\mathcal{M}(EL', M'))_{fi}^*. \quad (15.60)$$

Each matrix element is proportional to the corresponding CGC, the summation selects $L' = L, M' = M$, and the result does not depend on M . Then it is the same as the reduced probability (14.96),

$$\begin{aligned} \Sigma_{LM,L'M'} &= \frac{1}{2J_i + 1} \sum_{M_f M_i} |(\mathcal{M}(EL, M))_{fi}|^2 \delta_{LL'} \delta_{MM'} \\ &= \frac{B(EL; i \rightarrow f)}{2L + 1} \delta_{LL'} \delta_{MM'}. \end{aligned} \quad (15.61)$$

Coulomb excitation is especially useful for studying collective states with enhanced reduced probabilities. The total excitation probability is

$$w_{fi} = \left(\frac{4\pi Z_2 e}{\hbar} \right)^2 \sum_{L>0} \frac{B(EL; i \rightarrow f)}{(2L + 1)^3} \sum_M |I_{LM}(\omega_{fi})|^2. \quad (15.62)$$

From the projectile viewpoint, the process is inelastic scattering. The Coulomb trajectory defines the deflection angle θ and the Rutherford cross section that, in terms of the closest approach distance (15.52), is

$$d\sigma_R = \left(\frac{R_0}{4\sin^2(\theta/2)} \right)^2 d\Omega. \quad (15.63)$$

In our approximation, the trajectory is not influenced by the target excitation so that the inelastic cross section is factorized into the product of the Rutherford cross section (15.63) and the excitation probability (15.62),

$$d\sigma_{fi} = d\sigma_R w_{fi} = \sum_{L>0} d\sigma_{fi}(EL), \quad (15.64)$$

where the cross section for the excitation of multipolarity L is equal to

$$\frac{d\sigma_{fi}(EL)}{d\Omega} = \left(\frac{\pi Z_2 e R_0}{\hbar \sin^2(\theta/2)} \right)^2 \frac{B(EL; i \rightarrow f)}{(2L + 1)^3} \sum_M |I_{LM}(\omega_{fi})|^2. \quad (15.65)$$

We can make a crude estimate of the cross section for Coulomb excitation. The trajectory integral (15.59), after changing the variable to $dR = vdt$, gives the dimensional factor R^{-L}/v . It has to be taken near the closest approach point (15.52) that is the most effective for excitation. The constants from the Rutherford cross section can be combined into the Coulomb parameter (15.51). As a result,

$$\sigma(EL) \simeq \eta^2 \frac{B(EL)}{R_0^{2L-2}} f_L(\xi), \quad (15.66)$$

where the function $f_L(\xi)$ smoothly depends on L but contains the exponential cut-off at large values of the adiabaticity parameter ξ . We remember, Eq. (14.99), that in photoabsorption each consecutive multipole was suppressed by a factor $(kR)^2$. The situation for

exciting higher multipoles is easier in the Coulomb excitation because here

$$\frac{\sigma(\text{EL+1})}{\sigma(\text{EL})} \sim \frac{B(\text{EL+1})}{B(\text{EL})R_0^2} \sim \left(\frac{R}{R_0}\right)^2. \quad (15.67)$$

This ratio is significantly larger than $(kR)^2$.

This theory can be extended to consider quantum scattering instead of classical trajectories, use relativistic kinematics, take into account magnetic multipoles that become equally important for relativistic velocities, and include higher order processes of sequential excitation of nuclear states. The last generalization is necessary for excitation of rotational bands and overtones of giant resonances (quantum states with several vibrational quanta). The mutual excitation of the projectile and of the target can be studied as well. The fundamental review paper [5] contains a lot of information on the subject and does not look obsolete even now, 60 years after its publication.

15.9 Nuclear Photoeffect

When the absorbed photon frequency becomes greater than the lowest threshold of nuclear decay, the nucleus is excited to the continuum states. Those states decay either again emitting a photon or through particle emission or more complicated nuclear processes, such as fission. The same reactions are also possible after the nucleus absorbed a virtual photon in Coulomb excitation, see the previous section, or in electron scattering. If the photon is reemitted we speak about *photon scattering* that can be elastic, with the frequency of the final photon equal to that of the initial one, or inelastic when the final photon has lower energy, and the final nucleus is still in an excited state. Here we briefly discuss the process with the photon absorption resulting in the particle decay into continuum. This is a nuclear analog of the atomic *photoeffect*.

The energy conservation in the photoeffect case takes a form

$$E_i + \hbar\omega = E_f + \epsilon, \quad (15.68)$$

where the nucleus A makes the transition between the initial, usually ground, state with energy E_i to the final state of the nucleus $A - 1$ with energy E_f , and the particle in the continuum has energy $\epsilon = \mathbf{p}^2/2m$. If the initial nucleus is stable, the *separation energy* $E_f^{\min} - E_i > 0$ determines the threshold value (the analog of the ionization potential in atoms), and the reaction is allowed only if the photon frequency exceeds this value,

$$\hbar\omega_{\text{th}} = E_f^{\min} - E_i. \quad (15.69)$$

The main features of the photoeffect are connected to the fact that the process would be impossible if the nucleon was not bounded in the initial nucleus. For the photon absorption by a *free* particle, the energy and momentum conservation rules cannot be fulfilled.

Problem 15.3 Prove the last statement.

Solution

Using the relativistic units $\hbar = c = 1$, we can write a 4-momentum conservation law for this case as $p + k = p'$ with p, p' and k being 4-momentum vectors of the initial particle,

final particle, and the photon, respectively. The 4-square of this equation gives $(p \cdot k) = 0$ as $p^2 = p'^2 = m^2$ and $k^2 = 0$. In the rest frame of the particle, the invariant $(p \cdot k) = m\omega$ can vanish only if ω , and, consequently the momentum of the photon, vanishes. Therefore, the only way to satisfy the conservation law is to take $k = 0$.

Thus, the photon absorption is possible only for a *bound* particle when the third body, the residual nucleus in this case, accepts the leftover momentum. Then it is qualitatively clear that the probability of the photoabsorption should grow for tightly bound particles, if of course photon energy exceeds threshold (15.69). It is well known that in atoms [QP, II, 5.8], the photoeffect cross section (knock-out of an electron) is steeply rising when $\hbar\omega$ reaches the ionization threshold of the next atomic shell (M, L, K) but then decreases as the frequency increases further because the relative boundness of the electron is getting lower. After the so-called *red photoeffect edge* ($\hbar\omega$ equal to the ionization energy from the deepest K -shell), the cross section is decreasing monotonously, $\sigma \sim \omega^{-7/2}$; in the relativistic domain, $\hbar\omega \gg m_e c^2$, the drop becomes slower, $\sigma \sim \omega^{-1}$. By the same reason, the atomic photoeffect cross section is strongly, $\sim Z^5$, increasing with the nuclear charge that makes the electron more bound.

In contrast to the excitation of the discrete states that reveals the resonance dependence on photon energy, in the photoeffect we expect a more smooth dependence. Using our result in Section 15.7 for the final state in the continuum, we have to take into account the level density ρ_f of the emitted particle with the momentum \mathbf{p} in the solid angle element do ,

$$\rho_f = \frac{Vmp}{(2\pi\hbar)^3} do. \quad (15.70)$$

Then the differential photoeffect cross section is given by

$$d\sigma_{fi} = \frac{4\pi^2\hbar}{E_\gamma c} \left| \sum_a \frac{\mathbf{e}_a}{m_a} \langle f | (\mathbf{p}_a \cdot \mathbf{e}_{k\lambda}) e^{i(\mathbf{k} \cdot \mathbf{r}_a)} | i \rangle \right|^2 \rho_f. \quad (15.71)$$

Here the result is determined by the many-body structure of the initial and final states. In the final state, a particle in the continuum still interacts with the residual nucleus. Only the orbital current is taken into account in the photoabsorption matrix element in (15.71); the spin current can be added in a similar way if necessary.

As an important example, we can mention the deuteron electromagnetic break-up [6] at low energy of the photon. The general expression (15.71) can be presented as a sum of processes of different multipolarities. The simplest component corresponds to the electric dipole (E1) transition from the deuteron bound state into the state of continuum motion of the proton and the neutron with the reduced mass $m/2$. In the long wavelength limit, we set the exponential factor in the matrix element equal to 1 and express the matrix element of the relative momentum through the corresponding matrix element of the relative coordinate as in (14.52). As a result, Eq. (15.71) is reduced to (we set also $E_\gamma = \hbar\omega$, $V = 1$, and $\alpha = e^2/\hbar c$)

$$d\sigma_{E1} = \alpha \frac{mp\omega}{\hbar^2} \left| \sum_a (\mathbf{e} \cdot \mathbf{r}_a)_f \right|^2 \frac{do}{4\pi}, \quad (15.72)$$

where the solid angle do refers, for example, to the direction of motion of the proton. The proton coordinate is $\mathbf{r}/2$, where \mathbf{r} is the relative coordinate (compare the calculation of

the deuteron magnetic moment, Section 3.6). Also we consider the case of the unpolarized deuteron, when we have to average over initial spin states $((1/3)\sum_m)$, and count all final polarizations $(\sum_{m'})$ as the final state is still spin triplet because the dipole operator does not act on the spin variable,

$$\overline{d\sigma_{E1}} = \frac{1}{4} \alpha \frac{mp\omega}{\hbar^2} \frac{1}{3} \sum_{mm'} |(\mathbf{e} \cdot \mathbf{r})_{fi}|^2 \frac{do}{4\pi}. \quad (15.73)$$

The sums $\sum_{mm'}$ over initial and final spin projections of any spin operator \hat{O} can be reduced to the trace over spin variables,

$$\sum_{mm'} |O_{m'm}|^2 = \sum_{mm'} O_{m'm}^* O_{m'm} = \sum_{mm'} O_{mm'}^\dagger O_{m'm} = \sum_m (\hat{O}^\dagger \hat{O})_{mm} = \text{Tr} \{\hat{O}^\dagger \hat{O}\}. \quad (15.74)$$

Problem 15.4 Establish the quantum numbers of the final state in the dipole break-up of the deuteron. Argue that at low energy the final state of the proton and neutron can be approximated by the plane wave of relative motion and express the resulting differential and total cross sections in terms of the integrals containing the *s*- and *d*-components of the initial wave function (3.59) (perform averaging over spin projections of the initial deuteron and final nucleons, as well as over polarizations of the photon).

Solution

The final spin state after the E1 transition still remains triplet, $S = J = 1$, the orbital momentum and parity change; therefore, the final state corresponds to the *p*-wave of relative motion, $\ell = 1$. In this state, the low-energy nuclear forces are quite weak, and the wavelength of relative motion of final particles is much greater than the range of those forces. The magnitude of the wave vector k of relative motion in the final state is determined by the energy conservation,

$$\frac{\hbar^2 k^2}{2m} = \hbar\omega - \epsilon, \quad (15.75)$$

where ϵ is the binding energy of the deuteron. For a given direction of the relative momentum vector $\hbar\mathbf{k}$, the *p*-wave component of the plane wave normalized by unit density (we set $V = 1$) is expressed [QP, I, (17.91), (17.105)] through the Legendre polynomial $P_1(\cos \vartheta) = \cos \vartheta$, where ϑ is the angle between the relative coordinate \mathbf{r} and the wave vector \mathbf{k} , and the spherical Bessel function $j_{\ell=1}(kr)$:

$$\psi_f(r, \vartheta) = 3i \cos \vartheta j_1(kr) \chi_{m'}, \quad j_1(\rho) = \frac{\sin \rho - \rho \cos \rho}{\rho^2}. \quad (15.76)$$

In the *s*-wave integral, we integrate over angles of the unit vector $\mathbf{n} = \mathbf{r}/r$, using Eq. (3.1), and come to

$$\frac{1}{2} \langle f; m' | (\mathbf{e} \cdot \mathbf{r}) | \ell = 0; m \rangle = -i \frac{\sqrt{\pi}}{k} (\mathbf{e} \cdot \mathbf{k}) I_0 \delta_{mm'}, \quad (15.77)$$

where the radial integrals for the *s*- and *d*-components of the deuteron wave function (3.59) are

$$I_\ell = \int_0^\infty dr r^2 j_1(kr) u_\ell(r); \quad \ell = 0, 2. \quad (15.78)$$

In the d -wave integral, it is convenient to use the tensor operator S_{12} in the form (3.55). Here the angular integration contains four components of the unit vector \mathbf{n} and, using the symmetry arguments, can be found as

$$\int d\sigma n_i n_j n_k n_l = \frac{4\pi}{15} (\delta_{ij}\delta_{kl} + \delta_{ik}\delta_{jl} + \delta_{il}\delta_{jk}). \quad (15.79)$$

In terms of the deuteron spin operator $\mathbf{S} = \mathbf{s}_n + \mathbf{s}_p$, the angular integration leads to the d -wave contribution

$$\frac{1}{2} \langle f; m' | (\mathbf{e} \cdot \mathbf{r}) | \ell = 2; m \rangle = -i \frac{\sqrt{\pi}}{k} C_{m'm} I_2, \quad (15.80)$$

where the spin matrix element $C_{m'm}$ contains the operator

$$C = \frac{2\sqrt{2}}{5} \left\{ \frac{3}{4} [(\mathbf{k} \cdot \mathbf{S})(\mathbf{e} \cdot \mathbf{S}) + (\mathbf{e} \cdot \mathbf{S})(\mathbf{k} \cdot \mathbf{S})] - (\mathbf{e} \cdot \mathbf{k}) \right\}. \quad (15.81)$$

Now, according to (15.74), we have to calculate the necessary traces in the space of spin $S = 1$. Along the road, we need the traces of two and four spin components:

$$\text{Tr}[(\mathbf{k} \cdot \mathbf{S})(\mathbf{e} \cdot \mathbf{S})] = 2(\mathbf{e} \cdot \mathbf{k}), \quad (15.82)$$

$$\text{Tr}\{[(\mathbf{k} \cdot \mathbf{S})(\mathbf{e} \cdot \mathbf{S}) + (\mathbf{e} \cdot \mathbf{S})(\mathbf{k} \cdot \mathbf{S})]^2\} = 6(\mathbf{e} \cdot \mathbf{k})^2 + 2\mathbf{e}^2\mathbf{k}^2. \quad (15.83)$$

Since \mathbf{e} is the unit polarization vector of the photon, $\mathbf{e}^2 = 1$; if α is the angle between \mathbf{e} and the momentum \mathbf{k} of the final nucleon, the squared matrix element averaged over spin polarizations is equal to

$$\frac{1}{3} \sum_{mm'} |(\mathbf{e} \cdot \mathbf{r})_{fi}|^2 = 4\pi \left\{ I_0^2 \cos^2 \alpha + \frac{1}{25} I_2^2 (3 + \cos^2 \alpha) \right\}. \quad (15.84)$$

Similar to what was done for the angular distribution of dipole radiation, Section 14.6, we need to average over transverse polarizations of the initial photon; they are orthogonal to the direction \mathbf{n} of the photon:

$$\overline{e_i e_j} = \frac{1}{2} \sum_{\text{pol}} e_i e_j = \frac{1}{2} (\delta_{ij} - n_i n_j), \quad (15.85)$$

so that

$$\overline{\cos^2 \alpha} = \frac{1}{2k^2} \{ k^2 - (\mathbf{n} \cdot \mathbf{k})^2 \} = \frac{1}{2} \sin^2 \theta, \quad (15.86)$$

where θ is the experimentally observed angle between the directions of the photon and final nucleons.

Returning now to the cross section (15.72), we obtain

$$d\sigma = \frac{\pi}{2} \alpha \frac{mp\omega}{\hbar^2} \left[I_0^2 \sin^2 \theta + \frac{1}{25} (6 + \sin^2 \theta) I_2^2 \right] \frac{d\theta}{4\pi}. \quad (15.87)$$

The angular distribution of the break-up products is mainly determined by $\sin^2 \theta$ as characteristic for dipole-induced processes. The presence of tensor forces and therefore of the d -part of the deuteron wave function adds another component to the angular distribution. Finally, integrating over the angle of emitted nucleons, we derive the integral cross section of the deuteron photodisintegration,

$$\sigma = \frac{\pi}{3} \alpha \frac{mp\omega}{\hbar^2} \left(I_0^2 + \frac{2}{5} I_2^2 \right). \quad (15.88)$$

Problem 15.5 Neglect the contribution I_2 of the d -wave in the photodisintegration of the deuteron and estimate the cross section (15.88) using for the initial wave function the approximation of weak binding, when the wave function is substituted by its exponential tail outside the range of nuclear forces. Determine at what energy of the photon the cross section reaches the maximum and give the number for this maximum.

Solution

In this approximation, the initial coordinate wave function is

$$\psi_i = \sqrt{\frac{\kappa}{2\pi}} \frac{e^{-\kappa r}}{r}. \quad (15.89)$$

Here the factor κ of exponential decay is related to the binding energy ϵ ,

$$\epsilon = \frac{\hbar^2 \kappa^2}{2(M/2)} = \frac{\hbar^2 \kappa^2}{M}. \quad (15.90)$$

Calculating the integral I_0 and recalling the energy conservation (15.75), we obtain

$$\sigma = \frac{8\pi}{3} \alpha \frac{\hbar^2}{M} \frac{\sqrt{\epsilon(\hbar\omega - \epsilon)^{3/2}}}{(\hbar\omega)^3}. \quad (15.91)$$

The dependence $\sim E^{3/2} \propto k^3$ on the energy of the final particles is typical for the p -wave processes. In terms of the ratio $\xi = \hbar\omega/\epsilon$ of photon energy to the deuteron binding energy, we can give a numerical estimate of the cross section (15.91),

$$\sigma(\xi) \approx 1.2 \frac{(\xi - 1)^{3/2}}{\xi^3} \times 10^{-26} \text{ cm}^2. \quad (15.92)$$

Naturally, the cross section starts from zero at the threshold, $\xi = 1$, and reaches the maximum equal to

$$\sigma_{\max} \approx 0.15 \times 10^{-26} \text{ cm}^2 = 1.5 \text{ mb}, \quad (15.93)$$

where 1 barn (b) = 10^{-24} cm 2 and 1 millibarn (mb) = 10^{-3} b are typical units of nuclear cross sections.

15.10 Electron Scattering

This is the most powerful instrument for studying the electromagnetic structure of hadrons – nucleons and nuclei [7]. The *elastic* electron scattering gave the first detailed information on nuclear size and charge distribution inside the nucleus (Hofstadter experiments [8, 9]). The electrons are to be accelerated to high energy to have their quantum wavelength smaller than the spatial nuclear scale of interest.

The *inelastic* electron scattering allows one to study the excitation of various nuclear states. Here, in distinction to the photon excitation, we have an extra variable, the momentum transfer

$$\mathbf{q} = \mathbf{p} - \mathbf{p}' \quad (15.94)$$

from the scattered electron to the nucleus that in principle makes it possible by using the Fourier transformation to restore the spatial picture of the nuclear excitation at

the scale $R \sim 1/q$. This means that the fast electron scattering serves as a microscope for resolving the structure of the nucleus [10]; a relative weakness of electromagnetic interactions compared to strong forces means that the microscope will be less destructive with respect to the nuclear structure. At very large $|\mathbf{q}|$, one can study the internal structure of protons and neutrons that is outside of our interest here. It is possible to say that the elastic electron scattering is drawing the static charge distribution inside the nucleus, the charge form-factor (15.37), while the inelastic scattering determines the dynamic properties when the target nucleus is excited by the energy transfer from the electron,

$$\omega = \epsilon - \epsilon' \quad (15.95)$$

(In this section, we mainly use the relativistic units, $\hbar = c = 1$).

As the kinetic energy of the electron is usually much greater than its rest mass 0.5 MeV, we should use the relativistic kinematics. The 4-invariant for the transferred energy-momentum, neglecting the electron mass, can be expressed in terms of lab-frame measured quantities including the scattering angle θ ,

$$Q^2 = \omega^2 - \mathbf{q}^2 = 2m^2 + 2pp' \cos \theta - 2\epsilon\epsilon' \approx -2pp'(1 - \cos \theta) = -4pp' \sin^2 \frac{\theta}{2}. \quad (15.96)$$

Therefore the 4-momentum transfer Q is a space-like vector, $Q^2 < 0$, as characteristic for the scattering processes. If the nucleus was originally at rest, it acquires the recoil kinetic energy $\Delta E = E' - M$, which is also expressed in terms of the invariant (15.96):

$$Q^2 = (E' - M)^2 - (\mathbf{q})^2 = 2M^2 - 2E'M = -2M\Delta E. \quad (15.97)$$

The advantages of using the electron beam as a nuclear microscope come from obvious facts that we know quite well the electromagnetic interactions and that those interactions are relatively weak being characterized by the fine structure constant $\alpha = e^2/\hbar c = 1/137$; therefore an interaction event brings in the least distortion of nuclear structure. The second argument might be invalid for the scattering off very heavy nuclei with large Z . The obtained information is in general more rich than what we can learn in nuclear interactions of real photons. For example, in the photon scattering, the two kinematic variables, q and ω , are not independent while for the electrons the interaction mechanism includes the exchange by a *virtual photon* and the only restriction is that the 4-vector $Q = (\omega, \mathbf{q})$ is space-like, $\mathbf{q}^2 \geq \omega^2$. In particular, in the processes when the scattered electron knocks out from the nucleus a particle or cluster with the effective mass M^* , we expect to see in the spectrum of scattered electrons (dependence of the scattering cross section on ω at fixed q and scattering angle) a broad *quasielastic peak* at $\omega = Q^2/2M^*$.

Problem 15.6 Estimate the width of the quasielastic peak corresponding to the knock-out of a proton.

Solution

If the momentum of the knocked-out proton inside the nucleus was \mathbf{k} ,

$$\omega = \frac{(\mathbf{k} + \mathbf{q})^2 - k^2}{2M} = \frac{q^2}{2M} + \frac{(\mathbf{q} \cdot \mathbf{k})}{M}. \quad (15.98)$$

The width of the maximum is determined by possible angles between \mathbf{k} , where $k \sim k_F$ (Fermi momentum), and \mathbf{q} , so that

$$\Delta\omega \simeq \frac{2qk_F}{M}, \quad (15.99)$$

where M can be an *effective mass* of the proton in the medium.

The *elastic* electron scattering off the nucleus with zero spin can be described by the Mott formula that is derived from the standard result of Rutherford scattering [QP, II, 3.2], but with several necessary modifications. Without electron spin effects, the differential cross section for the elastic electron scattering by the infinitely heavy nucleus of charge Z would be given by

$$\frac{d\sigma}{d\omega} = \frac{Z^2 e^4}{4p^2 \sin^4(\theta/2)} |F(\mathbf{q})|^2. \quad (15.100)$$

Here the electron is considered an ultrarelativistic particle with energy much greater than its rest mass, so that in the denominator we have p instead of the nonrelativistic kinetic energy e . $F(\mathbf{q})$ in Eq. (15.100) is the charge form-factor of the nucleus (15.37) normalized to 1 at $q \rightarrow 0$,

$$F(\mathbf{q}) = \frac{1}{Z} \rho^{\text{ch}}(\mathbf{q}). \quad (15.101)$$

The additional change to be made in Eq. (15.100) is related to the electron spin that was not important for nonrelativistic electrons. At velocity close to c , the Dirac particles are longitudinally polarized, and the helicity is preserved. Since the Coulomb potential does not flip spin, the scattering backwards turns out to be forbidden. This adds the factor $1 - v^2 \sin^2(\theta/2) \approx \cos^2(\theta/2)$ to the cross section (15.100),

$$\frac{d\sigma}{d\omega} = \frac{Z^2 e^4 \cos^2(\theta/2)}{4p^2 \sin^4(\theta/2)} \frac{1}{1 + 2(p/M)\sin^2(\theta/2)} |F(\mathbf{q})|^2. \quad (15.102)$$

Problem 15.7 Show that the recoil energy of the target nucleus (originally at rest in the lab frame) adds the expression in the denominator of Eq. (15.102). This correction becomes important for very fast electrons and not too small scattering angles.

Solution

The momentum conservation can be easily reduced to

$$\frac{p'}{p} = \frac{1}{1 + (p/M)(1 - \cos\theta)}. \quad (15.103)$$

If we consider the charge density as an operator in the space of nuclear states, the form-factor (15.101) can describe the inelastic processes of the nuclear excitation induced by the Coulomb interaction of the electron with the target nucleus. The multipole expansion separates terms responsible for the excitation of states with certain values of the nuclear spin. Here we have to recall the standard expansion of the plane wave [QP, I, (17.106)],

$$e^{i(\mathbf{q} \cdot \mathbf{r})} = \sum_L \sqrt{4\pi(2L+1)} i^L j_L(qr) Y_{L0}(\mathbf{r}), \quad (15.104)$$

where we take the z -axis along the momentum transfer vector \mathbf{q} ; $j_L(qr)$ are spherical Bessel functions. The charge form-factor (in general inelastic) is an operator

$$F(\mathbf{q}) = \frac{1}{Z} \sum_L \sqrt{4\pi(2L+1)} i^L M_{L0}(q), \quad (15.105)$$

and the multipole operators are

$$M_{L\Lambda}(q) = \int d^3r j_L(qr) Y_{L\Lambda}(\mathbf{r}) \rho^{\text{ch}}(\mathbf{r}). \quad (15.106)$$

These operators are responsible for the excitation of nuclear states with spin quantum numbers $JM = L\Lambda$.

Problem 15.8 Find the cross section of exciting the low-lying vibrational states in the liquid drop model, Chapter 5, by the scattering of fast electrons [11].

Solution

It is sufficient to find the corresponding multipole operator. Using (15.106) (but without the long wavelength expansion of spherical Bessel functions), we find for $L \neq 0$

$$M_{L\Lambda}(q) = \frac{3Z}{4\pi} j_L(qR_0) \alpha_{L\Lambda}^\dagger, \quad (15.107)$$

where α^\dagger is the collective variable expressed as in Eq. (6.90) in terms of the phonon creation operators for the corresponding mode of multipole vibrations of the liquid drop. The oscillator parameters B_L and C_L require a special model of the liquid drop for their definition; for example, it was done in Chapter 5 with the use of irrotational kinetic energy, surface tension, and Coulomb energy of the drop. One can also use microscopic models for those oscillator parameters going beyond the liquid drop. A special case corresponds to $L = 0$ where we have the elastic process along with the two-phonon admixture, Eq. (5.23). However, the excitation with $L = 0$ (the giant monopole resonance) requires the knowledge of the compressibility of the drop removing the assumption of the volume conservation.

The full relativistic description of the electron scattering [12, 13] requires some elements of quantum electrodynamics, and we will not undertake this derivation here. Here we have to account for the *magnetic form-factor* of the target and excitation by the current carried over by transverse photons in addition to that due to the Coulomb interaction.

With high-energy electrons, a lot of information comes from the *quasielastic scattering*, or the processes like $(e, e'p)$, when the scattered electron is registered in coincidence with the knocked out proton. Analogous reactions, $(e, 2e)$, provide rich information about electron orbitals in atoms and molecules. In nuclear processes, we are interested in single-particle states inside the nucleus. A famous example is given by the comparison of the results for neighboring isotones, ^{206}Pb and ^{205}Tl [14, 15]. These nuclei differ by one proton which, according to the shell model in vicinity of the double-magic nucleus ^{208}Pb , occupies the $2s$ orbital. The ratio of the electron scattering cross sections and the corresponding density difference, Figure 15.6, show the real presence of the extra proton at this orbital that has a probability maximum in the center of the nucleus.

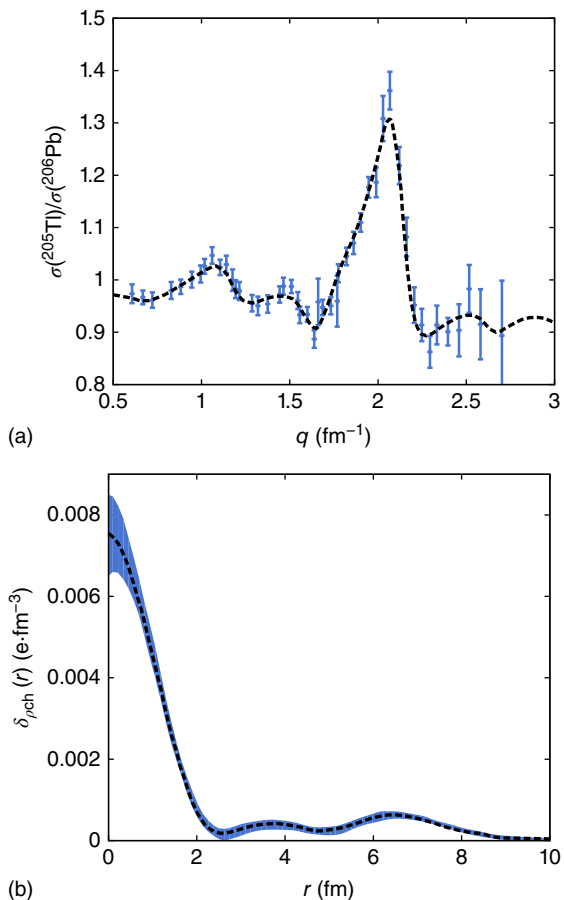


Figure 15.6 Ratio of $(e, e' p)$ cross sections for ^{206}Pb and ^{205}Tl shown in (a). The peak at $q = 2 \text{ fm}^{-1}$ corresponds to the Fourier image of the charge density for the $2s$ proton radial wave function. This wave function has two radial nodes and can be inferred from difference of charge densities $\delta\rho_{\text{ch}}(r)$ between ^{206}Pb and ^{205}Tl shown in (b). The fitted curves are shown by dashed lines, experimental data points with error bars are shown in (a) and the corresponding uncertainty in the Fourier image is shaded in (b), [14, 15].

In fact such experiments provide the so-called *spectroscopic factors* S_λ , which are overlaps of the final many-body wave function and the initial wave function without the removed particle,

$$S_\lambda = |\langle \Psi_{A-1} | a_\lambda | \Psi_A \rangle|^2. \quad (15.108)$$

In the above-mentioned example, the quantum numbers λ correspond to the $2s$ proton; one needs to separate correctly the angular momentum coupling coefficients to get the idea of the real filling factors of the orbital λ in the initial nucleus. In this case, we speak about a *quasihole* with quantum numbers of the $2s$ proton orbital created by the electron excitation. The width of the peak on the energy scale tells about the finite lifetime of this pure excitation that is not fully stationary because of the interactions with other particles.

The wealth of experimental data, mainly from the inelastic electron scattering, show that the spectroscopic factors of single-particle states near the Fermi surface in the nuclei in the vicinity of closed shells are typically around 0.7. The uncertainties from the $(e, e' p)$ experiments are mostly related to the final state interaction of the knocked out proton and the presence of meson currents that grows with the electron energy. The detailed analysis for the above-mentioned $2s$ proton orbital gives the occupation factor

0.76 ± 0.07 . Comparable results although with slightly bigger error bars were obtained from other types of nuclear reactions. The missing single-particle strength is transferred by residual interactions to higher energy; in this sense, it is even possible to loosely speak about temperature of the ground state based on the idea of thermalization of dynamics in a small isolated system (no contact with a heat bath).

References

- 1 A. Bohr and B.R. Mottelson, *Nuclear Structure*, Vol. **1**, Benjamin, New York, 1969.
- 2 U. Garg, Nucl. Phys. **A649**, 66c (1999).
- 3 R.S. Hager and E.C. Seltzer, Nucl. Data Sheets **4**, 1 (1968).
- 4 W.D. Loveland, D.J. Morrissey, and G.T. Seaborg, *Modern Nuclear Chemistry*, John Wiley & Sons, Inc., Hoboken, NJ, 2006.
- 5 K. Alder, A. Bohr, T. Huus, B. Mottelson, and A. Winther, Rev. Mod. Phys. **28**, 432 (1956).
- 6 W. Rarita and J. Schwinger, Phys. Rev. **59**, 436 (1941).
- 7 H. Überall, *Electron Scattering from Complex Nuclei*, Academic Press, New York, 1971.
- 8 R. Hofstadter, Rev. Mod. Phys. **28**, 214 (1956).
- 9 R. Hofstadter, Annu. Rev. Nucl. Sci. **7**, 231 (1957).
- 10 T.W. Donnelly and J.D. Walecka, Annu. Rev. Nucl. Sci. **25**, 329 (1975).
- 11 J.D. Walecka, Phys. Rev. **126**, 653 (1962).
- 12 T. De Forest and J.D. Walecka, Adv. Phys. **15**, 1 (1966).
- 13 A.I. Akhiezer, A.G. Sitenko, and V.K. Tartakovskii, *Nuclear Electrodynamics*, Springer-Verlag, Berlin, 1994.
- 14 J. Cavedon *et al.*, Phys. Rev. Lett. **49**, 978 (1982).
- 15 V.R. Pandharipande, I. Sick, and P.K.A. deWitt Huberts, Rev. Mod. Phys. **69**, 981 (1997).

16

Nuclear Rotation

It is really astonishing that there exists a set of characteristic collective states which are well separated from the thousands of neighboring excited states and are described by a simple rotating shell model.

F. Sakata, in *Nuclear Structure Models* (World Scientific, Singapore, 1992)

16.1 Introduction: Rotational Bands

Finite systems in free space have a specific collective degree of freedom – *rotation*. There is a crucial difference between rotational motion and translation. With no external fields, *translational motion* is characterized by the conserved total *momentum* \mathbf{P} . Translational energy of a *nonrelativistic* system of mass M is

$$E(\mathbf{P}) = \frac{\mathbf{P}^2}{2M}. \quad (16.1)$$

Of course, this is an eigenvalue of the kinetic part of a quantum Hamiltonian for motion of the center of mass. However, this part does not require any calculation. The Galilean relativity allows one to totally exclude global translational motion by the transformation to a moving inertial frame. The intrinsic excitations in this frame do not carry any memory of translations of the system as a whole; they do not depend on \mathbf{P} . The energy (16.1) is what is left of the total energy in a laboratory frame, where the object is moving with the momentum \mathbf{P} , after the intrinsic energy is subtracted. We know beforehand that, in the non-relativistic regime, the global kinetic energy is a quadratic function of \mathbf{P} and the *inertial parameter* M is merely a sum of masses of constituents,

$$M = \sum_a m_a. \quad (16.2)$$

The moving frame, where the object is at rest, is *inertial* and global motion is completely *decoupled* from other degrees of freedom.

The situation with *rotation* is much more complicated. Even uniform rotation cannot be fully excluded by a transition to a rotating frame because this frame is *noninertial*. For such a transition, we pay the price of earning the *centrifugal* and *Coriolis* forces which disturb intrinsic (nonrotational) degrees of freedom. Living on the Earth we feel its rotation. There still exist constants of motion, the components of the total *angular*

momentum \mathbf{J} (nuclear spin). But rotational energy E_J , in general, cannot be separated as an independent term similarly to what has been done in (16.1). It is not universal and depends on intrinsic structure. We know that solids and liquids behave quite differently under rotation.

Nevertheless, the mesoscopic objects with intrinsic deformation as nuclei and molecules have *rotational bands* in their spectra. These are the sequences of stationary states which differ by the quantum numbers of the rotation group J and M and have apparently very similar internal structure. We mentioned rotational bands in association with the selection rules for gamma-rays which strongly prefer *intraband* transitions due to the large overlap of the initial and final wave functions. The so-called Regge trajectory in elementary particle physics is a similar phenomenon.

Modern techniques of nuclear spectroscopy allow experimentalists to register *gamma-cascades* radiated by a rotating nucleus in the process of deexcitation. The observed bands in a number of cases stretch up to spins of 60 or 70 (in molecules the rotational bands may go beyond $J = 100$). For illustration we show, Figure 16.1, five low-lying rotational bands in the ^{168}Hf nucleus. In well-studied nuclei, one can find dozens of rotational bands. A band is characterized by a starting value of spin

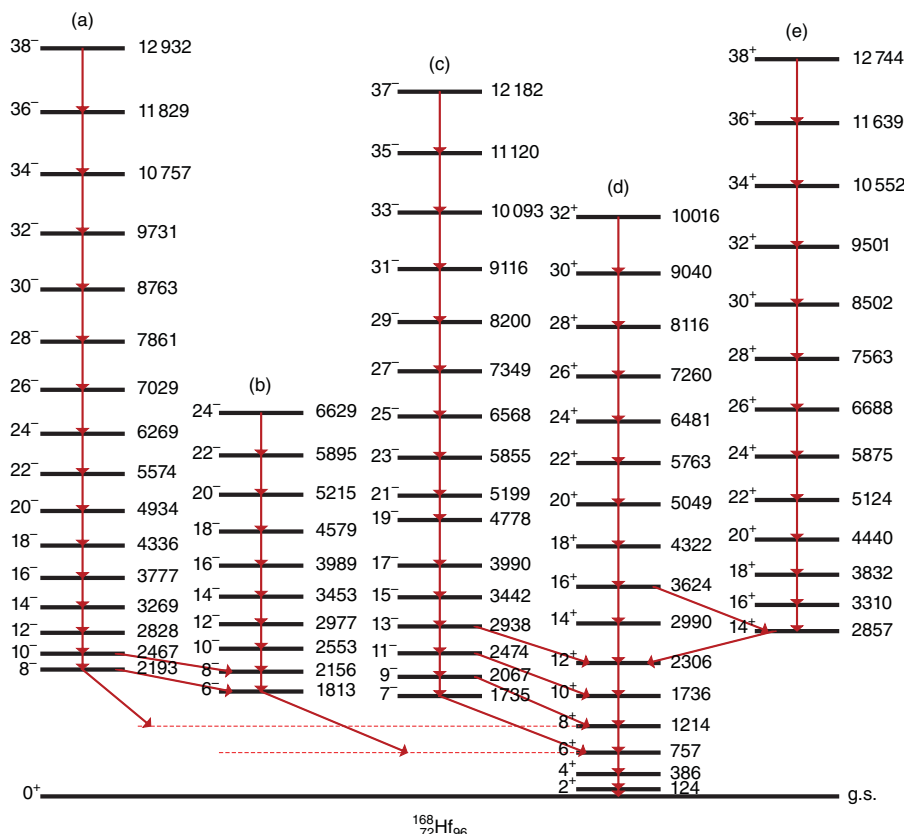


Figure 16.1 Low-lying rotational bands of ^{168}Hf . Spins and parities of states are indicated. Arrows correspond to gamma-transitions.

(*bandhead* J_0), monotonously increasing sequence of spins $J > J_0$, and parity which is the same for all members of the band.

All bands shown in Figure 16.1 have the angular momentum step $\Delta J = 2$ between adjacent states. Strong “stretched” E2 transitions proceed down the band from the upper state where the band was initially populated. The standard experimental methods use heavy ion reactions with the formation of a compound system that has large excitation energy and high spin equal to the initial relative angular momentum of a projectile and a target. The excitation energy is carried away by emitted particles and high energy, mostly E1, gamma-rays. They however take away only a small fraction of the original angular momentum. As a result, a nucleus is significantly cooled but still keeps high spin. At this stage, the nuclear states are populated with most of the excitation energy concentrated in collective degrees of freedom, particularly in high-spin rotation.

The reduced probabilities within a rotational band can reach hundreds of Weisskopf units that demonstrates the highly collective nature of E2 gamma-radiation. In other cases, when $\Delta J = 1$, M1 transitions can be allowed as well. At one of the lower states, the gamma-cascade jumps to another band and, at some point, reaches the *ground-state band* that eventually brings the nucleus to its ground state. Usually, weaker *interband* transitions between the bands of different parities can be of E1 type if this is allowed by ΔJ .

In the case of Figure 16.1, energies $E_b(J)$ of all bands b within a good accuracy can be described, analogously to (16.1), by the quadratic expression

$$E_b(J) = E_b(J_{0b}) + A_b[J(J+1) - J_{0b}(J_{0b}+1)] \quad (16.3)$$

where $E_b(J_{0b})$ is the energy of the bandhead with $J = J_{0b}$. Constants A_b are slightly different in different bands. For example, we can compare the energies of the gamma-transitions $20 \rightarrow 18$ in the two positive parity bands, ground-state band (d), and yrast band (e), to see that $A_d > A_e$. The word *yrast* refers to the lowest states for a given spin.

Equation (16.3) shows the energy spectrum of a quantum *rotor*. It can be described by the Hamiltonian

$$H_b = \text{const}(b) + \frac{\hbar^2 J^2}{2\mathcal{J}_b}. \quad (16.4)$$

The quantity

$$\mathcal{J}_b = \frac{\hbar^2}{2A_b} \quad (16.5)$$

is the inertial parameter for rotation that can be naturally called the *moment of inertia* of the band b . As seen from Figure 16.1, the ground-state band (d) shows the smallest moment of inertia. Typically, in even–even rare earth nuclei the moments of inertia are $30 \div 40 \hbar^2 \text{ MeV}^{-1}$; they are approximately twice as big in actinides. Later, we will encounter a more complicated notion of the *tensor of inertia*.

In contrast to classical rotation, we can have only discrete values of the angular momentum. Therefore, different empirical definitions of the moment of inertia are possible. The *static* moment of inertia $\mathcal{J}^{(1)}$ for a band with $\Delta J = 2$, where gamma-ray energies are $E_\gamma = E_J - E_{J-2}$, is defined usually as

$$\mathcal{J}^{(1)} = (2J-1) \frac{\hbar^2}{E_\gamma(J \rightarrow J-2)}. \quad (16.6)$$

The so-called *dynamical* moment of inertia is defined in terms of differences of sequential gamma-ray energies in the cascade,

$$\mathcal{J}^{(2)} = 4 \frac{\hbar^2}{E_\gamma(J \rightarrow J-2) - E_\gamma(J-2 \rightarrow J-4)}. \quad (16.7)$$

The first definition uses, in fact, the discrete analog of the first derivative of the energy spectrum and the second one utilizes the second derivative. Other treatments are possible as well.

For the *rigid rotor* (unperturbed by intrinsic motion) the moment of inertia is constant along the band, and all definitions coincide. A good example is given by the *superdeformed* bands, for example, in ^{152}Dy , where the spectrum of gamma-rays is almost *equidistant*. The moments of inertia in this superdeformed region are of the order of $(60 \div 85) \hbar^2 \text{ MeV}^{-1}$. Unfortunately, at high excitation, it can be hard to establish experimentally absolute excitation energies and spin values; only their differences are usually observed. The realistic gamma spectra, such as the one shown for ^{156}Dy in Figure 16.2 can be quite complicated and involve several bands and transitions between different shapes involving changes to the moment of inertia.

By definition, a *rotor* is a system that has only rotational degrees of freedom. In Figure 16.1, other degrees of freedom reveal themselves through the presence of several bands with different moments of inertia. One can think of bands as different intrinsic particle configurations. In this example, the bands are well segregated. In detailed analysis, one can notice that the rotor is not rigid and the rotational properties smoothly change along each band (the moment of inertia itself is a weak function of J). This is

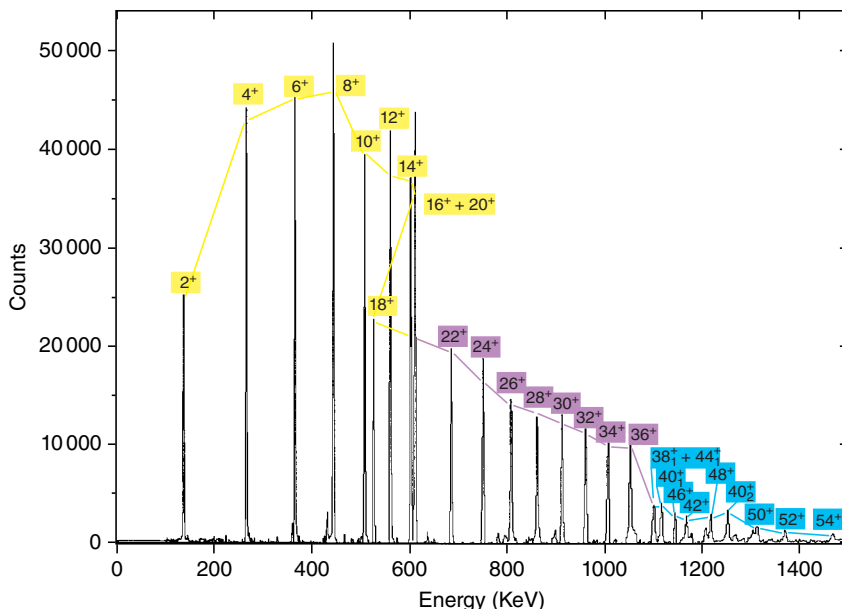


Figure 16.2 Gamma-ray spectrum for the lowest energy-positive parity (yrast) rotational structure in ^{156}Dy . The peaks are labeled with angular momenta of the corresponding gamma-emitting states and highlighted corresponding to different regions discussed in Figure 16.13. (Reproduced with permission of M. Riley [1], Florida State University.)

just a manifestation of *noninertial* effects. However, the band still keeps its identity: the difference of intrinsic configurations for different bands is, in this example, larger than their smooth evolution along the band. This is not always the case, see Figure 16.2.

In a classical system of particles with masses m_a attached to their positions in the points \mathbf{r}_a , the moment of inertia would be equal to the *rigid-body* value

$$\mathcal{J}_r = \sum_a m_a(x_{2a}^2 + x_{3a}^2), \quad (16.8)$$

or, for a continuous distribution of particles with the mass density $\rho_m(\mathbf{r})$,

$$\mathcal{J}_r = \int d^3r \rho_m(\mathbf{r})(x_2^2 + x_3^2). \quad (16.9)$$

Here we measure the particle coordinates in the frame rotating together with the object (*body-fixed frame*), and the 1-axis of the body-fixed frame is chosen as the rotation axis.

In contrast to the translational mass (16.2), the value of the moment of inertia as a parameter in the Hamiltonian (16.4) is not determined by any general principles and can drastically change when intrinsic structure is changed. In Figure 16.1, the moment of inertia of the ground-state band (d), $\mathcal{J} \approx 30\hbar^2 \text{ MeV}^{-1}$, is significantly smaller than the rigid-body value (16.9), $\mathcal{J}_r \approx 66\hbar^2 \text{ MeV}^{-1}$, for a known (axially deformed) nuclear shape. It is closer to \mathcal{J}_r in *excited* bands. Since the excited bands have no continuation to lower energies, we conclude that the angular momenta J_0 of the bandheads are carried by excitation of nonrotational degrees of freedom, presumably by *unpaired quasiparticles*. Their presence *increases* the moment of inertia. The systematics of the moments of inertia for ground-state rotational bands in well-deformed nuclei is shown in Figure 16.3.

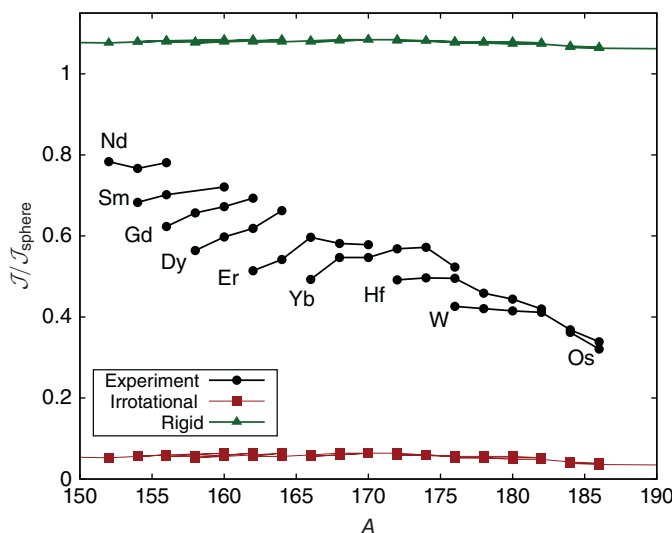


Figure 16.3 Systematics of moments of inertia in nuclei with $150 \leq A \leq 188$ relative to the sphere, $\mathcal{J}_{\text{sphere}} = 2/5MR^2$, where radius is taken from bulk properties (5.3) with $r_0 = 1.16 \text{ fm}$. The rigid and fluid moments of inertia are shown for the deformation parameter β corresponding to each nucleus. For small empirical deformation, the rigid moments of inertia are close to those of a sphere; the fluid moments of inertia discussed further in this chapter are small $\propto \beta^2 \mathcal{J}_{\text{sphere}}$.

The empirical values for even–even nuclei are lower than the corresponding rigid-body values, estimated for an axially symmetric quadrupole shape, by a factor $2 \div 3$. In odd- A and odd–odd nuclei, the moment of inertia is increased but still it does not reach the rigid-body value.

A physical reason which justifies the separation of rotational degrees of freedom is the *adiabaticity* of rotation. This is the extreme case of slow collective motion that disturbs intrinsic structure and interactions (interparticle bonds in molecules) in the minimum possible way. Energy required to excite such motion is lower than for other degrees of freedom. Although the adiabaticity factor is, in the nuclear case, not so strong as in molecules, rotation is rather adiabatic with respect to other types of excitations. We see in Figure 16.1 that typical energy of intrinsic excitations (heads of excited bands) is $2 \div 3$ MeV. This is the energy gap of approximately 2Δ necessary to break a pair and to create two quasiparticles. The first rotational states 2^+ of ground-state bands have energies of approximately 200 keV or less.

Problem 16.1 The first two excited states in ^{181}Ta have energies 136 and 303 keV. Find the moment of inertia, the ground-state spin and spins of these excited states assuming that all states belong to the same rotational band with nonrotational angular momentum $\neq 1/2$.

We need to stress that we consider here *collective* rotation. It is possible only if the object is deformed and the body-fixed rotation axis is not a symmetry axis of the system. There are no rotational bands in atoms because the strong central Coulomb field prevents noticeable intrinsic deformation. In molecules, the deformation is introduced by the heavy-ion skeleton that defines naturally the body-fixed frame for electrons. In nuclei, as we know, the deformation is a consequence of the self-consistent shell effects in a system of identical fermions. Therefore, it is much more vulnerable than in molecules.

Collective “rotation” *around the symmetry axis* does not create a variable field acting on particles and does not change their wave functions. Hence it does not generate a physical excited state. Equally, one can say that rotation of the charged ellipsoid around its symmetry axis does not lead to electric quadrupole radiation (no time-dependent field). For a linear molecule or an axially deformed nucleus, collective rotation is possible only around the axes *perpendicular* to the symmetry axis.

This does not mean that one cannot create angular momentum along the symmetry axis. It can be, for example, built of angular momenta of broken quasiparticle pairs. Collective rotation of such configurations adds the rotational angular momentum (perpendicular to the symmetry axis) to the quasiparticle angular momentum that can be aligned along the symmetry axis. In collective rotation, intrinsic structure changes smoothly as the angular momentum increases. Contrary to that, increase of intrinsic angular momentum requires redistribution of particles, that is, change of structure. It is only at high excitation energies in the semiclassical domain of high angular momenta that the qualitative difference of the two types of rotation vanishes because the relative change of structure becomes small in the noncollective case as well. This is what we should have expected, because in classical mechanics, the arguments against rotation around the symmetry axis lose their meaning.

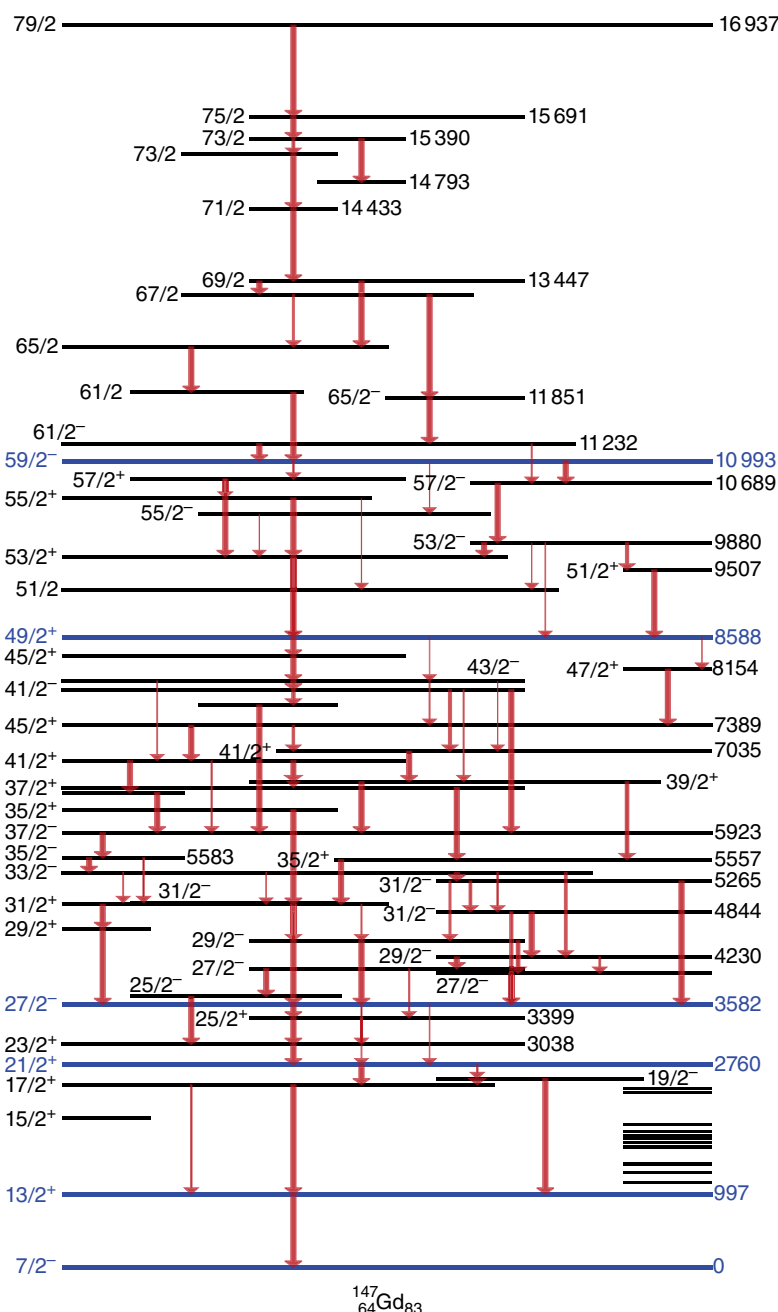


Figure 16.4 Level schemes near the yrast line in ^{147}Gd . Heavy lines indicate levels with lifetimes larger than (or about) 1 ns. Arrows show principal transitions in the cascade of electromagnetic decays from the state at the top.

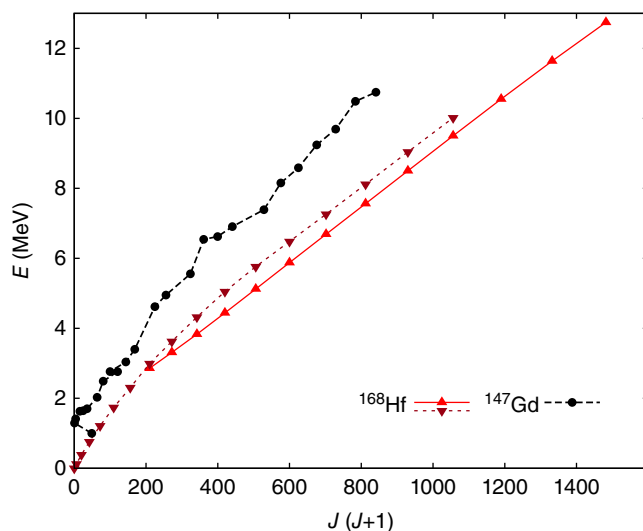


Figure 16.5 Excitation energy as a function of $J(J+1)$ in ^{147}Gd and ^{168}Hf . Yrast states in ^{147}Gd are shown by circles, and upward and downward pointing triangles show the yrast band (e) (in Figure 16.1) and ground band (d) in ^{168}Hf , respectively.

The difference between collective rotation and noncollective *alignment* is illustrated by Figure 16.4 where the spectrum of ^{147}Gd is shown to be compared with that of ^{168}Hf in Figure 16.1. In both cases, we consider the levels near the *yrast line*, that is, the locus of the states with lowest energy for each value of the angular momentum. The ^{147}Gd nucleus has one neutron above the core ^{146}Gd which reveals some signatures of a doubly magic nucleus ($Z = 64$ corresponds to a closure of proton spherical subshells). The ^{168}Hf nucleus has a normal prolate deformation. The angular momentum in the gadolinium case is built by quasiparticles, the energy intervals and even the level sequence are not monotonous functions of the angular momentum. It happens that violations of the natural spin sequence are capable of creating *traps*: inversion of even a pair of levels forces a state to decay by radiation of high multipolarity that considerably increases the lifetime. In contrast to that, two bands of ^{168}Hf display a regular picture of collective rotation with the larger moment of inertia in the two-quasiparticle band as compared to the ground-state band. The energy diagram of Figure 16.5 shows the fluctuating structure of the yrast line in ^{147}Gd and the smooth pattern in ^{168}Hf . Owing to the larger moment of inertia and, therefore, lower rotational energy, the two-quasiparticle band becomes actually the yrast band for $J > 14$.

The flexibility of the nuclear mean field leads to coexistence of different shapes and related different rotational patterns in the same nucleus and at close energies. The ^{152}Dy nucleus has *spherical* shape at low spin and low excitation energy. In this part of the spectrum, the angular momentum is created by quasiparticle excitations. At high spins, the *superdeformed* states with the axis ratio close to 2 : 1 occupy the yrast line. The moment of inertia of the superdeformed band is close to the rigid-body value for such a deformation. Heavier dysprosium isotopes, $N \geq 90$, are *normally deformed* in the low-lying part of the spectrum. The further high-spin evolution supposedly goes via *triaxial* shapes.

In general, one could envision different mean-field shapes of yrast configurations as a function of particle number and excitation energy.

Diversity and mutual transformation of nuclear shapes prevents us from an attempt to give a review of the whole area. In what follows, we concentrate mostly on basic ideas which allow us to describe rotation of a quantum system.

16.2 Finite Rotations

Among the most general symmetries which have been used extensively throughout the course, rotational invariance is especially important in studying a finite system that can freely orient itself in space. We mentioned that it is necessary to distinguish the orientational wave function of an object from its intrinsic shape that can be defined in the body-fixed frame. We need to formulate this idea in precise terms compatible with the spirit of quantum mechanics. Otherwise, it is impossible to understand physics of deformed nuclei and nuclear rotation.

Textbooks in quantum mechanics usually do not go into details after the statement that the orientational wave functions of a particle with correct quantum numbers l, m of the rotation group are spherical functions $Y_{\ell m}(\mathbf{n})$. This turns out to be just a particular case corresponding to intrinsic *axial symmetry*. On the other hand, more advanced books and monographs usually consider the subject as well-known to a reader. The goal of this section is to bridge the gap.

In the case of one particle, we also can introduce a *body-fixed* frame with the polar z' -axis along the radius \mathbf{r} . The frame will automatically follow the motion of the particle. Two angles θ, φ of the body-fixed polar axis with respect to the coordinate axes of a *space-fixed* frame are the rotational variables we need in order to describe the orientation. However, as we know, the general rotation in three-dimensional space requires three parameters for its description. For one particle, we have the degenerate case with two parameters only. Not defined yet is an angle corresponding to rotation around the radius vector \mathbf{r} that serves as a symmetry axis in the body-fixed frame. The orbital momentum ℓ generates particle rotations but it does not allow to rotate around the radial axis; its projection onto \mathbf{r} identically vanishes,

$$(\ell \cdot \mathbf{r}) = 0. \quad (16.10)$$

The same result follows in the momentum representation, $(\ell \cdot \mathbf{p}) = 0$. Thus, spherical harmonics $Y_{\ell m}$ describe cases with only one specified direction in space that can be taken as an intrinsic symmetry axis; rotation around this axis makes no sense so that the third rotation parameter would be redundant.

To study the general situation, we consider functions which transform according to an irreducible representation of the rotation group. We know that such functions form the multiplets $|JM\rangle$ of dimension $(2J + 1)$ with integer or half-integer J . An arbitrary rotation R is characterized by three parameters which we do not specify at this stage. The transformation of the functions $|JM\rangle$ among themselves under rotation R is given by the matrix $D^J(R)$ with elements $D_{M'M}^J(R)$. With the standard quantum definition of matrix elements,

$$R|JM\rangle = \sum_{M'} D_{M'M}^J(R)|JM'\rangle. \quad (16.11)$$

Since the states $|JM\rangle$ are orthogonal as eigenfunctions of Hermitian operators \mathbf{J}^2 and J_z and they are assumed to be normalized, we immediately see that

$$D_{M'M}^J(R) = \langle JM' | R | JM \rangle. \quad (16.12)$$

These functions are called *matrix elements of finite rotations*. Tensor operators $T_{\lambda\mu}$ are transformed under rotations in the same way as basis functions (16.11), that is, the coefficients are matrix elements of finite rotations for matrices D^λ of the corresponding rank λ ,

$$T'_{\lambda\mu} = RT_{\lambda\mu}R^{-1} = \sum_{\mu'} D_{\mu'\mu}^\lambda(R) T_{\lambda\mu'}. \quad (16.13)$$

The states $|JM\rangle$ are defined in the laboratory frame (x, y, z) so that $M = J_z$ is the projection onto the space-fixed quantization axis. One of possible parameterizations of the rotations R can be given in terms of the axis \mathbf{n} and angle α of rotation around this axis (three parameters!). Taking \mathbf{n} as the polar axis z , we find the diagonal elements of the matrix D^J from (16.12),

$$D_{M'M}^J(R_z(\alpha)) = e^{-iM\alpha} \delta_{M'M}. \quad (16.14)$$

We use *active* rotations here: the coordinate frame is fixed and we rotate the physical system. In *passive* rotations, the frame is rotated, which is equivalent to the inverse rotation of the system, $R \rightarrow R^{-1}$.

The D -matrices satisfy important relations which follow from the group properties of rotations and unitarity of the rotation operator R . The unitarity (equivalent to Hermiticity of the angular momentum operator as the generator of infinitesimal rotation) gives $R^{-1} = R^\dagger$. But we have from (16.12)

$$D_{M'M}^J(R^\dagger) = \langle JM' | R^\dagger | JM \rangle = \langle JM | R | JM' \rangle^*, \quad (16.15)$$

so that the matrix corresponding to the inverse rotation is

$$D_{M'M}^J(R^{-1}) = [D_{MM'}^J(R)]^* \rightsquigarrow D^J(R^{-1}) = D^J(R^\dagger) = [D^J(R)]^\dagger. \quad (16.16)$$

A rotation R_2R_1 composed of two consecutive rotations induces the matrix

$$D^J(R_2R_1) = D^J(R_2)D^J(R_1) \rightsquigarrow D^J(R^{-1}) = [D^J(R)]^{-1} \quad (16.17)$$

that follows from the completeness of the set of states $|JM\rangle$ used as an intermediate set in (16.12) for $D^J(R_2R_1)$. The D -matrices in (16.17) have to be ordered according to the order of rotations. All these equations are simply mathematical definitions of group properties. Matrices D^J repeat, in the subspace of a given representation, the geometrical properties of rotations.

16.3 Rotation Matrices as Functions on the Group

The matrix elements of finite rotations, $D_{M'M}^J(R)$, can be considered as functions defined on a *group manifold*, that is, space of continuously changing parameters of all possible rotations R . These functions are orthogonal in this space. To prove this, consider a fixed orientation \mathcal{O}_0 of the body-fixed frame that can be reached from an orientation \mathcal{O} by a corresponding rotation R so that $\mathcal{O}_0 = R\mathcal{O}$. Then each orientation is parameterized

by a rotation, $\mathcal{O} = R^{-1}\mathcal{O}_0$. The functions $D_{M'M}^J(R)$ at fixed M are now functions of the angles \mathcal{O} ,

$$D_{M'M}^J(R) = \Phi_{MM'}^J(\mathcal{O}), \quad \mathcal{O} = R^{-1}\mathcal{O}_0. \quad (16.18)$$

Now, we look at what happens to these functions under another rotation R' . The value of a function is simply carried to another point,

$$R' \Phi_{MM'}^J(\mathcal{O}) = \Phi_{MM'}^J(R'^{-1}\mathcal{O}) = \Phi_{MM'}^J(R'^{-1}R^{-1}\mathcal{O}_0) = \Phi_{MM'}^J((RR')^{-1}\mathcal{O}_0). \quad (16.19)$$

The result is a definition of the same function taken at the value RR' of the argument,

$$R' D_{M'M}^J(R) = D_{M'M}^J(RR') = \sum_{M''} D_{M'M''}^J(R) D_{M''M}^J(R'), \quad (16.20)$$

where we have used the group property (16.17) of D -matrices. Comparing (16.20) with the definition (16.11) we see that, for fixed M , the functions $D_{M'M}^J(R)$ transform under rotations as the members $|JM'\rangle$ of the irreducible rotational representation. As functions $|JM'\rangle$, they should be orthogonal on the space defined by their arguments R ,

$$\int dR D_{M'M}^{J*}(R) D_{K'K}^J(R) = \delta_{JJ'} \delta_{M'K'} C_{MK}^J \quad (16.21)$$

where C_{MK} are some numbers and dR means a volume element in space of rotational parameters. To find the coefficients C_{MK}^J , we take $J' = J, K' = M'$, and sum over M' using the conjugation property (16.16):

$$\sum_{M'} \int dR D_{M'M}^{J*}(R) D_{M'K}^J(R) = \sum_{M'} \int dR D_{MM'}^J(R^{-1}) D_{M'K}^J(R) = (2J+1) C_{MK}^J. \quad (16.22)$$

The sum over M' gives the matrix product of mutually inverse matrices, Eq. (16.17), that is, the unit matrix, and the result is

$$C_{MK}^J = \delta_{MK} \frac{\int dR}{2J+1} \quad (16.23)$$

where $\int dR$ is the *group volume* depending on the explicit parameterization of rotations. Finally, we obtain the orthogonality condition

$$\int dR D_{M'M}^{J*}(R) D_{K'K}^J(R) = \delta_{JJ'} \delta_{M'K'} \delta_{MK} \frac{\int dR}{2J+1}. \quad (16.24)$$

With rotations described by the two angles of the axis \mathbf{n} and one polar angle of rotation around \mathbf{n} , we obtain

$$\int dR = \int d\mathbf{n} \times (2\pi) = 8\pi^2. \quad (16.25)$$

16.4 Euler Angles

A convenient explicit parameterization of rotations is connected with the Euler angles. The definitions of various authors differ in details, so one has to be careful in borrowing

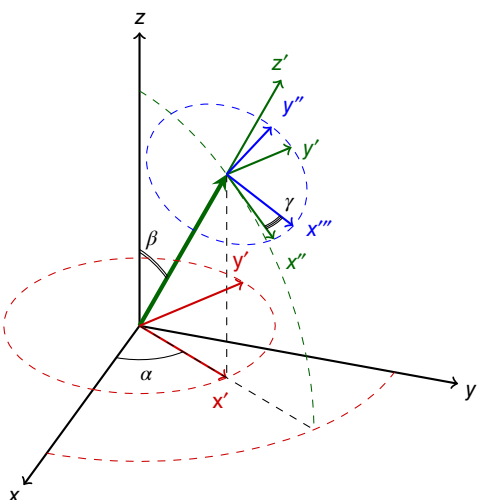


Figure 16.6 Illustration to the definition of Euler angles. The mobile (body-fixed) frame is formed by the axes (x', y', z') while the frame (x, y, z) (space-fixed) belongs to the laboratory.

equations from different sources, they can turn out to be incompatible. In the following, we use the system of notations adopted in Ref. [2]; see illustration in Figure 16.6.

We fix the origin and the space-fixed frame $S(x, y, z)$. It is characterized by the triplet of unit vectors $\mathbf{e}_{x,y,z}$. Let the body-fixed frame S' given by the triplet of unit vectors $\mathbf{e}^{(k)}$, $k = 1, 2, 3$, be combined initially with S . Both frames are assumed to be right handed. Any new orientation can be reached by the sequence of three rotations of the body-fixed frame considered as a rigid object. All rotations are performed in a positive (right-handed) direction.

First, we rotate in the xy -plane around the z -axis through an angle α that can take any value $0 \leq \alpha < 2\pi$. Then $\mathbf{e}^{(1)}$ and $\mathbf{e}^{(2)}$ take the directions x' and y' , respectively, and $\mathbf{e}^{(3)}$ still coincides with \mathbf{e}_z . The second rotation is made around the direction y' by an angle β that can be $0 \leq \beta < \pi$. The direction x' is transformed into x'' , while $\mathbf{e}^{(z)}$ takes the orientation z' that will be its final destination. Finally, we rotate by an angle γ , $0 \leq \gamma < 2\pi$, around the z' axis bringing the x'' and y' axes into their final positions $\mathbf{e}^{(1)}$ and $\mathbf{e}^{(2)}$, respectively. The Euler angles α, β, γ are the rotation parameters. The corresponding group volume to be used in the normalization (16.24) is again

$$\int dR = \int_0^{2\pi} d\gamma \int_0^\pi d\beta \sin \beta \int_0^{2\pi} d\alpha = 8\pi^2. \quad (16.26)$$

For half-integer spins, the representation of rotations by the D -functions is not single-valued because two matrices, $\pm D$, describe the same rotation. Indeed, for the angle 2π , $\exp(-i2\pi M) = -1$ if M is half-integer while physical rotations by α and $\alpha + 2\pi$ are identical. More precisely, this is a single-valued representation of the “covering” $SU(2)$ group that was mentioned in relation to isospin (Chapter 2). The representation can be made single-valued if only rotations α and $\alpha + 4\pi$ are considered as identical. For a major part of our applications, this does not lead to any significant difference.

The operator \mathbf{J} of total angular momentum of a system acts on the variables of the particles. To attach the frame S' to the body, we have to rotate the body in the same way.

The corresponding rotation operator is the product

$$R(\alpha, \beta, \gamma) = e^{-i\gamma J_z} e^{-i\beta J_y} e^{-i\alpha J_z}. \quad (16.27)$$

This can be converted into another form where all rotations are carried out around space-fixed axes only. Indeed, as any operator (16.13), the angular momentum components transform under rotations. After the first rotation $R_1 = \exp(-i\alpha J_z)$, the angular momentum J_y is transformed into $J_{y'}$ that has the same matrix elements in the new basis,

$$J_{y'} = R_1 J_y R_1^{-1} = e^{-i\alpha J_z} J_y e^{i\alpha J_z}. \quad (16.28)$$

The second rotation operator $R_2 = \exp(-i\beta J_{y'})$ results from the same transformation (16.28) applied to $\exp(-i\beta J_y)$. The operator $J_{z'}$ is the result of the second rotation R_2 only, because R_1 did not change this component,

$$J_{z'} = e^{-i\beta J_{y'}} J_z e^{i\beta J_{y'}}; \quad (16.29)$$

again the transformation of $\exp(-i\alpha J_{z'})$ follows from (16.29). Using (16.28) and (16.29) in (16.27), we come to the alternative representation that does not include the intermediate axis,

$$R(\alpha, \beta, \gamma) = e^{-i\alpha J_z} e^{-i\beta J_y} e^{-i\gamma J_z}. \quad (16.30)$$

The matrix elements of finite rotations (16.12) are now functions of the Euler angles,

$$D_{M'M}^J(\alpha, \beta, \gamma) = \langle JM' | e^{-i\alpha J_z} e^{-i\beta J_y} e^{-i\gamma J_z} | JM \rangle. \quad (16.31)$$

The inverse rotation corresponds to the set $(-\gamma, -\beta, -\alpha)$ of the Euler angles.

Using the obvious property (16.14) of rotations around the quantization axis, we come to

$$D_{M'M}^J(\alpha, \beta, \gamma) = e^{-iM'\alpha} d_{M'M}^J(\beta) e^{-iM\gamma} \quad (16.32)$$

where the only nontrivial angle dependence is concentrated in the function

$$d_{M'M}^J(\beta) = \langle JM' | e^{-i\beta J_y} | JM \rangle. \quad (16.33)$$

The representation introduced above is convenient because all matrices (16.33) are real owing to the standard (imaginary) choice of the matrix elements of J_y . At $\beta = \pi$, the same operator was used to define the time reversal operation. It follows from this definition that

$$d_{M'M}^J(\pi) = (-)^{J-M} \delta_{M', -M}. \quad (16.34)$$

Since d^J is a unitary real matrix, it follows that (d^J is a transposed matrix)

$$(d^J(\beta))^\dagger = (d^J(\beta))^T = (d^J(\beta))^{-1} = d^J(-\beta). \quad (16.35)$$

In matrix elements, this means

$$d_{MM'}^J(\beta) = d_{M'M}^J(-\beta). \quad (16.36)$$

A relation between the elements of d^J and $(d^J)^T$ can be derived in the following way (rotation by π around the z -axis changes the sign of J_y):

$$d_{M'M}^J(\beta) = \langle JM' | e^{i\pi J_z} e^{i\beta J_y} e^{-i\pi J_z} | JM \rangle = e^{i\pi(M'-M)} d_{M'M}^J(-\beta) = (-)^{M'-M} d_{MM'}^J(\beta), \quad (16.37)$$

where, in the last step, Eq. (16.36) was used. The \mathcal{T} -odd character of the angular momentum together with the selection rules $\Delta_M = \pm 1$ for J_y show that $\langle JM' | J_y | JM \rangle = -\langle J - M' | J_y | J - M \rangle$, which, of course, can be checked directly. This gives

$$d_{M'M}^J(\beta) = d_{-M',-M}^J(-\beta) = d_{-M,-M'}^J(\beta), \quad (16.38)$$

and, combined with the previous equation,

$$d_{M'M}^J(\beta) = (-)^{M'-M} d_{-M',-M}^J(\beta). \quad (16.39)$$

The d -functions can be calculated in a closed form (they are associated with Jacobi polynomials) constructing the system of $2J$ spins $1/2$ with total angular momentum J and rotating each constituent spin. We will not do it here; for complete information, see Ref. [3]. We just show the relation between the matrix elements of finite rotations $D_{M'M}^J(\alpha, \beta, \gamma)$ which are sometimes called *generalized spherical functions*, or Wigner functions, and the ordinary spherical functions $Y_{LM}(\theta, \varphi)$.

The spherical functions $Y_{LM}(\theta, \varphi)$ are determined on a sphere and they transform under rotations according to Eq. (16.11). Any direction $\mathbf{n}(\theta, \varphi)$ can be considered as a result of the rotation of the vector \mathbf{e}_z originally aligned along the polar axis,

$$\mathbf{n}(\theta, \varphi) = R(\varphi, \theta, 0)\mathbf{e}_z. \quad (16.40)$$

The same rotation can be presented as

$$\mathbf{n}(\theta, \varphi) = R^{-1}(0, -\theta, -\varphi)\mathbf{e}_z. \quad (16.41)$$

Therefore, a spherical function is

$$Y_{LM}(\mathbf{n}) = Y_{LM}(R^{-1}(0, -\theta, -\varphi)\mathbf{e}_z). \quad (16.42)$$

This is the same way of defining the function of the angles as in (16.18). Since the transformed function at any point has the same value as it had in the corresponding point before rotation,

$$R(0, -\theta, -\varphi)Y_{LM}(\mathbf{e}_z) = Y_{LM}(R^{-1}(0, -\theta, -\varphi)\mathbf{e}_z) = Y_{LM}(\mathbf{n}), \quad (16.43)$$

we explicitly relate the spherical functions with rotations parameterized by the Euler angles. On the other hand, the spherical functions transform in a normal way (16.11) as any eigenfunction $|LM\rangle$ of the angular momentum operator,

$$Y_{LM}(\mathbf{n}) = \sum_{M'} D_{M'M}^L(0, -\theta, -\varphi) Y_{LM'}(\mathbf{e}_z). \quad (16.44)$$

The values of spherical functions in the forward direction (\mathbf{e}_z) are well known; they do not vanish for $M' = 0$ only so that

$$Y_{LM}(\mathbf{n}) = \sqrt{\frac{2L+1}{4\pi}} D_{0M}^L(0, -\theta, -\varphi) = \sqrt{\frac{2L+1}{4\pi}} D_{M0}^{L*}(\varphi, \theta, 0) \quad (16.45)$$

where the conjugation property (16.16) was used. As is should be, spherical functions correspond to a particular case of rotations with two Euler angles. Equations (16.24) and (16.45) lead to the standard orthogonality of spherical functions.

16.5 Angular Momentum in Euler Angles

The advantage of using the Euler angles as new coordinates is the possibility to transfer all rotational properties onto the explicit dependence of the orientational wave function on those angles. This wave function determines the relative probabilities of various orientations of the body-fixed frame S' with respect to the space-fixed frame S . Since the frame S' always follows motion of the body, all intrinsic quantities referred to this frame are *scalars* which do not depend on orientation of the body in space. We discussed this separation of intrinsic and orientational variables in Section 12.5 in application to quadrupole shapes. A simpler prototype of this procedure is the standard separation of variables for a particle in a central field. We single out the angles θ, φ of the radius vector \mathbf{n} which is nothing but the vector $\mathbf{e}^{(3)}$ of the body-fixed frame (as we discussed, there are only two rather than three angles in this case). The orientational dependence is given by the universal spherical function $Y_{\ell m}(\mathbf{n})$. The remaining “intrinsic” variable is the length of the radius of the particle $r = (\mathbf{r} \cdot \mathbf{n})$ that is obviously defined in a “moving” frame and therefore is a scalar quantity. Unfortunately, there is no general recipe for explicitly separating the operators corresponding to the Euler angles in the general case of a *many-body* system.

We can find the angular momentum operator in the representation of Euler angles tracing the transformation of the unit vectors of the body-fixed frame under an arbitrary rotation. In the rotation by an angle γ around the space-fixed z -axis, the components (V_x, V_y, V_z) of a vector \mathbf{V} are transformed into (V'_x, V'_y, V'_z) according to a simple geometrical picture,

$$V'_x = V_x \cos \gamma - V_y \sin \gamma, \quad V'_y = V_y \cos \gamma + V_x \sin \gamma, \quad V'_z = V_z. \quad (16.46)$$

In the rotation by an angle β around the y -axis, we have

$$V'_x = V_x \cos \beta + V_z \sin \beta, \quad V'_y = V_y, \quad V'_z = V_z \cos \beta - V_x \sin \beta. \quad (16.47)$$

The third rotation is similar to the first one (16.46) with $\gamma \rightarrow \alpha$. The full result of the general rotation (16.30) is readily derived as the product of three steps.

In this way, we obtain the coordinates of the new basis vectors after they are rotated from the original position (coinciding with that of the space-fixed frame) to the instant orientation described by the Euler angles (α, β, γ) ,

$$\begin{aligned} \mathbf{e}^{(1)} &= \{c(\alpha)c(\beta)c(\gamma) - s(\alpha)s(\gamma), \quad c(\alpha)s(\gamma) + s(\alpha)c(\beta)c(\gamma), \quad -s(\beta)c(\gamma)\}, \\ \mathbf{e}^{(2)} &= \{-c(\alpha)c(\beta)s(\gamma) - s(\alpha)c(\gamma), \quad c(\alpha)c(\gamma) - s(\alpha)c(\beta)s(\gamma), \quad s(\beta)s(\gamma)\}, \\ \mathbf{e}^{(3)} &= \{c(\alpha)s(\beta), \quad s(\alpha)s(\beta), \quad c(\beta)\}. \end{aligned} \quad (16.48)$$

The meaning of the notations is evident: $c(\alpha) \equiv \cos \alpha, s(\alpha) \equiv \sin \alpha$, and so on. The triplet of body-fixed basic vectors is orthonormal,

$$(\mathbf{e}^{(j)} \cdot \mathbf{e}^{(k)}) = \delta_{jk}, \quad (16.49)$$

and right-handed,

$$[\mathbf{e}^{(j)} \times \mathbf{e}^{(k)}] = \epsilon_{jkl} \mathbf{e}^{(l)}. \quad (16.50)$$

Now it is a straightforward exercise to find the angular momentum operator $\hat{\mathbf{J}}$ in the representation of Euler angles. It transforms the components of any vector exactly as components of the angular momentum itself. In particular, components $e_m^{(j)}$ of $\mathbf{e}^{(j)}$ should transform among themselves,

$$[\hat{J}_l, e_m^{(j)}] = ie_{lmn} e_n^{(j)}. \quad (16.51)$$

It is clear that the angular momentum has to be a first-order differential operator with respect to the Euler angles, that is, a linear combination

$$\hat{J}_l = f_{l\alpha} \frac{\partial}{\partial \alpha} + f_{l\beta} \frac{\partial}{\partial \beta} + f_{l\gamma} \frac{\partial}{\partial \gamma}, \quad (16.52)$$

where the coefficients f are functions of the Euler angles which can be found from (16.49) and (16.51). As a result, we obtain

$$\begin{aligned} \hat{j}_x &= -\cos \alpha \cot \beta \frac{\partial}{\partial \alpha} - \sin \alpha \frac{\partial}{\partial \beta} + \frac{\cos \alpha}{\sin \beta} \frac{\partial}{\partial \gamma}, \\ \hat{j}_y &= -\sin \alpha \cot \beta \frac{\partial}{\partial \alpha} + \cos \alpha \frac{\partial}{\partial \beta} + \frac{\sin \alpha}{\sin \beta} \frac{\partial}{\partial \gamma}, \\ \hat{j}_z &= \frac{\partial}{\partial \alpha}. \end{aligned} \quad (16.53)$$

Of course, the commutation relations between the angular momentum components are automatically fulfilled. The operator of the squared angular momentum is, in these variables,

$$\hat{\mathbf{j}}^2 = - \left\{ \frac{1}{\sin \beta} \frac{\partial}{\partial \beta} \left(\sin \beta \frac{\partial}{\partial \beta} \right) + \frac{1}{\sin^2 \beta} \left(\frac{\partial^2}{\partial \alpha^2} + \frac{\partial^2}{\partial \gamma^2} \right) - 2 \frac{\cos \beta}{\sin^2 \beta} \frac{\partial^2}{\partial \alpha \partial \gamma} \right\}. \quad (16.54)$$

For the case of functions on a sphere, two Euler angles, $\beta \rightarrow \theta$ and $\alpha \rightarrow \varphi$, are sufficient. Then there is no γ -dependence, the corresponding derivative $\partial/\partial\gamma$ vanishes, and the angular momentum coincides with the textbook expression of the orbital momentum in terms of the polar angle θ and azimuthal angle φ .

We have at our disposal two frames, the space-fixed S and the body-fixed S' . The angular momentum $\hat{\mathbf{J}}$ derived above is a vector with the standard commutation relations between its components. We can also introduce the total angular momentum components referred to the *body-fixed* axes,

$$\hat{l}_i = (\hat{\mathbf{J}} \cdot \mathbf{e}^{(i)}). \quad (16.55)$$

These three operators are Hermitian and the order of the factors in the scalar products (16.55) is arbitrary because \hat{j}_k commute with components V_k of any vector \mathbf{V} along the same axis. Direct calculation with the aid of (16.49) and (16.53) gives

$$\begin{aligned} \hat{l}_1 &= -\frac{\cos \gamma}{\sin \beta} \frac{\partial}{\partial \alpha} + \sin \gamma \frac{\partial}{\partial \beta} + \cot \beta \cos \gamma \frac{\partial}{\partial \gamma}, \\ \hat{l}_2 &= \frac{\sin \gamma}{\sin \beta} \frac{\partial}{\partial \alpha} + \cos \gamma \frac{\partial}{\partial \beta} - \cot \beta \sin \gamma \frac{\partial}{\partial \gamma}, \\ \hat{l}_3 &= \frac{\partial}{\partial \gamma}. \end{aligned} \quad (16.56)$$

The simple relation between the two angular momentum operators is fulfilled,

$$\hat{I}_k(\alpha, \beta, \gamma) = [\hat{J}_k(-\gamma, -\beta, -\alpha)]^*. \quad (16.57)$$

It has the same geometrical meaning as the expression of the same physical rotation in two equivalent forms, (16.27) and (16.30). Of course, the angular momentum squared is the same in both frames,

$$\hat{\mathbf{J}}^2 = \sum_k (\hat{I}_k)^2. \quad (16.58)$$

The most important property of the operators (16.55) is that, with respect to rotations, they are *scalars* rather than components of a vector. It is clear that the scalar product of two vectors does not change under rotation. This follows formally from the commutation relations. Thus,

$$[\hat{J}_k, \hat{I}_l] = 0. \quad (16.59)$$

Using the definition (16.55) and the commutators (16.51), we obtain

$$[\hat{I}_l, e_k^{(n)}] = -ie_{lmn}e_k^{(m)} \quad (16.60)$$

(of course, components $e_k^{(n)}$ of the basic vectors commute among themselves). The operator \hat{I}_l is the generator of rotations around the body-fixed axis l . The sign in (16.60), opposite to that in (16.51), is connected to the fact that here we rotate not the body but the basic vectors of the same frame. Therefore, the transformation is actually a passive rotation, recall Eq. (16.14). This difference is seen in the result (16.60): the vector component $e_k^{(n)}$ acquires after rotation an admixture of the same component (k) of another vector $\mathbf{e}^{(m)}$, while in (16.51) it was an admixture of another component of the same vector. The same geometrical property is responsible for the relation (16.57).

Now we can calculate the commutator of two body-fixed components of the angular momentum,

$$[\hat{I}_l, \hat{I}_n] = [\hat{I}_l, \hat{J}_k e_k^{(n)}] = \hat{J}_k (-i) \epsilon_{lmn} e_k^{(m)} = -i \epsilon_{lmn} \hat{I}_m. \quad (16.61)$$

The resulting relation is quite similar to the normal one for the lab components of the angular momentum but differs in sign. We have almost the same algebra. It can be made identical to the algebra of the angular momentum in space-fixed axes by a substitution $\hat{I}_k = -\hat{I}'_k$, or by complex conjugation. Since in the standard representation only the y -component has imaginary matrix elements, it is enough to make a reflection in the xz -plane which changes $\hat{I}_2 \rightarrow -\hat{I}_2$. Then we simply interchange the lowering and raising operators. Only one of the projections in the body-fixed axes, say \hat{I}_3 , can have a certain value together with the magnitude (16.58) of the angular momentum.

We have to stress the difference between the angular momentum operators \hat{J}_k and \hat{I}_k acting on the Euler angles of the orientation of the body-fixed frame and the original angular momentum components J_k which act on variables of the particles in the system. The latter enter the general definitions (16.27) and (16.30) of the rotation operator of a physical system. Their commutation relations are the same regardless of the frame used for the calculations of their components, S or S' . To distinguish these operators, we introduced the hats in (16.51) and (16.55). We omit the hats if this does not cause any confusion.

16.6 Eigenfunctions of Angular Momentum

Describing a rotating body in terms of the Euler angles, we find the set of quantities which can have simultaneously certain values. The set includes two projections, \hat{J}_z and \hat{J}_3 , and the square of the angular momentum (16.58). The eigenvalues of these quantities are designated M, K and $J(J+1)$, respectively. Both projections, on the laboratory axis, M , and on the moving body-fixed axis, K , can vary between $-J$ and $+J$. The total number of possible states at a given J is $(2J+1)^2$.

In fact, we already know the functions of the Euler angles which are common eigenfunctions of all commuting operators. If R^{-1} is the rotation bringing the space-fixed frame \mathcal{O}_0 into the orientation \mathcal{O} characterized by the Euler angles (α, β, γ) , then the function (16.18),

$$\Phi_{MK}^J(\alpha, \beta, \gamma) = \sqrt{\frac{2J+1}{8\pi^2}} D_{KM}^J(-\gamma, -\beta, -\alpha) = \sqrt{\frac{2J+1}{8\pi^2}} D_{MK}^{J*}(\alpha, \beta, \gamma), \quad (16.62)$$

satisfies all the requirements. As was shown in (16.19), it is transformed according to the irreducible representation of the rotation group with angular momentum J from the explicit form (16.32), (16.36),

$$\Phi_{MK}^J(\alpha, \beta, \gamma) = \sqrt{\frac{2J+1}{8\pi^2}} e^{iK\gamma} e^{iM\alpha} d_{MK}^J(\beta). \quad (16.63)$$

The operator representations of the angular momentum components show that

$$\hat{J}_z \Phi_{MK}^J = M \Phi_{MK}^J, \quad \hat{J}_3 \Phi_{MK}^J = K \Phi_{MK}^J. \quad (16.64)$$

The functions (16.62) are normalized as [see (16.24)]

$$\int_0^{2\pi} d\alpha \int_0^\pi \sin \beta d\beta \int_0^{2\pi} d\gamma \Phi_{M'K'}^{J'*}(\alpha, \beta, \gamma) \Phi_{MK}^J(\alpha, \beta, \gamma) = \delta_{JJ'} \delta_{M'M} \delta_{K'K}. \quad (16.65)$$

Normal spherical functions, according to (16.45), are

$$Y_{LM}(\theta, \varphi) = \frac{1}{\sqrt{2\pi}} \Phi_{M0}^L(\varphi, \theta, 0), \quad (16.66)$$

where the normalization is taken with respect to the *three* Euler angles.

Let us go back to the definition (16.62) that can be written as

$$\Phi_{MK}^J(\alpha, \beta, \gamma) = \sqrt{\frac{2J+1}{8\pi^2}} \langle JK | e^{i\gamma J_z} e^{i\beta J_y} e^{i\alpha J_z} | JM \rangle. \quad (16.67)$$

According to the geometrical meaning of this definition, we take an initial state $|JM\rangle$ of the physical system and make a passive rotation of the frame combining its basis vectors with a certain orientation of the body-fixed vectors; projection onto $|JK\rangle$ determines the probability amplitude of getting the angular momentum component equal to K as required by (16.64). The operators J_k in the exponents are normal angular momentum components built as sums of angular momenta of all constituents. They act on the ket- and bra-vectors of a physical system rather than on the Euler angles that are parameters in this definition.

It is important that we now transfer the action of J_k from the particle variables onto the Euler angles; instead of rotating all the particles, we rotate the body-fixed frame attached to the system. The mutual equivalence of these operations is seen from (16.64):

$$\hat{J}_z \Phi_{MK}^J(\alpha, \beta, \gamma) = \sqrt{\frac{2J+1}{8\pi^2}} \langle JK|R(-\gamma, -\beta, -\alpha)J_z|JM\rangle, \quad (16.68)$$

$$\hat{J}_3 \Phi_{MK}^J(\alpha, \beta, \gamma) = \sqrt{\frac{2J+1}{8\pi^2}} \langle JK|J_zR(-\gamma, -\beta, -\alpha)|JM\rangle. \quad (16.69)$$

In the first case, we measure the angular momentum projection before the rotation of the frame and in the second, we measure it after the frame is rotated. Similar conclusions are valid for other components as well. For example,

$$\hat{J}_{\pm} \Phi_{MK}^J(\alpha, \beta, \gamma) = \sqrt{\frac{2J+1}{8\pi^2}} \langle JK|R(-\gamma, -\beta, -\alpha)J_{\pm}|JM\rangle, \quad (16.70)$$

$$\hat{J}_{\pm} \Phi_{MK}^J(\alpha, \beta, \gamma) = \sqrt{\frac{2J+1}{8\pi^2}} \langle JK|J_{\pm}R(-\gamma, -\beta, -\alpha)|JM\rangle. \quad (16.71)$$

The last equality means that the “raising” operator $\hat{J}_+ = \hat{J}_1 + i\hat{J}_2$ is in fact equivalent to the lowering operator $\hat{J}_+^\dagger = J_-$ acting on the bra-vector. This should be expected because of the specific algebra of operators \hat{J}_k [Eq. (16.61); see also the following sections].

16.7 Rigid Rotor

The simplest physical object for the application of general theory is a system with no intrinsic degrees of freedom. We can think of the perfect rigid body (a “top,” or rigid rotor) with intrinsic variables extremely weakly reacting to the noninertial effects of rotation. The coordinate origin is fixed at some point and the only dynamical variables are the Euler angles determining the orientation of the body, or the body-fixed frame, in space. The corresponding conjugate momenta are \hat{J}_k or \hat{l}_k .

The total angular momentum $\hat{\mathbf{J}}$ is a constant of motion if external forces are absent. We can choose an arbitrary space-fixed frame and take the states with certain values of J and $\hat{J}_z = M$. The Hamiltonian of the top has to be a scalar and therefore it cannot depend on the Euler angles (orientation of the top). However, it can be a function $H(\hat{J}_k)$ of scalar operators \hat{J}_k . These operators act only within the multiplet of the functions Φ_{MK}^J with given J as they commute with $\hat{\mathbf{J}}^2$. They commute as well with \hat{J}_z and cannot change M . However, the projection $\hat{J}_3 = K$ is not necessarily a constant of motion. The Hamiltonian matrix has, in general, a form $H'_{K'K}$ in the space of dimension $(2J+1)$ spanned, for given J and M , by the functions labeled by the values of K . As with any scalar, this matrix does not depend on M . Thus, the top dynamics are reduced to redistribution of the angular momentum between the body-fixed axes.

Additional information on the system may set some restrictions for the form of the Hamiltonian H . Time-reversal invariance and Hermiticity prevent appearance of terms with an odd number of factors \hat{J}_k . For instance, a linear term would be $\sum_k B_k \hat{J}_k$. To ensure

$H = H^\dagger$, the coefficients B_k have to be real, whereas for time-reversal invariance they have to be imaginary. The lowest nonvanishing term is *bilinear* in operators \hat{I}_k ,

$$H = A_{kl} \hat{I}_k \hat{I}_l, \quad (16.72)$$

with a *symmetric* matrix of coefficients $A_{kl} = A_{lk}$. An antisymmetric matrix would be equivalent to the commutator $[\hat{I}_k, \hat{I}_l]$ in (16.72) with the result linear in \hat{I} . A real symmetric matrix A_{kl} (inverse *inertia tensor*) can be transformed to its main axes which are most suitable for serving as those of the body-fixed frame. Then the Hamiltonian takes a standard form for the quantum top,

$$H = \sum_{k=1,2,3} A_k \hat{I}_k^2. \quad (16.73)$$

The numbers A_k are inverse values of the inertia tensor. They determine the *moments of inertia* along the main axes, the generalization of Eq. (16.5),

$$\mathcal{J}_k = \frac{\hbar^2}{2A_k}. \quad (16.74)$$

A comment might be appropriate here. A quantum top (rotor) can be considered as a good model for a physical system if it is *rigid* and, at least up to some excitation energy, one can neglect excitation of intrinsic degrees of freedom treating a rotating system as *structureless*. Even for a system with intrinsic structure, we can still use the top model if the rotation is adiabatic with respect to intrinsic excitations. The presence of the latter will be manifest as a change of the parameters of the rotational Hamiltonian along rotational bands. Such changes of the collective motion of a system as a whole can be gradual, being caused by excitation of individual particles or phonon modes. In this sense, the rotor model is useful for nuclear rotation.

The rotor is *symmetric* if all moments of inertia are equal, $A_k = A$. In this case, the Hamiltonian, owing to (16.58), is simply

$$H = AJ^2. \quad (16.75)$$

The energy spectrum consists of the multiplets $|JMK\rangle$ with degeneracy $(2J+1)^2$ and energies

$$E_J = AJ(J+1). \quad (16.76)$$

The corresponding wave functions in the Euler angle representation are Φ_{MK}^J , Eq. (19.62).

An *axially symmetric* case, with the intrinsic axis-3 as the symmetry axis, is also trivial. In this case, we have two equal rotational parameters, $A_1 = A_2 = A_\perp$ and $A_3 = A_\parallel$. Then $\hat{I}_3 = K$ is conserved, Φ_{MK}^J are still correct wave functions, but the multiplet is split in $|K|$,

$$\begin{aligned} E_{JK} &= \langle \Phi_{MK}^J | A_\perp (\hat{I}_1^2 + \hat{I}_2^2) + A_\parallel \hat{I}_3^2 | \Phi_{MK}^J \rangle = A_\perp [J(J+1) - K^2] + A_\parallel K^2 \\ &= A_\perp J(J+1) + (A_\parallel - A_\perp) K^2. \end{aligned} \quad (16.77)$$

The states are $2 \times (2J+1)$ -fold degenerate in M and sign of K , the latter being a consequence of time-reversal invariance.

For nuclear collective rotation, the moment of inertia along the symmetry axis, \mathcal{J}_3 , vanishes, $A_\parallel \rightarrow \infty$, and only the states with $K = 0$ have finite energy. Then the spectrum becomes that of a pure rotor (see Eqs (16.4) and (16.75) with $A = A_\perp$).

16.8 Symmetry Properties

Apart from rotational and time-reversal invariance, the general top Hamiltonian (16.73) displays *discrete symmetries* which subdivide the eigenstates into classes. We have here the same situation as the one discussed in Section 12.6. The choice of the main axes is not unique in the sense that a given quantum state can be described by different sets of the Euler angles. We have the same 24 symmetry operations as discussed in applications to quadrupole shapes (under restriction by right-handed frames (16.50)). Correspondingly, the Hamiltonian (16.73) is invariant under 24 discrete transformations of the basic triplet of unit vectors; they correspond to different Euler angles but the same physical orientation in space. Let us consider these symmetry properties for *integer J*. At *half-integer J*, the number of transformations is doubled because the rotation through 2π changes the sign of the wave function (this is the same as the negative sign of a fermion wave function under double time reversal).

It is convenient to express the symmetry transformations in terms of three basic ones, \mathcal{R}_1 , \mathcal{R}_2 , and \mathcal{R}_3 . The first is actually the time-reversal operation but in intrinsic axes,

$$\mathcal{R}_1 = e^{-i\pi\hat{l}_2}. \quad (16.78)$$

It transforms the axes according to $1 \rightarrow -1$, $2 \rightarrow 2$, $3 \rightarrow -3$; evidently, $\mathcal{R}_1^2 = 1$ for integer J . To find the transformation of Φ_{MK}^J under this operation, we convert \mathcal{R}_1 into its analog $\exp(-i\pi J_y)$ inside the matrix element with the help of (16.71), insert the complete set of states $|JK'\rangle$, and use (16.34). The result is

$$\mathcal{R}_1 \Phi_{MK}^J = (-)^{J+K} \Phi_{M-K}^J. \quad (16.79)$$

The second basic operation is the rotation around the 3-axis,

$$\mathcal{R}_2 = e^{-i(\pi/2)\hat{l}_3}. \quad (16.80)$$

Its action is trivial,

$$\mathcal{R}_2 \Phi_{MK}^J = e^{-i(\pi/2)K} \Phi_{MK}^J. \quad (16.81)$$

This operation transforms $1 \rightarrow 2$, $2 \rightarrow -1$, $3 \rightarrow 3$; whence, $\mathcal{R}_2^4 = 1$. The third basic operation \mathcal{R}_3 is taken as a cyclic permutation of the axes, $1 \rightarrow 2 \rightarrow 3 \rightarrow 1$. Therefore $\mathcal{R}_3^3 = 1$. An arbitrary symmetry transformation can be presented as

$$\mathcal{R} = \mathcal{R}_1^a \mathcal{R}_2^b \mathcal{R}_3^c \quad (16.82)$$

where $a = 1, 2$; $b = 1, 2, 3, 4$; $c = 1, 2, 3$.

For any set of the rotational constants A_k , the quantum top (16.73) is invariant with respect to the operations \mathcal{R}_1 and \mathcal{R}_2^2 which commute. Therefore, we can classify the eigenfunctions according to their behavior under these transformations. Let us call σ and ρ the eigenvalues of \mathcal{R}_1 and \mathcal{R}_2^2 , respectively. Since $\mathcal{R}_1^2 = \mathcal{R}_2^4 = 1$, these eigenvalues are $\sigma = \pm 1$ and $\rho = \pm 1$. All eigenfunctions are divided into four classes corresponding to four combinations of σ (called *signature*) and ρ . In group theory, these classes are designated as A, B₁, B₂, and B₃; the group itself is called D₂.

The angular momentum components \hat{l}_k have selection rules $\Delta K = 0, \pm 1$. Hence, the Hamiltonian (16.73) connects the states with $\Delta K = 0, \pm 2$ and conserves parity of K . As seen from (16.81), it is equivalent to the quantum number

$$\rho = e^{-i\pi K} = (-)^K. \quad (16.83)$$

Table 16.1 Symmetry classes of the D_2 group and corresponding combinations of other quantum numbers.

Class	σ	ρ	K	C_{-K}^J/C_K^J
A	+	+	Even	$(-)^J$
B ₁	-	+	Even	$(-)^{J+1}$
B ₂	+	-	Odd	$(-)^{J+1}$
B ₃	-	-	Odd	$(-)^J$

The classes of eigenstates and their characteristics are listed in Table 16.1.

16.9 Simplest Solutions

The eigenfunctions of the quantum top with quantum numbers of angular momentum J, M and discrete quantum numbers σ, ρ are superpositions

$$\Psi_M^J = \sum_{K=-J}^J C_K^J \Phi_{MK}^J. \quad (16.84)$$

The operation \mathcal{R}_1 , Eq. (16.79), gives

$$\mathcal{R}_1 \Psi_M^J = \sigma \Psi_M^J = \sum_K C_K^J (-)^{J+K} \Phi_{M-K}^J. \quad (16.85)$$

If this function has a certain value of ρ , Eq. (16.83), a number $(-)^K$ is the same for all components, and (16.85) can be rewritten as

$$\sigma \sum_K C_K^J \Phi_{MK}^J = \rho (-)^J \sum_K C_{-K}^J \Phi_{MK}^J. \quad (16.86)$$

We obtain the relation between the amplitudes C_K^J and C_{-K}^J of a given eigenfunctions stipulated by discrete symmetry,

$$C_{-K}^J = \rho \sigma (-)^J C_K^J = \sigma (-)^{J+K} C_K^J. \quad (16.87)$$

This is shown in the last column of Table 16.1.

The matrix elements of the Hamiltonian (16.73) in the basis of functions Φ_{MK}^J are

$$\langle \Phi_{MK}^J | H | \Phi_{MK}^J \rangle = \frac{1}{2}(A_1 + A_2)[J(J+1) - K^2] + A_3 K^2, \quad (16.88)$$

$$\langle \Phi_{MK}^J | H | \Phi_{MK+2}^J \rangle = \langle \Phi_{MK+2}^J | H | \Phi_{MK}^J \rangle \quad (16.89)$$

$$= \frac{1}{4}(A_1 - A_2) \sqrt{(J-K)(J-K-1)(J+K+1)(J+K+2)}.$$

In the axially symmetric case, $A_1 = A_2$, (16.88) reduces to (16.77), and off-diagonal elements (16.89) disappear owing to the conservation of the K quantum number. We can explicitly find the solutions for the lowest values of angular momentum when one does not need any numerical diagonalization (that is also straightforward).

At $J = 0$, we have $K = 0$, that is, classes A and B_1 are formally allowed but the function of the B_1 type vanishes, $C_0^0 = -C_0^0 = 0$. The only possible wave function $\Psi_0^0 = \Phi_{00}^0$ does not depend on the angles and belongs to the class A; its energy $E_0 = 0$.

At $J = 1$, the allowed values are $K = 0, \pm 1$. A state with $K = 0$ can belong to the classes A or B_1 while states with $|K| = 1$ can get into classes B_2 and B_3 . In the class A states, $K = 0$ with odd J are forbidden so that three states remain as it should be for $J = 1$. With the help of the symmetry conditions, we find

$$\begin{aligned} B_1 : \quad & \Psi_M^1 = \Phi_{M0}^1, \\ B_2 : \quad & \Psi_M^1 = \frac{1}{\sqrt{2}} (\Phi_{M1}^1 + \Phi_{M-1}^1), \\ B_3 : \quad & \Psi_M^1 = \frac{1}{\sqrt{2}} (\Phi_{M1}^1 - \Phi_{M-1}^1). \end{aligned} \quad (16.90)$$

The energies (16.75) of these states are

$$E_1(B_1) = A_1 + A_2, \quad E_1(B_2) = A_1 + A_3, \quad E_1(B_3) = A_2 + A_3. \quad (16.91)$$

At spherical or axial symmetry of the inertia tensor, we come back to (16.76) and (16.77), respectively. Energy eigenvalues of the class B_1 states are symmetric under the permutation $1 \leftrightarrow 2$, whereas energies of the states of the B_2 and B_3 types can be obtained from the energy of the B_1 type by the substitutions $2 \leftrightarrow 3$ and $1 \leftrightarrow 3$, respectively. This is a general property of spectra for any value of J .

Problem 16.2 Consider a quantum top with arbitrary inertial parameters $A_{1,2,3}$.

- a) Find the wave functions and energies of all states with angular momentum $J = 2$.
- b) Show that the state of class A with $J = 3$ is unique and find its energy. Show that energy of this state satisfies $E(3) = E(2_1) + E(2_2)$, where $2_{1,2}$ are $J = 2$ states, part a, belonging to the same class A.
- c) Consider the semiclassical case of large angular momentum $J \gg 1$. Let the axis 3 correspond to the largest moment of inertia, $A_3 < A_1, A_2$. What is the state with minimum energy at given J ("yrast state")?
- d) Write down the exact operator Heisenberg equations of motion for the angular momentum components \hat{l}_k . Compare these equations with the Euler equations for a classical top (look at the textbook [4] in classical mechanics if necessary).
- e) The operator equations of motion are nonlinear. Perform approximate linearization, substituting the component \hat{l}_3 in equations for \hat{l}_1 and \hat{l}_2 by a constant equal to its value in the yrast state of point c. Show that, as a result, you obtain a harmonic oscillator corresponding to small vibrations of the transverse components of the angular momentum. Find the frequency of oscillations (*wobbling* motion).

16.10 Ground-State Band

Accumulating some experience in basic models we can try to consider realistic examples. In well-deformed nuclei, rotation is *adiabatic* with respect to intrinsic excitations and we can start with the approximation of an isolated rotational band

(Section 16.1). Experimental data show that deformed even–even nuclei, as a rule, have *axially symmetric* shape. The low-lying excitations correspond to collective rotation that is possible only around the axis perpendicular to the symmetry axis 3. Thus we come to the case of the effective rotor with $A_3 \rightarrow \infty$.

Owing to pairing, there is no uncompensated intrinsic angular momenta in the ground state of an even–even system. Therefore, here $K = 0$. A collective rotational band contains the states with different J but close intrinsic structure, supposedly a specific configuration of particles in the mean field. This configuration may smoothly change adjusting itself to the increasing angular momentum through admixtures of other configurations. As we will see later, the mechanism of adjustment is provided by the Coriolis and centrifugal effects. For the ground-state band, these noninertial forces distort nucleon pairs creating the necessary angular momentum. Rotation around a perpendicular axis destroys axial symmetry. Therefore, the states with $J \neq 0$ in general acquire some admixtures of $K \neq 0$. However, the admixtures are small at not very high J , so we can in the first approximation label the ground-state band as the $K = 0$ band.

For $K = 0$, only states of class A with even J and the states of class B_1 with odd J are possible; see Table 16.1. Which case takes place, in reality, depends on the *intrinsic wave function* $\chi_{K=0}$ that should be specified. We have to combine intrinsic symmetry with symmetry of the rotor states to get a total single-valued wave function

$$\Psi_M^J = \Phi_{M0}^J \chi_{K=0} \propto Y_{JM} \chi_{K=0}. \quad (16.92)$$

It is simple for the ground-state band. The quadrupole deformation has a center of symmetry so that the wave function has certain parity, a product of rotational parity $(-)^J$ and parity of the intrinsic wave function that is positive for the paired ground state. For $K = 0$, parity coincides with the signature (16.79). The possible level sequences J^π in the ground-state band are therefore

$$\text{class A: } 0^+, 2^+, 4^+, \dots \quad \text{or} \quad \text{class } B_1 : \quad 1^-, 3^-, 5^-, \dots \quad (16.93)$$

The ground states of all even–even nuclei are completely paired – this selects the first option. The nucleus is symmetric under reflection in the plane perpendicular to the symmetry axis, analogously to the spectra of diatomic molecules with identical nuclei.

For the ideal rotor, we would have the energy spectrum (16.76) with characteristic level ratios

$$E_2 : E_4 : E_6 : E_8 \cdots = 1 : \frac{10}{3} : 7 : 12 \cdots \quad (16.94)$$

All nuclei selected for Figure 16.3 show spectra that are very close to (16.76). A typical example of ground-state band is seen in Figure 16.1. The energies of the 2^+ levels and other levels in the sequence allow for extraction of the moment of inertia.

16.11 Intensity Rules

After the global nuclear variables are subdivided into intrinsic ones and Euler orientation angles, we have to manipulate the observable physical quantities in the same way. It is sufficient to transform the multipole moments. In fact, we already did it for the quadrupole moment in our search for invariant deformation parameters (Section 12.5).

The general procedure is straightforward. The multipole moments $\mathcal{M}_{\lambda\mu}$ transform under rotations as indicated in (16.27). For rotation characterized by the angles (α, β, γ) , the transformation of tensor operators is

$$\mathcal{M}'_{\lambda\kappa} = \sum_{\mu} D_{\mu\kappa}^{\lambda}(\alpha, \beta, \gamma) \mathcal{M}_{\lambda\mu}. \quad (16.95)$$

The inverse expression can be found with the help of Eqs. (16.16) and (16.17),

$$\mathcal{M}_{\lambda\mu} = \sum_{\kappa} D_{\kappa\mu}^{\lambda}(-\gamma, -\beta, -\alpha) \mathcal{M}'_{\lambda\kappa}. \quad (16.96)$$

This gives the desired representation: an original operator \mathcal{M} contains the D -functions depending on the Euler angles and the intrinsic part \mathcal{M}' acting on the particle variables in the intrinsic frame. In particular, at $\mu = 0$, the D -functions do not depend on angle α , and we obtain the spherical functions

$$Y_{\lambda 0}(\theta) = \sum_{\kappa} D_{\kappa 0}^{\lambda}(-\gamma, -\beta, 0) Y_{\lambda\kappa}(\theta', \varphi'), \quad (16.97)$$

or, using (16.45),

$$Y_{\lambda 0}(\theta) = \sqrt{\frac{4\pi}{2\lambda + 1}} \sum_{\kappa} Y_{\lambda\kappa}^*(-\beta, -\gamma) Y_{\lambda\kappa}(\theta', \varphi'). \quad (16.98)$$

We come to the known *addition theorem*: the left-hand side of (16.98) is proportional to the Legendre polynomial $P_{\lambda}(\cos \theta)$ of the angle between the direction $\mathbf{n}'(\theta', \varphi')$ labeled by the angles in the body-fixed frame S' and the direction \mathbf{n}_0 that has angles $-\beta, -\gamma$ in the same frame and therefore is just a polar axis of the original frame S . θ is the polar angle of \mathbf{n} in the frame S that agrees with the geometrical meaning of the addition theorem.

Let a wave function of the system be represented by a product of the orientational and intrinsic parts [an example was given in Eq. (16.92) for the ground-state band],

$$\Psi_{MK}^J(\xi) = \Phi_{MK}^J(\alpha, \beta, \gamma) \chi_{JK}(\xi') \quad (16.99)$$

where ξ is a set of all variables and ξ' include only intrinsic variables invariant under rotations. In the adiabatic approximation, $\chi(\xi')$ does not depend on J being the same for all members of the band. According to (16.96), the matrix element of the multipole operator between two states (16.99) is given by

$$\langle \Psi_{M'K'}^{J'} | \mathcal{M}_{\lambda\mu} | \Psi_{MK}^J \rangle = \sum_{\kappa} \langle \Phi_{M'K'}^{J'} | D_{\kappa\mu}^{\lambda} | \Phi_{MK}^J \rangle \langle \chi_{J'K'} | \mathcal{M}'_{\lambda\kappa} | \chi_{JK} \rangle. \quad (16.100)$$

The orientational matrix element is *universal*, being determined exclusively by the rotational properties of the wave functions, similar to the Wigner–Eckart theorem. Using notation $R \equiv R(-\gamma, -\beta, -\alpha)$, we have

$$\langle \Phi_{M'K'}^{J'} | D_{\kappa\mu}^{\lambda} | \Phi_{MK}^J \rangle = \frac{\sqrt{(2J+1)(2J'+1)}}{8\pi^2} \int dR D_{K'M'}^{J'*}(R) D_{\kappa\mu}^{\lambda}(R) D_{KM}^J(R). \quad (16.101)$$

We can use arguments similar to those above for calculating this integral. The product of two D -functions is again the function of the Euler angles that can be expanded in terms of the D -functions. The angular momenta of two subsystems have to be coupled in agreement with the triangle conditions and with the algebraic addition of both

projections, \hat{J}_z and \hat{l}_3 . This dictates the form of the expansion,

$$D_{\kappa\mu}^{\lambda} D_{KM}^J = \sum_{J'K'M'} x(J'; \lambda J) C_{\lambda\kappa JK}^{J'K'} C_{\lambda\mu JM}^{J'M'} D_{K'M'}^{J'}. \quad (16.102)$$

Taking a particular case of the spherical functions (16.45) we see that all the coefficients $x(J'; \lambda J) = 1$. This, together with the orthogonality condition (16.24), (16.26), determines the integral of three D -functions,

$$\int dR D_{K'M'}^{J'*} D_{\kappa\mu}^{\lambda} D_{KM}^J = \frac{8\pi^2}{2J'+1} C_{\lambda\kappa JK}^{J'K'} C_{\lambda\mu JM}^{J'M'}. \quad (16.103)$$

This can be expressed in the form symmetric with respect to all three D -functions if one uses $3j$ -symbols instead of the Clebsch–Gordan coefficients. Substituting this universal result into (16.100), we obtain the matrix elements of the multipole operators,

$$\langle \Psi_{M'K'}^{J'} | \mathcal{M}_{\lambda\mu} | \Psi_{MK}^J \rangle = C_{\lambda\mu JM}^{J'M'} \sqrt{\frac{2J+1}{2J'+1}} \sum_{\mu} C_{\lambda\kappa JK}^{J'K'} \langle \chi_{J'K'} | \mathcal{M}'_{\lambda\kappa} | \chi_{JK} \rangle. \quad (16.104)$$

The first Clebsch–Gordan coefficient with the space-fixed projections expresses the requirement of the Wigner–Eckart theorem, while the rest plays the role of the reduced matrix element and contains all intrinsic dynamics. When applied to nuclear rotational bands, relations (16.104) are called Alaga intensity rules.

Along with the standard selection rules for J and M , we have here additional restrictions related to the K quantum number, $|\Delta K| = \mu \leq \lambda$. There exist isomer states with transitions hindered just by a large difference ΔK . A classical example is given by the state 8^- in ^{178}Hf that decays by E1 radiation to the state 8^+ but has a lifetime of 5.5 h. This transition is *K-forbidden* because the final state belongs to the ground-state rotational band with $K = 0$, whereas the initial excited state supposedly has excited quasiparticles with $K = 8$. The emitted gamma-quant has to carry away $\Delta K = 8$ and therefore have a high multipolarity $\lambda \geq 8$ that would make the transition improbable, if K were an exact constant of motion. However, Coriolis forces acting on the particles in the body-fixed frame violate axial symmetry and induce admixtures of the states with different K . Still the admixture of higher K to the state $8^+, K = 0$ is very small that explains the existence of the isomer. Even more impressive is the example [5] of the isomer excited state in the odd–odd nucleus ^{180}Ta that has a lifetime of 10^{15} years being the rarest naturally existing isotope on the Earth. The long lifetime is explained by the combination of a large difference between the K quantum numbers of this state, $K = 9$, and of the ground state, $K = 1$, and a very small excitation energy of only 75 keV that makes the gamma-transition of high multipolarity practically impossible. The question of K -mixing in excited states and its dependence on excitation energy is far from being solved [6].

The matrix elements within a given band built on a fixed intrinsic configuration χ_K are given by

$$\langle \Psi_{M'K'}^{J'} | \mathcal{M}_{\lambda\mu} | \Psi_{MK}^J \rangle = C_{\lambda\mu JM}^{J'M'} C_{\lambda 0 JK}^{J'K'} \sqrt{\frac{2J+1}{2J'+1}} \langle \chi_K | \mathcal{M}'_{\lambda 0} | \chi_K \rangle. \quad (16.105)$$

16.12 Electric Quadrupole Moment

The general expression (16.105) applied to the electric quadrupole moment determines both amplitudes of the E2 transitions within the rotational band and expectation values of the quadrupole moment for a given state of the band. Their interrelation is a remarkable feature of the rotational band built on a given deformed configuration. As a consequence of the common intrinsic state for all band members, diagonal as well as off-diagonal matrix elements are expressed in terms of the same *intrinsic quadrupole moment*

$$Q_0 = \langle \chi_K | Q'_{20} | \chi_K \rangle. \quad (16.106)$$

The tabular quadrupole moment for the band member with the angular momentum J is, by definition, taken for $M = J$,

$$Q(J) = C_{20J}^{JJ} C_{20JK}^{JK} Q_0. \quad (16.107)$$

A direct substitution of the Clebsch–Gordan coefficients leads to the final result

$$Q(J) = \frac{3K^2 - J(J+1)}{(J+1)(2J+3)} Q_0 \quad (16.108)$$

that can be also obtained by a simple derivation similar to the calculation of the single-particle quadrupole moment in Section 9.4.

Problem 16.3 Prove the result (16.108) without tables of Clebsch–Gordan coefficients at hand.

Solution

The effective quadrupole tensor within the multiplet of states with given J can be expressed in terms of the angular momentum components,

$$Q_{ik} = \frac{3Q(J)}{2J(2J-1)} \left(J_i J_k + J_k J_i - \frac{2}{3} \delta_{ik} \mathbf{J}^2 \right), \quad (16.109)$$

where the value $Q(J) = \langle JM = J | Q_{zz} | JM = J \rangle$ is the tabular number sought. In the body-fixed frame of an axially symmetric nucleus, the only available vector is that of the symmetry axis $\mathbf{e}^{(3)}$. Therefore, the symmetric traceless tensor of quadrupole moment has the form

$$Q_{ik} = b(3\mathbf{e}_i^{(3)}\mathbf{e}_k^{(3)} - \delta_{ik}). \quad (16.110)$$

The constant is defined by the intrinsic quadrupole moment (16.106), the component Q_{33} ,

$$Q_0 = Q_{33} = \mathbf{e}_i^{(3)} Q_{ik} \mathbf{e}_k^{(3)} = 2b. \quad (16.111)$$

Now, similar to (9.28), we consider the combination

$$A(J) = J_i Q_{ik} J_k = \frac{Q_0}{2} [3K^2 - J(J+1)], \quad (16.112)$$

where $K = I_3 = (\mathbf{J} \cdot \mathbf{e}^{(3)})$ is substituted. Since the multiplication by the components of \mathbf{J} still leaves us within the multiplet, we can make the same combination (16.112) using the space-fixed representation (16.109). Repeating the steps of Problem 9.2, we obtain

$$A(J) = \frac{1}{2} Q(J)(J+1)(2J+3). \quad (16.113)$$

Comparison of (16.113) with (16.112) results in (16.108).

In the ground-state band of an even–even nucleus, $K = 0$, the observable quadrupole moment has an opposite sign with respect to the intrinsic quadrupole moment,

$$Q(J) = -\frac{J}{2J+3} Q_0. \quad (16.114)$$

The origin of the negative sign is clear from the semiclassical picture of rotation ($J_z = J$) around the axis perpendicular to the symmetry axis: elongation along the 3-axis leads to the concentration in the equatorial plane for the rotation around the 1-axis. As it should be, the result disappears for $J = 0$ (of course, $J = 1/2$ is impossible for integer K). In the classical limit of $J \gg 1$, the quadrupole moment is $Q(J) = -(1/2)Q_0$. This means that two perpendicular components have certain values equal to $Q_{11} = Q_{22} = -Q_0/2$ as the tensor is traceless. A rotational band of an axially symmetric nucleus starts at the

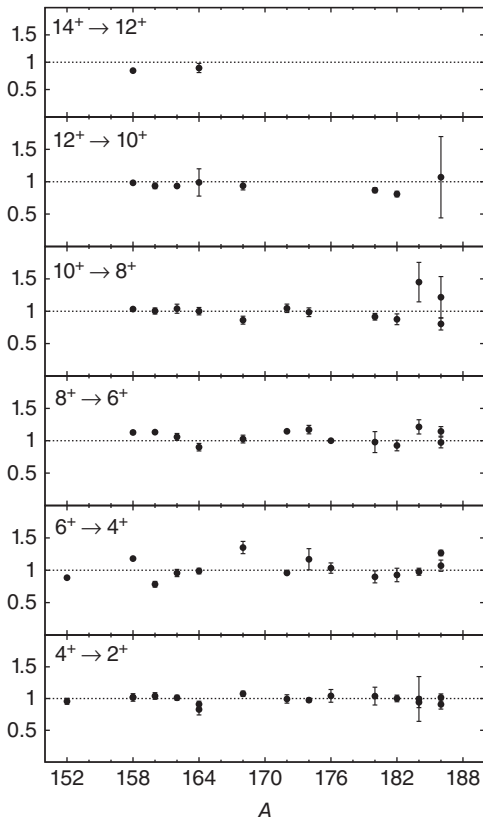


Figure 16.7 Reduced transition probabilities in units of the rotational value (16.116) for various E2 transitions in the ground-state bands of rare earth nuclei. The value of Q_0 is determined from the $B(E2, 2^+ \rightarrow 0^+)$ rate.

bandhead state $J = K$. For such a state

$$Q(J) = \frac{J(2J-1)}{(J+1)(2J+3)} Q_0. \quad (16.115)$$

In agreement with general selection rules, the quadrupole moment disappears for $J = 0$ and $J = 1/2$. The *projecting factor* from the body-fixed frame to the space-fixed one reflects quantum fluctuations which diminish the observed value. However, $Q(J)$ has the same sign and gradually approaches the intrinsic value in the classical limit of large J . Note the difference with the case $K = 0, J \neq 0$ of Eq. (16.114).

If the Alaga rules are valid, the same parameter of intrinsic quadrupole moment Q_0 determines the transition probabilities of gamma-cascades within the rotational band. Using the definition of the reduced transition probability and relation between the multipole moment $\mathcal{M}(\text{E2})$ and the quadrupole moment operator, we get from (16.105)

$$B(\text{E2}; J_i \rightarrow J_f) = \frac{5}{16\pi} e^2 Q_0^2 \left(C_{20J_iK}^{J_f K} \right)^2. \quad (16.116)$$

Thus, the intrinsic quadrupole moment can be measured both with the experiments using external fields (e.g., by the electric quadrupole hyperfine structure of atomic or molecular spectra [QP, I, 23.8]) and with the measurement of lifetimes in the gamma cascade. Figure 16.7 gives an idea of how well the rotational model based on a single intrinsic state reproduces the data in the yrast bands of deformed rare earth nuclei. The same quadrupole moment determines the transition probability in the processes such as Coulomb excitation (Section 15.8).

Problem 16.4 For a nucleus with triaxially deformed shape, using the shape variables (12.29) and expressing the electric quadrupole moment in terms of these variables (5.28), we arrive at the intrinsic quadrupole moment in the form

$$\mathcal{M}'_{20} = \mathcal{M}_0 \cos \gamma, \quad \mathcal{M}'_{2\pm 2} = \mathcal{M}_0 \frac{\sin \gamma}{\sqrt{2}}, \quad (16.117)$$

where

$$\mathcal{M}_0 = \sqrt{\frac{5}{16\pi}} Q_0 = \frac{3}{4\pi} Z e R_0^2 \beta, \quad (16.118)$$

and β and γ are deformation parameters (not to be confused with Euler angles). Our discussion related to the mass distributions (12.54)–(12.56) suggests an independent kinetic triaxiality parameter

$$\tan(\Gamma) = \frac{\sqrt{3}(A_1 - A_2)}{2A_3 - A_1 - A_2}. \quad (16.119)$$

- a) Show that $\Gamma/2$ is the mixing angle between $K = 0$ and $K = 2$ components of two states with $J = 2$.
- b) Show that in a rectangular triangle, where the catheti are given by the lengths of E2 matrix elements $0 \rightarrow 2_1$ and $0 \rightarrow 2_2$, the angle is $\gamma + \Gamma/2$. This gives the transition rate ratio as

$$\tan^2(\gamma + \Gamma/2) = \frac{B(\text{E2}; 2_2 \rightarrow 0)}{B(\text{E2}; 2_1 \rightarrow 0)}. \quad (16.120)$$

- c) If a rectangular triangle is formed where one cathetus is given by the off-diagonal matrix element of the quadrupole moment between the 2_1 and 2_2 states, and the other one is represented by the length of the diagonal matrix element (note that the lab quadrupole moments of the 2_1 and 2_2 states are equal but opposite in sign), then the angle opposite to the off-diagonal matrix element is $\gamma - \Gamma$,

$$\tan^2(\gamma - \Gamma) = \frac{B(E2; 2_2 \rightarrow 2_1)}{B(E2; 2_1 \rightarrow 2_1)}. \quad (16.121)$$

16.13 Magnetic Moment

For calculating the magnetic moment of a rotating nucleus, it is usually assumed that we can subdivide the system into a “core,” that creates the rotating deformed field, and the valence particle, or particles. This *particle(s) + rotor* model is a generalization of the deformed shell model where we worked in the intrinsic frame associated with the static deformed field – now the core can rotate. We denote the angular momentum of the core (rotor) as \mathbf{R} . The total angular momentum of the system is

$$\mathbf{J} = \mathbf{R} + \mathbf{j} \quad (16.122)$$

where \mathbf{j} is the angular momentum of the particle (or several valence particles).

In accordance with the decomposition of the angular momentum (16.122), the magnetic moment operator can be presented as the sum of two contributions, each with the specific gyromagnetic ratio,

$$\boldsymbol{\mu} = g_R \mathbf{R} + g_j \mathbf{j} = g_R \mathbf{J} + (g_j - g_R) \mathbf{j}. \quad (16.123)$$

In the rotational band of an axially symmetric nucleus, the effective operator \mathbf{j} is directed along the symmetry axis $\mathbf{e}^{(3)}$ – compare the similar arguments for the quadrupole moment (16.110). Its projection onto the symmetry axis is $j_3 = K$, so we put ($g_j \rightarrow g_K$)

$$\mathbf{j} = K \mathbf{e}^{(3)} \Leftrightarrow \boldsymbol{\mu} = g_R \mathbf{R} + g_K K \mathbf{e}^{(3)}. \quad (16.124)$$

Using (16.122) and the vector model, this can be reduced to

$$\boldsymbol{\mu} = (g_K - g_R) K \mathbf{e}^{(3)} + g_R \mathbf{J} = \left[(g_K - g_R) K \frac{(\mathbf{e}^{(3)} \cdot \mathbf{J})}{J(J+1)} + g_R \right] \mathbf{J}. \quad (16.125)$$

For the rotation around the perpendicular axis, $(\mathbf{R} \cdot \mathbf{e}^{(3)}) = 0$ and $(\mathbf{J} \cdot \mathbf{e}^{(3)}) = K$. Then the expectation value of the magnetic moment is given by the z -component of (16.125) for $J_z = M = J$,

$$\mu(J) = [(g_K - g_R) \frac{K^2}{J(J+1)} + g_R] J. \quad (16.126)$$

In particular, for the bandhead state $J = K$, the result is

$$\mu = g_K J - (g_K - g_R) \frac{J}{J+1}. \quad (16.127)$$

As follows from (16.123), the probabilities of M1 gamma-transitions between the levels of the band are proportional to $(g_K - g_R)^2$ because the total angular momentum

\mathbf{J} does not induce transitions. Combined information on the static magnetic moments and transition probabilities [plus an assumption about the sign of $(g_K - g_R)$] allows one to determine both gyromagnetic ratios. The valence part g_K can be calculated in the deformed shell model. The rotor part g_R is due to the current generated by collective rotation and also requires a microscopic model for its calculation. It is frequently assumed instead that this contribution is determined simply by the ratio of the total charge to the total mass, $g_R \approx Z/A$. This assumption is not seriously justified.

16.14 Symmetry Properties Revisited

The main feature of our picture of rotational bands in axially symmetric nuclei is that of adiabaticity of rotation: intrinsic degrees of freedom with relatively high typical frequencies of motion follow rotation of the axially deformed field described using the Euler angles. Therefore, the wave function is a product of the type (16.99) of the rotational function, which is, in fact, the Wigner D -function (16.62), and the intrinsic function is expressed in terms of scalar variables referred to the body-fixed frame.

The total angular momentum (16.122) rotates simultaneously the body-fixed frame (\mathbf{R}) and the intrinsic degrees of freedom. The intrinsic wave function in body-fixed variables is rotationally invariant. The operator $\hat{\mathbf{j}}$ acts therefore only on the Euler angles. The intrinsic angular momentum \mathbf{j} acts on the function χ_K . Its body-fixed components j_k satisfy normal angular momentum commutation relations and commute with the total angular momentum J_i . As for the total momentum \mathbf{J} , its space-fixed components J_k satisfy similar relations, whereas the body-fixed components I_k , Eq. (16.55), satisfy the commutators (16.61) with the opposite sign.

Rotation of the axially symmetric field around the symmetry axis cannot change the wave function (16.99). This means that

$$R_3 \Psi_{MK}^J = (\hat{I}_3 \Phi_{MK}^J) \chi_K - \Phi_{MK}^J (j_3 \chi_K) = 0. \quad (16.128)$$

Therefore, the intrinsic projection j_3 , usually called Ω (we prefer the notation m), is equal to K , which we have already taken into account in our notations (16.99).

The next symmetry operation is the *reflection* in the plane perpendicular to the symmetry axis. This is the operator \mathcal{R}_1 that was considered for a structureless rotor in (16.78). Its action on the rotational part Φ_{MK}^J is given by (16.79). However, it acts in a similar way on the intrinsic function as well. Let the intrinsic function χ_K be a superposition of the wave functions χ_{jK} of the *spherical* shell model corresponding to certain values of the angular momentum j . Then, similar to (16.81),

$$\mathcal{R}_1 \chi_K = \mathcal{R}_1 \sum C_j \chi_{jK} = \sum C_j (-)^{j+K} \chi_{j-K}, \quad (16.129)$$

or considering $(-\hat{j})$ as an operator that gives a phase factor $(-)^j$ to the corresponding spherical components,

$$\mathcal{R}_1 \Psi_{MK}^J = (-)^{J-\hat{j}} \Psi_{M-K}^J. \quad (16.130)$$

The invariance under the transformation \mathcal{R}_1 holds if the state is a combination, similar to the class A states of the top (Table 16.1),

$$\Psi_{JMK} = \frac{1}{\sqrt{2}} [\Psi_{MK}^J + (-)^{J-\hat{j}} \Psi_{M-K}^J]. \quad (16.131)$$

Thus, the subscript K of the total wave function

$$\Psi_{JMK} = \sqrt{\frac{2J+1}{16\pi^2}} [\Phi'_{MK}\chi_K + (-)^{J-j}\Phi'_{M-K}\chi_{-K}] \quad (16.132)$$

actually describes the linear combination of the components $\pm K$ that can lead to specific interference phenomena. In this case, parity of the orientational wave function coincides with the signature R_1 and is therefore positive. The total parity is that of the intrinsic function χ_K . The functions (16.132) with different $J = K, K+1, \dots$ form the rotational band with the common intrinsic function χ_K .

A special case corresponds to $K = 0$ when the wave function contains one term only. The invariance under R_1 requires, according to (16.130), that $(-)^{J-j}$ be an even number. Exactly as for the top, Eq. (16.93), two bands are possible, for even or odd states.

A new situation arises in the case when the intrinsic deformation has components of odd multipoles. There are indications that this is the case in nuclei such as ^{232}Th where octupole, $L = 3$, deformation is present in addition to quadrupole deformation. The intrinsic shape is *pearlike*. In the framework of the shell model, this can be interpreted as a component consisting of the doubly magic core ^{208}Pb and an additional cluster. Similar factors are responsible for *asymmetric fission* of many heavy nuclei when pear-shaped configurations present an important stage of the process. In such cases, the property of R_1 -invariance is lost. We have two nonidentical configurations, “right”- and “left”-oriented, similar to that in a diatomic molecule with *different nuclei*. These configurations have no definite parity.

To restore correct parity, we have to make linear combinations of the pear-shaped configurations with different orientations. It is possible because obviously these intrinsic adiabatic configurations are degenerate in energy. The way to construct proper combinations with parities (\pm) is explained in detail in Ref. [7]. In this approximation, we have degenerate *parity doublets*, a pair of states with the same J and both parity values. But nonadiabatic effects can mix the intrinsic states with opposite orientation. One can imagine a process of tunneling of the cluster that transforms the right pear into the left one. The same effect follows from the Coriolis forces. As a result, the doublets are split in energy. A similar phenomenon is known from elementary quantum mechanics. Consider a symmetric double potential well with a high barrier between the left and right minima. Neglecting the tunneling, we get the identical parallel sets of levels in isolated wells. The tunneling splits levels in pairs of the stationary states corresponding to (\pm) combinations of the original single-well levels. These correct combinations have certain parity. There are known examples of similar phenomena in molecular physics. The ammonium molecule NH_3 has two equivalent positions of the nitrogen atom, above and below the hydrogen plane. The tunneling through the plane creates the doublet of states and restores the parity. The weak interactions do not conserve parity and mix the states of opposite inversionsymmetry. The presence of close-in-energy parity doublets is predicted to facilitate this mixing and enhance the effects of parity nonconservation [8, 9].

16.15 Coriolis Mixing and Decoupling Parameter

Considering the core in (16.122) as a simple rotor (16.73) with axial symmetry, $A_1 = A_2 = A$, we have the rotational part of the total Hamiltonian as

$$H_{\text{rot}} = A(R_1^2 + R_2^2) + A_3R_3^2. \quad (16.133)$$

However, the operator R_3 vanishes on our class of functions (16.128). The remaining part can be written as

$$H_{\text{rot}} = A[J^2 + \mathbf{j}^2 - 2(\mathbf{j} \cdot \mathbf{J})]. \quad (16.134)$$

The operator $A\mathbf{j}^2$ gives a correction to the intrinsic Hamiltonian. The rotational term $A\mathbf{J}^2$ is responsible for the rotational spectrum (16.76). The new effect of the coupling between rotation and intrinsic motion is introduced by the Coriolis term

$$H_C = -2A(\mathbf{j} \cdot \mathbf{J}) = -2A[I_3 j_3 + (I_+ j_- + I_- j_+)]. \quad (16.135)$$

The first term in the brackets gives an energy shift $-2AK^2$. The second term has off-diagonal matrix elements. For example, j_- acting onto the state Ψ_{JMK} transforms the intrinsic state χ_K into another one χ_{K-1} . At the same time, I_+ , which is the *lowering* operator due to the properties of the body-fixed angular momentum components (16.57), transforms the angular function Φ'_{MK} into Φ'_{MK-1} . As a result, we get an admixture of the state Ψ_{JMK-1} with proper symmetry. Thus, the Coriolis interaction mixes the bands with $|\Delta K| = 1$. In the adiabatic case, we expect the spacings between different intrinsic configurations to be large compared to rotational energy. In this case, mixing is weak and the Coriolis interaction can be treated as a perturbation. The Coriolis mixing even in the lowest order leads to corrections to the intensity rules which are necessary to reproduce experimental data of high accuracy.

The specific case corresponds to $K = 1/2$. Our basis functions (16.132) contain both components, $\pm K$. The Coriolis interaction has matrix elements connecting these components. This results in the *diagonal* correction to the rotational energies in the band $K = 1/2$. The terms $I_+ j_-$ and $I_- j_+$ contribute equally so that the energy shift of the state (16.132) is given by

$$\Delta E_j = -2A\langle\Psi_{JM1/2}|I_- j_+|\Psi_{JM1/2}\rangle. \quad (16.136)$$

For the intrinsic function given by a superposition similar to (16.129),

$$\Delta E_j = -2A\sqrt{\frac{2J+1}{16\pi^2}}\langle\Psi_{JM1/2}|(I_- \Phi'_{M-1/2}) \sum C_j (-)^{j-j_+} (j_+ \chi_{j-1/2})\rangle. \quad (16.137)$$

The matrix elements of angular momenta give

$$I_- \Phi'_{M-1/2} = \left(J + \frac{1}{2}\right) \Phi'_{M1/2}, \quad j_+ \chi_{j-1/2} = \left(j + \frac{1}{2}\right) \chi_{j1/2}. \quad (16.138)$$

Taking the scalar product with the bra-vector and using the normalization of the Φ -functions and orthogonality of the intrinsic functions χ_{jk} , we find

$$\Delta E_j = A(-)^{j+1/2} \left(J + \frac{1}{2}\right) a, \quad (16.139)$$

where the *decoupling parameter*

$$a = \sum_j |C_j|^2 (-)^{j-1/2} \left(j + \frac{1}{2}\right) \quad (16.140)$$

depends on the intrinsic wave function. The term “decoupling” means that some particles are decoupled from the mean field and have their angular momenta aligned along the rotation axis rather than along the symmetry axis. In the present case, instead of the orbits with the projection $K = \pm 1/2$, we get their proper linear combinations. The

effect increases with J when perturbation theory might be insufficient and one needs to diagonalize the Coriolis interaction exactly.

In the linear approximation with respect to the rotation parameter A , that is the inverse moment of inertia (16.74), the energy spectrum of the band can be finally written as

$$E_J(K) = E^0(K) + A[J(J+1) + \alpha(-)^{J+1/2} \left(J + \frac{1}{2} \right) \delta_{K,1/2}] \quad (16.141)$$

In some cases, the presence of the decoupling parameter can change the normal sequence of levels in the rotational band. Similar terms corresponding to matrix elements connecting $\pm 1/2$ components of the wave functions appear in the calculation of the magnetic moment. The matrix elements between $\pm K$ parts exist in higher orders for other operators as well.

Problem 16.5 The ground-state spin of ^{183}W is $1/2$. The first two excited states have energies 46 and 99 keV. Find the moment of inertia and the decoupling parameter, and predict spins and energies of the two next excited states of the same band.

16.16 Classical Rotation and Routhian

Now we need to explicitly relate general geometric properties of the rotating nucleus with its intrinsic structure on the level of interacting particles. We return first to *classical* motion of a particle in the uniformly rotating anisotropic potential field [4]. The space-fixed coordinates of the particle are x, y, z and the kinetic energy is

$$K = \frac{m}{2} (\dot{x}^2 + \dot{y}^2 + \dot{z}^2). \quad (16.142)$$

We attach a body-fixed frame with coordinates x_1, x_2, x_3 to the potential field $U(x_1, x_2, x_3)$. Let the space-fixed frame and the body-fixed frame coincide at $t = 0$. If the 1 -axis is the rotation axis, it will always coincide with the space-fixed x -axis. Let $\Omega \mathbf{e}^{(1)}$ be the angular velocity vector of the body-fixed frame; Its magnitude is Ω and $\mathbf{e}^{(1)}$ is the unit vector along the rotation axis.

Particle coordinates in the body-fixed frame are expressed in terms of laboratory coordinates as

$$x_1 = x, \quad x_2 = y \cos \Omega t + z \sin \Omega t, \quad x_3 = -y \sin \Omega t + z \cos \Omega t. \quad (16.143)$$

Therefore, the kinetic energy (16.142) is transformed to

$$K = \frac{m}{2} [\dot{x}_1^2 + \dot{x}_2^2 + \dot{x}_3^2 - 2\Omega(\dot{x}_2 x_3 - \dot{x}_3 x_2) + \Omega^2(x_2^2 + x_3^2)]. \quad (16.144)$$

The equations of motion follow from the Lagrangian

$$\mathcal{L} = K - U(x_1, x_2, x_3), \quad (16.145)$$

where potential energy is created by the rotating field and therefore does not change its form if expressed via the coordinates attached to the field. The Lagrange equations,

$$\frac{d}{dt} \frac{\partial \mathcal{L}}{\partial \dot{x}_i} = \frac{\partial \mathcal{L}}{\partial x_i}, \quad (16.146)$$

determine particle motion in the rotating field,

$$\begin{aligned} m\ddot{x}_1 &= -\frac{\partial U}{\partial x_1}, \\ m\ddot{x}_2 &= -\frac{\partial U}{\partial x_2} + 2m\Omega\dot{x}_3 + m\Omega^2x_2, \\ m\ddot{x}_3 &= -\frac{\partial U}{\partial x_3} - 2m\Omega\dot{x}_2 + m\Omega^2x_3, \end{aligned} \quad (16.147)$$

or, in the vector form,

$$m\ddot{\mathbf{r}} = -\nabla U - 2m[\boldsymbol{\Omega} \times \mathbf{r}] - m[\boldsymbol{\Omega} \times [\boldsymbol{\Omega} \times \mathbf{r}]]. \quad (16.148)$$

Dynamics in the noninertial (rotating) frame are governed by the *Coriolis and centrifugal forces, apart from the normal potential force*.

To generalize the results for quantum mechanics, we need the Hamiltonian expressed in terms of conjugate momenta

$$p_i = \frac{\partial \mathcal{L}}{\partial \dot{x}_i} = \frac{\partial K}{\partial \dot{x}_i}, \quad (16.149)$$

or, in components,

$$p_1 = m\dot{x}_1, \quad p_2 = m(\dot{x}_2 - \Omega x_3), \quad p_3 = m(\dot{x}_3 + \Omega x_2). \quad (16.150)$$

This means that the particle velocity includes the *convective term*,

$$\mathbf{v} = (\dot{x}_1, \dot{x}_2, \dot{x}_3) = \frac{\mathbf{p}}{m} - [\boldsymbol{\Omega} \times \mathbf{r}]. \quad (16.151)$$

However, kinetic energy (16.144), expressed through canonical momenta (16.150) instead of velocities (16.151), acquires the standard form

$$K = \frac{1}{2m}(p_1^2 + p_2^2 + p_3^2) = \frac{\mathbf{p}^2}{2m}. \quad (16.152)$$

Finally, for the Hamilton function in the rotating frame,

$$H = \sum_i p_i \dot{x}_i - \mathcal{L}, \quad (16.153)$$

we obtain

$$H = \frac{\mathbf{p}^2}{2m} + U - \Omega(x_2 p_3 - x_3 p_2) \equiv H^o - \hbar(\boldsymbol{\Omega} \cdot \boldsymbol{\ell}), \quad (16.154)$$

where H^o is the Hamiltonian in the static field and $\hbar\boldsymbol{\ell}$ is the orbital angular momentum of the particle. This function H is sometimes called the *Routhian*. The last term in (16.154) is responsible for the Coriolis and centrifugal effects in the Hamiltonian description. The most important result is that the time dependence disappears and we look at *stationary* motion of the particle in a time-independent but velocity-dependent field. The energy of the particle is determined by the sum of its kinetic and potential energies and does not coincide with the Routhian,

$$E = \frac{\mathbf{p}^2}{2m} + U = H^o = H + \hbar(\boldsymbol{\Omega} \cdot \boldsymbol{\ell}). \quad (16.155)$$

Before we go to the quantum formulation, let us make two comments.

- 1) In the same way, one could consider a problem of translational motion. The transformation of coordinates $x_1 = x - ut, x_2 = y, x_3 = z$ to the frame moving with the velocity $\mathbf{u} = (u, 0, 0)$ would lead, instead of (16.154), to

$$H = H^0 - (\mathbf{u} \cdot \mathbf{p}). \quad (16.156)$$

This effect in a sense is trivial: we simply change the origin of the momentum scale (subtract the momentum of the system as a whole and the corresponding translational energy),

$$H = U + \frac{(\mathbf{p} - m\mathbf{u})^2}{2m} - \frac{mu^2}{2}. \quad (16.157)$$

There are no new coordinate-dependent forces that agree with the Galilean relativity: the dynamical laws do not depend on uniform motion of a system as a whole.

- 2) If the potential is *symmetric* with respect to the I -axis, the new term in (16.154) is, together with ℓ_1 , a constant of motion and does not influence the equations of motion. However, energy effectively does depend on the angular momentum because, in a many-body system, instead of ℓ in (16.155), we have to introduce the total angular momentum. Then we can consider only those particle configurations which are consistent with a chosen value of this angular momentum. The transition to another value requires a *redistribution* of the particles that changes energy. This corresponds to non-collective rotation mentioned in Section 16.1.

16.17 Cranked Rotation

Now we consider *quantum* collective rotation around an axis which is not the symmetry axis. Referring to our classical intuition, we assume that the intrinsic state of a rotating quantum system can be described in the lab frame by a wave function $\Psi(t)$ that corresponds to the orientation of the body-fixed frame uniformly rotating – together with the body(!) – with angular velocity Ω so that the rotation angle $\alpha = \Omega t$. Here we consider external, *cranked*, rotation.

Since the body-fixed rotation axis I is not the symmetry axis, the intrinsic Hamiltonian H_{intr} depends on time. The state vector $\Psi(t)$ satisfies the *nonstationary* Schrödinger equation

$$i\hbar \frac{\partial \Psi(t)}{\partial t} = H_{\text{intr}}(t)\Psi(t). \quad (16.158)$$

However, this time dependence comes exclusively from rotation of the body-fixed frame. The rotating object has a frozen intrinsic configuration ψ . The solution of (16.158) is merely a result of rotation of this intrinsic state,

$$\Psi(t) = R(t)\psi(t), \quad (16.159)$$

where the rotation operator is

$$R(t) = e^{-i\alpha(\mathbf{n} \cdot \mathbf{J})} = e^{-i\Omega t I_1}. \quad (16.160)$$

Here the generators of rotations around the body-fixed axes are the operators I_i , Eq. (16.55).

The new function ψ satisfies the equation

$$i\hbar \frac{\partial \psi}{\partial t} = \left[R^{-1}(t)H_{\text{intr}}(t)R(t) + i\hbar \frac{\partial R^{-1}(t)}{\partial t} R(t) \right] \psi(t). \quad (16.161)$$

The first term in square brackets is the frozen (turned-back) intrinsic Hamiltonian. In our picture, we should identify this Hamiltonian with the time-independent Hamiltonian H^0 of Eq. (16.154) that describes particles moving in a stopped deformed potential,

$$H^0 = e^{i\Omega t I_1} H_{\text{intr}}(t) e^{-i\Omega t I_1}. \quad (16.162)$$

The second term in (16.161) is precisely analogous to the change of the classical Hamiltonian (16.154) under the transformation to the rotating frame.

Thus, we get the Schrödinger equation (16.161) with the stationary Hamiltonian, or Routhian,

$$H = H^0 - \hbar\Omega I_1. \quad (16.163)$$

The additional Coriolis term [Eq. (16.163)] contains the total rotation generator, angular momentum I_1 that includes spins of the particles. If the rotation axis does not coincide with the symmetry axis, I_1 is not conserved and does not commute with the deformed Hamiltonian H^0 . Since the Routhian does not depend on time, we can look for the complete set of the stationary wave functions $\psi_k(t) = \exp(-i/\hbar)Ht)\psi_k$ with energies (Routhians) \tilde{E}_k ,

$$H\psi_k = (H^0 - \hbar\Omega I_1)\psi_k = \tilde{E}_k\psi_k. \quad (16.164)$$

Equation (16.164) is the starting point of the *cranking model* (see Figure 16.8). The solutions ψ_k , their energies, and the matrix elements of operators between the functions

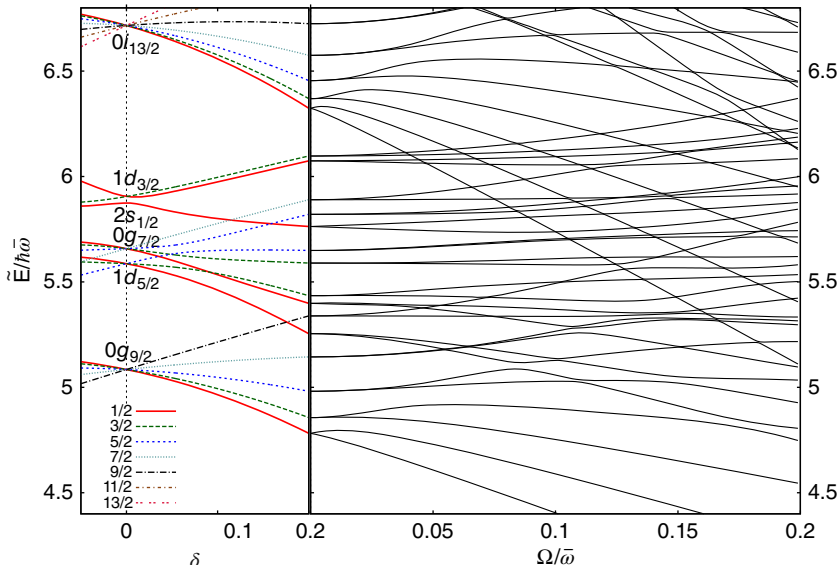


Figure 16.8 The left panel shows evolution of positive-parity eigenstates in the Nilsson potential (see Section 12.12) as a function of axially symmetric deformation δ along axis 3 with no rotation, $\Omega = 0$. The evolution of eigenvalues of the Routhian as a function of rotational frequency Ω along axis 1 at fixed deformation $\delta = 0.2$ is shown on the right.

of this set depend on Ω . The value of Ω is not fixed at this stage of external cranking. We are interested in describing a rotational state with a certain angular momentum J that is the result of *intrinsic* excitation. This angular momentum comes from (coherent or incoherent) accumulation of angular momenta of individual particles. Therefore, the *self-consistency* condition requires that the angular momentum operator I_1 used in the cranking formulation have, in the self-consistently constructed states ψ , an expectation value equal to the total angular momentum J ,

$$\langle \psi_k(\Omega) | I_1 | \psi_k(\Omega) \rangle = J. \quad (16.165)$$

In this way, we select an appropriate value of the angular velocity $\Omega = \Omega_k(J)$, in general different for different intrinsic configurations ψ_k . Finally, we express all observables through J instead of Ω obtaining an approximate self-consistent solution of the rotation problem.

The intrinsic “frozen” states with fixed orientation in space have no definite value of the angular momentum that is conserved only in average. Such a state is a wave packet of the states with different values of angular momentum. As seen from (16.163), the angular velocity plays the role of the Lagrange multiplier. Solving the Schrödinger equation in the frozen system, we look for the minimum of energy (Routhian) under constraint of the correct *mean value* of the angular momentum that in the exact solution would be a constant of motion.

The expectation value of energy has to be calculated in the lab frame and, because of the time dependence of the transformation $R(t)$, does not coincide with the eigenvalues \tilde{E} of the Routhian (16.163). Similarly to (16.154), we find

$$\begin{aligned} E &= \langle \Psi(t) | H_{\text{intr}}(t) | \Psi(t) \rangle = \langle \psi(t) | R^{-1}(t) H_{\text{intr}}(t) R(t) | \psi(t) \rangle \\ &= \langle \psi | H + \hbar \Omega I_1 | \psi \rangle = \tilde{E} + \hbar \Omega \langle \psi | I_1 | \psi \rangle. \end{aligned} \quad (16.166)$$

The last term is equal to $\hbar \Omega J(\Omega)$, where J is a function of Ω determined by the constraint (16.165). The connection between the genuine energy and the Routhian is the Legendre transformation from the cranking-model independent variable Ω to the physical constant of motion J . Such an approach is well known from statistical thermodynamics if the equilibrium ensemble is characterized by the conserved (in average) angular momentum.

In Eq. (16.164), the angular velocity was a *parameter*. In such cases, two important identities are valid which are very useful in many applications (the so-called Hellman–Feynman relations actually written by Pauli in the early years of quantum mechanics). Consider a complete set of stationary solutions ψ_k of the Schrödinger equation with the Hamiltonian $H(\Omega)$ depending on a parameter Ω ,

$$H(\Omega) \psi_k(\Omega) = E_k(\Omega) \psi_k(\Omega). \quad (16.167)$$

Energies E_k and the solutions ψ_k also depend on Ω . From the derivative of Eq. (16.167) with respect to this parameter, we obtain

$$\frac{\partial H}{\partial \Omega} \psi_k + H \frac{\partial \psi_k}{\partial \Omega} = \frac{\partial E_k}{\partial \Omega} \psi_k + E_k \frac{\partial \psi_k}{\partial \Omega}. \quad (16.168)$$

Let us take the scalar product (from the left) of this equation with the function $\psi_l(\Omega)$ that belongs to the same orthonormalized set (16.167),

$$\left\langle \psi_l \left| \frac{\partial H}{\partial \Omega} \right| \psi_k \right\rangle + E_l \left\langle \psi_l \left| \frac{\partial \psi_k}{\partial \Omega} \right. \right\rangle = \frac{\partial E_k}{\partial \Omega} \delta_{kl} + E_k \left\langle \psi_l \left| \frac{\partial \psi_k}{\partial \Omega} \right. \right\rangle. \quad (16.169)$$

If we put $l = k$ here, we obtain the energy derivative along the given energy term $E_k(\Omega)$ as the expectation value of the derivative of the Hamiltonian,

$$\frac{\partial E_k}{\partial \Omega} = \left\langle \psi_k \left| \frac{\partial H}{\partial \Omega} \right| \psi_k \right\rangle. \quad (16.170)$$

If we take $l \neq k$ in (16.169), we get the off-diagonal elements of the “operator” which differentiates with respect to a parameter,

$$\left\langle \psi_l \left| \frac{\partial}{\partial \Omega} \right| \psi_k \right\rangle = \frac{\left\langle \psi_l \left| \frac{\partial H}{\partial \Omega} \right| \psi_k \right\rangle}{E_k - E_l}, \quad l \neq k. \quad (16.171)$$

In accordance with (16.170), we obtain for our case (16.164)

$$\frac{\partial \tilde{E}}{\partial \Omega} = -\hbar \langle I_1 \rangle = -\hbar J. \quad (16.172)$$

Then the Legendre transformation (16.166) gives

$$\frac{\partial E}{\partial J} = \frac{\partial \tilde{E}}{\partial \Omega} \frac{\partial \Omega}{\partial J} + \frac{\partial \Omega}{\partial J} \hbar J + \hbar \Omega = \hbar \Omega \quad (16.173)$$

that coincides with the classical interpretation of the Lagrange multiplier Ω as angular velocity. Indeed, the result (16.173) is the Hamilton equation for Ω as the speed of the orientation changes with $\hbar J$ as a conjugate momentum.

16.18 Moment of Inertia

If the static Hamiltonian H^0 is time-reversal invariant, the only violation of \mathcal{T} -invariance is introduced by the Coriolis term $-\hbar \Omega I_1$. The expectation value of the angular momentum (16.165) is also a \mathcal{T} -odd quantity and changes its sign for the reversed rotation, $\Omega \rightarrow -\Omega$. We can write down the dependence of this expectation value on the angular velocity as

$$\hbar \langle \psi(\Omega) | I_1 | \psi(\Omega) \rangle = \Omega \mathcal{J}(\Omega^2), \quad (16.174)$$

where the coefficient of proportionality $\mathcal{J}(\Omega^2)$ is an *even* function of the angular velocity.

The coefficient \mathcal{J} is the ratio

$$\mathcal{J} = \mathcal{J}^{(1)} \equiv \frac{\hbar J}{\Omega} \quad (16.175)$$

of the angular momentum to the angular velocity found in the cranking model. It seems natural to call it the *moment of inertia*. Frequently, it is more convenient to introduce the so-called *dynamical moment of inertia* (see Section 16.1),

$$\mathcal{J}^{(2)} = \hbar \frac{dJ}{d\Omega} \quad (16.176)$$

that coincides with (16.175) in the case of no Ω -dependence of \mathcal{J} . Both moments of inertia are different for different intrinsic states ψ_k . Again, the whole construction bears clear physical meaning if one can trace the change of structure and of the moment of

inertia *along the rotational band* determined as a set of states interconnected by strong transitions (Section 16.1).

If the dependence of J on angular velocity is found from (16.165), energy of the rotational states (16.166) can be calculated by a simple integral,

$$E = \hbar \left(J\Omega - \int_0^{\Omega} d\Omega' J(\Omega') \right), \quad (16.177)$$

where, in the end, one should substitute the dependence $\Omega(J)$ extracted from (16.165). Indeed, the derivative $(\partial E / \partial J)$ taking into account $\Omega = \Omega(J)$ immediately leads to Eq. (16.173). If the static moment of inertia (16.165) is given by the expansion

$$\mathcal{J} = \sum_{n=0} \mathcal{J}_n \Omega^{2n}, \quad (16.178)$$

we get for the dynamic moment of inertia (16.176)

$$\mathcal{J}^{(2)} = \sum_{n=0} (2n+1) \mathcal{J}_n \Omega^{2n}, \quad (16.179)$$

and the energy along the band is

$$E = \sum_{n=0} \frac{2n+1}{2n+2} \mathcal{J}_n \Omega^{2n+2}. \quad (16.180)$$

In the simplest case of the *constant* moment of inertia,

$$\mathcal{J}^{(1)} = \mathcal{J}^{(2)} = \mathcal{J}_0, \quad E = \frac{1}{2} \mathcal{J}_0 \Omega^2 = \frac{\hbar^2 J^2}{2\mathcal{J}_0}. \quad (16.181)$$

Physically, this case corresponds to a rigid rotor that does not noticeably change as the angular velocity increases.

The whole concept of cranking is of a semiclassical character. The stationary states found in the framework of the cranking model are wave packets of actual stationary quantum states which could, in principle, be found by microscopic theory where rotation would appear as one of the intrinsic excitations rather than as a result of external cranking.

One easy step toward quantum theory is obvious – we should substitute an angular momentum J in formulae such as (16.165), (16.175), and (16.181) by $\sqrt{J(J+1)}$. If there exists a nonrotational angular momentum created by intrinsic excitations, it can be aligned around the symmetry axis-3. This part, $I_3 = K$, should be subtracted from the self-consistency condition (16.165). In this case, we would write

$$\langle \psi(\Omega) | I_1 | \psi(\Omega) \rangle = \sqrt{J(J+1) - K^2}. \quad (16.182)$$

To correct the internal physical deficiencies of the cranking model, much more work is needed. Until now, the cranking model is still the main tool for describing rotational bands. It can be shown [10] that the cranking model follows from the exact quantum operator equations of motion in the lowest order with respect to angular velocity under the assumption of the existence of an isolated rotational band where the quantum states are uniquely labeled by the angular momentum quantum numbers. But the model is valid as well in the classical limit of large angular momenta. Therefore, it can serve as a reasonable interpolation. The shortcomings of the cranking model become clear in the problems concerning mixing and crossing of rotational bands.

16.19 Adiabatic Expansion

We come now to the problem of actual microscopic calculation of the moment of inertia in the framework of the cranking model. At low angular momenta, we start from static configurations which are the stationary states ψ_k^o of the frozen deformed potential H^o ,

$$H^o \psi_k^o = E_k^o \psi_k^o. \quad (16.183)$$

We considered such configurations in our analysis of the deformed shell model. The Coriolis force makes the pure configurations *nonstationary*, bringing admixtures of other configurations which can be found, at low angular velocity, by perturbation theory.

The linear combinations of the first order are given by a standard expression

$$\psi_k = \psi_k^o + \hbar\Omega \sum_{k' \neq k} \frac{\langle \psi_{k'}^o | I_1 | \psi_k^o \rangle}{E_{k'}^o - E_k^o} \psi_{k'}^o. \quad (16.184)$$

An expectation value of a physical operator F in this rotating state is

$$\langle \psi_k | F | \psi_k \rangle = \langle \psi_k^o | F | \psi_k^o \rangle + \hbar\Omega \sum_{k' \neq k} \frac{\langle \psi_{k'}^o | F | \psi_{k'}^o \rangle \langle \psi_{k'}^o | I_1 | \psi_k^o \rangle + \langle \psi_k^o | I_1 | \psi_{k'}^o \rangle \langle \psi_{k'}^o | F | \psi_k^o \rangle}{E_{k'}^o - E_k^o}. \quad (16.185)$$

Such expressions, in general, determine the *linear response* of a system, in this case through the observable quantity F , to an external perturbation, specifically rotation.

Let us consider axially symmetric unperturbed configurations with the 3-axis as the symmetry axis. The projection I_3 of the angular momentum onto the body-fixed symmetry axis is a constant of motion K for each state ψ_k^o . The Coriolis term $-\hbar\Omega I_1$ leads to the admixture of states with $I_3 = K' = K \pm 1$. This can be understood as a trend toward *realignment* of particles in line with rotation and their gradual decoupling from the symmetry axis of the mean field. The collective nature of rotation is revealed by the fact that each single-particle orbit contributes a little to the rotational angular momentum along the axis perpendicular to the symmetry axis. For the cranking around the symmetry axis-3, we would have only diagonal matrix elements of the perturbation $-\hbar\Omega I_3$. The corresponding response would be reduced to the shifts of energies with no realignment. With a new level scheme, one might have to reshuffle the particles to reach the minimum energy at a given angular momentum. This means, as we mentioned earlier, that the angular momentum around the symmetry axis is created by the redistribution of particles rather than by collective rotation.

Take a rotational angular momentum I_1 as a response operator F in (16.185). The unperturbed expectation value vanishes,

$$\langle \psi_k^o | I_1 | \psi_k^o \rangle = 0, \quad (16.186)$$

owing to the axial symmetry of the frozen state and selection rules $\Delta K = \pm 1$ for the operator I_1 . We are left with

$$\langle \psi_k | I_1 | \psi_k \rangle = 2\hbar\Omega \sum_{k' \neq k} \frac{|\langle \psi_{k'}^o | I_1 | \psi_k^o \rangle|^2}{E_{k'}^o - E_k^o}. \quad (16.187)$$

Thus, we obtain the cranking model moment of inertia [11] in the adiabatic approximation of slow rotation,

$$\mathcal{J}[\psi_k] = 2\hbar^2 \sum_{k' \neq k} \frac{\left| \langle \psi_{k'}^o | I_1 | \psi_k^o \rangle \right|^2}{E_{k'}^o - E_k^o}. \quad (16.188)$$

In this order, the moment of inertia of a given configuration does not depend on angular velocity so that Eq. (16.181) are valid. The high-order perturbative corrections can be derived as well.

The angular momentum operator I_1 in the body-fixed frame is simply a derivative with respect to the conjugate rotation angle α in the (23)-plane. The intrinsic Hamiltonian H^o and its eigenfunctions ψ_k^o , Eq. (16.183), depend on this angle as a parameter (this dependence disappears if the rotation axis-1 is the symmetry axis). The derivative $\partial/\partial\alpha$ can be transferred to the Hamiltonian by the means of (16.171). It allows us to write down the moment of inertia (16.188) as

$$\mathcal{J}[\psi_k] = 2\hbar^2 \sum_{k' \neq k} \frac{\left| \langle \psi_{k'}^o | \frac{\partial H^o}{\partial \alpha} | \psi_k^o \rangle \right|^2}{(E_{k'}^o - E_k^o)^3}. \quad (16.189)$$

This is the general form of the *inertial parameter* in the linear response theory. The parameter corresponds to the field acting on the coordinate α .

Problem 16.6 Consider, similar to the cranking model, the so-called *pushing model* that describes uniform translational motion of a quantum system as a whole with the Hamiltonian

$$H = H^o - (\mathbf{u} \cdot \mathbf{P}), \quad (16.190)$$

where H^o is the intrinsic Hamiltonian of the system at rest, \mathbf{P} is the total momentum operator, and \mathbf{u} is the Lagrange multiplier that has a meaning of translational center-of-mass velocity.

- Define the total mass parameter M similar to the definition of the moment of inertia in the cranking model and derive, in the approximation of slow motion, the analog of Eq. (16.188).
- Assume that your system contains A particles of mass m interacting through velocity-independent forces. Show that the inertial parameter M for all unperturbed states coincides with the sum of particle masses, $M = Am$. (Use the operator equation of motion for the center-of-mass operator \mathbf{R} to exclude a matrix element of the total momentum and take into account the commutation relation between \mathbf{R} and \mathbf{P} .)

Perturbation theory is applicable if off-diagonal matrix elements of the perturbation are small compared to the unperturbed energy spacings of mixed levels. For the adiabatic cranking model, this means that

$$\hbar\Omega \left| \frac{\langle \psi_{k'}^o | I_1 | \psi_k^o \rangle}{E_{k'}^o - E_k^o} \right| \ll 1. \quad (16.191)$$

At small deformations, the intrinsic states with $|\Delta K| = 1$ coupled by the operator I_1 might belong to the same (slightly split) spherical rotational multiplet. Then the denominator in (16.191) is small. It approaches zero in the limit of vanishing deformation, as for example in the single-particle case (Section 12.4). In this case, as the numerator contains the deformation-independent matrix elements of the angular momentum, we have nearly degenerate states. Then one has to diagonalize exactly the states within this multiplet. But the result of diagonalization is obvious because the cranking term $-\hbar\Omega I_1$ is the only one breaking spherical symmetry. Therefore, we get axial symmetry around the rotation axis-1 and no collective rotation. In the basis of states quantized along the 1-axis, the operator I_1 has no off-diagonal matrix elements, and the moment of inertia vanishes. As seen from the last term in (16.181), the rotational levels with finite angular momentum J are pushed up to infinite energy. To apply the entire formalism based on the frozen intrinsic configurations, the deformation should be large enough.

An exceptional situation exists owing to the Kramers degeneracy as we know from our experience with the decoupling parameter (16.140). Quadrupole, or any time-reversal invariant, deformation keeps time-conjugate single-particle orbits degenerate. The states with angular momentum projections along the symmetry axis equal to $m = \pm 1/2$ are coupled by the matrix element of I_1 . In this 2×2 subspace we need to diagonalize the Coriolis interaction exactly. The correct linear combinations are

$$|\pm\rangle = \frac{1}{\sqrt{2}} \left[\left| m = +\frac{1}{2} \right\rangle \pm \left| m = -\frac{1}{2} \right\rangle \right]. \quad (16.192)$$

Their energies are split *linearly* in Ω ,

$$\Delta\epsilon_{\pm} = \mp \frac{\hbar\Omega}{2} (j + 1/2), \quad (16.193)$$

where it is assumed that the states belong to the same spherical j -level. The new quantum number (\pm) is the *signature* we mentioned earlier. Similar combinations can be constructed for any pair ($\pm m$) or ($\lambda \bar{\lambda}$) of time-conjugate orbits. The Coriolis interaction can never mix the states of type (+) with the states of type (-); this cuts the matrix in halves and facilitate the numerical work. The states with a certain signature are proper linear combinations for high-order calculations. Since the Coriolis interaction violates \mathcal{T} -invariance and axial symmetry, the only remaining constants of motion in the cranked deformed shell model are discrete ones, namely, parity and signature.

16.20 Rotation of a Perfect Fermi Gas

In the following, we calculate the moment of inertia of a perfect Fermi gas in a rotating deformed container. The remarkable result is that, for a normal distribution of particles over single-particle orbits, the moment of inertia is that of a *rigid body* of a given shape, Eq. (16.9).

Let an intrinsic state be a pure Slater determinant built on the single-particle states $|\lambda\rangle$ in a deformed potential $U(\mathbf{r})$. The single-particle energies are ϵ_{λ} . The angular momentum operator in the cranking model is the sum of single-particle operators,

$$I_1 = \sum_a (j_1)_a \Rightarrow I_1 = \sum_{\lambda\lambda'} (j_1)_{\lambda\lambda'} a_{\lambda'}^{\dagger} a_{\lambda}, \quad (16.194)$$

where we use the standard secondary quantized form of one-body operators (Section 11.2). Each term of (16.194) corresponds to a specific promotion $\lambda \rightarrow \lambda'$ of a particle from a filled state, $n_\lambda = 1$, to an empty state, $n_{\lambda'} = 0$. The matrix element of the transition contains the Pauli blocking factor $\sqrt{n_\lambda(1 - n_{\lambda'})}$. The change of unperturbed energy for this transition is $\epsilon_{\lambda'} - \epsilon_\lambda$.

The cranking formula (16.188) gives in this model

$$\mathcal{J} = 2\hbar^2 \sum_{\lambda\lambda'} \frac{n_\lambda(1 - n_{\lambda'})}{\epsilon_{\lambda'} - \epsilon_\lambda} |(j_1)_{\lambda'\lambda}|^2, \quad (16.195)$$

or, symmetrizing among λ and λ' ,

$$\mathcal{J} = -\hbar^2 \sum_{\lambda\lambda'} \frac{n_\lambda - n_{\lambda'}}{\epsilon_\lambda - \epsilon_{\lambda'}} |(j_1)_{\lambda'\lambda}|^2. \quad (16.196)$$

In fact, the same expression can be derived for nonzero temperature T of the gas but the ground-state occupation numbers n_λ equal to 0 or 1 have to be substituted in this case by the Fermi–Dirac occupation numbers $n_\lambda(T)$ smoothly changing between 0 and 1. Note that the moment of inertia (16.196) is positively defined only for a normal distribution when the occupancies n_λ decrease with increasing energy ϵ_λ .

We calculate the moment of inertia (16.196) in the semiclassical approach. Assume that the particle number A is sufficiently large and that, near the Fermi surface Σ_F , particles are mostly in single-particle states with large orbital angular momenta $\ell \approx A^{1/3} \gg 1$. Within the same accuracy, we can neglect spin effects taking $j \approx \ell$. The Coriolis force induces particle transitions across Σ_F , from occupied to empty orbits. The small denominators single out the states close to Σ_F . If the single-particle level density v_F is sufficiently high at Σ_F , we can replace the discrete numbers n_λ by a continuous function $n(\epsilon_\lambda)$ that has a derivative concentrated near Σ_F ,

$$\frac{n_\lambda - n_{\lambda'}}{\epsilon_\lambda - \epsilon_{\lambda'}} \approx \frac{dn(\epsilon_\lambda)}{d\epsilon_\lambda} \approx -\delta(\epsilon_\lambda - \epsilon_F). \quad (16.197)$$

In this semiclassical approximation, the moment of inertia (16.196) becomes

$$\mathcal{J} \approx \hbar^2 \sum_{\lambda\lambda'} |(\ell_1)_{\lambda'\lambda}|^2 \delta(\epsilon_\lambda - \epsilon_F). \quad (16.198)$$

Here the sum over λ' includes all orbits connected to λ by matrix elements of ℓ_1 . Using their completeness, we get

$$\mathcal{J} = \hbar^2 \sum_\lambda (\ell_1^2)_{\lambda\lambda} \delta(\epsilon_\lambda - \epsilon_F). \quad (16.199)$$

The semiclassical moment of inertia of the Fermi gas is equal to the sum of the expectation values of the squared angular momentum projections along the rotation axis for all particles at Σ_F .

In the semiclassical limit, the sum of (16.199) is equivalent to the integral

$$\mathcal{J} = g \int \frac{d^3r d^3p}{(2\pi\hbar)^3} (x_2 p_3 - x_3 p_2)^2 \delta(\epsilon(\mathbf{r}, \mathbf{p}) - \epsilon_F) \quad (16.200)$$

over the isoenergetic surface

$$\epsilon(\mathbf{r}, \mathbf{p}) \equiv \frac{\mathbf{p}^2}{2m} + U(\mathbf{r}) = \epsilon_F \quad (16.201)$$

in single-particle phase space; g is the spin–isospin degeneracy factor. Equation (16.201) defines the local Fermi momentum, the particle distribution function, and the local density.

The single-particle energy (16.201) is isotropic in momentum space, all directions of \mathbf{p} are equiprobable. As a result of integration over the momentum angles, the cross terms in (16.199) vanish,

$$\mathcal{J} = g \int \frac{d^3r d^3p}{(2\pi\hbar)^3} (x_2^2 p_3^2 + x_3^2 p_2^2) \delta(\epsilon(\mathbf{r}, \mathbf{p}) - \epsilon_F). \quad (16.202)$$

Owing to the same isotropy, the averaging of p_2^2 and p_3^2 over the spherical Fermi surface provides, at a given \mathbf{r} , identical results, $\overline{p_2^2} = \overline{p_3^2} = (1/3)p_F^2(\mathbf{r})$,

$$\mathcal{J} = \frac{g}{3} \int \frac{d^3r d^3p}{(2\pi\hbar)^3} (x_2^2 + x_3^2)p_F^2(\mathbf{r}) \delta(\epsilon(\mathbf{r}, \mathbf{p}) - \epsilon_F). \quad (16.203)$$

From the Fermi distribution, it is clear that the moment of inertia (16.203) can be rewritten as

$$\begin{aligned} \mathcal{J} &= \frac{g}{3} \int \frac{d^3r d^3p}{(2\pi\hbar)^3} (x_2^2 + x_3^2)p_F^2(\mathbf{r}) \frac{dn(\mathbf{r}, \mathbf{p})}{d\epsilon_F} \\ &= \frac{1}{3} \int d^3r (x_2^2 + x_3^2)p_F^2(\mathbf{r}) \frac{dn(\mathbf{r})}{d\epsilon_F}. \end{aligned} \quad (16.204)$$

The change of the density $n(\mathbf{r})$ due to the displacement of the Fermi energy is equal to

$$\frac{dn(\mathbf{r})}{d\epsilon_F} = \frac{dn(\mathbf{r})}{dp_F(\mathbf{r})} \frac{dp_F(\mathbf{r})}{d\epsilon_F} = \frac{3n(\mathbf{r})}{p_F(\mathbf{r})} \frac{m}{p_F(\mathbf{r})}, \quad (16.205)$$

so that (16.204) coincides with (16.9),

$$\mathcal{J} = \mathcal{J}_r = m \int d^3r (x_2^2 + x_3^2)n(\mathbf{r}). \quad (16.206)$$

We proved a theorem [12]: a perfect degenerate Fermi gas behaves in a slowly rotating deformed container as a rigid body of the same local density. This fundamental result is based on three main assumptions, (i) validity of the semiclassical description, at least in average; (ii) smooth character of the single-particle energy spectrum (16.201); and (iii) the distribution of particles ensuring the *isotropy of velocities*. The famous Bohr–van Leeuwen theorem on the absence of classical magnetism in the thermodynamical equilibrium [13] is based on the same fact of isotropy of the velocity distribution.

16.21 Perfect Bose Gas and Ideal Liquid

The moment of inertia crucially depends on the particle statistics and on how they are distributed over single-particle orbits. As can be seen from the simple calculation, the moment of inertia of a perfect *Bose gas* in its ground state in a rotating deformed container is proportional to the deformation parameter squared and therefore always is smaller than the rigid body value (16.8),

$$\mathcal{J} = \delta'^2 \mathcal{J}_r, \quad \mathcal{J}_r = Am[\langle x_2^2 \rangle + \langle x_3^2 \rangle]. \quad (16.207)$$

As earlier, the rotation proceeds around the I -axis, and the deformation parameter is defined as

$$\delta' = \frac{\langle x_3^2 \rangle - \langle x_2^2 \rangle}{\langle x_3^2 \rangle + \langle x_2^2 \rangle}. \quad (16.208)$$

The decrease of the moment of inertia compared to the rigid body value can be visualized as due to the fact that only the deformed “crust” of the liquid really takes part in rotation, while the spherical core is inert. The moment of inertia (16.207) is usually called *hydrodynamical*. Indeed, it corresponds to classical rotation of a *perfect incompressible liquid*.

In the ideal liquid, the velocity field $\mathbf{v}(\mathbf{r})$ is *irrotational*, $[\nabla \times \mathbf{v}] = 0$. We discussed this question briefly in Section 5.5, pointing out that this would be valid for a frictionless liquid in a single quantum state. The *incompressibility* of liquid means that $\operatorname{div} \mathbf{v} = 0$. Then the velocity field can be described by the potential, $\mathbf{v} = \nabla\phi$, that satisfies the Laplace equation. We have to solve this equation with the boundary conditions describing rotation of the container.

On the boundary of the container at rest, the normal (with respect to this boundary) component of the velocity field vanishes, $(\mathbf{n} \cdot \mathbf{v}) = 0$, where \mathbf{n} is a unit vector perpendicular to the surface at a given point. If the container is uniformly rotating with the angular velocity $\boldsymbol{\Omega}$, the velocity of the point \mathbf{R} of the wall is $[\boldsymbol{\Omega} \times \mathbf{R}]$. The normal component of this velocity should be equal to the normal component of the liquid velocity field,

$$(\mathbf{n} \cdot (\mathbf{v} - [\boldsymbol{\Omega} \times \mathbf{R}]))_{\text{surf}} = 0. \quad (16.209)$$

We see that in a *spherical* container, vectors \mathbf{n} and \mathbf{R} are parallel at all points of the wall; then the irrotational solution identically vanishes. As has appeared repeatedly in our arguments, collective quantum rotation is allowed only around an axis that is not the symmetry axis. Let us take an *ellipsoidal* container with 3 as a symmetry axis. The surface is described by

$$\frac{x_1^2 + x_2^2}{a^2} + \frac{x_3^2}{c^2} = 1. \quad (16.210)$$

The normal vector \mathbf{n} at the point \mathbf{r} of the surface (16.210) is proportional to $(x_1/a^2, x_2/a^2, x_3/c^2)$, and the boundary condition (16.209) with $\boldsymbol{\Omega} = \boldsymbol{\Omega}_x$ takes the form

$$\left[\frac{x_1}{a^2} \frac{\partial \phi}{\partial x_1} + \frac{x_2}{a^2} \left(\frac{\partial \phi}{\partial x_2} + \Omega x_3 \right) + \frac{x_3}{c^2} \left(\frac{\partial \phi}{\partial x_3} - \Omega x_2 \right) \right]_{\text{surf}} = 0. \quad (16.211)$$

The solution of the Laplace equation that is regular at the origin and obeys the condition (16.211) at the surface gives the potential ϕ of the velocity field,

$$\phi = \text{const} \cdot x_2 x_3, \quad \text{const} = \Omega \frac{a^2 - c^2}{a^2 + c^2}, \quad (16.212)$$

where the constant is determined by (16.211). Note that the condition (16.211) is fulfilled with this solution not only at the surface but in the entire volume as well.

For the found velocity field, the kinetic energy (Section 5.5) has to be identified with the rotational energy $(1/2)\mathcal{J}\Omega^2$, Eq. (16.181). This defines the *hydrodynamic moment*

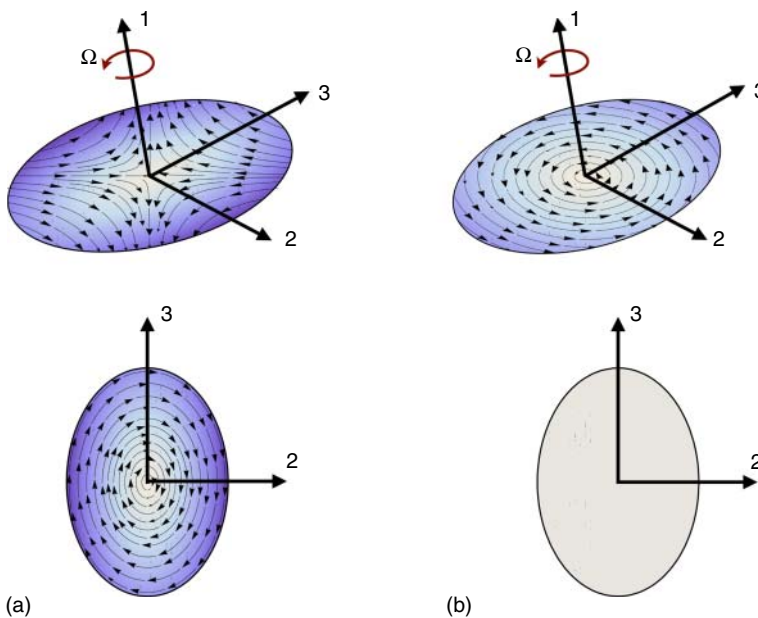


Figure 16.9 The velocity field in the rotating body of ellipsoidal shape. (a) View from the space-fixed frame for the irrotational flow, upper part, and the rigid-body rotation, lower part. (b) View of the same rotation from the body-fixed frame.

of inertia coinciding with (16.207),

$$\mathcal{J}_{\text{h-d}} = \left(\frac{c^2 - a^2}{c^2 + a^2} \right)^2 \int d^3r \rho_m (x_2^2 + x_3^2) = \delta'^2 \mathcal{J}_r. \quad (16.213)$$

We conclude that the Bose condensation transforms the perfect gas into the perfect liquid (as far as we discuss rotational properties). Figure 16.9 shows the velocity field in the rotating ellipsoidal body.

Problem 16.7 Consider a Fermi gas in the potential of an anisotropic harmonic oscillator. Apply the cranking model neglecting the spin of particles in the Coriolis term for the rotation around the x -axis that is not the symmetry axis.

- Find the contribution to the moment of inertia of a single particle on the orbit with the oscillator quantum numbers n_x, n_y, n_z . Look at the specific cases of $n_y = n_z$ and of the orbit with the isotropic velocity distribution around the rotation axis, $\langle v_y^2 \rangle = \langle v_z^2 \rangle$. In both cases, compare the result with the moment of inertia of a classical particle.
- Using the previous result, sum over all occupied orbits and calculate the total moment of inertia. Express the result in terms of the sums of oscillator quanta (Problem 12.4) and consider the case of the self-consistent particle distribution (12.71) and the case of the symmetric distribution, $W_y = W_z$.
- Calculate the same as in point b for the case of bosons in the ground state.

16.22 Pairing Effects

Superconducting pairing correlations (Chapter 13) modify the single-particle distribution function, energy spectrum of the single-particle (*quasiparticle*) excitations, as well as matrix elements of various operators. The moment of inertia turns out to be very sensitive to this modification.

The Cooper pair condensate discussed in Section 13.6 was constructed of the time-reversal invariant pairs on time-conjugate orbits ($\lambda\tilde{\lambda}$) which were filled with amplitudes v_λ , or empty with amplitudes u_λ , satisfying the normalization condition $u_\lambda^2 + v_\lambda^2 = 1$. The Coriolis term breaks time-reversal invariance. In the rotating container, one sense of rotation becomes preferable compared to the opposite one, and the system acquires a nonzero angular momentum (16.165). This cannot be the case unless the Cooper pairs are either broken or distorted. The first option corresponds to a rotational band built on the configuration with one or several quasiparticles. The second possibility is the one of *collective rotation*.

The Coriolis perturbation $-\hbar\Omega I_1$ is a one-body operator (16.194). In the BCS representation, it can transfer a quasiparticle, create or annihilate a pair of quasiparticles. If we consider the ground state of the BCS type of an even–even system (no quasiparticles), the only allowed possibility to excite it is the *breaking* of a vacuum pair that creates two quasiparticles. Therefore, the states $|\psi_k^0\rangle$ admixed by the Coriolis term are the states of seniority $s = 2$. In the axially symmetric case, they have the angular momentum projection onto the symmetry axis $|K| = 1$ (in the ground state $|\psi_k^0\rangle$ we have $s = 0$ and $K = 0$). In the adiabatic rotation, the quasiparticle states are only weakly admixed to the ground-state BCS wave function. Each vacuum pair is slightly distorted and contributes a small fraction of the collective angular momentum.

Let the newborn virtual quasiparticles be placed in the orbits λ and $\lambda' \neq \tilde{\lambda}$. The excitation energy of the admixed state with $s = 2$ is the sum $E_\lambda + E_{\lambda'}$ of the quasiparticle energies that exceeds the pair-breaking threshold 2Δ . The corresponding coherence factors in the matrix elements are to be borrowed from the \mathcal{T} -odd expression (Section 13.11). Then we obtain the result by Belyaev [14] for the cranking moment of inertia (16.188)

$$\mathcal{J} = \hbar^2 \sum_{\lambda\lambda'} \frac{(u_\lambda v_{\lambda'} - u_{\lambda'} v_\lambda)^2}{E_\lambda + E_{\lambda'}} |(j_1)_{\lambda'\lambda}|^2. \quad (16.214)$$

The matrix element of j_1 in (16.214) is to be calculated with unpaired single-particle states λ and λ' because pairing correlations are already accounted for explicitly. The formal limiting transition back to a system with no pairing correlations proceeds as follows. The product $u_\lambda v_{\lambda'}$ vanishes because the occupation numbers become 1 or 0. The coherence factors give $[n_\lambda(1 - n_{\lambda'})] + (\lambda \leftrightarrow \lambda')$. The denominator reduces to $|\epsilon_{\lambda'}| + |\epsilon_\lambda|$. We can leave only the first term in the numerator introducing the factor 2 in front. Then one of the energies in the denominator is positive and another one is negative (transitions across Σ_F). The result coincides with (16.195).

In comparison to the normal Fermi gas (16.196), the new expression (16.214) has larger energy denominators and the matrix elements suppressed by the coherence factors. Therefore, the moment of inertia is significantly *reduced* (by a factor of 2 or 3) from the rigid-body value. This reduction does not reach yet a hydrodynamic value (16.207) that would be by more than an order of magnitude lower at normal deformations of the

ground state ($\delta \approx 0.3$, $\delta' \approx \delta/2$). The systematics of empirical moments of inertia for the ground-state bands of even–even nuclei are shown in Figure 16.3.

As discussed in Section 16.1, the bands built on excited configurations have smaller rotational intervals, or larger moments of inertia, for the same angular momentum. The physical reason becomes clear if one takes into account pairing effects. An excited configuration includes broken Cooper pairs. The quasiparticles block a phase space volume available for the scattering of other pairs and diminish their pairing energy accordingly. As a result, the pairing effects become much weaker and the moment of inertia increases, evolving to the rigid body value. The deformation of the nucleus changes more slowly, being determined not by a small number of broken pairs but by a global core effects.

As rotation frequency increases, the Coriolis effects become exceedingly important. Their destructive influence on Cooper pairing brings new components into the wave function. In turn, this decreases the self-consistent value of the energy gap $\Delta(J)$ that depends on the angular momentum. This process of gradual destruction of the pair condensate carries some analogy to the destruction of superconductivity in metals by an external magnetic field. In nuclei, it is called *Coriolis antipairing* discussed by Mottelson and Valatin [15]. Similarly to the critical magnetic field in superconductors, the critical value of the angular velocity should exist where $\Delta(J) \rightarrow 0$. It corresponds to $J \approx 24$ in rare earth nuclei. However, owing to the relatively small number of particles, other phenomena shadow Coriolis antipairing in nuclei. It turns out to be easier to increase the moment of inertia and decrease the rotational energy by the rotational alignment of completely broken pairs along the rotation axis. We conclude this chapter with some examples of phenomena observed in high-spin nuclear states.

16.23 Band Crossing

The bands built on excited configurations have a larger moment of inertia and therefore lower rotational energy. For the same angular momentum J , rotation of an excited configuration requires less energy than that of a completely paired ground-state configuration. As a result, near some critical angular momentum J_c (much lower than it would be needed for the destruction of the pair condensate due to Coriolis antipairing), a gain in rotational energy for an excited band compensates an original loss of energy ΔE due to the pair breaking (Figure 16.10).

The crossing condition is

$$\frac{\hbar^2 J_c (J_c + 1)}{2J_{\text{g.s.}}} = \frac{\hbar^2 J_c (J_c + 1)}{2J_{\text{exc}}} + \Delta E. \quad (16.215)$$

At angular momenta $J > J_c$, the lowest band (*yrast band* or *yrast line*) is not anymore the ground-state band. It is replaced by the excited band where the moment of inertia is higher and the necessary angular velocity is lower. This situation can be recognized in Figure 16.1 where the ground-state band (*d*) is substituted as an yrast line by the excited band (*e*) around spin 14. Both of these bands shown in Figure 16.5.

For the same angular momentum, the increased moment of inertia requires lower angular velocity. Following the yrast line, we actually perform the transition from the ground-state band to the *S-band* built on the excited configuration. Near the

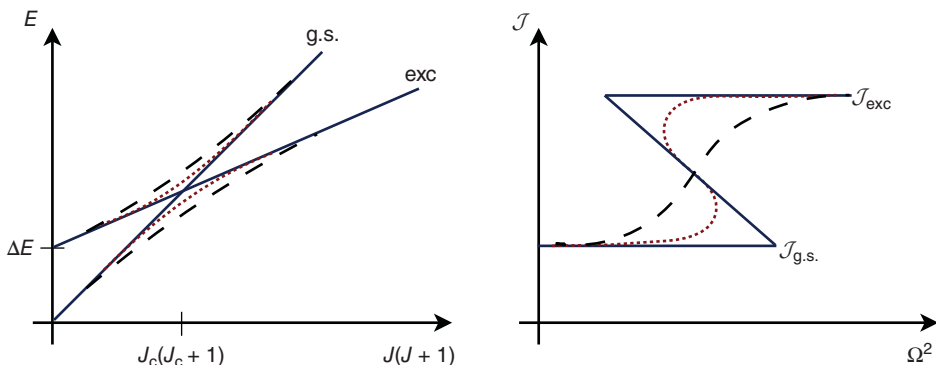


Figure 16.10 Schematic idea of the band crossing at the critical value of the angular momentum J_c .

intersection point, the moment of inertia considerably *increases*, while the angular velocity *decreases*. It gives rise to the *S*-shaped curve in the dependence of the moment of inertia on the angular velocity, or squared angular velocity, as seen on the right-hand part of Figure 16.10. This phenomenon is called *backbending*. Backbending is a common phenomenon and numerous examples have been identified experimentally.

The simple band crossing would lead to a sharp zigzag shape of the curve of the moment of inertia; see Figure 16.10. This is not the case experimentally. The intrinsic configurations corresponding to crossing bands interact via residual interaction and mix with each other. Near the crossing the stationary states are linear combinations of two bare bands. As follows from the simple two-level perturbation theory [QP, I, 10.5], the energy spacing between the mixed states taken as a function of a parameter, has a nonzero minimum determined by the matrix elements of the mixing interaction. The backbending is sharp if the mixing interaction is weak; in the case of a considerable strength of interaction, we have more smooth behavior. Typical matrix elements of mixing between the ground-state band and two-quasiparticle bands are of the order of dozens kiloelectronvolts. Unfortunately, the cranking model is not suited for exact calculations of band mixing in the vicinity of the crossing point. Here the states are mixed at a certain *angular frequency* that corresponds to *different angular momenta* in crossing bands. Exact microscopic calculations should consider the interaction at a *given angular momentum* that is an actual constant of motion.

In the two-quasiparticle *S*-band that becomes an *yраст* band after the backbending, the quasiparticles are decoupled from the symmetry axis-3 and aligned along the rotation axis-1. The schematic picture of the strong coupling case (normal deformed shell model with conserved angular momentum projection onto the symmetry axis) and *rotational alignment* [16], with a particle angular momentum oriented along the perpendicular axis, is shown in Figure 16.11.

This mechanism is well seen in odd-*A* nuclei where a valence particle in an orbit that is sensitive to the Coriolis perturbation aligns its angular momentum along the rotation axis. This gives rise to a specific band similar to the bands in neighboring even nuclei. Indeed, for the aligned particle with a certain value of j_1 , the Coriolis force does not induce any transitions. Only the deformed core reacts to the rotational perturbations and the band consists of states with angular momenta $j, j+2, j+4, \dots$ which are analogs of the corresponding states in the even core. In odd-*N* erbium isotopes, the

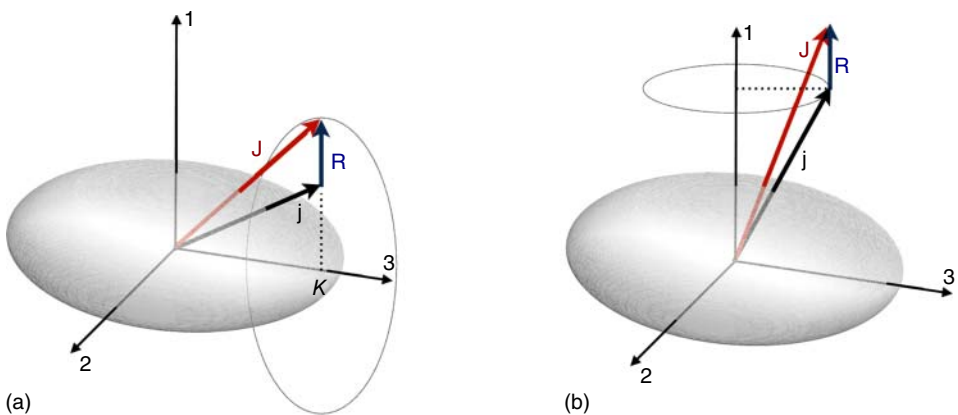


Figure 16.11 Strong-coupling (a) and rotational alignment coupling scheme (b).

neutron states near the Fermi surface Σ_F are originated from the $i_{13/2}$ spherical orbital that is a parity intruder and therefore keeps its almost pure character in a deformed nucleus. When the states with a small projection $m = j_3$ on the deformation axis turn out to be near Σ_F , their wave functions, expanded in the basis quantized along the rotation axis-1, have large components with big values of j_1 . Therefore, they feel the strong Coriolis perturbation and easily become aligned. The decoupled bands in $^{155,157,159}\text{Er}$ have the bandhead $J = j = 13/2$ that corresponds to the maximum $j_1 = j = 13/2$.

The microscopic picture of the pair decoupling in an even–even nucleus is presented in Figure 16.12. This is again the band crossing calculated in the cranking shell model. The model takes into account main effects only, the deformed mean field, pairing, and Coriolis forces. The energy (Routhian) of the two-quasiparticle state, which would correspond to low values of the projection j_3 , goes steeply down in the cranking model as a function of the rotation frequency. The Coriolis effects in the ground-state band are weak. At frequency Ω_c , the gain of rotational energy is sufficient to compensate the loss

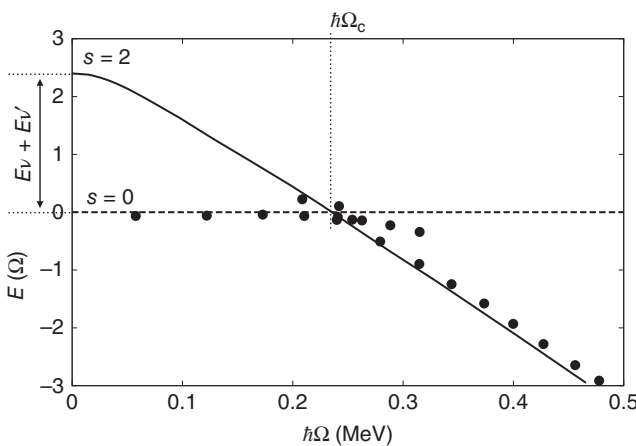


Figure 16.12 The Coriolis effects for the high- j configuration with small projection of the angular momentum along the symmetry axis. Experimental points are taken from the yrast band of ^{168}Hf .

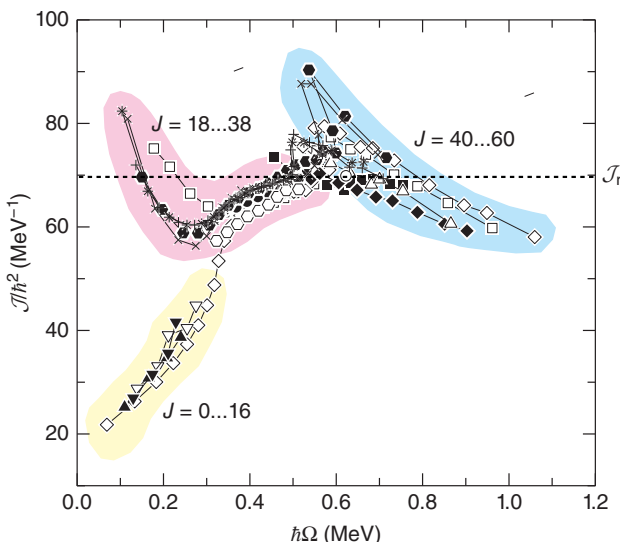


Figure 16.13 The moment of inertia for ^{156}Dy as a function of the rotational frequency. The data points are taken from Ref. [1] and references therein. The horizontal dashed line shows the moment of inertia for a rigid shape approximating ^{156}Dy . Different distinct groups of angular momentum are highlighted. (Reproduced with permission of M. Riley [1], Florida State University.)

of the pairing energy due to the pair breaking. At larger frequencies, the band built on the aligned pair of quasiparticles becomes the yrast band. The slope of the Routhian as a function of the angular velocity, according to (16.172), determines the aligned angular momentum.

At a higher rotational frequency, the second crossing can occur when it becomes energetically favorable to align another pair of quasiparticles. The strength of the remaining pairing sharply decreases and the moment of inertia approaches the rigid-body limit. In Figure 16.13, the behavior of the moment of inertia in ^{156}Dy as a function of rotational frequency is shown and various regions are highlighted. At low momenta, $J = 0 \dots 16$, the system displays properties of a slowly rotating superfluid drop. Higher rotational frequency leads to breaking of Cooper pairs, backbending, causing the transition from superconducting to a normal state for $J = 18 \dots 38$. Finally, another structural change, most likely shape change, occurs at even higher angular momentum, $J > 38$. We see the striking difference in phase transitions destroying superconductivity in bulk metals and finite Fermi systems as nuclei. The development of experimental techniques, especially study of gamma-correlations in cascades provide rich physical information [17–19]. The picture comes closer to classical expectations in the case of nuclear superdeformation [20].

References

- 1 M. Riley, *Gammasphere Online Booklet*, Florida State University, Tallahassee, 1998.
- 2 A.R. Edmonds, *Angular Momentum in Quantum Mechanics*, Princeton University Press, Princeton, NJ, 1974.

- 3 D.A. Varshalovich, A.N. Moskalev, and V.K. Khersonskii, *Quantum Theory of Angular Momentum*, World Scientific, Singapore, 1988.
- 4 L.D. Landau and E.M. Lifshitz, *Mechanics*, Vol. 1 of *Course of Theoretical Physics*, Vol. 1, 3rd edn, Butterworth-Heinemann, Oxford, 2005.
- 5 N. Auerbach and V. Zelevinsky, Phys. Rev. C **90**, 034315 (2014).
- 6 P.M. Walker and J.J. Carroll, Nucl. Phys. News **17**, 11 (2007).
- 7 A. Bohr and B.R. Mottelson, *Nuclear Structure*, Vol. 2, Benjamin, Reading, MA, 1975.
- 8 V. Spevak, N. Auerbach, and V.V. Flambaum, Phys. Rev. C **56**, 1357 (1997).
- 9 N. Auerbach and V. Zelevinsky, J. Phys. G **35**, 093101 (2008). (Topical review.)
- 10 S.T. Belyaev and V.G. Zelevinsky, Sov. J. Nucl. Phys. **17**, 269 (1973).
- 11 D. Inglis, Phys. Rev. **103**, 1786 (1956).
- 12 R.M. Rockmore, Phys. Rev. **116**, 469 (1959).
- 13 J.H. van Vleck, in *Nobel Lectures in Physics 1971–1980*, ed. S. Lundqvist, World Scientific, Singapore, 1992.
- 14 S.T. Belyaev, Kgl. Danske Vid. Selsk. Mat.-Fys. Medd. **31**, No. 11 (1959).
- 15 B.R. Mottelson and J.G. Valatin, Phys. Rev. Lett. **5**, 11 (1960).
- 16 F.S. Stephens and R.S. Simon, Nucl. Phys. **A183**, 157 (1972).
- 17 R.M. Lieder and H. Ryde, Adv. Nucl. Phys. **10**, 1 (1978).
- 18 R. Bengtsson and J.D. Garrett, in *Collective Phenomena in Atomic Nuclei*, International Review of Nuclear Physics, Vol. 2, p. 194, World Scientific, Singapore, 1984.
- 19 J.D. Garrett, in *The Response of Nuclei under Extreme Conditions*, eds. R.A. Broglia and G.F. Bertsch, p. 1, Plenum Press, New York, 1988.
- 20 P.J. Nolan, Nucl. Phys. **A553**, 107c (1993).

17

Self-Consistent Field

The independent particle motion, first introduced to describe the structure of atoms, has played a very important role in nuclear physics. In its most naive form it assumes that the nucleons occupy single-particle orbitals that are eigenstates of an average potential created by the interaction of the nucleons with each other.

I. Sick, in *Highlights of Modern Nuclear Structure*

(World Scientific, Singapore, 1999)

17.1 Exchange Interaction

The exact solution of the quantum many-body problem is attainable in exceptional cases only (noninteracting particles or specially constructed models like a degenerate seniority model, Section 13.4). The most direct method, diagonalization of the Hamiltonian in a truncated orbital space, may be impractical because of prohibitively large dimensions if the number of active particles is large. Usually, we need to do physical approximations based on general principles as well as on specific features of the system. Let us first note that the effective ratio of particle localization energy to the attractive interaction that keeps the nucleus as a whole, can be estimated as $\hbar^2/(Ma^2U_0)$, where the radius a is taken at the distance of maximum attraction, and U_0 the strength of this attraction. For a typical (not too light) nucleus, this parameter is about 0.4 [1], larger than in quantum liquids of helium isotopes ${}^3\text{He}$ and ${}^4\text{He}$, and by two orders of magnitude larger than in many solids. Therefore, we have to deal with a Fermi liquid rather than a piece of a crystal.

We consider the nucleus as a self-sustaining system of identical fermions. The original (vacuum) nucleon–nucleon interaction is very strong. It creates a many-body object that has some properties of a liquid drop. This certainly shows that the significant part of interaction is spent to form a mean field. The mean field is responsible for nuclear shape and main symmetry features. It accumulates the most smooth “coherent” components of interactions. We already know how the pairing interaction can be accounted for. In a sense, this can also be considered as a part of the mean field, the *pairing field*. But there also exist other collective phenomena along with incoherent collision-like processes, which are averaged out when the mean field is extracted. They are responsible for mixing of simple mean-field configurations that becomes more and more strong as excitation energy and level density increase.

The regular way of constructing a hierarchy of many-body approximations starts with the mean field. This is the base of microscopic calculations for nearly all many-body systems. There are several problems we have to solve on this way. The first one is related to identity of particles. The requirement of quantum statistics, antisymmetry of many-fermion wave functions in our case, leads to a specific contribution to the interaction. We have already learned how to handle symmetry properties in the pairing problem (Chapter 13). Now we apply the same approach to a general interaction of bound particles.

Let us consider identical particles moving in a common, at this stage *external*, field and interacting in some way. We write down the Hamiltonian in quite general (here two-body) form as

$$H = H^o + H' = \sum_a h_a + \frac{1}{2} \sum_{a \neq b} U_{ab}, \quad (17.1)$$

where h_a is a Hamiltonian of an isolated particle a and U_{ab} is the interaction of particles a and b . The identity of the particles is expressed by the obvious features of the Hamiltonian: the operators h_a are the same for all particles a , the interactions U_{ab} are identical for all pairs $a \neq b$, and the interaction operator is symmetric, $U_{ab} = U_{ba}$. The factor 1/2 in the interaction term, as in (12.4), prevents from counting the same pair twice.

The single-particle Hamiltonian h has a complete set of eigenfunctions $|\lambda\rangle$,

$$h|\lambda\rangle = h_\lambda|\lambda\rangle, \quad (17.2)$$

where h_λ are single-particle energies unperturbed by the interaction. For example, in the case of free motion, the quantum numbers λ are simply momentum and spin of a free particle, and h_λ is the kinetic energy. It might be practically convenient to include a potential well into H^o to deal from the very beginning with localized orbits rather than with plane waves. The corresponding counter-term can be subtracted from the interaction part.

Now we estimate the effect of the interaction. We do it first in *perturbation theory* calculating the expectation value of U for the unperturbed state of two particles. Consider the state

$$|\mu\nu\rangle = C_{\mu\nu} a_\mu^\dagger a_\nu^\dagger |0\rangle \quad (17.3)$$

with two particles placed on the orbits $|\mu\rangle$ and $|\nu\rangle$ by means of the creation operators acting onto the vacuum state with no particles. The normalization constant $C_{\mu\nu}$ depends on the type of statistics. For the Fermi case, we have $\mu \neq \nu$ (otherwise the state is impossible due to the Pauli principle) and $C_{\mu\nu} = 1$. The same result is valid for $\mu \neq \nu$ in the case of bosons, but for $\mu = \nu$ the properly normalized two-boson state reveals the stimulated emission effects, $C_{\mu\mu} = 1/\sqrt{2}$.

The interaction term contains all processes of scattering described by the matrix elements $(12|U|34)$, where the single-particle orbits are labeled by numbers instead of Greek letters. The matrix element for the transition of two fermions $|\mu\nu\rangle \rightarrow |\mu'\nu'\rangle$ between the two states of type (17.3),

$$\langle \mu' \nu' | H' | \mu \nu \rangle = \frac{1}{2} \sum_{1234} (12|U|34) \langle 0 | a_{\nu'} a_{\mu'} a_1^\dagger a_2^\dagger a_4 a_3 a_\mu^\dagger a_\nu | 0 \rangle, \quad (17.4)$$

follows directly from the fermion commutation rules, or the Wick theorem,

$$\langle \mu' \nu' | H' | \mu \nu \rangle = \frac{1}{2} [(\mu' \nu' | U | \mu \nu) + (\nu' \mu' | U | \nu \mu) - (\mu' \nu' | U | \nu \mu) - (\nu' \mu' | U | \mu \nu)]. \quad (17.5)$$

The presence of two last terms is simply a consequence of the permutational antisymmetry of two-particle states (17.3). Positive and negative contributions are pairwise equal as seen from the obvious symmetry of the matrix elements under permutations of pairs. Finally, the resulting amplitude is

$$\langle \mu' \nu' | H' | \mu \nu \rangle = (\mu' \nu' | U | \mu \nu) - (\nu' \mu' | U | \mu \nu). \quad (17.6)$$

We have already encountered this expression in Eq. (11.49). The first term in (17.6) is called *direct* interaction and the second one is *exchange* interaction. Due to the indistinguishability of particles, we have the sum of two *amplitudes* that interfere in observable *probabilities*. The interference is destructive for fermions; in the case of bosons, the similar terms would have constructive interference. The graphic image of this result is shown in Figure 17.1.

If the interaction $U = U(\mathbf{r}, \mathbf{r}')$ is of pure potential character and does not depend on spin, the result (17.6) nevertheless turns out to be spin dependent. This dependence comes solely from quantum statistics. We can write the single-particle wave function for the orbit $|\mu\rangle$ as a product $\psi_\mu(\mathbf{r})\chi_\mu$ of orthonormalized coordinate and spin functions. The interaction that depends only on coordinates cannot transfer the spin projections. This implies spin conservation and requires equalities

$$\sigma_{\mu'} = \sigma_\mu, \quad \sigma_{\nu'} = \sigma_\nu \text{ (direct);} \quad \sigma_{\nu'} = \sigma_\mu, \quad \sigma_{\mu'} = \sigma_\nu \text{ (exchange).} \quad (17.7)$$

Due to the spin conservation in the interaction, we have to construct the singlet and triplet combinations with the correct total spin $S = 0, 1$ and its projection S_z . In particular, two states with $S_z = 0$ are

$$|\mu \nu; S0\rangle = \frac{1}{\sqrt{2}} (\alpha_{\mu 1/2}^\dagger \alpha_{\nu -1/2}^\dagger + (-)^{S+1} \alpha_{\mu -1/2}^\dagger \alpha_{\nu 1/2}^\dagger) |0\rangle, \quad (17.8)$$

where quantum numbers μ, ν do not include the spin projection indicated explicitly.

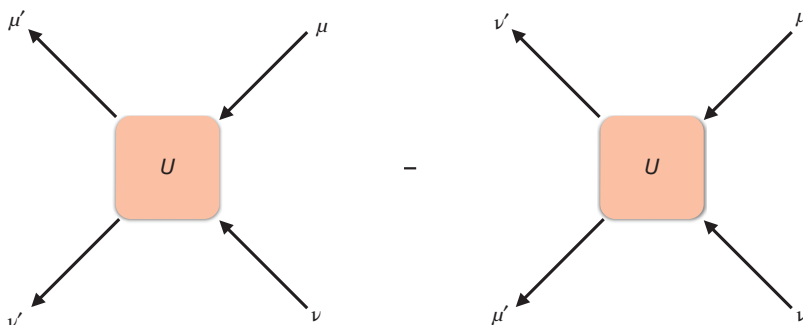


Figure 17.1 Direct and exchange contribution to the interaction of two fermions.

Without interaction, singlet and triplet states have the same energy equal to the sum of single-particle energies

$$E_{\mu\nu}^0 = h_\mu + h_\nu. \quad (17.9)$$

The interaction H' splits singlets from triplets. The energy shift is given by the expectation value of H' in the states (17.8). With the use of (17.6), we obtain

$$\Delta E_{\mu\nu}(S) = I_{\mu\nu}^d + (-)^S I_{\mu\nu}^e. \quad (17.10)$$

The direct contribution does not depend on spin projections,

$$I_{\mu\nu}^d = \int d^3r d^3r' |\psi_\mu(\mathbf{r})|^2 U(\mathbf{r}, \mathbf{r}') |\psi_\nu(\mathbf{r}')|^2. \quad (17.11)$$

This is what we would naively expect, the interaction of two clouds corresponding to the wave packets of two particles. The exchange integral is of quantum origin,

$$I_{\mu\nu}^e = \int d^3r d^3r' \psi_\nu^*(\mathbf{r}) \psi_\mu^*(\mathbf{r}') U(\mathbf{r}, \mathbf{r}') \psi_\nu(\mathbf{r}') \psi_\mu(\mathbf{r}), \quad (17.12)$$

see also (11.44) and (11.49). Note that for the very *short-range* interaction that can be approximated by $\delta(\mathbf{r} - \mathbf{r}')$, the direct and exchange integrals are equal. For the pair of nonequivalent spatial orbits μ and ν , the energy splitting of single and triplet states is $2I_{\mu\nu}^e$.

Recalling the spin exchange operator (2.5), the exchange part of the interaction can be rewritten as an effective *spin–spin* interaction (the original interaction had no spin dependence)

$$H' \Rightarrow -I^e \mathcal{P}^\sigma = -I^e \left(\frac{1}{2} + 2(\mathbf{s}_1 \cdot \mathbf{s}_2) \right). \quad (17.13)$$

For the positive exchange integral I^e , the parallel spin orientation is preferable, and for each pair of orbits $\mu \neq \nu$ the triplet state has lower energy than the singlet state. This is the case for two electrons in the helium atom. In the ground state, the electrons are in the $1s$ orbit and the spin triplet state is forbidden. In the excited configurations with $\psi_\mu \neq \psi_\nu$, both spin combinations are allowed. Since the exchange integral is positive (Coulomb repulsion), the triplet state goes down in energy. A qualitative way to understand this follows from the form of the wave function (17.8): the triplet combination, symmetric under the spin permutation, is antisymmetric under permutation $\mu \leftrightarrow \nu$ of the spatial variables as it should be for Fermi statistics. This means that in the coordinate representation the wave function $\psi(\mathbf{r}, \mathbf{r}')$ is antisymmetric with respect to $\mathbf{r} \leftrightarrow \mathbf{r}'$, and therefore $\psi(\mathbf{r}, \mathbf{r}) = 0$. The zero probability of small distances reduces the Coulomb repulsion and lowers the energy (which is again Coulomb energy as no original spin-dependent forces are present).

In complex atoms, this spin exchange gives rise to the so-called Hund's rule. For a given electron configuration (distribution of electrons over single-particle orbits), various coupling schemes for spin and orbital momentum are possible. Among them, the lowest energy corresponds to the state with the maximum total spin \mathbf{S} when the spatial wave function has the largest spatial antisymmetry and therefore the strongest suppression of the Coulomb repulsion.

For chemical binding, the opposite situation is generic. To combine two neutral atoms into a molecule, one has to concentrate the valence electron wave function between

the nuclei to suppress their Coulomb repulsion. Therefore, the electron state has to be spatially symmetric and antisymmetric in spins, $S = 0$. This is the well-known *covalent* binding via electron pairs with antiparallel spins; the simplest example is the hydrogen molecule H_2 . The Cooper pairing of electrons in superconducting metals has similar nature: an electron deforms a local state of a crystal lattice attracting ions, and another electron in the opposite spin state is attracted to the excess of the lattice positive charge that remains during a slow ion motion. The pairing in heavy nuclei prefers, Chapter 13, the pair states with $T = 1$ and $L = 0$ that implies $S = 0$.

The same spin–spin exchange interaction without spin–spin forces is responsible for the cooperative magnetic effects in condensed matter. The Heisenberg model is based on the effective spin–spin interaction (17.13) of localized spins. $I^e > 0$ prefers the *ferromagnetic* state with parallel spins, whereas $I^e < 0$ would lead to the *antiferromagnetic* ordering with antiparallel orientation of neighboring spins. The very possibility to see the magnetic order and various magnetic structures at rather high temperatures can be explained only by exchange interactions, which originate from Coulomb forces due to the statistical exchange effects. The magnetic dipole interactions are too weak to be capable of creating magnetic order at such high temperature.

17.2 Hartree–Fock Equations

If the interaction is not weak, it changes the energies of many-fermion states significantly. Moreover, it can change spatial symmetry and quantum numbers of stationary orbits. The original single-particle basis cannot be the best choice for the mean field. We need the procedure of extracting the mean field in the optimal way; it should appear as a result of the best selection rather than an *ad hoc* assumption. The Hartree–Fock (HF) method is a regular procedure that allows one to find the best mean field for a *given interaction Hamiltonian*.

The result can be understood very easily. The mean field has to be *self-consistent*. Its symmetry determines the single-particle orbits; the distribution of particles occupying these orbits creates, through their interaction, the average field that should coincide with the original choice. To obtain the HF equations, we simply write down these self-consistency conditions.

Since the proper mean field is unknown a priori, we assume that the single-particle basis $|\lambda\rangle$ exists that corresponds to the best choice. Consider an arbitrary orbit $|\lambda\rangle$ of this set occupied by a particle. In contrast to Eq. (17.2), this is not an eigenstate of the independent particle part h of the Hamiltonian. The operator h induces transitions through its off-diagonal matrix elements $h_{\lambda'\lambda}$. Similar transitions are caused by the interaction with other particles, both in direct and exchange processes (Figure 17.2). This is accompanied by the transitions of the interacting partners $v \rightarrow v'$. The process is *stationary* if (i) amplitudes of the transitions $\lambda \rightarrow \lambda'$ of “our” particle induced by kinetic energy h and by interaction H' compensate each other and, as a result, we have the stationary single-particle orbit, (ii) other particles occupy their orbits in a stationary way so that some orbits are permanently filled and others are permanently empty, and (iii) “our” orbit appears as a filled one in the similar consideration for all other orbits.

To write down explicitly the corresponding equations, we take into account both diagrams of Figure 17.2 and require the stationary conditions for the interacting partners,

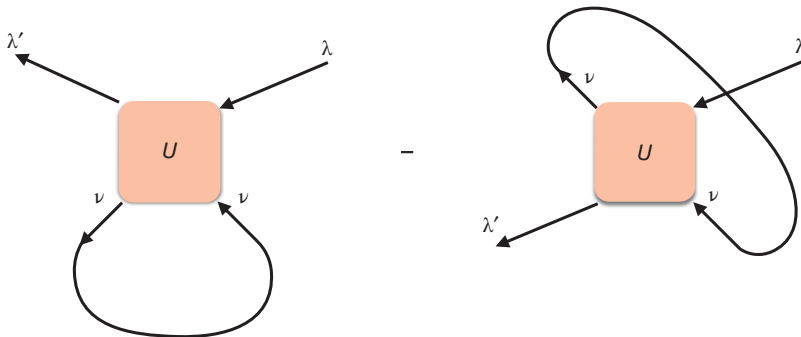


Figure 17.2 Processes contributing to the Hartree–Fock self-consistent field.

$\nu' = \nu$. Then we have to sum over all states occupied by the partners. This gives the average joint action of all of them that is nothing but a mean field sought for. Thus, the single-particle states $|\lambda\rangle$ have to satisfy the set of coupled HF equations,

$$(h + w)|\lambda\rangle = \epsilon_\lambda|\lambda\rangle, \quad (17.14)$$

where the self-consistent part of the mean field has matrix elements $w_{\lambda'\lambda}$ defined according to the standard quantum mechanical rule, see similar definition in Eq. (11.24),

$$w|\lambda\rangle = \sum_{\lambda'} w_{\lambda'\lambda}|\lambda'\rangle, \quad (17.15)$$

and explicitly corresponds to Figure 17.2,

$$w_{\lambda'\lambda} = \sum_v [(\lambda'v|U|\lambda v) - (\lambda'v|U|v\lambda)]. \quad (17.16)$$

The sum in (17.16) goes over *occupied* single-particle states $|\nu\rangle$. Let us introduce the occupation numbers n_ν of individual orbits in the ground state of the many-fermion system. This brings in the desired self-consistency: we assume that in the ground state, the lowest [with respect to the energies ϵ_λ found in (17.14)] single-particle orbits are filled, $n_\lambda = 1$, and the rest of the orbits are empty, $n_\lambda = 0$. Then the orbits are the eigenstates of the HF Hamiltonian

$$\epsilon = h + w, \quad (17.17)$$

where

$$w_{\lambda'\lambda} = \sum_v n_\nu (\lambda'v|\overline{U}|\lambda v), \quad (17.18)$$

and \overline{U} is the *antisymmetrized* interaction (11.49),

$$(\lambda'v'|\overline{U}|\lambda v) = (\lambda'v'|U|\lambda v) - (\lambda'v'|U|v\lambda). \quad (17.19)$$

which coincides with the amplitude in Eq. (17.6).

The set of equations (17.14) for the self-consistent field is *nonlinear*. One can solve them in an iterative way starting from some reasonable guess $h^{(0)}$ for the field, finding the single-particle eigenstates $|\lambda\rangle^{(0)}$ and the eigenvalues $\epsilon_\lambda^{(0)}$, filling the lowest states, and

calculating the resulting field $w^{(1)}$. With the Hamiltonian $\epsilon^{(1)} = h + w^{(1)}$, we repeat the whole cycle. The procedure is assumed to be convergent to the limit when the field $w^{(n+1)}$ coincides, up to some accuracy, with the input $w^{(n)}$. A simpler approach omitting the exchange contributions is called the Hartree approximation. It might be justified in some cases when the direct terms are responsible for the most coherent effects, as in the factorized models to be considered later.

17.3 Operator Formulation

It is clear that the solution of the HF equations gives, as a many-body ground state, a Slater determinant constructed of the self-consistent orbitals $|\lambda\rangle$. Moreover, this is the best approximation to the solution of the full original Schrödinger equation that can be represented by a single Slater determinant. Therefore, the *variational* approach is possible. One can consider the class of trial functions consisting of all Slater determinants built of all possible complete sets of single-particle orbitals. Among all these determinants, one can look for the determinant that minimizes the total energy of the system. This turns out to be just the solution of the HF equations [2].

Instead of performing the straightforward energy minimization, we show here another method that has great flexibility and can be applied to the excited states as well. We use the operator *equation of motion* for the particle creation and annihilation operators. Making certain approximations in the exact equations, we keep the possibilities of the regular improvement that is usually not easy in variational methods. We start with the Hamiltonian (17.1) written in an arbitrary single-particle basis that we label by numbers $|1\rangle, |2\rangle, \dots$

Let us consider a hole created by an annihilation operator a_1 of a particle with quantum numbers 1. This state is not stationary. Its evolution in time is described in the Heisenberg picture by the operator equation

$$i\hbar\dot{a}_1 = [a_1, H]. \quad (17.20)$$

Here all operators are time dependent being taken in the Heisenberg picture. Since the Hamiltonian (with no explicit time dependence) is in this picture the same as in the Schrödinger picture, we can keep the form of the secondary quantized Hamiltonian, simply assuming that all the operators are taken at the same time t . The right-hand side of (17.20) can be derived directly from the elementary commutation rules, which are valid for the Heisenberg operators at coinciding times.

The Hamiltonian (17.1), where we limit ourselves by two-body interactions, in the secondary quantization takes a form

$$H = \sum_{12} h_{12} a_1^\dagger a_2 + \frac{1}{2} \sum_{1234} (12|U|34) a_1^\dagger a_2^\dagger a_4 a_3. \quad (17.21)$$

Due to the antisymmetry of the Fermi operators, the interaction matrix elements in (17.21) can also be antisymmetrized by adding the exchange combination, as in (17.19), so that

$$H = \sum_{12} h_{12} a_1^\dagger a_2 + \frac{1}{4} \sum_{1234} (12|\bar{U}|34) a_1^\dagger a_2^\dagger a_4 a_3. \quad (17.22)$$

For an arbitrary annihilation operator a_1 , we have, using antisymmetry of the interaction \bar{U} ,

$$[a_1, H] = \sum_2 h_{12} a_2 + \frac{1}{2} \sum_{234} (12|\bar{U}|34) a_2^\dagger a_4 a_3. \quad (17.23)$$

This equation is exact but starting from the operator a_1 , we come to a more complicated operator $a_2^\dagger a_4 a_3$. The hole state is not stationary: after the interaction, we have already two holes, in the orbits 3 and 4, and one extra particle in the orbit 2 (our interaction preserves the total particle number).

We can write down similar equations of motion for a new operator $a_2^\dagger a_4 a_3$, but it is clear that the propagation of this complex will create more and more new particles and holes so that the set of equations is limited by the total particle number only. Since we cannot solve the full problem exactly, we introduce the appropriate approximations. If the variational many-body wave function of A particles would be a Slater determinant, the creation of the hole would lead us to another Slater determinant of $A - 1$ particles. Therefore, the equation of motion would be closed among the annihilation operators a . It can be the case if the creation operator a_2^\dagger compensates one of annihilation operators a_3 or a_4 ; both possibilities have to be taken into account and the corresponding contributions have opposite signs.

17.4 Single-Particle Density Matrix

To define accurately this procedure, we first introduce the *density matrix* as a set of particle–hole operators

$$R_{12} = a_2^\dagger a_1. \quad (17.24)$$

Note that these operators act in Hilbert space of *many-body* functions. At the same time, they form a matrix with respect to *single-particle* quantum numbers (1,2). An arbitrary one-body operator can be expressed as

$$Q = \sum_{12} (1|q|2) a_1^\dagger a_2 = \sum_{12} (1|q|2) R_{21} = \text{Tr}(qR). \quad (17.25)$$

Here the trace, Tr, is taken with respect to single-particle matrix subscripts only; the result is still an operator in the full Hilbert space.

We define the *single-particle density matrix* ρ_{12} of the ground state $|\emptyset\rangle$ as an expectation value of the operator matrix R_{12} in the ground state,

$$\rho_{12} = \langle \emptyset | R_{12} | \emptyset \rangle. \quad (17.26)$$

This is a *c*-number matrix rather than an operator. Its diagonal matrix elements,

$$\rho_{11} = \langle \emptyset | a_1^\dagger a_1 | \emptyset \rangle = \langle \emptyset | \hat{n}_1 | \emptyset \rangle, \quad (17.27)$$

are the mean occupation numbers of the orbits |1) in the ground state. But for an arbitrary basis |1) used as a representation in our equations, the off-diagonal matrix elements of the matrix (17.26) do not vanish.

According to our approach, the operator in the interaction term of the equations of motion (17.23) can be approximately reduced to the one-hole operator,

$$a_2^\dagger a_4 a_3 \approx \langle \emptyset | a_2^\dagger a_4 | \emptyset \rangle a_3 - \langle \emptyset | a_2^\dagger a_3 | \emptyset \rangle a_4 = \rho_{42} a_3 - \rho_{32} a_4. \quad (17.28)$$

Due to the antisymmetry of the interaction matrix elements, two terms (17.28) give equal contributions to (17.23) so that the equations of motion, now closed on the one-hole level, acquire the form (we rename the summation indices)

$$[\alpha_1, H] = \sum_2 h_{12} \alpha_2 + \sum_{234} (14|\bar{U}|23) \rho_{34} \alpha_2. \quad (17.29)$$

For any density matrix ρ , we can define the *field functional* $w\{\rho\}$ as a matrix in the single-particle space with elements

$$(w\{\rho\})_{12} = \sum_{34} (14|\bar{U}|23) \rho_{34}. \quad (17.30)$$

This is the field created by the particle distribution and determined by the density matrix ρ in the ground state via the interaction \bar{U} . Of course, this is the same operator as in (17.18) but written now in an arbitrary single-particle basis $|1\rangle$ instead of the final HF basis $|\lambda\rangle$. In this latter basis, the single-particle density matrix ρ_{12} is *diagonal* and its elements n_λ are simply 1 for occupied orbits and 0 for empty orbits. Then (17.30) coincides explicitly with (17.18).

With the aid of the total single-particle Hamiltonian ϵ , Eq. (17.17), that combines the independent particle part h and the self-consistent part $w\{\rho\}$, the equations of motion (17.20,17.29) become

$$i\hbar\dot{\alpha}_1 = [\alpha_1, H] = \sum_2 \epsilon_{12} \alpha_2. \quad (17.31)$$

In the same approximation, the equation for the extra particle produced by the creation operator α^\dagger is

$$i\hbar\dot{\alpha}_1^\dagger = [\alpha_1^\dagger, H] = - \sum_2 \alpha_2^\dagger \epsilon_{21}. \quad (17.32)$$

The HF equations (17.14) define eigenvectors $|\lambda\rangle$ of the single-particle operator ϵ and their eigenvalues ϵ_λ . These states are combinations of the original states $|1\rangle$ and vice versa,

$$|\lambda\rangle = \sum_1 u_{\lambda 1} |1\rangle, \quad |1\rangle = \sum_\lambda u_{\lambda 1}^* |\lambda\rangle. \quad (17.33)$$

The transformation matrix is unitary to guarantee the completeness and orthogonality of both bases,

$$\sum_\lambda u_{\lambda 1}^* u_{\lambda 2} = \delta_{12}, \quad \sum_1 u_{\lambda 1}^* u_{\lambda' 1} = \delta_{\lambda \lambda'}. \quad (17.34)$$

As we know from Chapter 11, the similar relations exist for the creation and annihilation operators, for example,

$$\alpha_1 = \sum_\lambda u_{\lambda 1} \alpha_\lambda, \quad \alpha_\lambda = \sum_1 u_{\lambda 1}^* \alpha_1. \quad (17.35)$$

The amplitudes $u_{\lambda 1}$ are the components of the eigenfunction $|\lambda\rangle$ in the basis $|1\rangle$,

$$\epsilon|\lambda\rangle = \epsilon_\lambda|\lambda\rangle \quad \Leftrightarrow \quad \sum_2 \epsilon_{12} u_{\lambda 2} = \epsilon_\lambda u_{\lambda 1}. \quad (17.36)$$

Therefore, Eqs. (17.31) and (17.32) take the form

$$i\hbar\dot{\alpha}_\lambda = \epsilon_\lambda \alpha_\lambda, \quad i\hbar\dot{\alpha}_\lambda^\dagger = -\epsilon_\lambda \alpha_\lambda^\dagger. \quad (17.37)$$

The creation and annihilation operators have thus the correct time dependence used, in particular, in the quantization of the electromagnetic field (Section 14.3).

Thus, we found an approximation where the ground state is a Slater determinant in the representation determined by the HF equations. Equations (17.31) and (17.32) allow us to find single-particle orbitals as the eigenstates (17.36) of the self-consistent field $\epsilon\{\rho\} = h + w\{\rho\}$. In the same single-particle basis, the density matrix ρ of the ground state is also diagonal with its eigenvalues being the occupation numbers. The operators $\epsilon\{\rho\}$ and ρ have a common basis of the eigenstates λ . This means that they commute,

$$[\epsilon\{\rho\}, \rho] = 0. \quad (17.38)$$

Apart from that, in the HF approximation, eigenvalues of ρ that are occupancies of the HF orbits are 1 or 0, that is, the operator identity is valid,

$$\rho^2 = \rho. \quad (17.39)$$

In terms of the transformation amplitudes (17.35) and occupation numbers n_λ in the HF ground state, the density matrix (17.26) expressed in an arbitrary basis is

$$\rho_{12} = \langle \emptyset | a_2^\dagger a_1 | \emptyset \rangle = \sum_\lambda u_{\lambda 2}^* u_{\lambda 1} n_\lambda. \quad (17.40)$$

In particular, the coordinate representation, $1 \Rightarrow \mathbf{r}$, is convenient when the interaction is given by a potential $V(\mathbf{r} - \mathbf{r}')$. Then the amplitudes $u_{\lambda 1}$ are ordinary wave functions $\psi_\lambda(\mathbf{r})$, and the density matrix (17.40) is

$$\rho(\mathbf{r}, \mathbf{r}') = \sum_\lambda \psi_\lambda(\mathbf{r}) \psi_\lambda^*(\mathbf{r}') n_\lambda. \quad (17.41)$$

The set of the HF equations (17.14) can be written in this case as

$$h\psi_\lambda(\mathbf{r}) + \int d^3 r' V(\mathbf{r} - \mathbf{r}') [\rho(\mathbf{r}', \mathbf{r}') \psi_\lambda(\mathbf{r}) - \rho(\mathbf{r}, \mathbf{r}') \psi_\lambda(\mathbf{r}')] = \epsilon_\lambda \psi_\lambda(\mathbf{r}). \quad (17.42)$$

The nonlinear HF equations have many solutions. Each of them provides a relative energy minimum as compared to the “nearest neighbors” in the space of the Slater determinants. The procedure does not determine which solution corresponds to an *absolute minimum* among Slater determinants. For example, spherical and deformed mean field are possible as solutions for the same original interaction. An additional investigation should show which solution is energetically favorable. One can also look for the solutions with the distribution of the empty and filled orbitals different from the normal Fermi gas in the ground state. For example, the solutions exist with some holes inside Σ_F . The self-consistent field determined by such a distribution of particles is different from the ground state field. Therefore, the single-particle states in these fields are not orthogonal that should be specially taken care of.

17.5 Hartree–Fock–Bogoliubov Approximation

As we know from Chapters 13 and 16, pairing correlations are very important for understanding all phenomena, both in single-particle motion and in collective modes as rotation. In the presence of developed pairing, the distribution of particles over orbitals changes considerably. Therefore, the “ordinary,” unrelated to pairing, residual forces

act in a different surrounding. As a result, the self-consistent field is different from what would be observed without pairing. Pairing influences nuclear shapes, moments of inertia, mass parameters, transition probabilities, and reaction cross sections. On the other hand, nuclear shape defines single-particle orbits and conditions for pairing. The energy gap is also a self-consistent quantity that depends on wave functions and energies of particle orbits. This complex interplay of various residual interactions is not accounted for in the HF approach that does not include pairing correlations on equal footing. The pairing added in the BCS model does not change the nuclear field that means a lack of self-consistency.

A more general approach that produces an advanced version of the self-consistent field method is the Hartree–Fock–Bogoliubov (HFB) approximation first developed by N.N. Bogoliubov, 1958–1959. It is widely used in condensed matter physics in order to take into account simultaneously effects of Coulomb forces or impurities and superconducting pairing.

We derive the HFB equations by the straightforward extension of the operator equations of motion. The canonical transformation (17.35) between the single-particle basis $|1\rangle$ and the HF quasiparticle basis $|\lambda\rangle$ conserves the particle number. In contrast to that, the HFB approximation takes into account the pair condensate and utilizes the general canonical transformation that, as its simplified version (Section 13.5), does not conserve the particle number. Therefore, we need to introduce chemical potentials for protons and neutrons that ensure correct nucleon numbers in average. The corresponding Hamiltonian of independent particles will be then $h' = h - \mu$.

We start with the exact equations of motion (17.23). We again linearize these equations by splitting the complicated operator into a single-particle operator and an expectation value of the remaining operator pair in the ground state. But now we have to take into account the possible existence of the pair condensate. Then the operators like aa or $a^\dagger a^\dagger$ have large matrix elements between the ground states of neighboring systems with $A \mp 2$ particles. In the framework of the seniority scheme, we discussed this problem in Section 13.5. Thus, we come, instead of (17.28), to the approximation for the *generalized density matrix*:

$$a_2^\dagger a_4 a_3 \approx \langle \emptyset | a_2^\dagger a_4 | \emptyset \rangle a_3 - \langle \emptyset | a_2^\dagger a_3 | \emptyset \rangle a_4 + \langle \emptyset | a_4 a_3 | \emptyset \rangle a_2^\dagger. \quad (17.43)$$

The new part of the density matrix,

$$P_{34} = \langle \emptyset | a_4 a_3 | \emptyset \rangle, \quad (17.44)$$

has the same meaning as matrix elements of the pair operator P in Section 13.5. The state $|\emptyset\rangle$ used as a model for the ground state includes now the pair condensate that serves as a reservoir for creating and annihilating correlated pairs. In this approximation, the linearization recipe is

$$a_2^\dagger a_4 a_3 \approx \rho_{42} a_3 - \rho_{32} a_4 + P_{34} a_2^\dagger. \quad (17.45)$$

The linearized equation of motion (17.23) becomes

$$[a_1, H] = \sum_2 \epsilon_{12} a_2 + \sum_2 \Delta_{12} a_2^\dagger, \quad (17.46)$$

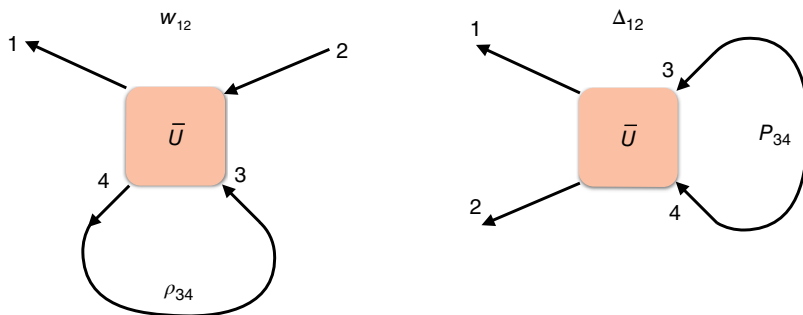


Figure 17.3 Scattering, Eq. (17.30), and pairing, Eq. (17.47), self-consistent potentials.

where the self-consistent field $\epsilon = h' + w$ is defined, as in the preceding section, by Eqs. (17.17) and (17.30), and the *pairing field* is

$$\Delta_{12} = \frac{1}{2} \sum_{34} (12|\bar{U}|34)P_{34}. \quad (17.47)$$

In the same way, we obtain the equation of motion for the creation operator, compare with (17.32),

$$[a_1^\dagger, H] = - \sum_2 a_2^\dagger \epsilon_{21} - \sum_2 \Delta_{12}^* a_2. \quad (17.48)$$

The self-consistent “potentials” $w\{\rho\}$ and $\Delta\{P\}$ are determined by different matrix elements of the same interaction \bar{U} . The averaging proceeds in the *particle-hole channel* for the scattering potential w and in the *particle-particle channel* for the pairing potential Δ (Figure 17.3).

The symmetry properties in those channels are also different. As seen from the definition (17.24), the full-density matrix operator R is Hermitian if considered in combined space, many-body Hilbert space plus single-particle space,

$$(R_{12})^\dagger = a_1^\dagger a_2 = R_{21}. \quad (17.49)$$

Since the single-particle density matrix is defined in (17.26) as a diagonal matrix element in Hilbert space, it is simply Hermitian in a standard sense in single-particle space, $\rho_{12}^\dagger = \rho_{21}^*$. The matrix P , Eq. (17.44), is antisymmetric, $P_{43} = -P_{34}$, because of the Fermi statistics. Since the interaction \bar{U} is Hermitian, the particle-hole potential w , Eq. (17.30), is Hermitian as well, while the particle-particle potential Δ , Eq. (17.47), is antisymmetric due to the antisymmetry of the interaction \bar{U} .

17.6 General Canonical Transformation

The set of coupled linear equations (17.46), (17.47) can be formally solved by the generalized canonical transformation to new Fermi operators b_λ and b_λ^\dagger . Our earlier transformation in the pairing problem, Section 13.5, involved only time-conjugate pairs, and therefore both old, a , and new, b , operators could be labeled by the same quantum numbers. The self-consistent field may change nuclear shape so that in general we have to

carry out a transformation to a completely new single-particle basis as in (17.35) but with the addition of the condensate part as in Section 13.5.

The general Bogoliubov transformation can be written as

$$a_1 = \sum_{\lambda} (u_{1\lambda} b_{\lambda} - v_{1\lambda} b_{\lambda}^{\dagger}), \quad a_1^{\dagger} = \sum_{\lambda} (u_{1\lambda}^* b_{\lambda}^{\dagger} - v_{1\lambda}^* b_{\lambda}). \quad (17.50)$$

The new operators $b_{\lambda}, b_{\lambda}^{\dagger}$ are supposed to be Fermi operators with the standard commutation rules. This imposes the unitarity conditions [generalization of (17.34)] onto the transformation coefficients. We consider these coefficients as “skew” matrices $u = \{u_{1\lambda}\}$ and $v = \{v_{1\lambda}\}$ with subscripts running over different bases of the same dimension. From the anticommutators $[a_1, a_2^{\dagger}]_+ = \delta_{12}$, we easily obtain

$$\sum_{\lambda} (u_{1\lambda} u_{2\lambda}^* + v_{1\lambda} v_{2\lambda}^*) = \delta_{12}, \quad (17.51)$$

or, in the matrix form,

$$uu^{\dagger} + vv^{\dagger} = 1, \quad (17.52)$$

which is an analog of the BCS normalization condition. Similarly, the anticommutator $[a_1, a_2] = 0$ gives (the superscript T means transposition of the matrix)

$$uv^T + vu^T = 0. \quad (17.53)$$

Due to the normalization (17.52) and (17.53), the inverse transformation from quasiparticles to original particles is easily checked to be

$$b_{\lambda} = \sum_1 (u_{1\lambda}^* a_1 - v_{1\lambda} a_1^{\dagger}), \quad b_{\lambda}^{\dagger} = \sum_1 (u_{1\lambda} a_1^{\dagger} - v_{1\lambda}^* a_1), \quad (17.54)$$

and the correct anticommutators of quasiparticle operators imply

$$u^T u^* + v^{\dagger} v = 1, \quad u^T v^* + v^{\dagger} u = 0. \quad (17.55)$$

Both components of the single-particle density matrix for the ground state can be expressed in terms of the transformation matrices. The ground state is considered to be the quasiparticle vacuum state. Then, using the transformation (17.50) in (17.40) and (17.44), we obtain

$$\rho_{12} = \sum_{\lambda} v_{2\lambda}^* v_{1\lambda} \rightsquigarrow \rho = vv^{\dagger} \quad (17.56)$$

and

$$P_{12} = - \sum_{\lambda} u_{2\lambda} v_{1\lambda} \rightsquigarrow P = -vu^T. \quad (17.57)$$

After the HFB equations are solved, the Hamiltonian (17.22) will be transformed to the form

$$H = E_0 + \sum_{\lambda} E_{\lambda} b_{\lambda}^{\dagger} b_{\lambda} + H'_{\text{HFB}}. \quad (17.58)$$

This can be done formally by means of the canonical transformation of the original fermion operators (17.50). We plug into the Hamiltonian the expressions of a, a^{\dagger} in terms of b, b^{\dagger} and, with the aid of commutation relations, rearrange all terms to the normal form with all b^{\dagger} 's to the left of all b 's.

All nonoperator terms comprise a constant in (17.58). With the density matrix given by (17.56) and (17.57), we get

$$E_0^{\text{HFB}} = \text{Tr} \left[\left(h' + \frac{1}{2} w \right) \rho + \frac{1}{2} \Delta P^\dagger \right]. \quad (17.59)$$

This can be obtained immediately from (17.22) taking the expectation value $\langle H \rangle$ in the HFB ground state and using the generalized Wick theorem,

$$\begin{aligned} \langle a_1^\dagger a_2^\dagger a_3 a_4 \rangle &= \langle a_1^\dagger a_4 \rangle \langle a_2^\dagger a_3 \rangle - \langle a_1^\dagger a_3 \rangle \langle a_2^\dagger a_4 \rangle + \langle a_1^\dagger a_2^\dagger \rangle \langle a_3 a_4 \rangle \\ &= \rho_{41}\rho_{32} - \rho_{31}\rho_{42} + P_{12}^\dagger P_{43}. \end{aligned} \quad (17.60)$$

The definitions (17.30) and (17.47) of the field components lead to the result (17.59). If there is no pairing, this reduces to the HF ground state energy

$$E_0^{\text{HF}} = \text{Tr} \left[\left(h + \frac{1}{2} w \right) \rho \right]. \quad (17.61)$$

Note that this energy is *not equal* to the sum of the HF quasiparticle energies

$$\sum_\lambda \epsilon_\lambda n_\lambda = \text{Tr}(\epsilon \rho) = \text{Tr}[(h + w)\rho], \quad (17.62)$$

where we have used the fact that ϵ and ρ are simultaneously diagonal, Eq. (17.38), in the HF basis $|\lambda\rangle$, and the trace does not depend on the representation of matrices. In the correct expression (17.61) of the HF energy, the interaction enters with the factor 1/2 as compared to the simple sum (17.62). This underlines the importance of self-consistency: the contribution of the self-consistent field w to the quasiparticle energy comes from the interaction with other quasiparticles. Summing all energies in (17.62), we account for all pairwise interactions twice.

The quasiparticle energy ϵ_λ is the difference between the ground state energy of A particles and the energy of the state of $A + 1$ particles where the extra particle is placed on the orbit λ . We used such a definition calculating the quasiparticle spectrum in the paired BCS state, Section 13.9. A similar approach should be used for determining the hole energy. According to this, the quasiparticle energy is the variational derivative of the total energy with respect to the quasiparticle occupation numbers,

$$\epsilon_\lambda = \frac{\delta E_0}{\delta n_\lambda}. \quad (17.63)$$

When applied to the HF expression (17.61), it has to include the change of the self-consistent field w , Eq. (17.18), in addition to the explicit change of the eigenvalues n_λ of the density matrix ρ . Due to the symmetry of the interaction $V_{ab} = V_{ba}$ both contributions are equal which cancels the factor 1/2 and leads to the correct value (17.14) of ϵ_λ .

17.7 Solutions

After the canonical transformation, the terms with two new operators in the Hamiltonian (17.58) include, apart from the quasiparticle energies of unpaired quasiparticles $E_\lambda b_\lambda^\dagger b_\lambda$, also terms of the same type with $b_\lambda^\dagger b_{\lambda'}^\dagger$, $\lambda \neq \lambda'$, and the terms creating ($\sim b^\dagger b^\dagger$) and annihilating ($\sim bb$) pairs. The latter *dangerous diagrams* were encountered in the

similar situation in the BCS theory as well. To make the Hamiltonian of the quasiparticles stable with respect to creation and annihilation of pairs, we have to find the set of the transformation amplitudes $u_{1\lambda}, v_{1\lambda}$ that will ensure the disappearance of the dangerous graphs and diagonalize the quasiparticle part. We do not need to do all the calculations in this way because our equations of motion (17.46) will give the same result.

We look for the solution of the equations of motion (17.46) as a superposition (17.50) of proper quasiparticle operators. The HFB approximation corresponds to the best choice of independent quasiparticles. In this approximation, we neglect the last term H'_{HFB} of the Hamiltonian (17.58) that includes four *normally ordered* quasiparticle operators b, b^\dagger . Then the equations of motion for the new operators are

$$[b_\lambda, H] = E_\lambda b_\lambda, \quad [b_\lambda^\dagger, H] = -E_\lambda b_\lambda^\dagger, \quad (17.64)$$

as it should be for independent annihilation and creation operators. Substituting (17.50) into (17.46), using (17.64) in the left-hand side and separating terms with the operators b_λ and b_λ^\dagger , we come to the set of coupled equations for the amplitudes $u_{1\lambda}$ and $v_{1\lambda}$,

$$\begin{aligned} u_{1\lambda} E_\lambda &= \sum_2 (\epsilon_{12} u_{2\lambda} - \Delta_{12} v_{2\lambda}^*), \\ v_{1\lambda} E_\lambda &= \sum_2 (-\epsilon_{12} v_{2\lambda} + \Delta_{12} u_{2\lambda}^*). \end{aligned} \quad (17.65)$$

It is easy to see that for the pure pairing interaction, we return to the results of the BCS model. Indeed, in this case, only two time-conjugate orbits are involved so that

$$\epsilon_{12} = \epsilon_1 \delta_{12}, \quad \Delta_{12} = \Delta_1 \delta_{21}, \quad (17.66)$$

and antisymmetry $\Delta_{12} = -\Delta_{21}$ is fulfilled due to the time-reversal operation. Then

$$v_{1\lambda} = \frac{1}{E_\lambda + \epsilon_1} \sum_2 \Delta_{12} u_{2\lambda}^* = \frac{\Delta_1}{E_\lambda + \epsilon_1} u_{1\lambda}^* \quad (17.67)$$

that is the correct relation between the u and v factors, compare the case of Section 13.7 where $u_1 = u_{\bar{1}}$. Now we use (17.67) to obtain the eigenvalue condition from the equation for $u_{1\lambda}$ and the same time-reversal condition,

$$u_{1\lambda} \left(E_\lambda - \epsilon_1 - \frac{|\Delta_1|^2}{E_\lambda + \epsilon_1} \right) = 0. \quad (17.68)$$

The quasiparticle energy E_λ coincides with what was found in the BCS theory; the definitions of Δ coincide as well. In this case, we do not need to go to a new single-particle basis; the quasiparticles are labeled by the same quantum numbers 1.

The coefficients u, v determine the wave function of the quasiparticle. It might be convenient to introduce the “spinor” notations. Each solution X_λ of the HFB equations (17.65) consists of the set of amplitudes, which are subdivided into two classes, $U_\lambda = \{u_{1\lambda}\}$ and $V_\lambda = \{v_{1\lambda}^*\}$,

$$X_\lambda = \begin{pmatrix} U_\lambda \\ V_\lambda \end{pmatrix} \quad (17.69)$$

This definition allows one to present the HFB equations (17.65) as a spinor Schrödinger equation for the wave function (17.69) with the Hamiltonian \mathcal{H} ,

$$\mathcal{H} X_\lambda = E_\lambda X_\lambda, \quad \mathcal{H} = \begin{pmatrix} \epsilon & -\Delta \\ \Delta^* & -\epsilon^* \end{pmatrix}. \quad (17.70)$$

Because of the antisymmetry of Δ , the effective Hamiltonian \mathcal{H} is Hermitian in spinor space, so that the eigenvalues E_λ are real. All eigenvalues appear in pairs $\pm E_\lambda$. Indeed, using the Pauli matrix σ_x , we can construct the vector

$$\bar{X}_\lambda = \sigma_x X_\lambda^* = \begin{pmatrix} V_\lambda^* \\ U_\lambda^* \end{pmatrix} = \begin{pmatrix} \{v_{1\lambda}\} \\ \{u_{1\lambda}^*\} \end{pmatrix}. \quad (17.71)$$

It satisfies the equation

$$(\sigma_x \mathcal{H}^* \sigma_x) \bar{X}_\lambda = E_\lambda \bar{X}_\lambda. \quad (17.72)$$

But the transformation of the Hamiltonian \mathcal{H} by σ_x gives

$$\sigma_x \mathcal{H} \sigma_x = -\mathcal{H}^*. \quad (17.73)$$

From hence the vector (17.71) is the eigenvector of the HFB Hamiltonian with the eigenvalue $-E_\lambda$,

$$\mathcal{H} \bar{X}_\lambda = -E_\lambda \bar{X}_\lambda. \quad (17.74)$$

Thus, for each solution X_λ with HFB energy E_λ , the partner exists, the solution \bar{X}_λ of the same HFB equations with the eigenvalue $-E_\lambda$.

The existence of such a mirror solution could be easily guessed because we have used the standard prescription (17.65) to distinguish between the quasiparticle creation and annihilation operators. They are eigenmodes of the same Hamiltonian with energies $\pm E_\lambda$. The mirror symmetry just corresponds to their mutual transformation as can be seen also from comparison of the solutions (17.69) and (17.71) with the canonical transformation (17.54). It seems now that we have twice as many solutions as in HF theory and two for each set of quasiparticle quantum numbers. This should be the case because we consider a system that has no certain particle number. As we discussed in Chapter 13, a quasiparticle with the same quantum characteristics can be generated with creation of a particle or with annihilation of the time-conjugate partner. Also in the BCS theory, one can consider $E_\lambda < 0$ that is connected with the transformation $u_\lambda \leftrightarrow v_\lambda$, that is, from empty to filled orbits.

The situation reminds that in relativistic theory [QP, II, 13.4] where creation of a particle and annihilation of an antiparticle produces the same charge of the system. The relativistic wave equations allow the solutions with energies $E = \pm \sqrt{c^2 \mathbf{p}^2 + m^2 c^4}$ for any momentum \mathbf{p} . A physical particle is described by the positive energy solution; the negative energy solution is reinterpreted as related to an antiparticle. As far as we consider the stable ground state, the quasiparticle excitations should correspond to positive energies. However, if quasiparticle energies depend on a variable parameter, some of them can go down as the value of the parameter changes. At some critical value, the former positive energy can cross the zero level from above and its partner becomes positive. This would correspond to instability of the HFB ground state when it becomes energetically profitable to create quasiparticles.

The Hamiltonian (17.58) describes a system of quasiparticles with their *residual interaction* expressed by the last term H'_{HFB} that contains four creation and annihilation quasiparticle operators in various combinations. The great advantage of the operator formulation is that the transformation is exact and we are able to take into account the terms H'_{HFB} going beyond the HFB approximation. The next step, Chapter 18, will be related to the random phase approximation.

17.8 Generalized Density Matrix

The formal scheme of the HFB approximation can be completed by a construction of the generalization of the single-particle density matrix (17.26). First, we define the operator spinors combining the creation and annihilation operators, both for the original basis, a_1^\dagger, a_1 , and for the HFB basis, $b_\lambda^\dagger, b_\lambda$,

$$B_\lambda^\dagger = \begin{pmatrix} b_\lambda^\dagger \\ b_\lambda \end{pmatrix}, \quad A_1^\dagger = \begin{pmatrix} a_1^\dagger \\ a_1 \end{pmatrix}. \quad (17.75)$$

In these terms, the canonical transformations (17.50) and (17.53) can be written in the matrix form,

$$A^\dagger = MB^\dagger, \quad B^\dagger = M^{-1}A^\dagger, \quad (17.76)$$

where, using notations of (17.52), (17.53) and (17.55),

$$M = \begin{pmatrix} u^* & -v^* \\ -v & u \end{pmatrix}, \quad M^{-1} = \begin{pmatrix} u^T & -v^\dagger \\ -v^T & u^\dagger \end{pmatrix}. \quad (17.77)$$

By direct multiplication with the use of canonical conditions (17.52)–(17.55), we see that the transformation is unitary, $M^\dagger M = 1$.

The density matrix, naturally generalized from (17.26) to the doubled space, is defined as

$$r_{12} = \langle \emptyset | A_2^\dagger A_1 | \emptyset \rangle. \quad (17.78)$$

This matrix, apart from the explicit single-particle indices, has also spinor indices obtained by the multiplication of the column A^\dagger by the row A . Its elements are the ordinary density matrix (17.40) and the pairing matrix (17.44),

$$r_{12} = \begin{pmatrix} a_2^\dagger a_1 & a_2^\dagger a_1^\dagger \\ a_2 a_1 & a_2 a_1^\dagger \end{pmatrix} = \begin{pmatrix} \rho_{12} & P_{12}^\dagger \\ P_{12} & \delta_{12} - \rho_{21} \end{pmatrix} = \begin{pmatrix} \rho & P^\dagger \\ P & 1 - \rho^T \end{pmatrix}_{12}. \quad (17.79)$$

After the canonical transformation, the density matrix acquires the simplest form because the ground state is the quasiparticle vacuum, $b_\lambda |\emptyset\rangle = 0$,

$$r_{\lambda\lambda'} = \begin{pmatrix} 0 & 0 \\ 0 & 1 \end{pmatrix}_{\lambda\lambda'}. \quad (17.80)$$

From (17.80), we see that the eigenvalues of the generalized density matrix are $r_\lambda = 0$ or 1, and it is diagonalized by the matrix M of the canonical transformation simultaneously with the effective Hamiltonian \mathcal{H} , Eq. (17.70). Thus, both main properties (17.38) and (17.39) of the HF approximation are preserved in the HFB approximation considered in the *doubled space*,

$$[\mathcal{H}\{r\}, r] = 0, \quad (17.81)$$

$$r^2 - r = 0. \quad (17.82)$$

The last equation is equivalent to the relations between the two parts of the generalized single-particle density matrix,

$$\rho - \rho^2 = P^\dagger P, \quad P\rho = \rho^T P. \quad (17.83)$$

The first of these equalities expresses that the ordinary occupation numbers are always between 0 and 1 as long as the pairing part does not vanish, that is, pairing smears out the Fermi surface (Figure 13.4).

The ground state of the HFB approximation is built in close analogy to the Fermi gas but in the doubled space. All states with negative energies $-E_\lambda$ [solutions \bar{X}_λ , Eq. (17.71)] are “occupied,” $r_\lambda = 1$, while their partners with positive energies E_λ (solutions X_λ , Eq.(17.70)) are “empty,” $r_\lambda = 0$.

The algebraic relations (17.83) allow one to prove the Bloch–Messiah theorem [3, 4] that shows that a special single-particle basis (sometimes called the *pointer basis* or canonical basis) does exist where the density matrix has a form similar to the BCS pairing case. Indeed, the Hermitian operator ρ can be diagonalized. Of course, at the same time, the transposed matrix ρ^T is getting diagonal as well and coincides with ρ . According to the first Eq. (17.83), the matrix $P^\dagger P$ is diagonal in the same basis. Factors P and P^\dagger are not diagonal in general, but due to the second Eq. (17.83) they have nonzero matrix elements only between the states with the same eigenvalue of ρ . But these matrices are antisymmetric so that their diagonal elements are always zero. If ρ has no degenerate eigenvalues, we have identically $P = 0$. The nondegenerate eigenvalues of ρ can be equal to 0 or 1 only. The normal case corresponds to the pairwise degeneracy between the single-particle states 1 and $\tilde{1}$. Let these two states have the same eigenvalue $\rho_1 = \rho_{\tilde{1}} \equiv n_1$. Then the operator $P^\dagger P$ has in the same 2×2 block the degenerate eigenvalue $n_1 - n_{\tilde{1}}^2$. This is the product of the off-diagonal matrix elements of P and P^\dagger ,

$$(P^\dagger P)_{11} = P_{1\tilde{1}}^\dagger P_{\tilde{1}1} = P_{\tilde{1}\tilde{1}}^* P_{\tilde{1}1} = |P_{\tilde{1}1}|^2. \quad (17.84)$$

It defines, compare Section 13.7,

$$|P_{\tilde{1}1}| = \sqrt{n_1(1 - n_1)}. \quad (17.85)$$

Here, as in the BCS model, the partners are occupied only pairwise so their occupancies are equal. The numbers n_1 correspond to v_1^2 in BCS theory, whereas the pairing amplitudes (17.85) are equivalent to $u_1 v_1$.

According to Bloch–Messiah theorem, the single-particle basis can be always decomposed by an additional transformation into the states with $n_1 = 0$ or 1 and no pairing, $P = 0$, and blocks 2×2 , which have the diagonal elements (occupation numbers $n_1 = n_{\tilde{1}}$) between 0 and 1 and the antisymmetric off-diagonal pairing matrix elements of magnitude (17.85). We can still call these partner states with the same occupancies “conjugate,” but in general they are not time-conjugate. Their HF energies (diagonal matrix elements of ϵ) can be different. The HF+BCS case is recovered if the diagonal, ϵ , and off-diagonal, Δ , parts of the HFB Hamiltonian (17.70) can be diagonalized simultaneously, and the pairing potential Δ has nonzero matrix elements only between the conjugate orbitals. This means that in Eq. (17.47), the summed states (3, 4) belong to the same pair being linked by the pairing operator P_{43} , but it does not mean that the same is valid for the states 1,2. However, this is the case for the spherical field and standard pairing of the time-conjugate orbits with the total angular momentum $J = 0$: starting with such a pair, we get a similar pair state after scattering.

17.9 Pairing and Particle Number Conservation

Although any realistic calculation for nuclear many-body physics includes the pairing correlations [5] and general computer programs are available [2, 6], the consideration along the lines discussed earlier is not always completely satisfactory. In finite systems, such as nuclei or atoms in traps, we do not enjoy universally the smooth dependence of properties on the number of particles. The exact evolution with the particle number can be of primary interest when we discuss loosely bound nuclei, especially close to the drip lines. Another obvious case when the particle number has to be exact is that of the shape instability. The transformation from spherical to deformed shape in some regions of periodic chart occurs quite sharply, for instance, the deformation appears like a phase transition between neodymium isotopes 148 and 150, or in the so-called *island of inversion* of rare neutron-rich isotopes at $N = 20$ [7]. In all such cases, the precise particle number is essential.

Many authors try to improve standard approaches to pairing and restore the precise particle number by a projection method. We have mentioned that the variational parameters u and v can be complex being characterized by a relative phase φ (the phase of the pair condensate wave function). The projection method considers the set of functions with identical structure but different phases. Integration over the phase with the factor $e^{i\hat{N}\varphi}$ works as a Fourier transformation. The transformed function is an eigenstate of the particle number operator \hat{N} . From a more abstract viewpoint, this procedure of rotation in the phase space corrects the spontaneous symmetry breaking related to a certain choice of the mean field. However, in this way, we lose the *variational* character of the whole approach – the projected function is not anymore the solution of the quantum problem which is guaranteed to be the best (in the sense of the lowest energy) on a certain class of trial functions.

Problem 17.1 A standard representation of a many-body coordinate wave function $\Psi(\mathbf{r}_1, \dots, \mathbf{r}_A)$ as a function of all coordinates violates the translational invariance by fixation of the center-of-mass position (all coordinates in this wave function are taken relative to this origin). A freely moving system has a definite value of the total momentum \mathbf{P} . Find the integral transformation of the many-body function that restores a certain value of \mathbf{P} .

Solution

We have to take a Fourier transform with respect to the center-of-mass coordinate \mathbf{R} ,

$$\Psi_{\mathbf{P}} = \int d^3 R e^{(i/\hbar)(\mathbf{P} \cdot \mathbf{R})} \Psi(\mathbf{r}_1 - \mathbf{R}, \dots, \mathbf{r}_A - \mathbf{R}). \quad (17.86)$$

We have also to remind that, in the framework of the BCS-type approach, the fundamental gap equation, recall (13.102), may not have a solution if the effective strength constant is smaller than a certain critical value. If so, the solution will be a normal Fermi-filling with lost pairing correlations. This happens, for example, in a standard consideration of the isotope ^{48}Ca where the BCS approximation has only the zero solution for the energy gap [8]. The shell-model solution based on the diagonalization of the Hamiltonian matrix in the same orbital space reveals a considerable energy related to the pairing correlations, ~ 2 MeV.

There are various ways how the traditional BCS-type description of pairing can be modified and improved by the exact particle number conservation [9]. One possible path to this goal is to use the equations of motion constantly keeping track of the exact particle number, see also our degenerate model example discussed in Section 13.5. The variational parameters $u_1(N)$ and $v_1(N)$ are defined as in Eq. (13.55), where the total particle number is fixed as

$$N = \langle N | \sum_1 a_1^\dagger a_1 | N \rangle \approx \langle N | a_1^\dagger | N - 1, \tilde{1} \rangle \langle N - 1, \tilde{1} | a_1 | N \rangle = \sum_1 |v_1(N)|^2. \quad (17.87)$$

Here the approximation consists in using only one intermediate state with a hole generated by the operator a_1 (a standard approach to pairing correlations which also can be extended for collective states), while the particle number is fixed for every state.

With the pairing interaction of a general type,

$$H = 2 \sum_1 \epsilon'_1 n_1 - \sum_{12} G_{12} a_1^\dagger a_1^\dagger a_2 a_2, \quad \epsilon'_1 = \epsilon_1 - \mu(N) - \frac{1}{2} G_{11}, \quad (17.88)$$

where the summation goes over the time-conjugate pairs, we come to the exact equations of motion,

$$[a_1, H] = \epsilon'_1 - \sum_2 G_{12} (a_2 a_2) a_1^\dagger, \quad (17.89)$$

and similarly for the creation operators. Leaving in the nonlinear term only intermediate states with seniority one, we obtain a set of linear equations,

$$\begin{aligned} [\epsilon_1(N) + \epsilon'_1(N)] v_1(N+2) - \Delta_1(N) u_1(N) &= 0, \\ [\epsilon_1(N) - \epsilon'_1(N)] u_1(N) - \Delta_1(N) v_1(N+2) &= 0. \end{aligned} \quad (17.90)$$

Here the gap function is defined as (we assume it to be real)

$$\Delta_1(N) = \frac{1}{2} \sum_2 G_{12} v_2(N+2) u_2(N), \quad (17.91)$$

while the excitation spectrum is expressed as earlier but for each value of N ,

$$\epsilon_1^2(N) = \epsilon'_1^2(N) + \Delta_1^2(N). \quad (17.92)$$

Problem 17.2 Derive equations for the gap parameter $\Delta_1(N)$ and occupancies $n_1(N) = v_1^2(N)$.

Solution

Using the expression of $v_1(N+2)$ from Eq. (17.91) and the occupancies from Eq. (17.87), we obtain (summation over pairs)

$$\Delta_1(N) = \sum_2 G_{12} \frac{\Delta_2(N)}{e_2(N) + \epsilon_2(N)} [1 - n_2(N)], \quad (17.93)$$

and

$$n_1(N+2) = \frac{\Delta_1^2(N)[1 - n_1(N)]}{[\epsilon_1(N) + \epsilon'_1(N)]^2} \quad (17.94)$$

with the normalization $\sum_1 n_1(N) = N$ for all N . It is easy to find that Eq. (17.94) reduces to the standard BCS scheme if we neglect the difference between occupancies in the

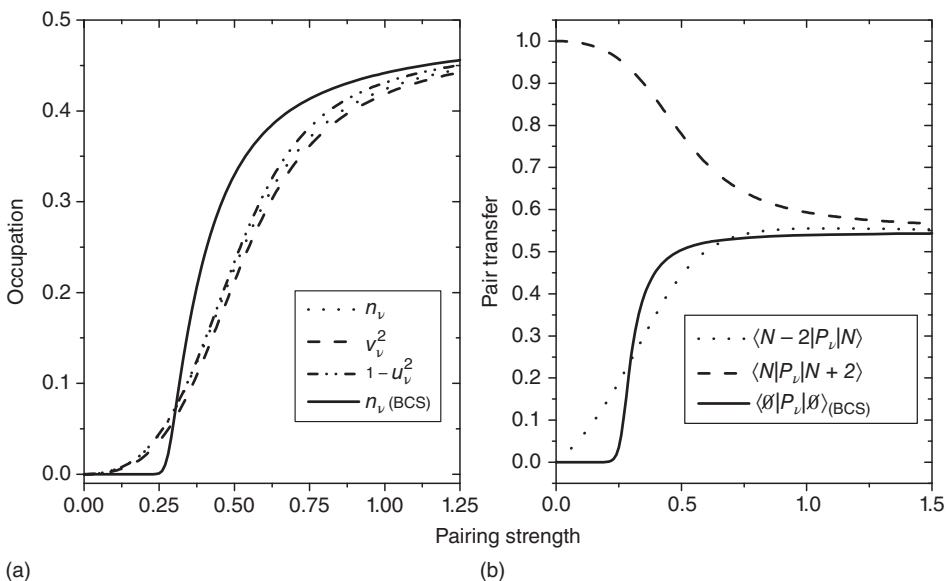


Figure 17.4 A model study of weak pairing limit. Panel (a) shows occupation numbers and related particle addition and removal amplitudes that are all equal within BCS theory, the BCS result is also shown. Panel (b) compares exact pair addition and pair removal amplitudes with that of BCS theory. The pairing strength is given in units of level spacing.

ground states of neighboring even nuclei. Otherwise we now have to solve the set of recurrence relations, for example, by iterations. As demonstrated in Section 13.5, the procedure reproduces the exact solution for the degenerate model.

Restoration of exact particle number is especially important in borderline situations when many-body structure is unstable and sensitive to small changes. For example, a proper treatment of pairing is critical for near-dripline nuclei, or in systems with an unstable mean field where several shapes can closely compete. Weak pairing, the limit when the embryo of the superconducting phase competes with single-particle motion, is another commonly encountered situation in nuclei and other mesoscopic systems. The latter situation and importance of particle number conservation are illustrated in Figure 17.4 where a model of 10 equally spaced double-degenerate single-particle states with $N = 10$ particles is considered. In Figure 17.4a, the occupancy of the first level above the Fermi surface is shown as a function of pairing strength G (in units of level spacing). In Figure 17.4b, the pair transfer matrix element is shown. In the limit of weak pairing, there could be a substantial difference between BCS and exact amplitudes. Similarly, the amplitudes for pair addition and pair removal are generally not equal when pairing is weak, right panel of Figure 17.4.

17.10 Effective Interaction

The most important practical question in application of the mean-field ideas is that of the interaction Hamiltonian. We have assumed that a “quite general” form of the Hamiltonian consists (i) of the independent particle part h , presumably the kinetic

energy of the bare particles, or a simple shell-model potential, and (ii) the residual pair interaction. Already here a strong approximation is made, namely that of the *pairwise* character of the residual interaction. Some average effects of three-body and four-body interactions can be included without large changes although the formalism becomes more involved [9].

However, even on the level of two-body interactions, many other possibilities were tried. In the region of relatively light nuclei, modern computational techniques allow the many-body calculations starting from first principles, *ab initio*, with the interaction taken from experiments with free nucleons, for example, *Argonne interaction* (Section 3.2). Such calculations are plausible only up to $A \approx 16$. There is an active recent development of the so-called *effective field theory* [10–13] where the nucleon interactions (two- and in principle many-body) are constructed using the symmetry of the light meson exchanges in quantum chromodynamics and adding few empirical constants modeling the short-range part of the interaction. This assumes that such a fundamental interaction can also serve in the nuclear medium as a base for real many-body theory. Nevertheless, until now, the question of renormalization of such an interaction along the periodic chart is far from being solved.

Very successful calculations were systematically performed with *semiempirical* interactions. Here it is possible, for a limited purpose of quantitative description of low-energy spectroscopic information, to make a direct diagonalization in the truncated space of single-particle orbits. For example, this space can include the major $1s-0d$ shell with three orbitals $1s_{1/2}$, $0d_{3/2}$, and $0d_{5/2}$ for both protons and neutrons. Within this space, there are only 63 independent two-body matrix elements $\langle (j_1 j_2)JT | H' | (j_3 j_4)JT \rangle$, which describe all scattering processes for the pair of nucleons with certain values of the constants of motion J and T in the field created by the inert core. If, at excitation energies of interest, there is no nuclear states that require the excitation of the core or the transfer of the valence particles into the next shell, one can find an *effective* two-body Hamiltonian that reproduces, in the many-body diagonalization, the observed levels and matrix elements of simple multipole operators. These 63 matrix elements can be fit to give the best overall description of hundreds known observables (level energies, transition rates, multipole moments) in many nuclei within the shell. Such a procedure fixes the Hamiltonian that subsequently can be used for calculating other quantities and making predictions for future experiments. The found matrix elements take into account effectively the influence of the coupling to the states outside the valence space.

In heavy nuclei, the dimensions of valence space become too large for such a procedure even inside one major shell. On the other hand, the direct application of the HF approximation with the realistic nucleon–nucleon forces is not satisfactory. It is impossible to obtain simultaneously a reasonable description of saturation of nuclear forces (nuclei do not collapse in spite of nuclear attraction) and binding energy in heavy nuclei or in the limit of infinite nuclear matter. The HF approximation does not take into account the short-range nucleon–nucleon correlations associated with the repulsive core. Such effects are averaged out in the mean-field description, but they are important for preventing a collapse. They cannot be included by perturbation theory because such a short-range scattering leads formally to infinite matrix elements.

Therefore, it is necessary either to include directly short-range correlations and give up the mean field approximation or to introduce effective interactions. Except for the light

nuclei, the last option is more attractive from both computational and conceptual points of view. The effective interaction should model the full nucleon–nucleon scattering amplitude *in nuclear medium*. To avoid difficulties with the perturbational approach to short-range correlations, one has to solve the two-body problem exactly but the results depend on the presence of other nucleons, partially because the intermediate states in the scattering process are up to a certain extent blocked due to the Pauli principle [14]. Such correlations are in fact *many-body effects*. The effective interactions in a truncated single-particle space cannot be absolutely universal. They necessarily depend on the next approximation as they have to take into account the truncation that is different in different approaches but practically always appears as a part of real computations.

However, due to the short range of interactions, the influence of the medium is *local*. In the same spirit of averaging the random components of dynamics as used for extracting the mean field [15], one can assume that the result will depend mainly on the *local density*. This gives rise to the so-called *energy density functional* method. In general, it is possible to show [QP, II, 19.10] that the ground state density of the particles given as a function of coordinates uniquely determines the ground state many-body wave function of the system. Here the universality can be reached although only for the ground (and special collective) states as we will discuss later. The problem is to convert this theorem of existence into a practical method of solution. This means that we have to determine this functional of density, which will play the role of the effective interaction.

17.11 Skyrme Functionals

The first and rather successful approach was developed with the use of the effective *momentum-dependent* forces by Skyrme [16]. The momentum dependence reflects the same effects of short-range correlations. Apart from that, usually three-body short-range forces are introduced; being averaged over the third particle, they are equivalent to the two-body forces with the density dependence.

In the coordinate representation, the two-body part of the Skyrme forces with their dependence on the relative distance \mathbf{r} and momentum (gradient operators acting onto the wave function of relative motion) can be written as

$$U(\mathbf{r}) = \hat{t}_0 \delta(\mathbf{r}) + \frac{1}{2} \hat{t}_1 [\delta(\mathbf{r}), \nabla^2]_+ + \hat{t}_2 (\nabla \cdot \delta(\mathbf{r}) \nabla). \quad (17.95)$$

Here the operators \hat{t}_i , $i = 0, 1, 2$, contain the mixture of the Wigner and Bartlett forces, Section 3.1,

$$\hat{t}_i = t_i (1 + x_i \mathcal{P}^\sigma), \quad (17.96)$$

where t_i and x_i are parameters. The forces contain also the spin–orbit part

$$U_{\ell s}(\mathbf{r}) = i\lambda (\nabla \cdot \delta(\mathbf{r}) [(\vec{\sigma}_1 + \vec{\sigma}_2) \times \nabla]), \quad (17.97)$$

and the local three-body interaction

$$U_3(\mathbf{r}_1, \mathbf{r}_2, \mathbf{r}_3) = t_3 \delta(\mathbf{r}_1 - \mathbf{r}_2) \delta(\mathbf{r}_2 - \mathbf{r}_3). \quad (17.98)$$

In practice, frequently the effective three-body forces of the type (17.98) are substituted by the density-dependent two-body forces with the coordinate dependence

$$U_3(\mathbf{r}_1, \mathbf{r}_2) \propto \delta(\mathbf{r}_1 - \mathbf{r}_2) \rho^\alpha \left(\frac{\mathbf{r}_1 + \mathbf{r}_2}{2} \right). \quad (17.99)$$

Here, the power α is also an empirical parameter taken by different authors as $1/3$, $2/3$, or 1 .

Problem 17.3 Show that the effective Skyrme-type two-body interaction can be written in terms of the matrix elements in the momentum space (here \mathbf{k} and \mathbf{k}' are final and initial relative momenta of the two-body interaction):

$$\langle \mathbf{k} | U | \mathbf{k}' \rangle = \hat{t}_0 + \frac{1}{2} \hat{t}_1 (k^2 + k'^2) + \hat{t}_2 (\mathbf{k} \cdot \mathbf{k}') + i\lambda (\vec{\sigma}_1 + \vec{\sigma}_2) \cdot [\mathbf{k} \times \mathbf{k}']. \quad (17.100)$$

In the HF approximation, the nucleon density as a function of coordinates \mathbf{r} , spin projection $\sigma \equiv \sigma_z$ and isospin $\tau \equiv \tau_3$, is given by the sum over the *occupied* single-particle states ϕ_λ (bispinors if we include spin and isospin variables),

$$\rho(\mathbf{r}, \sigma, \tau) = \sum_{\lambda} \phi_{\lambda}^\dagger(\mathbf{r}, \sigma, \tau) \phi_{\lambda}(\mathbf{r}, \sigma, \tau). \quad (17.101)$$

Problem 17.4 Show that for the ground state of an even–even nucleus, assuming the equal occupancy of time-reversed orbitals λ and $\tilde{\lambda}$,

$$\sum_{\lambda} \phi_{\lambda}^\dagger(\mathbf{r}, \sigma, \tau) \phi_{\lambda}(\mathbf{r}, \sigma', \tau) = \delta_{\sigma\sigma'} \rho_{\tau}(\mathbf{r}), \quad (17.102)$$

where the total density of neutrons or protons is, according to (17.101),

$$\rho_{\tau}(\mathbf{r}) = \sum_{\lambda; \sigma} |\phi_{\lambda}(\mathbf{r}, \sigma, \tau)|^2. \quad (17.103)$$

Problem 17.5 Show that the contribution of kinetic energy to the density functional is

$$K.E. = \sum_{\lambda} (\lambda |\hat{\mathbf{p}}|^2 / (2m)) |\lambda\rangle = \frac{\hbar^2}{2m} \int d^3 r \sum_{\lambda; \sigma, \tau} |\nabla \phi_{\lambda}(\mathbf{r}, \sigma, \tau)|^2 \equiv \frac{\hbar^2}{2m} \int d^3 r \kappa(r). \quad (17.104)$$

We mentioned that for the δ -interaction, the direct and exchange integrals give in fact the same result. Due to the local character of interaction, the matrix elements can be expressed explicitly in terms of the local density, momentum density, and spin density. The corresponding algebraic details (in application to even–even spherical nuclei) can be found in Ref. [17]. Therefore, the HF equations with Skyrme forces are actually differential equations rather than integrodifferential. The generalization of the HF method to density-dependent and many-body forces is straightforward, especially in models with a δ -interaction. A very similar interaction is introduced in the Landau–Migdal *Fermi-liquid theory* that is widely used in condensed matter physics as well as in nuclear physics [18, 19].

There are many versions of the Skyrme forces and many various parameter sets used in the literature. Figure 17.5 shows the results of solving the HF equations for proton and neutron single-particle energies with Skyrme forces from Ref. [20]. The nucleon density distribution and the effective potential from the same study are shown in Figure 17.6.

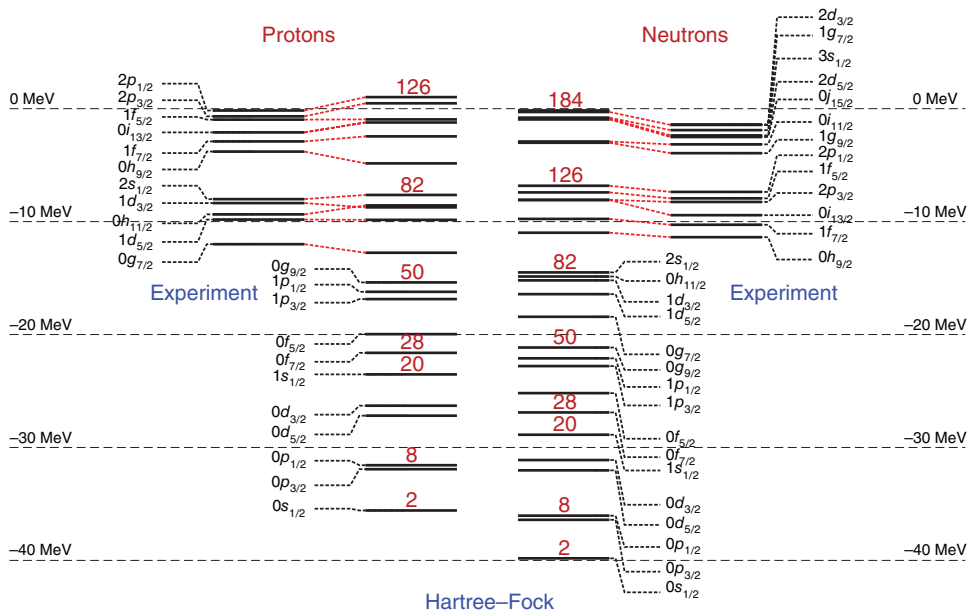


Figure 17.5 Proton, left panel, and neutron, right panel, single-particle levels in the doubly-magic nucleus ^{208}Pb . Hartree–Fock calculations are compared to experiment.

The role of pairing and the difference between HF and HFB approximations was highlighted earlier in Figure 13.7. The main effect from pairing for open-shell nuclei comes from redistribution of nucleons (Figure 13.6). The density is significantly smoothed, and the moment of inertia is decreased by a factor of 3 as compared to the HF case. This pushes up all rotational levels, in agreement with experimental spectra (see Figure 16.3).

The simplest situation takes place for the model of infinite symmetric *nuclear matter* where the orbitals are plane waves occupied up to the Fermi momentum k_F , or Fermi energy $\epsilon_F = \hbar^2 k_F^2 / (2m)$, total density $\rho = (2/3)\pi^2 k_F^3$, and total energy per particle can be expressed as

$$\frac{E}{A} = \frac{3}{5} \epsilon_F + a\rho + b\rho^2 + c\rho k_F^2, \quad (17.105)$$

where the constants a , b , and c are linear functions of parameters t in the Skyrme functional; the term $b\rho^2$ contains only t_3 and comes from the three-body forces with linear dependence on density, $\alpha = 1$ in Eq. (17.99). Three parameters of Eq. (17.105) can be found from E/A , the saturation condition – minimum E/A with respect to the density,

$$\frac{\partial(E/A)}{\partial k_F} = 0, \quad (17.106)$$

and the parameter of the nuclear-matter *incompressibility*,

$$K = k_F^2 \frac{\partial^2(E/A)}{\partial k_F^2}. \quad (17.107)$$

By construction, it is clear that the incompressibility and the parameter t_3 of three-body forces are related linearly.

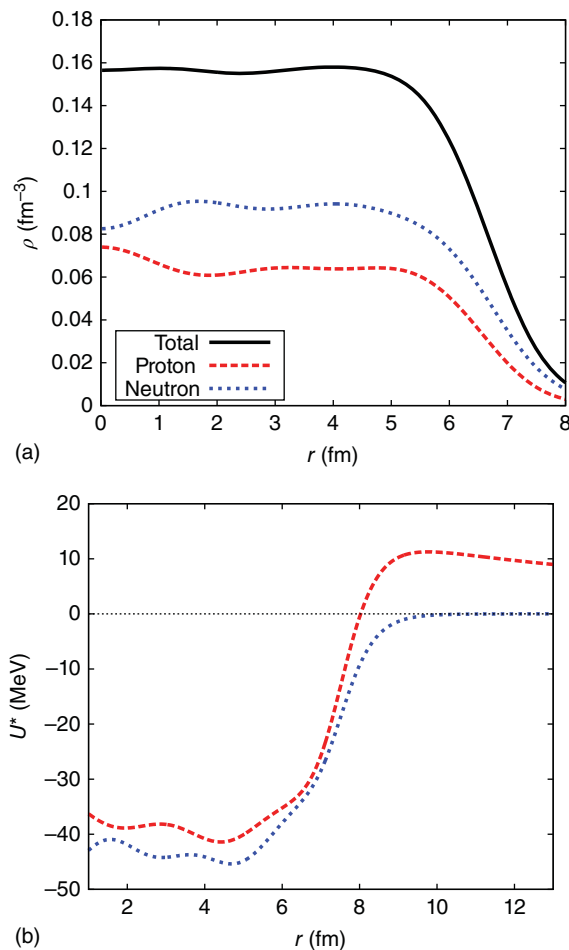


Figure 17.6 Hartree–Fock calculations for ^{208}Pb , same Skyrme functional as in Figure 17.5. (a) Proton, neutron and total density as a function of r . (b) Proton and neutron effective potential computed self-consistently for nucleon in $0s_{1/2}$ orbit.

For the finite nuclei, the effective orbitals $\phi_\lambda(\mathbf{r}, \sigma, \tau)$ are to be found from the HF equation that will have a form of the single-particle Schrödinger equation with kinetic energy [do not confuse the operator \hat{K} with incompressibility K in Eq. (17.107)],

$$\hat{K} = -\nabla \cdot \frac{\hbar^2}{2m_\tau^*(\mathbf{r})} \nabla, \quad (17.108)$$

that contains the effective density-dependent mass m_τ^* . The HF equation contains the effective potential $U_\tau(\mathbf{r})$ depending on ρ and on ρ^2 (through t_3) and also on gradients of ρ , Coulomb interaction, and currents of particles. The terms proportional to $(\nabla\rho)^2$ determine the surface properties (the thickness of the surface layer). For the self-conjugate nuclei ($N = Z$) and neglecting the Coulomb interaction, the equations are independent of τ .

Especially simple are the results for the double-magic nuclei. Here the density is spherically symmetric so that the solutions for the orbitals ϕ_λ are standard single-particle

functions in a spherical field with spin–orbit coupling,

$$\phi_\lambda(\mathbf{r}, \sigma, \tau) = \frac{u_{n\ell j\tau}(r)}{r} [Y_\ell \chi]_{j\ell m}, \quad (17.109)$$

where the quantum numbers are $\lambda = (n, \ell, j, m, \tau)$, and the symbol [...] means the vector coupling of spin and orbital momentum into a total angular momentum j . Due to spherical symmetry, the current can be only radial, and the effective mass m^* can depend on r only.

Problem 17.6 Express the total density and the kinetic part (17.104) for the spherically symmetric ansatz (17.109).

Solution

$$\rho(r) = \frac{1}{4\pi} \sum_{n\ell j\tau} (2j+1) \frac{u_{n\ell j\tau}^2(r)}{r^2}, \quad (17.110)$$

$$\kappa(r) = \frac{1}{4\pi} \sum_{n\ell j\tau} (2j+1) \left[\left(\frac{d(u_{n\ell j\tau}/r)}{dr} \right)^2 + \frac{\ell(\ell+1)}{r^4} u_{n\ell j\tau}^2 \right]. \quad (17.111)$$

The radial differential equation can be written as a regular Schrödinger equation with constant mass but with energy-dependent potential U^* and then solved self-consistently; such a potential for energy of $0s_{1/2}$ orbit is shown in Figure 17.6b.

Problem 17.7 The Hartree–Fock radial wave function in a spherically symmetric case satisfies the differential equation

$$\left\{ -\frac{\hbar^2}{2m^*(r)} \frac{d^2}{dr^2} + U(r) \right\} u(r) - \frac{du}{dr} \frac{d}{dr} \left(\frac{\hbar^2}{2m^*(r)} \right) = \epsilon u(r), \quad (17.112)$$

where $U(r)$ is the HF effective potential that includes the usual centrifugal part. Show that with substitution $u(r) = \sqrt{m^*(r)/m} u^*(r)$ this equation can be brought to a traditional, regular Schrödinger equation with the energy-dependent potential $U^*(r, \epsilon)$.

Solution

$$\begin{aligned} U^*(r, \epsilon) &= \frac{m^*(r)}{m} \left[U(r) + \left(\frac{d^2}{dr^2} \frac{\hbar^2}{4m^*(r)} \right) - \frac{m^*(r)}{2\hbar^2} \left(\frac{d}{dr} \frac{\hbar^2}{2m^*(r)} \right)^2 \right] \\ &+ \left[1 - \frac{m^*(r)}{m} \right] \epsilon. \end{aligned} \quad (17.113)$$

There exist more than a hundred different versions of the Skyrme functionals that provide a reasonable agreement on the properties of nuclei and nuclear matter close to the line of stability but diverge in their predictions on the loosely bound nuclei and for nuclear matter of high density in neutron stars [22]. In practical calculations, one usually starts with the harmonic oscillator trial functions and calculates the necessary densities created by the new self-consistent field. This field generates the new set of

orbitals and the iterations continue up to a good convergence when the resulting field agrees with the input field. The converged nuclear density can be compared with the empirical information on nucleon orbitals, spin–orbital splitting, nuclear masses, and nuclear form-factors extracted from the experiments on electron scattering.

17.12 Generalization to Nonzero Temperature

The description of nuclear reactions and nuclear matter in astrophysical conditions requires the generalization of the density functional method to finite temperature. The simplest way of doing this is to apply the same semiclassical approach as earlier but combine it with the Darwin–Fowler method of the statistical description. Anyway, here our physical interest is, by its nature, statistical.

In a standard Fermi-gas description, the temperature-dependent occupation numbers of single-particle orbitals λ are

$$n_\lambda = \frac{1}{1 + e^{(\epsilon_\lambda - \mu)/T}}. \quad (17.114)$$

Here the chemical potential is necessary because the total particle number N has to be fixed, at least in the statistical sense,

$$N = \sum_\lambda n_\lambda \Rightarrow \mu = \mu(N, T). \quad (17.115)$$

In fact, we need two chemical potentials, μ_τ , to fix the numbers N_τ of protons and neutrons. We always measure temperature T in energy units, $k_B \rightarrow 1$.

Problem 17.8 At zero temperature, we have used the single-particle level density $v(\epsilon) = \sum_\lambda \delta(\epsilon - \epsilon_\lambda)$ that is defined only through the discrete single-particle spectrum of orbitals. At $T \neq 0$, it might be convenient [21] to define another, effective, level density $v^T(\epsilon)$ that will depend on temperature and excitation energy. Introduce it by

$$N = \int_{-\infty}^{\mu} d\epsilon v^T(\epsilon). \quad (17.116)$$

Find $v^T(\epsilon)$.

Solution

At finite T , we still have $N = \sum_\lambda n_\lambda$. At $T = 0$, the single-particle occupation numbers n_λ changed from 1 to 0 by a jump if the chemical potential μ moved up crossing the level $\epsilon = \epsilon_\lambda$. At $T > 0$, the occupancies are changing continuously; instead of $\delta(\epsilon - \epsilon_\lambda)$, we have here a function

$$\left(\frac{\partial n_\lambda}{\partial \mu} \right)_{\mu=\epsilon} \equiv f(\epsilon - \epsilon_\lambda). \quad (17.117)$$

Therefore, the full accumulation of the particle probability at the level λ when we build the Fermi occupation is

$$n_\lambda = \int_{-\infty}^{\mu} d\epsilon f(\epsilon - \epsilon_\lambda). \quad (17.118)$$

Accordingly,

$$N = \sum_{\lambda} n_{\lambda} = \sum_{\lambda} \int_{-\infty}^{\mu} d\epsilon f(\epsilon - \epsilon_{\lambda}). \quad (17.119)$$

This determines function v^T , Eq. (17.116),

$$v^T(\epsilon) = \sum_{\lambda} \left(\frac{\partial n_{\lambda}}{\partial \mu} \right)_{\mu=\epsilon} = \frac{1}{4T} \sum_{\lambda} \frac{1}{\cosh^2[(\epsilon - \epsilon_{\lambda})/2T]}. \quad (17.120)$$

Problem 17.9 Find the function $v^T(\epsilon)$ for the paired system with the energy spectrum

$$\epsilon_{\lambda} \Rightarrow E_{\lambda} = \sqrt{(\epsilon_{\lambda} - \mu)^2 + \Delta_{\lambda}^2}. \quad (17.121)$$

Solution

$$v^T(\epsilon) = \frac{\Delta_{\lambda}^2}{2E_{\lambda}^3} \tanh \left(\frac{E_{\lambda}}{2T} \right) + \frac{(\epsilon - \epsilon_{\lambda})^2}{4TE_{\lambda}^2 \cosh^2(E_{\lambda}/2T)}. \quad (17.122)$$

Instead of the ground state density matrix ρ (17.101), where only the single-particle orbitals ϕ_{λ} occupied in the ground state of the Fermi-liquid contribute, we use the so-called Bloch density matrix $\tilde{\rho}$ depending on the statistical parameter β that has the dimension of inverse energy,

$$\tilde{\rho}(I, I'; \beta) = \sum_{\lambda} \phi_{\lambda}^{\dagger}(I) \phi_{\lambda}(I') e^{-\beta \epsilon_{\lambda}}. \quad (17.123)$$

For simplicity of formulae, we use here the combined argument $I = (\mathbf{r}, \sigma, \tau)$.

The main change compared to the previous definition (17.101) is in the summation that now completely covers the infinite Hilbert space of single-particle orbitals λ , including even the continuum states. The contributions of higher states are weighted by the statistical factor $e^{-\beta \epsilon_{\lambda}}$, where β is just a variable parameter playing the role of inverse temperature but still arbitrary.

The problems of the genetic connection between the effective forces used for calculating nuclear mean field properties and realistic vacuum forces on nucleon–nucleon, meson, and quark levels are still far from being fully understood.

References

- 1 B.R. Mottelson, Nucl. Phys. **A649**, 45c (1999).
- 2 C.J. Cramer, *Essentials of Computational Chemistry*, John Wiley & Sons, Ltd., Chichester, 2002.
- 3 C. Bloch and A. Messiah, Nucl. Phys. **39**, 95 (1962).
- 4 A.L. Goodman, Adv. Nucl. Phys. **11**, 263 (1979).
- 5 R.A. Broglia and V. Zelevinsky, eds. *Fifty Years of Nuclear BCS*, World Scientific, Singapore, 2013.
- 6 C. Froese Fischer, Comput. Phys. Commun. **43**, 355 (1987).

- 7 B.A. Brown and W.A. Richter, Phys. Rev. C **74**, 034315 (2006).
- 8 A. Volya, B.A. Brown, and V. Zelevinsky, Phys. Lett. **B509**, 37 (2001).
- 9 A. Volya and V. Zelevinsky, *Fifty Years of Nuclear BCS*, World Scientific, Singapore, 2013, p. 73.
- 10 C.P. Burgess, Annu. Rev. Nucl. Part. Sci. **57**, 329 (2007).
- 11 S.K. Bogner, T.T.S. Kuo, and A. Schwenk, Phys. Rep. **386**, 1 (2003).
- 12 E. Epelbaum, H.W. Hammer, and U.G. Meissner, Rev. Mod. Phys. **81**, 1773 (2009).
- 13 R. Machleidt and D.R. Entem, Phys. Rep. **503**, 1 (2011).
- 14 H.A. Bethe, Annu. Rev. Nucl. Sci. **21**, 93 (1971).
- 15 V.G. Zelevinsky, Nucl. Phys. **A555**, 109 (1993).
- 16 T.H.R. Skyrme, Nucl. Phys. **9**, 615 (1959).
- 17 D. Vautherin and D.M. Brink, Phys. Rev. C **5**, 626 (1972).
- 18 A.B. Migdal, *Theory of Finite Fermi Systems and Application to Atomic Nuclei*, John Wiley & Sons, Inc., New York, 1967.
- 19 S.P. Kamerdzhiev, J. Speth, and G. Tertychny, Phys. Rep. **393**, 1 (2004).
- 20 B.A. Brown, Phys. Rev. C **58**, 220 (1998).
- 21 M. Brack and P. Quentin, Nucl. Phys. **A361**, 35 (1981).
- 22 J.R. Stone and P.G. Reinhard, Prog. Part. Nucl. Phys. **58**, 587 (2007).

18

Collective Modes

.. the plastic behavior of the nucleus depends on subtle effects like the detailed occupation of single-particle levels close to the Fermi energy, the superfluidity of the system, the surface tension, and so on.

P.F. Bortignon, A. Bracco, R.A. Broglia, *Giant Resonances* (Harwood, Amsterdam, 1998)

18.1 Schematic Model

As we discussed in Section 15.2, the interactions in the system can form the eigenstates which are *coherent superpositions* of many simple states used as a basis in the absence of interactions. The coherence property is formulated as a special feature of the components of an eigenfunction: they are “parallel” to the matrix elements of a simple physical operator, such as a multipole moment, between this “parent” state and a “daughter” state connected by a strong transition amplitude. We can trace in detail how such a state emerges as a result of residual interactions if we consider a scheme of mixing of original noninteracting states. The scheme turns out to be quite generic for various many-body systems.

Let us assume that the Hamiltonian H of the system is subdivided into an unperturbed part (in practice, independent quasiparticles in the mean field) and the residual interaction,

$$H = H^o + H'. \quad (18.1)$$

The mean field creates a set of configurations $|k\rangle$ with energies ϵ_k ,

$$H^o|k\rangle = \epsilon_k|k\rangle, \quad (18.2)$$

whereas the interaction H' generates their mixing via matrix elements H'_{kl} . We can look for the solution of the Schrödinger equation for the exact eigenfunctions $|\alpha\rangle$ of the total Hamiltonian (18.1),

$$H|\alpha\rangle = E_\alpha|\alpha\rangle, \quad (18.3)$$

in terms of the complete set of “simple” states $|k\rangle$,

$$|\alpha\rangle = \sum_k C_k^\alpha |k\rangle. \quad (18.4)$$

Unitarity of the transformation between the original basis and the eigenbasis implies the orthonormality properties,

$$\sum_k C_k^{\alpha*} C_k^{\alpha'} = \delta_{\alpha\alpha'}, \quad \sum_{\alpha} C_k^{\alpha*} C_k^{\alpha} = \delta_{kk'}. \quad (18.5)$$

The Schrödinger equation (18.3) rewritten in the matrix form as a set of coupled equations for the amplitudes C_k^{α} reads

$$\epsilon_k C_k^{\alpha} + \sum_l H'_{kl} C_l^{\alpha} = E_{\alpha} C_k^{\alpha}. \quad (18.6)$$

All exact quantum numbers (constants of motion of the total Hamiltonian H , such as angular momentum, parity, isospin) are the same for the states $|k\rangle$ as well as for the eigenstates $|\alpha\rangle$. The formal solution of (18.6) is

$$C_k^{\alpha} = \frac{1}{E_{\alpha} - \epsilon_k} \sum_l H'_{kl} C_l^{\alpha}. \quad (18.7)$$

The emergence of the collective state is possible if the interaction itself reveals some coherence properties. The simplest situation when it occurs is the following. Assume that there exists a *subset* of simple states $|k\rangle$ of similar nature and with the same values of exact constants of motion. For example, these states are generated from the unperturbed ground state $|0\rangle$ by the action of similar operators \hat{q}_k^{\dagger} so that

$$|k\rangle = \hat{q}_k^{\dagger} |0\rangle. \quad (18.8)$$

The operators \hat{q}_k can be multipole one-body operators creating one-particle–one-hole ($1p-1h$) states of a given multipolarity (quantum numbers $J^{\Pi}T$) from the shell model ground state, or breaking a pair in the presence of developed pairing. In the secondary quantization language, they are separate contributions to the total multipole operator \hat{Q} .

If the states $|k\rangle$ belong to a certain class of $1p-1h$ states, their unperturbed energies are $\epsilon_k = \epsilon(p) - \epsilon(h)$, where both terms are counted from Σ_F so that $\epsilon(p) > 0$, $\epsilon(h) < 0$. If we limit ourselves in a shell model by the hole states from one occupied major shell below Σ_F , the selection rules usually place possible particle states into a certain empty shell above Σ_F . Thus, for the isovector dipole operator, the allowed particle states belong to the next shell that contains mostly orbits of the opposite parity. The picture is more smeared in deformed nuclei but it still keeps the same general character. In superdeformed states we have in fact different shell structure that also will concentrate $1p-1h$ states with specific quantum numbers in a certain energy region.

In such a situation, the main part of the mixing Hamiltonian H' acting between the states $|l\rangle$ and $|k\rangle$ should have the structure of the product of the operators annihilating one excitation (l) and creating another one (k). Therefore it can be modeled as a product of the corresponding multipole matrix elements,

$$H'_{kl} \approx \kappa q_k q_l, \quad (18.9)$$

where κ shows the common strength of the mixing interaction. Note that this is nothing but the multipole–multipole interaction that already has appeared in our discussion of onset of deformation (Section 12.4). The model (18.9) allows one to solve the problem exactly (for simplicity, we assume the Hermiticity $\hat{q} = \hat{q}^{\dagger}$ and take the matrix elements $q_k = \langle k | \hat{q} | 0 \rangle = \langle 0 | \hat{q} | k \rangle$ and therefore the amplitudes C_k^{α} as real).

The solution (18.7) explicitly determines all coefficients up to a normalization constant A_α ,

$$C_k^\alpha = \frac{q_k}{E_\alpha - \epsilon_k} A_\alpha, \quad (18.10)$$

the latter being expressed as a sum of the same amplitudes,

$$A_\alpha = \kappa \sum_l q_l C_l^\alpha. \quad (18.11)$$

Changing the summation index and using (18.10) again, we obtain

$$A_\alpha = \kappa \sum_k q_k C_k^\alpha = \kappa \sum_k \frac{q_k^2}{E_\alpha - \epsilon_k} A_\alpha. \quad (18.12)$$

There are three types of solutions for Eq. (18.12). The *trivial* solutions are those with $A_\alpha = 0$. As seen from (18.10), then $C_k^\alpha(E_\alpha - \epsilon_k) = 0$. The amplitude C_k^α can be nonzero if the energy of the state coincides with unperturbed energy of one of the simple states, $E_\alpha = \epsilon_k$. If the spectrum of the simple states is nondegenerate, it happens for one component k only. Therefore, for this solution, the eigenfunction $|\alpha\rangle$ is simply one of the unperturbed states $|k\rangle$. But then, from (18.11), A_α is equal to $\kappa q_k C_k^\alpha$ and can be zero only if $q_k = 0$. These are the states with zero multipole matrix elements from the ground state which do not participate in the interaction.

The non-trivial solutions, collective and non-collective, are more interesting. Assume that $A_\alpha \neq 0$. Then (18.12) leads to the *secular (characteristic) equation*

$$\frac{1}{\kappa} = \sum_k \frac{q_k^2}{E_\alpha - \epsilon_k} \quad (18.13)$$

that determines the energies E_α of the eigenstates. It is easy to get an idea of the character of the solutions by a graphic construction, Figure 18.1. We consider both parts of (18.13) as a function of energy E . The right-hand side is a function $F(E)$ that has N poles at all points of unperturbed energies ϵ_k involved in the interaction ($q_k \neq 0$). The derivative dF/dE is negative, so between the poles, the function goes from $+\infty$ to $-\infty$. Assuming that the energy interval ΔE , where all poles with considerably large residues

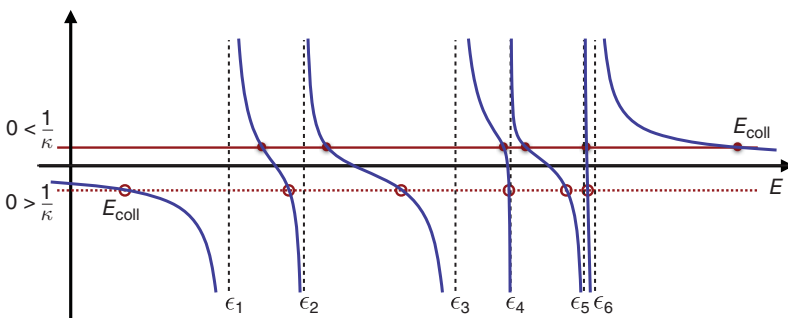


Figure 18.1 The graphic solution of the secular equation (18.13). The function $F(E)$ on the right-hand side of (18.13) is shown by a solid line, the points of intercept with the horizontal line $1/\kappa$ being the roots of interest. The solutions are shown by circles for $\kappa > 0$ and $\kappa < 0$, respectively.

q_k^2 are located, is finite, we can sketch the monotonous behavior of $F(E)$ on both sides of this interval. The horizontal line $1/\kappa$ intersects all internal branches of $F(E)$. These intersections define two types of solutions, $N - 1$ roots of the secular equation (18.13) located intermittently between unperturbed energies, and a single root outside this *quasicontinuum*. The latter corresponds to the energy E_α shifted up (for positive κ) or down (for negative κ) from the quasicontinuum. For significantly large κ , the horizontal line is close to the energy axis, and the energy shift from the unperturbed region is large.

The root with a large shift defines the *collective* state. For attractive interaction between the simple ($1p-1h$ in the example above) states, the energy is *lower* than that of the lowest simple state. In the repulsion case, the energy is *higher* than that of the highest state. In both cases, all components C_k^α of the wave function (18.10) have the same signs as the corresponding multipole matrix elements q_k . Using the language of Section 15.2, the vectors of the amplitudes, \mathbf{C} , and of the transition amplitudes, \mathbf{q} , are *parallel*. Therefore we expect an enhancement of the transition probability from the collective state to the ground state (for a given multipolarity). Looking back, we see that the physical reason for the collectivization is the presence of a strong (large κ) component of this multipolarity in the factorized form of the residual interaction (18.9).

To complete the solution, we normalize the wave function $|\alpha\rangle$ by the condition $\sum_k (C_k^\alpha)^2 = 1$ that gives

$$A_\alpha^2 = \left[\sum_k \frac{q_k^2}{(E_\alpha - \epsilon_k)^2} \right]^{-1}. \quad (18.14)$$

In the case of weak interaction, the external root is close to the borderline ϵ_m of the quasicontinuum, only one term in the sum (18.14) is important, $E_\alpha \approx \epsilon_m + \kappa q_m^2$, and $A_\alpha \approx (E_\alpha - \epsilon_m)/q_m^2$. Then, according to (18.10), $C_m^\alpha \approx 1$, and, instead of collectivization, we get an almost pure simple state $|m\rangle$. The same conclusion is valid for the internal roots that correspond to the combinations of the nearest simple states. The transition probability from such states is of the order of typical single-particle values.

In the case of a strong energy shift ΔE , the resulting state is *collective*, indeed. Consider the limiting case when the energy shift exceeds the energy spread $\delta\epsilon$ of the simple states. Then we can substitute all bare energies ϵ_k by their centroid $\bar{\epsilon}$, and Eq. (18.13) gives

$$E_{\text{coll}} \approx \bar{\epsilon} + \kappa \sum_k q_k^2 \equiv \bar{\epsilon} + \Delta E. \quad (18.15)$$

The normalization condition (18.14) determines

$$A_{\text{coll}}^2 \approx \frac{(\Delta E)^2}{\sum_k q_k^2} = \kappa \Delta E, \quad (18.16)$$

and the weights of the components (18.10) turn out to be

$$(C_k^{\text{coll}})^2 \approx \frac{q_k^2}{\sum_k q_k^2}. \quad (18.17)$$

These weights are determined by the relative multipole strengths of the basic states. In general, they depend on bare energies as well. If the multipole matrix elements q_k have the typical order of magnitude q and their effective number is N_c , we obtain from

(18.17) the weights $|C|^2$ of the order of $1/N_c$. The number N_c determines the collective enhancement (Section 15.2).

More accurately, we have for the transition probability induced by the full multipole operator $\hat{Q} = \sum \hat{q}$ between an eigenstate $|\alpha\rangle$ and the ground state,

$$B(\hat{Q}; \alpha \rightarrow 0) = \left| \langle 0 | \hat{Q} | \alpha \rangle \right|^2 = \left| \sum_k C_k^\alpha q_k \right|^2. \quad (18.18)$$

The simple *sum rule* is valid: the sum of transition probabilities from all eigenstates is the same as it would be for unperturbed states. It follows from the orthonormalization conditions (18.5),

$$\sum_\alpha B(\hat{Q}; \alpha \rightarrow 0) = \sum_\alpha \left(\sum_{kl} C_k^\alpha C_l^\alpha q_k q_l \right) = \sum_k q_k^2. \quad (18.19)$$

In the extreme collective limit (18.17), the probability of the transition from a single collective state reaches the value given by the sum rule (18.19),

$$B(\hat{Q}; \text{coll} \rightarrow 0) = \left| \sum_k C_k^{\text{coll}} q_k \right|^2 = \sum_k q_k^2. \quad (18.20)$$

It follows that, in this limit, the whole summed transition strength (18.19) is accumulated by a single collective state. All noncollective states $|\alpha\rangle$ have zero transition probabilities. Of course, in a realistic case, they also carry a fraction of the strength.

It is easy to find the corrections to the limiting solution (18.15). If we take into account the finite spread of the bare energies, we can introduce the distance of a specific bare state from the centroid, $\epsilon_k = \bar{\epsilon} + \delta\epsilon_k$. Performing the expansion of the denominator in (18.13), we obtain

$$E_{\text{coll}} - \bar{\epsilon} = \Delta E + \frac{\kappa}{E_{\text{coll}} - \bar{\epsilon}} \sum_k q_k^2 \delta\epsilon_k + \frac{\kappa}{(E_{\text{coll}} - \bar{\epsilon})^2} \sum_k q_k^2 (\delta\epsilon_k)^2. \quad (18.21)$$

We can choose the position of the centroid suitably to get rid of the term linear in $\delta\epsilon$,

$$\sum_k q_k^2 \delta\epsilon_k = 0 \Leftrightarrow \bar{\epsilon} = \frac{\sum_k q_k^2 \epsilon_k}{\sum_k q_k^2}. \quad (18.22)$$

The appropriate averaging in (18.22) proceeds with the strengths of the partial multipole transitions taken as weights (compare (18.17)). With such a choice,

$$E_{\text{coll}} \approx \bar{\epsilon} + \Delta E(1 + \xi), \quad \xi = \sum_k (C_k^{\text{coll}})^2 \left(\frac{\delta\epsilon_k}{\Delta E} \right)^2, \quad (18.23)$$

where the amplitudes in the last sum are those from (18.17). Calculating the collective transition probability within the same approximation, instead of (18.20), we get

$$B(\hat{Q}; \text{coll} \rightarrow 0) = (1 - \xi) \sum_k q_k^2. \quad (18.24)$$

The rest, as compared to the sum rule (18.19), belong to $(N - 1)$ noncollective states. Their typical transition probabilities are of the order of

$$\frac{B_{\text{noncoll}}}{B_{\text{coll}}} \simeq (C^{\text{coll}})^2 \left(\frac{\delta\epsilon}{\Delta E} \right)^2 \simeq \frac{1}{N_c} \left(\frac{\delta\epsilon}{\Delta E} \right)^2. \quad (18.25)$$

The schematic model considered in this section, in spite of its rough approximations, shows the generic mechanism of collective excitations in a complicated system. We have to stress again that the resulting state is collective (coherent) with respect to the specific type of operators only. The type of operator depends on the experimental method used for exciting these states. For example, take photonuclear or electronuclear reactions at energies which correspond to the wavelength of the photon (real in the first case and virtual in the second case) that is comparable or greater than the nuclear size. Then the main excitation mechanism is dipole, and the collective state (moved up in energy from the distance between the shells with opposite parity) forms the *giant dipole resonance*. The remaining dipole states still carry some dipole strength and one can see this concentration of strength as the so-called *pygmy dipole resonance*. Similar types of excitations, often not as easily detectable, create resonances with different quantum numbers, Section 6.4.

18.2 Random Phase Approximation

The regular way of looking for collective excitations is through the so-called *random phase approximation* (RPA). It was first suggested (D. Bohm and D. Pines, 1953) in relation to the problem of waves propagating in the electron gas or plasmas [QP, II, 20.7]. The RPA allows one to find collective modes of small amplitude in a quantum many-body system [1–5]. The RPA can be developed in many equivalent ways. In the following, we use the method of equations of motion that permits further extensions.

Let us consider a slight perturbation of the ground state described in the mean-field approximation, HF or HFB. The perturbed state is not a stationary state any longer. Instead it is a wave packet changing in time. Different Fourier components of the packet correspond to beating frequencies which are defined by the differences in energies between various stationary components of the packet. If the perturbation is weak, the main component still originates from the ground state, but we see also the energy differences between the ground state and excited states which are admixed by the perturbation.

The same result can also be obtained in the *linear response* approach, recall Section 6.3 for a static response, or the calculation of the moment of inertia in the cranking model (Section 16.18). Now we impose a weak external *time-dependent field* and look for the response of the system proportional to the perturbation (linear approximation). The response is an admixture of excited states to the unperturbed state of the system. Changing the frequency ω of the external field we see the resonances in the response. They appear when real transitions with energy conservation are possible, $E_f = E_i + \hbar\omega$. Therefore we again find the excitation spectrum of the system. In the next order, transitions between the excited states appear that, in general, show no resonance with the external field. This is the (neglected in the RPA) *noise* superimposed onto the coherent response; here we see the origin of the term *random phases*.

The RPA equations of motion follow from the linearization of the exact operator equations near the mean-field ground state. Instead of the density matrix (17.26) of the ground state we are now interested in that of the wave packet $\Psi(t)$,

$$\rho_{12}(t) = \langle \Psi(t) | R_{12} | \Psi(t) \rangle = \langle \Psi(0) | a_2^\dagger(t) a_1(t) | \Psi(0) \rangle, \quad (18.26)$$

where the time evolution is transferred to the operators in the Heisenberg picture. We write down the exact equations of motion for creation and annihilation operators and linearize them as in (17.28). This is based on the assumption that the resulting density matrix is close to that of the ground state and the admixtures are small. Thus, the equations of motion for the Fermi operators are still given by (17.31) and (17.32).

In this way, the evolution of the density matrix (18.26) is described by

$$i\hbar\dot{\rho}_{12} = \sum_3 (\epsilon_{13}\rho_{32} - \rho_{13}\epsilon_{32}), \quad (18.27)$$

or, using the matrix notations (17.38),

$$i\hbar\dot{\rho} = [\epsilon\{\rho\}, \rho]. \quad (18.28)$$

The nuclear field $\epsilon\{\rho\}$ as given earlier by Eqs. (17.17), (17.30) is *self-consistent*. It is defined by the particle distribution and therefore it is also *time dependent*. Therefore the whole approach is also a version of the *time-dependent mean field* method for small deviations from the ground state (or from statistical equilibrium at nonzero temperature).

If we are interested in *small* deviations from the ground state only,

$$\rho(t) = \rho^0 + \delta\rho(t), \quad (18.29)$$

where ρ^0 is the time-independent mean-field density matrix and $\delta\rho(t)$ contains the small time-dependent components. The nuclear field is the functional of the density matrix that should be linearized in the same way,

$$\epsilon\{\rho\} = h + w\{\rho\} = h + w\{\rho^0\} + \delta w = \epsilon\{\rho^0\} + \delta w. \quad (18.30)$$

In our case of the two-body interaction, we obtain from (17.30)

$$(\delta w)_{12} = \sum_{34} (14|\overline{U}|23)(\delta\rho)_{34}, \quad (18.31)$$

this is the same linear functional (17.30) of the deviation $\delta\rho$,

$$\delta w = w\{\delta\rho\}. \quad (18.32)$$

We use here all notations for the HF case. But the method works exactly in the same way for the HFB approximation. The single-particle space is doubled (17.76), the density matrix in this space is r , Eq. (17.79), and the self-consistent Hamiltonian is $\mathcal{H}\{r\}$, Eq. (17.71), including the pairing field (17.47), but the form of all equations stays the same. Since the excitations in this approach are quasiparticles from broken pairs, the method in this case is usually called *quasiparticle random phase approximation* (QRPA).

18.3 Canonical Form of the RPA

The stationary part of the density matrix ρ^0 and the corresponding self-consistent field $\epsilon\{\rho^0\}$ satisfy the mean-field equation (17.38). For the time-dependent part we have from (18.28),

$$i\hbar \frac{d}{dt} \delta\rho = [\delta w, \rho^0] + [\epsilon\{\rho^0\}, \delta\rho] + [\delta w, \delta\rho]. \quad (18.33)$$

The RPA neglects the last term of (18.33) assuming that the deviations from the stationary picture are small, having random phases. This linearization results in the matrix RPA equations

$$i\hbar \frac{d}{dt} \delta\rho = [\epsilon^o, \delta\rho] + [\delta w, \rho^o], \quad \epsilon^o \equiv \epsilon\{\rho^o\}. \quad (18.34)$$

Because of (18.31), the RPA equations are *linear* in the components of $\delta\rho$. We look for the solutions that give the *normal excitation modes* of the mean field,

$$\delta\rho(t) = \rho_\omega e^{-i\omega t}, \quad (18.35)$$

where ρ_ω is a time-independent matrix with matrix elements labeled by the pairs (12) of single-particle states contributing to this mode. Correspondingly, the variable field (18.32) has a form

$$\delta w(t) = w_\omega e^{-i\omega t}, \quad w_\omega = w\{\rho_\omega\}. \quad (18.36)$$

The single-particle basis can be taken arbitrarily and we use the freedom of its choice to simplify the equations and clarify their meaning.

As we know from (17.36) and (17.38), there exists a quasiparticle basis $|\lambda\rangle$, doubled in the HFB case, that is the common eigenbasis of the static density matrix ρ^o and the static mean field ϵ^o . Their eigenvalues are the ground-state occupation numbers n_λ and the quasiparticle energies ϵ_λ , respectively. Taking the matrix elements $(\lambda| \dots | \lambda')$ in (18.34) and introducing the eigenvalues of ϵ^o and ρ^o , we obtain

$$i\hbar \frac{d}{dt} (\delta\rho)_{\lambda\lambda'} = (\epsilon_\lambda - \epsilon_{\lambda'}) (\delta\rho)_{\lambda\lambda'} + (\delta w)_{\lambda\lambda'} (n_{\lambda'} - n_\lambda). \quad (18.37)$$

The Fourier components (18.35), (18.36) of the density matrix obey

$$\hbar\omega(\rho_\omega)_{\lambda\lambda'} = (\epsilon_\lambda - \epsilon_{\lambda'}) (\rho_\omega)_{\lambda\lambda'} - (n_\lambda - n_{\lambda'}) (w_\omega)_{\lambda\lambda'}. \quad (18.38)$$

Using the appropriate occupation numbers and reasonable truncation of single-particle space, we can solve the algebraic set of equations (18.38). The structure simplifies for the ground state filled as in the Fermi gas when the basis can be subdivided into the particle (p -) states, $n_p = 0$, $\epsilon_p > 0$, and hole (h -) states, $n_h = 1$, $\epsilon_h < 0$.

In the schematic model of the preceding section, we saw the existence of the trivial solution with unperturbed energy. Looking for nontrivial solutions based on the unperturbed Fermi sphere, we have $\omega \neq \epsilon_\lambda - \epsilon_{\lambda'}$, while the matrix elements between the states on the same side of Σ_F vanish because, for them, $n_\lambda = n_{\lambda'}$,

$$(\rho_\omega)_{pp'} = (\rho_\omega)_{hh'} = 0. \quad (18.39)$$

For the matrix elements across Σ_F , we obtain the coupled set,

$$\hbar\omega(\rho_\omega)_{ph} = (\epsilon_p - \epsilon_h) (\rho_\omega)_{ph} + \sum_{p'h'} \left[(ph'| \overline{U} | hp') (\rho_\omega)_{p'h'} + (pp' | \overline{U} | hh') (\rho_\omega)_{h'p'} \right], \quad (18.40)$$

$$\hbar\omega(\rho_\omega)_{hp} = (\epsilon_h - \epsilon_p) (\rho_\omega)_{hp} - \sum_{p'h'} \left((hh' | \overline{U} | pp') (\rho_\omega)_{p'h'} + (hp' | \overline{U} | ph') (\rho_\omega)_{h'p'} \right). \quad (18.41)$$

The standard form of the RPA equations can be reached if one considers the set $(ph) \equiv k$ as a unified label of the $p-h$ excitation and introduces the notations for the matrix elements,

$$(\rho_\omega)_{ph} = X_k^\omega, \quad (\rho_\omega)_{hp} = Y_k^\omega, \quad (18.42)$$

and for the transition amplitudes,

$$\begin{aligned} A_{kk'} &\equiv A_{ph,p'h'} = \epsilon_k \delta_{kk'} + (ph'|\bar{U}|hp'), \\ B_{kk'} &\equiv B_{ph,p'h'} = (pp'|\bar{U}|hh'). \end{aligned} \quad (18.43)$$

Here $\epsilon_k \equiv \epsilon_{ph} = \epsilon_p - \epsilon_h$ is the energy of the bare $p-h$ excitation. We come to the canonical RPA equations written as

$$\begin{pmatrix} A & B \\ B^* & A^* \end{pmatrix} \begin{pmatrix} X^\omega \\ Y^\omega \end{pmatrix} = \hbar\omega \begin{pmatrix} 1 & 0 \\ 0 & -1 \end{pmatrix} \begin{pmatrix} X^\omega \\ Y^\omega \end{pmatrix}. \quad (18.44)$$

This eigenvalue problem does not correspond to the diagonalization of a Hermitian operator [because of the matrix σ_z on the right-hand side of (18.44)]. Therefore we cannot guarantee that the eigenvalues $\hbar\omega$ are necessarily real. An imaginary part of frequency would signal the instability of the mean field placed in the base of the RPA.

A new element as compared to the schematic model is the presence of the *backward* amplitudes Y_k . They incorporate *correlations in the ground state*. To be consistent and to take into account all coherent contributions of the same order, we need to correct the ground state as well (these corrections were neglected in the schematic model). Namely, the nonzero backward amplitudes reveal the presence of the holes below Σ_F and of the particles above Σ_F in the *actual ground state* that does not coincide anymore with the HF vacuum. The *forward* amplitude X_{ph}^ω corresponds to the matrix element $\langle 0 | a_h^\dagger a_p | \omega \rangle$ between the excited state at the excitation energy $\hbar\omega$ and the actual ground state. This matrix element does not vanish even if the ground state is a pure HF vacuum. It simply means that the state $|\omega\rangle$ contains a particle in the orbit p above Σ_F and a hole in the orbit h below Σ_F . However, the backward amplitude Y_{ph}^ω is the matrix element $\langle 0 | a_p^\dagger a_h | \omega \rangle$. For this matrix element, we need the presence of $p-h$ pairs in the ground state. From this viewpoint, the schematic model corresponds to the so-called Tamm–Dancoff approximation when the backward contributions and the renormalization of the ground state are neglected.

Although the canonical form (18.44) of the RPA equations with decomposition into forward and backward graphs is useful, especially for numerical calculations, we can also use the original form (18.38). The formal RPA solution in this form is still an integral equation,

$$(\rho_\omega)_{\lambda\lambda'} = \frac{n_\lambda - n_{\lambda'}}{\epsilon_\lambda - \epsilon_{\lambda'} - \hbar\omega} (w_\omega)_{\lambda\lambda'}, \quad (18.45)$$

because the unknown matrix elements of the density matrix enter the right-hand side through w_ω . This form has to be used when the mean-field state is approximated differently from the HF ground state and the occupation numbers are given by a function different from the Fermi–Dirac step function. Then the subdivision into backward and

forward amplitudes loses its absolute meaning. This is the case for the so-called *thermal RPA* when the occupation numbers are given by the equilibrium Fermi–Dirac distribution depending on temperature.

18.4 Model with Factorized Forces

Here we again consider the simplified model of the residual interaction just to illustrate the character of the RPA solutions. The factorized forces have appeared in the discussion of deformation (Section 12.2) and in the schematic model of Section 18.1. They are nicely adjusted to single out the coherent components of interaction. However, they do not satisfy the requirements of antisymmetry (17.19). This drawback is not very important for our purpose here as the RPA is meant for the extraction of collective modes where the direct matrix elements are usually the most coherent. As we know from Chapter 5, the collective modes are typically concentrated on the surface of a nucleus. The multipole operators grow to the surface and therefore contain the main important contributions. A more realistic interaction has to be taken for detailed quantitative studies.

In the factorizable model, the matrix elements of the residual interaction are approximated by (18.9)

$$(12|\bar{U}|34) \approx \kappa q_{13}q_{24}, \quad (18.46)$$

where the particle–hole amplitudes q_{12} for simplicity can be taken as real and symmetric. In terms of one-body operators, this means the approximation of the particle interaction by

$$H_Q = \frac{\kappa}{2} Q \cdot Q, \quad Q = \sum_a q_a; \quad (18.47)$$

For the multipole operators of nonzero multipolarity, this includes the proper angular momentum coupling to the total scalar. Of course, this has to be understood as only one term of the expansion of the interaction over multipole–multipole terms in the *particle–hole* channel. But in the framework of the RPA, the multipoles are not mixed and each of them contributes to the excited states selected by the quantum numbers of the mode under study.

Similar to this, one might use the expansion over the multipoles in the *particle–particle* channel, $\sim p_{12}p_{34}$. The simplest term of this series is the standard pairing with scalar time-reversal invariant pairs. In principle, both expansions are complete. However, the consideration of the angular momentum coupling in these channels shows that the terms with large angular momenta in the *p–h* channel mainly correspond to the low angular momentum terms in the *p–p* channel and vice versa. Therefore for a long time, a model introduced by S.T. Belyaev [6, 7] was popular that combines the most important low-angular-momentum terms in *both* channels, quadrupole–quadrupole forces in the *p–h* channel and the BCS-type pairing, sometimes also quadrupole pairing $L = 2$, in the *p–p* channel. This allows one to interpolate successfully the main collective effects, low-lying quadrupole vibrations and deformation, on the one hand, and pairing on the other. The realistic effective interaction of quasiparticles automatically contains these effects. Similarly to (18.46), one can find the normal modes generated mostly in the *p–p* channel (*pairing vibrations*) [8].

With the model interaction (18.46), the self-consistent field component $w\{\rho\}$ induced by any part ρ of the density matrix is

$$(w\{\rho\})_{14} = \kappa q_{14} \sum_{23} q_{23} \rho_{32} = \kappa q_{14} \text{Tr}(q\rho). \quad (18.48)$$

The RPA equations (18.44) look now quite simple,

$$\epsilon_k X_k + \kappa q_k \sum_{k'} q_{k'} (X_{k'} + Y_{k'}) = \hbar\omega X_k, \quad (18.49)$$

$$\epsilon_k Y_k + \kappa q_k \sum_{k'} q_{k'} (X_{k'} + Y_{k'}) = -\hbar\omega Y_k. \quad (18.50)$$

Here we omitted the superscript ω . In the Tamm–Dancoff approximation, we consider only the upper equation (18.49) with $Y = 0$. Then we come back to our schematic model (18.6).

It is convenient to introduce the symmetrized and antisymmetrized amplitudes

$$Z_k^{(\pm)} = X_k \pm Y_k \quad (18.51)$$

and rewrite the set of the RPA equations as

$$\hbar\omega Z_k^{(+)} = \epsilon_k Z_k^{(-)}, \quad (18.52)$$

$$\hbar\omega Z_k^{(-)} = \epsilon_k Z_k^{(+)} + \kappa q_k \sum_{k'} q_{k'} Z_{k'}^{(+)}. \quad (18.53)$$

The solution of this set is obvious,

$$Z_k^{(+)} = \frac{q_k \epsilon_k}{(\hbar\omega)^2 - (\epsilon_k)^2} S, \quad Z_k^{(-)} = \frac{\hbar\omega}{\epsilon_k} Z_k^{(+)}. \quad (18.54)$$

Here the constant S is the sum analogous to (18.11),

$$S = \kappa \sum_{k'} q_{k'} Z_{k'}^{(+)}. \quad (18.55)$$

For the nontrivial solutions, $S \neq 0$, we obtain the secular equation for the eigenfrequencies of normal modes,

$$\frac{1}{\kappa} = \sum_k \frac{q_k^2 \epsilon_k}{(\hbar\omega)^2 - (\epsilon_k)^2}. \quad (18.56)$$

Note that all frequencies appear pairwise, $\pm\omega$, as the secular equation contains only ω^2 .

The procedure to obtain the qualitative solution of the secular equation is similar to that used in the schematic model, Figure 18.1. The results are also similar in the case of the repulsive interaction, $\kappa > 0$, as it is the case for the isovector giant resonances (Section 6.2). The frequency is shifted up from the upper boundary of the quasicontinuum; in the limit of strong collectivization, $(\hbar\omega)^2 \rightarrow \kappa \sum_k q_k^2 \epsilon_k$ (recall that the energies of the $p-h$ excitations ϵ_k are positive). In this limit, $Z^{(-)} \gg Z^{(+)}$ and $X \approx -Y$, which means that for the collective root the backward diagrams are not small and the Tamm–Dancoff approximation is invalid.

Completely new effects emerge in the attraction case, $\kappa < 0$. The lowest root is repelled down by the quasicontinuum. Its lower boundary ϵ_{\min} is determined by the major shell gap in magic nuclei and by the pair breaking energy 2Δ in nuclei with

developed pairing. Thus, we obtain the collective mode within the pairing gap (see illustration in Figure 13.3). Its frequency can be calculated from (18.56) if the appropriate coherence factors (Section 13.11) are taken into account in the multipole matrix elements q_k . The collective mode in the paired system coherently combines the states of a broken pair with the background components localized on some single-particle orbits. The interaction between the quasiparticles (in the channels different from pairing) again is of attractive character and creates a coherent superposition with the pair spread over different orbits. The large multipole moment of this superposition tells us that the vibration is collective although of nonhydrodynamic nature. This vibration might be interpreted as a soundlike wave of the deformation of pairs specific for paired systems. Such a wave cannot propagate coherently in a Fermi gas with no pairing, when the gap in the single-particle spectrum is absent.

The physical region of $\omega^2 > 0$ is bounded from below. At this threshold, the sum in (18.56) takes a finite negative value. If the attractive interaction is too strong, $\kappa < \kappa_c < 0$, the low-lying root crosses the vertical axis and goes into the unphysical region $\omega^2 < 0$. This is equivalent to the exponentially increasing amplitude $\rho(t) \propto e^{|\omega|t}$, that is, the ground state is *unstable* with respect to this RPA mode. The critical value of the interaction strength is

$$\kappa_c = - \left[\sum_k \frac{q_k^2}{\epsilon_k} \right]^{-1}. \quad (18.57)$$

Such a phenomenon is known to be associated with the quadrupole vibrations of transitional nuclei when the spherical shape becomes unstable. We need to have in mind however that we found the instability only in the *small amplitude* approximation. We do not know from the RPA what happens after the frequency of normal vibrations becomes too low and, correspondingly, the amplitude of the dangerous mode increases. The actual stable configuration is determined by the high-order terms outside of the domain of validity of the RPA. But the RPA itself signals the danger.

For the low-lying collective mode again, the backward diagrams are quite important because at $|\omega| \ll \epsilon_{\min}$ we have $X \approx Y$. We conclude that we need to use the RPA rather than the Tamm–Danoff approximation as long as we are interested in strongly collectivized states. If the frequency is close to one of the unperturbed $p-h$ energies, $Y \rightarrow 0$.

18.5 Collective Modes as Bosons

For collective RPA modes, the contribution of each quasiparticle component is small, $\sim N_c^{-1/2}$. Therefore the operator generating this mode from the ground state can be applied *repeatedly* with no strong violation of the Pauli principle. This would be impossible for noncollective modes which are almost pure single-particle excitations and cannot be repeated. The collective RPA mode gives rise to a series of excited states which form a *vibrational band* and can be interpreted as many-quantum states of the same mode. This is well known in low-lying spectra of spherical (non-magic) nuclei where the vibrational multiplets corresponding to several quadrupole quanta (phonons) form the majority of low-energy states. *Multiple* giant dipole resonance states, which are overtones of

high-lying collective RPA roots, were observed in Coulomb excitation and pion-induced reactions. By considering the quanta of next generations as identical to the lowest excitations, we can approximately treat them as *bosons* [9, 10].

The RPA can be reinterpreted as a tool of extracting *Bose-excitations* from the spectrum of interacting fermions. This gives also a convenient way to normalize our RPA solutions. From the dynamical point of view, the RPA corresponds to the *harmonic approximation* of noninteracting ideal bosons. Going beyond RPA, one can analyze effects of *anharmonicity*.

Our goal is to construct the collective Hamiltonian of vibrational modes,

$$H_c = \frac{1}{2}C\alpha^2 + \frac{1}{2B}\pi^2, \quad (18.58)$$

starting with the microscopic equations of motion for the fermions. Here α and π are quantum operators of the collective coordinate and the collective momentum that can be transformed to the Bose-operators of phonons. C and B are the restoring force and the mass parameter, respectively. Their values have to be found microscopically. For simplicity, we omit all quantum numbers related to multipolarity. In the harmonic approximation, they do not add any complications as the way of coupling the quadratic terms of (18.58) into rotational scalars is unique.

The equations of motion for the collective operators are the same for classical and quantum oscillators. On the other hand, we have the dynamics of fermions in the linearized approximation (18.37). The multipole moment Q can be expressed in both languages: phenomenologically it is proportional to the collective coordinate (Section 5.4) and microscopically it is a sum of the matrix elements of the density matrix (17.25),

$$Q = Q^o\alpha \Leftrightarrow Q = \text{Tr}(qR). \quad (18.59)$$

Therefore we can perform the *mapping* of microscopic dynamics governed by the total Hamiltonian (17.21) onto collective dynamics governed by (18.58). The description in terms of collective operators can be good until, at increased excitation energy and level density, the mixing with the states of the same symmetry but different nature becomes important.

For small amplitude vibrations, the part of the density matrix R responsible for the transitions to excited states is approximated by $\delta\rho$, see Eq. (18.34). Assuming that these excited states are one-phonon states, the operators $\delta\rho$ and δw act, in the boson language, as creation and annihilation operators, or as the operators α and π . We discriminate between them using their behavior under time reversal. The collective coordinate is \mathcal{T} -even while the collective momentum is \mathcal{T} -odd.

18.6 Mapping of Dynamics

Consider the RPA equations in the mean-field basis (18.37). If the mean field is \mathcal{T} -invariant, each quasiparticle orbit $|\lambda\rangle$ has a time-conjugate partner $|\tilde{\lambda}\rangle$ with the same energy, $\epsilon_\lambda = \epsilon_{\tilde{\lambda}}$. We also assume that the occupation numbers of the partners are equal, $n_\lambda = n_{\tilde{\lambda}}$, as it is the case in the ground state of an even–even nucleus. The interaction U is assumed to be \mathcal{T} -invariant as well; it is easy to generalize the procedure for the

cranking shell model where the Coriolis force destroys \mathcal{T} -invariance. We introduce \mathcal{T} -even, $\rho^{(+)}$, and \mathcal{T} -odd, $\rho^{(-)}$, parts of the density matrix according to

$$\rho_{\lambda\lambda'}^{(\pm)} = \frac{1}{2} [(\delta\rho)_{\lambda\lambda'} \pm (\delta\rho)_{\tilde{\lambda}\tilde{\lambda}}]. \quad (18.60)$$

In the same manner, we define the subdivision of the mean field w . Owing to the \mathcal{T} -invariance of the interaction, the even (odd) component of the oscillating density matrix induces the even (odd) component of the oscillating field,

$$w^{(\pm)} = w\{\rho^{(\pm)}\}. \quad (18.61)$$

The even and odd components satisfy the coupled set of equations that follows from (18.37),

$$i\hbar \frac{d}{dt} \rho_{\lambda\lambda'}^{(\pm)} = (\epsilon_\lambda - \epsilon_{\lambda'}) \rho_{\lambda\lambda'}^{(\mp)} - (n_\lambda - n_{\lambda'}) w_{\lambda\lambda'}^{(\mp)}. \quad (18.62)$$

According to the idea of mapping, the same equations would follow from the collective Hamiltonian if the density matrix would act in the Hilbert space as collective operators α and π . Because of the \mathcal{T} -invariance, the correspondence should have a form

$$\rho^{(+)} = R^{(+)}\alpha, \quad \rho^{(-)} = R^{(-)}\pi \quad (18.63)$$

where $R^{(\pm)}$ are matrices in quasiparticle space. The corresponding field components are

$$w^{(+)} = W^{(+)}\alpha, \quad w^{(-)} = W^{(-)}\pi, \quad W^{(\pm)} = w\{R^{(\pm)}\}. \quad (18.64)$$

Using these definitions in the left-hand side of (18.62) together with the phenomenological equations of motion for the oscillator Hamiltonian (18.58), we obtain the matrix equations

$$-i\hbar CR^{(-)} = [\epsilon^o, R^{(+)}] - [\rho^o, W^{(+)}], \quad \frac{i\hbar}{B} R^{(+)} = [\epsilon^o, R^{(-)}] - [\rho^o, W^{(-)}]. \quad (18.65)$$

In the matrix elements (18.62), the solution can be readily found,

$$R_{\lambda\lambda'}^{(+)} = \frac{n_\lambda - n_{\lambda'}}{(\epsilon_\lambda - \epsilon_{\lambda'})^2 - (\hbar\omega)^2} \left(-i\hbar CW_{\lambda\lambda'}^{(-)} + (\epsilon_\lambda - \epsilon_{\lambda'}) W_{\lambda\lambda'}^{(+)} \right), \quad (18.66)$$

$$R_{\lambda\lambda'}^{(-)} = \frac{n_\lambda - n_{\lambda'}}{(\epsilon_\lambda - \epsilon_{\lambda'})^2 - (\hbar\omega)^2} \left(\frac{i\hbar}{B} W_{\lambda\lambda'}^{(+)} + (\epsilon_\lambda - \epsilon_{\lambda'}) W_{\lambda\lambda'}^{(-)} \right). \quad (18.67)$$

Here the collective frequency ω is defined as in Section 5.6.

These equations can be solved for any specific model of the interaction \overline{U} . In the factorized model (18.46) with the \mathcal{T} -even multipole operator q , we have

$$W_{\lambda\lambda'}^{(-)} = 0, \quad W_{\lambda\lambda'}^{(+)} = \kappa q_{\lambda\lambda'} Q^o, \quad (18.68)$$

where the constant $Q^o = \text{Tr}(qR^{(+)})$ is the analog of (18.55) and coincides with the coefficient in (18.59),

$$Q = \text{Tr}(q\rho^{(+)}) = \text{Tr}(qR^{(+)})\alpha = Q^o\alpha. \quad (18.69)$$

In this case, the RPA equation (18.67) is easily solved and the secular equation for the frequency ω follows from the self-consistency condition (18.69),

$$1 = \kappa\Sigma_1(\omega^2), \quad (18.70)$$

where the set of sums Σ_n is defined as

$$\Sigma_n(\omega^2) = \sum_{\lambda\lambda'} q_{\lambda\lambda'}^2 \frac{(n_\lambda - n_{\lambda'})(\epsilon_\lambda - \epsilon_{\lambda'})}{[(\epsilon_\lambda - \epsilon_{\lambda'})^2 - (\hbar\omega)^2]^n}. \quad (18.71)$$

For the normal particle distribution, the secular equation (18.70) coincides with (18.56).

18.7 Normalization and the Mass Parameter

To properly normalize the solution, it is convenient to solve in parallel the inverse problem, namely, to express the collective coordinate and momentum as

$$\alpha = \text{Tr}(x\rho^{(+)}) , \quad \pi = \text{Tr}(p\rho^{(-)}) \quad (18.72)$$

where x and p are intrinsic images of collective variables in the same sense as the single-particle operator q is with respect to the total multipole operator Q (18.49). Obviously, x and p are \mathcal{T} -even and \mathcal{T} -odd operators, respectively.

The following procedure is straightforward. The equation of motion for α gives, from (18.62),

$$\frac{i\hbar}{B}\pi = \text{Tr} \left\{ x \left([\epsilon^o, \rho^{(-)}] + [w^{(-)}, \rho^o] \right) \right\}. \quad (18.73)$$

The first term in the trace can be transformed with the aid of the cyclic invariance,

$$\text{Tr} (x[\epsilon^o, \rho^{(-)}]) = \text{Tr} ([x, \epsilon^o]\rho^{(-)}). \quad (18.74)$$

In the second term of (18.73), we can use the simple property of the interaction that is symmetric with respect to two participating particles,

$$\text{Tr}(Aw\{B\}) = \sum_{13} A_{31} \sum_{24} (12|\overline{U}|34)B_{42} = \text{Tr}(w\{A\}B). \quad (18.75)$$

It allows one to transform the second term of the trace in (18.74) as

$$\text{Tr} (x[w^{(-)}, \rho^o]) = \text{Tr} ([\rho^o, x]w^{(-)}) = \text{Tr} (w\{[\rho^o, x]\}\rho^{(-)}). \quad (18.76)$$

All terms in (18.73) now contain $\rho^{(-)}$, and their comparison determines the equation for the operator p ,

$$\frac{i\hbar}{B}p = [x, \epsilon^o] - w\{[x, \rho^o]\}. \quad (18.77)$$

In exactly the same way, we find from the equation for π

$$-i\hbar Cx = [p, \epsilon^o] - w\{[p, \rho^o]\}. \quad (18.78)$$

Finally, the solution in matrix elements is

$$x_{\lambda\lambda'} = \frac{(i\hbar/B)(w\{[p, \rho^o]\})_{\lambda\lambda'} - (\epsilon_\lambda - \epsilon_{\lambda'})(w\{[x, \rho^o]\})_{\lambda\lambda'}}{(\epsilon_\lambda - \epsilon_{\lambda'})^2 - (\hbar\omega)^2}, \quad (18.79)$$

$$p_{\lambda\lambda'} = \frac{-i\hbar C(w\{[x, \rho^o]\})_{\lambda\lambda'} - (\epsilon_\lambda - \epsilon_{\lambda'})(w\{[p, \rho^o]\})_{\lambda\lambda'}}{(\epsilon_\lambda - \epsilon_{\lambda'})^2 - (\hbar\omega)^2}. \quad (18.80)$$

The RPA normalization comes from the original commutation relations of the density matrix (17.24). The commutator

$$[R_{12}, R_{34}] = \delta_{14}R_{32} - \delta_{23}R_{14} \quad (18.81)$$

holds in an arbitrary basis. For any one-body operators $Q = \text{Tr}(qR)$ and $Q' = \text{Tr}(q'R)$, the commutation relations in the global Hilbert space are simply copied from the intrinsic (single-particle) space,

$$[Q, Q'] = \sum_{1234} q_{21}q'_{43}[R_{12}, R_{34}] = \text{Tr}([q, q']R). \quad (18.82)$$

When applied to our collective operators, the main term in the right-hand side contains the static density matrix ρ^0 . Therefore the RPA normalization is

$$[\alpha, \pi] = i\hbar = \text{Tr}([x, p]\rho^0). \quad (18.83)$$

Our definitions will be self-consistent if Eqs. (18.63) and (18.72) are compatible, that is,

$$\text{Tr}(xR^{(+)}) = 1, \quad \text{Tr}(pR^{(-)}) = 1. \quad (18.84)$$

Cross quantities $\text{Tr}(xR^{(-)})$ and $\text{Tr}(pR^{(+)})$ vanish owing to the proper discrimination of \mathcal{T} -even and \mathcal{T} -odd terms.

Everything is seen clearly in the factorized model. Because of the commutator, the quantity $[x, \rho^0]$ is \mathcal{T} -odd so that the corresponding field $w\{[x, \rho^0]\}$ vanishes. Using the notation

$$w\{[p, \rho^0]\} = \kappa qT, \quad T \equiv \text{Tr}(q[p, \rho^0]), \quad (18.85)$$

we find the intrinsic operators

$$x_{\lambda\lambda'} = \frac{i\hbar\kappa T}{B} \frac{q_{\lambda\lambda'}}{(\epsilon_\lambda - \epsilon_{\lambda'})^2 - (\hbar\omega)^2}, \quad p_{\lambda\lambda'} = -\kappa T \frac{q_{\lambda\lambda'}(\epsilon_\lambda - \epsilon_{\lambda'})}{(\epsilon_\lambda - \epsilon_{\lambda'})^2 - (\hbar\omega)^2}. \quad (18.86)$$

The self-consistency conditions for T , Eqs. (18.85), (18.86), again lead to the secular equation (18.70). The normalization (18.83) gives

$$i\hbar = \frac{i\hbar\kappa^2 T^2}{B} \Sigma_2(\omega^2), \quad (18.87)$$

where the sums Σ_n are defined by Eq. (18.71). Finally, the two definitions (18.84) of collective variables give, together with (18.69), the same relation

$$1 = \frac{i\hbar\kappa^2 T Q^0}{B} \Sigma_2(\omega^2). \quad (18.88)$$

From (18.87) and (18.88) we find

$$T = i\hbar Q^0, \quad (18.89)$$

and the mass parameter for the given collective mode,

$$B = -\hbar^2(Q^0)^2 \Sigma_2(\omega^2). \quad (18.90)$$

Note that for the normal particle distribution function the occupation numbers n_λ decrease with growing energy ϵ_λ so that the mass parameter B is positive. We know

from our experience with the moment of inertia that the inertial parameters for quantum collective motion are not universal and depend on the configuration.

In the *adiabatic* limit of low frequency ω that corresponds to large negative κ , the expression (18.90) coincides with that given by the cranking model if we crank the system by the external force $-Q^\rho \alpha$ conjugate to the collective coordinate α . At low frequency, we have

$$\Sigma_1(\omega^2) \approx \Sigma_1(0) + (\hbar\omega)^2 \Sigma_2(\omega^2), \quad (18.91)$$

and the restoring force parameter is given by

$$C = -\frac{(Q^\rho)^2}{\kappa} (1 - \kappa \Sigma_1(0)). \quad (18.92)$$

We see the same instability (18.57) at a critical value κ_c of the interaction strength when the restoring force disappears.

We constructed the Hamiltonian H_c that can be rewritten in a *bosonic* form with the aid of standard secondary quantization. One has to remember that such a representation might be useful for collective modes only. The excitations corresponding to the noncollective roots of the RPA cannot be repeated and have no good Bose analogs (although in the literature, sometimes, all roots of the secular equation are called “phonons”).

In the critical region, the oscillation amplitude grows proportionally to $\omega^{-1/2}$, and we have to go beyond the RPA. The mapping procedure is probably the most regular way to calculate the next terms in a microscopic approach. They appear as the high-order corrections in (18.63), proportional to $\alpha^2, \pi^2, \alpha\pi$, and so on. Accordingly, the collective Hamiltonian is no more than that of the harmonic oscillator. It contains cubic, quartic, and higher terms [11]. They come from the dynamic interaction between different modes as well as from commutation relations which reflect the Pauli principle and cannot be fully implemented in any finite order of boson expansions. Although the mapping procedure is straightforward, the corresponding calculations turn out to be very cumbersome [12]. One of the reasons is that the factorized interaction adjusted to a linear RPA approximation hardly can be a realistic model for the description of strong anharmonicity. Other incoherent interactions can contribute considerably in high orders. This is related to the large vibrational amplitude that may strongly renormalize other degrees of freedom. On the other hand, the admixture of incoherent excitations is the first step along the road to *quantum chaos* (Chapter 25).

Problem 18.1 Consider a Lipkin–Meshkov–Glick (LMG) model of two Ω -degenerate levels labeled $\sigma = \pm 1$, with single-particle energies $\pm\epsilon/2$, and the interaction Hamiltonian

$$H = \frac{\epsilon}{2} \sum_{\nu} \sum_{\sigma=\pm 1} \sigma a_{\sigma\nu}^\dagger a_{\sigma\nu} + \frac{U}{2} \sum_{\sigma=\pm 1} \sum_{\nu\nu'} a_{\sigma\nu}^\dagger a_{\sigma\nu'}^\dagger a_{-\sigma\nu'} a_{-\sigma\nu}. \quad (18.93)$$

Assume $N = \Omega \gg 1$ particles so that the Fermi surface is exactly between the two levels.

- Solve the RPA equations and find the critical value of the interaction strength U when the RPA frequency approaches zero.
- Determine the anharmonic term proportional to α^4 added to the collective Hamiltonian of type (18.58).

Solution

- a) The model Hamiltonian (18.93) is of the factorized type discussed in Section 18.4. Similar to the degenerate model in Chapter 13, the symmetry with respect to index v allows one to limit consideration to only three particle–hole density operators (17.24)

$$R_- = \sum_v a_{-\sigma v}^\dagger a_{+\sigma v}, \quad R_+ = R_-^\dagger = \sum_v a_{+\sigma v}^\dagger a_{-\sigma v}, \quad R_0 = \frac{1}{2} \sum_{v \sigma=\pm 1} \sigma a_{\sigma v}^\dagger a_{\sigma v}. \quad (18.94)$$

The first two operators lower and raise the number of holes and excited particles, while the third one evaluates the particle–hole excitation. The Hamiltonian (18.93) in terms of these operators can be expressed as

$$H = \epsilon R_0 + \frac{U}{2} (R_+^2 + R_-^2); \quad (18.95)$$

The interaction part contains two factorized terms that are complex conjugates to each other. The RPA solution following Eqs. (18.48)–(18.56) leads to $(\hbar\omega)^2 = (\epsilon^2 - U^2\Omega^2)$. The RPA frequency approaches zero at critical interaction strength $U_{\text{cr}} = \epsilon/\Omega$, when the effective potential becomes flat and the collective potential should be considered up to higher orders.

- b) Building a collective Hamiltonian beyond RPA, we note from the commutation relations (18.81) that the three density operators form a closed $\mathcal{SU}(2)$ algebra of angular momentum. In order to obtain a bosonic expansion of (18.58), we can use the Holstein–Primakoff transformation [QP, I, Problem 16.8] that maps the $\mathcal{SU}(2)$ algebra onto bosonic creation and annihilation operators b^\dagger and b ,

$$R_+ = R_-^\dagger = b^\dagger(\Omega - b^\dagger b)^{1/2} = (\Omega + 1 - b^\dagger b)^{1/2} b^\dagger, \quad R_0 = b^\dagger b - \Omega/2, \quad (18.96)$$

where $\Omega/2$ represents the J quantum number of the $\mathcal{SU}(2)$ algebra; for $N = \Omega$, this is the largest possible eigenvalue of R_0 . Direct expansion of the Hamiltonian (18.95) determines its collective form with a quartic component

$$H = \frac{\pi^2}{2} + (\epsilon^2 - U^2\Omega^2) \frac{a^2}{2} + U(\epsilon + U\Omega)^2 \frac{a^4}{4}. \quad (18.97)$$

Here we have ignored some renormalization corrections of the order $\sim 1/\Omega$. In this example, consideration of the collective Hamiltonian to quartic order substantially improves the results in the soft limit when the RPA frequency approaches zero; this is illustrated in Figure 18.2.

18.8 Symmetry Breaking

The mean field found in the HF or HFB approximation, as a rule, violates some exact conservation laws. The HFB method by construction does not conserve the particle number. A deformed field is not invariant under rotations. Any mean field is related to the fixed position of the center of mass; because of this, the translational symmetry is broken. The violation of symmetries is a feature inherent in the density functional method in general.

The broken symmetry is restored by specific collective modes. For example, the violation of *translational* symmetry is physically corrected by the presence of states which

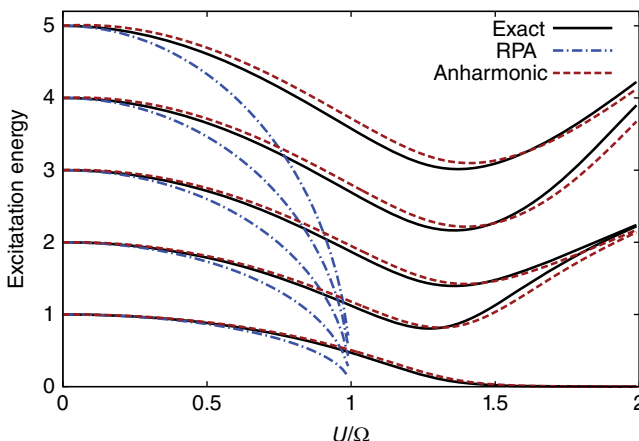


Figure 18.2 Excitation energies of the lowest five excited states in the LMG model ($\Omega = N = 40$) are shown as a function of interaction U and compared with those of RPA and with eigenstates of the collective Hamiltonian (18.97). All energies are expressed in units of ϵ .

are attached to other positions of the center of mass but have the same intrinsic energy. All such states are degenerate from the viewpoint of the mean field. The connection between the degenerate states is accomplished via translations of the system as a whole. We know from our introduction to rotations that translational motion is universal and its energy approaches zero in the limit of vanishing momentum or infinite wavelength.

This is a manifestation of the general Nambu–Goldstone theorem which states that the *spontaneous breaking* of a continuous symmetry (a choice of one fixed mean field among an infinite number of equivalent configurations) leads to a new branch of the excitation spectrum, the *Goldstone mode*, that has zero energy in the long wavelength limit [13]. For violation of *rotational* invariance, the symmetry is restored by collective rotation. In this case, the broken conservation law is that of the angular momentum. The Goldstone mode starts from zero energy at angular momentum equal to zero. For the pairing case, we have a pair condensate with the characteristic quantity Δ that would vanish identically for a system with the exactly fixed particle number. This quantity has a certain phase; we took it as real. The freedom of choice for this phase (*gauge rotation*) restores the violated symmetry.

The RPA displays the mechanism of the symmetry restoration quite clearly. In the presence of degenerate mean-field configurations, a transition between them has zero energy. If these configurations are taken infinitesimally close to each other, the transition requires only a small perturbation of the density matrix and of the corresponding nuclear field. Then we are in the area of validity of the RPA. The RPA mode obtained in this case should have zero energy. We can show that indeed such a mode does exist in the case of broken continuous symmetry.

Let a quantity $J = \sum_a j_a$ be a broken constant of motion corresponding to a generator of continuous symmetry transformations. It can be a component of the momentum for translational symmetry or that of the angular momentum for rotational symmetry. The particle interaction U_{ab} respects this symmetry that can be expressed as

$$[U_{ab}, j_a + j_b] = 0. \quad (18.98)$$

We also assume that the independent particle part h of the mean-field Hamiltonian $\epsilon\{\rho^o\}$ in Eq. (18.30) is invariant,

$$[h, j] = 0, \quad (18.99)$$

so that the symmetry breaking is induced by the interaction part w of the mean field.

The actual solution reveals *lower* symmetry than that of the Hamiltonian. The nuclear field obtained in the mean-field approximation is not invariant under transformations generated by the operator j . The continuous transformation of the single-particle state is

$$\psi \rightarrow \psi' = e^{-i\eta j} \psi \approx (1 - i\eta j)\psi, \quad (18.100)$$

where η is an infinitesimal parameter of the transformation (displacement or rotation angle). The corresponding transformation of the single-particle operators is

$$q \rightarrow q' = e^{-i\eta j} q e^{i\eta j} \approx q + i\eta [q, j]. \quad (18.101)$$

Let us transform the particle distribution, given by the mean-field density matrix ρ^o , by means of the “rotation” (18.101) so that we have a small variation

$$\delta\rho = i\eta [\rho^o, j]. \quad (18.102)$$

The nuclear field is created by the particles and, if it is self-consistent, it should automatically follow the particle distribution. The field transformation is

$$\delta w = w\{\delta\rho\} = i\eta w\{[\rho^o, j]\}. \quad (18.103)$$

To see the machinery of this transformation, it is convenient to write the self-consistency condition for the field (18.31) as

$$w_a\{\rho\} = \text{Tr}_b U_{ab} \rho_b. \quad (18.104)$$

This means that the field acting on a particle a is determined by the interaction U_{ab} of this particle with the distribution of all other particles ρ_b . According to (18.103), we need to find

$$w_a\{[\rho^o, j]\} = \text{Tr}_b U_{ab} [\rho_b^o, j_b]. \quad (18.105)$$

Using the cyclic invariance of the trace over the variables of particles b , this equals

$$w_a\{[\rho^o, j]\} = -\text{Tr}_b [U_{ab}, j_b] \rho_b^o. \quad (18.106)$$

Since, according to (18.98), particle interaction is invariant under simultaneous rotation of both interacting particles, we can transfer the transformation of other particles b to the probing particle a ,

$$w_a\{[\rho^o, j]\} = \text{Tr}_b [U_{ab}, j_a] \rho_b^o, \quad (18.107)$$

or, taking j_a out of Tr_b and using the definition of the field $w\{\rho\}$ before the transformation,

$$w_a\{[\rho^o, j]\} = [\text{Tr}_b (U_{ab} \rho_b^o), j_a] = [w_a\{\rho^o\}, j_a]. \quad (18.108)$$

Thus, as it should be, the field variation (18.103) due to the rotation (18.101) of the particle distribution is the same as the rotation (18.101) of the field itself,

$$\delta w = i\eta [w^o, j]. \quad (18.109)$$

The RPA equation (18.34) for the Fourier component $\delta\rho$ of frequency ω is

$$\hbar\omega\delta\rho = [\epsilon\{\rho^o\}, \delta\rho] + [\delta w, \rho^o]. \quad (18.110)$$

For the perturbation $\delta\rho$ of the density matrix in the form (18.102), the first term in the right-hand side can be rewritten as

$$[\epsilon\{\rho^o\}, [\rho^o, j]] = [[\epsilon\{\rho^o\}, \rho^o], j] + [\rho^o, [\epsilon\{\rho^o\}, j]]. \quad (18.111)$$

The first item in (18.111) vanishes owing to the mean-field equations (17.38). Since the independent particle Hamiltonian h is invariant (18.99), the second item reduces to

$$[\rho^o, [h + w\{\rho^o\}, j]] = [\rho^o, [w\{\rho^o\}, j]]. \quad (18.112)$$

This exactly compensates the second term in (18.110). Therefore, for $\delta\rho$ and δw taken self-consistently as a result of small rotation, the RPA equation is satisfied at $\omega = 0$. This *zero mode*, as we discussed above, restores symmetry broken by the choice of the mean field.

The existence of the zero mode can be used to find the self-consistent value of the coupling constant κ in the factorized model (18.46). If the interaction in the channel with the quantum numbers of the zero mode is modeled in this way, the value of κ should be equal to the critical one (18.57) to guarantee that the lowest frequency is equal to zero and the Goldstone theorem is fulfilled. In the general RPA solution for the factorized forces (18.70), the critical value is defined by

$$1 = \kappa \Sigma_1(0) = \kappa \sum_{\lambda\lambda'} q_{\lambda\lambda'}^2 \frac{n_\lambda - n_{\lambda'}}{\epsilon_\lambda - \epsilon_{\lambda'}}. \quad (18.113)$$

Note that this condition coincides with the equation for the moment of inertia found in the cranking model (Section 16.19). Indeed, to eliminate rotation and find the intrinsic Hamiltonian, we can simply subtract from the full original Hamiltonian the rotational term approximated by that for a rigid rotor,

$$H_{\text{intr}} = H - \frac{\hbar^2}{2J} (\mathbf{J} \cdot \mathbf{J}) \quad (18.114)$$

with the total angular momentum $\mathbf{J} = \sum_a \mathbf{j}_a$ in the role of the multipole operator Q . We get an effective factorizable interaction (18.47) with the forces generated by the operator $q \Rightarrow j$ and the coupling constant $\kappa \Rightarrow -\hbar^2/J$. The cranking value for the moment of inertia corresponds to the condition for rotation to be a Goldstone mode that restores the rotational symmetry broken by a deformed field. Remember that the zero mode was pushed down from the quasicontinuum of quasiparticle excitations and therefore κ has to be negative.

The coupling constant κ satisfying (18.113) can be easily estimated in the semiclassical approximation as it was done for the moment of inertia in Section 16.20. For the normal Fermi distribution, we obtain the inverse coupling constant equal to the total mean value of q^2 on the Fermi surface,

$$\frac{1}{\kappa} = - \sum_{\lambda} (q^2)_{\lambda\lambda} \delta(\epsilon_{\lambda} - \epsilon_F). \quad (18.115)$$

For the operator q that is a function of coordinates, we follow the same way as that for the moment of inertia to obtain in the end the volume-averaged value

$$\frac{1}{\kappa} = - \frac{3m}{p_F^2} \int d^3r q^2(\mathbf{r}) n(\mathbf{r}). \quad (18.116)$$

In non-magic nuclei, the pairing correlations modify this value but the arguments are the same.

For isoscalar dipole excitations, $q \Rightarrow \mathbf{r}$, the collective frequency should be equal to zero because the center-of-mass motion does not induce any intrinsic excitation as we have mentioned repeatedly. The self-consistent estimate (18.116) gives, in this case,

$$\kappa = -\frac{p_F^2}{3mA\langle r^2 \rangle} = -\frac{2\epsilon_F}{3A\langle r^2 \rangle}. \quad (18.117)$$

For quadrupole excitations, there are no Goldstone modes. But practically, in non-magic spherical nuclei the frequency of the low-lying quadrupole vibrations is quite small and we still are able to estimate the effective factorized coupling strength by its critical value (18.116).

Another branch of collective quadrupole motion appears as *giant resonances* (Chapter 6). This type of nuclear spectrum emerges as a coherent superposition of single-particle excitations with quantum numbers 2^+ across two oscillator shells (in order to preserve positive parity). Similar excitations are present in the spectrum for other combinations of quantum numbers, including spin-related modes. These excitations are at energy already in the continuum but their coherence allows the nucleus to perform several periods of collective vibrations before decay. In this chapter, we do not consider the continuum effects, so the giant resonances appear here as discrete lines of the vibrational spectrum; in reality, the experiment shows rather broad peaks corresponding to the finite lifetime. However, the position of the peak which is seen in all nuclei is a smooth function of energy and mass number revealing the collective nature of the excitation that is less sensitive to microscopic details (recall our epigraph).

Problem 18.2 Assume that the multipole resonances with angular momentum L are generated by multipole forces (18.46). In the coordinate representation,

$$U(\mathbf{r}, \mathbf{r}') = -\kappa_L Q_{LM}(\mathbf{r}) Q_{LM}^*(\mathbf{r}'), \quad Q_{LM}(\mathbf{r}) = r^L Y_{LM}(\mathbf{r}/r). \quad (18.118)$$

Considering the irrotational motion of incompressible nuclear liquid (Chapter 6) and the static harmonic oscillator mean-field potential, make a numerical estimate of the multipole constant κ_L [1, 5].

Solution

The local motion of the nuclear liquid corresponds to the time-dependent deformation (Section 12.1); the local displacement is proportional to the gradient of the self-consistent potential,

$$\mathbf{u}(\mathbf{r}, t) = a(t) \nabla Q_{LM}(\mathbf{r}), \quad (18.119)$$

where $a(t)$ plays the role of the collective vibrational coordinate. The incompressibility condition, $\nabla \cdot \mathbf{u} = 0$, is fulfilled as Q_{LM} satisfy the Laplace equation. The local change of the density is given by

$$\delta\rho(\mathbf{r}, t) = \rho(\mathbf{r} + \mathbf{u}(\mathbf{r}, t)) - \rho(\mathbf{r}) = (\mathbf{u}(\mathbf{r}, t) \cdot \nabla) \rho. \quad (18.120)$$

The unperturbed mean-field potential is assumed to be

$$U_{mf.}(\mathbf{r}) = \frac{1}{2} m\omega_0^2 r^2, \quad (18.121)$$

so that its local perturbation equals

$$\delta U = (\mathbf{u} \cdot \nabla U_{mf.}) = a(t)(\nabla Q_{LM} \cdot m\omega_0^2 \mathbf{r}) = a(t)m\omega_0^2 L Q_{LM}, \quad (18.122)$$

where only the radial component of the gradient contributes. On the other hand, this perturbation of the nuclear field comes self-consistently from the interaction (18.118) with other parts of nuclear density,

$$\delta U(\mathbf{r}) = \kappa_L Q_{LM}(\mathbf{r}) \int d^3 r' \delta\rho(\mathbf{r}') Q_{LM}^*(\mathbf{r}'). \quad (18.123)$$

The integral here can be directly calculated with integration by parts and use of $\delta\rho$, Eq. (18.120),

$$\int d^3 r Q_{LM}^*(\mathbf{r})(\nabla Q_{LM} \cdot \nabla\rho) = - \int d^3 r' |\nabla Q_{LM}|^2 \rho; \quad (18.124)$$

here $\nabla^2 Q_{LM} = 0$ is accounted for. With spherically symmetric unperturbed density ρ and the abbreviation

$$\int d^3 r r^n \rho(\mathbf{r}) = \frac{A}{4\pi} \langle r^n \rangle, \quad (18.125)$$

we find

$$\int d^3 r Q_{LM}^*(\mathbf{r})(\nabla Q_{LM} \cdot \nabla\rho) = - \frac{A}{4\pi} L(2L+1) \langle r^{2L-2} \rangle. \quad (18.126)$$

Comparison of the results (18.122) and (18.123) determines

$$\kappa_L = \frac{4\pi}{2L+1} \frac{m\omega_0^2}{A \langle r^{2L-2} \rangle}. \quad (18.127)$$

Problem 18.3 With the self-consistent estimate (18.127) of the multipole–multipole interaction constant and the energy-weighted sum rule [QP, I, 7.9], see also Eq. (6.11), for the quadrupole operator, evaluate the centroid energy of the giant quadrupole resonance (GQR).

Solution

In the harmonic oscillator field, the unperturbed excited states reached by the quadrupole operator have energy $2\hbar\omega_0$. The energy-weighted sum rule which can be found as in Eqs. (6.11), (6.13) and [QP, I, (7.133)],

$$S[Q_{LM}] = \sum_n (E_n - E_0) |\langle 0 | Q_{LM} | n \rangle|^2 = \frac{\hbar^2}{2m} \frac{L(2L+1)^2}{4\pi} A \langle r^{2L-2} \rangle, \quad (18.128)$$

is valid if we assume that there are no velocity-dependent forces, as in our case. In the quadrupole case,

$$S[Q_{2M}] = \frac{15}{4\pi} \frac{\hbar^2}{m} A R_0^2, \quad (18.129)$$

where for a spherical unperturbed shape, $\langle r^n \rangle = [3/(3+n)]R_0^n$. The denominator of the secular equation (18.70) has, for the harmonic oscillator field, all unperturbed transition energies equal to $2\hbar\omega_0$. Then simple algebra gives the GQR centroid energy

$$\hbar\omega_{GQR} = \sqrt{2}\hbar\omega_0 \approx \frac{58}{A^{1/3}} \text{ MeV}. \quad (18.130)$$

The experimental data better agree with a slightly different number $63 A^{-1/3}$. The found energy is below the unperturbed oscillator value of $2\hbar\omega_0$. This is regulated by the sign of the coupling constant κ_2 in the Hamiltonian (18.118) which corresponds to attraction in isoscalar channels and repulsion for isovector modes.

18.9 Generator Coordinate Method

Considering the self-consistent field, we tacitly assumed that such a field found as a solution of the HF or HFB equation is uniquely defined. This semiclassical feature of the approach is not always satisfactory. We know, for example, that the equilibrium nuclear shape can undergo a transition from spherical to deformed. In such cases, there are two (in more general cases, several) competing shapes with corresponding different mean fields and quantum numbers of single-particle orbitals. In some nuclei, it is experimentally known that the states of three quite different nuclear shapes coexist at low energy (the most clear example is given by the neutron-deficient isotope ^{186}Pb [14]).

We know how to describe the single-particle motion and corresponding collective modes in a pure case of a given mean field. However, if the ground-state energies of different mean-field solutions are not too different, there is unavoidable *quantum mixing* of configurations. A typical schematic example is shown in Figure 18.3 where various ground-state energies are qualitatively presented as a function of the axial deformation parameter. Two minima, spherical and deformed, are not separated by a large energy. A quantum many-body state built on the spherical minimum has orbitals which penetrate the deformed sector, and vice versa. The overlap is even greater for excited states.

The variables characterizing the mean field and interpolating from one configuration to another are called *generator coordinates*. The better approximation for a wave function would be reached by such an extension of the variational procedure where this function is a superposition of functions corresponding to various values of the generator coordinates along a certain trajectory in the parameter space. An approach of this

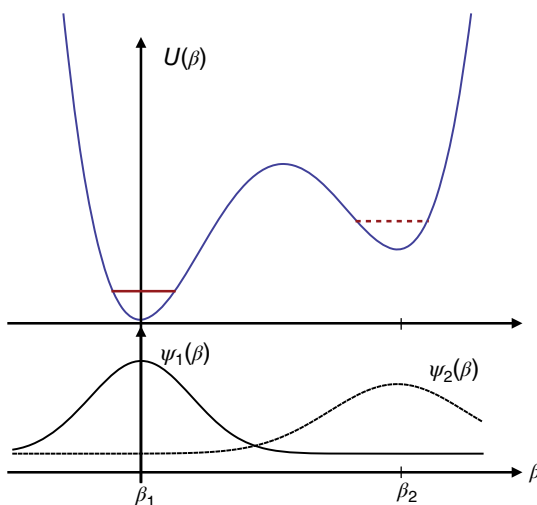


Figure 18.3 The upper plot shows typical energy terms as a function of the deformation parameter with two minima at deformation β_1 and β_2 . The lower plot shows the wave functions corresponding to lowest solutions in the first and second minima.

type was applied to the fission and related processes in the classical paper [15]. In the following, we give a simplified description of the procedure.

The wave functions Ψ_n are taken as superpositions of contributions $\psi_n(\beta)$ for different values of the generator coordinate(s) β ,

$$\Psi_n = \int d\beta f_n(\beta) \psi_n(\beta). \quad (18.131)$$

Here, the generator function $f_n(\beta)$ has to be found from the variational principle minimizing the expectation value of the Hamiltonian

$$E_n = \frac{\langle \Psi_n | H | \Psi_n \rangle}{\langle \Psi_n | \Psi_n \rangle}, \quad (18.132)$$

where we recall that the function (18.131) has to be normalized. The usual mean field corresponds to the ground-state generator function $f_0(\beta) = \delta(\beta - \beta_0)$ with a fixed value β_0 of the generator coordinate that is to be determined by energy minimization.

The direct variation of the functional (18.132) with respect to the function f_n leads to an analog of the Schrödinger equation, sometimes called the Hill–Wheeler equation,

$$\int d\beta' \mathcal{K}_n(\beta, \beta') f_n(\beta') = E_n \int d\beta' \mathcal{N}_n(\beta, \beta') f_n(\beta'). \quad (18.133)$$

Here, two integral kernels are introduced, the energy kernel,

$$\mathcal{K}_n(\beta, \beta') = \langle \psi_n(\beta) | H | \psi_n(\beta') \rangle, \quad (18.134)$$

and the overlap kernel,

$$\mathcal{N}_n(\beta, \beta') = \langle \psi_n(\beta) | \psi_n(\beta') \rangle, \quad (18.135)$$

If our trial functions ψ are taken from the BCS or HFB approach, while the generator coordinate corresponds to the axially symmetric deformation, many results can be obtained analytically [16]. Analytical calculations are also possible if the operators (18.134) and (18.135) can be approximated by the Gaussian functions of β, β' ; then one can easily solve technical problems related to nonorthogonality of functions which belong to different values of the generator coordinates.

A warning is appropriate here. The generator coordinate method in the form outlined above does not guarantee the best choice of the variational manifold – here our trial trajectory goes only through the ground states constructed as mean-field states for each preselected value of the collective parameter(s) β . For example, for the description of fission, such an approach would lead through the states located along the minimum valley of the potential for the elongated shapes, while even in the semiclassical framework, it would be more correct to find the path that gives the least action (the difference is that the effective mass parameter can be very sensitive to the shape and the pairing situation). This is seen also in the application of the method to the rotational motion: we come to the incorrect value of the moment of inertia [17] while the right answer comes out in the cranking model (Chapter 16). Later, computationally more advanced methods were developed that were based on combinations of the variational approach with the shell-model diagonalization, for example, the MONSTER scheme [18] and the multiparticle–multihole approximation [19]. The idea is that the one needs to select self-consistently the most important excited configurations, which form, along with the ground state, a basis for the subsequent variational procedure.

References

- 1 A. Bohr and B.R. Mottelson, *Nuclear Structure*, Vol. **1**, Chapter 1, p. 5; vol. **2**, Chapter 6, Benjamin, Reading, 1975.
- 2 K. Goeke and J. Speth, Annu. Rev. Nucl. Part. Sci. **32**, 65 (1982).
- 3 A.M. Saruis, Phys. Rep. **235**, 57 (1993).
- 4 G.F. Bertsch and R.A. Broglia, *Oscillations in Finite Quantum Systems*, Cambridge University Press, Cambridge, 1994.
- 5 P.F. Bortignon, A. Bracco, and R.A. Broglia, *Giant Resonances*, Harwood, Amsterdam, 1998.
- 6 S.T. Belyaev, Mat. Fys. Medd. Dan. Vid. Selsk. **31**, No. 11 (1959).
- 7 L.S. Kisslinger and R.A. Sorensen, Rev. Mod. Phys. **35**, 853 (1963).
- 8 D.M. Brink and R.A. Broglia, *Nuclear Superfluidity*, Cambridge University Press, Cambridge, 2005.
- 9 S.T. Belyaev and V.G. Zelevinsky, Nucl. Phys. **39**, 582 (1962).
- 10 A. Klein and E.R. Marshalek, Rev. Mod. Phys. **63**, 375 (1991).
- 11 O.K. Vorov and V.G. Zelevinsky, Nucl. Phys. **A439**, 207 (1985).
- 12 Y. Jia and V.G. Zelevinsky, Phys. Rev. C **84**, 064311 (2011).
- 13 J. Goldstone, A. Salam, and S. Weinberg, Phys. Rev. **127**, 965 (1962).
- 14 A.N. Andreyev *et al.*, Nature **405**, 430 (2000).
- 15 D.L. Hill and J.A. Wheeler, Phys. Rev. **89**, 1102 (1953).
- 16 N. Onishi and S. Yoshida, Nucl. Phys. **80**, 367 (1966).
- 17 R.E. Peierls and J. Yoccoz, Proc. Phys. Soc. **A70**, 381 (1957).
- 18 E. Bender, K.W. Schmid, and A. Faessler, Prog. Part. Nucl. Phys. **38**, 159 (1997).
- 19 N. Pillet, V.G. Zelevinsky, M. Dupuis, J.-F. Berger, and J.M. Daugas, Phys. Rev. C **85**, 044315 (2012).

19

Bosons, Symmetries and Group Models

Since the beginning of physics, symmetry considerations provided us an extremely powerful and useful tool in our efforts to understand nature. Gradually they have become the backbone of our theoretical formulation of physical laws.

T.D. Lee, *Particle Physics and Introduction to Field Theory* (Harwood Academic Publishers, 1981)

19.1 Introduction

In this chapter, we summarize what has been mentioned in several chapters concerning low-energy excitations in complex nuclei which are usually of *collective* character – rotations, vibrations, and their complicated combinations. The energy is low because many particles coherently take part in this motion and their relative configurations change very little. On a deeper level this is, of course, the motion of fermions – protons and neutrons. However, in such excitations, the quantum numbers of the states are changed as if this would correspond to the formation of *boson quasiparticles*. Because of the collective character of the excitation, the contribution of any individual particle is small, and the violations of the Fermi statistics emerging when we artificially introduce bosons are relatively small. For example, in the degenerate model (Section 13.2), fermion pairs show bosonic behavior and only a small N/Ω correction in their commutation relations reminds us of their composite nature. On the other hand, the description is highly simplified with the introduction of bosons, and we are rewarded by the convenience, clarity, and simplicity of the resulting, even if approximate, pattern. Some corrections can later be added to the original picture.

As was discussed earlier, a wave function $|\Psi_\alpha\rangle$ of a collective excitation is a coherent superposition of many single-particle or few-particle excitations $|\psi_k\rangle$,

$$|\Psi_\alpha\rangle = \sum_k C_k^\alpha |\psi_k\rangle, \quad \sum_k |C_k^\alpha|^2 = 1. \quad (19.1)$$

The effective number N_α of simple states $|\psi_k\rangle$ contributing to the wave packet (19.1) is large, $N_\alpha \gg 1$, but the weight of each of these is small,

$$|C_k^\alpha| \sim \frac{1}{\sqrt{N_\alpha}} \ll 1. \quad (19.2)$$

Therefore, the presence of a collective excitation typically only little distorts the single-particle motion. In the presence of developed pairing, the energies of the simplest low-energy collective modes are located inside the pairing gap. Therefore, they are not strongly mixed with single-particle excitations with energy above the gap and manifest a certain stability. In such cases, we can speak of new elementary excitations b_α^\dagger of the ground state $|0\rangle$,

$$|\Psi_\alpha\rangle = b_\alpha^\dagger|0\rangle. \quad (19.3)$$

We start with the simplest assumption that the coupling of those quasiparticles to single-particle excitations is weak; in reality, the situation cannot be that simple, especially if the vibrational amplitude gets large.

If the distortion of single-particle motion by the collective mode is relatively weak, we can repeat the action of the operator b_α^\dagger and construct *multiquantum* collective excitations. In this approximation, we come to the gas of the Bose quanta. Their older cousins in macroscopic systems are well known: phonons and magnons in solids, phonons in quantum liquids, such as helium isotopes ^4He and ^3He below the degeneracy temperature, and plasmons in an electron liquid. In a small system, such as a nucleus, the surface plays a special role, and low-lying vibrations are essentially shape modes we considered earlier, analogs of surface sound waves in a liquid drop.

The gas of independent bosons is just the starting approximation to reality. It is necessary to take the next step and consider the interaction of collective modes among themselves and with noncollective degrees of freedom. The interaction effects could be of dynamical origin (one can imagine the waves interacting at their spatial overlap) and kinematical – still our excitations are not genuine bosons all being formed of the same fermions. Even in a macroscopic ferromagnetic medium, where magnons are propagating spin-flip waves, the two-magnon state has to be corrected by subtraction of the effect of the formal double flip of the same spin. With increase of excitation energy, the interaction effects also grow; in macroscopic bodies, they accumulate and play the main role near the phase-transition points. In the interaction processes, the number of bosons is not conserved, they can appear and disappear.

In this chapter, we consider mainly the low-lying Bose-type excitations. Coherent interactions of quasiparticles lead also to collective modes of relatively high energy, which we called *giant resonances*. They are, to some extent, analogous to the *zero sound* in macroscopic Fermi systems (Chapters 5 and 6). New physics is then related to reactions needed to excite such a mode and to the finite lifetime due to the damping (decay into more complex configurations and decay into continuum). In this situation, the multiple (double and triple) excitations can be observed only rarely. The main tool for the analysis of giant resonances is the so-called *strength function*, which is discussed separately.

19.2 Low-Lying Quadrupole Excitations as Interacting Bosons

Limiting ourselves for definiteness to even–even complex nuclei, we notice that the low-lying states reveal, on the background of the simple shell-model picture, a clear collective structure. The pattern of such states is regular, changing systematically along

the nuclear chart, the most characteristic features being low energy and enhanced (compared to single-particle estimates) electromagnetic transition rates (Chapter 6). Quantum numbers $J^{\Pi} = 2^+$ of the first excited state, its low energy $E(2_1^+)$ rapidly going down as we move from a magic nucleus, growing collectivization measured by the large reduced probability $B(E2; 2_1^+ \rightarrow 0_1^+)$ of the electric quadrupole (E2) transition to the ground state 0_1^+ , and finally the emergence of static quadrupole deformation in nuclei at sufficiently large number of valence nucleons, all these specify a particular role of quadrupole symmetry in nuclear collective motion. The nearest classical relative of such collective motion is the surface vibrational wave of the nuclear drop considered by N. Bohr and J. Wheeler [1].

The quantized theory of quadrupole motion was stated by A. Bohr [2]. The main results, in fact, do not use a hydrodynamic picture, being based on the symmetry properties. Therefore, they are valid for collective quadrupole excitations of arbitrary microscopic structure. The lowest excitations are built, similarly to Eq. (19.3), as states of independent quadrupole bosons (perfect gas or *harmonic approximation*), while the interactions lead to *anharmonicity* and finally to static deformation that corresponds to the nonspherical condensate. In a fully microscopic approach, we work with interacting fermions and the most coherent particle–hole excitations form coherent bosonic modes (recall the random-phase approximation). In the nuclear case, it is important to correctly take into account strong monopole pairing that stabilizes the spherical shape, while the quadrupole polarization of the core by the valence nucleons leads to the deformation at some degree of occupation of the valence shell [3].

The reasonable *phenomenological* idea of the *interacting boson model* (IBM) is to take into account only monopole and quadrupole bosons [4] with their interactions. The bosons should personify combinations of nucleon pairs coupled to the angular momentum $L = 0$ and pairs excited to the angular momentum $L = 2$. These images of nucleon pairs can be called *s*- and *d*-bosons, respectively. Usually (not necessarily), the total number of bosons,

$$N = N_s + N_d, \quad (19.4)$$

is conserved, being taken equal to the number $N_f/2$ of fermionic pairs above the magic core. If the number N_f of valence nucleons is greater than half of the shell capacity Ω , one counts hole pairs taking $N = (\Omega - N_f)/2$. In a more detailed version of the model [5], [6], there are two types of fermions and correspondingly two types of bosons, proton and neutron ones.

The states generated by the boson creation operators \hat{s}^\dagger and \hat{d}_m^\dagger , where $m = 0, \pm 1, \pm 2$ is the angular momentum projection of the *d*-boson, are fixed by the boson number N , total angular momentum J , its projection $J_z = M$, and additional quantum numbers ζ which describe the coupling scheme for *d*-bosons as *s*-bosons do not carry angular momentum. In general, the state is a superposition of the type

$$|N, N_d, JM, \zeta\rangle = \sum_{N_d=0}^N C^J(N_d, \zeta) (\hat{s}^\dagger)^{N-N_d} [(\hat{d}^\dagger)^{N_d}]_{JM\zeta} |0\rangle, \quad (19.5)$$

where $|0\rangle$ is the boson vacuum, in practice identified in the IBM with the double-magic core. The model Hamiltonian can be constructed phenomenologically as a scalar conserving N . In principle, it is possible to exclude monopole bosons as they do not change

angular momentum quantum numbers and we can set

$$\hat{s} \Rightarrow \sqrt{N - \hat{N}_d}, \quad \hat{s}\hat{s} \Rightarrow \sqrt{(N - \hat{N}_d)(N - \hat{N}_d - 1)}, \dots \quad (19.6)$$

Here and later, we use the number operators for bosons,

$$\hat{N}_s = \hat{s}^\dagger \hat{s} = N - \hat{N}_d, \quad \hat{N}_d = \sum_m \hat{d}_m^\dagger \hat{d}_m. \quad (19.7)$$

The substitution (19.6) would lead to the inconvenient collective phenomenological Hamiltonian that contains nonlinear square-root operator factors truncating the d -boson space at a required value of N . The explicit use of s -bosons is practically more convenient. Before constructing the IBM Hamiltonian(s), let us look at the problem of multipole bosons from a more general viewpoint. A more rigorous group-theoretical consideration can be found in Ref. [7].

19.3 Algebra of Boson Operators

Let the indices i, j, \dots include all quantum numbers of bosons. The boson Hilbert space consists of states derived from the boson vacuum $|0\rangle$ by the repeated action of creation operators b_i^\dagger on the vacuum state. The standard commutation relations between the bosons are

$$[b_i, b_j^\dagger] = \delta_{ij}, \quad [b_i, b_j] = [b_i^\dagger, b_j^\dagger] = 0. \quad (19.8)$$

Any transformation in a subspace with a fixed total boson number N ,

$$\hat{N} = \sum_i \hat{N}_i = \sum_i b_i^\dagger b_i, \quad (19.9)$$

can be achieved by the sequence of elementary operations (*generators*)

$$B_{ij} = b_i^\dagger b_j = B_{ji}^\dagger, \quad (19.10)$$

which replace a boson j by its analog i keeping the same total boson number. The algebra of operators (19.10) is closed: their commutators are reduced to the operators of the same type,

$$[B_{ij}, B_{kl}] = \delta_{jk} B_{il} - \delta_{il} B_{kj}. \quad (19.11)$$

If we have bosons of D types, the operators B_{ij} (there are D^2 of them) generate the group $\mathcal{U}(D)$ of *unitary transformations* of the boson D -dimensional space. If we separate a trivial phase transformation related to the conservation of N , the group $\mathcal{U}(D)$ can be reduced to the *special unitary group* $S\mathcal{U}(D)$ of transformations which can be represented by matrices with a determinant equal to 1. The group $S\mathcal{U}(D)$ has $D^2 - 1$ generators. While the physics of boson systems is different from that of fermions, the underlying mathematics of the group theory associated with $\mathcal{U}(D)$ groups is the same and this discussion continues our earlier comments in Section 9.6.

In physical problems, we need to find quantum numbers of states which form a complete multiboson basis. The appropriate path goes through *invariant subgroups* of the total group $\mathcal{U}(D)$. They are characterized by smaller algebraically closed sets of operators. Each subgroup has its own *Casimir operators* commuting with all generators of the subgroup. In the subsequent classification of wave functions by

irreducible representations of subgroups, the values of these Casimir operators will be the quantum numbers. Such a reduction can usually be done in many ways; in physical applications we select the paths which are the closest to the symmetry of the actual Hamiltonian. We did not specify the dynamics yet, so that at this stage all reduction chains are equally good; each of them provides a complete basis for the wave functions.

We assume that, working in a finite, many-body system, we can classify our bosons by angular momentum quantum numbers, when the boson characteristics i are its angular momentum ℓ_i , projection m_i , and, if needed, additional marks x_i , so that $b_i \Rightarrow b_{\ell_i m_i x_i}$. Then the multiboson operators are classified as tensor operators of multipolarity (LM) obtained by the vector coupling of boson operators.

Similar to multipole operators made out of fermions (11.91), we define

$$B_{LM}^\dagger(\ell_1 x_1; \ell_2 x_2) = \sum_{m_1 m_2} (-)^{\ell_2 - m_2} C_{\ell_1 m_1 \ell_2 - m_2}^{LM} b_{\ell_1 m_1 x_1}^\dagger b_{\ell_2 m_2 x_2} \equiv (b_1^\dagger \tilde{b}_2)_{LM}. \quad (19.12)$$

Here, B_{LM}^\dagger is seen as a creation operator increasing the magnetic projection of the state by M . Action of the boson annihilation operator is seen as addition of reversed angular momentum (subtraction), thus tilde as in Eq. (11.76) is used to indicate that $\tilde{b}_{\ell m} = (-1)^{\ell - m} b_{\ell - m}$. B_{LM} are defined as destruction operators diminishing the projection by M . It follows from the definition that

$$B_{LM}^\dagger(\ell_1 x_1; \ell_2 x_2) = (-)^{\ell_1 - \ell_2 - M} B_{L-M}(\ell_2 x_2; \ell_1 x_1) \quad (19.13)$$

Problem 19.1 Show that the pair operator with $L = 1$, diagonal with respect to ℓ and x , is proportional to the total angular momentum of the system [see also (11.94)],

$$J_\mu = \sum_{\ell x} \sqrt{\frac{\ell(\ell+1)(2\ell+1)}{3}} B_{1\mu}^\dagger(\ell x; \ell x). \quad (19.14)$$

Problem 19.2 Using the standard techniques of angular momentum recoupling with the $6j$ -symbols, prove that the commutator relations (19.11) can be presented as

$$\begin{aligned} [B_{LM}^\dagger(12), B_{L'M'}^\dagger(1'2')] &= \sqrt{(2L+1)(2L'+1)} \sum_{\Lambda\mu} C_{LM L'M'}^{\Lambda\mu} \\ &\times \left[\delta_{21'} (-)^{\ell_1 - \ell'_1 + \Lambda} \begin{Bmatrix} L & L' & \Lambda \\ \ell'_1 & \ell_1 & \ell_2 \end{Bmatrix} B_{\Lambda\mu}^\dagger(12') \right. \\ &\left. - \delta_{12'} (-)^{\ell_2 - \ell'_2 + L + L'} \begin{Bmatrix} L & L' & \Lambda \\ \ell'_2 & \ell_2 & \ell_1 \end{Bmatrix} B_{\Lambda\mu}^\dagger(1'2) \right]. \end{aligned} \quad (19.15)$$

In certain applications, it might be convenient to introduce the combinations of the pair operators (19.10) with certain symmetry under time reversal (inverting the signs of the projections and interchanging initial and final states),

$$B_{ij}^{(\pm)} = \frac{1}{2}(B_{ij} \pm B_{\bar{i}\bar{j}}^\dagger). \quad (19.16)$$

or explicitly,

$$B_{\ell mx, \ell' m' x'}^{(\pm)} = \frac{1}{2}(B_{\ell mx, \ell' m' x'} \pm (-)^{\ell-m+\ell'-m'} B_{\ell' -m' x', \ell-m x}). \quad (19.17)$$

For D types of bosons, there are $D(D + 1)/2$ symmetric combinations $B^{(+)}$ and $D(D - 1)/2$ antisymmetric combinations $B^{(-)}$. The corresponding tensor operators (19.12) have the following symmetry properties:

$$B_{LM}^{(\pm)\dagger}(12) = \frac{1}{2} [B_{LM}^\dagger(12) \pm (-)^{\ell_1 + \ell_2 - L} B_{LM}^\dagger(21)] = \pm (-)^{\ell_1 + \ell_2 - L} B_{LM}^{(\pm)\dagger}(21). \quad (19.18)$$

These properties simply reflect the permutational symmetry of the Clebsch–Gordan coefficients. In particular, the diagonal in (ℓx) combinations $B_{LM}^{(\pm)\dagger}(11), (\ell_1 x_1) = (\ell_2 x_2)$, contains only even values of L , while $B_{LM}^{(-)\dagger}(11)$ contains only odd values of L . The results discussed here, including relations (19.15), are also valid for fermion operators and thus can be applied in classifications discussed in Chapter 11.

Problem 19.3 Rewrite the commutators (19.15) in terms of the pairs of certain symmetry, $B_{LM}^{(\pm)\dagger}(12)$.

19.4 Subgroups and Casimir Operators

The commutator structure (19.15) and an example of the angular momentum operators (19.14) reveal subsets of generators closed with respect to commutators. Among such subsets we can mention the following:

- All antisymmetric operators $B_{ij}^{(-)}$ form a closed subgroup of \mathcal{T} -odd generators: the commutator of two \mathcal{T} -odd operators is again \mathcal{T} -odd. The corresponding group operations involve only orthogonal transformations generated by real D -dimensional matrices. This group is the rotation group $\mathcal{O}(D)$ of D -dimensional space; the operators $B^{(-)}$ changing sign under time reversal play the role of the D -dimensional angular momentum. The number of these generators, $D(D - 1)/2$, is the number of planes for independent rotations in this space.
- Three components (19.14) generate the standard three-dimensional rotation group $\mathcal{O}(3)$.
- For each type of bosons with spin ℓ , $(2\ell + 1)^2$ operators containing only these particular bosons, $B_{\ell mx} \ell_{m'x} = B_{mm'}$, or in spherical form, $B_{LM}^\dagger(\ell x; \ell x)$, with $L = 0, 1, \dots, 2\ell$, generate the unitary group $\mathcal{U}(2\ell + 1)$. Without the corresponding phase transformation generated by the scalar boson number operator, the group is $S\mathcal{U}(2\ell + 1)$.
- For each type of bosons with spin ℓ , the antisymmetric operators $B_{mm'}^{(-)}$ generate the orthogonal group $\mathcal{O}(2\ell + 1)$. The generators of this group have odd L as dictated by the permutational symmetry of the Clebsch–Gordan coefficients, see Eq. (19.18). For $\ell > 1$, this group contains the subgroup $\mathcal{O}(3)$ of partial rotations among bosons of a given type (ℓx) generated by the $L = 1$ operators $B_{1\mu}^\dagger$.

For a given group algebra (19.11), it is straightforward to construct a *Casimir operator* quadratic in generators B_{ij} that commutes with every individual generator B_{ij} ,

$$\begin{aligned} C_{\mathcal{U}(D)} &= \sum_{ij} B_{ij}^\dagger B_{ij} = \sum_{ij} B_{ji} B_{ij} \\ &= 4 \sum_{ij} B_{ij}^{(+)\dagger} B_{ij}^{(+)} + 4 \sum_{ij} B_{ij}^{(-)\dagger} B_{ij}^{(-)}. \end{aligned} \quad (19.19)$$

For unitary and orthogonal groups of interest, this construction is nothing more than a length conserved under unitary or orthogonal transformations. As a rotational tensor, the Casimir operator must be a scalar, and we generalize the standard recipe of constructing scalars [QP, I, Problem 22.5] which leads to

$$C_{U(D)} = \sum_{12;LM} (-)^M B_{LM}^\dagger(12) B_{L-M}^\dagger(21) = \sum_{12;LM} (-)^{\ell_2 - \ell_1} B_{LM}^\dagger(12) B_{LM}(12). \quad (19.20)$$

The group $\mathcal{O}(D)$ is a subgroup of $U(D)$ with the Casimir operator containing only \mathcal{T} -odd generators; we define it as (sometimes an additional factor of 2 is used making it a part of (19.19))

$$C_{\mathcal{O}(D)} = 2 \sum_{12;LM} B_{ij}^{(-)\dagger} B_{ij}^{(-)} = 2 \sum_{12;LM} (-)^M B_{LM}^{(-)\dagger}(12) B_{L-M}^{(-)\dagger}(21). \quad (19.21)$$

In particular, similarly to usual three-dimensional rotations, the square of the D -dimensional momentum commutes with all partial rotation generators $B_{ij}^{(-)}$, so this is the Casimir operator $C_{\mathcal{O}(D)}$ of the group $\mathcal{O}(D)$.

Analogously to the fermion pairing (Chapter 13), we can introduce the operators for boson pairs coupled to zero angular momentum,

$$P_D = \frac{1}{2} \sum_{\ell mx} (-)^{\ell-m} b_{\ell-mx} b_{\ell mx}, \quad P_D^\dagger = \frac{1}{2} \sum_{\ell mx} (-)^{\ell-m} b_{\ell mx}^\dagger b_{\ell-mx}^\dagger. \quad (19.22)$$

If we regroup the boson operators in Eq. (19.20) and use the number operator (19.9), we find the useful expression for the Casimir operator,

$$C_{\mathcal{O}(D)} = N(N + D - 2) - 4P_D^\dagger P_D. \quad (19.23)$$

Let us take as basis states those with a certain number n of boson pairs with zero angular momentum, so that

$$N = 2n + \sigma, \quad (19.24)$$

where σ is the number of unpaired bosons. The pair destruction operator P_D reduces n by 1 and N by 2 without changing σ . The consecutive action by this lowering operator will bring us to the vacuum with respect to pairs, $n = 0$ and $N = \sigma$. The next action by P_D gives zero. As in this process the Casimir operator does not change, Eq. (19.23) determines the spectrum of its eigenvalues

$$C_{\mathcal{O}(D)} = \sigma(\sigma + D - 2), \quad \sigma = 0, 1, 2, \dots \quad (19.25)$$

The quantum number σ is an analog of the three-dimensional angular momentum J ; indeed, for $D = 3$, $C_{\mathcal{O}(3)} = \sigma(\sigma + 1)$. It follows now from Eq. (19.23) that, in the state with certain values of N and σ ,

$$P_D^\dagger P_D = \frac{1}{4} (N - \sigma)(N + \sigma + D - 2). \quad (19.26)$$

Problem 19.4 Consider a system with D degrees of freedom described by coordinates x_a and conjugate momenta p_a , $a = 1, \dots, D$, with standard commutation relations, $[x_a, p_b] = i\hbar\delta_{ab}$. Construct the components of the multidimensional angular momenta as generators of rotations in different planes,

$$\hbar L_{ab} = x_a p_b - x_b p_a. \quad (19.27)$$

Define the total square of the angular momentum as

$$L^2 = \frac{1}{2} \sum_{ab} L_{ab}^2. \quad (19.28)$$

Show that the eigenvalues of the operator (19.28) are quantized according to

$$L^2 = J(J + D - 2), \quad J = 0, 1, 2, \dots, \quad D \geq 2. \quad (19.29)$$

The analogy with the concept of seniority from the pairing problem can be useful.

Solution

One can introduce the annihilation, A_a , and creation, A_a^\dagger , operators as for the harmonic oscillators,

$$x_a = \sqrt{\frac{\hbar}{2}} (A_a + A_a^\dagger), \quad p_a = -i \sqrt{\frac{\hbar}{2}} (A_a - A_a^\dagger), \quad (19.30)$$

with commutation relations

$$[A_a, A_b^\dagger] = \delta_{ab}. \quad (19.31)$$

Using the standard ladder construction, we show that the number operators

$$N_a = A_a^\dagger A_a, \quad N = \sum_a N_a, \quad (19.32)$$

have a non-negative integer eigenvalue spectrum. After simple algebra, we find

$$L^2 = N(N + D - 2) - P^\dagger P, \quad (19.33)$$

where the pair operators are

$$P = \sum_a P_a, \quad P_a = A_a A_a^\dagger. \quad (19.34)$$

The operator L^2 is the Casimir operator commuting with all generators L_{ab} . The proof then just repeats what was earlier used in Eqs. (19.23)–(19.26).

Problem 19.5 The close analogy with the pairing problem can be established if we consider the algebra of pair operators and introduce an analog of quasispin \mathbf{S} ,

$$S_1 = \frac{1}{4} (P + P^\dagger), \quad S_2 = -\frac{i}{4} (P^\dagger - P), \quad S_3 = \frac{1}{2} n + \frac{1}{4} D. \quad (19.35)$$

Find their commutation relations and the Casimir operator.

Solution

The operators S_k satisfy the commutation relations of the noncompact (because the number of quanta is not restricted) algebra of the quasispin group $SU(1, 1)$ that differs from the $SU(2)$ algebra of angular momentum by some signs in the commutators,

$$[S_1, S_2] = -iS_3, \quad [S_2, S_3] = iS_1, \quad [S_3, S_1] = iS_2. \quad (19.36)$$

The Casimir operator of this noncompact group is the “*hyperbolic momentum*”

$$C = S_3^2 - S_1^2 - S_2^2. \quad (19.37)$$

19.5 s-d Model

The most widely used version of the IBM is restricted by two kinds of bosons,

$$b_{00} = s, \quad b_{00}^\dagger = s^\dagger; \quad b_{2m} = d_m, \quad b_{2m}^\dagger = d_m^\dagger. \quad (19.38)$$

These degrees of freedom are boson counterparts of paired fermions (monopole and quadrupole pairing). The direct identification of bosons with valence fermion pairs, as done by many practitioners, is dangerous because then the limiting angular momentum in many cases turns out to be smaller than observed in collective bands in the experiment. But, without this identification, the model presents a reasonable, simplified image of real collective dynamics.

Six (1+5) pairs of creation and annihilation operators (19.38) form 36 two-boson combinations (19.10). They, in turn, generate the unitary group $\mathcal{U}(6)$, or $S\mathcal{U}(6)$ for a fixed total boson number. We can classify the two-boson operators by their rotational properties (19.12) and time-reversal symmetry (19.18). Then we naturally come to the decomposition of 36 operators $B_{\ell m \ell' m'}$ into

- a) Twenty-one *symmetric* combinations including the following:
two monopole ones (numbers of quanta)

$$B_{00}^{(+)}(00) = N_s, \quad B_{00}^{(+)}(22) = \frac{1}{\sqrt{5}} N_d, \quad (19.39)$$

$5 + 5 = 10$ quadrupole operators of two types,

$$Q_M^{(+)} = \frac{1}{2} (B_{2M}^\dagger(20) + B_{2M}^\dagger(02)) = \frac{1}{2} (d_M^\dagger s + (-)^M s^\dagger d_{-M}), \quad (19.40)$$

and

$$Q_M = B_{2M}^\dagger(22) = (d^\dagger \tilde{d})_{2M}, \quad (19.41)$$

plus 9 hexadecapole ($L = 4$) operators

$$Q_{4M} = B_{4M}^\dagger(22) = (d^\dagger \tilde{d})_{4M}; \quad (19.42)$$

and

- b) Fifteen *antisymmetric* combinations:

three components of angular momentum (19.14) which are created by d -bosons only,

$$J_M = \sqrt{10} B_{1M}^\dagger(22) = \sqrt{10} (d^\dagger \tilde{d})_{1M}, \quad (19.43)$$

five quadrupole operators

$$Q_M^{(-)} = \frac{i}{2} (B_{2M}^\dagger(20) - B_{2M}^\dagger(02)) = \frac{i}{2} (d_M^\dagger s - (-)^M s^\dagger d_{-M}) \quad (19.44)$$

and seven octupole operators

$$Q_{3M} = B_{3M}^\dagger(22) = (d^\dagger \tilde{d})_{3M}. \quad (19.45)$$

Note that the phase change $s^\dagger \rightarrow -is^\dagger$ makes (19.44) dynamically equivalent to (19.40). This change has no significant effect on our following discussion and for the most part we can use the form (19.40) for the generators of $\mathcal{O}(6)$ and for all other purposes. Attention should only be paid to the cases where we encounter non-Hermitian quadratic terms ss

or $s^\dagger s^\dagger$ which should change sign (equivalent to the choice of sign in Eq. (19.6)); the most relevant place is the definition of the pairing operator for $\mathcal{O}(6)$ following (19.26).

We summarize how these operators can be organized into sets of generators for different groups as follows:

$$\mathcal{U}(6) = \{(s^\dagger \tilde{s})_0, (s^\dagger \tilde{d})_2, (d^\dagger \tilde{s})_2, (d^\dagger \tilde{d})_{L=0,1,2,3,4}\}; \quad 36 \text{ generators} \quad (19.46)$$

$$\mathcal{U}(5) = \{(d^\dagger \tilde{d})_{L=0,1,2,3,4}\}; \quad 25 \text{ generators} \quad (19.47)$$

$$SU(5) = \{(d^\dagger \tilde{d})_{L=1,2,3,4}\}; \quad 24 \text{ generators} \quad (19.48)$$

$$\begin{aligned} \mathcal{U}(3) = & \{(s^\dagger \tilde{s})_0 + \sqrt{5}(d^\dagger \tilde{d})_0, (d^\dagger \tilde{d})_1, (s^\dagger \tilde{d})_2 + (d^\dagger \tilde{s})_2 \\ & - \sqrt{7/4}(d^\dagger \tilde{d})_2\}; \end{aligned} \quad 9 \text{ generators} \quad (19.49)$$

$$SU(3) = \{(d^\dagger \tilde{d})_1, (s^\dagger \tilde{d})_2 + (d^\dagger \tilde{s})_2 - \sqrt{7/4}(d^\dagger \tilde{d})_2\}; \quad 8 \text{ generators} \quad (19.50)$$

$$\mathcal{O}(6) = \{(d^\dagger \tilde{d})_1, (d^\dagger \tilde{d})_3, ((s^\dagger \tilde{d})_2 + (d^\dagger \tilde{s})_2)\}; \quad 15 \text{ generators} \quad (19.51)$$

$$\mathcal{O}(5) = \{(d^\dagger \tilde{d})_1, (d^\dagger \tilde{d})_3\}; \quad 10 \text{ generators} \quad (19.52)$$

$$\mathcal{O}(3) = \{(d^\dagger \tilde{d})_1\}; \quad 3 \text{ generators} \quad (19.53)$$

Here, the subscripts $(\dots)_L$ indicate coupling to angular momentum L and for each L there exist $2L+1$ possible magnetic projections which are not labeled separately; we recall that the tilde sign is used to reverse angular momentum of the annihilation operator (11.76), $\tilde{d}_m = (-1)^m d_{-m}$. The number of generators is D^2 for $\mathcal{U}(D)$; $D^2 - 1$ for $SU(D)$; and $D(D-1)/2$ for $\mathcal{O}(D)$. The presence of the factor $\sqrt{7/4}$ will become clear in relation to Eq. (19.63).

In the $s-d$ model, the Hamiltonian conserves the total number of bosons. Its most general rotationally invariant form containing one- and two-boson parts can be written as

$$H = H_s^\circ + H'_s + H_d^\circ + H'_d + H'_{sd}, \quad (19.54)$$

where one- and two-body terms involving the s -boson are

$$H_s^\circ = \omega_s \left(s^\dagger s + \frac{1}{2} \right) \quad H'_s = U(s^\dagger s^\dagger)(ss). \quad (19.55)$$

For the d -boson, we have

$$H_d^\circ = \omega_d \sum_m \left(d_m^\dagger d_m + \frac{1}{2} \right), \quad H'_d = \frac{1}{2} \sum_{L=0,2,4} V_L \sum_M (d^\dagger d^\dagger)_{LM} (dd)_{LM}. \quad (19.56)$$

The two-body sd -interaction has three possible terms:

$$\begin{aligned} H'_{sd} = & \frac{U_1}{\sqrt{2}} \left[((d^\dagger d^\dagger)_2 (\tilde{d} \tilde{s})_2)_0 + ((s^\dagger d^\dagger)_2 (\tilde{d} \tilde{d})_2)_0 \right] \\ & + \frac{U_2}{\sqrt{2}} \left[((d^\dagger d^\dagger)_0 (\tilde{s} \tilde{s})_0)_0 + ((s^\dagger s^\dagger)_0 (\tilde{d} \tilde{d})_0)_0 \right] + U_3 ((d^\dagger s^\dagger)_2 (\tilde{s} \tilde{d})_2)_0. \end{aligned} \quad (19.57)$$

Altogether, there are nine parameters in the $s-d$ IBM version. However, as we discussed earlier, if the total number of bosons is fixed, the s -boson number can be defined in terms of d -bosons and H_s° and H'_s terms are not independent; in addition to that, the U_3 term can be recoupled and expressed in terms of boson number operators. Thus, there are only six independent parameters. The interaction Hamiltonian can be also expressed

as a linear combination of the d -boson number operator and the second-order Casimir operators $\mathcal{U}(5)$, $S\mathcal{U}(3)$, $\mathcal{O}(6)$, $\mathcal{O}(5)$, and $\mathcal{O}(3)$,

$$H = \epsilon N_d + \alpha C_{\mathcal{U}(5)} + \beta C_{S\mathcal{U}(3)} + \gamma C_{\mathcal{O}(6)} + \delta C_{\mathcal{O}(5)} + \eta C_{\mathcal{O}(3)} + \text{const.} \quad (19.58)$$

Problem 19.6 Establish a relation between the two types of the boson–boson interactions similar to the particle–hole and particle–particle channel for fermions:

$$\begin{aligned} \sum_{\Lambda} (-)^{\Lambda} (d^\dagger \tilde{d})_{K\Lambda} (d^\dagger \tilde{d})_{K-\Lambda} &= \frac{1}{5} (2K+1) N_d \\ &+ (2K+1) \sum_L \left\{ \begin{matrix} 2 & 2 & L \\ 2 & 2 & K \end{matrix} \right\} \sum_M (dd)_{LM}^\dagger (dd)_{LM}. \end{aligned} \quad (19.59)$$

See also Problem 11.10.

In general, all the operators shown above do not commute and cannot simultaneously have certain values. In practice, the problem has to be solved numerically, similarly to the fermion shell model but, as a rule, for much smaller dimensions. Various choices of basis can be used for this purpose. A strategy based on the canonical reduction of $\mathcal{U}(N)$ group has been discussed for fermions in Section 9.6. Similar to the many-fermion problem, one should use the basis that is most relevant for the specific system. Various choices select different reduction chains possible in the framework of the s – d model going from the general form to the rotational $\mathcal{O}(3)$ group that has to be always present as a final point of reduction. Different choices of intermediate symmetries can be seen as specific limits reflecting different physical pictures possible in the general boson s – d framework.

The simplest reduction starts with separating quadrupole bosons. There are 25 operators (19.47) formed exclusively by the d -bosons. They correspond to the group $\mathcal{U}(5)$, or $S\mathcal{U}(5)$ for fixed N_d , Eq. (19.48). Here we have a unique quadrupole operator $(d^\dagger \tilde{d})_2$, Eq. (19.41). The antisymmetric operators with odd L , angular momentum (19.43) and octupole (19.45), generate the orthogonal group $\mathcal{O}(5)$, Eq. (19.52), with the usual rotation group $\mathcal{O}(3)$, Eq. (19.53), as its subgroup. In this way, we obtain the group reduction chain which we label I,

$$I : S\mathcal{U}(6) \supset S\mathcal{U}(5) \supset \mathcal{O}(5) \supset \mathcal{O}(3). \quad (19.60)$$

The emerging picture of conserved quadrupole bosons may be juxtaposed with the vibrations of near-spherical nuclei (*vibrational limit*).

Two other chains include the operators $Q_M^{(\pm)}$, Eqs. (19.40) and (19.44), and mix s - and d -bosons. Taking all 15 antisymmetric operators (19.43)–(19.45), we come to the orthogonal group $\mathcal{O}(6)$, Eq. (19.51). The next reduction goes, as in the case I, along smaller orthogonal groups $\mathcal{O}(5)$ and $\mathcal{O}(3)$ and leads to the case II,

$$II: S\mathcal{U}(6) \supset \mathcal{O}(6) \supset \mathcal{O}(5) \supset \mathcal{O}(3). \quad (19.61)$$

The dynamics compatible with the $\mathcal{O}(6)$ symmetry is close to the so-called γ -unstable.

The third reduction possibility, also not conserving separately s - and d -bosons, is combined by angular momentum (that has to be present in any physical realization) and

the quadrupole. This is impossible using the d -bosons only because the commutator $[Q_M, Q_{M'}]$ of the components of the quadrupole moment of d -bosons (19.41) contains, apart from the angular momentum ($\Lambda = 1$), also the octupole ($\Lambda = 3$). However, it is possible to construct a specific combination of quadrupole operators (19.40) and (19.41) that includes $s-d$ transitions,

$$\tilde{Q}_M = \sqrt{2} \left[2Q_M^{(+)} + \frac{\sqrt{7}}{2} Q_M \right]. \quad (19.62)$$

For such an operator, the octupole drops from the algebra,

$$[\tilde{Q}_M, \tilde{Q}_{M'}] = \frac{3\sqrt{30}}{4} \sum_{\lambda} (-)^{\lambda} \begin{pmatrix} 2 & 2 & 1 \\ M & M' & -\lambda \end{pmatrix} J_{\lambda}. \quad (19.63)$$

Eight operators $\{\mathbf{J}, \tilde{Q}_M\}$ generate a popular realization of the $SU(3)$ group (19.50), [8]. Here we have the third group reduction:

$$\text{III: } SU(6) \supset SU(3) \supset O(3). \quad (19.64)$$

This is appropriate for the rotational limit.

As the group $O(6)$ is isomorphic to $SU(4)$, we exhausted the nonequivalent reduction chains proceeding from $SU(6)$ to $SU(5)$, $SU(4)$, and $SU(3)$, respectively in cases I, II, and III.

19.6 Irreducible Representations and Quantum Numbers

The final destination of all three reduction chains is the normal rotation group $O(3)$. Therefore, the basis functions can be labeled by the angular momentum quantum numbers J and M . The additional quantum numbers depend on the reduction path. Let us first consider the chain $O(5) \supset O(3)$ that is common for cases I and II.

For the $O(5)$ group of rotations in the space of d -bosons, the number of unpaired bosons (19.24) traditionally is called *seniority* v (compare with the fermion seniority in the pairing problem). According to (19.25), (19.26), we have here

$$C_{O(5)} = v(v+3), P_5^{\dagger}P_5 = \frac{1}{4} (N-v)(N+v+3). \quad (19.65)$$

For the Casimir operator of the $O(6)$ group we preserve the notation (19.24),

$$C_{O(6)} = \sigma(\sigma+4). \quad (19.66)$$

Now the problem is to determine what values of the angular momentum J can be found in the irreducible representation of the $O(5)$ group with seniority v . For a given total number N_d , we have here $n = (N_d - v)/2$ bosonic pairs coupled to zero angular momentum. Recalling the coordinate representation of the quadrupole variables (Section 12.6), we find that such pairs correspond to the global invariant variable β . There exists only one additional invariant $\beta^3 \cos(3\gamma)$ that corresponds to the cubic scalar combination of the quadrupole coordinates. This means that the unpaired bosons can couple in trios generated by the operator

$$P_5^{(3)\dagger} = (d^{\dagger} d^{\dagger} d^{\dagger})_{00}, \quad (19.67)$$

while the bigger scalar complexes can always be presented by some number of pairs and trios. The number n' of trios can change from zero to the integer part of $v/3$. Finally, we are left with $f = v - 3n'$ active bosons. Only these free quanta can give a nonzero angular momentum. They can have various projections $J_z = M$ but only in combinations which cannot be reduced to the operators of pairs or trios.

Let us construct the boson state with the maximum total projection $M = J$ for even J . This state is built uniquely by the product of creation operators

$$(d_2^\dagger)^{J-f} (d^\dagger d^\dagger)_{22}^{f-J/2}. \quad (19.68)$$

Indeed, here the powers of operator combinations are taken in such a way that the number of active phonons is $J - f + 2(f - J/2) = f$ and the angular momentum projection $M = 2(J - f) + 2(f - J/2) = J$. It follows from here that even values of J are possible from f (if f is even) or $f + 1$ (if f is odd) up to $2f$. Analogously, for odd values of J , the corresponding function instead of (19.68) should be

$$(d_2^\dagger)^{J-f} (d^\dagger d^\dagger)_{22}^{f-J/2-3/2} (d^\dagger d^\dagger d^\dagger)_{33}. \quad (19.69)$$

Here the odd values of J can run from f (if f is odd) or $f + 1$ (if f is even) up to $2f - 3$. Combining the results (19.68) and (19.69), we see that, at a fixed value of f , the allowed values of the total angular momentum are

$$J = f, f + 1, \dots, 2f - 3, 2f - 2, 2f. \quad (19.70)$$

An interesting conclusion is that states with $J = 1$ cannot be built of quadrupole bosons independently of the number f of active quanta; also, for a given f , the state with $J = 2f - 1$ is absent.

Problem 19.7 Count the total number of states, $D(v)$, with possible values of n', J , and M for a given value of seniority v and the total number of states of N_d quadrupole bosons.

Solution

The answer is

$$D(v) = \frac{1}{6} v(v+1)(2v+3), \quad (19.71)$$

while the total number of states is given by the standard count for Bose statistics, if each boson has five intrinsic states,

$$D(N_d) = \frac{(N_d + 4)!}{4! N_d!}. \quad (19.72)$$

We conclude that the states of quadrupole bosons transforming according to irreducible representations of the $SU(5)$ group are uniquely labeled by the set of quantum numbers N_d, v, n', J, M ; the seniority $v \leq N_d$ is even (odd) for even (odd) N_d . Because of the Bose statistics, for any reduction chain, the states belong to the fully symmetric representation of the $SU(6)$ group labeled as $[N]$, Section 9.6. Finally, we can fix the basis for the chain I, Eq. (19.60):

$$|[N]N_dvn'JM\rangle. \quad (19.73)$$

In the chain II, Eq. (19.61), the number N_d is not conserved. We can juxtapose the Casimir operators of the orthogonal groups $\mathcal{O}(5)$ and $\mathcal{O}(6)$, Eq. (19.20):

$$C_{\mathcal{O}(5)} = 2 \sum_{L=1,3} \sum_M (d^\dagger \tilde{d})_{LM}^\dagger (d^\dagger \tilde{d})_{LM} = \frac{1}{5} \mathbf{J}^2 + 2 \sum_M (-)^M Q_{3-M} Q_{3M} \quad (19.74)$$

and

$$C_{\mathcal{O}(6)} = C_{\mathcal{O}(5)} + \sum_M (-)^M Q_{-M}^{(-)} Q_M^{(-)}. \quad (19.75)$$

Here the antisymmetric quadrupole moment (19.44) is included with the selection rules $\Delta N_s = -\Delta N_d = \pm 1$. As we have seen earlier, Eq. (19.66), $C_{\mathcal{O}(6)}$ takes values $\sigma(\sigma+4)$, where the number of unpaired bosons $\sigma \leq N$ is even (odd) for even (odd) N . Then the seniority v (the number of unpaired d -bosons) runs from zero to σ , while the allowed values n' and J at given v can take the same values as in the chain I. Similarly to (19.73), we have here the basis

$$|[N]\sigma v n' JM\rangle. \quad (19.76)$$

For the chain III, Eq. (19.64), we need irreducible representations of the group $SU(3)$ which are described in the literature [8, 9], see also Section 9.6. In the boson realization (19.62), (19.63), the representation is characterized by two even numbers (λ, μ) . Here $\lambda/2$ has a meaning of the number of “freely rotating” quanta. In the rotational picture, these quanta create the angular momentum perpendicular to the symmetry axis. The magnitude of this momentum is restricted by $2 \cdot (\lambda/2) = \lambda$; in this limiting case, all quanta are in the d -mode with the maximum projection 2 onto the rotation axis. The quantum number μ can be interpreted as the number of bosons with the fixed angular momentum projection onto the symmetry axis. In the unified fermionic model, this would be analogous to the quanta of β - and γ -vibrations.

For a given boson number N , the series of representations (λ, μ) is allowed when we fix the numbers of rotating bosons in terms of these quantum numbers assuming that the rest is combined in triplets with zero angular momentum so that

$$N = \lambda + \mu + 3n', \quad (19.77)$$

where n' is the number of those triplets. If J_{\min} and J_{\max} are, respectively, the smallest and the largest of the numbers λ and μ , the (λ, μ) representation consists of several rotational bands. The heads of those bands have even angular momenta J_0 changing from zero to J_{\min} , while inside the band with given J_0 , the angular momentum takes all values $J = J_0, J_0 + 1, \dots, J_0 + J_{\max}$ if $J_0 \neq 0$. In the case of $J_0 = 0$, the band accepts only angular momenta of the same parity as J_{\max} , so that, going down, $J = J_{\max}, J_{\max} - 2, \dots, 1$ or 0, see Eqs. (9.46) and (9.47). Therefore, the states in the chain III can be listed as

$$|[N]\lambda\mu J_0 JM\rangle. \quad (19.78)$$

One can approximately identify J_0 with the quantum number $I_3 = K$ of an axially deformed nucleus, in agreement with the above-mentioned rule for $J \geq J_0$. However, in the unified model of the axially symmetric nucleus, K is an exact constant of motion, whereas in the $SU(3)$ classification the states which differ only by the value of J_0 but have the same values J, λ, μ still require orthogonalization. They are precisely orthogonal and fully analogous to the bands with the quantum number K only in the limit $J_{\max} \rightarrow \infty$ [8].

With normalization of generators \tilde{Q}_M according to Eq. (19.63), the Casimir operator of the group $SU(3)$ can be written as

$$C_{SU(3)} = \frac{3}{4} J^2 + \sum_M (-)^M \tilde{Q}_M \tilde{Q}_{-M}; \quad (19.79)$$

in the (λ, μ) representation

$$C_{SU(3)} = \lambda(\lambda + 3) + \mu(\mu + 3) + \lambda\mu. \quad (19.80)$$

The overall normalization here is not important, although an additional factor $2/3$ is commonly used in line with general group theory. We remind also that our Casimir operator for $O(D)$ group is defined to give $J(J+1)$ for $O(3)$ but it is less by a factor of 2 than some definitions found in literature [4, 6]. The dimension of $SU(3)$ representation (λ, μ) is given by Eq. (9.45).

19.7 Vibrational Limit

The symmetry of type I is exact if the boson Hamiltonian preserves the number N_d . The simplest possible example is given by the system of noninteracting quadrupole bosons,

$$H_d^\circ = \omega \sum_m \left(d_m^\dagger d_m + \frac{1}{2} \right), \quad (19.81)$$

where ω is a single-boson energy (below we set $\hbar = 1$). Here, we have equidistant multiplets of states with certain N_d . The energies of stationary states depend only on the total number N_d of bosons being degenerate with respect to the quantum numbers v, n' and angular momentum J . We have already encountered this model in Chapter 6 discussing phonon excitations. Figure 19.1 shows the energy spectrum of phonon multiplets up to $N_d = 4$ and relative rates $B(E2)$ of quadrupole transitions. As in the geometric model of Chapter 6, we assume that the quadrupole operator Q_μ is proportional to the d -boson coordinate operator $d_\mu + (-)^\mu d_{-\mu}^\dagger$, the transitions down are induced by the phonon destruction operator being shown in units of the lowest transition from the one-phonon state to the ground (vacuum) state, $(J=2)_1 \rightarrow (J=0)_1$, as discussed later in more detail.

The model is made more realistic if one includes the interaction of bosons still keeping their number conserved. The simplest two-boson interaction describes scattering processes. The general $SU(5)$ -symmetric Hamiltonian can depend on Casimir operators of the chain I, $C_{O(5)}$, Eq. (19.74), and J^2 . Then the energy spectrum will depend on $N, N_d, v(v+3)$, and $J(J+1)$ but not on n' . In practice, it is difficult to check this prediction as in the low-energy part of the spectrum, Figure 19.1, for given v every value of J appears just once: there are two states with different values of $n' = 0$ and $n' = 1$ only for $N_d = v = 6$ and $J = 6$.

The scattering interaction is the most natural as long as the number of quanta is not too high and we can imagine their pairwise “collisions,” similar to the fermionic ones in Figure 11.1. Here we can also consider both forms, direct (“particle–particle”), Figure 11.1a, and exchange (“particle–hole”), Figure 11.1b, with recoupling in Eq. (19.59).

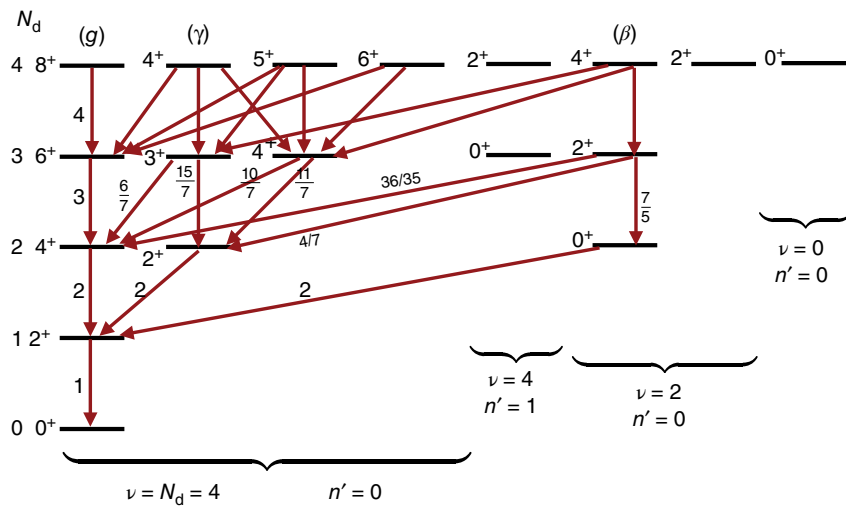


Figure 19.1 The energy scheme and relative quadrupole transition probabilities for the perfect $SU(5)$ symmetry and harmonic Hamiltonian (19.81) of noninteracting d -bosons, case I. The states are classified by quantum numbers of Eq. (19.73).

Since two identical d -bosons can have only even total angular momenta, there are only three coupling constants $V_L, L = 0, 2, 4$ in the direct channel, which determine the most general interaction Hamiltonian

$$H'_d = \frac{1}{2} \sum_{L=0,2,4} V_L \sum_M (d^\dagger d^\dagger)_{LM} (dd)_{LM}. \quad (19.82)$$

Problem 19.8 Find the energy spectrum of the d -boson Hamiltonian $H_d^0 + H'_d$ given by (19.81) and (19.82).

Solution

This has been done in Refs. [4, 10]. The result can be expressed as a function of quantum numbers N_d, J , and v :

$$\begin{aligned} E(N_d, v, J) = & \omega N_d + \alpha \frac{N_d(N_d - 1)}{2} \\ & + \beta(N_d - v)(N_d + v + 3) + \gamma[J(J + 1) - 6N_d], \end{aligned} \quad (19.83)$$

where three new constants are the combinations of V_L ,

$$\alpha = \frac{4}{7} V_2 + \frac{3}{7} V_4, \quad \beta = \frac{1}{10} V_0 - \frac{1}{7} V_2 + \frac{3}{70} V_4, \quad \gamma = \frac{1}{14}(V_4 - V_2), \quad (19.84)$$

or, inversely,

$$V_L = \alpha + 10\beta\delta_{L0} + \gamma[L(L + 1) - 12]. \quad (19.85)$$

To get the result (19.83), one needs to regroup in the Hamiltonian (19.82) by commutations and angular momentum recoupling, inverse to that in Eq. (19.59), the boson operators to the form $(d^\dagger d)(d^\dagger d)$ with three new independent combinations, namely, N_d^2, J^2 , and $P_5^\dagger P_5$ [Eq. (19.74)].

To predict the transition probabilities we have first to define the transition operators. In the phonon scheme introduced in Chapter 6, it is natural to assume that the quadrupole electromagnetic transitions are realized by the operator $Q_M^{(+)}$, Eq. (6.90), that changes $N_d \rightarrow N_d \pm 1$. This would correspond to the observed strongly enhanced quadrupole transitions with $|\Delta N_d| = 1$ between the states at least approximately described by the vibrational limit. Following Eq. (6.90) and similarly to Eq. (19.30), we can introduce quadrupole collective coordinates α_m and momenta π_m ,

$$\alpha_m = \frac{1}{\sqrt{2\omega}} [d_m + (-)^m d_{-m}^\dagger] \equiv \frac{1}{\sqrt{2\omega}} d_m^{(+)}, \quad (19.86)$$

$$\pi_m = i \sqrt{\frac{\omega}{2}} [d_m - (-)^m d_{-m}^\dagger] \equiv i \sqrt{\frac{\omega}{2}} d_m^{(-)}, \quad (19.87)$$

The discrimination between the coordinates and momenta, as always, is made by their behavior under time reversal. The quadrupole transition operator is taken as

$$T_m^{(E2)} = \bar{Q} d_m^{(+)}; \quad (19.88)$$

As it originates from the operator (19.40), this definition carries over the collective enhancement: the amplitude \bar{Q} is enhanced proportional to \sqrt{N} (this factor of collectivity is of the order $\sqrt{\Omega/2}$, where $\Omega \gg 1$ is the capacity of the valence nucleon shell) and, in addition, as follows from (19.86), by $1/\sqrt{\omega}$ for low-lying collective modes. These enhancement factors earmark *soft vibrational nuclei* with a large quadrupole amplitude and transition rates significantly greater than for a simple single-particle transition.

Problem 19.9 Show that, in the units of Figure 19.1, the transition probability in the yrast band (the states with maximum J for given N_d , labeled as “ground,” g -band in that figure) is given by

$$B(E2; J = 2N_d \rightarrow J = 2N_d - 2) = N_d. \quad (19.89)$$

See also Problem 6.5.

Solution

The g -band contains states with $N_d = N$, $J = 2N_d$. Since the reduced transition probability does not depend on projections of angular momentum, consider the state with the maximum projection, $M = J = 2N_d$. It can contain only the *aligned* bosons with all maximum individual projections, $m = +2$. Therefore, the state is a *condensate* of identical bosons d_2 , similar to the states of a one-dimensional oscillator,

$$|N_d, J = M = 2N_d\rangle = \frac{1}{\sqrt{N_d!}} (d_2^\dagger)^{N_d} |0\rangle. \quad (19.90)$$

Any boson pair taken from this state has the projection 4, so that only the interaction V_4 is active here. The energy (that does not depend on M) is equal to

$$E(J = 2N_d) = \omega N_d + \frac{1}{2} V_4 N_d (N_d - 1) = \frac{1}{2} \left(\omega - \frac{3}{4} V_4 \right) J + \frac{1}{8} V_4 J(J+1). \quad (19.91)$$

The formula of this type,

$$E_J = aJ + bJ^2, \quad (19.92)$$

was suggested phenomenologically long ago [11] as an interpolation between equidistant vibrational and quadratic rotational spectra. It can be approximately used for the yrast bands of spherical nuclei; in typical cases, $E_2 \approx 0.5 \text{ MeV}$, $E_4/E_2 \approx 2.2$, so that $V_4 \approx 0.1 \text{ MeV}$, and one can roughly use perturbation theory. The oscillator structure of the g -states defines the transition probability (19.86) for destruction of one quantum.

Problem 19.10 Show that for the operator (19.88) the total sum of the reduced probabilities $B(E2)$ for the transition to the next lower level satisfies the simple bosonic rule

$$\sum_{J'} B(E2; N_d + 1, J \rightarrow N_d, J') = (N_d + 1)B(E2; 2_1^+ \rightarrow 0_1^+). \quad (19.93)$$

The result (19.93) is a generalization of the rule (19.89) derived for the yrast band when the sum is reduced to a single transition. But the transition probabilities in other bands of Figure 19.1, such as the X -band or the β -band with one boson pair, $v = N_d - 2$, also grow with N_d because of the same “stimulated radiation.” However, the interband transitions into the yrast band, for example $X \rightarrow g$ or $\beta \rightarrow g$, do not grow with N_d as they require destruction of a single phonon that is different from others. The transitions between the sidebands even diminish with N_d . As a result, the bands with large seniority become more and more segregated when N_d and J increase.

Problem 19.11 Assume that the quadrupole transition operator contains, apart from the main term (19.88), also *anharmonic* corrections, such as

$$T_m'^{(E2)} = q'(d^\dagger d)_{2m} \quad (19.94)$$

and

$$T_m''^{(E2)} = q''[(dd)_{2m} + (d^\dagger d^\dagger)_{2-m}(-)^m]. \quad (19.95)$$

Calculate

- the mean quadrupole moment of the states in the yrast band;
- the relation between the values of the mean quadrupole momentum of the first and second states with $J = 2$;
- reduced probabilities of E2 transitions inside the two-phonon triplet;
- reduced probability of the E2 crossover transition from the two-phonon state $J = 2$ to the ground state;
- reduced probability of the E2 crossover transition from the three-phonon states with spin J to the first excited state.

Solution

Using the operators (19.94) and (19.95) and the Wigner–Eckart theorem, we find

a)

$$Q(J = 2N_d) = \sqrt{\frac{16\pi}{5}} \sqrt{\frac{5}{2}} \begin{pmatrix} 2 & 2 & 2 \\ -2 & 0 & 2 \end{pmatrix} q' J = \sqrt{\frac{16\pi}{70}} q' J; \quad (19.96)$$

b)

$$Q(2_2^+) = -\frac{3}{70} Q(2_1^+); \quad (19.97)$$

c)

$$B(\text{E2}; 0_2^+ \rightarrow 2_2^+) = 4q'^2, B(\text{E2}; 2_2^+ \rightarrow 4_1^+) = \frac{144}{175} q'^2; \quad (19.98)$$

d)

$$B(\text{E2}; 2_2^+ \rightarrow 0_1^+) = 2q''^2; \quad (19.99)$$

e)

$$B(\text{E2}; N_d = 3, J \rightarrow 2_1^+) = 2q''^2 \left[1 + 10 \begin{Bmatrix} 2 & 2 & J \\ 2 & 2 & 2 \end{Bmatrix} \right]. \quad (19.100)$$

In the last case, J takes values 0,2,3, and 4 (from the state $J = 6$ the quadrupole transition is not possible).

Let us assume that the deviations from the phonon scheme of Figure 19.1 are generated by anharmonic terms in the collective Hamiltonian, which are similar to the interaction (19.82), but change the boson number N_d . The eigenstates of the total Hamiltonian will acquire some mixtures of the states with various values of N_d . There exists some unitary transformation from the basis of Figure 19.1 to the eigenbasis of the full Hamiltonian, $|\psi\rangle \rightarrow U|\psi\rangle$. In principle, for calculating the matrix elements of observables, such as $\langle U\psi|Q|U\psi\rangle$, using the exact stationary wave functions, one can instead keep the wave functions unchanged but change the operators, $Q \rightarrow U^{-1}QU$. The normal quadrupole operator Q will be modified, so that it can contain now not only one-phonon terms, as in (19.92), but also high-order terms in boson operators. In particular, the additions to the Hamiltonian violating the phonon number conservation can bring in quadratic terms, such as (19.94) and (19.95) in the quadrupole operator.

Problem 19.12 Assume that the lowest correction to the harmonic Hamiltonian (19.81) comes from the *cubic anharmonicity*,

$$H^{(3)} = \text{const} \cdot (d^{(+)})_{00}^3. \quad (19.101)$$

Using perturbation theory, show that in this case the amplitudes q' and q'' in Eqs. (19.94) and (19.95) are interrelated, $q'' = q'/6$, and there is a universal relation between the mean quadrupole moment of the first excited state and reduced crossover transition probability (19.99):

$$\frac{|Q(2_1^+)|}{\sqrt{B(\text{E2}; 2_2^+ \rightarrow 0_1^+)}} = 24 \sqrt{\frac{\pi}{35}}. \quad (19.102)$$

In a broad class of spherical nuclei, this ratio of two small quantities fluctuates around this predicted value not more than by a factor of 2 [12].

Problem 19.13 Find the relation between the mean quadrupole moments of the first and second excited states 2^+ assuming that they are mixed by the weak perturbation [e.g., of the type (19.101)].

Solution

If the quadrupole operator is proportional to the phonon coordinate, then the perturbation theory predicts that these mean values are equal in magnitude and opposite in sign, which is close to what is seen in (unfortunately, poor) experimental data.

The data on matrix elements for monopole (E0) and magnetic dipole (M1) transitions in spherical nuclei are incomplete. The simplest E0 operator is a scalar proportional to N_d . Accepting this, we should expect a linearly increasing with N_d *isomeric shift* – change of the mean square charge radius $\langle r^2 \rangle$ for excited collective states (such data are practically absent). The monopole transitions in the main order are given by the boson pair operator P_5 , Eqs. (19.22) and (19.65). In the $SU(5)$ limit, such transitions proceed with conservation of seniority, $\Delta\nu = 0$, $\Delta n = \Delta N_d = \pm 2$, for example $2_3^+ \rightarrow 2_1^+$ or $0_2^+ \rightarrow 0_1^+$ (for this transition from the second $J = 0$ state to the ground state, limited experimental data do exist). However, E0 transitions $2_2^+ \rightarrow 2_1^+$ are not allowed by this mechanism.

The simplest M1 operator in this scheme is $(d^\dagger d)_{1M}$ which is nothing but the angular momentum. In this approximation, M1 transitions are forbidden, while the gyromagnetic ratios are the same for all states. Since there are several possible combinations of three- and four-boson operators with M1 quantum numbers, the phenomenological analysis here is uncertain. We can just note that appropriate boson operators should change sign under time reversal and therefore have to contain the momentum operator (19.87) in an odd power.

We add here a comment on the IBM approach where the *total* number of s - and d -bosons is conserved. Our geometrical consideration motivated by Chapter 6 involves only d -bosons and the quadrupole operator of type (19.88) is not strictly the same as the one of the IBM (19.40) where annihilation of a d -boson is accompanied with creation of an s -boson and vice versa. However, to deal with the s -boson condensate is trivial. For example, for E2 transitions, annihilation of a d -boson in the geometric model leads to an enhancement factor N_d ; in the IBM, this process is associated with an operator $\sim s^\dagger d_m$ and leads to a combined factor $(N_s + 1)N_d = [N - (N_d - 1)]N_d$. Therefore, we can relate the transition rates for a finite number of bosons N in IBM with those of the geometric model (formally corresponding to $N \rightarrow \infty$) as $B(E2)_N = (1 - N_d/N)B(E2)$, where N_d is the number of d -bosons in the final state. Thus, the finite model space of the IBM leads to suppression of bosonic collectivity, while there are data with phonon-like bands continuing up higher than the formal limit of the IBM, for example in even-even cadmium isotopes.

19.8 $\mathcal{O}(6)$ Limit

Here we consider the dynamics generated by the reduction chain II. The low-lying levels in this scheme are presented in Figure 19.2. If we still keep only pairwise boson interactions, the exact $\mathcal{O}(6)$ symmetry preserves the operators $C_{\mathcal{O}(6)}$, $C_{\mathcal{O}(5)}$, and \mathbf{J}^2 . Then, similar to the case I, we come to the simplest mass formula with three parameters,

$$E(\sigma, \nu, n', J) = \zeta \sigma(\sigma + 4) + \eta \nu(\nu + 3) + \xi J(J + 1). \quad (19.103)$$

Consider, for example, the yrast band, where $J = 2\nu$ and $\sigma = N$ (this common term for all levels of the band determines the ground-state energy). The spectrum of this band is

given by the expression analogous to (19.92),

$$E_J = 2\eta J + (4\eta + \xi)J(J+1). \quad (19.104)$$

Problem 19.14 Show that the energies of the first excited states 2_1^+ , 2_2^+ , and 4_1^+ satisfy in this limit

$$\frac{9}{5} E_4 + E_{2_2} = 7E_{2_1}. \quad (19.105)$$

This relation is roughly valid in mercury isotopes $^{190-196}\text{Hg}$.

The calculation of wave functions and matrix elements here is slightly more complicated than in case I, see, for example, Refs [13] and [14]. Without proof, we cite one important result: in the states without boson pairs, $\sigma = N$, the mean number of d -bosons depends only on v but not on J ,

$$\langle N_d \rangle = \frac{N(N-1) + v(v+3)}{2(N+1)}. \quad (19.106)$$

The fraction $\langle N_d \rangle / N$ of d -quanta changes from $(N-1)/[2(N+1)] \approx 1/2$ in the ground state to 1 at $v = N$.

The simplest candidate for the quadrupole operator is the generator (19.40) changing the number of quadrupole bosons by ± 1 (the antisymmetric operator (19.44) is dynamically equivalent as one can make a canonic transformation $s \rightarrow is$, $s^\dagger \rightarrow -is^\dagger$). For such an operator, the selection rule for E2 transitions is valid, $\Delta\sigma = 0$, as a generator of an algebra cannot have nonzero matrix elements between different irreducible representations. Owing to the $s \leftrightarrow d$ structure of this operator, we have another selection rule, $\Delta v = \pm 1$. Therefore, in this limit, the expectation values of the quadrupole moment vanish, $\langle Q \rangle = 0$. The calculated branchings of E2 transitions are shown in Figure 19.2. For

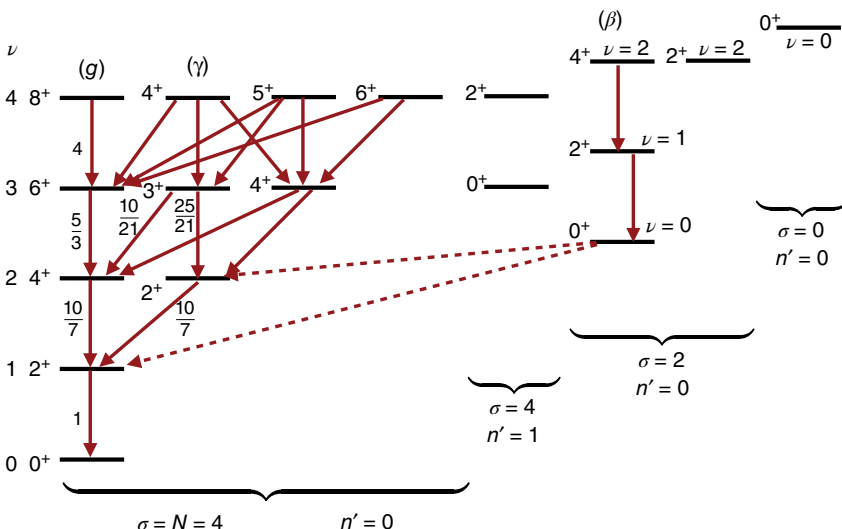


Figure 19.2 Energies of low-lying states and reduced probabilities of quadrupole transitions for the $\mathcal{O}(6)$ symmetry (case II).

low-lying states, the intensities of the transitions are close to those in case I but here they do not grow in the upward direction, being of the same order of magnitude for all $J \ll N$. The vertical transitions survive with increase of J , while the side transitions, such as $\Delta v = -1, \Delta J = 0$, die off proportionally to $1/J$. In the yrast band ($\sigma = N, v = J/2$), the transition probabilities contain a terminating factor $(1 - J/2N)$. The absolute transition probabilities are enhanced proportionally to N^2 .

The peculiarities of this case are due to the fact of the presence of two condensates, s and d_0 , of comparable power. The absence of the mean quadrupole moment is similar to the spherical phonon picture. At the same time, the pattern of quadrupole transitions is closer to that in a deformed nucleus with the intrinsic quadrupole moment $Q_0 \sim N$. Comparing the low-lying spectrum with a pure phonon case, we see that the d -boson multiplets are destroyed; for example, the former two-phonon state 0_2^+ belongs now to a different representation, $\sigma = N - 2$, and does not have an allowed transition to the single-phonon state 2_1^+ .

19.9 $SU(3)$ Limit

Here the pattern of degenerate rotational bands arises, which, at allowed values of quantum numbers λ and μ , does not depend on the statistics: for bosons it refers to the scheme with the specific quadrupole operator (19.62), while for fermions it emerges, strictly speaking, only in the model of a harmonic isotropic oscillator with specific quadrupole forces, where the operators \tilde{Q}_μ commute as in (19.63) (see Section 9.6). Such quadrupole operators can be constructed as a special mixture of coordinates and momenta that annihilates the contribution of the octupole to the result of commuting. However, this can also be derived with an approximate truncation of the exact operator equations of motion.

The simplest $SU(3)$ Hamiltonian contains two parameters,

$$H = -\kappa \sum_M (-)^M \tilde{Q}_M \tilde{Q}_{-M} - \kappa' \mathbf{J}^2. \quad (19.107)$$

According to Eqs. (19.79) and (19.80), the energy spectrum of stationary states is labeled by the quantum numbers λ, μ of the $SU(3)$ irreducible representation and rotational quantum numbers inside this representation,

$$E(N, \lambda, \mu; KJM) = -\kappa C(\lambda, \mu) + \left(\frac{3}{4} \kappa - \kappa' \right) \mathbf{J}^2. \quad (19.108)$$

The total boson number N determines the allowed representations (λ, μ) . The diagram of low-lying levels is shown in Figure 19.3.

The ground-state rotational band corresponds to $\lambda = 2N$ ($\lambda = 16$ in our graph) and $\mu = 0$. The first excited band $(\lambda, \mu) = (2N - 4, 2)$ should be juxtaposed with β - and γ -vibrations, $K = 0$ and $K = 2$, respectively. The excitation energy compared to the ground band is

$$\omega_\beta = -\kappa [C(2N - 4, 2) - C(2N, 0)] = 6\kappa(2N - 1). \quad (19.109)$$

This vibrational energy is large compared to the rotational intervals $\sim \kappa J$ if the rotational momentum is far from saturation, $J \ll 2N$, and $\kappa' \leq \kappa$. The scheme predicts the universal moment of inertia,

$$\mathcal{J} = \frac{2}{3\kappa - 4\kappa'} = \frac{3}{\omega_\gamma - \omega_\beta}. \quad (19.110)$$

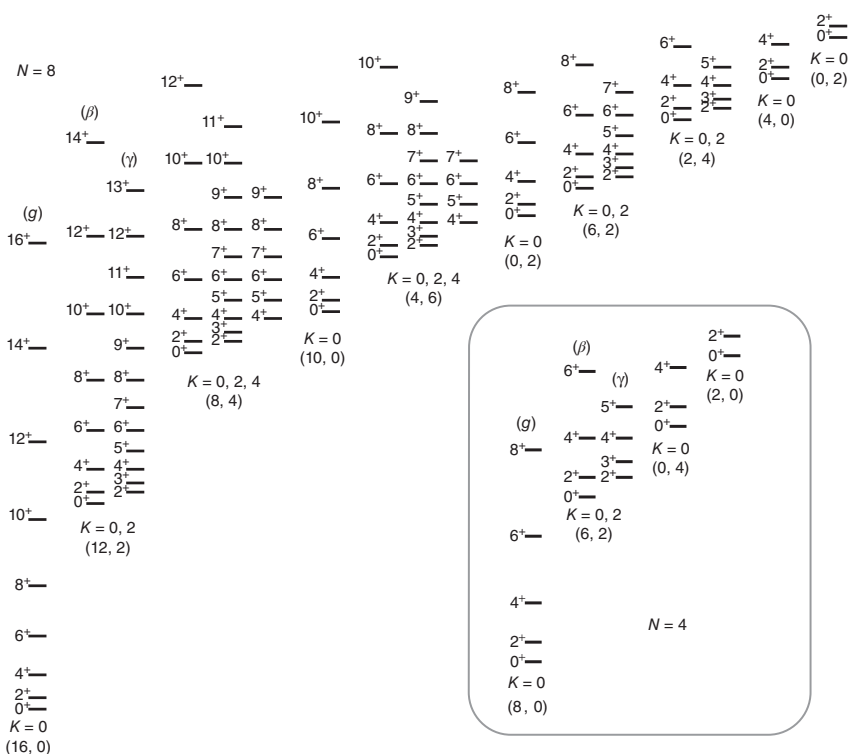


Figure 19.3 Energy spectrum for $N = 8$, $SU(3)$ symmetry (case III). The case for $N = 4$ for comparison with Figures 19.1 and 19.2 is shown in the inset.

In real nuclei with well-developed rotational spectra, one cannot see such a rigid relation between the moment of inertia and distance between β - and γ -frequencies. In fact, there is no appreciable correlation between these observables; also, the ordering of the 0^+_0 and 2^+_0 states is not defined uniquely. The many-phonon bands (at $N \gg \mu$) are predicted to be approximately equidistant with the energy step between their headbands equal to ω_β , Eq. (19.109).

The natural choice for the quadrupole operator is the generator of the group,

$$T_m^{(E2)} = \tilde{q} \tilde{Q}_m. \quad (19.111)$$

Then the E2 transitions are allowed only within the representation (λ, μ) . Therefore, the transitions between vibrational bands (β, γ) and the ground band (g) are forbidden. In reality, such transitions are well observed, and their rates, being weaker than those inside a rotational band, are still enhanced compared to single-particle estimates. We interpret such weakly collective states as shape vibrations of the deformed nucleus. Still this enhancement is noticeably smaller than between phonon states in spherical nuclei. For the rigid rotor, the E2 transition probability within a rotational band is written usually as

$$B_{\text{rot}}(\text{E2}; J+2 \rightarrow J) = \frac{5}{16\pi} Q_0^2 (2J+1) \begin{pmatrix} J+2 & 2 & J \\ 0 & 0 & 0 \end{pmatrix}^2. \quad (19.112)$$

Without going into details of calculations for the $SU(3)$ scheme, we mention that, after a natural identification of the amplitude \tilde{q} in the operator (19.111) with $\sqrt{5/16\pi} Q_0$, we would come to the similar result, however, with an additional factor that enforces saturation at the end of the rotational band,

$$B(E2; J+2 \rightarrow J) = B_{\text{rot}}(\text{E2}; J+2 \rightarrow J) \left[\left(\lambda + \frac{3}{2} \right)^2 - \left(J + \frac{3}{2} \right)^2 \right]. \quad (19.113)$$

Precisely the same relation exists between the expectation values of the quadrupole moment. In a pure rotational band,

$$Q_{\text{rot}}(J) = -Q_0 \frac{J}{2J+3}, \quad (19.114)$$

where the sign, as discussed in Chapter 12, is due to the definition of the mean quadrupole moment as the expectation value of Q_{zz} in the state of maximum projection, $J_z = M = J$, of angular momentum (then, with respect to the x -axis of rotation, the system with $Q_0 > 0$ is oblate). In the $SU(3)$ scheme, the result is

$$Q(J) = \left(\lambda + \frac{3}{2} \right) Q_{\text{rot}}(J). \quad (19.115)$$

Thus, the $SU(3)$ scheme, for not very high spin J and $N = 2\lambda \gg J$, is equivalent to the rotor with

$$Q_0 = \tilde{q} \sqrt{\frac{16\pi}{5}} \frac{N+3}{2}, \quad (19.116)$$

but for finite N , we expect the saturation effect when J approaches λ . A similar situation takes place inside the bands in other representations (λ, μ) . At large λ , the bands with different values of K decouple, so that transitions between β - and γ -bands disappear.

We can also notice that, owing to the presence of the d -boson condensate (it is possible to show that the fraction of d -bosons grows from approximately $2/3$ at small J to 1 at saturation), the monopole matrix elements between the ground and β -bands grow proportionally to those of the operator N_d ,

$$\langle N, g | N_d | N, \beta \rangle \propto \langle N, g | d^\dagger | N-1, g \rangle \langle N-1, g | d | N, \beta \rangle \propto \sqrt{N} \cdot 1 \propto \sqrt{N}. \quad (19.117)$$

At the same time, the isomeric shift is proportional to the difference of $\langle N_d \rangle$ between the ground and excited states and therefore should be small $\propto 1/N$.

We do not discuss here the possible generalizations for the odd systems [5] and for the doubling of the phonon numbers introducing “proton” and “neutron” bosons, which is tentatively justified by the observation of the so-called *scissors modes* interpreted as out-of-phase oscillations of proton and neutron liquids [15].

19.10 Shapes and Phase Transitions in the IBM

The IBM Hamiltonian along with its extensions provide a unique perspective on a general picture of collective dynamics that involves different shapes, their interplay, and phase transitions [16]. Without going into an in-depth discussion (further details can

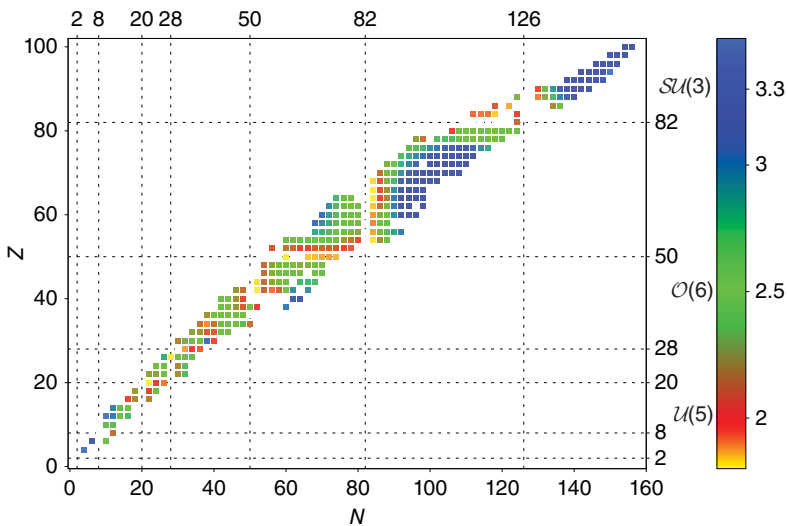


Figure 19.4 Systematics of excitation energy ratio E_4/E_2 for even–even nuclei.

be found in the literature) here, we limit our consideration to the simplest observable, the ratio of excitation energies $E(4^+_1)/E(2^+_1)$ that can be directly compared with the data.

The color map of this ratio for even–even nuclei shown in Figure 19.4 roughly distinguishes the different limits of the IBM. In the $\mathcal{U}(5)$ or $S\mathcal{U}(5)$ limit of noninteracting d -bosons, we have pure vibrational spectra slightly modified by interactions. Overall, we expect $E_4/E_2 \approx 2$. A series of cadmium isotopes in Figure 6.3 is a good example of the $\mathcal{U}(5)$ limit. The $S\mathcal{U}(3)$ leads to rotational-like spectra, see Eqs. (19.108)–(19.116), therefore $E_4/E_2 \approx 3.3$. As discussed in Chapter 11, Eqs. (11.57) and (11.58), the (λ, μ) quantum numbers can be related to quadrupole deformation parameters. There are many examples of $S\mathcal{U}(3)$ symmetry: from light nuclei, such as those in the $1s0d$ shell, to rare earth and heavier regions discussed in Chapter 16. In the third limit, a broad region of near $\mathcal{O}(6)$ nuclei is observed around $A = 130$ for xenon ($Z = 54$) and barium ($Z = 56$) isotopes. Another similar region is known near $^{196}_{78}\text{Pt}$ and in $^{194}_{80}\text{Hg}$. We identify the $\mathcal{O}(6)$ limit with $E_4/E_2 \approx 2.5$.

A limited form of the IBM Hamiltonian, the so-called *Consistent Q Formalism* provides a simplified form for exploration of different shapes and symmetries. The approach uses a generalized quadrupole operator as a linear combination of the two available quadrupole operators, one built from s - and d -bosons (19.40) and another one constructed from d -bosons only (19.41),

$$Q_M(\xi) = \left[(s^\dagger \tilde{d})_{2M} + (d^\dagger \tilde{s})_{2M} - \chi \frac{\sqrt{7}}{2} (d^\dagger \tilde{d})_{2M} \right]. \quad (19.118)$$

In the limit $\chi = 0$, we obtain a generator of $\mathcal{O}(6)$ in Eq. (19.49). At $\chi = 1$, we recover a generator of $S\mathcal{U}(3)$ group (19.50); this is a “prolate” limit. The “oblate” $\chi = -1$ limit leads to the conjugate $S\mathcal{U}(3)$ group with just the opposite sign of quadrupole moment. The use of the generalized quadrupole operator (19.118) is encouraged by numerous

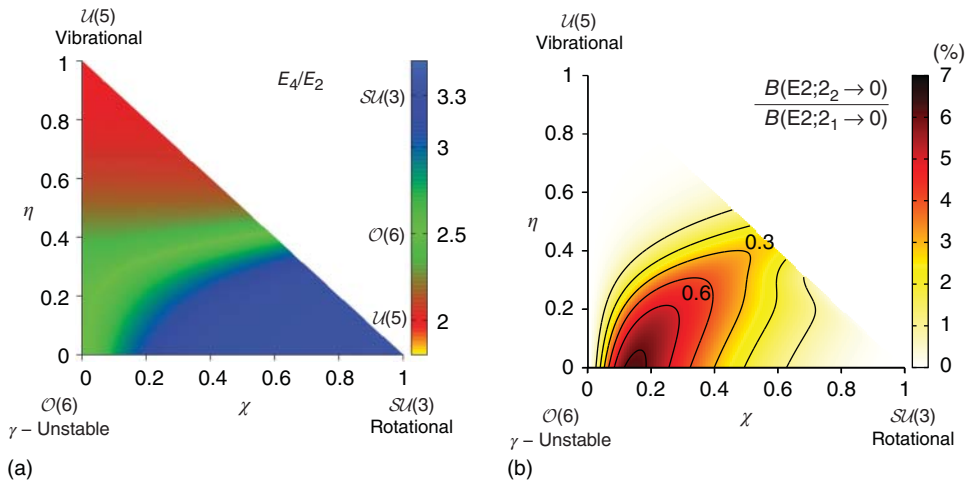


Figure 19.5 (a) Color map of excitation energy ratios E_4/E_2 . (b) Map of the quadrupole transition ratios $B(E2;2_2^- \rightarrow 0)/B(E2;2_1^- \rightarrow 0)$. Both phase diagrams correspond to the Hamiltonian (19.119) with $N = 10$.

empirical results. Thus, it makes sense to consider a quadrupole–quadrupole interaction involving the generalized operator

$$H = \varepsilon \left(\eta \sum_m d_m^\dagger d_m - \frac{1-\eta}{4N} \sum_M Q_M^\dagger(\chi) Q_M(\chi) \right). \quad (19.119)$$

This interaction Hamiltonian, apart from an overall scaling ε , is controlled by two parameters η and χ . The first parameter η determines the relative weights of the two terms; the second term of a two-body type is scaled proportional to $1/N$. At $\eta \rightarrow 0$ we have two limits $\mathcal{O}(6)$ and $SU(3)$ for $\chi = 0$ and $\chi = 1$, respectively; we do not consider a mirror domain when $\chi < 0$. With $\eta = 1$ we recover a vibrational $\mathcal{U}(5)$ limit.

In Figure 19.5a, using the ratio E_4/E_2 , we show the phase diagram for the Hamiltonian (19.119). Figure 19.5b shows the ratio of reduced E2 transition probabilities from the two lowest $J = 2$ states to the ground state. In Figure 19.5a, the different physical regions are illustrated by the color map, similar to that used in Figure 19.4. In Figure 19.5b the peak is evident. The peak is evident along the path from the $SU(3)$ rotational limit to the $\mathcal{U}(6)$ γ -soft shape. A similar behavior is seen in the rotor model, Eq. (16.120). At $\chi = 1$, the ground state associated with $\lambda = 2N$ and $\mu = 0$ has features of the axially deformed rotor, Eq. (12.58). The state 2_1^+ belongs to the ground state g -band, while 2_2^+ belongs to the β -band; transitions between these bands are forbidden. Moving away from this limit by reducing χ effectively increases the nonaxiality parameter γ , and the relative strength of the transition from the second excited 2_2^+ state grows. Toward the $\chi = 0$, $\mathcal{U}(6)$ limit, the transition ratio is decreasing again, and the situation resembles $\gamma = 30^\circ$; for the irrotational flow of inertia, $B(E2;2_2^- \rightarrow 0)/B(E2;2_1^- \rightarrow 0) = 0$ in this limit (moments of inertia along body-fixed axes 2 and 3 turn out to be equal). Finally, further decrease of χ toward $\chi = -1$, which would be a symmetric reflection of the triangle in Figure 19.5, can be seen as proceeding to the oblate limit $\gamma \rightarrow 60^\circ$, Figure 12.2.

Finally, we repeat that the direct identification of the total number N of bosons with one half of the number of valence fermions is too restrictive. In many cases, experiments

display the ground band of vibrational excitations continuing, in an almost equidistant way, up to spins higher than can be constructed under this limitation. This lays the ground for the boson Hamiltonians not conserving the total boson number. The main anharmonicity of this type is *quartic*, proportional to $(d + d^\dagger)^4$ [17]. Such terms (with a positive coefficient) restore the stability of the spherical shape when the harmonic frequency ω becomes too small. There are cases when one can set $\omega \rightarrow 0$ and consider only the combination of phonon kinetic energy and quartic anharmonicity. This is the situation close to the one experimentally observed in the region Ru–Pd–Cd. The isotope ^{100}Pd has the long vibrational band built on the ground state with energies exactly described by this simplest model of quartic anharmonicity. In neighboring nuclei of this region, one needs small corrections describing the so-called virtual rotation (at large vibrational amplitude, the nucleus spends significant time with slowly changing deformation and therefore is capable of rotational motion).

References

- 1 N. Bohr and J. Wheeler, Phys. Rev. **56**, 426 (1939).
- 2 A. Bohr, Kgl. Dan. Vid. Selsk. Mat.-fys. Medd. **26**, No. 14 (1952).
- 3 S.T. Belyaev, Kgl. Dan. Vid. Selsk. Mat.-fys. Medd. **31**, No. 11 (1959).
- 4 F. Iachello and A. Arima, *The Interacting Boson Model*, Cambridge University Press, Cambridge, 1987.
- 5 F. Iachello and P. Van Isacker, *The Interacting Boson-Fermion Model*, Cambridge University Press, Cambridge, 1991.
- 6 R. Casten (ed.) *Algebraic Approaches to Nuclear Structure, Interacting Boson and Fermion Models*, Harwood Academic Publishers, Switzerland, 1993.
- 7 A. Frank, J. Jolie, and P. Van Isacker, *Symmetries in Atomic Nuclei*, Springer-Verlag, New York, 2009.
- 8 J.P. Elliott, in *Selected Topics in Nuclear Theory*, International Atomic Energy, Vienna, 1963, p. 157.
- 9 M. Harvey, Adv. Nucl. Phys. **1**, 67 (1968).
- 10 F. Iachello and A. Arima, Phys. Lett. B **53**, 309 (1974).
- 11 H. Ejiri *et al.*, J. Phys. Soc. (Japan) **24**, 1189 (1968).
- 12 B.E. Stepanov, Yad. Fiz. **18**, 999 (1973).
- 13 A. Arima and F. Iachello, Ann. Phys. **123**, 468 (1979).
- 14 O. Castanos, E. Chancon, A. Frank, and M. Moshinsky, J. Math. Phys. **20**, 35 (1979).
- 15 E.B. Balbutsev and P. Schuck, Phys. At. Nucl. **68**, 1497 (2005).
- 16 R.F. Casten, Nat. Phys. **2**, 811 (2006).
- 17 O.K. Vorov and V.G. Zelevinsky, Nucl. Phys. **A439**, 207 (1985).

20

Statistical Properties

This is a contribution related to statistical physics; we emphasize systems with fluctuations rather than those which follow purely deterministic laws of evolution.

*R. Landauer, in Statistical Physics
(North Holland, Amsterdam, 1993)*

20.1 Introduction

As excitation energy and level density in a many-body system increase, it becomes practically impossible to describe the detailed properties of every stationary state. Moreover, the experiment, as a rule, cannot resolve individual states in regions of high level density. In nuclei, the exception is given by the *neutron resonances* seen individually in the elastic scattering of very slow neutrons (energy in the electronvolt range) off heavy nuclei. The energies of these resonances can be interpreted as corresponding to *quasistationary* states of a system “target+neutron.” Such *compound states* have very long lifetimes compared to typical nuclear processes governed by strong interactions. This occurs because of the complex many-body dynamics inside the nucleus which rapidly distribute the excitation energy (a little bigger than neutron separation energy) between various degrees of freedom. The interactions at this excitation energy (7–8 MeV) are very efficient because of the high *level density* that will be our first subject of attention. Here we deal with the *many-body* level density $\rho(E)$ of the whole system that should not be confused with the *single-particle* level density $v(\epsilon)$ discussed in Chapter 7.

For stationary quantum states, we assume a fixed value for the energy. Even for the quasistationary nuclear states mentioned above, the resonance energy is determined with high precision because of long lifetimes τ of compound states and therefore small level width $\Gamma \sim \hbar/\tau$. In contrast, in *macroscopic* systems, the energy spectrum is so dense that this assumption never can be strictly fulfilled. There are several interrelated reasons for this. To ensure that a system is in a given stationary state, the energy uncertainty ΔE has to be smaller than the distance D between the neighboring energy levels with the same values of exact constants of motion. This implies that the observation time is longer than the so-called Weisskopf *recurrence time*

$$t_r \simeq \frac{2\pi\hbar}{D}. \quad (20.1)$$

In macroscopic systems, t_r is extremely long, and, as a rule, the experimentally involved energy range ΔE covers a large number $\Delta \mathcal{N} \sim \Delta E/D$ of eigenstates. Then we have a wave packet representing an actual microstate as a very complicated superposition of stationary states which does not have certain energy although the relative uncertainty can be negligibly small, $\Delta E \ll E$.

Since the state of the system is, strictly speaking, nonstationary, the time-dependent description apparently would be more appropriate. However, it is impossible to precisely specify the *initial conditions* for such a wave function of an astronomical number of variables. Any new experiment with “the same” system would actually start with new microscopic initial conditions (the amplitudes and phases of the components of the superposition) which are absolutely irreproducible. Therefore, the exact dynamics on the microscopic level are completely different for each new copy of the same macroscopic system. As the developments over recent decades show, almost all mechanical systems, except for a small number of idealized examples, are unstable with respect to small variations in the initial conditions. In classical mechanics, the phase space trajectories, having started infinitesimally close to each other and deterministically evolving according the equations of motion, diverge exponentially in time. This *deterministic chaos* [1, 2], which can develop even in systems with two degrees of freedom, amplifies any tiny initial error, including roundoff errors in simulations, making such dynamics unpredictable. The quantum counterpart of classical chaos has its own specific features [QP, II, Ch. 24] but, at least at times shorter than the recurrence time (20.1), the dynamics of the initial wave packet are also very sensitive to the initial conditions and practically unpredictable. We shall devote Chapter 25 to this *quantum chaos* but here it is sufficient to admit that it is completely useless to look for an *exact* description of many-body systems at the microscopic level.

In addition, macroscopic systems cannot be considered as completely isolated from the outside world. Any weak external perturbation acting on the system is enhanced owing to the high level density that facilitates the perturbative mixing of adjacent microstates. For a closed system, the quantum dynamics are actually *phase dynamics* as the individual stationary components of the initial packet independently rotate their phases and the entire picture is that of a very complicated interference of many components. For a system interacting with the surroundings, the magnitudes of components are changing as well because the perturbation induces quantum transitions. This interaction certainly is of a *random* character and cannot be directly included in the dynamical equations for the system.

However, experience shows that the complexity of the system, making an exact dynamical description impossible and useless, reveals regularities of a different type, namely, *statistical* ones. In reality, we are never interested in the enormous amount of information hidden in the exact microscopic description, especially because this information is irreproducible. Important physical questions are usually connected to simple fields acting as agents for studying the system in the process of its response. Such fields probe a limited range of physical parameters. The point is that the vast majority of microscopic eigenstates, which are very different with respect to details of their structure, “look the same” as far as the simple observables are concerned [3]. This is the result of *decoherence* of the original wave packet even if it was produced initially with strict although random phase relationships. Owing to interaction with the environment or chaotic interaction within the system, the expectation values of

observables on average smoothly change along the energy spectrum. As an example, we mention the occupation numbers of single-particle orbitals. After mixing, almost all neighboring microstates manifest close values of such observables [4].

This makes a detailed knowledge of the microscopic population of individual many-body states within the uncertainty interval ΔE simply irrelevant because the results for observables are not sensitive to this ephemeral information. The only possible and reasonable description is *statistical*. We introduce an *ensemble* of systems with a different microscopic population in such a way that our observables are correctly predicted by averaging over the ensemble. Moreover, we need to predict not only the mean values of the observables but also their characteristic deviations from the mean values, that is, the *fluctuations*. The properties of the ensemble are quite simple if we describe the system at times longer than the *equilibration* scale necessary for the decoherence. Macroscopic conditions (with extremely reduced amount of information) determine a set of similar systems. On the basis of very general arguments of large numbers, such *equilibrium* ensembles assume, in fact, the uniform representation of all microstates compatible with those conditions. Enriching the available information, we are able to restrict the allowed class of systems and come to less general ensembles. In particular, if different variables have different decoherence (*relaxation*) timescales, we can consider partial equilibria with equilibrated fast variables and slow variables fixed at some nonequilibrium values.

In equilibrated macroscopic systems the *mean* observable properties do not change with time anymore. Therefore, the averaging over the statistical ensemble will give the same result as time averaging if the period of averaging exceeds the relaxation time (*ergodicity* property). Avoiding mathematical subtleties, we can simply say that a typical chaotic trajectory covers the whole available space visiting different regions with the probability determined by the equilibrium ensemble. The overwhelming accuracy of the equilibrium statistical predictions for mean values of observables in macroscopic systems shows that the fluctuations of the observables around their mean values are relatively small, except maybe for narrow regions near the phase-transition points where the structure of the system gets unstable.

The situation is different in some aspects when the statistical approach is applied to *mesoscopic* objects. They belong to the intermediate scale between macroscopic and microscopic physics. We refer to the systems with a number of degrees of freedom which is large enough to make the statistical description desirable and practically necessary. At the same time, in such systems it is still possible to study, experimentally and theoretically, the individual wave functions or classical trajectories. The unique combination of statistical and dynamical properties determines the theoretical interest and practical applications of mesoscopic physics. Typical objects which belong to this category are atomic clusters, small solid-state devices and atomic traps, metallic particles, heavy atoms, molecules, and nuclei.

The obvious new element here is a relatively low number of degrees of freedom, usually from tens to hundreds or thousands. This makes all fluctuational effects more pronounced and the predictions of standard equilibrium ensembles less accurate. For example, the number of electrons in a piece of metal is never fixed exactly, so the appropriate ensemble should allow the fluctuations of this number. In contrast, the particle number in a mesoscopic system can be strictly constant so that the use of the same ensemble would introduce unphysical fluctuations. We have already encountered

this difficulty in the BCS theory of pairing correlations, Chapter 13. Of course, the actual error introduced by such approximations is different in different cases. The regions near the phase transitions where the fluctuations are very important can be much wider in mesoscopic systems which leads to the pattern of a smooth transition between different structures (“*crossover*”) rather than that of a sharp structural transformation.

For a mesoscopic object, in some situations, the energy uncertainty can be made smaller than the level spacing. Then we deal, in a good approximation, with a single, almost stationary, wave function. This happens not only at low excitation energy but, for instance, in the above-mentioned nuclear reactions induced by slow neutrons which can be prepared within a very narrow energy spread. In such a case, we can study an individual wave function as a representative of the ensemble of chaotic states created by the interaction inside the system, with no environment involved. If the equilibrium properties are indeed determined by the most general characteristics of the system that are typical for the microstates in the given energy window, we expect the average over a generic compound wave function to coincide with the predictions of the statistical ensemble. This can be empirically checked by scanning the energy region from one resonance to another. Still we have to remember that the resonance states have a finite, even if relatively long, lifetime and after that decay; all excited states are *quasistationary*.

20.2 Level Density: General Properties

The many-body level density $\rho(E)$ increases very fast, roughly exponentially, with the number f of degrees of freedom of the system and total energy E (here we speak about *excitation energy* with respect to the ground-state energy E_0 taken as the origin of the energy scale). The fast growth of the level density is explained mainly by *combinatorial* reasons because available energy can be distributed between the degrees of freedom in many ways.

Indeed, as we saw in Section 7.2, the single-particle level density increases usually as a small power of single-particle energy, $v(\epsilon) \propto \epsilon^\eta$; the power law depends on the single-particle spectrum, see [QP, I, 3.7–3.9], but always $\eta \sim 1$. Assuming a uniform distribution of total energy over A particles (the number of degrees of freedom $f = 3A$ without spin), the energy per particle is $\epsilon \simeq E/A$. The single-particle orbitals can be occupied in different ways to form various many-particle configurations, and the number of available combinations grows, at given ϵ , approximately as the product $\prod[\epsilon v(\epsilon)]$, that is, exponentially with f . This estimate is made for noninteracting constituents but the presence of interactions does not change the total number of states, although it can significantly redistribute them. The effects of indistinguishability of particles and quantum statistics are crucial for the level density but still keep valid the general conclusion of its very fast growth.

In the following, we discuss the simplest approach to the theoretical determination of the level density in a complex quantum system. This method, strictly valid for macroscopic systems in the thermodynamic limit of a large particle number N and large volume V , at fixed density N/V , is based on the *saddle point approximation* that might not be sufficiently accurate for a finite system. Nevertheless, it gives a good qualitative description.

Let the time-independent Hamiltonian \hat{H} of the system possess exact constants of motion, namely, the energy E and some additional quantum numbers $I^{(i)}, i = 1, \dots, r$, the eigenvalues of the conserving (commuting with the Hamiltonian and among themselves) operators $\hat{I}^{(i)}$, for example, particle number \hat{N} , total angular momentum, and similar observables. Then the stationary states $|\alpha\rangle$ of \hat{H} can be characterized by E_α and $I_\alpha^{(i)}$ as well as by their specific characteristics. Suppose we are interested in the density $\rho(E, I^{(i)})$ of states with given values of energy and (some of the) quantum numbers $I^{(i)}$. As the first step, we make a *Legendre transformation* from $I^{(i)}$ to the corresponding *Lagrange multipliers* μ_i , introducing the new Hamiltonian

$$\hat{H}'(\mu_i) = \hat{H} - \sum_i \mu_i \hat{I}^{(i)}. \quad (20.2)$$

The trace over the full Hilbert space of the system of the *statistical operator* $\exp(-\beta \hat{H}')$, where β is the Lagrange multiplier corresponding to energy, is called the *partition function*, or statistical sum,

$$\Xi(\beta, \mu_i) = \text{Tr} e^{-\beta \hat{H}'(\mu_i)} = \sum_{\alpha} e^{-\beta(E_\alpha - \sum_i \mu_i I_\alpha^{(i)})}. \quad (20.3)$$

If the set of $\hat{I}^{(i)}$ includes the particle number \hat{N} , the partition function corresponds to the *grand canonical ensemble*, and the function

$$\Omega(\beta, \mu_i) = -\frac{1}{\beta} \ln \Xi \quad (20.4)$$

is the *thermodynamic potential* of this ensemble.

The *density of states* with energy E and quantum numbers $I^{(i)}$ is given by another trace,

$$\rho(E, I^{(i)}) = \text{Tr} \left\{ \delta(E - \hat{H}) \prod_i \delta(I^{(i)} - \hat{I}^{(i)}) \right\} = \sum_{\alpha} \delta(E - E_\alpha) \prod_i \delta(I^{(i)} - I_\alpha^{(i)}). \quad (20.5)$$

Then the partition function (20.3) can be formally rewritten as

$$\Xi(\beta, \mu_i) = \int dE \prod_i dI^{(i)} \rho(E, I^{(i)}) e^{-\beta(E - \sum_i \mu_i I^{(i)})}. \quad (20.6)$$

This means that the density of states (20.5) is the $(r+1)$ -dimensional *Laplace transform* of the partition function (20.3) to the quantum numbers – variables E and $I^{(i)}$. The inverse transformation determines

$$\rho(E, \{I\}) = \int_{\sigma-i\infty}^{\sigma+i\infty} \frac{d\beta \prod_i d\gamma_i}{(2\pi i)^{r+1}} \Xi(\beta, \{\gamma\}) e^{\beta E - \sum_i \gamma_i I^{(i)}}, \quad (20.7)$$

where the integration proceeds along vertical lines in the complex planes of variables β and $\gamma_i \equiv \beta \mu_i$ to the right of all singularities of the integrand [5]. Now we can apply the *Darwin–Fowler approximation* for calculating this integral. As a result, we obtain the smeared state density $\rho(E, \{I\})$ as a smooth function of energy and constants of motion, rather than the formally exact set of the δ -peaks (20.5). But this is precisely what we need for all statistical considerations. We need also to mention that we have here the density of *states* rather than of energy *levels* which are usually *degenerate* with respect to some quantum numbers, for example, the projection M of the total angular momentum of the system.

20.3 Darwin–Fowler Method

The characteristics E and $I^{(i)}$ are typically additive (*extensive*) quantities being expressed as sums of the contributions of individual particles or their small groups, for example, of interacting pairs of particles. This is clear with respect to total energy, particle number N , linear momentum \mathbf{P} , angular momentum \mathbf{J} , and so on. In contrast, the parameters β and μ_i , or γ_i , are *intensive* quantities. This distinction is obvious when applied to a macroscopic system in the thermodynamic limit of large volume and particle number, where the extensive characteristics are proportional to V and N . In a finite *mesoscopic* system, such a distinction becomes fuzzy near the ground state. For example, ground states of all even–even nuclei, regardless of the particle number, have spin $J_0 = 0$. However, near the ground state one usually has large gaps between the levels, and the smooth representation of the level density is not very useful. At higher excitation energy, the density of states grows very fast, usually exponentially with E and N , so that even in the mesoscopic systems, where it is possible in principle to resolve the individual states, the statistical approach makes sense, although the fluctuations from the average statistical predictions become more significant than for macroscopic systems.

Formally, we proceed in the following way. Let us define *nonequilibrium entropy* \tilde{S} as a function of given characteristics of the states E and $I^{(i)}$, and of the parameters β and γ_i :

$$\tilde{S}(E, \{I\}; \beta, \{\gamma\}) = \beta[E - \Omega(\beta, \{\gamma\})] - \sum_i \gamma_i I^{(i)}. \quad (20.8)$$

Then the density of states (20.7) is given by

$$\rho(E, \{I\}) = \int_{\sigma-i\infty}^{\sigma+i\infty} \frac{d\beta \prod_i d\gamma_i}{(2\pi i)^{r+1}} e^{\tilde{S}(E, \{I\}; \beta, \{\gamma\})}. \quad (20.9)$$

The main contribution to the integral (20.9) is expected to come from the point, or the points, in parameter space where the exponent \tilde{S} has a maximum. The maximum is very sharp in the case of macroscopic systems where the typical values of interest for the additive constants of motion are large (proportional to the particle number). Assuming that it is approximately valid for mesoscopic systems, we look for the vicinity of the point $(\beta = \bar{\beta}, \gamma_i = \bar{\gamma}_i)$ where

$$\frac{\partial \tilde{S}}{\partial \beta} = 0, \quad \frac{\partial \tilde{S}}{\partial \gamma_i} = 0, \quad (20.10)$$

or explicitly

$$E = \Omega(\beta, \{\gamma\}) + \beta \frac{\partial \Omega(\beta, \{\gamma\})}{\partial \beta}, \quad (20.11)$$

and

$$I^{(i)} = -\beta \frac{\partial \Omega(\beta, \{\gamma\})}{\partial \gamma_i}. \quad (20.12)$$

The solutions of these extremum equations determine the point

$$(\bar{\beta}(E, \{I\}), \{\bar{\gamma}(E, \{I\})\})$$

which can be identified with that of *thermal equilibrium* for given values of additive constants E and $\{I\}$. Selecting this set of equilibrium points in the parameter space we,

define the *equilibrium* entropy

$$S(E, \{I\}) = \tilde{S}(E, \{I\}; \bar{\beta}(E, \{I\}), \{\bar{\gamma}(E, \{I\})\}). \quad (20.13)$$

Since the derivatives of entropy \tilde{S} with respect to the parameters β and γ vanish at equilibrium,

$$\frac{\partial S}{\partial E} = \frac{\partial \tilde{S}}{\partial E} + \left(\frac{\partial \tilde{S}}{\partial \beta} \right)_{\beta=\bar{\beta}} \frac{\partial \bar{\beta}}{\partial E} + \sum_i \left(\frac{\partial \tilde{S}}{\partial \gamma_i} \right)_{\{\gamma\}=\{\bar{\gamma}\}} \frac{\partial \bar{\gamma}_i}{\partial E} = \left(\frac{\partial \tilde{S}}{\partial E} \right)_{\bar{\beta}, \{\bar{\gamma}\}}. \quad (20.14)$$

Consequently, we obtain from (20.8):

$$\frac{\partial S}{\partial E} = \bar{\beta}, \quad (20.15)$$

and, analogously,

$$\frac{\partial S}{\partial I^{(i)}} = -\bar{\gamma}_i. \quad (20.16)$$

Assuming that the extremum point (20.10) corresponds to the sharp maximum of entropy (positively defined matrix \mathcal{B} with the elements

$$b_{ij} = -\left(\frac{\partial^2 \tilde{S}}{\partial \gamma_i \partial \gamma_j} \right)_{\{\gamma\}=\{\bar{\gamma}\}}, \quad i, j = 0, \dots, r, \quad (20.17)$$

of the second derivatives, where we denote for uniformity $\beta = \gamma_0$), we can write the entropy in the vicinity of the extremum point as

$$\tilde{S}(E, \{I\}; \{\gamma\}) \approx S(E, \{I\}) - \frac{1}{2} \sum_{i,j=0}^r b_{ij} \eta_i \eta_j, \quad \eta_i = \gamma_i - \bar{\gamma}_i. \quad (20.18)$$

Going back to the density of states (20.9), we come to the Gaussian $(r+1)$ -dimensional integral

$$\rho(E, \{I\}) = e^S \int \frac{\prod_i d\eta_i}{(2\pi)^{r+1}} e^{-(1/2)\eta \cdot \mathcal{B} \cdot \eta}, \quad (20.19)$$

where the presumed sharpness of the maximum in the integrand allows one to extend the limits of integration up to $\pm\infty$, and the quadratic form in the exponent is written with the use of the matrix \mathcal{B} ,

$$\eta \cdot \mathcal{B} \cdot \eta \equiv \sum_{i,j=0}^r \eta_i \eta_j b_{ij}. \quad (20.20)$$

The integral in (20.19) can be easily calculated in general form. Indeed, the symmetric matrix \mathcal{B} can be diagonalized by the orthogonal linear transformation of variables $\{\eta_i\} \rightarrow \{\xi_i\}$. Then, instead of (20.20), we obtain $\sum_i \lambda_i \xi_i^2$ where λ_i are the eigenvalues of the matrix \mathcal{B} . If we work in the vicinity of the maximum of entropy, all λ_i are positive, and the integral converges. The Jacobian of the orthogonal transformation is equal to 1 (rotation of the basis), so that

$$\int \prod_i d\eta_i e^{-(1/2)\eta \cdot \mathcal{B} \cdot \eta} = \prod_i \int d\xi_i e^{-(1/2)\lambda_i \xi_i^2} = \prod_i \sqrt{\frac{2\pi}{\lambda_i}} = \frac{(2\pi)^{(r+1)/2}}{(\det \mathcal{B})^{1/2}}. \quad (20.21)$$

The result is expressed in the invariant form in terms of the determinant of the matrix \mathcal{B} . Thus, the level density (20.19) is found to be

$$\rho(E, \{I\}) = \frac{\exp(S)}{[(2\pi)^{r+1} \det \mathcal{B}]^{1/2}}, \quad (20.22)$$

where equilibrium entropy $S(E, \{I\})$ is given by Eq. (20.13), and the required values of the Lagrange multipliers are determined by the derivatives (20.15) and (20.16) of this entropy. Let us stress that the equilibrium entropy is determined by the maximum of the integrand, while the determinant of \mathcal{B} in the denominator of (20.22) reflects the contributions of the Gaussian fluctuations around this maximum.

20.4 Relation to Statistical Thermodynamics

The Darwin–Fowler method formally developed in the previous section can be put in the foundation of statistical thermodynamics (statistical mechanics of thermal equilibrium). According to the *second law of thermodynamics*, the equilibrium state is determined by the maximum entropy found under actual constraints for the system under study. We have fixed the constraints by the values of the constants of motion.

For a macroscopic particle number N , the maximum of entropy that gives the main contribution in the Darwin–Fowler method is so sharp that, among many microstates which would be in principle compatible with given constraints, only those in the vicinity of the maximum can be relatively important. This is the intrinsic meaning of the phenomenological second law (equilibrium corresponds to the maximum of entropy under given macroscopic conditions).

If we identify the maximum point with actual thermodynamic equilibrium, it is quite natural to establish a correspondence between the formal development above and thermodynamic observables. For this purpose, we can use the definitions (20.11) and (20.12) of the parameters $\bar{\beta}$ and $\bar{\gamma}_i$, corresponding at equilibrium to the given values of energy and other constraints, along with the derivatives of physical equilibrium entropy at this point, Eqs. (20.15) and (20.16). The latter equations coincide with those in phenomenological thermodynamics that define temperature, chemical potential, and other similar *intensive* quantities. The value of absolute *temperature* T corresponding to average energy E is therefore

$$T = \frac{1}{\bar{\beta}} \quad (20.23)$$

so that

$$\frac{\partial S}{\partial E} = \frac{1}{T}. \quad (20.24)$$

Taking $I^{(i)}$ equal to the particle number A_i of sort i , we introduce the corresponding *chemical potential* μ_i according to

$$\bar{\gamma}_i = \bar{\beta} \mu_i = \frac{\mu_i}{T}; \quad (20.25)$$

then

$$\frac{\partial S}{\partial A_i} = - \frac{\mu_i}{T}. \quad (20.26)$$

Analogously, the Lagrange multiplier $\bar{\gamma}_V$, being constrained by a fixed externally volume V of the system, has to be associated with *pressure* P ,

$$\bar{\gamma}_V = \frac{P}{T}, \quad (20.27)$$

and

$$\frac{\partial S}{\partial V} = P. \quad (20.28)$$

Here, as in thermodynamics, equilibrium entropy has to be considered as a function of extensive constraints, $S = S(E, V, A_i)$.

According to the results above, a small change of extensive variables leads to a corresponding variation of equilibrium entropy,

$$dS = \frac{1}{T} dE + \frac{P}{T} dV - \sum_i \frac{\mu_i}{T} dA_i. \quad (20.29)$$

This differential relation allows one to consider equilibrium thermal energy $E(S, V, A_i)$ as a function of entropy, volume, and particle numbers:

$$dE = TdS - PdV + \sum_i \mu_i dA_i. \quad (20.30)$$

This is the usual form of the second law of thermodynamics when TdS is interpreted as heat supplied to the system and PdV as work changing the volume.

20.5 Thermodynamics of a Nuclear Fermi Gas

The effective nuclear temperature is much lower than the Fermi energy of the nucleons $\sim \hbar^2 n^{2/3}/m$ at the normal nuclear density n , Eq. (7.19). Therefore, it is natural to consider the nucleons as particles of the *degenerate* Fermi system. Of course, this is not a perfect gas but rather a *Fermi liquid*, where the interaction between the nucleons is extremely important. However, at least above excitation energy of several megaelectronvolts, where the pairing is already not effective, the spectrum of a Fermi liquid is qualitatively similar to that of a gas of *quasiparticles*, fermions dressed by the average interactions. Such ideas lead to the simplest approach to the problem of level density [6, 7].

At zero temperature, entropy and heat capacity approach zero. The exception is an odd- A nucleus where the ground state is degenerate by spin $J \neq 0$ and the entropy at $T = 0$ equals $\ln(2J+1)$. In a Fermi gas, with the single-particle level density v_F at the Fermi surface, only the levels in the interval of excitation energy $\Delta\epsilon \sim T$ are unfrozen at temperature $T \ll \epsilon_F$. The number of these levels is $\sim v_F T$, so that the corresponding excitation energy of the nucleus grows as $v_F T^2$, a quadratic function of temperature. This determines a *linear* growth of heat capacity that is usually written as (we always set the Boltzmann constant $k = 1$ measuring temperature in energy units)

$$C = 2\alpha T, \quad (20.31)$$

where the constant α is proportional to v_F .

Problem 20.1 Find the constant α in the Fermi-gas model.

Solution.

$$\alpha = \frac{\pi^2}{6} v_F, \quad (20.32)$$

In this way, we come to excitation energy E and entropy S of the system, Eqs. (20.23) and (20.24), and to the corresponding estimate of the exponentially growing many-body level density (20.22) as a function of energy,

$$E = \alpha T^2, \quad S = 2\alpha T = 2\sqrt{\alpha E}, \quad \rho(E) \propto e^{2\sqrt{\alpha E}}, \quad (20.33)$$

where we omitted the preexponential factor that requires more detailed calculations.

Problem 20.2 Using Eq. (20.22) calculate the level density in the Fermi-gas model.

Solution.

$$\rho(E) = \frac{1}{\sqrt{48}} \frac{e^{2\sqrt{\alpha E}}}{E}. \quad (20.34)$$

There have been many semiphenomenological attempts to improve the oversimplified Fermi-gas model in order to apply it to real nuclei. The easiest thing is to take into account two kinds of nucleons which can have different single-particle level densities at the Fermi surface, $v_F(n)$ and $v_F(p)$. Correspondingly, the parameter α becomes $(\pi^2/6)(v_F(n) + v_F(p))$. This simply increases the dimension of the determinant in Eq. (20.22). The result (20.34) is then modified to (see Ref. [8])

$$\rho(E) = \frac{6^{1/4}}{12} \frac{v_F^2}{2\sqrt{v_F(n)v_F(p)}} \frac{e^{2\sqrt{\alpha E}}}{(v_F E)^{5/4}}, \quad v_F = v_F(n) + v_F(p). \quad (20.35)$$

Another improvement comes from substituting the excitation energy E by introducing the *backshift*, $E \rightarrow U = E - \Delta$, where Δ mimics the pairing energy that is either taken from the liquid drop model or fitted empirically. This takes into account that there are very few levels within the superconducting energy gap. At low energy, the Darwin–Fowler method formally breaks down because of the singular denominator. Therefore practitioners frequently use the so-called *constant temperature model* at low excitation energy, where the level density grows simply as $\exp(U/T)$ with an empirical temperature parameter T . At some excitation energy, this expression is continuously matched to the Fermi-gas formula. In some sense, this approach tries to account for the melting of pairing [9], while the temperature parameter is close to the value $\Delta/1.78$ corresponding to the critical temperature in the BCS theory.

The level density parameter α should grow with the mass number A . However, the nuclear shell model that determines nuclear spectroscopy immediately tells us that this growth cannot be monotonic. We expect that magic nuclei (and those close to them)

would have lower level density at similar excitation energy. It seems natural to expect also that the level density at low energies away from magic nuclei can be enhanced compared to those simple estimates due to collective degrees of freedom, rotation, and vibrations, which have low-lying bands of states. This *collective enhancement* effect is not accounted for in a simple Fermi-gas estimate. On the other hand, the excess of collective levels at low energies should be compensated by the corresponding depletion at higher energies and by mixing with noncollective excitations at growing general level density.

The above estimate counts all excited states independently of their quantum numbers. In practice, specific reactions can excite only subsets of states corresponding to certain quantum numbers of angular momentum (nuclear spin), its projection, isospin, and parity. The aforementioned reaction induced by slow neutrons can bring in only very low spin (the neutron orbital momentum is 0 or 1) and correspondingly change (*p*-wave) or not change (*s*-wave) nuclear parity. Therefore, it is important to know the *partial* level density corresponding to a given set of quantum numbers.

Selected examples of nuclear level densities are shown in Figure 20.1. These level densities are obtained indirectly [10] from the data using Fermi's golden rule, which states that the reaction rate is proportional to the density of final states (see Section 14.5). Figure 20.1 shows that the nuclear level densities, especially at high excitation energy, generally follow the exponential trend described by Eq. (20.33). The coefficient a slowly increases with mass number A . From ^{148}Sm and ^{149}Sm , we infer that the extra unpaired particle increases the level density by nearly a constant factor. At lower energies, structural effects are important; for example, peaks in the level density of ^{122}Sn are believed to be associated with pair breaking that occur with increasing temperature similar to pair breaking in rotating systems discussed in Chapter 16. We will return to theoretical predictions of level densities in the last chapter, where the statistical approach will be discussed on the basis of ideas of quantum chaos [QP, II, Ch. 24].

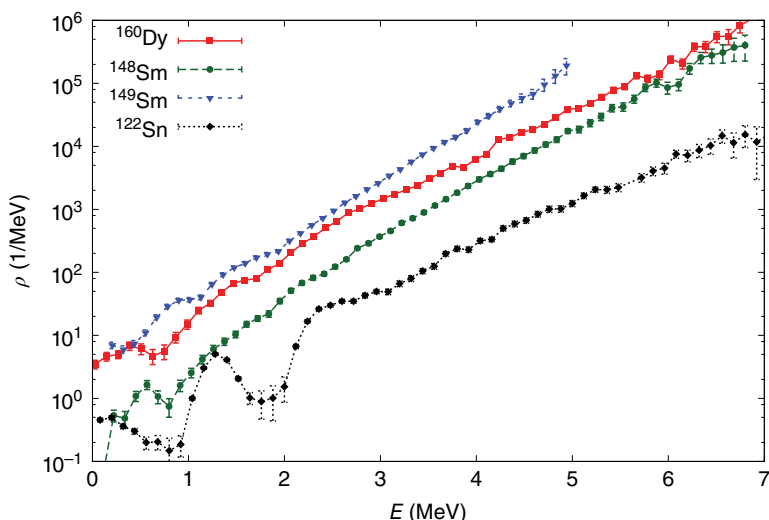


Figure 20.1 Density of states as a function of excitation energy for selected nuclei. The data are from compilation [10].

20.6 Statistics of Angular Momentum

As discussed in Section 20.2, the energy levels are labeled by quantum numbers $I^{(i)}$ that include angular momentum J (nuclear spin) and its projection M on an arbitrary quantization axis. The total spin \mathbf{J} is a result of the vector coupling of angular momenta \mathbf{j}_a of individual nucleons. The total projection is also the sum, but a simpler one, as the projections are added algebraically,

$$M = \sum_a m_a. \quad (20.36)$$

The simplest prediction concerning the distribution function of quantum numbers J and M can be made using the idea of *random coupling* of individual spins [11]. This idea is expected to work in the Fermi gas of independent quasiparticles and, in average, survive even in the presence of their interactions. If for n valence particles the probability of having the total projection M is $w_n(M)$, then the logical identity expressing the independent addition of individual projections should have a form

$$w_N(M) = \sum_{M'} w_n(M') w_{N-n}(M - M'). \quad (20.37)$$

This identity contains the sum over possible intermediate values of M' but should be valid for any decomposition of N particles into two groups of n and $N - n$. In fact, from the mathematical viewpoint, we assume here a *discrete Markovian process*. The crucial assumption is that the process of angular momentum coupling is random and it can proceed through many competing paths. Therefore, we add here incoherently the probabilities of individual steps but not their quantum amplitudes.

For a noticeable number of particles (and of possible M -values), one can, following Bethe [11], substitute the sum in Eq. (20.37) by an integral and, assuming a rather sharp maximum of the distribution we are looking for around some average value M^2 (obviously, the distribution function should be an even function of M), extend the integration to infinity:

$$w_N(M) = \int_{-\infty}^{\infty} dM' w_n(M') w_{N-n}(M - M'). \quad (20.38)$$

The solution of Eq. (20.38) is given by the Gaussian distribution which is essentially a particular case of the standard *central limit theorem* [12].

Problem 20.3 Prove that the distribution function satisfying Eq. (20.38) is

$$w_N(M) = c_N e^{-\alpha_N M^2}, \quad (20.39)$$

where the normalization is given by

$$\int_{-\infty}^{\infty} dM w_N(M) = 1 \quad \Rightarrow \quad c_N = \sqrt{\frac{\alpha_N}{\pi}}, \quad (20.40)$$

whereas

$$\alpha_N = \frac{\alpha}{N}, \quad (20.41)$$

and α is a constant characteristic for the system.

According to the randomness of the process, the average value of M^2 is proportional to the effective number of contributing particles,

$$\overline{M^2} = \frac{1}{2\alpha_N} = \frac{N}{2\alpha}, \quad (20.42)$$

which determines the physical meaning of the constant α . At not very high temperature T , the number N can be estimated as $N \Rightarrow v_F T$ through the mean single-particle level density v_F at the Fermi surface. This result is typical for consideration of statistical fluctuations of additive random variables. Indeed, if the angular momentum projections m_a of particles are *statistically independent* and their average value is $\overline{m_a} = 0$, while the mean square is $\overline{m^2}$ defined by the available single-particle levels, for the total projection $M = \sum_a m_a$, we find

$$\overline{M^2} = \overline{\sum_a m_a \sum_b m_b} = \overline{\sum_a m_a^2} + \overline{\sum_{a,b(a \neq b)} m_a m_b} = \overline{\sum_a m_a^2} = N \overline{m^2}. \quad (20.43)$$

This defines the width parameter $\alpha = 1/2\sigma^2$ in the distribution (20.41),

$$\alpha = \frac{1}{2\overline{m^2}}. \quad (20.44)$$

For example, in the simplest case of a single j -level available for the particles (of course it should be $j \gg 1$ in order for the statistical consideration to be meaningful),

$$\overline{m^2} = \frac{1}{2j+1} \sum_{m=-j}^j m^2 = \frac{j(j+1)}{3}. \quad (20.45)$$

This expression can be used for estimates in the cases of a realistic set of j -levels, substituting for j some average value and having in mind that each j -level has its single-particle energy and the statistical weight $(2j+1)$.

The distribution we just derived neglects all correlations between angular momenta of individual particles and therefore has a limited applicability. Nevertheless, it could be reasonable at sufficiently high excitation energy when the level density is high including the levels of different origins with practically all possible values of the total spin J .

If we would know the density of states ρ_M for various values of the total projection M , we can immediately find the level density $\rho(J)$ for a fixed value of total spin J . It is easy to understand that the projection M is present in all angular momentum multiplets with $J \geq M$. In the multiplets with $J = M$ it is the highest possible projection. But among states with projection M , there are states which belong to bigger values of J , starting with $(J+1)$, where M is not the highest projection. The number of levels with spin J is given by the corresponding difference, Eq. (9.43),

$$\rho(J) = \rho_{M=J} - \rho_{M=J+1}. \quad (20.46)$$

Since the distribution $w(M)$ is normalized, the level density as a function of energy and projection M can be written as

$$\rho(E; M) = \rho(E)w(M) = \rho(E)\sqrt{\frac{\alpha}{\pi}} e^{-\alpha M^2}, \quad (20.47)$$

where $w(M)$ can also depend on energy through its parameter α that can change because new single-particle levels become populated at higher energy. Equation (20.16) can now be written approximately [8] as

$$\rho(J) \approx \rho(E) \frac{2J+1}{\sqrt{\pi}} \alpha^{3/2} e^{-\alpha J(J+1)}. \quad (20.48)$$

The density of *states* rather than levels would include an additional factor $(2J+1)$ (the factor $(2J+1)$ in Eq. (20.48) comes, as argued in Ref. [8], from semiclassical integration over the volume of the sphere, $4\pi J^2 dJ$, in the space of the angular momentum J). The characteristic width σ is sometimes called the *spin cut-off factor*.

Problem 20.4 The result (20.48) can be interpreted as the correction to the excitation energy E where the genuine thermal part E^* results from subtraction of collective rotational energy $\hbar^2 J^2 / 2J$ from E . Derive the effective value of the moment of inertia J assuming that the rotational energy is small compared to total energy at nuclear temperature T [8].

Solution.

Under the assumption formulated in the problem, the level density can be written as

$$\rho(E, J) = \rho_0(E^*), \quad E^* = E - \frac{\hbar^2 J^2}{2J}. \quad (20.49)$$

With exponential (thermodynamic) dependence of the level density on temperature,

$$\rho(E, J) \approx \rho_0(E) e^{-(\hbar^2 J^2 / 2J T)}. \quad (20.50)$$

Comparing the exponential parts in Eqs. (20.50), (20.43), and (20.48) we identify

$$J = \frac{\hbar^2 \sigma^2}{T}. \quad (20.51)$$

With the previous estimate, $N \approx v_F T$, $\sigma^2 \approx v_F T \overline{m^2}$, we obtain

$$J = \hbar^2 v_F \overline{m^2}. \quad (20.52)$$

As an additional exercise, it is easy to show that the result (20.52) coincides with the rigid body moment of inertia found in Section 16.20.

The moment of inertia found above should be understood as some mean value. In an axially deformed nucleus, one has to introduce two effective moments of inertia whose contributions will be determined by the nuclear spin J and by the K -quantum number that gives (Chapter 16) the angular momentum projection onto the symmetry axis. The direct generalization of Eq. (20.50) gives

$$\rho(E, J, K) = \rho_0(E) e^{-(\hbar^2 / 2T) [J(J+1)/J_{\perp} - K^2(1/J_{\parallel} - 1/J_{\perp})]}. \quad (20.53)$$

20.7 Shell Model Monte Carlo Approach

As already mentioned, the direct large-scale diagonalization of the shell-model Hamiltonian is practically impossible for very large Hilbert spaces – the dimensions become

enormous. One of the possible ways to overcome this problem is given by the *Shell Model Monte Carlo* method [13].

The method is essentially a version of the path integral representation of quantum mechanics [QP, I, 7.11]. Here one cannot study the detailed spectroscopy but the method can be convenient for finding the ground state of the system and its statistical properties. The starting point of the approach is the evolution operator of the system $U(t)$ taken at *imaginary time*, $t \rightarrow -i\beta/\hbar$,

$$U(t) = e^{-(i/\hbar)Ht} \Rightarrow e^{-\beta H}, \quad \beta \geq 0. \quad (20.54)$$

The trace of this operator gives the partition function $Z(T) = \text{Tr}(e^{-H/T})$ for temperature $T = 1/\beta$. The idea of application to finding the ground state for a given Hamiltonian H can be stated quite simply. Take an arbitrary function of your system Ψ_0 (a trial state) and evolve in imaginary time with the evolution operator (20.54). The starting function is a superposition of stationary eigenstates Ψ_k of H , where Ψ_k with energies E_k form a complete basis,

$$\Psi_0 = \sum_k C_k \Psi_k \Rightarrow e^{-\beta H} \Psi_0 = \sum_k C_k e^{-\beta E_k} \Psi_k. \quad (20.55)$$

At the end of this evolution, $\beta \rightarrow \infty$, the main surviving contribution to the sum (20.55) will be that with the smallest energy – the ground state. We just need that the ground state be present in the initial superposition, $C_0 \neq 0$; we also assume that it is not degenerate. Of course, it would be better if the starting function could already remind the genuine ground state. In the statistical analogy, the process means that we steadily lower temperature and in the absolute zero limit the system turns out to become frozen in its ground state.

In practice, one splits the evolution of the parameter β into small steps $\Delta\beta$ as in the path integrals. For example, the Hamiltonian, taken in the second quantization (Chapter 11), contains operators of the type $a^\dagger a$ and at least their pairwise combinations. These operators in general do not commute. The way to handle this situation is through introduction of *auxiliary fields* which reduce the dynamics to the propagation of only elementary operators $\sim a^\dagger a$ in imaginary time and in the presence of external fields; then one has to integrate over this fields. For example, a typical two-body interaction term is first presented as a sum of linear and quadratic (with respect to the pairs of Fermi operators) expressions:

$$a_1^\dagger a_2^\dagger a_3 a_4 \equiv -\delta_{24} M_{13} + \frac{1}{4} (M_{14} + M_{23})^2 - \frac{1}{4} (M_{14} - M_{23})^2 + \frac{1}{2} [M_{14}, M_{23}], \quad (20.56)$$

where $M_{12} = a_1^\dagger a_2$ and the last term in (20.56) is a commutator which is again an M -operator. Along with the one-body part of the Hamiltonian, we come to the structure

$$H = \sum_\alpha \left[h_\alpha M_\alpha + \frac{1}{2} V_\alpha M_\alpha^2 \right]. \quad (20.57)$$

Each quadratic term in the evolution operator (20.54) can be presented as an integral of linear terms over an auxiliary field ξ with the help of the Gaussian identity (the Hubbard–Stratonovich transformation)

$$e^{(1/2)VM^2} = \sqrt{\frac{|V|}{\pi}} \int d\xi e^{-(1/2)|V|\xi^2 + sVM\xi}, \quad (20.58)$$

where $s = \pm 1$ for $V \geq 0$ and $s = \pm i$ for $V < 0$. As operators M do not commute among themselves, one has to subdivide the whole evolution into many (in principle, infinitely many) small pieces $\Delta\beta$, while the contributions of the commutators will be of a higher order. Then we come to the path integral in imaginary time. Finally, the result has to be integrated over time-dependent auxiliary fields ξ . This multidimensional integral is calculated using Monte Carlo techniques [14]. In this way, it turns out to be possible to handle much larger model spaces than in the shell model but for a limited set of problems including the level density. For the technical problems along this road and the current state of the work in this direction, we refer to the article [15] and references therein.

20.8 Thermodynamics of Compound Reactions

Using statistical ideas, Landau and Smorodinsky [16] gave simple estimates for the energy spectrum of neutrons evaporated from the compound nucleus. We can imagine the heated nucleus in thermodynamic equilibrium with the vapor of low-energy neutrons. This vapor is similar to the Maxwellian gas with energy distribution

$$f(\epsilon)d\epsilon \propto e^{-\epsilon/T} p^2 dp \propto e^{-\epsilon/T} \sqrt{\epsilon} d\epsilon. \quad (20.59)$$

The flux of neutrons attacking the nucleus from outside is then proportional to this distribution and neutron velocity,

$$j(\epsilon)d\epsilon \propto v f(\epsilon)d\epsilon \propto e^{-\epsilon/T} \epsilon d\epsilon. \quad (20.60)$$

The thermodynamic equilibrium requires that evaporating neutrons create the same flux from inside. Of course, the whole discussion here is based on the picture *averaged over resonances*.

Problem 20.5

- Assuming the equilibrium, find the average energy of evaporating neutrons.
- Such a consideration assumes essentially that the nucleus is *black* absorbing all neutron flux. In reality, there is an energy-dependent probability of capture given by the nuclear optical potential; at low energy, we expect [QP, II, Ch. 10] this probability to be inversely proportional to the neutron velocity. Determine, in this case, the average evaporation energy.

Solution.

$$(a) \bar{\epsilon} = 2T, \quad (b) \bar{\epsilon} = \frac{5}{2} T. \quad (20.61)$$

As stressed by Landau, the temperature parameter entering such estimates should be identified with the state of the *final* nucleus after evaporation – in such mesoscopic systems, the evaporation of a single particle can noticeably change the temperature of the system.

The basic relations between processes of decay of a compound nucleus and its level density were established by Weisskopf [17] and Bethe [18]. The energy conservation

in the process of the decay of a compound nucleus A into a daughter nucleus B and a particle x (e.g., a nucleon) is simply

$$E_A = E_B + Q + \epsilon, \quad (20.62)$$

where Q is the separation energy of a particle from the nucleus A , and ϵ is energy of relative motion of the particle in the continuum and residual nucleus B . Probabilities P_{\rightarrow} of the decay $A \rightarrow B + x$ and P_{\leftarrow} of recombination $B + x \rightarrow A$ are interrelated in the equilibrium:

$$P_{\rightarrow} g_A = P_{\leftarrow} g_B g_x, \quad (20.63)$$

where the quantities g are the statistical weights of the states of corresponding nuclei. For example, if the nucleus B is in the continuum with internal energy between E_B and $E_B + dE_B$ and has a momentum \mathbf{p}_B as a whole,

$$g_B = \frac{V}{(2\pi\hbar)^3} \rho(E_B) dE_B d^3 p_B, \quad (20.64)$$

where $\rho(E_B)$ is the state density of the nucleus B , and V is a normalization volume that has to be canceled in the final expression through observable quantities; the state density and level density differ by the degree of degeneracy of each level, for example, by the factor $(2J + 1)$ for a level with nuclear spin J .

If we are interested in energy distribution $w(\epsilon)$ of evaporated particles x , we write the condition of equilibrium (20.63) as

$$w(\epsilon) d\epsilon \rho_A(E_A) V \frac{d^3 p_A}{(2\pi\hbar)^3} = P_{\leftarrow} \rho_B dE_B V^2 (2J_x + 1) \frac{d^3 p_B d^3 p_x}{(2\pi\hbar)^6}. \quad (20.65)$$

Here, J_x is spin of the particle (or nucleus) x . The transformation from momenta $\mathbf{p}_B, \mathbf{p}_x$ to \mathbf{p}_A and relative momentum in the final state of B and x has a Jacobian equal to 1, then it is easy to derive

$$w(\epsilon) d\epsilon = (2J_x + 1) \frac{M_{Bx}\epsilon}{\pi^2\hbar^3} \frac{\rho_B(E_B)}{\rho_A(E_A)} \sigma_{\leftarrow} d\epsilon. \quad (20.66)$$

Here, M_{Bx} is the reduced mass. The cross section of formation of the compound nucleus is determined by the corresponding probability P_{\leftarrow} and the flux of relative motion in this channel,

$$\sigma_{\leftarrow} = \frac{P_{\leftarrow}}{v_{\text{rel}}/V}. \quad (20.67)$$

If we now return to thermodynamical description, the ratio of the level densities ρ_B/ρ_A in Eq. (20.41) can be substituted by $\exp[S_B(E_B) - S_A(E_A)]$. If the kinetic energy of a particle x is low, then

$$\begin{aligned} S_B(E_B) &= S_B(E_A - Q - \epsilon) \approx S_B(E_A - Q) - \epsilon \left(\frac{dS}{dE} \right)_{E=E_A-Q} \\ &= S_B(E_A - Q) \frac{1}{T_B(E_A - Q)}. \end{aligned} \quad (20.68)$$

In this way, we come to the Maxwellian distribution as in (20.59),

$$w(\epsilon) d\epsilon = \text{const } \sigma_{\leftarrow} e^{-\epsilon/T_B(E_A - Q)} \epsilon d\epsilon. \quad (20.69)$$

Here,

$$\text{const} = \frac{(2J_x + 1)M_{Bx}}{\pi^2 \hbar^3} e^{S_B(E_A - Q) - S_A(E_A)}. \quad (20.70)$$

As mentioned earlier, here we have the temperature of the *daughter* nucleus after emission of the particle x . In reactions with several megaelectronvolt neutrons, the cross section of formation of the compound nucleus weakly depends on energy and the evaporating neutrons have a distribution close to Maxwellian with average energy $\approx 2T_B$, considerably lower than their energy in the formation channel.

20.9 Statistical Description of Resonances

The presence of many sharp resonances in slow neutron scattering excludes a simple description of this process as the interaction of a neutron with a potential well of nuclear size: in this case, the resonance density would be much smaller corresponding to the single-particle motion in the well. We interpret these resonances, Figure 20.2, as *quasistationary many-body* states; the distance of the order of electronvolts between them corresponds to the level density of the nucleus as a whole that emerges, as we discussed above, from the nucleon–nucleon interactions. The typical small widths Γ of resonances indicate the lifetime $\tau \sim \hbar/\Gamma$ of the compound system that is much longer than the motion time of a neutron through the nuclear well.

The condition $\Gamma \ll D$, where D is a typical spacing between the resonances allows us to speak of the quasidiscrete levels of the intermediate system formed after the capture of the neutron. If the Weisskopf time $\sim \hbar/D$ characterizes the typical period of motion of the wave packet created by the captured neutron, here the lifetime is much longer. This certainly allows us to consider the isolated resonances as quasistationary states which are not much different from the discrete states below the threshold for neutron decay. Moreover, strictly speaking, both classes of states are in the continuum as in both cases gamma decay to low-lying states is possible. The neutron and gamma decay channels of the same initial state compete. The situation starts changing with increase of

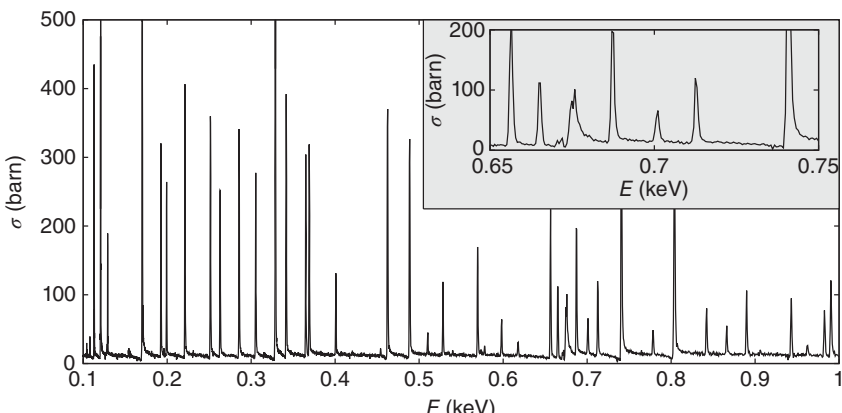


Figure 20.2 Neutron resonance cross section (note the large magnitudes of resonances) for $^{232}\text{Th}+n$ as a function of energy, the selected region is magnified in the inset. The data are from Ref. [19].

energy up to few megaelectronvolts: D goes down, Γ goes up, new decay channels are opened, the broadened resonances become overlapping. Then the whole picture is governed by random fluctuative processes because of unpredictable phases of interfering resonances [20].

We denote the channels of the reaction that open at given energy as a, b, c, \dots . The channel is characterized by the asymptotic fragments, their spins, and internal wave functions as well as the angular momenta of motion in the continuum. The compound state can decay through any open channel b , corresponding width Γ_b determining the probability Γ_b/Γ of the decay into this channel, where Γ gives the total decay rate. If the neutron capture and decay of the compound system are separated in time, we can expect that the cross section σ_{ba} of the compound nucleus formation from channel a with decay into channel b can be written as

$$\sigma_{ba} = \sigma_{\text{comp}}(a) \frac{\Gamma_b}{\Gamma}, \quad (20.71)$$

where $\sigma_{\text{comp}}(a)$ is the total cross section of the compound nucleus formation from the initial channel a . The evaporation of particles from the compound nucleus considered above is a natural result of this picture. The whole consideration can be described as *memory loss* by the compound nucleus that leads to thermodynamic equilibrium and makes the decay statistically independent of formation. This is a limiting case of possible processes. An opposite limiting case corresponds to *direct reactions* [21], such as (d, p) where the incoming weakly bound deuteron releases its neutron in the (probably localized at the nuclear surface) simple collision, with no compound nucleus being formed. The whole process of the compound nucleus formation can end at any moment by *preequilibrium emission* of a particle or photon and can be considered in a kinetic approach [22] which is outside of our consideration. We need also to keep in mind that, in principle, any final channel can be populated through the compound nucleus as well as through a direct reaction.

As a typical example, we can use the slow neutron s -wave scattering (no long-range Coulomb forces). The radial wave function $R(r) = u(r)/r$ of the neutron in the asymptotic region outside of the nuclear potential contains [QP, II, Ch. 10] the incoming and outgoing waves,

$$u(r) = \text{const} \cdot (e^{-ikr} - S(E)e^{ikr}), \quad E = \frac{\hbar^2 k^2}{2m}, \quad (20.72)$$

and $S(E)$ (the diagonal element of the scattering matrix for the elastic neutron channel, not to be confused with the entropy) defines the observable cross sections. The elements of the S -matrix are in general complex. The value $S(E) = 1$ corresponds to the absence of actual scattering. In the presence of only the elastic channel, $S = \exp[2i\delta(E)]$, where $\delta(E)$ is the real phase. The elastic scattering is determined by the difference $1 - S$,

$$\sigma_{\text{el}} = \frac{\pi}{k^2} |1 - S|^2. \quad (20.73)$$

If inelastic processes, including gamma radiation, are possible, the outgoing flux is present in other channels, $|S|^2 \neq 1$, and the corresponding reaction cross section is given by

$$\sigma_r = \frac{\pi}{k^2} (1 - |S|^2). \quad (20.74)$$

The sum of the two determines the total cross section of the process,

$$\sigma_{\text{tot}} = \sigma_{\text{el}} + \sigma_r = \frac{2\pi}{k^2} (1 - \text{Re } S). \quad (20.75)$$

In the case of an *isolated* resonance, the Breir–Wigner approximation for the reaction cross section $a \rightarrow b$ contains the entrance, A^a , and exit, A^b , amplitudes and the typical resonance denominator that corresponds to the pole $\mathcal{E} = E_r - (i/2)\Gamma_r$ in the lower part of the complex energy plane,

$$\sigma_r^{ba} = \frac{\pi}{k_a^2} \left| \frac{A^b A^{a*}}{E - E_r + (i/2)\Gamma_r} \right|^2. \quad (20.76)$$

The wave function in this approximation is that of the decaying resonance with the time dependence proportional to $\exp\{(-i/\hbar)[E_r - (i/2)\Gamma_r]t\}$. In a general case of the target nucleus spin J_A , spin of the projectile J_a and the spin J of the resonance in the compound nucleus, the cross section for nonpolarized particles, summed over final spin projections and averaged over initial projections, can be written, again in the resonance approximation, as

$$\sigma_J^{ba}(E) = \frac{\pi}{k_a^2} \frac{2J+1}{(2J_a+1)(2J_A+1)} \frac{\Gamma_J^b \Gamma_J^a}{(E - E_r)^2 + \Gamma_J^2/4}. \quad (20.77)$$

The partial widths here are $\Gamma^{a,b} = |A^{a,b}|^2$. In realistic cases, there is also a nonresonant part of the scattering amplitude that comes from direct processes, pure potential scattering, and the tails of other resonances. This part with its smooth energy dependence interferes with the resonance so that the total cross section has a more complicated form with a background and distorted wings.

To consider the case of many interfering (not necessarily completely overlapping) resonances, we can use the old *statistical averaging method* [23–26]. Let the interval I of energy contain many resonances of similar nature and with identical global quantum numbers. For simplicity, we will not average the factor k^2 in the definition of cross sections as it changes much slower than resonance curves (to avoid this, one can average $k^2\sigma$ instead of σ). The averaging goes in a simple way,

$$\bar{S} = \frac{1}{I} \int_I dE S(E). \quad (20.78)$$

For the S -matrix, we find the fluctuational part of the scattering matrix

$$|\Delta S|^2 = |\bar{S}|^2 - |\bar{S}|^2. \quad (20.79)$$

Accordingly, we have now the *fluctuational part* σ_{fl} of the reaction cross section (20.74),

$$\bar{\sigma}_r = \frac{\pi}{k^2} \left[1 - |\bar{S}|^2 \right] - \sigma_{\text{fl}}, \quad \sigma_{\text{fl}} = \frac{\pi}{k^2} |\Delta S|^2. \quad (20.80)$$

The average total cross section (20.75) should be identified with

$$\overline{\sigma_{\text{tot}}} = \frac{2\pi}{k^2} (1 - \text{Re } \bar{S}). \quad (20.81)$$

The formation of the compound nucleus can be ended by any reaction or by the decay in the elastic channel. The last possibility is called *compound elastic* with the

cross section $\sigma_{\text{comp-el}}$. The total average cross section of the processes going through the compound stage is then

$$\overline{\sigma_{\text{comp}}} = \overline{\sigma_r} + \overline{\sigma_{\text{comp-el}}} = \frac{\pi}{k^2} \left[1 - |\bar{S}|^2 \right] - \sigma_{\text{fl}} + \overline{\sigma_{\text{comp-el}}}. \quad (20.82)$$

The main idea in such arguments is the long-lived character of the compound nucleus that allows us to neglect the interference of the compound processes with the rapid scattering of the initial wave packet.

If we consider the elastic process, σ^{aa} , the fluctuations come from the formation of the compound nucleus. Then the simplest approximation – that of the *optical model* – is that the two last terms of Eq. (20.82) express the same physics and therefore cancel each other [24], so that the result is what is called the *shape-elastic scattering*,

$$\sigma_{\text{shape-el}}^{aa} = \frac{\pi}{k^2} \left| 1 - \overline{S^{aa}} \right|^2. \quad (20.83)$$

To explain the road to the practical description of a many-resonance situation, let us go back to Eq. (20.77) and rewrite it in terms of the total cross section $a \rightarrow b$ given by the sum of all resonances r with given quantum numbers contributing at given energy,

$$\sigma_J^{ba}(E) = \frac{\pi}{k_a^2} g \sum_r \frac{\Gamma_r^b \Gamma_r^a}{(E - E_r)^2 + \Gamma_r^2/4}. \quad (20.84)$$

Here g is the spin factor of Eq. (20.77), while in the denominator we have a total width,

$$\Gamma_r = \sum_c \Gamma_r^c. \quad (20.85)$$

The energy averaging (20.78) is performed over the interval I containing many individual resonances with the same quantum numbers. For any given resonance r , we have

$$\frac{1}{I} \int_{E-I/2}^{E+I/2} \frac{\Gamma_r^b \Gamma_r^a}{(E - E_r)^2 + \Gamma_r^2/4} \approx 2\pi \Gamma_r^b \Gamma_r^a, \quad (20.86)$$

where we assume that (i) the widths weakly change on the interval I of energy and (ii) the integration effectively covers energy from zero (threshold) to infinity so that the arctangent gives the factor of π .

Now the cross section is presented by averaging over resonances contributing to the interval I , and in this approximation the exact quantity I is not essential,

$$\overline{\sigma_J^{ba}} = \frac{\pi}{k^2} \frac{2\pi}{D} g \overline{\frac{\Gamma^a \Gamma^b}{\Gamma}}. \quad (20.87)$$

Here D is the mean energy distance between the resonances and the averaging is over I/D resonances so that the result does not contain the length I explicitly.

Problem 20.6 In the same way, work out the total reaction cross section started at the channel a .

Solution.

Here we sum over all channels b of the reaction,

$$\sigma_J^a(E) = \frac{\pi}{k_a^2} g \sum_r \frac{\Gamma_r \Gamma_r^a}{(E - E_r)^2 + \Gamma_r^2/4}. \quad (20.88)$$

The averaging gives

$$\overline{\sigma_J^a} = \frac{\pi}{k^2} g 2\pi \frac{\overline{\Gamma^a}}{D}. \quad (20.89)$$

The nuclear reactions are frequently described in terms of the *optical potential* [QP, II, 9.7]. This is an energy-dependent *complex* and *energy-dependent* potential V_{opt} for a given type of colliding particles that describes the elastic channel and the disappearance of projectiles due to the presence of other reaction channels modeled by the imaginary part of V_{opt} . This approach substitutes the explicit consideration of specific reaction channels. Defining the reaction cross section according to Eq. (20.74) and introducing the *transmission coefficient*, sometimes called *adhesion coefficient* for a given channel,

$$T^a = 1 - |S^a|^2, \quad (20.90)$$

the reaction cross section in a channel a can be written as

$$\sigma_r^a = \frac{\pi}{k_a^2} g T^a, \quad (20.91)$$

and the result of averaging (20.89) allows to identify

$$T^a = 2\pi \frac{\overline{\Gamma^a}}{D}. \quad (20.92)$$

In order to not violate the unitarity conditions, the coefficients T^a have to be between zero and one and this places limitations on the ratios $\overline{\Gamma^a}/D$ which cannot be too large, when the whole approach breaks down. Note that this does not limit the total resonance width (20.85).

The further approximation assumes a weak correlation between different reaction channels when the complicated averaged quantity in Eq. (20.80) can be factorized as

$$\frac{\overline{\Gamma^a \Gamma^b}}{\Gamma} \Rightarrow \frac{\overline{\Gamma^a} \cdot \overline{\Gamma^b}}{\overline{\Gamma}}. \quad (20.93)$$

This leads us to the Hauser–Feshbach approximation [23] for the average cross sections summed over allowed values of the total spin J of the system:

$$\overline{\sigma^{ba}} = \sum_J \overline{\sigma_J^{ba}} \Rightarrow \frac{\pi}{k_a^2} \sum_J g_J \frac{T^a T^b}{\sum_c T^c}. \quad (20.94)$$

The sum here should include also different parities of the compound system possible in the reaction, in particular, those due to the superposition of waves corresponding to various orbital momenta ℓ in the entrance channel. This approach is widely used in practice for estimates of cross sections, especially when the total experimental information is not available, for example, for astrophysical reactions.

To correct the crudeness of the approach, an additional factor W^{ba} can be introduced under the sum in Eq. (20.94) in order to account for the correlations between different channels neglected in Eq. (20.93). One thing that is rather obvious is the so-called *elastic enhancement* factor. Indeed, the derivation of Eq. (20.94) assumed the simple factorization (20.93) of the average product of the partial widths into the product of average values. But those widths are *squares* of the amplitudes, similarly to what we had in Eq. (20.77). The amplitude A^a can connect the channel a with many complicated

intrinsic states $|\mu\rangle$ and the product of two widths contains the expression such as $(A^a)^2(A^b)^2$. Different channels could be only weakly correlated as it was assumed in the previous consideration but this is certainly not right for $a = b$. For example, for the Gaussian distribution, $\overline{A^4} = 3(\overline{A^2})^2$, which would lead to the elastic enhancement factor $W^{aa} = 3$. If the sum over many intrinsic states plays the main role, which almost certainly happens at large widths, $\Gamma^a > D$, this factor turns out to be equal 2 [27].

References

- 1 M.C. Gutzwiller, *Chaos in Classical and Quantum Dynamics*, Springer-Verlag, New York, 1990.
- 2 N. Hall (ed.) *Exploring Chaos*, W.W. Norton, New York, 1991.
- 3 I.C. Percival, J. Phys. **B6**, L229 (1973).
- 4 V. Zelevinsky, B.A. Brown, N. Frazier, and M. Horoi, Phys. Rep. **276**, 315 (1996).
- 5 B. Davies, *Integral Transforms and their Applications*, 3rd edn, Springer-Verlag, New York, 2002.
- 6 Ya. Frenkel, Sow. Phys. **9**, 533 (1936).
- 7 L. Landau, JETP Lett. **7**, 819 (1937).
- 8 T. Ericson, Adv. Phys. **9**, 425 (1960).
- 9 L.G. Moretto, A.C. Larsen, F. Giacoppo, M. Guttormsen, and S. Siem, J. Phys. Conf. Ser. **580**, 012048 (2015).
- 10 (a) S. Siem *et al.*, Phys. Rev. C **65**, 044318 (2002); (b) M. Guttormsen *et al.*, Phys. Rev. C **68**, 064306 (2003); (c) H.K. Toft *et al.*, Phys. Rev. C **83**, 044320 (2011).
- 11 H.A. Bethe, Phys. Rev. **50**, 332 (1936).
- 12 R. Durrett, *Probability: Theory and Examples*, 4th edn, Cambridge University Press, Cambridge, 2004.
- 13 G.H. Lang, C.W. Johnson, S.E. Koonin, and W.E. Ormand, Phys. Rev. C **48**, 1518 (1993).
- 14 M.H. Kalos and P.A. Whitlock, *Monte Carlo Methods*, Wiley-VCH, Berlin, 2008.
- 15 Y. Alhassid, Eur. Phys. J. A **51**, 171 (2015).
- 16 L. Landau and Ya. Smorodinsky, *Lectures on Theory of the Atomic Nucleus*, Gostekhizdat, Moscow, 1955.
- 17 V.F. Weisskopf, Phys. Rev. **52**, 295 (1937).
- 18 H.A. Bethe, Rev. Mod. Phys. **9**, 69 (1937).
- 19 J.B. Garg, J. Rainwater, J.S. Petersen, and W.W. Havens Jr., Phys. Rev. **134**, B985 (1964).
- 20 T. Ericson and T. Mayer-Kuckuk, Annu. Rev. Nucl. Sci. **16**, 183 (1966).
- 21 N.K. Glendenning, *Direct Nuclear Reactions*, World Scientific, Singapore, 2004.
- 22 D. Agassi, H.A. Weidenmüller, and G. Mantzouranis, Phys. Rep. **22**, 145 (1975).
- 23 W. Hauser and H. Feshbach, Phys. Rev. **87**, 366 (1952).
- 24 F.L. Friedman and V.F. Weisskopf, in *Niels Bohr and the Development of Physics*, eds. W. Pauli, L. Rosenfeld, and V. Weisskopf, Pergamon Press, London, 1955.
- 25 G.E. Brown, Rev. Mod. Phys. **31**, 894 (1959).
- 26 J. Blatt and V. Weisskopf, *Theoretical Nuclear Physics*, Springer-Verlag, New York, 1979.
- 27 V.V. Sokolov and O.V. Zhirov, Phys. Rev. E **91**, 052917 (2015).

21

Nuclear Fission

At first, very approximately a sphere, the figure of this mass will become an ellipsoid of revolution which will flatten more and more, then, at a certain moment, it will be transformed into an ellipsoid with three unequal axes. Later, the figure will cease to be an ellipsoid and will become pear-shaped until at last the mass, hollowing out more and more at its “waist”, will separate into two distinct and unequal bodies.

Henri Poincaré, cited in E.T. Bell, *Men of Mathematics*,
A Touchstone Book. N.Y. 1986.

21.1 Introduction

Our epigraph shows that nuclear fission was qualitatively described by Henri Poincaré in his study of a problem of fluid dynamics (1910) before the discovery of atomic nuclei... In the discussion of the liquid drop model (LDM), Chapter 5, it was explained that, when we move along the nuclear chart, the heavy nuclei become more and more unstable with respect to fission into smaller fragments (the term *fission*, borrowed from the cell biology, was introduced by O. Frisch and L. Meitner, 1939). The driving force here is certainly the Coulomb repulsion that becomes very strong for heavy nuclei with a large electric charge Z . As discussed in Section 5.7, the *fissility* of the nucleus is mainly determined by the parameter $x = Z^2/A$ that comes from the ratio of Coulomb to surface energy.

As the binding energy per nucleon is lower by approximately 1 MeV at the large- A end of the mass curve, see Figure 5.1, in the fission process of a heavy nucleus, $A > 200$, we obtain about 200 MeV of released energy, mainly in the form of kinetic energy of the products. We have also to take into account that the symmetry energy does not change during the fission process. Extra neutrons in the fragments in many cases undergo beta-decay; excited fragments also emit several gamma-rays. Fragments overloaded by neutrons emit them (e.g., in each fission act of ^{235}U , in average, 2.5 neutrons with different energies are emitted). This is a precondition for the *chain reaction*.

The nucleus of mass M becomes unstable with respect to the separation of nuclear fragments of mass M_1 and M_2 if the process is accompanied by energy liberation, $M > M_1 + M_2$. The nuclei with a large electric charge can undergo *spontaneous fission* (K.L. Petrzhak and G.N. Flerov, 1940) and the lifetime with respect to spontaneous fission rapidly falls along the nuclear chart, from the enormous time $\sim 10^{22}$ years for ^{232}Th , $Z = 90$, to hours for ^{256}Fm (fermium), $Z = 100$. Although fission is energetically

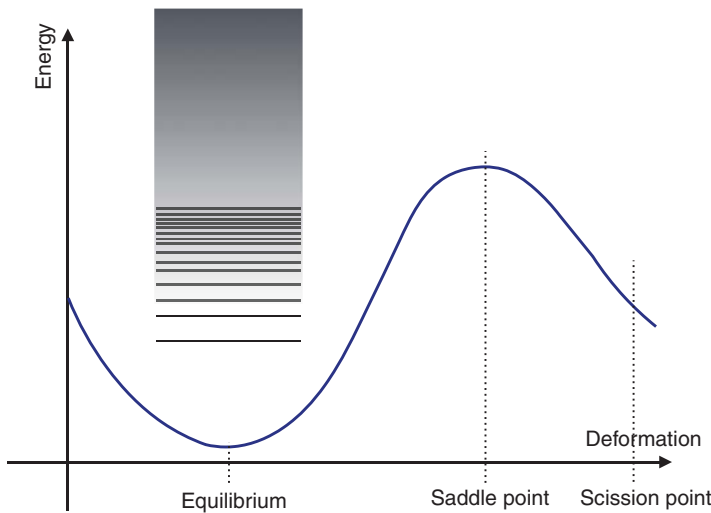


Figure 21.1 Fission barrier (a qualitative picture).

favorable for the majority of nuclei heavier than iron, it does not occur as a fast observable process because of the *fission barrier*. The fissioning nucleus has to go through the process of increasing deformation, Figure 21.1, before the *scission point* where first a neck and then two independent fragments are formed. Because of growing surface energy, this leads to the maximum in the total curve of potential energy as a function of deformation. The nucleus has to proceed through very elongated shapes on its way from normal deformation to fission, with the axes ratio 2:1 and greater. This creates the fission barrier. To overcome this barrier, the nucleus either has to be *activated* by an external agent or has to penetrate through the barrier using quantum tunneling. The barrier effectively disappears at $x_c \approx 46$ when the nucleus becomes absolutely unstable. In actinide nuclei, this parameter is still on the level of 0.7–0.8 of the critical value.

Problem 21.1 In the simplest approximation, the fission barrier can be presented by the inverted parabola taking the Hamiltonian of collective motion along the fission coordinate as

$$\hat{H} = \hat{K} + U(Q) = E_0 - \frac{\hbar^2}{2B} \frac{\partial^2}{\partial Q^2} - \frac{1}{2} B\omega^2 Q^2, \quad (21.1)$$

where E_0 is the top energy of the barrier, Q is the generalized deformation parameter, and B the corresponding mass parameter (for small amplitude vibrations, this was introduced in Section 5.6). In typical cases of spontaneous fission, the curvature of the barrier is characterized by $\hbar\omega \approx 0.4$ MeV so that the effective mass parameter B exceeds the irrotational value found in Chapter 5. For the Hamiltonian (21.1), find the barrier penetrability as a function of energy.

Solution

The problem was solved in [QP, I, 15.11]. The semiclassical transmission probability at energy E is

$$T(E) = \frac{1}{1 + e^{2\gamma}}, \quad \gamma = \pi \frac{E_0 - E}{\hbar\omega}. \quad (21.2)$$

The fission process can be accelerated by artificial excitation of the nucleus that helps in penetrating the barrier. In practical applications, the role of the excitation agents is frequently given to neutrons or photons [1], but the efficiency of this process depends on the nucleus and neutron (or photon) energy. Practically all fissioning nuclei can fission under the action of neutrons with energies higher than 50–100 MeV. The heaviest nuclei, including the odd uranium isotopes $^{233,235}\text{U}$, can fission on being irradiated by very slow neutrons (electronvolt energy). Indeed, the neutron with practically zero kinetic energy, being captured by the nucleus, excites the nucleus by the neutron separation energy $S_n \approx 6–8$ MeV that can exceed the height of the fission barrier. Slow neutrons interact with nuclear targets mainly in the s -wave of relative motion, and the capture cross section grows at low energy inversely proportional to the neutron velocity [QP, II, 10.4], see Figure 21.2. Up to neutron energy of the order of kiloelectronvolts, the capture cross section consists of many narrow resonances corresponding to the long-lived compound states (the level density at this excitation energy of the compound nucleus is very high, $\sim 10^6$ states per megaelectronvolt). Typical resonance cross sections for *thermal neutrons* (energy 1/40 eV) are quite large, up to 10^3 barn.

At low energy, there are several types of processes allowed for the decay of the compound nucleus formed after neutron capture: elastic scattering, fission, radiative decay

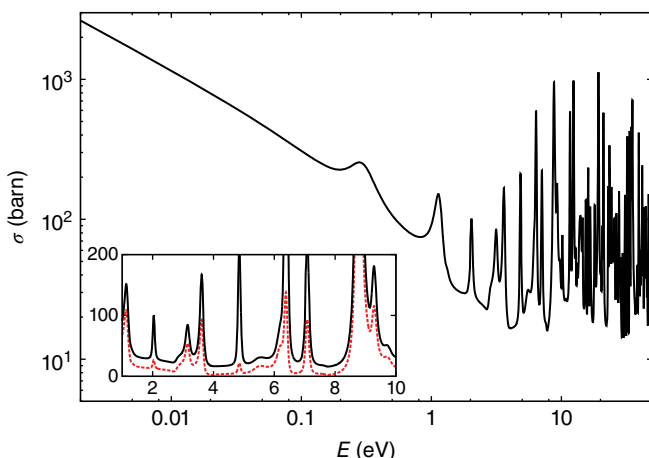


Figure 21.2 Total low-energy neutron scattering cross section of ^{235}U . The inset, using linear scale, shows the energy region between 1 and 10 eV, where fission cross section is also shown by a dashed line.

when the excitation energy is released by the emission of a photon with the nucleus left in one of the lower excited states of the discrete spectrum, and alpha-decay. In many practically important cases, fission is the most probable channel (probability > 80% for thermal neutrons captured by ^{235}U).

In all applications, the difference between odd- A and even–even nuclear targets is of extreme importance. The natural mixture of uranium isotopes, $Z = 92$, consists mostly (99.3%) of even–even ^{238}U and only 0.7% of ^{235}U . The lighter isotope undergoes fission even with thermal neutrons, while for fission of ^{238}U , the neutrons have to be more energetic than 1.1 MeV (in neutron physics such neutrons are called “fast,” Section 21.3). The main effect to be blamed for this difference is nuclear pairing. After the neutron is captured, the compound nucleus, ^{236}U or ^{239}U respectively, is formed for those uranium isotopes. The ground state of ^{236}U has all neutrons paired, while the ground state of ^{239}U contains an unpaired nucleon, therefore losing the energy Δ of the pairing gap (Chapter 13). Therefore, the compound nucleus ^{236}U has larger excitation energy than ^{239}U ; one has also to add here the effect of a slightly bigger fissility parameter x . As a result, only ^{235}U undergoes fission by thermal neutrons. This is the reason for the necessity of *enrichment* of the natural uranium by the fissioning isotope ^{235}U .

A heavy fissioning nucleus has a large neutron excess. As a result, many fission fragments have neutron numbers that are too large compared to that typical for stable lighter nuclei. Because of this, the fission fragments are active beta-emitters in many cases; getting rid of extra neutrons by beta-decay, they move across the nuclear chart to the stability line. Excitation energy of the fragments is also directly emitted in the form of neutrons (as mentioned above, 2–3 neutrons per act of fission of ^{235}U with energies up to few megaelectronvolts) which can lead to a chain reaction. In addition, during every fission act, several photons are emitted. If, on the way to the stability line by beta-decay, at some intermediate stage, a nucleus unstable with respect to the neutron emission is born, the process gives rise to the so-called *delayed neutrons*. The total balance of energy released during one fission act and the following transformations includes kinetic energies of all emitted particles and gamma-rays, being equal to about 200 MeV, as expected, for the ^{235}U fission.

The nuclear fission fragments (usually there are two of them, although *ternary fission* with three fragments has also been observed) reveal a broad distribution by their mass and kinetic energy [2]. The preferred type of fission is *asymmetric* with the fragment masses close to the magic numbers, Figure 21.3. In fission at higher excitation energy, the distribution usually becomes more symmetric. In this chapter, we limit ourselves to low-energy fission when the process takes place at energy comparable with the barrier height [3]. This means that there are only few fission channels at the transition point near the top of the barrier. The final mass and kinetic energy distributions are formed during the sliding from the barrier to the scission when the deformation energy is transformed into intrinsic degrees of freedom by all kinds of dissipative mechanisms.

21.2 Alpha-Decay

Before going to the real fission process, we briefly discuss its junior relative, the alpha-decay, when the smaller fragment is simply the ^4He nucleus. Alpha-radioactivity was discovered even before the first realistic nuclear models were articulated. On

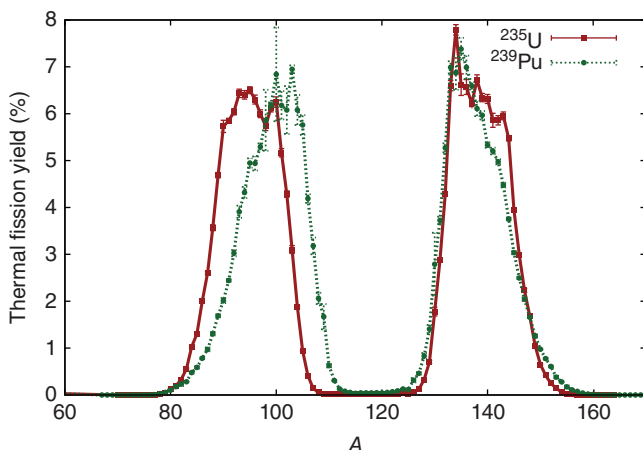


Figure 21.3 Mass distribution for fragments in the thermal fission process of ^{235}U and ^{239}Pu .

comparing the binding energies, one can see that for many nuclei, alpha-decay is energetically allowed. The superheavy nuclei frequently decay by a series of consecutive alpha-decays. The alpha-decay does not require such a large deformation of the decaying nucleus as genuine fission into two comparable fragments. Sometimes, there are also alpha-particles coming from the neck of the double system in the fission process (*ternary fission*). We expect that alpha-particles are formed close to the surface.

In many cases, the alpha-particles coming from this decay form groups with different energies. They correspond to different states of the daughter or mother nuclei. The decay probability is extremely sensitive to the energy released in the decay, which depends on the binding energies of the mother and daughter nuclei. For different nuclei, the lifetimes of alpha-active nuclei differ by many orders of magnitude. The natural linewidth, $\Gamma_\alpha = \hbar/\tau$, where τ is the lifetime for alpha-decay, is usually smaller than megaelectron-volts.

For a simple estimate, we can use an old Gamow theory where the main part of the decay probability is due to the penetration of the Coulomb barrier. If the alpha-particle is already formed inside a big nucleus, for the decay outside, it has to overcome the potential barrier that can be taken in a simple form as

$$U_C(r) = \frac{2Ze^2}{r}, \quad r > R, \quad (21.3)$$

while the potential is negative and constant inside, $r < R$, where R is the sum of the radii of the alpha-particle and the daughter nucleus of charge Z . Because of the crude approximation (21.3), it makes no sense to try to solve exactly the Schrödinger equation for the alpha-particle in this field. But the semiclassical approach, similar to that in Problem 21.1, gives a reasonable estimate.

Problem 21.2 Assuming the s -wave for the alpha-particle, find the barrier penetration probability in the standard semiclassical approximation [QP, I, 2.7, 15.10].

Solution

The turning points r_1 and r_2 are given by the conditions, $U(r_1) = U_C(r_2) = E$, where E is the energy of the alpha-particle counted from the bottom of the inner well.

The probability of barrier penetration is calculated as

$$P_\alpha = \exp \left\{ -\frac{2}{\hbar} \int_{r_1}^{r_2} dr \sqrt{2m[U_C(r) - E]} \right\}, r_1 = R, r_2 = \frac{2Ze^2}{R}, r_2 > r_1. \quad (21.4)$$

The result is

$$P_\alpha = \exp \left\{ -\frac{4Ze^2}{\hbar v} [\pi - 2\chi - \sin(2\chi)] \right\}, \sin \chi = \sqrt{\frac{ER}{2Ze^2}}, \quad (21.5)$$

and $v = \sqrt{2E/m}$ is the velocity of the alpha-particle at a large distance, m the reduced mass of the alpha-particle and the daughter nucleus.

The full probability of the alpha-decay includes also the preexponential factor for semiclassical tunneling (21.4). This is a very complicated theoretical problem that requires a good knowledge of the wave function of the mother nucleus and the probability of internal formation of the alpha-cluster. The estimates can be made [4, 5] in the best classical example of ^{212}Po , when the ground-state wave function clearly contains components of the low-lying states of the double magic nucleus ^{208}Pb plus a $2p-2n$ cluster, an embryo of the future alpha-particle. Usually, this is considered to be the most appropriate region of the nuclear chart, well adjusted for alpha-decay. The theoretical consideration unavoidably is quite involved as it is dependent on the shell structure, residual interactions forming the alpha-cluster, the Coulomb forces at the nuclear surface, and the optical potential for the alpha-cluster at this surface.

However, it turns out that the largest internal probability of alpha-decay [if we divide out the barrier penetration factor (21.5)] is observed for an exotic decay far from the line of stability, $^{105}\text{Te} \Rightarrow ^{101}\text{Sn}$. This is related to an interesting unsolved problem of behavior of the collective quadrupole degrees of freedom in the region of $^{100}_{50}\text{Sn}_{50}$, which is the last double-magic nucleus with $Z = N$ and beyond. Typically, the probability $B(\text{E}2; 2^+ \rightarrow 0^+)$ displays a collective behavior: it is small at the beginning of a new shell and at the end when the shell is almost full, having a maximum in the middle of the shell. Although the experimental situation is not clear (the measurements for such exotic nuclei far from the valley of stability are very difficult), it seems that this transition probability in tin isotopes beyond ^{100}Sn is greater than expected from standard collective models. One idea is that there exists an increased promotion of protons to the upper shell that would be empty for the magic number $Z = 50$. This would increase the probabilities of electromagnetic transitions. The mechanism of increase can be related to the easy formation, due to the condition $Z = N$, of alpha-type clusters [6]. The existence of strong alpha-decays in this region of the nuclear chart adds serious arguments to this idea.

The preexponential factor in the probability of alpha-decay with dimension of inverse time should define the lifetime of an alpha-emitter. The statistical approach leads to the Landau estimate of $D/2\pi\hbar$ which, as we know, is the inverse Weisskopf time for the typical frequency of the wave packet composed of compound states with appropriate quantum numbers in the given energy region, where D is the characteristic spacing between these levels. The very sensitive energy dependence comes mainly from the penetration factor.

Interesting physical questions are related to the electromagnetic radiation by the alpha-particle when it is accelerated by Coulomb repulsion after emission. The delicate experiments [7] showed that a part of the radiation comes from the classically forbidden

region under the barrier, and the interference of this radiation with the normal classical radiation after the barrier is destructive; the detailed theory is given in Ref. [8]. The radiative corrections, both from real radiation and from processes with virtual photons, also influence the results. In particular, the so-called *quantum Munchausen process* [9] when the tunneling particle first absorbs the virtual photon and then, after tunneling, returns it by emission, increases the tunneling probability (the barrier penetration occurs at a higher energy).

An approximate phenomenological Geiger–Nuttall law for the half-life $\tau_{1/2}$ of alpha-emitters as a function of energy E of alpha-decay was established long ago,

$$\ln \tau_{1/2} = A - \frac{BZ}{\sqrt{E}}. \quad (21.6)$$

It works relatively well, especially for crude estimates, describing the experimental data for transitions between ground states of even–even nuclei (typical values of constants are $A \approx 50$ and B between 1.4 and 1.5 if energy E is taken in megaelectronvolt and $\tau_{1/2}$ in second), and less well for odd–even cases. Equation (21.6) follows from the barrier penetration formula (21.5) neglecting the energy-dependent quantity χ . Transitions to excited states of the daughter nuclei are practically noticeable for the low-lying levels of the main rotational band. Energy of alpha-decay goes down from the nuclei with filled neutron shells to the isotopes with unfilled shells. From the qualitative picture of alpha-decay, it is natural that the decay preserves the K quantum number of the spin projection onto the symmetry axis ($K = 0$ for ground-state bands of even–even nuclei and the alpha-particle preserves $K = 0$ and parity). This selection rule explains also that in some cases, alpha-decay prefers excited levels of the daughter nucleus. For example, the ground state ^{241}Am , $J = K = 5/2^+$, decays mainly into the third excited level of ^{137}Np with the same quantum numbers, while the first two excited states of ^{137}Np have negative parity.

The theory of alpha-decay in its deep relation to nuclear structure is still not developed fully satisfactorily. Another set of questions refers to the relation of alpha-decay to the electronic structure of atomic shells in daughter nuclei where the Coulomb field of the daughter nucleus can be considerably modified.

21.3 Neutron Fission

Fission is one of the most important channels in reactions of slow neutrons with heavy nuclei. A compound system formed after the capture of a slow neutron by a heavy nucleus can undergo neutron evaporation, gamma-radiation, or fission. There is only one (elastic) channel for neutron emission, many gamma-channels which end at different final states, and just few fission channels if the excitation energy only slightly exceeds the barrier height. These channels can be called *transition states*, the states built on the large deformation reached in the fission process. In this situation, the motion of a heavy nucleus in the barrier region is slow (adiabatic) and the possible intrinsic states are similar to those we discussed while introducing normal nuclear deformation.

If D is the mean level spacing for the transitional channels, the beat period of the wave packet here is given by the Weisskopf time $2\pi\hbar/D$. The number of fission channels can

be estimated as the integral

$$\mathcal{N}(E) = \int_{E_0}^E dE' \rho_f(E' - E_0), \quad (21.7)$$

where we use the density ρ_f of the transition states at the barrier. For each channel c , there is a transmission coefficient t_c , and the typical lifetime per channel is $\tau_c \sim 2\pi\hbar/(Dt_c)$. The inverse quantity is the *fission width* $\Gamma_c \approx \hbar/\tau_c = (D/2\pi)t_c$. For the case of several fission channels above the barrier, $t_c \approx 1$, and we come to the *Bohr–Wheeler estimate* of the fission width,

$$\Gamma_f \approx \frac{D}{2\pi} \mathcal{N}(E). \quad (21.8)$$

Such estimates are always approximate as the fission process is possible by tunneling below the barrier, but they give reasonable numbers.

We can also arrive at the same result by using slightly different arguments [10]. Consider the energy region between E and $E + dE$. For the level density $\rho(E)$ there are $\rho(E)dE$ states in this region. The fission width Γ_f can be defined through the typical fission time \hbar/Γ_f , so that the fraction of nuclei from the energy interval dE undergoing fission per unit time is

$$\frac{\rho(E)dE}{\hbar/\Gamma_f} = \rho(E) \frac{\Gamma_f}{\hbar} dE. \quad (21.9)$$

Now, let p and Q be the conjugate momentum and coordinate describing the fission from the transition state, while E_Q is the energy available for the fragments. The transition state corresponds to the energy $E - E_f - E_Q$, where E_f is the fission barrier. The density of transition states is $\rho_f(E - E_f - E_Q)$. The number of transition states in the interval $dp dQ$ and total energy dE is

$$dN_t = \frac{dp dQ}{2\pi\hbar} \rho_f(E - E_f - E_Q) dE. \quad (21.10)$$

Using the velocity of the collective process \dot{Q} and its relation to the collective energy, $\dot{Q}dp = dE_Q$, we arrive at

$$dN(t) = \frac{dE}{2\pi\hbar} \int dE_Q \rho_f(E - E_f - E_Q) = \frac{dE}{2\pi\hbar} \mathcal{N}(E), \quad (21.11)$$

where $\mathcal{N}(E)$ is actually, as in Eq. (21.4), the cumulative number of transition states up to energy $E - E_f$. The comparison of (21.9) and (21.11) gives the same result (21.8) with $D = 1/\rho(E)$.

If the density of transition states, by order of magnitude, is the same as near the ground state in heavy deformed nuclei, $\sim 10/\text{MeV}$, then close to the top of the barrier $\mathcal{N} \sim 1$, and Γ_f is of the order of few electronvolts noticeably growing with excitation energy, almost exponentially as the level density. The neutron width Γ_n corresponds to elastic or inelastic scattering of the neutron. At neutron energy smaller than the excitation energy of the low-lying nuclear states, only elastic scattering is possible, and Γ_n is small. It grows along with the level density close to the ground state due to various inelastic neutron channels; above neutron energy of about 1 MeV, Γ_n is comparable to Γ_f . As predicted by Bohr [11], at excitation energy greater than the sum of the neutron separation energy E_n and fission barrier E_f , fission is possible even after the neutron emission.

As the interactions between neutrons and nuclei are very sensitive to the exact value of the neutron energy, there are traditional names for neutrons of various energies, for example *ultracold*, energy $< 10^{-7}$ eV, used in particular for precision measurements of fundamental constants; *cold*, $E \ll (1/40)$ eV (room temperature), which have a wavelength greater than atomic sizes or typical spatial periods of crystal lattices but large nuclear cross sections of radiative capture in agreement with the $1/v$ rule (the elastic cross section has a constant low-energy limit); *thermal*, energy up to 1 eV, the interval widely used in nuclear technology, in particular $E \approx (1/40)$ eV corresponds to the wavelength that makes such neutrons a useful instrument in condensed matter physics; *resonance*, energy up to 1 keV, the interval of observation of large neutron cross sections visible through isolated narrow resonances (still the main processes are those of radiation capture); *intermediate*, energy up to 100 keV, when the resonances, except for the lightest nuclei, become overlapping, and neutron scattering becomes more probable than radiative capture; and *fast*, energy up to 14 MeV that corresponds to the results of the fission processes; energy higher than ~ 10 MeV can be sufficient for the $(n, 2n)$ reactions multiplying the available neutron number. Neutrons of even higher energy have smaller nuclear cross sections and can be used for studying specific nuclear and particle reactions. Here we can also mention the *delayed* neutrons which emerge after beta-decay of some isotopes produced in the fission process, with the delay time of milliseconds or even seconds.

In this chapter, we are mostly interested in fission process. As mentioned earlier, if energetically allowed, the fission cross section by neutrons grows $\sim 1/v$ at low neutron energy. For some isotopes, such as $^{233,235}\text{U}$, ^{239}Pu , and many transuranium elements, fission is possible at practically zero neutron energy. The fission cross section by thermal neutrons for ^{235}U is 600 b (1 barn = 10^{-24} cm 2). Upon capture in the compound state, the fission process becomes allowed already at excitation energy as small as 2 MeV (for ^{233}U), while the neutron capture introduces energy about 6 MeV. Such *fission thresholds* can be studied, instead of using free neutron beams, with the help of other processes, for example the deuteron, or the triton, break-up reaction when the released neutron is captured by the target nucleus from the deuteron (tritium) bound state and forces the nucleus to fission. Then the excitation energy of the nucleus is lower by the neutron binding energy in the deuteron (triton) and one can come closer to the actual fission threshold [the standard notations for such reactions are (d, pf) and (t, pf)].

As fission is possible even below the neutron threshold and the tunneling of the fragments becomes more and more probable with energy approaching the saddle point, the notion of the fission channels becomes less definite, and one can speak about the effective number of these channels. Traditionally [12], the effective number of channels v is defined through the statistical distribution of fission widths Γ as the χ -square distribution with v degrees of freedom,

$$P_v(\Gamma) = A_v \Gamma^{(v/2)-1} e^{-v\Gamma/2\bar{\Gamma}}, \quad (21.12)$$

where $\bar{\Gamma}$ is the mean value of the width, the normalization constant is

$$A_v = \frac{1}{\Gamma(v/2)} \left(\frac{v}{2\bar{\Gamma}} \right)^{v/2}, \quad (21.13)$$

and the first factor in (21.13) contains the Gamma-function rather than the width Γ . This distribution corresponds to the most random, *chaotic*, structure of compound states $|\alpha\rangle$

populated after the neutron capture (before the saddle point),

$$|\alpha\rangle = \sum_k C_k^\alpha |k\rangle, \quad \sum_k (C_k^\alpha)^2 = 1. \quad (21.14)$$

The random amplitudes C_k^α are supposed to have a Gaussian distribution with the mean value $\overline{(C_k^\alpha)^2} = 1/N$, where N is a large number of significant components in the normalized superposition (21.14).

Problem 21.3 Let one of the components of the superposition (21.14) describe the fission channel $|c\rangle$. Assuming that the fission width is proportional to the probability of the corresponding amplitude $\Gamma \propto |\langle c|\alpha\rangle|^2$ and the compound state $|\alpha\rangle$ can be viewed as having a random orientation in the N -dimensional Hilbert space, find the fission width distribution.

Solution

Define the projection of interest $x = \langle c|\alpha\rangle$; it is a real number. In the two-dimensional case ($N = 2$), for example, the orientation angle θ has a uniform distribution between 0 and 2π and the corresponding amplitude $x = \cos \theta$ is distributed according to

$$P(x) = \frac{1}{\pi \sqrt{1-x^2}}. \quad (21.15)$$

In order to generalize this to the multidimensional case, define a surface area of a unit-radius multidimensional sphere

$$S_N = \int dx_1 \cdots dx_N \delta(x_1^2 + \cdots + x_N^2 - 1) = \frac{N \pi^{N/2}}{\Gamma(N/2 + 1)}. \quad (21.16)$$

The distribution of a single $x = x_1$ component is

$$P(x_1) = \frac{1}{S_N} \int dx_2 \cdots dx_N \delta(x_1^2 + \cdots + x_N^2 - 1). \quad (21.17)$$

The radial integration in $N - 1$ dimensions with $r^2 = x_2^2 + \cdots + x_N^2$ leads to

$$P(x) = \frac{S_{N-1}}{S_N} (1-x^2)^{(N-3)/2}. \quad (21.18)$$

Expanding the above expression for large N , we recover the normal distribution

$$P(x) \simeq \frac{1}{\sqrt{2\pi N}} e^{-x^2/(2N)}. \quad (21.19)$$

The distribution of widths $\Gamma \propto x^2$ is the χ^2 -distribution with $v = 1$ degree of freedom, called usually the Porter–Thomas distribution (PTD),

$$P_1(\Gamma) = \sqrt{\frac{1}{2\pi\bar{\Gamma}}} \frac{1}{\sqrt{\Gamma}} e^{-\Gamma/(2\bar{\Gamma})}. \quad (21.20)$$

The numerical value $\Gamma(1/2) = \sqrt{\pi}$ can be derived from the definition of the Γ -function,

$$\Gamma(\xi) = \int_0^\infty dx e^{-x} x^{\xi-1}; \quad (21.21)$$

the integral for $\xi = 1/2$ can be squared and then calculated in polar coordinates.

Problem 21.4 Show that the distribution (21.12) for v channels can be found by convolution if the amplitudes C^α are statistically independent (except for the normalization),

$$P_v(\Gamma) = \int_0^\Gamma d\Gamma' P_1(\Gamma') P_{v-1}(\Gamma - \Gamma'). \quad (21.22)$$

Note the similarity to the random process used in Section 20.6.

Problem 21.5 Show that the effective number of channels can be found from the average value $\bar{\Gamma}$ and the mean square fluctuation $(\Delta\Gamma)^2$ which can be determined from experimental data,

$$v = \frac{2\bar{\Gamma}^2}{(\Delta\Gamma)^2}, \quad (\Delta\Gamma)^2 = \bar{\Gamma}^2 - \bar{\Gamma}^2. \quad (21.23)$$

In the case of the width distribution that does not exactly coincide with the PTD, Eq. (21.23) frequently serves as an empirical estimate for the channel number [13].

The estimates discussed above should be applied for each class of states with given spin and parity. The parameter v found in this way is usually a number less than 5. This confirms the ideology related to the process going through few transition states at the saddle point.

21.4 Photofission

Another process that can be used for exciting the nucleus to (or above) the fission barrier is electromagnetic radiation. The photon absorption by the nucleus in the ground state can produce fission even below the neutron separation threshold. It is sufficient to excite the target nucleus close to the saddle point when the tunneling, Problem 21.1, becomes sufficiently probable.

Problem 21.6 Consider a process of photofission if the photon energy is close to the threshold (the nucleus is excited only slightly higher than the top of the fission barrier). What is the preferential direction of the fission fragments? Assume axially symmetric deformation of the even–even nucleus at the barrier and the E1 character of the photoabsorption.

Solution

The lowest states of the axially deformed nucleus have the $K = 0$ quantum number of the total spin projection on the symmetry axis. On the other hand, the dipole photoabsorption brings in the angular momentum projection ± 1 along the photon momentum (analog of the photon helicity). Therefore, the direction of the deformation symmetry, and hence of the fission products, is in average perpendicular to the photon direction. In other words, in such a process, the fission direction is defined by the electric field of the incident photon. The cone is broadened with the increase of the photon energy when the transitional states with higher values of the K quantum number become accessible.

The formal consideration allows us to express the angular distribution of the fission fragments in terms of the Wigner D -functions (Section 16.3). Under a simple assumption that the fission proceeds mainly in an axially symmetric way, as we did in Problem 21.6, and the fissioning nucleus keeps constants of total spin J , its projection K onto the symmetry axis, and projection M on the laboratory axis, the angular distribution is determined as

$$W(\theta) \propto |D_{MK}^J(\theta)|^2. \quad (21.24)$$

In the most probable case of *dipole* photoabsorption by an even–even nucleus in its ground state, $J_0 = K = 0$, the fissioning nucleus at the barrier has $J = 1, M = \pm 1$, and we arrive at what was explained earlier in words, the maximum at 90° with respect to the photon beam,

$$W(\theta) \propto |D_{\pm 1 \ 0}^1(\theta)|^2 \propto \sin^2 \theta. \quad (21.25)$$

This was observed experimentally and then explained by A. Bohr.

Typically, the probability of the *quadrupole* photoabsorption is two orders of magnitude lower than that of the dipole process. However, this photoprocess can excite a state $J^{\Pi} = 2^+$ near the barrier that is usually lower than the state 1^- excited in the dipole photoabsorption. Therefore, in some (rather small, ~ 0.5 MeV) interval of energies, the quadrupole process can be important. In this case, the angular distribution of fragments is close to

$$W(\theta) \propto |D_{\pm 1 \ 0}^2(\theta)|^2 \propto \sin^2(2\theta), \quad (21.26)$$

with the maximum at $\theta = 45^\circ$ with respect to the beam. At higher photon energies, many transitional states become available and the angular distribution is averaged close to isotropy. A similar angular averaging takes place also in photofission for odd- A or odd–odd nuclei when the ground-state spin can be coupled in many ways with the photon spin, especially if the target spin is relatively large.

Problem 21.7 Assume that the target nucleus has the ground-state spin $1/2$, while at the barrier, the band with $K = 3/2$ is lower than the band $K = 1/2$. Show that, after the dipole photoabsorption, the advantage for the $3/2$ band leads to the angular distribution peaked forward,

$$\frac{W(0)}{W(\pi/2)} = 2. \quad (21.27)$$

The situation is inverse if the fission proceeds through the band $K = 1/2$; it becomes more uniform if both bands contribute.

21.5 Fission as a Large-Amplitude Collective Motion

In order to obtain at least a qualitative description of the fission process, we can use the analogy to the liquid drop, recall the epigraph to this chapter. The drop, starting, as a rule, from the normal ground-state deformation, proceeds through the sequence of more deformed shapes to the saddle point. This process is relatively slow and we

can use the ideas of adiabatic collective motion parameterized by the shape characteristics $\{Q_i\}$. The shape variables are considered to be slow compared to single-particle motion. In the simplest approximation, we can assume that the dynamics is described just by the few shape variables which can be considered as an additional restriction on the motion of the particles. In order to avoid introduction of extra dynamic variables, the self-consistency conditions have to be imposed, namely, that these collective variables are average multipole parameters of the slowly evolving distribution of particles.

In fact, this philosophy of large-amplitude global motion is not much different from what we have used earlier in Chapters 5, 6, and 12, in our discussion of collective motion of small amplitude. While considering nuclear deformations, we still have to take into account only low multipolarities, $\lambda \leq A^{1/3}$, approximately 6 in heavy nuclei, Eq. (5.15). However, the calculational procedure is much more involved owing to the large amplitude. Only close to the bottom of the potential well or to the top of the barrier, the quadratic approximation with respect to the deformation parameters, as used in Eq. (21.1), can make sense.

The operators of collective variables \hat{Q}_i can be introduced with corresponding Lagrange multipliers into the Hamiltonian of particles [14]. We recall what we have discussed for the generator coordinate method in Section 18.9. The Hamiltonian acquires the form

$$H(Q) = H_0 - \sum_i \kappa_i \hat{Q}_i, \quad (21.28)$$

where H_0 is the microscopic many-body Hamiltonian, and the Lagrange multipliers κ_i are to be found from the requirement that the expectation values $\langle \hat{Q}_i \rangle$ take given values Q_i . The eigenstates of $H(Q)$ are similar to the Nilsson single-particle levels (Section 12.12), as a function of deformation parameters. However, they are *many-body* quantum states and the physical values of collective parameters are to be determined self-consistently. In practical terms, the operators \hat{Q}_i can be multipole moments of the deformed nucleus going through large-amplitude collective motion.

In the time-dependent formulation [QP, II, 1.5], we start with the Schrödinger equation

$$i\hbar \frac{\partial \Psi}{\partial t} = H(Q(t))\Psi. \quad (21.29)$$

At fixed collective parameters, we have a complete orthonormal set of instantaneous wave functions $\Psi_\alpha(Q(t))$ with “energies” $E_\alpha(t)$. The full solution is given by a superposition

$$\Psi(t) = \sum_\alpha C_\alpha(t) \Psi_\alpha e^{-(i/\hbar) \int^t dt' E_\alpha(t')}. \quad (21.30)$$

The time dependence of the amplitudes comes from the evolving deformation,

$$\dot{C}_\alpha = \dot{Q} \sum_{\alpha'} C_{\alpha'} \left(\frac{\partial}{\partial Q} \right)_{\alpha\alpha'} e^{-(i/\hbar) \int^t dt' (E_{\alpha'} - E_\alpha)}, \quad (21.31)$$

where, for simplicity, we use just a single parameter Q ; the generalization for many parameters is straightforward. The matrix elements of $\partial/\partial Q$ are taken for instantaneous wave functions.

We are interested in slow (*adiabatic*) motion along collective coordinates. Starting with the state Ψ_{α_0} , we can try to use the perturbation theory valid for a smooth change of collective parameters. Then [QP, II, 1.5]

$$C_\alpha = i\hbar \dot{Q} \frac{(\partial/\partial Q)_{\alpha\alpha_0}}{E_\alpha - E_{\alpha_0}} e^{-(i/\hbar)\int^t dt' (E_{\alpha_0} - E_{\alpha'})}, \quad (21.32)$$

The energy of collective motion is changing owing to the corresponding evolution of internal particle distribution being given by the effective collective Hamiltonian

$$H_{\text{coll}} = \sum_\alpha |C_\alpha(t)|^2 E_\alpha(t) = E_{\alpha_0}(Q) + \frac{1}{2} B(Q) \dot{Q}^2. \quad (21.33)$$

The mass parameter $B(Q)$ can be written in two equivalent forms [QP, I, 19.5]:

$$B(Q) = 2\hbar^2 \sum_\alpha \frac{|(\partial/\partial Q)_{\alpha\alpha_0}|^2}{E_\alpha - E_{\alpha_0}} = 2\hbar^2 \sum_\alpha \frac{|(\partial H_{\text{coll}}/\partial Q)_{\alpha\alpha_0}|^2}{(E_\alpha - E_{\alpha_0})^3}. \quad (21.34)$$

This result can also be applied to the collective rotation of a deformed nucleus at normal deformation; in fact, this mass parameter gives the cranking-model moment of inertia (Sections 16.18 and 16.19).

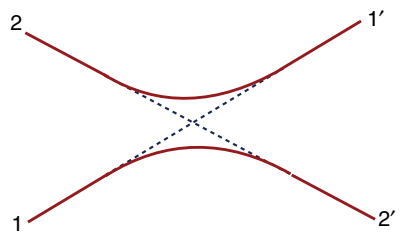
It is easy to understand that, in the fission process, the influence of pairing becomes effectively stronger when the nucleus traverses regions of greater deformation – this is due to the growing level density [15]. If we identify the collective parameter Q with quadrupole deformation and try to compare the mass coefficient in Eq. (21.33) with the mass parameter for low-lying quadrupole oscillations, we have to take into account that the big deformation is mixing the single-particle states with the energy difference of two oscillator shell $2\hbar\omega_0$, while the lower limit of the energy summation (integration) is $\sim 2\Delta$. Then we see that the corresponding mass parameter is bigger than for low-lying vibrations by the factor $\sim (1/4)(\hbar\omega_0/2\Delta)^2$. This confirms the slow character of motion, especially in the vicinity of the saddle point.

In spontaneous fission of an axially deformed nucleus, the K quantum number may still approximately be conserved. For fission of an even–even nucleus, the lowest adiabatic trajectory has a large probability to keep full pairing up to the scission point. The lowest adiabatic trajectory for odd- A nuclei is higher by the pairing energy which is responsible for the greater time for spontaneous fission. It is necessary to mention that the whole approach with collective variables (and there are several of them in a realistic treatment) is very involved computationally, see, for example, Ref. [16].

21.6 Nonadiabatic Effects and Dissipation

In the extreme adiabatic process, the quantum system moves along the lowest trajectory in the space of collective parameters. The wave function of the system smoothly changes during this process. Because the collective parameters are self-consistently determined by the particle distribution (this is the gradual change of the wave function described in the previous section), the intrinsic character of the state evolves but the ground state remains ground and so on. Certainly, this picture is valid only in a fully adiabatic evolution.

Figure 21.4 Quasicrossing of two energy terms as a function of the interaction parameters.



If an energy term for a given state turns out to be close in energy to another term, the probability of their mixing grows. The mixing is possible if the terms have the same values of exact constants of motion, in the evolution of a fissioning nucleus these constants are J, M and parity (also the K quantum number in an axially symmetric process). We mentioned this phenomenon in the discussion of the Nilsson scheme of single-particle terms in a function of deformation parameters (Section 12.12). Now we are following the evolution process of a many-body system but quantum mechanics works in a similar way. At close contact of two energy terms of the same symmetry, there is a chance of a real transition.

If the previous evolution proceeded along the lowest term, in the vicinity of the contact, the actual state becomes a superposition of two close terms. There is no real crossing if there is a mixing interaction, the terms repel each other so that the minimal approach distance is decided by a matrix element of this interaction [QP, I, 10.5]. However, in this area, the states mix and lose their individuality. In the motion beyond this quasicrossing point, the system can move along any trajectory (Figure 21.4). The lowest path $1 \rightarrow 2'$ corresponds to the adiabatic motion when the system continues to live in the less energetic state which however now has a wave function $|2\rangle$ as a continuation of the trajectory that was higher before the crossing. The *diabatic* path $1 \rightarrow 1'$ after the crossing corresponds to the previously lower state that continues its motion keeping the same function but being now higher in energy. The geometric picture of quasicrossing becomes more complicated in the case of many collective parameters [17] when multidimensional surfaces can cross.

In the evolution driven by the collective parameter $Q(t)$, the effective two-dimensional Hamiltonian $\mathcal{H}(t)$ including only these two close states, has a characteristic form

$$\mathcal{H}(t) = \begin{pmatrix} E_1(t) = E_0 + \kappa_1 [Q(t) - Q_0] & V \\ V^* & E_2(t) = E_0 + \kappa_2 [Q(t) - Q_0]. \end{pmatrix}. \quad (21.35)$$

Here the point $t = 0$ with collective coordinate Q_0 and energy E_0 corresponds to the crossing that would happen in the absence of the mixing interaction V . The probability of a jump between the trajectories is similar to the tunneling probability through a classically forbidden potential region. If the collective velocity can be approximated by a constant \dot{Q} in the vicinity of the crossing point, the jump probability is given by the Landau–Zener formula [QP, II, 1.6]

$$P_{12} = P_{21} \approx e^{-(2\pi/\hbar)|V|^2/|\dot{Q}(\kappa_1 - \kappa_2)|}. \quad (21.36)$$

The adiabatic evolution is a good approximation only if P_{12} or $(|\dot{Q}|)$ is small. In the opposite case, we have many crossings and frequent jumps between intrinsic states. Then the whole description can be simplified to the situation similar to a *random walk*.

with the system frequently jumping up or down. The result is diffusion over the levels so that the changes of internal energy are roughly proportional to time,

$$\overline{(\delta E)^2} \Rightarrow 2D t, \quad (21.37)$$

where the diffusion coefficient D is determined by the average value of the level density ρ , jump probability (21.36), and the number of crossings $(dc/dQ)\dot{Q}$ per unit time,

$$2D = \overline{\rho^2 P_{12}(dc/dQ)\dot{Q}}. \quad (21.38)$$

For validity of the adiabatic approximation with rare individual quasicrossings, the residual interaction V has to be sufficiently weak, as well as the typical deformation velocity \dot{Q} . A simple sliding from the saddle point without excitation usually has a low probability.

In general, multiple crossings with their probabilities of violation of adiabaticity during large-amplitude shape evolution lead to partial damping of collective motion. The collective energy partially goes to excitation of intrinsic degrees of freedom which is equivalent to increase of effective temperature. Then the problem becomes similar to that of Brownian motion. The collective degrees of freedom feel frequent fluctuations which we described above as level crossings. The averaging of these jumps, Eq. (21.38), can be described by stochastic differential equations of the Langevin type, with a random force [18].

One of the modern approaches [19] formulates the consideration of multidimensional dynamics accompanied by dissipation. Technically, it is realized as the set of dynamic equations for collective variables Q_i governed by the driving forces from deformation, shell effects and pairing, and the Langevin random force $F(Q, \dot{Q}) = \bar{F} + f$. The mean value \bar{F} of this force (averaged over fast changes, in fact, over the level crossings) plays the role of friction (viscosity) proportional to \dot{Q} ; the fluctuations are assumed to be delta-correlated,

$$\overline{f(Q, t)f(Q, t')} = C(Q)\delta(t - t'). \quad (21.39)$$

This approximation assumes that the whole process is *Markovian* where the memory of previous motion is immediately forgotten. This Brownian shape evolution allows one to predict, with a complicated computation, the charge distributions for many fissioning nuclei. The questionable feature of this and other similar approaches is just in the delta-force (21.39). If the evolution excites collective modes, which is almost certainly occurring, they keep significant memory and create after-action, which was neglected in the Langevin formulation.

21.7 Fission Isomers

This phenomenon was experimentally discovered in Dubna by Polikanov *et al.* [20] and, after further studies, explained by Strutinsky [21]. Earlier, we referred to the fission barrier that separates the normal ground-state deformation of the nucleus from the transition state (“*saddle point*”) leading later on to scission.

We know (Chapter 12) that nuclear deformation is related to the shell structure of nuclei emerging from the balance of the nucleon shell energy diminished by the core polarization. The liquid drop description (Chapter 5) assumes the smooth change of

particle occupancies from one nucleus to another. This description loses the shell effects which can be restored by the so-called *shell correction*, the difference of the sum of single-particle energies of occupied orbitals and the energy of the smooth occupation corresponding to the average single-particle level density [22]. The shell correction, in a simplified form, adds necessary effects to the smooth mass formula that follows from the traditional liquid drop description.

The semiclassical limit of the shell structure (Section 8.10) is related to the resonances between different degrees of freedom of single-particle motion. The simplest oscillator-like shell structure has equal frequencies of motion along different directions. At increasing deformation, new resonances appear, creating the new stabilized shell structure. The simplest resonances of this type correspond to the ratios of axes 2:1 and 3:1, compare Figure 12.5 and [QP, I, Figure 11.4]. In the course of increasing deformation during the fission process, the nucleus will traverse the regions with such resonance conditions. At an appropriate number of particles, this would correspond to a “second potential well,” first of all at *superdeformation* 2:1. There are two main ways out from the second well – either to continue the fission process by overcoming the right-hand side (second barrier) of the deformation potential or to radiate photon(s) and return to the states of normal deformation. However, the gamma-transitions to the first potential well are strongly suppressed by the very different shell structure and therefore quite small overlap of the many-body wave functions. Therefore, there should be cases when the nucleus will continue its way to fission after living for a considerable time in the second well.

This is exactly what was found in the experiments. The first discovery was that of the isomeric state in the odd–odd isotope ^{242}Am that revealed spontaneous fission as the main decay mode with lifetime of 14 ms. For the neighboring isotope ^{241}Am , the half-life is 2×10^4 years. The bottom of the second well corresponds to excitation energy of about 3 MeV, while the second barrier has approximately the same height as the first one. The isomeric effect cannot be explained by the large spin of the excited state as the gamma-transition would then be allowed to known lower excited states in ^{242}Am having spins 11 and 12. In addition, the neutron reaction, $(n, 2n)$ with 14 MeV neutrons in this case, is not capable of populating such large spins. Therefore, the spin of the isomer cannot be much greater than the ground-state spin. Many fission isomers with lifetimes from milliseconds to nanoseconds have been found and studied, but the experiments are difficult as the ratio of isomeric to normal fission events is typically only 10^{-4} [3, 23]. In Figure 21.5, the threshold effect in the $(p, 2n)$ reaction populating the isomeric state in ^{237}Am is shown, which allows to determine the excitation energy of the isomeric state.

Both the first and the second well have their own vibrational and rotational structure as illustrated in Figure 21.6, which shows the ^{240}Pu example. The moment of inertia of the second well is approximately twice as large as that in the ground-state band. There are some indications that even the third well may exist with *hyperdeformation* and the axis ratio 3:1. With excitation energy increasing, the mixing of superdeformed and normal bands grows because the excited states of normal deformation can acquire tails penetrating far into the superdeformed region so that the isomers disappear, getting a chance to decay by radiation into the well of normal states. In agreement with the explanation above, the fission isomers are frequently called *shape isomers*.

The calculation of the fission lifetime at energy below the height of the barriers includes a cumbersome quantum-mechanical problem of tunneling through two

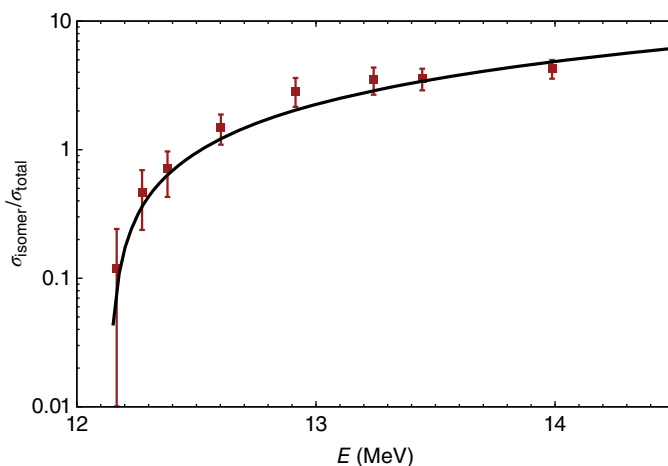


Figure 21.5 Ratio of the delayed to prompt fusion cross section for the isomer in ^{237}Am excited in the $^{238}\text{Pu}(p, 2n)$ reaction [24]; the threshold for isomeric excitation is clearly seen. The solid line shows the linear fit near the threshold.

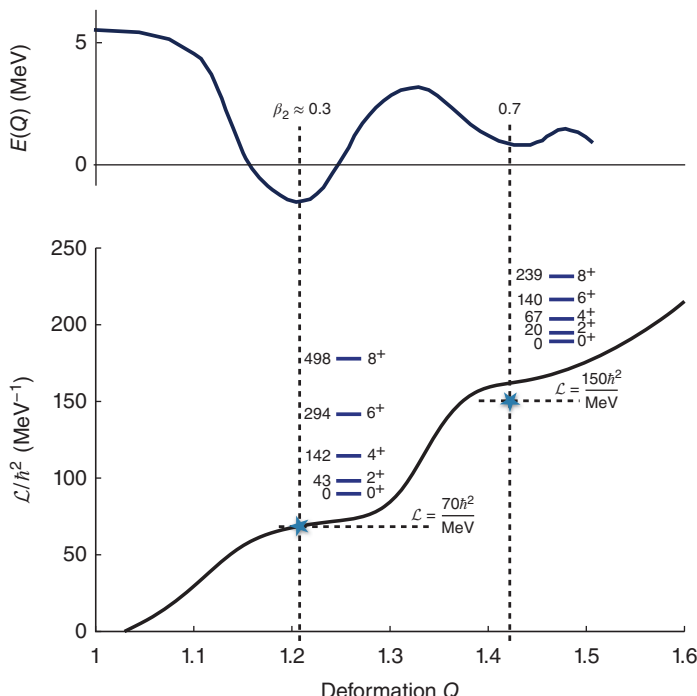


Figure 21.6 The deformation energy, Eq. (21.46), (upper plot) and the moment of inertia, Eq. (16.214), (lower plot) are shown as a function of deformational elongation Q . Vertical lines show approximate values of the quadrupole β_2 parameter for the ground and isomeric states in ^{240}Pu . Rotational bands in both wells are also shown along with the corresponding moments of inertia indicated by the horizontal grid lines. Stars indicate locations of ground and isomeric states.

barriers with the potential well in between. This requires a generalization of the semiclassical theory [QP, I, Ch. 15] but the important part of such a theory is the knowledge of the effective mass parameter for the fission coordinate (or coordinates) as the shape of the nucleus evolves in the process. The fully satisfactory theory has to account for the coupling of the fission coordinate to intrinsic (quasiparticle) degrees of freedom and corresponding dissipation of collective energy as mentioned in Section 21.6. Apparently, the restructuring of pairing plays an essential role in this process. The full theory is still absent. In the following, we briefly describe the shell correction method which is a semiclassical picture of the finite Fermi system with a slowly evolving shape [21, 22].

Having in mind the network of single-particle orbitals $|\lambda\rangle$ moving as a function of mean-field deformation parameters $\{Q\}$, one can find the sum of single-particle energies $\epsilon_\lambda(Q)$ occupied by the particles,

$$E_{\text{s.p.}}(Q) = \sum_{\text{occ}} n_\lambda \epsilon_\lambda(Q), \quad (21.40)$$

where n_λ are the occupancies of adiabatic orbitals. Certainly, this is not the total energy of the nucleus at a given deformation. In particular, the comparison with the Hartree–Fock approximation (Section 17.2) shows that the interaction part of the self-consistent field is counted twice. But this energy is related to the density of single-particle states near the Fermi surface. We can recall magic nuclei which are more stable with respect to the perturbation acting on individual nucleons. The actual deformation comes only at a certain degree of occupation of upper shells when the level density at the Fermi surface is large, which can lead to restructuring in the direction of deformation. An even simpler analogy can be found in solid-state physics. A weak electric field cannot excite a current in insulators where a gap exists between the lowest occupied and highest empty electron orbitals. But an electric current appears in metals where there is no such gap. It is important that single-particle orbitals change with the deformation and new gaps appear and disappear.

The single-particle level density can be defined for any set of deformation parameters,

$$v(\epsilon; Q) = \sum_\lambda \delta(\epsilon - \epsilon_\lambda(Q)). \quad (21.41)$$

The next step is to smooth out this set of δ -peaks, folding it with an averaging factor $g(\epsilon - \epsilon')$, for example, Gaussian (but not necessarily) with the width σ covering few single-particle orbitals, in practice maybe 1–2 MeV,

$$v(\epsilon; Q) \Rightarrow \bar{v}(\epsilon; Q) = \int_{-\infty}^{\infty} d\epsilon' v(\epsilon; Q) g(\epsilon - \epsilon'). \quad (21.42)$$

In addition to this, a broader smoothing is introduced in the same way but with the averaging function $\tilde{g}(\epsilon - \epsilon')$ that has a width up to 10 MeV,

$$\tilde{v}(\epsilon; Q) = \int_{-\infty}^{\infty} d\epsilon' v(\epsilon; Q) \tilde{g}(\epsilon - \epsilon'). \quad (21.43)$$

The second averaging creates a smooth function \tilde{g} where the whole shell structure is already smeared and no oscillations are present. The shell structure emerges [25] as a difference,

$$\delta v(\epsilon; Q) = \bar{v}(\epsilon; Q) - \tilde{v}(\epsilon; Q), \quad (21.44)$$

with shell gaps corresponding to the negative values of δv .

According to the shell correction prescription, the full energy corresponding to the deformation parameters $\{Q\}$ can be evaluated adding the shell correction to the energy of the liquid drop model (LDM)

$$\Delta E(Q) = \int^{\mu_0} d\epsilon \ \epsilon v(\epsilon, Q) - \int^{\mu} d\epsilon \ \epsilon \tilde{v}(\epsilon, Q). \quad (21.45)$$

Both chemical potentials, μ_0 and μ , are to be estimated from the total particle number; the level densities take into account the pairing factors and both kinds of nucleons. Finally, the total deformation energy is found as a sum of the LDM energy and the shell correction (21.45),

$$E(Q) = E_{\text{LDM}}(Q) + \Delta E(Q). \quad (21.46)$$

The subtraction in Eq. (21.45) essentially removes the energy of the smooth level occupation that was already accounted for in the LDM.

This approach allows one to qualitatively understand the physics of fission isomers. We interpret them as the consequence of the existence in many fissioning nuclei of the second potential minimum with a larger deformation. As a result, the potential curve becomes double (or even triple) humped. If, after the initial excitation, the nucleus turns out to be in the well between the first and second maxima, the gamma-decay into the normal deformed states is less probable because of the small overlap of corresponding many-body wave functions. The tunneling outside is facilitated by the necessity to overcome only one external barrier (Figure 21.6).

From a more general viewpoint, fission isomers are a particular case of the close coexistence of states with very different spatial structure, shape isomers. Even the deformed 0^+ state at energy 6.06 MeV in ^{16}O can be counted in this category in comparison with the double-magic spherical ground state of oxygen. The neutron-deficient isotope ^{186}Pb has three low-lying 0^+ states of different shape [26]; many examples are discussed in the review article [27]. The fission mode appearing in the transuranium region makes shape isomers into fission isomers. Similarly to the different fission behavior of odd- A and even–even isotopes excited from the ground state, the fission half-life of the odd isotopes is usually by few orders of magnitude longer than that of the even ones. We have however to mention that various cases of heavy fissioning nuclei have their individual features which require detailed experimental information accompanied by specific complicated calculations.

21.8 Parity Violation in Fission

Nuclear and electromagnetic interactions conserve parity. This puts certain limitations on various symmetries seen in nuclear processes. But the weak interactions are known to violate parity as will be discussed in a Chapter 24. An interesting question, however, is whether some violations of parity can be observed in fission. The first desire is to answer in negative – the weak interactions are indeed quite weak, whereas fission is essentially a macroscopic process governing the motion of hundreds of nucleons. This answer turns out to be wrong as shown by experiments [28]. Here we follow the logics of the article [29] where the first experiments were discussed. We will also give references to later experiments which are very convincing.

The strength of the weak interaction of nucleons is determined by the Fermi constant G_F ,

$$\frac{G_F}{(\hbar c)^3} = 1.1663787(\pm 6) \times 10^{-5} \text{ GeV}^{-2}. \quad (21.47)$$

The parity-violating effect on a nucleon inside the nucleus is described by the effective Hamiltonian

$$H_{\text{weak}} \sim G_F \frac{(\boldsymbol{\sigma} \cdot \mathbf{p})}{2m} \rho(\mathbf{r}), \quad (21.48)$$

which is the only time-reversal invariant *pseudoscalar* that can be built using spin and momentum operators. This is the largest possible effect being proportional to the total nuclear density $\rho(\mathbf{r})$ at the position of the nucleon. Being considered as a perturbation, this term, summed over nucleons, generates in a standard nuclear wave function a small component of opposite parity. In perturbation theory, we have to compare the typical matrix elements of the operator (21.48) with the characteristic distance between the unperturbed levels of opposite parity. For the single-particle operator and states at normal deformation, the parity partners usually belong to the next oscillator shell so that the energy denominator in perturbation theory would be of the order of oscillator frequency, at least several megaelectronvolts. With the weak constant (21.47), the admixture of opposite parity is expected here to be on the level of 10^{-7} to 10^{-8} .

The large observed effect comes from the *statistical*, or *chaotic* enhancement. In the “hot” compound nucleus with very complicated quasistationary wave functions emerged after neutron capture, the high level density contains states of both parities which can be populated as *s*- and *p*-wave neutron resonances. The corresponding level spacings that can serve as an energy denominator in perturbation theory are therefore of the order of electronvolts. This means that the perturbations can be strongly enhanced owing to the very high level density. However, the real question is in the mixing matrix element – we expect it to be quite small because of the very complicated, almost random, nature of compound states. A rough estimate shows that the small denominators win, bringing as a result strongly enhanced action of perturbation.

The main line of the reasoning goes as follows. The compound wave function $|\alpha\rangle$ is an extremely complex combination (21.14) of a large number $N \gg 1$ of “simple” (mean-field) states $|k\rangle$, as we used in the discussion of the Porter–Thomas distribution. The typical amplitude of individual components is $1/\sqrt{N}$. Consider a matrix element $F_{l\alpha}$ of a simple (one-body or two-body) operator F between such a state and one of the basis (mean-field) states $|l\rangle$. Because of its single-particle nature and always present angular momentum restrictions, this operator can connect $|l\rangle$ with only few, say, v , simple components in the chaotic wave function $|\alpha\rangle$. If nonzero matrix elements F_{lk} are on average estimated as f , we have

$$\langle l|F|\alpha\rangle = \sum_k C_k^\alpha F_{lk} \sim \frac{vf}{\sqrt{N}}. \quad (21.49)$$

We see the chaotic suppression $\propto N^{-1/2}$. Now let us consider a matrix element between two complicated states, for example, neutron resonances,

$$\langle \alpha'|F|\alpha\rangle = \sum_{lk} C_l^{\alpha'} C_k^\alpha F_{lk}. \quad (21.50)$$

Again, the single-particle selection rules for given k leave in average v nonzero contributions $F_{lk} \sim f$. The amplitudes C and C' here are of the order $1/\sqrt{N}$. The remaining sum over k of the pairwise products of $C'C$ is *incoherent* (this is a great difference from the collective states of Chapter 18) and therefore it is of the order \sqrt{N} instead of N . The resulting estimate of the matrix element (21.50) is again of the same order vf/\sqrt{N} as in (21.49). The general conclusion for perturbation theory is that the mixing of close in energy, $\Delta E \propto 1/N$, chaotic states by simple operators can be *enhanced* by a factor of \sqrt{N} (the effect sometimes called *N-scaling*). In the region of our interest with $N \sim 10^6$, this mechanism (originally called “dynamical,” which is not really appropriate) can provide about three orders of enhancement in mixing for two compound states.

With such estimates we come to the conclusion that the mixing of close compound states of opposite parity can be enhanced by about three orders of magnitude to give effects of the order 10^{-4} . The parity violation should be of a resonance character, being better developed during the long life of the compound state. A small energy uncertainty allows one to consider the time evolution of the individual resonance wave functions. As discussed earlier, the fission process goes through the highly deformed stage when the whole energy is absorbed by the shape variables and only few fission channels are available. The parity violation resulting in a small admixture of opposite parity in the compound stage is kept in the wave function during its almost adiabatic evolution and should be visible in the final fragments. But then we need to have an observational signal of parity violation.

If only momenta of the fission fragments going back to back in the frame of the fissioning mother nucleus are registered, there are no pseudoscalar correlations which would demonstrate parity violation (a pseudoscalar combination of three momenta including the momentum of the starting neutron would violate time-reversal invariance). We need some spin asymmetries. Convincing experiments are performed with longitudinally polarized neutrons. The correlation of the neutron spin with the fragment momentum, $(\sigma_n \cdot \mathbf{p}_f)$, is a good signal for parity violation. Indeed, the presence of such an additional term along with the main, independent of neutron spin, part of the fission cross section shows the asymmetry of fragment motion that changes sign under spatial inversion (different probability of the fragment motion along and against the neutron spin). It is quite impressive that the direction of an individual neutron spin can influence almost macroscopic motion.

The Grenoble experiments [30] confirm the physics of the phenomenon. The asymmetry of the fragments with respect to the helicity of the starting neutron is on the level between 10^{-3} and 10^{-4} in agreement with our estimates. What is important, this asymmetry is practically the same for all masses of the fragments and independent of kinetic energy distribution (Figure 21.7). Indeed, the weak interactions create parity mixing enhanced by the high level density at the “hot” compound stage and the following nuclear evolution through fission channels and real scission just keeps this admixture unchanged. The result here is on the same level as some parity-conserving correlations. Equally spectacular are the results of experiments [31, 32] measuring just the total cross sections of interaction of longitudinally polarized neutrons with heavy nuclei. With parity conserved, the cross sections for neutrons of opposite helicity, σ_{\pm} , are to be equal.

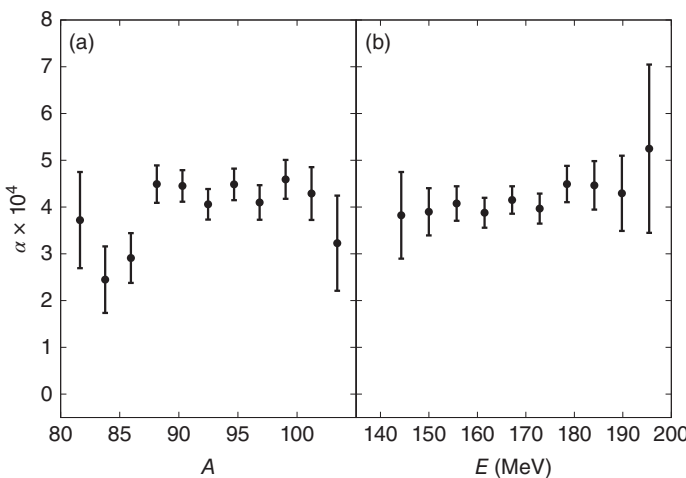


Figure 21.7 The fragment asymmetry in various fission events with different mass (a) or kinetic energy (b) distributions, found in the experiment [30].

The experiment shows that they are not,

$$\mathcal{P} = \frac{\sigma_+ - \sigma_-}{\sigma_+ + \sigma_-} \neq 0. \quad (21.51)$$

This effect, which can be seen by the naked eye, is shown in Figure 21.8 for ^{238}U . The table alongside shows that the difference of cross sections is noticeable only at energies of neutron resonances where the asymmetry \mathcal{P} is on the level 10^{-2} ; it reaches the 10% level in lanthanum. As discussed, we need an almost stationary wave function of a given resonance. The reason for further enhancement over and above the chaotic effect discussed earlier is the resonance character of the event: the neutron is absorbed in a

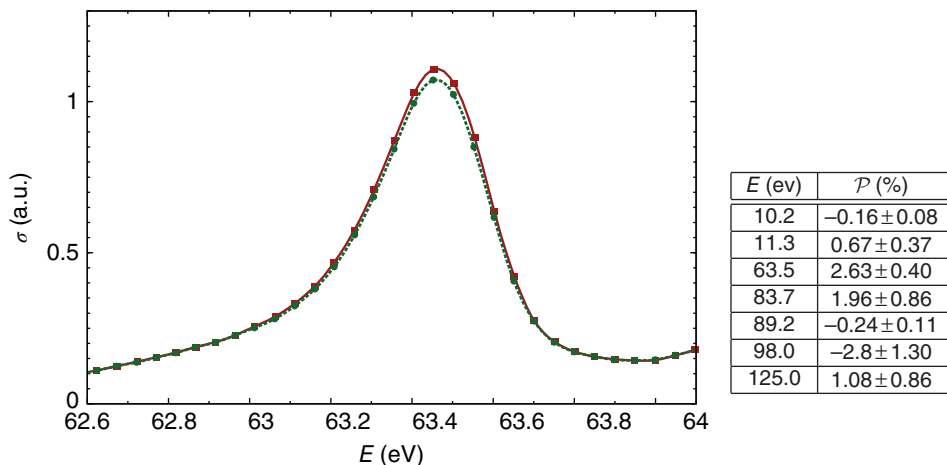


Figure 21.8 The absorption peak around 63.5 eV resonance in the transmission of polarized neutrons of two helicity states in ^{238}U . The table on the right summarizes asymmetries observed for various resonances, see Refs. [33, 34].

p-wave resonance but, after parity mixing, can be reemitted in the *s*-wave. The standard factor of the *s*-wave radial amplitude, $\Gamma_s/\Gamma_p \sim (kR)^2$ adds two orders of magnitude to the chaotic enhancement. Such a kinematic factor is absent in the fragment asymmetry.

Chaotic enhancement works in many processes where mixing is necessary of states of different nature at high level density, for example, in gamma-transitions between the superdeformed states and the states at normal deformation [35], or in excitation of nuclear isomers [36] unrelated to fission. In the last example, the isomer can live for a very long time because of a big spin or/and structure difference with lower states that forbids a gamma-radiation. For artificial deexcitation, the isomer should be excited to the chaotic region where the mixing and therefore decay become possible. As mentioned in Chapter 16, the best example is given by the rarest natural isotope ^{180}Ta with spin 9/2 and excitation energy only 75 keV that cannot undergo radiation transition to the ground state with spin 1/2 and very different *K* quantum number, so its lifetime is 10^{15} years, while the ground state undergoes beta-decay with the lifetime of 8 h.

References

- 1 J.J. Griffin, Phys. Rev. **116**, 107 (1959).
- 2 P. Möller, D.G. Madland, A.J. Sierk, and A. Iwamoto, Nature **409**, 785 (2001).
- 3 S. Bjørnholm and J.E. Lynn, Rev. Mod. Phys. **52**, 725 (1980).
- 4 F.A. Janouch and R. Liotta, Phys. Rev. C **27**, 896 (1983).
- 5 S.G. Kadmensky, Z. Phys. A **312**, 113 (1983).
- 6 R.A. Sen'kov and V.G. Zelevinsky, Phys. At. Nucl. **74**, 1296 (2011).
- 7 J. Kasagi *et al.*, Phys. Rev. Lett. **79**, 371 (1997).
- 8 N. Takigawa, Y. Nozawa, K. Hagino, A. Ono and D.M. Brink, Phys. Rev. C **59**, R593 (1999).
- 9 V.V. Flambaum and V.G. Zelevinsky, Phys. Rev. Lett. **83** (1999) 3108.
- 10 A. Akhiezer and I. Pomeranchuk, *Certain Problems of Nuclear Theory*, 2nd edn, Gostekhizdat, Moscow, 1950.
- 11 N. Bohr, Phys. Rev. **58**, 864 (1940).
- 12 C.E. Porter and R.G. Thomas, Phys. Rev. **104**, 483 (1956).
- 13 L. Wilets, Rev. Mod. Phys. **30**, 542 (1958).
- 14 A.K. Kerman, Ann. Phys. **12**, 300 (1961).
- 15 L. Wilets, *Theories of Nuclear Fission*, Clarendon Press, Oxford, 1964.
- 16 P. Möller, J. Randrup, and A.J. Sierk, Phys. Rev. C **85**, 024306 (2012).
- 17 D. Hill and J. Wheeler, Phys. Rev. **89**, 1102 (1953).
- 18 N.G. Van Kampen, *Stochastic Processes in Physics and Chemistry*, Elsevier, Amsterdam, 1992.
- 19 J. Randrup and P. Möller, Phys. Rev. C **88**, 064606 (2013).
- 20 S.M. Polikanov *et al.*, Sov. Phys. JETP **15**, 1016 (1962).
- 21 V.M. Strutinsky, Nucl. Phys. **A95**, 420 (1967).
- 22 M. Brack and R.K. Bhaduri, *Semiclassical Physics*, Addison-Wesley, Reading, MA, 1997.
- 23 A. Michaudon, Adv. Nucl. Phys. **6**, 1 (1973).
- 24 S.M. Polikanov and G. Sletten, Nucl. Phys. **A151**, 656 (1970).
- 25 V.M. Strutinsky, Nucl. Phys. **A122**, 1 (1968).

- 26 A.N. Andreev *et al.*, Nature **405**, 430 (2000).
- 27 K. Heyde and J.L. Wood, Rev. Mod. Phys. **83**, 1467 (2011).
- 28 G.V. Danilyan, Sov. Phys. Usp. **23**, 323 (1980).
- 29 O.P. Sushkov and V.V. Flambaum, Sov. Phys. Usp. **25**, 1 (1982).
- 30 A. Koetzle *et al.*, Nucl. Instrum. Methods A **440**, 750 (2000).
- 31 V.P. Alfimenkov *et al.*, Nucl. Phys. **A398**, 93 (1983).
- 32 J.D. Bowman, G.T. Garvey, M.B. Johnson, and G.E. Mitchell, Annu. Rev. Nucl. Sci. **43**, 829 (1993).
- 33 B.E. Crawford *et al.*, Phys. Rev. C **58**, 1225 (1998).
- 34 G.E. Mitchell, J.D. Bowman, and H.A. Weidenmüller, Rev. Mod. Phys. **71**, 445 (1999).
- 35 J.-Z. Gu and H.A. Weidenmüller, Nucl. Phys. **A660**, 197 (1999).
- 36 N. Auerbach and V. Zelevinsky, Phys. Rev. C **90**, 034315 (2014).

22

Heavy-ion Reactions: Selected Topics

The atomic nucleus is the playground of quantum mechanics and is probably the most complex system in the whole of physics. The richness of phenomenon and variety of structure within atomic nuclei is such that no single theoretical model can describe all nuclei.

J.S. Al-Khalili, *Nucl. Phys.* **A751**, 469 (2005).

22.1 Introduction

Heavy-ion reactions are currently in the mainstream of experimental efforts in nuclear science. This area of studies is very important as leading nuclear laboratories are interested in the production of isotopes outside the valley of stability, the so-called exotic nuclei, and heavy-ion collisions provide one of the most efficient paths to this goal. The related physics and astrophysics are very broad and cannot be covered here.

In this chapter, we discuss the interactions between complex nuclei which are sufficiently “large” systems and frequently can be described with the help of macroscopic and statistical concepts. One example of such a theory we have already seen when we briefly considered the Coulomb excitation (Section 15.8): the colliding nuclei being repelled by their electric charges move outside the range of nuclear forces and therefore their relative motion can be approximately described with the use of classical hyperbolic trajectories. Intrinsic excitations of the colliding nuclei by time-dependent Coulomb forces have to be studied quantum-mechanically, referring to nucleon degrees of freedom, both single-particle and collective. At energies around and above the Coulomb barrier, such a clear segregation of global and internal degrees of freedom is impossible and the problem becomes more complicated but also more interesting.

With heavy ions, our consideration should include statistical elements as it is usually difficult and frequently not necessary to consider all individual microscopic quantum states involved in the process. On the other hand, to a great extent, the statistical ideas utilized in such an analysis have an intuitive origin, being not strictly justified from first principles.

For example, the colliding heavy nuclei can fuse; this opens the road to statistical equilibration that can lead to the formation of a compound nucleus or, at least, of a temporary existing double-nuclear system. We can try to formulate rough criteria of applicability of statistical arguments. The typical quantum states of the double system are not stationary,

they can be characterized by the notion of widths: the *spreading width*, Γ^\downarrow , and the *decay width*, Γ^\uparrow . The decay width refers to the probability of return to one of the many open continuum channels. The spreading width describes the process of mixing the entrance configuration with more and more complex states of intrinsic motion – the process we would identify with proper thermodynamic equilibration. The spreading width shows the energy interval covered by the expansion of the initial wave function over stationary states of the Hamiltonian. One can speak of statistical equilibrium if both widths are greater than the spacings $D(E)$ between stationary states. This means that the density of states of the system, $\rho(E) = 1/D(E)$, has to be sufficiently high.

As in the fission problem (Chapter 21), we can translate such arguments into the language of time evolution. The decay width determines the lifetime, $t^\uparrow \sim \hbar/\Gamma^\uparrow$, of the compound nucleus, while $t^\downarrow \sim \hbar/\Gamma^\downarrow$ corresponds to the characteristic time of establishing statistical equilibrium between various degrees of freedom. The intrinsic temporal scale of a system is measured by the *Weisskopf time*, $\tau \sim 2\pi\hbar/D$, a period of quantum beats for a wave packet formed in a given energy region (an analog of the classical return time). These ideas have been used for fission near the ground state as well. According to such loose arguments, for equilibrium, it is necessary to have both t^\uparrow and t^\downarrow to be much shorter than τ , while the relation between rates of decay and spreading is not fixed by these inequalities. But it is clear that only at $\Gamma^\downarrow \gg \Gamma^\uparrow$ or $t^\downarrow \gg t^\uparrow$, we can speak of statistically equilibrated system, while in the opposite case the preequilibrium decay dominates. The existence of processes intermediate between direct reactions and compound reactions leads to the problem of *nuclear kinetics*.

22.2 Experimental Indications

As an example of typical dynamics, we consider heavy-ion scattering processes at the projectile energy 5–10 MeV per nucleon, which means several hundred megaelectron-volts for a medium nucleus. At collision, we can observe the transfer of few nucleons, mutual excitation of the projectile and the target, formation and departure of various fragments, and fusion (full or temporary) when the kinetic energy of the relative motion partially or completely is transformed into “heat,” namely, intrinsic excitations.

Usually, only average information is accessible concerning intrinsic nuclear states. If the final fragments are detected, the experimenter may know their charges and mass numbers; and their energies and angular distributions (but sometimes only specific combinations of such observables). One can distinguish elastic, quasielastic, and deep-inelastic processes. In quasielastic reactions, the main effect comes from the Coulomb interaction, whereas the nuclear forces only perturb the trajectories. In deep-inelastic processes, the nuclear forces are responsible for dissipation and drive to equilibrium.

The characteristic length parameters in the problem are (i) the distance of the closest approach in the head-on collision,

$$R_{\min} = \frac{Z_1 Z_2 e^2}{E}, \quad (22.1)$$

where $eZ_{1,2}$ are the charges of the colliding nuclei and E is the energy of relative motion in the center-of-mass frame, if this energy is below the Coulomb barrier; and (ii) the

global radius of the unperturbed double system,

$$R = r_0(A_1^{1/3} + A_2^{1/3}), \quad (22.2)$$

where $A_{1,2}$ are nuclear masses and r_0 is a parameter of the order 1.2–1.5 fm, if the energy is above the Coulomb barrier. The quantum effects in the relative motion are determined by the de Broglie wavelength, $\lambda \sim \hbar/(Mv)$, where M is the reduced mass of two nuclei and v is their relative velocity. In the reactions that we are interested in here, this wavelength is approximately two orders of magnitude smaller than the global radii defined in Eqs. (22.1) and (22.2). Therefore, the scattering can be considered in a semiclassical manner.

The role of nuclear forces grows for smaller values of the orbital momentum

$$\ell = \frac{Mvb}{\hbar}, \quad (22.3)$$

where b is the impact parameter. Then the probability of fusion increases as well. At not very high energy (say, not more than few dozen megaelectronvolt above the Coulomb barrier and for not too heavy nuclei), the fusion happens with considerable probability. A “hot” compound nucleus is formed and what is detected is a set of evaporation fragments or fission products at the end of the life of the compound nucleus. Typical features of the fission process are the fissionlike mass distribution, proximity of the kinetic energy of fragments to the Coulomb energy at the rapture time, and specific angular distributions. In such cases, the total reaction cross section σ_R is close to the cross section σ_{comp} of formation of the compound nucleus.

Classically, one can define σ_R through the value ℓ_{\max} of orbital momentum (or the corresponding value b_{\max} of the impact parameter), when the nuclei with energy E of relative motion still penetrate into the region of mutual attraction. If the total potential barrier is denoted as $V_I = V_{\text{Coul}} + V_{\text{nuc}}$, we can take its maximum, where $dV_I/dr = 0$, as the geometric size R_I that determines the reaction cross section,

$$\sigma_R = \pi b_{\max}^2 = \pi \lambda^2 \ell_{\max}^2 = \pi R_I^2 \left(1 - \frac{V_I}{E}\right). \quad (22.4)$$

The critical orbital momentum is defined by the radial turning point,

$$\frac{\hbar^2 \ell_{\max}^2}{2MR_I^2} + V_I = E. \quad (22.5)$$

The experimental data which extract the interaction radius R_I from the energy dependence of the cross section (22.4) indicate the value to be slightly smaller than the formal radius (22.2) of the double system. It is especially small for magic nuclei. The effective potential is illustrated in Figure 22.4 which we discuss later.

At energy greater than V_I , the compound cross section σ_{comp} gets smaller than σ_R . Most probably, there exists a critical value of orbital momentum, $\ell_{\text{cr}} < \ell_{\max}$, such that for $\ell > \ell_{\text{cr}}$, the overlap of nuclear densities is not sufficient for formation of the compound nucleus. Then

$$\sigma_{\text{comp}} = \pi \lambda^2 \ell_{\text{cr}}^2. \quad (22.6)$$

Experiments show that ℓ_{cr}^2 is approximately proportional to kinetic energy in the entrance channel. Therefore, it is possible to introduce the critical radius $R_{\text{cr}} < R_I$ and

the corresponding potential $V_{\text{cr}} = V(R_{\text{cr}})$ in such a way that

$$\ell_{\text{cr}}^2 = \frac{2M}{\hbar^2} R_{\text{cr}}^2 (E - V_{\text{cr}}). \quad (22.7)$$

The critical radius grows along with the target mass. This can be roughly described similarly to Eq. (22.2) with the aid of another parameter, r_{cr} ,

$$R_{\text{cr}} = r_{\text{cr}} (A_1^{1/3} + A_2^{1/3}), \quad r_{\text{cr}} \approx 1.05 \text{ fm}. \quad (22.8)$$

Another limitation for the formation of a compound nucleus [1] may come from small angular momenta. Here the fragments flying away do not correspond to the equilibrium fissionlike mass distribution; they retain the memory of initial values of A_1 and A_2 . The lifetime of the double system is too short (*quasifission*). The relaxation of kinetic energy could already proceed, and we can judge this by the proximity of the fragment kinetic energy to that of Coulomb repulsion. The angular distribution of fragments shows the trend to equilibrium with the growing rotation angle of the double system (essentially, its lifetime). From the grazing scattering (sliding contact) with pure Coulomb forces, the double system is rotating to smaller angles.

Probably the deep-inelastic processes are the most interesting. They occupy the region $\ell_{\text{max}} > \ell > \ell_{\text{cr}}$. The cross section for such collisions amounts to a large fraction of the reaction cross section σ_R . If the decay products differ from the initial nuclei by few nucleons, the energy spectra of light fragments reveal two components (Figure 22.1). For the higher energy component, the energy is close to that of elastic scattering. In the lower energy part, the energy is close to the Coulomb repulsion energy in the grazing collision. For the processes with transfer of many nucleons, only the low-energy peak survives, and its mean energy does not depend on the initial energy.

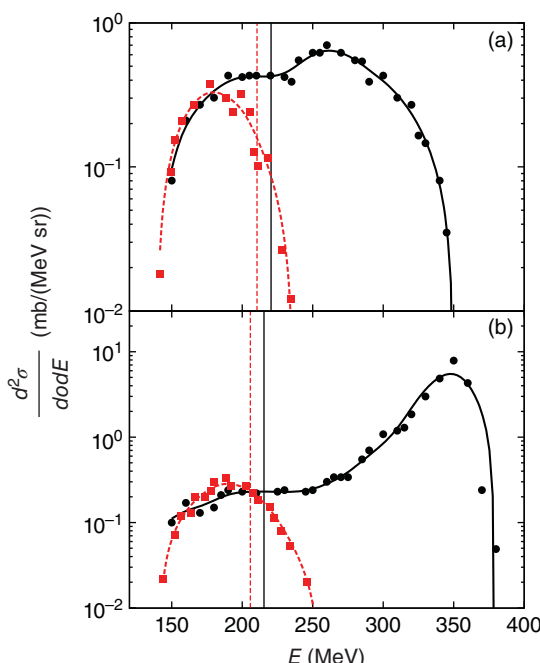


Figure 22.1 Comparison of spectra of potassium fragments for two energies of the bombarding ions of ${}^{40}\text{Ar}$ on the ${}^{232}\text{Th}$ target [2, 3]. Circles and solid lines outlining the general behavior of the cross section reflect the data for incident lab energy $E = 388 \text{ MeV}$; squares and dashed lines show data for energy $E = 297 \text{ MeV}$. Exit Coulomb barriers are shown by vertical grid lines: dashed for $E = 297 \text{ MeV}$ and solid for $E = 388 \text{ MeV}$. Panels (a) and (b) correspond to differential cross section at angles 20° and 30° , respectively.

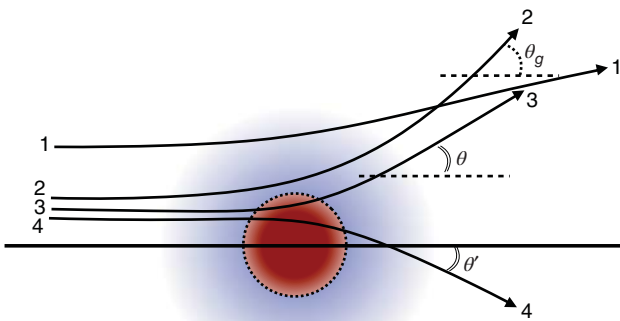


Figure 22.2 Classical scattering trajectories at different impact parameters for peripheral heavy-ion collisions. The Coulomb trajectory (1) is followed at a large impact parameter. Nuclear interactions become important for lower impact parameters (2), at grazing angle θ_g . Further reduction of impact parameter increases the role of attractive nuclear forces that quickly reduce the deflection angle from outward (trajectory (3), angle θ), to inward (trajectory (4), angle θ').

The whole picture can be qualitatively interpreted in terms of the formation of a *double nuclear system*. During its lifetime, the diffusion processes of exchange by energy and nucleons between the counterparts take place. The existing angular momentum continues rotating the system. The departure of fragments will occur at angles θ smaller than the angle θ_g for the grazing collision. The turning of the system can be sufficiently large so that the experiment will register at a given angle θ both events with $\theta > 0$ and those for the rotation “to the opposite side from the incident beam,” $\theta' = -|\theta| < 0$ (Figure 22.2). The quasielastic collisions are concentrated mainly around θ_g , while the negative θ correspond to the large lifetime of the double system. For the lightest fragments, the energy distribution smoothly changes as a function of angle as the time necessary for the multiple nucleon transfer could be comparable to the full rotation period of the double system which is equivalent to averaging over θ . This recalls the *orbiting* known in classical mechanics.

One interesting feature observed in deep inelastic processes is the so-called Q_{gg} -systematics. At the fixed angle θ , the differential cross sections for production of individual isotopes are well approximated by the exponential functions,

$$\frac{d\sigma}{d\theta} \propto \exp\left(\frac{Q_{gg} + \Delta E_C}{T}\right), \quad (22.9)$$

where Q_{gg} is the mass difference between the ground-state energies of the initial and final nucleus, and ΔE_C the change of Coulomb interaction energy after the transfer of a certain number of protons. The quantity Q_{gg} can be up to few dozens of megaelectron-volts, especially under multiparticle transfer. The parameter T of the order 2 MeV plays the role of temperature for the double system. This systematics is shown in Figure 22.3 for the reactions of ^{16}O with ^{232}Th . This dependence manifests specific statistical equilibrium with respect to the main macroscopic degrees of freedom.

Most probably, quasifission is a similar process. It was shown in a number of experiments that the summed kinetic energy of the fragments does not depend on the initial energy. This means that full relaxation occurs with respect to energy. However, the

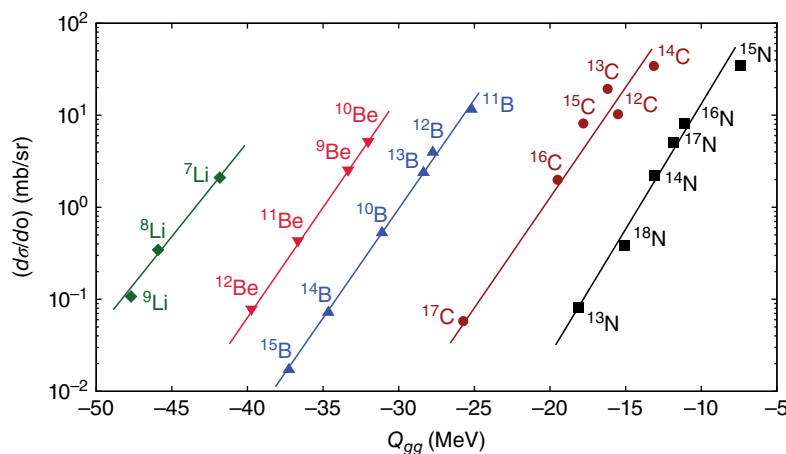


Figure 22.3 Q_{gg} -systematics after introduction of pairing corrections for the reaction ${}^{16}\text{O} + {}^{232}\text{Th}$. Here the differential cross sections at angle 40° are shown [4].

contribution of events which have to be attributed to $\theta < 0$ (orbiting) grows with energy. Also, one sees the increase of events with the symmetric mass distribution.

In the reactions of heavy nuclei, for example, for scattering of the krypton nuclei off lead or bismuth at energies of order 500–700 MeV, the observed results show the transitional picture from quasielastic to deep inelastic processes. At increase of energy, the energy of the deep inelastic peak also grows, and this peak gradually merges with the elastic one (decrease of dissipation).

In the vicinity of θ_g , it becomes difficult to earmark the deep inelastic events. The angular distribution is rather narrow, especially at large initial energy. Here the *focusing* effect works: at smaller ℓ , the Coulomb repulsion is stronger, trying to increase θ . But the nuclear attraction is also stronger, acting in the opposite direction. At large ℓ , both interactions are weaker, and the concentration of many partial waves takes place in the narrow interval of angles. This interval moves forward as energy increases. At greater energy, one can see a shoulder in the direction of smaller angles. This can be related to the orbiting that still plays a minor role for large Z_1 and Z_2 in this region of energy. A small tail in the direction of large angles can be related to the fission after fusion that provides only a small fraction of the total cross section here.

22.3 Macroscopic Description

The simplest description of such heavy ion reactions can be given in terms of classical equations of motion. Indeed, the global motion is semiclassical, and the density of states in the energy region appropriate for deep inelastic processes, 100–200 MeV, is very high. Therefore, one can expect that it is sufficient to find the averaged action of a large number of intrinsic degrees of freedom onto relative motion.

The relative motion is governed by the effective potential. For a given partial wave, we have the sum of nuclear, Coulomb, and centrifugal terms,

$$U_\ell(r) = V_{\text{nuc}}(r) + \frac{Z_1 Z_2 e^2}{r} + \frac{\hbar^2 \ell^2}{2 M r^2}. \quad (22.10)$$

For typical values of ℓ , this potential will resemble what is shown in Figure 29.4.

Starting from some distance, the nuclear forces begin distorting a Coulomb trajectory. At the extremum point $r = R_\ell$, where $dU_\ell/dr = 0$, the nuclear attraction compensates the Coulomb and centrifugal repulsion. In a crude approximation, this point serves as a threshold for nuclear fusion. After that, we expect the sliding down to the left along the potential curve. Then the overlap of nuclear densities grows and the formation of unified shells for the compound systems starts (a process inverse to fission). At r smaller than R_ℓ , the potential curve $U_\ell(r)$ has only conventional meaning because here the radial motion is strongly coupled to intrinsic degrees of freedom. Note that the point R_I defined in Eq. (22.2) is located a little to the right of R_ℓ , as

$$\frac{d}{dr} (V_{\text{nuc}} + V_{\text{Coul}})_{R_I} = 0 \Leftrightarrow \left(\frac{dU_\ell}{dr} \right)_{R_I} < 0. \quad (22.11)$$

A simple model can help understand the role of frictional forces and their relation to the phenomenon of orbiting. Let us assume that in Figure 22.4 the nuclei come to the point $r = R_I$ from the right with velocity

$$\dot{r} = -u = -\sqrt{\frac{2[E - U_\ell(R_I)]}{M}}. \quad (22.12)$$

This velocity would vanish for $\ell = \ell_{\max}(E)$, so that, according to Eq. (22.5),

$$u = \frac{\hbar}{MR_I} \sqrt{\ell_{\max}^2 - \ell^2}. \quad (22.13)$$

To the left of $r = R_I$, the potential barrier starts, and we can conveniently model it as an inverted parabola,

$$U_\ell(r) = U_\ell(R_I) + \frac{1}{2} M\omega^2 [(R_I - R_\ell)^2 - (r - R_\ell)^2]. \quad (22.14)$$

In this region, friction appears and nuclear reactions come into existence. Let us assume that the friction force is proportional to the velocity,

$$f = -M\gamma\dot{r}, \quad (22.15)$$

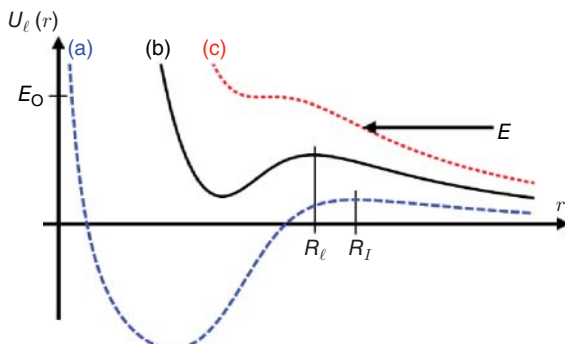


Figure 22.4 Qualitative behavior of the global potential for different partial waves (a), (b), and (c), where $0 = \ell_a < \ell_b < \ell_c$. The maximum for $\ell_a = 0$ defines R_I . The position of the maximum R_ℓ is shown for (b). For the incident energy E shown by an arrow, $\ell_{\max} = \ell_c$ as at this energy the classical closest approach distance R_{\min} coincides with R_I . The potential U_ℓ for ℓ_c has a flat area, and at scattering energy E_0 a classical particle can be temporarily captured leading to orbiting.

and does not depend on coordinates in the relatively narrow region $R_\ell < r < R_I$. We then come to the classical equation of motion for a damped inverted oscillator,

$$\ddot{r} + \gamma \dot{r} - \omega^2(r - R_\ell) = 0. \quad (22.16)$$

Problem 22.1 Solve the equation (22.16) with appropriate initial conditions.

Solution

The standard solution can be written as

$$r(t) = R_\ell + Ae^{\alpha t} + Be^{-\beta t}, \quad (22.17)$$

where the positive exponents are given by

$$\alpha = \frac{1}{2} \left(\sqrt{4\omega^2 + \gamma^2} - \gamma \right), \quad \beta = \frac{1}{2} \left(\sqrt{4\omega^2 + \gamma^2} + \gamma \right). \quad (22.18)$$

The coefficients A and B are determined by the initial conditions:

$$A = \frac{\beta(R_I - R_\ell) - u}{\sqrt{4\omega^2 + \gamma^2}}, \quad B = \frac{\alpha(R_I - R_\ell) + u}{\sqrt{4\omega^2 + \gamma^2}}. \quad (22.19)$$

If the entrance velocity u is sufficiently high, $u > \beta(R_I - R_\ell)$ (e.g., if the orbital momentum ℓ is not very large), the trajectory crosses over the top point $r = R_\ell$ and reaches the fusion region. In the case of a smaller velocity, $u < \beta(R_I - R_\ell)$, the trajectory stays on the right slope of the barrier, $r < R_\ell$: first it moves to the left of the point $r = R_I$, then the repulsive barrier stops the motion and reverses it to the right. The boundary between these two types of motion is defined by $A = 0$, when

$$u = u_{\text{cr}} = \beta(R_I - R_\ell). \quad (22.20)$$

The orbital momentum ℓ corresponding, according to Eq. (22.13), to this velocity should be identified with the critical value (22.7) that determines the cross section for the formation of a compound system,

$$\ell_{\text{cr}}^2 = \ell_{\text{max}}^2 - \frac{M^2 R_I^2}{\hbar^2} \beta^2 (R_I^2 - R_\ell^2)^2. \quad (22.21)$$

It is natural that friction, which increases the damping coefficient β , diminishes the value ℓ_{cr} and the cross section σ_{comp} . This was named *nuclear viscosity*, the main obstacle in the way to synthesis of superheavy elements.

As ℓ is slightly higher than ℓ_{cr} , the amplitude A is still small but positive. The second term in Eq. (22.17) responsible for the outgoing motion is also small. At small $A > 0$, the system will live in the region $R_\ell < r < R_I$ for a long time. This stage corresponds to *orbiting*; the orbital momentum rotates the system with angular velocity

$$\dot{\theta} = - \frac{\hbar \ell}{Mr^2}. \quad (22.22)$$

The time duration τ , when (for $A > 0$) the system still lives in the region $r < R_I$, can be juxtaposed to the lifetime of the double nuclear system. Continuing this logic, we can identify the process with small $A > 0$ and therefore long τ with the deep-inelastic collision. If the damping is noticeable, $\beta\tau > 1$, we find the lifetime from Eq. (22.17):

$$\tau = \frac{1}{\alpha} \ln \frac{R_I - R_\ell}{A} = \frac{1}{\alpha} \ln \left[\frac{\sqrt{4\omega^2 + \gamma^2}}{\beta} \frac{\ell_{\text{max}}^2 - \ell_{\text{cr}}^2}{\ell(\ell - \ell_{\text{cr}})} \right]. \quad (22.23)$$

At a small excess of the orbital momentum ℓ over its critical value, ℓ_{cr} , the orbiting time is long, in agreement with the condition $\beta\tau > 1$. The argument of the logarithm in Eq. (22.23) depends on friction only weakly. But the coefficient α , Eq. (22.18), changes significantly, from $\alpha = \omega$ in the absence of friction, to $\omega^2/\gamma \ll \omega$ at strong friction, $\gamma \gg \omega$. This may considerably increase the lifetime τ of the double system.

Let θ_g be the scattering angle due to the Coulomb and centrifugal potentials acting at $r > R_I$; this angle does not have any singularity at ℓ approaching ℓ_{cr} . The final scattering angle after orbiting (22.22) is given by

$$\theta = \theta_g - \frac{\hbar\ell}{M} \int_0^\tau \frac{dt}{r^2(t)}. \quad (22.24)$$

With some distance \bar{R} taken between R_ℓ and R_I , we can write down this angle as

$$\theta = \theta_g - \frac{\hbar\ell\tau}{M\bar{R}}. \quad (22.25)$$

As discussed earlier, we can ascribe the events with negative angles, $\theta = -|\theta|$, to deep inelastic scattering. The cross section at $\ell \rightarrow \ell_{\text{cr}}$ is

$$\frac{d\sigma}{d\theta} = 2\pi b \frac{db}{d\theta} \approx 2\pi\lambda^2\ell_{\text{cr}} \frac{d\ell}{d\theta}. \quad (22.26)$$

Using Eqs. (22.23) and (22.25), we find

$$\frac{d\theta}{d\ell} \approx \frac{\hbar\ell_{\text{cr}}}{M\bar{R}^2} \frac{1}{\ell - \ell_{\text{cr}}}, \quad (22.27)$$

and, introducing the parameters

$$z = \frac{\sqrt{4\omega^2 + \gamma^2}}{\beta} \frac{\ell_{\text{max}}^2 - \ell_{\text{cr}}^2}{\ell_{\text{cr}}^2}, \quad y = \frac{\hbar\ell_{\text{cr}}}{M\bar{R}}, \quad (22.28)$$

the cross section is expressed as

$$\frac{d\sigma}{d\theta} = 2\pi\lambda^2\ell_{\text{cr}}^2 \frac{z}{y} e^{-(\theta_g + |\theta|)/y}. \quad (22.29)$$

The total cross section for scattering to negative angles,

$$\sigma_{<0} = \int_0^{-\infty} d\theta \frac{d\sigma}{d\theta} = 2\pi\lambda^2\ell_{\text{cr}}^2 z e^{-\theta_g/y}, \quad (22.30)$$

grows with increase of friction ($y \propto 1/\alpha$). The exponential angular distribution (22.29) roughly represents experimental data with $y \approx 0.2$. For larger values of y , the lifetime τ could become greater than the time of a full rotation. Then the experimental cross section $d\sigma/d\theta$ would have to account for the contributions of scattering by angles $-|\theta| - 2n\pi$ which would give an additional factor $[1 - \exp(-2n/y)]^{-1}$ in Eq. (22.29).

The whole consideration is purely phenomenological so that other parameters are also to be found from experimental data. In typical collisions of relatively light projectiles (carbon, oxygen, and neon) with heavy targets (uranium, thorium, etc.) at energy of the order 10 MeV per nucleon, the characteristic values are $\ell_{\text{max}} \sim 200$, $\ell_{\text{cr}} \sim 90$; for $\bar{R} \approx 14$ fm, $\theta_g \approx 30^\circ$. The value of the prefactor $\sqrt{4\omega^2 + \gamma^2}/\beta$ in Eq. (22.28) is between

1 (for strong friction) and 2 (in the case of weak friction). Such estimates lead to the friction parameter $\hbar\gamma \approx 1 \div 2$ MeV. Then this description does not have much freedom to fit the cross section (22.29) which turns out to be 2–3 times lower than the typical experimental value of approximately 100 mb sr^{-1} (the sum over all reaction products). The mean value of the lifetime of the double system is $\tau \approx (0.5 \div 1) \times 10^{-21} \text{ s}$, while the damping of the energy of relative motion occurs faster, with characteristic time $1/\gamma \sim (3 \div 5) \times 10^{-22} \text{ s}$.

Of course, even in the classical framework, the previous consideration was oversimplified. Apart from radial friction, some *tangential friction* should have been present. This is an agent that transforms the original orbital momentum of relative motion into the rotational angular momentum of the double system and internal momenta of nuclear excitations. If this friction is considerable, the relative angular motion will be strongly damped, so that the total system will rotate as a whole with a moment of inertia that can be estimated through the moments of inertia of the original nuclei,

$$\mathcal{J} = \mathcal{J}_1 + \mathcal{J}_2 + M\bar{R}^2. \quad (22.31)$$

The tangential friction reduces the value of ℓ and shifts the system on the new curve of the effective potential. The assumption of nuclear fusion at $r < R_\ell$ was rather arbitrary. Other possibilities also exist, such as reflection into continuum from the intrinsic barrier with dissipation of energy and angular momentum; the compound nucleus can be unstable for a certain value of angular momentum. Various effects related to nucleon transfers and propagation of wavelike perturbations from the overlap region were neglected. The dynamics outside this approach leads to the evolution of the self-consistent field which, in turn, can reduce the height of the barrier.

Among some incorrect predictions of the classical approach we can mention the following: (i) energy loss is always noticeably, 40–50 MeV, smaller than in the experiment, while the final energy is always higher than the exit barrier; (ii) angular distributions are too narrow; (iii) cross sections are smaller than in the experiment. One direction of improvement can be found in the consideration of collective degrees of freedom (deformation and collective vibrations). Strong deformation lowers the Coulomb barrier and makes possible the events with energy below the exit barrier calculated for the original nuclei. The main contribution can be expected from *giant resonances* of surface nature. They are easily excited and the total energy transfer into such modes is of the same order as total dissipated energy. Phonons also transfer angular momentum and broaden angular and energy distributions. Because of the strong Coulomb field, both isoscalar and isovector modes, including the giant dipole resonance, can be excited. One can also note that in the double system, the common vibrations can exist with approximately doubled wavelength, their frequencies are lower, and the excitation probabilities are higher.

22.4 Equilibration as a Diffusion Process

During the lifetime τ , the double system moves to statistical equilibrium. By necessity, this process is *random* and diffusion-like, proceeding through many uncorrelated nucleon–nucleon interactions. If we associate the rotation angle θ of the double system with the duration τ , the events with different scattering angles can be interpreted as resulting from the dissociation of the double system at different stages of relaxation.

There are two ways for describing such processes: either in terms of the time-dependent random variables $x(t)$ (*stochastic differential equations* of Langevin type) or in terms of the evolution of the *distribution function* $w(x, t)$ that determines the probability of various values $x(t)$. We have briefly discussed such random processes in application to the fissioning nucleus (Section 21.6).

The Langevin-type equation has the form

$$\dot{x} = F + f + \zeta, \quad (22.32)$$

where x is a set of random variables governed by the conservative force F , friction (drag) force f , and random force ζ . In the classical model of *Brownian motion*, x is the velocity of the particle, the force F creates a dynamical acceleration, f leads to damping and therefore to stationary motion with terminal velocity, while ζ is responsible for the velocity spread and relaxation to the Maxwellian distribution determined by the temperature of the medium. Both terms f and ζ are due to the numerous collisions with the particles of the medium but $f \neq 0$ only for the moving particle (a difference in the momentum transfer to the particles hitting from the backward and forward directions) while $\zeta \neq 0$ even for a particle “at rest” (no macroscopic velocity).

The random force ζ should be specified by its probabilistic distribution. Usually, it is taken as the *white noise*:

$$\overline{\zeta(t)} = 0, \quad \overline{\zeta(t)\zeta(t')} = C\delta(t - t'), \quad (22.33)$$

where the noise intensity C is proportional to the temperature of the medium, T . The delta-function in Eq. (22.33) should not be understood literally – the ensemble averaging (22.33) is meaningful only if $|t - t'| \gg \tau_c$, where τ_c is an interval between individual random hits; at smaller time intervals, the ballistic motion still retains its memory of the last hit. In other words, the noise is *white*, uniformly reproducing all frequencies ω of perturbations, only approximately; very large frequencies $\omega \gg 1/\tau_c$ with the period smaller than τ_c are outside of our interest, having no physical source. Since the random forces of separate hits are uncorrelated after averaging over the memory time τ_c , the prehistory of motion becomes irrelevant. Such a random process is called *Markovian* [after the Russian mathematician A.A. Markov (1856–1922), sometimes also spelled in English as Markoff]. In the discrete version, such a process appeared in our consideration of random angular momentum coupling (Section 20.6).

A Markovian process is described by the *transition probability* $W(x, t|x_0, t_0)$ which is a conditional probability (or probability density, if the variables x are continuous) of having at time $t > t_0$ the value x of the random variable if initially $x(t_0) = x_0$. If we select any intermediate time moment ϑ between t_0 and t , the process consists of two intervals with the possible intermediate values y of the random variable. The final probability distribution satisfies a logical identity (the *Smolukhowsky equation*),

$$W(x, t|x_0, t_0) = \int dy W(x, t|y, \vartheta)W(y, \vartheta|x_0, t_0) \quad (22.34)$$

for any time moment ϑ between t_0 and t . If we define the initial distribution function, $w(x_0) = w_0(x_0)$, and integrate Eq. (22.34) over x_0 with this initial distribution, we come to the equivalent equation for the final distribution,

$$w(x, t) \equiv \int dx_0 W(x, t|x_0, t_0)w_0(x_0) = \int dy W(x, t|y, \vartheta)w(y, \vartheta). \quad (22.35)$$

The whole process is fully characterized by the transition probability $W(x, t|y, \vartheta)$.

The Markovian process that is equivalent to the dynamics described by the Langevin equation contains two components, *drift* and *diffusion*. We take a “physically small” time interval τ that covers many elementary collisions, $\tau \gg \tau_c$. Then, instead of the transition probability, we can consider its first moments: the mean displacement during time τ ,

$$\overline{\Delta x} \equiv \overline{x - y} = \int dy (x - y) W(x, t + \tau | y, t), \quad (22.36)$$

and the mean square displacement,

$$\overline{(\Delta x)^2} \equiv \overline{(x - y)^2} = \int dy (x - y)^2 W(x, t + \tau | y, t). \quad (22.37)$$

In the case of the Langevin process, the dynamic force leads to the *linear* growth of the displacement,

$$\overline{\Delta x} = A(x, t)\tau, \quad (22.38)$$

and the fluctuations are increased in the same way by the random noise,

$$\overline{(\Delta x)^2} = 2D(x, t)\tau. \quad (22.39)$$

The higher moments, $\overline{(x - y)^{n>2}}$, grow as higher powers of the small time τ .

In this approximation, taking the short time interval $t - t_0$ and calculating the time derivatives in Eq. (22.34), we come to the differential *Fokker–Planck equation* in partial derivatives,

$$\frac{\partial W}{\partial t} = - \frac{\partial}{\partial x} (AW) + \frac{\partial^2}{\partial x^2} (DW). \quad (22.40)$$

If we multiply this equation by $w_0(x_0)$ and integrate over x_0 , we obtain the analogous equation for the final distribution function $w(x, t)$,

$$\frac{\partial w}{\partial t} = - \frac{\partial}{\partial x} (Aw) + \frac{\partial^2}{\partial x^2} (Dw). \quad (22.41)$$

This is nothing but a *continuity equation*,

$$\frac{\partial w}{\partial t} + \operatorname{div} j = 0, \quad (22.42)$$

where the effective current, in general multidimensional, contains the drift and diffusion components,

$$j = Aw - \frac{\partial}{\partial x} (Dw). \quad (22.43)$$

We can establish the equivalence of the Langevin equation with a delta-correlated force (22.33) to the Fokker–Planck equation by direct juxtaposition of the moments of random quantities \bar{x} and $\overline{(\Delta x)^2} = \bar{x}^2 - \bar{x}^2$ calculated with the aid of Eqs. (22.32) and (22.41). This immediately gives

$$A(x, t) = F + f, \quad D(x, t) = \frac{1}{2} C(x, t). \quad (22.44)$$

Now we consider the special case of a *stationary* random process when the coefficients A and D do not contain explicit time dependence. Moreover, to get a simple solution, we

assume even that those coefficients do not depend on random variables, being constants of drift and diffusion. In this case, setting $t_0 = 0$,

$$\bar{x} = x_0 + At, \quad \overline{(\Delta x)^2} = 2Dt. \quad (22.45)$$

The localized initial state, $w_0(x) = \delta(x - x_0)$, reveals Gaussian spreading with parameters defined by Eq. (22.45),

$$w(x, t) = \frac{1}{\sqrt{4\pi Dt}} e^{-(x-x_0-At)^2/4Dt}. \quad (22.46)$$

Problem 22.2 Find the solution if the drift coefficient A contains the linear friction force $f = -\gamma x$.

Solution

Here $A = F - \gamma x$; the distribution is still Gaussian at all times,

$$w(x, t) = \frac{1}{\sqrt{2\pi\overline{(\Delta x)^2}}} e^{-(x-\bar{x})^2/2\overline{(\Delta x)^2}}. \quad (22.47)$$

The drift and the memory of initial state gradually disappear:

$$\bar{x} = x_0 e^{-\gamma t} + \frac{F}{\gamma} (1 - e^{-\gamma t}), \quad (22.48)$$

while the dispersion has a constant limit,

$$\overline{(\Delta x)^2} = \frac{D}{\gamma} (1 - e^{-2\gamma t}) \Rightarrow \frac{D}{\gamma} \text{ at } t \gg \frac{1}{2\gamma}. \quad (22.49)$$

The process of the last problem is *ergodic* (the limit does not depend on the initial state). If the random variable is the velocity of a Brownian particle, the stationary limit (22.47) is actually the Maxwell distribution if we set

$$D = \frac{\gamma}{m} T, \quad (22.50)$$

the *Einstein relation*, where m is the mass of the Brownian particle, and T the temperature of the surrounding fluid. The relaxation to equilibrium proceeds exponentially with the characteristic time determined by the friction intensity, $\tau_{\text{rel}} \sim 1/\gamma$.

In this framework, we have the freedom of choosing the random variables. They will be useful if it would be possible to follow their change by “large-scale” (macroscopic) observables straightforwardly related to experiments. The large-scale formulation describes not an individual quantum state but a wave packet built of many microscopic states close in energy. The natural choice of global observables is that of the excitation energy and the number of transferred nucleons. One practical possibility is to look at the cross section of the process where a light fragment (Z, A) emerges at the angle θ at excitation energy E^* in an energy interval determined by the experimental accuracy but, at any rate, covering many microscopic states. The timescale, $\tau = \tau(\theta)$, is defined, according to our preliminary consideration, Eq. (22.24), by the angle accumulated after the start of the collision.

As an example, we can show the distributions $w(Z, E^*, \tau)$ for the reaction ${}^{40}\text{Ar} + {}^{232}\text{Th}$ at energy of the projectile nucleus 388 MeV [5]. The curves $P(E^*)$ are constructed from

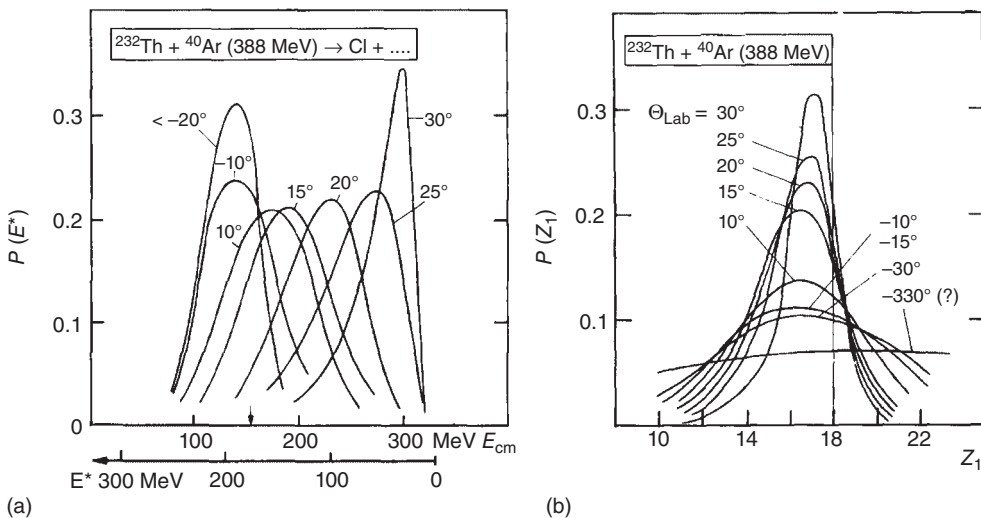


Figure 22.5 (a) Distribution functions for the energy of the chlorine fragment in reaction $^{40}\text{Ar}+^{232}\text{Th}$ at 388 MeV for angles θ changing from θ_g to $\theta < 0$. (b) Distribution functions for the charge of the light fragment in the same reaction. (Norenberg [5]. Reproduced with permission of Elsevier.)

the experimental angular and energy distributions of products; the variables Z and E^* are considered as independent, and the corresponding random forces (22.33) uncorrelated. For the analysis, one has to isolate the contribution of deep-inelastic processes for various angles which change from θ_g to $\theta < 0$. For each independent value (Z, E^*) , one has two parameters, the drift velocity A and the diffusion coefficient D ; the resulting patterns are shown in Figure 22.5. As the angle diminishes, the energy distribution for a typical product chlorine (Figure 22.5a) is shifting to larger E^* and broadening. The estimates of the drift and diffusion parameters give

$$A_E \approx 4 \times 10^{23} \text{ MeV s}^{-1}, \quad D_E \approx 4 \times 10^{24} (\text{MeV})^2 \text{ s}^{-1}. \quad (22.51)$$

The spreading Gaussian fit works also for the distribution in Z (Figure 22.5b); here the drift is almost absent,

$$|A_Z| \leq 10^{21} \text{ 1/s}, \quad D_Z \approx 10^{22} \text{ 1/s}. \quad (22.52)$$

As already mentioned, the translation of the angular distribution into the timescale used here a simple linear dependence $\tau = (\theta_g - \theta)/\Omega$, where the angles are referred to the center-of-mass frame and the angular velocity $\Omega \approx \hbar\ell/J$. Both from this formula and from the broadening of the curves, one can get $\Omega \approx 10^{21} \text{ 1/s}$. The diffusion coefficient D_E is almost independent of the projectile energy. Figure 22.6 shows linear broadening of the width squared, in agreement with the diffusion law.

In order to improve the description, one needs to introduce the friction force and related loss of memory about initial conditions. The drift and diffusion exponentially die out at $\gamma\tau \geq 1$. The experiment allows to obtain $\hbar\gamma \approx 1 \text{ MeV}$, in agreement with our previous estimate. Many experiments with heavy nuclei and energy not much higher than the Coulomb barrier support the idea of the diffusionlike process. If the charge dispersion is still far from its limiting value, one can use for $(\Delta Z)^2$ the simple expression $2D_z t$.

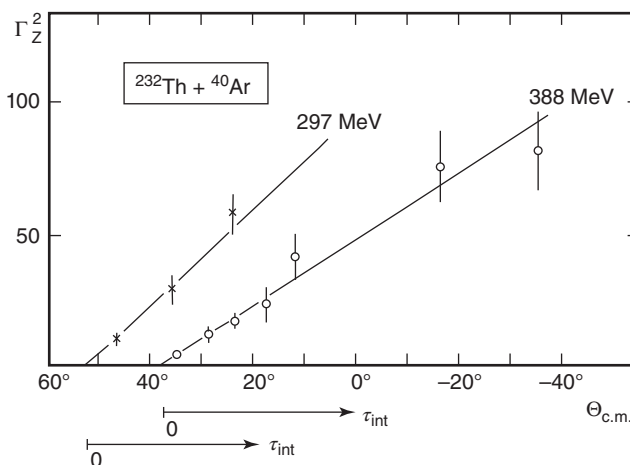
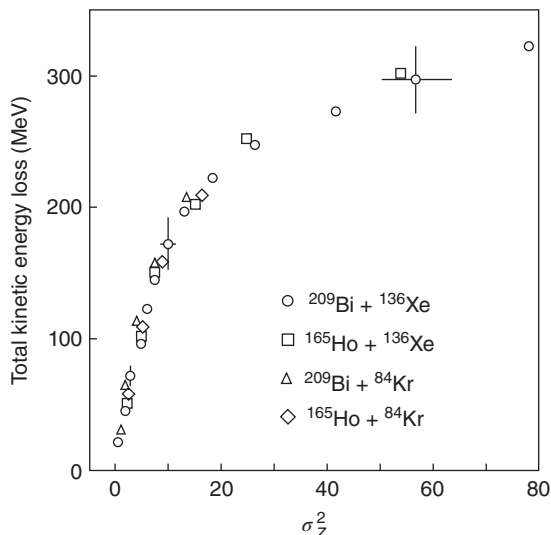


Figure 22.6 Extrapolation of the widths for the same reaction as in Figure 22.5 for two values of the projectile energy. (Norenberg [5]. Reproduced with permission of Elsevier.)

At the same time, the energy damping is already strong, so the kinetic energy satisfies the law similar to (22.48). Eliminating the time t , one can find the correlation of energy loss and the width of the charge distribution. As seen in Figure 22.7, the agreement with data is quite good in the collisions of heavy nuclei. Then the diffusion coefficient is $D_Z = (0.7 \pm 0.3) \times 10^{-22} \text{ 1/s}$, close to our previous estimate for lighter colliding nuclei, and the friction strength is $\gamma \approx (1/M)0.6 \times 10^{-21} \text{ MeV s fm}^{-2}$, which corresponds to $\hbar\gamma \approx 0.5 \text{ MeV}$, slightly lower than for a smaller value of Z_1Z_2 . This friction is not sufficiently strong to justify the previously discussed classical model with instantaneous loss of kinetic energy.

Such an analysis, as limited as it is, still leads to the conclusion that the energy relaxation is practically complete in a deep-inelastic process. The process is close

Figure 22.7 Correlation of the energy loss and the width of the charge distribution in collisions of heavy nuclei (Berkeley experiments [6]). (Huizenga 1976. Reproduced with permission of American Physical Society.)



to Markovian at times, τ satisfying a double inequality $\tau_c \ll \tau < \tau_{\text{rel}}$. During this process, the phase memory is lost, while the time is too short for a large change of dynamical variables. As we have mentioned, the time τ_c of phase memory should be estimated with transformation to large-scale quantities. One can subdivide the phase space in cells A, B, \dots corresponding to many quantum levels with practically identical values of macroscopic quantities (in Chapter 25 on quantum chaos we discuss the thermalization in a mesoscopic system of interacting particles). The relative motion of colliding nuclei introduces a time-dependent interaction $V(t)$ that induces transitions between the cells, mainly those of valence nucleons (but the shells themselves evolve with the interaction process). Such considerations usually provide estimates $\tau_c \sim 10^{-23}$ s, sufficiently short to justify the Markovian character of the relaxation process.

22.5 Toward a Microscopic Description

The current microscopic approach to the theory of heavy-ion reactions is usually the direct solution of the many-body Schrödinger equation in the approximation of time-dependent self-consistent fields; the simplest version is called *time-dependent Hartree–Fock approximation* (TDHF) [7].

The system of $A_1 + A_2 = A$ nucleons is described by the A -body variational wave function $\Psi_A(t)$ in the form of a Slater determinant formed by A filled single-particle orbitals $\psi_v(\mathbf{r}, t)$. Every function ψ_v evolves in time according to

$$i\hbar\dot{\psi}_v(\mathbf{r}, t) = \hat{h}(t)\psi_v(\mathbf{r}, t), \quad (22.53)$$

where the operator \hat{h} contains kinetic energy of the nucleons and their direct and exchange interactions. This effective Hamiltonian has to be self-consistently determined through the time-dependent single-particle density matrix

$$\rho(\mathbf{r}, \mathbf{r}', t) = \sum_v n_v \psi_v(\mathbf{r}, t) \psi_v^*(\mathbf{r}', t). \quad (22.54)$$

Here n_v are occupancies (equal to 0 or 1) of single-particle orbitals.

The usual (time-independent) Hartree–Fock approximation or its modern form of the energy density functional is already a complicated nonlinear problem of many-body physics (the variables we denote \mathbf{r} in fact include also spins of the nucleons). It should be solved by iterations which hopefully converge to the genuine energy minimum. In the TDHF method applied to the scattering problem, the task is even more difficult as the initial state is to be constructed on a two-center shell model. The initial conditions should be given by the static solutions of the self-consistent field for two separated nuclei plus the velocity of relative motion. When the nuclei approach each other and enter the interaction region, the total Slater determinant is constructed on *nonorthogonal* functions. Another problem is related to the necessity to take into account the pairing interaction and therefore at least introduce the BCS-like description.

Apart from technical problems, the method suffers from serious principal deficiencies. In the standard formulation, the reaction channels are absent. After starting with two isolated nuclei and solving the TDHF equations, we come to a complex final state, where the density $\rho(\mathbf{r})$ can be uniform, grouped into clusters, or oscillating between

them. This state has to be analyzed with respect to allowed decay channels with the aid of some special physical procedure.

Another big and still unsolved problem of the TDHF method is related to the occupation numbers n_ν . In the standard formulation (22.54) of the method, the single-particle orbitals are populated at the start of the process and do not change anymore while the function ψ_ν evolves with time. If so, the originally occupied orbitals are occupied during the whole process, while those which were initially empty remain empty. However, along the many-body trajectory the single-particle levels evolve in quite complicated way and undergo *multiple crossings*. Since the probability of filling the originally empty evolving orbitals is neglected, a big question is up to what extent the TDHF solution corresponds to a real physical situation.

At fast collisions (probably at energy higher than in the deep-inelastic regime discussed earlier) the time-dependent single-particle “levels” are *adiabatic* terms rapidly moving through crossings. The level crossings are efficient only during relatively short time intervals when the hopping of particles between the close levels can have an appreciable probability. At sufficiently high energy, those crossing regions are passed too quickly and the transitions are suppressed. This situation can be analyzed again with the aid of the Landau–Zener theory [QP, II, 1.6], which appeared in Section 21.6. Near the crossing point, the residual interaction not included in the mean-field Hamiltonian \hat{h} becomes essential. In this region, the levels are mixed and their correct linear combinations repel each other making the crossing *avoided*. The occupancy of the levels after the crossing region depends on the passage speed. At slow passage, the lower level remains occupied while its wave function is the adiabatically changed ground state. In the case of rapid passage, or rather weak interaction, the probability of hopping without change of the wave function is close to 1, the system gets excited while the lower level becomes empty. The situation is more favorable for the mean-field approximation at a later stage of the collision when the speed of dissipation of relative motion is reduced.

The whole process of collision with formation of the fused system starts and ends in a situation of regular (two-center or one-center) motion. In between, we have a turbulent level dynamics similar to quantum chaos. It seems that a reasonable way of treating the multiple level crossings should be to use a statistical element defining the probability of hopping between the levels in the spirit of the Landau–Zener formula. A separate question is related to the quantum spreading of the Slater determinant that can occur during the time comparable to the collision time.

22.6 Sketch of a More General Approach

Time-dependent effects of intrinsic restructuring during the reaction process can be approximately divided into *distortion* and *mixing*. “Distortion” means the continuous evolution of structure in a time-dependent perturbing field. At not very high energy, this can be accounted for by the *adiabatic* perturbation theory. The mixing is a nonadiabatic effect, such as in the Landau–Zener approach, which depends critically on the local speed of the change of the nuclear field. Here, we schematically show the way of possible construction of the theory.

First let us separate *global degrees of freedom* of the system of colliding nuclei which have large amplitudes but relatively low velocities of change as compared, for example, to

characteristic nucleon velocities (Fermi velocity). We can include here relative motion, mass transfer, shape deformation, and so on. These degrees of freedom can be described by generalized coordinates X_i and corresponding momenta P_i . The adiabatic expansion over small velocities (or momenta) provides the main terms of the Hamiltonian for the global motion,

$$H_0(X, P) = U(X) + \frac{1}{2} P_i B_{ik}^{-1}(X) P_k + \dots \quad (22.55)$$

where $U(X)$ is the effective potential energy and $B_{ik}^{-1}(X)$ is the inverse tensor of effective masses corresponding to the global degrees of freedom. For simplicity, we consider here the global motion as classical, neglecting noncommutativity of the operators X and P . This approximation can be easily removed.

In addition, we introduce the set $\{\xi\}$ of intrinsic degrees of freedom interacting with the global variables. Apart from the global part (22.55), the full Hamiltonian has to include the intrinsic Hamiltonian $h(\xi)$ and interaction V ,

$$H = H_0(X, P) + h(\xi) + V(X, P; \xi). \quad (22.56)$$

Now we can derive the dissipation of the global motion. In the classical approximation, the global variables are time-dependent functions $X_i(t)$ which should be found from the equation of motion

$$v_i = \dot{X}_i = B_{ik}^{-1} P_k + \overline{\frac{\partial V}{\partial P_i}}, \quad (22.57)$$

where the overline describes averaging over the microscopic state of intrinsic variables at a given instant. The Newton equations for classical variables are

$$\dot{P}_i = - \frac{\partial U}{\partial X_i} - \frac{1}{2} P_j \frac{\partial B_{jk}^{-1}}{\partial X_i} P_k - \overline{\frac{\partial V}{\partial X_i}}. \quad (22.58)$$

This defines the dissipation of the global energy,

$$\dot{H}_0 = - \overline{\frac{\partial V}{\partial X_i}} B_{ik}^{-1} P_k + \overline{\frac{\partial V}{\partial P_i}} \left(\frac{\partial U}{\partial X_i} + \frac{1}{2} P_j \frac{\partial B_{jk}^{-1}}{\partial X_i} P_k \right). \quad (22.59)$$

We will look for the solution in the form of expansion in powers of classical velocities v_i , Eq. (22.57), or corresponding momenta P_i . In this way, we present the interaction operator V as

$$V(X, P; \xi) = V_0(X; \xi) + \frac{1}{2} [V_i(X; \xi), P_i]_+ + \frac{1}{4} [V_{ik}(X; \xi), P_i P_k]_+ + \dots, \quad (22.60)$$

where in quantum consideration $[\dots, \dots]_+$ will be an anticommutator of operators inside the brackets. Because of the invariance with respect to time reversal, the expansion of $V_i(X; \xi)$ after the averaging over intrinsic variables should start with the terms linear in v_k . Using (22.60) in the equation of motion (22.57), we come to the collective momentum

$$P_k = M_{kl}(v_l - \overline{V_l}). \quad (22.61)$$

This can be interpreted as the effective mass of collective motion created by the medium,

$$M_{ik}^{-1} = B_{ik}^{-1} + \overline{V_{ik}}, \quad (22.62)$$

and the effective vector potential as seen from the difference of the kinetic momentum $M_{kl}v_l$ from the canonical momentum P_k in Eq. (22.61).

For the adiabatic expansion to be applicable, the averaged parameters of the Hamiltonian (22.60) have to be smooth functions of coordinates X_i . This leads to the estimates $v \sim (\partial/\partial X)$. In this classification, equations of motion (22.58) contain the first-order terms

$$\dot{P}_i^{(1)} = -\frac{\partial U}{\partial X_i} - \overline{\frac{\partial V_0}{\partial X_i}}, \quad (22.63)$$

and terms of higher orders, starting from the third one. The corresponding leading order term in the energy dissipation (22.59) is

$$\dot{H}_0^{(1)} = -v_i \overline{\frac{\partial V_0}{\partial X_i}} + \overline{V_i} \left(\frac{\partial U}{\partial X_i} - \overline{\frac{\partial V_0}{\partial X_i}} \right). \quad (22.64)$$

The first item in the right-hand side here is the usual work of the force of interaction with the medium. The second item is fully generated by the terms proportional to velocity in Eq. (22.60); this is a *counterflow* emerging in the system; $\overline{V_i}$ plays the role of the local velocity, while the second term in (22.64) separates this local motion as friction has to be determined just by the *relative* velocity.

Now we can formulate a *self-consistent* problem of evolution of a microsystem in a given nonstationary classical field that itself is to be determined through equations of motion (22.57), (22.58), which depend on the forces acting from the microsystem. The evolution of the microscopic variables can be found in adiabatic perturbation theory. The wave function $\Psi(\xi, t)$ of microscopic degrees of freedom satisfies the nonstationary Schrödinger equation,

$$i\hbar \frac{\partial \Psi(\xi, t)}{\partial t} = [\mathcal{H}(\xi) + V(X, P; \xi)]\Psi(\xi, t). \quad (22.65)$$

At this stage, $X_i(t)$ and $P_i(t)$ are considered as given functions of time. We expand the solution of Eq. (22.65) over the complete orthonormalized set of functions $\psi_\alpha(\xi; X)$ which are *instantaneous* eigenfunctions of the Hamiltonian $\mathcal{H} + V_0(X)$ with *instantaneous energies* $E_\alpha(X)$,

$$[\mathcal{H}(\xi) + V_0(X; \xi)]\psi_\alpha(\xi; X) = E_\alpha(X)\psi_\alpha(\xi; X). \quad (22.66)$$

The coefficients of the expansion are functions of time and it is convenient to separate the phase created by the change of levels $E_\alpha(X)$ at adiabatic evolution of the field $X(t)$, analogously to what was considered for fission (Section 21.5),

$$\Psi(\xi, t) = \sum_\alpha c_\alpha(t)\psi_\alpha(\xi; X(t))e^{-i\Phi_\alpha(t)}, \quad (22.67)$$

where

$$\Phi_\alpha(t) = \frac{1}{\hbar} \int_{t_0}^t dt' E_\alpha(X(t')). \quad (22.68)$$

The set of equations (22.65)–(22.68) leads to the coupled equations for coefficients $c_\alpha(t)$:

$$\dot{c}_\alpha(t) = - \sum_\beta c_\beta D_{\alpha\beta}(t) e^{i\Phi_{\alpha\beta}(t)}, \quad (22.69)$$

where $D_{\alpha\beta}$ is the time-dependent matrix element taken between the running functions ψ_α and ψ_β ,

$$D_{\alpha\beta}(t) = \left(\frac{\partial}{\partial t} \right)_{\alpha\beta} + \frac{i}{\hbar} \left\{ P_i(V_i(X))_{\alpha\beta} + \frac{1}{2} P_i P_k (V_{ik}(X))_{\alpha\beta} + \dots \right\}, \quad (22.70)$$

and the time dependence of items in the sum (22.69) is determined by the phase difference of instantaneous wave functions,

$$\Phi_{\alpha,\beta}(t) = \Phi_\alpha(t) - \Phi_\beta(t). \quad (22.71)$$

Taking the time derivative in (22.66), we derive the known results of the adiabatic perturbation theory, for diagonal,

$$\dot{E}_\alpha = v_i \left(\psi_\alpha, \frac{\partial V_0}{\partial X_i} \psi_\alpha \right) \equiv v_i (\nabla_i V_0)_{\alpha\alpha}, \quad (22.72)$$

and off-diagonal,

$$(\psi_\alpha, \dot{\psi}_\beta) = v_i \frac{(\nabla_i V_0)_{\alpha\beta}}{E_\beta - E_\alpha}, \quad \alpha \neq \beta, \quad (22.73)$$

quantities. The quantities $(\psi_\alpha, \dot{\psi}_\alpha)$ can be excluded by the choice of phases of functions (this follows from the normalization condition).

In the first order of adiabatic perturbation theory, we find the coefficients of the superposition (22.68),

$$c_\alpha(t) = c_\alpha^\circ + c_\alpha^{(1)}(t), \quad c_\alpha^{(1)}(t) = - \sum_\beta c_\beta^\circ \Lambda_{\alpha\beta}(t), \quad (22.74)$$

where the operator $\Lambda(t)$ is defined by its matrix elements,

$$\Lambda_{\alpha\beta}(t) = \int_{t_0}^t dt' \left\{ v_i \frac{(\nabla_i V_0)_{\alpha\beta}}{E_\beta - E_\alpha} + \frac{i}{\hbar} P_i (V_i)_{\alpha\beta} \right\}_{t'} e^{i\Phi_{\alpha\beta}(t')}. \quad (22.75)$$

In this approximation, the expectation value of any microscopic operator $Q(\xi)$, which can also contain an explicit time dependence through collective variables $X(t)$ and $P(t)$, can be found as

$$\langle Q \rangle = \langle Q \rangle^\circ + \sum_{\alpha\beta} [c^{(1)*}(t) c_\beta^\circ + c_\alpha^\circ c_\beta^{(1)*}(t)] \tilde{Q}_{\alpha\beta}(t), \quad (22.76)$$

where

$$\tilde{Q}_{\alpha\beta}(t) = Q_{\alpha\beta}(t) e^{i\Phi_{\alpha\beta}(t)}. \quad (22.77)$$

Introducing the evolution operator Λ from Eq. (22.75), the result takes the form

$$\langle Q \rangle = \langle Q \rangle^\circ - \langle \Lambda^\dagger \tilde{Q} + \tilde{Q} \Lambda \rangle^\circ, \quad (22.78)$$

where we use the averaging $\langle \dots \rangle^\circ = \text{Tr}(\rho^\circ \dots)$ of time-dependent operators over the density matrix $\rho_{\alpha\beta}^\circ = c_\beta^{*\circ} c_\alpha^\circ$ of the initial state.

Let us stress two important physical features of this approach. First, the result depends on the history of the process, an analog of the hydrodynamic viscose after-action, when a particle feels the influence of waves excited earlier in the medium by its own motion. Second, the collective velocity V_i enters on equal footing into the resulting friction force (the second item in the curly brackets of Eq. (22.75)). In general, one can develop a

kind of perturbation theory and the corresponding diagram technique for higher-order contributions, where new vertices appear in each order owing to higher terms of the Hamiltonian (60).

22.7 A Simple Model

In order to illustrate the physics discussed in an abstract form in the previous section, we consider here a simple example of a particle moving through a spatially uniform medium. Let the interaction of the particle with the medium be defined in a simplified potential form,

$$V = V_0(\mathbf{r}; \{\mathbf{r}_a\}) = \sum_a \phi(\mathbf{r} - \mathbf{r}_a), \quad (22.79)$$

where \mathbf{r} and \mathbf{r}_a are coordinates of a trial particle and constituents of the medium, respectively. We will neglect the direct influence of the intruder particle on the energy levels of the medium; then ψ_α and E_α are time-independent characteristics of the unperturbed medium.

The interaction (22.79) can be conveniently written in terms of the Fourier components $\phi_{\mathbf{k}}$ of the single-particle potential (22.79) and operators

$$\rho_{\mathbf{k}} = \sum_a e^{-i(\mathbf{k} \cdot \mathbf{r}_a)} \quad (22.80)$$

of the density fluctuations in the system,

$$V_0(\mathbf{r}) = \sum_{\mathbf{k}} \phi_{\mathbf{k}} \rho_{\mathbf{k}} e^{i(\mathbf{k} \cdot \mathbf{r})}. \quad (22.81)$$

In perturbation theory, we will encounter the operator $\zeta_{\mathbf{k}}$ with matrix elements

$$(\zeta_{\mathbf{k}})_{\alpha\beta} = \frac{(\rho_{\mathbf{k}})_{\alpha\beta}}{E_\beta - E_\alpha}. \quad (22.82)$$

As the energy difference corresponds to the time derivative, the operator (22.82) describes the integral over time of the density fluctuations.

Problem 22.3 Derive the equation of motion for the particle,

$$\dot{v}_i(t) = - \int_{t_0}^t dt' \Gamma_{ij}(t, t') v_j(t'), \quad (22.83)$$

where we have the *viscosity tensor* with retardation for a particle of mass m ,

$$\Gamma_{ij}(t, t') = \sum_{\mathbf{k}} \frac{k_i k_j}{m} |\phi_{\mathbf{k}}|^2 e^{i(\mathbf{k} \cdot (\mathbf{r}(t) - \mathbf{r}(t')))} \langle [\rho_{\mathbf{k}}(t), \zeta_{\mathbf{k}}^\dagger(t')] \rangle. \quad (22.84)$$

Physical properties of the medium are concentrated in the correlation function

$$G_{\mathbf{k}}(t, t') = \langle [\rho_{\mathbf{k}}(t), \zeta_{\mathbf{k}}^\dagger(t')] \rangle. \quad (22.85)$$

This is a response of the system at time t to an integrated action of density fluctuations during the previous time $t' < t$. There is an important *fluctuation-dissipation theorem*

in statistical mechanics [8, 9] that relates a spectral composition and intensity of fluctuations in a system to the dissipation of the external perturbation (the fluctuations have to decay in the same way as the system evolves to equilibrium). The result above extends this to the case of slow (but not necessarily weak) perturbations. One can show that it is equivalent to the classical results [10, 11] for Brownian motion in the medium with the given temperature.

In our problem, where ψ_α and E_α do not depend on time, the correlator (22.85) depends only on the difference $\tau = t - t'$. We can consider two cases of special interest. First, we assume that the density fluctuation operator $\rho_{\mathbf{k}}$ has many incoherent matrix elements which chaotically excite intrinsic degrees of freedom of the medium. Then the correlator of density fluctuations has to decay with time and it can be approximated by the Gaussian distribution,

$$G_{\mathbf{k}}(\tau) = G_{\mathbf{k}} e^{-(\tau/\tau_{\mathbf{k}})^2}. \quad (22.86)$$

Here the correlation (memory) time $\tau_{\mathbf{k}}$ is of the order $\hbar/V_{\mathbf{k}}$, where $V_{\mathbf{k}}$ are matrix elements of the particle interaction with the chaotic excitations of the medium with the wave vector \mathbf{k} .

Owing to a large number of degrees of freedom in the medium, the characteristic time intervals τ can be sufficiently small, at least for the wave vectors $k \sim 1/r_0$ which are the most effective for excitation of single-particle modes (r_0 is the average distance between particles). If the motion does not considerably change during such time intervals, we come to the usual Newtonian equation of motion with dissipation without retardation,

$$\dot{v}_i = -\gamma_{ij} v_j, \quad (22.87)$$

where

$$\gamma_{ij} = \frac{\sqrt{\pi}}{2} \sum_{\mathbf{k}} \frac{k_i k_j}{m} |\phi_{\mathbf{k}}|^2 G_{\mathbf{k}} \tau_{\mathbf{k}} e^{-(\mathbf{k} \cdot \mathbf{v})^2 \tau^2}. \quad (22.88)$$

This part of dissipation is generated by multistep incoherent processes with the average energy transfer in a single act

$$\Delta\epsilon \sim \hbar(\mathbf{k} \cdot \mathbf{v}) \leq \frac{\hbar}{\tau_{\mathbf{k}}}. \quad (22.89)$$

In the motion of a particle in a viscose medium, $kv \sim v/r_0 \ll (1/\tau_k)$, where τ_k is, by order of magnitude, a mean free path time between collisions with particles of the medium. Then we have the isotropic velocity-independent friction,

$$\gamma_{ij} = \frac{\sqrt{\pi}}{6} \sum_{\mathbf{k}} \frac{k^2}{m} |\phi_{\mathbf{k}}|^2 G_{\mathbf{k}} \tau_{\mathbf{k}} \delta_{ij}. \quad (22.90)$$

There exists another possible contribution to the correlation function $G_{\mathbf{k}}(t, t')$ due to the excitation of weakly damping collective modes, in this problem, longitudinal waves propagating in the medium. A wave packet with wave vector \mathbf{k} , typical frequency $\omega_{\mathbf{k}}$, and damping $\gamma_{\mathbf{k}}$ gives a typical contribution

$$\overline{|\rho_{\mathbf{k}}|^2} \frac{e^{-i(\omega_{\mathbf{k}} - i\gamma_{\mathbf{k}})(t-t')}}{\omega_{\mathbf{k}}}. \quad (22.91)$$

Then the equation of motion is quite complicated,

$$\dot{v}_i(t) = - \frac{k_i k_j}{m \omega_{\mathbf{k}}} |\phi_{\mathbf{k}}|^2 \overline{|\rho_{\mathbf{k}}|^2} \int_{t_0}^t dt' v_j(t') e^{i(\mathbf{k} \cdot \int_{t'}^t dt'' \mathbf{v}(t'')) - i(\omega_{\mathbf{k}} - i\gamma_{\mathbf{k}})(t-t')}.$$
 (22.92)

In the limit of long time t , the main contribution comes from the time moments t' when it becomes possible for the particle to emit the real wave (Cherenkov effect) with laws of conservation of momentum and energy fulfilled, $\omega_{\mathbf{k}} = (\mathbf{k} \cdot \mathbf{v}(t'))$. Such waves are emitted with Cherenkov angle in the direction of the particle trajectory, while the velocity of the particle exceeds the phase velocity ω_k/k of this wave. This analogy is valid if the dissipation of the wave and corresponding deceleration of the particle are sufficiently small. Owing to the resonance condition, the denominator $\omega_{\mathbf{k}}$ cancels the factor $(\mathbf{k} \cdot \mathbf{v}(t'))$, and the result is not proportional to the particle velocity; it does not resemble a primitive friction force giving, instead, the losses proportional to the distance of propagation.

In the physics of deep-inelastic processes, certainly both dissipation mechanisms coexist, namely, incoherent excitation of many chaotic degrees of freedom (uncorrelated superposition of particle–hole excitations in the Fermi system) and coherent excitation of collective waves. In agreement with the observed picture, one can expect the important contributions from the states of the giant-resonance type excited in the double-nuclear system.

22.8 Nuclear Multifragmentation

Here we briefly discuss a phenomenon that takes place at higher excitation energies. By an usual relation between energy and nuclear temperature in heavy nuclei, such energies would correspond to high temperature around 10 MeV. This is already higher than the typical binding energy per nucleon, 6–8 MeV. In fact, the mean-field calculations using the Skyrme parameterizations (but usually for symmetric nuclear matter with $N = Z$) predict even higher temperature at approximately 16 MeV but the surface and Coulomb effects of a finite size make the temperature lower. Indeed, in the LDM, we have a similar drop of the nucleon binding energy from the volume term to actual values. The analogs of the multifragmentation phenomenon can be found in physics of atomic clusters and even in stellar processes with a great role of gravitation.

Essentially, we have to deal here with the nuclear phase transition from Fermi liquid to Fermi gas, or, as it is sometimes called, *liquid–fog* transition [12]. It is natural to look for the analogy with a classical liquid–gas first-order phase transition in van der Waals gas. The common physical background comes from the qualitative similarity of typical particle–particle interactions: sharp repulsion at short distances and milder attraction at characteristic interparticle distances. The difference between macroscopic gas–liquid systems and the nuclear processes with not more than hundreds of particles is important and analogies can serve only as a hint. The chance of the whole dismantling of the nucleus at high excitation was envisaged by Niels Bohr as early as in 1936, but with more semblance to a nuclear explosion.

The term *multifragmentation* proper means the emission of nuclear fragments of different sizes and charges in a heavy-ion collision at sufficiently high energy. The expression “intermediate mass fragments” (IMF) is frequently used for the fragments

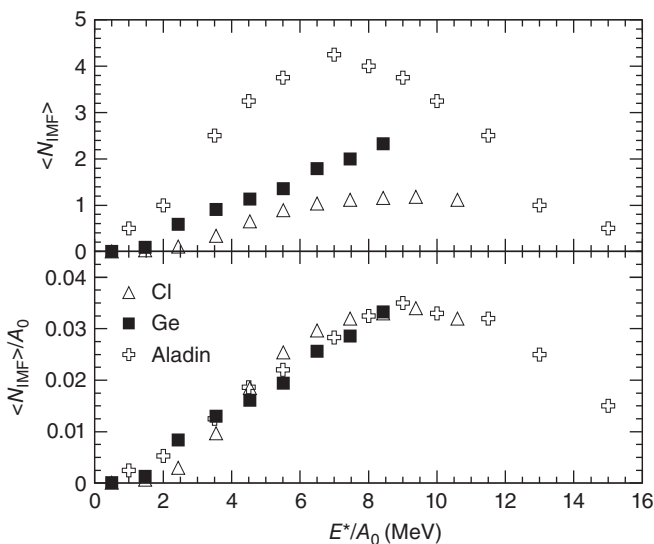


Figure 22.8 The average IMF number as a function of excitation energy (upper part); the same scaled by the size of the emitting source A_0 (lower part). (Beaulieu *et al.* [13]. Reproduced with permission of American Physical Society.)

heavier than alpha particles, $Z > 2$. Figure 22.8 shows the IMF production in a peripheral collision of a fast projectile with a nuclear target [13]. The fast projectile becomes an emitter, and the emission products are selected and analyzed. The number of IMF normalized to the size A_0 of the emission source shows a universal function of excitation energy per nucleon. The number of IMF scaled in this way grows linearly with energy up to approximately 9 MeV (excitation energy is found event by event as it is frequently done in particle experiments) and then goes down. In the emitter frame, the distribution of the fragments is close to isotropic and energy distribution is Maxwellian. The similarity covers very different processes including the scattering of uranium projectiles off a gold target at energy 600 MeV per nucleon (the process at the lowest energy was at 35 MeV per nucleon). This scaling would contradict to the idea of sequential decay with a strong size dependence.

Although the peak of experimental and theoretical interest to nuclear multifragmentation occurred about 20 years ago, until now there is no fully convincing theoretical description of this phenomenon. This interest was shielded by the experiments at the Relativistic Heavy Ion Collider (RHIC) and later at the Large Hadron Collider (LHC) directed at the study of quark–gluon matter created in nuclear collisions with much higher energies. A review of experimental data on multifragmentation and related physics can be found in Ref. [14].

Among several theoretical constructions aimed at the physics of multifragmentation, we can mention the *percolation* model [15] and the *lattice gas* model [16]. It is instructive to understand how the mechanism of the phase transition comes from the rough properties of the nucleon interactions considered within the simplest, essentially classical, mean-field approximation [16].

Dividing the partition function (statistical sum) of the heated nucleus (temperature T) into the kinetic part and the part due to the interparticle interaction U , we understand

that the phase transitions can come only from the second part that is usually called, as in the theory of the virial coefficients, the *configuration integral*,

$$Q(T) = \int \prod_a d^3 r_a e^{-U/T}. \quad (22.93)$$

As in the classical *lattice gas* model, each particle can occupy \mathcal{N} positions which give the total volume $V = r_0^3 \mathcal{N}$. Here r_0 is the characteristic size of the volume per particle at normal nuclear density, somewhat bigger than the size of the repulsive core of the nucleon. The volume of the cold nucleus with N nucleons then is $V_0 = r_0^3 N$. The particles in neighboring sites interact attractively, with effective mean energy $-\epsilon$ that should be of the order of the binding energy per particle in a normal nucleus. The number of neighboring sites in a three-dimensional lattice is $z = 6$. The average number of neighbors to interact with is zN/\mathcal{N} which means that the number of interacting pairs in the system equals $(1/2)N \times zN/\mathcal{N}$, while the degeneracy of this configuration leads to the configuration integral (22.93) as

$$Q = \frac{\mathcal{N}!}{N!(\mathcal{N}-N)!} e^{\epsilon z(N^2/\mathcal{N})/(2T)}. \quad (22.94)$$

Problem 22.4 Using the Stirling formula for the factorials in Eq. (22.94), derive the equation of state for the system.

Solution

Pressure at constant temperature is found as

$$P = T \left(\frac{\partial \ln Q}{\partial V} \right)_T \quad (22.95)$$

(the kinetic part of the partition function does not depend on the volume). The Stirling formula for factorials leads to

$$P = \frac{T}{r_0^3} \ln \frac{\mathcal{N}}{\mathcal{N}-N} - \frac{z\epsilon}{2r_0^3} \left(\frac{N}{\mathcal{N}} \right)^2, \quad (22.96)$$

or introducing the rarefied density $\rho = \rho_0(N/\mathcal{N}) = \rho_0(V_0/V)$, we come to the equation of state

$$P = T \rho_0 \ln \frac{V}{V - V_0} - \frac{z}{2} \epsilon \rho_0 \left(\frac{V_0}{V} \right)^2. \quad (22.97)$$

This is qualitatively similar to the van der Waals model, where

$$P = \frac{NT}{V-b} - \frac{a}{V^2}. \quad (22.98)$$

The constant b (increase of pressure due to short-range repulsion) is similar to V_0 ; the constant a reflects the attraction part of the interaction.

Problem 22.5 Determine the critical point of the lattice gas described by the equation of state (22.97).

Solution

The critical point $\rho = \rho_c$ corresponds to

$$\frac{\partial P}{\partial \rho} = 0, \quad \frac{\partial^2 P}{\partial \rho^2} = 0. \quad (22.99)$$

The algebra with Eq. (22.97) defines the critical density and critical temperature:

$$\rho_c = \frac{1}{2} \rho_0, \quad T_c = \frac{z\epsilon}{4}. \quad (22.100)$$

The isotherms $P(V)$ derived from this oversimplified model agree with those obtained from more detailed considerations.

The kinetic part of the statistical partition function is necessary for modeling the fragment distributions. This is typically done by Monte Carlo sampling that generates clusters according to some thermodynamic conditions, the simplest one would be the requirement for the pair of nucleons to belong to the same cluster if the kinetic energy of their relative motion in the Maxwell distribution is smaller than ϵ . Of course, the realistic models are much more elaborate in the attempt to cover many experimental observables including the collective flow, which we did not discuss here.

22.9 More about Fusion Reactions

The last section in this chapter we devote to a brief description of some ideas which can influence the fusion reactions including those of thermonuclear type. To find a real (not a notorious “*cold fusion*”) mechanism of enhancement of the fusion reactions would be extremely important for the most important applications of nuclear physics as well as for understanding astrophysical processes.

There are reliable experimental results showing that at low energy, the fusion processes in some cases have probabilities exceeding the predictions of the elementary barrier penetration models [17]. Interesting and still not fully understood results were obtained in studies of deuteron fusion in certain environments. It is known that some substances, for example, titanium and palladium (the best seems to be palladium oxide), can accommodate incorporated protons or deuterons in a concentration comparable to the atomic concentration of the host. It was observed [18] that normal chemical reactions in such cases are accompanied by neutron emission from the fusion reaction $d + d \rightarrow {}^3\text{He} + n$. The neutron production (as well as that of protons in the charge conjugate reaction ended with ${}^3\text{He} + p$) grows compared to the normal prediction based on the Coulomb barrier penetration by one to two orders of magnitude [19].

There exist several solid-state aspects [20], including electron screening, that can enhance the fusion probability compared to the simple barrier estimate for the reaction in vacuum, especially at low energy (where, regrettably, the absolute fusion cross section is also low). In particular, we can mention the *colliding beam mechanism*. The deuteron implanted in a solid and localized near the heavy host nucleus has a wave function that contains the relatively large momentum components. Then there is a probability of interaction with an external deuteron in the regime of colliding beams. In a limiting case, this transition to the relative velocity in the $d-d$ collision will change the barrier penetration exponent by a factor of $\sqrt{2}$.

Unrelated to the effects of matter, there are pure nuclear physics factors which enhance the low-energy fusion probability compared to the pure barrier exponents. This is confirmed, for example, in the fusion experiments with exotic helium isotopes, ^6He and ^8He , as projectiles [21–23]. At low projectile energy, below the Coulomb barrier, the fusion cross section with the heavy target nucleus is noticeably higher than the simple barrier estimates. There are nuclear effects responsible for such an enhancement just at low energy.

We can understand the underlying physics with a simple one-dimensional model [24]. Let a compound particle being a loosely bound state of two constituents, x and y (an analog of the deuteron), slowly move in an external potential that is acting differently on the two components. The Hamiltonian of the system can be written as

$$H = K_x + K_y + V(x - y) + U_x(x) + U_y(y), \quad (22.101)$$

with obvious notations. The wave function $\Psi(R, r)$ of the system in variables R of the center of mass and r of relative motion (corresponding masses are M and μ) satisfies the stationary Schrödinger equation

$$\left\{ -\frac{\hbar^2}{2M} \frac{\partial^2}{\partial R^2} - \frac{\hbar^2}{2\mu} \frac{\partial^2}{\partial r^2} + V(r) + U_x(R_+) + U_y(R_-) - E \right\} \Psi(R, r) = 0, \quad (22.102)$$

where $R_{\pm} = R \pm r(m_y/M)$.

The variables r and R cannot be separated but we are interested in a special case of slow motion of the system as a whole. Then we can use the *adiabatic* approximation considering the intrinsic state of the system at the slow changing global coordinate R in the same spirit as in the fission problem where we have treated intrinsic wave functions at slow changing deformation parameters.

Problem 22.6

- a) Formulate an adiabatic variational ansatz as $\Psi(R, r) = \psi(R)\chi(r; R)$, where the intrinsic function χ at fixed R satisfies

$$\left\{ -\frac{\hbar^2}{2\mu} \frac{\partial^2}{\partial r^2} + V(r) + U_x(R_+) + U_y(R_-) - \epsilon(R) \right\} \chi(r; R) = 0, \quad (22.103)$$

where we have now the evolving energy term $\epsilon(R)$.

- b) Multiply Eq. (22.103) by $\chi^*(r; R)$, integrate over r at fixed R , and derive the new equation for the slow variable R ,

$$\psi'' + 2\alpha(R)\psi' + \beta(R)\psi + \frac{2M}{\hbar^2} [E - \epsilon(R)]\psi = 0, \quad (22.104)$$

where the notations are introduced for the integrals over the intrinsic variable,

$$\alpha(R) = \frac{\langle \chi | (\partial \chi / \partial R) \rangle}{\langle \chi | \chi \rangle}, \quad \beta(R) = \frac{\langle \chi | (\partial^2 \chi / \partial R^2) \rangle}{\langle \chi | \chi \rangle}. \quad (22.105)$$

- c) Transform the result to the standard quantum form

$$\phi'' + \frac{2M}{\hbar^2} [E - \tilde{U}(R)]\phi = 0, \quad (22.106)$$

where the new function is

$$\phi(R) = \psi(R)e^{\int \alpha(R) dR}, \quad (22.107)$$

and the new effective potential for the global motion of the system is

$$\tilde{U}(R) = \epsilon(R) - \epsilon(\infty) + \frac{\hbar^2}{2M} [\alpha^2(R) + \alpha'(R) - \beta(R)]. \quad (22.108)$$

A simple but instructive case [24] is a crude model of the deuteron penetrating the barrier; the relative interaction $V(r)$ was taken as a well with the deuteronlike bound state. If the barrier is of the Coulomb origin, the neutron, the y -particle, does not feel it but the proton, the x -particle, does. For the model of a rectangular barrier, the comparison of the original barrier U_x with the effective one, \tilde{U} , is shown in Figure 22.9a. The effective barrier is significantly lower and smoother. Figure 22.9b shows the transmission probability through such a barrier as a function of energy E . A considerable enhancement at low energy is clear.

The effect shown in this model example demonstrates the general mechanism of fusion enhancement in the case of a loosely bound nuclear projectile. In the adiabatic case of low energy (note that the solution of Problem 22.6 takes into account nonadiabatic corrections), the complex system, the deuteron in this model and in the experiment [19], has enough time to restructure itself. As a result, the neutron, not feeling the Coulomb barrier, travels inside the target at a distance larger than the size of the original loosely bound system. Then the proton being stripped of a heavy load can tunnel with a smaller mass and therefore with greater transmission. This mechanism seems to be of a very general character. It was also studied [25] in a problem where the proton has to be fully reflected from the infinite barrier, while the neutron (bound to the proton) can penetrate but still has to return because of energy conservation. This problem is really difficult computationally because the reflection of the neutron comes as a sum of very many virtual neutron states behind the barrier; the solution requires special mathematical treatment. This mechanism can act in the solid-state environment as well.

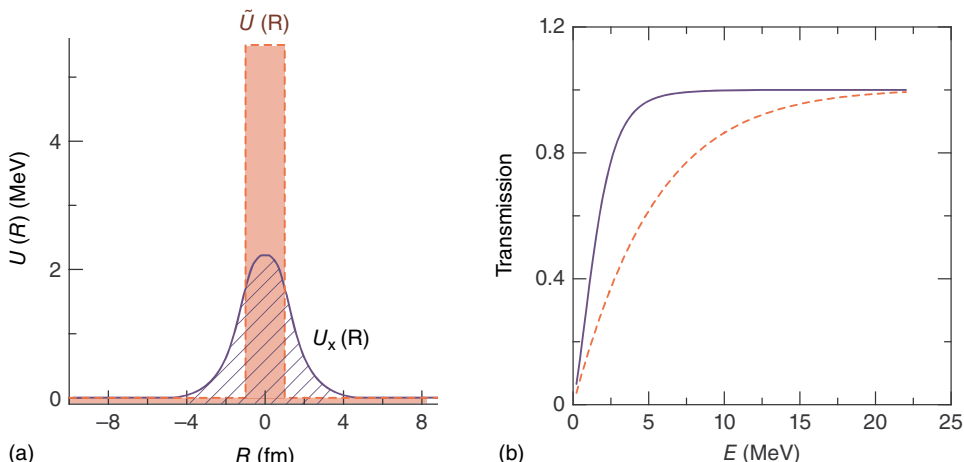


Figure 22.9 (a) Original potential (solid line) and effective potential experienced by the composite system (dashed line); (b) corresponding tunneling probability; see Ref. [24].

References

- 1 M.I. Sobel *et al.*, Nucl. Phys. **A251**, 502 (1975).
- 2 K.K. Gudima and V.D. Toneev, in *Proceedings of the International Conference on Selected Problems in Nuclear Structure* Dubna, 1976, p. 169.
- 3 A.G. Artukh *et al.*, Nucl. Phys. **A215**, 91 (1973).
- 4 V.V. Volkov, Nukleonika **21**, 53 (1976).
- 5 W. Nörenberg, Phys. Lett. B **52**, 289 (1974).
- 6 (a) W.U. Schröder *et al.*, Phys. Rev. Lett. **36**, 514 (1976); (b) L.G. Moretto *et al.*, Phys. Rev. Lett. **36**, 1069 (1976); (c) J.R. Huizenga *et al.*, Phys. Rev. Lett. **37**, 885 (1976).
- 7 P. Bonche, S. Koonin, and J.W. Negele, Phys. Rev. C **13**, 1226 (1976).
- 8 H.B. Callen and T. A. Welton, Phys. Rev. **83**, 34 (1951).
- 9 L.E. Reichl, *A Modern Course in Statistical Physics*, 3rd edn, John Wiley & Sons, Inc., New York, 2009.
- 10 J.G. Kirkwood, J. Chem. Phys. **14**, 180 (1946).
- 11 R. Eisenschitz, *Statistical Theory of Irreversible Processes*, Oxford University Press, London, 1958.
- 12 P.J. Siemens, Nature **305**, 410 (1983).
- 13 L. Beaulieu *et al.*, Phys. Rev. C **54**, R973 (1996).
- 14 B. Borderie and M.F. Rivet, Prog. Part. Nucl. Phys. **61**, 551 (2008).
- 15 W. Bauer, Phys. Rev. C **38**, 1297 (1988).
- 16 J. Pan and S. Das Gupta, Phys. Rev. C **51**, 1384 (1995).
- 17 S.E. Jones, E.P. Palmer, J.B. Czirr, D.L. Decker, G.L. Jensen, J.M. Thorne, S.P. Taylor, and J. Rafelski, Nature **338**, 737 (1989).
- 18 A. Arzhannikov and G. Kezerashvili, Phys. Lett. A **156**, 514 (1991).
- 19 H. Yuki, J. Kasagi, A.G. Lipson, T. Ohisuki, T. Baba, T. Noda, B.F. Lyakhov, and N. Asami, JETP Lett. **68**, 823 (1998).
- 20 B.L. Altshuler, V.V. Flambaum, M.Yu. Kuchiev, and V.G. Zelevinsky, J. Phys. G **27**, 2345 (2001).
- 21 A. Lemasson *et al.*, Phys. Rev. Lett. **103**, 232701 (2009).
- 22 D. Ackermann and H. Simon, Physics **2**, 101 (2009).
- 23 A. Lemasson *et al.*, Phys. Lett. B **697**, 454 (2011).
- 24 C.A. Bertulani, V.V. Flambaum, and V. Zelevinsky, J. Phys. G **34**, 2289 (2007).
- 25 N. Ahsan and A. Volya, Phys. Rev. C **82**, 064607 (2010).

23

Configuration Interaction Approach

The effectiveness of quantum science depends on its accuracy in predicting phenomena detected in apparatus, even if we never personally witness quantum fields at work.

Phillip F. Schewe, *Maverick Genius*, St. Martin's Press, 2013

23.1 Center-of-Mass Problem

In this chapter, we will discuss in more detail certain questions related to the shell-model calculations (borrowing the term from quantum chemistry, these approaches are often referred to as *configuration interaction*). From a general point of view, here we select, on the basis of physical grounds, a set of many-body configurations, accept (or derive from more fundamental principles) a many-body Hamiltonian, and solve the Schrödinger equation to find the stationary wave functions, their energies, possible decay widths, expectation values of various observables, and transition probabilities. We have to remind the reader that the basic discussions of the nuclear shell model can be found in Chapters 8 (empirical evidence, harmonic oscillator, and more realistic potentials, corresponding single-particle orbitals, semiclassical limit), 9 (many-body configurations, observables, group properties), 11 (formalism of secondary quantization), 12 (deformed shell model), 13 (pairing interaction as a part of the effective shell-model Hamiltonian), 14 and 15 (electromagnetic transitions between shell-model states). We also introduced physical approximation for certain classes of states (mean field, collective rotational and vibrational states, etc.) Here we will touch more specific problems of this approach in real action.

We start with a general nonrelativistic Hamiltonian

$$H = \sum_a \frac{\mathbf{p}_a^2}{2M} + \frac{1}{2} \sum_{a \neq b} U_{ab} \quad (23.1)$$

that consists of kinetic energy and two-body interaction terms (later we will comment on many-body interactions). A technical problem is associated with the motion of the system as a whole. It is not a subject of our interest but the Hamiltonian (23.1) for a finite system contains this motion as well; it should be fully separated from the physics of intrinsic states which are the subject of our interest. A formal solution would be the construction of the many-body eigenfunctions $\Psi(\mathbf{r}_1, \dots, \mathbf{r}_A; \mathbf{R})$ for an arbitrary choice

of the coordinate origin \mathbf{R} and projection of this function that depends only on relative distances $\mathbf{r}_a - \mathbf{R}$ on a plane-wave state of the uniform motion of the entire system with momentum $\mathbf{P} = \sum_a \mathbf{p}_a$:

$$\Psi_{\mathbf{P}}(\mathbf{r}_1, \dots, \mathbf{r}_A) = \int d^3R e^{i(\mathbf{P} \cdot \mathbf{R})} \Psi(\mathbf{r}_1, \dots, \mathbf{r}_A; \mathbf{R}); \quad (23.2)$$

the choice $\mathbf{P} = 0$ corresponding to the system at rest, $\hbar = 1$. The kinetic energy operator applied to such an A -nucleon function will separate the center-of-mass energy. This formal method can be practically applied only to the lightest few-body systems.

The Hamiltonian (1) contains a continuum spectrum corresponding to the center-of-mass kinetic energy. In the shell-model applications, we can rewrite the Hamiltonian as

$$H = \frac{\mathbf{P}^2}{2MA} + H_{\text{int}}, \quad (23.3)$$

where the center-of-mass kinetic energy, defined by the total momentum operator is separated from the intrinsic part using the following identity:

$$\sum_a \frac{\mathbf{p}_a^2}{2M} = \frac{\mathbf{P}^2}{2MA} + \frac{1}{2A} \sum_{a,b} \frac{(\mathbf{p}_a - \mathbf{p}_b)^2}{2M}. \quad (23.4)$$

Therefore,

$$H_{\text{int}} = \frac{1}{2A} \sum_{a,b} \frac{(\mathbf{p}_a - \mathbf{p}_b)^2}{2M} + \frac{1}{2} \sum_{a \neq b} U_{ab}. \quad (23.5)$$

The intrinsic part does not depend on the center-of-mass coordinate $\mathbf{R} = (1/A) \sum_a \mathbf{r}_a$. Thus, the wave function of the whole system is a product of the intrinsic wave function and the trivial center-of-mass part $e^{i\mathbf{P} \cdot \mathbf{R}}$.

We are interested only in the intrinsic part of the wave function that describes relative motion of nucleons, but the many-body states built as Slater determinants of single-particle wave functions depend on all A single-nucleon variables and separating intrinsic and center-of-mass parts becomes difficult. The intrinsic Hamiltonian by itself is degenerate with respect to center-of-mass motion. The truncation of basis inherently present in the shell-model applications usually leads to multiple spurious states; we will encounter this problem again in the calculation of the level density.

In order to break the center-of-mass degeneracy, one can localize the center of mass, adding a potential part for the center-of-mass variable. The harmonic oscillator center-of-mass Hamiltonian

$$H_{\text{cm}}(\omega_0) = \frac{\mathbf{P}^2}{2MA} + \frac{AM\omega_0^2}{2} \mathbf{R}^2 \quad (23.6)$$

is a good choice that retains the two-body nature of Hamiltonian operator; therefore, we consider an auxiliary Hamiltonian defined as

$$H(\omega_0) = H + \frac{AM\omega_0^2}{2} \mathbf{R}^2 = H_{\text{cm}}(\omega_0) + H_{\text{int}} \quad (23.7)$$

that depends on the frequency parameter ω_0 . The spectrum of $H(\omega_0)$ consists of intrinsic excitations repeated for every center-of-mass excitation energy $\hbar\omega_0(N_{\text{cm}} + 3/2)$; many-body eigenstates contain intrinsic wave functions multiplied by the harmonic

oscillator wave functions for the center-of-mass variable. We select only the states with $N_{\text{cm}} = 0$, while the states with $N_{\text{cm}} > 0$ are referred to as *spurious*.

At this stage, the single-particle basis can be selected arbitrarily; however, using the harmonic oscillator with the same frequency ω_0 for single-particle basis states simplifies the problem. The Hamiltonian (23.7) can be expressed also as

$$H(\omega_0) = \sum_a \hat{\epsilon}_a + \frac{1}{2} \sum_{a \neq b} U'_{ab} \quad (23.8)$$

where the single-particle Hamiltonian for the particle a is

$$\hat{\epsilon}_a = \frac{\mathbf{p}_a^2}{2M} + \frac{M\omega_0^2}{2} \mathbf{r}_a^2, \quad (23.9)$$

and the residual interaction between particles a and b is defined as

$$U'_{ab} = U_{ab} - \frac{M\omega_0^2}{2} (\mathbf{r}_a - \mathbf{r}_b)^2. \quad (23.10)$$

If $\hat{\epsilon}$ is used to define basis states, then the entire kinetic part becomes diagonal. In addition to that, the harmonic oscillator basis provides a systematic way for treating the center-of-mass problem as expansion over the basis states. It is important that the projection operation, which selects the part of space spanned by the basis states, commute with the center-of-mass Hamiltonian and harmonic excitations of the center of mass are not broken by partial truncation. In the case of the harmonic oscillator, the total number of oscillator excitation quanta is known for each many-body basis state, and this number is shared between the center-of-mass and intrinsic excitations.

Problem 23.1 Consider a single-oscillator shell valence space where all states below this shell are completely occupied and all states above are empty. In this space, the many-body states are made by redistributing particles within the valence oscillator shell. Show that this valence space contains no spurious states, namely, there are no states other than those with $N_{\text{cm}} = 0$.

Solution

Let us act with the operator annihilating the quanta of the center-of-mass oscillator. Using terminology of the second quantization, this is a sum of one-body operators which annihilate a nucleon from a given oscillator shell and create one on the oscillator shell below. In this valence space, the action of this operator onto any state gives zero because the final states are Pauli blocked. This proves that $N_{\text{cm}} = 0$.

These arguments can be extended to provide a general many-body truncation scheme. Starting with a Fermi configuration where all states within a single shell have a given total number of oscillator quanta N_0 , as a next step in expanding basis, we consider all one-particle-hole excitations to the next shell. These are the states of opposite parity with $N_0 + 1$ oscillator quanta where one particle is promoted to a higher shell (either from the valence shell up or from the shell below into the valence shell). The annihilation operator of the center-of-mass oscillator quantum can act only once, therefore such space, along with the states with $N_{\text{cm}} = 0$, contains also spurious states with $N_{\text{cm}} = 1$. In practice, the basis states are restricted by a maximum number of oscillator quanta N_{max} , and these states can contain center-of-mass excitations with $N_{\text{cm}} \leq N_{\text{max}} - N_0$.

Problem 23.2 The low-lying excited states in the doubly magic ^{16}O nucleus are particle–hole excitations with one nucleon promoted from the $0p$ shell into the $1s\ 0d$ oscillator shell. What is the total number of such states, what is the number of spurious states, and what are the quantum numbers of the spurious states?

Solution

Counting all possible couplings of quantum numbers of one hole and one particle we determine that there are 32 angular momentum multiplets, 16 of those having isospin $T = 0$ and 16 with $T = 1$; all states having negative parity. There is only one spurious state with quantum numbers $J^\Pi = 1^-, T = 0$. The only possible way to make such a state is to act with the center-of-mass oscillator creation operator onto a nonspurious 0^+ ground state of ^{16}O . This operator is a linear combination of \mathbf{R} and $i\mathbf{P}$, which determine the quantum numbers of the $N_{\text{cm}} = 1$ spurious state.

While ω_0 is just a parameter, a good physically relevant choice of the single-particle potential can substantially improve convergence; this choice can be guided by Eq. (8.16). When ω_0 is smaller than the energies of nonspurious excited states, it may be convenient to consider a more general Hamiltonian $H_{\text{int}} + \beta H_{\text{cm}}$; the $H(\omega_0)$ described above would then correspond to the $\beta = 1$ case. The additional term pushes spurious states further up in the spectrum. This procedure [1] can be used for approximate separation of the center-of-mass motion in situations where exact decoupling of spurious states is not possible.

23.2 Matrix Elements of Two-Body Interactions

If the two-body interactions U_{ab} are known, then one can evaluate matrix elements of the interaction Hamiltonian as discussed in Chapter 11 and apply the formalism of the second quantization to treat the full many-body problem. The number of matrix elements can be very large and the center-of-mass separation available for harmonic oscillator states is quite helpful. For brevity, in this section, we omit spin and isospin degrees of freedom.

The translationally invariant interaction depends only on the relative interparticle distance, $U_{ab} = U(\mathbf{r}_a - \mathbf{r}_b)$, making it appealing to evaluate it in the center-of-mass frame of the interacting particles. It is obvious that the Hamiltonian $\sum_a \hat{\epsilon}_a$ is invariant with respect to any orthogonal transformation of coordinates \mathbf{r}_a . In particular, for two particles, we can use a linear transformation $\mathbf{r}_\pm = (\mathbf{r}_1 \pm \mathbf{r}_2)/\sqrt{2}$ to express products of two harmonic oscillator wave functions $\psi_{n_1 \ell_1 m_1}(\mathbf{r}_1) \psi_{n_2 \ell_2 m_2}(\mathbf{r}_2)$ in terms of products $\psi_{n_+ \ell_+ m_+}(\mathbf{r}_+) \psi_{n_- \ell_- m_-}(\mathbf{r}_-)$. This rotation of coordinates is a symmetry operation and the two-nucleon states mix only within a given irreducible representation. The irreducible representation and its dimensionality is inferred from the degeneracy of eigenstates which in turn is given by the number of quanta. Thus we can formally write

$$|n_1 \ell_1, n_2 \ell_2; L\Lambda\rangle = \sum |n_+ \ell_+, n_- \ell_-; L\Lambda\rangle \langle n_+ \ell_+, n_- \ell_-; L| n_1 \ell_1, n_2 \ell_2; L\rangle, \quad (23.11)$$

where the summation goes over all n_\pm and ℓ_\pm allowed by angular momentum and restricted by oscillator quanta $2n_1 + \ell_1 + 2n_2 + \ell_2 = 2n_+ + \ell_+ + 2n_- + \ell_-$.

The coefficients $\langle n_+ \ell_+, n_- \ell_-; L | n_1 \ell_1, n_2 \ell_2; L \rangle$ are known as oscillator brackets or Talmi–Moshinsky coefficients; they are analogous to the rotational D -matrices with a specific angle of rotation 45° between \mathbf{r}_1 and \mathbf{r}_2 . This procedure can be generalized for particles of different masses, which would require a different angle. Therefore, similar to the discussion in momentum space, Eq. (11.58), with the help of center-of-mass separation in two-nucleon states, the integrals of type (12.44) are all reduced to one integration over the relative variable [2].

In many shell-model versions, the residual interaction is not characterized by explicit potentials depending on coordinates and spins. Instead, the two-body matrix elements allowed by the conservation laws (angular momentum, parity, isospin) in a selected orbital space are just fitted by experimental data and some theoretical arguments. Using the Wigner–Eckart theorem, we need to fit only reduced matrix elements because the dependence of magnetic quantum numbers is completely fixed by the Clebsch–Gordan coefficients. But the number of nonzero matrix elements rapidly grows with the size of the space. One of the best examples is given by the sd -space with only three orbitals for protons and the same for neutrons. Here one has 63 two-body matrix elements [3] and not all of them are practically well defined. The number increases if small isospin-violating matrix elements are allowed. We will return to this example later.

23.3 *Ab initio* Approach

As a first illustration, we demonstrate the combined many-body approach using a three-body model of the positronium ion, a system of two electrons and one positron. This simplest well-defined three-body system driven exclusively by the Coulomb interaction, where relativity and other QED effects are all ignored, has been commonly used to benchmark many-body techniques. The exact ground-state energy of this model system, known with high precision, is shown in Figure 23.1 by a dashed horizontal grid line. The ground-state energies as a function of oscillator length, or equivalently oscillator frequency $\hbar\omega_0$, are shown for different truncations N_{\max} .

Numerous similar *ab initio* no-core (which means that the orbital space includes all occupied orbitals without truncation from below) studies have been done for light nuclei; one of such examples is shown in Figure 23.2; here, the convergence of the ground-state energy as a function of upper truncation N_{\max} is explored. The solid black curve shows the convergence of the method discussed here, using “bare” (unmodified) two-body Argonne v_{18} potential (Section 3.2). One can observe that the convergence is poor and it is generally difficult to obtain good results using the direct expansion; this is also evident from Figure 23.1. In order to improve the situation, we need to understand what information about the nuclear Hamiltonian and which truncation scheme provide the best path to solutions.

By including highly excited oscillator states in our basis, we go to higher energies involving wave functions which have more nodes and provide higher and higher spatial resolution. If we used plane waves, or basis states of a large infinite square well, then the behavior of the matrix elements of the Coulomb potential is inversely proportional to the momentum transfer squared. This suggests that we should expect a power-law convergence. The convergence shown in Figure 23.2 is given by the power law proportional to $1/N_{\max}^3$. By including high-energy basis states we inadvertently probe

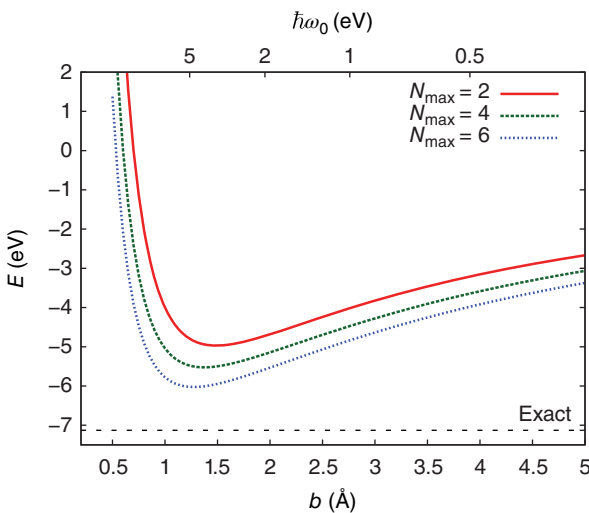


Figure 23.1 *Ab initio* no-core study of the positronium ion. The curves show ground-state energy as a function of oscillator length b (the top axis shows the corresponding $\omega_0 = \hbar/m b^2$) for different truncations N_{\max} ; the dashed grid line indicates the exact result.

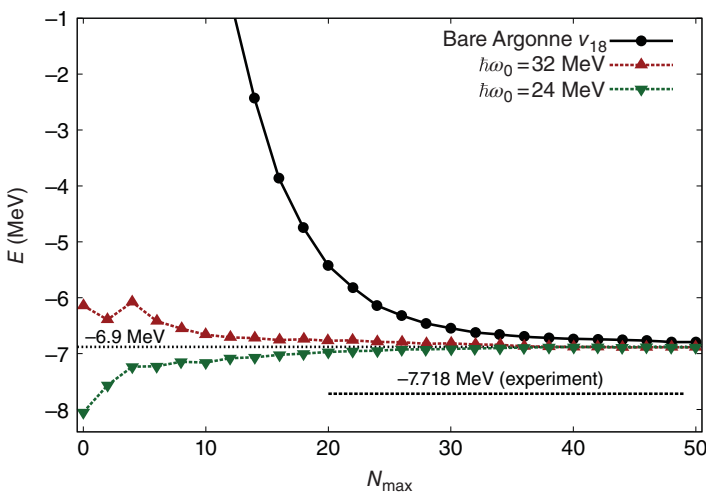


Figure 23.2 Convergence of ground-state energy of ${}^3\text{He}$ as a function of N_{\max} using the Argonne v_{18} nucleon–nucleon potential. One curve shows convergence when “bare” potential is used, and two other curves with $\hbar\omega_0 = 32$ and 24 MeV show results of calculations when interactions are renormalized. The data and details of these calculations are from Ref. [4].

the nucleon–nucleon interaction at shorter distances where it has a strong repulsive core that brings high-momentum components. The interactions at short distances are often not known and defined by physics outside our low-energy domain. We expect the answers to the low-energy questions to be insensitive to details of the behavior at high energy. The so-called *soft-core* versions of nucleon–nucleon potentials or direct removal of high-momentum components are among the methods used to control this problem. However, changes to the potential modify low-energy observables of interest and, while new fits to data can be performed, the procedure becomes cumbersome if one needs to control softness using continuous cutoff variables.

An alternative, and a rather general, approach is to renormalize interactions by a *similarity* transformation

$$H(\lambda) = \mathcal{U}(\lambda)H\mathcal{U}^\dagger(\lambda), \quad (23.12)$$

where $\mathcal{U}(\lambda)$ is a reasonable unitary operator as a function of a control parameter λ . Application of the unitary operator would keep all observables unchanged, whereas the freedom of choosing the form of this operator can be used to transform interaction, eliminating or suppressing hard components. A unitary transformation can be taken in the form $\mathcal{U}(\lambda) = e^{i\xi(\lambda)}$ with the Hermitian operator $\xi(\lambda)$.

In the *similarity renormalization group approach*, the evolution of the parameter-dependent operator (23.12) is considered analogously to the Heisenberg picture of quantum mechanics: the derivative of the Hamiltonian with respect to the parameter amounts to the flow equation

$$\frac{dH(\lambda)}{d\lambda} = [\eta(\lambda), H(\lambda)] \quad (23.13)$$

with the initial condition $H(0) \equiv H$. Here η is an anti-Hermitian operator

$$\eta(\lambda) \equiv i \frac{d\xi(\lambda)}{d\lambda} = -\eta^\dagger(\lambda) = \frac{d\mathcal{U}(\lambda)}{d\lambda} \mathcal{U}^\dagger(\lambda). \quad (23.14)$$

As an example, consider the evolution of a Hamiltonian $H(\lambda) = H_0 + V$ where H_0 is the diagonal part of H with matrix elements ϵ_1 and V contains all off-diagonal matrix elements V_{12} . Under unitary transformations, the trace of the H^2 remains unchanged:

$$\frac{d}{d\lambda} \text{Tr}(H^2) = \frac{d}{d\lambda} \text{Tr}(H_0^2) + \frac{d}{d\lambda} \text{Tr}(V^2) = 0. \quad (23.15)$$

Let us choose $\eta = [H_0, H]$ which in terms of matrix elements gives $\eta_{12} = (\epsilon_1 - \epsilon_2)H_{12}(\lambda)$. One can then show that

$$\frac{d}{d\lambda} \text{Tr}(H_0^2) = \frac{d}{d\lambda} \sum_1 \epsilon_1^2 = 2 \sum_{12} (\epsilon_1 - \epsilon_2)^2 |H_{12}|^2 \geq 0, \quad (23.16)$$

which, owing to Eq. (23.15), makes the sum of squares of all off-diagonal matrix elements diminish with increasing λ ,

$$\frac{d}{d\lambda} \text{Tr}(V^2) = \frac{d}{d\lambda} \sum_{1 \neq 2} |V_{12}|^2 \leq 0. \quad (23.17)$$

Projection techniques make it possible to project the dynamics onto a specific subspace of interest. Let us call this projection operator \mathcal{P} and the projection operator onto the remaining space \mathcal{Q} . Naturally, $\mathcal{P} + \mathcal{Q} = 1$, $\mathcal{P}^2 = \mathcal{P}$, $\mathcal{Q}^2 = \mathcal{Q}$, and $\mathcal{Q}\mathcal{P} = \mathcal{P}\mathcal{Q} = 0$. Then, starting from the Schrödinger equation $H|\Psi\rangle = E|\Psi\rangle$ as a block equation for the subspaces

$$\mathcal{P}H\mathcal{P}|\Psi\rangle + \mathcal{P}H\mathcal{Q}|\Psi\rangle = E\mathcal{P}|\Psi\rangle, \quad (23.18)$$

$$\mathcal{Q}H\mathcal{Q}|\Psi\rangle + \mathcal{Q}H\mathcal{P}|\Psi\rangle = E\mathcal{Q}|\Psi\rangle, \quad (23.19)$$

and using

$$\mathcal{Q}|\Psi\rangle = \frac{1}{E - QHQ} QH\mathcal{P}|\Psi\rangle \quad (23.20)$$

in Eq. (23.18), we arrive at the effective equation $\mathcal{H}(E)\mathcal{P}|\Psi\rangle = E\mathcal{P}|\Psi\rangle$ in the subspace \mathcal{P} . The effective Hamiltonian $\mathcal{H}(E)$ built of the original \mathcal{P} -state part and the part describing the series of excursions to the Q space and back,

$$\mathcal{H}(E) = \mathcal{P}\mathcal{H}\mathcal{P} + \mathcal{P}\mathcal{H}Q\frac{1}{E - Q\mathcal{H}Q}\mathcal{Q}\mathcal{H}\mathcal{P}, \quad (23.21)$$

is energy dependent, which makes the eigenvalue problem nonlinear. This formalism suggested by Feshbach [5] is often used to project out the continuum of reaction states [6], where the effective Hamiltonian becomes non-Hermitian due to the finite lifetime of resonance states. The projection approach, in spite of the energy dependence, can be used to construct a low-momentum nucleon–nucleon interaction (the Bloch–Horowitz method [7]).

In order to obtain effective interactions in the projected space we assume that $H = H_0 + V$, where H_0 corresponds to noninteracting particles and commutes with both projection operators \mathcal{P} and \mathcal{Q} . The effective interaction that comes from (23.21) is the so-called *G-matrix* [8],

$$G(E) = V + V\frac{\mathcal{Q}}{E - \mathcal{Q}H_0\mathcal{Q}}G(E). \quad (23.22)$$

In analogy to the Born series in quantum scattering theory, this integral equation can be solved iteratively. The operator $G(E)$ works in full space and the projected \mathcal{P} -space part of it recovers the effective Hamiltonian (23.21), $\mathcal{P}[H_0 + G(E)]\mathcal{P} = \mathcal{H}(E)$.

The *G*-matrix approach going back to Brueckner can be applied to a Fermi system near its ground state; in this way, the projector \mathcal{Q} essentially enforces Pauli blocking, assuring that interacting particles would not scatter into occupied states below the Fermi surface. The result not only incorporates the presence of the core but also alleviates the problem associated with the hard-core nature of nucleon–nucleon interactions.

The perturbative expansion of the effective nucleon–nucleon interaction in the presence of other nucleons can be done diagrammatically. Special approximations are possible summing only over a subclass of *ladder diagrams*. These are diagrams that repeat a certain pattern, such as shown in Figure 23.3, making them equivalent to a summation of a geometric series where the two-body scattering, including the short-range interaction, is accounted for in all orders. An example of this kind of re-summation is discussed in Problem 23.6.

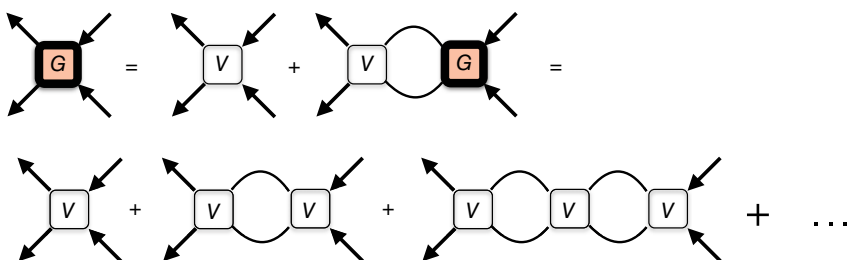


Figure 23.3 A series of ladder diagrams showing the element of the effective *G*-matrix for scattering of two nucleons influenced by the presence of other nucleons. The illustration shows the consecutive two-nucleon scattering, such as in Figure 11.1, but with intermediate scatterings traversing through Q -space.

The Lee–Suzuki similarity transformation [9] is a popular approach where the decoupling of spaces leads to an energy-independent effective Hamiltonian. The basis transformation

$$\begin{pmatrix} 1 & 0 \\ -\Omega & 1 \end{pmatrix} = 1 - Q\Omega P \quad (23.23)$$

is written here as the block matrix with the upper part for P -space and lower part for Q -space. The off-diagonal operator Ω only works one way from P to Q , therefore $\Omega = Q\Omega P$. This means that it cannot be repeated, $\Omega^2 = 0$, and $e^{-\Omega} = 1 - Q\Omega P$.

We select the operator Ω so that the desired set of low-lying eigenstates $|k\rangle$ gets decoupled from Q -space under this transformation, namely, $P e^{-\Omega} |k\rangle = e^{-\Omega} |k\rangle$, and thus the Q component vanishes,

$$Q e^{-\Omega} |k\rangle = Q(1 - Q\Omega P) |k\rangle = 0. \quad (23.24)$$

In terms of the basis states $|p\rangle$ and $|q\rangle$ that span the corresponding spaces, $Q = \sum_q |q\rangle \langle q|$ and $P = \sum_p |p\rangle \langle p|$, we obtain a linear equation for matrix elements of Ω :

$$\langle q|k\rangle = \sum_p \langle q|\Omega|p\rangle \langle p|k\rangle. \quad (23.25)$$

This procedure defines the decoupling transformation.

The transformation operator $e^{-\Omega}$ is not unitary, which means that the transformed states $|\check{k}\rangle \equiv e^{-\Omega}|k\rangle$, while all in P -space, are not orthonormal. Thus, the original eigenvalue equation $\langle k'|H|k\rangle = E_k \langle k'|k\rangle$, where $\langle k'|k\rangle = \delta_{kk'}$, becomes generalized to

$$\langle \check{k}|e^{\Omega^\dagger} H e^\Omega |\check{k}\rangle = E_k \langle \check{k}|e^{\Omega^\dagger} e^\Omega |\check{k}\rangle. \quad (23.26)$$

We can use a norm operator to transform this equation into a regular eigenvalue equation, keeping in mind that all operators should be limited to P space. We define an effective Hamiltonian as

$$\mathcal{H} = P \mathcal{N}^{-1/2} e^{\Omega^\dagger} H e^\Omega \mathcal{N}^{-1/2} P, \quad \text{where} \quad \mathcal{N} = P e^{\Omega^\dagger} e^\Omega P = P(1 + \Omega^\dagger \Omega)P. \quad (23.27)$$

The combined action of the projector and the unitary transformation operator,

$$P \mathcal{N}^{-1/2} e^{\Omega^\dagger} = P(1 + \Omega^\dagger \Omega)^{-1/2}(1 + \Omega^\dagger), \quad (23.28)$$

can be further simplified using the fact that $P\Omega = 0$:

$$P(1 + \Omega^\dagger \Omega + \Omega \Omega^\dagger)^{-1/2}(1 + \Omega^\dagger - \Omega) = P \frac{(1 + \Omega^\dagger - \Omega)^{1/2}}{(1 + \Omega - \Omega^\dagger)^{1/2}}. \quad (23.29)$$

Therefore, the effective Hamiltonian takes the form

$$\mathcal{H} = P \mathcal{U} H \mathcal{U}^\dagger P, \quad \text{where} \quad \mathcal{U} = \frac{(1 + \Omega^\dagger - \Omega)^{1/2}}{(1 + \Omega - \Omega^\dagger)^{1/2}}. \quad (23.30)$$

The use of the effective interaction can significantly speed up the convergence as demonstrated in Figure 23.4. However, we should make several comments about projection methods. First, unlike the expansion over complete sets of basis states, renormalization of interactions and projections make the approach *nonvariational*, and therefore the resulting convergence to the ground state can be both from above and from below.

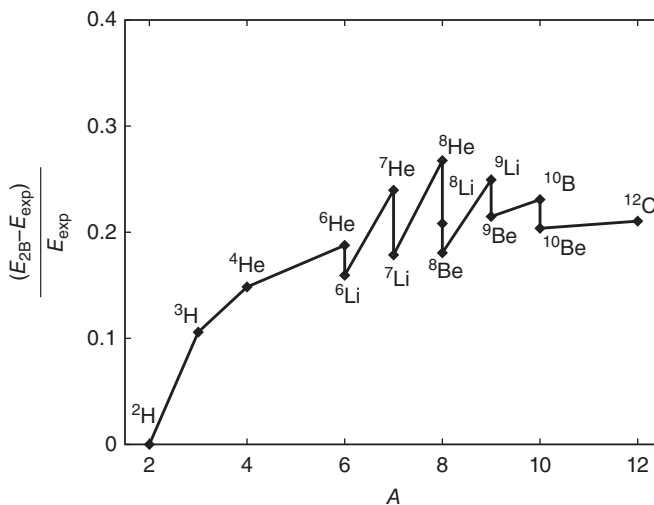


Figure 23.4 Fraction of binding energy associated with many-body forces. The many-body problem with two-body Argonne v_{18} potential is solved exactly and compared with the experiment. The fraction that represents the missing part in binding is shown as a function of the mass number A . (Data from Ref. [11]).

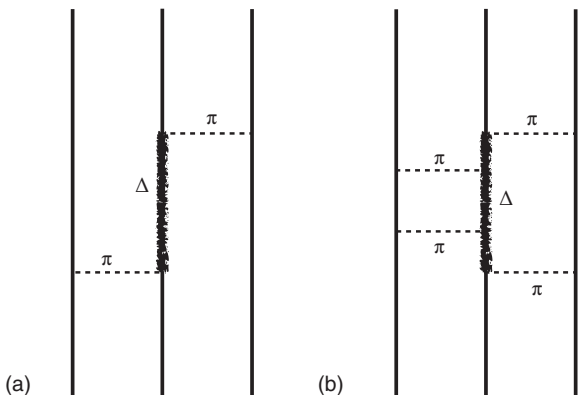
Second, unitary transformations and projections modify the original two-body Hamiltonian so that the effective interaction may acquire many-body forces. These forces are the artifacts of the approach and depend on the specifics of the transformations involved in renormalizations. Third, the observable quantities of interest are to be obtained using operators that are renormalized correspondingly.

23.4 Three-Body Forces

Now let us discuss the quality of the final results. In the case of the positronium ion, the discrepancy with the experiment is too small to be measured, effects of relativity and QED can be estimated (and introduced in the Hamiltonian) but they are smaller at least by three orders of magnitude. In contrast, as evident from Figure 23.2, in the nuclear case, the discrepancy with the experiment is substantial. The nucleon–nucleon forces here were constructed using mesons as mediators of the interactions; the parameters were fitted to two-body experimental data (see Chapter 3). A more systematic approach uses a *chiral perturbation theory* and there is some initial success in obtaining nucleon–nucleon interactions directly from the numerical lattice QCD solutions with only a few constants defined by a fit.

Nevertheless, numerous *ab initio* studies cross-checked by employing various methods demonstrate that no two-body forces can correctly reproduce three-body and heavier systems. As we see in Figure 23.2, the Argonne v_{18} Hamiltonian underbinds ${}^3\text{He}$ by around 0.8 MeV. The systematics presented in Figure 23.4 shows that about 20% of the binding energy is missing in calculations based on this two-body interaction. Thus, our *ab initio* approach must be extended to three-body forces and perhaps even to forces of higher ranks. These forces reflect the virtual excitations of nucleons and their complex composite nature (see the example in Figure 23.5). The Urbana model

Figure 23.5 Examples of processes where the three-body nucleon–nucleon interaction proceeds through the virtual excitation of the Delta-resonance ($J = 3/2, T = 3/2$) that cannot be reduced to two-body forces.



[10] offers a series of three-body interactions that have been successfully used together with Argonne two-nucleon potentials.

There is an active recent development of the so-called *effective field theory* where the nucleon interactions (two- and, in principle, many-body) are constructed using the symmetry of the light meson exchanges in quantum chromodynamics and adding few empirical constants modeling the short-range part of the interaction. This assumes that such a fundamental interaction can serve also in the nuclear medium as a base for the full many-body theory although the problems of the further modifications of the forces in the nuclear medium are far from being fully understood.

23.5 Semiempirical Effective Interactions

As follows from our discussion, the most important practical question in constructing successful nuclear many-body theory is that of the interaction Hamiltonian. So far we assumed that a “quite general” form of the Hamiltonian consists of the independent particle part h , (either the kinetic energy of the bare particles, or, probably better, of mean-field orbitals in a reasonable potential) and the effective residual interaction H' . A strong approximation has already been made here, namely, that of the *pairwise* character of the residual interaction. With this effective interaction, the goal is to find out the energy spectrum, static observables, and transition rates, at least up to some excitation energy.

Even on the level of two-body interactions, many different possibilities were tried. As shown above, for light nuclei, the modern computational techniques make feasible the many-body calculations starting from first principles with the interaction taken from experiments on free nucleons, as, for example, the *Argonne interaction* (Section 3.2). Such calculations are generally very difficult, often involve complex renormalization procedures, and lack precision once overall binding energy becomes large compared to nuclear many-body excitations of interest.

Very successful calculations are systematically performed with *semiempirical* interactions. Here it is possible, for a limited purpose of quantitative description of low-energy spectroscopic information, to use a truncated valence space of several single-particle orbits, where matrix elements of two-body interactions are adjusted on the basis of empirical data.

To give an example, we return to the above-mentioned *sd*-shell model, including the major $1s - 0d$ shell with three orbitals $1s_{1/2}$, $0d_{3/2}$, and $0d_{5/2}$, both for protons and for neutrons. Within this space, assuming isospin invariance, there are 63 independent two-body reduced matrix elements $\langle (j_1 j_2)JT \| H' \| (j_3 j_4)JT \rangle$ which describe all scattering processes for a pair of nucleons with certain values of the constants of motion J and T allowed in the field of the inert core of ^{16}O . If, at excitation energies of interest, there are no nuclear states which require the noticeable excitation of the core or the transfer of the valence particles into the next shell, one can find an *effective* two-body Hamiltonian that reproduces, in the many-body diagonalization, the observed levels and matrix elements of multipole operators. In practice, this is a good approximation up to the excitation energy of 10–15 MeV. This covers the area of experimental nuclear spectroscopy and many significant nuclear reactions, including astrophysical ones.

One can start with the matrix elements obtained by some *ab initio* strategy but then they can be adjusted for the best overall description of hundreds of known observables in many nuclei across the shell. Such a procedure fixes the Hamiltonian that subsequently can be used for calculating other quantities and making predictions for future experiments. The found matrix elements effectively take into account the influence of the coupling to the states outside the valence space.

In Figure 23.6, the matrix elements coming from the original *G*-matrix are compared with the adjusted ones, the points are scattered along the diagonal which highlights that the empirical adjustment generally represents a small change, well within the errors of *ab initio* procedures. However, these changes lead to great improvement in the description of experimental data and in the predictive power. In Figure 23.7 *ab initio* approaches with two- and three-body forces, empirical shell model, liquid drop mass formula (see Chapter 5), and mean-field calculations (see Chapter 17) are compared with experimental data for oxygen. Most of the theoretical results predate the experimental results for heavy oxygen isotopes that were only recently obtained.

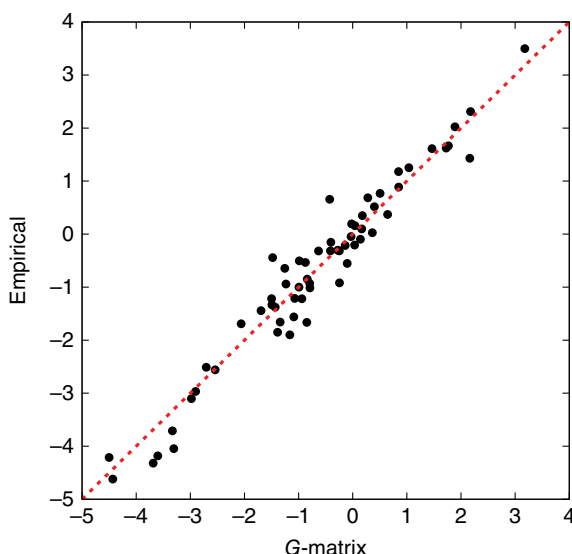


Figure 23.6 The 63 two-body matrix elements for the shell model fitted [12] to experimental data for the $1s - 0d$ orbital space are compared with the *G*-matrix values [8]; all energies are in megaelectronvolts. The dots are scattered along the diagonal shown by the dashed line, which indicates close agreement.

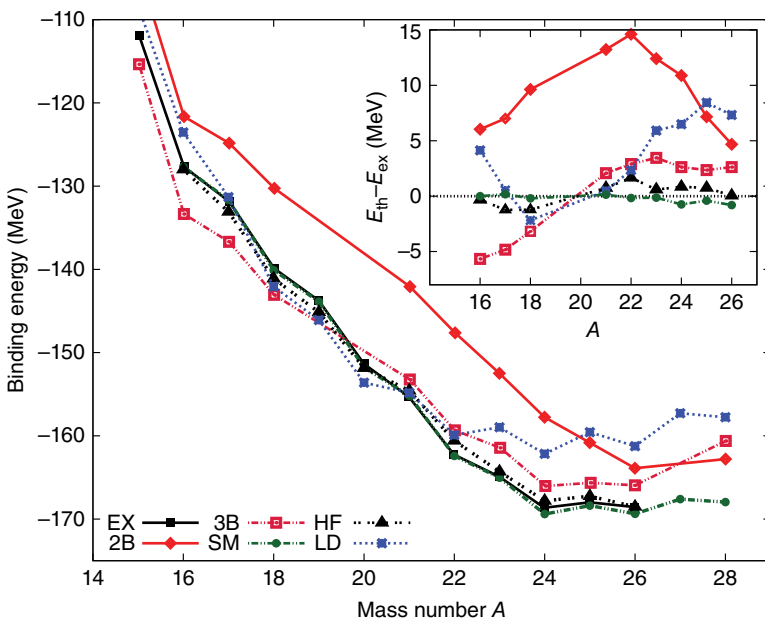


Figure 23.7 Comparison of theoretically predicted ground-state binding energies and experimental data for oxygen isotopes; the inset shows the energy deviations. The points connected by lines are labeled as follows: 2B – *ab initio* calculation with two-body Hamiltonian [13]; 3B – *ab initio* calculation that includes two- and three-body forces [13]; HF – Hartree–Fock mean-field calculation [14]; LD – results from the liquid drop model [15]; SM – results from the semiempirical *sd*-shell model [20] that includes treatment of the neutron states in the continuum discussed in Section 23.7. The inset shows the difference in binding energy between theory and experiment.

Besides binding energies, the 63 matrix elements along with three single-particle energies describe very well thousands of data for ground and excited states observed in nuclei between ^{16}O and ^{40}Ca . The quality of agreement varies but is typically within few hundred kiloelectronvolts. Because of the superior overall agreement with the experiment, excellent predictive power, and clear correspondence between theory and observations, the semiempirical shell model in various modifications is widely used in nuclear studies. In Figure 23.8, we compare theory and experiment for excited states in ^{24}Mg . Not only is there a good overall agreement but also the rotational features of this triaxially deformed nucleus are described very well within the approach that starts with the spherical mean field. The same semiempirical approach is used for the operators and matrix elements. However, the transition rates usually require additional adjusted parameters of *effective charges* coming from admixtures of the states outside the orbital space.

Problem 23.3

- Using a shell-model code with the USD interaction (see Ref. [12]), predict the spectrum of the lowest four states in the ^{24}Mg nucleus. Compare the results with the experimental data.
- Compute the quadrupole moments of excited states and possible E2 transitions between them. Assume the harmonic oscillator potential for basis states and

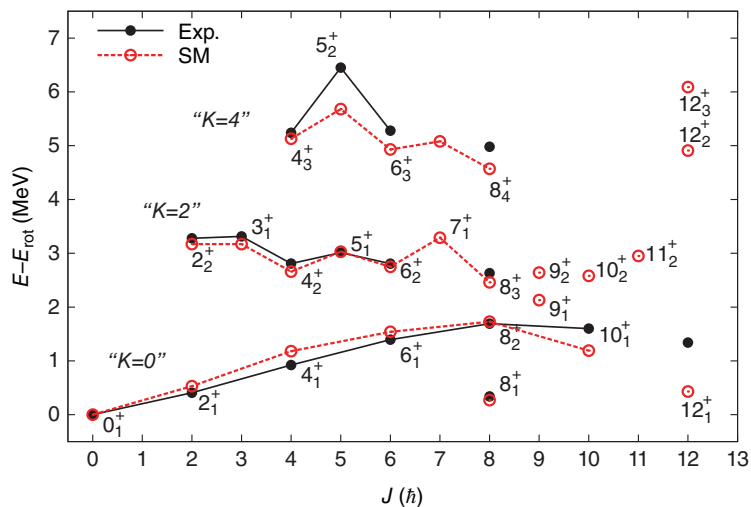


Figure 23.8 Excitation energies in ^{24}Mg from data [16] and predictions by the shell model. The energies are plotted relative to the rotor energies defined as $E_{\text{rot}} = 0.16(J + 1)$ MeV. Selected states are linked into bands which are traced experimentally by consecutive E2 transitions and theoretically can be related through $\mathcal{SU}(3)$ symmetry.

estimate the oscillator length for the nuclear mass number $A = 24$. Use effective charges $0.5e$ for neutrons and $1.5e$ for protons. Compare to the experimentally observed rates.

- Estimate the lifetime of the first excited state.
- Examine the Alaga rule (rigid rotor prediction, Section 16.12) for the quadrupole moment and the E2 transition probability down from the first excited state. Assuming a rotor model, determine the intrinsic quadrupole moment. Does this intrinsic moment determine the laboratory moments of all four states? Is this nucleus prolate or oblate? Comment on the collective structure of these four states, assuming a triaxial rotor shape.

Solution

- The low-lying spectrum of ^{24}Mg is summarized in the following table (energies in megaelectronvolts).

State	T	E_x	E (binding)	Experiment
0_1^+	0	0	-87.090	
2_1^+	0	1.509	-85.581	1.369
2_2^+	0	4.122	-82.967	4.238
4_1^+	0	4.378	-82.711	4.123

- In the following table, the E2 transitions between the four low-lying states are presented. Each row corresponds to a given initial state, column to a final state.

$i\backslash f$	0_1^+	2_1^+	2_2^+	4_1^+
0_1^+		44.5	3.98	
2_1^+	8.90	-5.84*	1.94	21.3
2_2^+	0.76	1.94	5.93*	0.11
4_1^+		11.8	0.06	-7.10*

The values in the table are expressed in units of the oscillator length b . The reduced transition rates are in units of $e^2 b^4$ and the quadrupole moments (listed on the diagonal and marked with the *) are in units of eb^2 . The oscillator frequency and the oscillator length scale for the nuclear mass number A are (see Eq. (8.16))

$$\hbar\omega \simeq \frac{41}{A^{1/3}} \text{ MeV}, \quad b = \sqrt{\frac{\hbar}{m\omega}} \simeq 1.01 A^{1/6} \text{ fm}.$$

For the ^{24}Mg nucleus, $b = 1.715 \text{ fm}$.

The predicted value

$$B(\text{E2}; 2_1^+ \rightarrow 0_1^+) = 77 e^2 \text{ fm}^4$$

is quite close to the observed value $B(\text{E2}; 0_1^+ \rightarrow 2_1^+) = 80.6 e^2 \text{ fm}^4$.

- c) The lifetime of the 2_1^+ state is determined, Eq. (14.99), as

$$\tau = \frac{8.16204 \times 10^{-10}}{E^5 B(\text{E2})}, \quad (23.31)$$

where $B(\text{E2})$ is in $e^2 \text{ fm}^4$, the energy in megaelectronvolts, and the result in seconds. The shell-model prediction is $\tau = 1.35 \times 10^{-12} \text{ s}$, the measured value is $\tau = 2 \times 10^{-12} \text{ s}$.

- d) The states 0_1^+ , 2_1^+ , and 4_1^+ form a nearly perfect rotational band with $K = 0$. The Alaga ratio for a rotor (see Section 16.12) is

$$A = \frac{Q^2(2_1^+)}{B(\text{E2}, 0^+ \rightarrow 2_1^+)} = \frac{16\pi}{5} \frac{4}{49} \approx 0.82 \quad (23.32)$$

and the shell model gives $A = 0.77$. The quadrupole moment

$$Q(J) = -Q_0 \frac{J}{2J+3} \quad (23.33)$$

can be used to determine the intrinsic deformation. For the 2_1^+ state we get $Q_0 = 20.5 eb^2$. Then from the rotor model $Q(4_1^+) = 7.4 eb^2$, the shell-model calculation leads to a similar value of $7.1 eb^2$. This nucleus is prolate, as follows from the positive intrinsic quadrupole moment.

The states 0_1^+ , 2_1^+ , and 4_1^+ form a $K = 0$ rotational band, the state 2_2^+ is a $K = 2$ bandhead. The transition $2_2^+ \rightarrow 0_2^+$ does not vanish, indicating some K mixing which is a signature of triaxiality. Note that for the triaxial rotor model $Q(2_1^+) = -Q(2_2^+)$, the same follows from the simple perturbational mixing of one- and two-phonon states 2^+ .

23.6 Shell-Model Hamiltonian, Properties and Solutions

In this section, we briefly address the way to solve the actual many-body problem. Very often, it is reduced to the diagonalization of a large matrix. We emphasize that this is a variational procedure – in any class of exact quantum numbers, the ground state obtained as a linear combination of basis states minimizes the energy [QP, I, Ch. 10]. Generally, the number of basis configurations is very large: in the ^{24}Mg example of the sd -shell model, the number of the m -scheme states with the total spin projection $M = 0$ is 28 503; for ^{56}Ni , in the middle of the $0f - 1p$ shell this number is already 1 087 455 228. As mentioned in Section 20.2, the combinatorics imply that the density of states grows exponentially with the number of particles and with the size of the valence space. A full diagonalization of a matrix of a very large size is not feasible and actually of no interest as only small subsets of low-lying states are physically meaningful.

In practice, the Hamiltonian matrices are very *sparse*; in the m -scheme in particular, the number of nonzero matrix elements is small. Indeed, a matrix element of a two-body Hamiltonian between two Slater determinants is only nonzero if these states can be connected by relocating at most two particles. The remaining, spectator, particles do not change their positions so that the same matrix element of two-body interaction appears in the Hamiltonian matrix many times, attached to different spectators. In addition, initial and final states have to have the same magnetic and isospin projections. The matrix elements for the m -scheme many-body Hamiltonian are shown in Figure 23.9. The matrices are sparse (a lot of white space), and the nonzero matrix elements form patterns associated with partitions (see Chapter 9); these are blocks of states corresponding

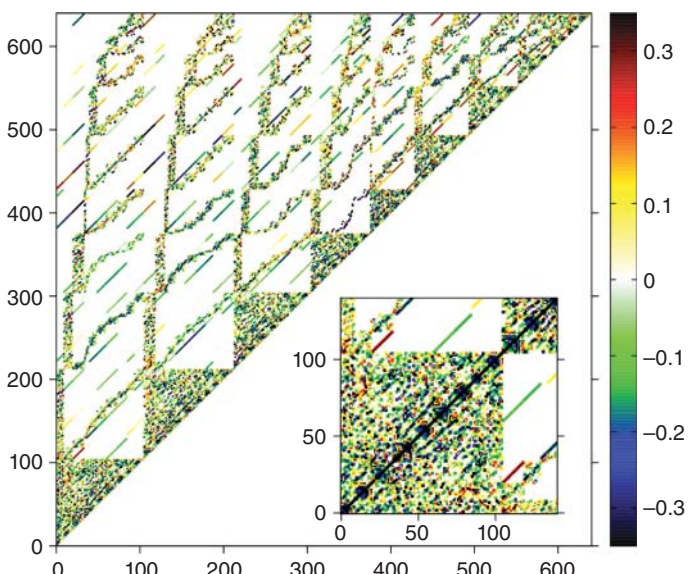


Figure 23.9 A 640×640 Hamiltonian matrix in the m -scheme for ^{20}Ne in sd -shell with realistic semiempirical interactions. The matrix is symmetric and only the upper part is shown. The inset magnifies the area containing the first 140 states. The color map shows scale in megaelectronvolts; note that the diagonal matrix elements (in black) are typically much larger.

to a specific distribution of particles over degenerate orbits in mean field potential; without two-body interactions these many-body states would be degenerate.

The sparseness of Hamiltonian matrices, and the interest limited usually to low-lying states make iterative *power-method* algorithms, such as the Lanczos algorithms very appealing. These iterative techniques are based on generating a Krylov subspace of states $|\Psi_0\rangle, H|\Psi_0\rangle, H^2|\Psi_0\rangle, \dots, H^{k-1}|\Psi_0\rangle$, where $|\Psi_0\rangle$ can be an arbitrary initial many-body state, supposedly nonorthogonal to the state we are searching for. Then the Hamiltonian matrix is diagonalized in the $k \times k$ subspace spanned by these vectors. For sparse matrices, the matrix–vector multiplication is among the most computationally inexpensive operations; powers of the Hamiltonian matrix favor eigenstates with a large absolute value of eigenvalues. Typically, ground-state convergence is reached for $k \approx 50$. There are numerous variations of the method; other operators, not just Hamiltonian, can be included in the process; block structure of the matrices allows for efficient parallel implementations; iterative procedures can be constructed to make other operators containing the Hamiltonian including propagators and evolution operators.

As discussed in Chapter 9, many-body states can be reorganized on the basis of their symmetries. The classes of states with different angular momentum can be treated separately. In the ^{56}Ni example, the number of states with $J = 0$ is only 15 443 684 (nearly two orders of magnitude smaller than the total of 1 087 455 228). The J -schemes are commonly used; however, the construction of states with good symmetry can be computationally challenging and, most noticeably, the Hamiltonian matrices are no longer as sparse. The m -scheme solutions should provide $(2J + 1)$ degeneracy as a confirmation of rotational symmetry.

Finally, the appropriate choice of the valence space and truncation of many-body states is a crucial part of successful strategy. Uncertainty in the effective Hamiltonian, the center-of-mass problem, and other similar issues often make exact or high-precision diagonalization unnecessary. The *chaotic* nature of highly excited states makes their admixture to low-lying states of interest only in a statistical sense. Owing to the variational character of the approach, expansion of the orbital space drives the low-lying states down. Analytic models, studies of ensembles of randomly interacting systems, as well as empirical studies show that in low-lying states, components of remote basis states are exponentially small although their cumulative result in high orders of perturbation theory can bring a considerable shift of the energy eigenvalues. The resulting *exponential convergence* of observables as a function of truncation [17] is an important and practically useful feature.

23.7 Effective Non-Hermitian Hamiltonian

The standard shell-model versions, although extremely helpful for all structure problems, frequently suffer from the fact that they are based exclusively on the discrete spectrum of the problem, especially in widely used methods utilizing the harmonic oscillator potential. The asymptotic properties of oscillator eigenfunctions are incorrect for the description of realistic continuum states. A nucleus excited above threshold opens to the decay channel(s) and has therefore a finite lifetime. Virtual admixtures of continuum states make questionable the shell-model results in many cases, especially for nuclei outside the valley of stability. Those exotic nuclei often have very few (or none) discrete excited states, so that the entire dynamics takes place in the virtual or real continuum.

There are several practically useful methods to enrich the configuration interaction machinery by including continuum effects. A characteristic feature of many of them is the appearance of *complex energies* in the formalism. As we know, the states with a finite lifetime τ do not have certain real energy E . Their time evolution is close to the exponential decay,

$$\Psi(t) \propto e^{(-i/\hbar)[E - (i/2)\Gamma]t}, \quad (23.34)$$

where the state width, Γ , is the corresponding energy uncertainty, and $\tau \sim \hbar/\Gamma$. This idea appeared in our previous chapters, including radiation and fission. Some approaches, such as the so-called *Gamow shell model* [18], from the very beginning work in the complex energy plane. Here we describe the *continuum shell model* [19–22] as a straightforward generalization of the shell model for an *open* system with some decay channels.

The convenient way of including the continuum dynamics is through the effective non-Hermitian Hamiltonian [6] derived with the help of the projection formalism (23.22); the details can be found in [23]. This formal procedure does not require any explicit expressions for the projection operators although it can be done in many ways, both in Hilbert space and in configuration space. Keeping the same notations, we assume that the states of the P -space belong to our standard shell model, whereas the Q -space includes the continuum states. The effective Hamiltonian nontrivially depends on running energy E . If it is above threshold for some channel(s), it belongs to the set of eigenvalues of QHQ . Then the second term of Eq. (23.21) has a singular denominator. The standard rule to handle such poles is to add to the energy E in this denominator an infinitesimal imaginary term $i\delta$, $\delta = +0$ (a vanishing but negative shift of the pole into the complex plane). The known identity is valid

$$\frac{1}{E - x + i\delta} = \text{P.v. } \frac{1}{E - x} - i\pi\delta(E - x), \quad (23.35)$$

where the symbol P.v. means that an integral with this expression in the integrand has to be taken in the sense of principal value (the symmetric limit to approach the singular point which is excluded). This handling of the singularity corresponds to the outgoing wave function in open channels (the singularity is present only if our running energy corresponds to a continuum state, that is, it belongs to the Q -space).

Using Eq. (23.35) in the effective Hamiltonian (23.21), we arrive at two energy-dependent terms in addition to the internal (e.g., standard shell-model) term PHP which we can identify with the shell-model Hamiltonian H ,

$$\mathcal{H}(E) = H + \Delta(E) - \frac{i}{2} W(E) \equiv \overline{H} - \frac{i}{2} W(E). \quad (23.36)$$

This formal expression includes the continuum structure which we can classify by the asymptotic channel states $|E, c, \tau\rangle$ (total energy above threshold E_c for each channel c , final particles and their intrinsic states, spins, and orbital momenta included in a symbol τ). Here we assume that H_{QQ} is diagonal, $H_{QQ}|c, \tau, E\rangle = E|c, \tau, E\rangle$. Then the Hermitian part of the effective Hamiltonian can be written as the set of matrix elements in the shell-model basis

$$\begin{aligned} \overline{H}_{12} &= H_{12} + \Delta_{12}(E), \\ \Delta_{12}(E) &= \text{P.v.} \sum_c \int (d\tau) dE' \langle 1 | H_{PQ} | c, \tau, E' \rangle \frac{1}{E - E'(c, \tau)} \langle c, \tau, E' | H_{QP} | 2 \rangle. \end{aligned} \quad (23.37)$$

This renormalization of the shell-model matrix elements results in *virtual, off-shell* transitions, similar to the standard perturbation theory, from the discrete spectrum to *all possible* (open or closed at given energy E) decay channels. The imaginary part $W(E)$ comes from *on-shell* transitions to *all open* channels, $E \geq E_c$, which require, as seen from the delta-functions in (23.35), energy conservation. Combining all kinematic factors in the integral, we introduce the effective amplitudes $A_1^c(E) = \langle 1 | H_{PQ} | c, \tau, E \rangle$ for the decay of the internal state $|1\rangle$ into the channel c at given energy; we can write the matrix elements of the on-shell part of the effective Hamiltonian as

$$W_{12} = 2\pi \sum_{c(\text{open})} A_1^c(E) A_2^{c*}(E). \quad (23.38)$$

At the threshold of a channel c , the kinematic factors cut off the available phase space for the decay $1 \rightarrow c$, and the corresponding amplitudes $A_1^c(E_c)$ have to vanish.

Problem 23.4 Consider a shell-model state with a single particle in the valence space on an orbit with orbital angular momentum ℓ and the radial wave function $u_\ell(r)/r$. This quasistationary state is just above the decay threshold, and the nuclear mean-field potential that drives this decay is $V(r)$. With the help of projection formalism, determine the decay width.

Solution

The radial wave function in the continuum $|\ell, E\rangle$ is given by a regular function $\sqrt{2M/(\hbar^2 \pi k)} f_\ell(kr)/r$. The function f_ℓ (see [QP, I, Ch. 17]), coincides with the Coulomb function for a charged particle and is related to a spherical Bessel function, $f_\ell(kr) = kr j_\ell(kr)$, for a neutral particle. The normalized functions f_ℓ are normalized to the asymptotics as a sine function with some phase. Our formalism assumes normalization by the Dirac delta function in energy which explains an additional factor. Here M is the reduced mass and k is the wave vector. For one open channel, we obtain

$$A_{sp}(E) = \sqrt{\frac{2M}{\hbar^2 \pi k}} \int_0^\infty V(r) f_\ell(kr) u_\ell(kr) dr, \quad \Gamma_{sp} = 2\pi |A_{sp}(E)|^2. \quad (23.39)$$

This expression, which is equivalent to a Fermi golden rule, is commonly used for determining the decay width of narrow quasistationary states. The potential V includes the nuclear potential and the difference of the actual Coulomb potential from that of a point charge.

Problem 23.5 Let the effective shell-model Hamiltonian represent \bar{H} and $|i\rangle$ be the initial state that decays into $|f\rangle$; both states are eigenstates of \bar{H} . Determine the decay width of the many-body state $|i\rangle$, assuming that W can be treated perturbatively and that the single-particle decay process is mediated by the mean-field potential of Problem 23.4.

Solution

Following Problem 23.4, the decay amplitude in the \mathcal{P} space is represented by a state $|A^c(E)\rangle = A_{sp}^c(E) a_{jm}^\dagger |f\rangle$. Here $W = 2\pi \sum_c |A^c(E)\rangle \langle A^c(E)|$. Here we first consider all magnetic substates as independent channels; then the channel label c includes angular momentum quantum numbers of the emitted particle, jm , and of the final daughter

state, $J_f M_f$. For the partial decay width between fixed initial and final states, the summation over channels goes only over magnetic substates m and M_f . Thus,

$$\Gamma = \Gamma_{\text{sp}}^j S_j, \quad (23.40)$$

where Γ_{sp}^j is the single-particle decay width, Eq. (23.39), and the *spectroscopic factor* S_j (see also Eq. (15.108)), is defined as

$$S_j = \sum_{m, M_f} |\langle i, J_t M_i | a_{jm}^\dagger | f, J_f M_f \rangle|^2 = \frac{|\langle i | a_j^\dagger | f \rangle|^2}{2J_i + 1}. \quad (23.41)$$

Note that the width of states in electromagnetic decays, Eqs. (14.97) and (14.99), has the same form. It is common to consider angular momentum coupled channels

$$|c, J_c M_c \rangle = \sum_{m, M_f} C_{jm}^{J_c M_c} a_{jm}^\dagger |f, J_f M_f \rangle, \quad (23.42)$$

in which case, $S_j = |\langle i, J_t M_i | c, J_c = J_t M_c = M_i \rangle|^2$.

The amplitudes A_1^c form a rectangular matrix \mathbf{A} (a column for each channel c), so that the operator (23.38) is $W = 2\pi \mathbf{A} \mathbf{A}^\dagger$. An important mathematic property of the operator W is its *factorization*. The number of terms in this expression is the number M of open channels so it has only M nonzero eigenvalues. This factorized structure guarantees the unitarity of the scattering matrix S_{ab} in the channel space. This follows from the comparison of two propagators (Green's functions),

$$G(z) = \frac{1}{z - H} \quad (23.43)$$

that includes only the Hermitian part and

$$\mathcal{G}(z) = \frac{1}{z - \mathcal{H}} \quad (23.44)$$

with the full effective Hamiltonian, both work in the \mathcal{P} -space. Here z is a complex variable; the physical reactions correspond to $z \rightarrow E + i\delta$.

Problem 23.6 Prove the algebraic relation between the two Green's functions:

$$\mathcal{G}(z) = G(z) - i\pi G(z) \mathbf{A} \frac{1}{1 + i\pi \hat{K}(z)} \mathbf{A}^\dagger G(z), \quad (23.45)$$

where the \hat{K} -matrix in the channel space describes the propagation inside the system between two excursions to the continuum,

$$\hat{K}(z) = \mathbf{A}^\dagger G(z) \mathbf{A}. \quad (23.46)$$

The denominator in Eq. (23.45) accounts for the full internal propagation history with any number of virtual continuum visits.

Solution

It follows from (23.43) and (23.44) that $\mathcal{G}(z) = G(z) - (i/2)G(z)W\mathcal{G}(z)$. Factorization of W allows to sum the geometric series that emerges from iterations

$$\mathcal{G}(z) = G(z) - i\pi G(z) \mathbf{A} [1 - i\pi \hat{K}(z) + (-i\pi \hat{K}(z))^2 + \dots] \mathbf{A}^\dagger. \quad (23.47)$$

The part of the amplitude for the reaction $b \rightarrow a$ that proceeds through the \mathcal{P} -space is the element T^{ab} of the $M \times M$ transmission matrix

$$\hat{T}(z) = \mathbf{A}^\dagger \mathcal{G}(z) \mathbf{A} = \hat{K}(z) \frac{1}{1 + i\pi \hat{K}(z)}. \quad (23.48)$$

The scattering matrix defined as $\hat{S} = 1 - 2\pi i \hat{T}$ is therefore explicitly unitary,

$$\hat{S} = 1 - 2\pi i \hat{T} = \frac{1 - i\pi \hat{K}}{1 + i\pi \hat{K}}. \quad (23.49)$$

A more complete consideration has to include also processes unrelated to the excitation of the P -space, such as potential scattering and direct reactions but they certainly do not violate unitarity.

Problem 23.7 Show that in the perturbative limit of weak decay discussed in Problems 23.4 and 23.5, the total cross section for single-particle scattering $c \rightarrow c'$ that proceeds through an isolated narrow resonance r has a Breit–Wigner form

$$\sigma(c \rightarrow c') = \frac{\pi}{k_c^2} \frac{2J_r + 1}{(2j_c + 1)(2J_c + 1)} \frac{\Gamma_r^c \Gamma_r'}{(E - E_r)^2 + \Gamma_r^2/4}, \quad (23.50)$$

where $\Gamma_r = \sum_c \Gamma_r^c$ is the total decay width.

Solution

See [QP, II, Ch. 10] and Eq. (20.77). Note that in contrast to a traditional Breit–Wigner shape the decay widths here are energy dependent and, if a resonance near threshold is sufficiently broad, the energy dependence assures that the cross section approaches zero at threshold.

With running energy E in the continuum, the eigenvalue problem for the effective Hamiltonian (23.36) produces complex eigenvalues $\mathcal{E}_r = E_r - (i/2)\Gamma_r$ in the low part of the complex energy plane. These poles are, in general, moving in the complex plane as a function of the real energy E of the experiment. As the Hamiltonian $\mathcal{H}(E)$ is non-Hermitian, the eigenfunctions for different poles are not orthogonal. Instead, there is a *biorthogonal* set (χ_r, χ_r^*) of right and left eigenfunctions of \mathcal{H} found through the corresponding shift of the energy parameter, $E \rightarrow E^{(\mp)} = E \mp i\delta$. The standard choice of this shift corresponds to the outgoing wave boundary condition. The resonant *Gamow state* [18], the right eigenstate here, can be defined using a boundary condition such that the wave function is regular inside and has an outgoing wave asymptotic. Unlike boundary conditions for bound states, this condition can only be satisfied when energy is complex. Physically, this represents a decaying resonance. The complex conjugate, left eigenstate, corresponds to a time-reversed process with incoming wave asymptotics representing a capturing state. The resonances and a possible background mentioned earlier form the resulting cross section picture.

Problem 23.8 Using the biorthogonal partners, derive the Bell–Steinberger relation for the width of the resonance r ,

$$\mathcal{E}_r - \mathcal{E}_r^* = \left\langle \chi_r^* \left| H_{PQ} \left(\frac{1}{E^+ - H_{QQ}} - \frac{1}{E^- - H_{QQ}} \right) H_{QP} \right| \chi_r \right\rangle, \quad (23.51)$$

or equivalently,

$$\Gamma_r = 2\pi \langle \chi_r^* | H_{PQ} \delta(E - H_{QQ}) H_{QP} | \chi_r \rangle. \quad (23.52)$$

23.8 From Isolated to Overlapping Resonances

The resonances in the cross section above thresholds are given by the poles of the S -matrix or the roots of the denominator (23.49),

$$\text{Det}[1 + i\pi \hat{K}(z)] = 0, \quad (23.53)$$

where the determinant is taken in the channel space. There are two limiting pictures of the resulting physics depending on the relative strength of the amplitudes A_1^c .

Below all thresholds, the discrete energies are just the real poles of the Green's function (23.43), where the influence of the existence of continuum is only in the appearance of the shift operator $\Delta(E)$, Eq. (23.37). To understand the evolution of the picture above threshold(s), let us first diagonalize the Hermitian part \bar{H} of the total effective Hamiltonian \bar{H} ,

$$\bar{H}|\alpha\rangle = \epsilon_\alpha |\alpha\rangle. \quad (23.54)$$

In this “internal” representation, the full Hamiltonian (23.36) still has a factorized imaginary part,

$$\bar{H}_{\alpha\beta} = \epsilon_\alpha \delta_{\alpha\beta} - \frac{i}{2} 2\pi \sum_{c(\text{open})} B_\alpha^c B_\beta^{c*}, \quad B_\alpha^c = \sum_1 \langle \alpha | 1 \rangle A_1^c. \quad (23.55)$$

Let N intrinsic states $|\alpha\rangle$ coupled to the decay channels cover the energy interval ND , where D is the mean spacing between these levels. We first revisit the *weak continuum coupling* limit exemplified by Problems 23.4, 23.5, and 23.7. In this limit, the anti-Hermitian part of the effective Hamiltonian is small and, in the lowest order of perturbation theory, we can limit ourselves by its diagonal part, so that the complex energies \mathcal{E}_r can be labeled by the intrinsic quantum numbers α and

$$\mathcal{E}_r \Rightarrow \mathcal{E}_\alpha = \epsilon_\alpha - \frac{i}{2} \Gamma_\alpha, \quad \Gamma_\alpha = 2\pi \sum_{c(\text{open})} |B_\alpha^c|^2. \quad (23.56)$$

This is the regime of isolated resonances with *partial widths* in a certain channel c ,

$$\gamma_\alpha^c = 2\pi |B_\alpha^c|^2, \quad \Gamma_\alpha = \sum_c \gamma_\alpha^c. \quad (23.57)$$

The trace w of the operator W , Eq. (23.38), is preserved in the internal transformation to the basis $|\alpha\rangle$ and we can estimate it as $w \sim NT$ in terms of the mean value of the resonance width Γ . The approximation (23.56) of narrow isolated resonances can be valid if the characteristic parameter

$$\kappa = \frac{\Gamma}{D} \ll 1. \quad (23.58)$$

The continuum coupling here is weak and the resonances correspond to long-lived compound states as, for example, typical neutron resonances at low energy (Figure 20.2).

The situation changes when the coupling to the continuum becomes strong and mean widths approach or even go beyond the limit of $\kappa \sim 1$. Instead of perturbation theory,

one has to fully consider the dynamics described by the operator (23.55). For illustrative purposes, consider just a single-channel case when the equation (23.53) is

$$1 + \frac{i}{2} \sum_{\alpha} \frac{\gamma_{\alpha}}{z - \epsilon_{\alpha}} = 0. \quad (23.59)$$

The parameter (23.58) here is simply $\kappa \sim \gamma/D$, where γ is the mean value of γ_{α} , Eq. (23.57).

Problem 23.9 Find the solution for the largest width in the limit $\kappa \sim w/ND \gg 1$.

Solution

The sum of the widths covers the whole spectral interval of levels coupled to the continuum. It is convenient to define the centroid of the internal spectrum weighted with the widths γ_{α} ,

$$\bar{\epsilon} = \sum_{\alpha} \epsilon_{\alpha} \frac{\gamma_{\alpha}}{w}, \quad (23.60)$$

and assume that the root z contains a large imaginary part much greater than the typical level spacing D . If we fully neglect the real spread of the internal spectrum, we come from Eq. (23.59) to

$$z = \bar{\epsilon} - \frac{i}{2} \sum_{\alpha} \gamma_{\alpha} = \bar{\epsilon} - \frac{i}{2} w, \quad (23.61)$$

a “giant resonance,” a broad pole in the center of the spectrum absorbing the whole summed width, $\Gamma = w$. It is easy to find the correction to this solution accounting for the spread of spectrum around the centroid and redistribution of widths, $z = E_{s.r.} - (i/2)\Gamma_{s.r.}$,

$$\Gamma_{s.r.} = w - 4 \sum_{\alpha} \gamma_{\alpha} \left(\frac{\epsilon_{\alpha} - \bar{\epsilon}}{w} \right)^2, \quad (23.62)$$

and

$$E_{s.r.} = \bar{\epsilon} + \sum_{\alpha} \gamma_{\alpha} \frac{\epsilon_{\alpha}(\epsilon_{\alpha} - \bar{\epsilon})^2}{w^3}. \quad (23.63)$$

This limit we will call *superradiance* (the subscript *s.r.*). One resonance absorbs almost the whole width, becoming very short-lived. The rest of resonances become very narrow, their typical widths, according to Eq. (23.62) where the sum should be divided between $N - 1$ resonances, are of the order of $(w/(N\kappa^2))$, much smaller at $\kappa \gg 1$ than the original “unperturbed” width $\gamma \sim w/N$. These *trapped* states have a very long lifetime, longer than the Weisskopf time we used for estimates in the past. Therefore, one can expect that the trapped states live long enough to undergo statistical equilibration that was supposed for the compound nucleus.

The term *superradiance* comes from quantum optics [24]. This class of phenomena was predicted [25] by R. Dicke and then observed and studied experimentally. Originally, a confined system of N two-level atoms in a volume smaller than the wavelength of the atomic transition was considered. If a typical width of this transition is γ , there exist a coherent combination of quantum atomic states that forms a very wide state with

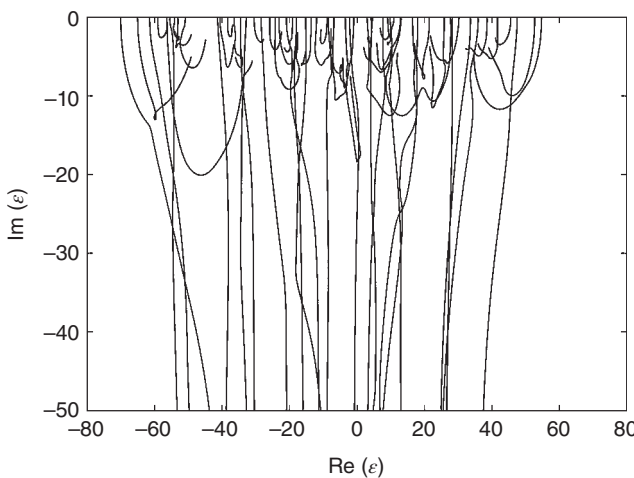


Figure 23.10 Trajectories of the energies and widths for an interacting system of $n = 3$ particles spread over $N = 8$ single-particle levels with the upper one having a direct access to continuum as a function of the growing strength of the continuum coupling.

the width $\propto N\gamma$. If this state is reached in the process of evolution, a burst of radiation is observed. The effect is not based on the direct interaction between atoms. The coherence is reached through the resonance exchange of atoms by virtual photons and enhanced by the fact of degeneracy of levels in identical atoms.

In the nuclear example, we have many intrinsic states with the same quantum numbers coupled to the same decay channel. These states are not degenerate but, for sufficiently large individual widths, their energy distributions overlap. This gives rise to the intense interaction through virtual transitions into continuum and back. Then the same mechanism we have seen in the emergence of collective states due to the normal Hermitian interaction (Chapter 18), creates the collectivization of the widths. One state absorbs the main strength of the decay, while others return to the trapped regime.

A simple model helps understand the dynamics of this process. Assume the shell-model set of few fermionic particles placed onto several single-particle orbitals where the upper orbital is already in the continuum with the width γ . The Kramers degeneracy of orbits and the fact that a physical system would have to have several decay channels with different spin orientation do not change this qualitative pattern. Switch on the interaction between the orbitals giving to many states access to continuum through the upper level. Then we can watch (Figure 23.10) the evolution of the complex energies of many-body states. When continuum coupling is allowed, the many-body states acquire widths. At a certain strength of continuum coupling, many trajectories invert their direction of motion in the complex plane, so that their widths get smaller, while the remaining states become superradiant and further increase their widths.

Problem 23.10 Predict the number of states of each class, superradiant and trapped.

Solution

The total number of many-body states, $N!/[n!(N-n)!]$, is given by Fermi statistics. The superradiant states are those where a particle occupies the upper level with direct access

to continuum. Their number is the number of many-body combinations available for the remaining $n - 1$ particles distributed over $N - 1$ levels, $(N - 1)!/[(n - 1)!(N - n)!]$.

It is difficult to reach full superradiance in nuclear applications because one needs large widths which appear, except for lightest nuclei, at sufficiently high excitation energy. But then new decay channels, frequently with different quantum numbers, get open, and the state widths are distributed over these channels. Then the resonances can overlap without reaching superradiance. In the one-channel case, the onset of superradiance would preclude the regime of overlapping resonances. In the low-energy neutron resonances, when only elastic neutron scattering is possible, the main width comes from many open gamma-radiation channels. The neutron width distribution is still modified from the standard Porter–Thomas distribution (Section 21.3) by the trend to superradiance, as seen experimentally [26] but the full theory of this change is not available yet [27].

As an illustration of effects related to the effective non-Hermitian Hamiltonian, we mention the two-level example [19]. Here two intrinsic states with the same quantum numbers are coupled to a single decay channel, a reasonable approximation to various problems in nuclear structure, atomic physics, and experiments with microwave cavities [23, 28]. A relevant nuclear example is the $^{11}\text{Li}_8$ isotope that has a neutron pair on top of the $^9\text{Li}_6$ core, while the intermediate isotope $^{10}\text{Li}_7$ is unbound, see Section 10.5. The ^{11}Li turns out to be bound mainly owing to the pairing forces between extra neutrons and their interaction through the collective excitations of the core. The pairing force mixes the $(0p_{1/2})^2$ and $(1s_{1/2})^2$ states of the valence neutron pair but these orbitals are already in the continuum.

Problem 23.11 Construct a general effective Hamiltonian matrix for the pair states with a common decay channel and find its complex eigenvalues.

Solution

The Hamiltonian includes unperturbed energies $\epsilon_{1,2}$, the Hermitian interaction v , and decay amplitudes $A_{1,2}$ which enter in the factorized form (23.38), where we include the factor 2π in their definition, so that it is given by

$$\mathcal{H} = \begin{pmatrix} \epsilon_1 - (i/2)A_1^2 & v - (i/2)A_1A_2 \\ v - (i/2)A_1A_2 & \epsilon_2 - (i/2)A_2^2 \end{pmatrix}. \quad (23.64)$$

The determinant of this matrix defines its complex eigenvalues,

$$\begin{aligned} \mathcal{E}_{\pm} = & \frac{1}{2} \left[\epsilon_1 + \epsilon_2 - \frac{i}{2} (\gamma_1 + \gamma_2) \right] \\ & \pm \frac{1}{2} \sqrt{(\epsilon_1 - \epsilon_2)^2 + 4v^2 - \frac{(\gamma_1 + \gamma_2)^2}{4} - i[(\epsilon_1 - \epsilon_2)(\gamma_1 - \gamma_2) + 4vA_1A_2]}, \end{aligned} \quad (23.65)$$

where $\gamma_{1,2} = A_{1,2}^2$.

The general feature is that while, according to the usual perturbation theory, a real perturbation, v in this case, repels the levels and, owing to the mixing of the wave functions, attracts their widths (the wave functions become more similar), an imaginary perturbation acts in the opposite way: energies are attracted but the widths are repelled, a trend to superradiance and segregation of the lifetimes. In the case of originally degenerate

noninteracting levels, $\epsilon_1 = \epsilon_2 \equiv \epsilon$, $v = 0$, the superradiance mechanism works immediately giving

$$\mathcal{E}_+ = \epsilon \text{ (stable)}, \quad \mathcal{E}_- = \epsilon - \frac{i}{2}(\gamma_1 + \gamma_2) \text{ (superradiant).} \quad (23.66)$$

Here we arrived at the bound state *embedded in the continuum* while the partner state absorbs the superradiance. The whole analysis is more complicated [19] if we take into account that the amplitudes A depend on energy, especially close to thresholds.

Problem 23.12

- For the same system as in the previous problem, find the condition when the two resonances cross in the complex plane.
- For a specific combination of the parameters, a state in the continuum (when neither of the amplitudes is zero) can be stable because of interference; find the condition for this to happen.

Solution

- a) Consider the discriminant in (23.65) $X = 2\text{Tr}(\mathcal{H}^2) - (\text{Tr}(\mathcal{H}))^2 = (\mathcal{E}_+ - \mathcal{E}_-)^2$. The crossing happens when $X = 0$; equations $\text{Re}(X) = \text{Im}(X) = 0$ can be brought to

$$(\gamma_1 - \gamma_2)^2 = 16v^2 \text{ and } (\epsilon_1 - \epsilon_2)^2 = \gamma_1 \gamma_2. \quad (23.67)$$

For the energy-independent non-Hermitian Hamiltonian, the partial crossing occurs when $\text{Im}(X) = 0$; then either widths (if $\text{Re}(X) > 0$) or real energies (if $\text{Re}(X) < 0$) cross.

- b) The eigenvalue equation for Hamiltonian (23.65) is equivalent to two coupled equations for real and imaginary parts of energy $\mathcal{E} = E - (i/2)\Gamma$,

$$E^2 - E(\epsilon_1 + \epsilon_2) - \frac{\Gamma}{4}(\Gamma - \gamma_1 - \gamma_2) + \epsilon_1 \epsilon_2 - v^2 = 0, \quad (23.68)$$

and

$$\Gamma = \frac{E(\gamma_1 + \gamma_2) - \gamma_1 \epsilon_2 - \gamma_2 \epsilon_1 + 2vA_1 A_2}{2E - \epsilon_1 - \epsilon_2}. \quad (23.69)$$

The condition $\Gamma_- = 0$ leads to the following relation:

$$v(\gamma_1 - \gamma_2) = A_1 A_2 (\epsilon_1 - \epsilon_2). \quad (23.70)$$

Problem 23.13

For the same system as in problem 23.11, find the resonance part of the scattering amplitude.

Solution

Using Eq. (23.48), we find

$$T(E) = \frac{E(\gamma_1 + \gamma_2) - \gamma_1 \epsilon_2 - \gamma_2 \epsilon_1 + v A_1 A_2}{(E - \mathcal{E}_+)(E - \mathcal{E}_-)}. \quad (23.71)$$

The degenerate case (23.66) displays pure transmission through the superradiant state,

$$T(E) = \frac{\gamma_1 + \gamma_2}{E - \epsilon + (i/2)(\gamma_1 + \gamma_2)}. \quad (23.72)$$

Before showing the effective Hamiltonian at work for realistic nuclear calculations, we have to mention that there are many applications of this approach to general problems of the quantum signal transmission through periodic structures, waveguides, two- and three-dimensional networks, and biological molecules (see [23, 29] and references therein). We will revisit the effective Hamiltonian in Chapter 25, devoted to the chaotic features of nuclear dynamics.

23.9 Realistic Nuclear Calculations

The effective non-Hermitian Hamiltonian is one of the possible synthetic paths to the unified description of nuclear structure and reactions. Using Figure 23.11, we illustrate the perspectives of this approach.

The ${}^8\text{B}$ nucleus has a 2^+ ground state (g.s.) which beta decays with a half-life of about 0.77 s. The proton decay threshold (proton separation energy) is at 0.137 MeV; above this energy, the states can decay to $3/2^-$ ground state of ${}^7\text{Be}$ and a proton. The next threshold is located at 0.567 MeV where proton decay to the first excited $1/2^-$ state in ${}^7\text{Be}$ becomes possible. At higher energy, other channels open up but their contribution is not significant for the region of energies discussed here although it can explain some discrepancy seen in Figure 23.11. The thresholds for the two decay channels mentioned are shown by the vertical grid lines. The upper plot shows the elastic scattering

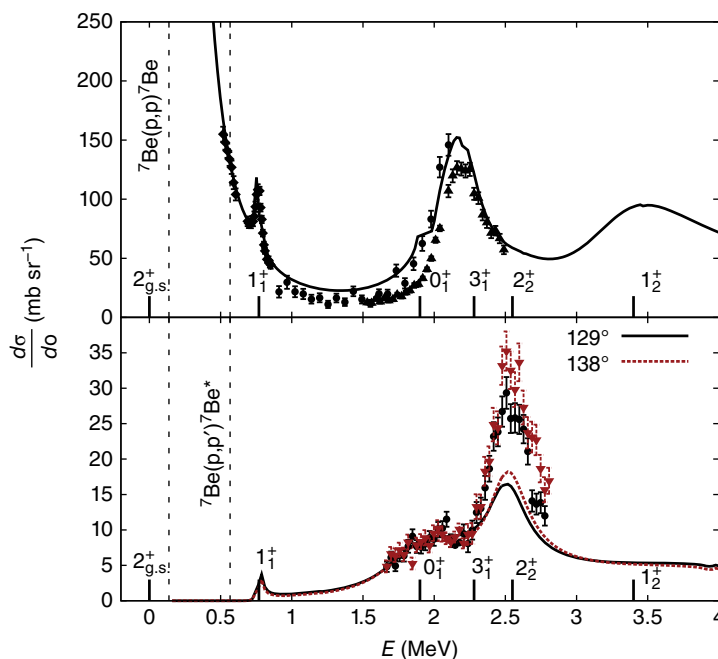


Figure 23.11 Differential scattering cross section for $p+{}^7\text{Be}$ reaction populating resonances in ${}^8\text{B}$ as a function of excitation energy. The top panel shows elastic scattering. The lower panel shows inelastic scattering leading to excited $1/2^-$ state in ${}^7\text{Be}$. The points give experimental results [30–32] and curves show continuum shell-model calculations.

cross section ${}^7\text{Be}(\text{p},\text{p}){}^7\text{Be}(\text{g.s.})$ at 148° scattering angle as a function of energy (excitation function). Experimental points from three experiments [30–32] are shown by squares, circles, and triangles, respectively. The inelastic cross section populating the first excited state in ${}^7\text{Be}$, ${}^7\text{Be}(\text{p},\text{p}){}^7\text{Be}(1/2^-)$, is shown in the lower panel. Here experimental points are from the study in Ref. [32].

The continuum shell-model calculations [22, 32] are shown with curves of corresponding style. The analysis is based on the p -shell effective shell-model Hamiltonian for the \bar{H} (internal part) [33]. The Woods–Saxon potential (Section 8.9) is used to obtain amplitudes (see Problems 23.4 and 23.5). This example is limited to the p -wave proton continuum; the lowest negative parity resonance 2^- that could involve s -wave protons appears as a very broad structure at around 3.2 MeV of excitation and has little effect on the features of the excitation function discussed here.

The low-energy part of the elastic cross section is dominated by the divergent Coulomb scattering cross section (Section 4.8), and the first excited state 1_1^+ appears as a narrow resonance. The behavior of the cross section near this narrow resonance is well described by the Breit–Wigner shape (23.50) with partial widths 34 and 1 keV for the elastic and inelastic channels, respectively. At higher energy and without additional theoretical input, it is impossible to interpret the structure of the excitation functions with multiple overlapping resonances. The analysis using the continuum shell model described here provides an invaluable tool. A good agreement with experiment for both elastic and inelastic scattering cross sections seen in Figure 23.11 allows us to infer nuclear structure in the continuum, positions, widths, and spin parities of the resonances labeled in the figure. Apart from varying the decay energies, the theoretical study has no fitted parameters, being based on a well-established effective Hamiltonian [33] dating back to 1965; this Hamiltonian has been used in multiple studies of p -shell nuclei. The model describes the behavior of the differential cross section as a function of energy and as a function of angle in both channels. For example, the inelastic cross section around 2_2^+ state grows as a function of the decreasing scattering angle. This indicates a specific structure of the resonance that is different from predictions of some other models [32]. While the structure studies are usually limited to positions of states and spectroscopic factors, reaction studies of overlapping resonances allow one to address the interference and signs of coupling amplitudes. Similar methods permit observation of very broad resonances that could manifest the superradiance phenomenon; these resonances do not appear as separate peaks but their presence can be inferred from angular dependence and interference patterns in the cross sections.

In practical applications of the continuum shell model, one can study problems starting from both directions, structure and reactions. For bound states and for narrow resonances, the effective non-Hermitian Hamiltonian can be diagonalized, leading, in general, to eigenstates with complex energy. Because of the energy dependence, the procedure has to be performed iteratively. It is important that the decay channels also involve many-body solutions for states of the decay products. This opens up a possibility of sequential decays. As the example above illustrates, for broad resonances the positions of poles of the scattering matrix, although mathematically well defined, become less connected to the observables. Then one can approach from the reaction side and target directly the scattering matrix and its energy behavior.

Derivation of the transmission matrix (23.48) involves a matrix inversion operation (23.44) as a function of running energy. For large dimensions, this procedure is not only

impractical but also highly numerically unstable because bound states and resonances with widths that differ by orders of magnitude have to be treated in the same process. A good strategy here [22] is to build the Green's function (23.43) using its time-dependent representation

$$G(E) = \frac{1}{E - \bar{H}} = -i \int_0^\infty dt \exp(iEt) \exp(-i\bar{H}t), \quad (23.73)$$

and then construct the evolution operator using the identity

$$\exp(-i\bar{H}t) = \sum_{n=0}^{\infty} (-i)^n (2 - \delta_{n0}) J_n(t) T_n(\bar{H}). \quad (23.74)$$

Here $J_n(t)$ is the Bessel function of the first kind and T_n stand for the *Chebyshev polynomials* defined as $T_n(\cos \theta) = \cos(n\theta)$. These polynomials obey an “angular addition” identity

$$2T_n(x)T_m(x) = T_{n+m}(x) + T_{n-m}(x), \quad n \geq m. \quad (23.75)$$

The \hat{K} -matrix in (23.46) and the corresponding \hat{T} -matrix from (23.48), both as functions of energy, can be found by evaluating the matrix elements $\langle c' | T_n(\bar{H}) | c \rangle$ between various channels (23.42). The recurrence relations between polynomials define an algorithm similar to those discussed in Section 23.6:

$$|c_0\rangle = |c\rangle, |c_1\rangle = \bar{H}|c\rangle, \text{ and } |c_{n+1}\rangle = 2\bar{H}|c_n\rangle - |c_{n-1}\rangle, \quad (23.76)$$

where $|c_n\rangle = T_n(\bar{H})|c\rangle$. The successive iterations allow to include terms with higher n in the sum (23.74), which in turn allows one to evaluate the evolution operator at more remote times. Each iteration improves the energy resolution and the process can be stopped when the desired precision is obtained. This method is also convenient for evaluation of strength distributions which, for an arbitrary state Ψ and with the help of Eq. (23.35), can be defined as

$$F_\Psi(E) = \langle \Psi | \delta(\bar{H} - E) | \Psi \rangle = -\frac{1}{\pi} \text{Im} \langle \Psi | G(E) | \Psi \rangle. \quad (23.77)$$

References

- 1 D. Gloeckner and R. Lawson, Phys. Lett. B **53**, 313 (1974).
- 2 A. de-Shalit and I. Talmi, *Nuclear Shell Theory*, Dover Publications, Mineola, N.Y., 2004.
- 3 B.A. Brown and B.H. Wildenthal, Annu. Rev. Nucl. Part. Sci. **38**, 29 (1988).
- 4 B. Barrett *et al.*, Lawrence Livermore National Laboratory report UCRL-PROC-210305, 2005.
- 5 H. Feshbach, Ann. Phys. **19**, 287 (1962).
- 6 C. Mahaux and H.A. Weidenmüller, *Shell-Model Approach to Nuclear Reactions*, North-Holland, Amsterdam, 1969.
- 7 T.C. Luu, J. Phys. G **31**, S1311 (2005).
- 8 M. Hjorth-Jensen, T. Kuo, and E. Osnes, Phys. Rep. **261**, 125 (1995).
- 9 K. Suzuki and S.Y. Lee, Progr. Theor. Phys. **64**, 2091 (1980).
- 10 J. Carlson, V.R. Pandharipande, and R.B. Wiringa, Nucl. Phys. **A401**, 59 (1983).

- 11 S.C. Pieper and R.B. Wiringa, Annu. Rev. Nucl. Part. Sci. **51**, 53 (2001).
- 12 B.A. Brown and W.A. Richter, Phys. Rev. C **74**, 034315 (2006).
- 13 G. Hagen, M. Hjorth-Jensen, G.R. Jansen, R. Machleidt, and T. Papenbrock, Phys. Rev. Lett. **108**, 242501 (2012).
- 14 J.-P. Delaroche, M. Girod, J. Libert, H. Goutte, S. Hilaire, S. Péru, N. Pillet, and G.F. Bertsch, Phys. Rev. C **81**, 014303 (2010); data from <http://www-phynu.cea.fr>.
- 15 W.D. Myers and W.J. Swiatecki, Nucl. Phys. **81**, 1 (1966).
- 16 E.S. Diffenderfer *et al.*, Phys. Rev. C **85**, 034311 (2012).
- 17 M. Horoi, A. Volya, and V. Zelevinsky, Phys. Rev. Lett. **82**, 2064 (1999).
- 18 N. Michel, W. Nazarewicz, and M. Ploszajczak, Phys. Rev. C **75**, 031301 (2007).
- 19 A. Volya and V. Zelevinsky, Phys. Rev. C **67**, 054322 (2003).
- 20 A. Volya and V. Zelevinsky, Phys. Rev. Lett. **94**, 052501 (2005).
- 21 A. Volya and V. Zelevinsky, Phys. Rev. C **74**, 064314 (2006).
- 22 A. Volya, Phys. Rev. C **79**, 044308 (2009).
- 23 N. Auerbach and V. Zelevinsky, Rep. Prog. Phys. **74**, 106301 (2011).
- 24 A.V. Andreev, V.I. Emel'yanov, and Yu.A. Il'inskii, *Cooperative Effects in Optics*, IOP, Bristol, 1993.
- 25 R.H. Dicke, Phys. Rev. **93**, 99 (1954).
- 26 (a) P.E. Koehler, F. Becvar, M. Krticka, J.A. Harvey, and K.H. Guber, Phys. Rev. Lett. **105**, 072502 (2010); (b) P.E. Koehler, Phys. Rev. C **84**, 034312 (2011).
- 27 A. Volya, H.A. Weidenmüller, and V. Zelevinsky, Phys. Rev. Lett. **115**, 052501 (2015).
- 28 M. Philipp, P. von Brentano, G. Paskovici, and A. Richter, Phys. Rev. E **62**, 1922 (2000).
- 29 V. Zelevinsky and A. Volya, Phys. Scr. **91**, 033006 (2016).
- 30 C. Angulino *et al.*, Nucl. Phys. A**716**, 211 (2003).
- 31 G. Rogachev *et al.*, Phys. Rev. C **64**, 061601 (2001).
- 32 J.P. Mitchell *et al.*, Phys. Rev. C **87**, 054617 (2013).
- 33 S. Cohen and D. Kurath, Nucl. Phys. A**73**, 1 (1965).

24

Weak Interactions

It is remarkable that this variety of physical fields, which play such different roles at the phenomenological level, are all manifestations of the same simple principle and even more remarkable that the way in which they interact with matter is prescribed in advance.

Lochlainn O’Raifeartaigh, *The Dawning of Gauge Theory*, Princeton, 1997

24.1 Introduction

The simplest and the earliest discovered type of the transformations caused by weak interactions is *beta-decay* of the nucleus by the same scheme as the decay of the neutron, mentioned in Sections 1.6 and 1.7,



Of course, at the early stage of development of nuclear science after the discovery of radioactivity and identification of negatively charged beta-particles with electrons, there was no idea of existence of the neutrino. Much later, the *continuous energy spectrum* of beta-electrons gave W. Pauli (1931) the thought of a light neutral particle of spin 1/2 accompanying the appearance of the beta-electron. The neutrino in beta-decay (24.1) more precisely should be called, as it is reflected in our notations, *electron antineutrino*. It was introduced in order to guarantee the energy (and spin) conservation, as well as correct statistics of nuclei, which became clear after discovery of the neutron (J. Chadwick, 1932).

For nuclei with excess of protons, charge-conjugate *positron decay* is possible,



with the emission of the *electron neutrino*. This terminology goes back to the concept of conservation of the *lepton charge*, L , that ascribes $L = 1$ to particles (electron and neutrino) and $L = -1$ to antiparticles (positron and antineutrino). It is not known yet if neutrino and antineutrino are in fact two faces of the same particle (the so-called Majorana fermion [QP, II, Ch. 14]). It is almost certain that the neutrino has nonzero mass, which is, however, so small, less than 1 eV, that in the beginning we will neglect this mass. Then the neutrino and antineutrino can be considered as the particle and antiparticle for the massless Dirac fermion. This will be appropriate for our initial consideration.

Traditionally, decays along the schemes (24.1) and (24.2) are called β^- and β^+ , respectively. The same states in final nuclei can be populated also in *charge exchange reactions* driven by strong nuclear forces, using processes (p, n) and (n, p) , correspondingly.

In the three-body decay as in (24.1) and (24.2), we have a continuous energy distribution between two emitted particles (plus also a small kinetic energy of the recoil nucleus that is, however, responsible for the momentum conservation). The sum of these energies is called the *Q-value*, or the thermal effect of the reaction, which is the difference of total intrinsic energies (masses) of the daughter and parent nuclei. The third type of beta-process, *orbital electron capture*, is allowed in all cases when positron decay (24.2) is possible (the energy threshold here is lower by $2m_e c^2$). This process occurs in the atom: an atomic electron can be absorbed according to



In this case, the released energy is the difference of corresponding nuclear masses minus binding energy of the captured electron and $2m_e c^2$. Usually, the captured electron comes from the lowest atomic orbits (*K*- or *L*-shells), and the atomic structure acquires a hole which is later either filled in by an outer electron with emission of *X*-rays or the hole excitation energy is transmitted to another atomic electron that is knocked out from the atom (Auger electrons). This process can be eliminated if the unstable nucleus is completely stripped of atomic electrons; the experiments with only one remaining electron and the radioactive nucleus in the storage ring were performed at GSI (Darmstadt). The historically first experiment [1] by Cowan and Reines that proved the existence of the neutrino registered the capture by protons of the antineutrino emitted from the nuclear reactor,



Recent GSI experiments [2] working with the unique arrangement of almost completely ionized heavy atoms report an observation of oscillations during times comparable with the half-life in beta-decay neutrino emission have fueled speculations that mixing of two radiating states that are close in energy could lead to exponential decay modulated by neutrino oscillations (Section 24.12). This observation remains yet to be fully confirmed and explained.

There are cases when beta-decays of standard types are forbidden because the energy of the neighboring nucleus, which would have been the daughter in the decay, is higher than the energy of the parent nucleus but the *double beta-decay* is still allowed owing to pairing effects. Decay of this type with emission of two electrons and two neutrinos was observed in 11 nuclei. We discuss this in more detail in the last section of this chapter.

Processes driven by weak interactions play a leading role in the nucleosynthesis of medium and heavy chemical elements in stellar astrophysics. The very first step on the long journey along the periodic table starts with deuteron formation by the fusion of two protons through a weak interaction,



Various channels of the nucleosynthesis proceed through combinations of proton and neutron capture, photonuclear reactions, and beta-decay that bring the exotic isotopes formed as intermediate products with a nonequilibrium neutron/proton ratio to the

valley of stability. We have also to mention various scattering processes governed by weak interactions, especially with participation of neutrinos, which play important roles in astrophysics.

Weak interactions do not respect *fundamental symmetries* firmly established for strong and electromagnetic processes. They violate parity conservation (invariance with respect to the coordinate inversion) and charge conjugation symmetry; both violations occur not as a little correction but as a hundred percent effect related to the nature of currents involved in weak processes. There exist many-body nuclear mechanisms which can, in some cases, magnify these effects and make them clearly observable, as was discussed in Chapter 21 for fission. Currently, there are experimental efforts to use symmetry-violating weak processes with evidently pronounced specific signals as an instrument for studying “normal” nuclear properties, such as matter distribution in nuclei.

The term *weak interactions* is quite justified by the small magnitude of the fundamental constants defining characteristic amplitudes of weak processes and long lifetimes of nuclei with respect to beta-decay. Typically, the lifetime of beta-unstable nuclei is of the order of normal “human” time intervals – from milliseconds to years and even longer. Such times are extremely long on the nuclear intrinsic timescale. As a rule, we can use the amplitudes of the lowest perturbational order to calculate the corresponding probabilities. According to the *standard model* of the microworld, the weak interactions are mediated by the heavy intermediate vector mesons, W^\pm and Z^0 , with masses approximately 80 and 90 GeV, respectively, the uncertainty relations immediately show that such virtual particles make the interaction range very short ($\sim (\hbar/Mc) \sim 10^{-16}$ cm). Therefore, it is usually possible to consider weak nuclear processes as *contact* interactions when the acts of emission and absorption of a virtual vector meson happen *at a point*. This brings us to the original four-fermion theory of weak interactions going back to Fermi (1934). The standard *electroweak* theory shows the common nature of the electromagnetism mediated by massless photons and weak interactions mediated by W^\pm and Z^0 bosons. In Section 24.10, we give a sketch of this theory.

24.2 Beta-Spectrum in the Simplest Case

We start with the discussion of the simplest case of the so-called *superallowed* and *allowed* transitions. We assume that in the beta-decay process all four participating fermions (initial neutron and final proton, electron, and antineutrino) interact in a point-like way. The amplitude of this process should be averaged out over the nuclear volume with appropriate nucleonic wave functions. The superallowed transition involves nuclear states where the coordinate nucleon wave function does not change, the neutron is simply transformed into the proton, or vice versa, at a point (only spin can be flipped). In Section 6.4, we already discussed the two possible coordinate-independent nucleon operators that generate such transformations, Fermi (F), Eq. (6.53), and Gamow–Teller (GT), Eq. (6.54), respectively.

Describing the electron and antineutrino by plane waves whose wavelengths are much greater than the nuclear size, the corresponding exponents can be set equal to 1 in the integral over the nuclear volume. In Fermi transitions, the nuclear matrix elements contain the operators τ^\mp transforming $n \leftrightarrow p$. This is possible only if the global quantum numbers of the nuclear state do not change: the leptons (electron and antineutrino) do

not carry away any orbital momentum while their spins are antiparallel, their total spin being zero. If the leptons carry away spin 1, the spin of the nucleon can change, and the transition operators are $\sigma\tau^\mp$ (Gamow–Teller transitions). Frequently, both F and GT matrix elements are contributing. If the isospin invariance is exact, the initial and final nuclear states have a certain isospin. Then the transitions generated by the Fermi and Gamow–Teller operators (Section 2.7) satisfy important *sum rules* derived in Problems of Section 6.4.

The beta-process transition probability can be calculated by the *golden rule* [QP, II, 2.1]. The counting rate for the decay electrons is given by

$$dN_e = \frac{2\pi}{\hbar} [|\mathcal{M}_F|^2 + |\mathcal{M}_{GT}|^2] \rho(E_e) dE_e, \quad (24.6)$$

where, in general, both Fermi and Gamow–Teller transitions contribute and the nuclear matrix elements are \mathcal{M}_F and \mathcal{M}_{GT} . The electron and antineutrino density of final states in the continuum is determined by the distribution of energy between the electron and antineutrino [QP, II, 2.5],

$$\rho(E_e) dE_e = \int dE_{\bar{\nu}} \delta(E - E_e - E_{\bar{\nu}}) \frac{V d^3 p_e}{(2\pi\hbar)^3} \frac{V d^3 p_{\bar{\nu}}}{(2\pi\hbar)^3}, \quad (24.7)$$

where E is the total decay energy and V is the normalization volume used for the wave functions in the continuum. The lepton plane waves will be $e^{i(\mathbf{k}\cdot\mathbf{r})}/\sqrt{V} \approx 1/\sqrt{V}$, and the final answer has to be independent of V . The Coulomb distortion of the electron wave function is discussed in the next section. The momentum of the recoiling nucleus guarantees the conservation of momentum, while the nuclear recoil energy can be neglected.

Using $p_e dp_e = (E_e/c^2) dE_e$ (and similarly for neutrino) and integrating over angles, we come to

$$\rho(E_e) dE_e = \frac{E_e E_{\bar{\nu}} p_e p_{\bar{\nu}}}{4\pi^4 \hbar^6 c^4} dE_e = \frac{g(E_e; E; m_{\bar{\nu}})}{4\pi^4 \hbar^6 c^6} dE_e. \quad (24.8)$$

The energy spectrum of electrons in the decay with total energy release E is given by

$$g(E_e; E; m_{\bar{\nu}}) = (E - E_e) E_e \sqrt{[(E - E_e)^2 - m_{\bar{\nu}}^2 c^4](E_e^2 - m_e^2 c^4)}. \quad (24.9)$$

If we neglect the antineutrino mass, assuming $E_{\bar{\nu}} = cp_{\bar{\nu}} = E - E_e$, we obtain

$$g(E_e; E) = (E - E_e)^2 E_e \sqrt{E_e^2 - m_e^2 c^4}. \quad (24.10)$$

Because of the smallness of $m_{\bar{\nu}}$, the distortion of the electron energy spectrum can be experimentally noticed only at the very end of this spectrum. The most favorable case is the decay with the lowest energy release. Therefore, the experimental efforts in this direction are concentrated on the tritium beta-decay,



where the Q -value is very low, only 18.6 keV, which implies a long half-life of 12.3 years. The effect of *neutrino oscillations* (Section 24.12), can make the situation even more complicated as the electron antineutrino is then a coherent superposition of at least two quantum states of certain mass with the amplitudes $\cos\theta$ and $\sin\theta$ that depend on the mixing angle θ , so that [QP, II, Problem 2.3], in the experiment that is capable of measuring the mass of the neutrino,

$$g(E_e; E) \rightarrow g(E_e; E; m_1) \cos^2\theta + g(E_e; E; m_2) \sin^2\theta. \quad (24.12)$$

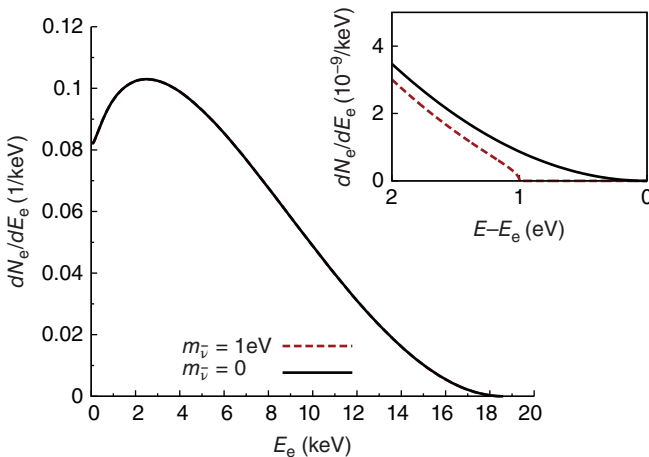


Figure 24.1 Normalized spectrum of electrons expected in tritium beta-decay, Eq. (24.11), for massless (solid curve) and massive, $m_{\bar{\nu}} = 1$ eV, (dashed curve) neutrino. Area near the endpoint is magnified in inset.

With the wavelength of the electron much larger than the nuclear size, $kR \sim 10^{-2}$, and the lepton wave functions being practically constant in the nuclear volume, the electron energy spectrum, according to this density of states, approaches zero at both ends, $E_e = 0$ and $E_e = E$, and has a maximum in between; this was the primary indication of the presence of another particle not seen directly. Frequently, the phase space factor (24.8) is expressed in terms of the spectrum of the electron momentum p ,

$$\rho(p)dp = \frac{E_{\bar{\nu}}p_{\bar{\nu}}p^2}{4\pi^4\hbar^6c^4} dp \equiv \frac{g(p)}{4\pi^4\hbar^6c^3} dp. \quad (24.13)$$

If the electron spectrum would be determined by the phase space only, the experimentally measured quantity $\sqrt{g(p)/p}$ would show up as a straight line in a function of E_e intersecting the energy axis at the end point $E_e = E$; this is called the Curie plot. With $m_{\bar{\nu}} \neq 0$, the line near the endpoint bends down and the intersection is shifted to $E_{\max} = E - m_{\bar{\nu}}c^2$. Figure 24.1 shows the electron energy distribution in tritium beta-decay, with Coulomb distortion included. The area near the end point is magnified to show the effect of massive neutrino. Practically, the difference is hard to detect; under assumption of $m_{\bar{\nu}} = 1$ eV, the chance of an electron being produced within 1 eV from the endpoint is only about 2×10^{-13} .

The integral of the spectrum over energy or momentum of the electron determines the total decay rate. If the decay energy is large, $E \gg mc^2$ for the relativistic electron, we can set $E \approx cp$, and the integral over the electron spectrum is $\propto E^5$.

In the process of orbital capture, the final state contains the neutrino and the recoil nucleus. The Q -value of the reaction is here

$$Q = E_{\nu} + E_{\text{rec}} + |E_b|, \quad (24.14)$$

where $|E_b|$ is the electron binding energy in a certain atomic shell. The density of final states brings only the factor $d^3p_{\nu}/(2\pi\hbar)^3$, while the recoil momentum of the final nucleus is compensated by the momentum of the neutrino.

24.3 Nuclear Transitions

To write down the total transition rate we have to apply the golden rule (24.6) and integrate over the electron spectrum. This requires the knowledge of the nuclear matrix element \mathcal{M} that contains the integral over initial and final nuclear wave functions.

The *allowed* transitions are generated by the same Fermi and Gamow–Teller operators (24.6) but they are weaker because the initial and final nuclear wave functions are slightly different and thus transition is suppressed by the overlap. For our discussion, it is convenient to separate from the matrix element $\mathcal{M} = GM$ the fundamental constant G of the weak interaction. Here we can discuss Fermi and Gamow–Teller transitions separately, with independent matrix elements and coupling constants. The full theory is addressed in Section 24.5.

The matrix element is an amplitude of the process where the four particles – initial and final nucleons, electron (or positron) and (anti)neutrino – are taken at the same point, which is afterwards averaged over the nuclear wave functions. Figure 1.2 in Section 1.6 shows examples of various weak processes; a typical diagram of the four-fermion weak process and its detailed structure accounting for an intermediate vector boson are shown in (b) and (a), respectively. The diagram for neutron decay from a quark structure perspective is shown in Figure 24.2a. The diagram for muon decay, which is another type of pure leptonic beta decay, is shown in Figure 24.2b. For allowed transitions, this coupling amplitude does not depend on the energy distribution between the electron and neutrino.

The electron spectrum found in the previous subsection is distorted by the Coulomb field of the nucleus; this can be expressed by a special distortion function $F(Z, p)$, where Z is the nuclear charge of the daughter nucleus. In this way, we arrive at a useful formula for the transition rate,

$$\dot{\omega} = \frac{2\pi}{\hbar} \frac{1}{4\pi^4 \hbar^6 c^3} G^2 |M|^2 \int_0^{p_{\max}} dp g(p) F(Z, p). \quad (24.15)$$

The function $F(Z, p)$, often referred to as *Fermi function*, can be roughly estimated as a squared ratio of the actual wave function of the electron, or the positron, in the atom,

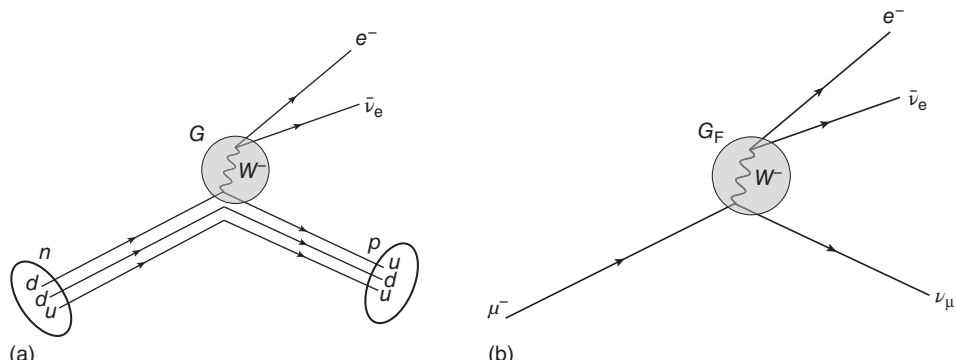


Figure 24.2 Weak interaction diagrams: (a) neutron beta-decay, (b) muon decay. The shaded circle shows the four-fermion interaction vertex. The detailed structure involving the vector boson exchange is shown inside.

to the wave function of free motion. For example, for a nonrelativistic electron, the spherically symmetric scattered state in the continuum can be represented by a regular Coulomb function with $\ell = 0$ (see Problem 23.4). This gives

$$F(Z, p) \approx \lim_{x \rightarrow 0} |F_0(x)/x|^2 = \frac{2\pi\eta}{e^{2\pi\eta} - 1}, \quad (24.16)$$

Here $\eta = \pm Ze^2 m_e / (\hbar p)$ is the Sommerfeld parameter (see Section 4.8), which is positive for the positron and negative for the electron. The qualitative effect can be described as additional acceleration of positrons and deceleration of electrons; as a result, the low-energy part of the electron (positron) spectrum is enhanced (reduced).

In the electron capture from the K -shell, the function $F(Z, p)$ would be just the electron density at the nucleus, $2Z^3/\pi a^3$, where $a = \hbar^2/(m_e e^2)$ is the Bohr radius. In heavy atoms, the relativistic effects are important; the results of realistic atomic calculations have been tabulated [3]; there are also useful analytical approximations, see, for example Ref. [4].

It is convenient to rewrite the integral in dimensionless variables, $\tilde{p} = p/m_e c$. According to (24.13), this separates the factor $m_e^5 c^7$ and leaves a dimensionless integral,

$$f(Z, \tilde{p}_{\max}) = \int_0^{\tilde{p}_{\max}} d\tilde{p} F(Z, \tilde{p}) g(\tilde{p}). \quad (24.17)$$

The transition rate (24.15) becomes (its dimension is inverse time)

$$\dot{w} = \frac{m_e^5 c^4}{2\pi^3 \hbar^7} G^2 |M|^2 f. \quad (24.18)$$

Traditionally, the half-life time $t_{1/2}$ is introduced here, $\dot{w} = \ln(2)/t_{1/2}$, and the decays are characterized by the quantity

$$ft_{1/2} = \frac{K}{G^2 |M|^2}, \quad (24.19)$$

where the universal constant K is defined by

$$\frac{K}{(\hbar c)^6} = \frac{2\pi^3 \hbar \ln 2}{(m_e c^2)^5} = (8120.2776 \pm 0.0009) \times 10^{-10} \text{ s GeV}^{-4}. \quad (24.20)$$

If time is taken in seconds, the quantity $ft_{1/2}$ is usually a large number. Therefore it is common to use $\log_{10}(ft_{1/2})$ instead, which typically changes from 3 to 20. A histogram showing the number of nuclei with different $\log(ft_{1/2})$ values is shown in Figure 24.4.

The superallowed transitions are those with $\log(ft_{1/2})$ close to 3. The neutron beta-decay has $\log(ft_{1/2}) = 3.075$; a very close value 3.06 characterizes the tritium beta-decay (24.11); for the heavy helium isotope the transition ${}^6\text{He} \rightarrow {}^6\text{Li}$ has $\log(ft_{1/2}) = 2.91$; so far, the lowest $\log(ft_{1/2}) = 2.6 \pm 0.1$ has been seen in the decay of ${}^{100}\text{Sn} \rightarrow {}^{100}\text{In}$, see Ref. [5]. In all superallowed transitions, the nuclear parity does not change and the angular momentum change can be only 0 or ± 1 . For $\log(ft_{1/2})$ up to 5, usually, the term *allowed transition* is used, although there is no strict naming rule.

If neutron and proton wave functions would be identical, the Fermi matrix element would be simply 1. For *Fermi transitions*, sometimes the notation is used

$$M_f(F) \equiv \int 1 \equiv \langle f | T^\pm | i \rangle. \quad (24.21)$$

where the operator $T^\pm = \sum_a \tau_a^\pm$ changes only the total isospin projection leaving the nucleus in a different charge state within the same isospin multiplet. Here we can have only $\Delta J = 0$. The transitions of *Gamow–Teller type* are described by the vector matrix element

$$\mathbf{M}_f(GT) \equiv \int \sigma \equiv \langle f | \sum_a \sigma_a \tau_a^\pm | i \rangle. \quad (24.22)$$

Here we can also have spin-flip with $|\Delta J| = 1$ (e.g., decay of ${}^6\text{He}$), but in this case, the transition $(J_i = 0) \rightarrow (J_f = 0)$ is forbidden because the matrix element is generated by the axial vector operator similar to angular momentum. For $\Delta J = 0$, both decays are present but, as the amplitudes correspond to different quantum numbers, these are effectively different decay channels adding up to the total decay rate, Eq. (24.6).

Since Gamow–Teller transitions are of vector type, in decays where final $J_f \neq 0$, the lifetime, in full analogy with electromagnetic and particle decays, Eqs. (14.97) and (23.42), is characterized by the reduced transition probability $B^\pm(GT; i \rightarrow f)$ (see also Eq. (6.56)), which involves the matrix element squared and summation over final magnetic substates that can be reached by different vector components of the Gamow–Teller operator. The lifetime of the initial state does not depend on its orientation; thus it is also common to average over initial magnetic substates. For scalar Fermi transitions, we always have $B^\pm(F; i \rightarrow f) = B^\mp(F; f \rightarrow i) = |M_f(F)|^2$.

Let us briefly give examples of allowed nuclear transitions [6]. We have already discussed the transitions in the $A = 18$ isobaric multiplet (Figure 6.2). If isospin is viewed as a good quantum number, and in practice it is violated only at a level of few percent, the Fermi transitions occur only between two isobaric analog states. In Figure 6.2, the $0^+ \rightarrow 0^+$ transition from the $T = 1$ ground state of ${}^{18}\text{Ne}$ is a Fermi transition. As stated above, in the $0^+ \rightarrow 0^+$ cases, Gamow–Teller transitions are not allowed. However, Gamow–Teller decay of 0^+ ground state occurs to two ($T = 0, 1^+$) states in ${}^{19}\text{F}$. In this case, the vector operator can populate only the 1^+ final states and there is some fragmentation of the strength. This decay pattern is quite typical: in low-lying nuclear states, the isospin takes the lowest allowed value $T = |N - Z|/2$. If one of the nuclei taking part in such a transition has a neutron or proton excess $|N - Z| \geq 3$, the isospin has to change and therefore Fermi transitions are forbidden. Indeed, the Fermi matrix elements in all such cases are smaller by at least two orders of magnitude being related to small violations of isospin invariance. The selection rules for allowed beta-decay often provide strong evidence for spin-parity assignments. In addition to that, excited final states are unstable themselves. For instance, in the *beta delayed neutron decay* the 0^+ ground state of ${}^8\text{He}$ beta-decays populating several 1^+ resonances in ${}^8\text{Li}$ that immediately neutron decay to ${}^7\text{Li}$.

The typical superallowed transitions occur between the odd nuclei which are the members of an isospin multiplet $T = 1/2$ (*mirror transitions*). Here the main part of the nuclear transition is the isospin transformation of the single unpaired nucleon. The nucleus ${}^9\text{F}_8$ undergoes the electron capture process resulting in ${}^8\text{O}_9$. In the framework of the simple shell model, the identical ground-state spin-parity quantum numbers of these nuclei, $J^\Pi = 5/2^+$, are defined by the single nucleon in the $d_{5/2}$ orbital above the inert magic core of ${}^{16}\text{O}_8$. In this process, the maximum energy of the positron is only 1.75 MeV, essentially the difference of neutron and proton masses and extra Coulomb energy of the fluorine nucleus, the half-life time is 66 s, and $\log(f t_{1/2}) = 3.38$. Here both

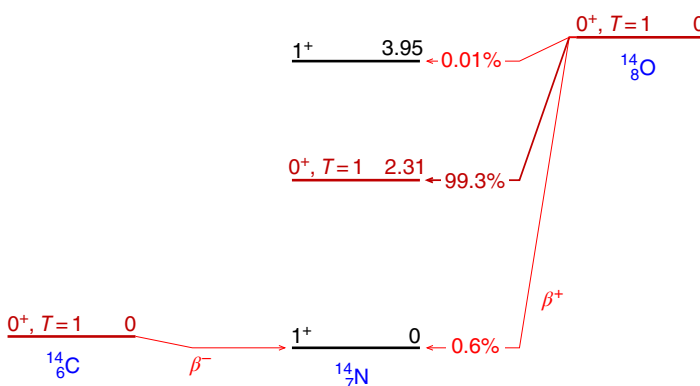


Figure 24.3 The isobaric triplet in $A = 14$ nuclei; the $T = 1$ states are highlighted and beta-decay branching is shown. The states are aligned on the basis of relative beta decay Q -values (in contrast to Figure 2.3).

Fermi and Gamow–Teller operators contribute, and the Fermi matrix element is equal to 1 in the simple shell model.

As we have already mentioned, if spins of both nuclei are $J = 0$, only the Fermi operator is at work in the β -transition between them. Another good example is given by the isospin triplet, $T = 1, J = 0$, that consists of the ground state of the light oxygen isotope $^{14}\text{O}_6$, excited state of nitrogen, $^{14}\text{N}_7$, and the ground state of $^{14}\text{C}_8$ (Figure 24.3). The ^{14}N ground state has spin $J = 1$, similarly to the deuteron having the $n-p$ pair with isospin $T = 0$. The ground state of $^{14}\text{O}_6$ decays nearly exclusively via $0^+ \rightarrow 0^+ \beta^+$ Fermi transition to its isobaric analog excited state in nitrogen. The Gamow–Teller decay to the $J = 1$ ground state of ^{14}N is also allowed but it is very weak in comparison; the branching ratio is only about 0.6%. From the other side of this isobaric triplet, there is β^- decay of ^{14}C ($T_3 = +1$) to the $T = 0$ ground state of ^{14}N . In this case, the state $J = 0$ of ^{14}N that belongs to the isospin triplet is higher in energy than the ground state of ^{14}C . Because of the spin and isospin change, the decay of ^{14}C can be only of Gamow–Teller type; the half-life time here is quite long (5600 years), allowing for the use of the radioactive isotope ^{14}C for geochronology. Another classical example of the Gamow–Teller transition is given by the β^- decay of the heavy helium isotope $^6\text{He}(0^+, T = 1) \rightarrow ^7\text{Li}(1^+, T = 0)$.

Problem 24.1 Assuming exact isospin conservation, calculate the squared nuclear matrix element in the following Fermi transitions

- for the decay $^{14}\text{O} \rightarrow ^{14}\text{N}$;
- for the mirror transition.

Solution

For the pure Fermi transition (24.21), the operator algebra fully determines the matrix elements,

$$B(F) = |M_f(F)|^2 = |\langle T = 1, T_3 = 0 | T_{\pm} | T = 1, T_3 = \mp 1 \rangle|^2 = T(T + 1). \quad (24.23)$$

- a) For this decay, the result is $B(F; {}^{14}\text{O} \rightarrow {}^{14}\text{N}) = |\int 1|^2 = 2$.
b) For a mirror transition, $T_3 = \pm 1/2 \rightarrow T'_3 = \mp 1/2$, $B(F) = 1$. For a general Fermi transition, $|\langle T, T_3 \rangle| \rightarrow |\langle T, T'_3 = T_3 \pm 1 \rangle|^2$,

$$B(F; T_3 \rightarrow T'_3) = T(T+1) - T_3 T'_3. \quad (24.24)$$

In transitions between the two states with $J^\Pi = 0^+$ the Gamow–Teller matrix elements vanish, while Fermi matrix elements are universal, Eq. (24.24). Therefore, for all such cases, the value $ft_{1/2}$ has to be the same, assuming the same T, T_3 , and T'_3 , which is confirmed by the experiment (see Refs. [7, 8]) where the data include necessary small calculable corrections. Thus, in addition to ${}^{14}\text{O}$ discussed in the previous problem, superallowed Fermi transitions have been studied in a series of other $T = 1$ nuclei [7] leading to an average value of $ft_{1/2} = 3072.3 \pm 0.7$ s. This allows to estimate the coupling constant, Eq. (24.19), labeled in Fermi transitions as G_V ,

$$G_V = 1.1494 \times 10^{-5} (\hbar c)^3 / \text{GeV}^2. \quad (24.25)$$

For estimates, one can use $G_V = 10^{-5}/m_p^2$ in units $\hbar = c = 1$.

Problem 24.2 Consider a mirror transition assuming that the nucleon taking part in this process changes its isospin projection but keeps the quantum numbers n, j , and ℓ of its shell-model wave function. Find the reduced Gamow–Teller transition probability for single-particle transitions.

Solution

We have to calculate, for example, for the $n \rightarrow p$ decay,

$$B^-(GT; i \rightarrow f) = \frac{1}{2j+1} \sum_{\mu m m'} |\langle f | \sigma_\mu T^{(-)} | i \rangle|^2, \quad (24.26)$$

where the initial and final states correspond to a nucleon in a certain spherical orbital with quantum numbers j, ℓ but, in general, changing the angular momentum projection $j_z = m \rightarrow m'$. Because of the spin–orbit coupling between spin and orbital momentum,

$$\boldsymbol{\ell} + \mathbf{s} = \mathbf{j}, \quad (24.27)$$

we can use the vector model [QP, I, 22.8] and find the effective spin operator for a transition without change of absolute values j and ℓ ,

$$\boldsymbol{\sigma}_{\text{eff}} = 2 \mathbf{s}_{\text{eff}} = 2 \frac{(\mathbf{s} \cdot \mathbf{j})}{j(j+1)} \mathbf{j} \equiv \zeta \mathbf{j}. \quad (24.28)$$

Using the squared Eq. (24.27), we find the proportionality factor ζ in Eq. (24.28),

$$\zeta = \begin{cases} \frac{1}{j}, & j = \ell + 1/2, \\ -\frac{1}{j+1}, & j = \ell - 1/2. \end{cases} \quad (24.29)$$

Therefore,

$$B^-(GT; i \rightarrow f) = \frac{\zeta^2}{2j+1} \sum_{\mu m' m} |\langle p; jm' | j_\mu T^{(-)} | n; jm \rangle|^2. \quad (24.30)$$

The isospin matrix element here equals $\langle p|T^{(-)}|n\rangle = 1$, and the sum over projections is reduced to the trace $\text{tr}(\mathbf{j}^\dagger \mathbf{j}) = (2j+1)j(j+1)$. As a result,

$$B^-(GT; i \rightarrow f) = \zeta^2 j(j+1) = \begin{cases} \frac{j+1}{j}, & j = \ell + 1/2, \\ \frac{j}{j+1}, & j = \ell - 1/2. \end{cases} \quad (24.31)$$

Through isospin invariance, the Gamow–Teller operator is related to the isovector part of the spin operator involved in the magnetic dipole. A Gamow–Teller transition between spin–orbit partners cannot be worked out with a vector model because $j \rightarrow j \pm 1$, but we can use recoupling described in Section 11.6, which gives

$$B(GT; i \rightarrow f) = \frac{2j_f + 1}{\ell + 1/2}. \quad (24.32)$$

A significant difference between this prediction and the experimentally established value of the matrix element would tell us that, in this case, the single-particle description of the transition is invalid and one has to use more realistic many-body wave functions. For example, in the decay ${}^{11}\text{C} \rightarrow {}^{11}\text{B}$, the quantity (24.26) is smaller by a factor close to 5 than the estimate $5/3$ (an upper line of the array (24.31)) under an assumption that the odd nucleon is in the $p_{3/2}$ orbital.

The neutron decay involves both Fermi and Gamow–Teller processes. Here the best estimate for the phase space factor gives $f = 1.7148 \pm 2$ and the neutron half-life is $t_{1/2} = 613 \pm 3$ s. Taking $B(F) = 1$ and $B(GT) = 3$ from (24.24) and (24.31), respectively, we can evaluate the coupling constant for the Gamow–Teller operator. This coupling constant is usually referred to as G_A ; it comes with an axial operator that has an opposite, relative to Fermi, behavior under spatial inversion. It is convenient to express $G_A = \lambda_A G_V$, where we find $\lambda_A = 1.27$ from neutron decay. Summarizing this phenomenological approach, the allowed and superallowed transitions can be described with the following expression which actually works reasonably well in practice:

$$ft_{1/2} = \frac{\mathcal{T}_{1/2}}{B(F) + \lambda_A^2 B(GT)} \text{ where } \mathcal{T}_{1/2} = 6145 \text{ s.} \quad (24.33)$$

In Figure 24.4, we show statistics of $\log(ft_{1/2})$ values for different types of transitions. The figure also includes the so-called *forbidden* transitions with higher values of $\log(ft_{1/2})$.

24.4 Dirac Formalism

At energy much lower than masses of W^\pm and Z^0 bosons, we still can use the Fermi interaction that substitutes the emission and absorption of the intermediate boson by the effective four-fermion vertex. As the range of propagation of these very heavy bosons is limited by their Compton wave length $\hbar/(Mc) \sim 10^{-16}$ cm, in nuclear processes at low energy this is essentially a contact interaction (Figures 24.2 and 1.2b). The wave functions of light fermions, electron (positron) and (anti)neutrino are to be taken in the relativistic form. Therefore, in this auxiliary section we recall the main properties of the

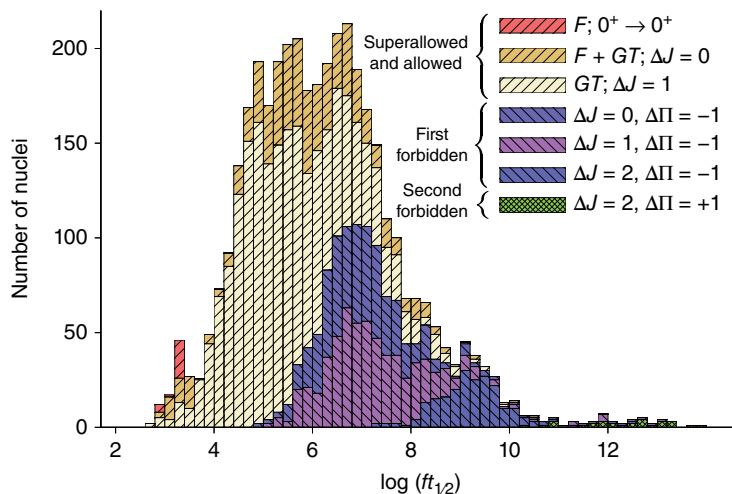


Figure 24.4 Stacked histogram showing the statistics of $\log(f_{t_{1/2}})$ values, where the height of each bin shows the number of nuclei observed with a given beta-decay $\log(f_{t_{1/2}})$. Different colors and shading patterns are used to identify the types of transitions using angular momentum and parity change (ΔJ and $\Delta \Pi$).

Dirac equation that governs the free relativistic motion of a fermion with spin 1/2; more detailed explanations can be found in [QP, II, Chapters 11–14].

We write the Dirac Hamiltonian as

$$\hat{H} = mc^2\beta + c(\boldsymbol{\alpha} \cdot \hat{\mathbf{p}}), \quad (24.34)$$

where the 4×4 Dirac matrices will be taken in the *standard representation*: in the block 2×2 form, they are given by

$$\beta = \begin{pmatrix} \hat{1} & \hat{0} \\ \hat{0} & -\hat{1} \end{pmatrix}, \quad \boldsymbol{\alpha} = \begin{pmatrix} \hat{0} & \boldsymbol{\sigma} \\ \boldsymbol{\sigma} & \hat{0} \end{pmatrix}, \quad (24.35)$$

where $\boldsymbol{\sigma}$ are the usual Pauli matrices of spin 1/2. The Dirac matrices anticommute,

$$[\beta, \alpha_j]_+ = 0, [\alpha_i, \alpha_j]_+ = 0 \text{ for } i \neq j, \quad (24.36)$$

while

$$\beta^2 = \alpha_1^2 = \alpha_2^2 = \alpha_3^2 = 1. \quad (24.37)$$

The single-particle wave functions ψ are four-component *bispinors*. For free motion with momentum \mathbf{p} , the stationary state with positive energy $\epsilon = \sqrt{m^2c^4 + c^2\mathbf{p}^2}$ has a normalized wave function

$$\psi = e^{(i/\hbar)(\mathbf{p} \cdot \mathbf{r})} u(\mathbf{p}), \quad u(\mathbf{p}) = \sqrt{\frac{\epsilon + mc^2}{2\epsilon}} \begin{pmatrix} \phi \\ \frac{c(\boldsymbol{\sigma} \cdot \mathbf{p})}{\epsilon + mc^2} \phi \end{pmatrix}. \quad (24.38)$$

The bispinor is normalized as $u^\dagger u = 1$ if, for the two-component spinor, $\phi^\dagger \phi = 1$. Similar bispinors $v(\mathbf{p})$ can be constructed for antiparticle states with negative energy. Starting from this moment, we, as a rule, simplify our equations going to the system of

units that is usually introduced for relativistic problems: we set $\hbar = c = 1$. Then energy, mass, and momentum have the same dimension, which is inverse to the dimensions of length and time. The relativistic invariance of the theory becomes natural in these units. For example, we have the *four-vectors* x^μ , $\mu = 0, 1, 2, 3$, of coordinate (t, \mathbf{r}) and energy–momentum $p^\mu = (\epsilon, \mathbf{p})$, with Lorentz invariants of interval, $t^2 - \mathbf{r}^2$, between two events, and mass, $m^2 = \epsilon^2 - \mathbf{p}^2$. In general, the four-scalars (invariants) are constructed of two vectors $a^\mu = (a^0, \mathbf{a})$ and $b^\mu = (b^0, \mathbf{b})$ as their scalar products with the metrics $(+, -, -, -)$, namely, $a^0 b^0 - \mathbf{a} \cdot \mathbf{b} \equiv a^\mu b_\mu$. Here we have the relativistic contraction: the summation over repeated indices is implied and application of the diagonal matrix (see Eq. (24.41) in the following), lowers or raises the index, namely, $a^0 = a_0$ and $a^k = -a_k$ for spatial index $k = 1, 2, 3$.

Instead of the matrices β and α_i , one can use another set of matrices, $\gamma^\mu = \{\gamma^0, \boldsymbol{\gamma}\}$, where

$$\gamma^0 = \beta, \quad \boldsymbol{\gamma} = \beta \boldsymbol{\alpha}. \quad (24.39)$$

With the Hamiltonian (24.34), the Dirac equation for the bispinor ψ of free motion, $\hat{H}\psi = \epsilon\psi$, acquires the form (after multiplication by the matrix $\beta = \gamma^0$):

$$(\not{p} - m)\psi = 0, \quad \not{p} \equiv \gamma^\mu p_\mu = \gamma_0 \epsilon - (\boldsymbol{\gamma} \cdot \mathbf{p}). \quad (24.40)$$

Each component of the bispinor satisfies the normal energy–momentum relation as can be easily seen after multiplying the Dirac equation (24.40) by $(\not{p} + m)$ and using the anticommutation relations, which follow from (24.36), (24.37), and (24.39),

$$[\gamma_\mu, \gamma_\nu]_+ = 2g_{\mu\nu} = 2 \begin{pmatrix} 1 & 0 & 0 & 0 \\ 0 & -1 & 0 & 0 \\ 0 & 0 & -1 & 0 \\ 0 & 0 & 0 & -1 \end{pmatrix}. \quad (24.41)$$

In this representation, only the matrix γ_2 changes sign under complex conjugation, while the matrices $\gamma_{0,1,3}$ do not change; under Hermitian conjugation (complex conjugation and transposition), all spatial matrices $\boldsymbol{\gamma}$ change sign but γ_0 does not. We will need also the matrix

$$\gamma^5 = i\gamma^0\gamma^1\gamma^2\gamma^3 = \begin{pmatrix} \hat{0} & \hat{1} \\ \hat{1} & \hat{0} \end{pmatrix}, \quad (24.42)$$

that anticommutes with all γ_μ and has a square equal to the unit matrix. With this definition, the matrix γ^5 is Hermitian, real, and symmetric.

In order to consider physical characteristics given by matrix elements of various operators sandwiched between the solutions of the Dirac equation, we introduce the Dirac-conjugate bispinor (a row) $\bar{u} = u^\dagger \gamma_0$ that satisfies

$$\bar{u}(\not{p} - m) = 0. \quad (24.43)$$

There are $4 \times 4 = 16$ independent bilinear combinations $\bar{u}\Gamma u$ constructed for a given spinor u and various products Γ of the Dirac matrices. They are grouped according to their properties under Lorentz transformation:

scalar $S = \bar{u}u$ (1 component),

polar 4-vector $V_\mu = \bar{u}\gamma_\mu u$ (4 components),

antisymmetric tensor $T_{\mu\nu} = (1/2)\bar{u}[\gamma_\mu, \gamma_\nu]u$ (6 components),

axial 4-vector $A_\mu = \bar{u} \gamma_\mu \gamma^5 u$ (4 components),
 pseudoscalar $P = \bar{u} \gamma^5 u$ (1 component).

It is shown in [QP, II, 12.7] that their names indeed correspond to their Lorentz transformation properties.

Since the weak interactions are extremely dependent on the neutrino properties, the matrix γ^5 plays a special role [QP, II, 14.4, 14.5]. For *massless* particles in free motion, the spin polarization is preserved. Let us redefine the Dirac matrices (24.39) as

$$\gamma_0 = \begin{pmatrix} \hat{0} & -\hat{1} \\ -\hat{1} & \hat{0} \end{pmatrix}, \quad \gamma = \begin{pmatrix} \hat{0} & \sigma \\ -\sigma & \hat{0} \end{pmatrix}. \quad (24.44)$$

It is easy to check that the transformation to new matrices is unitary, preserving the commutation relations. This representation is often called the spinor, chiral, or Weyl representation.

Problem 24.3 Find the γ^5 matrix in the spinor representation.

Solution

According to the definitions (24.42) and (24.44),

$$\gamma^5 = \begin{pmatrix} \hat{1} & \hat{0} \\ \hat{0} & -\hat{1} \end{pmatrix}. \quad (24.45)$$

The upper and lower components of the transformed bispinor ψ now can be called *right* and *left* spinors,

$$\psi = \begin{pmatrix} \psi_R \\ \psi_L \end{pmatrix}. \quad (24.46)$$

Correspondingly, the operators

$$\Lambda^{(\pm)} = \frac{1}{2} (1 \pm \gamma^5). \quad (24.47)$$

are projection operators for the states $\psi_R = \psi^+$ and $\psi_L = \psi^-$.

Problem 24.4 Find the relation between the left and right spinors for free motion according to the Dirac equation.

Solution

For energy E that can be of any sign (using the units $\hbar = c = 1$),

$$m\psi_R = [E + (\boldsymbol{\sigma} \cdot \mathbf{p})]\psi_L, \quad m\psi_L = [E - (\boldsymbol{\sigma} \cdot \mathbf{p})]\psi_R. \quad (24.48)$$

For $m \rightarrow 0$ and positive energy $E = p > 0$, the solution ψ_L describes the particle with left helicity and ψ_R corresponds to the particle with right helicity. At $m \neq 0$, the right and left solutions are not independent.

For massless particles, the Dirac equation is reduced to the Weyl equation,

$$(\boldsymbol{\Sigma} \cdot \mathbf{n})\psi^{(\pm)} = \pm\psi^{(\pm)}, \quad (24.49)$$

where the 4×4 spin matrix is used,

$$\Sigma = \begin{pmatrix} \sigma & 0 \\ 0 & \sigma \end{pmatrix}, \quad (24.50)$$

and

$$\mathbf{n} = \frac{c\mathbf{p}}{E} = \frac{\mathbf{p}}{p} \operatorname{sign} E \quad (24.51)$$

is the unit vector defining the *helicity* ($\sigma \cdot \mathbf{n}$) that is Lorentz invariant for massless particles, similarly to circular polarization of the photon. The matrix γ^5 , *chirality* or *handedness*, plays the analogous role for massive particles. In the massless case, $(\Sigma \cdot \mathbf{n}) = \gamma^5$.

24.5 Four-Fermion Theory

Historically, starting from the first calculations by Fermi, the interaction responsible for beta decay is used in the current–current form, where the currents of different tensor nature are written using 16 possible tensor structures,

$$H_\beta = \frac{G_F}{\sqrt{2}} J J^\dagger. \quad (24.52)$$

Here G_F is the Fermi constant used earlier and the coefficient $1/\sqrt{2}$ is traditionally included in the definition. The current J , in principle, can contain any of the combinations indicated above. However, we should obtain a *relativistic scalar* so that our possibilities are limited by the combinations SS, PP, PS, VV, VA, AA, and TT, where all Lorentz indices are contracted (summed over with the relativistic metric).

In the *secondary quantized* form, the bispinors ψ become operators of destruction of a fermion or creation of an antifermion, while their Hermitian conjugate operators ψ^\dagger describe creation of a fermion or annihilation of an antifermion. The neutron beta-decay, analogous to the nuclear process (24.1), contains therefore the operators $\psi_p^\dagger \psi_e^\dagger \psi_n \psi_\nu$, where the destruction of the neutrino will describe the creation of the antineutrino. The nucleon operators belong to the hadron current h_μ^c , while the electron and neutrino operators belong to the lepton current l_μ^c ; those currents (superscript c) are *charged* which means that they change the electric charges in a complementary way so that the total charge is conserved. Later, we will also use *neutral currents*. The total charged current is the sum

$$J_\mu^c = h_\mu^c + l_\mu^c, \quad (24.53)$$

and the product of the currents in Eq. (24.52) contains, apart from the beta-decay, also pure hadronic and pure leptonic processes.

Various operator structures listed above can generate different types of interactions. Numerous experiments on beta-decay and related processes, after earlier trials and errors, selected the combinations realized in nature. It turned out that the lepton current consists of the vector, V_μ , and axial, A_μ , parts, which come in equal proportion,

$$l_\mu^c = \bar{\psi}_e \gamma_\mu (1 - \gamma^5) \psi_\nu, \quad (24.54)$$

where the bispinors are defined in Eq. (24.38). This variant of the Hamiltonian is called $V - A$. A similar operator structure is established for the hadron current. The only

difference is that the axial part of this current is renormalized by strong interactions getting a factor $\lambda_A \approx 1.27$,

$$h_\mu^c = \bar{\psi}_p \gamma_\mu (1 - \lambda_A \gamma^5) \psi_n. \quad (24.55)$$

The vector current V_μ is not renormalized. This idea of *conservation of vector current (CVC)*, was originally formulated by Feynman, Gell-Mann, and independently by Zel'dovich in analogy with the electromagnetic current that has exactly the same vector structure. The strong interactions cannot change the electromagnetic current operator because it is proportional to the electric charge of the particle that is strictly conserved, including strong interaction processes. As is usually argued, strong interactions can generate the virtual process of proton transformation into neutron and positive pion. The electric charge is of course conserved and the pion will take part in weak interactions adding the portion of the current lost in the disappearance of the proton; the positive pion can decay into the positron and neutrino through the same interaction. As will become clear a little later, practically much more probable is the pion decay into the positive muon (with the same positive charge as the positron) and muonic neutrino, but both electronic and muonic decays are governed by the same weak interaction as they are identical from the viewpoint of electric charge. In a modern electroweak theory (Section 24.10), we have the unification of electromagnetic and weak interactions.

As an example, we can write down the total matrix element for the process of beta-decay going on between the initial, $|i\rangle$, and the final, $|f\rangle$, nuclear states,

$$H_{fi} = \frac{G_F}{\sqrt{2}} \left\langle f \left| \int d^4x (\bar{\psi}_p(x) \gamma_\mu (1 - \lambda_A \gamma^5) \psi_n(x)) (\bar{\psi}_e(x) \gamma^\mu (1 - \gamma^5) \psi_v(x)) \right| i \right\rangle. \quad (24.56)$$

This decay is generated by the cross term between leptonic and hadronic currents.

The original motivation and strong confirmation of theoretical ideas presented here comes from muon decay (Figure 24.2b),

$$\mu^- \rightarrow e^- + \bar{\nu}_e + \nu_\mu. \quad (24.57)$$

The muons are heavy leptons analogous to electrons, $m_\mu/m_e = 206.77$. This process is driven by the four-fermion interaction involving two leptonic currents (24.54) but otherwise the matrix element is identical to the one in Eq. (24.56). There is a convenient set of Feynman rules that one could apply in order to obtain amplitudes for processes represented by diagrams such as in Figure 24.2; the whole procedure of muon lifetime calculation is outlined in a number of textbooks, see, for example, Ref. [9]. In the rest frame of the decaying muon, ignoring the electron and neutrino masses and integrating over angles leads to the following electron energy distribution and the total decay width (equal to the decay rate \dot{w} since here $\hbar = 1$) as

$$\frac{d\dot{w}}{dE_e} = \frac{G_F^2}{12\pi^3} m_\mu^2 E_e^2 \left(3 - \frac{4E_e}{m_\mu} \right), \quad \Rightarrow \quad \dot{w} = \frac{G_F^2 m_\mu^5}{192\pi^3}. \quad (24.58)$$

Measurements of the muon lifetime along with calculations including higher-order corrections allow one to determine the G_F , Ref. [10],

$$\tau_\mu = 2.196980(2) \times 10^{-6} \text{ s}, \quad G_F = 1.1663787 \times 10^{-5} (\hbar c)^3 / \text{GeV}^2. \quad (24.59)$$

We obtained close values, $G_F \approx G_V$ (Eq. (24.25)). The small difference between G_F and the constant G_V for hadronic current suggests that states of various quark generations are actually slightly mixed relative to weak decay processes. This mixing is described by the Cabibbo–Kobayashi–Maskawa matrix and the whole idea is quite similar to neutrino mixing discussed later.

Problem 24.5 Consider beta decay of the unpolarized neutron. Calculate the matrix element for the neutron beta-decay following the diagram in Figure 24.2a and assuming that spectator quarks lead to renormalization of the axial current with λ_A as in Eq. (24.56). Find the lifetime for the decay in terms of the phase space integral (24.17).

Solution

Here the mathematical steps are similar to those involved in the muon lifetime calculation, see Ref. [9], although the situation is complicated by the λ_A term. One noteworthy intermediate result,

$$\frac{d\dot{w}}{dE_e d\omega_e d\omega_\nu} = \frac{G_F^2}{(2\pi)^5} (1 + 3\lambda_A^2) g(E_e; E) \left[1 + \alpha \frac{\mathbf{p}_e \cdot \mathbf{p}_\nu}{E_e E_\nu} \right], \text{ where } \alpha = \frac{1 - \lambda_A^2}{1 + 3\lambda_A^2}, \quad (24.60)$$

is the electron–neutrino angular correlation coefficient, the deviation from the exact $V - A$ result, $\lambda_A \neq 1$. An additional angle-independent small term proportional to m_e/E_e (the so called Fierz interference term) is ignored here. The $e - \nu$ angular correlation that can be measured by the directions of the electron and recoiled proton provides information on λ_A but it does not contribute to the total angular integrated rate. The decay rate of a free neutron is given by

$$\dot{w} = \frac{G_F^2 m_e^5}{2\pi^3} f(E) (1 + 3\lambda_A^2), \quad (24.61)$$

which coincides with our earlier result in Eq. (24.30).

24.6 Nuclear Structure Effects

In order to apply this theory to complex nuclei, we assume that, due to the very short range of weak forces, the weak interaction processes occur at such small distances that the presence of other nucleons does not change the character of this elementary act. The actual nuclear wave function just determines the spatial distribution of those acts and Pauli principle for the final nucleon. This means that we use the same hadronic currents as secondary-quantized operators applied to actual many-body wave functions. At this stage, the nuclear structure has a decisive influence upon the decay rate. The nuclear matrix elements for β^- and β^+ processes are essentially identical, except for interchange of neutrons and protons. In realistic nuclear calculations, pairing effects are an important ingredient. Of course, the kinematics are different in the electron capture with only two final particles, the neutrino and the final nucleus. That process depends on the atomic wave function of the captured electron taken at the nucleus (and on the filling of electron shells in the atom).

The beta-decay serves as a powerful source of information about some features of nuclear structure. A simple example of how the forbidden transition can emerge because of the structure of corresponding nuclear states was discussed long ago by Wigner [11]. Let the initial state have a valence configuration of two paired neutrons and an unpaired proton in the same orbital state. For simplicity, assume that spin–orbital coupling is absent and the neutrons have just opposite spin projections. If we have a decay $n \rightarrow p$, the transition will be completely allowed. But if the beta-transition proceeds as $p \rightarrow n$, it will be forbidden by the Pauli principle because the required final neutron states are blocked.

If the nuclear spin changes by more than one unit, or if the parity of the nuclear state changes in the transition, both Fermi and Gamow–Teller matrix elements vanish, and we come to *forbidden* beta-decays. The transition still can occur if the leptons carry away the necessary angular momentum. The lepton wave functions with orbital momentum ℓ approach zero inside the nucleus as $(kr)^\ell$, which leads to a much smaller nuclear matrix element proportional to $(kR)^{2\ell} \ll 1$. The shape of the energy spectrum also changes. For the *first forbidden decays*, $\ell = 1$, we have to take the dipole terms of the lepton plane waves in the nuclear matrix element. Then nuclear parity changes; the characteristic values of $\log(ft_{1/2})$ increase to 6–8. As a typical example, we can mention the β^- transition between the ground states $^{141}_{58}\text{Ce}_{83} \rightarrow {^{141}_{59}\text{Pr}_{82}}$. In the single-particle scheme, the neutron from the valence orbit $f_{7/2}$ just above the magic number $N = 82$ is transformed into the proton at the orbit $d_{5/2}$ of opposite parity; in this transition, $\Delta j = 1$ and $\log(ft_{1/2}) = 7.7$.

The phenomenological description of Fermi and Gamow–Teller transitions in Section 24.3 can be extended to include more general multipole operators classified by their symmetries, similarly to the discussion in Section 6.4. The procedure requires a specific hierarchy of approximations, but one can find some analogy to electromagnetic transitions (Chapter 14). In electromagnetic transitions, the interaction involves a vector coupling (14.43) which leads to electric and magnetic multipoles that in the long wavelength limit can be reduced to Eqs. (14.94) and (14.91). The relative suppression of transitions can be roughly classified by the combined power (forbiddenness) of the nucleon coordinate r and velocity \mathbf{v} involved; as already stated, the coordinate gives a long wavelength suppression kR and the velocity indicates relativistic effect with a factor v/c . The parity change in a given transition coincides with parity of forbiddenness.

The vector current is an isovector and our discussion above suggests that it could be viewed as being proportional to the isovector part of the regular electric current. The Fermi operator, for example, could be generalized to include the charge density coupling in higher multipoles,

$$\mathcal{M}(\rho_V; \lambda\mu) = \sqrt{4\pi} G_V \sum_a \tau_a^\pm r_a^\lambda Y_{\lambda\mu}(\hat{\mathbf{n}}_a). \quad (24.62)$$

The axial vector current is expected to couple via the following multipole operators:

$$\mathcal{M}(\rho_A; \lambda\mu) = \frac{\sqrt{4\pi} G_A}{c} \sum_a \tau_a^\pm (\boldsymbol{\sigma}_a \cdot \mathbf{v}_a) r_a^\lambda Y_{\lambda\mu}(\hat{\mathbf{n}}_a), \quad (24.63)$$

and

$$\mathcal{M}(j_A; \kappa, \lambda\mu) = \sqrt{4\pi} G_A \sum_a \tau_a^\pm r_a^\kappa [Y_\kappa(\hat{\mathbf{n}}_a) \otimes \boldsymbol{\sigma}_a]_{\lambda\mu}. \quad (24.64)$$

Here the square brackets with a subscript indicate the angular momentum coupling, Eq. (6.49), and the Gamow–Teller operator is just a specific $\kappa = 0$ and $\lambda = 1$ case of (24.64). Typical $\log(f_{1/2})$ values for the first and second forbidden transitions can be inferred from Figure 24.4.

In well-deformed, axially symmetric nuclei (Chapter 16), the rotational bands are characterized by the quantum number K of the angular momentum projection onto the intrinsic symmetry axis. In the first forbidden transition, $|\Delta K| = 1$. The states of the mother nucleus with the K quantum number significantly different from that in the low-lying states of the daughter have typically a very long lifetime because of the required restructuring in the transition. In the odd–odd nucleus ^{176}Lu , the ground state has $J = K = 7$, while the low-lying states of the even–even daughter nucleus ^{176}Hf belong to the rotational band with $K = 0$. Owing this mismatch, the lifetime of the mother nucleus is 2×10^{10} years. As mentioned at the end of Section 21.8, the record belongs to the famous isotope ^{180}Ta , which is the rarest *naturally occurring* isotope [12] that exists in the *isomeric* excited state from which the beta decay is extremely forbidden. The neighboring even–even nuclei have the ground-state rotational bands built with $K = 0$, while the isomeric state is the almost pure Nilsson configuration of the odd proton $9/2[504]$ and the odd neutron $9/2[624]$ with $K = 9$ (recall the Nilsson scheme, Section 12.12).

The superallowed Fermi beta-decay leads to the *isobaric analog* of the mother state. Because of Coulomb energy, the members of the isospin multiplet with a larger proton number Z have higher energy. Therefore, the Fermi decay cannot be β^- (of the type $n \rightarrow p$). The only possibility for the Fermi decay is β^+ , or electron capture, of the type $p \rightarrow n$, which requires $Z > N$. Indeed, if $N > Z$, and, as usually in the ground state, the isospin takes its maximum possible value, $T = T_3 = (N - Z)/2$, the β^+ decay would lead to the projection $T_3 + 1$ that exists only in a different isospin multiplet, $T \rightarrow T + 1$, inaccessible in the Fermi process if isospin is precisely conserved.

There is no strict conservation law that would select a certain state in the daughter nucleus for the Gamow–Teller decay; the isospin can change. But in many cases, the action by the Gamow–Teller operator leads to the final states concentrated in a relatively narrow region of the daughter nucleus. This strength concentration is similar to giant resonances discussed earlier (Chapter 6), and sometimes called the *Gamow–Teller giant resonance* [13]. However, this strength typically does not exhaust the sum rule (Section 6.4), and its noticeable part spreads to higher energy, the so-called *quenching* of the Gamow–Teller strength, which is still not fully understood as it continues to be a subject of theoretical and experimental discussions. Of course, the highly excited part of this strength is experimentally accessible only in charge–exchange reactions but not in beta-decays. This resonance would be narrow if the nuclear forces would have exact $SU(4)$ spin–isospin symmetry; then the Gamow–Teller operator would belong to generators of this group.

Problem 24.6 Consider a Gamow–Teller decay of β^- type in a nucleus with a neutron excess. Argue that the geometry of Clebsch–Gordan coefficients in isospin space makes the transitions with $\Delta T = \Delta T_3 = -1$ preferable.

Solution

This transition amplitude contains the Clebsch–Gordan coefficient $C_{TT_3-1-1}^{T'T_3'}$, where $T = T_3 = (N - Z)/2 > 0$, and the isospin of the final nucleus can be $T' = T$ or $T' = T \pm 1$,

while $T'_3 = T_3 - 1$. Then the corresponding coefficients behave as $1/T$ for $T' = T + 1$, as $1/\sqrt{T}$ for $T' = T$, and 1 for $T' = T - 1$.

Problem 24.7 Consider a Gamow–Teller β^- decay in the nucleus with no valence protons in the orbit with angular momentum j and n neutron pairs on the analogous orbit. Find the quantum numbers J^Π of the final nuclear state and compare the transition probability B_{GT} with the probability in the case when there is only one neutron in the initial state.

Solution

The final state has quantum numbers $J^\Pi = 1^+$ and the transition probability is greater by a factor $2n$.

24.7 Parity Violation

Although for many years it was “naturally” assumed that all interactions in nature are invariant under spatial inversion \mathcal{P} , a detailed analysis in 1956 [14] of all available experimental information revealed that there are no direct confirmations of this symmetry in weak interactions. Very soon after that (in the course of 1 year), three decisive experiments clearly demonstrated that both parity \mathcal{P} and charge-conjugation symmetry C are violated in weak interactions. The first experiment by Wu *et al.* [15] has shown the asymmetry, $(\mathbf{p}_e \cdot \mathbf{J})$, of electrons in the beta-decay with respect to the spin direction \mathbf{J} of the decaying polarized nucleus. Second, the electrons in beta-decay turn out to be polarized [16]. Finally, the same conclusion followed [17] from the muon decay.

Nuclei ^{60}Co have the ground-state quantum numbers $J^\Pi = 5^+$ and decay into ^{60}Ni , electron and antineutrino (Figure 24.5). The main decay branch arrives at the excited state 4^+ of ^{60}Ni . The nuclear parity does not change and $\Delta J = 1$, so that this is a pure allowed Gamow–Teller transition. Initial nuclei were cooled and spin-polarized by a magnetic field (the degree of polarization was 60%). The experiment revealed a large asymmetry of the decay electrons with respect to the direction of the polarizing magnetic field, and therefore nuclear spin; the electrons evidently prefer to move in the direction opposite to the polarization of the initial nucleus. The directional distribution of the electrons is given by

$$\frac{dN}{d\theta} \propto (1 - \alpha \cos \theta), \quad (24.65)$$

where θ is the angle between the electron momentum and the direction of nuclear polarization, and the asymmetry coefficient $\alpha \approx v/c$ for the electrons with velocity v (in the experiment, fast electrons had $v/c \approx 0.6$). For relativistic electrons with $v/c \approx 1$, one would therefore expect the asymmetry coefficient close to 1 with no electrons flying in the direction of the original nuclear spin.

This result evidences full parity violation in this process. Indeed, fast electrons have, according to this observation, asymmetry characterized by the combination of a scalar (the isotropic term in (24.65)) and pseudoscalar ($\mathbf{J} \cdot \mathbf{n}_e$), where \mathbf{n}_e is the unit vector along the electron momentum. The cross section which is a combination

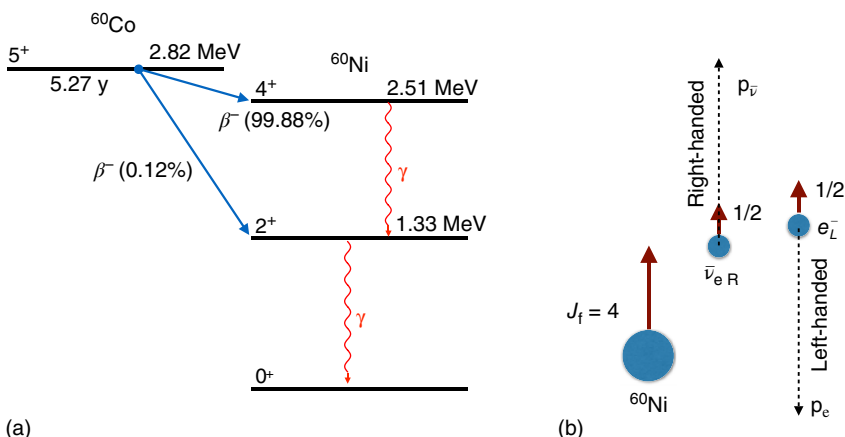


Figure 24.5 (a) Decay scheme of the ^{60}Co nucleus. (b) Illustration showing parity violation in the final state. Thick arrows show directions of aligned spins that add up to the initial $J_i = 5$ of the polarized ^{60}Co nucleus. Dashed arrows show direction of motion that has to be right handed for antineutrino and correspondingly left handed for electron (assuming masses of both leptons are negligible).

(scalar)+(pseudoscalar) becomes, in the frame with inverted coordinate axes, (scalar)-(pseudoscalar). This means that this process completely violates invariance with respect to spatial inversion. With the pseudoscalar amplitude a of the order unity, we have essentially maximum parity violation.

This discovery can be understood assuming that the antineutrino, the electron counterpart in the beta-decay, has zero mass, $|E| = cp$. For the *massless* Dirac fermions, one can use the description [QP, II, 14.4] using the Weyl equations (24.49) for two-component spinors,

$$(\boldsymbol{\sigma} \cdot \mathbf{n})\psi^{(\pm)} = \psi^{(\pm)}, \quad (24.66)$$

where the unit vector \mathbf{n} has an opposite meaning for the particle and the antiparticle, Eq. (24.51). Such particles are uniquely attached to their *helicity* $(\boldsymbol{\sigma} \cdot \mathbf{p})/p$. In principle, we could have four types of particles: neutrino, solutions with $E > 0$, and antineutrino, solutions with $E < 0$, each of them with positive or negative helicity. If parity is completely violated, nature supplies only one helicity, negative ("left") for the neutrino and positive ("right") for the antineutrino. The two other alternatives are not realized in nature. As shown by the ^{60}Ca decay (and many subsequent experiments), the antineutrino here comes always right polarized, while in the positron decays, or electron capture, the neutrino is left polarized. Therefore, it is said that this interaction is carried by the *left currents*.

In the pure Gamow–Teller ^{60}Co decay, no orbital momentum is carried away by the leptons. The total change of the nuclear spin, equal to 1, should be compensated by the parallel spins of the electron and antineutrino; see illustration in Figure 24.5. The right-polarized antineutrino therefore has to move in the polarization direction, while the electron is doomed to move in the opposite direction as shown by the experiment and, for the spin conservation, with negative helicity. In fact, in this limit, the fast electrons, $E \gg mc^2$, are similar to neutrinos being compulsory left polarized.

Problem 24.8 For the left-handed electron created in the beta-decay process determine the probability for spin orientation along and against the direction of motion. Find the coefficient a in Eq. (24.65).

Solution

It is convenient to choose the quantization axis along \mathbf{p} . Starting from the normalized bispinors (24.38) for both spin orientations \pm , we calculate the corresponding probabilities P^\pm and the ratio determining the correlation amplitude a :

$$P^\pm = u^{(\pm)\dagger}(\mathbf{p}) \frac{1}{2}(1 - \gamma^5) u^{(\pm)}(\mathbf{p}) = \frac{E \mp p}{2E}, \quad \frac{P^+ - P^-}{P^+ + P^-} = -\frac{v}{c} = -a. \quad (24.67)$$

The negative sign here indicates that spins of electrons are predominantly oriented against the direction of motion.

These ideas are confirmed by the decays of pions and muons. A comprehensive summary of particle data, overview of current experimental information as well as description of theoretical and experimental methods can be found in publications of the Particle Data Group [18]. In the decay [17] of the zero-spin pion,

$$\pi^- \rightarrow \mu^- + \bar{\nu}_\mu, \quad (24.68)$$

the spins of the muon and muonic antineutrino have to be antiparallel. Moving back to back, the products have to compensate their spins, which means here that their helicities are the same. With the right-handed antineutrino, the negative muon automatically has to be also right handed. This means that kinematics constrains muons to a “wrong” polarization; only left-handed ones are produced in the weak decay and therefore, according to Eq. (24.67), the decay is suppressed by a factor $1 - v/c$.

This explains the overwhelming probability of the pion decay according to Eq. (24.68), contrary to the natural idea that similar pion decay to the electron and electronic antineutrino $\pi^- \rightarrow e^- + \bar{\nu}_e$ seems to be much more probable because, owing to the very small mass of the electron, the decay energy and therefore the available phase space volume would be much bigger than in the muonic decay. But this would contradict the necessity to have left polarization for the relativistic electron. The heavier muon in the decay (24.68) is not ultrarelativistic and can easier carry the “wrong” polarization.

The muons from the pion decay in turn also decay according to (24.57). In the decay events with the most energetic decay electrons, the electronic antineutrino and muonic neutrino move together, while the momentum of the electron is opposite to the summed momentum of this pair. The neutrino and the antineutrino with opposite helicities do not carry any spin. Then the electron has to inherit the spin of the muon. But the natural helicity of the decay electron is left so that it should be opposite to the helicity of the muon from the decay (24.57).

Similar arguments can be used to understand the electron–neutrino angular correlation in the decay of unpolarized neutrons under a simplifying assumption of massless electron and neutrino, Eq. (24.60). From the nonrelativistic limit, we know that the Gamow–Teller transition is associated with λ_A^2 strength and the leptons in this case carry the net spin angular momentum 1. The Fermi transition has a unit relative strength and leptons come out with spins coupled to zero. As in the previously discussed

Gamow–Teller ${}^{60}\text{Co}$ decay, when the spins of two leptons are aligned (the net magnetic projection is ± 1), they are moving in the opposite directions; thus we associate this with probability $P^- = 2\lambda_A^2$. When the spins of two leptons are antialigned, they have to move in the same direction. The probability $P^+ = 1 + \lambda_A^2$ in this case comes from the Fermi transition and from the Gamow–Teller transition with the net zero magnetic spin projection of leptons. The total probability $P^- + P^+ = 1 + 3\lambda_A^2$ correctly reproduces the corresponding combination in Eq. (24.61); and the angular correlation coefficient is $\alpha = (P^+ - P^-)/(P^+ + P^-)$.

The parity violation in the beta-decay is accompanied by a similarly complete violation of charge conjugation symmetry C , the transformation of particles into antiparticles and vice versa. In the massless limit, this operation, without changing the helicity, transforms the left-handed neutrino into a nonexistent left-handed antineutrino. Therefore, the C -symmetry is also broken. According to the idea of Landau [19], the nature is symmetric with respect to the *combined inversion* CP , spatial inversion accompanied by the transition to antiparticles.

The quantum field theory concludes [20] that the requirements of relativistic invariance and unitarity (conservation of probability summed over all reaction channels) lead to the CPT -symmetry where the combined inversion CP is supplemented by the time reversal operation T . This corresponds to Feynman's picture of antiparticles as particles moving backward in time, or to the natural classical picture of the positron moving in the same electric field exactly opposite to the trajectory of the electron and repeating in the opposite order all intermediate values of momentum and coordinate. Therefore, the later discovery [21] of the rather weak, on the level of 10^{-3} , violation of the CP -symmetry in some meson decays [20, 22, 23] speaks in favor of T -violation. The CP violation is one of the famous Sakharov conditions [24] for explaining the strong matter–antimatter asymmetry in the visible Universe. So, CP is also only an approximate symmetry, although violated quite weakly, in comparison with P - and C -symmetries completely violated in weak processes.

Beta-decay is not a unique nuclear process with parity violation. Weak interactions responsible for beta-decay, as a rule, do not effectively contribute to the nuclear structure observables. These interactions are indeed weak and can give some corrections to nuclear observables typically on the level $10^{-(7\pm 8)}$. However, there are effects where the contribution of the weak interaction is *enhanced* by specific features of the nucleus as discussed in Section 21.8.

24.8 Electric Dipole Moment

The theorem by Purcell and Ramsay [25] shows that an expectation value of the electric dipole moment (EDM) in any stationary quantum state with a certain value of angular momentum is twice forbidden. Indeed, let us consider such an expectation value given by the diagonal (in all quantum numbers except maybe the angular momentum projection) matrix element of the dipole operator $\hat{\mathbf{d}}$:

$$\mathbf{d} = \langle JM' | \hat{\mathbf{d}} | JM \rangle. \quad (24.69)$$

The rotational invariance, formally expressed through the Wigner–Eckart theorem (*vector model* [QP, I, 22.8]), tells us that any such vector matrix element is proportional to the

same matrix element of the angular momentum as the only conserving vector operator,

$$\mathbf{d} = \frac{\langle J | (\mathbf{d} \cdot \mathbf{J}) | J \rangle}{J(J+1)} \langle JM' | \hat{\mathbf{J}} | JM \rangle. \quad (24.70)$$

Here the matrix element of the scalar $(\mathbf{d} \cdot \mathbf{J})$ preserves the projection M and does not depend on M . But this is a *pseudoscalar* rather than a genuine scalar: the scalar product of the polar vector \mathbf{d} and the axial vector \mathbf{J} changes sign under the inversion of coordinates. Therefore, the nonzero dipole moment automatically requires that the stationary state does not have certain parity.

This is the first limitation for the stationary dipole moment: parity has to be violated. We already know that weak interactions indeed do not respect parity. However the Purcell–Ramsay theorem claims more. Consider the time reversal operation when $\mathbf{J} \rightarrow -\mathbf{J}$, $M \rightarrow -M$ but \mathbf{d} does not change. The rotationally invariant product $(\mathbf{d} \cdot \mathbf{J})$ does not depend on M but, on the other hand, it has to change sign. Therefore, the dipole moment vanishes along with this scalar product. This means that the EDM is forbidden twice – by P and by T symmetry.

As both symmetries are violated in nature, the search for the EDM of elementary quantum systems is a legitimate direction of experimental efforts. Of course, this quantity has to be very small and this search is extremely difficult as can be seen from current boundaries obtained after decades of hard labor; the EDM of a free neutron is $d_n < 2.9 \times 10^{-26}$, for the electron $d_e < 8.7 \times 10^{-29}$, and for an atom $d < 3.1 \times 10^{-29}$ as measured in ^{199}Hg (all numbers in the units $e\text{ cm}$). It is amazing that it is experimentally possible to study their nature at such a small scale. The current standard model of elementary particles contains a prediction of the EDM on the very low level of 10^{-38} which is far below experimental feasibility. On the other hand, some theories beyond the standard model predict effects as large as 10^{-28} so that such variants are already rejected.

For nuclear and atomic dipole moments, the situation is further aggravated by the following consideration. The experiment searching for the dipole moment will use an external electric field \mathcal{E} . Even if the nuclear dipole moment \mathbf{d}_N is present, in the electric field applied to an atom, electrons will be rearranged screening the nuclear dipole moment. This is the essence of the Schiff theorem [26, 27]. Below we provide the simple proof of this statement.

The Hamiltonian of a neutral atom in the external electric field \mathcal{E} can be written as a sum of contributions from Z atomic electrons (coordinates \mathbf{r}_a) and from the nucleus,

$$H = H_{\text{el}} + H_{\text{nucl}} + \sum_{a=1}^Z e\Phi(\mathbf{r}_a) - (\mathcal{E} \cdot (\mathbf{d} + e \sum_{a=1}^Z \mathbf{r}_a)), \quad (24.71)$$

where the electrostatic potential acting on atomic electrons is created by the nuclear charge density $\rho(\mathbf{x})$,

$$\Phi(\mathbf{r}) = \int d^3x \frac{\rho(\mathbf{x})}{|\mathbf{r} - \mathbf{x}|}. \quad (24.72)$$

To come to the Schiff theorem, let us make a unitary transformation of the Hamiltonian,

$$H \Rightarrow H' = e^{(i/\hbar)G} H e^{-(i/\hbar)G} \approx H + \frac{i}{\hbar} [G, H], \quad (24.73)$$

where we take the generator G of the transformation proportional to the (very small) expectation value $\langle \mathbf{d} \rangle$ of the nuclear dipole moment which justifies the approximation made in Eq. (24.73).

We choose the generator G as acting only on atomic variables,

$$G = \frac{\langle \mathbf{d} \rangle}{Z|e|} \cdot \sum_{a=1}^Z \mathbf{p}_a, \quad (24.74)$$

where $\langle \mathbf{d} \rangle$ is the mean value of the nuclear dipole moment sought for and \mathbf{p}_a are the momentum operators of atomic electrons combined to their total momentum. The commutator in (24.73) involves the electron coordinates,

$$\frac{i}{\hbar} [G, H] = \langle \mathbf{d} \rangle \cdot \left(\mathcal{E} - \frac{1}{Z} \sum_{a=1}^Z \nabla_a \Phi(\mathbf{r}_a) \right). \quad (24.75)$$

The vector multiplied in Eq. (24.75) by the dipole moment is nothing but the total field $\mathcal{E} + \mathcal{E}'$ acting at the nucleus, the sum of the external field and the field of the electrons. But the expectation value of the left-hand side is vanishing as a mean value of the commutator with the Hamiltonian taken for the stationary state. This leads to the Schiff result,

$$\mathcal{E} + \mathcal{E}' = 0. \quad (24.76)$$

The electrons are redistributed in the external field in such a way that they screen the field acting at the nucleus. After the transformation, the dipole term in the Hamiltonian becomes $(\mathbf{d} - \langle \mathbf{d} \rangle) \cdot \mathcal{E}$ which disappears in the first order.

The main contribution to the observable EDM will come from the next vector term of the expansion of the nuclear charge density which is usually called the Schiff moment, the dipole moment weighted with the radial distribution of the nuclear charge density,

$$\mathbf{S} = \frac{1}{10} \int d^3x \rho(\mathbf{x}) \left(x^2 - \frac{5}{3} \langle x^2 \rangle \right) \mathbf{x}, \quad (24.77)$$

where corrections from the expectation value of the nuclear quadrupole moment also are to be added (we do not discuss here the effects of the hyperfine interactions which can be essential in light nuclei, while the collective enhancement discussed below is expected in heavy nuclei).

24.9 Nuclear Enhancement

The nonzero EDM possible only due to the simultaneous \mathcal{P} - and \mathcal{T} -violation is certainly minuscule. The chances of getting significant enhancement in a nucleus are related either to the more or less accidental close proximity of levels mixed by the weak interactions or to possible collective effects which could coherently enhance the atomic EDM. In this problem, the desired effects might be associated with the combination of the quadrupole and octupole collectivity, either in the form of static deformation or in the interplay of corresponding soft vibrational modes.

The expectation value of the nuclear Schiff moment, similar to the dipole moment, is given by the effective operator of the vector model for the nuclear ground state with nonzero spin J ,

$$\mathbf{S} = \frac{\langle J | (\mathbf{S} \cdot \mathbf{J}) | J \rangle}{J(J+1)} \mathbf{J}. \quad (24.78)$$

The exact nuclear state $|JM\rangle$ should be a superposition of the ground state $|JM; 0\rangle$ found with no weak interactions and admixtures of opposite parity states with the same spin J induced by the \mathcal{PT} -violating weak interaction W ,

$$|J\rangle = |J; 0\rangle + \sum_{k \neq 0} \frac{\langle J; k | W | J; 0 \rangle}{E_0 - E_k} |J; k\rangle. \quad (24.79)$$

The weak perturbation creates the nonzero expectation value of the Schiff moment,

$$\langle \mathbf{S} \rangle = 2 \operatorname{Re} \sum_{k \neq 0} \frac{\langle J; 0 | \mathbf{S} | J : k \rangle \langle J; k | W | J; 0 \rangle}{E_0 - E_k}. \quad (24.80)$$

The Schiff moment influences the atomic electrons and generates the EDM of the atom.

Now let us recall main properties of the deformed nuclear field. In the well-deformed case, we consider the *intrinsic* reference frame rotating together with the body. This rotational motion defines the orientational wave function D_{MK}^J , where J and $J_z = M$ are total nuclear spin and its projection onto the laboratory quantization axis, respectively. We assume that the nuclear shape has axial symmetry characterized by the unit vector \mathbf{n} and one can define the conserved component $(\mathbf{J} \cdot \mathbf{n}) = K$ of the total spin along the symmetry axis. The single-particle states in this case are Nilsson orbitals with a certain angular momentum projection $j_z = \kappa$. Owing to the \mathcal{T} -invariance of strong forces, the orbitals $\pm\kappa$ are degenerate (Kramers theorem).

In the body-fixed frame, any polar vector, such as the Schiff moment \mathbf{S} , can have a nonzero expectation value S_{intr} without any \mathcal{P} - or \mathcal{T} -violation. The symmetry dictates the direction of this vector along the symmetry axis, $\mathbf{S}_{\text{intr}} = S_{\text{intr}} \mathbf{n}$. However, this intrinsic vector is averaged out by rotation because the only possible combination in the space-fixed frame is proportional to the pseudoscalar product $(\mathbf{n} \cdot \mathbf{J})$ that violates \mathcal{P} - and \mathcal{T} -invariance. If the weak forces create an admixture α of states of the same spin and opposite parity, the average orientation of the nuclear axis arises. In the linear approximation with respect to α ,

$$\langle (\mathbf{n} \cdot \mathbf{J}) \rangle = 2\alpha K, \quad (24.81)$$

and, therefore, we acquire the space-fixed Schiff moment (24.78) along the laboratory quantization axis,

$$\langle JM | S_z | JM \rangle = \frac{2\alpha KM}{J(J+1)} S_{\text{intr}}. \quad (24.82)$$

In order to have a significant value of the intrinsic Schiff moment, it is not sufficient to have a standard quadrupole deformation. We need a type of deformation that distinguishes the two directions of the axis violating the symmetry with respect to the reflection in the equatorial plane perpendicular to the symmetry axis. The needed effect may emerge in the simultaneous presence of quadrupole and octupole deformation, the latter creating a pear-shaped intrinsic mean field. The octupole deformation near the transition point of the fission process is important for the physics of fission isomers (Section 21.7), but here we need the octupole deformation in the ground state.

Problem 24.9 Consider a nucleus with the axially symmetric surface shape described by the liquid drop parameters,

$$R(\theta) = R \left[1 + \sum_{\ell=1}^{\infty} \beta_{\ell} Y_{\ell 0}(\theta) \right]. \quad (24.83)$$

Find the dipole deformation of this shape and the corresponding Schiff moment (in terms of the lowest contributing multipoles).

Solution

The vector terms $\ell = 1$ emerge, after excluding the center-of-mass displacement, through bilinear combinations of even and odd multipoles,

$$\beta_1 = -\sqrt{\frac{27}{4\pi}} \sum_{\ell=2} \frac{\ell+1}{\sqrt{(2\ell+1)(2\ell+3)}} \beta_\ell \beta_{\ell+1}. \quad (24.84)$$

The main contribution to the Schiff moment comes from $\ell = 2$,

$$S_{\text{intr}} = \frac{9}{20\sqrt{35\pi}} eZR^3 \beta_2 \beta_3. \quad (24.85)$$

We see the importance of the simultaneous presence of quadrupole and octupole deformation.

The significant enhancement comes in the presence of close levels of opposite parity mixed by the interaction W . The small splitting, $\Delta_{\pm} = |E_+ - E_-|$, exists, for example, in ^{225}Ra ($\Delta_{\pm} = 55 \text{ keV}, J = 1/2$) and in ^{223}Ra ($\Delta_{\pm} = 50 \text{ keV}, J = 3/2$). Radium and radon isotopes seem to be promising because of clear manifestations of octupole collectivity. In addition, the large nuclear charge is favorable for the relativistic enhancement of atomic effects (large electron wave functions in the vicinity of the nucleus). Note that the parameter α , Eq. (24.81), already requires \mathcal{PT} -violation and therefore it contains β_3 , so the final effect is proportional to β_3^2 .

The mixing can be particularly enhanced if the admixed states are *parity doublets*. In the presence of the octupole deformation (or for any axially symmetric shape with no reflection symmetry in the equatorial plane), the states of certain parity are even and odd combinations of intrinsic states $\chi_{\pm K}$ with the quantum numbers $K \neq 0$. The intrinsic wave functions which differ just by the “right” or “left” orientation of the pear-shape configuration should be combined in the states with definite parity Π ,

$$|JMK; \Pi\rangle = \sqrt{\frac{2J+1}{8\pi}} [D'_{MK} \chi_K + \Pi(-)^{J+K} D'_{M-K} \chi_{-K}]. \quad (24.86)$$

Such doublets, in fact, do not even require axial symmetry; the label K may have a more general meaning. The intrinsic partners are time-conjugate and, according to the Kramers theorem, they are degenerate in the adiabatic approximation. In the nonaxial case, one can write the wave function as a sum over K of items similar to those in equation (24.86). In reality, the doublets are split by additional interactions. This can be accomplished by Coriolis forces (the body-fixed frame of the rotating nucleus is non-inertial) or by the tunneling between the two orientations. Such a splitting is not large and the similarity of intrinsic structure should help in increasing the mixing by the weak interactions. However, only the interaction violating both \mathcal{P} - and \mathcal{T} -invariance can mix the doublet partners because

$$\langle JMK; -\Pi | JMK; \Pi \rangle = \frac{1}{2} [\langle \chi_K | W | \chi_K \rangle - \langle \chi_{-K} | W | \chi_{-K} \rangle]. \quad (24.87)$$

The matrix elements of the pseudoscalar W change sign together with K which is possible only if the \mathcal{T} -invariance is violated, along with parity. The “normal” weak interaction is \mathcal{T} -invariant. Therefore, it is capable of mixing the parity doublets only with the help of a mediator, a regular \mathcal{P}, \mathcal{T} -conserving interaction, including the one responsible for the doublet splitting. In contrast to this, the \mathcal{P}, \mathcal{T} -violating interaction can mix the parity doublets directly, which is important for the enhancement of the Schiff moment. The total enhancement factor, by estimates [28], can reach few thousand in the cases with small Δ_{\pm} . The experimental search for the EDM along the lines explained above is currently under way using ^{225}Ra , Ref. [29]; other idea are also pursued. Similar estimates show that the effect can be large also in the cases without static deformation but with the combination of low-lying collective quadrupole and octupole modes [30].

24.10 On the Way to Electroweak Theory

The four-fermion formulation for weak interactions (Section 24.5) is only the low-energy reduction of a more general theory based on the exchange by heavy W^{\pm} and Z^0 bosons where weak and electromagnetic interactions are naturally unified. Here we can only present a rough scheme of the modern approach not using the full quantum relativistic field theory [9, 31].

We know that in the limit of small fermion masses, the left-polarized and right-polarized Dirac states are almost separated. The fermions we will have to deal with here, neutrino, electron, u - and d -quark, all have masses much smaller than masses of intermediate bosons. Therefore, it is convenient to make a transformation to a form (*spinor representation*, Eq. (24.44)) of the Dirac equation where the polarization properties appear as natural. As follows from Eq. (24.48), the mass term $m\bar{\psi}\psi$ can be interpreted as corresponding to mixing of left and right polarizations. Under \mathcal{P} -transformation, the spinors ψ_R and ψ_L are transformed among themselves. For $m = 0$, the particle is forever left or right (there is no rest frame where it would be possible to change the helicity). In weak interactions, only left-polarized neutrino and right-polarized antineutrino appear, even if they have nonzero masses. This is the property of the weak interaction rather than of the masslessness. The neutrino and antineutrino can be even the same particle (Majorana fermion). The structure of the interaction makes also the choice of the electron helicity taking ψ_{eL} although right-polarized electrons certainly do exist as well.

Problem 24.10 Assuming that the vector current of a Dirac particle is given by [QP, II, Eq. (12.31)],

$$j^\mu = \bar{\psi} \gamma^\mu \psi, \quad (24.88)$$

express it in terms of left and right spinors.

Solution

It is convenient first to show that projectors (24.47) satisfy the relation $\Lambda^{(\pm)} \gamma^\mu = \gamma^\mu \Lambda^{(\mp)}$. This gives

$$j^\mu = \bar{\psi}_L \gamma^\mu \psi_L + \bar{\psi}_R \gamma^\mu \psi_R \equiv j_L^\mu + j_R^\mu. \quad (24.89)$$

Therefore, the interactions through the current, contrary to the mass term, preserve the helicity. Left and right currents (24.89) can be written in terms of the full bispinor ψ as

$$j_L^\mu = \bar{\psi} \gamma^\mu \frac{1 - \gamma^5}{2} \psi, \quad j_R^\mu = \bar{\psi} \gamma^\mu \frac{1 + \gamma^5}{2} \psi. \quad (24.90)$$

The left current automatically has a structure $V - A$ of the weak interaction.

The next idea needed for the advancement on our road is the *gauge invariance*. Already in nonrelativistic quantum theory, we have a *global phase invariance*, $\psi \rightarrow e^{-ia}\psi$. Such a trivial transformation with a constant phase a does not change the physical properties of the system. However, a similar *local* transformation with the phase function $a(\mathbf{x}, t)$ is not innocent as the quantum dynamics contain the operators $\partial/\partial t$ and ∇ acting on the phase as well. The new effects can be compensated for the wave function of a charged particle in the presence of the *gauge vector field* $A^\mu = (\phi, \mathbf{A})$ that is added to the four-momentum operator [QP, I, 13.2]. The electromagnetic field A^μ serves as the gauge field restoring the local invariance by the gauge transformation,

$$\psi(\mathbf{x}, t) \rightarrow \psi'(\mathbf{x}, t) = e^{-ia(\mathbf{x}, t)} \psi(\mathbf{x}, t), \quad (24.91)$$

$$\mathbf{A} \rightarrow \mathbf{A}' = \mathbf{A} + \frac{1}{e} \nabla a, \quad \phi \rightarrow \phi' = \phi - \frac{1}{e} \frac{\partial a}{\partial t}, \quad (24.92)$$

where e is the absolute value of the electric charge. In the modern logic, the existence of the four-vector electromagnetic field is justified by the restoration of the local gauge invariance; the gauge transformation $A^\mu \rightarrow A'^\mu = A^\mu - (1/e)\partial^\mu a$ is universal for all particles (the charge e is specific for a given type of particles).

In more general cases, the particle can have intrinsic degrees of freedom. A general gauge field A^μ also can contain matrices acting on these variables. The generalization of the gauge transformation will include the *covariant derivative*,

$$D^\mu = \partial^\mu - igA^\mu, \quad (24.93)$$

where g is the new “charge” of a particle under consideration.

Problem 24.11 Find the transformation of the gauge field A^μ necessary for the gauge invariance under the transformation of an arbitrary wave function ψ :

$$\psi \rightarrow \psi' = U\psi, \quad D'^\mu \psi' = U(D^\mu \psi). \quad (24.94)$$

Solution

Here U can act also on the intrinsic variables. The gauge field transforms as

$$A'^\mu = UA^\mu U^{-1} - \frac{i}{g} (\partial^\mu U) U^{-1}. \quad (24.95)$$

Generally, the gauge field A^μ can have several intrinsic components A_a^μ , where the index a refers to some transformation group, analog of the isospin $SU(2)$ group (Chapter 2). Then the gauge transformation will act on these degrees freedom as well through the noncommuting generators of this *non-Abelian* group. In the standard model, three independent groups are involved, so that the covariant derivative can be

written as a sum of corresponding transformations with three coupling constants $g_{1,2,3}$ and three Lorentz-vector gauge fields,

$$D^\mu = \partial^\mu - ig_1 \frac{Y}{2} B^\mu - ig_2 \frac{\tau_a}{2} W_a^\mu - ig_3 \frac{\lambda_b}{2} G_b^\mu. \quad (24.96)$$

The constants $g_{1,2,3}$ are to be determined from the experiment. The first transformation group here is Abelian $\mathcal{U}(1)$ with the constant hypercharge generator Y ; later it will give rise to the electromagnetic field. The Pauli matrices $\tau_a, a = 1, 2, 3$, generate the $S\mathcal{U}(2)$ group of *electroweak isospin*. The corresponding three vector bosons W_a^μ can be regrouped into states with a certain charge,

$$W_\pm^\mu = \mp \frac{1}{\sqrt{2}} (W_1^\mu \pm W_2^\mu), \quad W_0^\mu = W_3^\mu. \quad (24.97)$$

This group will generate the intermediate W - and Z -bosons. Finally, the third group, $S\mathcal{U}(3)$, generates bosons responsible for strong interactions, *gluons*, with $b = 1, \dots, 8$ which change the quantum number of *color* in quark interactions of quantum chromodynamics (QCD). The corresponding λ_b matrices are $S\mathcal{U}(3)$ analogs of spin or isospin matrices of the $S\mathcal{U}(2)$ group, but here we do not study their detailed properties.

The weak interaction involves only the left-polarized leptons, electron and neutrino. The right particles do not participate in these interactions. To formalize this, we introduce the aforementioned electroweak isospin combining the left particles in the $S\mathcal{U}(2)$ doublet

$$l = \begin{pmatrix} v_e \\ e_L \end{pmatrix}. \quad (24.98)$$

The right electrons go to the weak isospin scalar e_R . The bosons (24.97) are accompanied by the matrices τ_a which can convert electrons into neutrino and back, generating the weak currents. An analogous construction is valid for higher lepton families (muon and tau-lepton with their neutrinos) and for quarks. Different classification of left and right fermions is responsible for the parity violation.

The Lagrangian of free fermions can be written as

$$L = -\bar{\psi} (i\gamma_\mu \partial^\mu - m) \psi; \quad (24.99)$$

Indeed, the variation over $\bar{\psi}$ leads to the free Dirac equation. The interactions should be introduced in the gauge-invariant way (24.96). The $\mathcal{U}(1)$ terms for leptons (e_L, e_R , and v) contain

$$L[\mathcal{U}(1)] = \frac{g_1}{2} \{ Y_L (\bar{e}_L \gamma_\mu e_L + \bar{v}_e \gamma_\mu v_e) + Y_R (\bar{e}_R \gamma_\mu e_R) \} B^\mu. \quad (24.100)$$

Here two hypercharges are introduced, Y_L for the left doublet and Y_R for the right singlet. The same doublet (left) leptons interact with W -bosons through the $S\mathcal{U}(2)$ part of Eq. (24.96),

$$L[S\mathcal{U}(2)] = \frac{g_2}{2} \{ \sqrt{2} (\bar{v}_e \gamma_\mu e_L W_+^\mu + \bar{e}_L \gamma_\mu v_e W_-^\mu) + (\bar{v}_e \gamma_\mu v_e - \bar{e}_L \gamma_\mu e_L) W_0^\mu \}. \quad (24.101)$$

The diagonal terms like $\bar{v}_e \gamma_\mu v_e$ reveal, in the sum of these equations, the interaction with the *neutral current*, which we will normalize in a convenient way,

$$Z^\mu = \frac{g_1 Y_L B^\mu + g_2 W_0^\mu}{\sqrt{(g_1 Y_L)^2 + g_2^2}}. \quad (24.102)$$

The electromagnetic current should have the same expression for left and right electrons. The corresponding terms are

$$\frac{1}{2} \{(g_1 Y_L B^\mu - g_2 W_0^\mu)(\bar{e}_L \gamma_\mu e_L) + g_1 Y_R (\bar{e}_R \gamma_\mu e_R) B^\mu\}. \quad (24.103)$$

We define the electromagnetic field as “orthogonal” to the neutral boson (24.102),

$$A^\mu = \frac{g_2 B^\mu - g_1 Y_L W_0^\mu}{\sqrt{(g_1 Y_L)^2 + g_2^2}}. \quad (24.104)$$

It is more convenient to express the primary neutral fields in terms of the physical fields A^μ and Z^μ :

$$B^\mu = \frac{g_1 Y_L Z^\mu + g_2 A^\mu}{\sqrt{(g_1 Y_L)^2 + g_2^2}}, \quad W_0^\mu = \frac{g_2 Z^\mu - g_1 Y_L A^\mu}{\sqrt{(g_1 Y_L)^2 + g_2^2}}. \quad (24.105)$$

Then the electromagnetic component of the electron terms (24.103) is

$$A_\mu = \frac{g_1 g_2}{\sqrt{(g_1 Y_L)^2 + g_2^2}} \left\{ Y_L (\bar{e}_L \gamma_\mu e_L) + \frac{Y_R}{2} (\bar{e}_R \gamma_\mu e_R) \right\}. \quad (24.106)$$

With $Y_R = 2Y_L$, we can identify the physical electric charge with

$$-e = \frac{g_1 g_2 Y_L}{\sqrt{(g_1 Y_L)^2 + g_2^2}}; \quad (24.107)$$

and later we can simply put $Y_L = -1$. Finally, the neutral current component of Eq. (24.103) is given by

$$Z_\mu = \frac{1}{\sqrt{g_1^2 + g_2^2}} \left\{ \frac{g_1^2 - g_2^2}{2} (\bar{e}_L \gamma_\mu e_L) + g_1^2 (\bar{e}_R \gamma_\mu e_R) \right\}. \quad (24.108)$$

Usually, the Weinberg angle θ_W is introduced according to

$$\sin \theta_W = \frac{g_1}{\sqrt{g_1^2 + g_2^2}}, \quad \cos \theta_W = \frac{g_2}{\sqrt{g_1^2 + g_2^2}}. \quad (24.109)$$

This quantity is not determined theoretically – it has to be extracted from the experiment; its currently accepted value is $\sin^2 \theta_W = 0.222$ but it evolves as a function of the momentum transfer in a given experiment.

Problem 24.12 The neutrino interacts (without transformation to electron) only with the neutral current; the corresponding term in the Lagrangian can be written as $f_\nu Z^\mu (\bar{\nu} \gamma_\mu \nu)$. Determine the constant f_ν (the electroweak neutrino charge).

Solution

$$f_\nu = \frac{g_2}{2 \cos \theta_W} = \frac{1}{2} \sqrt{g_1^2 + g_2^2} = \frac{e}{2 \sin \theta_W \cos \theta_W}. \quad (24.110)$$

For all fermions, the weak charge can be written in a general form as

$$f = \frac{e}{\sin \theta_W \cos \theta_W} (t_3^{\text{weak}} - q \sin^2 \theta_W). \quad (24.111)$$

Here q is the electric charge of the fermion (-1 for the electron and 0 for the neutrino), and t_3^{weak} is the weak isospin projection ($1/2$ for the neutrino, $-1/2$ for the left electron, and 0 for the right electron).

Collecting neutron and proton from quarks (ddu and uud , correspondingly, with electric charges $q_u = 2/3$ and $q_d = -1/3$), one can see that the nucleon weak charge ratio is

$$\frac{f_n}{f_p} = - \frac{1}{1 - 4 \sin^2 \theta_W}. \quad (24.112)$$

The weak charge of the proton almost vanishes because the Weinberg angle is very close to 30° as measured by the parity-violating scattering of polarized electrons from a proton target [32]. This is the source of the modern idea that the electron parity-violating scattering off exotic nuclei with a large excess of neutrons will be able to measure the size of the neutron skin.

24.11 Higgs Mechanism

The main problem of the electroweak theory as we have discussed up to now is that of masses of particles. The whole hierarchy of symmetry groups and gauge invariance is based on the absence of the mass terms which, as we have seen in Eq. (24.48), lead to the mixing of right and left components. In electrodynamics, it is well known that gauge invariance is related to the massless character of the photon. The masses of massive particles can be introduced by the so-called *Higgs mechanism* [33] which we just outline below. This idea shows how it is possible to keep one gauge field massless (photon) while three other fields acquire their masses (W_\pm and Z bosons).

The simplest version of this theory assumes the existence of a complex boson field $\mathcal{H}_\alpha(x)$, $\alpha = 1, 2, Y = 1$. The covariant derivative (24.96) acts on this doublet as

$$D^\mu \mathcal{H}_\alpha(x) = \partial^\mu \mathcal{H}_\alpha(x) - i \frac{g_1}{2} B^\mu(x) \mathcal{H}_\alpha(x) - i \frac{g_2}{2} (\tau_\alpha)_{\alpha\beta} W_a^\mu(x) \mathcal{H}_\beta(x), \quad (24.113)$$

where we do not show the action of the $SU(3)$ operators. Then it is assumed that the Higgs field \mathcal{H} has a nonlinear *self-action* term so that the Lagrangian part of this field can be written, with the simplest choice, a difference of kinetic and potential terms,

$$L_{\mathcal{H}} = K(\mathcal{H}) - U(\mathcal{H}) = (D_\mu \mathcal{H}^\dagger)(D^\mu \mathcal{H}) - \frac{\lambda}{2} \left(\mathcal{H}^\dagger \mathcal{H} - \frac{v^2}{2} \right)^2. \quad (24.114)$$

The chosen potential U here has a minimum at $\lambda > 0$ with a nonzero value

$$\mathcal{H}^\dagger \mathcal{H} = \frac{v^2}{2}. \quad (24.115)$$

In fact, this defines a degenerate manifold of possibilities for the field \mathcal{H} which are interconnected by the group operators. We can fix the gauge for the Higgs field by introducing a new, real, scalar field $h(x)$ and setting

$$\mathcal{H}(x) = \frac{1}{\sqrt{2}} \begin{pmatrix} 0 \\ v + h(x) \end{pmatrix}. \quad (24.116)$$

Problem 24.13 The choice (24.116) violates gauge symmetry but still keeps an invariance with respect to the subgroup of the full $U(1) \times SU(2)$ group that corresponds to the charge operator $Y + \tau_3$. Check that this solution is invariant under the action of the product $e^{(i/2)\alpha(x)} e^{(i/2)\alpha(x)\tau_3}$.

With the choice (24.116), the potential of the Higgs field becomes

$$U(h) = \frac{1}{2} \lambda v^2 h^2 + \frac{1}{2} \lambda v h^3 + \frac{1}{8} \lambda h^4. \quad (24.117)$$

The first term here determines the mass of the Higgs field,

$$m_h = \lambda v^2. \quad (24.118)$$

This quantity was measured by the Large Hadron Collider in 2012 to be equal to 125.1 GeV. The vacuum value v of the Higgs field determines nonzero masses of vector bosons W_{\pm} and Z .

Problem 24.14 Calculate the kinetic term $K(\mathcal{H})$.

Solution

$$K(\mathcal{H}) = \frac{1}{2} (\partial^\mu h)^2 + \frac{(v + h)^2}{8} (g_1 B^\mu - g_2 W_0^\mu)^2 + \frac{g_2^2 (v + h)^2}{8} ((W_1^\mu)^2 + (W_2^\mu)^2). \quad (24.119)$$

Here the first term is the kinetic energy of the Higgs boson and we also come to the *massive* vector mesons. Their squared masses of W_{\pm} are given by the terms proportional to the vacuum Higgs condensate (the coefficients for $v^2/2$),

$$M(W_{\pm}) = \frac{1}{2} g_2 v. \quad (24.120)$$

The second term in Eq. (24.119) has a massive combination of original vector particles B^μ and W_3^μ which we attribute to the Z -boson; in the normalized form (24.102),

$$Z^\mu(x) = \cos \theta_W W_0^\mu(x) - \sin \theta_W B^\mu(x), \quad (24.121)$$

where, as in Eq. (24.109),

$$\tan \theta_W = \frac{g_1}{g_2}. \quad (24.122)$$

The corresponding mass is

$$M_Z = \frac{1}{2} v \sqrt{g_1^2 + g_2^2}. \quad (24.123)$$

The orthogonal to the Z^μ combination,

$$A^\mu(x) = \sin \theta_W W_0^\mu(x) + \cos \theta_W B^\mu(x), \quad (24.124)$$

does not have a mass term and defines the massless electromagnetic field. Finally, the Weinberg angle determines the ratio of boson masses,

$$\cos \theta_W = \frac{M_W}{M_Z}, \quad (24.125)$$

The masses are measured experimentally, for example, the neutral Z -boson appears as a strong resonance in the electron–positron collider experiments, and then the Weinberg angle is extracted. The main conclusion is that the nuclear weak interaction is not weak by itself – just its mediators have very large masses. It is seen that the squared masses M_Z^2 and $M_\gamma^2 = 0$ are the eigenvalues of the mixing 2×2 matrix

$$M^2 = \frac{v^2}{4} \begin{pmatrix} g_2^2 & -g_2 g_1 \\ -g_2 g_1 & g_1^2 \end{pmatrix}. \quad (24.126)$$

The same matrix structure appeared in the example (23.55) of the two-resonance problem when one of the eigenstates had zero width (here zero mass).

Looking for the coupling of the vector mesons to the electromagnetic current, we again come to the definition of the electric charge (24.107) that does not carry explicitly the Higgs characteristics. The Fermi effective constant of the four-fermion weak interaction (charged currents) appears as a result of the exchange by the W mesons modeled by the contact process; see Figure 24.2. The direct evaluation of the exchange diagram under assumption that M_W is very large allows to establish that

$$\frac{G_F}{\sqrt{2}} = \frac{e^2}{8M_W^2 \sin^2 \theta_W}. \quad (24.127)$$

This is actually the measure of the Higgs condensate because

$$\frac{G_F}{\sqrt{2}} = \frac{1}{2v^2}. \quad (24.128)$$

It is easy to see that the effective constant for the weak neutral currents has exactly the same value, in agreement with experiments. This gives the numerical value for the condensate parameter, $v = 246$ GeV. The same mechanism is responsible for the masses of fermions (electrons and quarks) – here the color $SU(3)$ part of the theory enters the game. But the problem of the actual mass spectrum is still unsolved, requiring a more deep theory beyond the current standard model.

24.12 Neutrino: Oscillations

Toward the end of this long chapter, we briefly discuss problems related to neutrino physics [34, 35]. Until now, the neutrino appeared in the text as a very light neutral particle that was needed to fill the gap in the description of weak interactions. Its own role was reduced to the energy, spin, and statistics conservation; its polarization was a signal of the left-handed nature of weak processes. Currently, it is well known that neutrinos play a very important role in nuclear astrophysics appearing in weak processes in the stellar

cores, creating the “neutrino wind” in supernovae, and bringing to the Earth (including the special detector under the ice of Antarctica) signals of amazing cosmic events. But the physical properties of the neutrinos are still not clearly defined by experiments. We will touch on two problems – neutrino oscillations and the possible Majorana nature of the neutrino.

Earlier, we could take the neutrino mass to be zero; now we come to the physics based on its nonzero mass. Neutrino oscillations are the consequence of the fact that the neutrinos produced in a weak process with a certain *flavor* – electron, muon, or tau – are not stationary particle states with certain mass m . Instead, the stationary particle states are their linear combinations. In the free propagation from the source to the detector, or in a secondary reaction, there is a normal quantum interference of the stationary components contained in the initial state. The clearest consequence of this situation is the deficit of solar neutrino coming after various weak processes in the Sun: the terrestrial detector registers only the neutrinos in their “electronic” phase, which leads to approximately 1/3 of the expected solar neutrino flux.

For simplicity, consider the mixing of only two types of neutrino. The electronic neutrino born in a weak process at $t = 0$ is a linear combination

$$|\nu; t = 0\rangle = \cos \vartheta |\nu_1\rangle + \sin \vartheta |\nu_2\rangle. \quad (24.129)$$

The components $|\nu_1\rangle$ and $|\nu_2\rangle$ have certain masses m_1 and m_2 , and during the vacuum propagation with a certain momentum \mathbf{p} , their wave functions acquire phases

$$\varphi_{1,2} = (\mathbf{p} \cdot \mathbf{r}) - E_{1,2}(p)t, \quad (24.130)$$

where we use the units $\hbar = c = 1$. Certainly, the neutrino masses are very small, <1 eV, and the energy can be presented as

$$E_{1,2}(p) = \sqrt{p^2 + m_{1,2}^2} \approx p + \frac{m_{1,2}^2}{2p}. \quad (24.131)$$

With the squared mass difference $\Delta^2 = m_2^2 - m_1^2$ and the mean value $m^2 = (m_1^2 + m_2^2)/2$, the evolution of the initial state acquires the form

$$|\nu; t > 0\rangle = e^{i[(\mathbf{p} \cdot \mathbf{r}) - m^2 t / (2p)]} (e^{i\Delta^2 t / (4p)} \cos \vartheta |\nu_1\rangle + e^{-i\Delta^2 t / (4p)} \sin \vartheta |\nu_2\rangle). \quad (24.132)$$

Problem 24.15 Assume that the initial state is the electron neutrino. Determine the probability to find the electron neutrino at time $t > 0$ and define the oscillation length L for the period of oscillation of this probability.

Solution

The probability of the neutrino to be in the electronic mode equals

$$P(\nu_e) = 1 - \sin^2(2\vartheta) \sin^2\left(\frac{\Delta^2}{4E}t\right), \quad (24.133)$$

or, introducing all units and mean energy $E = cp$, the oscillation length is found as

$$L = 4\pi \frac{\hbar c E}{\Delta^2 c^4}. \quad (24.134)$$

The oscillations become more complicated if three types of neutrino are involved; then there are three mixing angles and additional phases which are not all determined by current experiments. The processes with solar neutrinos are influenced by the fact that neutrinos born inside the Sun should traverse a lot of dense matter. Another physics comes into the picture, namely, the so-called Mikheev–Smirnov–Wolfenstein (MSW) mechanism [36, 37] that can significantly enhance flavor oscillations.

The density of the solar medium is responsible for changing the effective mass of neutrino flavors. The electron neutrinos interact with electrons in a dense medium, being scattered through both charged and neutral weak currents, while other flavors interact only through neutral currents. The effect is sensitive to the density of the medium. It is easy to understand that, instead of the simple mixing (24.129), the density effect converts the matrix equation of two-flavor mixing into

$$i \frac{d}{dt} \begin{pmatrix} a_1 \\ a_2 \end{pmatrix} = \begin{pmatrix} m_1^2/(2p) + \kappa \cos^2 \vartheta & \kappa \cos \vartheta \sin \vartheta \\ \kappa \cos \vartheta \sin \vartheta & m_2^2/(2p) + \kappa \sin^2 \vartheta \end{pmatrix} \begin{pmatrix} a_1 \\ a_2 \end{pmatrix}, \quad (24.135)$$

where the approximation (24.131) is used and the medium interaction constant κ is proportional to the local density $\rho(t)$ and weak Fermi constant G_F (in fact, $\kappa = \sqrt{2}G_F\rho$).

Problem 24.16 Find the effective mixing angle $\tilde{\vartheta}$ defined as in Eq. (24.132) in the approximation of constant density ρ .

Solution

$$\tan(2\tilde{\vartheta}(\rho)) = \frac{\sin(2\vartheta)}{\cos(2\vartheta) + 2\kappa p/(m_1^2 - m_2^2)} \quad (24.136)$$

For $\kappa \rightarrow 0$, we return to the previous result, $\tilde{\vartheta} \rightarrow \vartheta$.

The solution (24.136) is valid in the adiabatic approximation of slowly changing density (recall Sections 21.5 and 21.6). Starting in the state $|1\rangle$, and propagating slowly through the dense regions to the solar exterior, the neutrino remaining on the lower energy term will change its nature more efficiently than in vacuum. The current set of experimental data including reactor neutrinos, solar neutrinos, and atmospheric neutrinos [38] is sufficient only for establishing the differences of the squared neutrino masses (Figure 24.6). The absolute scale of the masses is still not determined, and the confident choice between the two hierarchies of these masses is still impossible. The best candidate for the direct (but very hard) measurement in the terrestrial laboratory is the tritium beta-decay (Figure 24.1), with the half-life of 4500 days and small energy release of 18.6 keV. The laboratory results just indicate that the upper boundary for the neutrino mass is smaller than 2 eV.

24.13 Neutrino: Majorana or Dirac?

The presence of oscillations tells us that the neutrinos have nonzero, even if minuscule on the standard particle scale, mass. The massless Dirac neutrinos have certain helicity – recall the Weil equation (24.49). The existence, in this massless limit, of the left-handed neutrino and right-handed antineutrino, violates C and P symmetry but

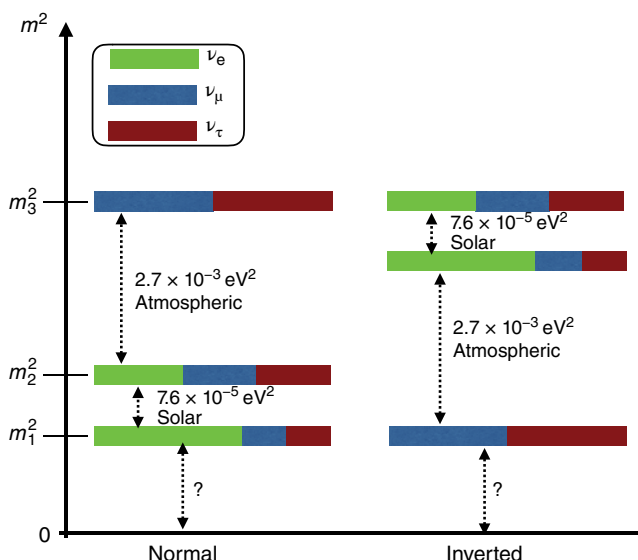


Figure 24.6 Two possible hierarchies of neutrino masses.

keeps the combined \mathcal{CP} invariance. The helicity conservation is a general property of massless particles, including photons and gravitons, from relativistic arguments as follows: the maximum spin projection on the direction of motion, $\pm 1/2$ for massless neutrinos, ± 1 for photons, ± 2 for gravitons is the only possible one as the angles 0 and π are relativistically invariant.

This argument does not work if the neutrino is massive, and there exists a rest frame for the neutrino. In this sense, the certain neutrino helicity is the property of the interaction, namely, of the weak force that is driven by left currents. However, we then lose the qualitative difference between the neutrino and antineutrino, each of them could, in principle, have any helicity if the nature of the weak interaction is different. This opens the possibility for the neutrino and antineutrino to be *the same* particle, $\nu = \bar{\nu}$. The formal distinction between such Majorana particles and usual Dirac fermions is that the combined inversion has opposite signs for the Dirac particles and antiparticles, $\mathcal{CP} = -\mathcal{P}\mathcal{C}$, while $\mathcal{CP} = \mathcal{P}\mathcal{C}$ for Majorana particles [QP, II, Ch. 14].

Currently, we do not have the answer to the question on the nature of the neutrino. The only realistic experimental possibility to solve this problem is to observe the *neutrinoless double beta-decay* of a nucleus. There are many cases when an even–even nucleus cannot undergo normal beta-decay because the neighboring odd–odd nuclei have ground states with higher energy (mainly because of an unpaired couple of nucleons). A typical example is given by $^{76}_{32}\text{Ge}_{44}$ that has too many neutrons and would like to go through β^- decay. However, the ground state of the appropriate daughter nucleus $^{76}_{33}\text{As}_{43}$ is higher in energy and undergoes its own β^- decay (lifetime 26 h) to the next even–even nucleus $^{76}_{34}\text{Se}_{42}$ which is stable with the ground-state energy even lower than that of ^{76}Ge . This makes the *double beta-decay* from ^{76}Ge directly to ^{76}Se energetically allowed (Figure 24.7). In fact, this double beta-decay branches also to two low-lying excited collective states 2^+_1 and 0^+_2 in ^{76}Se .

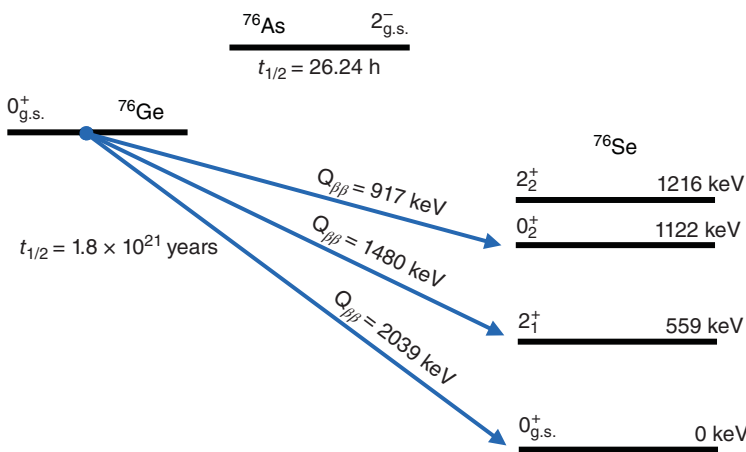


Figure 24.7 A part of the nuclear chart around ^{76}Se ; known beta-transitions in ^{76}Ge are shown.

There are about 35 cases in the nuclear chart with the double beta-decay energetically allowed, and more than 10 examples are currently measured experimentally. This is a process of the second order in weak interaction and therefore the corresponding lifetime is quite long. For example, the half-life for the ^{76}Ge decay is 1.8×10^{21} years; the fastest case is the double beta-decay of ^{100}Mo with the half-life 7×10^{18} years. The standard scheme of such a process is

$$(Z, A) \Rightarrow (Z + 2, A) + 2e^- + 2\bar{\nu}_e. \quad (24.137)$$

The second order of perturbation theory with respect to weak interaction can be applied here directly. Although the possibility of such a process was understood long ago (M. Goeppert-Mayer, 1935), the first direct experimental observation came much later, for ^{82}Se [39] with the half-life of 10^{20} years. As commented in the historical review [40], “*This result was very important, particularly from the psychological point of view.*”

If the neutrino belongs to the Majorana type, it is easy to imagine that the massive antineutrino born in the first act of the double decay along with the electron can appear in the role of the neutrino and activate the second act of the weak process where it is converted into the second electron. As a result, we would observe the *neutrinoless double beta-decay* (Figure 24.8), where we can see only the final nucleus and two electrons. The total energy of two electrons is fixed in this case by the conservation law and should be revealed as a separate furthermost peak in the energy spectrum, while the decay (24.137) gives a smooth distribution of the electron energy. This is possible only if the neutrino and antineutrino are identical Majorana particles. Moreover, it was shown [41] that, even if the internal process of the double beta-decay does not contain the neutrino being driven by a different mechanism, the existence of this process indicates the Majorana nature of the neutrino.

The probability of the neutrinoless double beta-decay, usually designated as $\beta\beta(0\nu)$, can be also predicted by the second-order perturbation theory [34, 42]. The virtual particle produced in the first act of the β^- decay is the right-polarized electron antineutrino, $\bar{\nu}_{eR}$, helicity $h = +1$, with a small admixture proportional to the ratio of mass to energy,

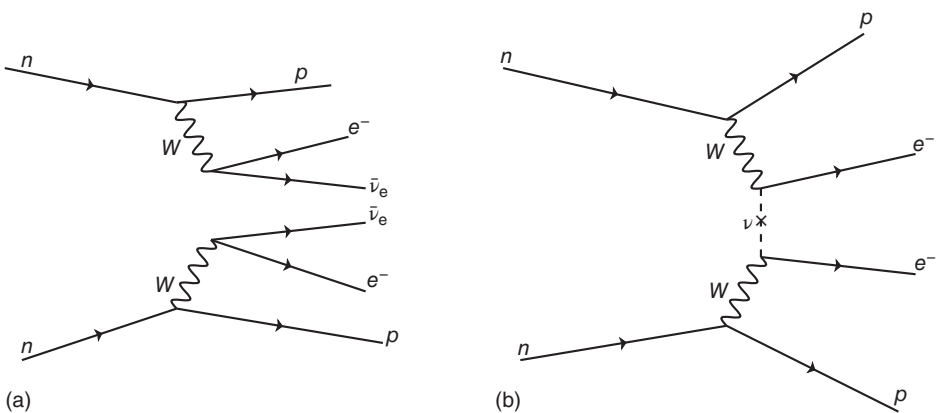


Figure 24.8 Schematic view of the two types of double beta-decay, a normal one, Eq. (24.137), and neutrinoless one.

of the left antineutrino. In terms of the mixing matrix U_{ei} (the two-dimensional version of this matrix was used in Eq. (24.129)),

$$\bar{\nu}_{eR} = \Lambda^{(+)} \sum_{i=1}^3 U_{ei} \bar{\nu}_i. \quad (24.138)$$

Then the helicity-forbidden small component $\propto (1 - v/c) \sim m/E$ can induce the second act of weak interaction. The quantity that can be extracted from the experiment would be the effective Majorana mass

$$m_{\beta\beta} = \left| \sum_{i=1}^3 U_{ei}^2 m_i \right|. \quad (24.139)$$

Certainly this decay would show the violation of the lepton charge by two units.

The resulting probability suppression proportional to $(m/E)^2$ depends on energy but is, anyway, very strong, approximately 10^{-14} for the neutrino mass of about 0.1 eV and energy of about 1 MeV. In fact, the virtual neutrino energy can be up to 100 MeV. This is related to the main practical problem of calculation of the $\beta\beta(0\nu)$ probability as it is necessary to sum over all possible virtual nuclear states contributing to the second-order perturbation theory. A review of the current status can be found in Ref. [43]; the detailed nuclear calculations are shown in Ref. [44]. Reliable observation of the $\beta\beta(0\nu)$ will not only solve the Dirac–Majorana dichotomy of the nature of the neutrino but also add to the understanding of the source of this mass outside of the standard model and to some cosmological problems [43].

References

- 1 C. Cowan and F. Reines, Phys. Rev. **107**, 528 (1957).
- 2 (a) Yu.A. Litvinov *et al.*, Phys. Lett. B **664**, 162 (2008); (b) P. Kienle *et al.*, Phys. Lett. B **726**, 638 (2013).
- 3 N.B. Gove and M.J. Martin, At. Data Nucl. Data Tables **10**, 205 (1971).

- 4 G.K. Schenter and P. Vogel, Nucl. Sci. Eng. **83**, 393 (1983).
- 5 C.B. Hinke *et al.*, Nature **486**, 341 (2012).
- 6 C.S. Wu and S.A. Moszkowski, *Beta Decay*, Interscience, New York, 1965.
- 7 J.C. Hardy and I.S. Towner, Phys. Rev. C **91**, 025501 (2015).
- 8 I.S. Towner and J.C. Hardy, Phys. Rev. C **82**, 065501 (2010).
- 9 F. Halzen and A.D. Martin, *Quarks and Leptons*, John Wiley & Sons, Inc., New York, 1984.
- 10 V. Tishchenko *et al.* (MuLan Collaboration) Phys. Rev. D **87**, 052003 (2013).
- 11 E.P. Wigner, Phys. Rev. **56**, 519 (1939).
- 12 N. Auerbach and V. Zelevinsky, Phys. Rev. C **90**, 034315 (2014).
- 13 J.C. Hardy, in *Nuclear Spectroscopy and Reactions, Part C*, ed. J. Cerny, Academic Press, New York, 1974, p. 417.
- 14 T.D. Lee and C.N. Yang, Phys. Rev. **104**, 254 (1956).
- 15 C.S. Wu, E. Ambler, R.W. Hayward, D.D. Hoppes, and R.F. Hudson, Phys. Rev. **105**, 1413 (1957).
- 16 H. Frauenfelder, R. Bobone, E. von Goeler, N. Levine, H.R. Lewis, R.N. Peacock, A. Rossi, and G. de Pasquali, Phys. Rev. **106**, 386 (1957).
- 17 R. Garwin, L. Lederman, and M. Weinrich, Phys. Rev. **105**, 1415 (1957).
- 18 K.A. Olive *et al.* (Particle Data Group), Chin. Phys. C **38**, 090001 (2014) and 2015 update; <http://pdg.lbl.gov>.
- 19 L.D. Landau, Nucl. Phys. **3**, 127 (1957).
- 20 M.S. Sozzi, *Discrete Symmetries and CP violation*, Oxford University Press, New York, 2008.
- 21 J.M. Christensen, J.W. Cronin, V.L. Fitch, and R. Turlay, Phys. Rev. Lett. **13**, 138 (1964).
- 22 L. Wolfenstein, *CP Violation*, North Holland, Amsterdam, 1989.
- 23 M. Beyer (ed.) *CP Violation in Particle, Nuclear and Astrophysics*, Springer-Verlag, Berlin, 2002.
- 24 A.D. Sakharov, JETP Lett. **5**, 24 (1967).
- 25 E.M. Purcell and N.F. Ramsey, Phys. Rev. **78**, 807 (1950).
- 26 L.I. Schiff, Phys. Rev. **132**, 2194 (1963).
- 27 R.A. Sen'kov, N. Auerbach, V.V. Flambaum, and V.G. Zelevinsky, Phys. Rev. A **77**, 014101 (2008).
- 28 V. Spevak, N. Auerbach, and V.V. Flambaum, Phys. Rev. C **56**, 1357 (1997).
- 29 Y.L. Singh and B.K. Sahoo, Phys. Rev. A **92**, 022502 (2015).
- 30 V. Zelevinsky, A. Volya, and N. Auerbach, Phys. Rev. C **78**, 014310 (2008).
- 31 G. Kane, *Modern Elementary Particle Physics*, Addison-Wesley, New York, 1987.
- 32 Qweak collaboration, Phys. Rev. Lett. **111**, 141803 (2013).
- 33 G.D. Coughlan, J.E. Dodd, and B.M. Gripaios, *The Ideas of Particle Physics: An Introduction for Scientists*, 3rd edn, Cambridge University Press, Cambridge, 2006.
- 34 F. Boehm and P. Vogel, *Physics of Massive Neutrinos*, Cambridge University Press, Cambridge, 1987.
- 35 Y. Fukugita and T. Yanagida, *Physics of Neutrinos and Application to Astrophysics*, Springer-Verlag, Berlin, 2003.
- 36 S.P. Mikheev and A.Yu. Smirnov, Sov. J. Nucl. Phys. **42**, 913 (1985); Nuovo Cimento **9**, 17 (1986).
- 37 L. Wolfenstein, Phys. Rev. D **17**, 2369 (1978).

- 38** W. Haxton, arXiv:1209.3743.
- 39** S.R. Elliott, A.A. Hahn, and M.K. Moe, Phys. Rev. Lett. **59**, 2020 (1987).
- 40** A.S. Barabash, arXiv: 1104.2714.
- 41** J. Schechter and J.W.F. Valle, Phys. Rev. D **25**, 2951 (1982).
- 42** M. Doi, T. Kotani, and E. Takasugi, Prog. Theor. Phys. Suppl. **83**, 1 (1985).
- 43** S.M. Bilenky and C. Giunti, Int. J. Mod. Phys. A **30**, 153000 (2015).
- 44** R.A. Sen'kov, M. Horoi, and B.A. Brown, Phys. Rev. C **89**, 054304 (2014).

25

Nucleus as a Chaotic System

It has become increasingly difficult for experts in a given field to keep up with the current literature; the novice can only be confused. What is needed is both a consistent account of a field and a presentation of a definite “point of view” concerning it.

David Pines, *Editor’s Foreword* to the series *Frontiers in Physics*,
Addison-Wesley, 1997

25.1 Introduction

In this last chapter, we present our “*point of view*” that perhaps is neither orthodox nor yet generally accepted; this presentation reflects our longstanding experience and perception of timeliness on the subject. Usually, the words *deterministic chaos* are applied [1] to *classical* systems where the exact solution of Hamilton equations of motion is incapable of predicting the trajectory of the system in its phase space because of the extreme sensitivity of the solution to initial conditions. After some time, trajectories that start extremely close in phase space diverge exponentially. As initial conditions can be practically defined only with some precision, even inevitable round-off errors become critical, the formally exact solution turns out useless in the long run, and we come to chaotic dynamics. Then only statistical distributions provide a practical tool for the analysis. Incidentally, the majority of physical systems have this property although the characteristic time of chaotization can be quite long, as for example in most problems in celestial mechanics. From this widely prevalent viewpoint, in application to quantum systems one can only speak about quantum signatures of classical chaos [2, 3]. There are simple arguments in favor of such statements. Indeed, for a quantum system, uncertainty relations do not allow at all to specify precisely the initial position in phase space. It is easy to show that, in any finite Hilbert space, the quantum dynamics of the Schrödinger equation is formally regular [QP, II, 24.1] from the viewpoint of classical criteria – it is reduced to a system of linear oscillators.

Another viewpoint stems from the fundamental quantum laws. The classical chaotic systems with their dynamics can appear in the appropriate limit only. For a sufficiently complex quantum system (and this complexity does not require the system to be macroscopic with very many degrees of freedom), the signatures of essentially chaotic dynamics appear either from boundary conditions, or, especially in self-bound systems,

as a consequence of interactions between the constituents. This last situation will be the subject of our interest. In the most frequently encountered nuclear shapes (spherical or ellipsoidal), the single-particle quantum dynamics is regular. The whole complexity with its seemingly chaotic features comes from the interaction.

Historically, the ideas of quantum chaos were attached to the mathematical theory of *random matrices* [4–6]. These are matrices with given statistical distributions of random elements, usually satisfying only the most general symmetry requirements, for example, hermiticity. Indeed, the Hamiltonian matrix of a realistic nuclear or atomic system expressed in an arbitrary basis usually resembles a set of random numbers, at least starting from some excitation level. However, in the appropriate mean-field basis, this matrix reveals certain symmetries and clear repeated structures; see Figure 23.9. This occurs because of the mostly two-body character of interaction when the matrix element of a certain process can be repeated on any background of other particles. Nevertheless, in a not too large spectral interval, statistical characteristics of the energy spectra are indeed close to the universal predictions of the random matrix theory. Still, this is only the first and the weakest criterion of quantum chaos. The deeper features are related to the properties of stationary wave functions which allow us to use quantum chaos as a practical tool. Many impressive mathematical results concerning random matrices and their generalizations for various applications can be found in Ref. [7].

Instead of starting with random matrices we begin by demonstrating the actual complexity of nuclear dynamics which has already been mentioned in our previous considerations. The complexity often comes from the high level density that rapidly grows with excitation energy simply owing to combinatorial reasons (Chapter 20) even in a system of noninteracting particles. At this stage, the wave functions are still relatively simple combinations of several particle–hole excitations. But here even weak interactions become effectively strong by mixing configurations which are close in energy. As a result, the wave functions acquire a complexity which is the real signature of quantum chaos. The discussion of parity violation by weak interactions in fission (Section 21.8) had already demonstrated the new physical aspects of the emerging situation: the mixing of very complicated states close in energy by simple perturbations is effectively enhanced.

25.2 Strength Function

This was the subject of original interest by E. Wigner which lead him to random matrices. First, we define this concept. We consider a finite system of interacting constituents governed by the Hermitian Hamiltonian H , its eigenstates $|\alpha\rangle$ satisfy

$$H|\alpha\rangle = E^\alpha |\alpha\rangle. \quad (25.1)$$

The strength function $F_k(E)$ refers to a certain complete orthogonal basis $|k\rangle$ which we use for the expansion

$$|\alpha\rangle = \sum_k C_k^\alpha |k\rangle, \quad |k\rangle = \sum_\alpha C_k^{\alpha*} |\alpha\rangle. \quad (25.2)$$

Our formal definition is

$$F_k(E) = \sum_\alpha |C_k^\alpha|^2 \delta(E - E^\alpha). \quad (25.3)$$

Here we fix a basis state $|k\rangle$ and look at the spread of the wave function of this state over exact stationary states $|\alpha\rangle$ measuring the fraction of this spread found at energy E . This explains the normalization

$$\int dE F_k(E) = \sum_{\alpha} |C_k^{\alpha}|^2 = \langle k|k \rangle = 1. \quad (25.4)$$

In condensed matter physics, the quantity equivalent to $F_k(E)$ is often called the *local density of states* (LDOS); if the basis $|k\rangle$ is that of localized states on a regular lattice, the proper stationary states $|\alpha\rangle$ are delocalized Bloch waves, and the strength of each localized state is spread over these waves of different energies. If the level density, formally singular,

$$\rho(E) = \sum_{\alpha} \delta(E - E^{\alpha}), \quad (25.5)$$

is, after small averaging, a smooth function of energy, the strength function (25.3) can be understood as

$$F_k(E) = \overline{|C_k^{\alpha}|^2} \rho(E), \quad (25.6)$$

where the average is taken over the energy interval close to E . This gives the meaning for the term LDOS.

Problem 25.1 For a given basis state $|k\rangle$, express the mean value of energy \bar{E}_k and its mean square fluctuation σ_k^2 in terms of the matrix elements of the original Hamiltonian H .

Solution

We find from the definitions,

$$\bar{E}_k \equiv \int dE F_k(E)E = \sum_{\alpha} |C_k^{\alpha}|^2 E^{\alpha} = H_{kk} \quad (25.7)$$

(the *diagonal* element of the original Hamiltonian matrix), and

$$\sigma_k^2 \equiv \int dE F_k(E)(E - \bar{E}_k)^2 = \sum_{l \neq k} H_{kl}^2 \quad (25.8)$$

(the sum of squared *off-diagonal* matrix elements along the row k).

These results show that the primary statistical characteristics of the interrelation between the original basis and the basis of stationary states can be read from the Hamiltonian matrix without diagonalization. The strength function reveals the interrelation between the selected basis and exact eigenstates being strongly dependent on the choice of the basis $|k\rangle$. If we guess the genuine set of stationary states and take them as a basis, we come to a trivial result, $C_k^{\alpha} \rightarrow \delta_{\alpha k}$. In applications to interacting systems of nuclear (or atomic) type, it is reasonable to select an appropriate mean field and take the states of noninteracting particles in this field as our basis $|k\rangle$. The stationary basis $|\alpha\rangle$ then differs by the effects of the interparticle interaction, and the strength function demonstrates the signatures of physical complexity measured relative to the mean-field picture.

To obtain an idea of the dependence of the strength function on the main parameters, we can use a simple procedure of the two-step diagonalization [8]. We single out

an arbitrary state $|k\rangle \equiv |1\rangle$ with the corresponding row and column of the Hamiltonian matrix and assume that, after temporary removal of the state $|1\rangle$, the remaining submatrix is prediagonalized producing the intermediate eigenfunctions $|\nu\rangle$ and their energies ϵ_ν . The diagonal matrix element H_{11} is, according to Eq. (25.7), equals \bar{E}_1 . The selected state interacts with the states $|\nu\rangle$ through matrix elements obtained from the off-diagonal elements of the original representation after prediagonalization,

$$V_{1\nu} = \sum_{k \neq 1} \langle 1|H|k\rangle\langle k|\nu\rangle, \quad (25.9)$$

so that the Hamiltonian matrix in the new basis takes the following form:

$$H = \begin{pmatrix} H_{11} & V_{12} & V_{13} & \dots \\ V_{21} & \epsilon_{\nu=2} & 0 & 0 \\ V_{31} & 0 & \epsilon_{\nu=3} & 0 \\ \vdots & 0 & 0 & \ddots \end{pmatrix}. \quad (25.10)$$

The main assumption is that the elimination of a single state does not change significantly the average properties of a large Hamiltonian matrix. The eigenvalue problem now can be solved analytically.

Problem 25.2 Write down the Schrödinger equation in the new basis and show that exact eigenvalues E^α of the full Hamiltonian are the roots of the following equation:

$$E^\alpha = \bar{E}_1 + \Phi_1(E^\alpha), \quad \Phi_1(E) = \sum_\nu \frac{|V_{1\nu}|^2}{E - \epsilon_\nu}, \quad (25.11)$$

while the squared amplitudes of the stationary states are expressed in terms of energies (25.11) as

$$|C_1^\alpha|^2 = \frac{1}{1 - (d\Phi_1(E^\alpha)/dE^\alpha)}. \quad (25.12)$$

An interesting limit corresponds to a very strong interaction when the shift of the exact eigenvalue E^α from the centroid \bar{E}_1 exceeds the interval $\Delta\epsilon$ of basis states. In this limit,

$$(E^\alpha - \bar{E}_1)^2 \approx \sum_\nu |V_{1\nu}|^2. \quad (25.13)$$

This predicts two peaks combining the whole strength of the original state. Physically, we can understand this as a result of collective interactions: the basis states coherently form the collective state that repels the original state and the whole strength is equally divided between the two. This *doubling phase transition* is known in quantum optics and, in some situations, is theoretically possible with excited nuclear states; see Refs. [9, 10] and references therein.

The “*standard model*” of the strength function [8] is a very useful estimate. The big sum $\Phi(E)$ in the secular equation (25.11), as a function of E , has many poles at the points ϵ_ν found in prediagonalization. Between the poles, this function goes from $-\infty$ to $+\infty$, the behavior similar to that shown in Figure 18.1. We can approximately model this behavior by a function $\cot(\pi E/D)$ if many poles appear with more or less uniform spacings D between them so that the level density can be considered in some interval as a constant,

$\rho(E) \approx 1/D$. Further, we will also approximately substitute the matrix elements by an effective constant, $|V_{1v}|^2 \rightarrow V^2$, covering a noticeable set of intermediate levels. Then the cotangent behavior indeed appears owing to the algebraic relation

$$\cot \varphi = \sum_{n=-\infty}^{\infty} \frac{1}{\varphi - n\pi} \quad (25.14)$$

that is proven by comparing the poles and residues on both sides. Now the squared amplitudes (25.12) can be considered as functions of energy,

$$|C(E)|^2 = \frac{1}{1 + (\pi^2 V^2 / D^2)[1 + \cot^2(\pi E / D)]}. \quad (25.15)$$

With the useful notation for the *spreading width*,

$$\Gamma = 2\pi \frac{V^2}{D}, \quad (25.16)$$

we come to the important answer,

$$|C_1(E)|^2 = \frac{D}{2\pi} \frac{\Gamma}{(E - \bar{E}_1)^2 + \Gamma^2/4}, \quad (25.17)$$

and, with the help of Eq. (25.6),

$$F_1(E) = \frac{1}{2\pi} \frac{\Gamma}{(E - \bar{E}_1)^2 + \Gamma^2/4}. \quad (25.18)$$

The standard model leads to the Breit–Wigner shape of the strength function with the centroid given by the first moment (25.7) and the width (25.16) that brings to mind the *golden rule* of the standard time-dependent perturbation theory [QP, II, 2.1] and of reaction physics with an effective non-Hermitian Hamiltonian (Section 23.7). Here we can think of the original basis state $|1\rangle$ as being embedded in the “continuum” of eigenstates $|v\rangle$ and thus acquiring the spreading width Γ . Contrary to perturbation theory, for this picture to be valid, the “coupling amplitude” V should be strong enough so that $V \gg D$. At the same time, the spreading width Γ is finite, keeping the state $|1\rangle$ still localized.

In spite of crude assumptions in the derivation, the result for the spreading width works well for qualitative estimates. Of course, under these approximations, the tails of the function (25.18) are going down too slowly and the higher moments of this function do not exist, so we can apply it only when close enough to the centroid.

The distribution (25.18) is not applicable when the matrix elements V or/and the level spacing D change significantly along the width Γ . Then the shape becomes close to Gaussian as the result of a random walk according to the central limit theorem of mathematical physics (recall Section 20.6). One interesting indication of this transformation comes from the double giant resonances (a second harmonic) seen in some experiments [9]. The giant resonances, found, for example, in the random phase approximation (RPA), acquire their width due to the interaction with more complicated states in the same energy range. Using the boson approximation for the collective giant resonances, one can think of the repeated excitation of similar quanta. The so-called Brink–Axel hypothesis even assumes that the collective giant resonance can be excited on the background of any other (not very high-lying) state. If the width of the original resonance comes from admixtures of more complex states, the second harmonic will, in a good approximation, contain the first one plus the same excitations

of complex nature. The width of the *double* excitations is expected to be a *convolution* of two almost identical shape functions, where the result is different for Breit–Wigner and Gaussian shapes of the individual resonances.

Problem 25.3 Show that the convolution of two resonances at centroids E and $2E$ (interpreted as one- and two-phonon states created by the sequential one-phonon excitation) leads to a width 2Γ for the Breit–Wigner shape and $\sqrt{2}\Gamma$ for the Gaussian shape. The second prediction is closer to the experimental results although here we neglect the width due to the irreversible decay into continuum (usually still not big at typical energy).

Solution

If the anharmonic effects are weak, the convolution of the single-phonon strength functions gives the strength function of the double resonance,

$$F^{(2)}(E) = \int dE_1 dE_2 \delta(E - E_1 - E_2) F^{(1)}(E_1) F^{(1)}(E_2). \quad (25.19)$$

Shell-model examples allow us to find the actual strength functions (25.3) of stationary states resulting from the exact diagonalization of a realistic many-body Hamiltonian in truncated space. Because of truncation, the upper states do not correspond to real data, being an artifact of the truncation. However, this is still a good model of many-body complexity coming from interacting particles. As seen, for example, from the results in the full solution of the *sd* nuclear shell model [11], individual stationary states have irregular strength functions but the averaging for several neighboring states reveals a characteristic bell-shaped picture. Essentially, just this average strength function is a subject of physical interest.

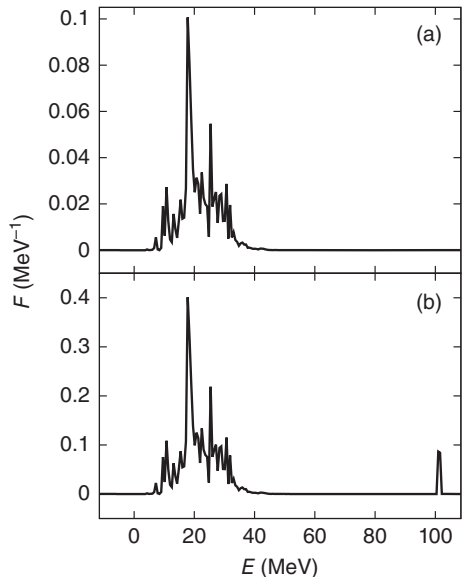
The concept of strength function and strength distribution has already been mentioned a number of times. The alternative expression, valid for any state k , can be useful:

$$F_k(E) = \sum_{\alpha} |C_k^{\alpha}|^2 \delta(E - E^{\alpha}) = \langle k | \delta(E - H) | k \rangle = -\frac{1}{\pi} \text{Im} \left\langle k \left| \frac{1}{E - H + i\delta} \right| k \right\rangle. \quad (25.20)$$

Green's function $G(E) = 1/(E - H + i\delta)$ involves here an infinitesimal imaginary part; in the continuum shell-model approach (Section 23.7), it would be replaced by $G(E) = 1/(E - \mathcal{H}(E))$ with an effective non-Hermitian Hamiltonian $\mathcal{H}(E)$. The strength function evaluated relative to physical channels expresses the strength distribution for particular reactions; the total integrated strength is normalized by the norm of the channel vector which is not necessarily equal to 1 as in Eq. (25.4). For example, the strength in particle channels defined by Eq. (23.42) gives the distribution of spectroscopic factors for the transition into a given channel. Similarly, the channels involving various multipole operators for electromagnetic and weak decays can be constructed and studied. As mentioned in Section 23.8, the time-dependent techniques, Eqs. (23.73)–(23.77), offer an effective method for evaluating strength functions.

A typical strength function is illustrated in Figure 25.1. Here the upper panel (a) shows the strength function for the isovector dipole excitation of 1^- states in ${}^{22}\text{O}$ from the ground state. This figure essentially represents the distribution of $B(\text{E}1, 1_i^- \rightarrow 0_{\text{g.s.}}^+)$.

Figure 25.1 Dipole strength function in ^{22}O in the p - sd - fp model space that allows for particle–hole excitations; see also Ref. [12]. (a) The strength function for isovector dipole operator with effective charges from Eq. (2.61), where giant dipole resonance is seen. (b) This panel shows that an unphysical operator which contains an isoscalar part leads to spurious strength in the center-of-mass excitation; here the spurious states artificially shifted to about 100 MeV of excitation energy.



The broad Breit–Wigner peak (25.18) at about 20 MeV of excitation energy is a giant dipole resonance; see Section 6.2 and Figure 6.1. Here the resonance emerges from multiple particle–hole excitations involving the valence sd , the lower $0p$, and upper $0f$ – $1p$ shells. As discussed in Section 23.1, this p - sd - fp model space contains spurious states; here these states are pushed to higher excitation energy, about 100 MeV, using an artificial term in the Hamiltonian. As seen from panel (a), the physical isovector dipole operator with effective charges from Eq. (2.61) does not contain spurious strength; however, this is not the case in panel (b) where the strength of an unphysical dipole operator with $e_n = -1$ and $e_p = 1$ is shown. The latter operator has both isovector and isoscalar components and the isoscalar component excites spurious center-of-mass states at high energy.

25.3 Level Density Revisited

The level density is among the most important statistical characteristics of nuclei and quantum many-body systems in general. The nuclear level density was discussed in Chapter 20 using statistical ideas and mean-field arguments in the form of Fermi-gas combinatorics. We should emphasize a close connection between symmetries, classical periodic orbits, and the single-particle density of states discussed in Section 8.10, as well as point out to a chaotic nature of one-body mean-field levels (see Figure 12.8 in Section 12.13), emerging when symmetries are broken. Going beyond the mean field, chaotic and collective nucleon–nucleon interactions play a critical role. The framework of the nuclear shell model allows for this more advanced study to be conducted. This branch of studies is called *statistical spectroscopy* [13]; its history and main contributions are collected in the books [14, 15].

We consider the usual shell-model Hamiltonian as a sum

$$H = H_0 + U \quad (25.21)$$

of the mean-field part H_0 and residual interaction U . We assume that the Hamiltonian H is known, either from theory or by empirical fit of its matrix elements to the experimental data. The spherically symmetric mean field with the pronounced shell structure leads to partitions (distributions of a given particle number over orbitals) as mentioned in Chapter 17. In the absence of U , all many-body states in each partition are degenerate, and the density of states has sharp peaks corresponding to sets of states with different numbers of particle–hole excitations. The states within each partition can be further classified by symmetry, in particular, by total spin J .

The level density is formed not only by single-particle shell structure but on equal footing by all parts of interparticle interactions. Owing to the interaction U , the states in each partition are no longer degenerate, the density of states is broadened, and partitions overlap in energy; with the growing particle number, the dimensions of partitions grow and the statistical properties become more evident. A large number of small matrix elements corresponding to incoherent collision-like processes, to a large extent, level off the partition peaks present on the level of the mean-field combinatorics [16]. The effect is illustrated in Figure 25.2a. Here the dashed line shows the level density in ^{24}Mg which follows from the realistic shell-model Hamiltonian restricted to the sd shell (see Section 23.5). This includes states of all spins. The two other results in panel (a) show the density of states for the Hamiltonian $H \rightarrow H_0 + \lambda_{2b} U$ where the two-body interaction is

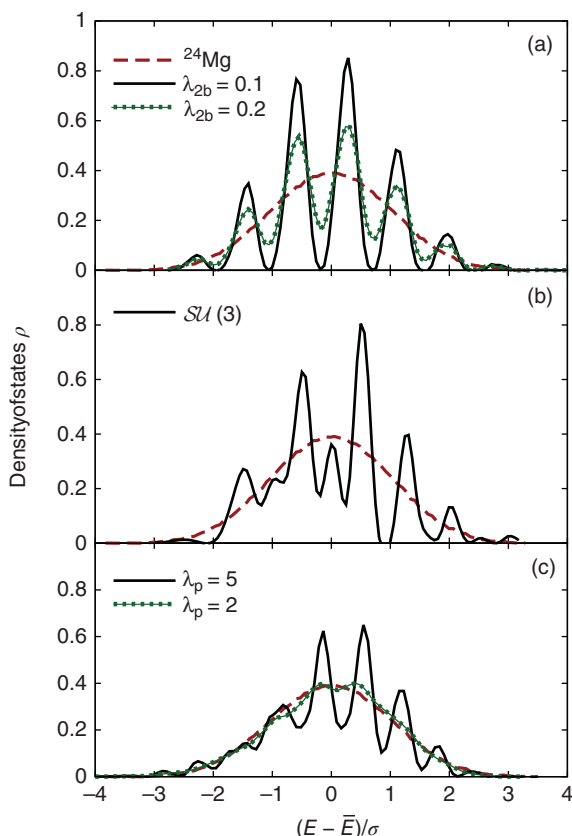


Figure 25.2 Density of states, including all spins and isospins, for the ^{24}Mg model in the sd valence space: (a) for the Hamiltonian where two-body interactions are reduced by a factor of λ_{2b} ; (b) for the Hamiltonian comprised exclusively of the components that conserve the $SU(3)$ symmetry; (c) the density of states as a function of the isovector pairing strength λ_p where all nonpairing matrix elements are weakened by a scaling factor 0.1, while H_0 is unchanged. In all panels, the result for the realistic Hamiltonian is shown by a dashed line; this curve has a smooth shape close to Gaussian.

weakened by a factor of λ_{2b} . The peaks are quickly smoothed out with the increased strength of the two-body interaction and disappear around $\lambda_{2b} \approx 0.5$. Here the density of states is plotted relative to the mean energy \bar{E} and is normalized by the variance σ .

Changes to the Hamiltonian have significant effects on the lowest moments. The monopole mean-field component of the two-body interaction shifts the mean energy \bar{E} , while any additional interaction generally spreads the levels apart, leading to increased variance. For example, for $\lambda_{2b} = 0.2$, $\sigma = 7.2$ MeV and $\bar{E} = -20.0$ MeV, while in the realistic limit, $\lambda_{2b} = 1$, $\sigma = 11.3$ MeV, and $\bar{E} = -43.5$ MeV.

Coherent components in the two-body interaction can act in a different way, for example, one can provoke the deformation phase transition that requires the significant mixing of single-particle orbitals, mainly by matrix elements of single-particle transfer; recall the Nilsson scheme, Section 12.12. Then the effect of the *collective enhancement* of the low-energy level density emerges owing to the appearance of low-lying rotational bands built on simple excited states. As we know from our discussion in Section 12.8 and Problems 12.6 and 23.3, the ^{24}Mg nucleus is deformed and the onset of this deformation can be described by the quadrupole–quadrupole interaction Hamiltonian that preserves $SU(3)$ symmetry as clearly seen in the harmonic oscillator basis. Onset of this symmetry indeed leads to significant irregularities in the density of states as illustrated in Figure 25.2b. While this symmetry persists in the rotational structure of states (Figure 23.8), its effect on the density of states is also partially washed out by the incoherent nucleon–nucleon scattering in other channels.

Pairing interaction is another limiting case that should be mentioned; this interaction leads to gaps in the spectrum and states with different seniority separately leading again to peaks in the density of states (Figure 25.2c, see also Ref. [17]). In the ^{24}Mg example, the role of seniority is weak. However, as it is a macroscopic phenomenon, the effect can grow with increasing particle number and can prevail at low temperatures as it happens in the the macroscopic superconductors. Paring effects are among most likely possible explanations of the features in the nuclear level densities shown in Figure 20.1.

Direct computation of the level density by full diagonalization of the shell-model Hamiltonian is a daunting task and can only be done for relatively small systems. Development of effective methods for the density of states in an interacting many-body system is an active subject of research. To mention a few directions, the shell-model Monte Carlo approach (Section 20.7) can be used to obtain level densities with the help of traditional thermodynamic relations [18]; stochastic sampling of random states and averaging strength functions obtained using the time-dependent technique (Section 23.8) is another potential avenue; recursion relations provide alternative strategy for tackling thermodynamic properties of interacting systems [19].

A simple and practically useful statistical method for level density evaluation is developed for the cases where one has a reliable shell-model Hamiltonian and the calculation of the moments of the Hamiltonian is quite feasible even if the Hamiltonian matrix is prohibitively large for diagonalization. This statistical spectroscopy is based on the central limit theorem: the sums of random quantities rapidly approach the Gaussian distribution; for a given partition, this is illustrated in Ref. [20]. This offers an opportunity for a fast and effective method to predict the shell-model level density: the near-Gaussian level densities for different partitions are to be superimposed and interaction between the partitions can be included similarly to what we have in the second moment (25.8).

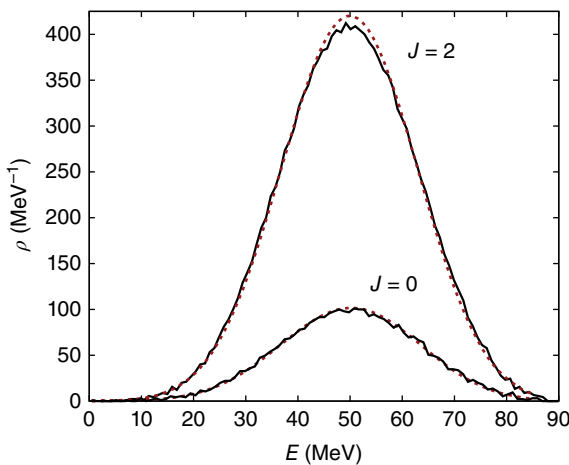


Figure 25.3 Level density for the ^{28}Si nucleus for spins $J = 0$ and $J = 2$ with the effective shell-model interaction in the sd valence space. The results from exact diagonalization shown by solid lines are compared with the density of states found with the moments method, dashed lines; Ref. [22].

In practice [21], one has to calculate two first moments to get a reliable prediction for the shell-model level density presented as

$$\rho_\alpha(E) = \sum_p d_{ap} G_{ap}(E). \quad (25.22)$$

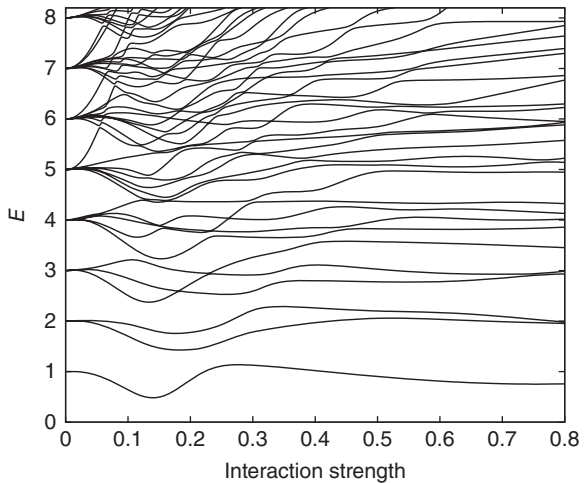
Here the energy E is counted from the ground-state energy. The sum in (25.22) is taken over partitions, d_{ap} is the dimension of a given class of states α in the partition p , and the Gaussian G has a centroid at the first moment (25.7), while its width is determined by the second moment (25.8), where the off-diagonal interaction elements between different partitions are accounted for. As mentioned earlier, the calculation of the moments uses the Hamiltonian matrix without diagonalization.

There are additional subtle elements to the method such as treatment of the unphysical tails in Gaussians, removal of the center-of-mass spurious states, and applications that involve many-body forces; see Ref. [22]. Figure 25.3 demonstrates a very good reproduction of the exact shell-model level density by the moments method. In the cases where experimental information up to some energy is nearly complete, the result of such statistical calculation with the appropriate shell-model version is quite close to the data. In spite of the space limitations, the shell model can cover the regions of excitation where the knowledge of the level density is necessary for understanding the reaction cross sections, including those needed for technology and astrophysics. The computational algorithm for calculating shell-model level densities and links to computer codes can be found in the Ref. [21].

25.4 Complexity of Wave Functions

As seen from the behavior of the level density in different classes of states, the smoothness of the bell-shaped curve and its energy dependence show the interplay of many processes. If we assume that the interaction is switched on adiabatically, the energy of a many-body state evolves through many crossings with other levels. As we know (recall the Landau–Zener crossing physics, Section 21.6), the levels with the same constants of motion in general do not cross; the crossing is *avoided*. As a result, the wave functions exchange their physical contents. This process (plus, of course, weak but frequent

Figure 25.4 Evolution of the energy spectrum as a function of the intensity of interactions. Note similar behavior of levels in Figure 12.8.



mixing with many remote levels) rapidly transforms the original pure shell-model wave function into a very complicated superposition of Eq. (25.2).

There are two main features in the spreading process. The energy spectrum undergoing the “turbulent” sequence of multiple avoided crossings arrives at the visible picture of “laminar” motion with the level spacings weakly fluctuating around some kind of a picket fence structure and forming an *aperiodic crystal* (Figure 25.4). At the same time, the strength functions (25.3) of the original basis states acquires wider spreading. Simple quantitative estimates of the degree of complexity have already appeared in the discussion of enhancement of weak interaction effects (Section 21.8). The simplest characteristic is the effective number N^α of components C_k^α in direct and inverse expansions (25.2),

$$\overline{w_k^\alpha} \equiv \overline{|C_k^\alpha|^2} = (N^\alpha)^{-1}. \quad (25.23)$$

The physics of neutron near-threshold compound resonances in heavy nuclei shows that this number is of the order 10^6 . With $N^\alpha \gg 1$, we expect the normal distribution of the components C_k^α of a typical wave function and therefore the Porter–Thomas distribution of the weights w_k^α (Section (20.9)),

$$P_C^\alpha = \sqrt{\frac{N^\alpha}{2\pi}} e^{-(N^\alpha/2)C^2}, \quad P_w^\alpha = \sqrt{\frac{N^\alpha}{2\pi w}} e^{-(N^\alpha/2)w}. \quad (25.24)$$

The shell-model study [23] shows that the structures of various complicated states are practically uncorrelated; the situation is quite similar for complex atoms [24].

To formalize such estimates and compare the complexity of different states, we can introduce the *information* (Shannon) entropy of a given state $|\alpha\rangle$,

$$I^\alpha = - \sum_k w_k^\alpha \ln(w_k^\alpha). \quad (25.25)$$

This is a measure of the complexity jump from pure states $|k\rangle$ to the stationary eigenstate $|\alpha\rangle$ and as such it depends on the choice of the reference basis $|k\rangle$. Without interactions, this entropy vanishes similarly to thermodynamical entropy at a temperature of absolute zero. The same happens if we start from the basis of stationary states identifying k and α .

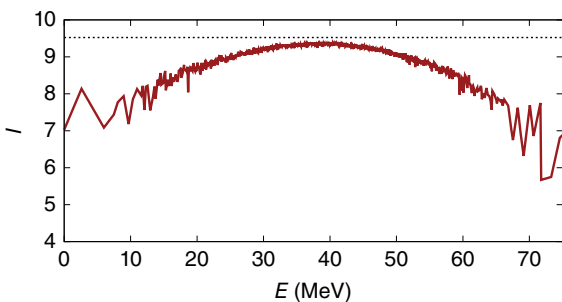


Figure 25.5 Information entropy for all $J = 2, T = 0$ positive parity states in ^{24}Mg found in the exact diagonalization of the shell-model Hamiltonian in the sd valence space shown as a function of excitation energy of the state. The dotted line shows the Gaussian distribution limit of $\ln(0.48N)$.

The useful physical information comes if we choose k as the mean-field basis; then the growth of entropy is a signal of complexity coming from residual interactions.

Figure 25.5 shows the behavior of entropy (25.25) as a function of energy E^α in a certain class of states of ^{24}Mg nucleus. Because of the practically truncated space, the lowest and the highest states have quite low entropy. Entropy maximum in the middle of the spectrum illustrates the monotonous (with small fluctuations suppressed for larger spaces) growth of complexity. Note that, up to small fluctuations, this entropy is a function of the excitation energy – a *thermodynamic quantity* which can be compared to thermodynamic entropy of a heated system.

If many close-in-energy states have a similar degree of complexity (the same N^α) and the Gaussian distribution (25.24) is valid (note that the Porter–Thomas distribution (25.24) of weights $w_k^\alpha = |C_k^\alpha|^2$ emerges from the Gaussian distribution of amplitudes C_k^α ; see Problem 21.3), one can find out the mean entropy \bar{I}^α of these states by integration:

$$\bar{I}^\alpha = -2 \sqrt{\frac{2N^\alpha}{\pi}} N^\alpha \int_0^\infty dC C^2 \ln C e^{-(N^\alpha/2)C^2} = \ln \left(\xi \frac{N^\alpha}{2} \right), \quad (25.26)$$

where the universal constant is

$$\xi = \exp \left(-\frac{8}{\sqrt{\pi}} \int_0^\infty dx x^2 e^{-x^2} \ln x \right) = 0.964. \quad (25.27)$$

In this limit, $\bar{I}^\alpha = \ln(0.482 N^\alpha)$. The smooth behavior of the information entropy in Figure 25.5 displays a maximum at the center of the spectrum with the value close to the limit (25.27) and N^α close to the total dimension N of the space: these functions indeed have a very high degree of complexity.

Instead of information entropy, one can use equivalent measures of complexity. The simplest among them is the so-called *inverse participation ratio*, the next moment of w_k^α , which is also called the *number of principal components*,

$$(\text{NPC})^\alpha = \sum_k (w_k^\alpha)^2 = \sum_k |C_k^\alpha|^4. \quad (25.28)$$

With the Gaussian distribution of components, this equals $N^\alpha/3$; in this limit, we have the universal (independent of N^α) ratio

$$\frac{\exp(\bar{I}^\alpha)}{(\text{NPC})^\alpha} = 1.44. \quad (25.29)$$

A possible objection to such measures of complexity, or chaoticity, emerges if we recall that the collective states, such as those considered in Chapter 18, have, similarly to (25.2),

the wave functions as superpositions of many simpler excitations. According to the definitions (25.25), (25.28), such states will be characterized by a large information entropy and inverse participation ratio. The statistical weight of such a state in the total level density is usually small but indeed the admixture of many small components to an RPA-type collective state does exist. One possible theoretical way to distinguish these two types of rich superpositions is to look at the correlations of components rather than only the weights [23]. The *phase correlator* for a certain stationary state $|\alpha\rangle$ can be defined as [25]

$$P^\alpha = \frac{1}{N} \sum_{k,k'=1}^N C_k^\alpha C_{k'}^{\alpha*}. \quad (25.30)$$

This quantity can reach its maximum equal to 1 for a “supercollective” state with all amplitudes of the same sign and equal to $1/\sqrt{N}$, where N is the full dimension of the space. In the chaotic situation with uncorrelated amplitudes C_k^α , their random phases result in the correlator (25.30) of the order $1/N$.

We can now briefly return to the problem of the strength function. The standard golden-rule model is oversimplified even if it frequently provides a good instrument for semiquantitative estimates. If we look at the chaoticization process, as in Figure 25.4, starting from a basis state $|k\rangle$, at the first mixing it acquires components of particle–hole states provided by the interaction. These states serve as the *doorway* states of the whole process and they define the main part ΔE of the spreading width for the progenitor state $|k\rangle$. The doorway states have their own spreading widths but outside the primary interval, the matrix elements V usually decrease. A theory of transition from the standard model and the Breit–Wigner distribution to the Gaussian limit and even further to the so-called semicircle strength function in the case $\Gamma \gg \Delta E$ can be found in Ref. [26]; more examples outside of nuclear physics are discussed in the review [27].

25.5 Correlations between Classes of States

In the diagonalization of a Hamiltonian matrix, exact constants of motion divide the common Hilbert space into nonoverlapping classes. However, the dynamics in all classes is usually governed by the same many-body Hamiltonian so that we expect certain correlations between different subsets, at least in a statistical sense. This would not be the case if, for example, we would consider a scattering problem introducing different spherical potentials for different values of orbital momentum. But in many-body physics, as a rule, we have the same few-body Hamiltonian for all states of the system as a whole.

Although a specific experiment typically is sensitive to the certain subclasses of states, the theoretical analysis can vary the Hamiltonian and study the changes in physical observables including the correlations between the classes. This opens the way to various computational experiments which can elucidate the underlying physics, giving food for thought. One simple series of such experiments was started in Ref. [28] and stimulated a lively reaction [29, 30]. Consider a small orbital space, even one degenerate j -level with a relatively large value of angular momentum j , and put there a few (for simplicity, an even number) of identical nucleons. Introduce the most general set of two-body matrix elements allowed by the rotational invariance and consider their amplitudes as random quantities with a simple distribution symmetric with respect to their signs; this can be

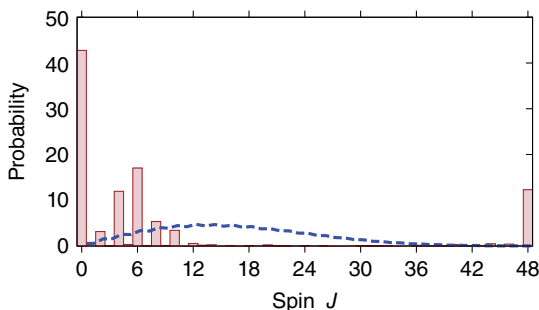


Figure 25.6 The multiplicity of states as a function of their spin J , dashed line, and the probability of their appearance at an extremal energy (both in percent) for a system of eight identical fermions on $j = 19/2$ level with the Gaussian distribution of two-body matrix elements.

a Gaussian or even uniform ± 1 distribution. As an example discussed in Figure 25.6, we could take a single j -level model space with the Hamiltonian from Chapter 11, Eq. (11.96), and create a random two-body ensemble by randomly generating interaction matrix elements U_L for all $L = 0, 2, \dots, 2j - 1$ with the Gaussian distribution.

Every choice of this ensemble of matrix elements defines the energy spectrum and the set of stationary states. An interesting question to address is – what are, averaged over very many random choices, the preferential quantum numbers (in the simplest case, just total spin J) of the ground state? Owing to the symmetry of the ensemble, this will be also the most frequent spin of the highest state.

The simplest “natural” idea would be that after many random tries the probability to have the lowest energy will be the largest for the value of J that has the maximum multiplicity $D(J)$ of appearance in a given Hilbert space; see discussion in Section 9.6. This turns out to be wrong. In spite of a low multiplicity, the spin $J = 0$ has the largest probability to appear at the edge of the spectrum, practically independently of the distribution function used to generate the ensemble (Figure 25.6). Among the two-body matrix elements, there is pairing but it is easy to check that it is not a reason for the victory of $J = 0$ states; even if the sign of the pairing matrix element proportional to $(a^\dagger a^\dagger)_{00}(aa)_{00}$ is always positive (increasing the energy), the decrease in percentage of the $J = 0$ ground states is very small.

A qualitative understanding of the situation is suggested in terms of *geometric chaoticity*. The multiplicities are defined by chaotic angular momentum coupling that leads to the Gaussian distribution of spin projections in the combinatorial approach to the level density in a fermionic system with no interaction (Section 20.6). The mean field emerges after averaging over incoherent collisions driven by almost any reasonable Hamiltonian – this can be shown by the alternative derivation of the mean field equations [31]. This is also seen in the simpler picture [32] of the interacting boson model (Chapter 19) with a clear geometric structure of available mean-field configurations and phase transitions between them under change of the parameters. The simplest effective spin interaction in the mean field limit is of the Heisenberg type,

$$H_s = A \sum_{ab} (\mathbf{j}_a \cdot \mathbf{j}_b) \quad (25.31)$$

which gives, for a random coupling constant A , 1/2 probability for the ground-state spin $J_0 = 0$ (antiferromagnetic situation, $A > 0$) and 1/2 probability for the maximum possible ground-state spin (ferromagnetic situation, $A < 0$). Since the maximum spin in the shell model is realized by one state only (maximum alignment compatible with

Fermi statistics), the zero ground-state spin has a clear advantage. The Kramers theorem on degeneracy of the stationary states in a system of an odd fermion number with a time-reversal invariant Hamiltonian acts in the same direction: for any shape of a mean field it is energetically favorable to populate the orbitals pairwise.

Therefore, the current hypothesis on predominance of ground state with zero total spin, being still a hypothesis describing the available data but with no strict proof, seems quite attractive: for the ground state it is statistically preferable to have the lowest possible exact symmetry.

An ensemble of Hamiltonians with given general properties of certain symmetry and random numerical parameters can also serve another purpose. Using such models, it is possible to establish which parts of the complicated Hamiltonian are responsible for certain values of observables. The first nuclear structure question is that about the ground-state shape of the nucleus. A spherical shape and well-deformed shape, at the same ground state spin $J = 0$, give rise to quite different spectral properties of low-lying states. The same ensemble of random parameters contains in itself all such possibilities defined by subsets of values of certain interaction parts which play the role of control parameters as they are usually termed in general theory of quantum phase transitions. Figure 25.7 illustrates the wealth of nuclear shapes possible under random variation of the Hamiltonian parameters in the same orbital space [33].

Here the distribution of reduced probabilities of quadrupole transitions from the 0^+ ground state to the first excited 2^+ state is shown in Figure 25.7a for an ensemble with six fermions on the $j = 19/2$ level. The reduced transition rate is expressed as a fraction of the total sum rule (sum of $B(E2)$ from the ground state to all 2^+ states). In addition to the predominance of $J = 0$ ground states, the probability for the first excited state to be $J = 2$ is quite high; this sequence is seen in more than 10% of realizations. The shaded peak where $B(E2; 0_{\text{g.s.}}^+ \rightarrow 2_1^+) > 0.7$ indicates that most of these realizations have collective dynamics, saturating the significant fraction of the sum rule related to the lowest

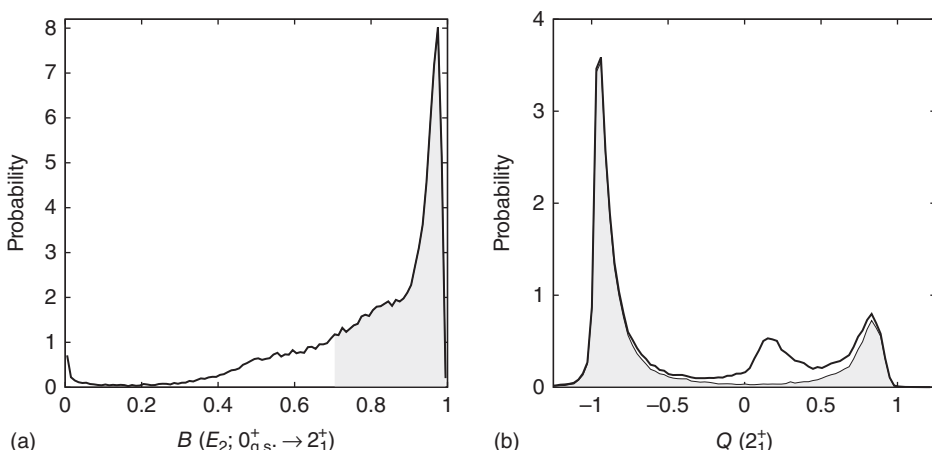


Figure 25.7 Distribution of the normalized reduced transition rates (a) and quadrupole moments (b) for an ensemble with six fermions on $j = 19/2$ level, see the text. The shaded area in both panels highlights collective realization. The sequence of interest, $J = 0$ ground state and $J = 2$ first excited state, is realized in 10.4% of cases.

2^+ state. In Figure 25.7b, the distribution of the quadrupole moment in the first 2^+ state is shown. The quadrupole moment is also expressed in relative units using the rotor model (Section 16.12), where the sum rule determines the scale of intrinsic deformation. Thus, the values of the quadrupole moment -1 and $+1$ correspond to prolate and oblate shapes, respectively. The two peaks seen in the distribution on the right panel confirm that most collective (shaded area) realizations are indeed either prolate or, with a smaller probability, oblate deformed. Various collective structures, such as spherical vibrational with $E(4_1^+)/E(2_1^+)$ close to 2 and triaxial deformed, have considerable probabilities compared to all intermediate cases.

The emergence of shapes and regular systematics in low-lying states generated by random ensembles is reproduced here; partly, this behavior can be traced to coherent components in the interaction. For example, in a single- j system we can transform the interaction to the particle–hole channel (see Problems 11.9 and 11.10). The $K = 1$ component amounts to an effective moment of inertia so that the contribution to energy is proportional to $\tilde{U}_1 J(J + 1)$. As follows from Eqs. (11.94)–(11.97), the $K = 1$ term leads to

$$E = AJ^2 \quad \text{where} \quad J^2 \equiv J(J + 1) \quad \text{and} \quad (25.32)$$

$$A = \frac{3}{\{2(2j + 1)\mathbf{j}^2\}^2} \sum_{L=0,2,\dots}^{2j-1} (2L + 1)U_L\{\mathbf{L}^2 - 2\mathbf{j}^2\}. \quad (25.33)$$

This can be interpreted as a preference for either zero or maximally aligned ground-state spin depending on the sign of A . Realizations with attractive “short range,” lower L , and repulsive “long range,” higher L , components would favor low spin. The opposite situation is similar to Hund’s rule in atomic physics favoring maximal value of the ground-state spin. The systematics observed in shapes and quadrupole transitions has connection to the $K = 2$ quadrupole–quadrupole interaction and $SU(3)$ symmetry.

The empirical fact that almost all stable deformed nuclei have *prolate* shape raises a related question about the sign of quadrupole deformation, prolate versus oblate. Any model with particle–hole symmetry would have the prolate–oblate symmetry of allowed many-body states. The ground states in the beginning of the shell occupation (less than half-occupied shells) are prolate, while hole-type states (more than half-occupied shells) should be oblate. It follows from a similar study [34] that the quadrupole deformation is driven mainly by the matrix elements where one particle is transferred to another orbit of the same parity, the *pf*-mixing in that specific case. This is a reflection of the Nilsson-scheme mixing of neighboring orbitals by quadrupole deformation (Section 12.12). When we start filling the *p*-orbit and probe the deformation where this state is close to one of the *f*-orbitals (split by the projection $j_z = m$ onto the symmetry axis and going down as a function of deformation), the Nilsson scheme shows that for low- $|m|$ orbitals the prolate deformation is energetically favorable. This leads to a qualitative explanation of the empirical fact that almost all stable deformed nuclei have *prolate* shape. The oblate shape is preferred by the same mixing for large $|m|$ values, which means the second half of the shell filling. However, at this point, in many cases, the split levels from the next oscillator shells steeply go down and again induce mostly prolate shapes; additionally, the shell spacing decreases with energy. One could also argue that while for the harmonic oscillator mean field there is exact prolate–oblate symmetry, the realistic nuclear potential is more flat

and has a pronounced surface so that there is a preference to higher ℓ ; recall term $v_{\ell\ell}$ in the Nilsson potential, Eq. (11.97). The situation can be different in nuclei far away from stability with large neutron–proton asymmetry; here one can expect more oblate-deformed nuclei.

The ground-state deformation induced by the single-particle transfer matrix elements should lead to the accumulation of rotational bands with relatively low spacings between the levels. This is the above-mentioned *collective enhancement* of the level density often introduced in a phenomenological way.

25.6 Invariant Entropy

The information entropy (25.25), as was already stressed, shows the statistical interrelation between the eigenstates of the Hamiltonian and the starting basis. This degree of complexity obviously is *relative*. Another way of looking at the problem of statistical complexity can be found with the use of the *density matrix* instead of a pure wave function [QP, II, Chapter 23].

Here the density matrix will be defined for a given energy term $|\alpha\rangle$ that evolves as a function of some parameters λ . At each realization of the parameters, we define the continuously changing wave function

$$|\alpha; \lambda\rangle = \sum_k C_k^\alpha(\lambda) |k\rangle. \quad (25.34)$$

The coefficients $C_k^\alpha(\lambda)$ depend on the reference basis and on the parameters. They define the instantaneous (for a given set of λ) density matrix of a given state,

$$\rho_{kk'}^\alpha(\lambda) = C_k^\alpha(\lambda) C_{k'}^{\alpha*}(\lambda). \quad (25.35)$$

At given values of λ , this does not give anything new compared to the pure wave function. The density matrix (25.35) in k -space has a trace equal to 1 and eigenvalues equal to 1 (this eigenstate is of course $|\alpha\rangle$ itself) or zero for any orthogonal state.

The new physics comes if we take the average of the matrix elements (25.35) over some interval of change of the parameters λ with a reasonable normalized distribution function $\mathcal{P}(\lambda)$. This leads to a nontrivial density matrix [35] (still referring to a certain energy term α),

$$\rho_{kk'}^\alpha \Rightarrow \overline{C_k^\alpha(\lambda) C_{k'}^{\alpha*}(\lambda)} \equiv \int d\lambda \mathcal{P}(\lambda) C_k^\alpha(\lambda) C_{k'}^{\alpha*}(\lambda). \quad (25.36)$$

The orthonormalized eigenstates $|v\rangle$ of this Hermitian matrix differ from the states $|\alpha\rangle$; they form the so-called *pointer basis* that plays a role in theory of measurements where the parameters λ mimic the interaction of the system with a measuring apparatus [QP, II, 25.7]. The eigenvalues ρ_v^α of this density matrix are real numbers between 0 and 1. In general, they describe the influence of noise on a certain energy term of our deterministic system.

Using the density matrix (25.36), we can introduce another entropy,

$$S^\alpha = - \text{Tr } \rho^\alpha \ln(\rho^\alpha) = - \sum_v \rho_v^\alpha \ln(\rho_v^\alpha). \quad (25.37)$$

This entropy, still being attributed to a single original energy term α , reflects correlational properties of the system subject to different levels of noise. Therefore, we can call it *correlational entropy*, although the definition (25.37) is quite similar to that of standard thermodynamic entropy in canonical thermal ensembles. Expressed by a trace, this quantity does not depend on the choice of the primary basis $|k\rangle$ – it is an invariant characteristics although specific for the choice $\mathcal{P}(\lambda)$ of the applied noise.

If the interactions of the starting state $|k\rangle$ with other basis states are weak, so that the genuine stationary state $|\alpha\rangle$ is close to $|k\rangle$, only one eigenvalue of the density matrix is still large (close to 1), the rest of them are small, being proportional to the perturbational admixtures of other components and the mean square fluctuation $(\Delta\lambda)^2$ of the noise.

Problem 25.4 Consider a two-level system where the noise is imposed on the diagonal matrix elements (random perturbation of original energy, similar to a random magnetic field splitting the spin projections or fluctuations of the energy levels in crystal cells in a disordered solid). With the help of Pauli matrices, the Hamiltonian can be written as

$$H = \frac{1}{2} (\epsilon - \lambda) \sigma_z + V \sigma_x. \quad (25.38)$$

Find invariant entropy (25.37) for two eigenstates of this Hamiltonian in terms of quantities averaged over λ with some distribution function $\mathcal{P}(\lambda)$. In parallel find also information entropy of the eigenstates of the Hamiltonian (25.38).

Solution

The diagonalization in this two-dimensional space at fixed value of λ is reached by the rotation of the basis through an angle $\varphi/2$, where

$$\sin \varphi = \frac{2V}{\Delta}, \quad \cos \varphi = \frac{\epsilon - \lambda}{\Delta}, \quad \Delta = \sqrt{(\epsilon - \lambda)^2 + 4V^2}. \quad (25.39)$$

After averaging over λ , we obtain

$$c = \overline{\cos \varphi}, \quad s = \overline{\sin \varphi}, \quad (25.40)$$

where, in general, $\sqrt{c^2 + s^2} \equiv r \neq 1$. This determines the entropy (25.37) that has the same value for the two eigenstates,

$$S = - \frac{1+r}{2} \ln \frac{1+r}{2} - \frac{1-r}{2} \ln \frac{1-r}{2}, \quad (25.41)$$

that is equal to zero without averaging ($r = 1$) and to $\ln 2$ for $r \rightarrow 0$ (equipartition of occupancies, maximum of “thermalization”). It is important for the result whether or not the range of averaging covers the original spacing between the levels.

The information entropy (here we can set $\lambda = 0$) equals

$$I = - \frac{1+c}{2} \ln \frac{1+c}{2} - \frac{1-c}{2} \ln \frac{1-c}{2}, \quad c^2 + s^2 = 1. \quad (25.42)$$

This quantity measures the quantum-mechanical mixing which we have discussed earlier in relation to the process of complexity growth; for weak mixing (V as a perturbation), information entropy goes to zero, while it reaches its maximum value $\ln 2$ at strong mixing, describing the spreading of the strength function at strong interaction.

Figure 25.8 Invariant correlational entropy (arbitrary scale) for state α being the ground state of ^{24}Mg is plotted as a function of scaling λ for isovector and isoscalar pairing components, and for all other (nonpairing) matrix elements.

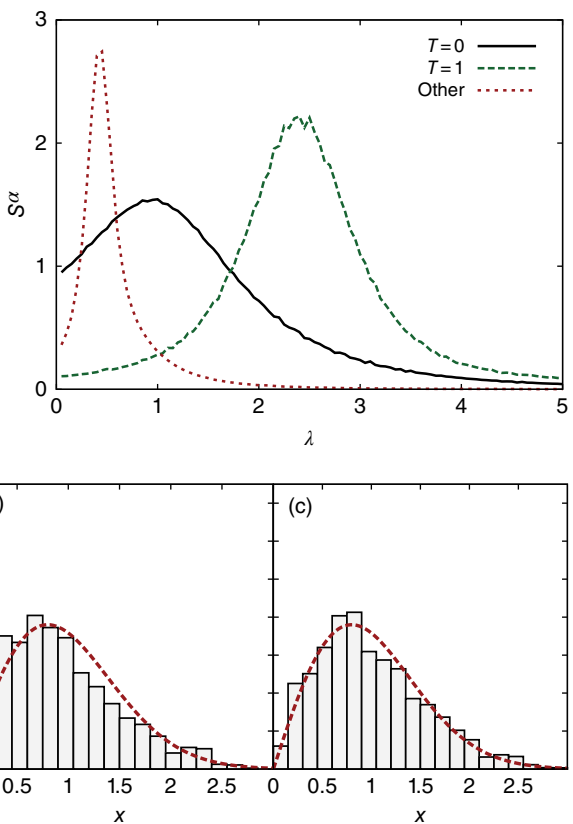


Figure 25.9 The nearest level spacing distribution for the states $J^{\pi} = 2^+$ found in the exact diagonalization of the sd -shell model for ^{28}Si [23]. The panels correspond to the gradual increase of the interaction part of the Hamiltonian scaled by the common strength $\lambda = 0, 0.1$, and 0.2 for panels (a), (b), and (c), respectively. Wigner–Dyson and Poisson distributions are shown by dashed and dotted lines, respectively.

If the system changes its structure (e.g., shape of the nuclear mean field) at some value of parameters, this *quantum phase transition*, which we have observed through the collective enhancement of the level density, should be seen in the behavior of invariant entropy S . Here we can take the term(s) of the Hamiltonian responsible for this phase transition as our noise parameters. Varying them around the phase transition point, we randomly visit different phases with large changes of the structure. These large fluctuations will be reflected in the growth of S . It is easy to notice that we have here a smoothed version of a macroscopic second-order phase transition with characteristic growth (frequently even singularity) of susceptibilities, heat capacity, and entropy. This opens the way to see quantum phase transitions by the behavior of the correlational entropy as a function of corresponding control parameters. In Figure 25.8, we take the two-body interaction Hamiltonian as a sum of isoscalar pairing, isovector pairing, and all other two-body matrix elements: $U = \lambda_{T=0} U_{T=0} + \lambda_{T=1} U_{T=1} + \lambda_{\text{other}} U_{\text{other}}$. The realistic case corresponds to $\lambda_{T=0} = \lambda_{T=1} = \lambda_{\text{other}} = 1$. Figure 25.8 shows the behavior of the invariant correlational entropy for the ground state of ^{24}Mg as a function of one of these

scaling parameters, while the other two are kept at unity. The peaks indicate phase transitions, although describing the single state. We infer from here that only a relatively weak strength of nonpairing interaction $\lambda_{\text{other}} \approx 0.5$ is sufficient to change the structure; this is consistent with our findings in Section 25.3 and results in Figure 25.9. With respect to isovector pairing, the realistic ^{24}Mg is right in the middle of a transitional region, while with respect to isoscalar pairing it is in the “normal” phase, quite far from the $\lambda_{T=0} \approx 2.5$ transitional region.

25.7 Random Matrix Ensembles

As seen from our experience with statistical properties of many-body excited states, the typical features are large level density, a rather uniform spectral picture of closest states with very similar strength functions, and high complexity of each wave function. As formulated, probably for the first time, by Percival [36], the stationary states in a certain region of spectrum (and belonging to the same sector by exact quantum numbers) are very similar in their degree complexity and typical values of observables. These properties smoothly evolve along the spectrum but they are very similar along a substantial energy interval containing many levels.

This situation justifies the idea of introducing, as standard candles in astronomy, standard examples of Hamiltonians whose statistical properties well simulate, with an appropriate choice of few parameters, those features of realistic systems which are typical for complicated quantum dynamics. In this way, we come to the *random matrices* [4–7, 14] which reflect only the most general requirements to the stable quantum system and produce necessary observable statistical features. We made here a new far-reaching step from usual statistical mechanics, where the system with a certain Hamiltonian is described by a density matrix (e.g., corresponding to usual thermodynamic equilibrium, Section 20.4). The system reaches equilibrium with maximum of entropy that corresponds to a given set of external conditions. The next generalization includes the statistics of Hamiltonians of a given class that is selected by very general physical principles only.

The simplest of *canonical* random matrix ensembles is the Gaussian orthogonal ensemble (GOE). Here we assume that the Hamiltonians belonging to the ensemble are Hermitian and time-reversal invariant. Then it is always possible to select the phases of the basis functions in such a way that the matrix elements of the Hamiltonian are real, so that the matrices are symmetric. All choices of the basis are assumed to be equally good in the sense that the distribution functions of the matrix elements are invariant under unitary (in this case orthogonal) transformations of the basis. This invariance determines the distribution function $P(H)$ for the matrix elements H_{ij} .

The traditional derivation introduces the *ensemble entropy* corresponding to the distribution we are looking for:

$$S_{\text{GOE}} = - \int dH P(H) \ln P(H), \quad (25.43)$$

The integral goes over all matrix elements, N diagonal and $N(N - 1)/2$ non-trivial off-diagonal ones. The probability distribution has to be normalized,

$$I_0 \equiv \int dH P(H) = 1. \quad (25.44)$$

To compare different distributions of matrix elements, we assume that they have the same centroid, which can be taken at zero. The orthogonal invariance requirement tells us that the distribution $P(H)$ should depend on invariant characteristics; in this role, we select the lowest one, the trace of H^2 (the linear trace is fixed by the centroid),

$$I_2 \equiv \int dH P(H) \text{Tr}(H^2). \quad (25.45)$$

The minimum of ensemble entropy (25.43) can be found with two Lagrange multipliers that fix the conditions for I_0 and I_2 ,

$$S_{\text{GOE}} \Rightarrow \tilde{S}_{\text{GOE}} = S_{\text{GOE}} - \mu_0 I_0 - \mu_2 I_2. \quad (25.46)$$

Problem 25.5 Show that the minimization of conditional entropy with the minimum of information available (25.46) determines the GOE distribution function

$$P(H) = e^{-(1+\mu_0)} e^{-\mu_2 \text{Tr}(H^2)}, \quad (25.47)$$

where μ_0 and μ_2 are to be determined by the normalization and the choice of the dispersion I_2 .

After normalization, we have here the Gaussian distributions of matrix elements, diagonal

$$P(H_{jj}) = \sqrt{\frac{C}{4\pi}} e^{-CH_{jj}^2/4}, \quad \overline{H_{\text{diag}}^2} = \frac{2}{C}, \quad (25.48)$$

and off-diagonal,

$$P(H_{ij}) = \sqrt{\frac{C}{2\pi}} e^{-CH_{ij}^2/2}, \quad \overline{H_{\text{off-diag}}^2} = \frac{1}{C}, \quad (25.49)$$

The absence of correlations between matrix elements can be formulated as

$$\overline{H_{ij} H_{kl}} = \frac{1}{C} (\delta_{ij} \delta_{kl} + \delta_{ik} \delta_{jl}). \quad (25.50)$$

Problem 25.6 Consider a two-dimensional example and express the GOE distribution functions of matrix elements in terms of energy eigenvalues E_1 and E_2 and the rotation angle θ from the original basis to the eigenbasis.

Solution

The eigenvalue distribution is given by

$$P(E_1, E_2, \theta) = \text{const} |E_1 - E_2| e^{-(2/a^2)(E_1^2 + E_2^2)}, \quad (25.51)$$

where the convenient parametrization is $C = 4N/a^2$ with dimension N equal to 2 in this case. Note that the result does not depend on θ (another sign of orthogonal invariance of the ensemble).

For large dimensions N , the distribution of energy levels is a natural generalization of Eq. (25.51). The probability vanishes for any coincidence of two energies. This is a result of the standard level repulsion in any process of mixing. For the degeneracy of two states with the same exact quantum numbers, both their diagonal distance and the mixing matrix element have to vanish at the same point of the parameter space. This is the

same as what we would expect, for a random walk in the plane (x, y) to get precisely at the origin; this is an event with probability of measure zero. From the mathematical viewpoint, the coincidence of eigenvalues tells us that the Jacobian of transformation from the original basis is equal to zero, and the unique inverse transformation is impossible.

Now we can recall the process of evolution of the network of levels from the mean-field picture to the realistic “disordered crystal” of levels. At sufficiently strong interaction, the close contacts of two eigenvalues become quite improbable, in agreement with the trend seen in Eq. (25.51). The GOE predicts the distribution of the spacings s between neighboring levels which is well approximated by the *Wigner–Dyson distribution*

$$P_x(x) = \frac{\pi x}{2} e^{-(\pi/4)x^2}, \quad (25.52)$$

that, in agreement with Eq. (25.51), combines the short-range linear repulsion $\propto x$ with the Gaussian behavior at large distances. For a practical comparison with actual spectra, one needs to *unfold* the energy spectrum expressing the spacings s in units of the *local* mean level spacing D , $x = s/D$. In all applications, it is important to remember that there is no global spectral evolution in canonical random matrix ensembles so that any direct confrontation of ensemble theory with real data makes sense only locally. The gradual increase of the strength of interaction matrix elements rapidly brings the nearest level spacing distribution (inside of a certain class of states) to agreement with Eq. (25.52). If one tries to combine spectra of many subsets with different quantum numbers into one basket and then look at the nearest level spacing distribution, the result will be close to the *Poisson distribution* $\propto e^{-x}$ because of the absence of repulsion between the levels of different classes [QP, II, 24.2].

The distribution function of spacings between the nearest levels is the first, although not the strongest, signal of chaotic dynamics. It becomes close to the distribution (25.52) already at a rather weak interaction strength (Figure 25.9). There are also more refined tools. In the presence of level repulsion, a sufficiently long sequence of states with the same quantum numbers reveals fluctuations around the staircase function of the cumulative state number,

$$\mathcal{N}(E) = \int_{E_{\min}}^E dE' \rho(E'), \quad (25.53)$$

which, after unfolding, would be just a straight line. The deviations grow with the length of the level sequence but quite slowly in the GOE ensemble, only logarithmically, while they increase much faster, linearly, for the Poisson-like sequence [5, 7]. The neutron resonances close to the neutron separation energy, present an appropriate example of an experimental ensemble to compare with canonical ensembles [37]. The study of level sequences in search of fluctuations (the so-called Δ_3 statistics [5]) turns out to be a sensitive instrument in a search for levels missing in the experiment or for incorrectly ascribed quantum numbers.

The amplitudes C_k^α of stationary states are uncorrelated and obey, for a sufficiently large dimensions N of the ensemble, a simple Gaussian distribution

$$P_C(C) = \sqrt{\frac{N}{2\pi}} e^{-NC^2/2}, \quad \overline{C^2} = \frac{1}{N}. \quad (25.54)$$

The typical complexity of eigenstates is fixed in the mathematical ensemble by the dimension, but in realistic examples, the effective number N evolves along the spectrum

defining the spreading width of the corresponding strength function. It can be shown that the distributions of information entropy and inverse participation ratio satisfy the properties discussed in the previous section.

In the approximation (25.54), the probabilities C^2 are described by the Porter–Thomas distribution (Section 21.3). Along with the nearest level spacing distribution, this property can be used for recovery of the level density with given quantum numbers in an experiment with relatively poor resolution ΔE [38]. This works if the states under consideration being in reality already in the continuum, still have their decay widths Γ much smaller than the typical level spacings D , so that the double inequality is fulfilled, $\Gamma \ll D \ll \Delta E$.

In general, the presence of the continuum (instability of states with respect to decay outside the space under consideration) distorts the statistical properties found in canonical ensembles. Only at small decay widths and for a single decay channel, the width statistics can be identified with the statistics of corresponding components C^2 . Recent experiments on neutron resonances indicate deviations from the Porter–Thomas statistics; both the openness to neutron decay and the unavoidable presence of gamma-decay of neutron resonances make the theoretical description quite complicated [39] and still open for discussion. Another important change due to the continuum coupling is that the level repulsion at small energy spacings is now absent: the possibility of decay means that level energies are defined only up to their widths so that the real parts of complex energies $E - (i/2)\Gamma$ of two levels can now coincide. This effect disappears at very strong continuum coupling – as we know, in this case the total channel width is concentrated in the superradiant state, while the trapped states return to the no-crossing regime. Until now, we do not have an experimentally measured distribution of complex energies.

One can conclude that the GOE provides valuable information describing the limiting case of quantum chaos. Here chaos emerged naturally in a many-body interacting system without any chaotic elements in the Hamiltonian. The realistic nuclei at energies higher than breaking few pairs are indeed demonstrating the qualitative agreement with the main properties of mathematical chaos. In many cases, one can use the GOE predictions as a remarkable theoretical and experimental tool. Probably, now the deviations from this extreme limit are mainly of practical interest.

We do not discuss here other canonical random matrix ensembles [5, 7, 14]. The *Gaussian unitary ensemble* (GUE) does not assume time-reversal invariance; therefore, the Hermitian Hamiltonian matrices contain complex off-diagonal elements. Many properties in this case are similar to those in GOE. Among differences we note that, as follows from our discussion of level crossings, in this case the crossing requires that three quantities are to vanish simultaneously, the original level spacing, and real and imaginary parts of the mixing matrix element. This makes the probability of crossing proportional to x^2 at small x rather than to x as in Eq. (25.52). Here an unusual opportunity arises – to look for the violation of the fundamental time-reversal symmetry in the statistics of short-range repulsion of nuclear levels. Unfortunately, here the statistics are rather poor already because of the linear repulsion so that it is difficult to find the symmetry violations on the level better than is known from more specific experiments. The third canonical ensemble, the *Gaussian symplectic ensemble* (GSE), can describe the systems with time-reversal invariance but, for example, an odd- A nucleus with half-integer spins.

The Kramers degeneracy makes the energy levels doublets (time-conjugate states). Here the repulsion at small distances is even less probable, proportional to x^4 . This ensemble has not yet found many applications.

Generally, we feel that what is now important for many-body physics is not the set of exact beautiful mathematical predictions of canonical ensembles but the set of ideas related to physical complexity of eigenstates. This is confirmed by the fact that essentially the same effects are observed in the so-called TBRI (two-body random interaction) ensembles. Here one works with normal many-body (in this case two-body) interactions and only the parameters of the Hamiltonian run over some sets of values. As already mentioned, this allows one to study various physical situations which are possible in the systems of this type. New regularities and interesting physics here go beyond canonical ensembles which, however, have played a great role in attracting physicists to this area. The reader is referred here to the reviews of applications of random matrix theory to nuclear problems [40, 41].

25.8 Thermalization

In Chapter 20, we applied regular statistical mechanics, including the Darwin–Fowler method, to the problems of nuclear physics. Many textbooks traditionally limit the applications of such approaches to large systems in the *thermodynamic limit* of given density, the finite ratio of large particle number N to the large volume V . Then the application of statistical ideas to complex nuclei (and complex atoms or molecules) becomes questionable. It is impossible, for example, to apply the property of thermodynamic fluctuations of the particle number as it is usually done for a systems in a heat bath described by the grand canonical ensemble. The energy of a closed system does not fluctuate either (it obviously does in a standard canonical ensemble). Then it seems that we can use only the microcanonical ensemble of an isolated system but then we lose simple computational tools of statistical mechanics.

Such questions are directly related to the fundamental problems of justification of statistical mechanics. Starting from Boltzmann, equilibration in a complex system was attached to *chaos*, the set of ideas carrying the flavor of randomness and absence of clear predictability substituted by a probabilistic forecast. This was developed, in different form, by many great physicists. We can recall a not widely known statement from *Statistical Physics* by Landau and Lifshitz: "... according to the fundamental principles of statistical physics, the result of the averaging is independent of whether it is done mechanically over the exact wave function of the stationary state of the system or statistically by means of the Gibbs distribution. The only difference is that in the former case the result is expressed in terms of the energy of the body, and in the latter case as a function of its temperature". This is exactly the conclusion one can come to considering the complicated dynamics of an excited many-body system, such as an atomic nucleus.

With the standard definition of thermodynamic entropy S_{th} through the logarithm of the level density which, as we have seen, is close to a Gaussian in any class of states (centroid E_0 and width σ), we come to thermodynamic temperature in the finite orbital space,

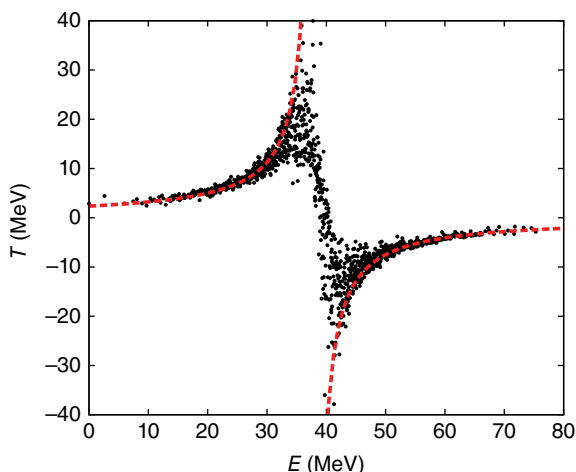
$$T_{\text{th}} = \frac{\sigma^2}{E_0 - E}. \quad (25.55)$$

The left branch of the Gaussian, $E < E_0$, corresponds to the positive temperature; in the maximum of the level density, temperature T_{th} becomes infinite and after that jumps to negative values, the typical behavior for systems with a finite space. We have seen already that information entropy, being a characteristic of a single stationary state, has essentially the same typical energy dependence which, in the spirit of Landau–Lifshitz, can be interpreted as a thermodynamic function found through individual quantum states. This can be simply interpreted as another temperature scale (as, for example, Fahrenheit against Celsius).

This is the point when we have to be careful. The equivalence of such quasi-thermodynamic scales takes place only in the presence of *quantum chaos*. If the residual interactions are too weak, we are still in the mean-field (or Fermi-gas) regime, information entropy is too low to clearly characterize thermal excitations. In the opposite case of excessively strong interaction, the information entropy for the majority of states will be on the level of the GOE without thermal evolution. The appropriate self-consistent description in terms of informational entropy (recall that it defines the relative information of eigenstates with respect to the mean-field basis) takes place if the residual interactions and the mean field are self-consistent so that the mean field includes the main part of regular interactions leaving incoherent collisions to the interaction part.

In the self-consistent case, we can move further asking the question of equilibrium particle distribution in excited states of chaotic nature. The computational experiments within the shell model of atoms [24], nuclei [23, 41], and Fermi gas with TBRI [42] show that the particle distribution in individual stationary states is practically equivalent to the Fermi-gas distribution with the effective temperature that agrees with thermodynamic or informational scales. The computational experiment finds the particle distribution for each eigenstate and fits for this shell-model state the parameters of chemical potential and temperature. The sequence of effective temperature values found in this way for individual states agrees quite closely with thermodynamic and informational temperature scales (Figure 25.10). The broad field of questions related to thermalization in small systems is discussed in the review article [27]. The chaotic dynamics

Figure 25.10 Comparison of single-particle (scattered dots) and thermodynamic (dashed line) temperatures of individual $J = 2, T = 0$ many-body states in ^{25}Mg , the same model as in Figure 25.5. Both temperatures are shown as a function of excitation energy [23, 41].



related to the continuum coupling and open decay channels still contains many unsolved problems. Here nuclear physics overlaps with condensed matter physics with its conductance fluctuations [43, 44].

References

- 1 H.G. Schuster and W. Just, *Deterministic Chaos: An Introduction*, John Wiley & Sons, Inc., New York, 2006.
- 2 F. Haake, *Quantum Signatures of Chaos*, 3rd edn, Springer-Verlag, Heidelberg, 2010.
- 3 H.-J. Stöckmann, *Quantum Chaos: An Introduction*, Cambridge University Press, Cambridge, 1999.
- 4 E.P. Wigner, Ann. Math. **62**, 548 (1955); **65**, 203 (1957).
- 5 M.L. Mehta, *Random Matrices*, 3rd edn, Elsevier, Amsterdam, 2004.
- 6 F.J. Dyson, J. Math. Phys. **3**, 140,157,166 (1962); 1199 (1963).
- 7 V.K.B. Kota, *Embedded Random Matrix Ensembles in Quantum Physics*, Springer, Cham, 2014.
- 8 A. Bohr and B.R. Mottelson, *Nuclear Structure*, Vol. **1**, Benjamin, New York, 1969.
- 9 C.H. Lewenkopf and V.G. Zelevinsky, Nucl. Phys. **A569**, 183 (1994).
- 10 Ch. Stoyanov and V. Zelevinsky, Phys. Rev. C **70**, 014302 (2004).
- 11 N. Frazier, B.A. Brown, and V. Zelevinsky, Phys. Rev. C **54**, 1665 (1996).
- 12 A. Volya, Phys. Rev. C **79**, 044308 (2009).
- 13 S.S.M. Wong, *Nuclear Statistical Spectroscopy*, Oxford University Press, New York, 1986.
- 14 C.E. Porter (ed.) *Statistical Properties of Spectra: Fluctuations*, Academic Press, New York, 1965.
- 15 V.K.B. Kota, and R.U. Haq (eds.) *Spectral Distributions in Nuclei and Statistical Spectroscopy*, World Scientific, Singapore, 2010.
- 16 S. Hilaire, M. Girod, S. Goriely, and A.J. Koning, Phys. Rev. C **86**, 064317 (2012).
- 17 V. Zelevinsky and A. Volya, Phys. At. Nucl. **66**, 1781 (2003).
- 18 Y. Alhassid, M. Bonett-Matiz, S. Liu, and H. Nakada, Phys. Rev. C **92**, 024307 (2015).
- 19 S. Pratt, Phys. Rev. Lett. **84**, 4255 (2000).
- 20 T.A. Brody, J. Flores, J.B. French, P.A. Mello, A. Pandey, and S.S.M. Wong, Rev. Mod. Phys. **53**, 385 (1981).
- 21 R.A. Sen'kov, M. Horoi, and V.G. Zelevinsky, Comput. Phys. Commun. **184**, 215 (2013).
- 22 R. Sen'kov and V. Zelevinsky, Phys. Rev. C **93**, 064304 (2016).
- 23 V. Zelevinsky, B.A. Brown, N. Frazier, and M. Horoi, Phys. Rep. **276**, 315 (1996).
- 24 V.V. Flambaum, A.A. Gribakina, G.F. Gribakin, and M.G. Kozlov, Phys. Rev. A **50**, 267 (1994).
- 25 J.R. Armstrong, S. Åberg, S.M. Reimann, and V.G. Zelevinsky, Phys. Rev. E **86**, 066204 (2012).
- 26 B. Lauritzen, P.F. Bortignon, R.A. Broglia, and V.G. Zelevinsky, Phys. Rev. Lett. **74**, 5190 (1995).
- 27 F. Borgonovi, F.M. Izrailev, L.F. Santos, and V.G. Zelevinsky, Phys. Rep. **626**, 1 (2016).
- 28 C.W. Johnson, G.F. Bertsch, and D.J. Dean, Phys. Rev. Lett. **80**, (1998) 2749.

- 29 V. Zelevinsky and A. Volya, Phys. Rep. **391**, 311 (2004).
- 30 Y.M. Zhao, A. Arima, and N. Yoshinaga, Phys. Rep. **400**, 1 (2004).
- 31 V. Zelevinsky, Nucl. Phys. **A555**, 109 (1993).
- 32 R. Bijker and A. Frank, Phys. Rev. C **65**, 044316 (2002).
- 33 V. Abramkina and A. Volya, Phys. Rev. C **84**, 024322 (2011).
- 34 M. Horoi and V. Zelevinsky, Phys. Rev. C **81**, 034306 (2010).
- 35 V.V. Sokolov, B.A. Brown, and V. Zelevinsky, Phys. Rev. E **58**, 56 (1998).
- 36 I.C. Percival, J. Phys. B **6**, L229 (1973).
- 37 D. Mulhall, Z. Huard, and V. Zelevinsky, Phys. Rev. C **76**, 064611 (2007).
- 38 G. Kilgus, G. Kühner, S. Müller, A. Richter, and W. Knüpfer, Z. Phys. A **326**, 41 (1987).
- 39 A. Volya, H.A. Weidenmüller, and V. Zelevinsky, Phys. Rev. Lett. **115**, 052501 (2015).
- 40 H.A. Weidenmüller and G.E. Mitchell, Rev. Mod. Phys. **81**, 539 (2009).
- 41 V. Zelevinsky and A. Volya, Phys. Scr. **91**, 033006 (2016).
- 42 V.V. Flambaum and F.M. Izrailev, Phys. Rev. E **55**, R13 (1997).
- 43 C.W.J. Beenakker, Rev. Mod. Phys. **69**, 731 (1997).
- 44 S. Sorathia, F.M. Izrailev, G.L. Celardo, V.G. Zelevinsky, and G.P. Berman, EPL (Europhys. Lett.) **88**, 27003 (2009).

General Nuclear Data Resources

Particle Data Group, Lawrence Berkeley National Laboratory.

<http://www-pdg.lbl.gov>

Particle listings, tables, reviews.

National Nuclear Data Center, Brookhaven National Laboratory.

<http://www.nndc.bnl.gov>

Nuclear structure, decay, and reaction data. Databases, evaluations, codes and tools.

Nuclear Data Evaluation Project, Triangle Universities Nuclear Laboratory.

<http://www.tunl.duke.edu/nucldata>

Energy Levels of Light Nuclei, $A = 3 - 20$.

Nuclear Data Services, at Nuclear Energy Agency.

<http://www.oecd-nea.org>

Nuclear information databases.

Nuclear Data Services at the International Atomic Energy Agency.

<https://www-nds.iaea.org>

Large collection of nuclear data and references.

Atomic Mass Data Center, Institute of Modern Physics, Chinese Academy of Sciences (IMP), Lanzhou, China.

<http://amdc.impcas.ac.cn>

Evaluations and database of nuclear masses.

Computer Physics Communications Program Library.

<http://www.cpc.cs.qub.ac.uk>

Library of programs in physics and related science.

Reference Input Parameter Library

<https://www-nds.iaea.org/RIPL-2/>

Masses, deformations, levels, resonances, level densities, strength functions, GDR parameters, fission barriers.

NN-online, Radboud University Nijmegen,

<http://nn-online.org>

Nucleon–nucleon and hyperon–nucleon interactions, phase shifts, observables data, codes.

Resources from authors' research.

<http://www.volya.net>

Shell model, miscellaneous tools, and links.

Index

a

Ab initio approach 559–564
 adhesion coefficient 496
 adiabatic approximation 226–228
 adiabatic expansion, nuclear rotation 377–379
 adiabatic perturbation theory 544
 Alaga intensity rules 362
 alpha-decay 502–505
 angular momentum 217
 classification 132–134
 conservation 213
 eigenfunctions 354–355
 Euler angles 351–353
 operators 79, 221
 recoupling of 215–222
 statistics of 486–488
 annihilation operators 205, 397, 398, 400
 anticommutators 268
 Argonne interaction 45–48, 565
 asymptotic quantum numbers 245–246
 asymptotic two-body wave function 53, 57, 200
 atomic spectroscopy 7, 8, 22, 320, 321
 Auger electrons 586

b

backbending 386
 baryonic charge 4, 14
 BCS theory 269–271, 308, 478, 484
 beta-decay process 13, 587, 588, 600, 606
 binding energy 91–95, 251
 black-body radiation 283

Bloch–Horowitz method 562
 body-fixed frame 345, 351, 370
 Bogoliubov transformation 269, 403
 Bohr radius 7, 8
 Bohr–Sommerfeld quantization 167
 Borromean nuclei 198
 Bose gas, ideal liquid rotation 381–383
 Bose quanta 448
 Bose statistics 84, 128, 132, 204, 287, 459
 bosonic approximation 130
 bosons
 collective modes as 432–433
 operators, algebra of 449–452
 quasiparticle 447
 Breir–Wigner approximation 494
 Breit–Wigner shape 196, 582, 631
 Brink–Axel hypothesis 631
 Brownian motion 514, 535

c

canonical form, RPA 427–430
 canonical transformation 265–269, 402–404
 Cartesian coordinates 241
 Casimir operators 450, 451–454, 458, 460
 second-order 457
 center-of-mass
 motion 21
 problem 555–558
 central density 91
 central limit theorem 631, 635
 CGC *see* Clebsch–Gordan coefficients (CGC)

- chaotic enhancement 522
 chaotic system 627–652
 complexity of wave functions 636–639
 correlations between classes of states
 639–643
 invariant entropy 643–646
 level density 633–636
 random matrix ensembles 646–650
 strength function 628–633
 thermalization 650–652
- charge
 baryonic 4, 14
 density, multipoles 98, 301, 602, 609
 distribution 5–10
 weak 615, 616
- chemical equilibrium, Fermi gas model 143–146
- chemical potential 92
- Cherenkov effect 547
- circular polarizations 285
- Clebsch–Gordan coefficients (CGC) 32, 64, 130, 170, 175, 213–216, 253, 254, 306, 452, 559
- coherence factors 267
- coherent superpositions 421
- collective enhancement effect 485
- collective rotation 342, 344
- collective RPA modes 432–433
- collective transitions 308–310
- compound elastic process 494
- condensation energy 278–279
- configuration interaction
 Ab initio approach 559–564
 center-of-mass problem 555–558
 effective non-Hermitian Hamiltonian
 571–576
 isolated to overlapping resonances
 576–581
 many-body Hamiltonian 570–571
 semiempirical effective interactions
 565–569
 three-body forces 564–565
 two-body interactions 558–559
- configuration mixing 174
- constant temperature model 484
- core polarization 307
- Coriolis antipairing 385
- Coriolis mixing 368–370
- Coulomb barrier penetration 15, 16, 530
- Coulomb energy 5
- Coulomb excitation 322–326
- Coulomb field 160
- Coulomb interaction 86
- Coulomb-nuclear interference 87–89
- Coulomb scattering 86–87
- cranked model 372–375
- Curie plot 589
- d**
- Darwin–Fowler method 418, 479–482, 650
- de Broglie wavelength 527
- decoherence 476, 477
- decoupling parameter 368–370
- deep-inelastic process 526, 528, 538, 547
- delayed neutrons 502
- Δ -resonance 34, 48, 565
- density
 general properties 478–479
 operators 98
- density matrix
 evolution of 427
 Fourier components 428
 generalized 407–408
 of ground state 426
 single-particle 398–400
- deuterium 28
- deuteron 27, 51–55
- deuteron magnetic moment 58
- deuteron quadrupole moment 60
- diamagnetic effect 318
- diffusion process, equilibration as 534–540
- dipole operator 115, 116, 293
- dipole polarization 119
- Dirac equation 596–598
- Dirac formalism 595–599
- direct interaction 393
- dissipation, nuclear fission 512–514
- double-magic nuclei 154, 416
- drip lines 192, 193
- deuteron d -wave 55–58
- dynamical moment of inertia 340, 375
- dynamics mapping 433–435

e

effective field theory 412, 565
 effective radius 82–83
 Efimov states 199–202
eigenfunction *see eigenstates*
 eigenstates
 angular momentum 347, 354–355
 collective modes 421, 423, 465
 degenerate model 262
 deuteron 56
 independent particles 169
 many-body Hamiltonian 571
 mean-field 169
 rotor Hamiltonian 356
 elastic enhancement factor 496
 elastic scattering 68, 79
 electric charge 4
 electric dipole 120
 radiation 292–295
 transitions 307
 electric dipole moment (EDM) 607–609
 electric multipole moment 129
 electric quadrupole moment 59–65, 172,
 363–366
 electric quadrupole radiation 295–296
 electric quadrupole transitions 307
 electromagnetic field, and gauge invariance
 283–284
 electromagnetic interactions 5–10
 electromagnetic radiation 283
 electron antineutrinos 13
 electron mass 9
 electron scattering 2, 5, 236, 330–335
 electron wave function 7–8
 electrostatic repulsion energy 108
 electroweak theory 612–616
 energy conservation 321
 energy density functional method
 413
 energy gap 228, 273–276
 energy minimization 271–272
 enhancement, nuclear 609–612
 ensembles 477
 equilibrium 477
 properties of 477
 random matrix 646–650
 entropy, invariant 643–646

equilibration, diffusion process 534–540

equilibrium ensemble 477
 equilibrium entropy 482, 483
 ergodicity 477
 Euler angles 231, 347–350
 angular momentum in 351–353
 exchange interaction 391–395
 exotic nuclei 188, 525

f

factorized forces, model with 430–432
 Fermi energy 244
 Fermi gas 428
 description 418
 nuclear 483–485
 nuclear rotation of 379–381
 Fermi gas model 167, 170
 asymmetric systems 143–146
 chemical equilibrium 143–146
 correlation between particles 142–143
 density of 484
 gravitational equilibrium 148–150
 ground state 138–141
 mean field and quasiparticles 135–136
 nuclear matter equation of state
 150–151
 perfect 137–138
 pressure and speed of sound 146–148
 Fermi golden rule 485
 fermion transfer operator 305
 Fermi operator 38, 122, 253, 427
 Fermi process 603
 Fermi statistics 3, 26, 29, 78, 148,
 205, 447
 Feshbach resonance 202
 Fierz interference term 601
 finite rotations 345–346
 matrix elements of 346
 fission barrier 500
 fission isomers 514–518
 fission process 501, 527
 fluctuation–dissipation theorem 545
 Fock space 204
 forbidden transitions 595
 form-factor 332, 333
 four-fermion theory 599–601
 Fourier transformation 330

full width at half maximum (FWHM)

197

fusion reactions 550–552

g

Galilean invariance 100

gamma-radiation 283–303

 electric dipole radiation 292–295

 electric quadrupole radiation 295–296

 magnetic dipole radiation 296–297

 multipole expansion 299–303

 photoabsorption 298–299

 photons 285–288

 radiation probability 291–292

gamma-ray spectrum 340

Gamow factor 88

Gamow–Teller giant resonance 603

Gamow–Teller operators 38

Gamow–Teller transitions 123, 588,
590, 592, 593, 595, 602, 604,
606, 607

gauge transformation 284

Geiger–Nuttall law 505

generalized spherical functions 350

generator coordinate method 444–445

geometric chaoticity 640

giant dipole resonance (GDR) 121

giant resonances 119–121, 448

Goldstone mode 439, 441, 442

gravitational equilibrium, Fermi gas
model 148–150

Grenoble experiments, parity violation
520

ground state band 359–360

 moment of inertia 341

ground state, Fermi gas model 138–141

gyromagnetic ratio 11, 290

h

halos

 nuclear 192–193

 one-body 193–195

 in quantum systems 190–192

 two-body 195–199

harmonic oscillator potential 157–159

Hartree approximation 397

Hartree–Fock approximation 517, 540

Hartree–Fock–Bogoliubov (HFB)

 approximation 400–402

Hartree–Fock (HF) equations 395–397

 operator formulation 397–398

heavy ion reactions 525–552

 equilibration as diffusion process

534–540

 experimental indications 526–530

 fusion reactions 550–552

 general approach 541–545

 macroscopic description 530–534

 microscopic description 540–541

 nuclear multifragmentation 547–550

 simple model 545–547

Hellman–Feynman relations 374

Hermitian conjugation 127

Hermitian operator 268, 429

HFB approximation *see*

 Hartree–Fock–Bogoliubov (HFB)
 approximation

Higgs mechanism 616–618

high energy nuclear physics 2

Hill–Wheeler equation 445

hole-type operators 127

Hoyle state 190

Hubbard–Stratonovich transformation
489

Hund rule 394

hydrodynamic model 100

hydrogen atom 7, 8

i

IBM *see* interacting boson model (IBM)

ideal liquid, nuclear rotation 381–383

inelastic electron scattering 334

inelastic scattering process 325

inertial parameters 100–102

intensity rules, nuclear rotation 360–362

interacting boson model (IBM) 449, 450,
455, 456, 466

IBM Hamiltonian 450, 470, 471

 shapes and phase transitions in
 470–473

intermediate mass fragments (IMF)

547, 548

internal electron conversion 320–322

internal photoeffect 318

- intrinsic deformation 569
 invariant entropy 643–646
 inverse participation ratio 638
 irreducible representations 458–641
 irrotational flow 100
 island of inversion 409
 isobaric analog state (IAS) 122
 isomerism, nuclear 310–312
 isomers 17
 fission 514–518
 shape 515
 isoscalar 312, 314
 isospin 23–25, 312–315
 exchange 45
 multiplets 38–40
 selection rules 35–38
 isospin invariance 25–26
 classification 30–31
 relations between cross sections 31–34
 space–spin symmetry and 26–29
 isovector 312–314
 modes 117–119
- k**
- kinetic energy 100–102
 Klein–Gordon equation 48
 Kramers degeneracy 251
 Kramers theorem 96, 229
- l**
- Landau–Zener formula 513, 541
 Langevin equation 535, 536
 Laplace equation 101
 Laplace operator 106
 large-amplitude collective motion 510–512
 Large Hadron Collider (LHC) 548
 LDM *see* liquid drop model (LDM)
 Lee–Suzuki similarity transformation 563
 Legendre polynomials 228, 252, 273
 Legendre transformation 479
 leptons 13
 level density 633–636
 light nuclei
 Efimov states 199–202
 halo in quantum systems 190–192
 nuclear chart 185–190
- nuclear halos 192–193
 one-body halo 193–195
 two-body halos 195–199
 linear response 119–121
 Lipkin–Meshkov–Glick (LMG) model 437, 439
 liquid drop model (LDM) 97, 499, 518
 binding energies 91–95
 inertial parameters 100–102
 kinetic energy 100–102
 microscopic variables 97–98
 multipole moments 98–100
 shape variables 95–97
 shape vibrations 102–104
 stability of 104–111
 liquid–fog transition 547
 LMG model *see* Lipkin–Meshkov–Glick (LMG) model
 local density of states (LDOS) 629
 Lorentzian function 118
 low-energy Hamiltonian 43
 low-energy nuclear forces 43–45
 low-energy scattering 71
- m**
- magic numbers 96, 153
 magnetic dipole
 interactions 395
 moment 58–59
 operator 307, 308, 314
 radiation 296–297
 magnetic moment 172–174
 nuclear rotation 366–367
 Majorana fermion 585
 Majorana operator 45
 many-body Hamiltonian 570–571
 Markovian process 535, 536
 mass parameter 435–438
 matrix elements
 of finite rotations 346
 two-body interactions 558–559
 Maxwellian distribution 491
 mean field, Fermi gas model 135–136
 mean square radius 194
 mesoatom 28
 meson exchange 48–51
 mesoscopic 2, 92

- microscopic variables 97–98
 Mikheev–Smirnov–Wolfenstein (MSW) mechanism 620
 moment of inertia 339
 dynamical 340, 375
 ground state band 341
 nuclear rotation 375–376
 momentum conservation 212
 momentum transfer 9
 monopole operator 115, 116
 monopole transitions 318–320
 Moszkowski units 308
 multifragmentation 547–550
 multiparticle configurations 178–183
 multiphonon excitations 128–132
 multipole expansion 299–303
 multipole moments 98–100
 in seniority scheme 260–261
 multipole operators, of nonzero multipolarity 430
- n**
 Nambu–Goldstone theorem 439
 near-magic spherical nuclei 246
 neutrino
 Majorana/Dirac 620–623
 oscillations 618–620
 neutron-deficient isotope 444
 neutrons 1, 3
 decay 13–15
 fission 505–509
 resonance 475
 skin 199
 Nilsson potential 163, 246–247,
 373
 Nilsson scheme 511, 635
 non-adiabatic effects, nuclear fission 512–514
 nonequilibrium entropy 480
 non-Hermitian Hamiltonian 571–576,
 579
 non-orthogonal orbitals 208
 normalization, and mass parameter 435–438
 normal modes, classification of 121–125
- nuclear deformation 223–250
 adiabatic approximation 226–228
 anisotropic harmonic oscillator 240–245
 asymptotic quantum numbers 245–246
 collective model 224–226
 empirical deformation 235–239
 examples 247–250
 Nilsson potential 246–247
 onset of deformation 228–230
 quadrupole deformation 230–232
 quadrupole shapes 233–235
 quadrupole shape variables 232–233
 single-particle quantum numbers 239–240
 nuclear enhancement, weak interactions 609–612
 nuclear Fermi gas, thermodynamics of 483–485
 nuclear fission 499–522
 alpha-decay 502–505
 dissipation 512–514
 fragments 502
 isomers 514–518
 large-amplitude collective motion 510–512
 neutron fission 505–509
 non-adiabatic effects 512–514
 parity violation 518–522
 photofission 509–510
 nuclear halos 192–193
 nuclear isomerism 310–312
 nuclear multifragmentation 547–550
 nuclear photoeffect 326–330
 nuclear rotation
 adiabatic expansion 377–379
 classical rotation and Routhian 370–372
 Coriolis mixing 368–370
 cranked rotation 372–375
 decoupling parameter 368–370
 eigenfunctions of angular momentum 354–355
 electric quadrupole moment 363–366

- Euler angles 347–353
finite rotations 345–346
ground state band 359–360
ideal liquid 381–383
intensity rules 360–362
magnetic moment 366–367
matrices as functions on group 346–347
moment of inertia 375–376
pairing effects 384–385
perfect Bose gas 381–383
perfect Fermi gas 379–381
rigid rotor 355–356
rotational bands 337–345
simplest solutions 358–359
symmetry properties 357–358, 367–368
nuclear spectra, periodicity of 156–157
nuclear structure, effects 601–604
 gamma radiation 315
 weak interactions 601–604
nuclear transformations 17
nuclear transitions, weak interactions 590–595
nuclear vibrational modes, quantization of 125–127
nucleon–nucleon interaction 391
nucleon–nucleon scattering 71
nucleon pair operators 214
nucleon separation energy 155–156
nucleus
 charge distribution 5–10
 electromagnetic interactions 5–10
 magnetic properties 10–11
 neutron decay 13–15
 proton and neutron 3
 strong interactions 4–5
 weak interactions 1–2, 11–13
- o**
occupation number representation 203
odd-even effect 263
one-body halo 193–195
one-body operators 208–209
- orbital momentum 62
representation 160–162
oscillator brackets 559
oscillator eigenfunctions 571
- p**
pair annihilation operators 213
pairing correlations
BCS theory 269–271
canonical transformation 265–269
condensation energy 278–279
degenerate model 261–265
energy gap 273–276
energy minimization 271–282
excitation spectrum 276–278
multipole moments in seniority scheme 260–261
physical evidence 251–256
seniority scheme 256–259
transition amplitudes 279–281
pairing Hamiltonian 269
parity violation
 nuclear fission 518–522
 weak interactions 604–607
partial wave expansion 69
particle–hole symmetry 171–172
particle number conservation 269, 409–411
particle–particle channel 211
partition function 479
Pauli blocking 259
Pauli matrices 22
Pauli principle 128, 146, 178, 205
 limitations 206
periodicity of nuclear spectra 156–157
permutational symmetry 452
phase dynamics 476
phase shifts 69–71
phase transitions 478
phonons 127
phonon vacuum 128
photoabsorption 118, 298–299, 510
photoeffect
 energy conservation in 326
 nuclear 326–330

photofission 509–510
 photons 285–288
 pion–nucleon scattering 32–33
 Planck constant 9
 pointer basis 643
 Porter–Thomas distribution (PTD) 508, 519
 power-method algorithms 571
 preequilibrium emission 493
 proton–neutron separation 120
 proton–proton scattering 87
 protons 1, 3
 pushing model 378
 pygmy dipole resonance 301, 426

q

quadrupole
 bosons 457
 deformation 109, 230–232
 electromagnetic transitions 463
 excitations, low-lying 448–450
 moment 59–65, 174–177, 236
 operator 458, 468, 469
 phonon 128
 shape variables 232–233
 quadrupole–quadrupole interaction 472
 quantization
 Bohr–Sommerfeld 167
 of nuclear vibrational modes 125–127
 secondary 203–208
 quantized theory 449
 quantum chromodynamics (QCD) 4
 quantum electrodynamics (QED) effects 559
 quantum Munchausen process 505
 quantum numbers
 Interacting Boson Model 458–461
 multiparticle configurations 178–183
 nuclear states 17
 seniority 255
 single-particle 203, 239–240
 strong interactions 4
 two-body problem 21–23
 quantum scattering theory 67–69, 562
 quasielastic reactions 526, 529
 quasifission 529
 quasimolecular model 226

quasiparticle random phase approximation (QRPA) 427
 quasiparticles 268, 315
 boson 447
 energy 276, 404–406
 Fermi gas model 135–136
 unpaired 341
 quasispin 262–265
 quasistationary 475, 571–583
 quenching, Gamow–Teller strength 603

r

radial differential equation 417
 radial electron wave function 7
 radial form-factor 226
 radial wave functions 77
 radiation probability 100, 291–292
 random matrix ensembles 646–650
 random phase approximation (RPA) 426–427
 canonical form 427–430
 collective modes 432–433
 normalization and mass parameter 435–438
 symmetry breaking 438–444
 thermal 430
 reaction threshold 321, 572
 realistic level scheme 165–166
 recoil effects 177–178
 recoupling, of angular momentum 215–222
 recurrence time, Weisskopf 475
 Regge trajectory 338
 resonances
 energy 475
 Feshbach 202
 isolated 494
 scattering at low energies 80–81
 statistical description of 492–497
 rigid rotor 355–356
 rotational bands 337–345
 Routhian 371
 classical rotation 370–372
 function 371
 RPA *see* random phase approximation (RPA)

- Runge–Lenz vector 160
 Rydberg state 191
- s**
 scalar potential 284
 scattering
 Coulomb-nuclear interference 87–89
 Coulomb scattering 86–87
 effective radius 82–83
 of identical particles 83–86
 interaction 461
 length 71–77, 78–80
 at low energies 80–81
 phase shifts 69–71
 problem 67–69
 processes 273
 Schiff moment 314, 609
 Schmidt values 256
 Schrödinger equation 70, 73, 226, 227
 Schwinger representation 179
 scissors modes 470
 secondary quantization 203–208
 second-order Casimir operators 457
 self-consistent field
 effective interaction 411–413
 exchange interaction 391–395
 general canonical transformation 402–404
 generalization to non-zero temperature 418–419
 generalized density matrix 407–408
 generator coordinate method 444–445
 Hartree–Fock–Bogoliubov
 approximation 400–402
 Hartree–Fock equations 395–397
 operator formulation 397–398
 pairing and particle number conservation 409–411
 single-particle density matrix 398–400
 Skyrme functionals 413–418
 solutions 404–406
 semicircle strength function 639
 semiclassical theory 517
 semiempirical interactions 565
 seniority 458
 scheme 255
- separation energy 155–156
 shape-elastic scattering 495
 shape isomers 515
 shapes and phase transitions, IBM 470–473
 shape variables 95–97
 shape vibrations 102–104
 shell correction 515
 shell model *see* configuration interaction
 calculation 569, 582
 configurations 169–171, 185
 examples 632
 magnetic moment 172–174
 Monte Carlo approach 488–490
 multi-particle configurations 178–183
 particle–hole symmetry 171–172
 quadrupole moment 174–177
 recoil corrections 177–178
 solution 409
 shell structure 153
 semiclassical origins of 166–168
 single-boson energy 461
 single-nucleon adiabatic collective model 227
 single-particle degeneracy 251
 single-particle density matrix 398–400
 single-particle energies 272
 single-particle level density 517
 single-particle levels 241
 single-particle motion 448
 single-particle operator 208
 single-particle orbits 270
 single-particle problem 225
 single-particle quantum numbers 203, 239–240
 single-particle shell model 260
 single-particle transitions 305–308
 single-photon transitions 292
 Skyrme functionals 413–418
 sound waves 113–116
 space–spin symmetry 26–29, 44
 spatial density operator 209
 spectroscopic factors 334
 spherical basis, interaction in 213–215
 spherical Bessel function 9
 spherical liquid drop 104–111
 spherical shell model 305, 311

- spin-angular wave function 175
 spin cut-off factor 488
 spin exchange 45
 spin gyromagnetic ratios 59
 spin magnetic moments 58
 spin-orbit coupling/interaction 47, 163–165, 188, 217, 223, 240, 245, 305, 311
 spin-orbit potential 226
 spin symmetry 44
 spin-triplet fermions 85
 spontaneous radiation 283
 spreading width 526
 square well potential 162–163
 static polarizability 119
 statistical spectroscopy 633
 statistical thermodynamics:relation to 482–483
 Stern–Gerlach experiment 18
 strength function 448, 628–633
 structural selection rules 315–318
 subgroups 452–454
 superallowed 587
 superdeformed nuclei 238
 superradiance 577, 579
 surface velocity 101
 surface waves 113, 114
s-wave 51–55, 72
 symmetry breaking 438–444
 symmetry properties
 nuclear rotation 357–358
 revisited 367–368
- t**
 tabular quadrupole moment 60
 Talmi–Moshinsky coefficients 559
 Tamm–Dancoff approximation 429, 431
 TBRI *see* two-body random interaction (TBRI)
 TDHF *see* time-dependent Hartree–Fock approximation (TDHF)
 tensor forces 55–58
 tensor operator 44, 45
 thermalization, chaotic system 650–652
 thermal random phase approximation (RPA) 430
 thermodynamics
- compound reactions 490–492
 nuclear Fermi gas 483–485
 statistical 482–483
 Thomas–Reiche–Kuhn sum rule 116
 time-conjugate orbits 261
 time-dependent Coulomb forces 525
 time-dependent Hartree–Fock
 approximation (TDHF) 540
 time-independent Hamiltonian 479
 time-reversal invariant system 268
 transition amplitudes 279–281
 transition states 505
 density of 506
 transmission coefficient 496
 transversality condition 285
 triaxial deformation 238
 triple-alpha process 190
 two-alpha construction 237
 two-body halos 195–199
 two-body operators 209–210
 two-body random interaction (TBRI) 650
 two-nucleon function 29
 two-nucleon system 22, 47
- u**
 ultralow energy 72
 uniform macroscopic systems 273
 unitarity 422
 unpaired quasiparticles 341
 Urbana model 565
- v**
 velocity-dependent interactions 120
 vibrational limit 461–466
 vibrational quanta 127
 virtual rotation 473
 volume sound wave 114
 volume wave equation 118
- w**
 wave equation 285
 wave functions 424, 444, 445
 complexity of 636–639
 electron 7–8
 radial 7, 77
 spin-angular 175
 wavelike perturbations 534

- weak interactions 585–623
beta spectrum 587–589
Dirac formalism 595–599
electric dipole moment 607–609
electroweak theory 612–616
four-fermion theory 599–601
Higgs mechanism 616–618
neutrino 618–623
nuclear enhancement 609–612
nuclear structure effects 601–604
nuclear transitions 590–595
parity violation 604–607
- Weil equation 620
Weisskopf recurrence time 475
Weisskopf single-particle units 307
Wick theorem 258
Wigner–Eckart theorem 128, 265, 306,
313, 559
Wigner formula 75
Woods–Saxon potential 192, 195, 246

Z

- zero-point amplitude 230
zero-point vibrations 237